THE 23RD EDITION *of* THE MANUAL OF

MINERAL SCIENCE

CORNELIS KLEIN & BARBARA DUTROW

CD-ROM
VERSION 3.0

MINERALOGY TUTORIALS VERSION 3.0 CD

PC-Windows

MINERALOGY TUTORIALS INSTALLATION

1. Insert the CD into CD-ROM drive.
2. Installation should start automatically. If NOT, select My Computer, then the CD-ROM drive, then Select icon named "Mineralogy Tutorials"
3. Follow instructions on screen.

HARDWARE REQUIREMENTS

1. Pentium 500-MHz or higher processor.
2. 128 MB of RAM (256 MB RAM recommended)
3. 640x480 resolution with 256 colors or greater
4. 8x CD-ROM drive or faster
5. 15 MB of free disk space

SOFTWARE REQUIREMENTS

1. Windows OS, running - Windows ME, 98, 2000 or XP
2. QuickTime 6 or higher for Windows (QuickTime 6 included on CD-ROM.)

HOW TO RUN THE TUTORIALS

1. Insert the CD into CD-ROM drive.
2. Program should start automatically
3. If NOT, select My Computer, then the CD-ROM drive, then Select icon named "Mineralogy Tutorials"

MAC

MINERALOLOGY TUTORIALS INSTALLATION

1. Insert the CD into CD-ROM drive.
2. Auto Install follows

HARDWARE REQUIREMENTS

1. G3 model or better
2. 128 MB of RAM (256MB or more is recommended)
3. 640x480 resolution with 256 colors or greater
4. 8x speed CD-ROM drive or faster
5. 15 MB of free disk space

SOFTWARE REQUIREMENTS

1. Mac OS X v. 10.2.8 or higher
2. QuickTime 6 or higher (QuickTime 6 included on CD-ROM)

HOW TO RUN THE TUTORIALS

1. Insert the CD into CD-ROM drive
2. Double-click on "Mineralogy Tutorials" icon which is located in the same directory as the "Read Me" file in the CD-ROM

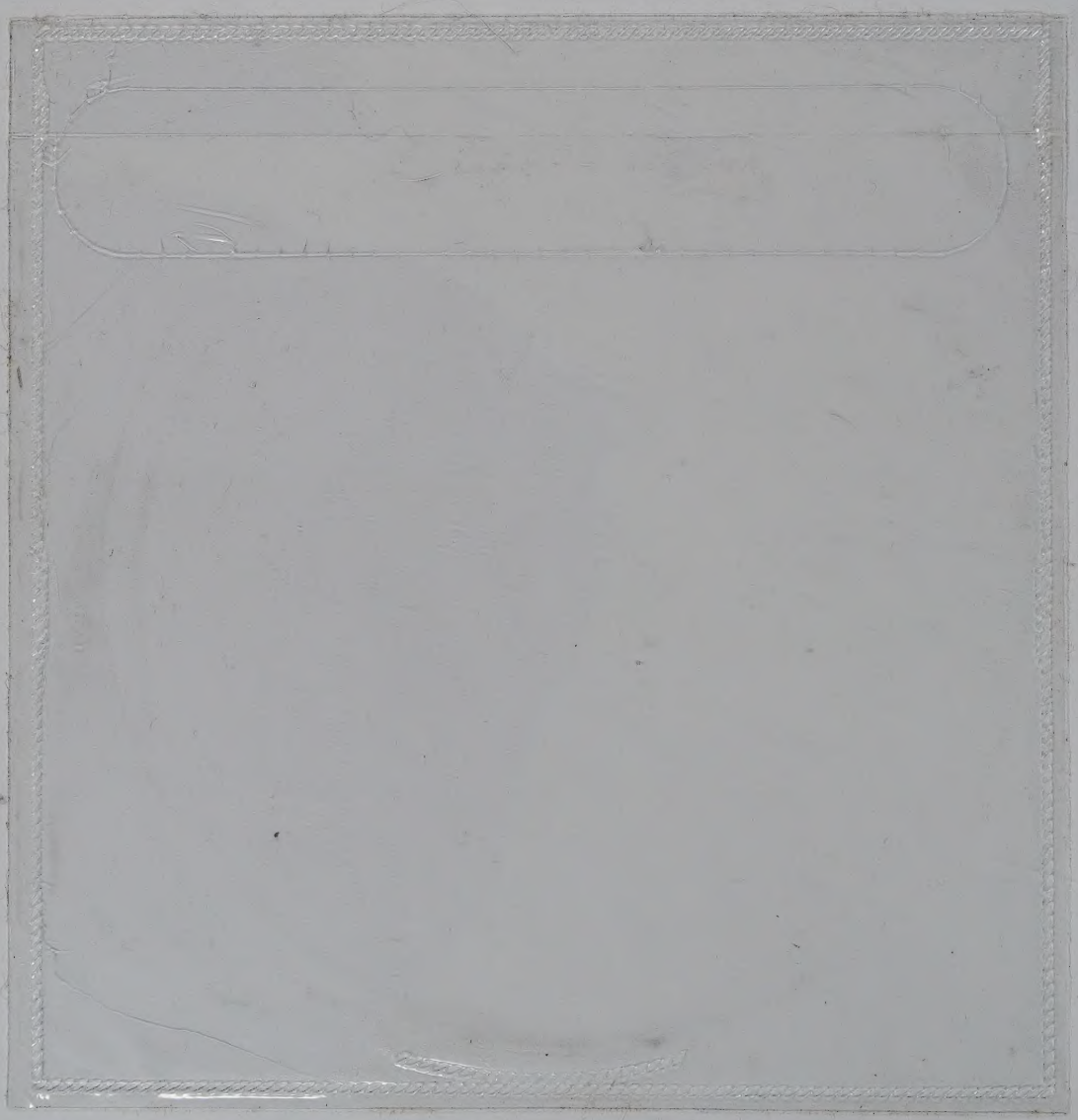

Accessing subject matter on the CD-ROM, MINERALOGY TUTORIALS (version 3.0)

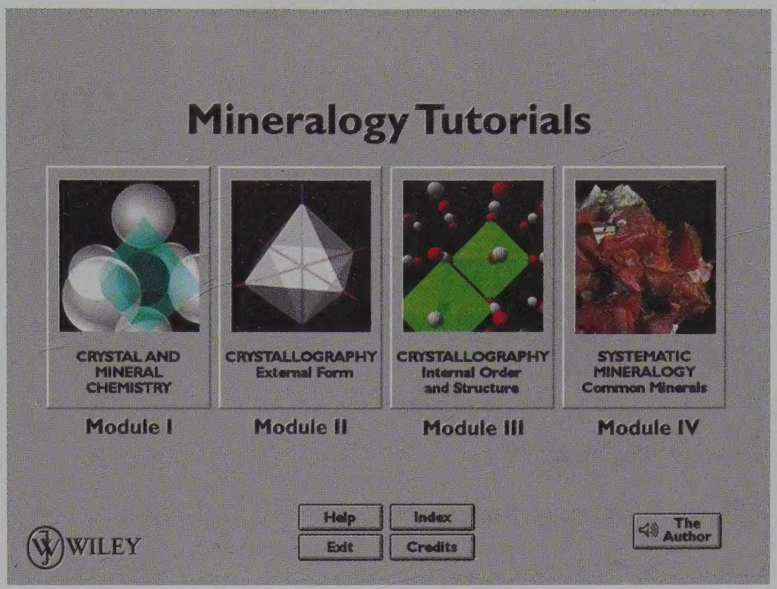

The first menu screen ▶ followed by the first subject screen ▼ in Module I

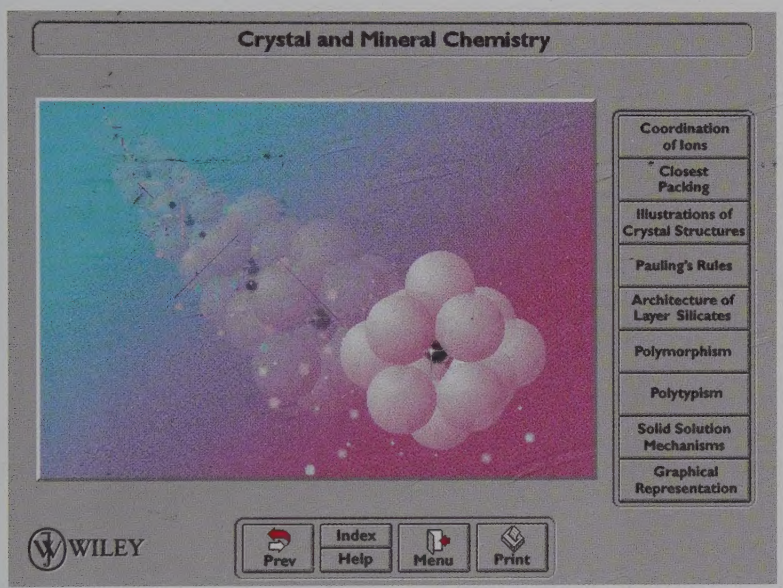

Examples of Index Screens

The main menu screen, showing major subject categories in the four modules ▶

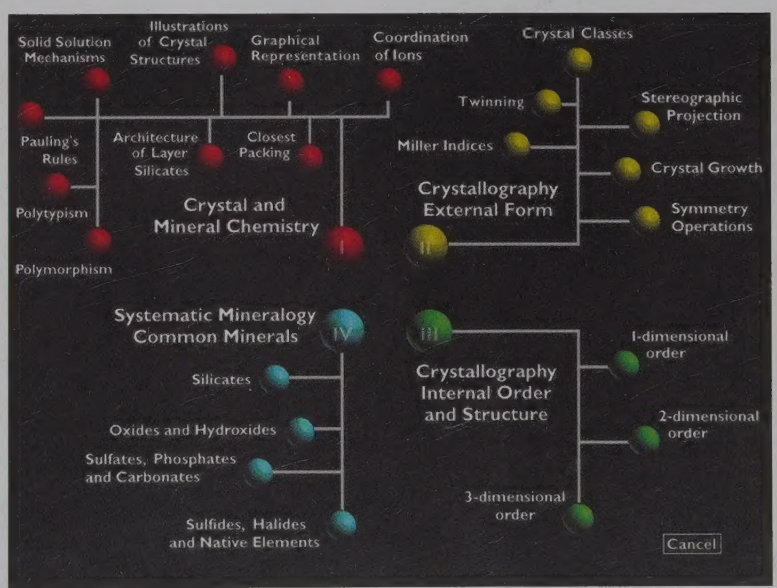

The colored spheres are "hot" and can be clicked with the mouse.

Examples of Index Screens

continued

The index screen for Module II shows a more detailed screen when the "Crystal Classes" button is clicked. ▶

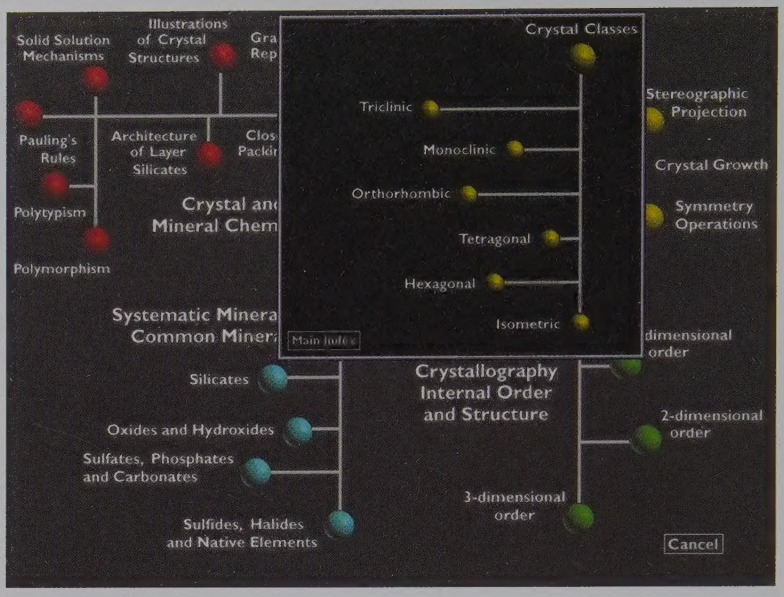

◀ The index screen for Module III shows a more detailed screen when the "3-dimensional order" button is clicked.

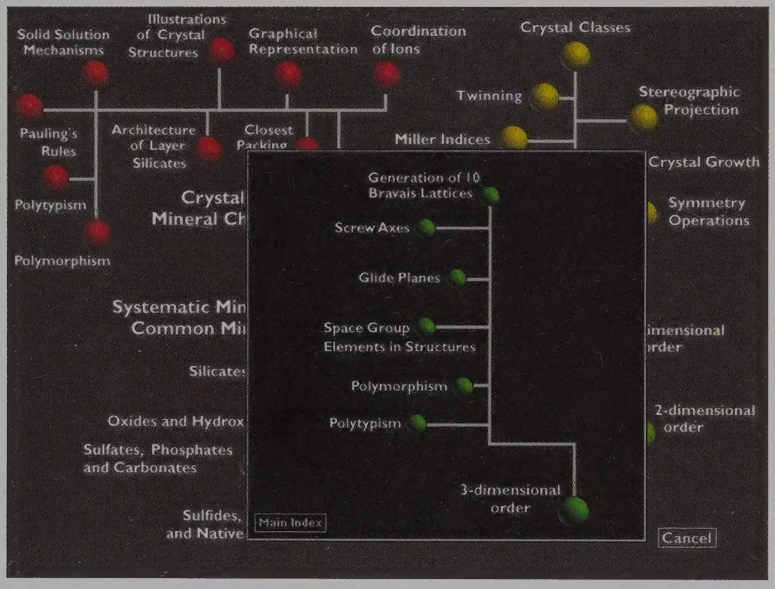

The index screen for Module IV shows the subdivision of the silicates when the "Silicates" button is clicked. ▶

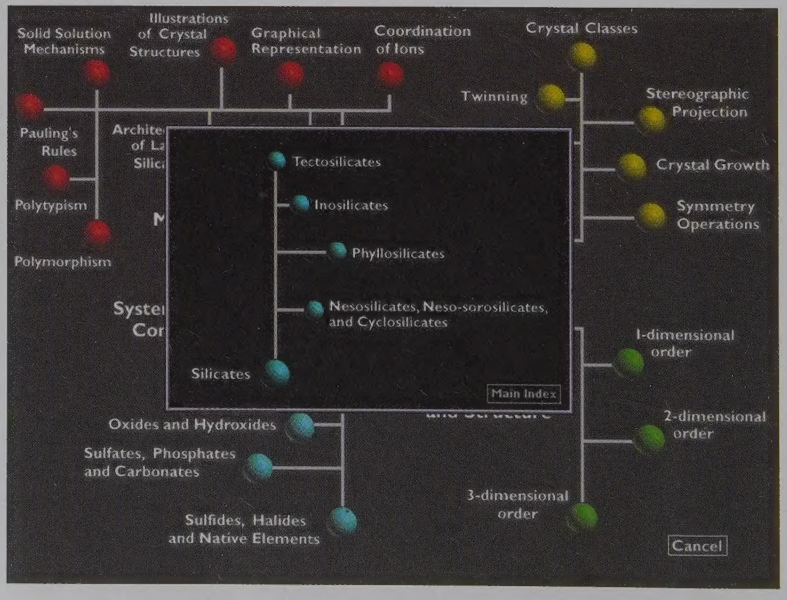

The colored spheres are "hot" and can be clicked with the mouse.

THE WILEY BICENTENNIAL–KNOWLEDGE FOR GENERATIONS

Each generation has its unique needs and aspirations. When Charles Wiley first opened his small printing shop in lower Manhattan in 1807, it was a generation of boundless potential searching for an identity. And we were there, helping to define a new American literary tradition. Over half a century later, in the midst of the Second Industrial Revolution, it was a generation focused on building the future. Once again, we were there, supplying the critical scientific, technical, and engineering knowledge that helped frame the world. Throughout the 20th Century, and into the new millennium, nations began to reach out beyond their own borders and a new international community was born. Wiley was there, expanding its operations around the world to enable a global exchange of ideas, opinions, and know-how.

For 200 years, Wiley has been an integral part of each generation's journey, enabling the flow of information and understanding necessary to meet their needs and fulfill their aspirations. Today, bold new technologies are changing the way we live and learn. Wiley will be there, providing you the must-have knowledge you need to imagine new worlds, new possibilities, and new opportunities.

Generations come and go, but you can always count on Wiley to provide you the knowledge you need, when and where you need it!

William J. Pesce

WILLIAM J. PESCE
PRESIDENT AND CHIEF EXECUTIVE OFFICER

Peter Booth Wiley

PETER BOOTH WILEY
CHAIRMAN OF THE BOARD

COVER

This represents a photograph of a thin (2 mm thick), polished slice of a tourmaline crystal cut across its length. This translucent slice, with more subtle natural coloring than shown here, was photographed on a light box that illuminated the slice from below. The intensity of the original color banding has been computer-enhanced.

The width of the total pattern on the text cover is approximately 23 cm, which corresponds to about 7 cm on the specimen, giving a magnification of approximately 3.2×. The 3-fold rotation axis (the *c* axis) of tourmaline coincides with the center of the tristar pattern. The rays of the tristar coincide with the traces of three vertical mirrors (*m*) and the triangular color banding is parallel to the prism form $\{11\bar{2}0\}$. The distinct coloration of the rays of the tristar and the different colors of the triangular zones result from minute chemical variations during outward growth of the crystal. Specimen from Anjanabonoina near Betafo, Madagascar (Harvard Mineralogical Museum).

SUPPLEMENTARY MATERIALS

For laboratory and homework assignments: Klein, C. 2008. *Minerals and rocks: Exercises in crystal and mineral chemistry, crystallography, X-ray powder diffraction, mineral and rock identification, and ore mineralogy*, 3rd ed. John Wiley and Sons, Hoboken, NJ. *A Solutions Manual* with completely worked answers to most of the assignments in *Minerals and Rocks: Exercises* is available to instructors who have adopted *Minerals and Rock: Exercises* from John Wiley and Sons.

For classroom instruction: www.wiley.com/college/klein

The *Manual of Mineralogy* was written by James D. Dana in 1848 and revised by him in 1857, in 1878 as the *Manual of Mineralogy and Lithology*, and in 1887 as the *Manual of Mineralogy and Petrography*. An edition number was given to some, but not all, reprintings of each revision. For example, the 1887 revision was reprinted in 1891 as the 10th Edition, but in 1893, 1895, and 1900 as the 12th Edition.* Each subsequent revision, as *Dana's Manual of Mineralogy*, has been given an edition number as follows: *13*, 1912, and *14*, 1929 by William E. Ford. *15*, 1941; *16*, 1952; *17*, 1959; and *18*, 1971 by C. S. Hurlbut, Jr. *19*, 1977 by C. S. Hurlbut, Jr. and C. Klein. *20*, 1985 by C. Klein and C. S. Hurlbut, Jr. *21*, 1993 by C. Klein and C. S. Hurlbut, Jr. *22*, 2002 by C. Klein. *23*, 2007 by C. Klein and B. Dutrow.

*The information regarding revisions by James D. Dana was supplied by Clifford J. Awald, Buffalo Museum of Science.

THE 23RD EDITION OF THE MANUAL OF

MINERAL SCIENCE

THE 23RD EDITION OF THE MANUAL OF

MINERAL SCIENCE

(after JAMES D. DANA)

Cornelis Klein
The University of New Mexico
Albuquerque, New Mexico

Barbara Dutrow
Louisiana State University
Baton Rouge, Louisiana

JOHN WILEY & SONS, INC.

Publisher **Jay O'Callaghan**
Acquisitions Editor **Ryan Flahive**
Marketing Manager **Emily Streutker**
Production Manager **Kelly Tavares**
Cover **Marc Klein**
Editorial Assistant **Courtney Nelson**
Senior Illustration Editor **Sandra Rigby**
Production Services **Jeanine Furino, GGS Book Services**

This book was set in Janson by GGS Book Services
and printed and bound by Courier Companies.

ISBN-13: 978-0-471-72157-4

Printed in the United States of America

10 9 8 7 6

In 1848, John Wiley & Sons, Inc., was beginning to shift from being primarily a literary publisher to being a scientific, technical, and engineering publisher. This shift was the first of many Wiley has made over the years as it has constantly adapted to meet the unique needs of each new generation.

This was also the year Wiley published one of its most enduring and notable titles: James D. Dana's *Manual of Mineralogy, including Observations on Mines, Rocks, Reduction of Ores, and the Application of the Science to the Arts*. Over the years, it too has continually adapted to meet the changing needs of all who use it. Now in its twenty-third edition, the *Manual of Mineral Science* remains the standard for teaching introductory mineralogy/mineral science.

ENHANCED ILLUSTRATIONS

This new twenty-third edition features many changes that enhance the text's trademark clarity and effectiveness. A great deal of effort was spent on improving the large number of illustrations, with almost all drawings of crystal structures re-rendered, and line drawings redesigned. The result is a crisp, new look that includes crystal structure illustrations, black line drawings, and many new photographs mainly of mineral specimens.

The illustration history of this classic text is particularly interesting. The first edition evolved through many reprintings and new editions. The earliest illustrations were of aspects of the external morphology of crystals, and many that still appear in the text have been used since 1912. Some examples can be seen in Fig. A(a).

In 1959, with the publication of the seventeenth edition of Dana's *Manual of Mineralogy* by C. S. Hurlbut, Jr., some basic crystallochemical concepts were introduced. These were illustrated by artist-drawn renderings of coordination polyhedra and the close packing of SiO_4 tetrahedra and various silicate linkages derived therefrom [see Fig. A (b)]. Several of these illustrations have been purposely retained in the present edition because of their artistic appeal and historical value.

In 1977, the nineteenth edition of Dana's *Manual of Mineralogy* was authored by C. S. Hurlbut, Jr., and C. Klein. At that time, the authors introduced a large number of polyhedral airbrush drawings of crystal structures [all done by graphic artists in Wiley's drafting and illustration department at that time—see Fig. A(c)]. Most of these are still in the present text, but many have since been re-rendered using computer techniques.

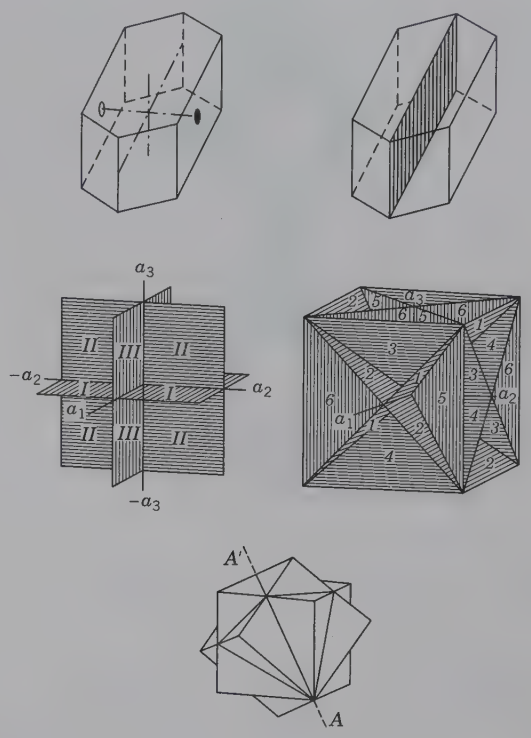

FIG. A (a) Morphological crystallography (1912)

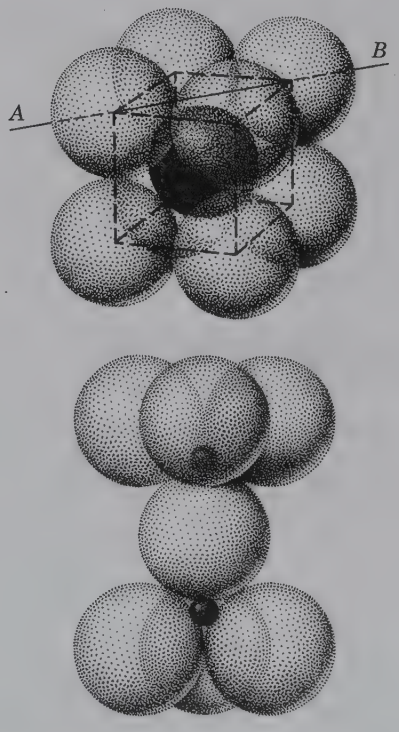

FIG. A (b) Crystal chemistry (1959)

FIG. A (c) Tetrahedral linkage in zeolites (1977)

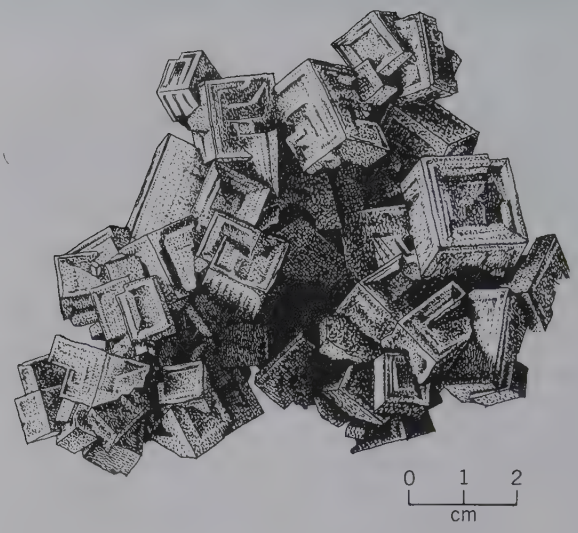

FIG. A (d) Halite (1949)

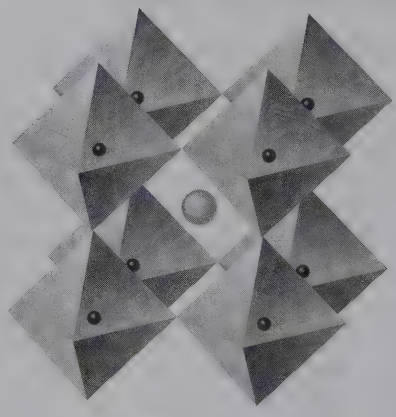

FIG. A (e) Perovskite structure (2008)

In 1983, while C. Klein was visiting with Connie Hurlbut in his office at Harvard University, he found two black pen (artist-sketched) mineral specimen drawings that had been used by Hurlbut in 1949 in *Minerals and How to Study Them*, Third Edition, by E. S. Dana and C. S. Hurlbut, Jr. They were so attractive that they were included as historic and artistic illustrations in the twentieth edition of *Manual of Mineralogy* [one is shown in Fig. A (d)]. Both remain in this new twenty-third edition.

New, computer-generated illustrations of crystal structures look really no different from the earlier, handcrafted airbrush drawings. Many of the structure illustrations in the twenty-third edition have been rerendered by computer to improve their contrast and clarity. An example is shown in Fig. A(e).

A REVISED ORGANIZATION FOR GREATER UTILITY

Another immediately obvious change in the new edition can be found in the Table of Contents. It now features 22 chapters instead of the 14 from the prior edition. This is the result of having packaged coherent subject matter into smaller, more easily accessible units. Each chapter has a new and expanded introductory statement, which gives the user a quick overview of what is to come. Just before these introductions, each chapter features a new illustration that highlights some aspect of the subject in that particular chapter. All such changes were made to make the text more readable, user-friendly, and searchable. The text continues to have a mineral and a subject index, and the twenty-third edition also has a new Glossary (available only on the Web site at www.wiley.com/college/klein).

Here is an overview of the new organization:

- Chapter 3 from the last edition ("Elements of Crystal Chemistry") is now subdivided, cutting its 61 pages into three chapters of more reasonable length—Chapter 3, "Elements of Crystal Chemistry;" Chapter 4, "Aspects of Crystal Structures;" and Chapter 5, "Chemical Composition of Minerals."

- Chapter 4 from the last edition ("Mineral Reactions, Stability, and Behavior") is similarly divided into three new chapters—Chapter 10, "Crystal Growth and Defects; Twinning, Color, and Magnetism;" Chapter 11,

"Mineral Stability and Phase Diagrams;" and Chapter 12, "Postcrystallization Processes in Minerals."

• The topic of crystallography is now covered in four chapters rather than two—Chapter 6, "External Symmetry of Minerals;" Chapter 7, "Internal Order and Symmetry in Minerals;" Chapter 8, "Crystal Projections;" and Chapter 9, "Selected Point Groups and Further Aspects of Space Groups."

• The prior chapter on analytical techniques is now two chapters—Chapter 13, "Optical Microscopy;" and Chapter 14, "Analytical and Imaging Methods in Mineral Science."

• Chapters 15 through 19 dealing with the descriptive and crystallochemical aspects of minerals have been updated, and Chapter 22, "Determinative Tables," includes this new information but is otherwise the same as before.

• Chapters 20, "Gem Minerals," has been retained from the prior edition. It provides a natural transition, from mineralogy to the fascinating world of gems.

• "Mineral Assemblages: Introduction to Rock Types" was omitted from the previous edition. It has been reinstated in this edition as Chapter 21. This means the text can now be used for mineralogy and earth materials courses covering rock types.

• Chapters on chemical aspects of mineral science (or mineralogy) precede those on crystallographic concepts. This was also the case in the previous edition because it appears that students are more comfortable if the course begins with chemical and crystal chemical subject matter, instead of crystallography. The main reason for this is that almost all undergraduate mineralogy courses have a college-level chemistry course as a prerequisite.

All of these changes will make access to, and introduction of, mineralogic concepts somewhat easier. Every effort has been made to ensure the level of topic discussion was not compromised by the organizational changes. Many of the first 14 chapters are independent of each other, and the instructor can cover them in his or her order of preference.

CD-ROM (VERSION 3.0)

A revised CD-ROM (entitled *Mineralogy Tutorials*, version 3.0) packaged with this text, provides additional study venues to the subject of mineralogy. Two sections, one on the "Graphical Representation of Mineral Chemistry" and a second on "Twinning" have been added in this new version. The CD-ROM is subdivided into four modules: I, "Crystal and Mineral Chemistry;" II, "Crystallography: External Form;" III, "Crystallography, Internal Order and Structure;" and IV, "Systematic Mineralogy." The first three modules provide many animations that deal with three-dimensional concepts (in crystal chemistry and crystallography) and which are difficult to explain or visualize using a two-dimensional, static book illustration. It appears that if students are required to review concepts on the CD-ROM in these three modules, at the same time as the instructor covers such material in class, the learning process can be improved. Furthermore, the CD-ROM serves a broader spectrum of learning styles than the text on its own.

Module IV contains brief text pages for 104 of the most common minerals. On these text pages are entries in green (hot) text that provide instant, clickable linkages to crystal structure illustrations, compositional and assemblage diagrams, stability and phase diagrams, solid solution mechanisms, and so on. This fourth module, therefore, is an excellent alternative way to review one's understanding of the crystallography, crystal chemistry, and paragenesis of rock-forming minerals by various instant pathways, through the click of a mouse on hot text. By such quickly branching pathways, one can call up images and concepts that have been developed in a much more linear sequence in the text.

This version of the CD-ROM also provides audio explanations by the senior author on about 50 screens to aid the user's understanding of presentations and/or animations that follow. One can access subject material on the CD-ROM in two ways. A click on one of the four "buttons" for modules I, II, III, and IV, found on the first menu screen, leads directly into the subject matter, as shown by the first screen for module I that follows the very first menu screen. These two screens are printed in color in the front piece of this text.

The other, more systematic way to subject matter on the CD-ROM, is via the index screens that link each subject "button" directly, through the click of a mouse, to the discussion of that subject. In several cases, subjects in the graphical index can be pursued in more detail with a graphical display of subcategories that is superimposed on the original index menu. Examples of four index screens are given in the front piece of the text.

Throughout the printed text of the *Manual of Mineral Science*, icons appear with the **Subject Headings**, (e.g., ) where concepts discussed in the text can also be located on the CD-ROM. In many places, written references specify locations within one of the four modules of the CD-ROM.

LABORATORY MANUAL

A new edition of the accompanying laboratory manual is available from Wiley for use in the mineralogy laboratory: C. Klein. 2008. *Minerals and Rocks: Exercises in Crystal and Mineral Chemistry, Crystallography, X-ray*

Powder Diffraction, Mineral and Rock Identification, and Ore Mineralogy, 3rd ed., ISBN 0471-77277-1

DIGITAL IMAGES FOR CLASSROOM PRESENTATION

The Instructor's Companion Site for the twenty-third edition features downloadable PowerPoint images—organized by chapter—to enhance your classroom presentation. The images include:

- 162 scientific illustrations.
- 72 color reproductions of color photos of mineral specimens taken from Plates I through VIII in the text.
- 20 new colored specimen photos of minerals—these appear as black and white photographs in the text but are in full color in the PowerPoint images.
- Gemstones taken from color Plates IX through XII in the text, as well as individual gems and gem groupings.

These images and all the black-and-white illustrations and photos from the text are available to instructors only and can be downloaded from the Instructor's Companion Site at www.wiley.com/college/klein.

A MINERALOGY EDUCATION

Although this edition has reorganized, streamlined, and simplified some concepts, it continues to provide what should be taught in a basic, one-semester mineralogy course. We addressed this coverage topic by asking "what should geology (or environmental science) B.A. or B.S. recipients be prepared to deal with?"—be it in subsequent graduate school or as professionals in the workforce. Our answer is that students who have taken a single undergraduate mineralogy course, should be reasonably comfortable in consulting much of what appears in *Reviews in Mineralogy and Geochemistry* (published by the Mineralogical Society of America) and in such reference volumes as *Rock-Forming Minerals* (the various volumes written by W. A. Deer, R. A. Howie, and J. Zussman), in *Dana's New Mineralogy*, by R. V. Gaines, H. C., Skinner, E. E. Foord, B. Mason, and A. Rosenzweig, or in the four-volume set entitled *Handbook of Mineralogy*, by J. W. Anthony, R. A. Bideaux, K. W. Bladh, and M. C. Nichols. To be reasonably comfortable in consulting any of these volumes, new graduates must have had a considerable background in concepts dealing with crystal chemistry, crystal structure, mineral behavior, and crystallography; and they must have some fundamental understanding of mineral stability and/or mineral assemblage diagrams. As part of this background, new graduates should have familiarity with point and space groups and their notation, statements about unit cell dimensions and content, atomic coordination, and so on—all of which is interwoven in every mineral description in the reference volumes previously mentioned here.

DEDICATION

The author and coauthor of many prior editions of this text, Cornelius S. Hurlbut, Jr., died on September 1, 2005, at the age of 99, in Lexington, Massachusetts. Connie, as he was known to family and friends, received his Ph.D. from Harvard University, joined the Harvard faculty in 1934, and continued his research and teaching there until his retirement in 1972.

In 1941, he was the author of a completely rewritten fifteenth edition of *Dana's Manual of Mineralogy*. Subsequent editions by him appeared in 1952, 1959, and 1971. Later, he was senior author on the nineteenth edition (1977), with C. Klein as coauthor, and became coauthor on the twentieth (1985) and twenty-first editions (1993). In addition, he twice revised *Minerals and How to Study Them* (1949, 1998; Wiley) and wrote *Minerals and Man* (1970; Random House), a coffee-table book with accounts of his worldwide travels to many major mining and mineral location, and lots of beautiful photographs. He was also the author of two editions of *Gemology* (1979 and 1991; Wiley); the

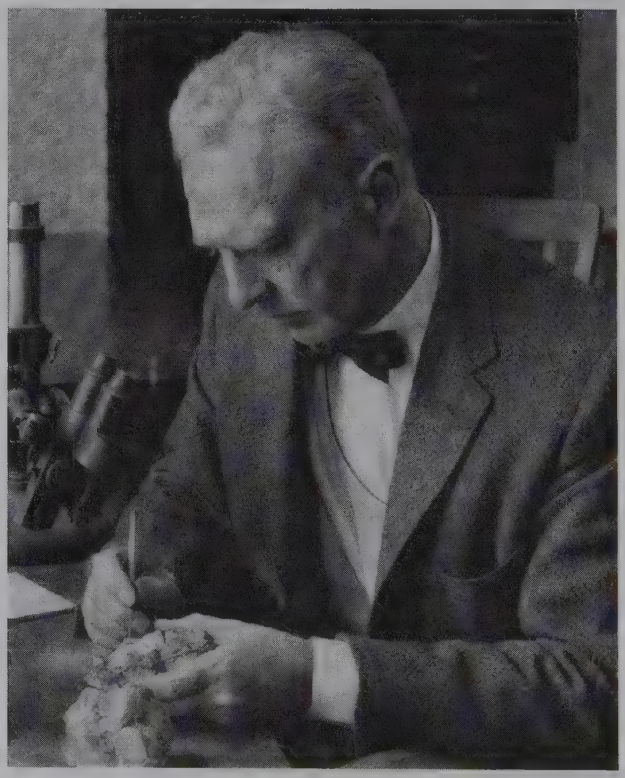

Cornelius S. Hurlbut, Jr., late 1960s.

first with George Switzer and the second edition with Robert C. Kammerling.

It was my (C. K.) good fortune to have been associated with Connie as coauthor of several prior editions of this text. Our cooperative efforts have been wonderful in every way; highly professional and respectful of each other. Having been able to be a partner in the development of several mineralogy texts has added much to my professional development as an instructor, and I much cherish the memories of my long-term friendship with Connie Hurlbut. As a tribute to Connie, I will now re-introduce a poem, written by him, that was originally part of the front matter of the nineteenth edition of the *Manual of Mineralogy*, 1977.

A Mineral

A mineral is a wondrous thing,
At least it is to me,
For in its ordered structure
Lies a world of mystery.
The secrets that it has withheld
For countless ages past
And clung to most tenaciously
Are being learned at last.
Each year using new techniques
Or with a new device,
We make our knowledge more complete,
Our data more precise.
But let us not in trying to solve
A mineral mystery
Forget that minerals are a part
Of natural history.
Nor in our quest for more detail
When probing an unknown,
Forget that every mineral
Has a beauty of its own.
With progress in technology
Each year sees new machines
That try to copy nature
By sophisticated means.
But for all these modern methods
We cannot yet compete
With the world of ordered beauty
That lies beneath our feet.

C.S.H.

ACKNOWLEDGMENTS

The revised twenty-third edition has benefited from professional reviews of the prior (twenty-second) edition as well as of early drafts of the present first five chapters.

We received student evaluations of various chapters in the twenty-second edition from two mineralogy courses. One, at the University of Michigan (Ann Arbor), as taught by Rodney C. Ewing and Udo Becker, and the other by Adrian Brearley at the University of New Mexico (Albuquerque). The student comments and the overall instructor evaluations were very helpful, and we are grateful to these three instructors for their input.

Subsequently, early in the writing stage of this edition, the first five chapters were sent out to four mineralogy instructors. These were: Lydia K. Fox, University of the Pacific, Stockton, California; Nancy J. McMillan, New Mexico State University, Las Cruces, New Mexico; Matthew Nyman, University of New Mexico, Albuquerque, New Mexico; and Thomas Sharp, Arizona State University, Tempe, Arizona. We thank these reviewers for their valuable input regarding content and style of these first five (draft) chapters.

We also thank Darrell Henry, Nancy McMillan, Denis Norton, Paul Spry, Malcolm Ross, and Tom Sharp for additional comments on selected portions of the text.

We wish to thank Carl A. Francis, Curator of the Harvard Mineralogical Museum in Cambridge, Massachusetts, for his generous help in the photography of about 20 Harvard mineral specimens of which photographs had appeared in earlier editions. These 20 earlier photographs now looked "fatigued," and it was decided that new pictures had to be taken. The specimens in question were shipped from Harvard to Albuquerque and were re-photographed by David Nufer Photography in Albuquerque. Carl Francis also provided us with a polished slab across a tourmaline crystal, which became the design for the cover of this text.

We thank Ryan Flahive, geology editor at John Wiley and Sons, for his continued guidance, support, and understanding; Sandra Rigby, illustration coordinator, for much help in the thorough revision of the illustration program; Kelly Tavares and Jeanine Furino, who were most effective production editors; and Madelyn Lesure, design director, for her various design suggestions, which have resulted in the new look of the present text. We are grateful to Marc A. Klein (C. K.'s son), of New York City, for the overall design of the present cover. He has designed every cover for the *Manual* since 1985.

We wish to thank Joe Mandarino for providing us with the latest information on the total number of mineral species and their distribution among the various mineral groups.

I am grateful to my wife, Shirley Morrison, for her support and understanding as well as her acceptance of my seemingly endless hours at the office during this text revision.

I (B. D.) am grateful to Darrell Henry for his generous support, understanding, and technical expertise. Nancy McMillan unselfishly provided additional reviews and unwavering encouragement. Corine Armstrong is thanked for her willingness to work long hours on many unglamorous aspects of text preparation. My thanks to the many colleagues and students who, over the years, helped refine my teaching, provided resources, and championed these efforts; especially Mike Holdaway, Susan Anderson, Kim Gunderson, Hallie Latham Graves, and Jennifer Whittington. Additional appreciation is extended to the LSU Department of Geology and Geophysics and to my research colleagues for tolerating my neglect while providing inspiration.

Most important, I thank my mother, Winifred Dutrow, for her kindness and understanding when her caregiver was not able to give more during the months of textbook writing.

Cornelis Klein
Albuquerque, New Mexico

Barbara Dutrow
Baton Rouge, Louisiana

ABOUT THE AUTHORS

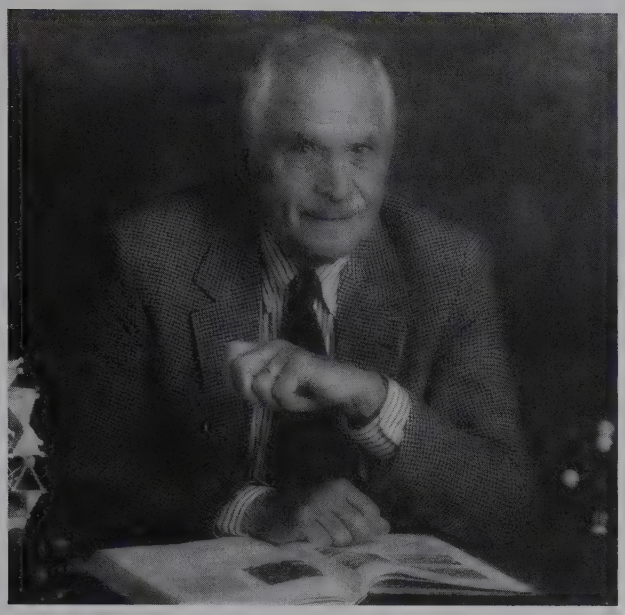

Cornelis Klein was born in the Netherlands and completed his primary and secondary education there. He received B.Sc. (with honors) and M.Sc. degrees in geology from McGill University in Montreal, Canada, and his Ph.D. degree from Harvard University, also in geology. He was a member of the geology faculty at Harvard (1965–1972), at Indiana University, Bloomington (1972–1984), and the University of New Mexico (1984–2002), where he is presently a research professor. His earliest research activities dealt with the geochemical and mineralogic aspects of the amphiboles. He served as coinvestigator, with the late Clifford Frondel of Harvard University, on lunar materials returned by the *Apollo* 11 through 14 missions. His subsequent, and very long-term research efforts have focused on the mineralogy, geochemistry, and origin of Precambrian banded iron-formations (BIFs) worldwide. That has taken him for many years of field seasons to Canada, Western Australia, South Africa, and Brazil. He was awarded a Guggenheim Fellowship (for field research in Western Australia) in 1978; he received the Carnegie Mineralogical Award (from the Carnegie Museum of Natural History, Pittsburgh, PA), in 1997; he was given two awards for excellence in teaching while at the University of New Mexico, the Burlington Resources Faculty Achievement Award in 1990, and the Presidential Teaching Award in 1995; and he served as president of the Mineralogical Society of America in 2001.

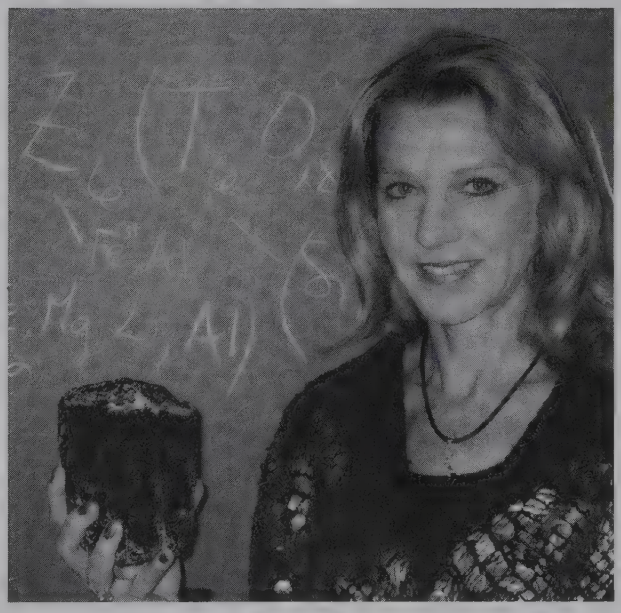

Barb Dutrow is the Adolphe G. Gueymard Professor of Geology at Louisiana State University in Baton Rouge. She was raised in northwestern Nebraska where she frequently visited nearby mineral localities in the Black Hills of South Dakota. She received her B.S. degree in earth science from Chadron State College in Nebraska and her M.S. and Ph.D. (1985) degrees in geology from Southern Methodist University in Dallas, Texas. Between degrees, she worked for Mobil Exploration evaluating the potential of rocks as traps for hydrocarbons. Her Ph.D. research, under M. J. Holdaway, focused on field, experimental, and theoretical studies of staurolite and associated metamorphic rocks. She carried out one of the earliest ion microprobe studies of light element concentrations (Li, H) in metamorphic minerals, which led to a new model for the crystal chemistry of staurolite. Subsequently, she was awarded an Alexander von Humboldt Fellowship (1985–1987) to continue high-pressure experimental and crystal chemical mineral studies in the lab of Professor Werner Schreyer at Ruhr-Univeristät in Bochum, Germany. As a research associate at the University of Arizona (1988–1990) with Professor Denis Norton, her focus expanded to include the effects of fluids on mineral development. She took a faculty position at the University of Iowa (1990–1992) prior to moving to LSU (1992–present). Her research now integrates field, theoretical, and computational modeling of heat and mass transfer in metamorphic rocks to decipher their textural and chemical development. Research has taken her to mountain belts on four continents with field work aided by her enjoyment of ultra distance running and multisport, expedition adventure racing. At LSU, she has received several University-wide teaching and research awards and consults to industry on matters related to minerals. She is currently serving as president of the Mineralogical Society of America.

CONTENTS

LOCATIONS OF SOME IMPORTANT TABLES AND ILLUSTRATIONS

THE 23RD EDITION OF THE MANUAL OF

MINERAL SCIENCE

CHAPTER 1

Introduction

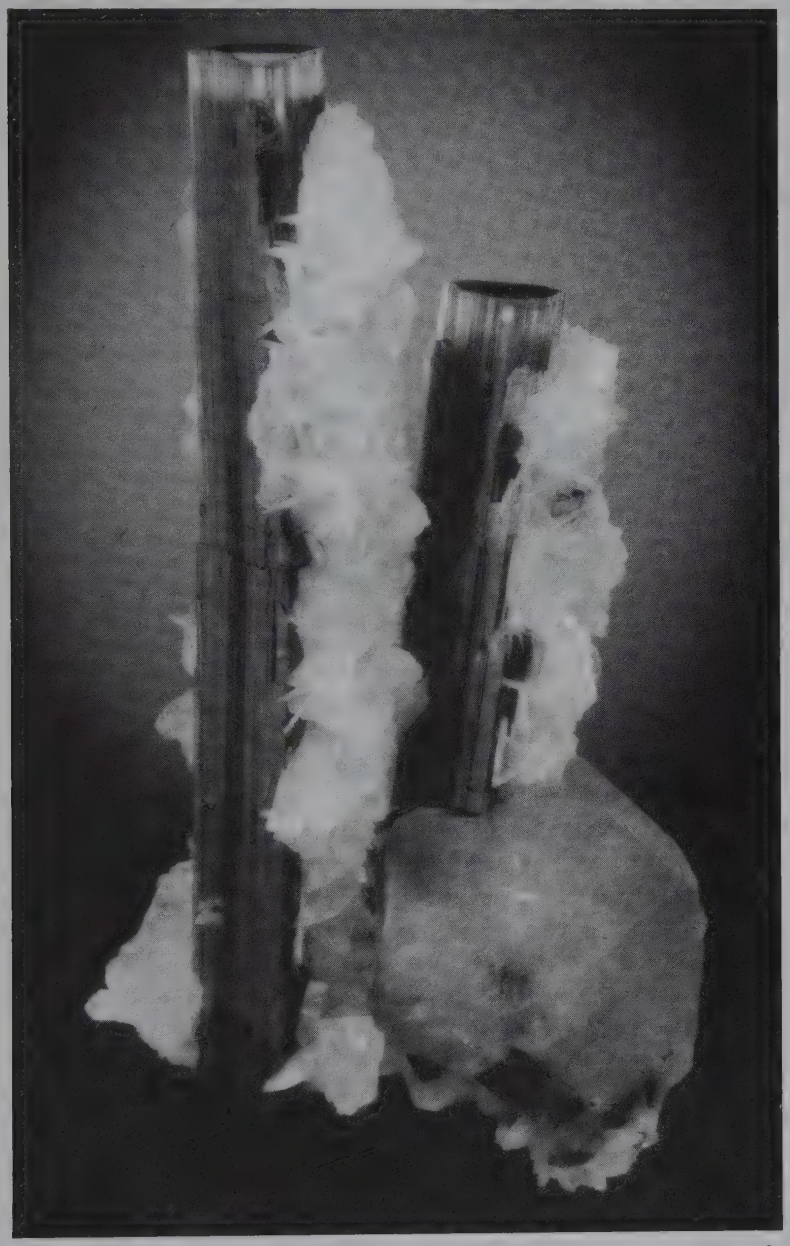

Well-formed, prismatic tourmaline, $Na(Fe,Li,Al)_3Al_6(BO_3)_3Si_6O_{18}(OH)_3(F,O)$, covered with white plates of albite, $NaAlSi_3O_8$, and one crystal of fluorite, CaF_2 (at the right bottom). Striated faces of tourmaline are caused by many slightly offset prism faces. The color change toward the top of the tourmaline crystals suggests a change in chemical composition. Specimen is 10.6 cm high. From Stak Nala, N.A., Pakistan (photograph courtesy of Jeff Scovil, collection © Jeff Scovil).

"Minerals are the basic stuff of the Earth, and their study will always remain at the core of the Earth Sciences." Frank C. Hawthorne, 1993

Minerals, and their chemical derivatives, are everywhere. We walk on them (along sand beaches or in mountain ranges), we wear them (as jewelry), we wash our clothes with them (as surfactants in detergent), and we brush our teeth with them (the abrasive in toothpaste). They bring electricity into our lives and provide the building materials for our homes and schools. Without minerals, we would not have a solid Earth on which to live nor have our present economic system.

Why are these materials such an integral portion of our lives, not just as students of geology but as citizens of the Earth? In this text you will discover what minerals are, how they form, how they are described and defined, how they are used in everyday life, how they relate to other fields of study in the arts and sciences, and how to extract clues that they hold about Earth and planetary processes. You will learn about minerals that make kitty litter absorb, duct tape strong, and microchips fast.

WHAT IS A MINERAL?

The word ***mineral*** is defined as follows.

> A mineral is a naturally occurring solid with a highly ordered atomic arrangement and a definite (but not necessarily fixed), homogeneous chemical composition. Minerals are usually formed by inorganic processes.

Mineral science, also referred to as **mineralogy**, is the study of these materials. This definition is restrictive and differentiates the use of the word *mineral* in geology and other sciences from uses (and misuses) of the word *mineral* in other fields. For example, nutritionists will use the term *mineral* when they actually mean chemical element or compound. Our bodies need calcium, iron, and potassium, which are chemical constituents essential to life. As such, they commonly are additives in nutritional supplements, breakfast cereals, sports drinks, and multivitamin capsules and are erroneously referred to as *minerals*. These are chemical elements and/or compounds, not minerals.

An analysis of the above definition will help to clarify the proper meaning of the word **mineral**.

- **Naturally occurring** indicates that a mineral must have been formed by natural processes. This is in contrast to those minerals made in the laboratory. Industrial and research laboratories routinely produce synthetic equivalents of many naturally occurring materials, including valuable gemstones, such as emeralds, rubies, and diamonds. If the minerals formed in the laboratory also have naturally occurring counterparts, they are referred to by their mineralogic name. A mineral produced in a laboratory should be qualified by the term *synthetic* (e.g., synthetic emerald). How does one refer to $CaCO_3$ (calcite) that sometimes forms in city water mains? The material is precipitated from water by natural processes but in a man-made system. Most mineralogists would refer to it by its mineral name, calcite, because humanity's part in its formation was inadvertent.
- **Solid** excludes materials that are gases and liquids. In solids, there is a fixed position for atoms. Thus, H_2O as ice in a glacier is a mineral, but H_2O as a liquid (water) is not. On the ocean floor, some gas molecules form solid structures termed gas hydrates. In this case, gas as a hydrate would be considered a mineral. Conversely, liquid mercury, found in some mercury deposits, is excluded as a mineral by the above definition.
- A **highly ordered atomic arrangement** indicates an internal structural framework of atoms (or ions) arranged in a regular, repeating, geometric pattern. Because this is the criterion of a crystalline solid, minerals are **crystalline**. Solids that lack an ordered atomic arrangement are called *amorphous*. Several natural solids are amorphous, and examples include volcanic glass (obsidian—which is not classified as a mineral because of its highly variable composition and lack of ordered atomic structure) and limonite (a mixture of various hydrous iron oxides that form rust). In some cases, the crystalline character of a mineral can be destroyed by the radioactive elements contained in it. Zircon, a well-ordered solid, may become amorphous after radioactive elements (e.g., U or Th) housed inside its structure decay. The release of radioactive energy may damage the crystal structure and lead to loss of its internal atomic order.
- A **definite (but not necessarily fixed) homogeneous chemical composition** that varies within limits, implies that the composition of a mineral can be expressed by a specific chemical formula. For example, quartz contains the chemical elements silicon and oxygen in a ratio of 1:2. Its composition is, therefore, expressed as SiO_2. Because quartz contains almost no chemical elements other than silicon and oxygen, its formula is *definite* and *fixed*, and quartz is referred to as a pure substance. Most minerals, however, do not have such well-defined compositions, and the amounts of chemical elements may vary extensively. For these minerals, the composition is not fixed but can vary between certain limits. An example of a chemical composition that varies within limits is given by the mineral dolomite. The formula for pure dolomite is $CaMg(CO_3)_2$. However, most dolomite is not a pure Ca-Mg-carbonate but instead contains considerable amounts of Fe and Mn in place of Mg. To represent this variability, the more general chemical formula for dolomite is typically written as $Ca(Mg,Fe,Mn)(CO_3)_2$ without specific subscripts for Mg, Fe, or Mn. The ideal formula has $Ca:Mg:CO_3$ in proportions of 1:1:2 and is definite. For the iron and manganese-containing variety of dolomite, $Ca:(Mg + Fe + Mn):CO_3$ is also 1:1:2. In other words, the overall atomic ratios in these formulas remain the same (*definite*) even though a range in chemical composition exists (*its composition is not fixed*). **Homogeneous** means that the mineral is of the same composition throughout its volume regardless of the location sampled.
- According to the traditional definition, minerals are formed by **inorganic processes**, but it is increasingly recognized that minerals may also be produced organically. A familiar example is the

calcium carbonate of mollusk shells. The oyster's shell and the pearl that may be inside are composed primarily of aragonite, $CaCO_3$. This material is identical to the inorganically formed mineral aragonite. Although several forms of $CaCO_3$ (calcite, aragonite, vaterite) and monohydrocalcite, $CaCO_3 \cdot H_2O$ are the most common *biogenic minerals* (which means "mineral formed by organisms"), many other biogenic mineral species are recognized. Magnetite, Fe_3O_4; fluorite, CaF_2; vivianite, $Fe_2(PO_4)_3 \cdot H_2O$ is a phosphate, and several other phosphates; some sulfates; Mn-oxides; pyrite, FeS_2; and elemental sulfur, S, are a few examples of minerals that can be precipitated by organisms (see Weiner and Dove, 2003). The human body also produces essential minerals. A form of apatite, $Ca_5(PO_4,CO_3)_3(OH,O,F)$, is the principle constituent of bones and teeth. The body can also produce mineral matter (calculi) in the urinary system. Such calculi consist predominantly of calcium phosphates (such as hydroxylapatite, carbonate-apatite, and whitlockite), calcium oxalates (that are very uncommon in the mineral world), and magnesium phosphates (see Gibson, 1974). Organisms have been manufacturing minerals for most of Earth's history. By the Cambrian period, 540 million years ago, organisms had produced at least 64 different minerals (see Weiner and Dove, 2003). Recognition of these materials has spawned a new research area, **biomineralization**, which is the study of the processes by which organisms produce minerals.

The definition of a mineral requires aspects of both crystal structure and chemistry, which are explored in the upcoming chapters. Because of this, one other related term is needed when discussing the definition and classification of natural materials. Substances that meet the other criteria of minerals but that lack long-range internal order are called **mineraloids**. Naturally occurring glasses are considered mineraloids. These include volcanic glass (obsidian) and fulgurites (where heat from a lightning strike melts rock and soil to produce a glass). Additional examples include the liquids, water and mercury, although some geologists suggest that mercury might be considered a mineral (see Nickel, 1995). Opal, $SiO_2 \cdot nH_2O$, was originally considered to be completely without internal structure (amorphous); however, careful electron beam studies have shown that it contains an ordered arrangement of small SiO_2 spheres (see Figs. 2.6 and 2.7).

DEFINING A MINERAL MORE BROADLY

Research in the mineral sciences is diverse and encompasses many fields of study. Consequently, a more expansive definition of a mineral is accepted in many research areas. Examples of these areas, from R. J. Hemly (1999), include: (1) synthesis of new "minerals" at high pressures and temperatures to simulate materials in the Earth's mantle and core that cannot be directly sampled (see also Hemley, 1998), such as the "post perovskite" phase of the lower mantle (see Chapter 5); (2) investigations of the transition from the crystalline to the amorphous (noncrystalline, disordered) state by application of extremely high pressures or by electron beam irradiation (to help determine minerals appropriate for storage of nuclear waste) (see for example, Ewing et al., 2004); (3) research on microorganisms that cause mineral precipitation or dissolution and control the distribution of elements in diverse environments at and below the surface of the Earth (see Banfield and Nealson, 1997; Dove et al., 2003); (4) study of mineral surfaces and their involvement in controlling chemical reactions that occur near the Earth's surface (see Hochella and White, 1990); and (5) synthetic production of zeolitic structures that can be used for industrial applications, such as molecular sieving, ion exchange, and catalysis. These wide-ranging research endeavors are part of mineral and materials science. Results from such investigations will provide the mineralogist and earth scientist with a fuller understanding of the complex and heterogeneous makeup of the Earth and other planets and the processes that control their geologic evolution.

For the purposes of this textbook, the more restrictive definition of a mineral is used. However, it is good to keep in mind these broader definitions.

WHERE DO WE FIND MINERALS AND WHAT CAN WE LEARN?

Minerals are found throughout our universe. They are the products of complex Earth and planetary processes that take place over a wide range of temperatures and pressures. They not only occur on beaches (black, green, and white "sand" beaches), covering the ocean floor, and in the cores of mountain belts but also on other planets, their moons, in asteroids, and far beyond. These mineral occurrences provide clues to the understanding of the origin, evolution, and behavior of planets in the solar system. For example, minerals found in meteorites contain chemical elements that record the evolution of our solar system. On Earth, mineralogic changes in the mantle might be responsible for deep earthquakes and for tectonic plate motion. As such, minerals are basic to earth science as well as to the evaluation of the sustainability of mineral resources.

MINERALS AS INTEGRAL TO EARTH SCIENCE

Mineral science is central to many branches of the earth sciences. The branches shown in Fig. 1.1 represent many subdisciplines and schematically illustrate that most of the earth sciences involve minerals in one way or another. This diagram also indicates that these subdisciplines, and their geologic applications, are interconnected. Beginning with the subject of petrology and going clockwise from there, one may ask, *"What are these branches of earth science, and how do minerals play a key role?"*

Petrology is the branch of geology that involves the study of rocks, their composition, and the processes that form them. A rock is a coherent, consolidated, naturally occurring aggregate of minerals. Deciphering a rock's composition, texture, condition of origin (the tectonic setting in which it occurs), and evolution requires an understanding of its constituents—minerals. *Experimental petrology* involves synthesizing, melting, and/or growing rocks and minerals in the laboratory to understand the physical and chemical conditions under which minerals form and are stable. For example, diamonds produced in the laboratory demonstrate that they require great pressure for formation. Thus, the rocks in which diamonds occur also have been subjected to high pressures. Petrology is also closely linked to geochemistry through the chemical elements contained in the rocks and to geochronology because geochronologic techniques provide age dates for the rocks. These interrelationships are shown by arrows that extend to and from mineralogy at the center of the diagram outward to each subdiscipline in Fig. 1.1. Arrows between subdisciplines in this figure indicate that each subdiscipline contributes valuable information to other areas.

Geochemistry deals with the relative abundance, distribution, and migration of chemical elements (and their isotopes) in Earth and planetary materials. These chemical elements are primarily contained in minerals, rocks, and soils. In addition, fluids within the Earth transport chemical components from one reservoir to another. Understanding the exchange of elements between these different reservoirs requires knowledge of minerals and how they react especially at the mineral-fluid interface. A subdiscipline of geochemistry, isotope geochemistry, involves the use of isotopes found in minerals to determine the geologic age of minerals (geochronology) or to decipher the evolution of the atmosphere. Evaluation of elemental abundances is also important in the study of the origin of planetary materials.

Meteoritics and Planetary Studies. The field of **meteoritics** is dedicated to the study of the chemistry and mineralogy of meteorite samples (Fig. 1.2). **Planetary studies** involve, in part, the study of rocks and other materials that were collected from scientific missions to other planets and moons (e.g., lunar rocks and regolith). It also includes the study of interplanetary dust particles that originate from comets, asteroids, and protoplanets. These studies help to unravel the geologic history of the planets, the origin of our solar system, and include the search for traces of life on other planets.

Paleontology is the study of ancient life. Fossils of plants and animals are preserved because many are replaced by minerals (Fig. 1.3). Examples of mineral replacements are petrified wood, silicified dinosaur bones, opalized clam shells, and emerald-filled snails. **Geomicrobiology** is a multidisciplinary field that

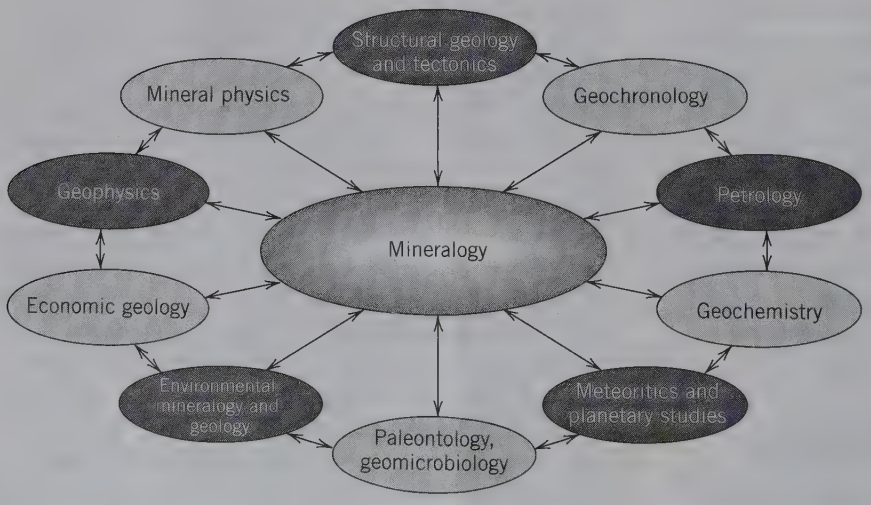

FIG. 1.1 The central role of mineral science in the earth sciences. The double arrows portray linkages of subdisciplines to one another and to mineral science; they indicate an especially close relationship between subdisciplines (see text for details.)

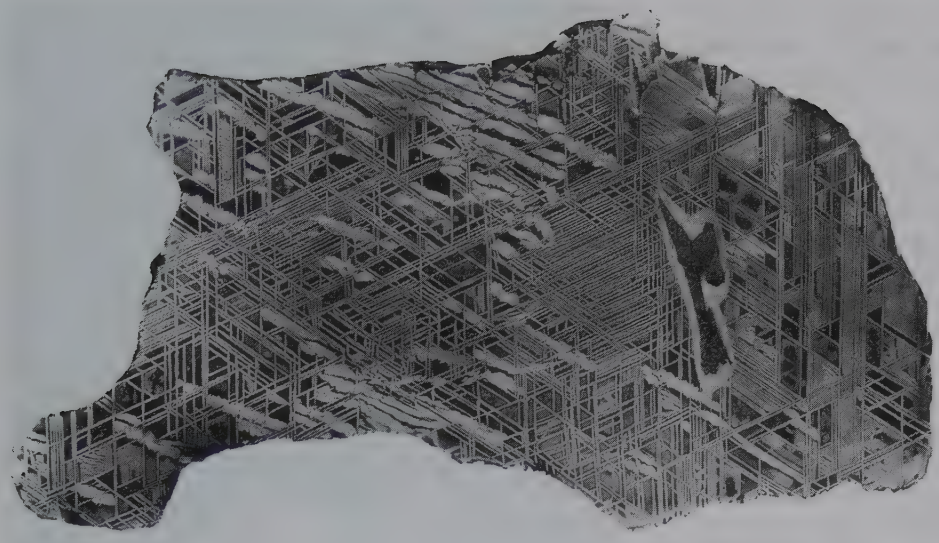

FIG. 1.2 A polished and chemically etched slab of the Edmonton (Kentucky) iron meteorite. The octahedral pattern displayed by this meteorite consists of a crystallographically controlled intergrowth of two types of Fe-Ni alloy: *kamacite*, which contains about 5.5 weight percent Ni, and *taenite*, which tends to have a variable Ni content ranging from about 27 to 65 weight percent. This texture is known as Widmanstätten pattern. The irregular inclusion at the right center consists of *troilite*, FeS. (Smithsonian Astrophysical Observatory, courtesy of J. A. Wood; Harvard Mineralogical Museum.)

involves the study of the interactions of geology, mineralogy, biology, and micro-organisms. Minerals may provide a life source for some microbes. For example, some bacteria respire by transferring electrons to iron-containing minerals, thereby reducing the iron in the mineral. This is shown in Fig. 1.4. Also, minerals may provide a substrate for microbial growth. In caves, microbes may increase the rate of cave formation by the etching and dissolution of minerals. Alternatively, microbes can affect crystal growth by trapping materials or becoming calcified and preserving their former presence. Microbes may manufacture minerals or convert one mineral to another (factors that can contribute

FIG. 1.3 Pinecones—recent (left) and fossilized (right). The Jurassic age pinecone has been replaced by quartz (SiO_2) and is about 208 million years old. Specimen is from Patagonia, Argentina (photograph courtesy of D. Henry, Louisiana State University, Baton Rouge).

FIG. 1.4 Minerals are used by microorganisms as food for growth and respiration. This photograph is a transmission electron micrograph (TEM) that shows metal-reducing bacteria (lobate features—one is outlined in white) in close association with iron oxide minerals (mainly hematite, Fe_2O_3, nanoparticles). The bacteria respire by transferring electrons to the ferric iron in the hematite, which reduces the iron. Scale bar is 1314 nm (131.4 Å) (photograph courtesy of M. Hochella, Virginia Tech, Blacksburg, Virginia).

to acid mine drainage), affect water quality, and impact environmental conditions. This area of research explores the complex interactions between the biological and physical worlds.

Environmental mineralogy and **geology** are scientific fields that apply geologic research to understanding and solving problems in our environment. Of great importance to our energy policy is the need to identify materials for the long-term storage of nuclear waste. For example, environmental mineralogy evaluates the stability of those minerals that might be used as stable hosts because they are reasonably resistant (over long time periods) to the radioactivity produced by nuclear waste. Another issue relates to reclamation of lands that were once mined to extract valuable minerals. Now, many of these areas have disturbed vegetation, may contain toxic elements accessible to the environment, and produce acid drainage that pollutes blue ribbon trout streams. Environmental geology seeks solutions to these problems, commonly through the use of minerals that may trap toxic elements. In addition, environmental mineralogy focuses on the interaction of minerals (their surfaces, fracture patterns, and particle size) with biological systems. An example of this is the role of mineral dust and the occurrence and severity of pulmonary diseases studied in the field of **medical mineralogy**.

A related emerging field is that of **forensic mineralogy**, in which minerals are used to help solve crimes. For example, minerals that characterize a specific geologic location may be used to provide a lead or authenticate the origin of a material (e.g., gems, marble, metals) found at a crime scene.

Economic geology is the study of the distribution of valuable mineral deposits, the economic considerations involved in their recovery, the assessment of available resources and reserves, and the impact of mining on the environment. Economic geology includes the extraction of all materials from the Earth, such as metal-rich ores (e.g., copper), fossil fuels, industrial materials (e.g., salt and gypsum for wallboard), building stone (for counter tops), and sand and gravel (for roads). Minerals are the fundamental materials of economic geology. The chemical elements extracted from minerals are used in many new materials that provide the basis for our technological advances and our high standard of living (Fig 1.5). Many of these resources are discovered through exploration geophysical techniques that allow for interpretation of the shallow subsurface as well as the deeper parts of the Earth's crust that are otherwise inaccessible.

Geophysics is the study of the physics of the Earth, emphasizing its physical nature and dynamic geologic behavior. The properties of minerals and rocks are basic

FIG. 1.5 Minerals provide the materials for our standard of living and for many products that are used everyday. Titanium is extracted from minerals, such as rutile, TiO_2, and ilmenite, $FeTiO_3$, and used to make products such as this titanium mountain bike (photograph courtesy of J. Schoomaker, American Bicycle Group, Inc., Chattanooga, Tennessee).

parameters that control geophysical processes. The temperature distribution of the Earth's interior, the source of earthquakes and the distribution of seismicity, the variability of the Earth's geomagnetic field, and the convection of the Earth's mantle, all require an understanding of how mineral properties vary over a wide range of temperature and pressure conditions.

An important link between mineralogy and geophysics is provided by the field of **mineral physics**. Geophysicists, together with mineralogists, explore mineral behavior under extremely high pressure and temperature conditions (produced in the laboratory) to understand the fundamental physical and chemical processes that determine mineral properties. Research in the field of mineral physics provides the physical property data needed to interpret geophysical observations and the Earth's deep dynamic behavior. In addition, it provides insights into the mineralogical makeup of the Earth's mantle and core.

Structural geology and tectonics evaluates rock movement and the resulting structures. Deformation features range in scale from submicroscopic lattice defects in crystals (measured in terms of nanometers) to the faulting and folding associated with mountain building (measured in terms of kilometers) to the upward and downward movements of the Earth's crust (on the scale of tens of kilometers). How a rock deforms and whether it breaks (i.e., is brittle) or bends

(i.e., is elastic) is determined, in part, by the minerals composing the rock formation. Commonly, these deformational events can be assigned an age based on the geochronological studies of the minerals contained in the rock.

Geochronology is the study of time as it relates to Earth's history. Earth's development can be unraveled through the study of the ages of Earth materials, and the timing of event sequences that occur in the formation and alteration of rocks and minerals. Earth scientists think about the 4.6 billion years of geologic time in two ways: *relative time*, in which specific rock units or events are simply older or younger than an other; and *absolute time*, in which a numerical age (in years, thousands of years, millions or even billions of years) is determined for a mineral. Thus, specific dates in the Earth's history can be recorded by minerals. Minerals contain chemical elements that undergo radioactive decay, and the abundance of these chemical components can be used to calculate an age for the mineral. How a mineral responds to radioactive decay and how chemical elements are bonded in a mineral significantly impact the quality and interpretation of the analyses used to acquire the age date. Understanding minerals, their composition and behavior, provides the geochronologist with the tools needed to interpret Earth's history as preserved in the rock record.

These areas of geology highlight the fundamental role that minerals play in the study of the Earth. Mineralogy is the link that connects these subdisciplines. As discoveries are made in the field of mineralogy, other disciplines advance and progress as a consequence.

MINERALOGY AS IMPORTANT TO OTHER FIELDS

It is easy to understand the importance of minerals to the disciplines of earth science, but minerals and their study are also important to the humanities and to other fields of science. The following are a few examples.

Mineral science is closely related to **inorganic chemistry**. Because minerals are composed entirely of chemical elements (that are of inorganic origin), they are inorganic chemical compounds. Minerals help chemists understand complicated inorganic materials because minerals are nature's own complex chemical solids. The same principles of how atoms bind together are shared between the two disciplines. Mineral science is different, however, in that the focus is mainly on naturally occurring solid substances, rather than on synthetic materials, liquids, or gases.

The discipline of **material science and engineering** is a multidisciplinary field focused on making new materials for a specific function. These functions may be chemical, optical, thermal, magnetic, electronic, structural, or a combination of these. Experimental mineralogists were among the first to synthesize superconducting materials. They also helped develop fiber optic materials, the tiny strands of glass that transmit light signals. (The mineral ulexite transmits light similar to that in a fiber optic cable; see Fig. 1.6). Material scientists also use minerals as examples for the development of new materials. For example, minerals that have survived 4.4 billion years on Earth, while having been bombarded by their own internal radioactive elements, suggest synthetically equivalent materials for storage of high-level radioactive waste (see Ewing et al., 2004). Material science uses many techniques developed by crystallographers and mineralogists. In many ways, mineralogy is the first material science.

Minerals are the materials of most gemstones. **Gemology** involves the study of gem minerals which are the most beautiful representatives of minerals found on Earth. The world of gems is easily visible: Wander through a jewelry store and see the gemstones that are for sale. From the earliest times, humanity has adorned itself with gems. Cleopatra loved emeralds. The crown jewels of nations are commonly comprised of precious gems, a visible sign of wealth and stature (see also Chapter 20).

Minerals and organic matter are the main constituents of soils. Thus, minerals are an integral part of the field of **soil science**. Minerals provide the principle source of nutrients, such as N, P, K, Se and other trace

FIG. 1.6 Nature's fiber optic, the mineral ulexite, $NaCaB_5O_6(OH)_6 \cdot 5H_2O$. A fiber optic material transmits light. This photograph shows that the word *fiber*, written on a sheet of paper beneath the specimen, is projected to its upper surface. The word *optic* is on the sheet of paper below. (Specimen courtesy of R. Sielecki, Ausrox, Melbourne, Australia; photograph by B. Dutrow.)

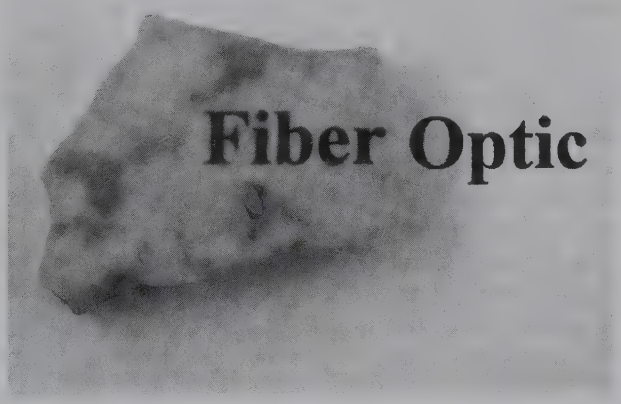

constituents, needed for plant growth. The quality of wine depends, in part, on the soil type used for grape growing. In some cases, a certain plant will only thrive in a specific type of soil because of the chemical elements and minerals it contains. A geologist may be able to map a specific rock unit by the appearance of an identifying plant. For example, in Madagascar, large aloe plants are restricted to growth on carbonate rocks and, thus, provide an obvious marker to the presence of buried carbonate units.

Minerals also play a role in **biology** and **paleobiology**. Best known are various compositions of apatite, the mineral that constitutes vertebrate bones and teeth. Other organisms also require minerals for function: Fish have otoliths (ears) composed, in part, of the calcium carbonate mineral, vaterite; and birds have magnetite to help their guidance system. Many invertebrates make their shells out of the minerals calcite and/or aragonite. In the case of one foraminifer, its "shell" is made of the mineral celestite, a strontium sulfate. Such materials also resist weathering to produce fossils that can be used to trace biological function back in time, as in the field of paleobiology.

The emerging discipline of **nanoscience** also involves mineralogy. Nanoscience is the scientific field that deals with very small particles, where a nanometer = 10^{-9}m (*nano* is from the Greek word meaning *dwarf*). It involves the study and manufacture of materials at approximately the molecular and atomic levels. At that scale, materials are measured in nanometers or billionths of a meter. Nanoparticles have physical (and thermodynamic) properties, and/or chemical reactivities that are distinctly different from those same properties for the same materials when they occur in a larger range of sizes from, for example, 0.1 mm upward (Banfield and Navrotsky, 2001; see also Figs. 1.4 and 1.7). Nanoscale particles, films, and confined fluids are ubiquitous in nature, on the continents, in the atmosphere, and in the oceans. Minerals, such as jade, apatite, magnetite, and hematite, may form nanocrystals. It has been suggested that nanoscience and technology are keys to the next generation of revolutionary research in the earth sciences (Hochella, 2006). Investigations in environmental geology using nanoscience for remediation are very promising. Nano-materials also appear to have unique properties that may be exploited industrially.

Art has always been associated with humans. From ancient cave paintings (their color derived from minerals), to sculptures of Egyptian kings carved of stone to recent pottery and their glazes, minerals are an integral ingredient of the art world (see Fig. 1.8). By knowing the physical properties of minerals and rocks, artists utilize these materials for specific purposes. Pottery is made of mineral mixtures (porcelain is primarily quartz, and earthenware is mainly clay), as are the many colorful glazes used for decoration (e.g., using copper, or rutile, TiO_2). Paintings may be viewed as recording human history. With their pigments derived from mineral material, early cave paintings display hunting scenes whereas prehistoric Egyptian paintings and Renaissance drawings may depict mining practices (see Figs. 1.8 and 1.10). Minerals have provided the color that sustains this artwork through the ages, but in the present day many colors are of synthetic (chemical) origin.

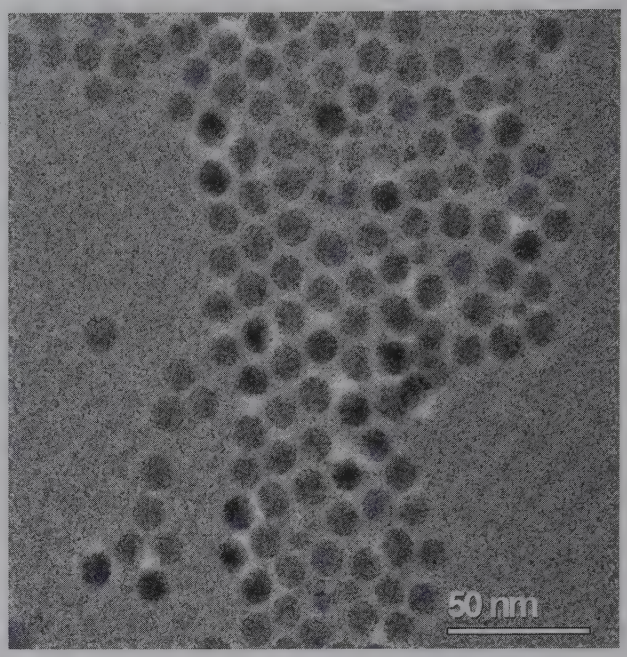

FIG. 1.7 Bright field transmission electron microscope (TEM) image of synthetic magnetite nanocrystals with an average diameter of 11 nm. (Photograph courtesy of Huifang Xu, University of Wisconsin, Madison.)

Archeology applies scientific principles to the study of ancient peoples and cultures. Minerals found in ancient sites help scientists deduce trade routes, determine sources of materials used for food gathering and preparation, and interpret the wealth of societies. In Central America, salt (halite) was an important trade item, whereas in Asia, it was turquoise. Chert was used for making arrowheads, and basalt was used for grinding corn.

The study of minerals allows insight into many other areas of the sciences and humanities. These are only a few examples of how mineralogy is part of many other endeavors.

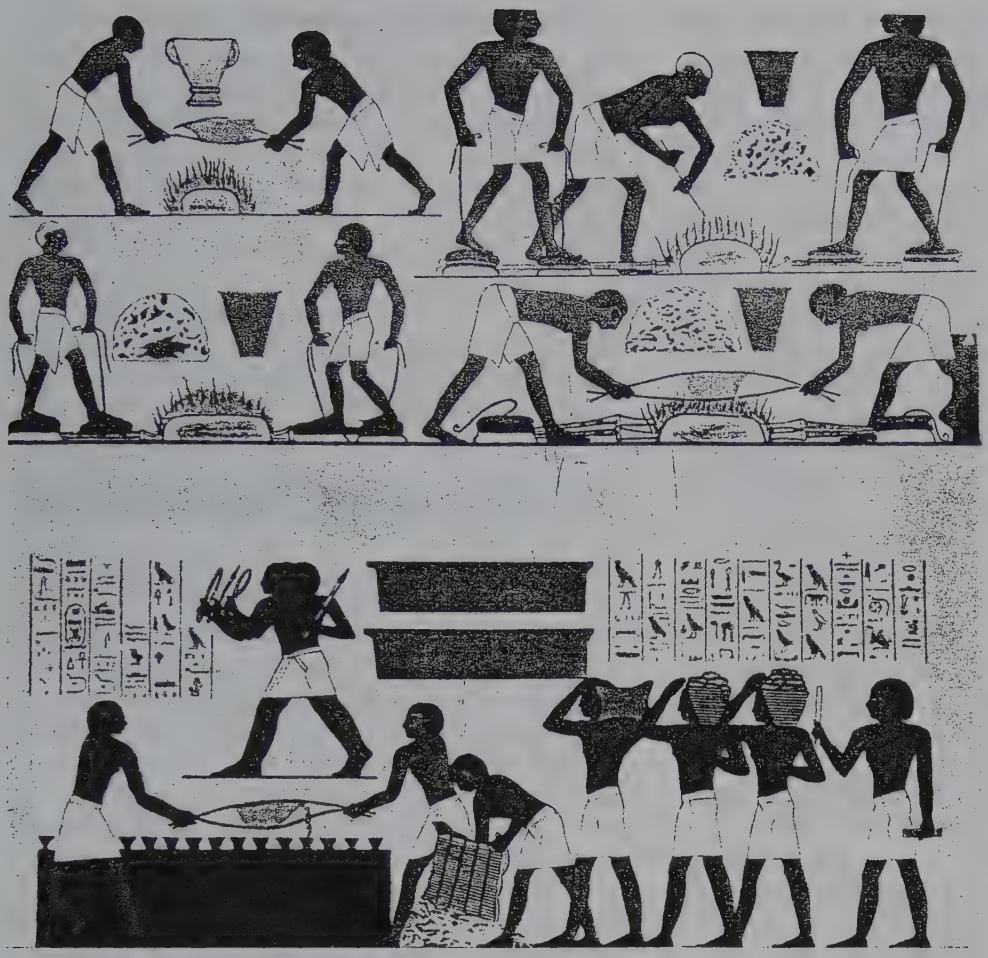

FIG. 1.8 The process of extracting metals from ores is very old. Shown here are the smelting stages of gold-bearing ore by ancient Egyptians. (From Hurlbut, C. S., Jr. *Minerals and Man.* Random House, New York.) This painting was created with pigments extracted from minerals.

DISCIPLINES OF MINERAL SCIENCE

The subject of mineral science encompasses five interrelated subfields (see Fig. 1.9). Each aspect leads to important information about minerals, and each field is integral to the next. These features are explored here and on the next page.

Descriptive mineralogy is the measurement and recording of physical properties that help describe and identify a mineral. Some features of a mineral, such as crystal form, hardness, color, and specific gravity (see Chapter 2), can be evaluated in hand specimens by looking at the mineral and/or using some basic testing equipment. Other, more objective aspects of a mineral, such as optical properties and the size of the unit cell (dimensions of the smallest building block of the atomic structure), require specialized techniques and equipment. Examples of equipment required for these measurements include the petrographic microscope and an X-ray diffraction system, respectively (explained in Chapters 13 and 14).

Crystallography is a broad branch of science that deals with the atomic arrangement of solid materials. Consequently, it links to other disciplines, such as material science and inorganic chemistry. Initially, crystallography focused on geometric form, external

FIG. 1.9 Diagram showing the major subdisciplines that constitute mineral science. Arrows imply a major contribution of one subfield to another.

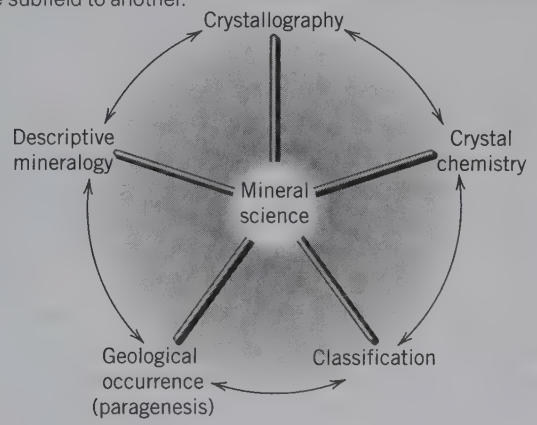

symmetry, and optical properties of crystals. The discovery of X-rays, and the subsequent experiments using X-rays, brought about a revolution in crystallography. Today, the aim of modern crystallographic techniques is the determination of the internal structure of crystalline materials, referred to as their *crystal structure*. Determination of the crystal structure provides information on the location of all the atoms, bond positions and bond types, internal symmetry, and the chemical composition of the basic building blocks of minerals. This information is fundamental to concepts in *crystal chemistry*, the interrelation of mineral chemistry and structure.

Crystal chemistry relates the chemical composition, the internal structure, and the physical properties of crystalline materials. A specific mineral is defined on the basis of its crystal structure and chemical composition. These, in turn, relate to the mineral's physical properties. In many mineral groups, the overall structure is relatively constant, but the chemical composition is highly variable. The assessment of the structure type, atomic bonding arrangement, chemical variability, and related changes in physical properties of crystalline materials are included in crystal chemistry.

Classification of minerals is the manner in which minerals are logically categorized, similar to what is done in biology or chemistry. There are approximately 4,200 valid mineral species and each has a distinctive name (see page 332). To make sense of the variable chemistries and structures represented by these minerals, it is customary to classify them according to a scheme that incorporates both chemistry and structure. After careful analysis, they are first classified by their anion or anionic group. This results in classifications, such as native elements, sulfides, oxides, carbonates, and silicates, for example (see Chapters 15 through 19). Second, in groups with many species and complex structures, such as the silicate group, further subclassifications are made. These subclassifications are primarily based on structural (atomic) arrangements, such as the various linkages of the silicate tetrahedra.

Geologic occurrence refers to the geologic setting in which a mineral is found and to its characteristic association with other minerals (often termed *paragenesis*). For example, a common occurrence for the mineral pyrite, FeS_2, would be reported as "in ore deposits of hydrothermal origin." Garnet, a chemically complex silicate, is especially characteristic of metamorphic rocks. Depending on a garnet's chemical makeup, its occurrence might be listed as "mainly in Al-rich rock types that are the product of regional metamorphism" or "as in Fe- and Ca-rich limestones that have been altered by contact metamorphism."

The field of **mineral science** now encompasses a very broad area of study. Major areas of mineralogically related research have been described above and in the section "Defining a Mineral More Broadly." Additional fields include X-ray, electron, and neutron diffraction analysis of minerals and mineral synthesis. Other study areas focus on the thermodynamic stability of minerals, the analysis of rocks and minerals under the microscope (petrography), and aspects of metallurgy and ceramics. The field of mineral science is expanding continually as more scientific discoveries are made and new experimental techniques and analytical tools are developed.

HISTORY OF MINERALOGY

The development of mineralogy spans centuries, and only a few highlights are presented here. The emergence of mineralogy as a science is relatively recent, but the practice of mineralogical arts is as old as human civilization. Natural pigments, made of red hematite and black manganese oxide, were used in cave paintings by early humans (ca. 40,000 YBP). Flint tools were prized possessions used for hunting during the Stone Age. Tomb paintings in the Nile Valley produced nearly 5,000 years ago (Fig. 1.8) show busy artificers weighing malachite and precious metals, smelting mineral ores, and making delicate gems of lapis lazuli and emerald (as worn by Cleopatra). As the Stone Age gave way to the Bronze Age, other minerals were sought from which metals could be extracted. Minerals were often the "money" of ancient times, and now they aid archeologists in the tracing of prehistoric trade routes.

Compilations of minerals existed as early as 700 B.C. in China and later in India (see Hawthorne, 1993 for details). The Greek philosopher Theophrastus (372–287 B.C.) provided the first written work on minerals, and Pliny, 400 years later, recorded the mineralogical thought of his time. During the following 1,300 years, the few works that were published on minerals contained much lore and fable with little factual information. Perhaps the single event signaling the emergence of mineralogy as a science was the 1556 publication of *De Re Metallica* by the German physician Georgius Agricola. This work provides a detailed account of the mining and ore smelting practices of the time and includes the first factual data on minerals. (*De Re Metallica* was translated into English from the Latin in 1912 by the former president of the United States, Herbert Hoover, and his wife, Lou Henry Hoover.) An illustration from it is reproduced in Fig. 1.10.

In 1669, an important contribution to crystallography was made by Nicolaus Steno (Fig. 1.11) through his

FIG. 1.10 An illustration from Agricola, *De Re Metallica* (1556) shows ore mined underground, moved through horizontal tunnels, and hoisted through vertical shafts. (From Agricola, *De Re Metallica*, translated into English. Published in 1950 by Dover Publications, Inc., New York.)

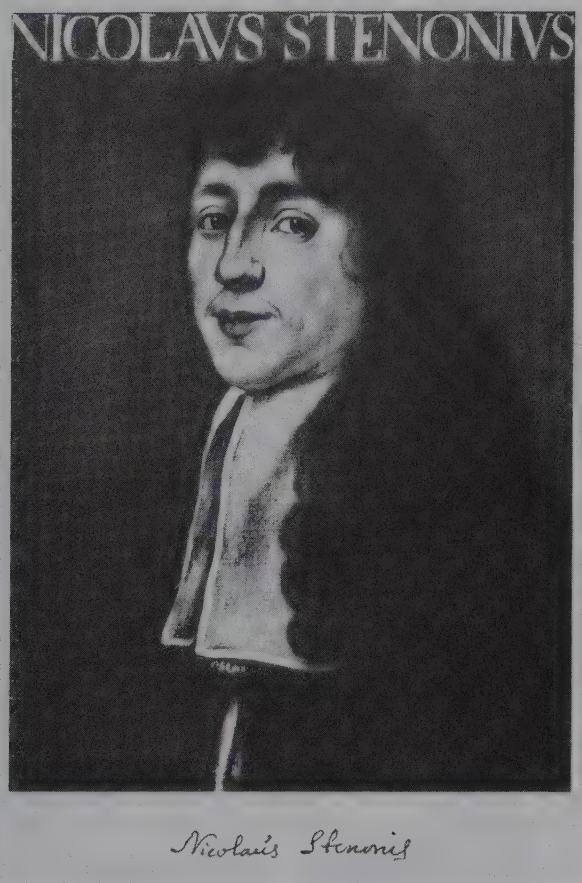

FIG. 1.11 Portrait of Niels Stensen (Latinized to Nicolaus Steno). Steno was born in Copenhagen, Denmark, in 1638 and died in 1686. He was beatified by the Roman Catholic Church in 1988 (from Scherz, G. 1969. *Steno, Geological Papers*. Odense University Press).

study of quartz crystals. He noted that despite differences in origin, size, or shape of quartz crystals, the angles between the same faces on different crystals were constant (Fig. 1.12). More than a century passed before the next major contributions were made. In 1780, Carangeot invented a device used to measure interfacial crystal angles, called the contact goniometer (Fig. 1.13a). In 1783, Romé de l'Isle used this device to make angular measurements on crystals confirming Steno's work and formulated the *law of the constancy of interfacial angles* now known as *Steno's Law* (discussed in Chapter 6). The following year, 1784, René J. Haüy showed that crystals were built by stacking together tiny identical building blocks, which he called integral molecules (Fig. 1.14). The concept of integral molecules survives almost in its original sense as the *unit cells* of modern crystallography (see Chapter 6). The *theory of rational indices for crystal faces* followed, in 1801, through Haüy's study of hundreds of crystals (discussed in Chapter 6).

In the early nineteenth century, rapid advances were made in the field of the physics and chemistry of minerals, commensurate with advances in instrumentation (Fig. 1.13b). In 1809, Wollaston (who is honored by the mineral name *wollastonite*) invented the reflecting goniometer, which permitted highly accurate and precise measurements of the positions of crystal faces. Where the contact goniometer had provided the necessary data for studies on crystal symmetry, the reflecting goniometer (Figs. 1.13c and d) provided extensive, highly accurate measurements on crystals. These data made crystallography an exact science. Between 1779 and 1848, Berzelius, a Swedish chemist, and his students studied the chemistry of minerals and developed the principles of our present chemical classification of minerals.

FIG. 1.12 Steno's drawings of various quartz and hematite crystals, illustrating the constancy of angles among crystals of different habits or shapes. (From Schafkranovski, J. J. 1971. *Die Kristallographischen Entdeckungen N. Stenens*, in *Steno as Geologist*. Odense University Press.)

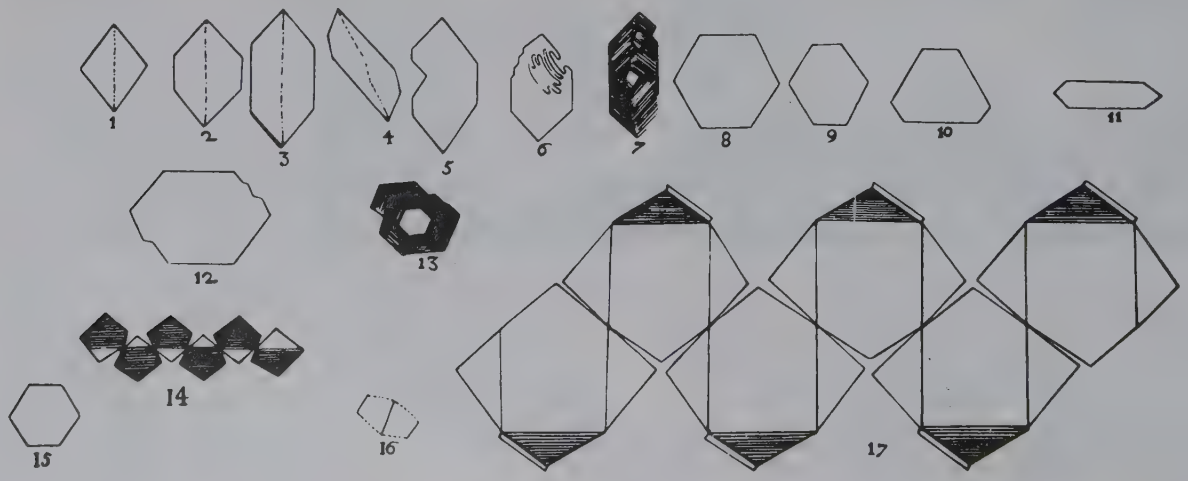

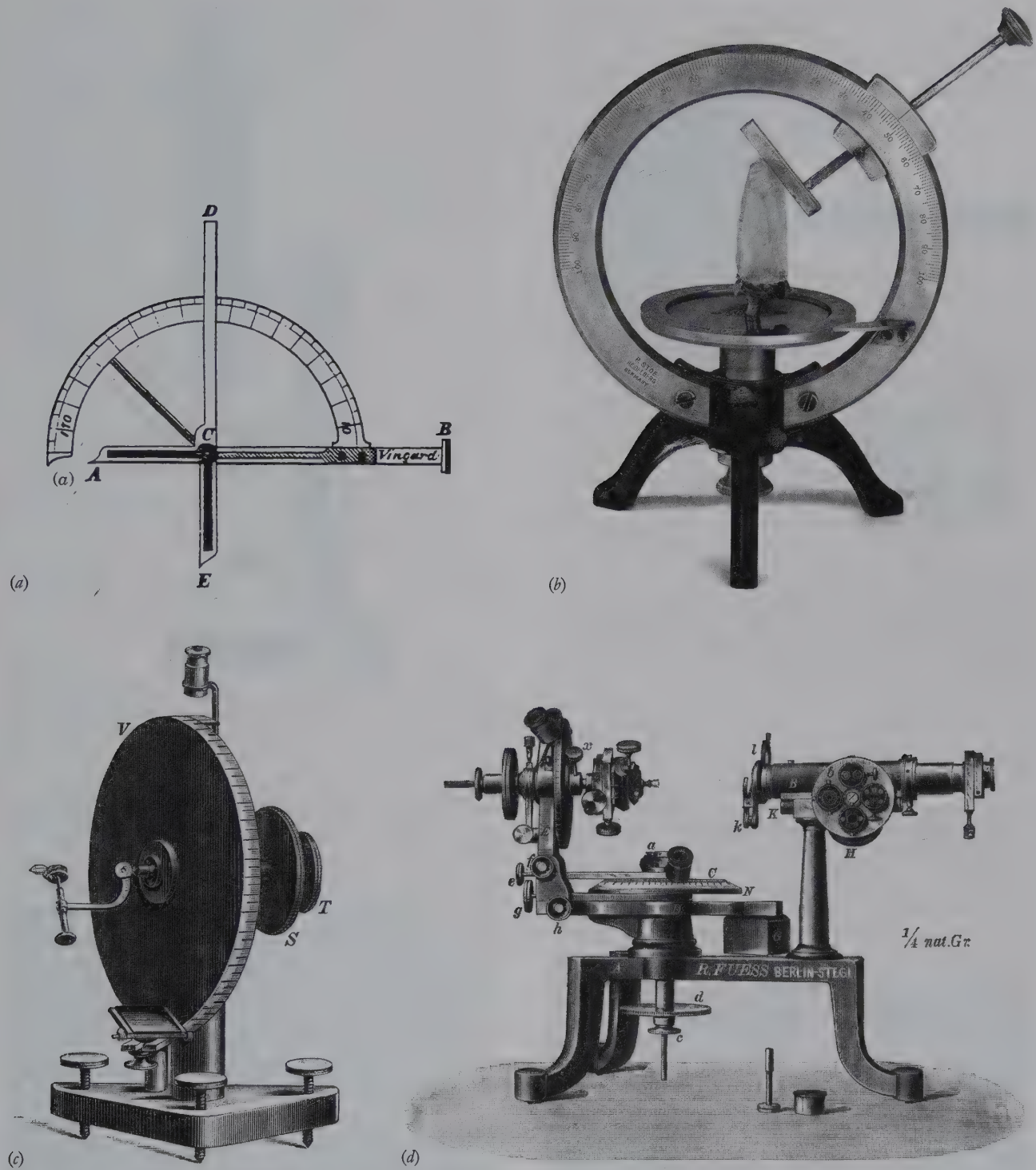

FIG. 1.13 Examples of instruments used for the measurement of angles between crystal faces. (a) Brass contact goniometer of the Carangeot type. This was used at Harvard University in 1797 (see Frondel, 1983). (b) A two-circle contact goniometer based on the 1896 design of Victor Goldschmidt. (c) The earliest reflecting one-circle goniometer as invented by W. H. Wollaston in 1809. (From Tschermak, G. and Becke, F. 1921. *Lehrbuch der Mineralogie*. Hölder-Pichler-Tempsky, Vienna.) (d) A two-circle reflecting goniometer developed in the latter part of the nineteenth century. (From Groth, P. 1895. *Physikalische Krystallographie*. Leipzig.)

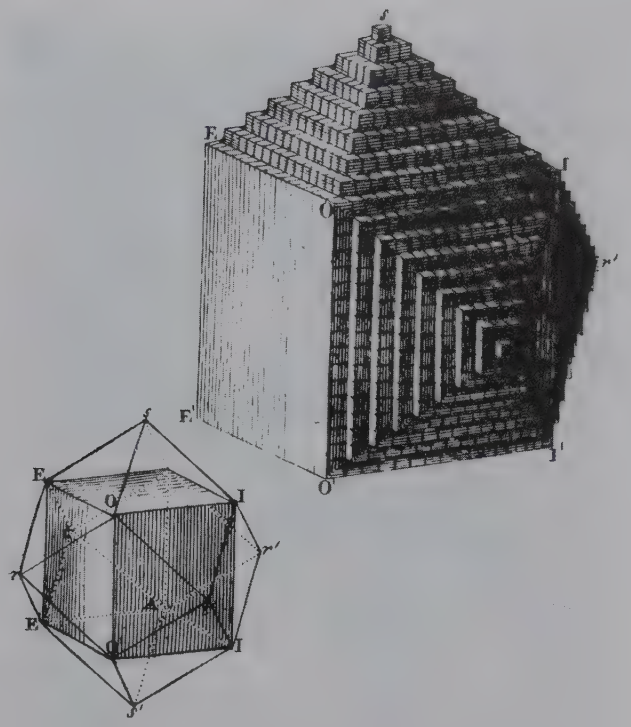

FIG. 1.14 Illustration of the concept developed by R. J. Haüy (1743–1826) of tiny identical building blocks underlying the external form of crystals. In this figure, the development of a dodecahedron of garnet is shown. (From Marr, G. M. 1970. *Geschichte der Kristallkunde.* Reprinted by Sandig, Walluf, Germany.)

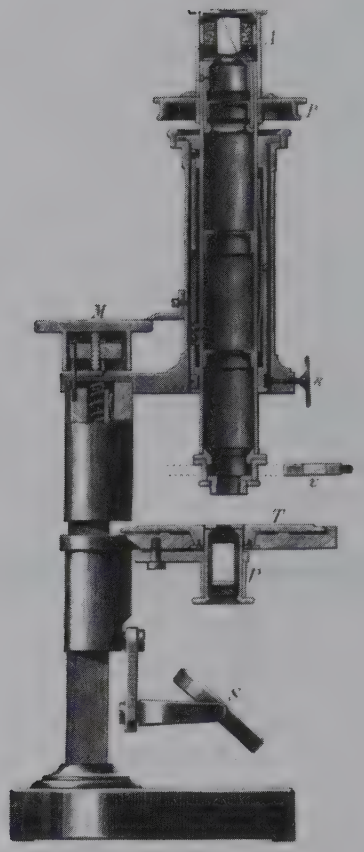

FIG. 1.15 Mid-nineteenth century polarizing microscope. (From Tschermak, G., and F. Becke. 1921. *Lehrbuch der Mineralogie.* Hölder-Pichler-Tempsky, Vienna.)

In 1815, the French naturalist Cordier (whose legacy to mineral science is honored by the name of the mineral *cordierite*) investigated crushed mineral fragments immersed in water under the microscope. This *immersion method* developed into an important technique for studying the optical properties of mineral fragments (see Chapter 13). The usefulness of the microscope for mineral study was greatly enhanced by the invention of a light-polarizing device that permitted the systematic study of the behavior of optical properties in crystalline substances (in 1828 by a Scotsman, William Nicol). The polarizing microscope became, and still is, a powerful determinative tool in mineralogical studies. An early model is illustrated in Fig. 1.15. In the latter part of the nineteenth century Fedorov, Schoenflies, and Barlow, all working independently, came to the same conclusions and simultaneously developed theories for the internal symmetry (refer to Chapter 7) and order within crystals. This work became the foundation for later work in X-ray crystallography (Chapter 14).

The most far-reaching discovery of the twentieth century with respect to minerals must be attributed to Max von Laue (of the University of Munich, Germany) for providing a technique to image the ordered arrangement of atoms in crystalline materials. In 1912, after the discovery of X-rays by Wilhelm Conrad Roentgen in 1895, an experiment was performed by Friedrich and Knipping at the suggestion of von Laue. This experiment demonstrated that crystals could diffract X-rays. To diffract X-rays, materials need an ordered and repeating structure. Thus, for the first time, it was proven that there is a regular and ordered arrangement of atoms in crystalline material. Almost immediately, X-ray diffraction became a powerful method for the study of minerals and all other crystalline substances (discussed in detail in Chapter 14). In 1914, the earliest crystal structure determinations were published by W. H. Bragg and W. L. Bragg (a father and son team) in England. Modern X-ray diffraction equipment and computer algorithms have made possible the relatively rapid acquisition of data necessary to determine highly complex crystal structures.

The advent of the electron microprobe in the early 1960s provided a powerful tool for the *in situ* chemical analysis of minerals, synthetic compounds, and glasses on the micrometer scale. The electron microprobe is

now used routinely for determination of the chemical composition of minerals. In the early 1970s, another electron beam instrument, the transmission electron microscope (TEM), was developed that could magnify the internal architecture of minerals many millions of times. TEMs have produced elegant and powerful visual images of atomic structures. High-resolution transmission electron microscopy (HRTEM) allows the study of crystalline materials at resolutions approaching the scale of atomic distances (see P. R. Buseck, 1983) and further illustrates that many minerals have infinitely extending, perfectly repeating, internal structural arrangements. An example of such a "perfect" structure is illustrated by the HRTEM image in Fig. 1.16 for the chemically complex mineral tourmaline (of which, a photograph of a transparent section was used for the cover of this text). New instruments allow us to see images of a material's surface (see Chapter 14 opening illustration) and to resolve structures at size levels approximating atoms (see opening image in Chapter 7). For further discussion of such analytical techniques see Chapter 14.

The science of minerals has been, and continues to be, influenced by many scientists from a variety of different fields. Because it is difficult to predict which contributions to the science of mineralogy will prove to be most enduring and important, a list of prominent mineralogists who have received the prestigious Roebling Medal, awarded annually by the Mineralogical Society of America for profound contributions to mineral science, is given in Appendix 1.

FIG. 1.16 High-resolution transmission electron microscope (HRTEM) image of the structure of tourmaline, the mineral illustrated on the cover of this text. (From Iijima, S., J. M. Cowley, and G. Donnay, 1973. High-resolution electron microscopy of tourmaline crystals. *Tschermaks Mineralogische Petrographische Mitteilungen* 20: 216–24.) The white areas in the photograph correspond to regions of low electron density in the structure of tourmaline. The six-fold "daisy" pattern is the image of the six-fold Si_6O_{18} rings in tourmaline; one such ring is schematically outlined in black (compare with Fig. 18.14a). The bar scale represents 150 nm.

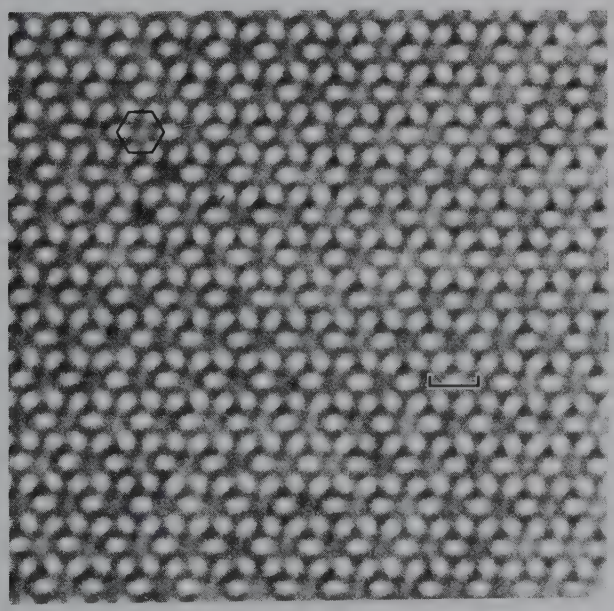

MINERALS IN OUR LIVES

Minerals are the raw materials on which much of society's technological development and economic productivity are based. Minerals have always played a major role in humanity's way of life and standard of living. The ages of man are named after the materials that they used, such as the Stone Age, Bronze Age, and Iron Age, and each relied on minerals for the materials. Flint and pyrite, two minerals, were first used to make fire.

With each successive century, minerals have become increasingly important, and today we depend on them in countless ways—from the construction of skyscrapers to the manufacture of computers and duct tape. Modern civilization depends on and necessitates the prodigious use of minerals. A few minerals, such as talc, halite (salt), and sulfur, are used essentially as they come from the ground. Most minerals, however, are first processed to obtain a usable material. This material is then incorporated into other compounds to produce products, such as aluminum foil, brick, glass, cement, plaster, kitty litter, or paper (Fig. 1.17). A score

FIG. 1.17 Minerals are found in products used every day, some of which are shown here. Such minerals include, from left to right in forefront, copper (for copper wiring), zeolites (white—as an absorbent in kitty litter), rutile (small dark block—as white coloring agent in M&Ms, toothpaste), and clay minerals (large white block in center—as a filler for glossy paper, deodorant). Bauxite is the source of aluminum used in aluminum foil; halite (NaCl) is the same as table salt.

of metals ranging from molybdenum to iron to titanium to gold are incorporated into a wide array of products, such as lubricants, airplanes, steel, or mountain bikes (see Fig. 1.2). Metallic ores and industrial minerals are mined on every continent, except Antarctica, wherever specific minerals are sufficiently concentrated to be economically extracted.

ANNUAL AVERAGE MINERAL USE IN THE UNITED STATES OF AMERICA

According to the U.S. Bureau of Mines (reported in *Geotimes*, 1989, v. 34, p. 19), "Each year, every American requires 40,000 pounds of new minerals. At that level of consumption, the average newborn infant will need a lifetime supply of 795 pounds of lead (mainly for car batteries, solder, and electronic components); 757 pounds of zinc (as an alloy of copper to make brass, as protective coatings on steel, and as chemical compounds in rubber and paints); 1,500 pounds of copper (mainly used in electrical motors, generators, communication equipment, and wiring); 3,593 pounds of aluminum (for all sorts of things, such as aluminum foil, beverage cans, folding lawn chairs, and aircraft); 32,700 pounds of iron (for kitchen utensils, automobiles, ships, and large buildings); 28,213 pounds of salt (for cooking, highway de-icing, and detergents); and 1,238,101 pounds of stone, sand, gravel, and cement (for building roads, homes, schools, offices, and factories)." Because the Earth has a limited supply of these materials, a worldwide commitment to recycling and reusing is necessary to lower many of the above estimates before the supplies are exhausted.

NAMING OF MINERALS

Minerals are most commonly *classified* on the basis of a major chemical component, either an *anion* or *anionic complex*. For example, categorizing on the basis of a dominant *anion* arranges minerals into the oxides, sulfides, and halides whereas a dominant *anionic complex* results in the silicates, carbonates, and phosphate groups. This is especially convenient because most minerals contain only one major anion. Consequently, the careful description and identification of new minerals require both the definition of the chemistry and of the structure. (Techniques for obtaining these data are given in Chapter 14.)

In contrast, the *naming* of minerals is not based on such a logical chemical scheme and names originate from a variety of sources. Minerals may be given names on the basis of some physical property or chemical aspect, or they may be named after a locality, a public figure, a mineralogist, or almost any other subject considered appropriate (see examples that follow). Typically, a mineral is given its name by the person who first discovers the new mineral and describes its properties.

Some examples of mineral names and their derivations are as follows.

Albite, $NaAlSi_3O_8$, from the Latin *albus* (white), an allusion to its color.

Rhodochrosite, $MnCO_3$, from the Greek *rhodon* (rose), an allusion to its characteristically pink color.

Chromite, $FeCr_2O_4$, because of the presence of a large amount of chromium in the mineral.

Magnetite, Fe_3O_4, because of its magnetic properties.

Pyrite, FeS_2, from the Greek *pyros* (fire) because it sparks when hit with another mineral.

Franklinite, $ZnFe_2O_4$, after a locality, Franklin, New Jersey, where it occurs as the dominant zinc mineral.

Sillimanite, Al_2SiO_5, after Professor Benjamin Silliman of Yale University (1779–1864).

Staurolite, $Fe_{3-4}Al_{18}Si_8O_{48}H_{2-4}$, from the Greek *stauros* (a cross) after the typical crossed crystals (twins) it displays.

An international committee, the Commission on New Minerals and Mineral Names of the International Mineralogical Association (CNMMN), now reviews all new mineral descriptions and judges the appropriateness of new mineral names as well as the scientific characterization of newly discovered mineral species. This commission maintains a website where the status of minerals is recorded (because the website address changes, search on IMA—CNMMN). The *Fleischer's Glossary of Minerals Species* (published in 2004 by Mandarino and Back) lists over 4,000 mineral entries as valid or probably valid mineral species. This text will use the names given in that listing. An alphabetical listing of about 3,800 mineral species is given in the *Encyclopedia of Mineral Names* (Blackburn and Dennen, 1997) and describes the origin of a mineral's name.

REFERENCES AND LITERATURE OF MINERALOGY

The first comprehensive book on mineralogy in English was *A System of Mineralogy* written by James D. Dana in 1837. Since then, through subsequent revisions, it has remained a standard reference work. The last complete edition (the sixth) was published in 1892, with supplements in 1899, 1909, and 1915. Parts of a seventh edition, known as *Dana's System of Mineralogy*,

appeared as three separate volumes in 1944, 1951, and 1962. The first two volumes cover the nonsilicate minerals, and volume three covers silica (quartz and its polymorphs). A more recent reference is the five-volume work, *Rock-Forming Minerals*, by W. A. Deer, R. A. Howie, and J. Zussman, published in 1962. Since then, eight completely revised volumes have appeared in this series in different years (see the reference listing at the end of this chapter). The treatment of the physical properties of all minerals in *Dana's System* is exhaustive. The coverage in *Rock-Forming Minerals*, however, is more topical and expansive in the areas of chemistry, structure, and experimental studies, but is essentially confined to the rock-forming minerals. Another useful reference on the chemistry and nomenclature of minerals is *Strunz Mineralogical Tables* (H. Strunz and E. H. Nickel, 2001). A useful tabulation of mineral data can be found in the four-volume set *Handbook of Mineralogy* (J. Anthony et al.). An in-depth treatment of topical subjects in mineralogy is provided by *Reviews in Mineralogy* (and *Reviews in Mineralogy and Geochemistry*), volumes 1 to 60, published by the Mineralogical Society of America.

More in-depth coverage of mineral science is found in papers published in scientific journals. The most widely circulated mineralogical journals are *American Mineralogist*, published by the Mineralogical Society of America; *The Canadian Mineralogist*, published by the Mineralogical Association of Canada; and *Mineralogical Magazine*, published by the Mineralogical Society of Great Britain. The *European Journal of Mineralogy* merged publications of the mineralogical societies of Germany, France, and Italy. Many other publications covering petrology and material science also include mineral science topics. *The Mineralogical Record* and *Rocks and Minerals* are devoted to mineralogical subjects that are often of more general appeal to hobbyists or mineral collectors than those found in the other journals listed previously.

WHAT'S TO COME

In the following chapters of this text, you will discover the world of minerals: their properties, their uses, and how they relate to our Earth and to our everyday life. Knowing about minerals can help you make wise decisions about many facets of life ranging from buying a gemstone to buying a house. Also, you will learn about the fundamental building blocks of minerals, how they are arranged, and how this atomic arrangement is manifest in their external form and their resultant properties. Once these basics are mastered, identification of minerals follows.

STANDARD MINERALOGICAL REFERENCE WORKS AND FURTHER READING

Anthony, J. W., R. A. Bideaux, K. W. Bladh, and M. C. Nichols. *Handbook of mineralogy.* Vol. 1, *Elements, sulfides, sulfosalts*, 1990. Vol. 2, *Silica, silicates*, 1995. Vol. 3, *Halides, hydroxides, oxides*, 1997. Vol. 4, *Arsenates, phosphates and vanadates*, 2000. Mineral Data Publishing, Tucson, Arizona. Online at: www.minsocam.org.

Blackburn, W. H., and W. H. Dennen. 1997. *Encyclopedia of mineral names.* The Canadian Mineralogist, Special Publication 1.

Dana, J. D. 1937. *A system of mineralogy.* Wiley, New York.

Dana, J. D. 1944–1962. *Dana's system of mineralogy.* 7th ed. 3 vols. Wiley., New York. Rewritten by C. Palache, H. Berman, and C. Frondel.

Deer, W. A., R. A. Howie, and J. Zussman. 1962. *Rock-forming minerals.* 5 vols. Wiley, New York. Eight completely revised volumes (nos. 1A, 1B, 2A, 2B, 3A, 4A, 4B, and 5B) have been published since 1962 and are available from the Geological Society, London, Great Britain.

Gaines, R. B., H. C. W. Skinner, E. E. Foord, B. Mason, and A. Rosenzweig. 1997. *Dana's new mineralogy.* Wiley, New York.

Mandarino, J. A., and M. E. Back. 2004. *Fleischer's glossary of mineral species 2004.* The Mineralogical Record, Inc., Tucson, Arizona.

Nickel, E. H., and M. C. Nichols. 1991. *Mineral reference manual.* Van Nostrand Reinhold, New York.

Reviews in Mineralogy and Geochemistry. 1974–2006, 60 vols. Mineralogical Society of America, Washington, D.C.

Strunz, H. and E. H. Nickel 2001. *Strunz Mineralogical Tables.* 9th ed. E. Schweizerbart'sche Verlagsbuchhandlung, Stuttgart.

Historical Accounts

Agricola, G. 1950. *De Re Metallica.* Translated from the first Latin edition of 1556 by Herbert C. Hoover and Lou H. Hoover. Dover Publications, New York.

Ford, W. E. 1918. The growth of mineralogy from 1818 to 1918. *American Journal of Science* 46: 240–54.

Frondel, C. 1983. An overview of crystallography in North America. In *Crystallography in North America*, 1–24. Edited by D. McLachlan and J. P. Glusker. American Crystallographic Association, New York.

Greene, F. C., and J. G. Burke. 1978. The science of minerals in the age of Jefferson. *American Philosophical Society* 68, pt. 4: 113.

Hazen, R. M. 1984. Mineralogy: A historical review. *Journal of Geological Education* 32: 288–98.

Knopf, A. 1941. Petrology. *Geology 1888–1938.* Geological Society of America, 50th anniversary vol.: 333–64.

Kraus, E. H. 1941. Mineralogy. *Geology 1888–1938.* Geological Society of America, 50th anniversary vol.: 307–32.

Pirsson, L. V. 1918. The rise of petrology as a science. *American Journal of Science* 46: 222–40.

Economic Geology/Natural Resources

Cameron, E. G. 1986. *At the crossroads: The mineral problems of the United States.* Wiley, New York.

Carr, D. C., ed. 1994. *Industrial minerals and rocks.* 6th ed. Society for Mining, Metallurgy, and Exploration, Inc., Littleton, Colorado.

Chang, L.L.Y. 2002. *Industrial mineralogy.* Prentice Hall, Upper Saddle River, New Jersey.

Evans, A. M. 1987. *Introduction to ore geology*, 2nd ed. Blackwell Scientific Publications, London.
Guilbert, J. M., and C. F. Park Jr. 1986. *The geology of ore deposits.* W. H. Freeman, New York.
Kessler, S. E. 1994. *Mineral resources, economics, and the environment.* Prentice Hall, Upper Saddle River, New Jersey.
U.S. Bureau of Mines. Various years. *Minerals yearbook.* U.S. Government Printing Office, Washington, D.C.

Additional References

Banfield, J. F., and K. H. Nealson, eds. 1997. Geomicrobiology: Interactions between rocks and minerals. *Reviews in Mineralogy* 35, Mineralogical Society of America, Washington, D.C.
Banfield, J. F., and A. Navrotsky, eds. 2001. Nanoparticles and the environment. *Reviews in Mineralogy and Geochemistry* 44, Mineralogical Society of America, Washington, D.C.
Buseck, P. R. 1983. Electron microscopy of minerals. *American Scientist* 71, no. 2: 175–85.
Dove, P.M., J. J. DeYoreo, and S. Weiner, eds. 2003. *Biomineralization. Reviews in Mineralogy and Geochemisty* 54, Mineralogical Society of America, Washington, D.C.
Ewing, R.C., W. J. Weber, and J. Lian. 2004. Nuclear waste disposal-pyrochlore (A(2)B(2)O(7)): Nuclear waste form for the immobilization of plutonium and "minor" actinides. *Journal of Applied Physics* 95: 5949–71.
Gibson, R. I. 1974. Descriptive human pathological mineralogy. *American Mineralogist* 59: 1177–82.
Hawthorne, F. C. 1993. Minerals, mineralogy, and mineralogists: Past, present, and future. *The Canadian Mineralogist* 31: 253–96.
Hemley, R. J. 1999. Mineralogy at the crossroads. *Science* 285: 1026–27.
Hemley, R. J., ed. 1998. *Ultrahigh-pressure mineralogy: Physics and chemistry of the Earth's deep interior. Reviews in Mineralogy* 37, Mineralogical Society of America, Washington, D.C.
Hochella, M.F., Jr. and A.F. White, eds. 1990, *Mineral-water interface geochemistry. Reviews in Mineralogy* 23, Mineralogical Society of America, Washington, D.C.
Hochella, M.F., Jr., 2002. Sustaining Earth: Thoughts on the present and future roles of mineralogy in environmental science. *Mineralogical Magazine* 66: 627–652.
Hochella, M.F., Jr. 2006. The case for nanogeoscience: Why it will be the centerpiece of geoscience research of the future (Abstract), *NNIN Conference on Nanoscale Processes in the Earth and Planetary Sciences*, Albuquerque, New Mexico, 25.
Lowenstam, H. A. 1981. Minerals formed by organisms. *Science* 211: 1126–31.
Nickel, E. J. 1995. The definition of a mineral. *The Canadian Mineralogist* 33: 689–90.
Papike, J. J., ed. 1998. *Planetary materials. Reviews in Mineralogy* 36, Mineralogical Society of America, Washington, D.C.
Weiner, S. and P. Dove, 2003. An overview of biomineralization processes and the problem of the vital effect. In *Biomineralization. Reviews in Mineralogy and Geochemistry* 54, Mineralogical Society of America, Washington, D.C.

CHAPTER 2

Physical Properties of Minerals

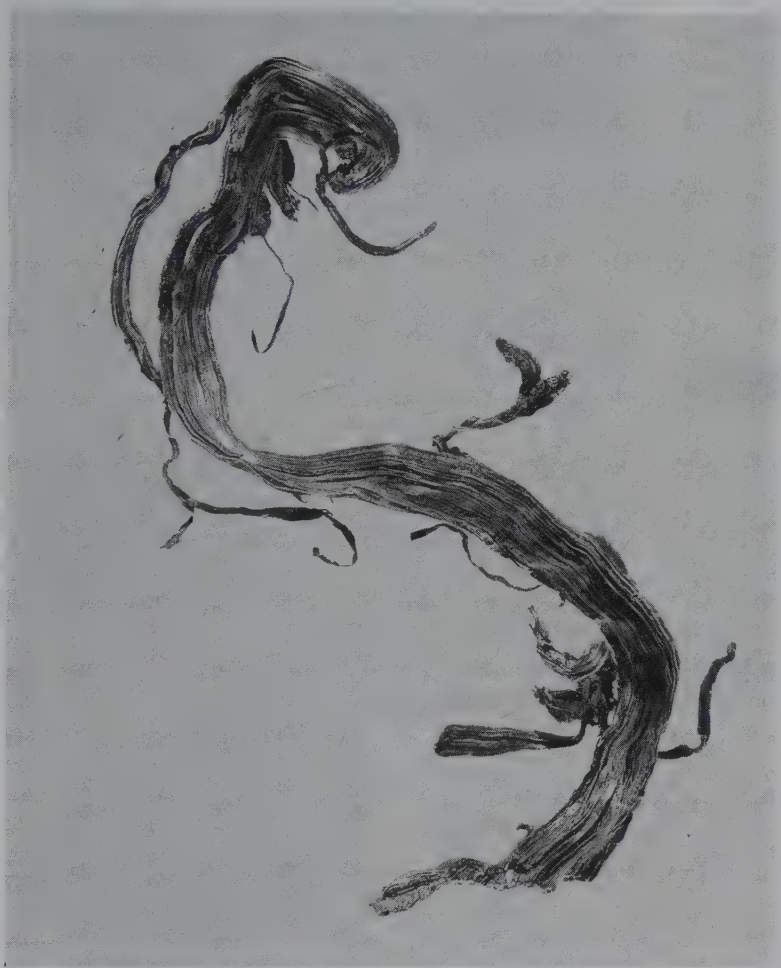

Silver, Ag. This specimen has a curved, wire-like habit. It is also soft, malleable, ductile, and sectile. These physical properties are unique to several of the native metals, such as gold, silver, and copper. The specimen is 12.7 cm high. From Kongsberg, Norway. (Photograph courtesy of Stuart and Donna Wilensky, Wilensky Fine Minerals, Wurtsboro, NY.)

The physical properties of a mineral are the macroscopic expression of its internal makeup, specifically its crystal structure and chemical composition. Because these are characteristic for each mineral, different samples of the same mineral should display similar physical properties and these can be used to determine the identity of a mineral. These physical features also make many minerals valuable; soft minerals are lubricants, hard minerals are abrasives. This chapter describes several important physical properties of minerals and outlines simple diagnostic tests that can be used for mineral identification. Building on this foundation, later chapters examine minerals at the atomic scale to provide an understanding of the origin of these properties.

The study of minerals in hand specimen is observational. The first step to identifying and studying minerals is visual inspection of hand-sized samples. Because the external properties of a mineral are a reflection of its atomic properties, that is, its chemistry and structure, a few simple determinative tests on these samples will probably lead you to a correct identification of the mineral under study. In subsequent chapters, we will study minerals at the atomic level to understand the origin of these properties.

In Chapters 15, 16, 17, and 19, mineral properties are grouped according to appearance (crystal form, habit), interaction with light (luster, color, streak, luminescence), mechanical properties (hardness, tenacity, cleavage, fracture and parting), mass (density and specific gravity), and other useful properties (magnetism, radioactivity, reactivity with acid, etc.). Examples of many physical properties are shown in the color photographs of minerals, Plates I–XII.

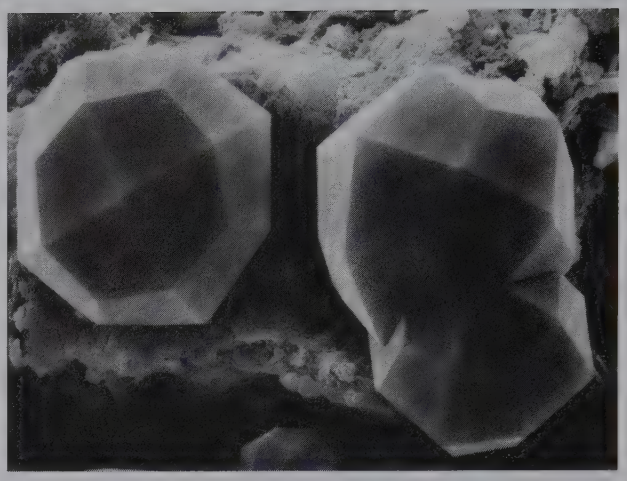

FIG. 2.1 Scanning electron microscope (SEM) photograph of three beautifully formed crystals of the mineral analcime, $NaAlSi_2O_6 \cdot H_2O$, from Ischia, Italy. Each crystal displays a single form, a trapezohedron that reflects a high symmetry content in the isometric system. The trapezohedron is composed of 24 trapezium-shaped faces. (From Gottardi, G., and E. Galli. 1985. *Natural zeolites.* Springer-Verlag, New York; with permission.)

CRYSTAL SHAPE

One of the most aesthetically pleasing aspects of well-formed mineral specimens is their occurrence in crystals or crystal groupings. Such crystals have smooth planar surfaces that assume geometric forms like a tetrahedon, octahedron, or a cube (Figs. 2.1 and 2.2). When the outward appearance of a mineral takes on a regular geometric shape, it is referred to as its **crystal form.** Crystal forms may be used as a diagnostic physical property because the external form is the outward expression of the internal ordered atomic arrangement. For example, garnets crystallize in the shape of a dodecahedron consisting of 12 diamond-shaped planes (Fig. 2.2a; Plate IV, no.7), whereas pyrite may form cubes or crystals with 12 smooth planes that each have five edges (Fig. 2.2b). These forms are also useful descriptive and determinative tools. Chapter 6 provides a more detailed discussion of *forms* as they relate to crys-

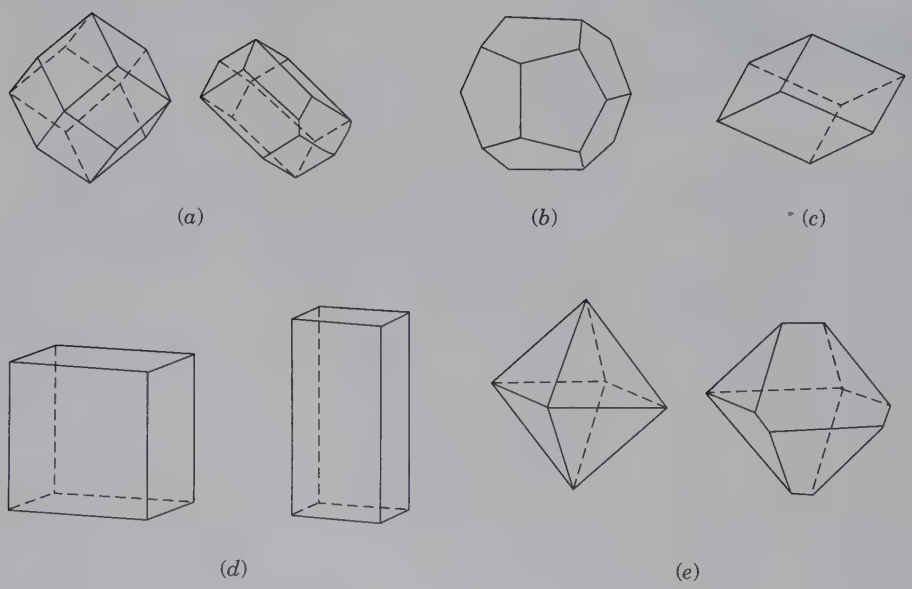

FIG. 2.2 Examples of perfect and distorted crystal forms that display diagnostic crystal shapes. (a) Dodecahedron and malformed dodecahedron. (b) Pyritohedron. (c) Rhombohedron. (d) Perfect and malformed cube. (e) Octahedron and malformed octahedron.

tallography. If mineral specimens display well-developed crystal forms, geometric form names are used to describe a mineral's outward appearance. For example (see also Figs. 2.2 and 2.3):

prismatic—for a crystal with one dimension much longer than the other two (Plate III, no. 8).

rhombohedral—with the external form of a rhombohedron (Plate III, nos. 6, 7).

cubic—with the external form of a cube (Plate 1, no. 8; Plate III, nos. 4, 5).

octahedral—with the external form of an octahedron (Plate 1, no. 5; Plate III, nos. 1, 5).

FIG. 2.3 Some common mineral habits. (Adapted from Klein, C. 2008. *Minerals and rocks: Exercises in crystal and mineral chemistry, crystallography, X-ray powder diffraction, mineral and rock identification, and ore mineralogy.* 3rd. ed. Wiley, New York. Originally modified after Sinkankas. 1964. *Mineralogy.* Van Nostrand Reinhold, New York, 94.)

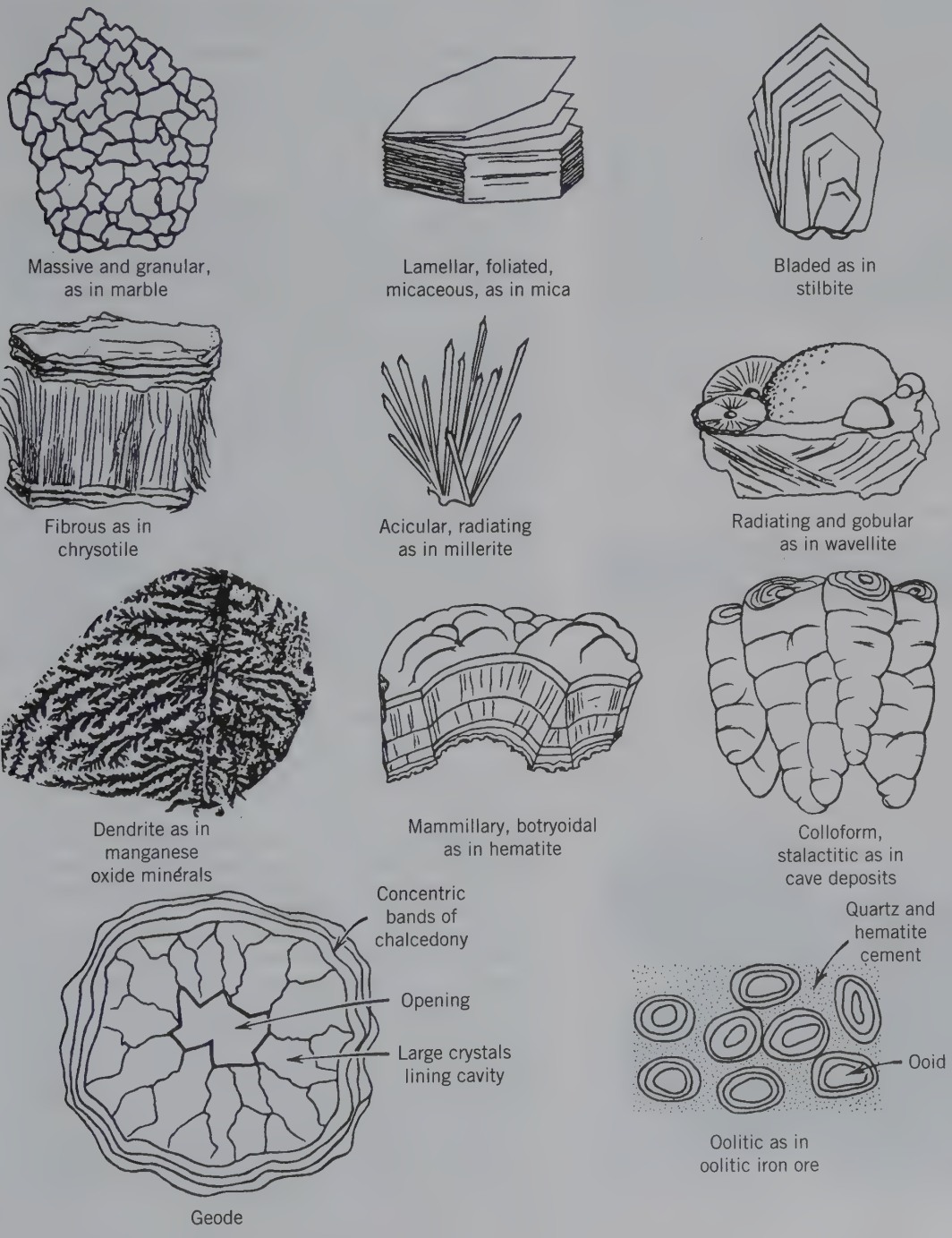

In contrast, **crystal habit** is the general shape of a mineral, which also includes irregularities due to growth (Chapter 10). Most natural crystals tend to be malformed so that well-defined geometric forms are rarely found (cf. Figs. 2.2 and 2.3).

The quality of development of the external planes (or faces) is described by three terms.

Euhedral: describing a mineral that is completely bounded by crystal faces (well-formed); from the Greek roots *eu*, meaning good, and *hedron*, meaning plane (Plate I, no. 4; Plate IV, no. 8; Plate V, no.3; Plate VI, no. 1).

Subhedral: describing a crystal or mineral grain that is partly bounded by crystal faces and partly by irregular surfaces; from the Latin root *sub*, meaning less than (Plate 1, no. 3; Plate VII, no. 4).

Anhedral: describing a mineral that lacks crystal faces and that may show rounded or irregular surfaces; from the Greek root *an*, meaning without (Plate IV, nos. 1, 5).

These qualities are a reflection of the space that was available to the crystal at the time of its growth. If there is no interference of other minerals while the mineral is growing, then it may be *euhedral*. Mineral drawings in this text are of euhedral crystals. Minerals that are intergrown, for example, in rocks, tend to be *aggregates* of many smaller grains, with crystals ranging from euhedral to anhedral. Such occurrences are traditionally described by the terms that relate to their overall appearance (in Table 2.1), or their *morphology* (see also Figs. 2.3, 2.4).

FIG. 2.4 Reniform hematite, Cumbria, England (Harvard Mineralogical Museum).

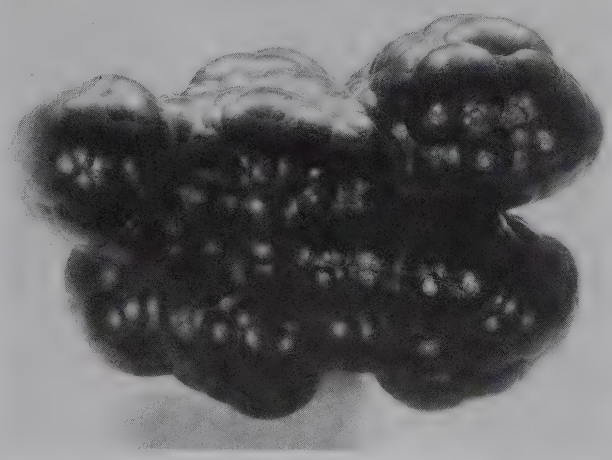

Table 2.1 Terms Used to Describe the Habit of Crystals or Aggregates of Crystals

Massive—a mineral specimen totally lacking crystal faces, often found in very fine-grained minerals (as in goethite).

Granular—mineral grains that are of approximately equal size. The term is mainly applied to minerals whose grains range in size from about 2 to 10 mm. If the individual grains are larger, the aggregate is described as *coarse-granular*; if smaller, it is *fine-granular* (Plate IV, no. 6).

Compact—a specimen so fine-grained that individual grains are not obvious to the eye (as in kaolinite; Plate VII, no. 1).

Lamellar—a specimen made up of layers, like the leaves in a book (as in graphite, molybdenite; Plate II, no. 5).

Micaceous—a mineral that separates into thin plates easily (as in mica; Plate VII, nos. 3–7).

Bladed—individual crystals (or grains) that are flattened, elongated crystals (as in kyanite, stibnite; Plate II, no. 3).

Fibrous—very thin, flexible thread-like grains or fibers (as in chrysotile; Plate VI, no. 9).

Acicular—a mineral with a needlelike shape; from the Latin root *acicula*, meaning needle (as in sillimanite; Plate V, no. 1).

Radiating—a mineral in which acicular crystals radiate from a central point (as in wavellite and goethite; Plate III, no. 3).

Dendritic—a mineral exhibiting a branching pattern like a fern; from the Greek root *dendron*, meaning tree (as in manganese oxides).

Banded—a mineral aggregate in which a single mineral may show thin and roughly parallel banding (as in banded malachite), or in which two or more minerals form a finely banded intergrowth (as in chert and hematite bands in banded iron-formation).

Concentric—when bands or layers are arranged concentrically about one or more centers (as in agates; Plate VII, no. 9).

Botryoidal—when a mineral appears as a bunch of grapes; from the Greek root *botrys*, meaning bunch or cluster of grapes. Botryoidal forms are common in smithsonite, chalcedony, and prehnite.

Globular—a surface made of little spheres or globules (as in smithsonite; shown in Plate IV, no. 1).

Stalactitic—made up of small stalactites, which are conical or cylindrical in form as is common on the ceilings of caves; from the Greek word *stalaktos*, meaning dripping.

Geode—a rock cavity lined with mineral matter but not completely filled. Geodes may be banded, as in agate, containing a central portion filled with euhedral crystals projecting into an open space.

Oolitic—a specimen that is made up of oolites, which are small, round, or ovate (meaning egg-shaped) accretionary bodies and resemble the roe of fish; from the Greek word *oön*, meaning egg. This appearance is common in some iron-rich specimens, made of hematite, known as oolitic iron ore.

Pisolitic—made of pea-sized grains; from the Greek word *pisos*, meaning pea; having a texture similar to that of an oolitic aggregate but somewhat coarser in grain size. Bauxite, the major source of aluminum ore, is commonly pisolitic.

PROPERTIES BASED ON INTERACTION WITH LIGHT

The properties of luster, color, streak, and luminescence relate to how light interacts with a mineral. Light can be scattered, reflected, transmitted, or absorbed (Fig. 2.5). The relative magnitude of these processes controls how we perceive light-related properties in minerals. Luster, color, and streak are easily observed, and in some cases, serve as distinguishing criteria. A more detailed discussion of color, and the causes of color in minerals, follows in Chapter 10.

Minerals are commonly described in terms of the amount of light they can transmit, or **diaphaneity**, meaning the light-transmitting qualities of a mineral. (This word originates from the Greek word *diaphanes*, meaning transparent.)

Transparent describes a mineral that transmits light and through which an object may be seen. Quartz and calcite are commonly transparent as is the ulexite shown in Fig. 1.6. Most gemstones are transparent and many are priced on the quality of their transparency (Plates IX to XII).

Translucent describes a mineral that is capable of transmitting light diffusely but is not transparent. Although a translucent mineral allows light to be transmitted, it will not show a sharp outline of an object seen through it. Some varieties of gypsum are translucent (Plate III, no. 5).

Opaque describes a mineral that is impervious to visible light, even on thin edges of the mineral. Most metallic minerals are opaque (Plate I, nos. 3, 6, 8).

LUSTER

Luster refers to the general appearance of a mineral surface in reflected light. There are two distinct types of luster: **metallic** and **nonmetallic**. **Metallic** is the luster of a polished metal surface, such as the appearance of chrome, steel, copper, and gold (Plate I, nos. 1–3, 8). Materials with a metallic luster reflect light like metals and are opaque to transmitted light. **Nonmetallic** luster is shown by many minerals that transmit light, at least through their edges. Nonmetallic luster varies widely in appearance ranging from a highly polished glass surface to a dull earthy-like appearance (Plate VII, nos. 8, 1, respectively). Minerals with an intermediate luster are said to be **submetallic**. Table 2.2 contains several useful terms that are used to further describe the luster of nonmetallic minerals.

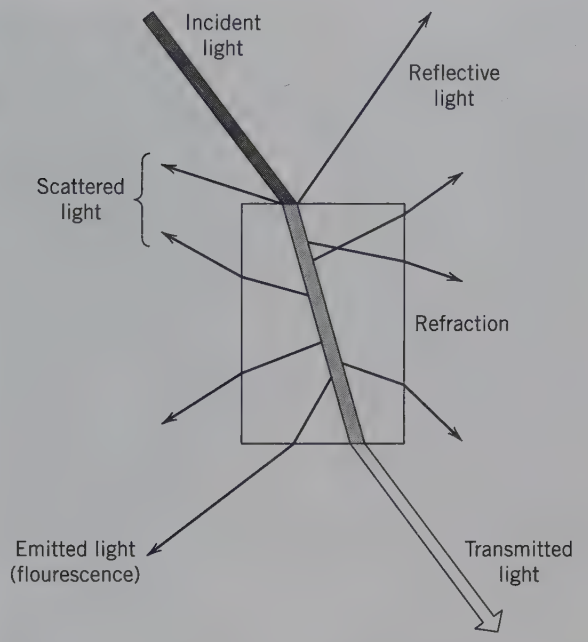

FIG. 2.5 Light interactions with minerals. Luster is a combination of scattered and reflected light, and color is transmitted light. Some absorbed light can be reemitted (usually at longer wavelengths) as fluorescence. (Adapted from Nassau, K. 1980. The causes of color. *Scientific American* 243: 124–156.)

Table 2.2 Terms Used to Describe the Luster of Nonmetallic Minerals

Adamantine—appears to have the luster of a diamond; from the Greek word *adamas*, meaning diamond. This is the brilliant luster shown by some minerals that also have a high refractive index, and as such refract light strongly, like a diamond (Plate IX, no. 1). Other examples are some garnets and the lead carbonate, cerussite.

Vitreous—appears as a piece of polished glass (as in quartz, Plate VII, no. 8; and emerald, Plate IX, no. 2).

Resinous—appears as a piece of resin (as in sphalerite, Plate I, no. 9).

Pearly—appears as a mother-of-pearl with an iridescent sheen. This is characteristic of mineral surfaces that are parallel to well-developed cleavage planes (as in talc and apophyllite).

Greasy—appears as if covered with a thin layer of oil (as in some milky quartz and nepheline). This luster results from light scattered by a microscopically rough surface (see halite, Plate III, no 4).

Silky—appears as a skein of silk or a piece of satin (as in fibrous gypsum). This is characteristic of some minerals in fibrous aggregates.

Earthy—appears dull (as in soil). This is characteristic of aggregates of very fine-grained materials (as in goethite and limonite).

COLOR

The color of a mineral is easily observed. For some minerals it is characteristic and serves as a distinguishing property. Many gemstones are recognized on the basis of their color alone (Plates IX to XII; Chapters 10, 20). In other minerals, color is highly variable and is unreliable as a diagnostic property. This discussion focuses on the use of color as a distinguishing criterion.

Color is directly related to the chemistry and structure of a mineral. *When the chemical element causing the color is essential to the mineral, color can be used as a diagnostic tool* because such a mineral has a constant color. Examples of nonmetallic minerals with essential elements that cause color are sulfur (yellow), malachite (green), azurite (blue), rhodonite and rhodochrosite (rose-red to pink), and turquoise (a greenish blue to blue-green.) A detailed discussion of the causes of color in minerals is given in Chapter 10.

Most minerals with a metallic luster vary little in color, and the color of a freshly broken surface of metallic minerals is diagnostic. However, many metallic minerals become tarnished with time. Tarnish dulls the color of some minerals while it changes the color of others. For example, galena has a bright, bluish, lead-gray color on a fresh surface and becomes a dull gray with exposure to air. Bornite has a brownish-bronze color when fresh, but when tarnished, shows iridescent metallic purples and blues. This characteristic and diagnostic tarnish gives bornite its nickname—peacock ore. For identification of minerals with a metallic luster, it is important to have a freshly broken surface to compare with a more tarnished surface.

In contrast, many minerals with nonmetallic luster vary in color. Therefore, in most nonmetallic minerals, color is a helpful property but not commonly a diagnostic property. Most nonmetallic minerals do, however, have a relatively narrow range in colors. Members of the plagioclase feldspar series range from almost pure white (albite), through light gray to darker gray (anorthite). Most common garnets show various shades of red to red-brown to brown (Plate XI, no. 2). Members of the pyroxene group range from almost white to light green (diopside; Plate V, no. 8), through dark green (hedenbergite), to almost black (augite; Plate VI, no. 1). On the other hand, some minerals show an entire spectrum of colors, such as tourmaline (clear, pink, blue, green, yellow, brown, and black), and some exhibit distinct color zonation within a single crystal (Plate X, no. 11). A spectacular example of such zonation is "watermelon" tourmaline because of its resemblance to a watermelon slice, where the core is pink and is surrounded by colorless and green rims. The front cover of this text illustrates a tourmaline with distinct green and pink color bands arranged in a crystallographically controlled pattern. Similarly, gem minerals, such as corundum (clear, yellow, orange, red, green, blue, purple), beryl (red, green; Plate XI, no. 8), quartz (Plate X, nos. 1 to 5), and numerous others occur in many colors. Gemstones are given varietal names such as sapphire (blue corundum) or ruby (red corundum), reflective of their color (Plate IX, nos. 6 and 7).

STREAK

A mineral's **streak** is the color of the finely powdered mineral on an unglazed white porcelain plate, called a *streak plate*. A streak is commonly a diagnostic property. However, if a mineral has a hardness higher than that of the streak plate (about 7, see discussion on hardness later in this chapter), it will simply scratch the streak plate leaving a white powder. The streak of a mineral remains constant, even if different specimens of the same mineral have different colors. For example, gray hematite has a red-brown streak as does red oolitic hematite. The streak is especially useful in the identification of metallic minerals because their streaks are characteristically colored. Most minerals with a nonmetallic luster will have a whitish streak even if the minerals themselves are colored. That is, the color and streak of a mineral need not be the same. The color of pyrite, for example, is gold whereas the streak is greenish black. The mineral sphalerite ranges in color from dark brownish black to light honey brown but always has a pale yellow streak.

PLAY OF COLORS

Interference of light either at the surface or in the interior of a mineral may produce a series of colors as the angle of the incident light changes. The brilliant flashes of varied color, against a white or black background, as seen in precious opal, are called **play of colors** (Plate X, no. 7; Chapter 10). This phenomenon is caused by diffraction of light from closely spaced features, such as packed spheres (as in the case of opal) or fine lamellae (as in the case of plagioclase; Plate VIII, no. 5) within the mineral. In opal, diffraction is produced by the regular three-dimensional array of equal-size amorphous silica (SiO_2) spheres packed together into domains and cemented together by amorphous silica containing variable water contents (Fig. 2.6). The variously oriented domains act as diffraction gratings for white light and resolve the light into its spectral colors (Fig. 2.7 and Chapter 14 for diffraction).

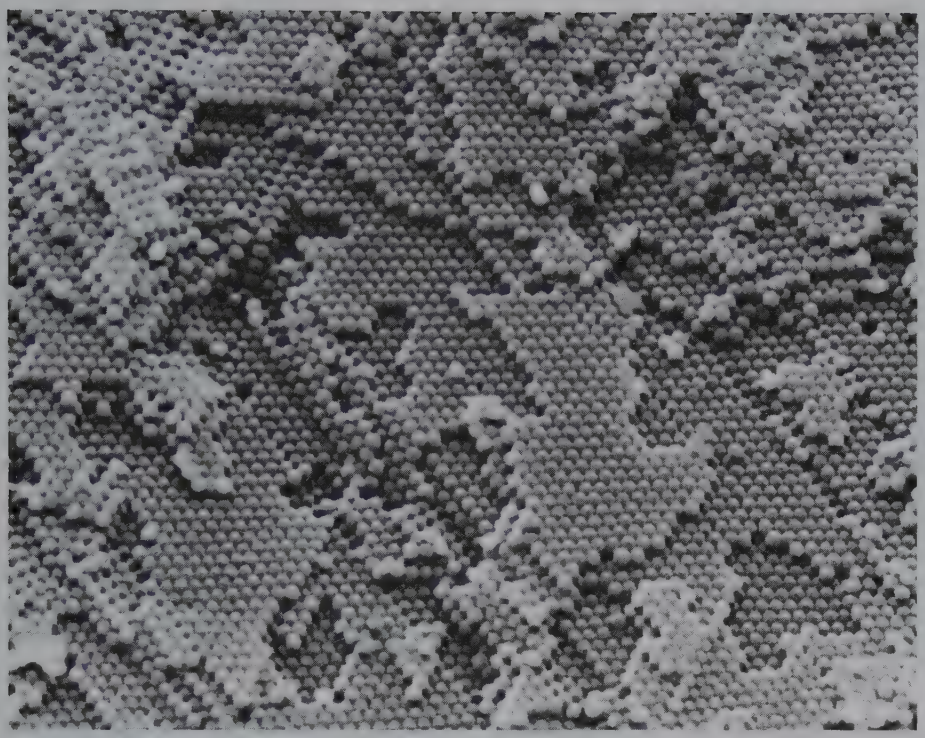

FIG. 2.6 Scanning electron micrograph of an opal with chalky appearance, showing hexagonal closest packing of silica spheres (diameter of spheres is approximately 3,000 Å). Because of weak bonding between the spheres, they are completely intact; in typical precious opal samples, many of the spheres are cleaved. (Courtesy of Darragh, P. J., A. J. Gaskin, and J. V. Sanders. 1976. Opals. *Scientific American* 234, no. 4: 84–95.)

FIG. 2.7 The spectral colors of precious opal are the result of diffraction by regularly spaced lattice planes. These planes result from amorphous spheres in a regular close-packed array. The spacing of the lattice planes is shown as *d*. The λ of the diffracted spectral line is a function of *d* and the angle θ. (Redrawn after Darragh, P. J., A. J. Gaskin, and J. V. Sanders. 1976. Opals. *Scientific American* 234: 84–95. Scientific American, Inc., copyright © George V. Kelvin.)

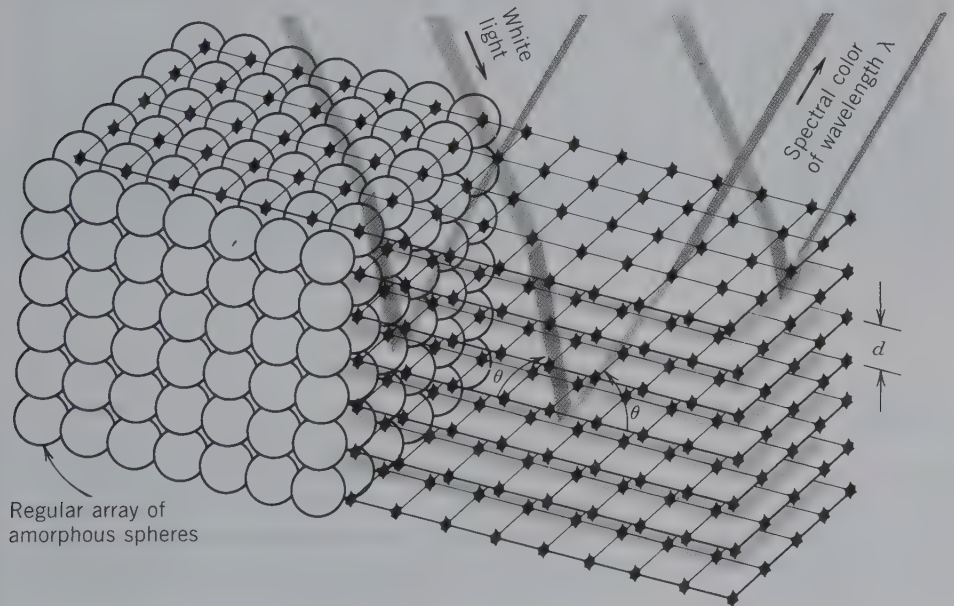

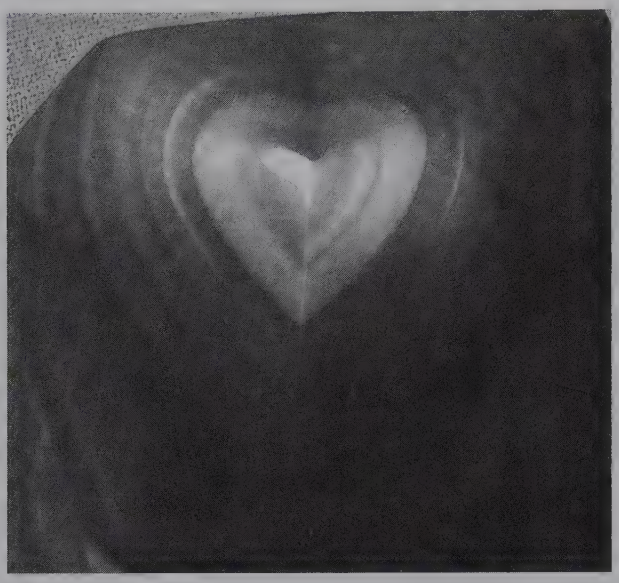

FIG. 2.8 Play of colors in rainbow obsidian (volcanic glass) caused by parallel alignment of very fine, needlelike rutile, TiO_2, inclusions. The specimen has been polished to highlight the concentric color bands. Field of view ~5 cm. (Photograph from B. Dutrow.)

A play of colors can also result from light diffracted and reflected from closely spaced fractures, cleavage planes, twin lamellae, exsolution lamellae (see Chapter 11), or minute foreign inclusions in parallel orientation (Fig. 2.8). Some specimens of plagioclase show spectacular colors ranging from blue to green or yellow and red that change as a function of the thickness of lamellar pairs. This iridescence, also called *labradorescence*, is the result of light scattered by extremely thin (less than 1/10 micron) exsolution lamellae (Fig. 2.9; Plate VIII, no. 5). Other varieties of plagioclase that are white may have a blue play of colors. These stones are often used as gems and are referred to as moonstone.

A surface iridescence similar to that produced by soap bubbles or thin films of oil on water is caused by interference of light as it is reflected from thin surface films. These films are produced by oxidation or alteration of the mineral. It is most commonly seen on metallic minerals, particularly hematite, bornite, limonite, and sphalerite.

CHATOYANCY AND ASTERISM

Some minerals display a silky appearance when viewed in reflected light. This feature results from closely packed parallel fibers or from a parallel arrangement of inclusions or cavities. When a mineral shows a band of light at right angles to the length of the fibers, or to the direction of the inclusions, it is known as **chatoyancy** (Fig. 2.8). Some gemstones are specifically cut and polished to show chatoyancy: Examples include *cat's eye*, a gem variety of chrysoberyl, and *tiger's eye*, quartz containing minute fibers of amphibole.

In some crystals, inclusions may be arranged in three directions at 120° to each other. A stone cut from such a crystal shows a six-pointed star. This phenomenon, seen in star rubies, sapphires, and garnets, is termed **asterism** (Fig. 2.10) and results from the scattering of light from small mineral inclusions properly oriented in three directions.

LUMINESCENCE

Minerals may also emit light that is not the direct result of incandescence. **Luminescence** is the phenomenon that results from a material absorbing a form of energy (thermal, mechanical, electromagnetic) and reemitting that energy as visible light. Most luminescence is faint and can be seen only in the dark.

Fluorescence and Phosphorescence

Fluorescent minerals emit light (luminesce) in the visible light spectrum during exposure to ultraviolet (UV) light, X-rays, or cathode rays. If the luminescence continues after the exciting rays are cut off, the mineral is said to be **phosphorescent**. The difference between fluorescence and phosphorescence is the time that light continues to be emitted by the material. However, there is no sharp distinction between fluorescence and phosphorescence because some minerals that appear only to fluoresce can be shown by refined methods to continue to glow for a small fraction of a second after the removal of the exciting radiation.

The cause of fluorescence is associated with ions of the transition metals that behave as effective activators. Electrons, excited by the invisible short radiation (e.g., ultraviolet light), are raised from their ground state to higher energy levels (excited state), but tend to drop back toward the lower initial energy state. When the electrons fall back to their initial (ground) state, visible light of the same wavelength is emitted. However, these excited electrons may fall back to an energy level intermediate between their excited state and the ground state (Fig. 2.11). When they do, they then emit a photon of light of lower energy (longer wavelength). This usually occurs in a very short time, on the order of 10^{-8} seconds. If the original excitation is produced by ultraviolet light, the fluorescence is commonly in the visible light range. In phosphorescent minerals, there is a time lag between the excitation of electrons to a higher energy level and their return to the ground

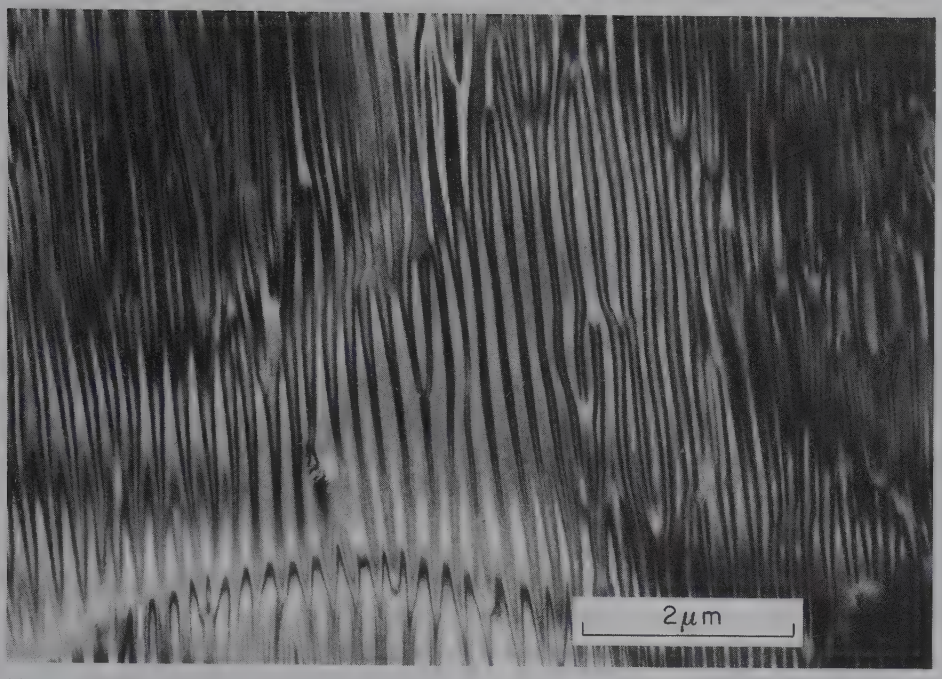

(*a*)

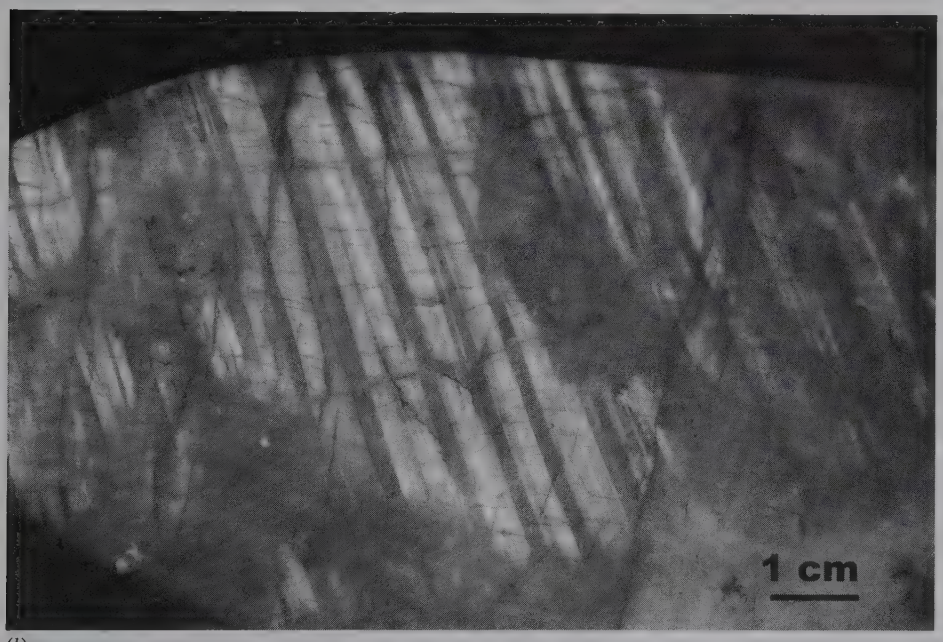

(*b*)

FIG. 2.9 (a) Microstructure in labradorite showing very fine essentially parallel lamellae. These lamellae act as a diffraction grating for white light, producing spectral colors known as *labradorescence.* This photograph was taken with a transmission electron microscope. (From Champness, P. E., and G. W. Lorimer. 1976. Exsolution in silicates. Chapter 4.1 in *Electron Microscopy in Mineralogy,* H. R. Wenk, ed. Springer-Verlag, New York.) (b) Parallel lamellae, as observed in a hand specimen of labradorite (from Madagascar) and the resultant labradorescence. Field of view is ~10 cm. (Specimen donated by R. Young, Natures Own, Boulder, Colorado; photograph by B. Dutrow.)

state. Hence, they continue to emit light long (up to hours or more) after the exciting rays cease. Minerals vary in their ability to absorb UV light at a given wavelength. Some fluoresce only in shortwave UV ($\lambda \sim 254$ nm), others may fluoresce only in longwave UV ($\lambda \sim 366$ nm), and still others will fluoresce under either UV wavelength. The color of the emitted light varies with the wavelengths or source of UV light.

Not all specimens of the same mineral exhibit fluorescence, even if specimens are from the same locality. For example, some fluorite (the mineral from which the property receives its name) will fluoresce. The cause of its usual blue fluorescence results from the presence of organic material or rare earth ions in the mineral structure. Other minerals that commonly fluoresce include: scheelite, willemite, calcite, scapolite, and diamond.

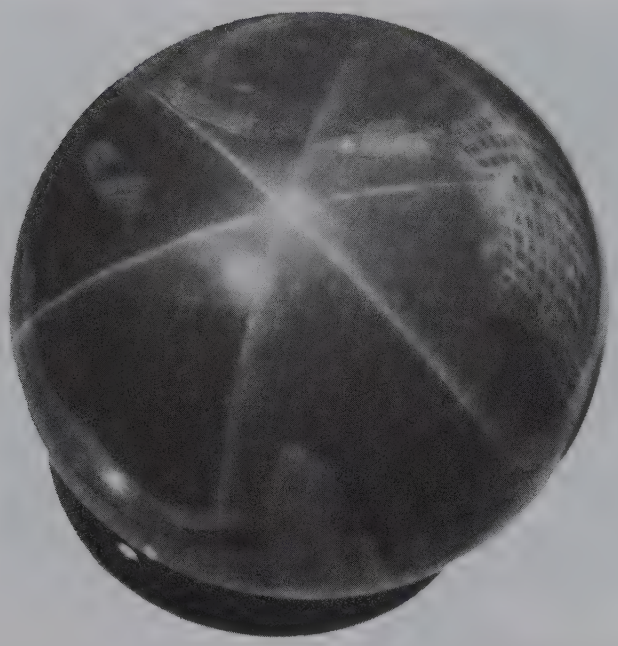

FIG. 2.10 Asterism in a sphere of rose quartz. Sphere diameter is 5.5 cm. The six-rayed star is caused by microscopic needlelike inclusions of rutile, TiO_2, that are oriented in three directions (at 120° to each other) by the quartz structure. These inclusions reflect a spotlight source yielding the six-rayed star (Harvard Mineralogical Museum).

With the development of synthetic phosphors, fluorescence is a commonly observed phenomenon in lamps, paints, cloth, and tapes. The fluorescent property of minerals also has practical applications in prospecting for valuable mineral deposits. With a portable UV light at night, one can detect scheelite in an outcrop, and underground, the amount of scheelite on a freshly blasted surface can be quickly estimated. Eucryptite is an ore of lithium. In white light it is indistinguishable from quartz, but under UV light it can be easily distinguished by its salmon pink fluorescence.

FIG. 2.11 Schematic energy level diagram for the absorption of ultraviolet radiation and resulting fluorescence in the visible light region.

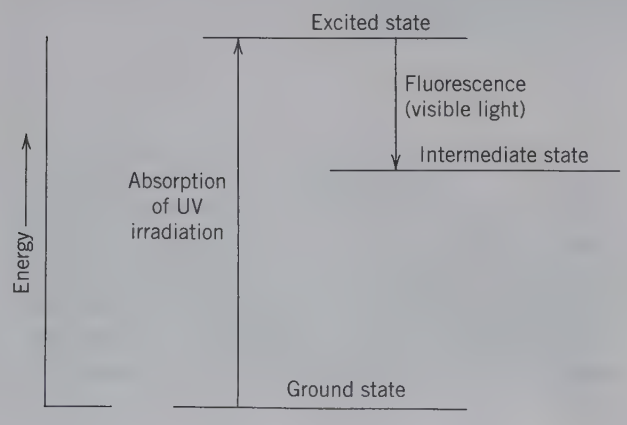

MECHANICAL PROPERTIES

Mechanical properties, such as cleavage, fracture, parting, and hardness, reflect the strength of the internal forces that hold the individual atoms together; in other words, they reflect the bond strength. Chapter 3 describes the internal atomic aspects of minerals so that the origin of these properties will be understood.

The properties of **cleavage, parting**, and **fracture** are the response of a crystalline material to an external force. When such a force is applied, a mineral is *stressed*. If the internal structure of the crystalline substance is deformed due to the stress, it is said to have undergone *strain*. Stress relates to the force applied and strain to the resultant deformation. Minerals break when the strain exceeds their overall strength.

CLEAVAGE

Cleavage is the tendency of minerals to break along parallel planes. Cleavage occurs because the mineral has weaker bonds holding the atoms together in specific directions; the mineral breaks preferentially along these directions. Thus, a mineral with cleavage may display a sequence of parallel steps along these directions (Plate III, no. 6). Cleavage is well displayed by layered structures, such as micas and graphite. These minerals are held tightly together within the layers, but between layers the bonds are much weaker and they will break. In these structures, perfect cleavage is parallel to the layering. Cleavage is an excellent diagnostic property.

Cleavage is described by the quality (perfect, good, fair, poor, absent), the number of cleavage directions (1 to 6), and the orientation of the cleavage planes (see Chapter 6). The quality of the cleavage refers to both the ease with which the mineral breaks and to the perfection of the broken surface. A mineral has *perfect cleavage* if it breaks easily and if the resulting surface is flat and reflects light well, as in micas. *Good cleavage* means that the cleavage surfaces are less continuous and may have some irregularities. *Poor cleavage* is difficult to see, and the cleavage surfaces are not well developed, as in beryl or apatite. *Fair cleavage* reflects properties between poor and good. In some minerals, cleavage is absent, as in quartz.

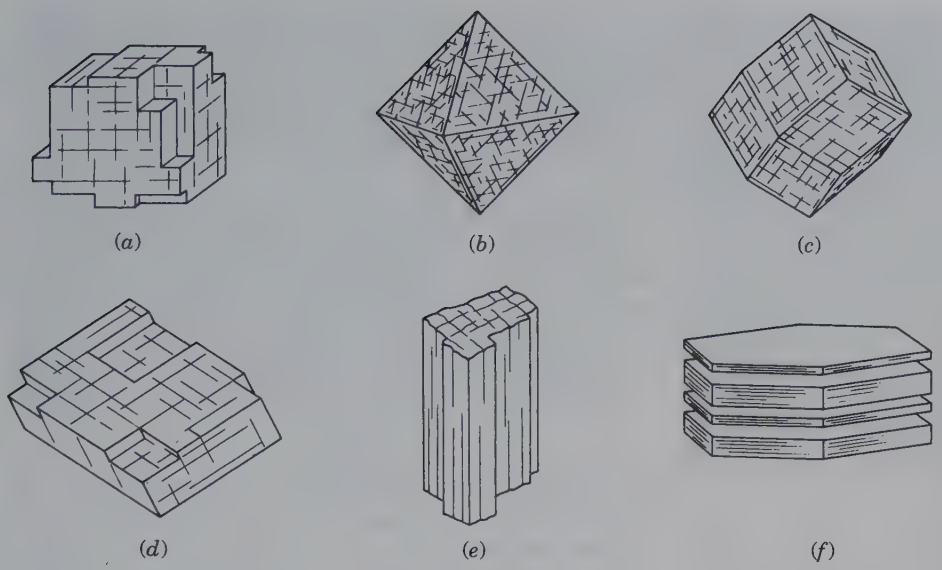

FIG. 2.12 Cleavage and its relationship to forms. (a) Cubic (3 cleavage directions parallel to faces of the cube). (b) Octahedral (4 directions). (c) Dodecahedral (6 directions). (d) Rhombohedral (3 directions). (e) Prismatic (2 directions) and pinacoidal (1 direction). (f) Pinacoidal, basal (1 direction).

In describing cleavage, the number of cleavage directions is identified. For example, halite has three directions of cleavage all at right angles whereas calcite has three directions of cleavage that are not perpendicular. An alternate method is to give the crystallographic direction along which the cleavage occurs. The description of the type of cleavage (six such types are illustrated in Fig. 2.12) is in crystallographic terms that relate to symmetry. This nomenclature uses Miller indices and is fully explained in Chapter 6. Briefly, cleavage is always consistent with the symmetry of a crystallographic form. For example, a cube has six sides, three sets of two parallel faces (top and bottom, front and back, and the two sides). These three directions are the three cleavage directions in minerals with cubic cleavage (Fig. 2.12a). Similarly, a dodecahedron has twelve sides (six sets of two parallel faces), which, divided by two, equals six directions of cleavage (Fig. 2.12c). Therefore, if dodecahedral cleavage is present, it implies that there must be six related cleavage directions in total. Sphalerite, ZnS, is an example of a mineral with excellent dodecahedral cleavage, with six different (but related) cleavage directions.

PARTING

Parting is similar to cleavage in that a mineral breaks along specific planes of structural weakness. However, such parting surfaces generally have discontinuities and are not smooth. While the internal structural weakness is parallel to specific planes in the mineral, it is not uniform. This is because the weakness may result from external pressure or internal defects. Parting, unlike cleavage, is not shown by all specimens of the same mineral but only by those that have been subjected to the proper pressure. Even in these specimens there are a limited number of planes in a given direction along which the mineral will break. Familiar examples are found in the basal parting of pyroxene and the rhombohedral parting of corundum (Fig. 2.13). *Basal parting*, observed in many minerals, occurs parallel to the "base" of a mineral.

FRACTURE

In some crystal structures, the strength of the bonds is approximately the same in all directions and breaking of these minerals generally will not follow a particular direction. The breakage of minerals when they do not yield along cleavage or parting surfaces is **fracture**. Fracture patterns can be distinctive and diagnostic in mineral identification.

FIG. 2.13 (a) Basal parting, pyroxene. (b) Rhombohedral parting, corundum.

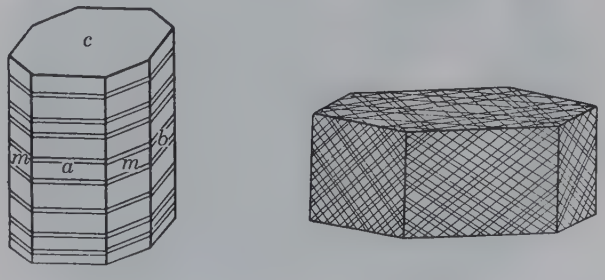

Fracture patterns are given names based on their appearance. A few examples follow.

Conchoidal fracture produces the smooth, curved ridges resembling the interior surface of a shell (Fig. 2.14). This is commonly observed in materials such as glass and quartz.

Fibrous and **splintery fracture** results in pieces that are fibrous or as splinters.

Hackly fracture produces a jagged and sharp edge.

Uneven or **irregular fractures** produce rough and irregular surfaces.

HARDNESS

Hardness (designated by **H**) is the resistance of a smooth surface of a mineral to scratching. The hardness of a mineral is determined by observing if a mineral is scratched by another material of known hardness. These materials commonly include a file, knife, or another mineral. The hardness of a mineral might then be said to be its "scratchability." Hardness is related to bond strength. The evaluation of hardness is the assessment of a crystal structure's response to stress without *rupture* (cleavage, parting, and fracture are various forms of rupture). In some minerals that can flow plastically, scratching results in a groove. However, brittle materials respond to stress (i.e., a hardness test) by microfracturing (rupture on a very fine scale). A crystal structure's overall strength is a composite of all of its bond types, whereas the hardness of that same structure is an expression of its weakest bonding.

FIG. 2.14 Conchoidal fracture, as seen in obsidian (volcanic glass).

A series of 10 common minerals was chosen for use in comparing mineral hardness by the Austrian mineralogist, F. Mohs, in 1824. The following minerals, arranged in order of *increasing* hardness (from soft to hard), are known as *Mohs scale of hardness*:

1. Talc	**6.** Orthoclase
2. Gypsum	**7.** Quartz
3. Calcite	**8.** Topaz
4. Fluorite	**9.** Corundum
5. Apatite	**10.** Diamond

Talc, number 1 in the Mohs scale, has a structure made up of plates so weakly bound to one another that the pressure of a fingernail is sufficient to slide one plate over the other. At the other end of the scale is diamond (**H** = 10), with its carbon atoms so firmly bound to each other that no other mineral can force them apart to cause a scratch.

By comparing one mineral to another, the relative hardness of any mineral can be determined. Hardness can also be measured by techniques more quantitative than a scratch test, and this leads to an absolute hardness scale as shown in Fig. 2.15. The relative position of the minerals in Mohs scale is preserved, but corundum, for example, is two times as hard as topaz and four times harder than quartz.

FIG. 2.15 Comparison of Mohs relative hardness scale and absolute measurements of hardness.

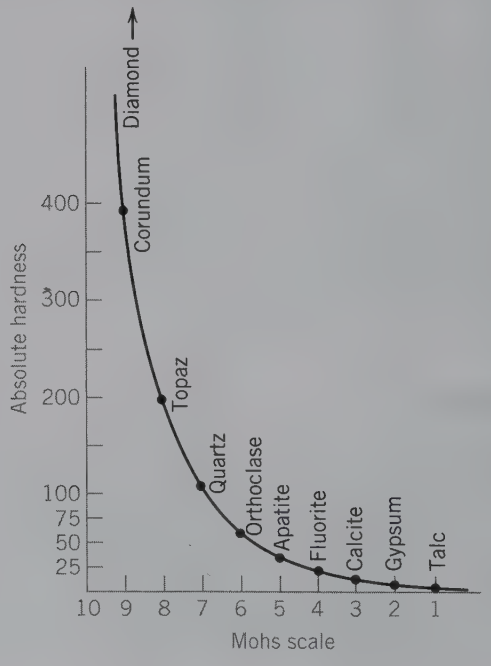

Table 2.3 Mohs Hardness Scale and Additional Observations (From C. Klein, 2008, *Minerals and rocks: Exercises in crystal and mineral chemistry, crystallography, X-ray powder diffraction, mineral and rock identification, and ore mineralogy*, 3rd ed. Wiley, New York.)

Mineral	Mohs Hardness	Other Materials	Observations on the Minerals
Talc	1		Very easily scratched by the fingernail; has a greasy feel
Gypsum	2	~2.2 fingernail	Can be scratched by the fingernail
Calcite	3	~3.2 copper penny	Very easily scratched with a knife and just scratched by a copper coin
Fluorite	4		Easily scratched with a knife but not as easily as calcite
Apatite	5	~5.1 pocket knife ~5.5 glass plate	Scratched with a knife, with difficulty
Orthoclase	6	~6.5 steel file	Cannot be scratched with a knife, but scratches glass
Quartz	7	~7.0 streak plate	Scratches glass easily
Topaz	8		Scratches glass very easily
Corundum	9		Cuts glass
Diamond	10		Used as a glass cutter

To determine the relative hardness of any mineral based on this scale, it is necessary to find which of these minerals the unknown mineral can and cannot scratch. Several common materials can be used in addition to the minerals listed. Table 2.3 lists the 10 minerals as well as several other materials that are highly useful in hardness testing.

Determination of the Hardness of a Mineral

In making a determination of hardness, one should always use a fresh mineral surface, and observe the following.

1. Sometimes, when one mineral is softer than another, portions of the first will leave a mark on the second that may be mistaken for a scratch. Such a mark can be rubbed off, whereas a true scratch will be permanent.

2. The surfaces of some minerals are frequently altered to a material that is much softer than the original mineral. A *fresh surface* of the specimen to be tested must be used.

3. The physical nature of a mineral may prevent a correct determination of its hardness. For instance, if a mineral is granular, or splintery, it may break but appear to be scratched by a mineral much softer than itself. It is always advisable when making the hardness test to confirm it by reversing the order of procedure; that is, try to scratch mineral *A* by mineral *B*, but also try to scratch *B* by *A*.

Hardness is a vectorial property, and some minerals show varying degrees of hardness depending on the directions in which they are scratched. In most common minerals, this difference is so slight that it is only detected through the use of sophisticated instruments. Two exceptions are kyanite and calcite. In kyanite, **H** = 5½ parallel to the length, but **H** = 7 across the length of the crystal. Consequently, a knife will scratch kyanite parallel to the blade but not across the blade. The hardness of calcite is 3 on all surfaces except on a planar surface that may appear at the top of a calcite crystal; on this face it can be scratched by a fingernail and has a hardness of 2.

Because there is a general link between hardness and chemical composition, the following generalizations can be made (see also Chapters 15 through 19).

1. Most hydrous minerals are relatively soft (**H** < 5).
2. Halides, carbonates, sulfates, and phosphates are also relatively soft (**H** < 5½).
3. Most sulfides are relatively soft (**H** < 5) with pyrite being an exception (**H** ~ 6 to 6½).
4. Most anhydrous oxides and silicates are hard (**H** > 5½).

Because hardness is a highly diagnostic property in mineral identification, most determinative tables use relative hardness as a primary sorting parameter, as is done in the Determinative Table 22.1 in Chapter 22. A discussion of why hardness varies follows in Chapter 3.

TENACITY

The resistance of a mineral to breaking or deforming, or its cohesiveness, is known as **tenacity**. The tenacity of a mineral also relates to its internal bonding (Chapter 3).

Table 2.4 Terms Used to Describe Tenacity of Minerals

Mineral	Description	Mineral Example
Brittle	A mineral that breaks and powders easily.	halite
Malleable	A mineral that can be hammered out into a thin sheet.	copper
Sectile	A mineral that can be cut into thin shavings with a knife.	chalcocite
Ductile	A mineral that can be drawn into a wire.	gold
Flexible	A mineral that bends but does not return to its original shape when pressure is released.	sheets of chlorite, talc
Elastic	A mineral that, after being bent, will resume its original position upon the release of the pressure.	micas

Tenacity in minerals is described by the terms given in Table 2.4. These properties may be useful, especially for identification of metallic minerals. However, to determine tenacity, a part of the specimen is destroyed.

PROPERTIES RELATED TO MASS

DENSITY AND SPECIFIC GRAVITY

The **density** (ρ) of a mineral, like that of any other substance, is defined as its mass (m) per unit volume (v):

$$\rho = m/v$$

Density is expressed in units; grams per cubic centimeter (g/cm^3) or in kg/m^3 (for standard international, S.I., units).

Specific gravity (**G**), or *relative density*, is a number that expresses the ratio of the weight of a substance and the weight of an equal volume of water at 4°C (the temperature of the maximum density of water).

$$\mathbf{G} = \rho/\rho_{H_2O}$$

G is a ratio of densities so the number has no units (units are the same for the numerator and the denominator and, thus, they cancel). Because the density of pure water at 4°C is nearly 1.0 g/cm^3 (0.999973 g/cm^3), the numeric values for specific gravity and density are nearly equal if g/cm^3 is used for density.

Consequently, a mineral with a specific gravity of 2 weighs twice as much as the same volume of water. **G** is frequently an important aid in mineral identification. Measuring **G** does not destroy a specimen. Therefore, **G** is very useful, particularly in working with fine crystals or gemstones, when other tests would harm the specimen. A listing of minerals arranged according to increasing specific gravity is given in Table 22.2.

Table 2.5 Specific Gravity Increase with Increasing Atomic Weight of Cation in Orthorhombic Carbonates

Mineral	Composition	Atomic Weight of Cation	Specific Gravity
Aragonite	$CaCO_3$	40.08	2.94
Strontianite	$SrCO_3$	87.62	3.78
Witherite	$BaCO_3$	137.34	4.31
Cerussite	$PbCO_3$	207.19	6.58

Factors That Affect Density and Specific Gravity

The specific gravity of a crystalline substance depends on (1) its chemical composition and (2) the packing of atoms in its crystal structure. In minerals with identical structures, the mineral composed of elements of higher atomic weight will usually have higher density and specific gravity. This is well illustrated by the orthorhombic carbonates listed in Table 2.5; there is a direct correlation between increasing atomic weight of the cation and increasing specific gravity of the mineral. If a single mineral varies in composition, there is usually a systematic variation in the chemistry of that mineral and its specific gravity. This is shown for Mg-Fe-rich amphiboles in Fig. 2.16.

How tightly the atoms are packed inside a structure also controls the specific gravity of the mineral; typically, the more tightly packed the atoms, the higher the density and specific gravity. This is observed in compounds that have the same composition but different structures (these minerals are called *polymorphs*, see Chapter 12).

FIG. 2.16 Variation of specific gravity with composition in the monoclinic cummingtonite-grunerite amphibole series ranging in composition from $Fe_2Mg_5Si_8O_{22}(OH)_2$ to $Fe_7Si_8O_{22}(OH)_2$. (After Klein, C. *American Mineralogist*, 1964.) Density and specific gravity are sometimes used interchangeably. However, density requires units of measurement, for example, grams per cubic centimeter or kilograms per meter.

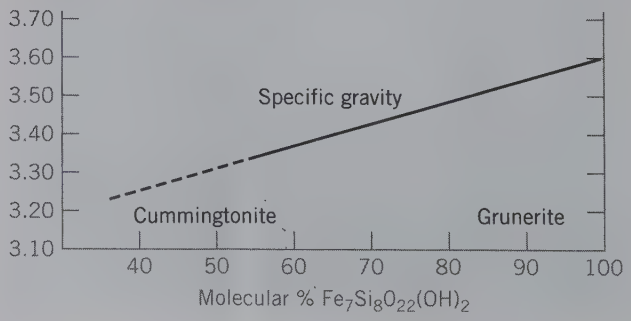

Among such polymorphs, the mineral formed at higher pressures usually has denser packing. The most dramatic example of this is given by diamond and graphite. Both minerals consist of elemental carbon (C). Diamond, formed at high pressures, has a specific gravity of 3.5 and a closely packed structure, giving a high density of atoms per unit volume. In contrast, graphite, formed at much lower pressures, has a specific gravity of 2.23 because the structure consists of loosely packed layers of carbon atoms, giving a lower density of atoms per unit volume.

Average Specific Gravity

A sense of the relative weight of the mineral is acquired by its *heft*. When you pick up ulexite (**G** = 1.96), for example, it seems light, whereas barite (**G** = 4.5) seems heavy for a nonmetallic mineral. This means that you have developed an idea of an average specific gravity or a feeling of what a nonmetallic mineral of a given size should weigh. The range of average specific gravity is between 2.65 and 2.75. The reason for this is that the specific gravities of quartz (**G** = 2.65), feldspar (**G** = 2.60–2.75), and calcite (**G** = 2.72), the most common and abundant nonmetallic minerals, fall mostly within this range. The same sense may be developed for metallic minerals: Graphite (**G** = 2.23) seems light, whereas silver (**G** = 10.5) seems heavy. The average specific gravity for metallic minerals is about 5.0, that of pyrite. With a little practice, one can, by merely lifting specimens, distinguish minerals that have comparatively small differences in specific gravity. This is often a useful diagnostic tool.

Measurement of Specific Gravity

To measure specific gravity (**G**) accurately, the mineral must be homogeneous, pure, and compact with no cracks or cavities within which bubbles or films of air could be trapped. These requirements are difficult to fulfill. For normal mineralogic work, the specimen should have a volume of about one cubic centimeter.

The necessary steps in making a specific gravity determination are, briefly, as follows: The mineral is first weighed in air. Let this weight be represented by W_a. It is then immersed in water and weighed again. Under these conditions it weighs less because in water, it is buoyed up by a force equivalent to the weight of the water displaced. Let the weight in water be represented by W_w. Then $W_a - W_w$ equals the apparent loss of weight in water or the weight of an equal volume of water. Therefore, the specific gravity of a sample can be calculated using the formula:

$$\mathbf{G} = W_a/(W_a - W_w)$$

where W_a is the weight of the sample in air and W_w is the weight of the sample when it is immersed in water.

Jolly Balance. Because specific gravity is a ratio, it is not necessary to determine the absolute weight of the specimen but merely values proportional to the weights in air and in water. A quick procedure for the determination of these weights involves a *Jolly balance* (Fig. 2.17; manufactured by Eberbach and Son, Ann Arbour, Michigan). A fragment is first placed on the upper scale pan and the elongation of the spring noted. This is proportional to the weight in air (W_a). The fragment is then transferred to the lower pan and immersed in water. The elongation of the spring is now proportional to the weight of the fragment in water (W_w). When the mineral is weighed immersed in water, it is buoyed up by the water and weighs less than it does in air; this weight loss is equal to the weight of water it displaces. Hence, if one first determines the weight of a mineral fragment in air and subsequently its weight while immersed in water (it being suspended on a pan by a thin wire thread), the difference in weights is the weight of the equal volume of water. For example, the weight of a small quartz fragment is 4.265 grams in air; in water it is 2.656 grams. The difference in weight, or weight of an equal volume of water, is therefore 1.609 grams; the specific gravity of quartz becomes 2.651.

The specific gravity is: $\mathbf{G} = W_a/W_a - W_w$

$$\frac{4.265}{4.265 - 2.656} = \frac{4.265}{1.609} = 2.651$$

Heavy Liquids. Another method for the determination of the specific gravity of a mineral is by comparing it with liquids of known specific gravity. These liquids have relatively high densities and are referred to

FIG. 2.17 Jolly balance.

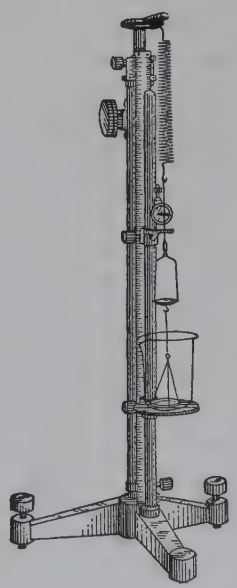

as **heavy liquids**. Liquids most commonly used are bromoform (**G** = 2.89), lithium metatungstate (**G** = 3.0), and methylene iodide (**G** = 3.33). (*Note:* although bromoform and methylene iodine are miscible, *do not mix* them. The mixture will become black.) A mineral can be placed directly into the heavy liquid; if it sinks it has a higher **G**, and if it floats, it has a lower **G** than the liquid. These heavy liquids are miscible with acetone (**G** = 0.79), and by mixing, a solution of any intermediate specific gravity may be obtained. A mineral grain is placed into the heavy liquid, and the liquid is diluted with acetone until the mineral neither rises nor sinks. The specific gravity of the liquid and the mineral are then the same. The density of the liquid (and by inference the mineral) is calculated from the proportions of the acetone and the heavy liquid.

Heavy liquids are commonly used in the separation of mineral grains from mixtures composed of several constituents. For example, the separation of the constituent mineral grains of a sand composed of quartz (**G** = 2.65), tourmaline (**G** = 3.20), and garnet (**G** = 4.25) can be made quickly. In bromoform, the quartz floats and the tourmaline and garnet sink; the heavier minerals can be separated from quartz using a separatory funnel. After removing and washing these "heavy minerals" in acetone, tourmaline and garnet can be separated from each other in methylene iodide (**G** = 3.33); the tourmaline floats, and the garnet sinks.

OTHER DIAGNOSTIC PROPERTIES

MAGNETISM

Few common minerals display magnetism, but for those that do, magnetism can be a diagnostic property. Magnetic strength in minerals ranges from being so strong as to lift steel bars, to barely deflecting a compass needle, to nonexistent. Most minerals experience no attraction to a magnetic field; these minerals are referred to as *diamagnetic*. A few minerals may be drawn to a magnetic field as long as the field is present; these are known as *paramagnetic*. The most magnetically active minerals are *ferromagnetic*. Magnetite is an excellent example of a ferromagnetic mineral. These types of minerals are important to geology, in part, because they can record the direction of the Earth's magnetic field through time (i.e., they remember their magnetic past) and help geophysicists to reconstruct plate tectonic motions. A more complete discussion of the origin of magnetism is given in Chapter 10.

In mineralogy, a small hand magnet is commonly used to determine magnetism in minerals. If a mineral is highly magnetic, it will strongly attract the magnet, as in the case of the mineral magnetite. If the mineral has weaker magnetism, it will attract the magnet but not so strongly, as in the case of the mineral pyrrhotite. If the mineral is mixed with other grains but present in small quantities, removing one or several grains from a specimen with a needle or a pocketknife will allow you to test the magnetism of individual grains.

Because minerals show a wide range of magnetic susceptibility, they can be separated from each other by placing them in a strong magnetic field. Seemingly diamagnetic minerals are weakly paramagnetic in such strong fields. A Franz Isodynamic Separator® is an instrument that uses a strong magnetic field to separate minerals that are paramagnetic from those that are diamagnetic. It can also be used to separate paramagnetic minerals with different magnetic susceptibilities. On a commercial scale, electromagnetic separation is used to separate ore minerals from waste.

RADIOACTIVITY

Minerals containing radioactive elements, such as uranium and thorium, will continually undergo decay reactions in which radioactive isotopes of U and Th form various daughter elements. During decay, they release energy in the form of alpha and beta particles and gamma radiation (refer to Chapter 12 for a detailed discussion). The radiation produced can be measured in the laboratory or in the field using a Geiger or a scintillation counter. A radiation counter is helpful in the identification of U- and Th-containing minerals. Examples of such minerals are uraninite, pitchblende, thorianite, and autunite.

SOLUBILITY IN ACIDS

Some minerals undergo a visible reaction with dilute hydrochloric acid. The positive identification of carbonate minerals is aided by this reaction. For calcite, the reaction is:

$$CaCO_3 + 2H^+ \rightarrow Ca^{2+} + CO_2^{\uparrow}\,(gas) + H_2O.$$

As the calcite dissolves, it releases carbon dioxide gas that bubbles in the liquid, producing the familiar "fizz." Calcite, aragonite, witherite, and strontianite, as well as Cu-carbonates, show bubbling or effervescence when a drop of dilute HCl is placed on the mineral. Other carbonates, such as dolomite, rhodochrosite, magnesite, and siderite, show effervescence only in hot HCl.

Reaction with HCl is an easy test, and many geologists add a bottle of dilute HCl to their field testing kit. Remember that HCl is an acid; use it carefully and wipe the specimen clean after testing.

OTHER SENSORY TESTS

Odor can often be helpful in identifying minerals. Sulfur, for example, smells like the gas produced by rotten eggs. Clay minerals commonly smell "earthy."

Taste can also be used. Halite, NaCl—rock salt—tastes salty, while sylvite, KCl, tastes salty and bitter.

The *feel* of a mineral can also be diagnostic. Some minerals have a characteristic feel, such as "greasy." Molybendite, graphite, and talc all feel greasy.

ELECTRICAL PROPERTIES (OF INDUSTRIAL USE)

PIEZOELECTRICITY

Under directed pressure, certain minerals will develop an electrical charge; they become positively charged on one side and negatively charged on the other. These minerals are referred to as **piezoelectric**. Common minerals that are piezoelectric include tourmaline and quartz. *Piezoelectricity* is extensively used in industrial applications for the control of radio frequencies in electronic circuits.

The property of piezoelectricity was first detected in quartz in 1881, by Pierre and Jacques Curie, but nearly 40 years passed before it was used in a practical way. Toward the end of World War I, it was found that sound waves produced by a submarine could be detected by the piezoelectric current generated when they impinged on a submerged quartz plate. The device was developed too late to have great value during the war, but it pointed the way to other applications. In 1921, the piezoelectric property of quartz was first used to control radio frequencies, and, since then, millions of quartz plates have been used for this purpose. When subjected to an alternating current, a properly cut slice of quartz is mechanically deformed and vibrates by being flexed first one way and then the other; the thinner the slice, the greater the frequency of vibration. By placing a quartz plate in the electric field generated by a radio circuit, the frequency of transmission or reception is controlled when the frequency of the quartz coincides with the oscillations of the circuit. The tiny quartz plate used in digital and analog quartz watches serves the same function as quartz oscillators used to control radio frequencies. The quartz mechanically vibrates at a constant frequency that is a function of the plate's thickness and the crystallographic orientation of the slicing within the original quartz crystal. This quartz frequency controls accurately the radio frequency of the electronic circuit in the watch. The circuit counts the crystal oscillation and provides the digital time display of the watch.

Figure 2.18 is an illustration of the basic schematic of a liquid crystal watch for the display of hours and minutes. The quartz crystal controls an oscillator circuit, which, in turn, generates pulses of one second in time. These "second" pulses are counted to produce "minute" and "hour" pulses. Each of these pulses is decoded to provide proper outputs for the digital watch display. Powered by a 1.5 V silver oxide battery, a quartz plate vibrates approximately 100,000 times per second. An inexpensive quartz watch today is more

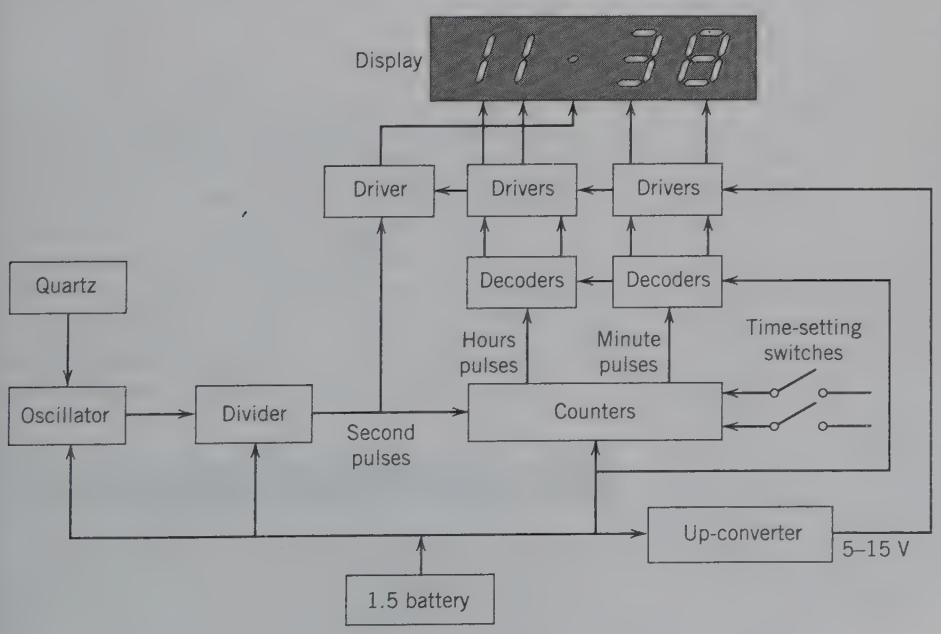

FIG. 2.18 Block diagram of a liquid crystal watch using the piezoelectric property of quartz. (Redrawn after Burfoot, J. C., and G. W. Taylor. 1979. *Polar dielectrics and their applications.* University of California Press, Berkeley, California. Copyright © 1979, Jack Burfoot and George Taylor.)

accurate than the best-made mechanical watch, and precision-manufactured quartz clocks are accurate to within one second per 10 years.

The piezoelectric property of tourmaline has been known almost as long as that of quartz, but compared with quartz, tourmaline is a less effective radio oscillator and is less abundant in occurrence. Nevertheless, small amounts of it are used today in piezoelectric pressure gauges. In tourmaline, which is hexagonal-rhombohedral in symmetry (see Chapter 6), the vertical *c* axis is a polar axis. Plates cut perpendicular to this direction will generate an electrical current when subjected to a transient pressure. The current generated is proportional to the area of the plate and to the pressure. Tourmaline gauges were developed to record the blast pressure of the first atomic bomb in 1945, and, since then, they have been used by the United States with each atomic explosion. Lesser pressures also can be recorded by them, such as those generated by firing a rifle or by surf beating on a sea wall.

PYROELECTRICITY

During heating, certain minerals can also develop an electric charge. These minerals are termed **pyroelectric**. Heat causes the mineral structure to distort and displaces the positive and negative charges relative to each other. Heat is nondirectional (unlike pressure); consequently, only minerals that have specific properties (such as a single polar crystallographic direction) may be pyroelectric. Tourmaline is pyroelectic as well as piezoelectric.

This chapter provides the basis for the evaluation of physical properties displayed by minerals. To understand the origin of each of these physical properties, a mineral must be examined on the atomic scale. The following chapters provide the basic concepts of mineral structures, which are fundamental to an understanding of macroscopic properties.

REFERENCES AND FURTHER READING

Broz, M. E., R. F. Cook, and D. L. Whitney. 2006. Microhardness, toughness, and modulus of Mohs scale minerals. *American Mineralogist* 91: 135–142.

Hochleitner, R. 1994. *Minerals, classifying and collecting them.* Barron's Educational Series, Inc. Hauppauge, New York.

Hurlbut, C. S., Jr., and W. E. Sharp. 1998. *Dana's minerals and how to study them.* 4th ed. Wiley, New York.

Keffer, F. 1967. The magnetic properties of materials. *Scientific American* 217: 222–38.

Klein, C. 2008. *Minerals and rocks: Exercises in crystal and mineral chemistry, crystallography, X-ray powder diffraction, mineral and rock identification, and ore mineralogy.* 3rd. ed. Wiley, New York.

Loeffler, B. M., and R. G. Burns. 1976. Shedding light on the color of gems and minerals. *American Scientist* 64: 636–47.

Simon and Schuster's guide to rocks and minerals. 2004. Simon and Schuster, New York.

Zussman, J. 1977. *Physical methods in determinative mineralogy.* Academic Press, New York.

CHAPTER 3

Elements of Crystal Chemistry

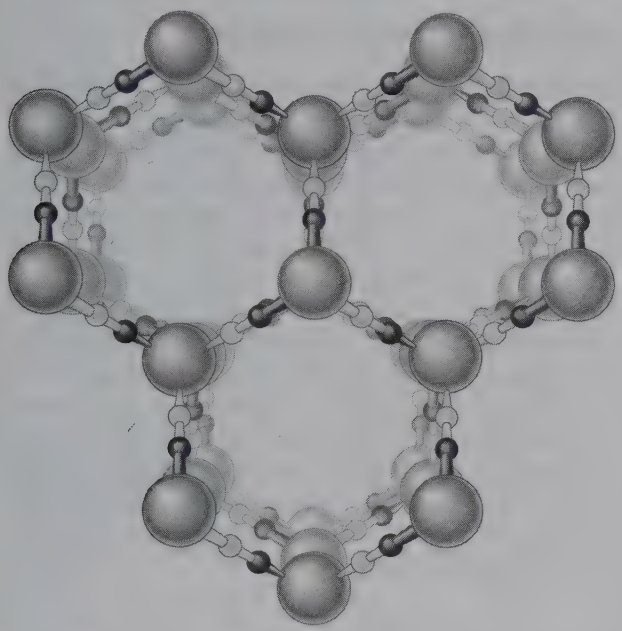

Perspective view of a small part of the crystal structure of ice I (hexagonal in symmetry). This structure is held together by hydrogen bonding. The large spheres are oxygen atoms, and the smaller spheres (dark and light) are hydrogen atoms. Each hydrogen lies between two oxygen atoms at one of two positions shown. Two are close at 1.0 Å, and two are far at 1.8Å, in a tetrahedral arrangement. Note the open "channels" in this structure, which explains the low density of ice (as compared with water) and its ability to float. Ice I is one of several forms of ice (known as polymorphs), and it crystallizes at atmospheric pressure.

Minerals are composites of chemical elements. Consequently, chemical principles are an essential component of the mineral sciences. The manner in which elements are held together, the chemical bond, determines many physical properties displayed by minerals. To understand these connections, this chapter reviews basic concepts of chemical elements, the mechanisms by which elements are bound together to form a solid, the relationship of bonding to mineral behavior and composition, and other important aspects of atoms and ions as they relate to minerals and the structures that they form.

Chemical elements combine in various ways to produce the many minerals that are the building blocks of the Earth. Therefore, understanding basic aspects of chemistry is essential to understanding mineral behavior and properties and deducing information about the Earth, planets, and other materials. A brief review of the fundamental aspects of the atom: protons, electrons, and neutrons, begins this chapter. While many other subatomic particles have been discovered, they are not important in an assessment of mineralogy.

THE ATOM

An **atom** is the smallest subdivision of matter that retains the characteristics of the element. It consists of a very small, massive nucleus composed of **protons** and **neutrons** (Table 3.1) surrounded by a much larger region thinly populated by **electrons**. Each proton carries a unit positive charge; the neutron, as the name implies, is electrically neutral; and each electron carries a unit negative charge (Table 3.1). The fundamental difference between atoms of the different elements lies in the electrical charge of the nucleus. This positive charge is the same as the number of protons. This number, equal to the number of electrons in an uncharged atom, is called the **atomic number (= Z)**. The sum of the number of protons and neutrons determines the **characteristic mass**, or mass number of an element and is based on *atomic mass units* (*amu*). The amu is defined as exactly $\frac{1}{12}$ of the mass of an atom of carbon-12 (^{12}C). Traditionally, this is termed *atomic weight* (*AW*), but the measurement is most properly termed a *mass* rather than *weight*. The mass of the atom

Table 3.1 Some Atomic Particles*

Particle	Symbol	Atomic Mass Units	Relative Change
Electron	*e*	0.0005486	−1
Proton	*p*	1.007276	+1
Neutron	*n*	1.008665	0

*Consideration of other particles discovered in studies of high-energy physics is unnecessary in this context.

is concentrated in the nucleus because the mass of an electron is only $\frac{1}{1837}$ that of the proton. The simplest atom is that of hydrogen, which consists of one proton and one electron (Fig. 3.1); Z = 1 and its atomic mass = 1.00794. Atoms of the other elements have from 2 protons (helium, He, Z = 2) to 116 protons (Uuh, Z = 116) (Table 3.2). These are arranged in the periodic table of elements (see the end paper at the back of this text for Z = 1 to Z = 109).

Atoms of the same element (with the same number of protons) but with differing numbers of neutrons are called **isotopes**. Adding a neutron does not change the electrical charge of the atom, but it does change its mass. For example, oxygen (Z = 8) has three isotopes, the most common of which has a nucleus with eight protons and eight neutrons; this is known as ^{16}O. Rarer and heavier isotopes of oxygen carry eight protons and nine or ten neutrons; these are ^{17}O and ^{18}O, respectively. Similarly, hydrogen, H, can exist in several isotopic forms. The element H (Z = 1) consists of one proton and one electron; the H isotope with one neutron in the nucleus is ^{2}H, known as deuterium (D), and the isotope with two neutrons in the nucleus is ^{3}H, tritium (T). A schematic illustration of selected isotopes is given in Fig. 3.2.

Although atoms are so small that their images can barely be resolved even with high-powered, high-resolution electron microscopes, their sizes can be deduced from measurements of interatomic distances. The atomic radii are expressed in nanometer or angstrom units [1 nanometer (nm) = 10 angstroms (Å)]. For example, the smallest atom, hydrogen, has a radius of only 0.46 Å, whereas the largest, cesium, has a radius of 2.72 Å. Although the electrons and nuclei are both extremely small, the diameter of the atom is approximately 10,000 times the diameter of its nucleus; almost all the volume of an atom is occupied by its electrons that fill the space around the nucleus. The distribution of electrons defines its size, and these electrons hold mineral structures together.

FIG. 3.1 Schematic representation of the hydrogen atom as based on the model of Niels Bohr. A single electron (e^-) moves in an orbit around the nucleus (composed of only a proton), as in a planetary system.

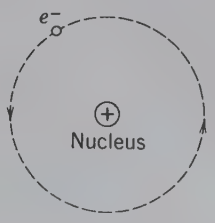

ELECTRON CONFIGURATION

Electrons orbit around the central nucleus. Their orbit is not random but is systematically organized. In the Bohr model of the atom (after Niels Bohr, 1913; see Appendix 2 for details), electrons are distributed in specific orbits of discrete energy levels, often referred to as shells. While the Bohr model gained wide acceptance, it did not satisfactorily explain important observations about the lack of energy radiating from orbiting electrons. In 1923, de Broglie demonstrated that electrons had properties identical to those of waves, and it became impossible to visualize electrons as being in a specific place at a particular time (the Heisenberg uncertainty principle). In 1926, all of these developments were incorporated into a new atomic model by Schrödinger and expressed as a wave equation (see Appendix 2 for more details).

FIG. 3.2 Schematic illustration of the content of protons and neutrons in the nucleus of several elements. The isotopes in the first column have equal numbers of protons and neutrons; those in the second column have an extra neutron; and the isotope in the third column has two extra neutrons.

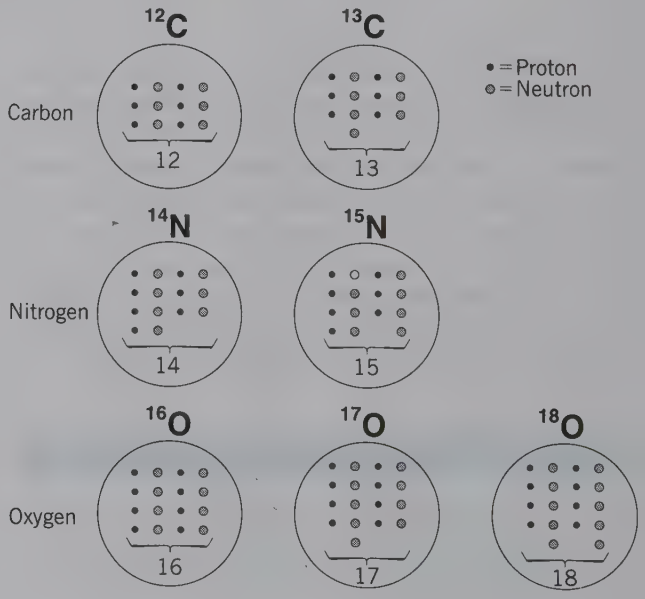

Table 3.2 Alphabetical Listing of the Elements, Their Symbols, Atomic Number, and Atomic Weights

Name	Symbol	Atomic Number, Z	Atomic Weight*
Actinium	Ac	89	227.0278
Aluminum	Al	13	26.98154
Americium	Am	95	(243)
Antimony	Sb	51	121.75
Argon	Ar	18	39.948
Arsenic	As	33	74.9216
Astatine	At	85	~210
Barium	Ba	56	137.33
Berkelium	Bk	97	(247)
Beryllium	Be	4	9.01218
Bismuth	Bi	83	208.9804
Bohrium	Bh	107	(264.12)
Boron	B	5	10.81
Bromine	Br	35	79.904
Cadmium	Cd	48	112.41
Calcium	Ca	20	40.08
Californium	Cf	98	(251)
Carbon	C	6	12.011
Cerium	Ce	58	140.12
Cesium	Cs	55	132.9054
Chlorine	Cl	17	35.453
Chromium	Cr	24	51.996
Cobalt	Co	27	58.9332
Copper	Cu	29	63.546
Curium	Cm	96	(247)
Darmstadtium	Ds	110	281
Dubnium	Db	105	(262.1144)
Dysprosium	Dy	66	162.50
Einsteinium	Es	99	(252)
Erbium	Er	68	167.26
Europium	Eu	63	151.96
Fermium	Fm	100	(257)
Fluorine	F	9	18.998403
Francium	Fr	87	(223)
Gadolinium	Gd	64	157.25
Gallium	Ga	31	69.72
Germanium	Ge	32	72.59
Gold	Au	79	196.9665
Hafnium	Hf	72	178.498
Hassium	Hs	108	(265.1306)
Helium	He	2	4.00260
Holmium	Ho	67	164.9304
Hydrogen	H	1	1.0079
Indium	In	49	114.82
Iodine	I	53	126.9045
Iridium	Ir	77	192.22
Iron	Fe	26	55.847
Krypton	Kr	36	83.80
Lanthanum	La	57	138.9055
Lawrencium	Lr	103	(260)
Lead	Pb	82	207.2
Lithium	Li	3	6.941
Lutetium	Lu	71	174.967
Magnesium	Mg	12	24.305
Maganese	Mn	25	54.9380
Meitnerium	Mt	109	(268)
Mendelevium	Md	101	(258)
Mercury	Hg	80	200.59
Molybdenum	Mo	42	95.94
Neodymium	Nd	60	144.24
Neon	Ne	10	20.179
Neptunium	Np	93	237.0482
Nickel	Ni	28	58.70
Niobium	Nb	41	92.9064
Nitrogen	N	7	14.0067
Nobelium	No	102	(259)
Osmium	Os	76	190.2
Oxygen	O	8	15.9994
Palladium	Pd	46	106.4
Phosphorus	P	15	30.97376
Platinum	Pt	78	195.09
Plutonium	Pu	94	(244)
Polonium	Po	84	(209)
Potassium	K	19	39.0983
Praeseodymium	Pr	59	140.9077
Promethium	Pm	61	(145)
Protoactinium	Pa	91	231.0359
Radium	Ra	88	226.0254
Radon	Rn	86	(222)
Rhenium	Re	75	186.207
Rhodium	Rh	45	102.9055
Roentgenium	Rg	111	272
Rubidium	Rb	37	85.4678
Ruthenium	Ru	44	101.07
Rutherfordium	Rf	104	(261.1089)
Samarium	Sm	62	150.4
Scandium	Sc	21	44.9559
Seaborgium	Sg	106	(263.1186)
Selenium	Se	34	78.96
Silicon	Si	14	28.0855
Silver	Ag	47	107.868
Sodium	Na	11	22.98977
Strontium	Sr	38	87.62
Sulfur	S	16	32.064
Tantalum	Ta	73	180.9479
Technetium	Tc	43	98.906
Tellurium	Te	52	127.60
Terbium	Tb	65	158.9254
Thallium	Tl	81	204.37
Thorium	Th	90	232.0381
Thulium	Tm	69	168.9342
Tin	Sn	50	118.69
Titanium	Ti	22	47.90
Tungsten	W	74	183.85
Ununbium	Uub	112	285
Ununtrium	Uut	113	284
Ununquadium	Uuq	114	289
Ununpentium	Uup	115	288
Ununhexium	Uuh	116	292
Uranium	U	92	238.029
Vanadium	V	23	50.9415
Xenon	Xe	54	131.30
Ytterbium	Yb	70	173.04
Yttrium	Y	39	88.9059
Zinc	Zn	30	65.38
Zirconium	Zr	40	91.22

*A value given in parantheses denotes the mass of the most stable known isotope.

The important aspects of these developments are as follows. To completely specify the position of an electron in three-dimensional space, *three quantum numbers* are needed:

1. The *principal quantum number*, n
2. The *azimuthal quantum number* (or *orbital shape quantum number*), l, and
3. The *magnetic quantum number*, m.

These three quantum numbers follow from the solution of the Schrödinger wave equation and represent parameters in the mathematical formulation of ψ (the electron probability density function; see Appendix 2 for more details).

In three dimensions, as in an atom, the *principal quantum number*, n, is a function of the distance r of the electron from the nucleus. Therefore, it reflects the effective volume (or mean radius) of an electron orbital and can have any positive integral value from 1 to infinity (1, 2, 3, . . . , ∞). It also reflects the energy levels in an atom. The larger the value of n, the greater the average energy of the levels belonging to the shell. As in the Bohr theory, n is correlated with shells: $n = 1$ defines the K shell; $n = 2$ defines the L shell; $n = 3$ defines the M shell; and so on. n determines the position of the horizontal rows of the periodic table (see end paper at the back of this text).

As an example, the probability of finding the electron at a distance r from the nucleus is given by $4\pi r^2\psi^2$ (where ψ is explained in Appendix 2). This is plotted for the s-orbital of the hydrogen atom (Fig. 3.3). (The wave functions that describe the motions of an electron are known as *orbitals*, to distinguish them from the *orbits* in the Bohr atomic model). This curve shows that the electron occupies all of the specified volume around the nucleus, but that it is most frequently found at distance r_0, the radius predicted in the Bohr model of the atom (refer to Appendix 2 for details).

The *azimuthal quantum number* (or *orbital shape* or *angular momentum quantum number*), l, determines the general shape of the region in which an electron moves (i.e., the shape of the orbital), and to some degree, its energy. For a given shell, l may have values of 0, 1, 2, 3, . . . , to a maximum of $(n - 1)$ for that shell. This means that for the K shell, with $n = 1$, the only value of l that is possible is $l = 0$. When $n = 2$ (L shell), two values of l are possible, 0 and 1, resulting in two **subshells** for the L shell. The values of l that are possible for each value of n are given in Table 3.3. It follows that the number of subshells in any given shell is equal to its value of n (see Table 3.3). Even though an electron can be in any location around its nucleus, it will statistically spend most of its time within the volume of its subshell. The subshells are represented by the letters $s, p, d, f, \ldots$. These letters distinguish subshells of different shapes; the s orbital is spherical in shape, the p orbital is quasi-dumbbell-shaped and axially directed, and the d orbital has various shapes (Fig. 3.4).

FIG. 3.3 The radial distribution function ($4\pi r^2\psi^2$) for the s-orbital plotted against increasing distance (r) from the nucleus. The vertical axis is a measure of the probability of finding the electron at a specific distance from the nucleus. The maximum in this function coincides with r_0, the radius of the smallest orbit in the Bohr atomic model.

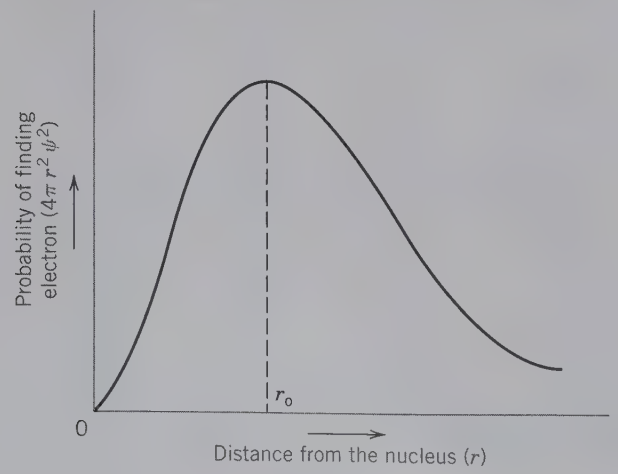

Table 3.3 Quantum Notation and Electron Distribution

Shell and Main Energy Levels (n)	Energy Sublevels	Number of Orbitals		Maximum Number of Electrons	
K ($n = 1$)	$1s$ ($l = 0$)	1	1	2	2
L ($n = 2$)	$2s$ ($l = 0$)	1	4	2	8
	$2p$ ($l = 1$)	3		6	
M ($n = 3$)	$3s$ ($l = 0$)	1	9	2	18
	$3p$ ($l = 1$)	3		6	
	$3d$ ($l = 2$)	5		10	
N ($n = 4$)*	$4s$ ($l = 0$)	1	16	2	32
	$4p$ ($l = 1$)	3		6	
	$4d$ ($l = 2$)	5		10	
	$4f$ ($l = 3$)	7		14	
O ($n = 5$)	$5s$ ($l = 0$)	1	16	2	50*
	$5p$ ($l = 1$)	3		6	
	$5d$ ($l = 2$)	5		10	
	$5f$ ($l = 3$)	7		14	
P ($n = 6$)	$6s$ ($l = 0$)	1		2	72*
	$6p$ ($l = 1$)	3		6	
	$6d$ ($l = 2$)	5		10	
Q ($n = 7$)	$7s$ ($l = 0$)	1		2	98*

*This number is not reached in naturally occurring atoms.

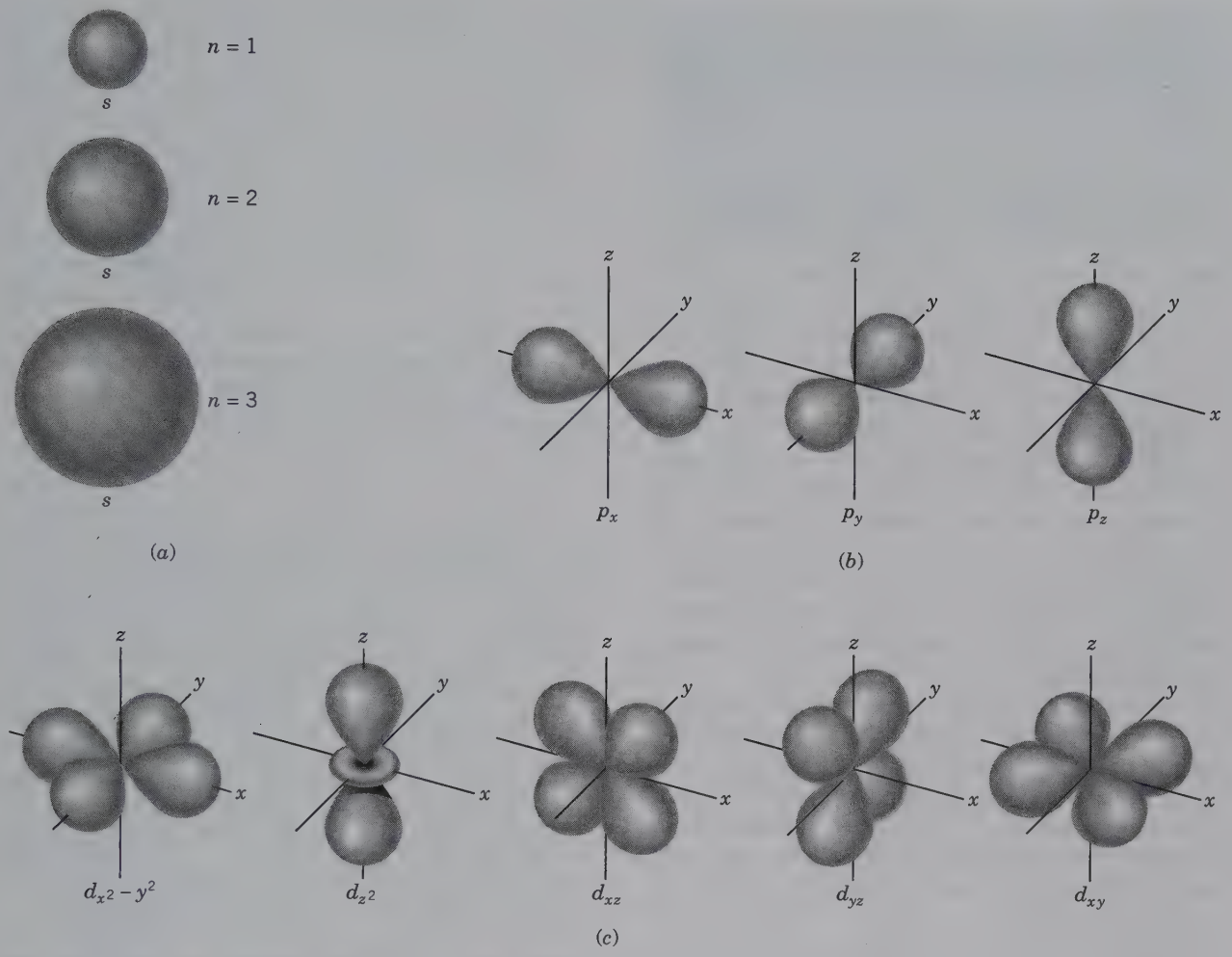

FIG. 3.4 Surfaces showing the angular dependence of the function ψ^2 for *s*, *p*, and *d* orbitals of the hydrogen atom. These angular wave functions can be regarded as probability distributions of electrons. (a) Spherical *s* orbitals. (b) Dumbbell-shaped *p* orbitals. (c) Various lobate-shaped *d* orbitals.

The various states of l (0, 1, 2, 3, . . . , $>n-1$) have been given letter designations as follows:

value of l	0	1	2	3	4	5	6 . . .
subshell designation	*s*	*p*	*d*	*f*	*g*	*h*	*i* . . .

The letters *s*, *p*, *d*, and *f* are abbreviations of the spectroscopic terms *sharp*, *principal*, *diffuse*, and *fundamental*, respectively. This discussion will be limited to the *s*, *p*, *d*, and *f* subshells because they are the ones populated by electrons in atoms in their lowest energy state, or ground state. To designate a subshell within a given shell, the value of n (for the shell) is followed by the letter designation of the subshell. That is, the 2 *s* subshell is a subshell of the second shell ($n = 2$), with $l = 0$. The 3*d* subshell is a subshell of the third shell ($n = 3$), with $l = 2$.

The *magnetic quantum number*, m, restricts the orientation and shape of each type of orbital. It has integer values that range from $-l$ to $+l$, so that the number of orbitals within a subshell is $2l + 1$. When $l = 0$, only one value of m is permitted, $m = 0$. This means that the *s* subshell has only one orbital (the *s* orbital) and is spherical in shape (Fig. 3.4a). For the *p* subshell $l = 1$ and results in an m of -1, 0, $+1$, or three orientations (bilobate orbitals as in Fig. 3.4b). The *d* subshell $l = 2$ results in an m of -2, -1, 0, $+1$, $+2$, or five orientations of orbitals (Fig. 3.4c; quadrilobate orbitals). The *f orbitals* are geometrically complex and difficult to illustrate.

In addition to the three quantum numbers, n, l, and m, (which follow from the solution of the wave equation; see Appendix 2), there is a fourth quantum number, the *spin quantum number*, s, which defines the direction of spin of the electron in space. Because an

electron can spin only in one of two directions around an axis, it has only two values, $+\frac{1}{2}$ and $-\frac{1}{2}$, generally representing a spin to the right and to the left, respectively. An orbiting electron can produce a magnetic field. A magnetic field is produced by movement of electrical charge, just like the magnetic field produced by an electric current moving through a coiled wire. A spinning electron behaves as a small magnet with a north and a south pole and can produce a magnetic field while moving around its orbit, both from its orbital motion and from its spin. In Fig. 3.5, which illustrates an electron orbital and the spinning motion of an electron, the overall magnetic field is represented by *H*. Because the spinning electron behaves as a small magnet, there will be an interaction between *H* (the magnetic field strength) and the field produced by the axial spin of the electron. The axial spin of the electron will either reinforce or oppose the field strength (*H*), depending on whether the spin is clockwise or counterclockwise. [Note that in this picture of the electron's spin (Fig. 3.5), the electron is depicted as a charged particle, not a wave function].

To record the electron spin directions in an atom, an electron with its associated spin (in one direction) is indicated by an arrow pointing up, ↑ , and an electron with a reverse spin (in the opposite direction) by an arrow pointing down, ↓. To indicate the distribution of electrons among orbitals, the arrows are placed over bars that symbolize orbitals, such as for

H $\frac{\uparrow}{1s}$ He $\frac{\uparrow\downarrow}{1s}$

Li $\frac{\uparrow\downarrow}{1s}\frac{\uparrow}{2s}$ Be $\frac{\uparrow\downarrow}{1s}\frac{\uparrow\downarrow}{2s}$

and

Ne $\frac{\uparrow\downarrow}{1s}\frac{\uparrow\downarrow}{2s}\frac{\uparrow\downarrow}{2p}\frac{\uparrow\downarrow}{2p}\frac{\uparrow\downarrow}{2p}$

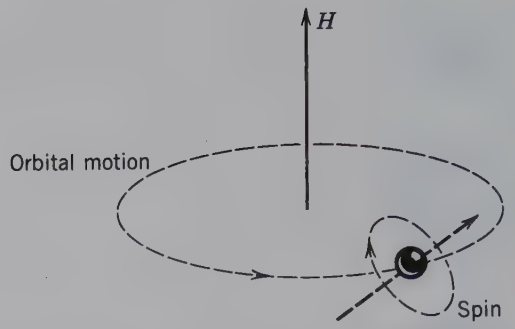

FIG. 3.5 The orbital and spin motions of an electron. The magnetic field *H* is the result of the electron moving along the orbital. The spin of the electron can reinforce or oppose the magnetic field *H*, depending on the rotation direction of the spin (clockwise or anticlockwise).

Two electrons paired in the same orbital have spin directions opposing each other (see the discussion of the Pauli exclusion principle that follows). The magnetic moments of such paired electrons nullify each other (Table 10.4), whereas an effective magnetic moment is the result of unpaired electrons in outer orbitals. In addition, when many atoms are together in bulk materials, and when the spins to the right and left are balanced, no net magnetic moment is produced. If the spins are not balanced, a net magnetic moment is produced and a magnetic field results. This magnetic moment gives rise to the magnetism found in some minerals, such as magnetite (see Chapter 10 for discussion of magnetism).

In summary, each electron in an atom can be assigned values for the four quantum numbers, *n*, *l*, *m*, and *s*, which determine the orbital in which the electron occurs and the direction in which the electron spins. There is, however, a restriction on the values these quantum numbers may have. The **Pauli exclusion principle** states that *no two electrons in any one atom can have all four*

Table 3.4 Summary of the Three Quantum Numbers

Principal Quantum Number, *n* (Shell)	Azimuthal Quantum Number, *l* (Subshell)	Subshell Designation	Magnetic Quantum Number, *m* (Orbital)	Number of Orbitals in Subshell	Maximum Number of Electrons	
1 (K)	0	1*s*	0	1	2	2
2 (L)	0	2*s*	0	1	2	8
	1	2*p*	−1, 0, +1	3	6	
3 (M)	0	3*s*	0	1	2	18
	1	3*p*	−1, 0, +1	3	6	
	2	3*d*	−2, −1, 0, +1, +2	5	10	
4 (N)	0	4*s*	0	1	2	32
	1	4*p*	−1, 0, +1	3	6	
	2	4*d*	−2, −1, 0, +1, +2	5	10	
	3	4*f*	−3, −2, −1, 0, +1, +2, +3	7	14	

quantum numbers the same. This limits the number of electrons in any given orbital to two, and requires the two electrons to spin in opposite directions (with *s* values of $+\frac{1}{2}$ and $-\frac{1}{2}$). Therefore, the maximum number of electrons that can occur in the various (*s*, *p*, *d*, and *f*) subshells is also limited. For example, the *s* subshell has only one orbital and, therefore, can house only a maximum of two electrons; the *p* subshell has three orbitals and, therefore, can house a maximum of six electrons. This is illustrated in Table 3.4.

The relative energies of shells, subshells, and orbitals in atoms with more than one electron, are illustrated in Fig. 3.6. This figure shows that the energy of a shell increases with the increasing value of the principal quantum number, *n*. It also shows that, as the value of *n* increases, there is an overlap in the energy levels of subshells for $n = 3$ and higher. That is, the 4*s* subshell has a lower relative energy level than the 3 *d* subshell. Such overlap becomes more common in the higher shells. This sequence of energy levels is critical in the arrangement of electrons in the atom. In general, those of lower energy are filled prior to higher energy shells; 4*s* will be filled before 3*d*, for example.

The symbolism for summarizing an atom's electron configuration is as follows: The symbol of each orbital is followed by an exponent indicating the number of electrons present in the orbital. The symbol for atomic silicon ($Z = 14$) is $1s^2 2s^2 2p^6 3s^2 3p^2$; signifying that there are two electrons in the 1*s* and 2*s* orbitals, six in the 2*p* orbital, and two each in the 3*s* and 3*p* orbitals.

FIG. 3.6 Relative energies of the orbitals in neutral, many-electron isolated atoms.

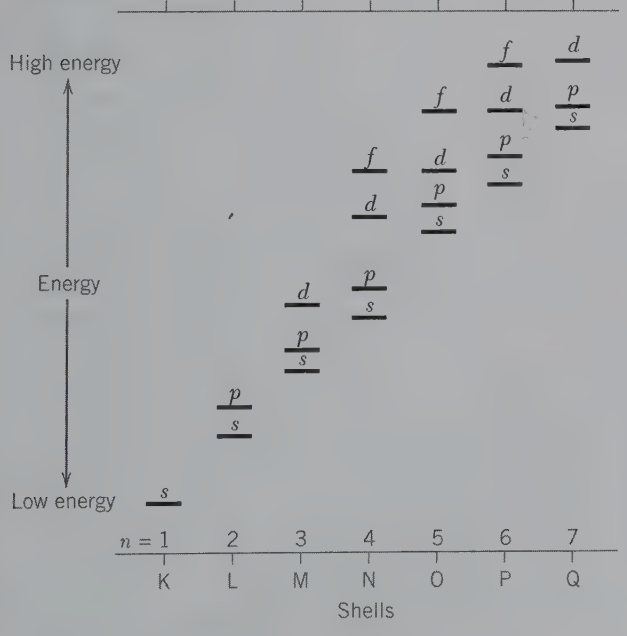

Table 3.5 First Ionization Potentials, Electronegativity Values, and Electronic Structure of the Elements Through Atomic Number 37

Z	Element	First Ionization Potential in Electron Volts (e.v.)*, †	Electro-negativity‡	Electronic Structure
1	H	13.598	2.1	$1s^1$
2	He	24.587	0	$1s^2$
3	Li	5.392	1.0	$1s^2 2s^1$
4	Be	9.322	1.5	$1s^2 2s^2$
5	B	8.298	2.0	$1s^2 2s^2 2p^1$
6	C	11.260	2.5	$1s^2 2s^2 2p^2$
7	N	14.534	3.1	$1s^2 2s^2 2p^3$
8	O	13.618	3.5	$1s^2 2s^2 2p^4$
9	F	17.422	4.1	$1s^2 2s^2 2p^5$
10	Ne	21.564	0	$1s^2 2s^2 2p^6$
11	Na	5.139	1.0	$[Ne]3s^1$
12	Mg	7.646	1.3	$[Ne]3s^2$
13	Al	5.986	1.5	$[Ne]3s^2 3p^1$
14	Si	8.151	1.8	$[Ne]3s^2 3p^2$
15	P	10.486	2.1	$[Ne]3s^2 3p^3$
16	S	10.360	2.4	$[Ne]3s^2 3p^4$
17	Cl	12.967	2.9	$[Ne]3s^2 3p^5$
18	Ar	15.759	0	$[Ne]3s^2 3p^6$
19	K	4.341	0.9	$[Ar]4s^1$
20	Ca	6.113	1.1	$[Ar]4s^2$
21	Sc	6.54	1.2	$[Ar]3d^1 4s^2$
22	Ti	6.82	1.3	$[Ar]3d^2 4s^2$
23	V	6.74	1.5	$[Ar]3d^3 4s^2$
24	Cr	6.766	1.6	$[Ar]3d^5 4s^1$
25	Mn	7.435	1.6	$[Ar]3d^5 4s^2$
26	Fe	7.870	1.7	$[Ar]3d^6 4s^2$
27	Co	7.86	1.7	$[Ar]3d^7 4s^2$
28	Ni	7.635	1.8	$[Ar]3d^8 4s^2$
29	Cu	7.726	1.8	$[Ar]3d^{10} 4s^1$
30	Zn	9.394	1.7	$[Ar]3d^{10} 4s^2$
31	Ga	5.999	1.8	$[Ar]3d^{10} 4s^2 4p^1$
32	Ge	7.899	2.0	$[Ar]3d^{10} 4s^2 4p^2$
33	As	9.81	2.2	$[Ar]3d^{10} 4s^2 4p^3$
34	Se	9.752	2.5	$[Ar]3d^{10} 4s^2 4p^4$
35	Br	11.814	2.8	$[Ar]3d^{10} 4s^2 4p^5$
36	Kr	13.999		$[Ar]3d^{10} 4s^2 4p^6$
37	Rb	4.177	0.9	$[Kr]5s^1$

*e.v. = electron volt = 23 kilocalories/mole.
†From Lide, D. R., ed., 1991. *CRC Handbook of Chemistry and Physics*, 72nd ed. CRC Press, Boca Raton, Florida.
‡From Brady, J. E., J. W. Russell, and J. R. Holum. 2000. *Chemistry, matter and its changes*, 3rd ed. Wiley, New York.

A listing of the symbolic notation of the electronic structure for elements $Z = 1$ to 37 is given in Table 3.5. A complete table of electron configurations of the elements is given in Table 3.6.

These basic features of chemical elements control structures of minerals and explain many physical properties ranging from magnetism to color. In addition, the periodic table is a valuable tool for understanding chemical bonding and the chemical variability in minerals.

Table 3.6 Electron Configurations of the Atoms

Element \ Shell	K	L		M			N				O					P			Q
	1*s*	2*s*	2*p*	3*s*	3*p*	3*d*	4*s*	4*p*	4*d*	4*f*	5*s*	5*p*	5*d*	5*f*	5*g*	6*s*	6*p*	6*d*	7*s*
1. H	1																		
2. He	2																		
3. Li	2	1																	
4. Be	2	2																	
5. B	2	2	1																
6. C	2	2	2																
7. N	2	2	3																
8. O	2	2	4																
9. F	2	2	5																
10. Ne	2	2	6																
11. Na	2	2	6	1															
12. Mg	2	2	6	2															
13. Al	2	2	6	2	1														
14. Si	2	2	6	2	2														
15. P	2	2	6	2	3														
16. S	2	2	6	2	4														
17. Cl	2	2	6	2	5														
18. Ar	2	2	6	2	6														
19. K	2	2	6	2	6		1												
20. Ca	2	2	6	2	6		2												
21. Sc	2	2	6	2	6	1	2												
22. Ti	2	2	6	2	6	2	2												
23. V	2	2	6	2	6	3	2												
24. Cr	2	2	6	2	6	5	1												
25. Mn	2	2	6	2	6	5	2												
26. Fe	2	2	6	2	6	6	2												
27. Co	2	2	6	2	6	7	2												
28. Ni	2	2	6	2	6	8	2												
29. Cu	2	2	6	2	6	10	1												
30. Zn	2	2	6	2	6	10	2												
31. Ga	2	2	6	2	6	10	2	1											
32. Ge	2	2	6	2	6	10	2	2											
33. As	2	2	6	2	6	10	2	3											
34. Se	2	2	6	2	6	10	2	4											
35. Br	2	2	6	2	6	10	2	5											
36. Kr	2	2	6	2	6	10	2	6											
37. Rb	2	2	6	2	6	10	2	6			1								
38. Sr	2	2	6	2	6	10	2	6			2								
39. Y	2	2	6	2	6	10	2	6	1		2								
40. Zr	2	2	6	2	6	10	2	6	2		2								
41. Nb	2	2	6	2	6	10	2	6	4		1								
42. Mo	2	2	6	2	6	10	2	6	5		1								
43. Tc	2	2	6	2	6	10	2	6	5		2								
44. Ru	2	2	6	2	6	10	2	6	7		1								
45. Rh	2	2	6	2	6	10	2	6	8		1								
46. Pd	2	2	6	2	6	10	2	6	10										
47. Ag	2	2	6	2	6	10	2	6	10		1								
48. Cd	2	2	6	2	6	10	2	6	10		2								
49. In	2	2	6	2	6	10	2	6	10		2	1							
50. Sn	2	2	6	2	6	10	2	6	10		2	2							
51. Sb	2	2	6	2	6	10	2	6	10		2	3							
52. Te	2	2	6	2	6	10	2	6	10		2	4							
53. I	2	2	6	2	6	10	2	6	10		2	5							
54. Xe	2	2	6	2	6	10	2	6	10		2	6							

Table 3.6 (continued)

Element \ Shell	K	L		M			N				O					P			Q
	1*s*	2*s*	2*p*	3*s*	3*p*	3*d*	4*s*	4*p*	4*d*	4*f*	5*s*	5*p*	5*d*	5*f*	5*g*	6*s*	6*p*	6*d*	7*s*
55. Cs	2	2	6	2	6	10	2	6	10		2	6				1			
56. Ba	2	2	6	2	6	10	2	6	10		2	6				2			
57. La	2	2	6	2	6	10	2	6	10		2	6	1			2			
*58. Ce	2	2	6	2	6	10	2	6	10	1	2	6	1			2			
*59. Pr	2	2	6	2	6	10	2	6	10	2	2	6	1			2			
*60. Nd	2	2	6	2	6	10	2	6	10	3	2	6	1			2			
*61. Pm	2	2	6	2	6	10	2	6	10	4	2	6	1			2			
*62. Sm	2	2	6	2	6	10	2	6	10	5	2	6	1			2			
*63. Eu	2	2	6	2	6	10	2	6	10	6	2	6	1			2			
*64. Gd	2	2	6	2	6	10	2	6	10	7	2	6	1			2			
*65. Tb	2	2	6	2	6	10	2	6	10	8	2	6	1			2			
*66. Dy	2	2	6	2	6	10	2	6	10	9	2	6	1			2			
*67. Ho	2	2	6	2	6	10	2	6	10	10	2	6	1			2			
*68. Er	2	2	6	2	6	10	2	6	10	11	2	6	1			2			
*69. Tm	2	2	6	2	6	10	2	6	10	12	2	6	1			2			
*70. Yb	2	2	6	2	6	10	2	6	10	13	2	6	1			2			
*71. Lu	2	2	6	2	6	10	2	6	10	14	2	6	1			2			
72. Hf	2	2	6	2	6	10	2	6	10	14	2	6	2			2			
73. Ta	2	2	6	2	6	10	2	6	10	14	2	6	3			2			
74. W	2	2	6	2	6	10	2	6	10	14	2	6	4			2			
75. Re	2	2	6	2	6	10	2	6	10	14	2	6	5			2			
76. Os	2	2	6	2	6	10	2	6	10	14	2	6	6			2			
77. Ir	2	2	6	2	6	10	2	6	10	14	2	6	7			2			
78. Pt	2	2	6	2	6	10	2	6	10	14	2	6	9			1			
79. Au	2	2	6	2	6	10	2	6	10	14	2	6	10			1			
80. Hg	2	2	6	2	6	10	2	6	10	14	2	6	10			2			
81. Tl	2	2	6	2	6	10	2	6	10	14	2	6	10			2	1		
82. Pb	2	2	6	2	6	10	2	6	10	14	2	6	10			2	2		
83. Bi	2	2	6	2	6	10	2	6	10	14	2	6	10			2	3		
84. Po	2	2	6	2	6	10	2	6	10	14	2	6	10			2	4		
85. At	2	2	6	2	6	10	2	6	10	14	2	6	10			2	5		
86. Rn	2	2	6	2	6	10	2	6	10	14	2	6	10			2	6		
87. Fr	2	2	6	2	6	10	2	6	10	14	2	6	10			2	6		1
88. Ra	2	2	6	2	6	10	2	6	10	14	2	6	10			2	6		2
89. Ac	2	2	6	2	6	10	2	6	10	14	2	6	10			2	6	1	2
*90. Th	2	2	6	2	6	10	2	6	10	14	2	6	10			2	6	2	2
*91. Pa	2	2	6	2	6	10	2	6	10	14	2	6	10	2		2	6	1	2
*92. U	2	2	6	2	6	10	2	6	10	14	2	6	10	3		2	6	1	2
*93. Np	2	2	6	2	6	10	2	6	10	14	2	6	10	4		2	6	1	2
*94. Pu	2	2	6	2	6	10	2	6	10	14	2	6	10	6		2	6	1	2
*95. Am	2	2	6	2	6	10	2	6	10	14	2	6	10	7		2	6		2
*96. Cm	2	2	6	2	6	10	2	6	10	14	2	6	10	7		2	6	1	2
*97. Bk	2	2	6	2	6	10	2	6	10	14	2	6	10	8		2	6	1	2
*98. Cf	2	2	6	2	6	10	2	6	10	14	2	6	10	10		2	6		2
*99. Es	2	2	6	2	6	10	2	6	10	14	2	6	10	11		2	6		2
*100. Fm	2	2	6	2	6	10	2	6	10	14	2	6	10	12		2	6		2
*101. Mv	2	2	6	2	6	10	2	6	10	14	2	6	10	13		2	6		2
*102. No	2	2	6	2	6	10	2	6	10	14	2	6	10	14		2	6		2

*Lanthanide and actinide elements; some configurations uncertain.

CHEMICAL ELEMENTS, ELECTRONIC CONFIGURATION AND THE PERIODIC TABLE

The periodic table is the ordered result of basic chemical properties that depend on the nature of the outer electrons, the **valence electrons**. These are the electrons available for chemical bonding so that atoms can combine to form crystalline solids. Thus, "electrons are the glue that holds minerals together."

The periodic table (see end paper at the back of this text) groups elements together that have a similar chemical character. And, as a result of this similarity (caused by their similarity in outer electron configurations), these elements generally have similar chemical behavior. When these elements are incorporated into minerals, they can be found in similar crystallographic sites within mineral structures and similar mineral behavior results.

Although the alphabetical listing of chemical elements (as in Table 3.2) is useful as a reference, it provides no insight into the regularity of their atomic build-up or electronic configuration. The *periodic table* (see end paper at the back of this text) is the widely used chemical listing of all the elements. In this table, the elements are arranged in order of increasing atomic number (Z) because this order exhibits best the periodic arrangement of chemical and physical properties of the elements. In other words, the charge on the nucleus (reflected in the atomic number) and the number of electrons in the neutral atom are what determines the order in which the elements occur. The table is organized into *vertical columns*, also called *groups*, with Roman numerals (I, II, . . . VIII). These numbers are equal to the numbers of electrons contained in the outermost shell of the atom. For example, all elements in column I (Z = 1, 3, 11, 19, 37, 55, and 87) have only one electron in the *s* orbital of the outer shell (see also Table 3.6). All elements in column II have two *s* orbital electrons in the outer shell; elements in column III contain three electrons (two *s* and one *p*). Those in column IV have four electrons (two *s* and two *p*), and so forth, until column VIII, which contains all those elements (except He) with eight outer shell electrons (two *s* and six *p*). Helium has two electrons in the *s* orbital, completely filling the K shell. Thus, the far right-hand column (VIII) contains atoms with completely filled shells, the inert, or **noble gases**.*This is the most stable electron configuration.* Within a column, atoms from the lower rows (i.e., those with greater principal quantum numbers) are larger. They have more electrons; these electrons repel each other and occupy a larger space around the nucleus. The volume of space occupied by electrons increases the size of the atom.

The *horizontal rows*, also known as *periods*, are designated by Arabic numerals 1 through 7. These are equivalent to the K, L, M, N, . . . shells. In a left-to-right sequence in any given row, the outer shell of an atom is progressively filled, beginning with the *s* orbital and ending with the *p* orbitals. Atoms with Z = 21 to 30 (in row 4), with Z = 39 to 48 (in row 5), and with Z = 57 to 80 (in row 6) are called the *transition elements* because the orbital electrons, in excess of those present in calcium (Z = 20), fill inner shells. For example, in row 4, elements with Z = 21 to 30 fill the 3*d* orbital of the more interior M shell; in row 6, elements with Z = 57 to 80 first fill 4*f* and subsequently 5*d* orbitals on the interior side of the P shell (Table 3.6). Atoms are larger in size on the sides and smaller toward the middle of the periodic table. This is because, as one proceeds from left to right, the charge on the nucleus increases due to the increasing number of protons. This charge pulls the electrons together until, at a critical number of electrons, interference between electrons occurs and their mutual repulsion overcomes the attraction to the protons of the nucleus. This leads to a diffuse electron cloud and a larger size of the atom.

The two long rows below the main part of the table are known as the *lanthanide series*, or *rare earth elements* (REE; Z = 58 through 71), and the *actinide series* (Z = 90 through 103). These elements belong in the body of the table but are placed below simply to conserve space. Most of the elements listed in the table occur naturally; however, elements with atomic numbers 43, 61, 85, 87, and 93 through 116 are radioactive, have no stable isotopes, and decay relatively quickly. Consequently, they are present in natural systems in only ultra trace quantities. (The end paper of this text shows elements up to 109.)

In the periodic table, most of the elements are *metals*, but those that are shaded, in the right-hand portion, are *nonmetals*. Metals have distinct properties, such as high electrical conductivity, high thermal conductivity, metallic luster, generally high melting points, ductility, and malleability. Nonmetals, in contrast, show poor electrical conductivity (except for C, graphite), do not have the characteristic luster of metals, and, as solids, are brittle. Chemists consider B, Si, Ge, As, Sb, Te, and At to be *metalloids*, with properties intermediate between those of metals and nonmetals (e.g., Whitten et al., 2004)

ATOMIC AND IONIC RADII

The sizes of atoms or ions are difficult to define but even more difficult to measure experimentally. The **radius** of an atom is defined by the radius of the maxi-

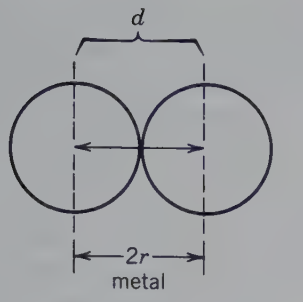

(a)

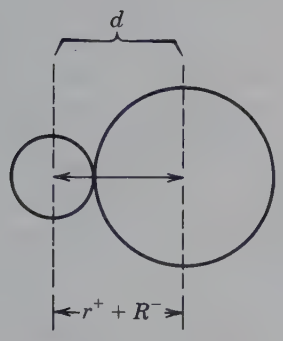

(b)

FIG. 3.7 (a) Metallic radii are half the distance between the centers of two adjoining metal atoms. (b) Ionic radii are defined as the distance between the centers of the cation and anion. If the radius of the anion is well established, such as for rO^{2-} in 3-fold coordination = 1.36 Å, the radius of the cation can be calculated. For example, the size of Mg^{2+} is obtained by subtracting 1.36 Å from the internuclear distance between Mg^{2+} and O^{2-} in MgO.

mum radial charge density of the outermost shells of the atom, but the **effective radius** of an atom (or ion) is also dependent on the type and number of neighboring atoms and/or ions, and on the charge of the ion. In a crystal of a pure metal, where identical atoms are bonded to each other, the radius of the individual atom is assumed to be one-half the bond length. Such measurements provide sizes for atomic radii (Fig. 3.7a and Table 3.7). In ionic crystals, where two oppositely charged ions are bonded together, however, the distance between a positive and a negative ion is the sum of two different radii (Fig. 3.7b). This distance is determined by electrostatic forces. There is, between any pair of oppositely charged ions, an attractive electrostatic force that is directly proportional to the product of their charges and inversely proportional to the square of the distance between their centers. This is known as Coulomb's law, formulated in 1787 by the French physicist Charles Coulomb. It is stated as follows:

$$F = k\frac{(q^+)(q_-)}{d^2}$$

where F is the force of attraction between two oppositely charged ions; q^+ and q^- are the charges on the ions, d is the distance between them, and k is a proportionality constant. A force operating over a certain distance can also be expressed as energy (E). In Fig. 3.8, the curve representing the attractive force is the lower one, with (−) energy values. When ions approach each other under the influence of these forces, *repulsive* forces are also set up. These repulsive forces arise from the interaction of the negatively charged electron clouds and from the opposition of the positively charged nuclei; they increase rapidly with diminishing internuclear distance. In Fig. 3.8, this is represented by the upper curve with (+) energy values. *The distance at which these repulsive forces balance the attractive forces is the characteristic interionic spacing (bond length) for a pair of ions.* This is shown in Fig. 3.8 by the minimum value in the curve that is the sum of the attractive and repulsive forces.

In the simplest case, when both cations and anions are fairly large, of low charge, and both have numerous symmetrically arranged neighbors of opposite sign, ions may be regarded as spheres in contact. Sodium chloride, NaCl, is a good example, where both the

Table 3.7 Metallic Radii (in Å)*

Li	Be													
1.57	1.12													
Na	Mg	Al												
1.91	1.60	1.43												
K	Ca	Sc	Ti	V	Cr	Mn	Fe	Co	Ni	Cu	Zn	Ga	Ge	
2.35	1.97	1.64	1.47	1.35	1.29	1.37	1.26	1.25	1.25	1.28	1.37	1.53	1.39	
Rb	Sr	Y	Zr	Nb	Mo	Tc	Ru	Rh	Pd	Ag	Cd	In	Sn	Sb
2.50	2.15	1.82	1.60	1.47	1.40	1.35	1.34	1.34	1.37	1.44	1.52	1.67	1.58	1.61
Cs	Ba	La	Hf	Ta	W	Re	Os	Ir	Pt	Au	Hg	Ti	Pb	Bi
2.72	2.24	1.88	1.59	1.47	1.41	1.37	1.35	1.36	1.39	1.44	1.55	1.71	1.75	1.82

*The values refer to 12-coordination. From Wells, A. F. 1991. *Structural Inorganic Chemistry*. 5th ed. Clarendon Press, Oxford, England, p. 1382.

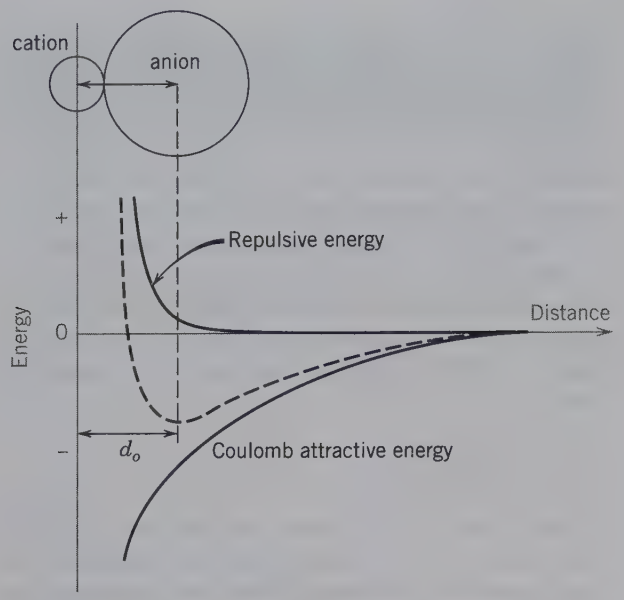

FIG. 3.8 Electrostatic interaction between a cation and anion. The attractive force acts over longer distances than the repulsion. The attractive and repulsive forces add to produce a resultant (dashed curve) in which the minimum value corresponds to the equilibrium distance (d_0) between the centers of the cation and anion.

cation and anion are monovalent, fairly large, and surrounded by six neighbors of opposite polarity. In such crystals, the interionic distance may be regarded as the sum of the radii of the two ions in contact.

If one of the ionic radii in an internuclear distance is well-known from prior experimental measurements, the radius of the other ion can be obtained by subtraction (Fig. 3.7b). For example, once Linus Pauling (in 1927) determined the radius of 6-coordinated O^{2-} to be 1.40 Å (that is the radius of an O with six other ions surrounding it, see Chapter 4 for details), the radii of many cations that are ionically bonded to oxygen were obtained by subtracting the value of 1.40 Å from the measured bond length between cation-oxygen pairs. Such measurements provide ionic radii. (In practice, the value of one anion, usually oxygen, is assumed. Cation radii are then calculated from interatomic distances in oxides. These cation radii are subsequently used to calculate other anion radii, from interatomic measurements of, for example, chlorides or sulfides. These are then used to calculate other cation radii, which, in turn, are used to calculate oxygen radii. The process is repeated iteratively so as to arrive at a self-consistent set of ionic radii.) However, the ionic radius of an ion may not be constant from one crystal structure to another. This is due to possible changes in bond type and **coordination number** (**C.N.** = the number of closest neighbors that surround a specific atom or ion in a structure as discussed in Chapter 4). Because of such influences, the values of ionic radii given in tabulations generally represent averaged values.

Shannon and Prewitt (1969; revised by Shannon, 1976) made a detailed evaluation of the variation of ionic size as a function of coordination number. It is clear from Table 3.8 that many of the radii (for anions or cations) vary as a function of *coordination number*. For example, they found considerable variation in the ionic size of O^{2-} as a function of coordination number, ranging from 1.35 Å when O^{2-} is in 2-fold coordination to 1.42 Å when it is in 8-fold coordination (Table 3.8). Cations also vary. For example, the K^+ radius is 1.38 Å for **C.N.** = 6, 1.51 Å for **C.N.** = 8, and 1.59 Å for **C.N.** = 10. The increase in the cation radius reflects the expansion of the cation into the space (or void) provided by the surrounding anions. Figure 3.9 graphically illustrates the expansion of the radii of some selected cations as a function of coordination number. Their ionic radius values (many of which are listed in Table 3.8; for a complete listing see Shannon's Table 1) are referred to as *effective* ionic radii. The term *effective* is used because they were determined empirically from highly accurate data for a very large number of oxide structures. According to Shannon and Prewitt (1969) and Shannon (1976), these radii may well represent the best possible fit because they reproduce interatomic distances in a wide variety of crystalline solids.

A comparison of the metallic radii (for neutral atoms), given in Table 3.7, with the ionic radii for the same elements, given in Table 3.8 shows that, in all cases, the ionic radius of cations is considerably smaller than the metallic radius, for the same element. This is the result of the loss of one or more outer electrons, and the resultant reduction in the overall size of the electron cloud. Anions, on the other hand, because they gain electrons, are larger than the corresponding neutral atom. In a specific crystal structure, the measured radius of a given element may be somewhere between the element's metallic and ionic radii because the bond type in that specific structure is a mixture of several bond types, such as ionic, covalent, and/or metallic (see Chapter 4).

A regular change in ionic size is reflected by the arrangement of the elements in the periodic table. For elements of the same column, the ionic radii increase as the atomic number (Z) increases. For example, in Table 3.8, column II, the smallest ion is Be^{2+}, with a radius of 0.16 to 0.45 Å, and the last ion in that column, Ba^{2+}, has a radius ranging from 1.35 to 1.61 Å. While ionic radii generally increase with increasing atomic number, the trivalent ions of the lanthanide elements decrease in radius with increasing atomic number, from La^{3+} (Z = 57), with a radius of 1.16 Å

Table 3.8 Effective Ionic Radii (in Å) for Ions Commonly Found in Minerals*

I	II											III	IV	V	VI	VII	←Column
Li^{+} 0.59 [4] 0.74 [6] 0.92 [8]	**Be^{2+}** 0.16 [3] 0.27 [4] 0.45 [6]											**B^{3+}** 0.11 [4] 0.27 [6]	**C^{4+}** −0.08 [3] 0.15 [4] 0.16 [6]	**N^{5+}** −0.10 [3] 0.13 [6]	**O^{2-}** 1.36 [3] 1.38 [4] 1.40 [6] 1.42 [8]	**F^{-}** 1.31 [4] 1.33 [6]	**Row** 2
Na^{+} 0.99 [4] 1.02 [6] 1.18 [8] 1.24 [9] 1.39 [12]	**Mg^{2+}** 0.57 [4] 0.72 [6] 0.89 [8]											**Al^{3+}** 0.39 [4] 0.48 [5] 0.54 [6]	**Si^{4+}** 0.26 [4] 0.40 [6]	**P^{5+}** 0.17 [4] 0.29 [5] 0.38 [6]	**S^{2-}** *1.84 [4]* **S^{6+}** 0.12 [4] 0.29 [6]	**Cl^{-}** *1.81 [6]*	**3**
K^{+} 1.38 [6] 1.51 [8] 1.55 [9] 1.59 [10] 1.64 [12]	**Ca^{2+}** 1.00 [6] 1.12 [8] 1.18 [9] 1.23 [10] 1.34 [12]	**Sc^{3+}** 0.75 [6] 0.87 [8]	**Ti^{4+}** 0.42 [4] 0.61 [6] 0.74 [8]	**V^{5+}** 0.36 [4] 0.46 [5] 0.54 [6]	**Cr^{3+}** 0.62 [6] **Cr^{4+}** 0.41 [4] 0.55 [6] **Cr^{6+}** 0.26 [4]	**Mn^{2+}** 0.83 [6] 0.96 [8] **Mn^{3+}** 0.65 [6] **Mn^{4+}** 0.53 [6]	**Fe^{2+}** 0.63 [4] 0.78 [6] 0.92 [8] **Fe^{3+}** 0.65 [6] 0.78 [8]	**Co^{2+}** 0.74 [6] 0.90 [8]	**Ni^{2+}** 0.55 [4] 0.69 [6]	**Cu^{+}** 0.46 [2] 0.77 [6] **Cu^{2+}** 0.57 [4] 0.65 [5] 0.73 [6]	**Zn^{2+}** 0.60 [4] 0.74 [6] 0.90 [8]	**Ga^{3+}** 0.47 [4] 0.55 [5] 0.62 [6]	**Ge^{4+}** 0.39 [4] 0.53 [6]	**As^{3+}** 0.58 [6] **As^{5+}** 0.34 [4] 0.46 [6]	**Se^{2+}** *1.98 [6]*	**Br^{-}** *1.96 [6]*	**4**
Rb^{+} 1.52 [6] 1.61 [8] 1.66 [10] 1.74 [12]	**Sr^{2+}** 1.18 [6] 1.26 [8] 1.36 [10] 1.44 [12]	**Y^{3+}** 0.90 [6] 1.02 [8]	**Zr^{4+}** 0.72 [6] 0.78 [7] 0.84 [8] 0.89 [9]	**Nb^{5+}** 0.64 [6] 0.69 [7] 0.74 [8]	**Mo^{4+}** 0.65 [6] **Mo^{6+}** 0.41 [4] 0.59 [6]			**Rh^{4+}** 0.60 [6]	**Pd^{2+}** 0.64 [4] 0.86 [6]	**Ag^{+}** 1.16 [6] 1.28 [8]	**Cd^{2+}** 0.58 [4] 0.74 [6] 0.90 [8]	**In^{3+}** 0.62 [4] 0.80 [6] 0.92 [8]	**Sn^{4+}** 0.69 [6] 0.81 [8]	**Sb^{3+}** *0.76 [6]* **Sb^{5+}** 0.60 [6]	**Te^{2-}** *2.21 [6]*	**I^{-}** *2.20 [6]*	**5**
Cs^{+} 1.67 [6] 1.74 [8] 1.81 [10] 1.85 [11] 1.88 [12]	**Ba^{2+}** 1.35 [6] 1.42 [8] 1.47 [9] 1.52 [10] 1.61 [12]	**La^{3+}** 1.03 [6] 1.16 [8] 1.22 [9] 1.27 [10]	**Hf^{4+}** 0.71 [6] 0.76 [7] 0.83 [8]	**Ta^{5+}** 0.64 [6] 0.69 [7] 0.74 [8]	**W^{6+}** 0.42 [4] 0.51 [5] 0.60 [6]	**Re^{4+}** 0.63 [6] **Re^{7+}** 0.38 [4] 0.53 [6]			**Pt^{2+}** 0.80 [6]		**Hg^{2+}** 0.94 [4] 1.01 [6] 1.14 [8]		**Pb^{2+}** 1.19 [6] 1.29 [8] 1.35 [9] 1.40 [10]	**Bi^{3+}** 0.96 [5] 1.03 [6] 1.17 [8]			**6**
			Th^{4+} 0.94 [6] 1.05 [8] 1.09 [9] 1.13 [10]		**U^{4+}** 0.89 [6[1.00 [8] **U^{6+}** 0.52 [4] 0.73 [6]												

Transition elements

*Numbers in square brackets are the coordination numbers of the ions. Radii in upright digits are from Shannon (1976). Radii in italics are from Pauling (1960), revised and supplemented by Ahrens (1952). For complete references see the reference list at the end of the chapter.

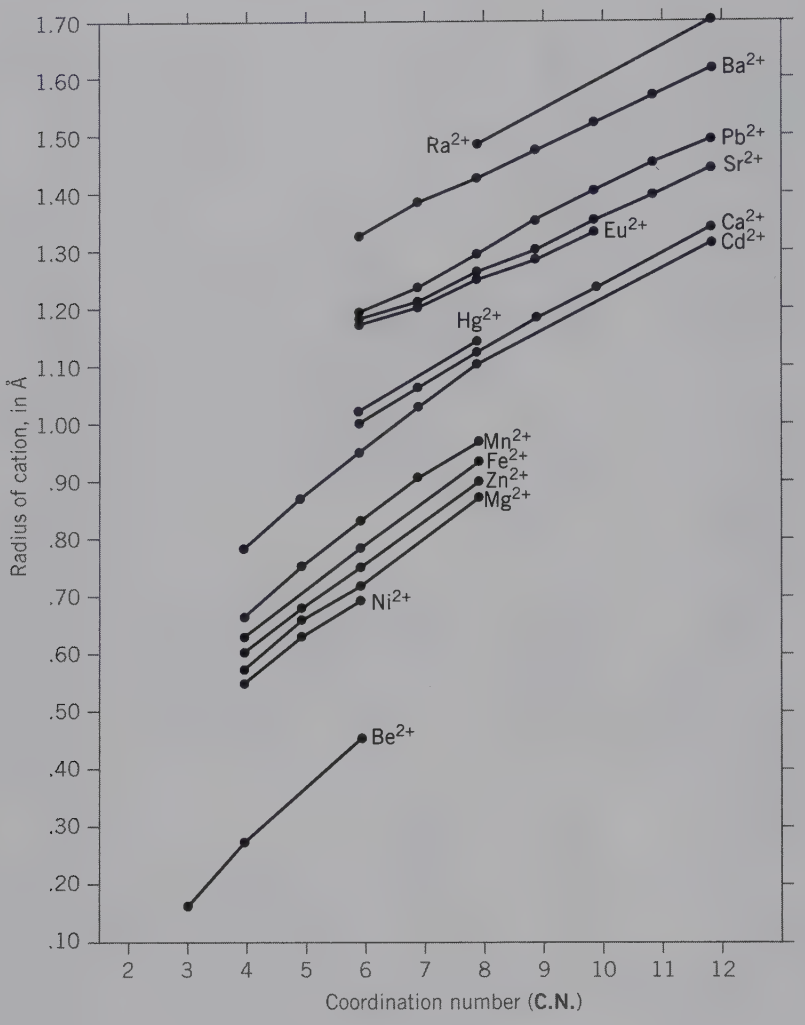

FIG. 3.9 The change in ionic radius as a function of coordination number (**C.N.**) for some selected cations. (From Shannon, 1976; for the complete reference see the list at the end of the chapter.)

(8-fold coordination), to Lu^{3+} ($Z = 71$), with a radius of 0.98 Å (8-fold coordination). This feature, known as the *lanthanide contraction*, is the result of building up inner electron orbitals before adding to a new outer orbital (Table 3.6). As a result of the increasing nuclear charge, and the fairly weak "shielding" of this positive charge by inner-shell 4*f* electrons, an increased attraction is exerted on the outer-shell 5*s*, 5*p*, and 5*d* electrons, which draws them in more tightly, causing a decrease in ionic radius.

For positive ions with the same electronic structure, the radii decrease with increasing charge. For example, the ionic radii of the metallic elements in the third horizontal row, all of which have two electrons in the first shell and eight in the second shell, decrease (for 6-fold coordination) from Na^{+}, with a radius of approximately 1.02 Å, to P^{5+}, with a radius of 0.38 Å. The size of these ions, with identical electron configurations of the K and L shells (but not M), decreases because the increased nuclear charge exerts a greater pull on the electrons, thus, decreasing the effective radius of the ion.

For an element that can exist in several valence states (ions of the same element with different charges), the higher the charge on the positive ion, the smaller its radius. For example, $Mn^{2+} = 0.83$ Å, $Mn^{3+} = 0.65$ Å, and $Mn^{4+} = 0.53$ Å. This decrease in size is due to the greater pull exerted by the nucleus on a reduced electron cloud.

In addition to variations in size as a function of coordination number and bond type, there can also be considerable change in the *shape* of some atoms and ions. Atoms and ions are not rigid bodies but respond to external electrical forces by dilation and deformation. A larger number of neighboring ions tend to distend the central ion as a function of increasing coordination number; a smaller number allows it to collapse a little. Some distortion of shape may accompany the distention of ions. These effects are collectively called *polarization* and are of considerable importance in crys-

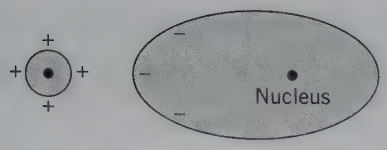

FIG. 3.10 Polarization effect of a small, highly charged cation on a large anion.

tal structures. If the apparent shape and size are strongly affected by its structural environment, the ion is said to have a high polarizability. If, on the other hand, it behaves essentially as a rigid sphere in all environments, it is said to have a low polarizability. Generally, large monovalent anions with a noble gas electronic structure are most easily polarized. The greater the polarization between two neighboring ions, the more the electron density is localized between the two nuclei and the more covalent the bond is between them. Figure 3.10 is a schematic illustration of polarization of a large monovalent anion by a highly charged smaller cation.

THE ION

Ions, unlike electrically neutral atoms with an equal number of protons and electrons, are charged particles. They have an excess or deficiency of electrons when compared to the numbers of protons. There are several ways to turn an atom into an ion, such as heat, light, or exchange of electrons with another atom. The charge on the ion is known as its **valence** or **oxidation state**. Electrons in the outermost shell are the *valence electrons*. When one or more electrons are lost from the electron configuration of an atom, a **cation** is formed (net positive charge, +), and when electrons are added, an **anion** results (with a net negative charge, −). This can be expressed as:

$$X_{atom} - e^- \rightarrow X^+_{cation}$$

and

$$X_{atom} + e^- \rightarrow X^-_{anion}$$

In either process, energy is involved in the transformation. The energy required to remove the most weakly held electron from a neutral atom (to infinity) is known as the **first ionization potential**. This value (listed for a representative number of elements in Table 3.5) expresses how strongly the nucleus of a neutral atom attracts an electron in a partially filled orbital.

Elements in the periodic table can be divided into two groups: those that have a tendency to give up electrons and those that are capable of acquiring electrons. Those that are electron donors are the **metals** (in the left-hand part of the periodic table, see the end paper at the back of this text) and those that are electron acceptors are the **nonmetals** (in the right-hand part of the periodic table). The first ionization potential values increase with increasing atomic number, within each period (as Fig. 3.11a illustrates). This increase coincides with the progressive filling of electron orbitals and expresses the reluctance of atoms to lose electrons from orbitals that are nearly completely filled. It also shows that inert gases (He, Ne, Ar, Kr) have maximal values and alkali metals (Li, Na, K, Rb) have minimal values. This means that the *electron configurations of the inert gases are the most stable*. The lack of chemical reactivity of the noble (inert) gases is attributable to the *extraordinary stability of configuration of 2, 10, 18, 36, 54, and 86 electrons about an atomic nucleus* (Table 3.6). Thus, *elements want to reach a noble gas configuration*. The alkali metals (in column I of the periodic table) carry one more electron than the noble-gas atom, and this electron is easily lost to achieve the noble-gas configuration. Only a small amount of energy is needed to remove this electron to produce a stable monovalent (1+) ion; such monovalent cations are Li^+, Na^+, K^+, and Rb^+. Similarly, the elements of column II of the periodic table have low ionization potential values suggesting that little energy is needed to lose two electrons to produce divalent ions (Be^{2+}, Mg^{2+}, Ca^{2+}, Sr^{2+}, Ba^{2+}) with a noble-gas structure (see Fig. 3.11 and Table 3.5). Similar considerations hold for the formation of trivalent (e.g., Al^{3+}) and tetravalent (e.g., Si^{4+}) cations. The halogens (which mean "salt formers") in column VII of the periodic table contain one less electron than a noble-gas atom, and they easily gain an electron.

In addition, it takes more energy to remove a paired electron (e.g., from beryllium, Be^{2+}) than it does to remove an unpaired electron (e.g., from lithium, Li^+, or boron, B^{3+}). An unpaired electron, whether it is in a 2*s* orbital (as in lithium) or in a 2*p* orbital (as in boron; Table 3.5), is evidently more weakly bonded to the atom than a paired electron, as in the filled 2*s* orbital of beryllium. A similar effect is seen in period 3 in the first ionization potential of magnesium versus that of sodium and aluminum. The ionization potentials of elements in period 4 with partially filled *d* orbitals (Table 3.5) vary little with atomic number. The general trend, within each period, is one of low ionization potentials (elements acting as electron donors and, as such, metallic in their character) to high ionization potentials (elements acting as electron acceptors and, as such, nonmetallic in character).

Ionization potentials that express the energy needed to remove additional electrons (i.e., more than one electron) are much larger than those of the first ionization reported in Table 3.5. Such higher values

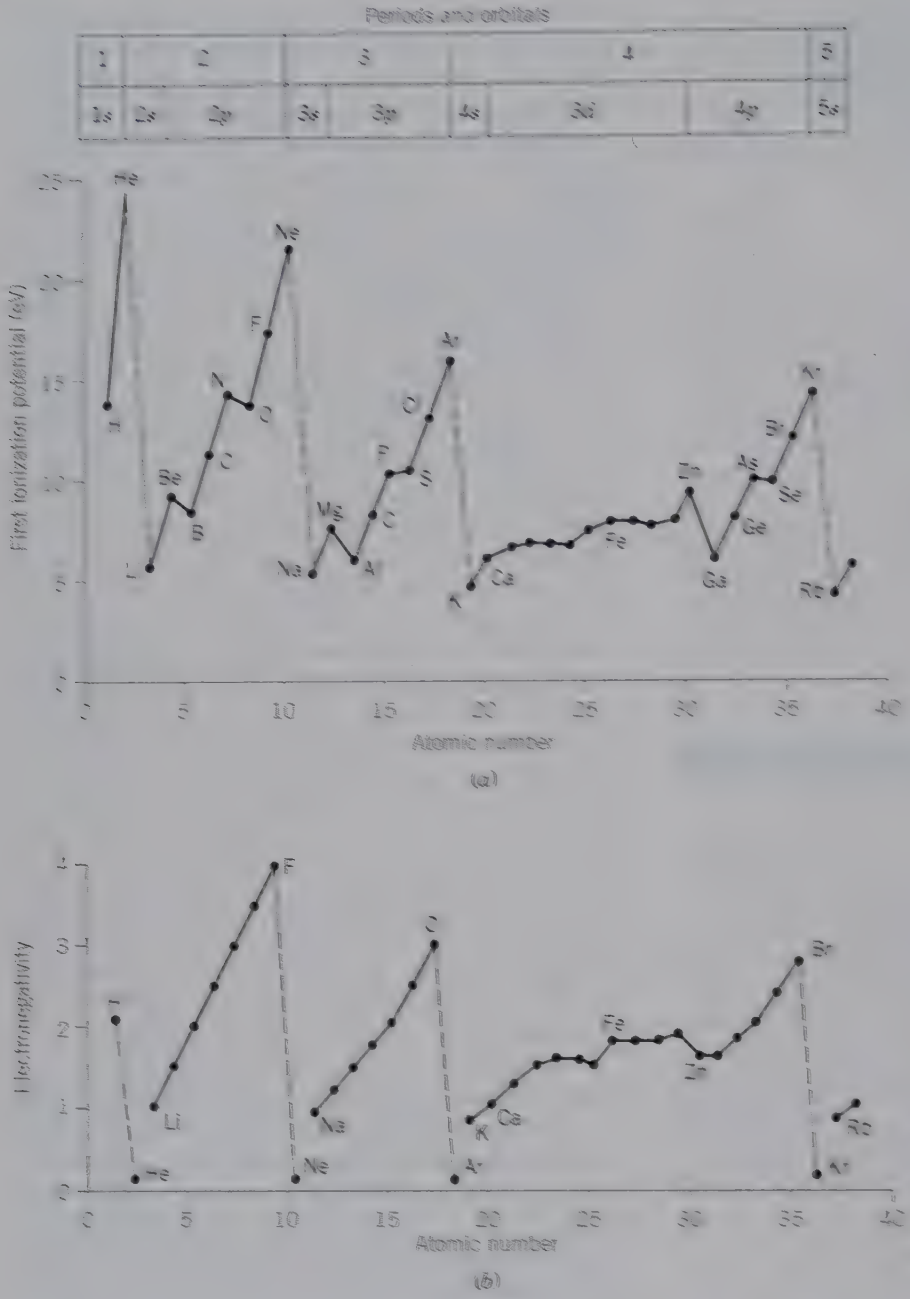

FIG. 3.11 (a) Variation of the first ionization potential as a function of increasing atomic number (Z) for the first 37 elements. (b) Variation of the electronegativity for the same elements as shown in (a).

reflect the much greater energy needed to remove an electron from an atom that has already acquired a positive charge, as well as the higher energy needed to remove an additional electron from remaining electrons that fill the orbital in which they occur. Because of these energy barriers, elements involved in chemical reactions tend to lose only their *valence* electrons, which are those that reside in unfilled orbitals.

Several elements are found in more than one valence or *oxidation state*. For example, iron (Fe) can occur in a divalent state (*ferrous* iron, Fe^{2+}) or in a more oxidized trivalent (*ferric* iron, Fe^{3+}) state. The electronic configuration of atomic Fe is $1s^2 2s^2 2p^6 3s^2 3p^6 3d^6 4s^2$ (Table 3.6). In Fe^{2+}, the atom loses the two $4s$ electrons, but it can lose one $3d$ electron as well, making Fe^{3+}, which then has a half-filled subshell. Other elements, such as Mn and Cr, most commonly occur in the divalent or trivalent state but can also occur in other, higher oxidation states, such as Mn^{4+} and Cr^{6+}. Because in a crystalline substance d orbitals have energy differences that are similar to wavelengths in visible light, transition elements, such as iron, tend to play a major role in the coloration of minerals (see Chapter 10). Table 3.9 lists the valence states of some common ions.

Table 3.9 The Valence States of Ions (and of Ionic Groups) That Occur Abundantly in Rock-Forming Minerals (see also Table 4.1).

CATIONS	
Na^{+}	Si^{4+}
K^{+}	Ti^{4+}
	C^{4+}
Mg^{2+}	
Fe^{2+} (also Fe^{3+})	P^{5+}
Ca^{2+}	
Mn^{2+} (also Mn^{3+}, Mn^{4+})	S^{6+}
Al^{3+}	

ANIONS AND ANIONIC GROUPS		
O^{2-}	$(SiO_4)^{4-}$	$(PO_4)^{3-}$
$(OH)^{1-}$	$(CO_3)^{2-}$	$(SO_4)^{2-}$

BONDING FORCES IN CRYSTALS

The outermost electrons, the *valence electrons*, are those perturbed by bringing other atoms in close proximity. Consequently, these are the electrons involved in bonding; that is, combining chemical elements to make mineral structures. A chemical bond results from a redistribution of electrons that leads to a more stable configuration between two or more atoms. When the electrons have reorganized themselves, and if the energy configuration is lower, then the atoms will stay together forming a **bond**. The attractive (bonding) forces that bind together the atoms (or ions, or ionic groups) in minerals are electrical in nature because they are formed by some distribution of + and − charges. *These electrical forces are chemical bonds.* Their type and intensity are largely responsible for the physical and chemical properties of minerals. Hardness, cleavage, fusibility, electrical and thermal conductivity, compressibility, and the coefficient of thermal expansion are all directly related to these binding forces. In general, *the stronger the average bond, the harder the crystal*, the higher its melting point, and the smaller its coefficient of thermal expansion. The great hardness of diamond (10 on Mohs scale; Chapter 2) is attributed to the very strong electrical forces, bonds, linking together its constituent carbon atoms. The minerals periclase, MgO, and halite, NaCl, both have the same structural arrangement of atoms yet periclase melts at 2820°C, whereas halite melts at 801°C. Which of these two minerals then, has the strongest bond? The greater amount of heat energy required to melt periclase (that is, separating its atoms) indicates that Mg-O forms a stronger electrical bond than Na-Cl in halite.

Chemical bonds, important to mineralogy, can be described as belonging to one of five principal bond types: **ionic, metallic, covalent, van der Waals**, or **hydrogen bonding**. Three of these bond types, ionic, covalent, and metallic, involve valence electrons while the other two, van der Waals and hydrogen, do not directly involve valence electrons. In reality, hybrid (mixed) bonds may exist between all bond types so the grouping of five bond types is one of efficiency.

BONDS WITH VALENCE ELECTRONS

In terms of their valence electrons, all atoms have a strong tendency to achieve a noble gas configuration because completely filled valence shells are almost completely inert (Table 3.6). This electron configuration is the lowest energy and most stable configuration. Other naturally occurring chemical elements would have lower energy and be more stable if they, too, could achieve a filled outer orbital. Elements do so by losing, gaining, or sharing their valence electrons through bonding.

Ionic Bond

> An **ionic bond** forms *when one or more electrons in the valence shell of an atom are transferred to the valence shell of another so that both elements achieve an inert gas configuration.*

For example, the sodium atom has a noble-gas core of neon with a single valence electron in its outer orbital (*3s*) that it loses readily. If it loses this electron, sodium then has the noble gas configuration of neon (Ne) and a positive charge of 1+; it becomes a cation. However, this electron cannot just be lost because electric neutrality must be maintained. Instead, the electron lost by the sodium is picked up by the chlorine. An atom of chlorine has five electrons in its outer *3p* orbital and needs to acquire one electron to achieve the noble gas structure of argon (see Tables 3.5 and 3.6). When Cl acquires this electron, it becomes negatively charged and an anion; it has the structure of Ar with a -1 charge.

These electron losses and gains can be stated as

$$Na\ (1s^2 2s^2 2p^6 3s^1) \rightarrow Na^{+}\ (1s^2 2s^2 2p^6) + e^{-}$$

$$Cl\ (1s^2 2s^2 2p^6 3s^2 3p^5) + e^{-} \rightarrow Cl^{-}\ (1s^2 2s^2 2p^6 3s^2 3p^6)$$

Once formed, the Na^{+} and Cl^{-} attract each other because of their opposite charges. *The attraction between oppositely charged ions constitutes the ionic (or electrostatic) bond* (Fig. 3.12). This bond forms as the result of *the exchange of electron(s) of the metal atom (forming a cation) to the nonmetal atom (forming an anion).* Therefore, the result of ionic bonding is that both atoms have filled shells and that both atoms end up with a charge, one negative and one positive (hence the term *ionic bonding*). Ionic bonds commonly form between atoms of columns I and VII and columns II and VI.

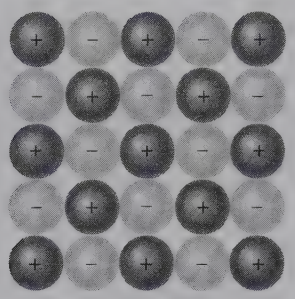

FIG. 3.12 An idealized structure image with ionic bonding. The NaCl (halite) structure shown here represents bonding between Na^+ and Cl^-. The distance between the centers of adjoining Na^+ and Cl^- ions is 2.8 Å.

The energy of the ionic bond, u, depends on two factors: (1) the center-to-center spacing between the ions (r), and (2) the product of their charges (q):

$$u = (Aq_1q_2)/r$$

where A is a numerical quantity, the *Madelung constant*. This expression is similar to that for the Coulombic force (F) operating over a distance d, where F is defined by the equation on page 47 in this chapter (see also Fig. 3.8).

As indicated by this equation, the strength of the bond is inversely proportional to its length. This is seen when we compare the different halides of sodium

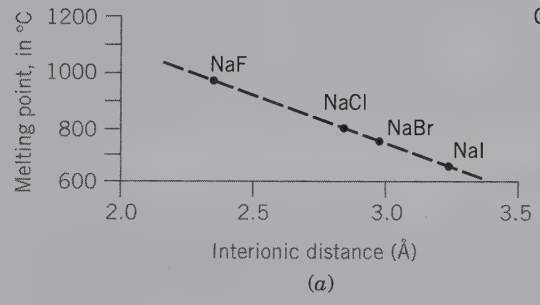

(*a*)

Compound	Interionic distance Å	M.P. (°C)
NaF	2.35	988
NaCl	2.83	801
NaBr	2.97	755
NaI	3.22	651

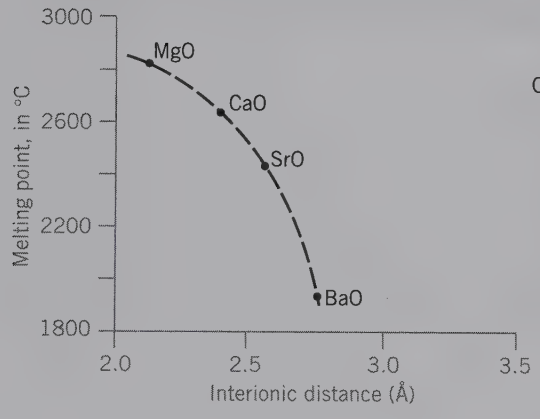

(*b*)

Compound	Interionic distance Å	M.P. (°C)
MgO	2.12	2820
CaO	2.40	2580
SrO	2.56	2430
BaO	2.76	1923

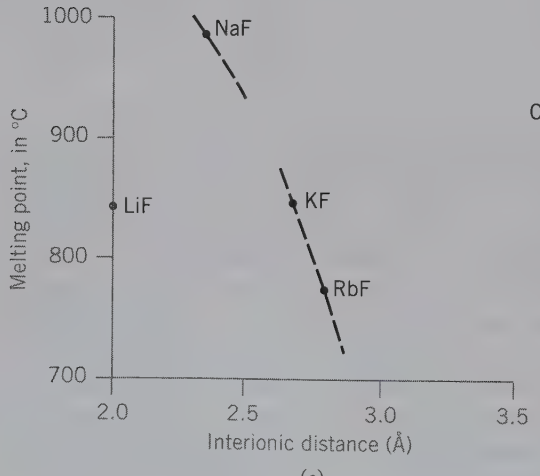

(*c*)

Compound	Interionic distance Å	M.P. (°C)
LiF	2.07	842
NaF	2.35	988
KF	2.69	846
RbF	2.80	775

FIG. 3.13 Melting point versus interionic distance in ionic-bonded compounds. (Data from *Handbook of chemistry and physics*. 1991. 72nd ed. CRC Press, Boca Raton, Florida.)

with anions that increase in size. As the distance (due to the size of the anion) increases, the bond strength decreases (as shown by melting points; the amount of energy needed to break these bonds) as a function of increasing interionic distances in these compounds (Fig. 3.13a). Similarly, oxide compounds with cations that increase in size also display a decrease in the strength of the bond (as measured by the melting temperature) as a function of increasing interionic distances (Fig. 3.13b). Fig. 3.13c shows that the melting temperatures of the fluorides of the alkali metals are a direct function of the size of the cation; the anions are all F^-. The compound with the smallest cation, Na^+ (=1.02 Å for **C.N.** = 6), has the highest melting temperature, and the one with the largest cation, Rb^+ (= 1.61 Å for **C.N.** = 6), has the lowest melting temperature (ionic radii from Table 3.8). LiF is an exception to this generalization, which is explained by anion-anion (*F-F*) repulsion in a structure having a very small cation (such as Li).

The charge of the coordinated ions (those ions in close proximity; see Chapter 4), has an even more powerful effect on the strength of the bond. The bonds uniting the more highly charged ions are much stronger. A comparison of the absolute values of the melting temperatures for the alkali-earth oxides (Fig. 3.13b), which are divalent compounds ($q = 2$), with the absolute values for the monovalent alkali fluorides ($q = 1$), in which the interionic spacings are closely comparable (Fig. 3.13c), reveals the magnitude of the valence charge effect. The interionic distance is almost the same for corresponding oxides and fluorides, but their bond strengths are very different (e.g., MgO has a melting temperature almost three times that of the monovalent fluoride). Figure 3.14 illustrates the effect of interionic spacing and charge on hardness. All substances grouped together in columns of these two figures have the same structure and may be regarded as ionically bonded.

Sodium chloride (halite) crystals exhibit several characteristic properties of the ionic bond: cubic crystal habit, cleavage, specific gravity, and so forth. Touching the halite crystal to the tongue yields the taste of a

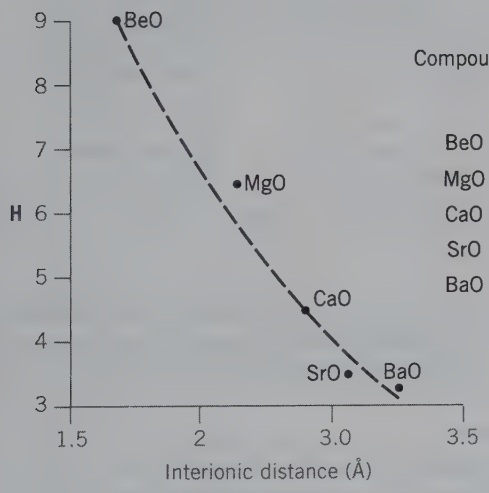

Compound	Interionic distance Å	H Hardness (Mohs)
BeO	1.67	9.0
MgO	2.12	6.5
CaO	2.40	4.5
SrO	2.56	3.5
BaO	2.76	3.3

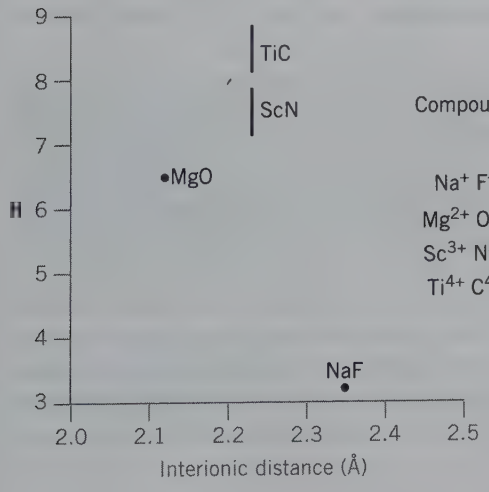

Compound	Interionic distance Å	H Hardness (Mohs)
$Na^+ F^-$	2.35	3.2
$Mg^{2+} O^{2-}$	2.12	6.5
$Sc^{3+} N^{3-}$	2.23	7-8
$Ti^{4+} C^{4-}$	2.23	8-9

FIG. 3.14 Hardness versus interionic distance and charge in ionic-bonded compounds. (Data from Evans, R. C. 1952. *Crystal chemistry.* Cambridge University Press, London.)

Table 3.10 Examples of Properties Conferred by the Principal Types of Chemical Bond

Property	Bond Type			
	Ionic (Electrostatic)	Metallic	Covalent (Electron-shared)	van der Waals (Residual)
Bond strength	Strong	Variable strength, generally moderate	Very strong	Weak
Mechanical	Hardness moderate to high, depending on interionic distance and charge; brittle	Hardness low to moderate; gliding common; high plasticity; sectile, ductile, malleable	Hardness great Brittle	Crystals soft and somewhat plastic
Electrical	Poor conductors in the solid state; melts and solutions conduct by ion transport	Good conductors; conduction by electron transport	Insulators in solid state and melt	Insulators in both solid and liquid state
Thermal (melting point = m.p.; coefficient of thermal expansion = coef.)	m.p. moderate to high depending on interionic distance and charge; low coef.	Variable m.p. and coef.; atoms in melt	m.p. high; low coef.; atoms and molecules in melt	Low m.p.; high coef.; liquid crystal molecules in melt
Solubility	Soluble in polar solvents to yield solutions containing ions	Insoluble, except in acids or alkalis by chemical reaction	Very low solubilities	Soluble in organic solvents to yield solutions
Structure	Nondirected; gives structures of high coordination and symmetry	Nondirected; gives structures of very high coordination and symmetry	Highly directional; gives structures of lower coordination and symmetry	Nondirected; symmetry low because of shape of molecules
Examples	Halite, NaCl; Fluorite, CaF_2; most minerals	Copper, Cu; silver, Ag; gold, Au; electrum, (Au, Ag); most metals	Diamond C; sphalerite; ZnS; molecules of O_2; organic molecules; graphite (strong bond)	Sulfur (weak bond); organic compounds; graphite (weak bond)

salt solution. These properties are in stark contrast to properties of the individual, uncombined elements; the shining metal (Na) or the greenish, acrid gas (Cl_2). In other words, the properties conveyed to the crystal by its constituent elements are the properties of the *ions*, not the elements.

Ionically bonded crystals are generally of moderate hardness and specific gravity, and have fairly high melting points. These crystals are strong when forced together but weak when cleaved or sheared. Once the bonds are broken, recombining them is difficult. They can be recombined by dissolving the ionic solid or by heating it sufficiently to excite the valence electrons. Ionic solids are poor conductors of electricity and heat. The lack of electrical conductivity is due to the stability of the ions, which neither gain nor lose electrons easily. Because the electrostatic charge constituting the ionic bond is evenly spread over the ion, a cation will tend to surround itself with as many anions as can fit around it. This means that the ionic bond is nondirectional, and the symmetry of the resultant crystals is generally high (see Fig. 3.12 and Table 3.10; Chapter 6 for a discussion of symmetry). Table 3.10 summarizes selected properties related to the different bond types.

Metallic Bond

In **metallic bonds**, the valence electrons owe no affinity to any particular nucleus and are free to drift through the structure or even out of it entirely, without disrupting the bonding mechanism.

The attractive force between the positively charged nuclei with their filled electron orbitals (but lacking valence electrons) and the cloud (or sea) of negative electrons that holds such crystal structures together is the **metallic bond**.

This bond is schematically illustrated in Figs. 3.15a and b, which shows positively charged spherical ions in a dense cloud of mobile, delocalized valence electrons. The atoms are depicted as having spherical cores because their valence electrons are lost to the crystal

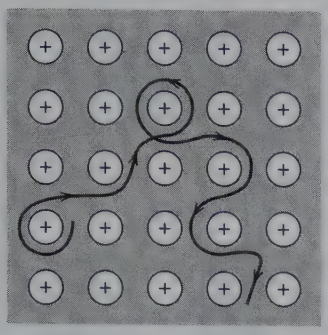

(*a*)

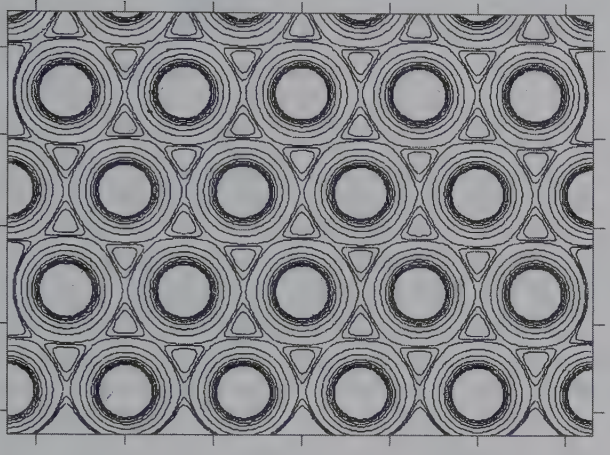

(*b*)

FIG. 3.15 (a) Schematic cross section through the structure of a metal. Each circle with a positive charge represents a nucleus with filled, nonvalence electron orbitals of the metal atoms. The mobile electrons are represented by the cloud around the atoms (light gray shading). A possible electron path between the nuclei is shown by the line. (b) An electron density map of copper atoms in copper metal showing the spherical nature and close packing of the positively charged nuclei (white circles) surrounded by a less dense cloud of electrons (contour lines). (Figure courtesy of R.T. Downs, University of Arizona, Tucson.)

structure as a whole. Several factors are the cause of the metallic bond. Metal atoms have valence electrons that are only weakly held and have similar energy. Therefore, instead of releasing the electrons to another specific atom, electrons are redistributed and shared by all atoms because they are free to move with few energy constraints.

These energy constraints, and the resulting properties of metals, are explained in terms of **band theory**. If there is infinite spacing between identical atoms in a crystal, then energy levels of electrons within each orbital and subshell are identical and discrete. As such distance decreases, atoms within close proximity to one another interact, but no two electrons can have the energy level, as dictated by the Pauli exclusion principle. Consequently, the energy that separates the discrete bonding (and nonbonding) orbitals lessens as the distance between atomic orbitals decreases. These interactions result in a series of very closely spaced molecular orbitals (e.g., $\sim 10^{23}$ for one mole of metal) that constitute a near continuum of energies (Fig. 3.16; see also Whitten et al., 2004; Nesse, 2000). This includes many electron orbitals that interpenetrate (Fig. 3.16). This continuous spectrum of energies is called a *band*.

For example, in an isolated Mg atom, the outer electron orbital ($3s$) is filled with two electrons (Table 3.6) so that all available energy levels are occupied. When Mg atoms impinge on one another, as in a magnesium crystal, the otherwise vacant $3p$ orbitals become available and electrons from the $3s$ orbital move into the open energy levels in the $3p$ band. This allows electrons to migrate easily throughout the crystal as a whole. In transition metals, such as iron, electrons migrate into the $3d$ orbital to produce metallic bonding. In metallic crystals, electrons occupy either a *partially filled band* or a *filled band that overlaps an empty band* (Fig. 3.16). The band, or orbital, into which the electrons migrate, is known as the **conduction band** (e.g., $3p$ orbital of Mg). The band that supplies the electrons is known as the **valence band** (e.g., $3s$ orbital of Mg). An energy barrier or **band gap** exists between the inner subshells and the outer bands eliminating the contribution of electrons from these shells (Fig. 3.16). When the energy difference between the filled orbitals and the lowest empty band is too large for electrons to jump into a conduction band, the material is an **insulator** and does not conduct electricity (Fig. 3.16). When the difference in energy between the filled band is only slightly below, but not overlapping, the empty band, the material is a **semiconductor** (Fig. 3.16). Thus, the structural units of true metals are the atomic nuclei plus nonvalence electron orbitals bound together by the aggregate electrical charge consisting of a cloud of valence electrons that surrounds the nuclei. These electrons are the "glue" that holds metals together.

Many of these low energy states are in the visible light range. Thus, in metallic objects, light is immediately absorbed as the electron jumps into an excited state. The continuum of unoccupied electronic states available results in a continuum of absorbed photon energies and, therefore, the metal is opaque. When the electron drops back to the ground state, a photon is emitted, and a reflection is observed. Thus, metals have metallic, reflective luster.

Metals owe their high plasticity, tenacity, ductility, and electrical conductivity, as well as their generally low hardness and metallic luster to the metallic bond. Because metals are made of spherical atoms in a cloud of electrons, atoms pack tightly, and bond strength is

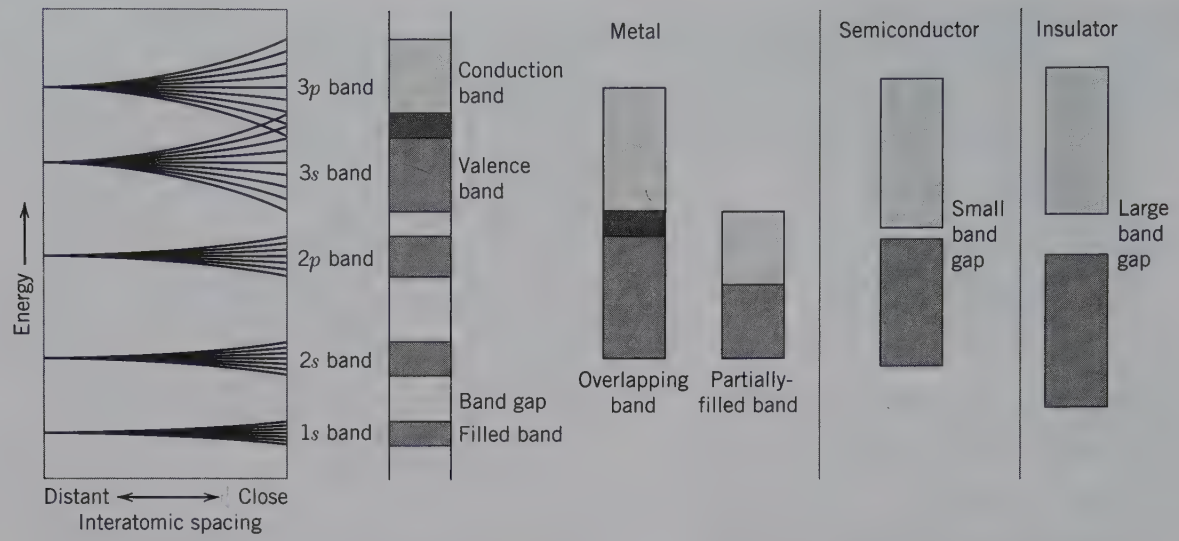

FIG. 3.16 Energy bands for metals, semiconductors, and insulators. Discrete energy levels are represented by single lines at the left of the diagram. When atoms are brought into close proximity, energy levels spread out and overlap, as shown here for magnesium. Electrons from the 3*s* orbital (valence band, gray) move into the overlapping 3*p* orbital (conduction band, light gray). Metals have partially filled or overlapping (dark gray) energy bands; semiconductors have only a small energy gap between conduction and valance bands; insulators have a large energy gap between bands. Unshaded bands represent conduction bands. (The left two columns of this diagram are a modification of Fig. 3.8 (p. 50) from *Introduction to Mineralogy*, 2000, by W. D. Nesse; and with permission from Oxford University Press, Oxford, U.K.; the four columns on the right are modified from *General Chemistry* (with CD-ROM and Info Trac), 7th ed., by WHITTEN/DAVIS/PECK/STANLEY, 2004. Reprinted with permission of Brooks/Cole, a division of Thomson Learning: www.thomsonrights.com Fax 800-730-2215.)

nearly equal in all directions. In addition, the tight packing of spherical atoms (as can be modeled with ping-pong balls) gives rise to a dense atomic arrangement and results in the high specific gravity of most metals. When a metal is hammered, it tends to deform rather than break (as in ionic crystals) because the atoms roll over each other without setting up repulsive electrostatic forces (see Table 3.10 for a summary of properties). This atomic property is responsible for the physical behavior of metals under stress. Some metals have yet another distinguishing property. So free with their electrons are sodium and its close relatives, cesium, rubidium, and potassium, that the impact of the radiant energy of light knocks a considerable number of electrons entirely free of the structure. This photoelectric effect, on which such instruments as exposure meters depend, demonstrates that the electrons are very weakly tied into the metal structure.

Among minerals, only the native metals display pure metallic bonding. These are gold, Au; silver, Ag; copper, Cu; etc. Table 3.10 gives a brief listing of some of the properties related to the metallic bond type in crystalline materials. However, hybrid (mixed) bonds also exist between metallic bonding and other bond types. Sulfide minerals, such as pyrite, exhibit partial metallic bonding which gives rise to their characteristic metallic luster.

Covalent Bond

Between the previously mentioned two bonding mechanisms, there exists another bond type that is intermediate between ionic and metallic bonding.

In many cases, *the stable inert gas configuration can be achieved if two (or more) atoms share their outer valence electrons.* This electron-sharing is the basis for the **covalent bond.**

The resulting noble gas configuration occurs simultaneously around each atom and the electron orbitals overlap. As discussed previously, a single atom of chlorine with an incomplete valence orbital is highly reactive. It seizes upon and combines with almost anything in its neighborhood. Generally, its nearest neighbor is another chlorine atom. When this occurs, the two Cl atoms unite in such a way that two electrons, one from each chlorine atom, do double duty in the outer orbitals of both atoms. By sharing electrons, both Cl atoms achieve the stable noble-gas configuration, and the two atoms of chlorine are strongly bound together by the covalent bond.

The bonding mechanism between two chlorine atoms can be symbolically shown as follows:

$$\cdot\ddot{\underset{\cdot\cdot}{\mathrm{Cl}}}: + \cdot\ddot{\underset{\cdot\cdot}{\mathrm{Cl}}}: \rightarrow :\ddot{\underset{\cdot\cdot}{\mathrm{Cl}}}:\ddot{\underset{\cdot\cdot}{\mathrm{Cl}}}:$$

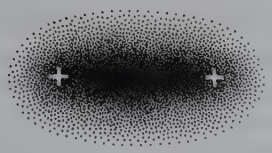

FIG. 3.17 Schematic representation of the electron distribution between two covalently bonded atoms.

The small dots represent the outer-shell (valence) electrons in the *s* and *p* orbitals of the M shell in chlorine (this notation is known as Lewis symbols, after the American chemist Gilbert N. Lewis, 1875–1946). The valency shell is completed by the sharing of electrons between the two Cl atoms on the right side of the equation. The bonding energy of the atom is entirely consumed in linking to one neighbor, and stable Cl_2 molecules show little tendency to link one to another. A schematic representation of this type of covalent bonding is shown in Fig. 3.17.

The number of covalent bonds that an atom may form can commonly be predicted by counting the number of electrons required to achieve a stable electron configuration (such as that of a noble gas). In general, those elements near the middle of the periodic table, such as carbon, silicon, aluminum, and sulfur, have two, three, and four vacancies in their outer orbitals. They can form up to four covalent bonds with neighboring atoms as is the case with carbon. Carbon has four electrons in its valence shell; through sharing four additional electrons, it achieves the noble-gas configuration of neon. (It cannot form an ionic bond because all the electrons have similar energies.) The four valence electrons in each carbon are sufficient to fill the bonding orbitals by electron sharing with four other carbon atoms. This forms a very stable, firmly bonded configuration having the shape of a tetrahedron with a central carbon atom bonded to four other carbon atoms at the apices (Fig. 3.18). Every carbon atom is linked to four others, forming a continuous network. Orbitals of the electrons have a large overlap, producing very strong bonds. The energy of the bonds is strongly localized in the vicinity of the shared electrons, producing a very rigid structure—that of diamond, the hardest natural substance. Because all the valence electrons in diamond are used for bonding, none can move freely to conduct electricity. Consequently, diamond is a good insulator.

FIG. 3.18 Schematic representation of the overlap of orbitals between a C atom (at the center of the illustration) with similar orbitals from four carbon atoms at the corners. This represents the covalent bonding in diamond.

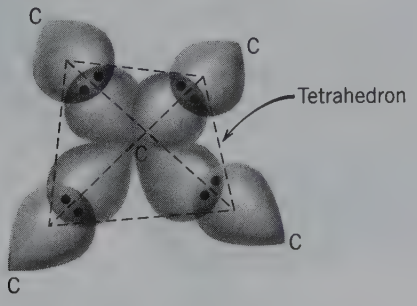

In covalently bonded structures, the interatomic distance is generally equal to the arithmetic mean of the interatomic distances in crystals of the elemental substances. In diamond, the C-C spacing is 1.54 Å; in silicon Si-Si distance is 2.34 Å. Therefore, if these atoms unite to form a compound, SiC, the silicon–carbon distance will be near 1.94 Å, the arithmetic mean of the elemental spacings (1.54 + 2.34 / 2). X-ray measurement (Chapter 14) confirms this spacing in the familiar synthetic abrasive, silicon carbide, as 1.93 Å.

This **electron-sharing** or **covalent** bond is the strongest of the chemical bonds. Minerals with covalent bonds are characterized, in general, by insolubility (there is generally slow reactivity), chemical and mechanical stability, and very high melting points. They do not yield ions in the dissolved state and are nonconductors of electricity, both in the solid state and in solution. The sharp localization of electrical forces in the vicinity of the shared electron, leads to a highly directional bond (Fig. 3.17). The ions are no longer spherical, and the symmetry of the resulting crystals is likely to be lower (less symmetric) than when ionic bonding occurs (Table 3.10).

ESTIMATION OF THE CHARACTER OF THE BONDING MECHANISM

Electronegativity

Hybrid (or mixed) bonds exist in many natural materials. There appears to be some electron sharing (covalent bonding) in most ionically bonded crystals, whereas atoms in covalently bonded substances commonly have some electrostatic charges (as in ionic bonding). Bonds between elements of the first and seventh columns of the periodic table and between the second and the sixth columns are dominantly ionic. Examples are the alkali halides (e.g., NaCl) and the alkali-earth oxides (e.g., MgO). Bonds between like atoms or atoms close together in the periodic table tend to be covalent (e.g., C). In addition, metallic bonds are similar to covalent bonds because both involve a sharing of electrons. Therefore, the degree of electron sharing suggests that there may be bonds with both covalent and metallic characteristics. This is

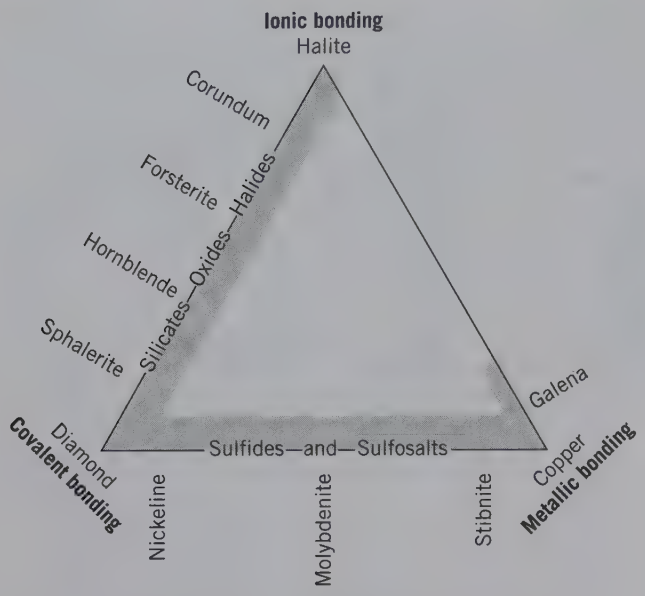

FIG. 3.19 The gradational and hybrid (mixed) nature of the chemical bonds in minerals. Each corner represents pure bonding of one type. The shading schematically represents the mixed nature of the bonding mechanisms. Bonding mechanisms for various minerals are shown. (Modified after Blackburn and Denner, *Principles of Mineraolgy, 2e,* Copyright 1994, William C. Brown Publishing. Reproduced with permission of the McGraw Hill Companies.

shown schematically in Fig. 3.19 using a triangular diagram with the three valence bond types placed at its corners. The shaded area between bonds represents the range of characteristics observed in minerals.

To evaluate the amount of ionic (or covalent) character between two bonding elements, Linus Pauling in 1939, developed a method by which the percentage of ionic character of a chemical bond can be estimated. The basis for this method is his scale of electronegativities of the elements. These values are based, in part, on *ionization potentials*.

Electronegativity *is a measure of the ability of an atom in a crystal structure (or molecule) to gain (or lose) electrons to its outer shell.*

It is expressed as a dimensionless number that is calculated from the known bond strength between atoms in molecules (see Table 3.5 for a partial listing of these values; see also Fig. 3.20). Elements with *low* electronegativity values are electron *donors*, they relinquish their outer valence electrons easily to form cations. Those with *high* values act as electron *acceptors* and have a high affinity for gaining electrons to form anions. Lithium (Li) has been assigned an electronegativity value of 1.0, carbon (C) has a value of 2.5, and fluorine (F) has an electronegativity of 4.0. The electronegativity values of the noble gases are set at zero because these atoms do not attract (or lose) electrons.

Within a specific period (in the periodic table), electronegativity values rise as a function of increasing atomic number (see Figs. 3.11b and 3.20). Electronegativity values of elements in column I (H, Li, Na, K, Rb, and so on; see Table 3.5) or in column II (Be, Mg, Ca, Sr, and so on) decrease with increasing atomic number as shown in Figs. 3.11b and 3.20. The same holds for their values of ionization potential. This suggests that the

FIG. 3.20 The electronegativities of the elements. (From Brady, J. E., J. W. Russell, and J. R. Holum. 2000. *Chemistry, matter and its changes*, 3rd ed., Wiley, New York.)

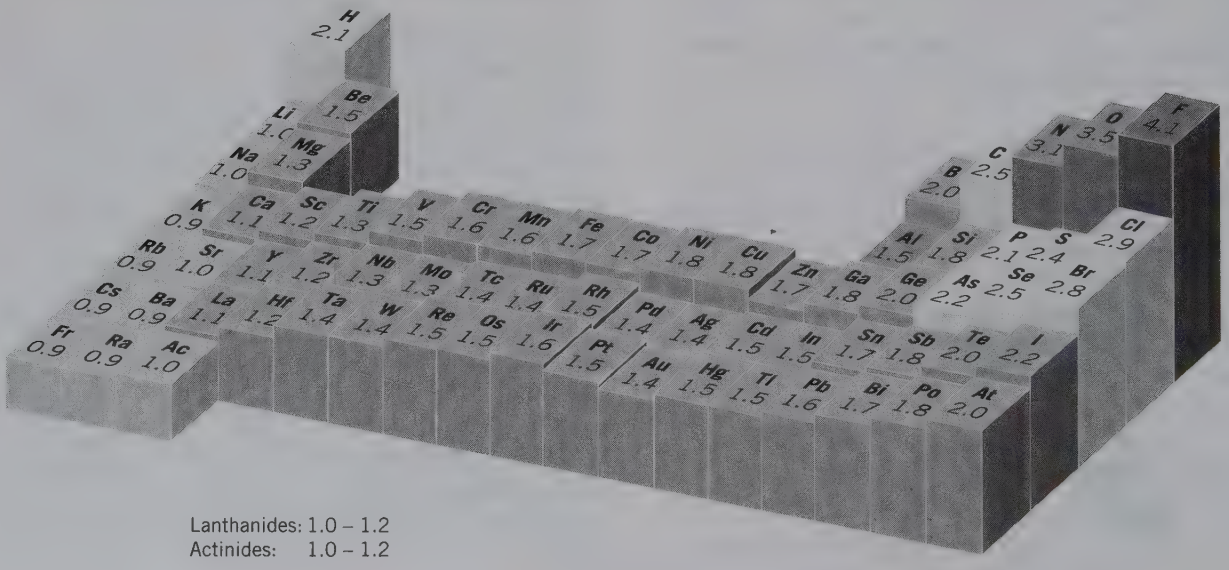

The noble gases are assigned electronegativities of zero and are omitted from this illustration.

binding energy between the nucleus and the first valence electron of an element (in a specified column) decreases as the volume of the atom in the column increases. This implies that large atoms hold their outer valence electrons more loosely than do smaller atoms. The concept of electronegativity is especially useful in assessing the type of bond formed between different atoms.

The *difference* in the electronegativity values of the elements is an expression of the ionic character of the bond formed by their atoms. This difference is expressed as the absolute value of $X_a - X_b$, where X_a is the electronegativity of element A bonded to element B with its own electronegativity value X_b. Linus Pauling used this difference in values of electronegativity to formulate an equation for estimating the ionic character of a single bond:

$$\text{Amount of ionic character} = 1 - e^{-0.25(X_a - X_b)^2}$$

This mathematical function is a curve shown in Fig. 3.21. By using this curve, the amount of ionic character of any bond can be estimated. First, calculate the difference in electronegativity, then find the corresponding fraction of ionic character on the curve. It follows from Fig. 3.21 that compounds made of elements with large differences in their electronegativity are more ionic than compounds made up of elements with similar values of electronegativity.

FIG. 3.21 Curve relating the percentage of ionic character of a bond *A–B* to the difference in electronegativity (X_A–X_B) of the atoms. (After Pauling, L. 1960. *The nature of chemical bond.* Cornell University Press, Ithaca, New York.)

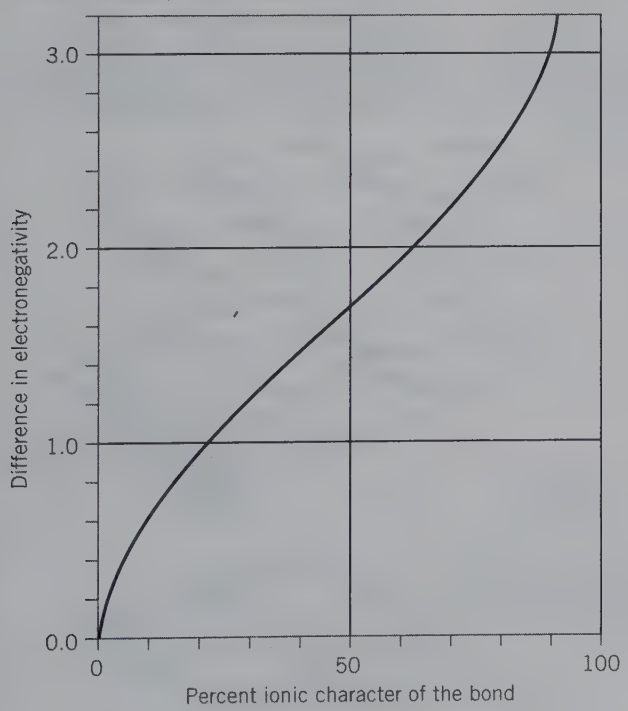

For example, the compound NaF is composed of Na (e.n. = 0.9) and F (e.n.= 4.0). The difference in electronegativity is 3.1, which corresponds to ~92% ionic character. Therefore, the NaF bond is essentially ionic. In contrast, TiC has an electronegativity difference of 1.2 , or about 30% ionic character. Therefore, TiC contains a more covalent bond type (70%). Similarly, one can evaluate the ionic character of the bond type between silicon and oxygen. The absolute value for (Si-O) turns out to be 1.7; this bond type is 50% ionic in character (and, therefore, 50% covalent in character; Fig. 3.21).

The Si-O hybrid (mixed) bond is found in the mineral quartz. The bonds linking the atoms of silicon and oxygen in quartz display characteristics of the ionic and the covalent bond in nearly equal amounts. The strong bonding between Si^{4+} and O^{2-} ions in SiO_2 causes the electron densities of the two ions to be localized between the nuclei of Si and O. Such distortions of the electron clouds from generally spherical to more ellipsoidal shapes have been determined directly from X-ray diffraction intensity measurements (see Chapter 14). Figure 3.22 shows a considerable build-up of charge density in the Si-O bond of coesite, SiO_2, with

FIG. 3.22 A map of the electron density distribution of an Si–O–Si bond in coesite, one of the high-pressure polymorphs of SiO_2. This map displays the difference between the total electron density and the electron density prior to formation of the bond. The solid contours represent positive electron density, the dotted contours negative density, and the long-dashed contour zero density. The contour interval is 0.1 electrons per Å^3. The distance between O and Si is 1.61 Å. (From Geisinger, K. L. and G. V. Gibbs. 1983. An X-ray diffraction study of the electron distribution in coesite. *Geological Society of America, Abstracts with Programs*, 15: 580.)

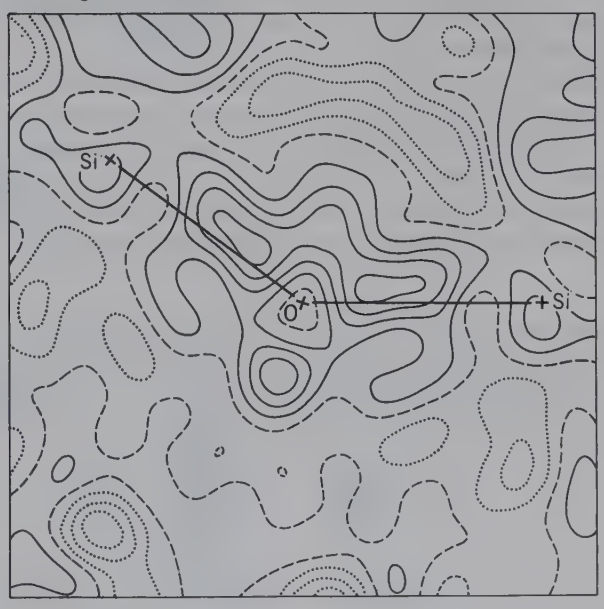

the strongest charge concentration in the vicinity of the more electronegative oxygen atoms. This shows that electronegativity, along with ionic size and valence, is helpful in predicting the chemical behavior of elements.

BONDS THAT DO NOT INVOLVE VALENCE ELECTRONS

Bonds can also form from relatively weak electrostatic forces developed because of an asymmetric charge distribution. Such bonding mechanisms do not rely on a transfer of valence electrons from one atom to another. The **van der Waals** and **hydrogen** bonds are two types of bonding mechanisms that result from asymmetric charge distributions.

van der Waals Bond

The **van der Waals** (or *residual*) bond is a bond due to residual charges.

It ties neutral molecules and essentially uncharged structural units into a cohesive structure by virtue of small residual electrical charges on their surfaces.

Electrons in the occupied orbitals of the interacting atoms synchronize their motions to avoid each other as much as possible such that an instantaneous and weak dipole attraction is produced between the two atoms (often referred to as a dynamic dipole; Fig. 3.23). This results in a small concentration of positive charge at one end, with a corresponding dearth of positive charge (which results in a small negative charge) at the other end. The net positive charge on one side of the molecule attracts electrons from the neighboring molecule. This weak dipole can induce a similar effect in neighboring atoms, which will cause the whole molecular structure to be bonded together by this weak dipole effect. Such bonding is especially effective over large distances in molecular structures. In the formation of crystals, these molecules are aligned with negative poles against positive poles of neighboring molecules. This is the mechanism that bonds the Cl_2 molecules in solid Cl_2 and in other neutral molecules, such as N_2 and O_2, to form molecular solids despite the fact that all the valence orbitals are occupied either by nonbonding electrons or by electrons used in covalent bonding to form *dimers* (a dimer is a molecule created from two identical simpler units). While common in organic compounds and solidified gases, this bonding type is much less common in minerals.

When van der Waals bonds are present in minerals, it generally defines a zone of cleavage and low hardness. It is the weakest of the chemical bonds. Two minerals, graphite and sulfur, contain van der Waals bonds. The mineral graphite consists of covalently bonded sheets of carbon atoms linked only by van der Waals bonds (Fig. 3.24 and Table 3.10). This weak bonding mechanism allows graphite to be used as the "lead" in pencils. The soft graphite cleaves easily, leaving a mark on paper. The most common form of crystalline sulfur is made up of discrete S_8 molecules with a cyclic structure (Figs. 3.25a, b). Within the rings, there is pure covalent bonding, but adjacent rings are held together by van der Waals forces, which account for the low hardness of sulfur (H = 1.5–2.5) and its low melting point (at 112.87°C) . Properties of minerals containing van der Waals bonds are given in Table 3.10.

It is the van der Waals bond that allows geckos to climb. Van der Waals bonds that occur between the fibers on their feet and the substrate over which they crawl, gives them their impressive ability to climb windows effortlessly.

FIG. 3.23 Polarization of one atom by another because of an increase in the concentration of electrons on one side of the atom. This causes a dipole effect. The weak dipole attraction is that of the van der Waals bond.

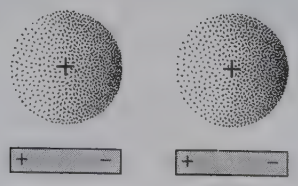

FIG. 3.24 Perspective sketch of the graphite structure with covalent bonding between carbon atoms within layers and residual (van der Waals) bonding between layers. Note the large separation (3.35 Å) between layers, which leads to cleavage.

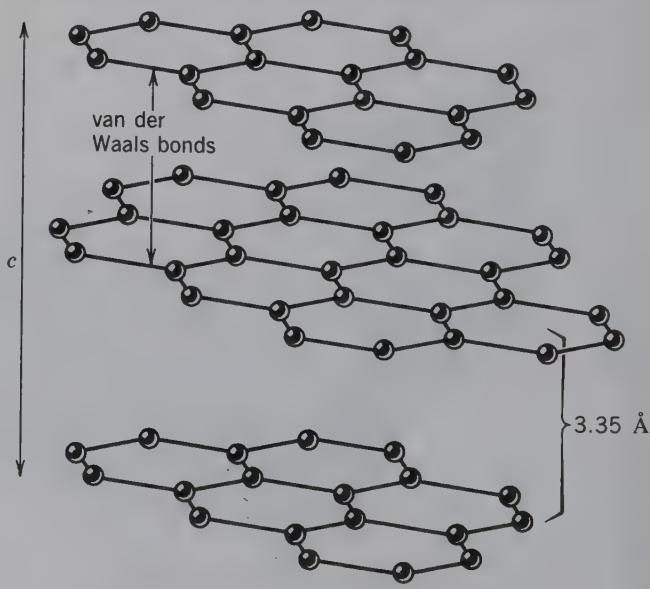

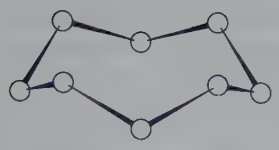

(a)

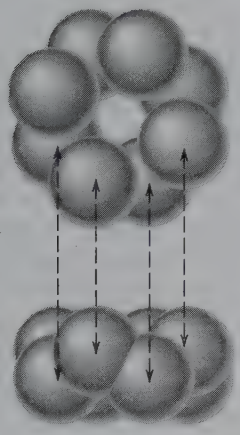

(b)

FIG. 3.25 (a) S_8 rings occur in the crystal structure of sulfur. These rings are linked to each other by van der Waals bonds. (b) The S_8 rings in plan view and in cross section.

Hydrogen Bond

Polar molecules, those that display some sort of dipole behavior, can form crystalline structures by the attraction between the oppositely charged ends of molecules (Fig. 3.26a). If the molecule bonds and leaves one part with more charge than another, a polar bond occurs. A special type of polar bond is the hydrogen bond.

The **hydrogen bond** *is an electrostatic bond between a positively charged hydrogen ion and a negatively charged ion*, such as O^{2-} or N^{3-}.

Because hydrogen has only one electron, when it transfers this electron to another more electronegative ion in ionic bonding, the remaining proton of the hydrogen nucleus becomes unshielded. This unshielded positive ion has the ability to form weak electrostatic bonds (hydrogen bonds) with other negative ions or with the negative ends of polar molecules, such as H_2O (Fig. 3.26b). The close approach allows the formation of a dipole-dipole bond, which is relatively weak when compared with an ionic or covalent bonding mechanism. However, the hydrogen bond is considerably stronger than the van der Waals bond.

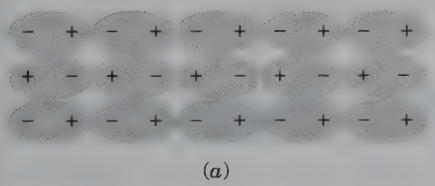

(a)

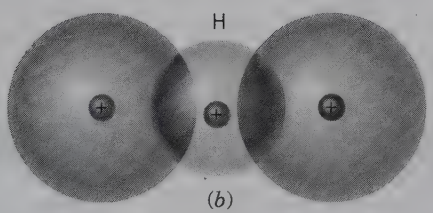

(b)

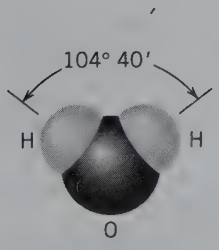

(c)

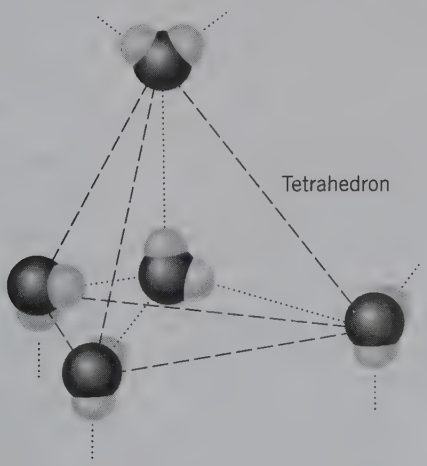

(d)

FIG. 3.26 (a) Schematic representation of the packing of polar molecules in a crystalline solid. Charges of opposite sign are arranged as closest neighbors. (b) Model of a hydrogen bond. (c) A water molecule and the bond angle between H–O–H. (d) Hydrogen bonding as shown by one of the polymorphs of ice. The coordination is tetrahedral and similar to that in diamond.

Ice is an especially good example of hydrogen bonding. The shape of an H_2O molecule is polar (Fig. 3.26c), with a concentration of positive charge on one side of the molecule. Because of this, the two hydrogen atoms in the H_2O molecule (net positive charge) can link to two negative charges concentrated on the oxygen side. Thus, two hydrogens provide the bonding to two other neighboring H_2O molecules. Two additional neighboring H_2O molecules, in turn, provide H atoms to make two more hydrogen bonds. Therefore, each oxygen atom is bound to four neighboring oxygen atoms, in a tetrahedral arrangement, by intervening hydrogen bonds (Fig. 3.26d illustrates the tetrahedrally bonded structure of one form of ice; see also the illustration at the very beginning of this chapter of the structure of ice I). Ice is less dense than water at the melting temperature. At the onset of melting, this relatively open network structure collapses, and in the resulting liquid, the H_2O molecules are more densely packed than in the solid. Hence, ice floats on liquid water.

As in the case of van der Waals bonds, the hydrogen bonds are weak, but there are many of them per unit volume of structure, which results in an overall, relatively strong material. Hydrogen bonding is common in hydroxides in which the $(OH)^-$ group does not behave strictly as a spherical anionic group but is more realistically represented by an asymmetrical coordination, which produces a dipole effect. Hydrogen bonding is also present in many of the layer silicates, such as micas and clay minerals, which contain hydroxyl groups.

CRYSTALS WITH MORE THAN ONE BOND TYPE

Among naturally occurring substances, with their tremendous diversity and complexity, the presence of only one type of bonding within a single mineral is rare, and two or more bond types coexist in most minerals. Whenever a mineral consists of more than one chemical element, the mineral may have more than one bond type and, as discussed, even in minerals with only one element, more than one bond type can occur. In gold (Au), all the atoms are gold, and metallic bonds exist between all gold atoms. In contrast, in the mineral graphite, C, two bond types exist, covalent and van der Waals. For minerals with more than one cation, more than one bond type commonly occurs. For example, calcite has the formula $CaCO_3$. Because cations are surrounded by anions, each Ca is bonded to O and each C is bonded to O. This provides the possibility for at least two bond types. We can estimate the character of the Ca–O and C–O bond types using electronegativities. For example, the Ca–O bond is ionic in character (based on e.n. values of 1.1–3.5 = absolute value of 2.5) whereas the C–O (e.n. of 2.5 and 3.5 = 1.0) bond is covalent in character. Many minerals, such as mica, contain two or more bond types of different character and strength. This difference in the strength of bonds is what leads to **cleavage**; *minerals cleave where bonds are weak*. If all bonds are of the same strength, minerals tend to fracture rather than cleave along well-defined planes.

When more than one bond type exists in a crystal structure, the crystal shares in the properties of the different bond types and commonly strongly directional properties result. Thus, in the mineral graphite, the mineral structure consists of thin sheets held together by strong covalent bonding *in* the plane of the sheets, whereas the excellent cleavage between the sheets reflects the weak van der Waals bonds *between* the sheets (Fig. 3.24). The layer silicates consist of sheets of strongly bonded silicon tetrahedra, with a relatively weak ionic and/or hydrogen bond, joining the sheets together. The layer silicates reflect, in their remarkable basal cleavage between the sheets, the difference in strength of two bond types (see Figs. 18.32, 18.34, and 18.36). The prismatic habit and cleavage of the pyroxenes and amphiboles, and the chunky, blocky habit and cleavage of the feldspars, are similarly the result of relatively weak bonds joining together more strongly bonded structure units having a chain, band, or block shape (see also Chapter 2). Galena, PbS, exhibits characteristics related to the metallic bond (Pb–Pb), as expressed by good electrical conductivity and bright metallic luster, and of the ionic bond (Pb–S), as shown by excellent cleavage and brittleness.

REFERENCES AND FURTHER READING

Ahrens, L. H. 1952. The use of ionization potentials. *Geochimica et Cosmochimica Acta* 2: 155–69.

Bloss, F. D. 1994. *Crystallography and crystal chemistry: An introduction.* Reprint of original text of 1971. Mineralogical Society of America, Washington, D.C.

Brady, J. E., J. W. Russell, and J. R. Holum. 2000. *Chemistry: The study of matter, and its changes.* 3rd ed. Wiley, New York.

Bragg, W. L., and G. F. Claringbull. 1965. *Crystal structure of minerals.* Cornell University Press, Ithaca, New York.

Brown, T. H., E. LeMay, and B. E. Bursten. 2005. *Chemistry: The central science.* 10th ed. Prentice Hall, Upper Saddle River, New Jersey.

Cotton, F. A., G. Wilkinson, and P. L. Gaus. 1995. *Basic inorganic chemistry.* 3rd ed. Wiley, New York.

Evans, R. C. 1966. *An introduction to crystal chemistry.* 2nd ed. Cambridge University Press, Cambridge, England.

Griffen, D. T. 1992. *Silicate crystal chemistry.* Oxford University Press, New York.

Klein, C. 2008. *Minerals and rocks: Exercises in crystal and mineral chemistry, crystallography, X-ray powder diffraction, mineral and rock identification, and ore mineralogy.* 3rd ed. Wiley, New York.

Liebau, F. 1985. *Structural chemistry of silicates, structure, bonding and classification.* Springer-Verlag, New York.

Mason, B., and C. B. Moore. 1982. *Principles of geochemistry.* 4th ed. Wiley, New York.

Nesse, W. D. 2000. *Introduction to mineralogy.* Oxford University Press, New York.

Pauling, L. 1960. *The nature of the chemical bond.* 3rd ed. Cornell University Press, Ithaca, New York.

Pimentel, G. C., and R. D. Spratley. 1969. *Chemical bonding clarified through quantum mechanics.* Holden Day, San Francisco.

Shannon, R. D., and C. T. Prewitt. 1969. Effective ionic radii in oxides and flourides. *Acta Crystallographica* 25: 925–46.

Shannon, R. D. 1976. Revised effective ionic radii and systematic studies of interatomic distances in halides and chalcogenides. *Acta Crystallographica* A32: 751–767.

Silberberg, M. S. 2004. *Chemistry: The molecular nature of matter and change.* 3rd ed. McGraw Hill, New York.

Smyth, J. R., and D. L. Bish. 1988. *Crystal structures and cation sites of the rock-forming minerals.* Allen & Unwin, Boston.

Wells, A. G. 1991. *Structural inorganic chemistry.* 5th ed. Clarendon Press, Oxford, England.

Whitten, K.W., R. E. Davis, M. L. Peck, and G. G. Stanley, 2004. *General chemisty.* 7th ed. Thomson-Brooks/Cole, Belmont, California.

CHAPTER 4

Aspects of Crystal Structures

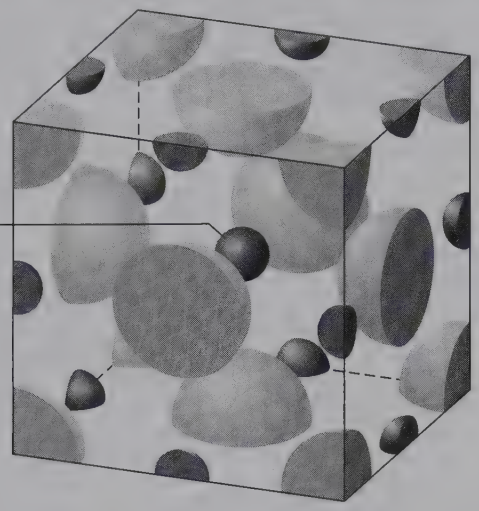

Exploded view of a unit cell of halite, NaCl, showing the location of the central Na^+ ion. In this representation of the unit cell, one can count the total number of ions that make up the unit cell. The Cl^- are located at the eight corners and in the centers of the six faces. That is, 8 corners $\times \frac{1}{8}$ $Cl^- = 1$ Cl^- and 6 faces $\times \frac{1}{2} = 3$ Cl^-, totaling 4 Cl^-. For the Na^+ ions, there is one along each of the 12 edges of the cube (contributing $\frac{1}{4}$ each to the cube) and one whole ion in the center. This totals $12 \times \frac{1}{4}$ $Na^+ = 3$ $Na^+ + 1$ Na^+ (in the center) $= 4$ Na^+. This means that the number of Na^+ ions is also four. This results in a 1:1 ratio for Na^+:Cl^- as required for electrical neutrality. (From Brady, J.E., and G.E. Humiston. 1982. General chemistry. *Wiley, New York. 265.)*

The structure of crystalline materials provides the linkage between the atomic (or ionic) makeup and the macroscopic manifestation of physical features. In the previous chapter, the fundamental building blocks of matter and their electronic properties were reviewed to elucidate how chemical constituents combine. The packing arrangements of the atoms and ions also influence the resulting mineral structure. This chapter discusses major controls on crystal structures; how atoms and ions nestle together in structures and how generalities known as "Pauling's Rules" apply. Methods for illustrating crystal structures as well as a presentation of common structure types, found in nature, follow. Aspects of the external symmetry of crystals, as an expression of their internal atomic arrangement, are discussed subsequently in Chapters 6 and 7.

The structure of crystalline materials is basic to the understanding of many physical properties, such as cleavage, hardness, density, melting point, and optical properties, such as refractive index. And, the inverse also holds true—one can deduce the basic elements of the crystal structure, in part, by observable physical properties, as discussed previously with respect to the bonding of chemical elements (refer to Chapter 3). Understanding a crystal structure also helps to predict aspects of the compositional variations that occur in minerals (see Chapter 5). Our knowledge of atomic and ionic sizes, and of the nature of the chemical bonds in crystals, is derived from the accurate determination of crystal structures.

The chemical bond is a primary parameter of a mineral structure. For ionic and metallic bonding, this bond is assumed to occur between cations and anions that behave as spheres (see Figs. 3.8, 3.12). These spheres are of diverse sizes, representing different elements, and pack together to make a mineral structure. Understanding how variably sized spheres are arranged is a successful approach to explaining controls on crystal structures.

COORDINATION OF IONS

For simplicity, the packing of atoms comprising metals is first discussed. In any given metal consisting of a single element, all atoms are assumed to be the same size and all are spherical in shape based on electron density maps (see Figs. 3.15b, 3.22). These metal atoms pack together in an ordered arrangement that minimizes void space. There are two primary packing arrangements, and the structures are termed collectively, **closest packing**. These structures are based on **hexagonal closest packing** (**HCP**) and **cubic closest packing** (**CCP**).

This is easily illustrated with a tray of identical spheres, such as marbles, ping-pong balls, or tennis

balls. Begin with a layer of spheres on a flat surface. When the spheres are arranged as compactly as possible, each sphere touches six other spheres in a close-packed layer, called a **monolayer**. This layer is labeled *A* (Fig. 4.1a). Between the spheres in the first (*A*) layer, two types of voids are created based on the orientation of their triangular shapes; voids that point up (*B*), and voids that point down (*C*). These voids create two equivalent positions, differing only in orientation, in which a second layer can snuggly fit into the first (lower, *A*) layer. When a second layer is added, nestled within the *B* voids, it is termed the *B* layer. The difference between *hexagonal closest packing* and *cubic closest packing* lies in the position taken by a *third* layer with respect to that of the first two layers.

In **hexagonal closest packing**, the third layer is positioned with the spheres resting in the dimples of the second layer, directly over the first layer (*A*). The spheres alternate between only two positions (*A* and *B*) and this sequence of stacking can be represented by the combination of letters *AB* (Fig. 4.1b). This can be extended upward by another layer of spheres on top of the *B* voids, giving rise to an infinite stacking sequence, *ABABAB*. . . . , which is known as *hexagonal closest pack-*

FIG. 4.1 Closest packing of like-sized spheres (**C.N.** = 12). (a) Monolayer *A* of same size spheres showing six spheres in contact with a central sphere producing two types of voids. (b) Addition of another layer over *B* voids. (c) Addition of a third layer over *C* voids. (d) Oblique vertical view of packing in (c).

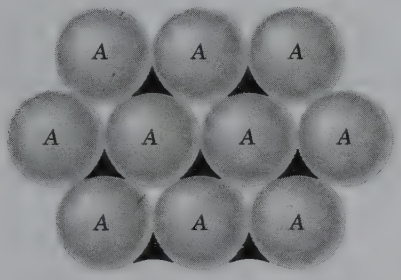

(*a*) Hexagonal closest packed layer

▲ *B* voids

▽ *C* voids

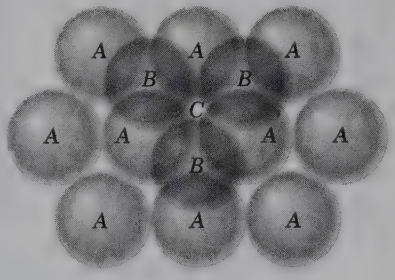

(*b*) Hexagonal closest packing sequence: *AB AB*.....

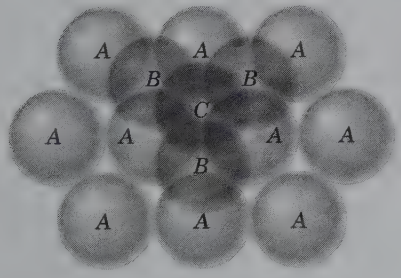

(*c*) Cubic closest packing sequence: *ABC ABC*.....

The plane of this drawing turns out to be perpendicular to the 3-fold axis at the corner of a cube

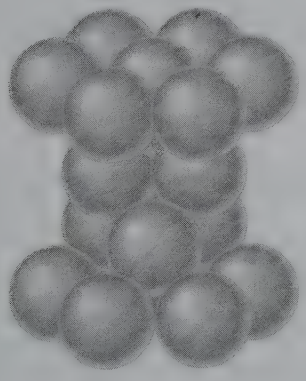

(*d*)

ing (*HCP*). This packing of atoms produces hexagonal symmetry (discussed in Chapter 6).

In **cubic closest packing**, every fourth layer repeats. Here, the third layer is stacked on top of the second layer of the *AB* sequence in the dimples that directly overlie the *C* voids in the first layer. This third layer, *C*, is not equivalent in position to layers *A* or *B* so that a three-layer sequence *ABC* is created, as in Fig. 4.1c. When this stacking sequence repeats infinitely, it results in an *ABCABCABC*. . . . sequence, or *cubic closest packing* (*CCP*).

In both *closest packing* arrangements, each sphere is in contact with 12 other spheres; 6 in the plane of the central sphere and 3 above and 3 below the central sphere (Fig. 4.1d). The atoms are said to coordinate with their nearest neighbors (those in direct contact), and in the case of closest packing, the coordination is described as 12-fold coordination. Atoms or ions must be nearly equal in size to result in 12-fold coordination. Such coordination is rare in minerals, with the exception of the native metals (see Chapter 15). For example, gold, silver, and copper acquire the CCP arrangement. If metal atoms are of similar size, they can substitute for each other in such a structure to form alloys (e.g., gold + silver). Some examples of HCP and CCP are given in Fig. 4.2. (Animations that build both closest packing types—HCP and CCP—can be found in module I of the CD-ROM, by clicking the button "Closest Packing".)

PAULING'S RULES

In both closest packing arrangements, void spaces (interstices) exist. These empty spaces can accommodate smaller spheres. It follows then, that most minerals are composed of numerous elements with various ionic or atomic sizes. The bonding in many of these minerals, such as those between oxygen and other common elements (e.g., Al, Na, K, Ca, Fe, Mg, excluding Si), is primarily ionic (as discussed in Chapter 3). Therefore, to a first approximation, mineral structures may be considered to consist of different size spheres packed tightly together.

In general, it is noted that anions form the closest-packed array, and the smaller cations fill the voids in

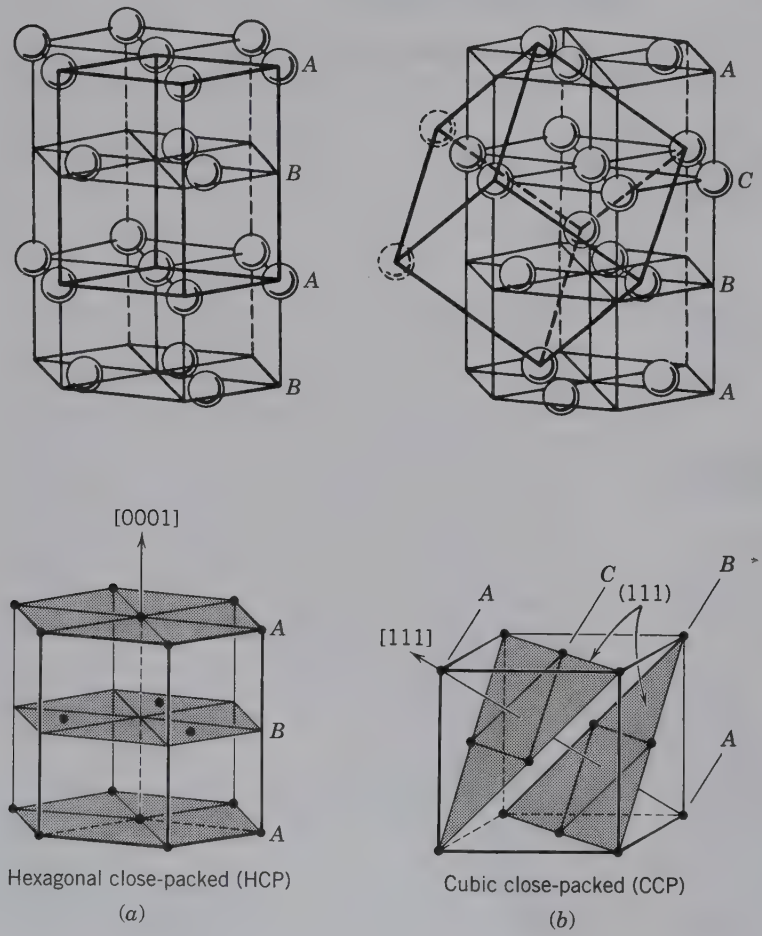

FIG. 4.2 (a) Two representations of a lattice based on hexagonal closest packing (HCP). (b) Two representations of a lattice based on cubic closest packing (CCP).

this closest-packed array. However, it is necessary to know which cations fit into which spaces. Furthermore, what are the nearest neighbor ions (or atoms)? Because of the relatively high symmetry resulting from ionic bonding (see Chapter 3), these bonds are regarded as nondirectional, which allows for the geometric assessment of the packing of variously sized spheres. Linus Pauling addressed many of these questions realizing that every stable crystal structure bears witness to the operation of some broad generalizations that determine the structure of solid matter. These principles were enunciated in 1929 by Pauling in the form of the following five rules, now known collectively as **Pauling's Rules**. (Animations of the rules are presented in module I of the CD-ROM under the heading "Pauling's Rules.")

Rule 1. **The Coordination Principle:** A coordination polyhedron of anions is formed about each cation, the cation-anion distance is determined by the radius sum, and the coordination number (i.e., number of nearest neighbors) of the cation by the radius ratio.

Rule 2. **The Electrostatic Valency Principle:** In a stable crystal structure, the total strength of the valency bonds that reach an anion from all the neighboring cations is equal to the charge of the anion.

Rule 3. **Sharing of Polyhedral Elements I:** The existence of edges, and particularly of faces, common to two anion polyhedra in a coordinated structure, decreases the stability of ionic structures.

Rule 4. **Sharing of Polyhedral Elements II:** In a crystal containing different cations, those of high valence and small coordination number tend *not* to share polyhedral elements with each other.

Rule 5. **The Principle of Parsimony:** The number of essentially different kinds of constituents in a crystal tends to be small.

These rules will now be discussed further.

RULE 1: THE COORDINATION PRINCIPLE

This principle states that the relative sizes of the cation and anion determine how they pack together, or coordinate. *When oppositely charged ions unite to form a crystal structure with dominantly ionic bonding, each ion tends to gather to itself as many ions of opposite sign as size permits.* The ion is said to **coordinate**, and those in contact are its *nearest neighbors*. When atoms are linked by ionic bonds, they approximate spheres, and the resulting geometry of coordination is simple. The coordinated ions always cluster about the central ion in such a way that their centers lie at the apices of a polyhedron (e.g., tetrahedron, octahedron, etc.). Thus, in a stable crystal structure, each cation lies at the approximate center of a **coordination polyhedron** of anions. The cation fits snuggly inside a "house" of anions. The number of anions in the polyhedron, surrounding the cation, is the **coordination number** (**C.N.**) of the cation with respect to the given anion. The largest coordination number is 12 and is described geometrically as a cuboctahedron. Other regular polyhedra are cubes, octahedra, and tetrahedra, in addition to triangles and lines, resulting from coordination numbers of 8, 6, 4, 3, and 2, respectively.

The coordination number, and the resulting geometric arrangement, is a function of the relative sizes of the cation and anion. The relative size of ions is generally expressed as a **radius ratio** (**R.R.**), $= R_A:R_X$, where R_A is the radius of the cation and R_X the radius of the anion (see Table 3.8 for ionic radii). The radius ratio dictates how many anions can fit snuggly around the cation. For example, the radius ratio of sodium and chlorine in halite, NaCl, is:

$R_{Na^+} = 1.02$ Å (for **C.N.** 6)
$R_{Cl^-} = 1.81$ Å (for **C.N.** 6)
$R_{Na^+}:R_{Cl^-} = 1.02/1.81 = 0.56$

The radius ratio of calcium and fluorine in fluorite, CaF_2, is

$R_{Ca^{2+}} = 1.12$ Å (for **C.N.** 8)
$R_{F^-} = 1.31$ Å (for **C.N.** 4)
$R_{Ca^{2+}}:R_{F^-} = 1.12/1.31 = 0.86$

The minimum number for nearest neighbors is not strictly limited. However, the maximum number of coordinating ions is limited by the requirement that the cation must maintain contact with all of the surrounding anions. In accordance with this rule, the cation will bond with as many anions as possible, size permitting. This also keeps bonds equal in strength. In order to evaluate the limits on coordination numbers, and to determine the shape of coordination polyhedra, we begin with a cation (assumed to be a sphere) and gradually increase its radius with respect to that of surrounding anions (of constant size). This allows us to calculate geometric limits for certain coordination types, illustrated in Fig. 4.3. (This same illustration is presented as an animation entitled "Coordination of Ions" in module I of the CD-ROM, and viewing that will clarify the concept.)

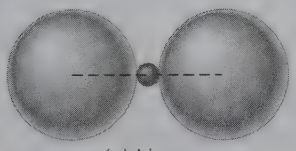

(*a*) Linear

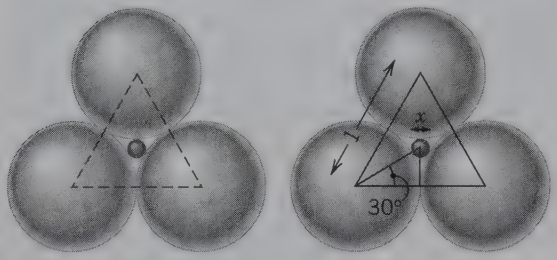

(*b*) Triangular

$$\cos 30° = \frac{\frac{1}{2}}{\frac{1}{2} + \frac{1}{2}x}$$

$$\frac{1}{2} + \frac{1}{2}x = \frac{\frac{1}{2}}{\cos 30°} = \frac{\frac{1}{2}}{0.8660} = 0.5774$$

$$\frac{1}{2}x = 0.5774 - 0.50 = 0.0774$$

$$x = 0.155$$

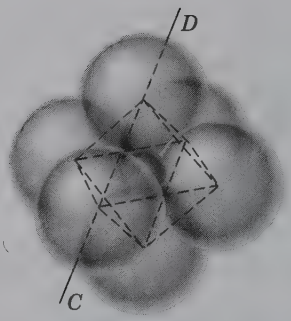

(*d*) Octahedral

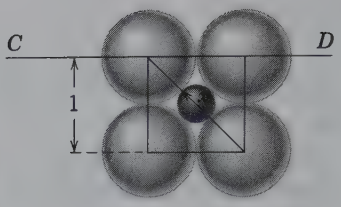

$$(1 + x)^2 = (1)^2 + (1)^2$$

$$1 + x = \sqrt{2} = 1.414$$

$$x = 0.414$$

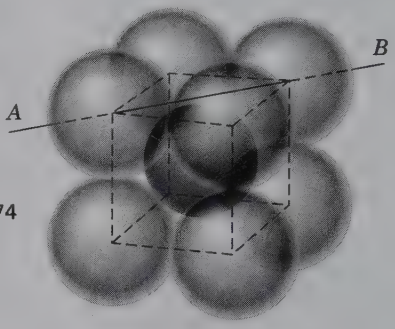

(*e*) Cubic

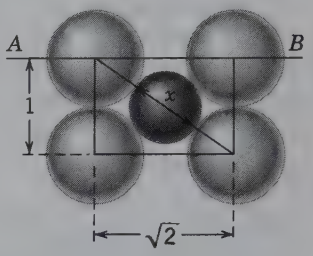

$$(1 + x)^2 = (1)^2 + (\sqrt{2})^2$$

$$1 + x = \sqrt{1 + 2} = 1.732$$

$$x = 0.732$$

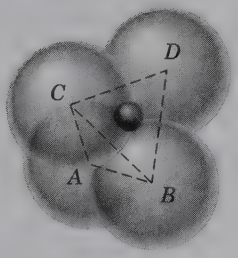

(*c*) Tetrahedral

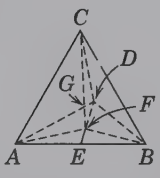

G is location of center of small ion, in center of tetrahedron

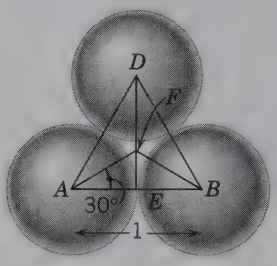

In base triangle

$$\cos 30° = \frac{AE}{AF}$$

$$\therefore AF = \frac{AE}{\cos 30°} = \frac{\frac{1}{2}}{\cos 30°}$$

$$= \frac{1}{2} \cdot \frac{2}{\sqrt{3}} = \frac{1}{\sqrt{3}}$$

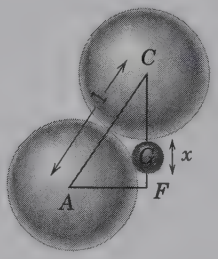

In vertical triangle CAF

$$CF = \sqrt{AC^2 - AF^2} =$$

$$\sqrt{(1)^2 - \left(\frac{1}{\sqrt{3}}\right)^2} = \sqrt{1 - \frac{1}{3}}$$

$$\sqrt{\frac{2}{3}} = .81649$$

Also $CG = \frac{3}{4}\ CF$, because center of tetrahedron *G* is $\frac{1}{4}\ CF$ from the base.

Furthermore $CG = \frac{1}{2} + \frac{1}{2}x$

$$\therefore \frac{1}{2} + \frac{1}{2}x = \frac{3}{4} \cdot .81649 = .6124$$

$$\therefore \frac{1}{2}x = .6124 - .5 = .1124$$

$$x = 0.225$$

2-Fold Coordination

The smallest coordination number is 2-fold coordination or **linear coordination** (Figs. 4.3a, 4.4). The cation only maintains contact with two anions. Here, the radius ratio is less than 0.155. Linear coordination is very rare in ionically bonded crystals. Examples are the uranyl group $(UO_2)^{2+}$, the nitrite group $(NO_2)^-$, and copper with respect to oxygen in cuprite, Cu_2O.

3-Fold Coordination

With an increase in the relative size of the central ion, three anions can fit around the central ion and **triangular coordination**, or 3-fold coordination, becomes stable. **C.N.** = 3 occurs between the radius ratio limits of 0.155 and 0.225 (Figs. 4.3b, 4.4). The centers of the anions form an equilateral triangle. Triangular coordination is common in minerals, such as those with CO_3, NO_3, and BO_3 groups.

4-Fold Coordination

When R_A:R_X becomes 0.225, four anions touch each other and the central cation. This results in a changeover from triangular coordination to 4-fold coordination (Figs. 4.3c, 4.4). The centers of the anions are at the corners of a tetrahedron, thus, 4-fold coordination is termed **tetrahedral coordination**.

Expanding the cation further (in tetrahedral coordination), results in the anions continuing to touch the central cation but not each other. Tetrahedral coordination is possible over the range of radius ratios from 0.225 to 0.414 (Fig. 4.4). Four-fold coordination is common in minerals and is typified by the SiO_4 group in silicates, and by the sphalerite, ZnS, and diamond structures.

6-Fold Coordination

When R_A:R_X reaches 0.414, 6-fold coodination becomes stable. The centers of the coordinated ions lie at the corners of an octahedron, thus, it is termed **octahedral coordination**. Remember, an octahedron has eight faces but only six apices, hence the **C.N.** is 6 (Figs. 4.3d, 4.4). Four anions are arranged in a square surrounding the central cation, and in addition, there is one anion above and one anion below, equaling six anion neighbors. At the radius ratio value of 0.414, the six coordinated anions touch each other and the central cation. The upper limit for 6-fold coordination turns out to be R_A:R_X = 0.732 (Fig. 4.3d). Therefore, **C.N.** = 6 occurs when the radius ratio lies between 0.414 and 0.732. Na and Cl in halite, Ca and O in calcite, and many cations in silicates are examples of 6-fold coordination.

8-Fold Coordination

When the radius ratio value reaches 0.732, eight anions touch each other as well as the central cation and 8-fold coordination results. The coordinating ions lie at the eight corners of a cube (Figs. 4.3e, 4.4), thus, 8-fold coordination is termed **cubic coordination**. Allowing the radius of the cation to increase further, such that its radius becomes equal to that of the anions, gives rise to a radius ratio value of 1.0, which is the stable ratio for 12-fold coordination. Consequently, cubic coordination occurs most commonly for radius ratios between 0.732 and 1.0.

An example of 8-fold coordination (as a distorted cube) is found in the *M2* crystallographic site of monoclinic pyroxenes (see Fig. 18.16). This site commonly houses relatively large cations, such as Ca^{2+} and Na^+.

12-Fold Coordination

When the anions and cations have similar sizes, the radius ratio is approximately 1.0, and 12-fold coordination is stable. Each cation can now be in contact with 12 anions (see Fig. 4.1). Two different packing sequences occur, HCP and CCP (Figs. 4.2 and 4.5), with **C.N.** = 12 (as discussed earlier.)

FIG. 4.3 Illustration of the geometric derivation of limiting ratios for R_A (cation) : R_X (anion) as a function of coordination (number). Note that the central cation gradually increases in size in going from (a) to (e), whereas the surrounding anions remain constant in size. The *x* is the diameter of the cation that increases in size from (a) to (e). (a) *Linear* or 2-fold coordination of anions around a cation. The radius of the cation may be minute and can range upward to a maximal size predicted by the R_A: R_X, 0.155, as derived for triangular coordination. (b) *Triangular* or 3-fold coordination of anions about a cation. The limiting value for the changeover from linear to triangular coordination is shown to be at R_A: R_X = 0.155. (c) *Tetrahedral* or 4-fold coordination of anions about a cation. The limiting value for the changeover from triangular to tetrahedral coordination is shown to be at R_A:R_X = 0.225. (d) *Octahedral* or 6-fold coordination of anions about a cation. The limiting value for the changeover from tetrahedral to octahedral coordination is shown to be at R_A:R_X = 0.414. (e) *Cubic* or 8-fold coordination of anions about a cation. The limiting value for the changeover from octahedral to cubic coordination is shown to be at R_A:R_X = 0.732.

Minimum Radius Ratio $R_A : R_X$	*Coordination Number* C.N.	*Packing Geometry*
< 0.155	2	Linear
0.155	3	Corners of an equilateral triangle (triangular coordination)
0.225	4	Corners of a tetrahedron (tetrahedral coordination)
0.414	6	Corners of an octahedron (octahedral coordination)
0.732	8	Corners of a cube (cubic coordination)
1.0	12	Corners of a cuboctahedron (close packing)

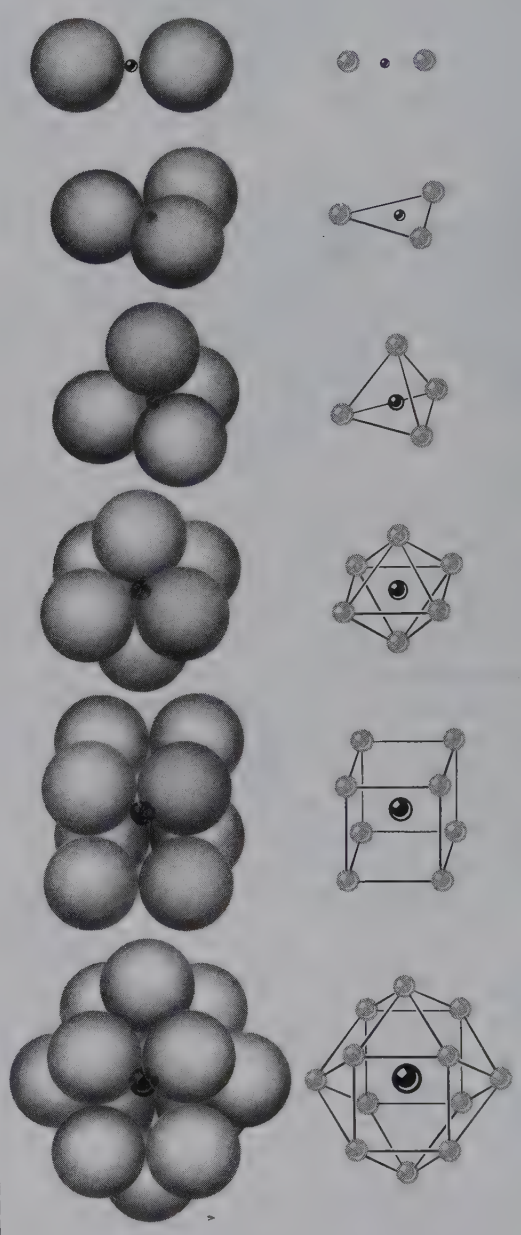

FIG. 4.4 Atomic packing schemes.

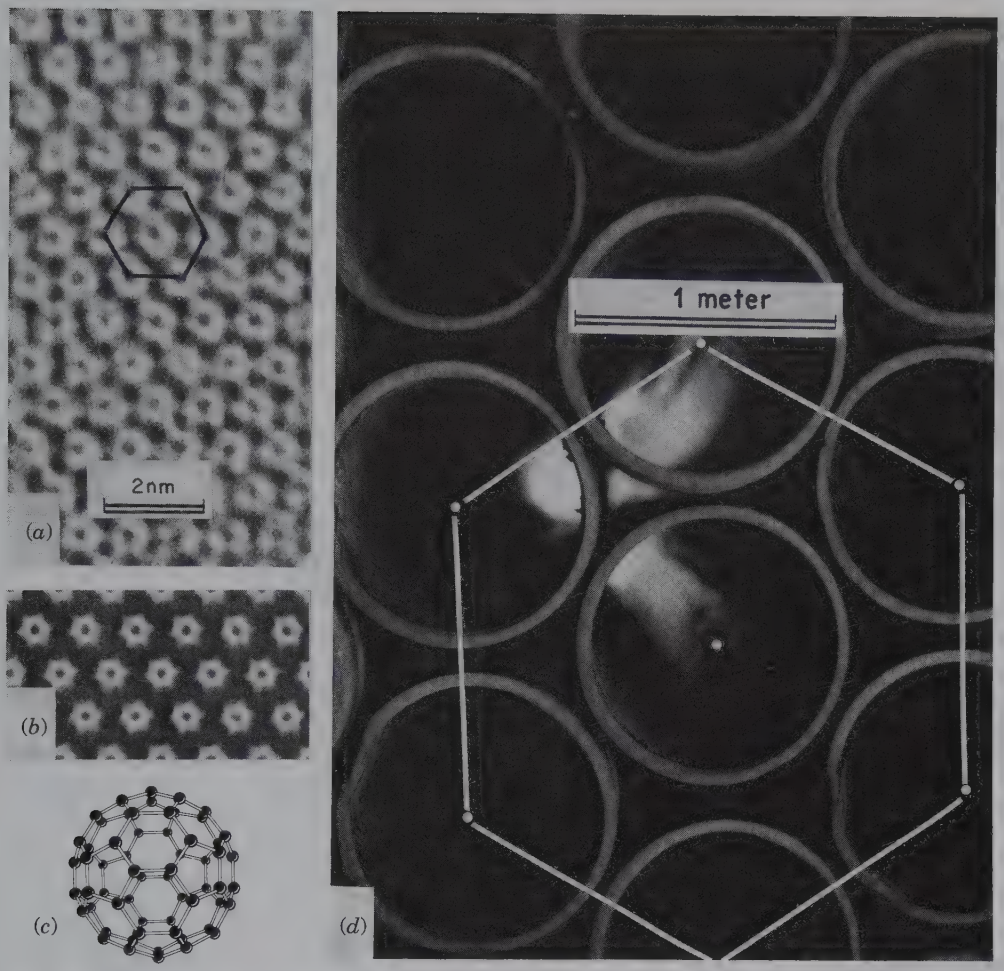

FIG. 4.5 Examples of hexagonal closest packing (HCP). (a) The hexagonal closest packing of C_{60} molecules ("buckminsterfullerene") as revealed by high-resolution transmission electron microscopy (HRTEM). These complex carbon molecules are of synthetic origin and have not been found in nature. Scale is in nanometers (nm): 1 nm = 10 Å. (For further discussion, see Curt, R. F., and R. E. Smalley. 1991. Fullerenes. *Scientific American* 265: 54–63.) (b) A computer calculated image that replicates the observed structure image in (a). (a and b from Wang, S., and P. R. Buseck. 1991. Packing of C_{60} molecules and related fullerenes in crystals: A direct view. *Chemical Physics Letters* 182: 1–4). (c) Illustration of the structure of C_{60} "buckminsterfullerene," named after the American engineer and philosopher R. Buckminster Fuller because of his invention of the geodesic dome that underlies the structure of C_{60}. (d) Hexagonal closest packing on a very large scale, as seen in everyday life when steel, concrete, or plastic pipes are stacked.

Other Coordination Geometries

Other coordination numbers are known, such as 5-, 7-, 9-, and 10-fold coordination. An example of 5-fold coordination is found in the mineral andalusite, Al_2SiO_5. Such coordination numbers are possible only in complex structures in which the anions are not closely packed, which results in distortions of the regular polyhedra. These geometries can also be related to bonds containing substantial covalent character, thus, leading to directional distortions.

The coordination polyhedra, as determined by X-ray structure analysis, are almost always distorted. The smaller and more strongly polarizing the coordinating cation, or the larger and more polarizable the anion, the greater the distortion and the wider the departure from the theoretical radius ratio limits. Also, *if the bonding mechanism is not dominantly ionic, radius ratio considerations may not be adequately used to determine the coordination number.*

Coordination of Common Cations

The most common ionic charges, coordination polyhedra, and ionic sizes of the 11 most common elements in the Earth's crust are given in Table 4.1. These coordination numbers and polyhedra are helpful in understanding mineral structures as well as various aspects of

Table 4.1 Some Common Ions (Exclusive of Hydrogen) That Occur in Rock-Forming Minerals, Arranged in Decreasing Ionic Size

Ion	Coordination Number with Oxygen		Ionic Radius in Å
O^{2-}			1.36 [3]
K^+	8–12		1.51 [8]–1.64 [12]
Na^+	8–6	cubic to	1.18 [8]–1.02 [6]
Ca^{2+}	8–6	octahedral	1.12 [8]–1.00 [6]
Mn^{2+}	6		0.83 [6]
Fe^{2+}	6		0.78 [6]
Mg^{2+}	6	octahedral	0.72 [6]
Fe^{3+}	6		0.65 [6]
Ti^{4+}	6		0.61 [6]
Al^{3+}	6		0.54 [6]
Al^{3+}	4		0.39 [4]
Si^{4+}	4	tetrahedral	0.26 [4]
P^{5+}	4		0.17 [4]
S^{6+}	4		0.12 [4]
C^{4+}	3	triangular	−0.08 [3]

*The first column lists the most common ionic (valency) states of the elements. The second column lists their most common coordination with respect to oxygen, and the third column lists ionic sizes for specific coordinations (the number in square brackets is **C.N.**). A complete listing of elemental abundances is given in Table 5.1.

compositional variation in minerals (see Chapter 5 for details).

RULE 2. THE ELECTROSTATIC VALENCY PRINCIPLE

This rule is a statement of bond strength. The strength of an electrostatic bond (e.v.) may be defined as an ion's valence charge (Z) divided by its coordination number (**C.N.**):

$$\text{Bond strength (e.v.)} = Z/\textbf{C.N.}$$

expressed as an absolute value. The resulting number, called the **electrostatic valency (e.v.)**, is a measure of the strength of any of the bonds that reach the coordinating ion from its nearest neighbors. For instance, in NaCl, the Cl^- is surrounded by six Na^+ neighbors in octahedral coordination. Therefore, using the formula above, each of the bonds reaching Na^+ has a strength (e.v.) of $\frac{1}{6}$. This means that six bonds between a central Na^+ and six octahedrally coordinated closest neighbors of Cl^- completely and exactly neutralize the charge on the central Na^+ (Fig. 4.6*a*). The Cl^- also has six neighbors (Na^+), so that the e.v. for each of the bonds reaching Cl^- is also $\frac{1}{6}$. As such, the charge on the $Cl^-(1^-)$ is neutralized by six bonds of $\frac{1}{6}$ $(6 \times \frac{1}{6} = 1)$ reaching the central ion from six (octahedrally coordinated) Na^+ ions. Figures 4.6b and c give examples of electrostatic

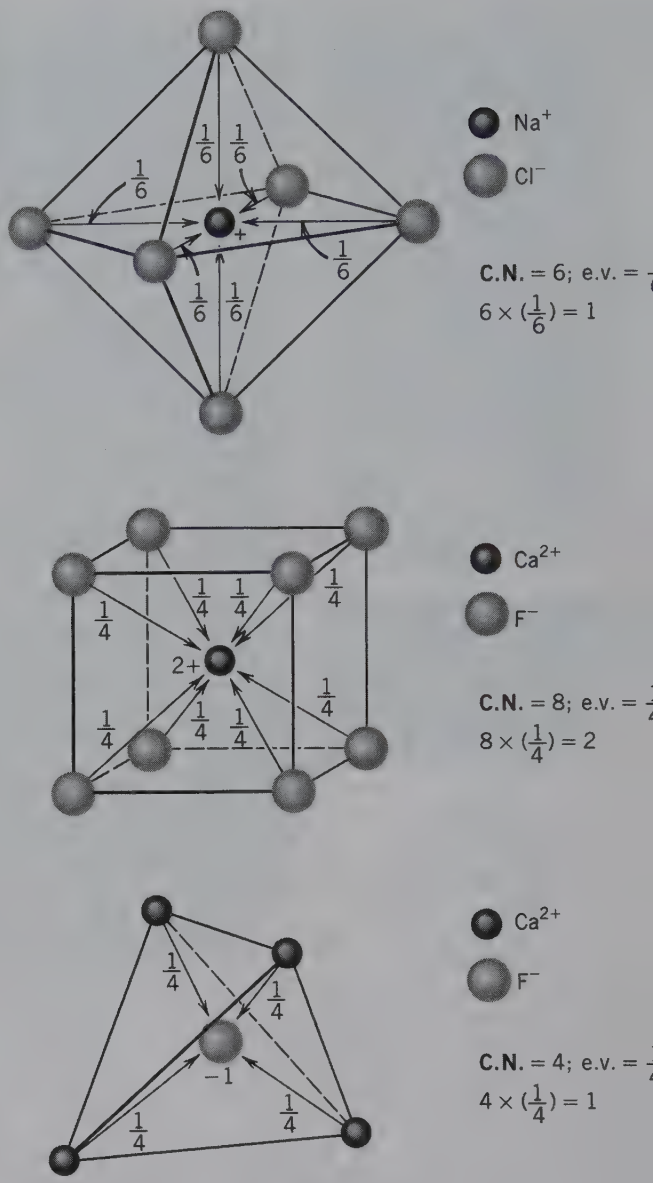

FIG. 4.6 Illustration of the neutralization of a central ion by bonds from nearest neighbors. Each of these bonds has an electrostatic valency (e.v.). The total of all bonds with specific e.v.s neutralizes the central ion. (a) Octahedral coordination in the halite structure (see Figs. 4.10a, 4.17b). (b) Cubic coordination of F^- around Ca^{2+} in the fluorite structure (see Figs. 4.10b, 4.20). (c) Tetrahedral coordination of Ca^{2+} around F^- in the fluorite structure (see Figs. 4.10b, 4.20).

valencies in additional coordination polyhedra. (Animations of this concept are given in module I of the CD-ROM under the heading "Pauling's Rules: Rule 2.")

The electrostatic valency rule is very helpful in evaluating the nature of crystal structures. In a stable structure, the sum of the electrostatic valencies from cations in coordination polyhedra exactly balances the charge on the anion that is shared among these coordi-

nation polyhedra. For example, in the structure of grossular garnet ($Ca_3Al_2Si_3O_{12}$), Ca^{2+} is in cubic coordination (**C.N.** = 8), Al^{3+} is in octahedral coordination (**C.N.** = 6), and Si^{4+} is in tetrahedral coordination (**C.N.** = 4), all of them with oxygen. Their bonds, therefore, have electrostatic valencies of $\frac{2}{8} = \frac{1}{4}$, $\frac{3}{6} = \frac{1}{2}$, and $\frac{4}{4} = 1$, respectively. In order to neutralize the 2^- charge on a shared oxygen, that oxygen ion must belong to *two* cubic Ca^{2+} polyhedra, *one* Al^{3+} octahedron, and *one* Si^{4+} tetrahedron ($2 \times \frac{1}{4} + \frac{1}{2} + 1 = 2$). Such is the linkage of coordination polyhedra in grossular garnet.

Uniform Bond Strength

Crystals in which all bonds are of equal strength are called **isodesmic**. This is the case for ionically bonded crystals that have a single cation and anion (e.g., NaCl). This may also be true for those with multiple cations and/or anions. Some unexpected results emerge from calculation of electrostatic valencies for isodesmic minerals. For example, minerals of the spinel group have a general formula of the type AB_2O_4, where A is a divalent cation, such as Mg^{2+} or Fe^{2+}, and B is a trivalent cation, such as Al^{3+} or Fe^{3+}. Such compounds have been called aluminates and ferrates, by analogy with such compounds as borates and oxalates. This nomenclature suggests that ionic clusters, or radicals, are present in the structure. Studies reveal that the A ions are in 4-fold coordination, whereas the B ions are in 6-fold coordination with oxygen. Hence, for the A ions, e.v. $= \frac{2}{4} = \frac{1}{2}$, and for B ions, e.v. $= \frac{3}{6} = \frac{1}{2}$. All bonds are of the same strength, and such crystals are isodesmic multiple oxides.

Nonuniform Bond Strength

When small, highly charged cations coordinate larger and less highly charged anions, compact, firmly bonded groups result; these are termed **radicals**. If the strength of the bonds within such groupings is calculated, the numerical value of the electrostatic valency is always greater than one-half the total charge on the anion. This means that in such groups, the anions are more strongly bonded to the central coordinating cation than to any other ion (because more than half of the charge is satisfied). For example, in the carbonate group, $(CO_3)^{2-}$, C^{4+} is in 3-fold coordination with O^{2-}. From the previously mentioned formula for bond strength, e.v. $= \frac{4}{3} = 1.33$. This value is greater than one-half the charge on the oxygen ion (2^-) leaving only 0.67 e.v. (2.0 e.v. − 1.33 e.v. = 0.67 e.v.) to bond with other cations. Therefore, a radical exists, the carbonate triangle, which is a basic structural unit of carbonate minerals (Fig. 4.7a). The mineral cleaves through the weaker bonds leaving the radical intact. Another example is the sulfate group, $(SO_4)^{2-}$. O^{2-} is in 4-fold coordination with S^{6+}; hence the e.v. $= \frac{6}{4} = 1.5$. Because this

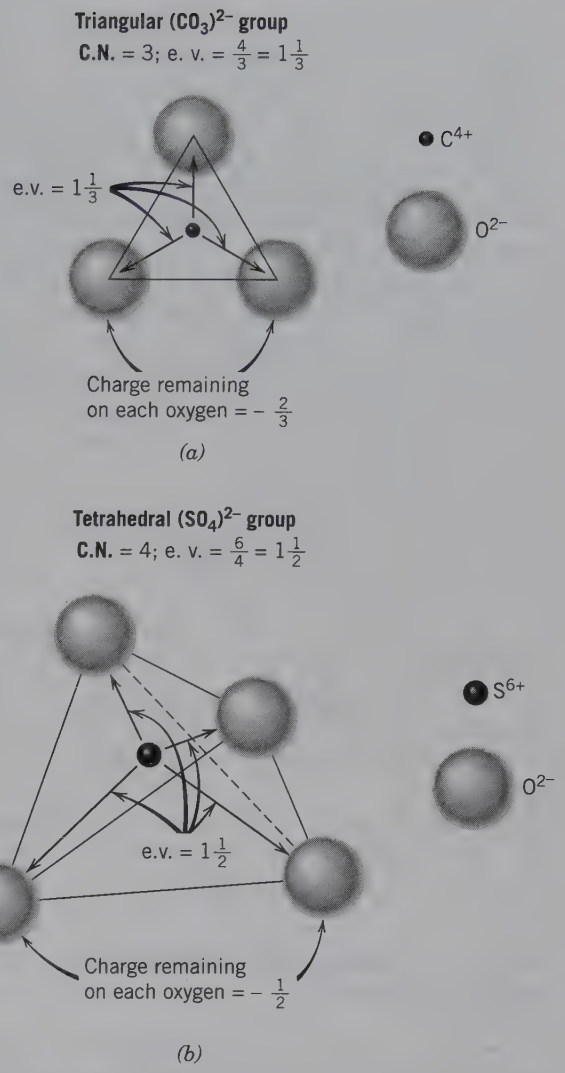

FIG. 4.7 Examples of polyhedral anionic groupings about a central cation, in which the electrostatic valency that the central cation contributes to each coordinating anion, is greater than half the anion's charge. Therefore, the anion is more tightly bonded to the central cation than it can be to any other cation in the structure. These discrete bonding units (or complex ions or radicals) occur in what are known as anisodesmic structures.

is also greater than one-half the charge on the oxygen ion, the sulfate radical forms a tightly knit group, and oxygen is more strongly bonded to sulfur (1.5 e.v.) than it can be bound to any other ion in the structure (0.5 e.v.). This is the tetrahedral unit (Fig. 4.7b), which is the fundamental unit of the sulfate structure. These strongly bonded units remain together during melting or dissolution of the mineral. In simple compounds, such as calcite, $CaCO_3$, all Ca to $(CO_3)^{2-}$ group bonds are of one strength, and the C–O bonds are of another. Such crystals are called **anisodesmic** because they contain bonds of differing strengths. In calcite, there are

strong C–O bonds and weaker Ca to $(CO_3)^{2-}$ group bonds. In barite, $BaSO_4$, there are strong S–O bonds and weaker Ba to $(SO_4)^{2-}$ group bonds.

When the strengths of bonds between the central cation and its coordinating anions equal exactly half the charge of the anion, the term **mesodesmic** is used. In this case each anion may be bonded to some other unit in the structure just as strongly as it is to the coordinating cation. The other unit may be an identical cation, and the anion shared between two cations may enter into the coordination polyhedra of both. For example, consider silicon-oxygen groupings, in which the oxygens are in tetrahedral coordination about the central Si^{4+} in every group. The e.v. of the bonds between O^{2-} and Si^{4+} is $\frac{4}{4} =$ 1 e.v. This is half the bonding strength available from the oxygen ion (2^-). Consequently, a SiO_4 tetrahedron may link to some other ion just as strongly as to the central Si^{4+} ion. If this ion is another Si^{4+}, two tetrahedra may combine, linked through a common oxygen to form a single $(Si_2O_7)^{6-}$ group. Similarily, SiO_4 tetrahedra may join, or **polymerize**, to form chains, sheets, or networks by sharing oxygen ions (Fig. 4.24). The most important examples of mesodesmic minerals are the silicates and the tetrahedral linkages found within this group.

All ionic crystals may be classified on the basis of the relative strengths of their bonds into isodesmic, anisodesmic, or mesodesmic structures.

RULE 3. SHARING OF POLYHEDRAL ELEMENTS, PART 1

The existence of edges, and particularly of faces, common to two anion polyhedra in a coordinated structure, decreases its stability (Fig. 4.8). This, in effect, is a reminder that cations like to be as far apart as possible because of cation repulsion. Recall that every ion in a crystal structure has some effect on every other ion—it is attracted if the charges are opposite, repulsed if the charges are the same. As such, ions tend to group themselves in crystal structures so that cations are as far apart as possible, yet consistent with a coordination of the anions that results in electrical neutrality. Thus, when cations share anions between them, they do so in such a way as to place themselves as far apart as possible. Consequently, the coordination polyhedra formed around each are linked commonly through corners and edges of the polyhedra but generally not through faces (Fig. 4.8). This is because sharing a face would put similarly charged ions too close together.

This effect is large for cations with high valency and small coordination number (e.g., C^{4+} in 3-fold coordination) and is especially large when the radius ratio approaches the lower limit of stability of the polyhedron. When coordination polyhedra share corners, the cations are farthest apart, followed by sharing an edge. When polyhedra share faces, the cations are moved close together, thus, decreasing the stability of the structure.

For example (shown in Fig. 4.8), if two octahedra are linked through a shared oxygen, the maximum distance separating the cation centers may be taken as 1.0. If they share edges, this distance drops to 0.71. If the octahedra share faces, the center-to-center distance is reduced to 0.58. However, this is much larger than the distance between centers of cations for shared tetrahedra, at 0.33. (Animations of these concepts are found in module I of the CD-ROM under the heading "Pauling's Rules: Rule 3.")

RULE 4. SHARING OF POLYHEDRAL ELEMENTS, PART 2

In a crystal containing different cations, those of high valence (charge) and small coordination number tend *not* to share polyhedral elements with each other. This maintains maximum distance between cations, as in Rule 3 (shown in Fig. 4.8). An additional consideration follows from Rule 2. Small, highly charged cations form low-coordination number anionic groups where more than half of the charge is neutralized within the group [e.g., $(CO_3)^{2-}$, $(PO_4)^{3-}$ groups]. Therefore, the oxygens can only bond with low valence cations in coordination polyhedra that are larger. This accounts for the lack of two Al–O tetrahedra bonding, through a bridging oxygen, in many silicates. The Al^{3+}–O bond in tetrahedral coordination has an e.v. $= \frac{3}{4}$. If there were a bridging oxygen between two (AlO_4) tetrahedra, it would receive *only* $2 \times \frac{3}{4} = 1.5$ e.v, and the O^{2-} would not be satisfied.

When sharing of edges occurs, the shared edge contracts (to reduce the repulsive charge between the cations), and the cations are displaced from their polyhedral centers, away from the shared edge (or face). (Animations of this concept are found in module I of the CD-ROM under the heading "Pauling's Rules: Rule 4.")

Rules 1 through 4 all reflect the tendency of crystal structures to maximize cation-anion attractions and to minimize anion-anion and cation-cation repulsion.

RULE 5. THE PRINCIPLE OF PARSIMONY

The number of essentially different kinds of constituents in a crystal tends to be small because, characteristically, there are only a few types of contrasting

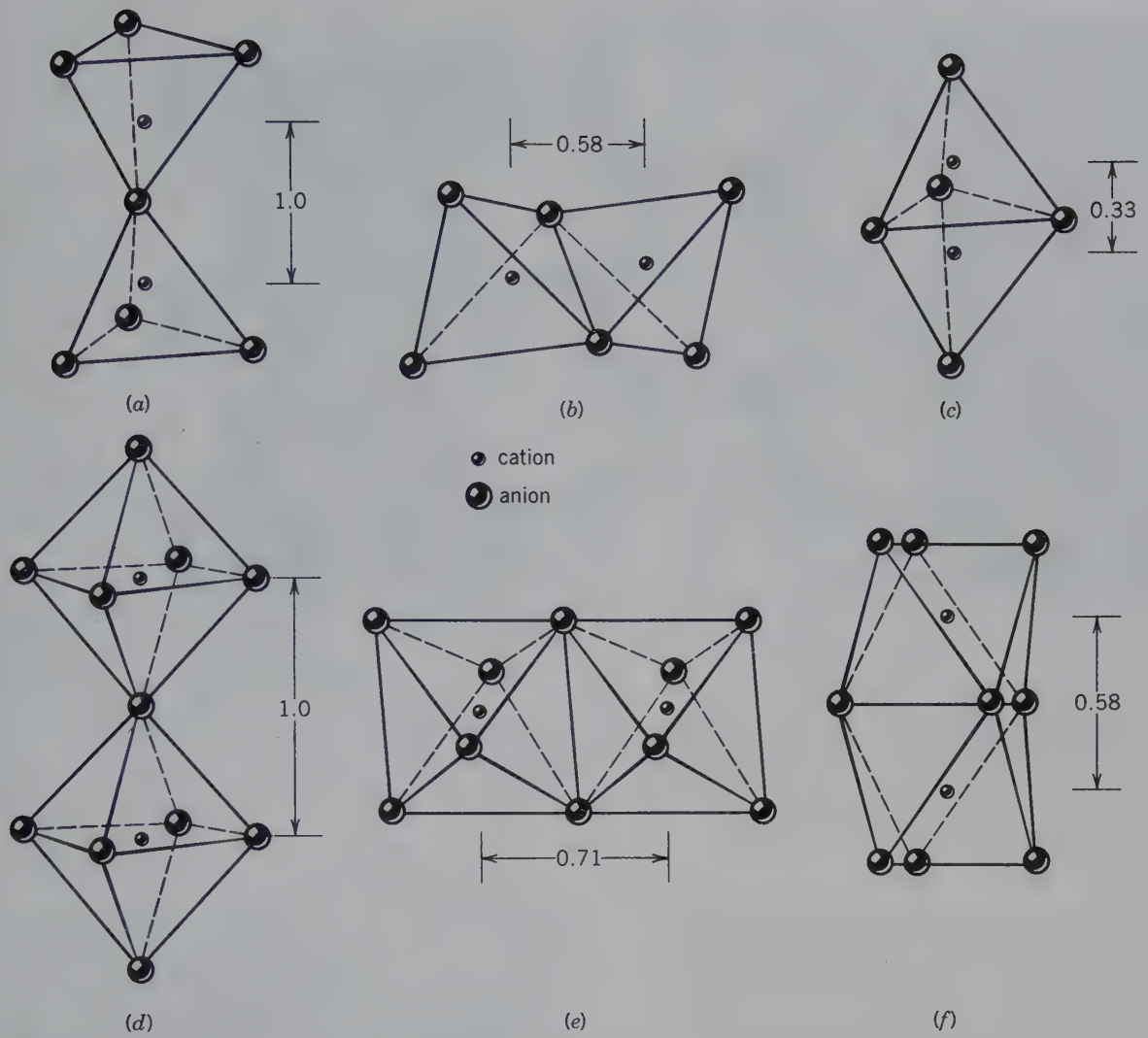

FIG. 4.8 (a) Tetrahedra sharing corners, as is commonly found in crystal structures. Here the cation-cation distance is given as 1.0. (b) Tetrahedra sharing edges; very uncommon. The cation-cation distance is reduced from 1.0 to 0.58. In this case cation-cation repulsion would occur, causing severe polyhedral distortion. (c) Tetrahedra sharing faces; this is never found when both tetrahedra are occupied by a cation. The cation–cation distance is reduced to 0.33 from 1.0 (in a) and 0.58 (in b). (d) Octahedra sharing corners, as is common in crystal structures. The cation-cation distance is given as 1.0. (e) Octahedra sharing edges is also common. The cation-cation distance is reduced to 0.71 (but the cations are still considerably farther apart than in the case of tetrahedra sharing edges; see b). (f) Octahedra sharing faces; this is not uncommon in crystal structures. The cation-cation distance is reduced to 0.58 from 1.0 (in d) and 0.71 (in e). Face-sharing of octrahedra is possible because the cation-cation distance is larger for octahedra than tetrahedra. Furthermore, cations in octahedral coordination tend to have lower charges (e.g., Mg^{2+}, Fe^{2+}) than cations in tetrahedral coordination (e.g., Si^{4+}, Al^{3+}). Therefore, the repulsive force between cations inside octahedra is generally less than that between cations inside tetrahedra.

cation and anion *sites*. Thus, in structures with complex chemical compositions, a number of different ions may occupy the same structural position (site). These ions are then considered as a single "constituent." This phenomenon leads to what is termed solid solution, discussed in detail in the next chapter.

This "rule" can be illustrated with respect to the polyhedral representation of the amphibole structure (Fig. 4.9; and also in module I of the CD-ROM under the heading "Pauling's Rules: Rule 5"). Amphiboles have a limited number of different crystallographic sites, but their range of chemical constituents is large. Figure 4.9

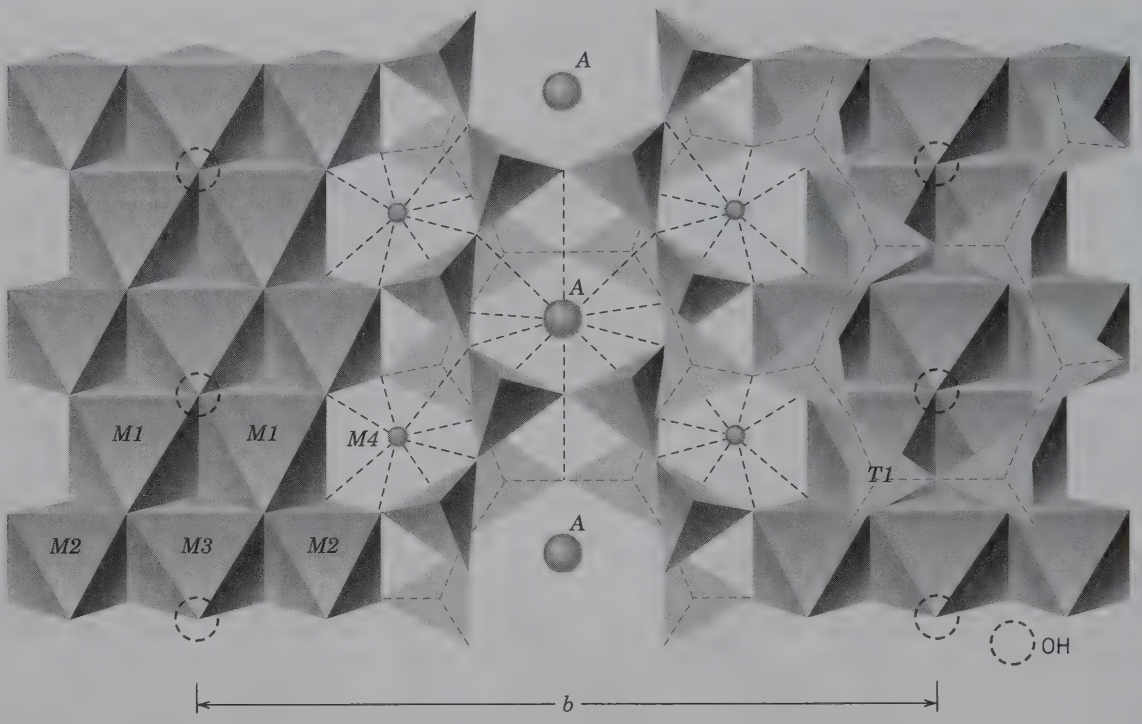

FIG. 4.9 Polyhedral representation of the structure of monoclinic amphibole projected down the *a*-axis. Polyhedral sites are marked as follows: *T1* and *T2* = tetrahedral; *M1*, *M2*, and *M3* = regular octahedral; *M4* = distorted cubic; *A* is in irregular coordination of 10 to 12 neighboring oxygens and (OH); (OH) notes the specific location of hydroxyl in the structure. (After J. J. Papike et al. 1969. *Mineralogical Society of America, Special Paper*, 2: 120.)

shows the presence of tetrahedral *T* sites (labeled *T1* and *T2*), octahedral *M* sites (labeled *M1*, *M2*, and *M3* because of slightly different octahedral sizes and shapes), an *M4* site (with irregular 8-fold coordination), a large and irregularly coordinated *A* site, and the location of $(OH)^-$ groups. The tetrahedral sites will accommodate Si^{4+} and Al^{3+}. The *M1*, *M2*, and *M3* sites house Mg^{2+}, Fe^{2+}, Mn^{2+}, Al^{3+}, Fe^{3+}, and Ti^{4+}. The *M4* sites can contain Mg^{2+}, Mn^{2+}, Fe^{2+}, Ca^{2+}, and Na^+. The *A* site may be occupied by Na^+ or K^+, and the $(OH)^-$ location also holds Cl^- and F^-. Therefore, 13 different ions may be distributed among only five distinctly different crystallographic sites [tetrahedral, regular octahedral, distorted cubic, the large *A* site, and the (OH) location]. (An interactive approach to the cation distribution in an amphibole structure is provided in module I of the CD-ROM. You can locate this by clicking on the button "Solid Solution Mechanisms" and subsequently the button "Substitutional Solid Solution in Amphiboles.")

Additional Controls on Mineral Structures

Anions may also be regarded as occupying the centers of coordination polyhedra formed by cations. In NaCl, each chloride ion has six sodium neighbors and is in 6-fold coordination with respect to sodium. Because both sodium and chlorine are in 6-fold coordination, there must be equal numbers of both, in agreement with the formula, NaCl. On the other hand, in the fluorite structure, each fluorine ion has four closest calcium neighbors and is in 4-fold coordination with respect to calcium (**C.N.** = 4). Although these four calcium ions do not touch each other, they form a definite coordination polyhedron about the central fluorine ion in such a way that the calcium ions lie at the apices of a regular tetrahedron (Fig. 4.10b). Because each calcium ion has eight fluorine neighbors (**C.N.** = 8), whereas each fluorine ion has only four calcium neighbors, there are twice as many fluorine as calcium ions in the structure and, therefore, the formula is CaF_2. In fluorite, only half the possible calcium sites are filled. This leads to an important restriction in crystal structures; *the total number of ions of all kinds in any stable ionic crystal structure must be such that the crystal as a whole is electrically neutral.* That is, the total number of positive charges must equal the total number of negative charges; therefore, in fluorite there can be only half as many divalent positive calcium ions as there are monovalent fluorine ions.

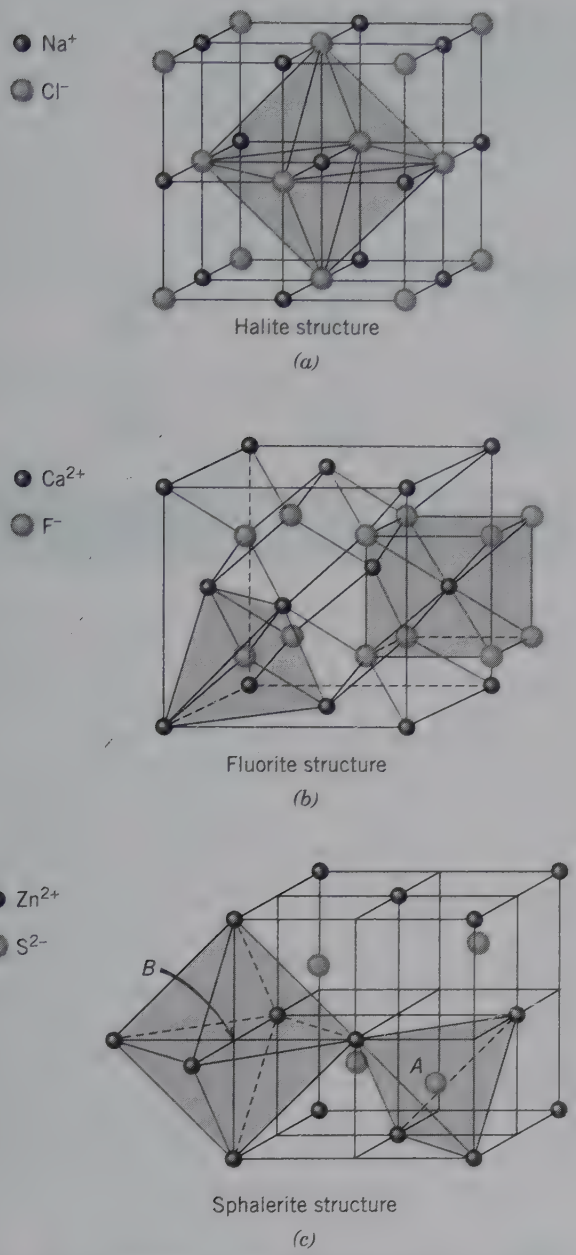

FIG. 4.10 Visualization of coordination polyhedra in various mineral structures represented by "ball and stick" structure drawings. (a) The halite, NaCl, structure where the ions are positioned in a cubic arrangement (with overall isometric symmetry). Both Na^+ and Cl^- are in 6-fold coordination (**C.N.** = 6) with each other. A coordination polyhedron about Na^+ is shown; it is an octahedron. (b) The fluorite, CaF_2, structure with overall isometric symmetry. Each Ca^{2+} is coordinated to eight neighboring F^- (**C.N.** = 8); this arrangement is a cube in shape. F^-, however, is coordinated only to four Ca^{2+} cations (**C.N.** = 4); this is tetrahedral in shape. (c) The sphalerite, ZnS, structure with overall isometric symmetry. Each S^{2-} (in position marked *A*) is surrounded by four Zn^{2+} ions, in tetrahedral coordination (**C.N.** = 4). The position marked *B* is empty and has octahedral surroundings.

ISOSTRUCTURALISM

Although it might seem that uraninite, UO_2, and fluorite, CaF_2, would have little in common, their structures are alike, but the spacings between the atoms are different. Structure analysis of uraninite reveals that there are four U^{4+} ions around each oxygen, whereas eight O^{2-} are grouped about each uranium. In fluorite, four Ca^{2+} are grouped about each fluorine, and eight F^- are packed about each calcium (Fig. 4.10b). These two substances are said to be **isostructural** or *isotypous*, because they express the same structure type. Occasionally the term *isomorphism* is used instead of *isostructuralism*, but this is not recommended.

Crystals in which the centers of the constituent atoms occupy geometrically similar positions, regardless of the size of the atoms or the absolute dimensions of the structure, are said to *belong to the same structure type*. For example, all isometric crystals in which there are equal numbers of cations and anions in 6-fold coordination belong to the NaCl (halite) structure type. Many minerals of diverse composition belong to this structure type. A few are: KCl, sylvite; MgO, periclase; PbS, galena; MnS, alabandite; AgCl, chlorargyrite; and TiN, osbornite.

The two minerals stishovite, SiO_2, and rutile, TiO_2, are also isostructural. In both structures, the cation (Si^{4+} or Ti^{4+}) is surrounded by six oxygen neighbors in octahedral coordination. In other known forms of SiO_2 (including quartz), as well as all other silicates found in the Earth's crust, silicon is surrounded by four neighboring oxygens, in tetrahedral coordination. Stishovite is a very high pressure polymorphic form of quartz, showing that higher coordination numbers commonly reflect higher pressures of origin (see discussion that accompanies Fig. 5.4).

Isostructural groups are groups of minerals related to each other by analogous structure, generally having a common anion but different cations. These groups commonly display extensive ionic substitution. Many groups of minerals are isostructural. Perhaps the best examples are the barite group of sulfates, the calcite group of carbonates, and the aragonite group of carbonates. The extremely close relationship that exists among the members of many groups, is illustrated by the aragonite group listed in Table 4.2.

POLYMORPHISM

When radius ratios are near limiting values, the cation may occur in structures in one of two different coordination polyhedra. At such limiting values, the cation

Table 4.2 Aragonite Group of Orthorhombic Isostructural Carbonates

Mineral	Chemical Composition	Cation	Size (Å)	Unit Cell Dimensions (Å)			Volume (Å^3)	Specific Gravity (G)	Cleavage Angle 110 ∧ 110
				a	*b*	*c*			
Aragonite	$CaCO_3$	Ca^{2+}	1.18	4.96	7.97	5.74	226.91	2.94	63°48′
Strontianite	$SrCO_3$	Sr^{2+}	1.34	5.11	8.41	6.03	259.14	3.78	62°41′
Cerussite	$PbCO_3$	Pb^{2+}	1.35	5.19	8.44	6.15	269.39	6.58	62°46′
Witherite	$BaCO_3$	Ba^{2+}	1.47	5.31	8.90	6.43	303.87	4.31	62°12′

*Because the metal ions are coordinated to nine oxygens, the ionic radii (see Table 3.8) are given for 9-fold coordination.

has a close fit for either coordination polyhedron. [For example, in $CaCO_3$, Ca:O has a radius ratio of 0.714 near the limiting value of 0.732 for the change-over from 6- to 8-fold coordination. Consequently, Ca may occur in two structure types. In calcite, $CaCO_3$, Ca is in 6-fold coordination with O whereas in aragonite, $CaCO_3$, Ca is in 9-fold coodination with O.] *When two minerals have the same chemical formula but different structures*, they are termed **polymorphs** (for the Greek word *poly* meaning many, and *morphe* meaning form). Rubidium, Rb, may be in either 6- or 8-fold coordination, and, thus, rubidium chloride is polymorphous (i.e., it is able to occur in two different structural arrangements). The change from 6- to 8-fold coordination in the alkali chlorides with increasing ionic radius of the cation is shown in Fig. 4.11. Li^+, Na^+, and K^+ have radius ratios with Cl^- between 0.414 and 0.732, and, therefore, go into 6-fold coordination with Cl^-. Cs^+has a radius ratio with Cl^- between 0.732 and 1.00 and, thus, goes into 8-fold coordination with Cl^-. Rb^+ has a radius ratio with Cl^- close to 0.732 and, therefore, can have either 6- or 8-fold coordination with Cl^-. Polymorphism and the transformation from one polymorph to another are considered more fully in Chapter 12. (Additional details are provided in module I of the CD-ROM under the heading "Polymorphism.")

ILLUSTRATION OF CRYSTAL STRUCTURES

A crystal structure is determined using many advanced analytical techniques that image, for example, atomic locations (discussed in Chapter 14). Typically, the accurate interpretation of a crystal structure requires additional information, such as the external symmetry (see Chapter 6), the chemical composition (see Chapter 5), as well as the density. The resulting crystal structure data locate the positions of all of the atoms (or ions) in the unit cell, and the bonding and coordination between them. These data are given in tables with bond angles, ion locations, etc. (see, for example, the American Mineralogist Crystallographic Database website).

Effective illustration of a three-dimensional structure image on a two-dimensional page is difficult. Several methods exist, and some that are commonly used are described here. One method is to illustrate a crystal structure in terms of coordination polyhedra, as in the amphibole structure (Fig. 4.9). The orientation and

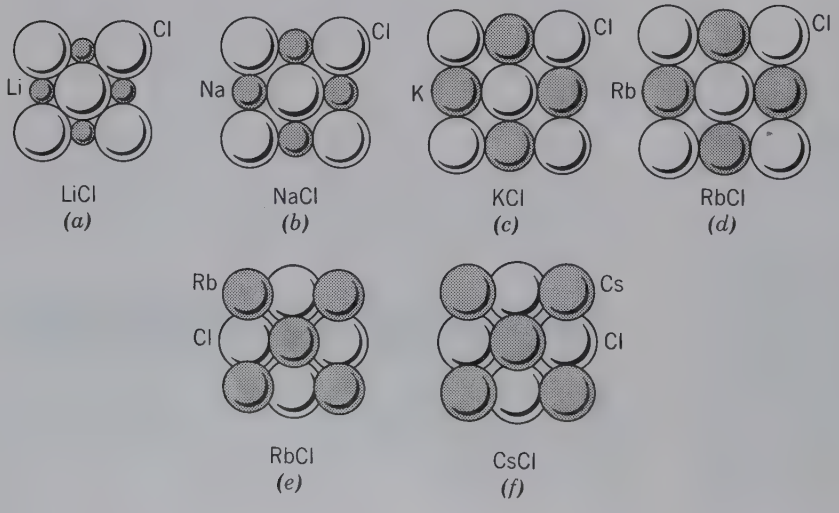

FIG. 4.11 Change in coordination from 6 to 8 in alkali chlorides as a function of increasing cation size. (a), (b), (c), and (d) have sodium chloride type structures with 6-fold coordination; (e) and (f) have cesium chloride type structures with 8-fold coordination.

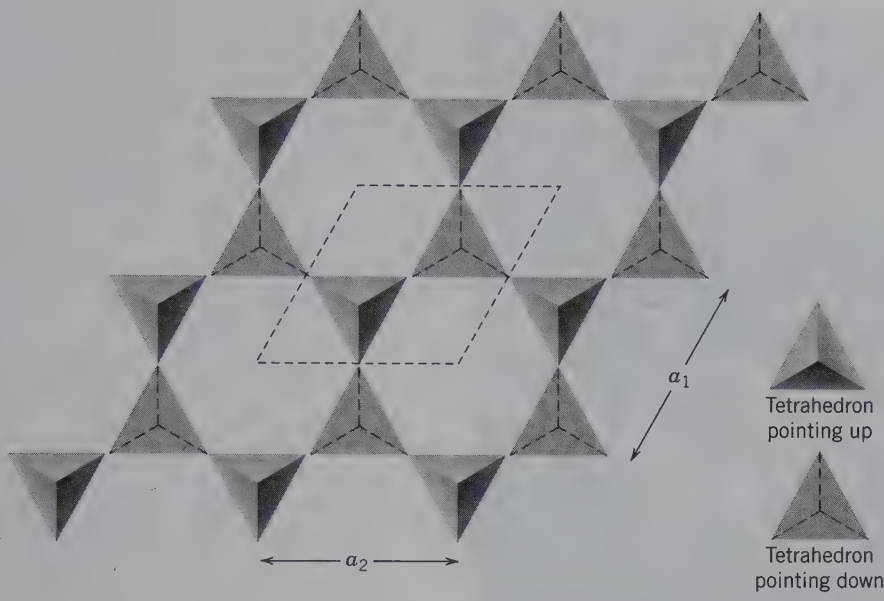

FIG. 4.12 A single sheet of the high tridymite structure (polymorph of SiO_2) projected onto the (0001) plane. Unit cell is outlined. Compare with Fig. 4.15b.

linkages of the coordination polyhedra are shown but typically only for a single layer of the structure. Also, the coordination polyhedra represent the anions but the cations are omitted for simplicity. A polyhedral representation of the structure of high tridymite, showing the linkage of SiO_4 tetrahedra, is shown in Fig. 4.12. For a three-dimensional representation and easier visualization of complex crystal structures, crystal structure models can be built or obtained commercially. Such models reproduce the internal atomic arrangement on an enormously magnified scale (e.g., 1 Å might be represented by 1 cm in a model). Several types of these models are illustrated in Figs. 4.13 and 4.14. A **close-packed model** is most realistic in terms of representing the filling of space on an atomic scale (Fig. 4.13a) although it is difficult to visualize the interior of these models. A **polyhedral model** (Figs. 4.13b and 4.14a) represents the coordination polyhedra instead of specific atomic locations. These two model types appear very different in the representation of the same mineral (e.g., Fig. 4.13 shows two representations of the NaCl structure). A polyhedral model of a complex structure (Fig. 4.14a) is most useful in visualizing the overall symmetry and the regular repeat units of the structure. This often-idealized regularity of the polyhedral arrangement also allows relatively easy identification of the space group elements in the structure (discussed in Chapters 7 and 9).

An **open "ball and stick" model** (Fig. 4.14b) allows a view of the coordination inside the model and portrays the irregularly coordinated environment of ions in a complex structure. In this type of model, a *ball* represents the atom (or ion) and a *stick* represents a bond. Neither of these features is displayed to scale.

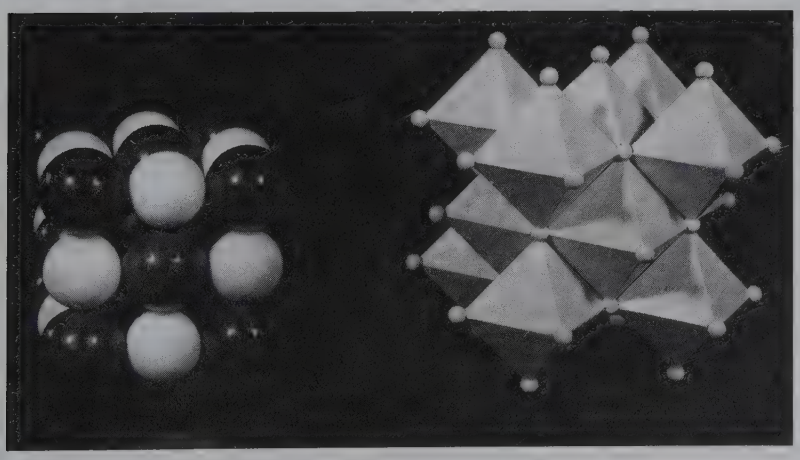

FIG. 4.13 (a) Close-packed model of the NaCl structure. Na^+ ions light; Cl^- ions dark. (b) Polyhedral representation of octahedral coordination of Cl^- about Na^+ (as well as Na^+ about Cl^-) in NaCl.

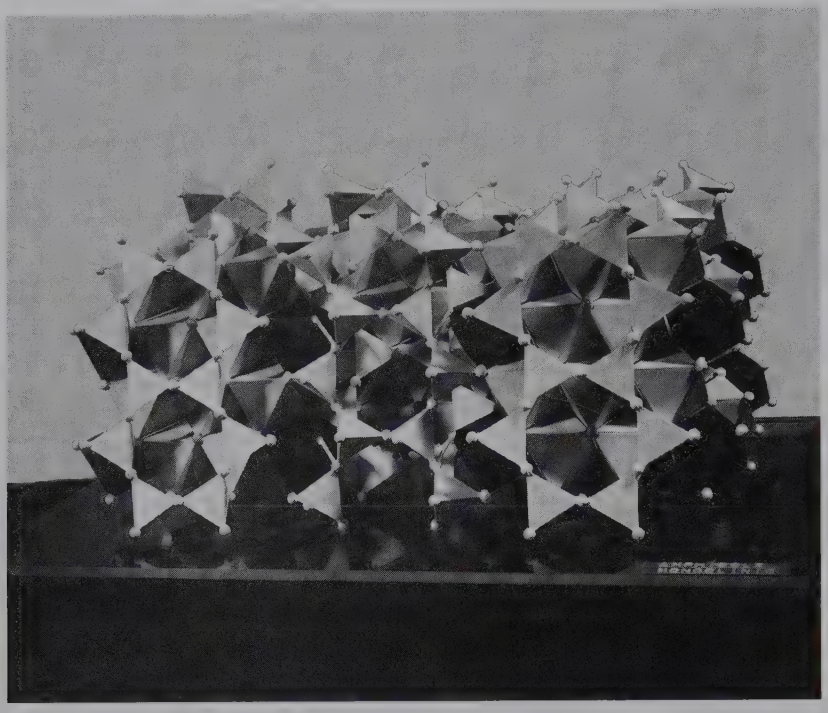

(*a*)

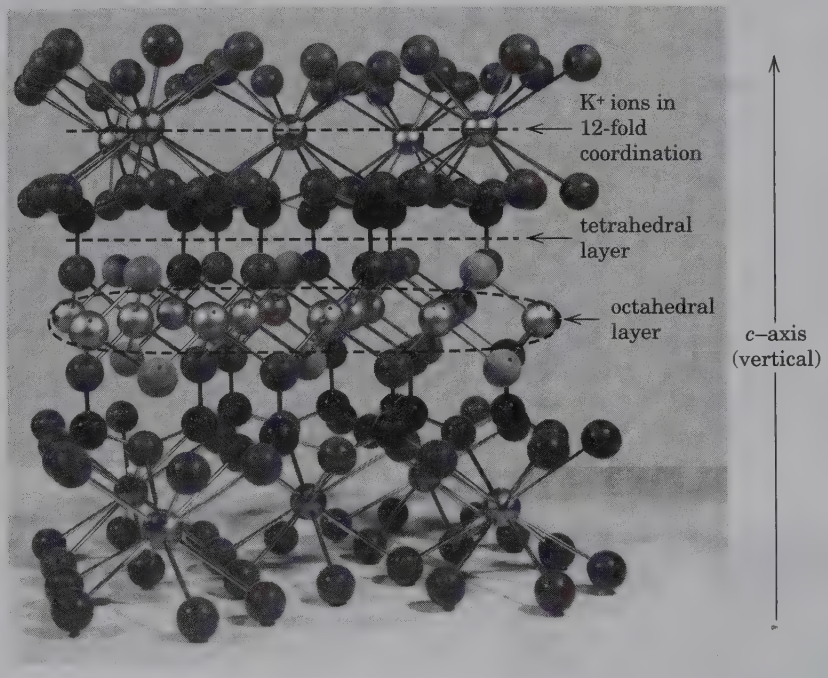

(*b*)

FIG. 4.14 (a) Polyhedral structure model representing a monoclinic amphibole. Tetrahedral linking of SiO_4 (Si_4O_{11} chains parallel to *c*-axis) and octahedral coordination of cations between chains. Dark octahedra represent *M4* positions in structure. (b) Expanded "ball and stick" model of the structure of biotite, $K(Mg,Fe)_3(AlSi_3O_{10})(OH)_2$. Top and bottom layers represent K^+ ions in 12-fold coordination with oxygen. Central layer represents Mg^{2+} and Fe^{2+} in 6-fold coordination with O^{2-} and $(OH)^-$.

An additional method for representing three-dimensional structures in two dimensions is through the use of **fractional coordinates**, x, y, and z. As an example, Fig. 4.15a shows the location of an atom within the outlined unit cell whose edges a, b, and c can be described in terms of distances from the origin (0, 0, 0) and whose components are parallel with the edges. These components are x', y', and z', where $x = x'/a$, $y = y'/b$, and $z = z'/c$; x, y, and z range from 0 to 1. Listing the fractional coordinates of all atoms (and/or ions) in a unit cell (this is the smallest unit of the structure that, when repeated regularly and indefinitely in three dimensions, yields the entire structure), defines the crystal structure. From such a listing, a two-dimensional projection can be constructed. Usually such projections are made onto one of the cell faces or onto planes perpendicular to a specific

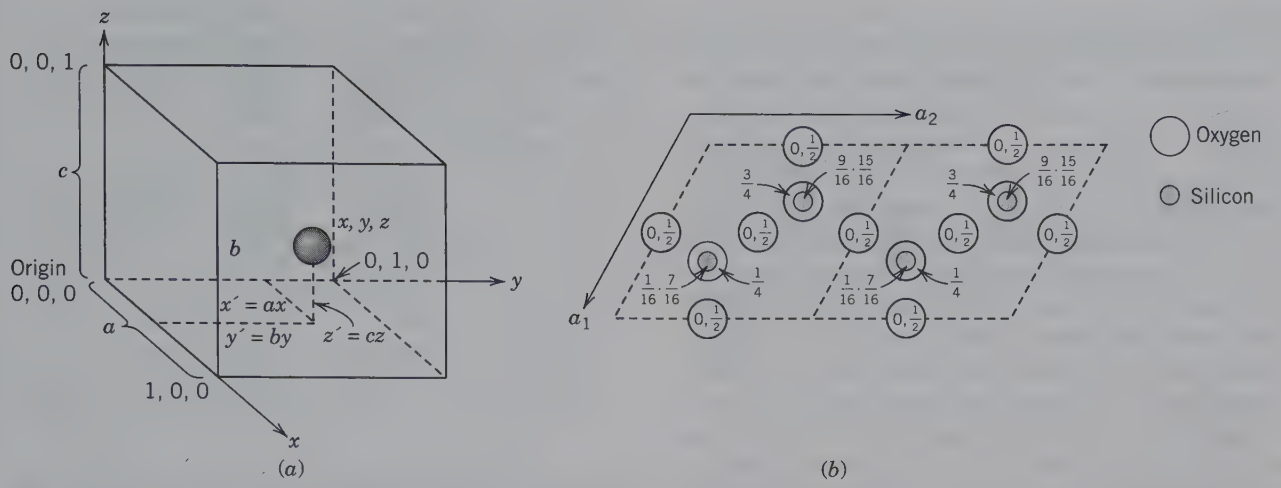

FIG. 4.15 (a) Fractional cell coordinates (x, y, z) of an atom in a unit cell as outlined. (b) Atomic arrangement in the high tridymite polymorph of SiO_2, projected on (0001). Oxygens occur in the base of the cell (0), one quarter ($\frac{1}{4}$), halfway ($\frac{1}{2}$), and three-quarters of the way up ($\frac{3}{4}$). In this projection some oxygen positions superimpose, as shown by the z coordinates 0, $\frac{1}{2}$. Silicon positions, above and below oxygen locations, occur at $\frac{1}{16}$, $\frac{7}{16}$, $\frac{9}{16}$, and $\frac{15}{16}$ of the z axis. (Note that vectors along a, b, c are often referred to as x, y, z).

direction in the crystal (e.g., the crystallographic axes). The fractional heights of atoms above the plane of projection are noted adjacent to them. The values of 0 to 1, corresponding to positions on the bottom and top faces of the unit cell, are commonly omitted. The coordinates (0, 0, 0) locate the origin of the unit cell.

As an example, a structure projection onto a horizontal plane of high tridymite, SiO_2, is shown in Fig. 4.15b. Two unit cells are shown (dashed lines). The x and y coordinates of the oxygen and silicon ions in the structure are shown by their locations in the a_1–a_2 plane. The z coordinates of the ions are shown by fractions indicating their locations above the plane of the projection (the page). Instead of using fractional coordinates, vertical structure projections may be also represented by atomic positions accompanied by numbers ranging from 0 to 100. An atom in the base of the unit cell is indicated by 0, one on the top face by 100, and intermediate heights are given accordingly. An atom marked 75, for example, is located three-quarters of the way up the unit cell based on fractional coordinates.

EXAMPLES OF SELECTED COMMON STRUCTURE TYPES

In the visualization of inorganic crystal structures, it is useful to view the larger anions as a closest packed array with the smaller cations housed in the interstitial positions. As demonstrated previously, close-packed layers of spheres can be stacked into a hexagonal closest packed sequence (HCP: *ABAB*. . .) or a cubic closest packed sequence (CCP: *ABCABC*. . .) (see Fig. 4.1). The interstices that arise in such close-packed sequences are tetrahedral and octahedral in coordination (Fig. 4.16). These tetrahedral and octahedral interstitial

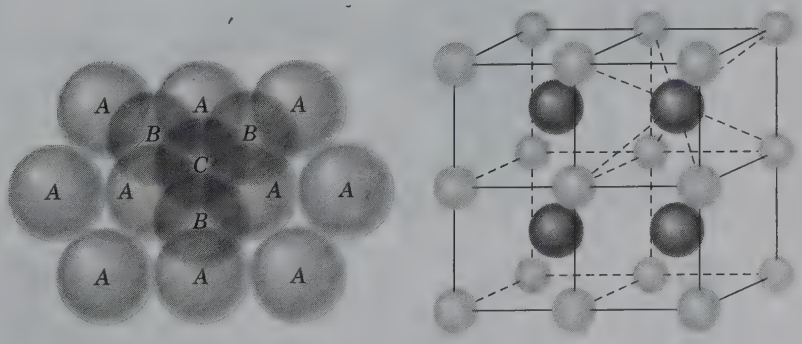

FIG. 4.16 (a) Hexagonal closest packing sequence (HCP) with tetrahedral interstices (or voids, marked *B*) and octahedral interstices (marked *C*). (b) Simple cubic packing (SCP) results when R_A:R_X is between 0.73 and 1.0. The relatively large cation is surrounded by eight nearest neighbors in cubic coordination. This coordination pattern is shown in four cubic units.

sites may or may not be fully occupied by cations, as will be seen in various examples of the following structures. In structures in which the cations are larger than can be housed in octahedral coordination (R_A:R_X values between 0.73 and 1.0; see Fig. 4.4), they commonly occur in **simple cubic packing** (**SCP**) with the cations at the center of a cube and the anions at the eight corners (Fig. 4.16b). This is equivalent to a coordination number of 8.

The important structure types summarized here are those of NaCl, halite; CsCl, cesium chloride; ZnS, sphalerite; CaF_2, fluorite; TiO_2, rutile; $CaTiO_3$, perovskite; $MgAl_2O_4$, spinel; and the silicates. The cations are referred to, in general, as *A* and *B*, and the anions, in general, as *X* with the appropriate subscripts. The names of the structure types are based on a specific mineral name (e.g., halite), but the term *halite structure type* encompasses any mineral that has this same structure (i.e., is isostructural). (Several of these structure types are found in module I of the CD-ROM under the heading "Illustrations of Crystal Structures.")

NaCl STRUCTURE

This structure type is adopted by a large number of *AX* (1 cation:1 anion) compounds in the appropriate radius ratio range. In this structure type, the anions are in cubic closest packing, with the cations filling all the octahedral sites. Values of the radius ratio in the range of 0.73 to 0.41 favor octahedral coordination (see Fig. 4.4). The cations and anions in this structure occur in edge-sharing octahedra (Fig. 4.17), with each of the 12 edges of an octahedron shared with a neighboring octahedron.

Examples of this structure type are:

Halides:	LiF, LiCl, LiBr, LiI NaF, NaCl (halite), NaBr, NaI KF, KCl (sylvite), KBr, KI RbF, RbCl, RbBr, RbI
Oxides:	MgO (periclase), CaO, SrO, BaO, NiO
Sulfides:	MgS, CaS, MnS, PbS (galena)

See page 66 for an illustration of the unit cell of halite and its atomic (ionic) content. The structure of pyrite, FeS_2, can be considered as a derivative of the NaCl structure (see Fig. 15.8) in which Fe^{2+} is in the Na position and covalently bonded S_2 (in pairs) is in the Cl position. (The halite structure type is found in module I of the CD-ROM under the heading "Illustrations of Crystal Structures: Halite.")

CsCl STRUCTURE

The cesium chloride structure is adopted by *AX* compounds when the radius ratio is greater than 0.73 (see Fig. 4.4). Therefore, the anions (*X*) are in SCP, and the cations fill the large interstices between them. The overall structure (Fig. 4.18) is made up of centered

FIG. 4.17 (a) The structure of NaCl, halite. The Na^+ and Cl^- ions are arranged in a face-centered cubic lattice. (b) The same structure showing the edge-sharing octahedra about the Na^+. Similar edge-sharing octahedra could be drawn about Cl^-.

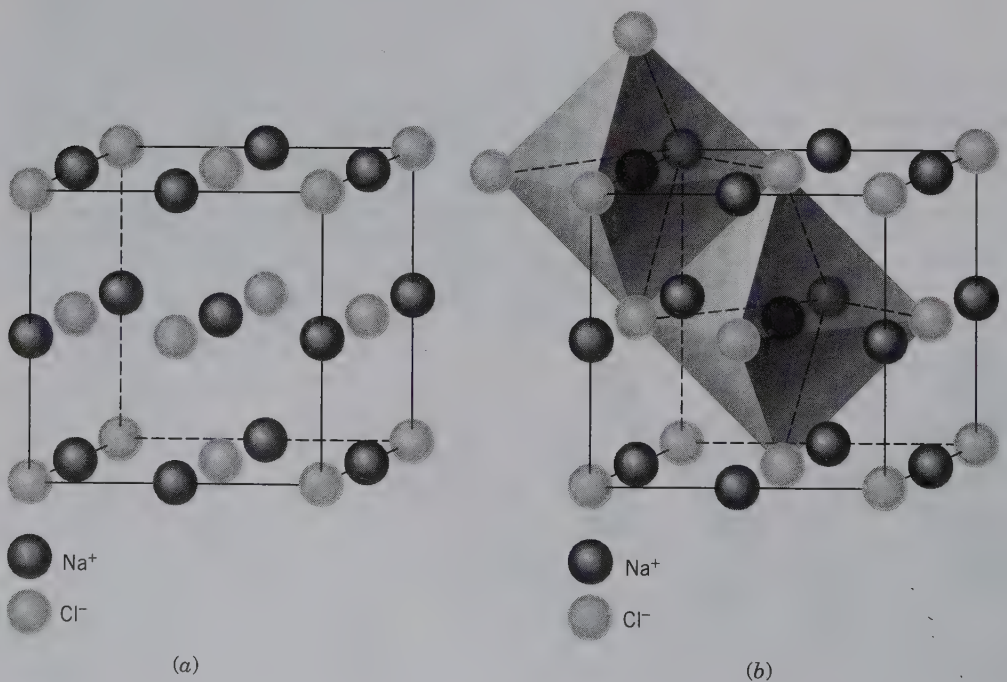

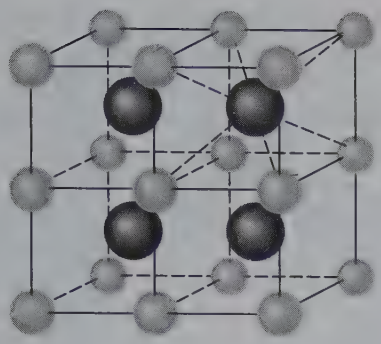

FIG. 4.18 The structure of CsCl. Each cation is surrounded by eight neighbors, and so is each anion.

cubes that share faces with six other neighboring cubes. This feature makes this structure an unattractive choice for highly charged cations (see Pauling's Rule 3). Examples of *AX* compounds that exhibit this structure are:

CsCl, CsBr, CsI, $(NH_4)Cl$, $(NH_4)Br$

SPHALERITE (ZnS) STRUCTURE

A radius ratio of 0.32 (calculated from the radius of Zn^{2+} = 0.60 Å in 4-fold coordination and S^{2-} = 1.84 Å in 4-fold coordination; see Table 3.8) predicts that Zn^{2+} is in tetrahedral coordination with the neighboring S^{2-} (Fig. 4.19a). The sphalerite structure may be considered as a derivative of the diamond, C, structure (Fig. 4.19b) in which half the carbon atoms in the diamond structure are replaced by Zn and the other half by S. In comparison with the sphalerite structure, diamond may be viewed as having C atoms in the cation positions of the *AX* compound, as well as C atoms in the anion positions. Derivatives of the sphalerite structure, such as chalcopyrite, $CuFeS_2$, and tetrahedrite, $Cu_{12}Sb_4S_{13}$, are illustrated in Fig. 15.5. SiC (silicon carbide; carborundum) is also isostructural with sphalerite.

CaF_2 STRUCTURE

For AX_2 compounds in which the radius ratio exceeds 0.73 (see Fig. 4.4), the fluorite structure may be adopted. In this structure, the Ca^{2+} ions are arranged at the corners and face centers of a cubic unit cell, and F^- ions are at the centers of the eight equal cubelets into which the cell may be mentally divided (Fig. 4.20). Each Ca^{2+} is surrounded by eight F^- in cubic coordination, and each F^- is surrounded by four Ca^{2+}at the corners of a tetrahedron. The fluorite structure may be derived from the CsCl structure by replacing Cl^- with F^- and *every other* Cs^+ with Ca^{2+}. This leaves alternate cubic interstices vacant and results in the octahedral cleavage of fluorite and its isostructural minerals. The cubic coordination of F^- about a central Ca^{2+} is the result of the radius ratio of $R_{Ca^{2+}}$: R_{F^-} being approximately 0.75. These cubic coordination polyhedra share edges only; similarly, the tetrahedral coordination polyhedra share only edges. This arrangement allows for the maximum separation of the Ca^{2+} cations from each other (Fig. 4.20). Because the *A* cation has double the charge of the *X* anion, the number of anions in the structure must be double that of the cations in order to achieve electrostatic neutrality. As such, the resulting general formula is AX_2. This structure type is adopted by a large number of AX_2 halides and oxides:

Halides: CaF_2 (fluorite), SrF_2, BaF_2, CuF_2, CdF_2, $SrCl_2$, $BaCl_2$
Oxides: ZrO_2, HfO_2, CeO_2, UO_2(uraninite)

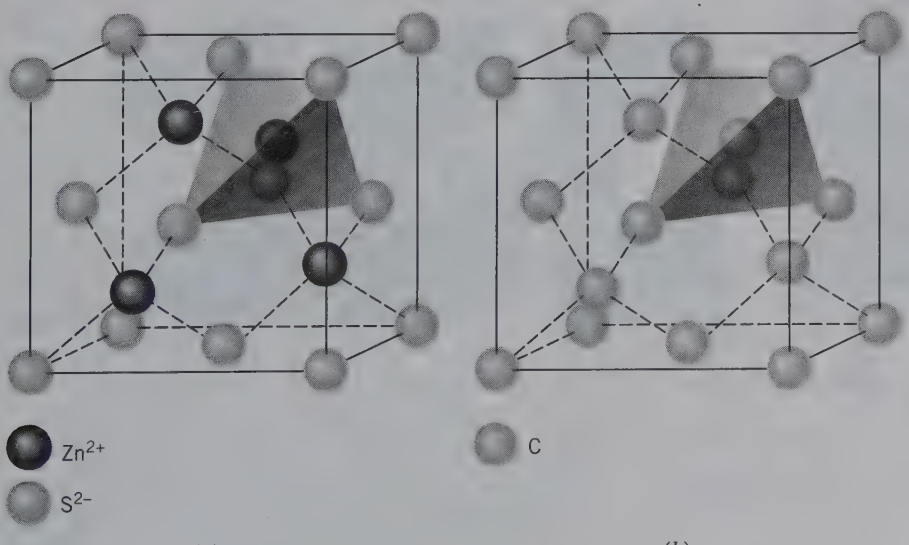

FIG. 4.19 (a) The structure of sphalerite, ZnS. Both Zn^{2+} and S^{2-} are in a face-centered cubic array. Zn^{2+} is in tetrahedral coordination with four S^{2-} neighbors (see also Fig. 4.10*c*). (b) The structure of diamond, C. The coordination of C by four nearest carbon neighbors is tetrahedral. (See also Fig. 3.18.)

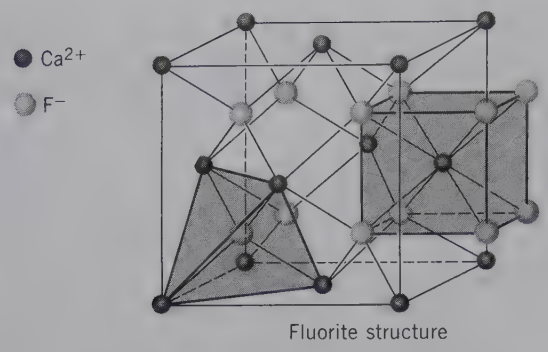

FIG. 4.20 The structure of fluorite, CaF_2. Ca^{2+} ions are arranged in a face-centered cubic lattice. The F^- ions are in simple cubic packing (SCP) with Ca^{2+} occupying the voids at the centers of *alternating* cubic interstices.

(This structure type is found in module I of the CD-ROM under "Illustrations of Crystal Structures: Fluorite.")

RUTILE (TiO_2) STRUCTURE

The rutile structure is based on HCP, with Ti filling half the octahedral interstitial positions. AX_2 compounds that exhibit radius ratios between about 0.73 and 0.41 (see Fig. 4.4) adopt the rutile structure in which the *A* cation is octahedrally coordinated (**C.N.** = 6) to the *X* anion (Fig. 4.21). The oxygen anions are coordinated by three cations in a triangular array (**C.N.** = 3). The structure consists of octahedra that are linked along horizontal edges. This linking pattern forms strips of octahedra parallel to the *c* axis, and these bands are cross-linked to each other by corner-sharing of neighboring octahedra. This structure results in the prismatic cleavage of rutile, parallel to *c*. A large number of inorganic compounds assume the rutile structure. Examples are:

MgF_2, NiF_2, CoF_2, FeF_2, MnF_2, ZnF_2
TiO_2 (rutile), MnO_2 (pyrolusite), SnO_2, WO_2, PbO_2, SiO_2 (stishovite)

PEROVSKITE (ABO_3) STRUCTURE

This structure type is based on CCP of oxygen, with one-quarter of the oxygens replaced by a large *A* cation. This large cation position is in 12-fold coordination with the surrounding oxygens. The *B* cations occur in octahedra that share only apices (Fig. 4.22). The valence of the *A* and *B* ions is not specified; however, the total valence of both ions ($A + B$) must be equal to 6 (to balance the $O^{2-}{}_3$ in the formula ABO_3). The perovskite structure type is adopted by many com-

FIG. 4.21 Two views of the structure of rutile, TiO_2. (a) Standard orientation of two unit cells of rutile stacked in the *c* direction. The octahedra share two horizontal edges with adjacent octahedra, forming bands parallel to the vertical *c* axis. (b) The array of bands of edge-sharing octahedra (parallel to *c*) running into the page. Chains of edge-sharing octahedra running parallel to *c* are clearly seen, cross-linked by corner-sharing octahedra. The HCP stacking is shown by *ABAB*. . . . (From Waychunas, G. A. 1991. Crystal chemistry of oxides and hydroxides, in *Oxide Minerals. Reviews in Mineralogy* 25: 11–68.)

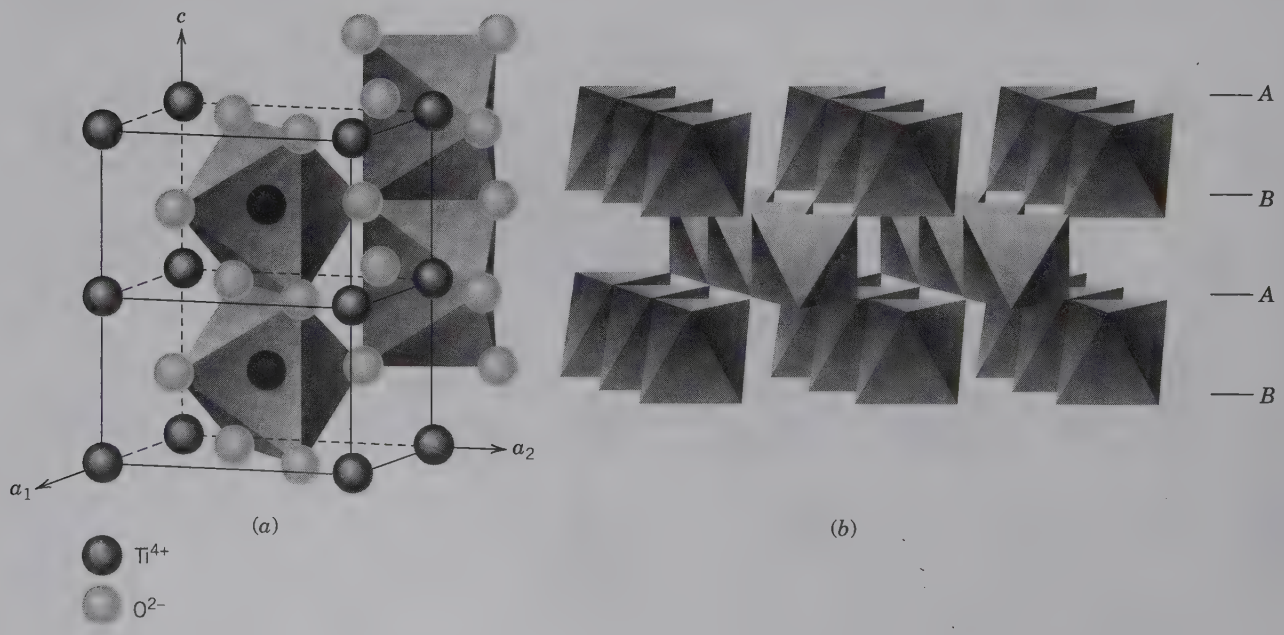

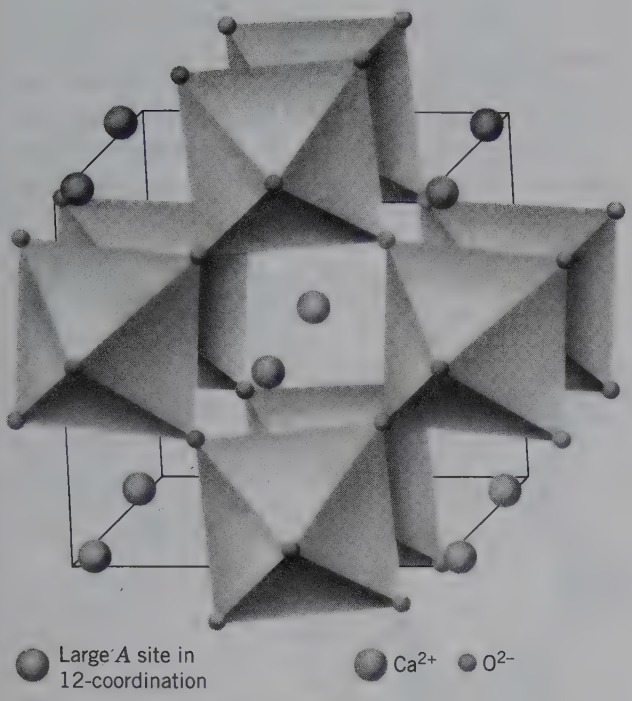

FIG. 4.22 The structure of perovskite, $CaTiO_3$, in a perspective projection looking down the *c* axis. Layers of anion-sharing octahedra (containing Ti^{4+}) are oriented perpendicular to the *c*-axis. Ca^{2+} is in 12-fold coordination. (Modified after Smyth, J. R., and D. L. Bish. 1988. *Crystal structures and cation sites of the rock-forming minerals.* Allen and Unwin, Boston).

pounds. These examples are arranged in columns based on the charge of the cations in the *A* and *B* sites:

$A^{1+}B^{5+}$	$A^{2+}B^{4+}$	$A^{3+}B^{3+}$
$NaNbO_3$	$CaTiO_3$	$LaCrO_3$
$KNbO_3$	$SrTiO_3$	$YAlO_3$
$KTaO_3$	$BaZrO_3$	$LaAlO_3$
	$BaTiO_3$	

The perovskite structure type is of special interest because it is considered to be a common structure type under very high-pressure conditions, as in the Earth's lower mantle (see Fig. 5.4).

SPINEL (AB_2O_4) STRUCTURE

The spinel structure type consists of a CCP array of oxygens in which one-eighth of the tetrahedral interstices (*A*) and half of the octahedral interstices (*B*) are occupied by cations. All spinels contain two differing cations, or at least two different valences of the same cation, in the ratio of 2:1. Spinels are classified as *normal* or *inverse* spinels, depending on where the more abundant of the cations is "housed." If it occurs in the octahedral site, it is classified as *normal*. If it is equally split between the octahedral and tetrahedral sites, it is *inverse*.

The CCP layers of oxygens are stacked parallel to octahedral planes, resulting in alternating layers of octahedral sites and tetrahedral sites (Fig. 4.23). Occupied octahedra are joined along edges to form rows and planes in the structure, and tetrahedra provide cross-links between layers of octahedra (Fig. 4.23a). A plan view of an oxygen layer parallel to the {111} plane (see Chapter 6 for notation) and its coordination with

FIG. 4.23 The spinel (AB_2O_4) structure. (a) Alternating layers parallel to {111} of octahedral and octahedral-tetrahedral polyhedra, as based upon approximate cubic closest packing. (b) A close-packed layer of oxygen in the spinel structure, projected onto the {111} plane. The large spheres are oxygen, and the cation layers on either side of the oxygen layer are shown as well. (a and b redrawn after Waychunas, G. A. 1991. Crystal chemistry of oxides and hydroxides, in *Oxide Minerals. Reviews in Mineralogy*, 25:11–68.)

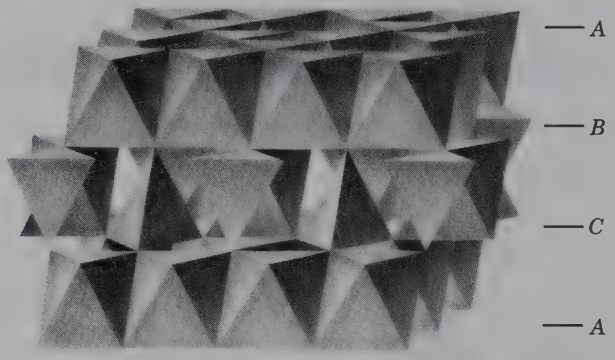

(*a*)

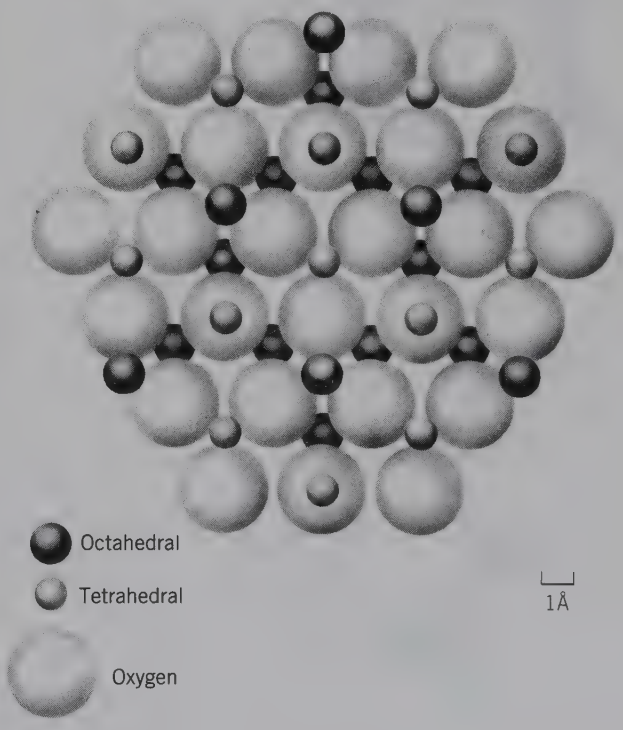

(*b*)

cations is given in Fig. 4.23b. In the general formula of spinel (AB_2O_4), the smaller tetrahedral *A* site is commonly occupied by Mg^{2+}, Fe^{2+}, Mn^{2+}, Zn^{2+} and the larger octahedral *B* site by Al^{3+}, Cr^{3+}, or Fe^{3+}. The coordination polyhedra about the various cations in spinel are not what might be predicted on the basis of the ionic sizes of the cations. Because Mg^{2+} is larger than Al^{3+}, one would expect Mg to occur in the octahedral *B* site and Al in the tetrahedral *A* site. In the normal spinel structure (e.g., $MgAl_2O_4$), however, the general concepts of radius ratio do not apply; the larger cation is in the smaller polyhedron, and vice versa.

FIG. 4.24 Examples of some common linkages of (SiO_4) tetrahedra in silicates. The oxygen that links two tetrahedra is known as the "bridging" oxygen.

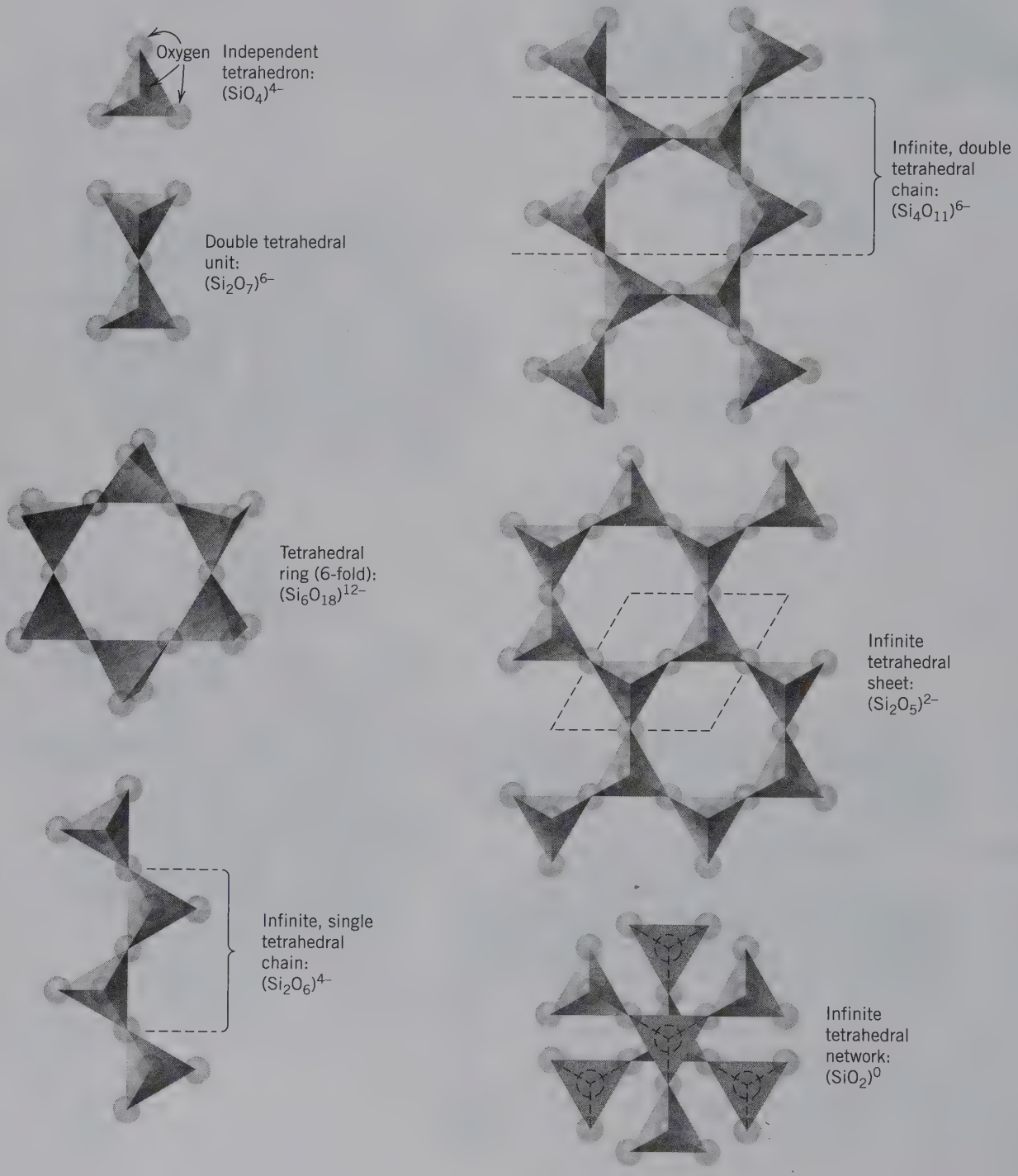

Only when crystal field stabilization energies are considered, instead of geometric aspects of the ions, does it become clear why the larger cation occupies tetrahedral sites.

The spinel structure has a coordination scheme similar to that of the silicates of the olivine series, Mg_2SiO_4 to Fe_2SiO_4. This compositional series can be represented as $X_2^{2+}Y^{4+}O_4$. Although this is not the same as $A^{2+}B_2^{3+}O_4$, as in spinel, in both cases the overall cation charge is identical. Comparison of the structure of an Mg–Fe olivine with that of a possible Mg–Fe spinel, shows that the spinel structure is about 12% denser than the olivine structure of the same composition. This leads to the conclusion that the spinel form of Mg_2SiO_4 must be abundant in the mantle as a result of very high confining pressures (see Chapter 5, Fig. 5.4). Some examples of spinel composition are:

Spinel	$MgAl_2^{3+}O_4$
Hercynite	$FeAl_2^{3+}O_4$
Gahnite	$ZnAl_2^{3+}O_4$
Chromite	$Fe^{2+}Cr_2^{3+}O_4$
Magnesiochromite	$MgCr_2^{3+}O_4$

For further discussion of spinel, see pages 372–373.

SILICATE STRUCTURES

Silicates, compounds consisting of abundant oxygen and silicon, are the major mineral components of the Earth's crust. The oxygen in these structures is in close packing with the cations in various coordination polyhedra (see Table 4.1). In *all* crustal silicates, silicon is in tetrahedral coordination with oxygen. Only in the high-pressure polymorph of SiO_2, stishovite, is Si found in octahedral coordination with oxygen. The various ways in which the tetrahedral $(SiO_4)^{4-}$ group can link itself to other $(SiO_4)^{4-}$ groups by sharing one, two, three, or all four oxygens of the tetrahedron are fundamental to any classification of silicates. An overview of these tetrahedral linking (or polymerization) schemes is given in Fig. 4.24. The basic underlying reason for the ability of the $(SiO_4)^{4-}$ tetrahedron to link itself in so many ways to other $(SiO_4)^{4-}$ tetrahedra is the fact that the e.v. of the bonds between Si^{4+} and oxygen is = 1. This is exactly half the bonding strength of the oxygen ion (2^-). Consequently, the SiO_4 tetrahedron may link itself through a "bridging" oxygen to another SiO_4 tetrahedron. Individual silicate structures are discussed in detail in Chapter 18. (An illustration of the quartz structure is found in module I of the CD-ROM under the heading "Illustration of Crystal Structures: Quartz.") In addition to the classification of silicates used in this text, there are other classifications proposed by Liebau (1985) and Zoltai (1960) (see the references at the end of this chapter).

REFERENCES AND FURTHER READING

Bloss, F. D. 1994. *Crystallography and crystal chemistry: An introduction.* Reprint of original text of 1971. Mineralogical Society of America, Washington, D.C.

Bragg, W. L., and G. F. Claringbull. 1965. *Crystal structure of minerals.* Cornell University Press, Ithaca, New York.

Evans, R. C. 1966. *An introduction to crystal chemistry.* 2nd ed. Cambridge University Press, Cambridge, England.

Griffen, D. T. 1992. *Silicate crystal chemistry.* Oxford University Press, New York.

Klein, C. 2008. *Minerals and rocks: Exercises in crystal and mineral chemistry, crystallography, X-ray powder diffraction, mineral and rock identification, and ore mineralogy.* 3rd. ed. Wiley, New York.

Liebau, F. 1985. *Structural chemistry of silicates, structure, bonding and classification.* Springer-Verlag, New York.

Silberberg, M. S. 2000. *Chemistry, the molecular nature of matter and change.* 2nd ed. McGraw Hill, New York.

Smyth, J. R., and D. L. Bish. 1988. *Crystal structures and cation sites of the rock-forming minerals.* Allen & Unwin, Boston.

Wells, A. G. 1991. *Structural inorganic chemistry.* 5th ed. Clarendon Press, Oxford, England.

Zoltai, T. 1960. Classification of silicates and other minerals, with tetrahedral structures. *American Mineralogist* 45: 960–73.

CHAPTER 5

Chemical Composition of Minerals

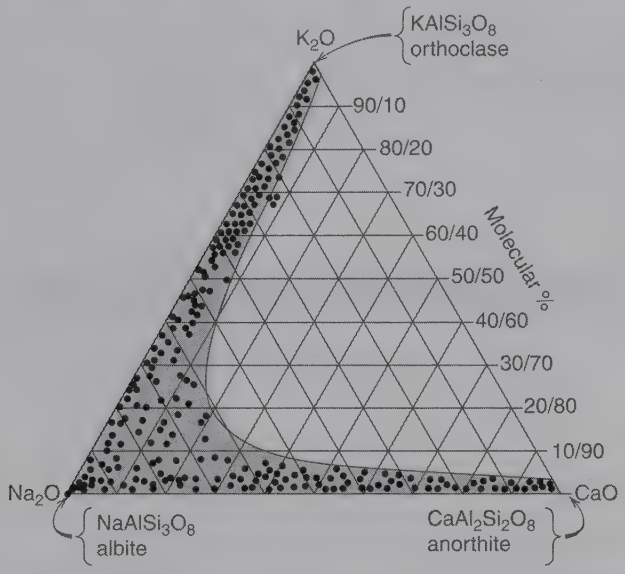

Representation of mineral compositions on a ternary (three-component) diagram. Several hundred dots represent chemical analyses for members of the feldspar series that were formed at high temperature. These are plotted in terms of three compound chemical components: K_2O (or $KAlSi_3O_8$, orthoclase), Na_2O (or $NaAlSi_2O_8$, albite) and CaO (or $CaAl_2Si_2O_8$, anorthite). The gray shaded area is the extent of atomic substitution (of the three components for each other; also known as "solid solution") in high-temperature feldspars.

As an introduction to the chemistry of minerals, this chapter begins with an overview of the chemical composition of the Earth. The chemical elements that are globally present are the same as those that make up the most common minerals. Compositional variability of these minerals is explored, and graphical techniques for displaying mineral composition are presented.

There are currently 116 known elements (see the periodic table on the end paper in the back of this text), including six inert gases and 28 elements that are not found naturally (or have no stable isotopes). Surprisingly, the most common minerals of the Earth are composed of only about 15 chemical elements. This chapter explores the reasons why most minerals contain only a small number of the known elements and how the less abundant elements are incorporated into crystal structures.

COMPOSITION OF THE EARTH

Geophysical investigations of the Earth's density and mass indicate a division of the Earth into a **crust, mantle**, and **core**. These divisions and the distance to their boundaries are shown in Fig. 5.1a. The crust has an average thickness of about 36 km on the continents, but varies in thickness from ~10 km under the oceans to ~100 km under mountains (Fig. 5.1b). The boundary between the crust and the underlying upper mantle is referred to as the Mohorovičić discontinuity, and is commonly known as the *Moho*. The mantle makes up about 80% of the planet's volume and extends from the base of the crust to the outer core at 2,891 km. It is divided into the upper and lower mantle, separated by the mantle transition zone (Fig. 5.1a). In the lower mantle, about 200 km above the mantle-core boundary, geophysical techniques suggest another division, the recently discovered D″ layer. The boundary between the lower mantle and core is not smooth (as depicted in Fig. 5.1a) but irregular. The core is divided into a liquid outer core and a solid inner core, extending to 6,371 km, the radius of the Earth. As minerals are buried deeper within the Earth, pressures and temperatures increase (to about 3,000 K in the lower mantle to, perhaps, 6,000–7,000 K in the core), which cause mineralogical changes. The overall density of materials in the core is considerably greater than in the Earth's

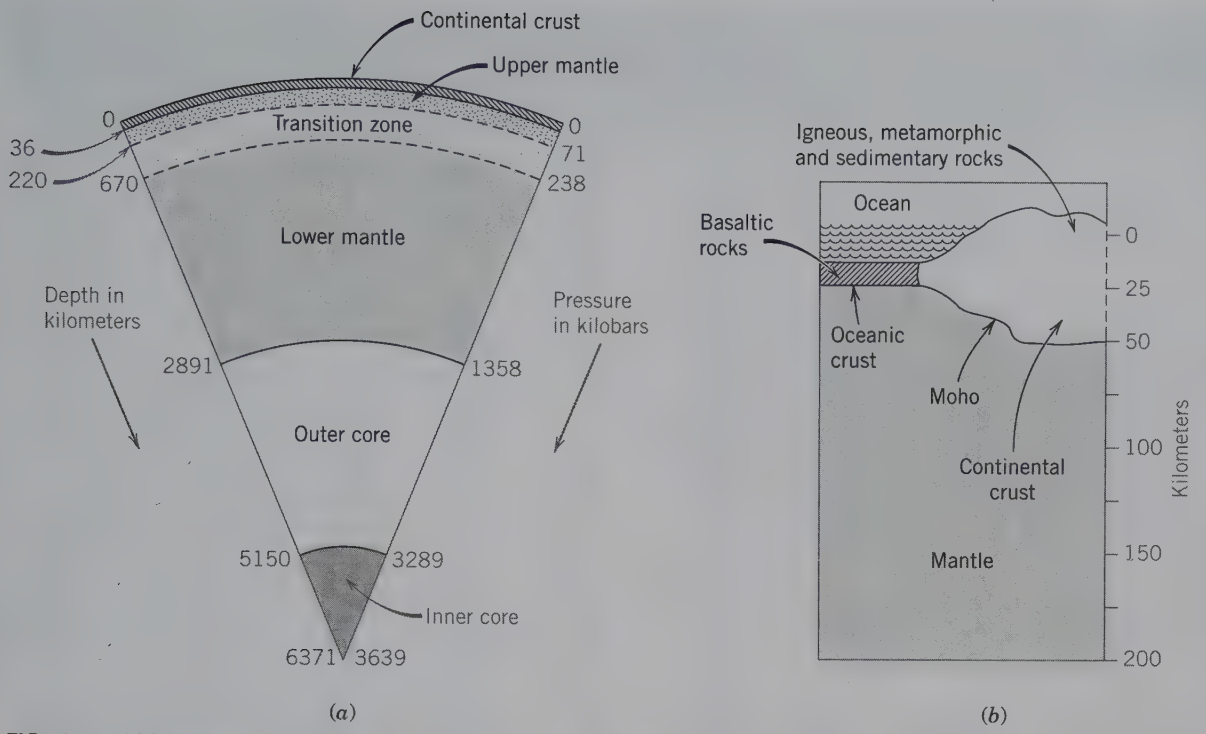

FIG. 5.1 (a) Major subdivisions of the Earth's interior. The pressure is expressed in kilobars, where 1 kilobar = 1,000 bars = 100 megapascals, and 1 bar = 0.987 atmosphere or 10,000 pascals. (From Liu, L., and W. A. Bassett, 1986. *Elements, oxides, silicates: High-pressure phases with implications for the earth's interior.* Oxford University Press, New York.) (b) Schematic representation of the Earth's lithosphere. Crustal rocks are less dense than the rocks of the mantle below. The crust is thicker beneath the continents than under the oceans.

crust. As such, the atomic packing schemes of minerals in the deep mantle and core must be denser than those observed in most crustal materials.

COMPOSITION OF THE EARTH'S CRUST

The upper part of the crust, consisting of the materials near the Earth's surface, is composed of a relatively large percentage of sedimentary rocks and unconsolidated material. However, this sedimentary cover forms only a thin veneer on an underlying basement of igneous and metamorphic rocks (see Chapter 21) that are exposed in mountain belts and on the sea floor. Clarke and Washington (1924) estimated that the upper 10 miles (16 km) of the crust consists of 95% igneous rocks (or their metamorphic equivalents), 4% shale, 0.75% sandstone, and 0.25% limestone. Therefore, the average composition of igneous rocks would closely approximate the average crustal composition. Clarke and Washington then compiled data on 5,159 complete chemical analyses of igneous rocks, which represent the average composition of the continental crust (Table 5.1). It turns out that this average composition is intermediate between that of a granite and a basalt, which are the two most common igneous rock types (see Chapter 21 and Box 19.1). These data did not, however, include an appropriate number of basalts from the ocean floor that would have made their average more representative of the average crust than of just the average *continental* crust. Inclusion of these extensive basalts would lower the average Si, K, and Na values and would increase the proportions of Fe, Mg, and Ca.

Of the 88 naturally occurring elements, a mere 8 elements make up approximately 99 weight percent of the Earth's crust (Fig. 5.2, Table 5.1). Of these, oxygen is by far the most abundant. This predominance is even more apparent when the original weight percentages are recalculated to atom percent and volume percent (Fig 5.2). As such, the Earth's crust consists almost entirely of oxygen compounds, which are primarily the silicate, carbonate, oxide, hydroxide, phosphate and sulfate minerals. In terms of the number of atoms, oxygen exceeds 60%. If the volumes of the most common ions are considered, oxygen is found to constitute about 94% of the total volume of the crust. In other words, the Earth's crust, on an atomic scale, consists essentially of a close packing of

Table 5.1 Average Amounts of the Elements in Crustal Rocks, in Weight Percent for the Common Elements (as indicated by %) and in Parts Per Million for the Less Abundant Elements*

Atomic Number	Element	Crustal Average	Granite (G-1)	Diabase (W-1)	Atomic Number	Element	Crustal Average	Granite (G-1)	Diabase (W-1)
1	H	0.14%	0.04%	0.06%	45	Rh	0.005		<0.001
3	Li	20	22	5	46	Pd	0.01	0.002	0.0025
4	Be	2.8	3	0.8	47	Ag	0.07	0.05	0.08
5	B	10	1.7	15	48	Cd	0.2	0.03	0.15
6	C	200	200	100	49	In	0.1	0.02	0.07
7	N	20	59	52	50	Sn	2	3.5	3.2
8	O	46.60%	48.50%	44.90%	51	Sb	0.2	0.31	1.01
9	F	625	700	250	52	Te	0.01	<1	<1
11	Na	2.83%	2.46%	1.60%	53	I	0.5	<0.03	<0.03
12	Mg	2.09%	0.24%	3.99%	55	Cs	3	1.5	0.9
13	Al	8.13%	7.43%	7.94%	56	Ba	0.04%	0.12%	0.02%
14	Si	27.72%	33.96%	24.61%	57	La	30	101	9.8
15	P	0.10%	0.04%	0.06%	58	Ce	60	170	23
16	S	260	58	123	59	Pr	8.2	19	3.4
17	Cl	130	70	200	60	Nd	28	55	15
19	K	2.59%	4.51%	0.53%	62	Sm	6.0	8.3	3.6
20	Ca	3.63%	0.99%	7.83%	63	Eu	1.2	1.3	1.1
21	Sc	22	2.9	35	64	Gd	5.4	5	4
22	Ti	0.44%	0.15%	0.64%	65	Tb	0.9	0.54	0.65
23	V	135	17	264	55	Dy	3.0	2.4	4
24	Cr	100	20	114	67	Ho	1.2	0.35	0.69
25	Mn	0.09%	0.02%	0.13%	68	Er	2.8	1.2	2.4
26	Fe	5.00%	1.37%	7.76%	69	Tm	0.5	0.15	0.30
27	Co	25	2.4	47	70	Yb	3.4	1.1	2.1
28	Ni	75	1	76	71	Lu	0.5	0.19	0.35
29	Cu	55	13	110	72	Hf	3	5.2	2.7
30	Zn	70	45	85	73	Ta	2	1.5	0.50
31	Ga	15	20	16	74	W	1.5	0.4	0.5
32	Ge	1.5	1.1	1.4	75	Re	0.001	<0.002	<0.002
33	As	1.8	0.5	1.9	76	Os	0.005	0.00007	0.0003
34	Se	0.05	0.007	0.3	77	Ir	0.001	0.00001	0.003
35	Br	2.5	0.4	0.4	78	Pt	0.01	0.0019	0.0012
37	Rb	90	22	21	79	Au	0.004	0.004	0.004
38	Sr	375	250	190	80	Hg	0.08	0.1	0.2
39	Y	33	13	25	81	Tl	0.5	1.2	0.11
40	Zr	165	210	105	82	Pb	13	48	7.8
41	Nb	20	24	9.5	83	Bi	0.2	0.07	0.05
42	Mo	1.5	6.5	0.57	90	Th	7.2	50	2.4
44	Ru	0.01			92	U	1.8	3.4	0.58

*From Mason, B. and Moore C. B., 1982, *Principles of geochemistry*. Copyright © 1982 by John Wiley & Sons, Inc., New York.

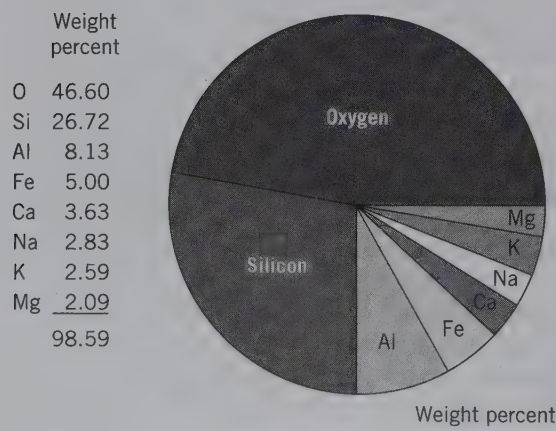

	Weight percent	Atom percent	Ionic+ radius (Å)	Volume percent
O	46.60	62.55	1.36	~ 94
Si	26.72	21.22	0.26 [4]	
Al	8.13	6.47	0.39 [4]	
Fe	5.00	1.92	0.78 [6]	
Ca	3.63	1.94	1.00 [6]	~ 6% in total
Na	2.83	2.64	1.02 [6]	
K	2.59	1.42	1.51 [8]	
Mg	2.09	1.84	0.72 [8]	
	98.59	100.00		

FIG. 5.2 The eight most common elements in the Earth's crust. (From Mason, B. and C. B. Moore. 1982. *Principles of geochemistry* 4th ed. (Wiley, New York). +Ionic radii taken from Table 3.8. Numbers in square brackets refer to coordination number.

oxygen anions with interstitial metal ions, primarily Si. Because of this high abundance of oxygen and other low atomic weight elements in the crust, the average mean density of the crust is about 2.8 g/cm^3(2,800 kg/m^3). Thus, the minerals referred to as the **rock-forming minerals** in the crust are, with few exceptions, members of the silicate, oxide, and carbonate groups that include oxygen as the major anion.

Quantitative chemical analyses of minerals allow for the grouping of elements on the basis of their abundance. When chemical elements occur in large amounts (>1 wt. %), they are considered to be **major elements** and are measured in weight percent (wt. %). **Minor elements** occur in smaller amounts (0.1–1.0 wt. %), but are also measured in weight percent. Other elements occur in minute amounts (< 0.1 wt. %), and are referred to as **trace elements**. Trace elements are measured in parts per million (ppm) or parts per billion (ppb). Despite their low abundance, trace elements may provide insights into geologic processes, such as the temperature or pressure at which minerals form.

Many elements important to our economy have very low average abundances in the crust (Table 5.1) and occur as *trace elements*. For example, in a typical crustal rock, Cu (atomic number, $Z = 29$) has an abundance of 55 ppm, Pb ($Z = 82$) = 13 ppm, and Hg ($Z = 80$) = 0.08 ppm. Interestingly, the less commonly used element, Zr ($Z = 40$), is more abundant (with an average of 165 ppm) than the commonly used element, Cu. The occurrence of trace elements in rocks is reflected in two different modes: (1) as elements that make their own minerals and (2) as elements that are only dispersed or taken up into other minerals. Some elements that are strongly concentrated in specific minerals include Zr (to make the mineral zircon, $ZrSiO_4$), and Ti (in rutile, TiO_2, and ilmenite, $FeTiO_3$.) In contrast, rubidium (Rb, $Z = 37$) generally does not form specific Rb compounds. Instead, it is dispersed throughout common K-bearing minerals. Therefore, Rb is an example of a **dispersed element**.

COMPOSITION OF THE MANTLE

The division between the crust and upper mantle (the Moho) is associated with a significant chemical change from a silica- and aluminum-rich crustal composition to a more silica-poor, magnesium-, and iron-richer mantle composition. Consequently, the upper mantle is dominated by the mineral olivine with lesser amounts of pyroxene and only trace amounts of aluminous minerals, such as feldspar, spinel, and garnet. It is possible for scientists to directly evaluate the mineralogy of the upper mantle (below the crust and down to about 220 km) by examining samples brought to the surface in volcanic eruptions and along large faults. Pieces of the mantle occur in basalts, such as at San Carlos, Arizona (Fig. 5.3) as well as in *kimberlite* pipes. Kimberlites are products of old, violent volcanic eruptions that blast to the surface at supersonic speeds from depths of 250 km to 350 km. This rapid ascent preserves minerals, such as diamond (see Chapter 15), formed deep within the Earth.

At greater depths and higher pressures, the mantle transition zone is marked by discontinuities associated with changes in material properties (thus, the use of the

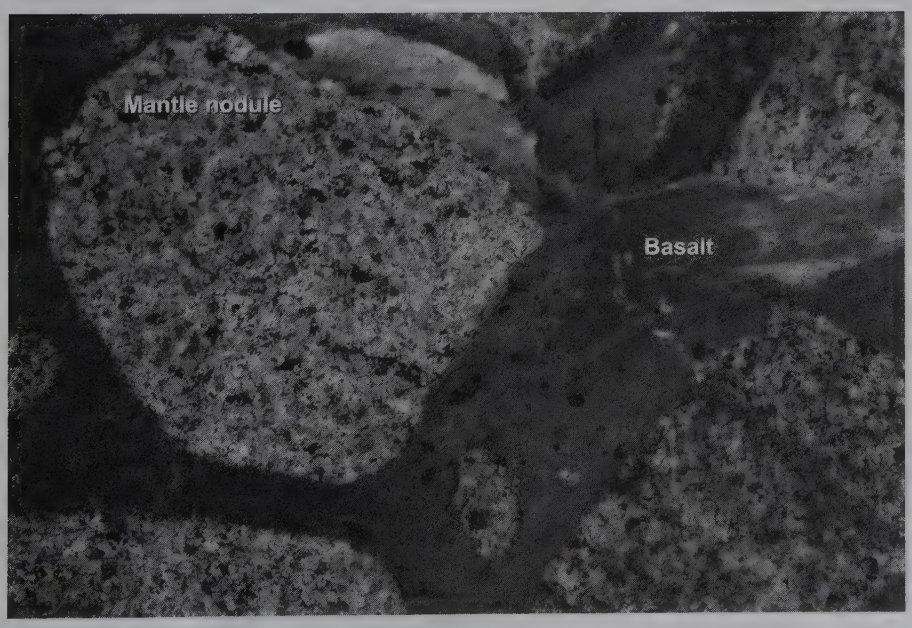

FIG. 5.3 Mantle nodules brought to the surface by basalt, from the San Carlos, Arizona, volcanic field. The nodules consist primarily of the minerals olivine, two pyroxenes (Mg- and Cr-rich), and spinel. The nodules are ~15 cm in width. (Photograph by B. Dutrow.)

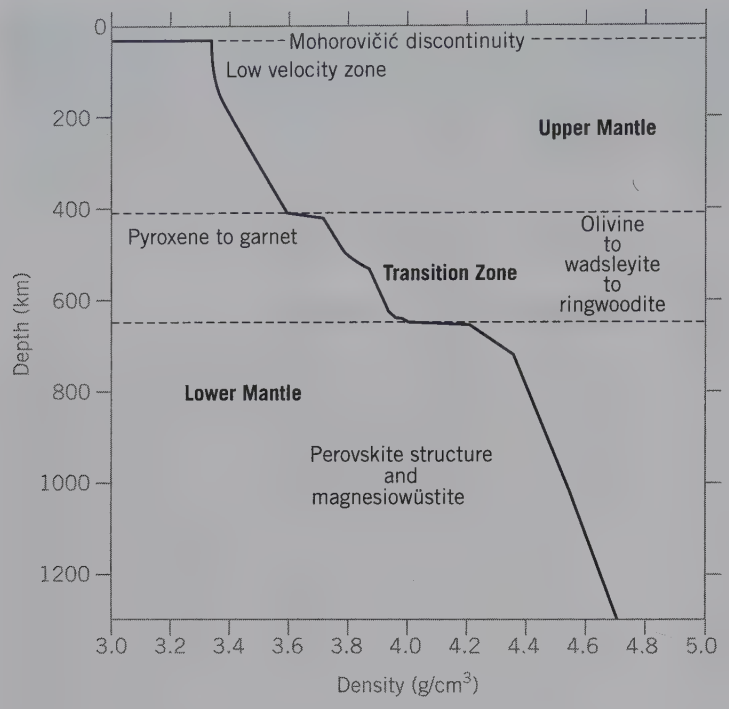

FIG. 5.4 Changes in mineralogy, structure packing and assemblages, as a function of depth within the mantle. Density is shown as the heavy black line. Below 660 km, it is likely that all silicon is in 6-fold coordination with oxygen. (Modified from Stixrude, L., and C. Lithgow-Bertelloni. 2005. Mineralogy and elasticity of the oceanic upper mantle: Origin of the low velocity zone. *Journal of Geophysical Research* 110:B03204.)

word *transition*) without a major change in overall chemical composition, as shown in Fig. 5.4. At about 400 km, olivine, Mg_2SiO_4, will isochemically transform to a denser structure with closer packing, a spinel structure, named ringwoodite. The intermediate phase in this reaction is another spinel, wadsleyite. This transformation sequence is:

$Mg_2^{[6]}Si^{[4]}O_4$	$\rightarrow Mg_2^{[6]}Si^{[4]}O_4$	$\rightarrow Mg_2^{[6]}Si^{[4]}O_4$
olivine structure	spinel structure (wadsleyite)	spinel structure (ringwoodite)
(ρ = 3.22 gm/cm^3)	(ρ = 3.47 gm/cm^3)	(ρ = 3.55 gm/cm^3)

ρ represents the density of the minerals. The density values reflect the closer packing (refer to Chapters 2 and 4). The superscripts in square brackets refer to the coordination numbers of the sites; where [6] = **C.N.** 6 and [4] = **C.N.** 4. Similarly, the pyroxene structure adopts a denser garnet-type structure at the 400 km discontinuity.

At still higher pressures, which exist at depth of about 660 km, silicates undergo another radical mineralogical and structural rearrangement, and silica goes from tetrahedral coordination [4] to octahedral coordination [6]. Below such depths, Si in Mg-silicates is probably only in stable octahedral coordination, **C.N.** = 6. This depth is also where spinel structures, and other Ca- and Mg-silicates, transform to the *perovskite* structure together with other oxide structures. In the perovskite structure (Fig. 5.5), six oxygens cluster around each Si and eight such octahedra are grouped around the Mg. Such a structure is in sharp contrast to those of silicate minerals in the Earth's crust, where four oxygens surround each Si in tetrahedral coordinaton. The general transformation sequence is:

$Mg_2^{[6]}Si^{[4]}O_4$	$\rightarrow Mg_2^{[8]}Si^{[6]}O_3$	$+Mg^{[6]}O$
spinel structure (ringwoodite)	perovskite structure	halite structure
(ρ = 3.55 gm/cm^3)	(ρ = 4.10 gm/cm^3)	

It is unclear whether the 660 km discontinuity represents only a change in composition or a structural change as well (see also Navrotsky, 1994).

FIG. 5.5 The perovskite structure type. The Si^{4+} (small black spheres) are located at the center of octahedra, where each octahedral corner represents one oxygen (**C.N.** = 6). The large cation in the center of the structure represents Mg^{2+}, Fe^{2+} and/or Ca^{2+} and is coordinated to eight SiO_6 octahedra packed around it. The coordination of this site is variable from **C.N.** = 8 to **C.N.** = 12.

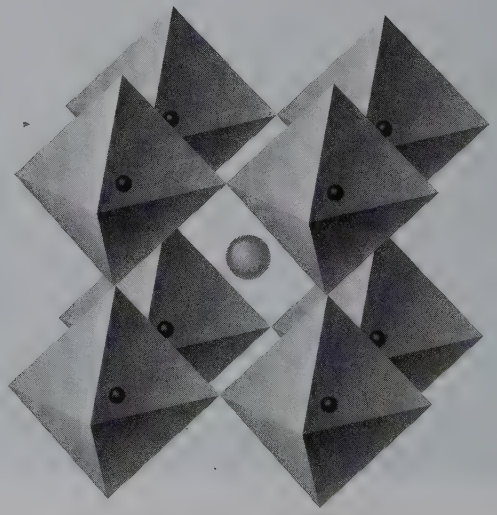

The lower mantle, below the 660 km discontinuity, consists of the mineral perovskite together with small amounts of the oxide mineral (Mg, Fe)O, magnesiowüstite, which is a high pressure product of ringwoodite. Because of the large predicted abundance of silicate perovskite (e.g., $Mg^{[8]}Si^{[6]}O_3$) in the lower mantle (80–100% by volume between 660–2,900 km), it is concluded that the silicate perovskite structure type may be the most abundant single phase in the planet. (However, the mineral perovskite, $CaTiO_3$, is a very uncommon mineral in the crust). The enigmatic D″ region occurs at about 200 km above the core-mantle boundary. Here, it is suggested that perovskite transforms to a more tightly packed structure, termed "post-perovskite," a synthetic mineral phase discovered in high temperature and pressure experiments (see Murakami et al., 2004). Examples of the greatly increased densities, reflecting much denser packing of structures at these pressures, are given for a few common silicate minerals in Table 5.2.

For the deeper mantle (e.g., below 250 km) from which no direct samples are obtainable, high temperature and high pressure laboratory experiments and computer simulations are used to determine which minerals are stable at these conditions (Fig. 5.4). These techniques, in combination with other geophysical tools, help to determine the composition and structure of minerals in the deeper portions of the mantle. Meteorites, samples of the ancient solar system, are also used to predict mantle mineralogy because they are thought to represent similar materials. Stony (silicate) meteorites (Fig. 5.6), with little metal, are probably analogous to materials in the mantle. The composition of iron meteorites (mainly FeNi alloy; see Fig. 1.2) is concluded to be very similar to the composition of the Earth's core.

Table 5.2 Compositions and Measured Densities of Three Common Crustal Mineral Types as Compared with Their Calculated Densities in High-Pressure Polymorphs with SiO_6 Octahedra*

Mineral	Density	C.N. (Si)
SiO_2 (quartz)	2.65	4
SiO_2 (stishovite)	4.29*	6 (rutile structure type)
$CaSiO_3$ (wollastonite)	2.91	4
$CaSiO_3$	4.25*	6 (perovskite structure type)
$MgSiO_3$ (enstatite)	3.21	4
$MgSiO_3$	4.10*	6 (perovskite structure type)

*High-pressure polymorphic data from Hazen, R. M., and L. W. Finger. 1991. Predicted high-pressure mineral structures with octahedral silicon. *Geophysical Laboratory Annual Report.* Carnegie Institution of Washington, no. 2250, 101–107.

FIG. 5.6 A polished and etched slab of the Imilac pallasite (a silicate-metal meteorite) displaying centimeter-sized, well-rounded olivines dispersed in metal (an iron-nickel alloy). The width of the sample is about 7 cm. (Photograph courtesy of the Smithsonian Institution, Washington, D.C.)

COMPOSITION OF THE CORE

The transition from the lower mantle to the core is a definite chemical discontinuity. The core is extremely dense and represents 30% of Earth's mass but only one-sixth (17%) of its volume. This core volume is larger than the entire planet Mars. The liquid outer core, from 2,900–5,100 km, consists primarily of iron plus about 2% nickel. Its well-known density (9.9 g/cm^3, or 9,900 kg/m^3) is slightly too low to represent the density of pure iron (10.6 g/cm^3, or 10,600 kg/m^3) and incorporation of 9% to 12% silica, or other light elements, produces a better fit with the known density. The solid inner core, from 5,100 km to 6,371 km, also consists of an Fe-Ni alloy, containing about 20% nickel. The core has pressures that are 3 million times atmospheric pressure and temperatures that rise to 7,600°C (13,700°F). Experimental studies of minerals at extremely high pressures and temperatures show that this environment causes very different mineral behavior from what is observed in the mantle or crust.

COMPOSITION OF THE EARTH

Although we cannot directly determine the average composition of the entire Earth, assumptions and calculations can be made using constraints that include the average compositions of different types of meteorites and the known volumes and compositions of the core, mantle, and crust. This provides an average estimate for the whole Earth composition. Based on this procedure, Mason and Moore (1982) calculated the average weight percentage composition of the Earth as: Fe, 34.63%; O, 29.53%; Si, 15.20%; Mg, 12.70%;

Ni, 2.39%; S, 1.93%; Ca, 1.13%; Al, 1.09%; and seven other elements (Na, K, Cr, Co, Mn, P, and Ti) each in amounts from 0.1% to 1%. Although all of these elements, in the calculated *average Earth abundance* (except for Ni and S), are also major elements in the *average crustal abundance* listing (Table 5.1 and Fig. 5.2), their order is altered because of the inclusion of materials from the Fe-Ni-S–rich core and the silicate-rich mantle. Thus, this means that *only about 10 to 15 chemical elements are the common chemical building blocks of most minerals* (Fig. 5.2).

VARIABILITY OF MINERAL COMPOSITIONS

Now that the major, common chemical constituents that comprise minerals are identified, the composition of individual minerals can be examined. A portion of the definition of a mineral states, "*. . . with a definite (but not necessarily fixed) chemical composition*" (see Chapter 1). This aspect of the definition reflects the fact that most minerals vary in their chemical composition. It is the exceptional mineral that is essentially a *pure substance*; quartz, SiO_2, and corundum, Al_2O_3, are two notable examples.

Compositional variation is known as **solid solution** and occurs in minerals as a result of chemical substitution in the crystal structure. One ion or ionic group can exchange or substitute with another ion or ionic group occupying a specific structural site in the mineral. This type of exchange process is referred to as **ionic** (or **atomic**) **substitution** or *solid solution*. Solid solution occurs among minerals that are *isostructural*, those minerals that have the same atomic structure (*iso* is the Greek word for equal; Chapter 4). *A solid solution is a range of composition in a mineral in which specific atomic site(s) are occupied by two or more different chemical elements (or ions) in variable proportions.* In other words, a mineral with solid solution has one (or more) element(s) or ion(s) that substitute in the same atomic site within the crystal structure. In a mineral formula, elements or ions that substitute for one another are grouped together in parentheses, for example, (Fe, Mg)O. At the end of the compositional spectrum of a solid solution series are **end members**; these are the *fixed* mineral formulae that show no chemical substitution.

The principle factors that determine the degree of solid solution in a mineral structure are:

1. *The* **relative sizes** *of the ions, atoms, or ionic groups that are substituting for each other.* Generally, a wide range of substitution is possible if the *size difference* between the ions (or atoms) replacing one another is *less than ~15%*. If the radii of the two elements differ by 15% to 30%, substitution is limited or rare, and if the radii differ by more than 30%, substitution is poor to nonexistent. The potential for solid solution to occur can be evaluated easily by determining the percentage difference between the size of the individual radii (given in Table 3.8).

2. *The* **charges** *of the ions involved in the substitution.* Mineral structures must maintain electrical neutrality. If the charges of the substituting ions are the same, as in Mg^{2+} and Fe^{2+}, the ionic replacement remains electrically neutral and is, therefore, more likely. If the charges are not the same, as in the case of Al^{3+} substituting for Si^{4+}, an additional ionic substitution in another structural site must take place in order to maintain overall electrostatic neutrality. One such example is:

$$Al^{3+} + Ca^{2+} \rightleftarrows Si^{4+} + Na^{+}$$

The total charge of the ions on the left portion of the equation is 5^+, and the same total charge, 5^+, is found on the right. This double substitution occurs because Al and Si are similar in size, as are Ca and Na. When two or more ions substitute in different structure sites to maintain charge balance, it is called **coupled substitution**.

3. *The* **temperature and pressure** *at which the substitution takes place.* Minerals, similar to other materials, tend to expand at higher temperatures and compress at greater pressures. There is, in general, a greater tolerance toward ionic substitution at higher temperatures when thermal vibrations (of the overall structure) are greater resulting in expanded structures. At elevated temperatures, the sizes of available atomic sites are larger and more tolerant of size differences. Therefore, in a given structure, one expects a larger variability in a mineral composition at higher temperature than at lower temperature. The converse occurs with increasing pressure. As pressure increases, crystal structures compress and are less tolerant of size discrepancies. As both temperature and pressure increase, temperature is typically the overriding factor.

4. *The* **availability** *of the ion(s).* For solid solution to occur, substituting ions must be readily available. In a chemical environment, for example, where Fe is rare and Mg abundant, little substitution of Fe^{2+} for Mg^{2+} would occur.

There are three types of solid solution mechanisms, referred to as **substitutional, interstitial,** and **omission** solid solution. (Extensive coverage of these concepts is found in module I of the CD-ROM under the heading "Solid Solution Mechanisms.")

SUBSTITUTIONAL SOLID SOLUTION

The simplest types of ionic substitutions are *simple cationic* or *anionic* substitutions. In a compound of the type A^+X^-, A^+ may be partly or completely replaced by B^+ with no valence change. An example of this type of substitution is the replacement of Rb^+ for K^+ in KCl, resulting in (K,Rb)Cl. Similarly, a simple anionic substitution can occur in an A^+X^- compound as some amount of X^- replaced by Y^-. An example of this is the incorporation of Br^- in the structure of KCl in place of Cl^-, resulting in K(Cl,Br). An example of a **complete binary solid solution series**, meaning that substitution of one ion by another occurs over the total possible compositional range as defined by two end member compositions, is the mineral olivine $(Mg,Fe)_2SiO_4$. In the olivine structure, Mg^{2+} can be replaced, in any proportion or completely, by Fe^{2+}. The *end members* of the olivine series are Mg_2SiO_4, forsterite, and Fe_2SiO_4, fayalite, and there is complete solid solution between these ends of the compositional range. Because the ionic radii of Mg^{2+} (= 0.72 Å for **C. N.** = 6) and Fe^{2+} (= 0.78 Å for **C. N.** = 6; both from Table 3.8) are so close, their size difference is only 0.06 Å. This can be stated in terms of the percentage difference of the size: 0.06/0.72 = 0.0833 or 8.33% (which is well within the 15% limit). They also are both divalent in charge, and for these reasons the two elements substitute for one another in many minerals. Another example of a complete solid solution series is $(Mn,Fe)CO_3$, which extends from $MnCO_3$, rhodochrosite, to $FeCO_3$, siderite. An example of a complete anionic series between two compounds is KCl and KBr. Here, the size of the two anions is within 10% of each other, allowing for complete substitution of Cl^- and Br^- (that is, the size of Br^- for **C. N.** = 1.96 Å and that of Cl^- for **C. N.** = 1.81 Å, with a difference in size of 0.15 Å; both values from Table 3.8). This recalculates to a percentage size difference as follows: 0.15/1.81 = 0.0828 or 8.28% (Fig. 5.7). An example of extensive, but not complete, simple cation solid solution is shown by the mineral sphalerite, (Zn,Fe)S, where Fe^{2+} replaces Zn^{2+} in the structure. This substitution is discussed in detail in the section that covers mineral formula calculations in Table 5.4.

Simple cationic:

$Mg^{2+} \rightleftarrows Fe^{2+}$ (complete)	Mg^{2+} [6] = 0.72Å
$Fe^{2+} \rightleftarrows Mn^{2+}$ (complete)	Fe^{2+} [6] = 0.78Å
$Na^+ \rightleftarrows K^+$ (partial)	Mn^{2+} [6] = 0.83Å
$Mg^{2+} \rightleftarrows Mn^{2+}$ (partial)	Na^+ [8] = 1.18Å
	K^+ [8] = 1.51Å

Simple anionic:

$Br^- \rightleftarrows Cl^-$ (complete)	Br^- [6] = 1.96Å
	Cl^- [6] = 1.81 Å
$I^- \rightleftarrows Cl^-$ (partial)	I^- [6] = 2.20Å

Coupled cationic:			***Extent of solid solution:***
Na^+Si^{4+}	$\rightleftarrows$	$Ca^{2+}Al^{3+}$	complete at high temperature in plagioclase
2 cations: total charge 5^+		2 cations: total charge 5^+	
$Ca^{2+}Mg^{2+}$	$\rightleftarrows$	Na^+Al^{3+}	limited, as in omphacite, a member of the pyroxene group
2 cations: total charge 4^+		2 cations: total charge 4^+	
$Mg^+Al_2^{3+}$	$\rightleftarrows$	$Fe^{2+}{}_2Ti^{4+}$	extensive, as in the spinel group
3 cations: total charge 8^+		3 cations: total charge 8^+	
$\square^\circ + Si^{4+}$	$\rightleftarrows$	Na^+Al^{3+}	extensive, as in arfvedsonite, a sodium amphibole
2 sites: total charge 4^+		2 cations in 2 sites: total charge 4^+	
$\square^\circ$ = vacancy			

FIG. 5.7 Examples of various types of substitutional solid solution. Ionic radii are taken from Table 3.8. Square brackets after the ions enclose the coordination number.

COUPLED SUBSTITUTION

If in a general composition of $A^{2+}X^{2-}$, a cation B^{3+} substitutes for some of A^{2+}, electrical neutrality is maintained if an identical amount of A^{2+} is simultaneously replaced by cation C^{+}. This is represented by

$$2A^{2+} \rightleftarrows 1B^{3+} + 1C^{+}$$

with identical total electrical charges on both sides of the equation. This type of substitution is known as **coupled substitution**. The substitution of Fe^{2+} and Ti^{4+} for $2Al^{3+}$ in the corundum, Al_2O_3, structure of gem sapphire is an example of a coupled substitution. The plagioclase feldspar series can be represented in terms of two end members, $NaAlSi_3O_8$, albite, and $CaAl_2Si_2O_8$, anorthite. A complete solid solution between these two end member compositions results from the coupled substitution:

$$Na^{+} + Si^{4+} \rightleftarrows Ca^{2+} + Al^{3+}$$

This means that for each Ca^{2+} that replaces Na^{+} in the feldspar structure, one Si^{4+} is replaced by Al^{3+} so that the structure remains electrically neutral. An example of only limited coupled solid solution is provided by two pyroxenes, diopside, $CaMgSi_2O_6$, and jadeite, $NaAlSi_2O_6$. This coupled replacement is represented as: $Ca^{2+}Mg^{2+} \rightleftarrows Na^{+}Al^{3+}$. Although the pyroxene structure is electrically neutral with either type of cation pair, the atomic sites and coordination polyhedra restrict the amount of solid solution that is possible (Fig. 5.7).

INTERSTITIAL SOLID SOLUTION

Between atoms, ions, or ionic groups of a crystal structure, interstices may exist that normally are empty. Occasionally, ions or atoms occupy these structural sites resulting in what is known as **interstitial substitution** or **interstitial solid solution**. In some crystal structures, these voids may be channel-like cavities as in beryl, $Be_3Al_2Si_6O_{18}$, a cyclosilicate (see Fig. 18.12). Large ions as well as molecules, such as Na^{+}, K^{+}, Rb^{+}, Cs^{+}, H_2O, and CO_2, can occupy the tubular cavities of the superimposed rings (Fig. 5.8). H_2O and CO_2 molecules are weakly bonded to the internal oxygens of the six-fold Si_6O_{18} rings. The large monovalent alkalis Na^{+}, K^{+}, Rb^{+}, and Cs^{+} are also located inside these rings, but they are much more strongly bonded than H_2O or CO_2 because of the following coupled substitutional mechanisms:

$$Si^{4+} \rightleftarrows Be^{2+} + 2R^{+}$$

$$Be^{2+} \rightleftarrows Li^{+} + R^{+}$$

and

$$Si^{4+} \rightleftarrows Al^{3+} + R^{+}$$

FIG. 5.8 Plan view of the hexagonal structure of beryl, $Be_3Al_2Si_6O_{18}$, projected onto the basal plane (0001). The Si_6O_{18} rings at two different heights are shown. The hexagonal channels are the locus for large alkali ions and neutral molecules, such as H_2O and CO_2. A unit cell is outlined by dashed lines.

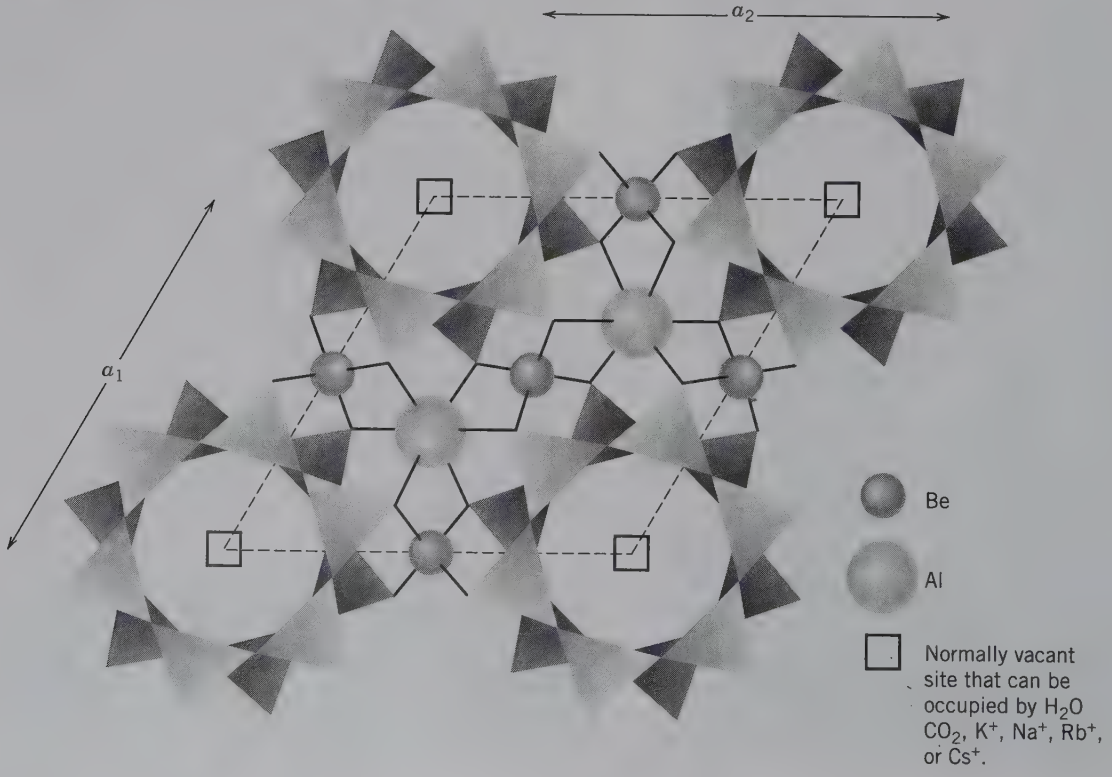

where R represents Na^+, K^+, Rb^+, or Cs^+. In the first substitution equation, two monovalent alkali cations are housed inside the openings (the interstices) of the hexagonal rings; in the second and third equations, only one cation is positioned there.

Another example of interstitial solid solution occurs in the zeolite group of silicates (see Chapter 18). The zeolites constitute a group of tectosilicates in which (SiO_4) and (AlO_4) tetrahedra are linked together in an open framework. Within this skeletal framework, there may be large voids and continuous channels with openings ranging from 2 to 9 Å in diameter. These channels provide easy access to the interior of the crystals, and they can accommodate large H_2O molecules.

OMISSION SOLID SOLUTION

Omission solid solution occurs when a more highly charged cation replaces two or more lower-charged cations. To maintain charge balance, another site (or sites) is left unfilled, or vacant (omitted). Here, the substitutional scheme is a coupled subsitution that involves a vacancy, which is shown as a □;. For instance, when Pb^{2+} substitutes for K^+ in the blue-green variety of microcline feldspar ($KAlSi_3O_8$), Pb^{2+} replaces two K^+ ions (for charge balance), but Pb^{2+} occupies only one site leaving the other original K^+ site vacant.

$$K^+ + K^+ \rightleftarrows Pb^{2+} + \square$$

This creates a lattice vacancy, □, which becomes a color center to produce the color (see Chapter 10 for details).

Another example is a partial coupled substitution that occurs in the amphibole tremolite, $\square Ca_2Mg_5Si_8O_{22}(OH)_2$. Here, the open box, □, represents the normally vacant A site in the structure that may be filled by some Na according to:

$$\square + Si^{4+} \rightleftarrows Na^+ + Al^{3+}$$

In this *coupled substitutional* scheme, Al^{3+} replaces Si^{4+} in the tetrahedral position, and the additional Na^+ is housed in the 10-12 fold site that is normally vacant (Fig. 5.7).

The best-known mineralogical example of **omission solid solution** is provided by the mineral pyrrhotite, $Fe_{(1-x)}S$. In pyrrhotite, sulfur occurs in hexagonal closest packing and iron in 6-fold coordination with sulfur. If all sites are fully occupied by Fe^{2+}, the formula of pyrrhotite would be FeS (the mineral troilite). However, in pyrrhotite, the number of octahedral site vacancies varies, causing the composition to range from Fe_6S_7 (where $x = 0.143$) through $Fe_{11}S_{12}$ (where $x = .084$) so that the formula is generally expressed as $Fe_{(1-x)}S$, with x ranging from 0 to ~0.2. When Fe^{2+} is absent from some of the octahedral sites, with the sulfur net completely intact, the structure is not electrically neutral. It is likely that some of the Fe is in the Fe^{3+} state to compensate for the deficiency in Fe^{2+}. If this is so, a neutral pyrrhotite formula can be written as $(Fe^{2+}_{1-3x}Fe^{3+}_{2x})\square_xS$, where □ represents vacancies in the cation position. If x in this example were 0.1, there would be 0.1 vacancies, 0.7 Fe^{2+}, and 0.2 Fe^{3+} in the pyrrhotite structure. In other words, Fe^{3+} is accommodated in the pyrrhotite structure by the following substitution: $Fe^{2+} + Fe^{2+} + Fe^{2+} = Fe^{3+}\ 1\ Fe^{3+} + \square$, which results in a vacancy □. Or, when every two Fe^{2+} are replaced by two Fe^{3+}, this results in two extra charges, so that one Fe^{2+} site is left vacant for charge compensation. Minerals, such as pyrrhotite in which a particular structural site is incompletely filled, are known as defect structures (see Fig. 5.9 for a structural image of pyrrhotite).

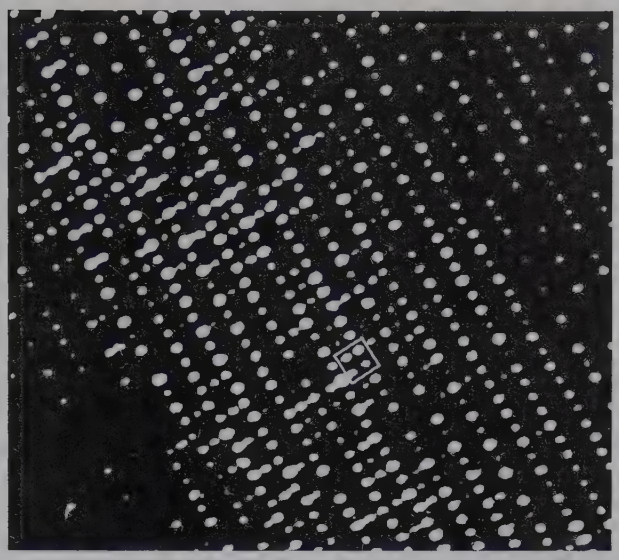

FIG. 5.9 High-resolution transmission electron microscope (HRTEM) structure image of pyrrhotite, $Fe_{1-x}S$, in which the white spots correspond to columns of iron atoms; these columns are aligned perpendicular to the plane of the photograph. The less intense spots represent columns from which some of the iron atoms are missing (omission solid solution). The columns are alternately more or less fully occupied by iron atoms. The white square is 3 Å to a side. (From Pierce, L., and P. R. Buseck. 1974. Electron imaging of pyrrhotite superstructures. *Science* 186: 1209–12; copyright 1974 by the AAAS. See also Buseck, P. R., 1983. Electron microscopy of minerals. *American Scientist* 7: 175–85.)

DETERMINATION OF A MINERAL FORMULA

Most minerals are solid solutions and, therefore, this chemical variability must be taken into account when determining their chemical composition. The procedure

Table 5.3 Chalcopyrite, $CuFeS_2$, Recalculations

	1 Weight Percent	2 Atomic Weights	3 Atomic Proportions	4 Atomic Ratios
Cu	34.30	63.55	0.53973	1
Fe	30.59	55.85	0.54772	1 approx.
S	34.82	32.06	1.08575	2
Total	99.71			

	Atomic Weights		
Cu	63.55	Cu (in %) = $\frac{63.55}{183.52} \times 100\% = 34.53$	
Fe	55.85	Fe (in %) = $\frac{55.85}{183.52} \times 100\% = 30.53$	
S (2×)	(32.06) × 2	S (in %) = $\frac{64.12}{183.52} \times 100\% = 34.94$	
Total	183.52		Total 100.00

by which the actual mineral formula is calculated, from a set of quantitative chemical data, follows. (Description of analytical techniques for obtaining such chemical analyses is given in Chapter 14). Beginning with simple compositions, the derivation of chemical formulae progresses to more complicated mineral compositions.

Elements, such as gold, arsenic, and sulfur, occur in the native state and their mineral formulae are the chemical symbols of the elements, that is Au, As, and S. Most minerals, however, are compounds composed of two or many more elements, and their chemical formulae indicate the atomic proportions of the elements present. For example, in galena, PbS, there is one atom of sulfur for each atom of lead, and in chalcopyrite, $CuFeS_2$, there is one atom of sulfur for each atom of copper and iron. Such specific atomic proportions underlie the definition of a mineral, "*. . . a definite chemical composition (but not necessarily fixed).*"

Calculation of these atomic proportions allows for the derivation of mineral formulae.

CALCULATION OF MINERAL FORMULAE FROM METAL PERCENTAGES

A quantitative chemical analysis provides the basic information for the atomic formula of a mineral (see Chapter 14 for analytical methods). Typically, a quantitative analysis is reported in weight percentages (wt. %) of metals, or oxides, and is a listing of which elements are present in what concentrations. An example of a quantitative analysis for chalcopyrite is given in Table 5.3, column 1. The analysis should add up to within 1% of 100%. Slight variations above or below 100% occur because of cumulative small errors inherent in the analytical procedure. For example, the total for the chalcopyrite analysis (in Table 5.3) is 99.71.

Because the elements have different atomic weights, these percentages do not represent the ratios of the numbers of different atoms. These must be calculated. To arrive at the relative proportions of the elements, the weight percentage in each element is divided by the atomic weight of the element. This gives the *atomic proportions* (column 3 in Table 5.3) from which the *atomic ratios* can be quickly derived (column 4). In the analysis of chalcopyrite, these ratios are Cu : Fe : S = 1 : 1 : 2; resulting in $CuFeS_2$ as the chemical formula. The reverse procedure, that of calculating the elements' weight percentages from the formula, is

Table 5.4 Recalculation of Several Sphalerite, ZnS, Analyses and of Troilite, FeS

	WEIGHT PERCENTAGE*				
	1	2	3	4	5
Fe	0	0.15	7.99	18.25	63.53
Mn	0	0	0	2.66	0
Cd	0	0	1.23	0.28	0
Zn	67.10	66.98	57.38	44.67	0
S	32.90	32.78	32.99	33.57	36.47
Total	100.00	99.91	99.59	99.43	100.00
	RECALCULATED IN TERMS OF ATOMIC PROPORTIONS				
Fe	0	0.003	0.143	0.327	1.137
Mn	0	0	0	0.048	0
Cd	0	0	0.0011	0.002	0
Zn	1.026	1.024	0.878	0.683	0
		0 1.027	1.032	1.060	
S	1.026	0.022	1.029	1.047	1.137
(Zn + Fe + Mn + Cd) : S	1 : 1	1 : 1	1 : 1	1 : 1	1 : 1
Formulas	ZnS	$(Zn_{0.997}Fe_{0.003})S$	$(Zn_{0.851}Fe_{0.138}Cd_{0.011})S$	$(Zn_{0.644}Fe_{0.308}Mn_{0.045}Cd_{0.002}S$	FeS
Fe : Zn	0 : 100	0.3 : 99.7	14.0 : 86.0	32.4 : 67.6	100 : 0

*Analysis 1–4 from *Dana's System*, v. 1, 1994; analysis 5 for pure troilite FeS.

shown in the lower half of Table 5.3. The formula of chalcopyrite is $CuFeS_2$; thus, the gram-formula weight (weight of one mole of chalcopyrite) is 183.52 (found by adding the atomic weights of Cu + Fe + 2S, column 2). Dividing the weight of each element by the total weight and converting these values to percentages, yields the calculated Cu, Fe, and S weight percentage values, very similar to the measured percentages reported in column 1 of Table 5.3. The calculated values are slightly different from the determined values, probably because of slight errors introduced by the analysis technique.

Another example is given by several sphalerite, ZnS, analyses, which show solid solution with Fe, Cd, and Mn, and a considerable range in Fe, toward the end-member troilite, FeS (Table 5.4). The upper half of the table shows a series of weight percentages for the various elements from five different analyses. The atomic proportions for each element are obtained by dividing each weight percentage by the atomic weight of the element. For sphalerite and troilite, the ratio of (Zn + Fe + Mn + Cd):S is a constant value of 1:1 (columns 1 and 5). However, the Zn in the sphalerite structure is partially substituted by variable amounts of Fe, Mn, and Cd (analyses 2, 3, 4). The maximum amount of Fe shown is 18.25 wt. % Fe (column 4). This corresponds to 0.327 atomic proportions out of a total of 1.060 atomic proportions for (Zn + Fe + Mn + Cd). These analyses of naturally occurring sphalerites show that the formula, ZnS, is an oversimplification. For the sphalerite with the largest amount of Fe solid solution (column 4), the total cation content (in atomic percentage) is 1.060. Fe is $0.327/1.060 \times 100 = 30.8\%$; similarly, Mn, Cd, and Zn values are 4.5, 0.2, and 64.4%, respectively. The cation proportion values can be used as subscripts to represent the composition of the sample of sphalerite in column 4; this leads to the formulation $(Zn_{0.644}Fe_{0.308}Mn_{0.045}Cd_{0.002})S$. The other formulae in Table 5.4 were obtained in a similar manner. If the percentage of Fe with respect to Zn is needed (to evaluate temperature of formation, for example), only the total of (Fe + Zn) is used. For example, in analysis 4 (Fe + Zn = 1.010, rather than 1.060 for Fe + Zn + Cd + Mn), the factor $(0.327/1.010) \times 100 = 32.4\%$ (last line of Table 5.4) is used. These Fe:Zn ratios show that this suite of sphalerites shows *a compositional range*, or *solid solution*, from pure ZnS to $(Zn_{0.68}Fe_{0.32})S$. The mineral troilite, FeS, is found only in meteorites and contains no Zn; it can be considered as an end member composition in this binary series.

MINERAL FORMULAE FROM OXIDE WEIGHT PERCENTAGES

The majority of minerals, such as silicates, oxides, carbonates, etc., are compounds containing large quantities of oxygen. By convention, the analyses of these minerals are reported as percentages of oxides, rather than as percentages of elements. To determine the proportions of elements from oxide components requires a few additional steps to those outlined previously. The end result is a statement of molecular proportions of the oxides, rather than atomic proportions of elements.

Table 5.5 gives an example of the recalculation of an analysis of gypsum. The analytically determined oxide components in column 1 are divided by the molecular weights of the corresponding oxides (column 2) to arrive at molecular proportions (column 3). From

Table 5.5 Recalculation of Gypsum, $CaSO_4 \cdot H_2O$, and Olivine, Mg_2SiO_4, Analyses

Gypsum	1 Weight Percent	2 Molecular Weights	3 Molecular Proportions	4 Molecular Ratios	
CaO	32.44	56.08	0.57846	1	approx.
SO_3	46.61	80.06	0.58219	1	
H_2O	20.74	18.0	1.15222	2	
Total	99.79				

Olivine	1 Weight Percent	2 Molecular Weights	3 Molecular Proportions	4 Atomic Proportions Cations	5 Atomic Proportions Oxygens	6 On Basis of 4 Oxygens		7 Atomic Ratios
SiO_2	34.96	60.09	0.58179	Si 0.5818	1.1636	0.989		1
FeO	36.77	71.85	0.51176	Fe^{2+} 0.5118	0.5118	0.870		
MnO	0.52	70.94	0.00733	Mn 0.0073	0.0073	0.012	2.022	2
MgO	27.04	40.31	0.67080	Mg 0.6708	0.6708	1.140		
Total	99.29				2.3535			

Olivine in terms of end-member compositions: Mg = 1.140, Fe = 0.870; total; 2.010. Percentage Mg = 56.7; percentage Fe = 43.3; percentage Mg_2SiO_4 = % fosterite = % Fo = 56.7%; percentage Fe_2SiO_4 = % Fayalite = % Fa = 43.3%.

Table 5.6 Recalculation of a Pyroxene, $CaMgSi_2O_6$, Analysis

	1	2	3	4	5		6		7
	Weight Percent	Molecular Proportions	Cation Proportions	Number of Oxygens	Cations on Basis of 6 Oxygens		Cation Assignment		End Member Recalculation
SiO_2	50.38	0.8384	0.8384	1.6768	1.875	Si	1.875	2.0	MgO as $MgSiO_3$
Al_2O_3	3.01	0.0295	0.0590	0.0885	0.132 →	Al	0.125		(enstatite = En)
					↘	Al	0.007		FeO as $FeSiO_3$
TiO_2	0.45	0.0056	0.0056	0.0112	0.012	Ti	0.012		(ferrosilite = Fs)
Fe_2O_3	1.95	0.0122	0.0244	0.0366	0.055	Fe^{3+}	0.055	1.033	CaO as $CaSiO_3$
FeO	4.53	0.0630	0.0630	0.0630	0.141	Fe^{2+}	0.141	≃ 1	(wollastonite = Wo)
MnO	0.09	0.0013	0.0013	0.0013	0.003	Mn	0.003		Using molecular
MgO	14.69	0.3643	0.3643	0.3643	0.815	Mg	0.815		proportions:
CaO	24.32	0.4321	0.4321	0.4321	0.966	Ca	0.966	1.006	MgO = 0.3644
Na_2O	0.46	0.0074	0.0148	0.0074	0.033	Na	0.033	≃ 1	FeO = 0.0630
K_2O	0.15	0.0016	0.0032	0.0016	0.007	K	0.007		CaO = 0.4321
Total	99.44		Total O =	2.6828					Total = 0.8595
									% En = 42.39
			Oxygen factor $\frac{6}{2.6828}$ = 2.236469						%Fs = 7.33
									%Wo = 50.27

the molecular ratios in column 4 we see that $CaO:SO_3:H_2O = 1:1:2$. This composition can be written as $CaO \cdot SO_3 \cdot 2H_2O$, or as $CaSO_4 \cdot 2H_2O$. The latter formula is preferred because it avoids creating the erroneous impression that the mineral is composed of discrete oxide molecules.

A more complicated procedure is required in the case of the chemical analysis of a member of the olivine series (lower portion of Table 5.5). The steps in going from columns 1 to 3 are the same as in the gypsum analysis. In addition, column 4 lists the values for the atomic proportions of the various atoms, based on the molecular proportions determined in column 3. To arrive at the numbers in columns 4 and 5, the molecular proportion of each element is multiplied by the number of cations and anions in the oxide. For example, one "molecule" of SiO_2 contributes one Si (1 × column 3 = atomic proportions of cation in column 4). Similarly, one "molecule" of SiO_2 contributes two oxygens (2 × column 3 = atomic proportions of O in column 5). The total number of oxygens, contributed by the atomic proportions of each oxide in column 5, is 2.3535. At this point, a mineral formula of $Mg_{0.6708}Mn_{.0073}Fe_{.5118}Si_{.5818}O_{2.3535}$ has been calculated. Olivine, with the general formula of $(Mg, Fe)_2SiO_4$, has four oxygens (per formula unit) based on crystal structure data. To arrive at the cation proportions in terms of four oxygens instead of 2.3535, one must multiply each of the cation numbers in column 4 with 1.699 (the ratio of 4/2.3535, referred to as the oxygen factor). This leads to the numbers in columns 6 and 7. (If the oxygens are multiplied by this amount to arrive at a simple whole number, then the cation proportions must be multiplied by the same amount to maintain the correct ratios). The final chemical formula for this olivine is $(Mg_{1.14}Fe_{.87}Mn_{.01})SiO_4$, when only significant digits are taken into account.

Commonly, the chemical composition is expressed in terms of *end member compositions*. In olivine these are Mg_2SiO_4, forsterite, and Fe_2SiO_4, fayalite. The amounts of forsterite (Fo) and fayalite (Fa) in the composition are directly proportional to the atomic proportions of Mg and Fe, or molecular proportions of MgO and FeO, in the analysis. For example, (Mg / Mg + Fe) × 100 = Fo and (Fe / Fe + Mg) × 100 = Fa. This leads to Fo_{57} and Fa_{43} (see footnote to Table 5.5).

In contrast to olivine, many silicates have various structural sites among which elements can be distributed, or in which solid solution can occur. An example would be a mineral in the diopside-hedenbergite series of the pyroxenes ($CaMgSi_2O_6$ - $CaFeSi_2O_6$). Table 5.6 gives a chemical analysis, as well as the various recalculation steps, for pyroxene similar to that outlined previously for olivine. In analyses made by many instrumental techniques, Fe^{3+} and Fe^{2+} cannot be distinguished, and total Fe is then reported as FeO only, or Fe_2O_3 only. Here, both are listed. Column 2 provides molecular proportions, obtained by dividing the weight percent oxides by the appropriate molecular weights. Column 3 lists the cation proportions for each oxide "molecule," taking into account the number of cations in each oxide (for example, as there are 2 Al in Al_2O_3, the number of cation proportions in column 3 becomes

0.0295 × 2 = 0.0590). Column 4 lists the number of oxygens contributed by each oxide "molecule." Note that Al_2O_3 contains three oxygens per "molecule," therefore, the molecular proportion value (0.0295) is multiplied by 3. The total number of oxygens, contributed by all the oxide "molecules" in column 4, sums to 2.6828. From crystal structure data, pyroxene of this type has a general formula of $Ca(Mg,Fe)(Si,Al)_2O_6$ with six oxygens. The formula is, therefore, recalculated on the basis of six oxygens (6/2.6828). To achieve this, the values in column 3 are multiplied by 2.23647 to obtain those in column 5. However, the analysis provides no direct information about the location of the elements (or ions) in specific sites within the mineral structure.

Subsequently, cations are assigned to specific atomic sites in the pyroxene structure, based, in part, on their size (refer to Table 3.8). If necessary, sufficient Al is added to Si so that the sum Si + Al = 2.0 in column 6; the remainder of the Al is added to the sum of the intermediate size cations. These cations (Al, Ti, Fe^{3+}, Fe^{2+}, Mn, Mg) are assigned to the *M*1 cation position (see Fig. 18.16) in the structure; the cation sum in the *M*1 site amounts to 1.033, in agreement with the general formula $Ca(Mg, Fe)(Si, Al)_2O_6$. The remaining larger cations (Ca, Na, K) are assigned to the *M*2 position in the pyroxene structure, and their total is 1.006, again approximately 1.0.

Pyroxene analyses are commonly recalculated in terms of *end member* compositions. In addition to SiO_2, the pyroxene in Table 5.6 consists mainly of CaO, MgO, and FeO and can be recalculated in terms of the percentage of $CaSiO_3$ (wollastonite, Wo), $MgSiO_3$ (enstatite, En), and $FeSiO_3$ (ferrosilite, Fs) end members. These calculations are given in column 7, showing that the weight percent analysis can be recast as $Wo_{50.3}En_{42.4}Fs_{7.3}$.

MINERAL FORMULAE FOR HYDROUS SILICATES

Complex hydrous silicates, such as amphiboles, are recalculated by the same sequence of steps as illustrated for olivine and pyroxene, but the H_2O content is evaluated as (OH) groups in the amphibole structure. Table 5.7 gives an example of an amphibole (actinolite) analysis. A general actinolite formula is $Ca_2(Mg,Fe)_5Si_8O_{22}(OH)_2$. Column 1 lists weight percentages for $H_2O(+)$ and $H_2O(-)$. The $H_2O(+)$ is considered part of the amphibole structure, but the $H_2O(-)$ is not and is, therefore, neglected in subsequent calculations (see footnote to Table 5.7). Column 2 lists the molecular proportions, column 3 the cation proportions, and column 4 gives the total contribution of (O, OH) for each of the "molecules" in column 2. An amphibole has 24 (O + OH) and the sum in column 4 (2.8301) divided into 24 gives the ratio by which the entire analysis must be multiplied to arrive at a basis of 24(O, OH). Column 3 is now multiplied by the factor 8.4803, giving the results in column 5 on the basis of 24(O, OH).

To distribute the various ions among structural sites, an ideal mineral formula is used as a guide, in addition to the size of the ions. For amphiboles, in general,

Table 5.7 Recalculation of an Amphibole, $Ca_2Mg_5Si_8O_{22}(OH)_2$, Analysis

	1	2	3	4	5		6
	Weight Percent	Molecular Proportions	Number of Cations	Total Number of (O, OH)	Cations on Basis of 24 (O, OH)		Cations on Basis of 23 Oxygens
SiO_2	56.16	0.9346	0.9346	1.8692	7.926	7.958	7.931
Al_2O_3	0.20	0.0019	0.0038	0.0057	0.032	≈ 8	0.032
Fe_2O_3	1.81	0.0113	0.0226	0.0339	0.192	5.111	0.192
FeO	6.32	0.0880	0.0880	0.0880	0.746	≈ 5	0.747
MgO	19.84	0.4921	0.4921	0.4921	4.173		4.176
MnO	2.30	0.0324	0.0324	0.0324	0.275		0.275
CaO	9.34	0.1665	0.1665	0.1665	1.412	2.068	1.413
Na_2O	1.30	0.0210	0.0420	0.0210	0.356	≈ 2	0.356
K_2O	0.14	0.0015	0.0030	0.0015	0.025		0.025
$H_2O(+)$	2.15	0.1198	0.2396	0.1198	2.032	≈ 2	
$H_2O(-)$*	0.48	—		—			
Total	100.05			2.8301			

$$\frac{24}{2.8301} = 8.4803; \quad 2.8301 - 0.1198 = 2.7103; \quad \frac{23}{2.7103} = 8.4861$$

*This H_2O is weakly held by the powdered sample and is removed by drying at low temperature. It is assumed to be absorbed from the atmosphere, not structurally bound.

Si is less than 8.0 and Al is added to bring (Si,Al) to 8.0. The remaining Al, if any, is added to the cation group immediately below consisting of the intermediate size cations Fe^{3+}, Fe^{2+}, and Mg^{2+} (similar size cations, Table 3.8). The total for this group is 5.111, close to 5.0, and the total for the remaining larger size cations is 2.068, close to 2.0. The intermediate size cations enter the *M*1, *M*2, and *M*3 sites in the amphibole structure, and the larger cations enter *M*4 (see Fig. 18.22). Mn can be distributed among *M*1, *M*2, and *M*3 as well as *M*4 because its ionic size lies between that of Ca^{2+} and Mg^{2+}. The (OH) content turns out to be about 2. The recalculated analysis now has the general form $(Ca,Na,Mn)_2(Fe,Mg)_5(Si,Al)_8O_{22}(OH)_2$.

Instrumental analyses of hydrous minerals, such as amphiboles, do not provide information on the oxidation state of ions (Fe^{2+} versus Fe^{3+}, for example), or on the presence of structural water. Such anhydrous analytical results are frequently recalculated on an anhydrous basis. For the analysis in Table 5.7, the anhydrous basis would be 23 oxygens, replacing two $(OH)^-$ by one O^{2-}. These results are shown in column 6 and are similar to the calculation in column 5. Although this is incorrect in terms of the amphibole structure, it does allow for comparison among analytical results in which H_2O was not determined.

Additional examples of recalculations of mineral analyses followed by recalculation exercises are given in Klein, 2008, *Minerals and Rocks* (see full reference at the end of the chapter).

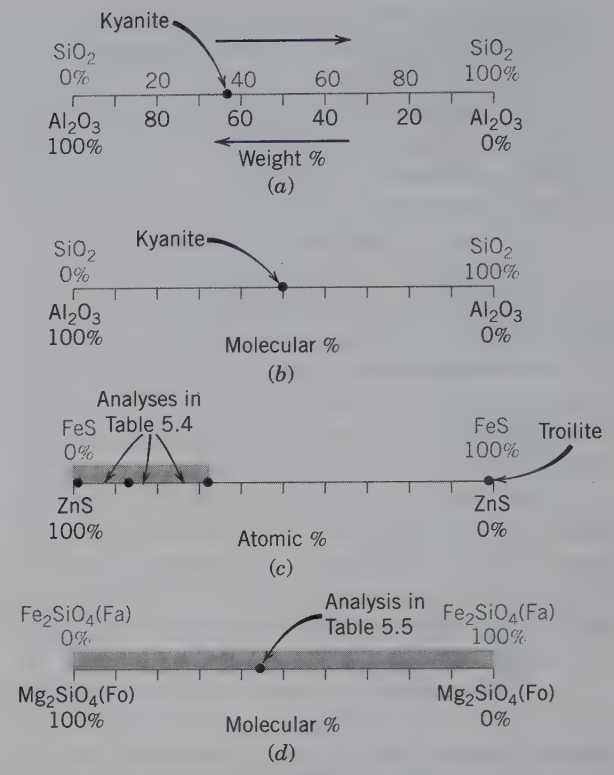

FIG. 5.10. Graphical representations of chemical compositions in terms of linear bar diagrams. (a) Kyanite, Al_2SiO_5, composition in terms of weight percentage of the oxides. (b) Kyanite in terms of molecular percentage of the oxides. (c) Sphalerite analyses from Table 5.4 in terms of atomic percentages of Zn and Fe. (d) Complete solid solution series of olivine and composition of olivine from Table 5.5 in terms of molecular percentages of forsterite (Fo) and fayalite (Fa).

GRAPHICAL REPRESENTATION OF MINERAL COMPOSITION

LINEAR OR BAR DIAGRAMS

It is commonly useful to display compositional variability in graphical form, because most minerals have partial to complete solid solution. (This subject is covered extensively in module I of the CD-ROM under the heading "Graphical Representation of Mineral Chemistry.") The first step is to choose the chemical components relevant to the mineral compositions to be graphed. These are often the major components in the mineral. For example, the mineral kyanite, Al_2SiO_5, is known to be essentially pure in composition. This leads one to select Al_2O_3 and SiO_2 as the two end components of a linear graph. One end represents 100% Al_2O_3 (= 0% SiO_2) and the other end 100% SiO_2 (= 0% Al_2O_3). A chemical analysis of a kyanite yields Al_2O_3 = 62.91, and SiO_2 = 37.08 wt. %. This can be plotted directly on the graph, if the graph is constructed in terms of weight percent oxides (Fig. 5.10a). Chemical formulae that provide direct information about atomic proportions of elements or molecular proportions of components can be used as well for graphing of compositions. The formula of kyanite can be written as $1Al_2O_3 + 1SiO_2 = 1Al_2SiO_5$ and expressed in terms of the molecular proportions of the oxide components Al_2O_3 and SiO_2. This is shown in Fig 5.10b.

Sphalerite analyses, recalculated in Table 5.4, are shown graphically (Fig. 5.10c) in terms of two end members, ZnS and FeS. Intermediate compositions can be obtained directly from the Zn:Fe ratios in the last line of Table 5.4. Sphalerite shows a partial solid solution series from ZnS to at least $Zn_{0.676}Fe_{0.324}S$ and that is shown graphically by the shading. Troilite, FeS, on the other hand, incorporates no Zn and must appear as a single point on the bar graph at Fe = 100%, indicating a total lack of Zn. The graph shows that between troilite and the most Fe-rich sphalerite plotted, there is a region in which compositions of more Fe-rich sphalerites are not found.

In the olivine analysis (Table 5.5), molecular percentages of MgO and FeO can also be expressed as Mg_2SiO_4 (Fo) and Fe_2SiO_4 (Fa), the two end member

compositions of the olivine solid solution series. For olivine, a complete solid solution series exists between Fo and Fa. Consequently, there is continuous shading along the entire compositional range (Figure 5.10d) in addition to the point for the specific composition of the olivine from Table 5.5. Linear diagrams of this type are the horizontal axis in *variation diagrams* that relate changes in physical properties to variation in composition (see Fig. 2.16). Composition bars also are the horizontal axis in temperature-composition diagrams (see Figs. 11.6, 11.7, and 11.8).

TRIANGULAR DIAGRAMS

Mineral analyses can be very complex and typically suggest substitution of several elements in the same atomic site of the structure. To portray the variation of three components instead of just two, a *triangular diagram* is used. (Triangular coordinate graph paper is available commercially from Keuffel and Esser Company.) Triangular diagrams are basically three linear diagrams, which share components, combined. For example, Figure 5.11a lists the mineral names, formulae, and compositions in terms of oxide weight percentages for the two end members of the orthopyroxene series, enstatite and ferrosilite, and the two end members of the olivine series, forsterite and fayalite. These contain three primary chemical components (MgO, FeO, SiO_2). Two choices exist for a triangular plot; on the basis of weight percentages, or on the basis of the relative cation proportions in the formulae.

For plotting in weight percent, the corners of the triangle are marked as 100 wt.% SiO_2, 100 wt.% MgO, and 100 wt.% FeO (Fig. 5.11b). The four minerals can be plotted because they contain only these three oxide components. Enstatite and forsterite contain 40.16 and 57.30 wt.% MgO, respectively. The MgO scale extends from 0% to 100% on the left side of the triangle, and it is along this side that the MgO values are directly plotted. Both minerals contain no FeO, so that they lie on the edge directly between SiO_2 and MgO. The right side of the triangle extends from 100% SiO_2 to 100% FeO; with FeO (from 0% to 100%) increasing along the right side from top to bottom. Along this side lie the compositions of the Fe-end members (given in Fig. 5.11a) on the basis of their FeO weight percentage values. The end members of both series are joined by a dashed line to portray the locations where intermediate compositions plot. The two lines are not exactly parallel because of the slight differences in MgO content (57.30 − 40.16 = 17.14 wt. %) and the FeO content (70.51 − 54.46 = 16.05 wt. %) of the Mg and Fe end-member compositions. The final plot, in weight percent, is easy enough to achieve *if* weight percentage values are available.

Enstatite Component	$MgSiO_3$ Weight Percent	*Ferrosilite* Component	$FeSiO_3$ Weight Percent
SiO_2	59.84	SiO_2	45.54
MgO	40.16	FeO	54.46
Total	100.00	Total	100.00

Forsterite Component	Mg_2SiO_4 Weight Percent	*Fayalite* Component	Fe_2SiO_4 Weight Percent
SiO_2	42.70	SiO_2	29.49
MgO	57.30	FeO	70.51
Total	100.00	Total	100.00

(*a*)

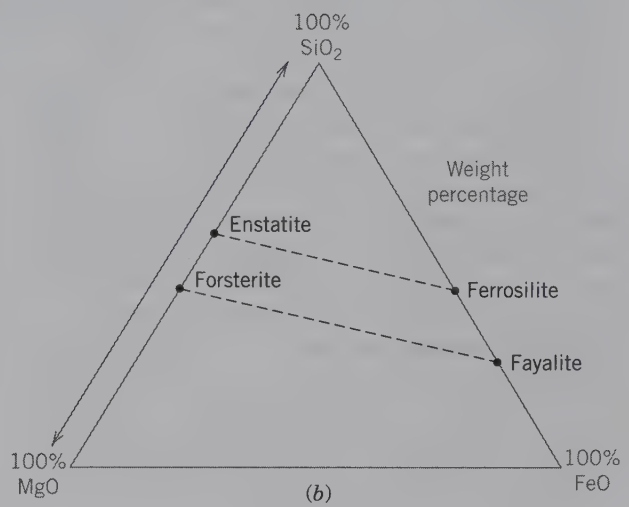

(*b*)

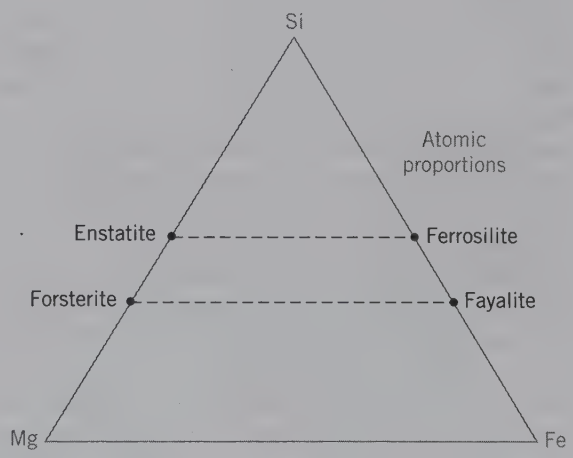

(*c*)

FIG. 5.11 Plotting of binary silicate composition ranges on triangular diagrams for the systems Mg–Fe–Si and MgO–FeO–SiO_2.

In Fig. 5.11c, the elements Si, Mg, and Fe are chosen for the corners. To plot the four minerals in terms of cation proportions, it would appear that each of the mineral analyses would have to be recalculated from weight percentage, via molecular proportions, to cation proportions, and so on, as shown in Tables 5.6

and 5.7 for two different silicates. This is the correct procedure for complex mineral compositions; for simple end member compositions for which the exact formulae are known, this is unnecessary.

Enstatite contains one Mg and one Si atom (or ion) per formula. The same ratio holds for ferrosilite, with one Fe and one Si. In other words, enstatite contains one Mg out of a total of two cations (Mg + Si = 2) or enstatite is 50% Mg and 50% Si; this is the same in ferrosilite with one Si to one Fe. Thus, enstatite plots halfway on the Mg–Si side of the triangle and ferrosilite plots at the same location on the Fe–Si side. The plotted positions are shown and are joined by a dashed line that is parallel to the bottom edge of the triangle.

For the olivine series, forsterite contains two Mg and one Si, for a total of three cations (2 + 1 = 3; 2 in 3 = 66.7%); fayalite contains two Fe and one Si, again a total of three cations. This means that the forsterite composition must lie on the Mg-Si side of the triangle, two-thirds of the way towards Mg, and that the fayalite composition plots at the equivalent position on the Fe–Si side. Forsterite plots at 66.7% MgO, 33.3% SiO_2, and fayalite plots at 66.7% FeO and 33.3% SiO_2. These two compositional points are shown and are connected by a dashed line, which again is parallel to the base and, as such, is also parallel to the line for intermediate compositions in the orthopyroxene series.

A weight percentage diagram, as in Fig. 5.11b, is commonly used in the plotting of rock and mineral compositions in igneous rocks because the investigator is mainly interested in the possible changes in composition of the melt from which an igneous rock formed. However, mineralogists and petrologists who deal with sedimentary and metamorphic rocks prefer the atomic representation. Such a diagram is especially easy to construct if end member formulae are known.

A more complex mineral composition, that of a pyroxene, is listed in Table 5.6. This analysis has been recalculated in terms of three components, $CaSiO_3$ (wollastonite, Wo), $MgSiO_3$ (enstatite, En), and $FeSiO_3$ (ferrosilite, Fs), used for corners of a triangular plot (Fig. 5.12). The ratios of these three components are the same as they would be for CaO, MgO, and FeO (these two sets of alternate components are completely interchangeable). Any pyroxene composition that involves only two of the three components will plot along an edge of the triangle, identical to the procedure in the bar graphs of Fig. 5.10. For example, diopside, $CaMgSi_2O_6$, will plot halfway along the left edge of the triangle: $1CaSiO_3 + 1MgSiO_3 = 1CaMgSi_2O_6$, or at 50% of each component. Similarly, hedenbergite, $CaFeSi_2O_6$, will plot along the right edge, midway, at $1CaSiO_3 + 1FeSiO_3 = 1CaFeSi_2O_6$. Compositions along the bottom edge contain no $CaSiO_3$ and are expressed, in general, as (Mg, Fe)SiO_3. A possible specific composition along this edge is $(Fe_{0.80}Mg_{0.20})SiO_3$, which restated as 80 molecular percent ferrosilite (Fs) and 20 molecular percent enstatite (En), plots along the bottom edge near $FeSiO_3$, shown in Fig. 5.12.

A more general pyroxene composition containing all three components can be expressed as $Wo_{45}En_{20}Fs_{35}$. This is shorthand for a pyroxene containing 45 molecular percent CaO (Wo), 20 molecular percent MgO (En), and 35 molecular percent FeO (Fs). Note that the join En–Wo (in Fig. 5.12) represents 0% Fs; similarly the En–Fs join represents 0% Wo, and the Wo–Fs join represents 0% En. The distance between the corner and the opposite side of the triangle is graduated in "%" lines from 100% at the corner to 0% along the join. For example, the $CaSiO_3$ corner represents 100% $CaSiO_3$ and horizontal lines between this corner and the base of the triangle mark the change from 100% to 0% $CaSiO_3$. To plot $Wo_{45}En_{20}Fs_{35}$, locate first the Wo_{45} line (marked on Fig. 5.12), then locate the En_{20} line (also marked) to find their intersection. This can be checked because the intersection of the Wo_{45} and the En_{20} lines will lie on the Fs_{35} line. If a mistake has been made, the lines will not intersect. The position of the composition, $Wo_{50}En_{43}Fs_7$, from Table 5.6 is also shown in Fig. 5.12.

Like linear graphs, triangular diagrams are frequently used to depict the extent of solid solution in minerals. The olivine series $(Mg,Fe)_2SiO_4$ and the orthopyroxene series $(Mg,Fe)SiO_3$, both of which show an essentially complete solid solution between the end-member compositions, is shown as a shaded bar across the diagram for SiO_2–MgO–FeO (Fig. 5.13). SiO_2 (quartz and its various polymorphs) shows no substitution in terms of FeO or MgO and is depicted as a point, indicating its constant composition. The illustration that opens this chapter depicts the extent of solid solution among the most common feldspars at high temperature.

Triangular Representation of More Than Three Components

Triangular diagrams limit representation to only three components, which may be simple elements, compound oxides, or more complex components as expressed by mineral formulae. To represent more than three components on one triangle, some components are commonly combined, and some may not be considered in the graphical representation. For example, to represent carbonate compositions in the system CaO–MgO–FeO–MnO–CO_2, the possible number of compositional variables must be reduced. Because all carbonates contain CO_2, no additional information is gained in using the CO_2 component to show the small

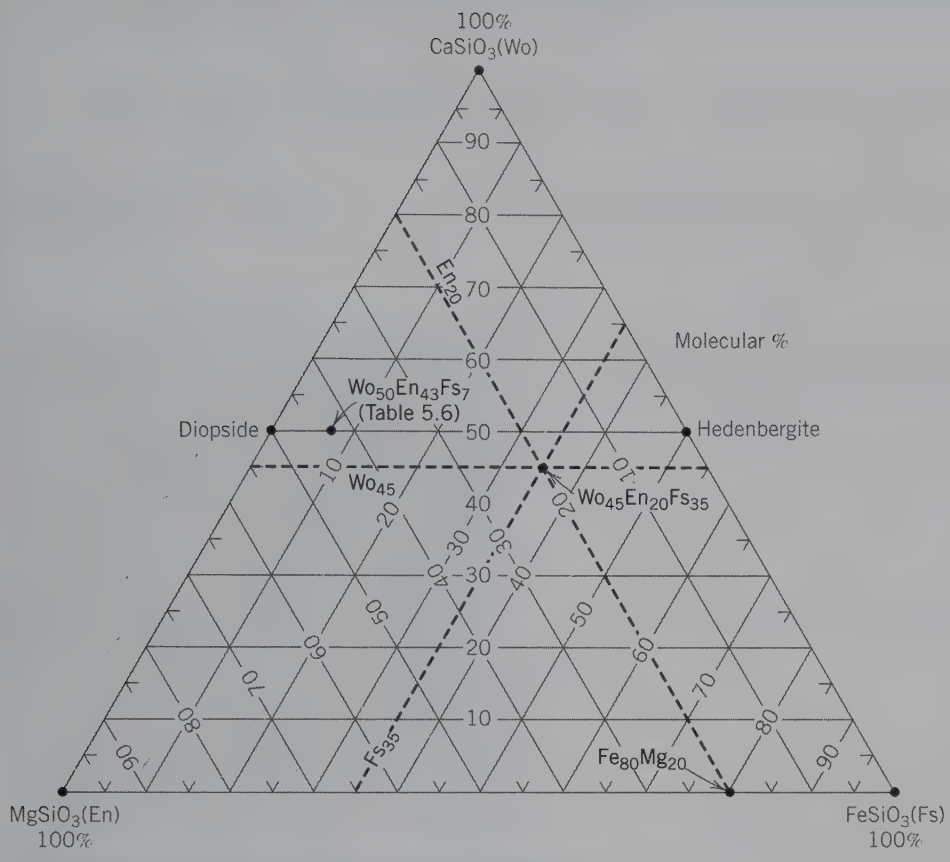

FIG. 5.12 Plotting of mineral compositions, with three components, on triangular diagrams. The specific compositions represented are for the pyroxene family of silicates.

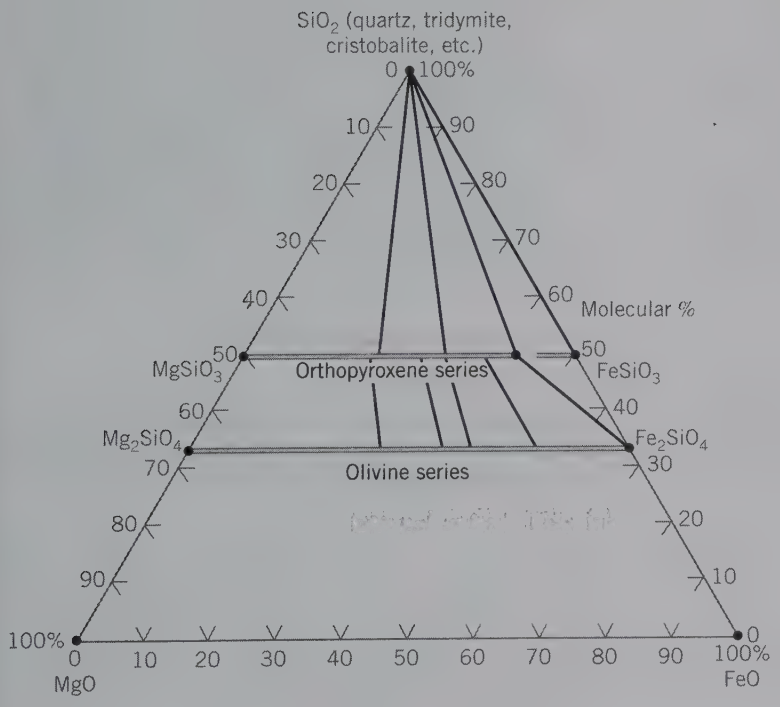

FIG. 5.13 Triangular representation, in terms of molecular percentage, of minerals in the chemical system MgO–FeO–SiO_2. The olivine and orthopyroxene series show complete solid solution series between Mg and Fe end members, as shown by the continuous shaded bars. Lines connecting SiO_2 to various orthopyroxene compositions, and between orthopyroxene and olivine compositions, are *tielines*; these connect coexisting minerals in rocks. The triangle outlines a cristobalite-orthopyroxene (Fs_{83})-fayalite coexistence.

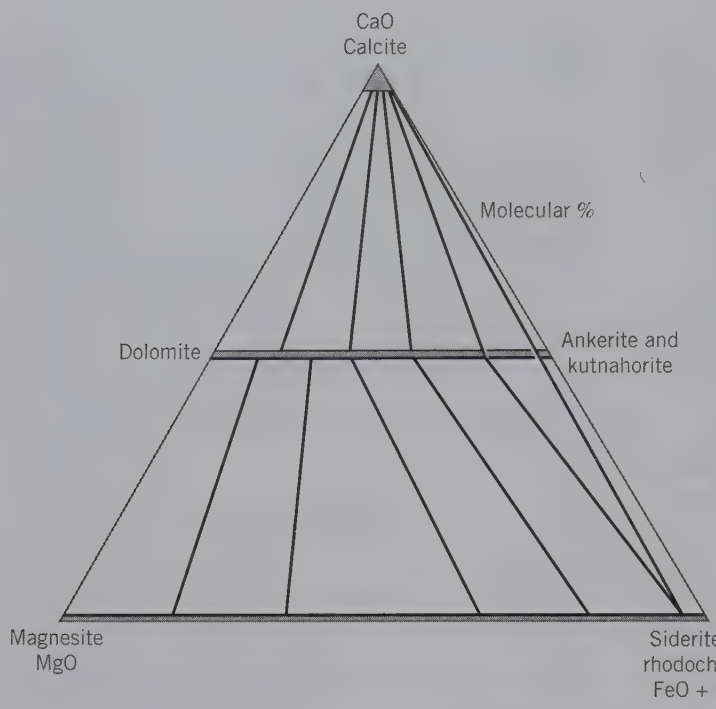

FIG. 5.14 Compositions of carbonates in the system CaO–MgO–FeO–MnO–CO_2. The CO_2 component is not considered in this diagram. (FeO + MnO) is a combined component. A complete solid solution series exists between dolomite, $CaMg(CO_3)_2$, and ankerite, $CaFe(CO_3)_2$, and between magnesite, $MgCO_3$, and siderite, $FeCO_3$ (shaded bars). Tielines connect possible coexisting carbonate members. The three-mineral triangle portrays the coexistence of calcite-ankerite-siderite.

CO_2 variations that exist. CO_2, therefore, is ignored in the graphical representation. Because Fe^{2+} and Mn^{2+} substitute easily for each other in the carbonate structure, and because Mn^{2+} typically is far less abundant in most environments than Fe^{2+}, FeO and MnO are combined. This leaves three components, CaO, MgO, and (FeO + MnO). Figure 5.14 shows that a complete solid solution series (shaded bar) exists between magnesite, $MgCO_3$, and siderite + rhodochrosite, $FeCO_3$ + $MnCO_3$; the full extent of this series is well documented (see also Fig. 17.5). The diagram also shows a nearly complete series between dolomite, $CaMg(CO_3)_2$, and ankerite, $CaFe(CO_3)_2$ + kutnahorite, $CaMn(CO_3)_2$. Calcite, $CaCO_3$, shows a very limited ionic substitution by Mg, Fe, and Mn, so that the shaded area is restricted to the top. Tielines show coexistences of magnesite-dolomite, calcite-dolomite, and calcite-ankerite-siderite in the triangle. This three-mineral assemblage is found in banded Precambrian iron formations. Additional discussion of the procedures in plotting mineral compositions on triangular diagrams, and exercises on the graphical representation of mineral compositions, are given in Klein (2008). (Coverage of these procedures is located in module I of the CD-ROM under the heading "Graphical Representation of Mineral Chemistry.")

REFERENCES AND FURTHER READING

Clarke, F. W., and H. S. Washington. 1924. *The composition of Earth's crust.* U.S. Geological Survey Professional Paper 127.

Hemley, R., and D. Mao (editors). 1999. *Ultrahigh pressure mineralogy. Reviews in Mineralogy* 37. Mineralogical Society of America, Washington D. C.

Klein, C. 2008. *Minerals and rocks: Exercises in crystal and mineral chemistry, crystallography, X-ray powder diffraction, mineral and rock identification, and ore mineralogy.* 3rd ed. Wiley, New York.

Mao, W. L. et al. 2004. Ferromagnesian postperovskite silicates in the D″ layer of the Earth. *Proceedings of the National Academy of Sciences* 101:15867–69.

Murakami, M. et al. 2004. Post-perovskite phase transition in $MgSiO_3$. *Science* 304:855–858.

Navrotsky, A. 1994. *Physics and chemistry of earth materials.* Cambridge University Press, New York.

Papike, J. J. (Editor). 1998. *Planetary Materials, Reviews in mineralogy and geochemistry* 26. Mineralogical Society of America, Washington D.C.

Taylor, S. R., and S. M. McLennan. 1985. *The Continental crust: Its composition and evolution.* Blackwell Scientific.

Smyth, J. R., and D. L. Bish. 1988. *Crystal structures and cation sites of the rock-forming minerals.* Allen & Unwin, Boston.

CHAPTER 6

Crystallography: External Symmetry of Minerals

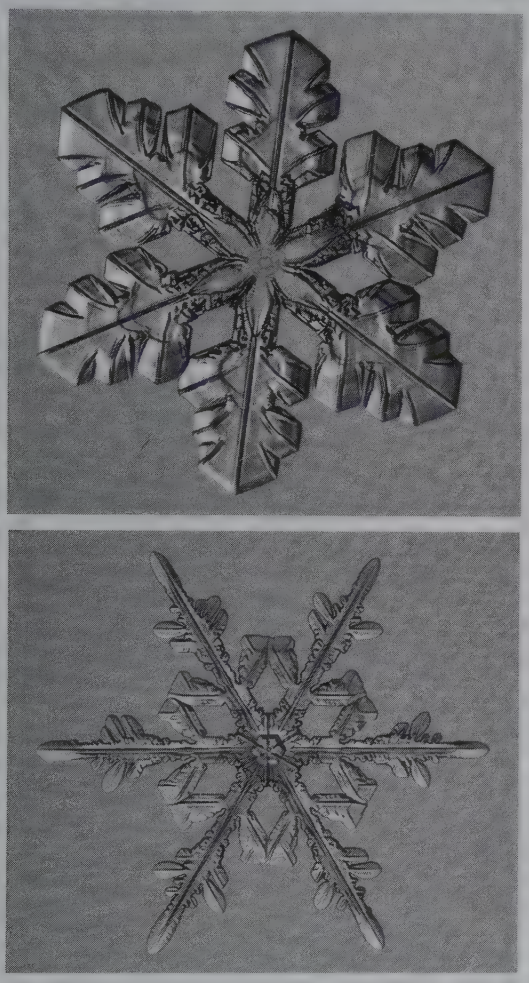

Exquisite external form (morphology) of two crystals of ice I as viewed under a microscope. Both display delicate branching patterns that clearly reflect hexagonal symmetry (photographs courtesy of Dr. Kenneth Libbrecht, California Institute of Technology; used with permission).

"... The main feature of crystal geometry is that it deals with orderly repetition. In fact, the geometry of crystals is the geometry of order." Martin J. Buerger, 1971.

"... The chief forms of beauty are order and symmetry and definiteness. ..." Aristotle, 384 BC–322 BC.

Eye-catching mineral specimens found in museums worldwide commonly have the characteristic of spectacularly well-developed external form (Fig. 6.1). This external form is the visible expression of a mineral's *"long-range, three-dimensional internal order."* This internal order (see Chapter 7) consists of ions or groups of atoms that are repeated at regular intervals throughout the mineral. These ordered geometric arrangements result in inherent internal symmetry that is expressed by the external form. Symmetry deals with the repetition of objects, through rotation, reflection, inversion, and translation. Symmetry is fundamental and pervasive in all types of chemical compounds (Fig. 6.2).

The study of the external form and internal atomic arrangement of crystalline solids and the principles that govern their growth, external shape, and internal structure is called *crystallography* (see Chapter 1). This chapter provides a broad overview of the most important crystallographic aspects that are expressed by the external morphology of crystals. This discussion of

FIG. 6.1 Photograph of a fluorite cube on galena cubes from Nicolai Mine, Dal'Negorsk, Russia. Specimen is ~3 inches in height (photograph courtesy of Stuart & Donna Wilensky, Wilensky Fine Minerals, Wurtsboro, New York).

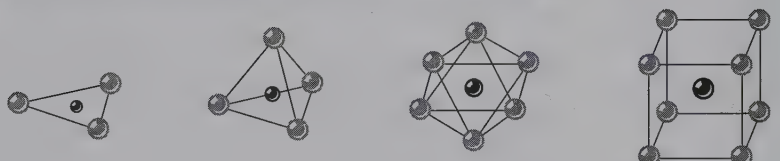

Some coordination polyhedra

(*a*)

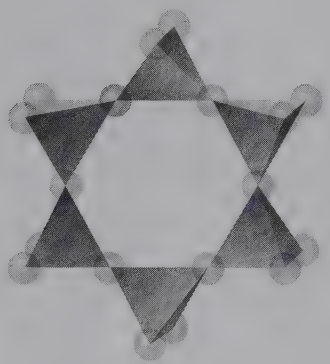

Si_6O_{18} ring in structure of beryl

(*b*)

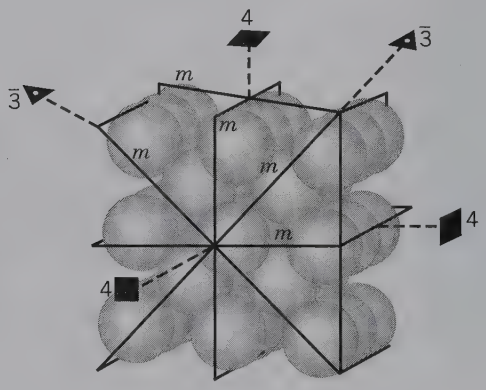

Atomic structure of metallic iron

(*c*)

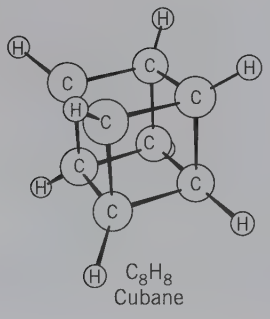

C_8H_8
Cubane

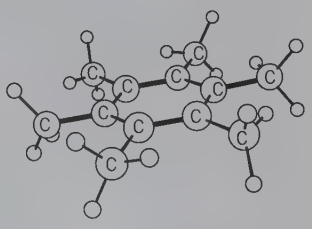

$(CH_3)_6C_6$
Hexamethylbenzene

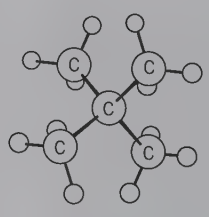

$C(CH_3)_4$
Neopentane

(*d*)

FIG. 6.2 Symmetry in chemistry. (a) Variable symmetry contents in some examples of regular coordination polyhedra (see also Fig. 4.4). (b) An (Si_6O_{18}) ring with six-fold rotational symmetry in the structure of beryl, $Be_3Al_2Si_6O_{18}$. (c) An illustration of the atomic structure of metallic iron. The iron atoms are arranged in body-centered cubic packing. This cubic structure has many symmetry elements; only a few are shown in the illustration. (d) Three different organic molecules with variable inherent symmetry contents. (Taken with permission of the author, from Bernal, I., W. C. Hamilton, and J. S. Ricci. 1972. *Symmetry: A stereoscopic guide for chemists.* W. H. Freeman and Co. New York, with permission).

external symmetry (also referred to as *morphological symmetry*) precedes aspects of internal structure because it is initially simpler to locate symmetry elements in physical objects (e.g., actual crystals or idealized wooden crystal models) than in patterns that represent internal structures. To understand concepts in crystallography requires an understanding of symmetry.

SYMMETRY

Symmetry can be seen in the world around us. Flowers and leaves of plants commonly exhibit symmetry in their external shapes. People and animals have bilateral symmetry, and the perfection of such symmetry leads to "facial attractiveness" that has genetic significance (see Box 6.1). Examples of symmetry in architecture are commonplace, especially the bilateral symmetry of classical Greek and Roman architecture (see Box 6.1).

External symmetry is an expression of the infinite repeat of regular building blocks that exist internally in minerals. The *three-dimensional internal order* of a crystal can be thought of as a *motif* (a single unit, such as an ion or atom, or a unit of pattern, such as a group of atoms) repeated regularly as an array of points in space. Each motif has an identical environment to each repeated motif. The spacing of motifs represents the translational component of the regular array and will be discussed further in Chapter 7. A simple and ordered arrangement of a motif in two dimensions is shown in Fig. 6.3. A comma is the motif and is repeated in space. In crystals, the motifs may be H_2O molecules (as in snow), anionic groups, such as $(CO_3)^{2-}$ or $(SiO_4)^{4+}$; cations, such as Ca^{2+} or Mg^{2+}; atoms, such as Cu; or combinations of these. When polyhedra combine, a regular (ordered) arrangement results. For example, a combination of triangular $(CO_3)^{2-}$ groups and Ca^{2+} ions manifests itself in the rhombohedral outline of calcite, $CaCO_3$ (Fig. 6.4).

The first scientist to demonstrate that the external crystal form (its morphology) of a well-developed mineral is an expression of its internal order was René-Just Haüy (1743–1822). Haüy's concept was that "integral molecules" are regularly stacked together to achieve various commonly developed forms (see Fig. 6.5; see also Fig. 1.14). Haüy coined the word *molécule*, which preceded the modern concept of **unit cell**.

FIG. 6.3 Two-dimensional order. The comma is the motif which is repeated regularly to make the complete pattern.

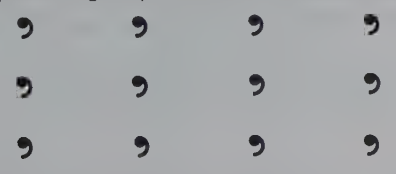

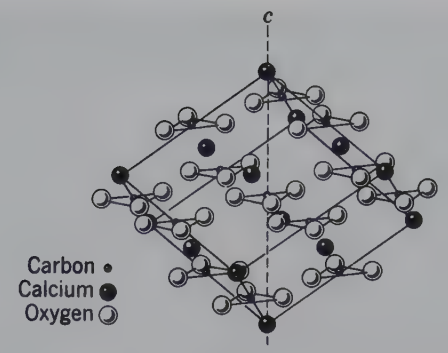

FIG. 6.4 The atomic structure of calcite, $CaCO_3$. The outline of the unit cell is rhombohedral in shape. The locations of the carbon, calcium, and oxygen are shown as spheres. The carbonate group, $(CO_3)^{2-}$, has the shape of an equilateral triangle with carbon at its center and oxygen at the three corners (**C.N.** = 3). The calcium ions and carbonate groups are the motif units of the structure, *c* represents an axis about which the motifs are repeated.

A **unit cell** is the smallest unit of a structure (or pattern) that can be infinitely repeated to generate the entire structure (or to generate the complete print of a pattern).

Because crystals are formed by the regular repetition in three dimensions of a unit cell, the limiting surfaces (external planes), which are known as the *faces* of a crystal, depend in part on the shape of the unit. (They also depend on the conditions under which the crystal grows.) If a cubic unit cell is repeated in three dimensions to build up a crystal with n units along each edge, a larger cube will result containing n^3 units (Fig. 6.5a). With a similar orderly repeat mechanism, different shapes may result, as shown in Fig. 6.5 for a cube, distorted cubes, an octahedron, and a dodecahedron. The octahedral and dodecahedral forms are common in many crystals, but because the unit cell dimensions are on the angstrom (10^{-10} m) level, the steps shown in Figs. 6.5c and d are invisible to the eye, resulting in faces that appear as smooth, planar surfaces.

With a given internal structure, a limited number of planes will bound the crystal, and only a comparatively few faces are common. In determining the types of faces that may develop on a crystal, the internal lattice must also be considered because the lattice represents the orderly repeat of a unit cell.

A **lattice** is an imaginary pattern of points (or nodes) in which every point (or node) has an environment that is identical to that of every other point (or node) in the pattern. A lattice has no specific origin as it can be shifted parallel to itself.

BOX 6.1 Bilateral Symmetry in Humans and Architecture

Leonardo da Vinci's famous drawing displays the proportions of the human body and stresses its bilateral symmetry. It now appears that human body symmetry is a parameter in sexual selection; the more symmetric the body the more attractive it is to a partner (R. Thornhill and S. W. Gangestad, 1994, Human fluctuating asymmetry and sexual behavior, *Psychological Science*, v. 5, pp. 297–302). The human face contains the same mirror symmetry as the overall body, and human facial symmetry is found to be linked to attractiveness as well. R. Thornhill and S. W. Gangestad, 1999, discuss this subject in their paper "Facial Attractiveness" published in *Trends in Cognitive Sciences*, vol. 3, pp. 452–460. They note that "when members of a species discriminate between potential mates with regard to their physical appearance, as humans do, a reasonable working hypothesis is that the discrimination reflects special-purpose adaptations responsive to cues that had mate value in evolutionary history." They review several studies that show that those with more symmetrical faces are generally rated as more attractive even though faces are not actually perfectly symmetrical.

Bilateral symmetry is also common in the buildings of many cultures. Examples shown here are: (a) The J. Paul Getty Museum in Malibu, California; this is a 1974 reconstruction and adaptation of the Roman Villa dei Papiri at Herculaneum, which was buried by the eruption of Mount Vesuvius in A.D. 79 (it is a highly symmetrical building with everything planted around it enhancing strict bilaterial symmetry as well) and (*b*) The Taj Mahal in Agra, India, which was built between 1630 and 1648 by the Mogul emperor Shah Jahan in memory of his wife who died in 1629. This specific photograph shows more than bilateral symmetry on account of the additional reflection in the pool in front.

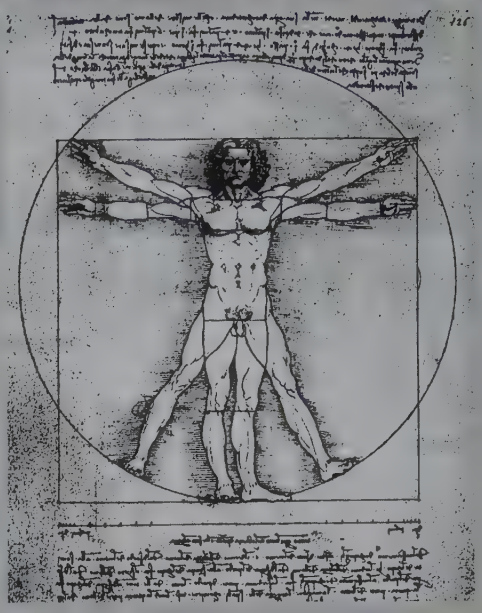

Leonardo da Vinci, 1452–1519, Schema delle proporzione del corpo umano.

(a) *The J. Paul Getty Museum, Malibu, California. Photograph by Jack Ross, used with permission.*

(b) *The Taj Mahal, Agra, Uttar Pradesh, India. Photograph by Wolfgang Kaehler, Corbis, used with permission.*

Faces that are most likely to develop are parallel to lattice planes that have a high density of **lattice points** (or *nodes*). The frequency with which a given face is observed is roughly proportional to the number of nodes it contains in the lattice: the larger the number of nodes, the more common the face, as is illustrated in Fig. 6.6. This rule, known as the **law of Bravais**, is generally confirmed by observations. (Exceptions to this law were pointed out by Donnay and Harker in 1937).

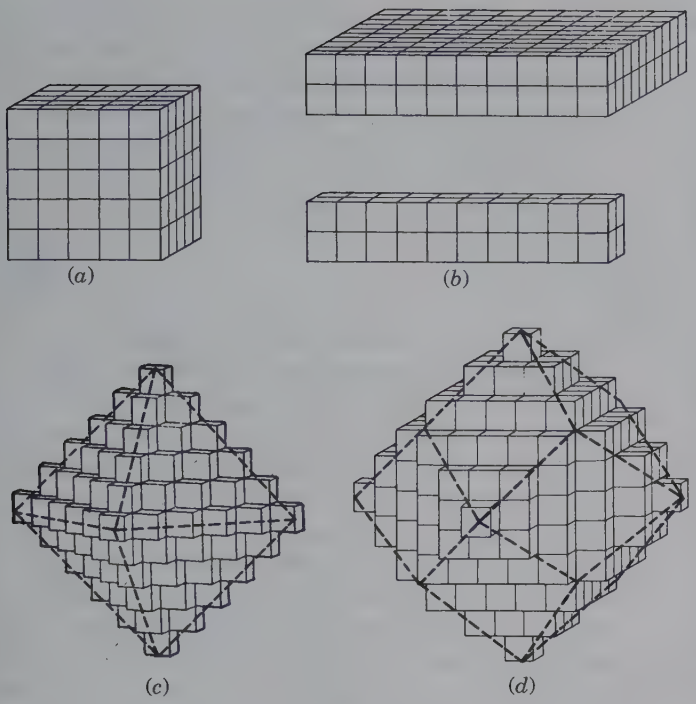

FIG. 6.5 Different external shapes produced by systematic stacking of square (cubic) unit cells. (a) Perfect cube, (b) distorted cubes, (c) octahedron, and (d) dodecahedron. The octahedral and dodecahedral forms are the result of systematic additions of units along directions of accelerated growth. Dashes outline the different faces on the crystal. Compare with Fig. 1.14.

Because crystal faces have a direct relationship to the internal structure, it follows that the faces have a definite relationship to each other. This fact was observed in 1669 by Nicolaus Steno, who pointed out that the angles between similar faces on different crystals of quartz were always the same (see Fig. 1.12). This observation is generalized today as **Steno's law of the constancy of interfacial angles**, which states: *The angles between equivalent faces of crystals of the same substance, measured at the same temperature, are constant* (Fig. 6.7). For this reason, crystal morphology is frequently a valuable tool in mineral identification. A mineral may be found in crystals of widely varying shapes and sizes, but the angles between pairs of corresponding faces are always the same. An illustration of such constancy of interfacial angles, in horizontal sections of two distinctly different quartz crystals, is given in Fig. 6.7. Despite their different appearance, the angle remains the same.

As noted previously, the internal structure of a crystalline material contains translations (on the order

FIG. 6.6 This figure represents one layer of *lattice points* in a cubic lattice. Several lines are possible through the net that include a greater or lesser number of *lattice points* (or nodes). These lines represent the traces of possible crystal planes. The planes with the highest density of lattice points tend to be the most common, such as *AB* and *AC*.

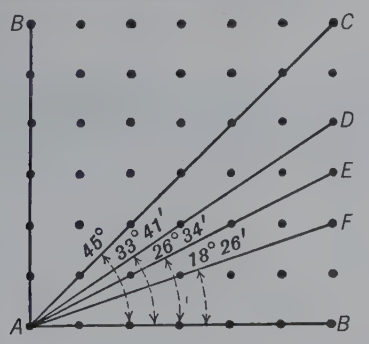

FIG. 6.7 Constancy of interfacial angles is shown by comparison of a well-formed and highly symmetric quartz crystal (a) with a distorted quartz crystal (b). The shaded sections across the direction of elongation show identical interfacial angles of 120° in both, irrespective of the asymmetric habit in (b).

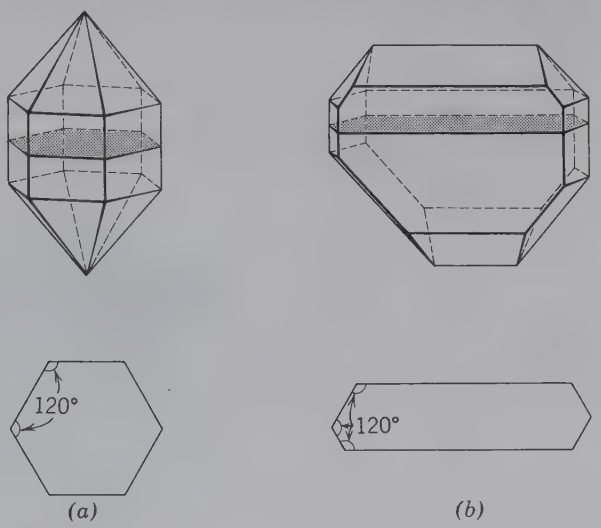

of the Å = 10^{-10} m scale; see Chapter 7) as well as symmetry elements. Such extremely small translations can be seen directly only with the very high resolution of a transmission electron microscope (TEM). As such, these translations are invisible to the naked eye, when observing the external morphology of a crystalline substance. Therefore, the external morphology of crystals expresses the presence (or absence) of symmetry elements, devoid of translational components.

SYMMETRY ELEMENTS (WITHOUT TRANSLATION)

The external shape of a well-formed crystal may reflect the presence or absence of symmetry. This morphological symmetry is referred to as **point symmetry** because it expresses how a motif (such as a crystal face) is repeated about a point. This point, the center of the crystal or the origin of the unit cell, is fixed in the crystal. The geometric feature that expresses the symmetry of an ordered arrangement is known as a **symmetry element**. Such symmetry elements are **rotation axes**, **mirror (reflection) planes**, **centers of symmetry**, and **rotoinversion axes**. Examples of each of these symmetry elements, as part of a well-formed crystal, are shown in Fig. 6.8. The processes of rotation about an axis, of reflection by a mirror, and of inversion about a central point are referred to as **symmetry operations**. These operations are illustrated in Fig. 6.9. Table 6.1 lists the symmetry elements (nouns), their operations (verbs), and the symbols used to describe them.

The presence of these symmetry elements can be detected, in a well-formed crystal, by the angular arrangement of the bounding faces, and sometimes, by their size and shape. (Many such aspects of morphological symmetry are treated, with animations, in module II of the CD-ROM under the heading "Crystallography: Symmetry Operations.")

ROTATION

The presence of **rotation** is established by rotating a motif (such as a specific crystal face) about an imaginary axis that intersects the crystal center (Fig. 6.8a). When rotational symmetry is present, a specific face on the crystal is repeated n times in a complete rotation of the crystal. The number n expresses the number of times a specific crystal face is repeated during a 360° (complete) rotation. Therefore, each rotation is characterized by an angle (α), the angle of rotation required to repeat the appearance of a specific crystal face. An **axis of rotation** is an imaginary line through the center of the crystal about which a specific crystal face repeats itself in appearance. This can be visualized as a thread stretching from one end of a crystal to the opposite end, passing through the crystal's center (Figs. 6.8a and 6.9a).

Rotational symmetry can be expressed by any whole number (n) from 1 to infinity. A rotational symmetry of $n = 1$ means that after a complete rotation of 360° about an axis, all aspects of an object (or figure) come into coincidence with themselves just once (Fig. 6.10). The other limiting case of rotational symmetry is that of a rotation about an axis of infinite

FIG. 6.8 Translation-free symmetry elements as expressed by the morphology of crystals. (a) Six-fold axis of rotation, (b) mirror plane, (c) center of symmetry (C), (d) four-fold axis of rotoinversion. See text for explanation.

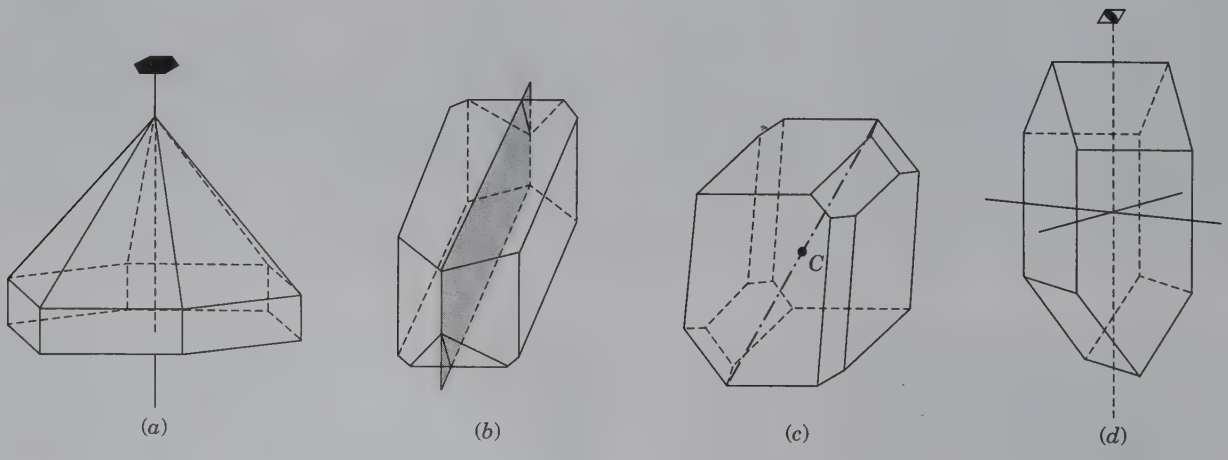

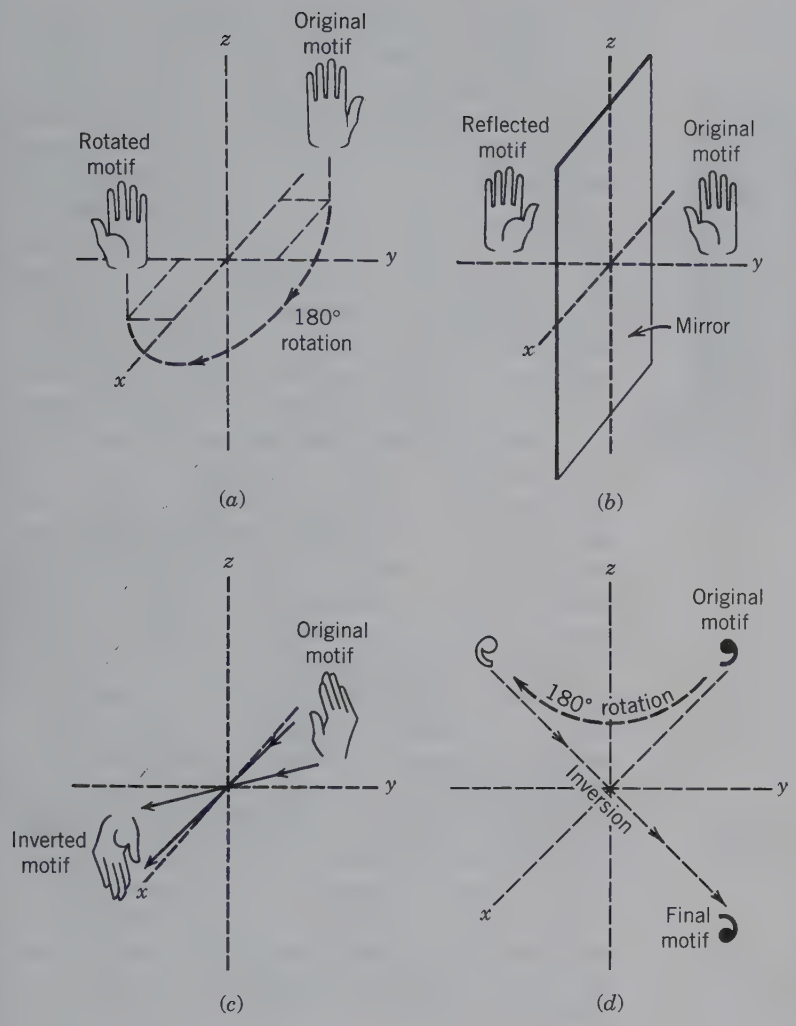

FIG. 6.9 Examples of symmetry operations. (a) Generation of a pattern by rotation of a motif through an angle of 180°. (b) Motifs as related by a mirror reflection. (c) Motifs related by inversion through a center. (d) Motifs related by 180° rotation and subsequent inversion; known as rotoinversion (see also Fig. 6.14a).

order ($n = \infty$). An object possessing this kind of an axis repeats itself by any angle of rotation, because the amount of rotation necessary is infinitely small (Fig. 6.10a). Many objects, or shapes, are found with rotational symmetries that lie between the two extremes of $n = 1$ and $n = \infty$ (where n is a whole number that is divisible into 360°, also known as an aliquot part). The rotational symmetries of some shapes and objects are illustrated in Fig. 6.11. Here, the axis of rotation is perpendicular to the plane of the page. Place a pencil point on the center of each figure and rotate the page around the pencil.

When consideration is given to the fact that the internal structure of minerals consists of motifs arranged in an ordered pattern, and that these motifs must fill space (see also page 150), only a small number of possible rotations results (see Table 6.1). The types of rotation found in internally ordered crystals, and also expressed in their external morphology, are repeats of a specific face 1, 2, 3, 4, or 6 times during a complete

Table 6.1 Nomenclature for Point Symmetry

Symmetry Element	Symmetry Operation	Symmetry Symbol	Hermann-Mauguin Notation
Rotation Axis	Rotation	A_1, A_2, A_3, A_4, A_6	1, 2, 3, 4, 6
Mirror Plane	Reflection	m	m
Center of Symmetry	Inversion	i	$\bar{1}$
Rotoinversion	Rotation + Inversion	$\bar{A}_1 = i, \bar{A}_2, \bar{A}_3, \bar{A}_4, \bar{A}_6,$	$\bar{1}, m(=\bar{2}), \bar{3}, \bar{4}, \bar{6}$

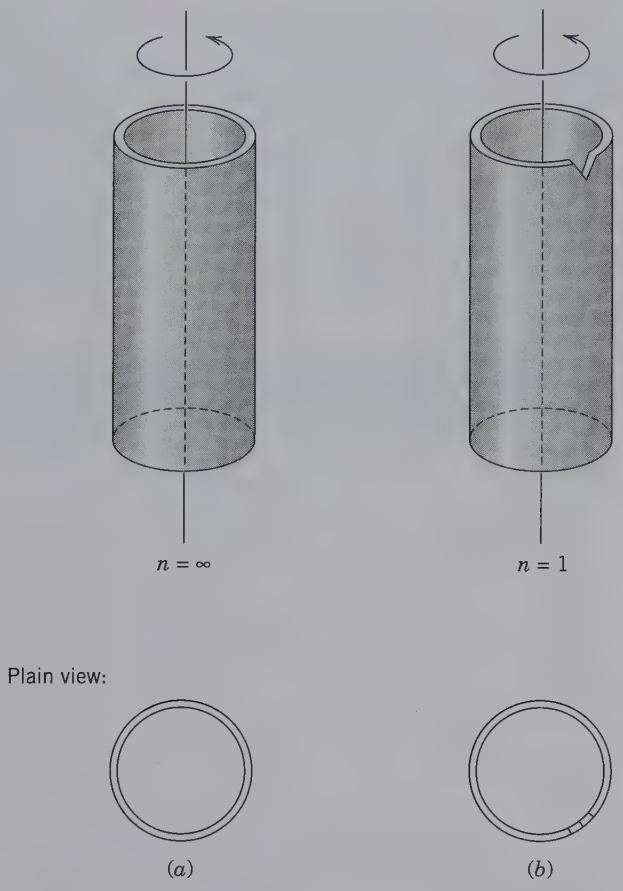

FIG. 6.10 The two extremes of rotational symmetry ($n = \infty$ and $n = 1$) as shown by: (a) a perfect, hollow cylinder and (b) a hollow cylinder with a *V*-shaped notch at the top.

360° rotation. The number of duplications of a specific face during a 360° rotation gives the rotation axis its name. For example, two equivalent faces per 360° rotation are related by a *two-fold rotation axis*. One-fold ($\alpha = 360°$) repeats once, two-fold ($\alpha = 180°$) repeats the face twice in 360°, three-fold ($\alpha = 120°$) repeats three times, four-fold ($\alpha = 90°$) repeats four times, and six-fold ($\alpha = 60°$) repeats six times in 360° (Fig. 6.8a where an upper face is repeated six times about the imaginary vertical six-fold axis). Rotation of an asymmetric motif produces patterns in which the original motif and those generated from it are identical in orientation with respect to each other (Fig. 6.12). In other words, the original motif and the newly generated one have the same "handedness" (Fig. 6.12).

A five-fold axis and seven- and higher-fold axes are not possible in crystalline materials. A geometric derivation for the absence of a five-fold symmetry axis in ordered patterns is given on page 150. Intuitively, this becomes clear when one tries to completely cover a planar surface with a five-sided motif, such as a pentagon, without mismatches and gaps (Fig. 6.13a). On the other hand, Fig. 6.13b shows how hexagons can completely cover a surface. The mismatches and gaps, illustrated in Fig. 6.13a, tend *not* to occur in the crystal structures of minerals. On an atomic scale, such gaps could represent unsatisfied chemical bonds or overstretched bonds between ions (or atoms), both of which are absent in ordered crystal structures. In contrast, mineral structures made of hexagons are common because the pattern fills space.

FIG. 6.11 Objects showing elements of rotational symmetry only. (a) A pinwheel with a four-fold axis (A_4) perpendicular to the face of the wheel. (b) A pattern of three lizards that are related to each other by a three-fold rotation axis (A_3) perpendicular to the page. The three-fold axis intersects the page at a point between the three heads. (M. C. Escher's "Symmetry Drawing E25 (Reptiles)" copyright © 2006, The M. C. Escher Company—Holland. All rights reserved www.mcescher.com.) (c) An apatite crystal viewed along its *c*-axis. This drawing shows a large basal face (with a dot marked in its center) and an array of modifying faces around it. The overall symmetry of this crystal reveals a six-fold rotation axis (A_6) at the location of the dot. There are no mirror planes visible in this orientation of an apatite crystal.

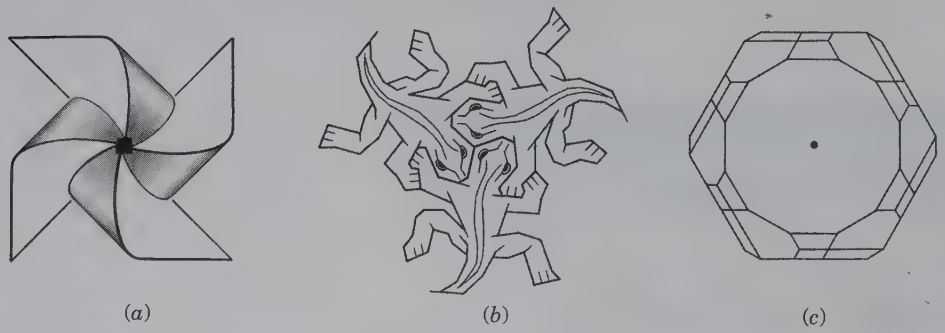

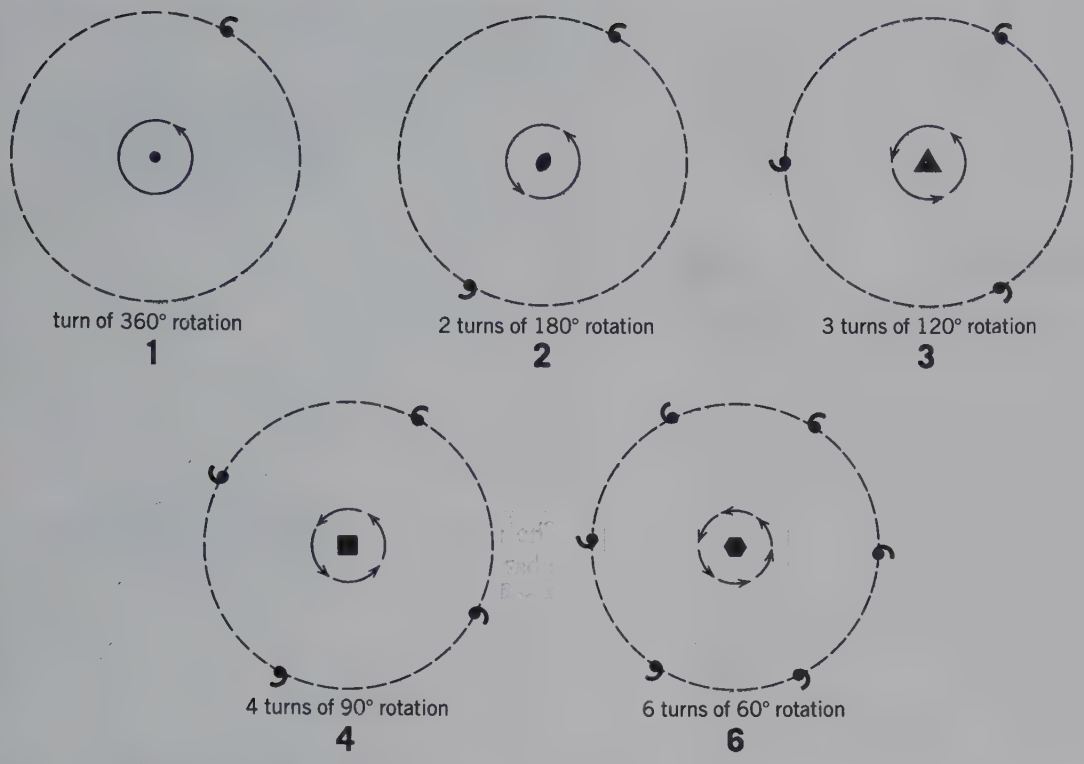

FIG. 6.12 Illustration of rotations that allow the motif to coincide with an identical unit for one-, two-, three-, four-, or six-fold rotation axes. Symbols in the circle centers are used to represent these axes. The diagram for **2** represents a projection onto the *xy* plane of Fig. 6.9a.

The shorthand notation used for a rotational symmetry axis is "A" followed by a subscript depicting the number of times a crystal face is repeated during a complete rotation, such as A_2, A_4, A_6 (see Table 6.1). In illustrations, this notation is shortened to simply the number of rotations, 1, 2, 3, 4, 6. Figure 6.12 shows not only these rotational numbers but also the graphical symbols used to represent them (e.g., 2-fold = ⬮, 3 = ▲, 4 = ■, 6 = ⬢).

REFLECTION (MIRROR)

A **mirror plane**, ***m***, is an imaginary plane that divides a crystal into two halves, each of which, in a perfectly developed crystal, is the mirror image of the other. A **reflection** across a mirror plane (Figs. 6.8b, 6.9b) produces a mirror image. A mirror plane is denoted by *m* (see Table 6.1). Figure 6.8b illustrates the position of a single mirror in a crystal, also called a *symmetry plane*.

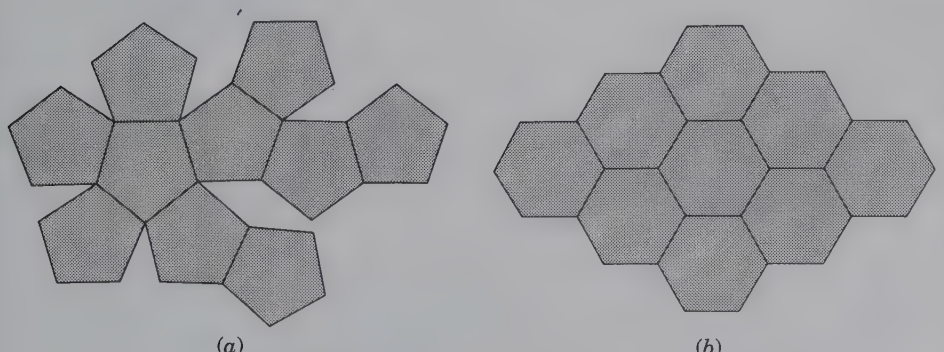

FIG. 6.13 (a) Arrangement of pentagons, which individually have five-fold symmetry axes perpendicular to the page, leads to gaps in the pattern. (b) Arrangement of hexagons with six-fold axes perpendicular to the page, as in honeycombs, completely fills the space.

Figure 6.9b illustrates the case of a generated motif that has the opposite handedness of the original motif; the two motifs make an *enantiomorphic pair* (they are related by a mirror, and they cannot be superimposed on each other). This is the same as the relationship between the right and the left hand.

CENTER OF SYMMETRY

A **center of symmetry**, *i*, is present in a crystal if an imaginary line can be passed from any point on its surface through its center and the same point is found on the line at an equal distance beyond the center on the opposite side (Fig. 6.8c). A *center of symmetry*, also known as an **inversion** (*i*), produces an inverted object through an *inversion center* (Fig. 6.9c). An inversion involves drawing imaginary lines from every point on the object through the inversion center and out an equal distance on the other side of the inversion center. The inverted object is then "recreated" by connecting the points (Fig. 6.9c). The presence of a center of symmetry is denoted by an *i* or $\bar{1}$ (see Table 6.1). Inversion, like reflection, produces an enantiomorphic pair. Two enantiomorphic motifs are related by mirror reflection or inversion.

ROTATION WITH INVERSION

In addition to the symmetry generated by operations of rotation, there are one-, two-, three-, four-, and six-fold rotations that can be combined with inversion to produce what are known as **rotoinversion operations** (Figs. 6.8d and 6.9d). To generate rotoinversion, rotate the motif through α (the rotation angle), then invert the motif through the center (Figs. 6.14 and 6.15). An axis of rotoinversion within a crystal is an imaginary line that relates rotation about an axis with inversion ($\bar{A}_2$, $\bar{A}_3$, $\bar{A}_4$, $\bar{A}_6$, read: A bar two, etc., see also Table 6.1). Figure 6.8d illustrates the morphological expression of a four-fold rotoinversion axis in a crystal.

A one-fold rotoinversion axis, symbolized as $\bar{1}$ (read: bar one), is the simplest. The original motif is rotated 360°, so that it returns to its original position, and is then inverted through a center, as shown in Fig. 6.14. This combination of operations produces the same result as does the presence of a *center of symmetry*. The operation is also referred to as a *center of symmetry* or *i* (for inversion). Figure 6.14c illustrates how the three-dimensional arrangement of the motif commas appears when projected on the equatorial plane of a globe in Fig. 6.14a.

The rotoinversion operations for $\bar{2}$, $\bar{3}$, $\bar{4}$, and $\bar{6}$ (read: bar two, bar three, etc.) are shown in Fig. 6.15. The $\bar{2}$ operation is equivalent to a mirror plane coincident with the equatorial plane of the globe (Fig. 6.15a). The $\bar{3}$ operation is the equivalent of a three-fold rotation axis (3) and inversion (*i*), which is the same as a three-fold rotation with a center of symmetry (Fig. 6.15b). The $\bar{4}$ operation is not resolvable into other operations and is unique (Fig. 6.15c). The $\bar{6}$ operation is equivalent to a three-fold axis of rotation with a mirror plane perpendicular to the rotation axis (Fig. 6.15d). Rotoinversion is best seen and evaluated in three-dimensional objects, such as wooden crystal models.

The original motif unit (denoted *A* in all illustrations of Figs. 6.14 and 6.15) has an enantiomorphic relationship with the second motif unit (denoted *B*), because of the inversion. The third motif unit (denoted *C*), however, is similar to the original motif unit (*A*). All of these symmetry operations (rotation, reflection, and

FIG. 6.14 (a) Illustration of an operation of rotoinversion, consisting of 360° rotation and subsequent inversion through the center of the globe. (b) Projection of the two motif units (*A* and *B*) from the outer skin of the globe onto the equatorial plane. (c) Location of the projected motifs on the equatorial plane (see also Fig. 6.15). Two enantiomorphic motifs are related by mirror reflection or inversion.

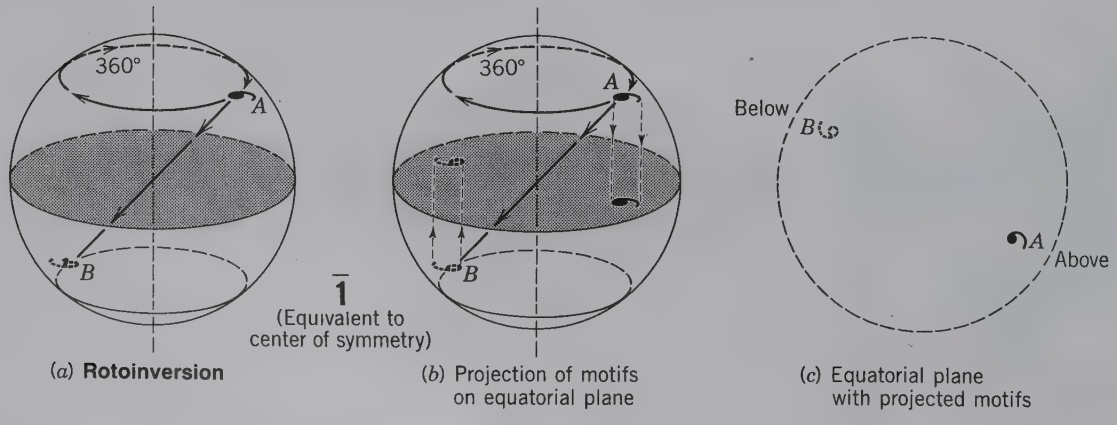

(*a*) **Rotoinversion** (*b*) Projection of motifs on equatorial plane (*c*) Equatorial plane with projected motifs

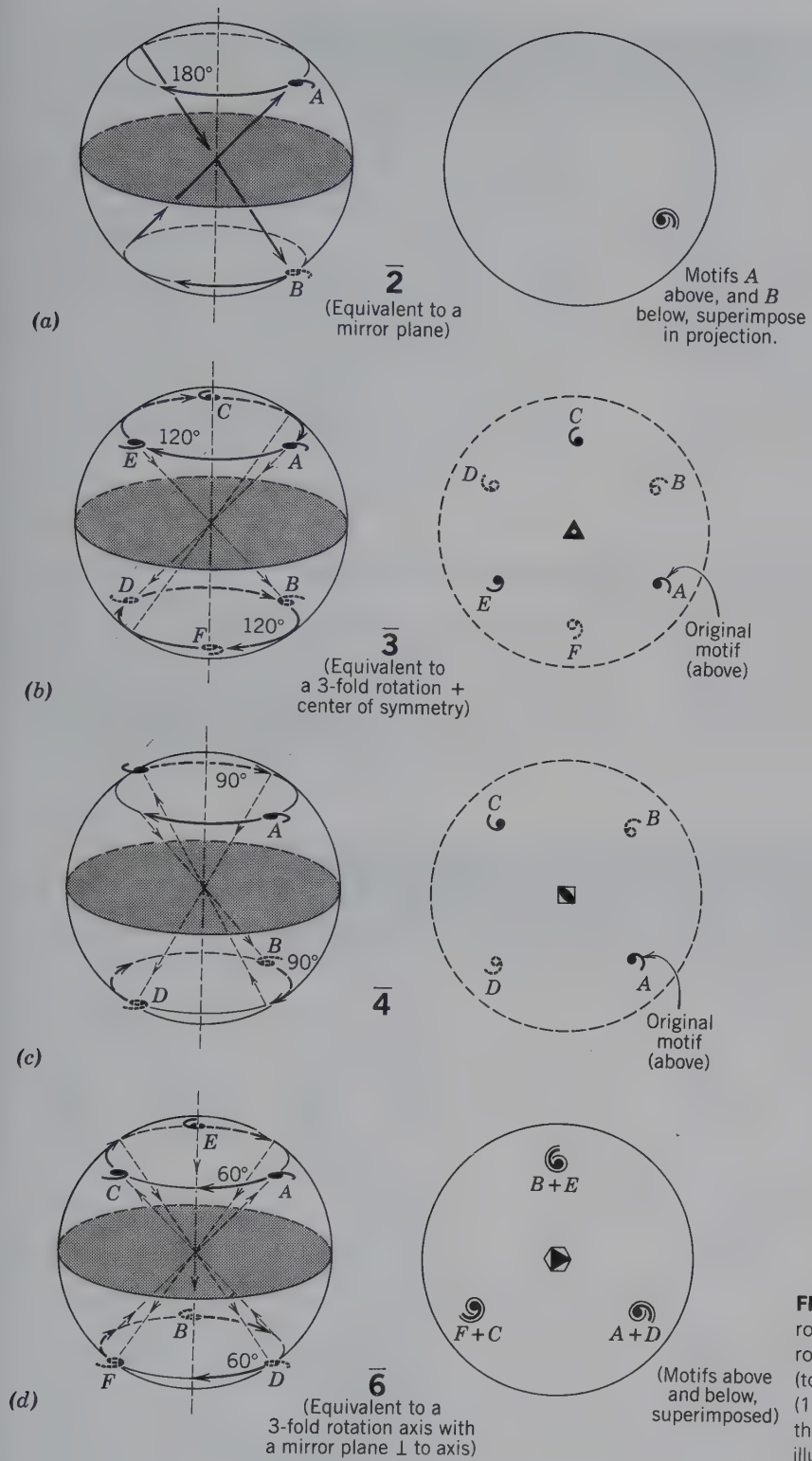

FIG. 6.15 Illustration of operations of rotoinversion on motif units for all possible rotoinversion axes. To go from unit *A* to *B* (to *C*, etc.) involves rotation through an angle (180°, 120°, 90°, or 60°) as well as inversion through the center (see Fig. 6.14 for illustration of projection scheme).

Table 6.2 The 32 Possible Symmetry Elements and Combinations of Symmetry Elements

	Increasing Rotational Symmetry →			
Rotation axis only	1	2	3	4	6
Rotoinversion axis only	$\bar{1}(=i)$	$\bar{2}(=m)$	$\bar{3}$	$\bar{4}$	$\bar{6}(=3/m)$
Combination of rotation axes		222	32	422	622
One rotation with perpendicular mirror		2/*m*	$3/m(=\bar{6})$	4/*m*	6/*m*
One rotation with parallel mirrors		2*mm*	3*m*	4*mm*	6*mm*
Rotoinversion with rotation and mirror			$\bar{3}2/m$	$\bar{4}2m$	$\bar{6}2m$
Three rotation axes and perpendicular mirrors		2/*m*2/*m*2/*m*		4/*m*2/*m*2/*m*	6/*m*2/*m*2/*m*
Additional symmetry combinations present in isometric patterns		23 $2/m\bar{3}$		432 (see Fig. 6.18) $\bar{4}3m$	$4/m\bar{3}2/m$

rotoinversion) generate only a finite number of motifs. On the other hand, translation, and translational symmetry operations (covered in Chapter 7) will repeat a motif infinitely. As such, rotation, reflection, and rotoinversion operations are classified as *without translation*. (These symmetry operations are illustrated, with animations, in module II of the CD-ROM under "Crystallography: Symmetry Operations.")

SYMMETRY NOTATION

The notation of symmetry is simplified by the use of symbols (see Tables 6.1 through 6.3). In the preceding discussion, various symmetry symbols were used to designate symmetry elements. For example, the complete symmetry of a crystal might be listed as:

i, $3A_4$, $4A_3$, $6A_2$, $9m$.

Table 6.3 The 32 Point Groups (Crystal Classes) and Their Symmetry Contents (Those listed in bold are presented in detail in Chapter 9)

Crystal System	Crystal Class	Symmetry Content	Crystal System	Crystal Class	Symmetry Content
Triclinic	$\bar{1}$	none	Hexagonal*	3	$1A_3$
	1	i		$\bar{3}$	$1\bar{A}_3(=i+1A_3)$
Monoclinic	2	$1A_2$		**32**	$1A_3, 3A_2$
	m	1*m*		**3*m***	$1A_3, 3m$
	2/*m*	$i, 1A_2, 1m$		**$\bar{3}$2/*m***	$1\bar{A}_3, 3A_2, 3m$
Orthorhombic	222	$3A_2$			$(1\bar{A}_3 = i + 1A_3)$
	***mm*2**	$1A_2, 2m$		$\bar{6}$	$1\bar{A}_6$
	2/*m*2/*m*2/*m*	$i, 3A_2, 3m$		$\bar{6}$	$1\bar{A}_6(=1A_3+m)$
Tetragonal	$\bar{4}$	$1\bar{A}_4$		**6/*m***	$i, 1A_6, 1m$
	$\bar{4}$	$1\bar{A}_4$		**622**	$1A_6, 6A_2$
	4/*m*	$i, 1A_4, m$		**6*mm***	$1A_6, 6m$
	422	$1A_4, 4A_2$		$\bar{6}$m2	$1\bar{A}_6, 3A_2, 3m$
	$\bar{4}mm$	$1\bar{A}_4, 4m$			$(1\bar{A}_6 = 1A_3 + m)$
	$\bar{4}$2*m*	$1\bar{A}_4, 2A_2, 2m$		**6/*m*2/*m*2/*m***	$i, 1A_6, 6A_2, 7m$
	4/*m*2/*m*2/*m*	$i, 1A_4, 4A_2, 5m$	Isometric	**23**	$3A_2, 4A_3$
				$2/m\bar{3}$	$3A_2, 3m, 4\bar{A}_3$
					$(1\bar{A}_3 = 1A_3 + i)$
				432	$3A_4, 4A_3, 6A_2$
				$\bar{4}3m$	$3\bar{A}_4\, 4A_3, 6m$
				4/$m\bar{3}$2/*m*	$3A_4, 4\bar{A}_3, 6A_2, 9m$
					$(1\bar{A}_3 = 1A_3 + i)$

*In this table all point groups beginning with 6, $\bar{6}$, 3, and $\bar{3}$ are grouped in the hexagonal system. In earlier editions of the *Manual of Mineralogy* the hexagonal system was divided into the hexagonal and rhombohedral divisions. The use of these two subdivisions, as based on the presence of 6 or $\bar{6}$ versus 3 or $\bar{3}$ axes in the morphological symmetry of a crystal, results in confusion when subsequent X-ray investigations show a specific crystal with, for example, 32 symmetry to be based on a hexagonal lattice. This is the case in low quartz, which shows morphological symmetry 32 but is based on a primitive hexagonal lattice, resulting in space group $P3_12$ (or $P3_22$).

This indicates that the crystal has a center of symmetry (i), three four-fold rotation axes ($3A_4$), four three-fold rotation axes ($4A_3$), six two-fold rotation axes ($6A_2$), and nine mirror planes ($9m$). In Tables 6.2 and 6.3, symbols for the overall symmetry content of a crystal are referred to as the *Hermann-Mauguin* (HM) *notation*, after the inventors. This internationally accepted notation recognizes that certain combinations of symmetry operations generate others (and are therefore implied) and are omitted. For example, symmetry of $4/m\ 2/m\ 2/m$ means that there is one four-fold rotation axis with perpendicular mirror plane and that there are two kinds of two-fold rotation axes each with a perpendicular mirror plane. The presence of the three perpendicular mirror planes implies that the mineral has a center of symmetry, but this is not explicitly stated by an i.

COMBINATIONS OF ROTATIONS

Until now, patterns generated by a *single* axis of rotation or rotoinversion have been considered. If various axes of rotation are combined, regular three-dimensional patterns are generated. Symmetry axes can only be put together in symmetrically consistent ways, such that an infinite set of axes is not generated. For instance, if one four-fold axis, A, is put at an acute angle to another four-fold axis, B, each will operate on the other, generating an infinite set of axes. To avoid this,

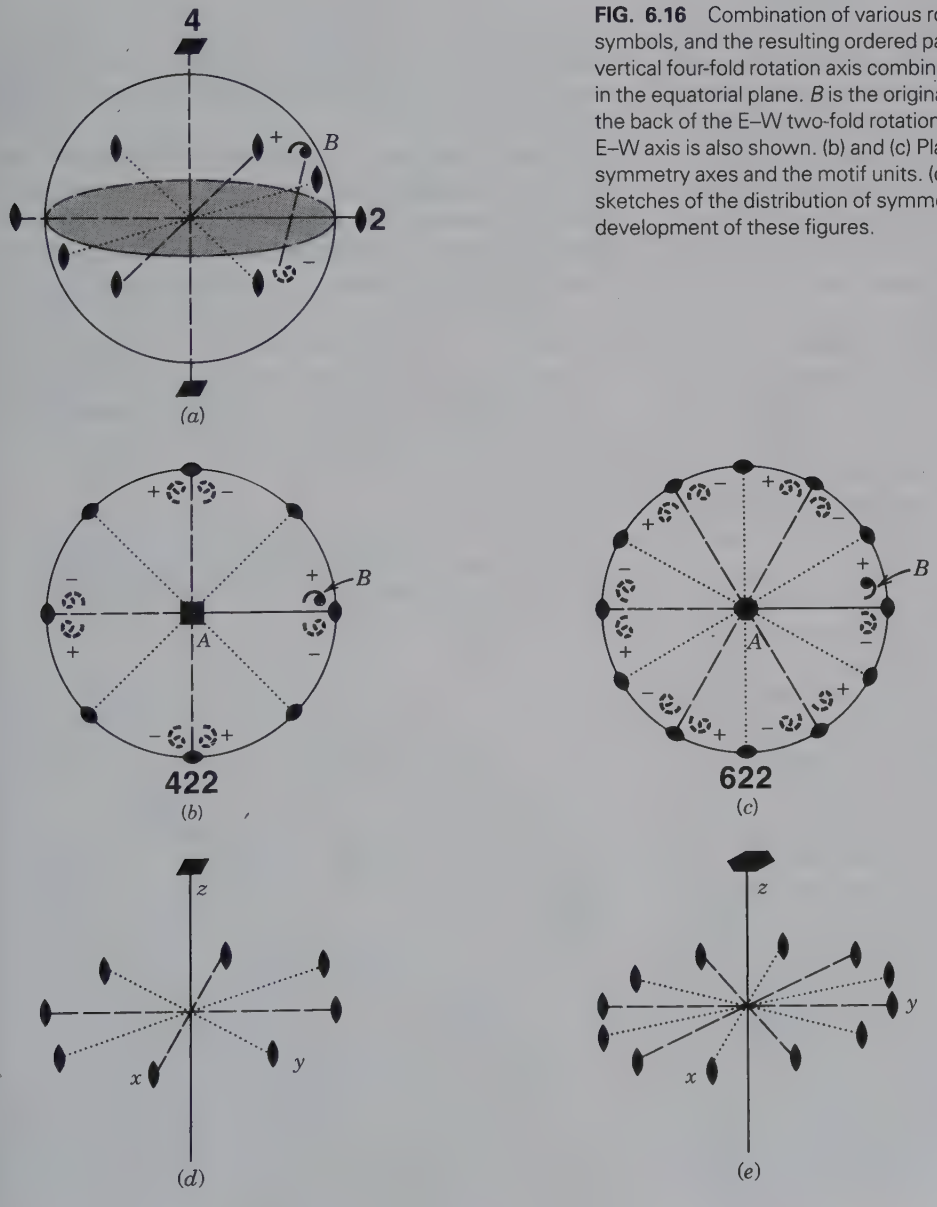

FIG. 6.16 Combination of various rotation axes, as designated by symbols, and the resulting ordered patterns. (a) Perspective view of a vertical four-fold rotation axis combined with a two-fold rotation axis E–W in the equatorial plane. B is the original motif above the equatorial plane to the back of the E–W two-fold rotation axis. One motif generated by this E–W axis is also shown. (b) and (c) Plan views of the location of the symmetry axes and the motif units. (d) and (e) Three-dimensional sketches of the distribution of symmetry axes. See text for the development of these figures.

axes must be put together at 90°, or at 54° 44′. All symmetry operators must intersect at a single point, and that point remains unchanged by operations (as is the case for point symmetry).

For example, a four-fold rotation axis (A_4) perpendicular to the plane of the page might be combined with a two-fold rotation axis (A_2) in the plane of the page. Another example would be a combination of a six-fold rotation axis (A_6) perpendicular to the plane of the page with a two-fold axis (A_2) in the plane of the page. Both examples are illustrated in Fig. 6.16. The locations of A_4 and A_6 in both symmetry combinations are at point *A*, the center of the circle, perpendicular to the page. The two-fold axis is to the right of *A*, along the east-west direction. The presence of the four- and six-fold axes will generate 3 and 5 more two-fold axes, respectively, shown as *dashed* lines. Although 3 and 5 two-fold axis extensions have been generated, they constitute only 2 two-fold axis directions at 90° to each other in Fig. 6.16b and 3 two-fold axis directions at 120° to each other in Fig. 6.16c.

With reference to Fig. 6.16a, note that there is a comma (marked by *B* in the drawings) above the page in a position slightly north of the original two-fold axis. This comma is marked (+) indicating that it lies above the page in the positive direction of the *z* axis. The original two-fold axis (in the east-west direction) will generate another comma from the one given at *B* and is accompanied by a minus (−) sign, indicating its position below the page. The four- and six-fold axes will generate 3 and 5 additional comma (motif) pairs, respectively, as shown by dashed commas in Figs. 6.16b and c. Carefully observing the arrangement of all of the commas shows that yet another set of two-fold axes is generated. These axes are dotted and at 45° to the original two-fold axes in Fig. 6.16b and at 30° to the original two-fold axes in Fig. 6.16c. The total symmetry in Figs. 6.16a and b, therefore, consists of a four-fold rotation axis perpendicular to the page and 2 sets of two-fold axes, the original set in the E–W, N–S directions, and the second at 45°. The total symmetry in Fig. 6.16c consists of a six-fold rotation axis ($1A_6$) perpendicular to the page and 2 sets of three A_2 in the plane of the page. The two sets of A_2 are at 30° to each other. In each case, each *set* of two-fold axes is symmetrically equivalent to the other set. That is, if 1 two-fold axis is given, the other symmetry elements will generate the other two-folds; in the example given, as 2 independent sets of two-folds. These types of combinations of axes can be represented by a sequence of digits for the types of rotation axes involved (see Table 6.2). In such symbols, each symmetrically equivalent set of symmetry elements is listed. For the examples in Fig. 6.16 this would result in 422 and 622, respectively. Three-

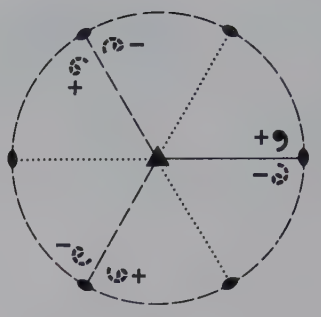

FIG. 6.17 Combination of a three-fold rotation axis perpendicular to the page and a two-fold rotation axis lying E–W in the page. The original motif units are on the right-hand side. Motif units generated by the symmetry and symmetry axes are indicated by dashes and dots. The resultant symmetry sequence is 32, not 322. Compare with Fig. 6.16.

dimensional representations of the locations of the rotation axes in the 422 and 622 combinations are given in Figs. 6.16d and e.

In contrast, some combinations of symmetry produce no additional axes. Figure 6.17 shows that combining a three-fold axis with a two-fold axis in a plane perpendicular to it, generates no symmetry axes in addition to 3 two-fold axes.

The 432 symmetry axis combination is one of high symmetry with the locations of the axes in specialized positions. Figure 6.18 shows the location of such axes with reference to a cube. The A_4 axes are perpendicular to the cube faces, the A_3 axes are at the corners of the

FIG. 6.18 The location of four- three- and two-fold symmetry axes with respect to a cubic outline for 432. Note that the axes connect symbols on opposite sides of the crystal and run through the center.

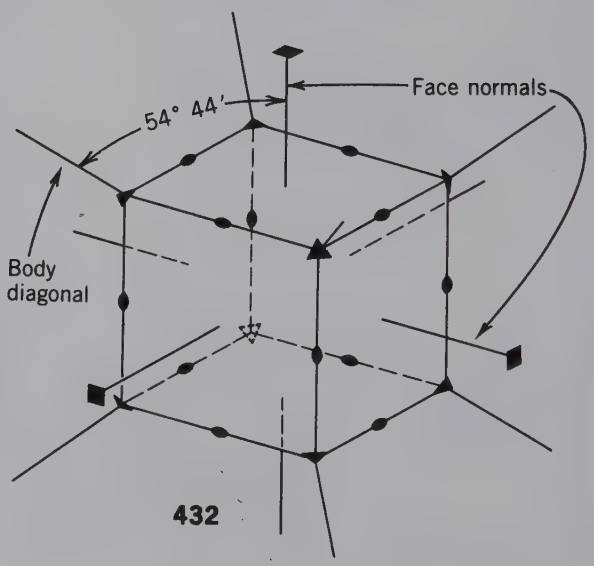

cube, and the A_2 axes are located at the centers of the edges of the cube. These A_3 axes meet the axes that are perpendicular to the cube faces at 54° 44′. For a rigorous derivation of the limits on combinations of rotational operators see Boisen and Gibbs (1990; complete reference is given at the end of this chapter).

COMBINATIONS OF ROTATION AXES AND MIRRORS

Many crystals show mirrors in addition to the combinations of rotation axes discussed previously. As a general rule, mirror planes are either perpendicular to or parallel to possible rotation axes. In Fig. 6.19a, a four-fold rotation axis is combined with a mirror plane perpendicular to the axis, and in Fig. 6.19b a six-fold axis is combined with a mirror perpendicular to it. In Fig. 6.19a, the arrangement of the motifs is compatible with the A_4 and is shown by commas above the mirror plane. These are reflected by the mirror plane giving rise to another set of four commas below, as shown by the dashed commas. Normally, the symmetry elements and motif units are shown in a two-dimensional projection, as on the right side of Fig. 6.19a. The motif units above the mirror as well as those below the mirror are projected onto the mirror itself. This causes the commas from above and below to coincide. To distinguish motif units that lie above the plane of projection (the mirror plane in this case) from those below the plane, motif units above the plane are generally shown as solid dots and those below the plane as small open circles. When this convention is used for the perspective drawing in Fig. 6.19a, it results in a four-fold rotation axis surrounded by four motif units (dots) above, and four identical motif units (circles) below the mirror plane (as shown on the right of Fig. 6.19a). The mirror plane is conventionally shown by a solid circle. This type of combination of symmetry elements is represented by $4/m$ (read: four over m) because the mirror plane is perpendicular to the axis. The symmetry combination in Fig. 6.19b is represented by $6/m$. Other similar combinations are $2/m$ and $3/m$. There are yet other symmetry combinations such as: $6/m2/m2/m$, $4/m2/m2/m$, and $2/m2/m2/m$. In Figs. 6.20a, b, and c, illustrations are given for the combinations 422, $4/m2/m2/m$, and $4mm$ (compare with Fig. 6.16). Additional symmetry combinations are shown in Fig. 6.21.

All of the nontranslational symmetry elements that have been introduced, as well as their combinations, are the easily observed expression (in well-formed crystals or wooden models) of the internal atomic arrangement of the mineral's structure. This is

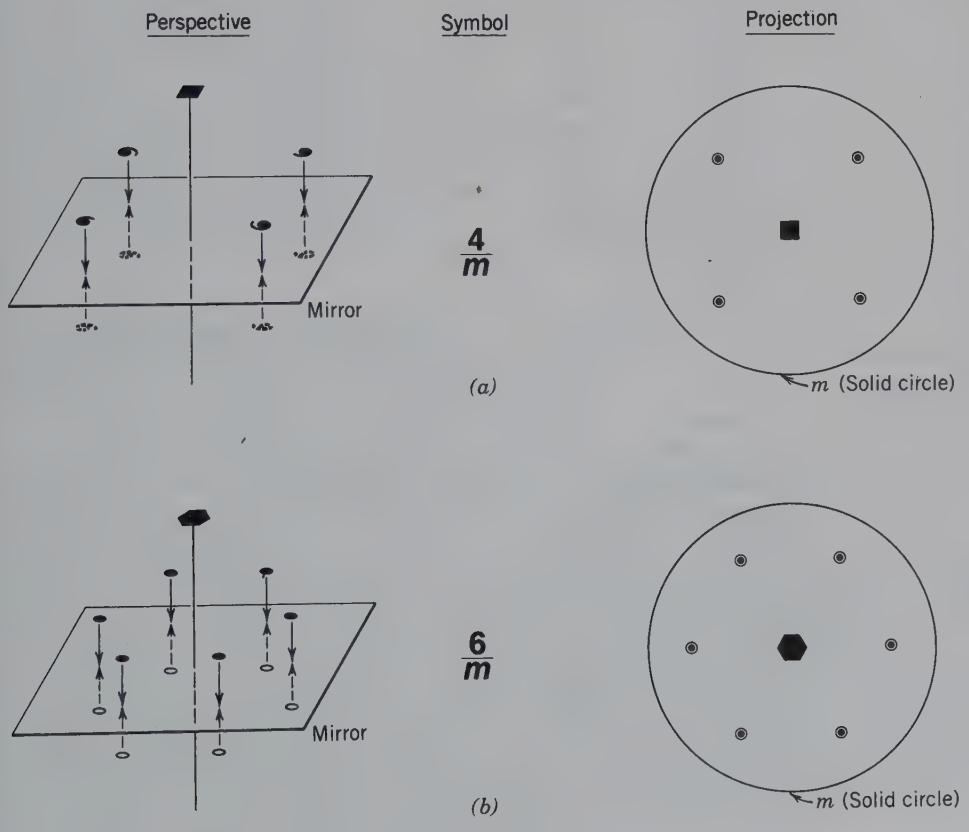

FIG. 6.19 (a) Combination of a four-fold symmetry axis with a perpendicular mirror plane. The motif units that can be represented by commas are more conventionally shown by solid dots and small open circles in order to differentiate motif units above and below the mirror plane, respectively. In the projection, the mirror plane is shown by the solid circle. (b) Combination of a six-fold rotation axis and a mirror plane perpendicular to it.

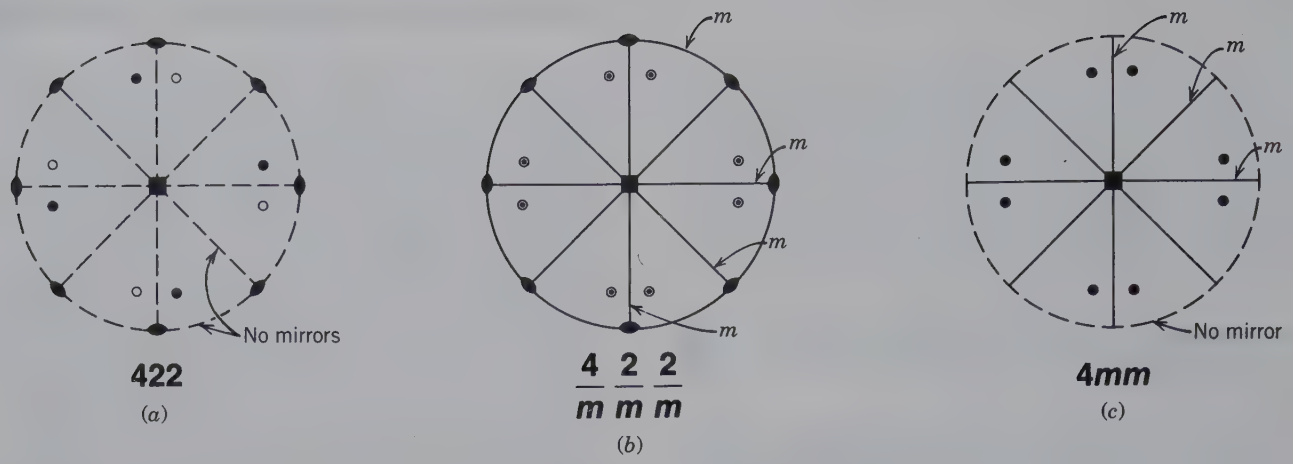

FIG. 6.20 (a) Combination of a four-fold rotation axis and 2 sets of two-fold rotation axes (see also Fig. 6.16). Motif units above the plane of the page are shown as solid dots, those below as open circles. (b) Combination of a four-fold rotation axis, 4 two-fold rotation axes, and mirror planes perpendicular to each of the axes. (c) Combination of a four-fold rotation axis and two sets of mirror planes parallel to the four-fold axis. The absence of a mirror plane is indicated by the dashed circle.

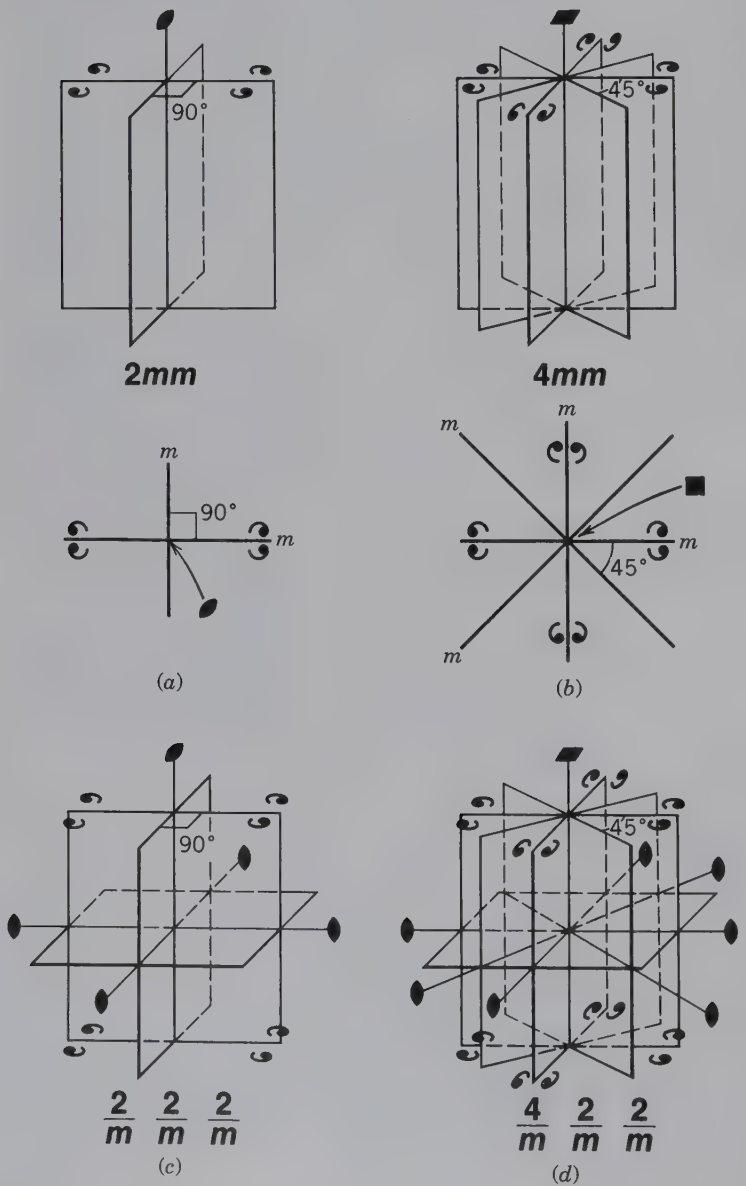

FIG. 6.21 Illustrations of intersecting mirrors and the resultant lines of intersection, equivalent to rotation axes. (a) and (b) Perspective and plan views of 2*mm* and 4*mm*. In (a) the vertical mirrors are at 90° to each other; in (b) the vertical mirrors are at 45° to each other. In (c) and (d) horizontal mirrors are added to the drawings in (a) and (b) respectively. The horizontal intersection lines become two-fold rotations in both illustrations. Compare Fig. 6.21d with the plan view in Fig. 6.20b.

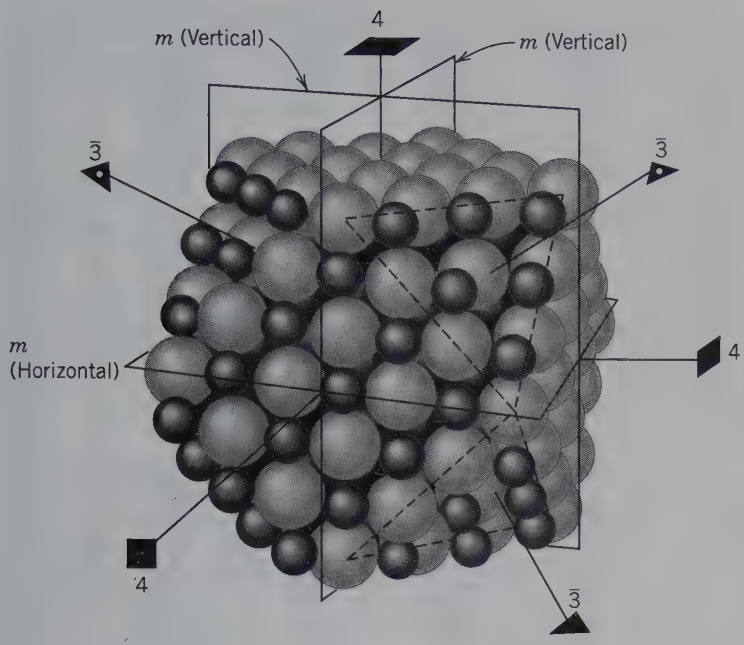

FIG. 6.22 A structure model of the packing of Na^+ (small spheres) and Cl^- (large spheres) in NaCl, halite. The model has a cubo-octahedral outline showing square cube faces and triangular octahedral faces at the corners of the cube. This structure contains all of the symmetry elements that are also present in the morphology of a cube, that is, 3 four-fold axes (all are shown), 4 three-fold rotoinversion axes (three are shown at corners of the cube), 6 two-fold axes (at the cube edge; none are shown), and nine mirror planes in various orientations (only three are shown that are perpendicular to each other).

shown in Fig. 6.22. This illustration depicts the regular packing of Na^+ and Cl^- ions in the structure of NaCl, halite. This specific ionic packing scheme is a function of relative ionic sizes (for Na^+ and Cl^-), their electrical charges, and the types of bonds between the ions. This structure also shows several of the symmetry elements that can be observed on the basis of its external morphology (compare with Fig. 6.18). Although the NaCl structure (as shown in Fig. 6.22) also contains translational elements, the symmetry operations discussed thus far are basic to an understanding of the morphology as well as the internal structure of crystalline materials.

COMBINATIONS OF SYMMETRY OPERATIONS WITHOUT TRANSLATION

The number of possible symmetry combinations, of *rotation axes*, *mirror planes*, a *center of symmetry*, and *rotoinversion axes* found in crystals, is not unlimited. The total number of symmetry elements and combinations of symmetry elements is only 32. These 32 combinations of symmetry elements describe the symmetry of all known minerals and are given in Tables 6.2 and 6.3. They are arranged in a sequence from the lowest rotational symmetry (A_1) to the highest rotational symmetry (A_6). These are shown graphically in Fig. 6.23. The possible 32 nonidentical symmetry elements and their combinations are also known as the **32 point groups.** The word *point* indicates that the symmetry operations leave, at least, one particular point of the pattern (at the center of the pattern) unmoved. The word *group* relates to the mathematical theory of groups that allows for a systematic and rigorous derivation of all of the possible and nonidentical symmetry combinations (see, for example, D. E. Sands 1975, or Boisen and Gibbs 1990).

A crystal, under favorable circumstances of growth, will develop smooth planes or "faces" that may assume regular geometric forms expressing its internal, regular (ordered), atomic arrangement. A systematic study of the external forms of crystals leads to 32 possible symmetries or symmetry combinations, which are the same 32 as the point groups, noted previously. These 32 point groups are identical to the 32 possible **crystal classes** to which crystals can be assigned on the basis of their morphology (Table 6.3).

A graphical illustration of all 32 symmetries in projection is given in Fig. 6.24. This figure precedes a more detailed discussion of crystal form (see page 134) because it is based solely on the distribution of motif units, without reference to crystals and their faces or crystallographic axes. In Fig. 6.24, the presence or absence of a center of symmetry ($\bar{1}$) is not indicated by a specific symbol. However, visual inspection of the circles (within which there are unique distributions of motif units) allows one to determine whether a center of symmetry is present or absent. Recall that a center of symmetry inverts the motif through the center of the circle. For example, a motif at the upper right (above the page) is balanced by a motif at the lower left (below the page).

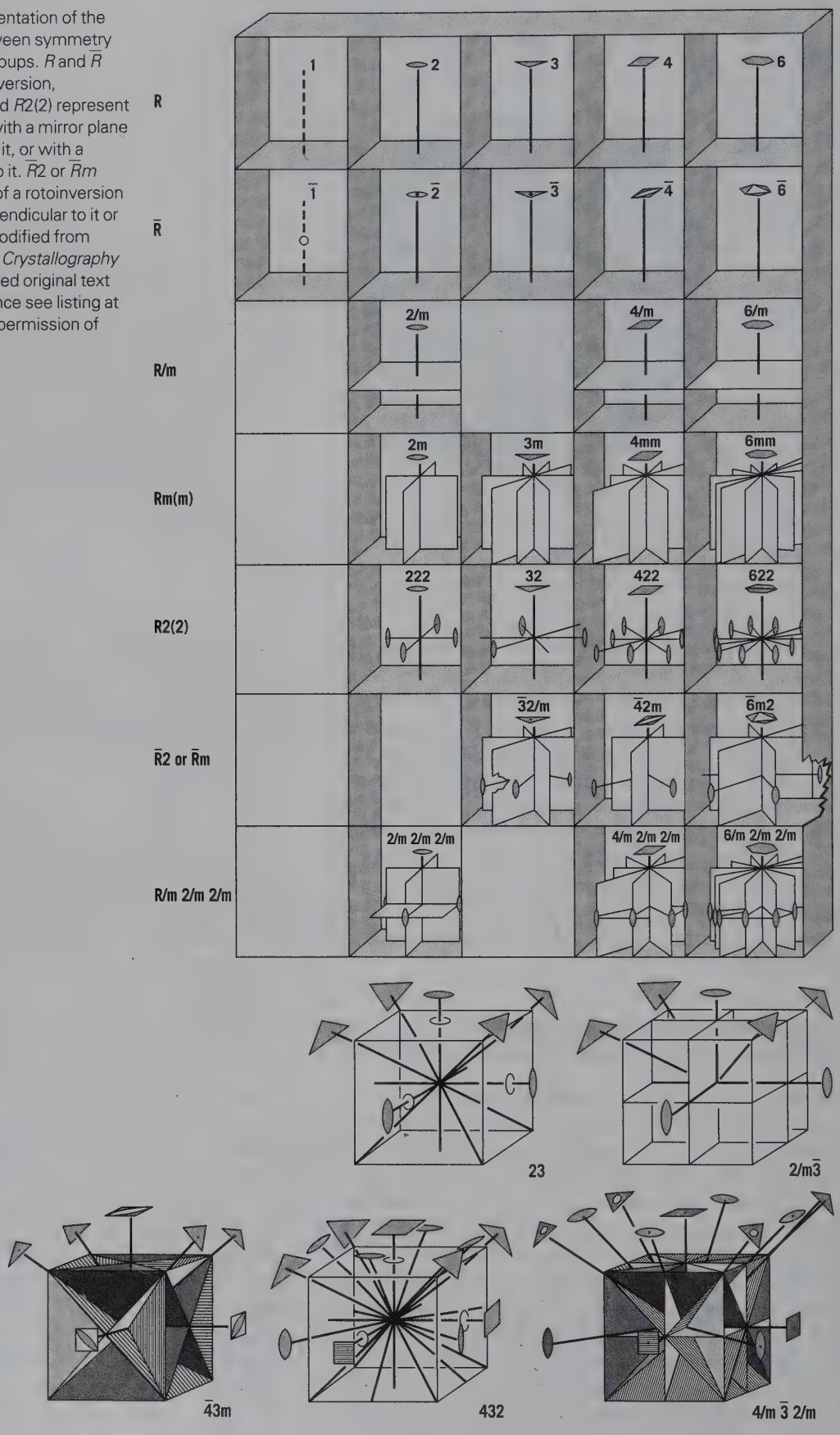

FIG. 6.23 Graphical representation of the geometric relationships between symmetry elements and the 32 point groups. *R* and $\bar{R}$ represent rotation and rotoinversion, respectively. R/*m*, *Rm*(*m*), and *R*2(2) represent the combination of rotation with a mirror plane perpendicular to it, parallel to it, or with a two-fold axis perpendicular to it. $\bar{R}2$ or $\bar{R}m$ represents the combination of a rotoinversion axis with a two-fold axis perpendicular to it or a mirror plane parallel to it (Modified from Fig. 1.15 in Bloss, F. D. 1994. *Crystallography and crystal chemistry*, reprinted original text of 1971; for complete reference see listing at the end of this chapter; with permission of the author).

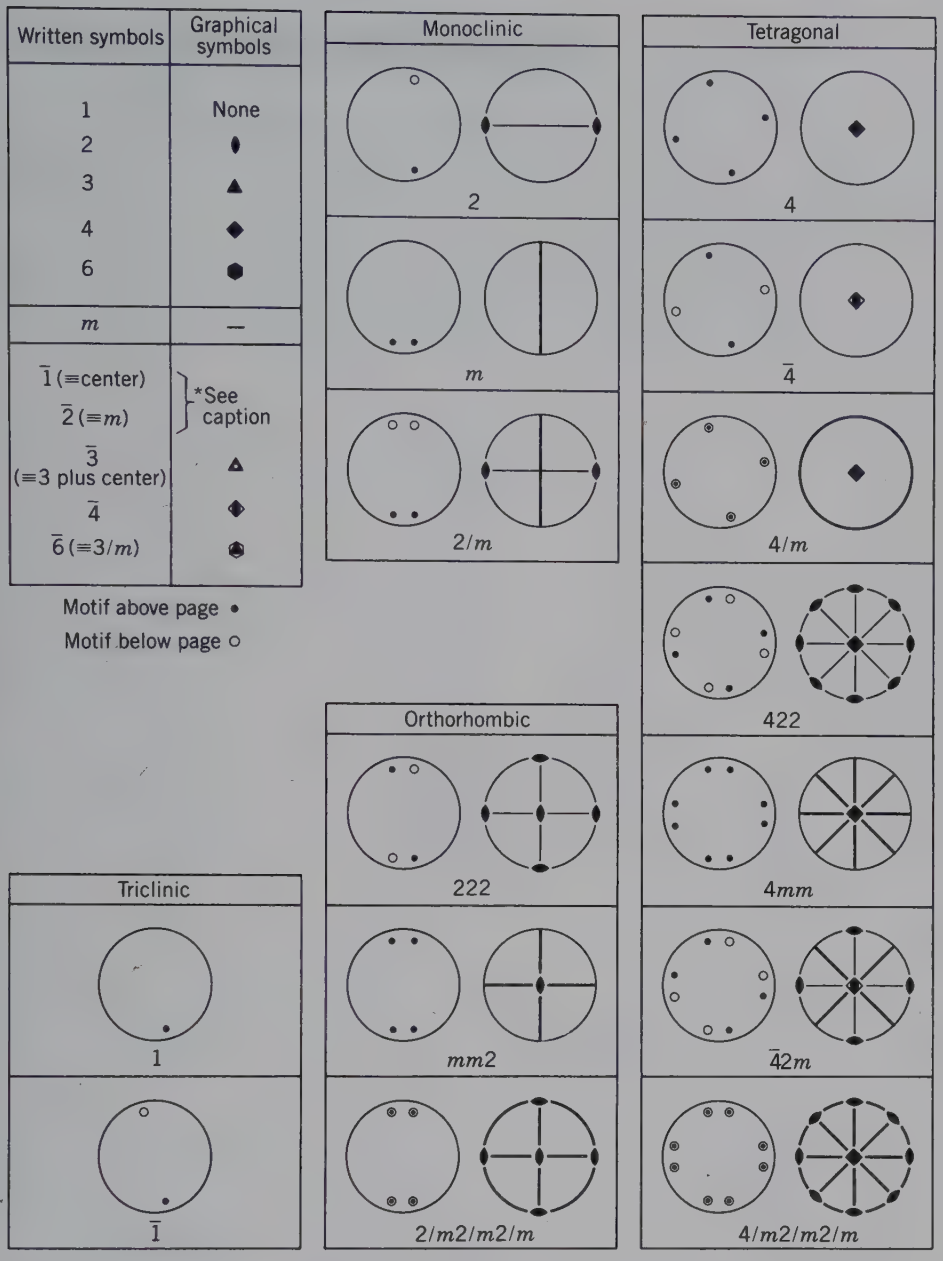

(continued)

FIG. 6.24 Graphical representation of the distribution of motif units compatible with the symmetry elements of each of the 32 crystal classes (point groups). The symbols for the symmetry elements are given at the top left corner of the diagram. For all crystal classes, excepting triclinic, there are two circular diagrams, with the left-hand diagram showing the distribution of motif units and the right-hand diagram illustrating the symmetry elements consistent with these motif units. The motif units above the page are equivalent to those below the page, but they are differentiated by dots (above the page) and circles (below the page). The presence of a center of symmetry is not shown by any symbol; its presence can be deduced from the arrangement of motif units. Instead of $\bar{2}$ the symbol for a mirror (m) is used. The diagrams for the monoclinic system are shown in what crystallographers refer to as the "second setting," with m vertical (perpendicular to the page) and the two-fold axis in an east-west orientation. Monoclinic symmetry can also be shown by setting the two-fold rotation axis perpendicular to the page, and orienting the mirror parallel to the page; this is referred to as the "first setting."

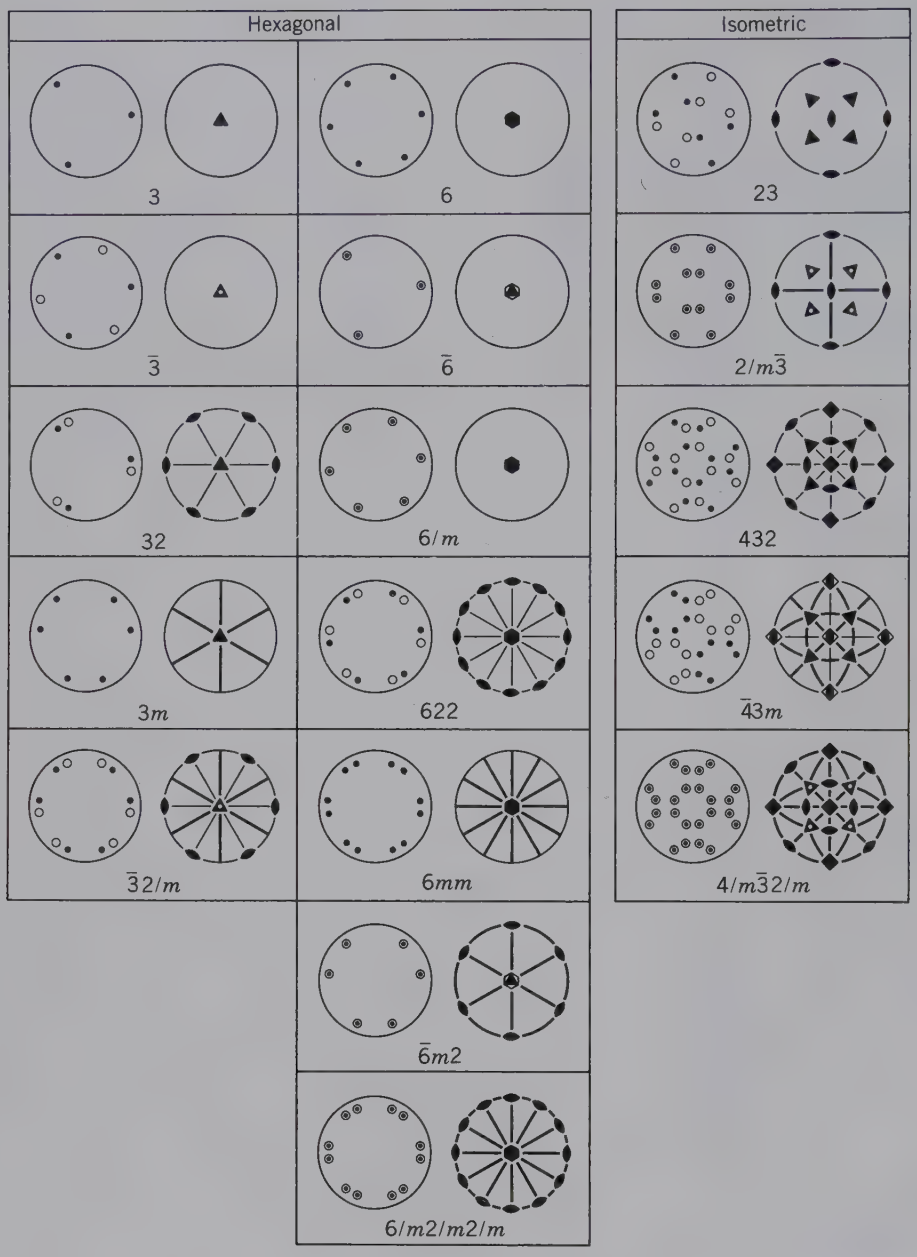

FIG. 6.24 *(continued)*

Of the 32 crystal classes, there are 21 without a center of symmetry and 11 with a center. Table 6.4 distinguishes the 32 crystal classes according to the absence or presence of a symmetry center. The 19 most important crystal classes (or point groups) are listed in bold type in Table 6.3. These are the point groups that contain the largest number of minerals (as well as synthetic compounds) or minerals of widespread geologic occurrence. In Chapter 9, the crystal morphology of these 19 crystal classes (point groups), as arranged within the six crystal systems, is covered in detail. (These same 19 crystal classes are shown in animations in module II of the CD-ROM under the heading "Crystallography: Crystal Classes.")

Table 6.4 The 32 Crystal Classes Grouped According to the Presence or Absence of a Center of Symmetry

Crystal System	No Center	Center Present
Triclinic	1	$\bar{1}$
Monoclinic	2, $\bar{2}$(= *m*)	2/*m*
Orthorhombic	222, *mm*2	2/*m*2/*m*2/*m*
Tetragonal	4, $\bar{4}$, 422	4/*m*, 4/*m*2/*m*2/*m*
	4*mm*, $\bar{4}$2*m*	
Hexagonal	3, 32, 3*m*	$\bar{3}$, $\bar{3}$2/*m*
	6, $\bar{6}$, 622	6/*m*, 6/*m*2/*m*2/*m*
	6*mm*, $\bar{6}$*m*2	
Isometric	23, 432, $\bar{4}$3*m*	2/*m*$\bar{3}$, 4/*m*$\bar{3}$2/*m*

CRYSTAL SYSTEMS

Several of the 32 *crystal classes* have common symmetry characteristics, permitting them to be grouped together in one of **six crystal systems**. (Table 6.3 shows the conventional arrangement of crystal systems and crystal classes). There are six crystal systems, but the hexagonal system has two subdivisions, hexagonal and rhombohedral. Each of the six crystal systems is defined by a set of crystallographic axes.

CRYSTALLOGRAPHIC AXES

In describing crystals it is convenient to refer the external forms or internal symmetry to a set of three (or four) reference axes. These imaginary reference lines are known as the **crystallographic axes** and are designated as ***a***, ***b***, and ***c***, except for the hexagonal system, which has four crystallographic axes, $\boldsymbol{a_1}$, $\boldsymbol{a_2}$, $\boldsymbol{a_3}$, and ***c*** (Figs. 6.25, 6.26). The notation of *a*, *b*, and *c* indicates that each axis is of a different length. The ends of the axes are designated plus (+) or minus (−), with the following orientation: The

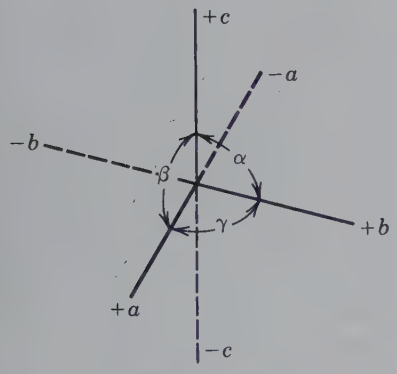

$a \neq^* b \neq c$
$\alpha \neq \beta \neq \gamma \neq 90°$

Triclinic

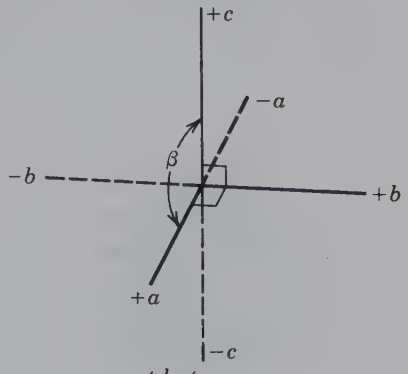

$a \neq b \neq c$
$\beta > 90°$; $\alpha = \gamma = 90°$

Monoclinic

FIG. 6.25 Illustrations of crystallographic axes for each of the six crystal systems. The three directions are labeled *a*, *b*, and *c*, unless symmetry makes them equivalent. The vertical is labeled *c* except in the isometric system where all axes are equal. The two horizontal axes are labeled *a* and *b*. If they are equal, they are labeled with the same letter, such as a_1 and a_2. In the hexagonal system, there are three equal horizontal axes labeled a_1, a_2, and a_3. See Table 6.5 for the relationship of symmetry notation (as in the Hermann–Mauguin system) and crystallographic axes.

*The sign ≠ implies nonequality by reason of symmetry; accidental equality may occur.

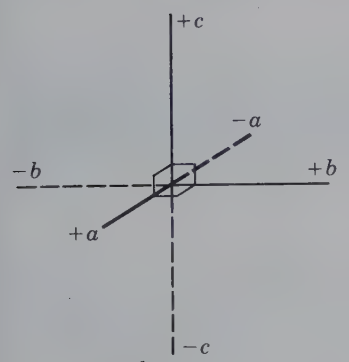

$a \neq b \neq c$
$\alpha = \beta = \gamma = 90°$

Orthorhombic

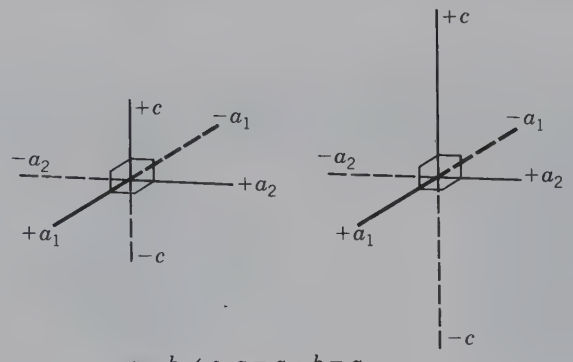

$a = b \neq c$; $a = a_1$; $b = a_2$
$\alpha = \beta = \gamma = 90°$

Tetragonal

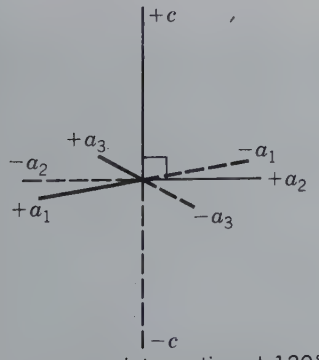

$a_1 = a_2 = a_3$, intersecting at 120°
c perpendicular to plane with a_1, a_2, a_3

Hexagonal

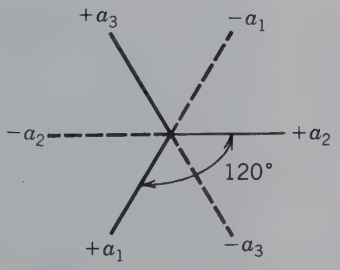

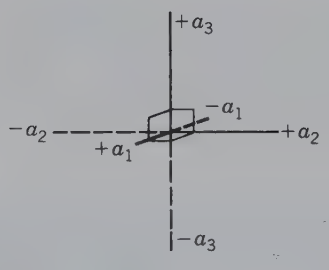

$a_1 = a_2 = a_3$; all axes at 90° to each other

Isometric

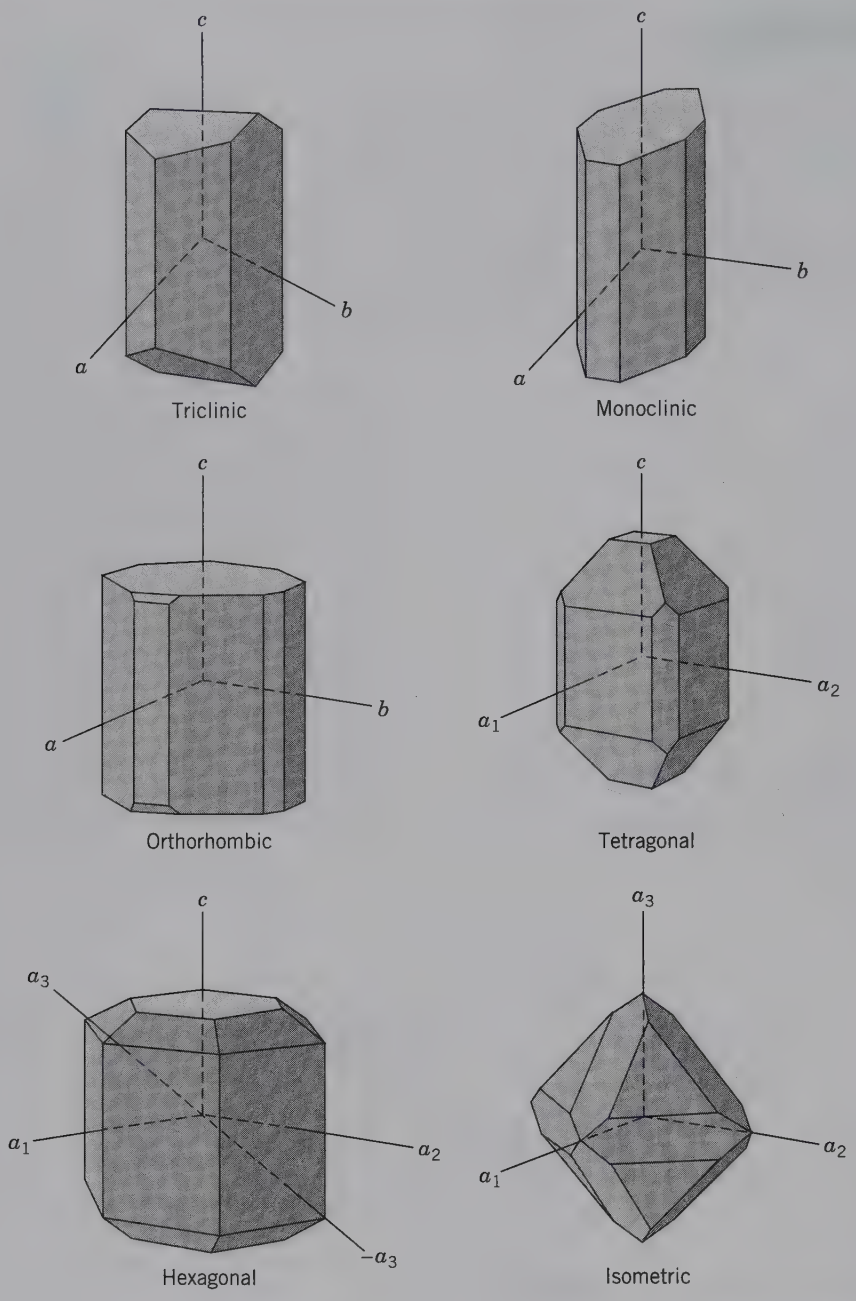

FIG. 6.26 Graphical representation of the relationship of the morphology of crystals and the choice of crystallographic axes. These perspective drawings provide only a qualitative impression. Fig. 6.25 gives relative lengths of axes and the angles between them.

positive end of *a* is to the front, positive *b* to the right, and positive *c* to the top; the opposite ends are negative. The angles between the positive ends of the axes are conventionally designated by the Greek letters α, β, and γ. The α angle is between axial directions *b* and *c*; β is between *a* and *c*; and γ is between *a* and *b*.

"The six crystal systems are defined on the basis of the symmetry present. In turn, the crystallographic axes are constrained to their different lengths or values of interaxial angles based on this symmetry."

Triclinic. Three axes of unequal length (*a*, *b*, *c*), all intersecting at different (oblique) angles ($\alpha \neq \beta \neq \gamma$).

Monoclinic. Three axes of unequal length (*a*, *b*, *c*), two of which are inclined to each other at an oblique angle and the third perpendicular to the plane of the other two ($\beta \neq 90°$, $\alpha = \gamma = 90°$).

Orthorhombic. Three mutually perpendicular axes all of different lengths (*a*, *b*, *c*; $\alpha = \beta = \gamma = 90°$).

Tetragonal. Three mutually perpendicular axes, two of which (the horizontal axes) are of equal length (a_1 and a_2), but the vertical axis (*c*) is shorter or longer than the other two ($a_1 = a_2 \neq c$; $\alpha = \beta = \gamma = 90°$).

Hexagonal. This system has four crystallographic axes; three equal horizontal axes (a_1, a_2, and a_3) that lie in a plane with their positive ends separated by angles of 120°; the fourth axis (vertical) is of different length (c) and is perpendicular to the plane of the other three ($a_1 = a_2 = a_3 \neq c$; $\beta = 90°$).

Isometric. Three mutually perpendicular axes of equal lengths (a_1, a_2, and a_3) ($a_1 = a_2 = a_3$; $\alpha = \beta = \gamma = 90°$).

In general, crystallographic axes are taken as parallel to the intersection of major crystal faces. These axes are, in most instances, fixed by the inherent symmetry of crystals and coincide with symmetry axes or with normals to symmetry planes (*mirror planes*). For example, in the monoclinic system, the two-fold rotation axis is set to be the *b* crystallographic axis, where *b* is perpendicular to the mirror plane. For the isometric system, the *a* axes are the 3 four-fold axes for the most symmetric isometric crystal class (see Table 6.5 for a synopsis of the interrelationship of symmetry elements to the choice of crystallographic axes). For some crystals, there may be more than one choice of crystallographic axes when the selection is made on morphology alone. Ideally, the axes should be parallel to, and their lengths proportional to, the edges of the unit cell. A graphical illustration of the relationship of the choice of crystallographic axes to morphology is shown in Fig. 6.26.

CRYSTALLOGRAPHIC NOTATION FOR PLANES

The system of notation that is used in crystallography for referring to planes and axes (or zones) as deduced from the external forms of crystals, is based on the proper choice of axes, and on making some simple measurements. This notation is a powerful tool when visualizing and working with crystals.

FACE INTERCEPTS

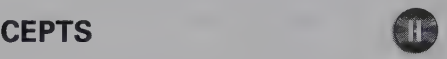

A crystal face can be defined by evaluating which crystallographic axis (or axes) it intersects. Thus, in describing a crystal face it is necessary to determine the crystal system to which the mineral belongs, to orient the crystal properly, and then to determine whether a face is parallel to, or intersects, the various crystallographic axes. For example, a face might be parallel to two axes and intersect the third, parallel to one axis and intersect the other two, or intersect all three axes. In

Table 6.5 Characteristic Symmetry, and Relationships Between Crystal Axes and Symmetry Notation of Crystal Systems

Crystal Class	System	Characteristic Symmetry	Hermann-Mauguin Notation
1, $\bar{1}$	Triclinic	1-fold (inversion or identity) symmetry only	Because of low symmetry, no crystallographic constraints.
2, *m*, 2/*m*	Monoclinic	1 two-fold rotation axis and/or mirror	The two-fold axis is taken as the b axis, and the mirror (the *a*–*c* plane) is vertical (second setting).
222, *mm*2 2/*m*2/*m*2/*m*	Orthorhombic	3 mutually perpendicular directions about which there is binary symmetry (2 or m)	The symbols refer to the symmetry elements in the order *a*, *b*, *c*; two-fold axes coincide with the crystallographic axes.
4, $\bar{4}$, 4/*m* 422, 4*mm* $\bar{4}$2*m*, 4/*m*2/*m*2/*m*	Tetragonal	1 four-fold axis	The four-fold axis refers to the *c* axis; the second symbol (if present) refers to the axial directions (a_1 and a_2); the third symbol (if present) to directions at 45° to a_1 and a_2.
6, $\bar{6}$, 6/*m* 622, 6*mm* $\bar{6}$*m*2, 6/*m*2/*m*2/*m*	Hexagonal*	1 six-fold axis 1 three-fold axis	The first number refers to the *c* axis; the second and third symbols (if present) refer respectively to symmetry elements parallel to and perpendicular to the crystallographic axes a_1, a_2, and a_3.
3, $\bar{3}$, 32, 3*m*, $\bar{3}$2/*m*			
23, 2/*m*$\bar{3}$, 432, $\bar{4}$3*m*, 4/*m*$\bar{3}$2/*m*	Isometric	4 three-fold axes each inclined at 54°44′ to the crystallographic axes (see Fig. 6.18)	The first number refers to the three crystallographic axes a_1, a_2, and a_3; the second number refers to 4 diagonal directions of three-fold symmetry (between corners of a cube); the third number or symbol (if present) refers to 6 directions between the edges of a cube.

*The accepted orientation of the symmetry elements in two crystal classes of the hexagonal system is not straightforward. These are $\bar{6}m2$ and $3m$. The location of the six- or three-fold axis is unambiguous. However, the location of the next symmetry element is not obvious. In $\bar{6}m2$, the third entry (two-fold rotation axes) coincides with the perpendiculars to a_1, a_2, and a_3; the *m*s are coincident with these same directions. In $3m$ the *m*s are located in directions perpendicular to a_1, a_2, and a_3.

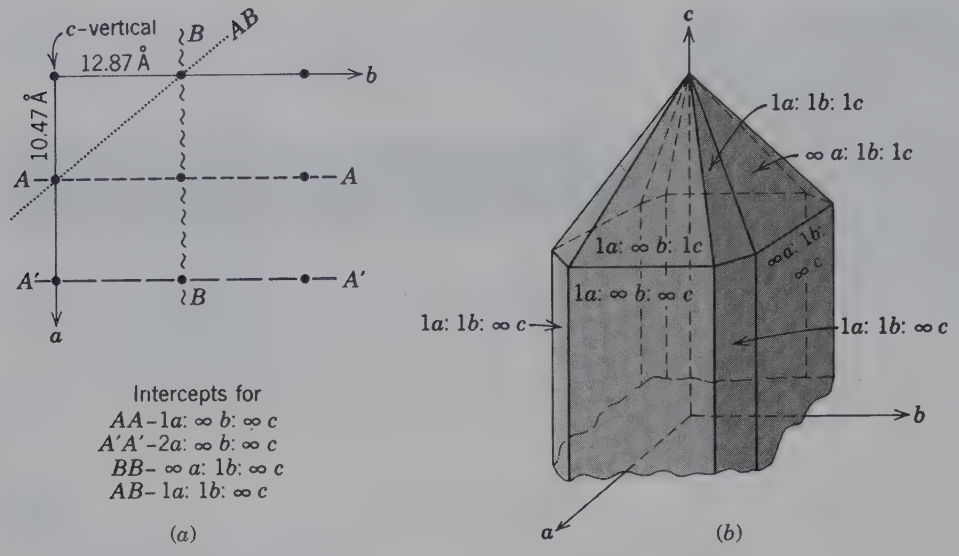

FIG. 6.27 (a) Intercepts for some planes (denoted by capital letters) in an orthorhombic lattice looking down the *c* axis. *a* and *b* represent crystallographic directions in the crystal and are equivalent to the *a* and *b* axes in the right figure. The upper left four dots outline a unit cell. (b) Intercepts for crystal faces on the upper half of an orthorhombic crystal. Some of these intercepts are shown in plan view in (a).

addition, one must determine at what *relative* distance the face intersects the different axes. Figure 6.27a illustrates an *a–b* plane (looking down *c*, as in plan view) for an orthorhombic crystal.

The lattice shown in Fig. 6.27a represents the repeat of a rectangular unit with an origin at the upper left corner. A lattice plane *AA* (short, dashed lines in Fig. 6.27a) is parallel to the *b* and *c* axes and intersects the *a* axis at one length from the origin (taken as unit length) along the *a* axis. To indicate that the face intersects an axis, the length at which the axis is intercepted is noted. To indicate that the face is parallel to an axis, and thus never intersects that axis, the symbol ∞ is used. The intercepts for the *AA* plane, therefore, become: 1∞, ∞*b*, ∞*c*. Similarly the plane *A'A'*, which is parallel to *AA* but intersects the *a* axis at two unit lengths (two nodes from the origin), would have intercepts: 2*a*, ∞*b*, ∞*c*. The plane *BB*, which is parallel to the *a* and *c* axes and intersects the *b* axis at unit distance, has intercepts: ∞*a*, 1*b*, ∞*c*. Plane *AB* intersects both horizontal axes (*a* and *b*) at unit distance but is parallel to *c*, which leads to the intercepts: 1*a*, 1*b*, ∞*c*. A plane that intersects all three axes at unit distances would have intercepts 1*a*, 1*b*, and 1*c*. Figure 6.27b shows various crystal faces on an orthorhombic crystal, some of which are parallel to the lattice planes shown in Fig. 6.27a. Recall that all crystallographic axes intersect one another in the center of the crystal. Therefore, to determine the relative length at which a face intersects an axis, the axis must begin in the crystal's center. Also, remember that face intercepts shown on the crystal faces (in Fig. 6.27b), are strictly *relative* values and do not indicate actual intersection lengths.

When intercepts are assigned to the faces of a crystal, without any knowledge of its unit cell dimensions, one face that cuts all three axes is arbitrarily assigned the units 1a, 1b, *and* 1c. This face, which is referred to as the **unit face**, is generally the largest, in case there are several faces that cut all three axes. Figure 6.28 shows an orthorhombic crystal that consists of faces, all of which cut all three crystallographic axes. The largest face (shaded) that intersects all three crystallographic axes at their positive ends is taken as the unit face. Its intercepts are 1*a*, 1*b*, and 1*c*, as shown. The intercepts of the smaller face above it can now be estimated by extending the edges of this face in the directions of the *a* and *b* axes noting the relative distances at which the axes are

FIG. 6.28 Relative intersections of faces on an orthorhombic crystal, all of which cut three crystallographic axes.

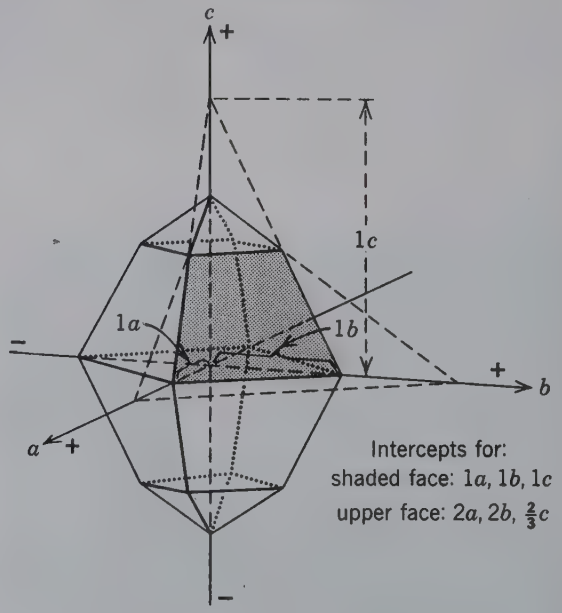

intersected relative to the unit face. This face intersects the *a* and *b* axis at twice the distance of the unit face but the *c* axis at 2/3 the distance. Therefore, the intercepts for the upper face become 2*a*, 2*b*, 2/3*c* with respect to the unit face. These intercepts can be divided by the common factor 2, resulting in 1*a*, 1*b*, 1/3*c*. This example illustrates that the units 1*a* and 1*b* do not represent actual distances at which the crystallographic axes are cut, but express only relative values. The intercepts of a face have no relation to its size, for *a face may be moved parallel to itself for any distance without changing the relative values of its intersections with the crystallographic axes.*

MILLER INDICES

Various methods of notation have been devised to express the intercepts of crystal faces upon the crystal axes. The most universally employed is the system of indices proposed by W. H. Miller which has many advantages over the system of face intercepts discussed previously.

The **Miller indices** of a face *consist of a series of whole numbers that have been derived from the intercepts by inverting and, if necessary, the subsequent clearing of fractions.*

The indices of a face are always given so that the three numbers (four in the hexagonal system) refer to the *a*, *b*, and *c* axes, respectively, and, therefore, the letters that indicate the different axes are omitted. Like the intercepts, the Miller indices express a ratio, but for the sake of brevity the ratio sign is also omitted.

With reference to Fig. 6.28, the two upper faces, which cut the positive segments of the crystallographic axes, have intercepts 1*a*, 1*b*, 1*c*, and 2*a*, 2*b*, 2/3*c*, respectively. Inverting these intercepts leads to 1/1 1/1 1/1 and 1/2 1/2 3/2, respectively. For the unit face, this reduces to a Miller index of (111). For the upper face, clearing the fractions by multiplying all by 2 leads to a Miller index of (113). The Miller index (111) is read as "one-one-one". Miller indices are placed in *parentheses* to distinguish them from similar symbols used to designate crystal forms, zones, and axial directions (see the text that follows). Commas are used in Miller indices only when two-digit numbers appear, as in (1, 14, 3).

Further examples of conversions of intercepts to Miller indices for an isometric lattice and crystal faces are given in Fig. 6.29. For faces that intersect negative ends of crystallographic axes, a bar is placed over the appropriate number, as shown in Fig. 6.30. For example, (1 $\bar{1}$ 1) reads "one, minus one, one" or "one, bar one, one." Note that when $\bar{1}$ ("bar one") is part of a Miller index representation, is *not* the same as a rotoinversion axis, which refers to a symmetry element. (An interactive animation on Miller index derivation is available in module II of the CD-ROM under the heading "Crystallography: Miller Indices.")

When the exact intercepts are unknown, it is sometimes convenient to use a *general symbol* (*hkl*) for the Miller indices. Here *h*, *k*, and *l* are, respectively, the reciprocals of rational but undefined intercepts along the *a*, *b*, and *c* axes. The symbol (*hkl*) would indicate that a face cuts all three crystallographic axes without implying relative units along the axes. If a face is parallel to one of the crystallographic axes, a 0 is used

FIG. 6.29 (a) A plan view showing intercepts and Miller indices for some planes in an isometric lattice. (b) Intercepts and Miller indices of some faces modifying the corner and edges of a cube.

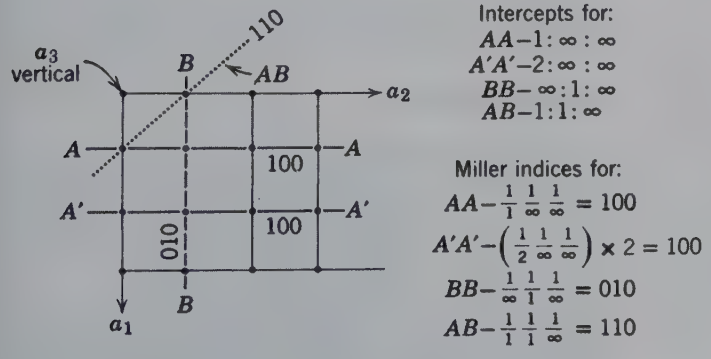

(a)

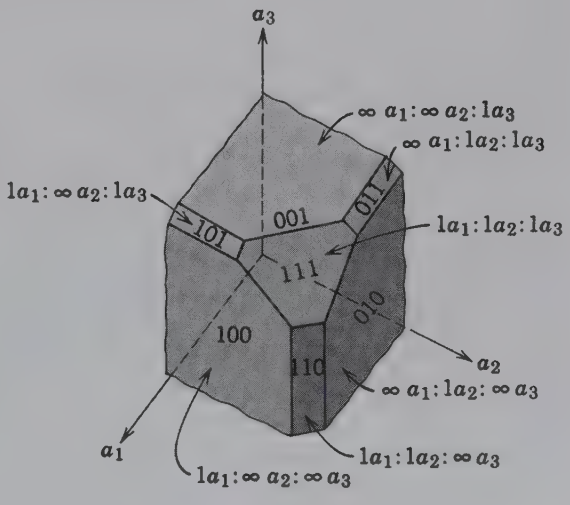

(b)

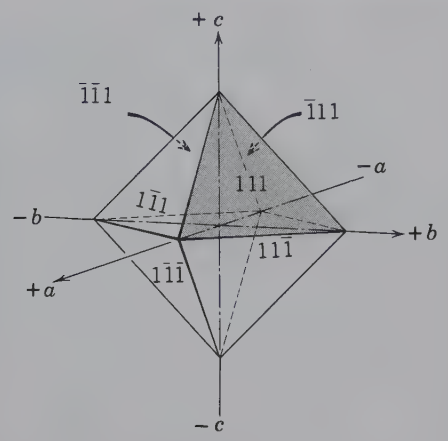

FIG. 6.30 Miller indices for faces with respect to positive and negative ends of crystallographic axes.

(because $1/\infty = 0$). And, if the face intersects the other two axes, the general symbols would be written as (0*kl*), (*h*0*l*), and (*hk*0). A face parallel to two of the axes may be considered to intersect the third at unity, and the indices would, therefore, be: (100), (010), or (001), as well as the negative equivalents such as $(\bar{1}00)$, $(0\bar{1}0)$, and $(00\bar{1})$.

Early in the study of crystals it was discovered that for a given face the indices could always be expressed by simple whole numbers or zero. This is known as the **law of rational indices.**

Crystals belonging to the hexagonal system are distinct from other systems because they possess one unique axis that is either six- or three-fold in symmetry. This unique axis is perpendicular to the plane which contains three identical axes, a_1, a_2, and a_3. Because of the presence of four crystallographic axes, instead of three as in the other crystal systems, a four-number system for indexing crystal faces was developed. This is known as the Bravais–Miller system of indexing. The indices are derived from the intercepts on the axes in the same way as the three-number Miller indices. Figure 6.31 illustrates the conversion of intercepts in the four-axis system to Bravais–Miller indices for three differently oriented crystal faces. The general symbol in this index system is ($h\ k\ \bar{i}\ l$) in which the first three letters refer to the a_1, a_2, and a_3 axes and the last letter to *c*. Recall that the positive ends of the *a* axes are separated by 120°, therefore, the negative end of a_3 bisects a_1 and a_2. In this notation $h + k + i = 0$ holds invariably. For example, with respect to the three faces indexed in Fig. 6.31:

$(1\ 0\ \bar{1}\ 0),\ 1 + 0 - 1 = 0$
$(1\ 1\ \bar{2}\ 0),\ 1 + 1 - 2 = 0$
$(1\ 1\ \bar{2}\ 1),\ 1 + 1 - 2 = 0$

ZONES

One of the conspicuous features on many crystals is the arrangement of a group of faces with parallel intersection edges. A **zone** is a collection of faces with parallel edges. A line through the center of the crystal that is parallel to the lines of face intersections is called the **zone axis**. In Fig. 6.32 the faces *m'*, *a*, *m*, and *b* are in one zone, and *b*, *r*, *c*, and *r'* are in another. The lines, designated [001] and [100], are the zone axes, respectively. This indicates that faces *m'*, *a*, *m*, *b* intersect in a line parallel to [001] and *b*, *r*, *c*, and *r'* parallel to [100].

A zone is indicated by a symbol similar to that for Miller indices of faces, but the zone symbols are enclosed in square brackets, such as the generalized expression [*uvw*], to distinguish them from face and form symbols (that is ( ) and { }, respectively). Any two nonparallel faces determine a zone. To determine the zone axis of two faces, (*hkl*) and (*pqr*), the method usually used is to write twice the symbol of one face and directly beneath, twice the symbol of the other face. The first and last digits of each line are disregarded and the remaining numbers, joined by sloping arrows, multiplied. In each set, the product of 2 is subtracted from the product of 1:

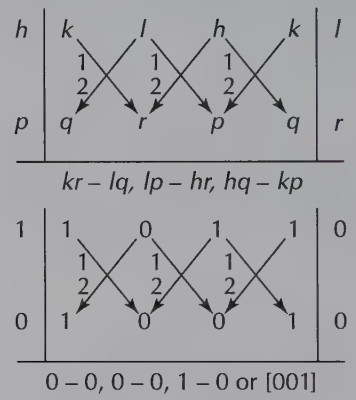

As a specific example assume *m*, Fig. 6.32 is (*hk*0) with index (110) and *b* is (010). The zone axis is thus [001], as shown in the figure, because all edges are parallel to *c*.

CRYSTAL FORM

The term **morphology** is commonly used to indicate the general outward appearance or shape of crystals. In crystallography, external shape is denoted by the word **habit** (refer to Chapter 2) whereas **form** is used in a special and restricted sense.

A **form** *consists of a group of like crystal faces, all of which have the same relation to the elements of symmetry.*

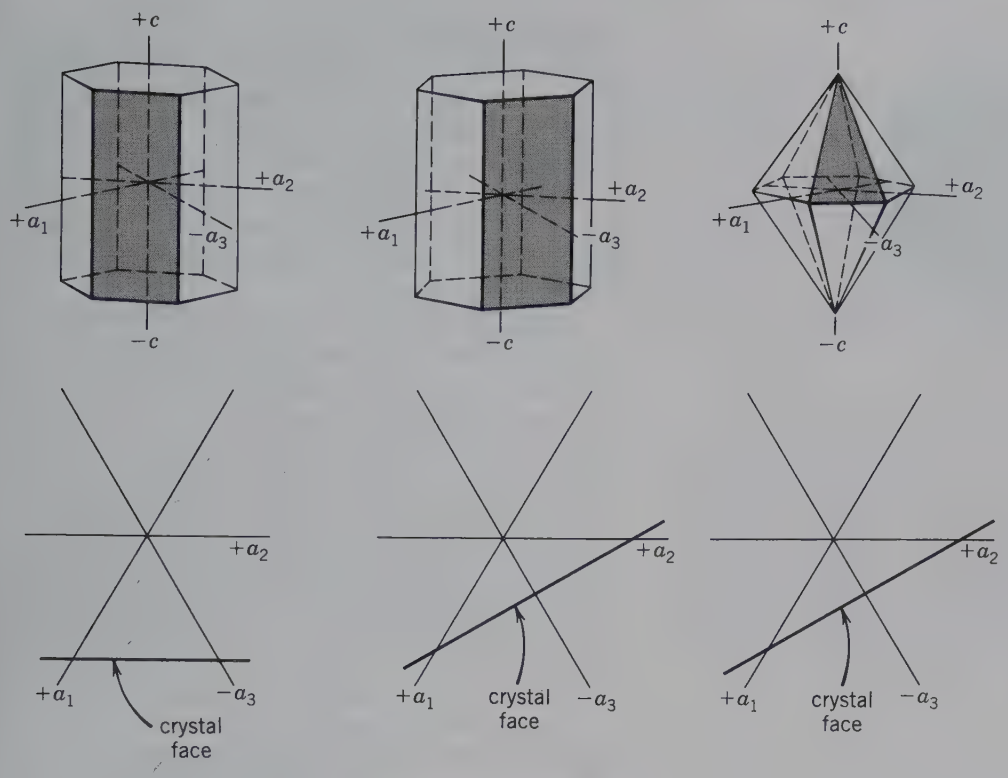

FIG. 6.31 Derivation of the four-digit Bravais–Miller index from the intercepts of three different crystal faces in the hexagonal system.

FIG. 6.32 Crystal zones and zone axes indicated by Miller indices in square brackets. Intersections of faces *m'*, *a*, *m*, and *b* belong to the [001] zone and those of faces *r'*, *c*, *r*, and *b* belong to the [100] zone.

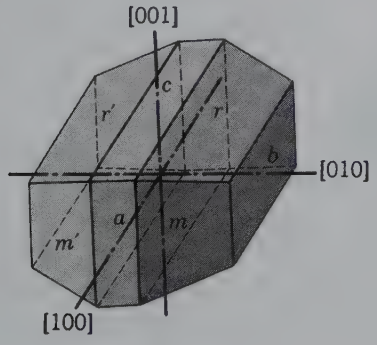

They display the same chemical and physical properties because all are underlain by like atoms in the same geometrical arrangement (see Fig. 6.22). On crystal drawings, each face that belongs to the same form is labeled with the same letter (Fig. 6.33).

The relationship between form and the symmetry content of a crystal is important to understand. By selecting one individual face in a form and performing all of the symmetry operations of the crystal class, one can generate the remaining faces in that form. For example, the full form development for the unit face (111), on the basis of the symmetry content of two crystal classes, $\bar{1}$ (in the triclinic system) and $4/m\,\bar{3}\,2/m$ (in the isometric system), is shown in Fig. 6.34. In the case of

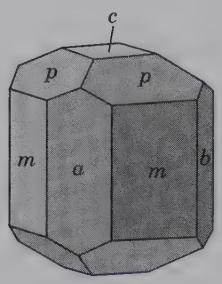

FIG. 6.33 Conventional lettering of forms on crystal drawings. Faces that belong to the same form are given the same letter.

the $\bar{1}$ symmetry (which is equivalent to a center of symmetry), one additional face is generated by inverting the original face (111) through the origin of the three crystallographic axes. This additional face will have indices $(\bar{1}\bar{1}\bar{1})$. This form consists of two parallel faces only, and is known as a **pinacoid**. For the (111) face in the isometric system, symmetry elements for $4/m\ \bar{3}\ 2/m$ will generate seven additional faces equivalent to $(1\bar{1}1)$ with indices $(\bar{1}11)$ $(1\bar{1}\bar{1})$ $(11\bar{1})$ $(\bar{1}\bar{1}1)$ $(\bar{1}1\bar{1})$ $(\bar{1}\bar{1}\bar{1})$ and $(\bar{1}11)$. Each face cuts all three crystallographic axes at equal lengths and, therefore, has the same relationship to the symmetry elements. This form is known as an **octahedron**. Therefore, *the number of faces that belong to a form is a function of the symmetry content of the crystal class (or point group)*. The distribution of forms in the 32 point groups is given in Tables A3.1 to A3.4 in Appendix 3.

Although faces of a form may be of different sizes and shapes because of distortion of the crystal (see Fig. 2.2), their similarity is frequently evidenced by natural striations, etchings, or growths, as shown in Fig. 6.35. A cube of pyrite has the form of a cube but on closer examination one sees that the six flat faces have striations in different directions and are related by three-fold rotation. On some crystals, the differences between faces of different forms can be seen only after etching with acid. In Figs. 6.35a and b, the crystals have three forms, each of which has a different physical appearance from

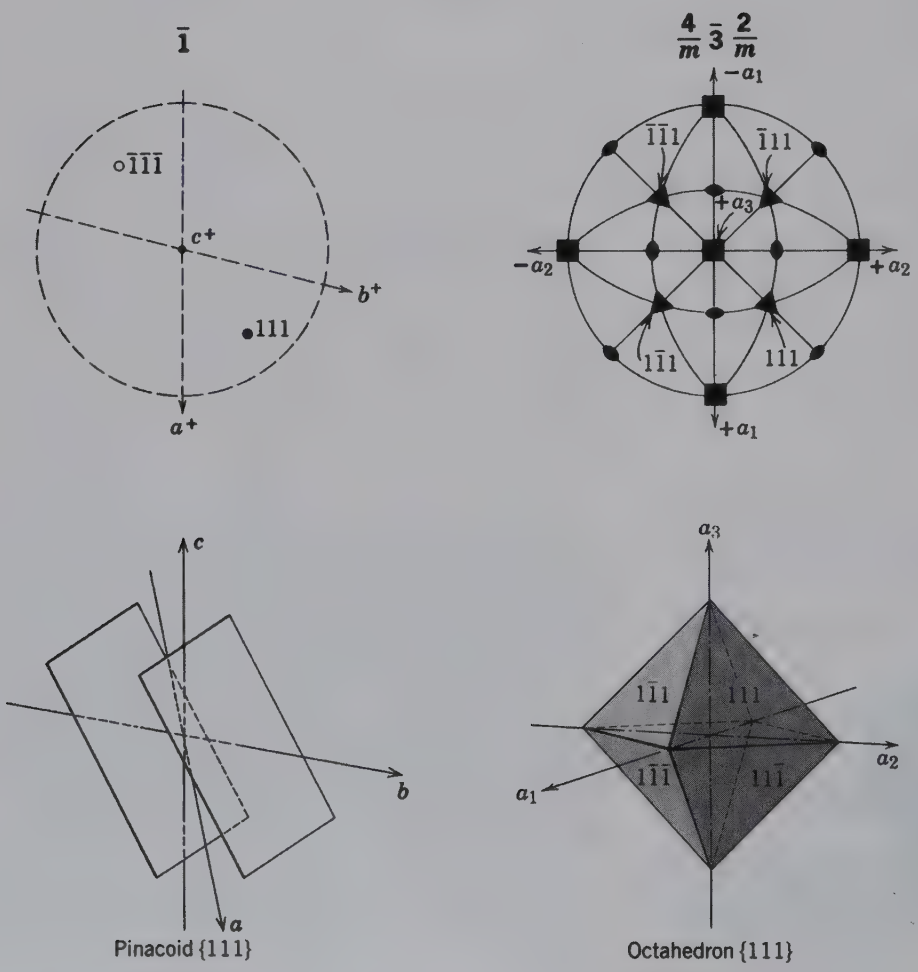

FIG. 6.34 Development of a form from one face with Miller index (111) in the $\bar{1}$ and the $4/m\ \bar{3}\ 2/m$ crystal classes. In the case of $\bar{1}$ symmetry only a two-faced form, a pinacoid, develops. For the $4/m\bar{3}2/m$ crystal class, seven more faces develop to make an octahedron. In the upper right illustration, the pole to the (111) face coincides with the position of the three-fold rotoinversion axis. Faces at the top of the crystal are generally shown by dots, those at the bottom by open circles. On the octahedron, only the positions of the four front faces are shown by Miller indices; there exists a similar set of four faces at the back.

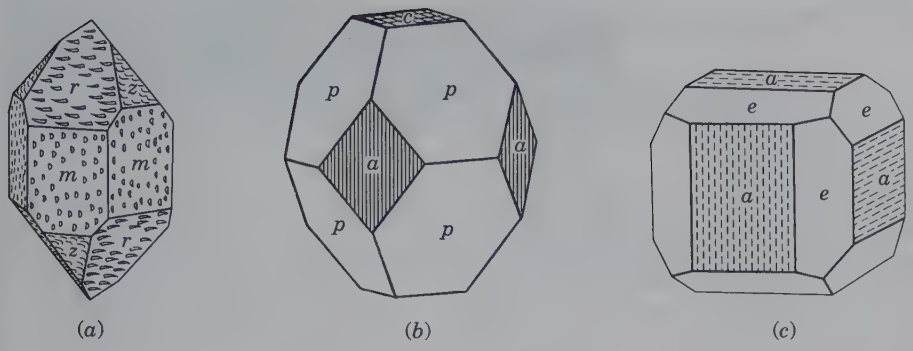

FIG. 6.35 Different forms are commonly manifested by different appearances such as striations. (a) Quartz—hexagonal. (b) Apophyllite—tetragonal. (c) Pyrite—isometric.

the others and is marked with a letter; and in Fig. 6.35c, there are two forms.

Miller indices also may be used as *form* symbols and are then enclosed in braces as {*hkl*}, or, for example {010}. Thus, in Fig. 6.34, (111) refers to a specific face, whereas {111} embraces all faces of that form. In choosing a form symbol, it is desirable to select, if possible, the face symbol with positive digits: {111} rather than $\{1\bar{1}1\}$. *In each crystal class there is a form, the faces of which intersect all of the crystallographic axes at different lengths*; this is the **general form**, {*hkl*}. All other forms that may be present are **special forms**. In the orthorhombic, monoclinic, and triclinic crystal systems, {111} is a general form because the unit lengths along each of the crystallographic axes are different ($a \neq b \neq c$). In crystal systems of higher symmetry in which the unit distances along two or more of the crystallographic axes are the same, a general form must intersect the like axes at different multiples of the unit length. Thus, {121} is a general form in the tetragonal system (because $a_1 = a_2 \neq c$) but a special form in the isometric system, and {123} is the general form in the isometric system (because $a_1 = a_2 = a_3$). The concept of a general form can also be related to the symmetry elements of a specific crystal class. *An* (hkl) *face will not be parallel or perpendicular to a symmetry axis or plane, regardless of the crystal class.* A special form, however, consists of faces that are parallel or perpendicular to the symmetry elements in the crystal class. For most crystal classes, the general form consists of a larger number of faces than any of the special forms of that same class (see also Tables A3.1 to A3.4 in Appendix 3).

In Fig. 6.34, a two-faced form and an eight-faced form were developed. The two-faced form {111} for crystal class $\bar{1}$ is referred to as an *open form* because it consists of two parallel faces that do not enclose space (see also Fig. 6.36). The eight-faced form {111} in crystal class $4/m\bar{3}2/m$ is a *closed form*, because the eight faces together enclose space (see Figs. 6.30 and 6.34).

A crystal may consist of only one form, if the form is closed. However, because any combination of forms must enclose space, a minimum of two open forms is necessary. The two may exist together or be in combination with other closed or open forms. The various combinations of compatible forms are given in Tables A3.1 to A3.4 in Appendix 3.

NAMES OF FORMS

A scheme of form nomenclature, originally proposed by Groth in 1895 and modified by A. F. Rogers in 1935, is used in this text. This scheme recognizes 48 kinds of crystal forms on the basis of the angular relations of the crystal faces. Of these 48 forms, 32 are the general forms in the 32 crystal classes (or point groups); 10 are special, closed forms of the isometric system; and 6 are special open forms (prisms) of the hexagonal and tetragonal systems. In this scheme of nomenclature, the name of each of the 32 general forms, {*hkl*} (or $\{h\bar{k}il\}$ in the hexagonal system), becomes the descriptive name of each of the 32 crystal classes. For example, in $\bar{1}$ the general form {*hkl*} is a two-faced form known as a *pinacoid*, and the descriptive name for $\bar{1}$ is *pinacoidal class*. Similarly, the name of the general form {*hkl*} in $4/m2/m2/m$ (of the tetragonal system) is *ditetragonal-dipyramid* ; accordingly, the class $4/m\ 2/m\ 2/m$ is commonly referred to as the *ditetragonal-dipyramidal class*. Further discussion of crystal classes and their forms are found in Chapter 9.

Another similar system of form nomenclature has been developed by crystallographers of the Fedorov Institute in Moscow, Russia. However, for reasons of simplicity the Groth–Rogers scheme is used in this text. Although form names are often useful, such names are not absolutely necessary because a form is uniquely defined by a combination of its Miller indices and the Hermann–Mauguin notation of its point group symmetry.

ILLUSTRATION AND DESCRIPTION OF FORMS

The forms listed in Tables 6.6 and 6.7 are illustrated in Fig. 6.36. In the case of prisms, pyramids, and dipyramids (numbers 5 through 25 in Fig. 6.36), the three-dimensional representations cannot properly convey the shapes of the cross-sections. For this reason, the various prisms numbered 5 through 11 are accompanied by a cross-section perpendicular to the long axis of the prism; the shapes of other cross-sections represent sections perpendicular to the long axes of the pyramids (numbers 12 through 18) and dipyramids (numbers 19 through 25). The total symmetry content of each of these forms is discussed in detail in Chapter 9 under the heading "Nineteen of the Thirty-Two Point Groups." A brief description of the 48 forms follows with the number referring to Fig. 6.36. For the distribution of these forms as a function of the 32 crystal classes, refer to Tables A3.1 to A3.4 in Appendix 3.

Table 6.6 The Names of the 33 Different Types of Nonisometric Crystal Forms*

Name According to System of Groth–Rogers	No. of Faces
1. Pedion	1
2. Pinacoid	2
3. Dome	2
4. Sphenoid	2
5. Rhombic prism	4
6. Trigonal prism	3
7. Ditrigonal prism	6
8. Tetragonal prism	4
9. Ditetragonal prism	8
10. Hexagonal prism	6
11. Dihexagonal prism	12
12. Rhombic pyramid	4
13. Trigonal pyramid	3
14. Ditrigonal pyramid	6
15. Tetragonal pyramid	4
16. Ditetragonal pyramid	8
17. Hexagonal pyramid	6
18. Dihexagonal pyramid	12
19. Rhombic dipyramid	8
20. Trigonal dipyramid	6
21. Ditrigonal dipyramid	12
22. Tetragonal dipyramid	8
23. Ditetragonal dipyramid	16
24. Hexagonal dipyramid	12
25. Dihexagonal dipyramid	24
26. Trigonal trapezohedron	6
27. Tetragonal trapezohedron	8
28. Hexagonal trapezohedron	12
29. Tetragonal scalenohedron	8
30. Hexagonal scalenohedron	12
31. Rhombohedron	6
32. Rhombic disphenoid	4
33. Tetragonal disphenoid	4
Total no. of forms = 33	

*The number of faces of each form is given. The numbers on the left refer to Fig. 6.36.

Table 6.7 The Names of the 15 Different Types of Forms in the Isometric System*

Name According to System of Groth–Rogers	No. of Faces
34. Cube	6
35. Octahedron	8
36. Dodecahedron (rhombic)	12
37. Tetrahexahedron	24
38. Trapezohedron	24
39. Trisoctahedron	24
40. Hexoctahedron	48
41. Tetrahedron	4
42. Tristetrahedron	12
43. Deltoid dodecahedron	12
44. Hextetrahedron	24
45. Gyroid	24
46. Pyritohedron	12
47. Diploid	24
48. Tetartoid	12

*The number of faces of each form is given. The numbers on the left refer to Fig. 6.36.

Pedion. A single face comprising a form (1).

Pinacoid. An open form made up of two parallel faces (2).

Dome. An open form consisting of two nonparallel faces symmetrical with respect to a mirror plane (*m*) (3).

Sphenoid. Two nonparallel faces symmetrical with respect to a two-fold rotation axis (4).

Prism. An open form composed of 3, 4, 6, 8, or 12 faces, all of which are parallel to the same axis. Except for certain prisms in the monoclinic system, the axis is one of the crystallographic axes (5–11).

Pyramid. An open form composed of 3, 4, 6, 8, or 12 nonparallel faces that meet at a point (12–18).

Dipyramid. A closed form having 6, 8, 12, 16, or 24 faces (19–25). A dipyramid can be considered as formed from two pyramids by reflection of one of them into the other across a horizontal mirror plane. Faces meet at two points.

Trapezohedron. A closed form that has 6, 8, or 12 faces in all, with 3, 4, or 6 upper faces offset from 3, 4, or 6 lower faces (26–28). These forms are the result of a three-, four-, or six-fold axis combined with perpendicular two-fold axes. In addition, there is an isometric *trapezohedron* (38), a 24-faced form. In a well-developed single trapezohedron, each face is a trapezium.

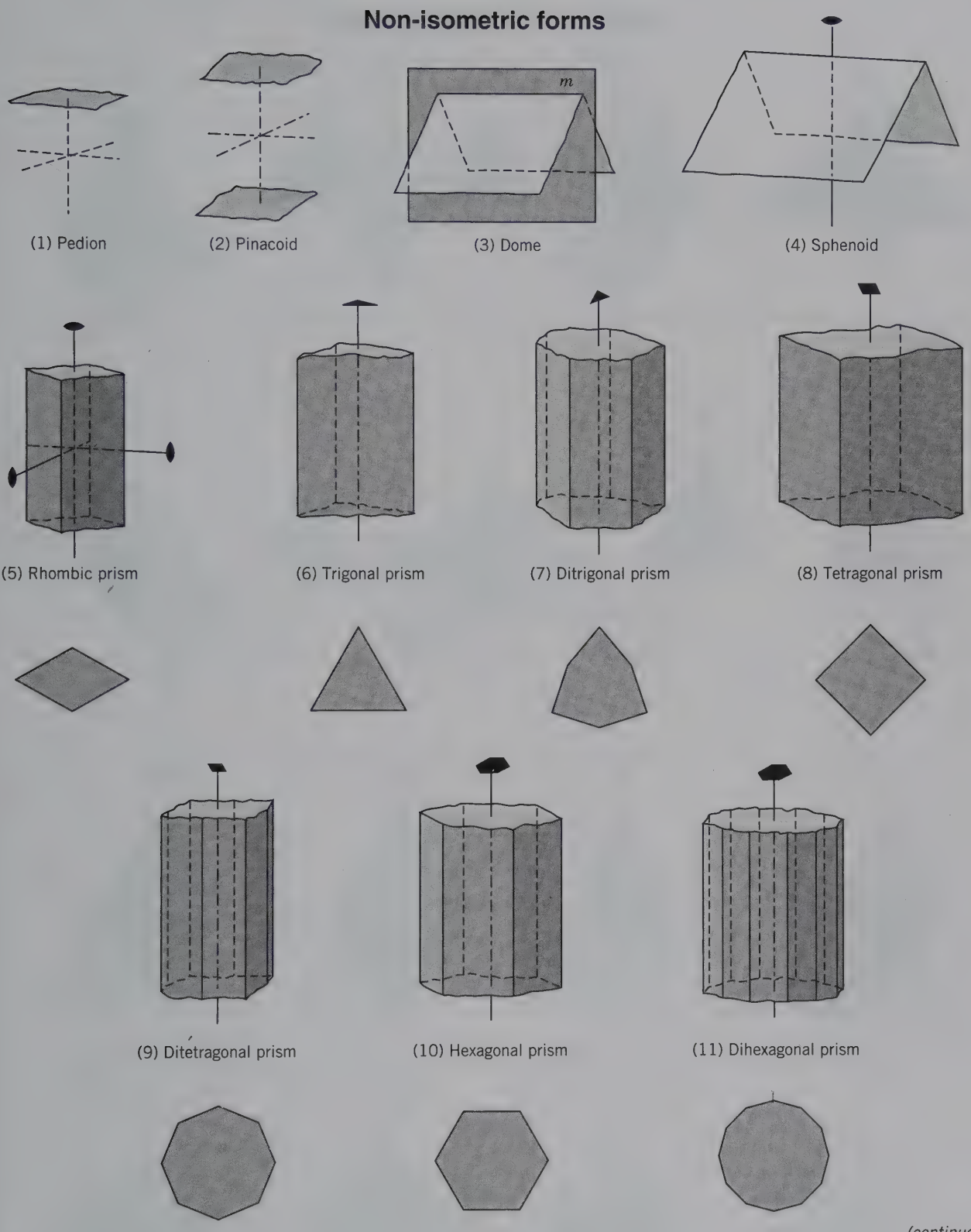

(continued)

FIG. 6.36 The 48 different crystal forms and some of their symmetry elements.

Non-isometric forms (cont'd)

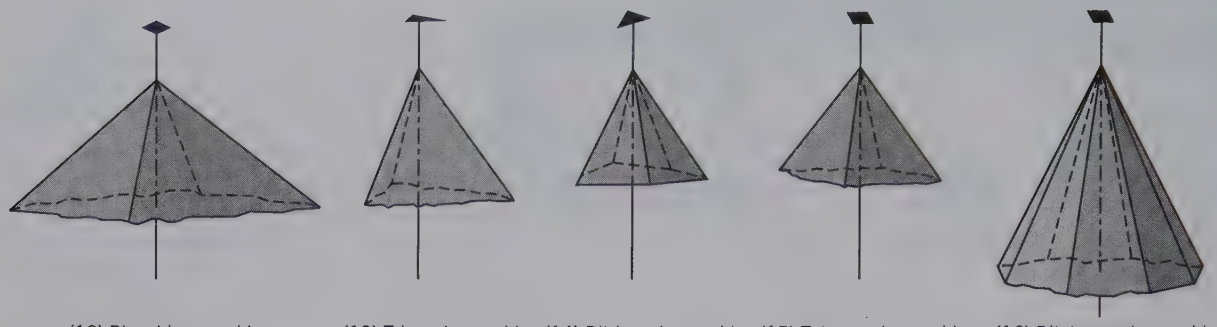

(12) Rhombic pyramid (13) Trigonal pyramid (14) Ditrigonal pyramid (15) Tetragonal pyramid (16) Ditetragonal pyramid

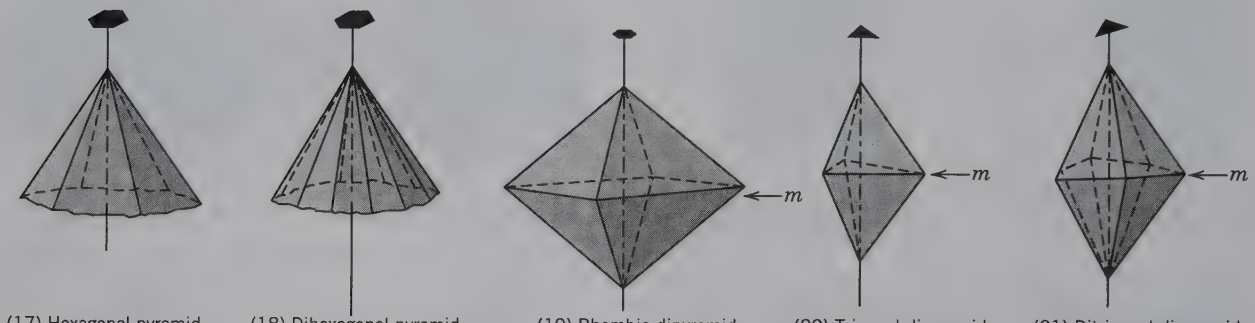

(17) Hexagonal pyramid (18) Dihexagonal pyramid (19) Rhombic dipyramid (20) Trigonal dipyramid (21) Ditrigonal dipyramid

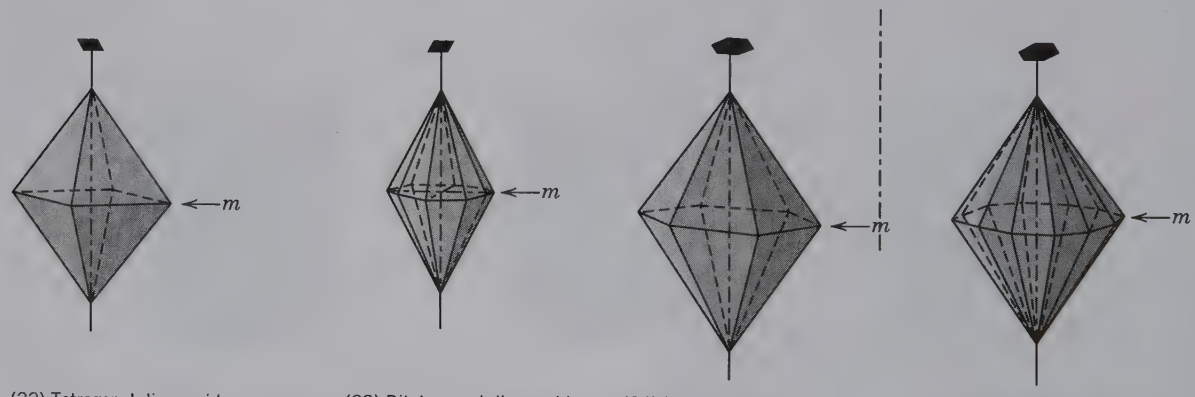

(22) Tetragonal dipyramid (23) Ditetragonal dipyramid (24) Hexagonal dipyramid (25) Dihexagonal dipyramid

(Fig. 6.36 continued)

Non-isometric forms (cont'd)

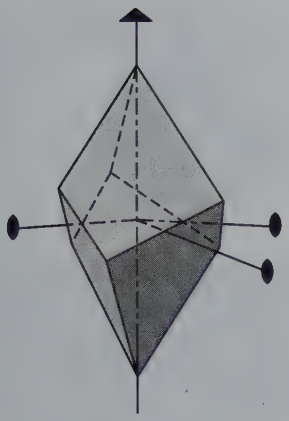

(26) Trigonal trapezohedron

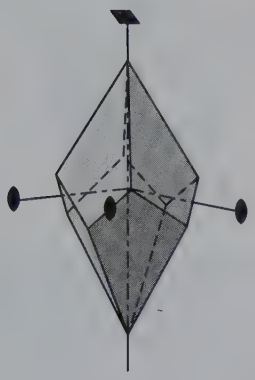

(27) Tetragonal trapezohedron

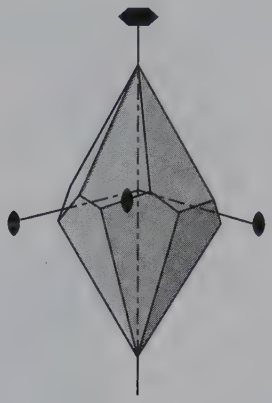

(28) Hexagonal trapezohedron

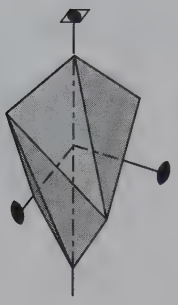

(29) Tetragonal scalenohedron

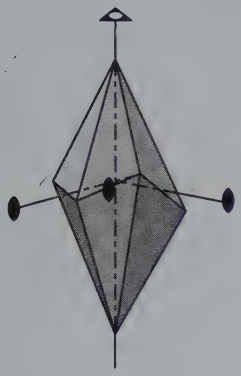

(30) Hexagonal scalenohedron

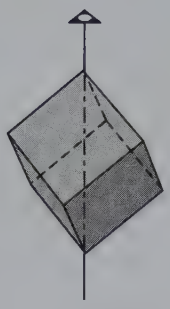

(31)Rhombohedron

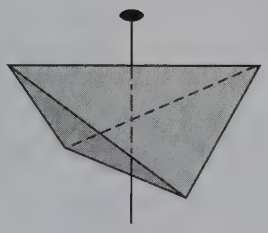

(32)Rhombic disphenoid

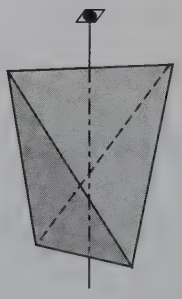

(33) Tetragonal disphenoid

Isometric forms

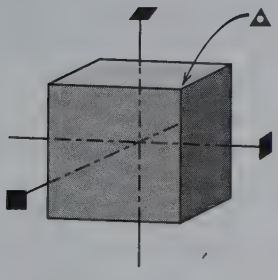

(34) Cube (hexahedron)

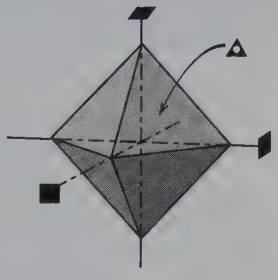

(35) Octahedron

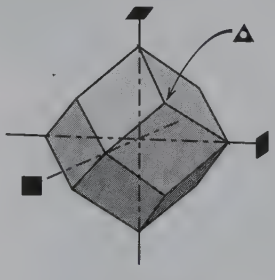

(36) Dodecahedron

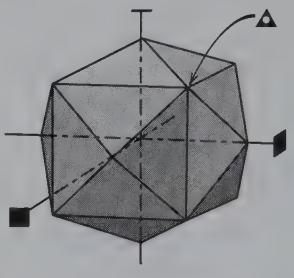

(37) Tetrahexahedron

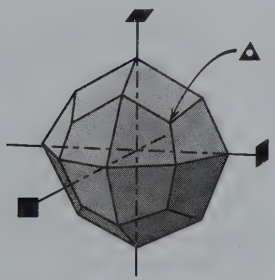

(38) Trapezohedron

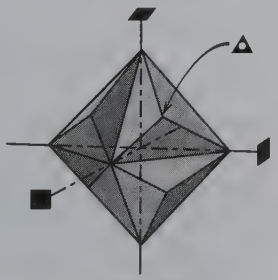

(39) Trisoctahedron

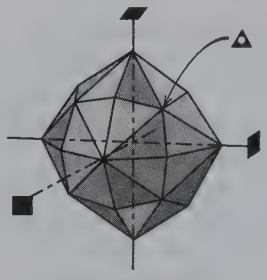

(40) Hexoctahedron

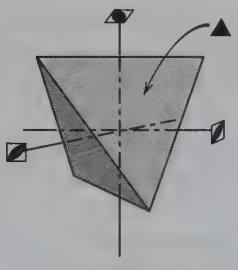

(41) Tetrahedron

(Fig. 6.36 continued)

Non-isometric forms (cont'd)

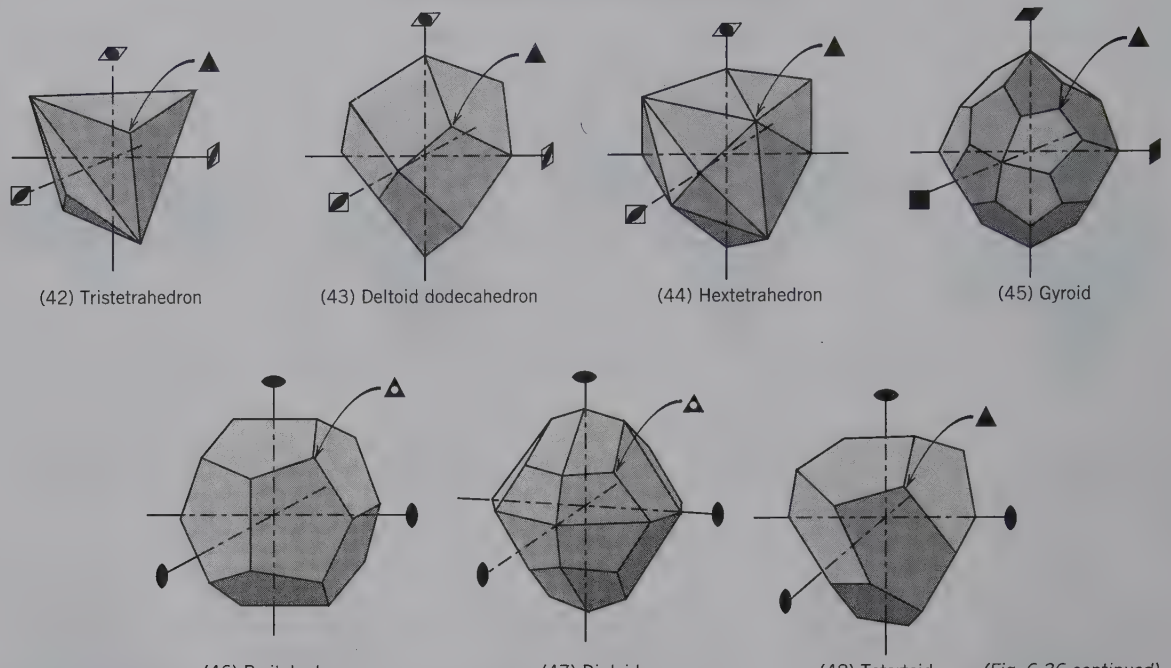

(42) Tristetrahedron (43) Deltoid dodecahedron (44) Hextetrahedron (45) Gyroid

(46) Pyritohedron (47) Diploid (48) Tetartoid *(Fig. 6.36 continued)*

Scalenohedron. A closed form with 8 or 12 faces (29 and 30), grouped in symmetrical pairs. In the *tetragonal scalenohedron*, pairs of upper faces are related by an axis of four-fold rotoinversion to pairs of lower faces. The 12 faces of the *hexagonal scalenohedron* display three pairs of upper faces and three pairs of lower faces in alternating positions. The pairs are related by a center of symmetry, which is part of a three-fold rotoinversion, $\bar{3}$. In an ideally developed scalenohedron, each face is a scalene triangle.

Rhombohedron. A closed form composed of six faces of which three faces at the top alternate with three faces at the bottom, the two sets of faces being offset by 60° (31). Rhombohedrons are found only in point groups $\bar{3}2/m$, 32, and $\bar{3}$.

Disphenoid. A closed form consisting of two upper faces that alternate with two lower faces, offset by 90° (32 and 33).

The specialized forms in the isometric system are numbered 34 through 48. Every one of these forms contains 4 three-fold rotation axes or rotoinversion axes. One such direction (in the upper right, positive quadrant) is indicated in the illustrations.

As noted before, the faces of a form are identified by the same letter in crystal drawings. The choice of which letter shall be assigned to a given form rests largely with the person who first describes the crystal. However, there are certain simple forms that, by convention, usually receive the same letter. Thus, the three pinacoids that cut the *a*, *b*, *c* axes are lettered respectively *a*, *b*, and *c*, the letter *m* is usually given to {110} and *p* to {111} (see Fig. 6.33). This lettering scheme is used throughout the remainder of this text.

REFERENCES AND FURTHER READING

Bernal, I., W. C. Hamilton, and J. Ricci. 1972. *Symmetry: A stereoscopic guide for chemists.* W. H. Freeman & Company, San Francisco.

Bloss, F. D. 1994. *Crystallography and crystal chemistry: An introduction.* Reprint of the original text of 1971 by the Mineralogical Society of America, Washington, D.C.

Boldyrev, A. K. 1936. Are there 47 or 48 simple forms possible in crystals? *American Mineralogist* 21: 731–34.

Bragg, W. L., and G. F. Claringbull. 1965. *Crystal structures of minerals.* Cornell University Press, Ithaca, New York.

Buerger, M. J. 1978. *Elementary crystallography: An Introduction to the fundamental geometric features of crystals.* Rev. ed. MIT Press, Cambridge, Massachusetts.

———, 1971. *Introduction to crystal geometry.* McGraw Hill, New York.

Cotteril, R. 1985. *The Cambridge guide to the material world.* Cambridge University Press, New York.

Goldschmidt, V. 1913–23. *Atlas der Kristallformen* (9 volumes and 9 atlases). Universitätsbuchhandlung, Heidelberg.

Hargittai, I., and M. Hargittai, 1994. *Symmetry: A unifying concept.* Shelter Publications, Bolinas, California.

Klein, C. 2008. *Minerals and rocks: Exercises in crystal and mineral chemistry, crystallography, x-ray powder diffraction, mineral and rock identification, and ore mineralogy.* 3rd ed. Wiley, New York.

Phillips, F. C. 1971. *An introduction to crystallography.* Wiley, New York.

CHAPTER 7

Internal Order and Symmetry in Minerals

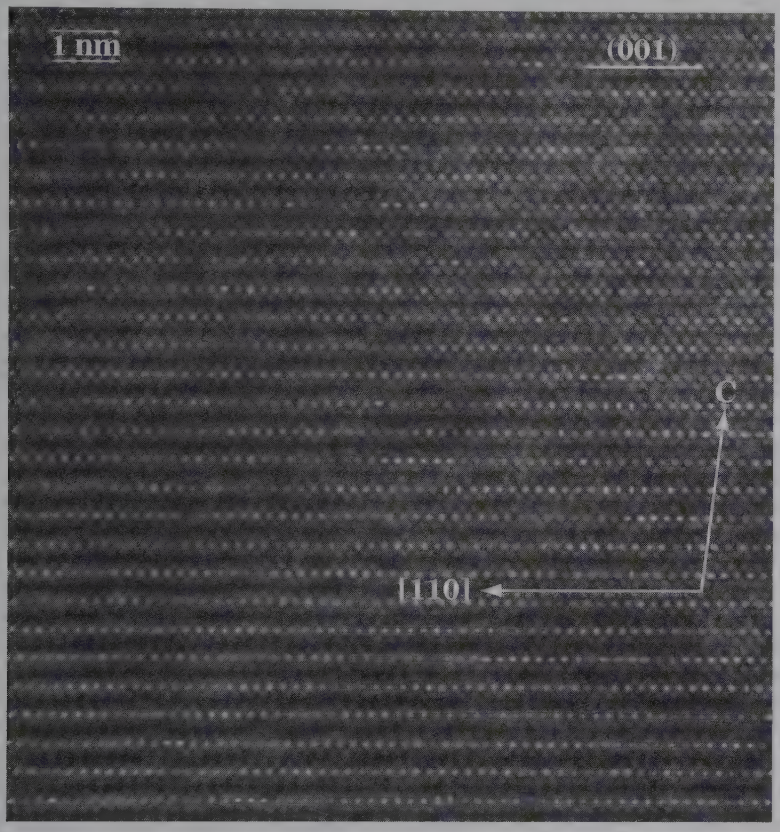

Perfect regularity in spacing (also known as periodicity) on the atomic level in a monoclinic layer silicate, biotite, as revealed in a high-resolution transmission electron microscopy (HRTEM) image. This is known as a 1M polytype. The spacing between the layers that appear as horizontal lines with white dots, is 1 nm (= 10 Å) as shown. These layers are parallel to (001). The c axis and the crystallographic zonal direction [110] are superimposed (Courtesy of Huifang Xu, University of Wisconsin, Madison.)

The morphology of a single crystal of almost any mineral commonly displays many crystal faces. Recreating an image of the external shape of such a well-formed crystal is achieved by the interaction of all of the symmetry operations (of the point group) with a face in each of its forms. Once accomplished, the complete crystal morphology is replicated. However, to fully evaluate a crystal structure at the atomic level, an additional operation is needed, that of translation. This chapter describes the operation of translation, the new symmetry elements produced by the addition of translation, the development of ordered patterns, and the motifs that comprise ordered crystal structures at the atomic level. These atomic scale features are observable only through very high powered electron microscopes and are invisible to the naked eye.

The internal structure of minerals contains many more symmetry elements than one can evaluate externally. This is the result of internal translations. One characteristic of a mineral is that it is a homogeneous solid possessing long-range, *three-dimensional internal order* (Chapter 1). Order, the opposite of randomness (also referred to as disorder, or even more specifically as total disorder), results from the repetition of motifs (chemical units in the case of minerals) in an infinite ordered array. Crystalline materials are based on patterns that represent a lower energy state than random patterns, and the lower energy state is the most stable state. Intuitively, a brick wall constructed with carefully positioned bricks in an ordered arrangement provides a more stable, and less energetic, configuration than a brick wall made with a less-ordered arrangement of identical bricks (Fig. 7.1a). The brick, in these walls, can be considered as the basic building block

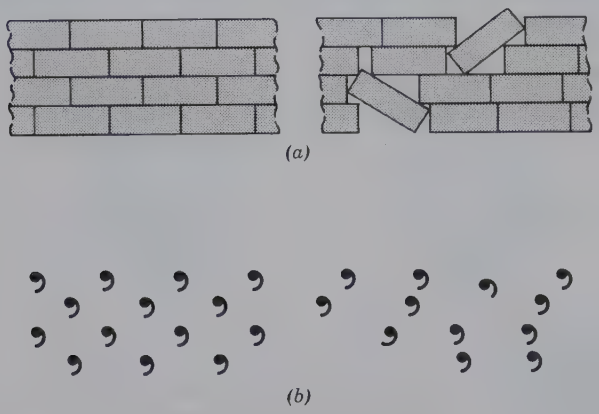

FIG. 7.1 (a) Two-dimensional ordered and more random (less-ordered) arrangement of bricks in a wall. (b) The brick patterns are represented by commas as motifs.

and, consequently, as the motif. If one simplifies this motif by replacing the center of each brick with a comma, the comma now represents the motif, as in Fig. 7.1b. This example shows how an ordered pattern is generated by a motif repeated in a regular sequence of new locations. This repetition is the result of regular translation. For example, many wallpaper designs are based on a two-dimensional pattern in which the motif (e.g., sprays of flowers, dots) is arranged in a regular geometrical array. Similarly, ordered patterns result from the regular repetition of a unit cell in a mineral.

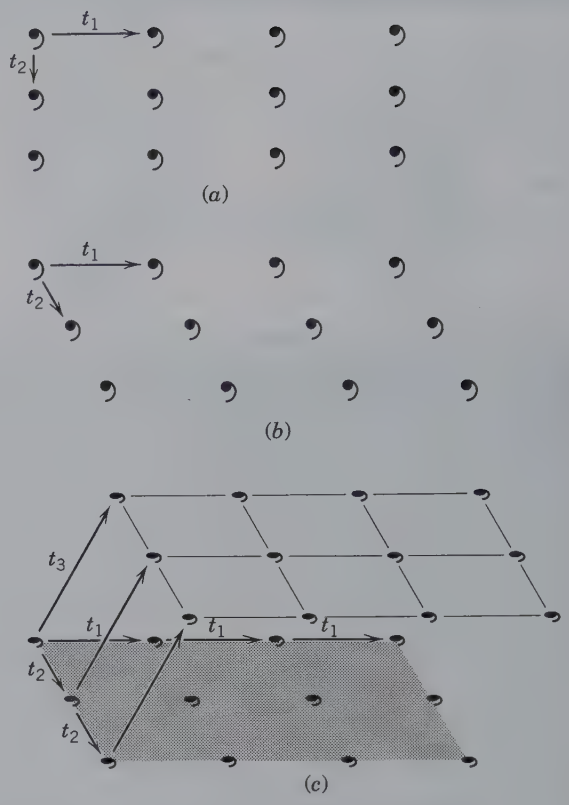

FIG. 7.2 (a) A two-dimensional pattern with translation components t_1 and t_2 at 90° to each other. (b) A two-dimensional pattern with translation components t_1 and t_2 at < 90° to each other. (c) A three-dimensional pattern with translation components t_1, t_2, and t_3. None of the translation components are at 90° to each other.

TRANSLATION DIRECTIONS AND DISTANCES

An ordered pattern can be generated by taking a motif (such as a comma) and repeating it or translating it a specific distance, t_1. This results in a linear row shown, for example, at the top in Fig. 7.2a. A two-dimensional array is created by translating such a row a specific distance, t_2, also in Fig. 7.2a. The order in this array can be expressed in terms of two translations (t_1 and t_2), with an angle of 90° between the translation directions. A different pattern of motifs results (Fig. 7.2b) when t_1 is the same as in Fig. 7.2a but the t_2 translation is at an angle < 90° to the t_1 translation. Both illustrations can be thought of as infinite strings of units along the t_1 direction that have been repeated by parallel and identical infinite strings along another translation direction, t_2. The translations, as marked by t_1 and t_2, are vectors (they have both direction and magnitude.)

A three-dimensional ordered pattern is obtained by adding yet another translation component, t_3, that does not lie in the plane of t_1 and t_2 (Fig. 7.2c). This results in a pattern of motifs that is infinite in three dimensions, as in a crystal structure. A three-dimensional crystal structure can be regarded as containing three-dimensional, noncoincident translations that repeat motif units (such as chemical units) in the atomic arrangement inside the crystal. These translations are extremely small, on the order of 1 to 10 angstroms (Å, where Å = 0.1 nm or 10^{-10} m), reflecting the size range of ionic radii in minerals (see Table 3.8). In crystals, such a pattern is not truly infinite, although it is generally considered so because of the large number of repeats. One centimeter in a crystal would contain approximately 100 million translations; that can be considered infinite.

The only way in which such extremely small distances (repeats) can be imaged is by high-powered electron microscopes (as shown in the image that opens this chapter and also Fig. 7.18). Consequently, it is very important to realize that *the external form of a crystal, although an expression of its internal structure, lacks any expression of translation.* The symmetry elements, observable in the external form of crystals, are, therefore, translation-free (as discussed in Chapter 6.)

In the evaluation of the geometry of the repeated motifs in a structure, it is often convenient to ignore the actual *shape* of the motif units in the pattern. If the motifs (commas in Fig. 7.2) are replaced by points (also called nodes), a regular pattern of points results that is referred to as a **lattice**.

A **lattice** is an imaginary pattern of points (or nodes) in which every point (node) has an environment that is identical to that of any other point (node) in the pattern.

A lattice has no specific origin, as it can be shifted parallel to itself. Beginning with one-dimensional rows, lattices will now be developed systematically. (Animations of these concepts are found in module III on the CD-ROM under the heading "Crystallography—Internal Order and Structure.")

ONE-DIMENSIONAL ORDER—ROWS

The simplest array of motifs, which might represent chemical clusters in a structure, is a sequence of equally-spaced motifs (or points) along a line (Fig. 7.3). This *row* represents order in one dimension. In a row, the magnitude of the *unit translation* (in this case, b, the repeat distance) determines the spacing between motifs. The motif, the unit of pattern representing a chemical unit at each lattice point, determines the ultimate pattern. Examples of objects with different motifs and different repeat distances, b, along a direction defined as y, are illustrated in Fig. 7.3. Such rows are common as borders along illustrations, in wallpaper, along friezes, but are not common in the structures of most crystalline materials. (Interactive animations of one-dimensional order are given in module III of the CD-ROM under the heading "1-Dimensional Order.")

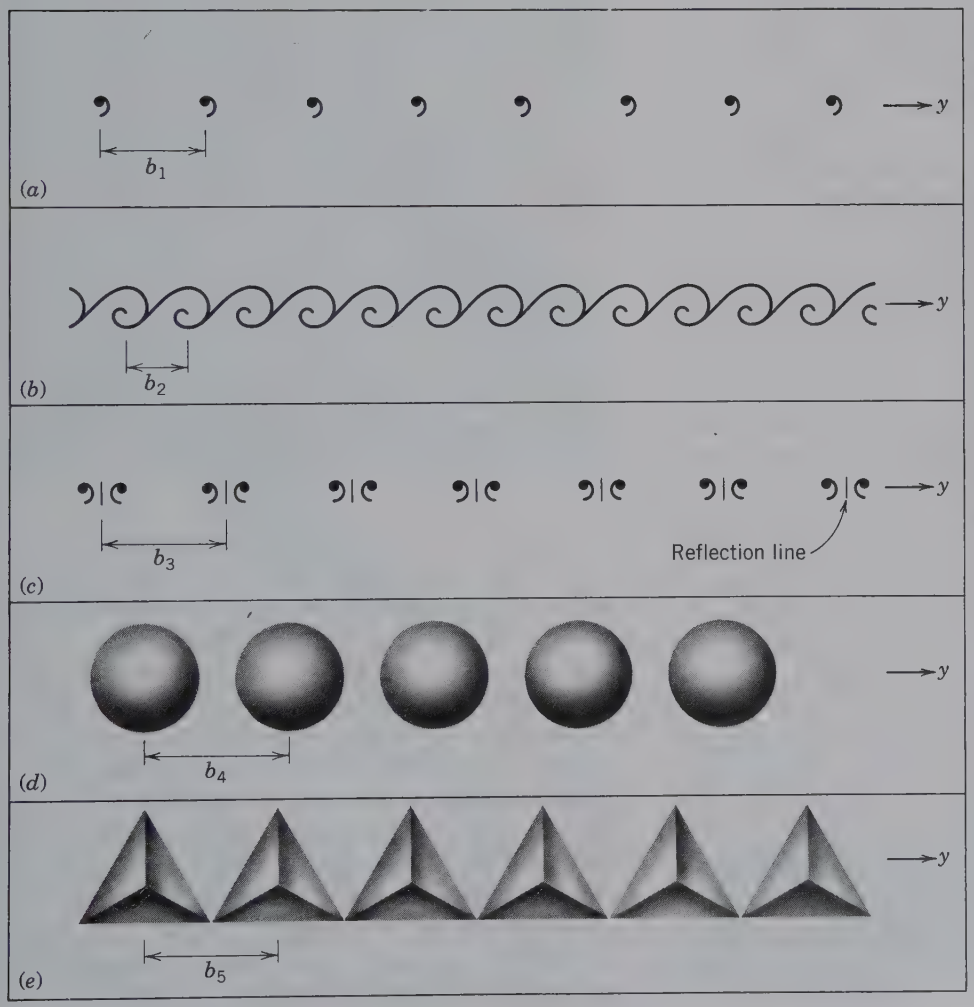

FIG. 7.3 Rows of objects (motifs) at various spacings, b, along translation direction, y. (a) Regularly spaced commas (repeat distance b_1) representing an asymmetric motif. (b) A scroll design of asymmetric motifs, repeated at distance b_2. (c) A row of equally spaced motifs, repeated at b_3, in which one part of the motif is related to the other by a mirror line (marked by a short line between pairs of motifs). (d) A row of spheres, repeated at b_4, that may represent atoms in a structure. (e) A row of tetrahedra, repeated at b_5, that represent anionic complexes, such as tetrahedral SiO_4 groups.

TWO-DIMENSIONAL ORDER—PLANE LATTICES

Two-dimensional order results from regular translations in two different directions, designated x and y. In a pattern, there are several ways to generate the array by a combination of different translation distances and directions. This is shown in Fig. 7.4a where various choices of as and bs have been superimposed on the coordinate axes along which the translations take place, x (x_1, x_2, x_3) and y (y_1, y_2). The translation distances are marked as a (or a_1, a_2, etc., along x) and b (or b_1, b_2, etc., along y). These translational patterns can be described by translation vectors: **a** and **b**, their magnitudes (translations) as a and b, and their directions (coordinate axes along which the translations are repeated) as x and y. The angle between the x and y axes is denoted by γ.

When the angle γ between the x and y directions is neither 90° nor 60° nor 120°, an oblique array of motifs results (as shown in Fig. 7.4b). This regular two-dimensional pattern is produced with two different spacings (the unit of translation along the row = b; the unit of translation between the rows = a). To better visualize the pattern of the array created by the motifs (commas), each motif is replaced with a point, and the points are connected by lines. This creates a two-dimensional *net* or *plane lattice* (as shown in Fig. 7.4c). The regularly spaced points (or nodes) represent the locations of motifs, which in minerals structures may be atoms, ions, molecules, or ionic complexes. The smallest building unit in the two-dimensional pattern of Fig. 7.4c is that of the shaded parallelogram; this is the **unit cell**. If this *unit cell* is repeated infinitely by translations a and b along directions x and y, the array (in Fig. 7.4b) and the lattice (Fig. 7.4c) will result.

There are only **five possible** and **distinct plane lattices** (also known as *nets*). The five choices are the result of repeating a row (with translation distance b along direction y) along direction x with repeat distance a. The resulting plane lattice types depend on the choice of the angle λ (i.e., whether λ = 90°, 60°, or some other angle) and on the length of a relative to b (i.e., whether $a = b$, or not). These five plane lattices (nets), illustrated in Fig. 7.5, represent the only possible ways to arrange points *periodically* in two dimensions. (Interactive animations that build these five net types are found in module III of the CD-ROM under the heading "2-Dimensional Order.")

An **oblique lattice** results when row number 1 (Fig. 7.5a) is infinitely repeated by translation distance a, along translation direction x, with $\gamma \neq 90°$. Here, $a \neq b$.

A primitive **rectangular lattice** results when row number 1 is infinitely repeated by a translation distance a, along translation direction x, with $a \neq b$ and γ = 90° (Fig. 7.5b). This type of lattice is termed a **primitive lattice** because *primitive* implies that nodes only occur at the corners of the chosen unit cell. This can be compared with a centered rectangular lattice, which follows.

Another rectangular lattice is possible, but this lattice also has a node in the center of the unit cell. This is known as a **centered rectangular lattice**. Row number 1 is infinitely repeated by translations along direction x, with translation distance a, and with γ such that $\cos\gamma = a/2b$. The resulting lattice is conventionally described in terms of two orthogonal directions (x and y'), with a centering node inside the rectangular unit cell choice. The same array of nodes can be described by two vectors (**a′** and **b′**, where **a′** = **b′** and $\gamma' \neq 90°, 60°$, or 120°); this results in a *primitive lattice* with a diamond shape. This alternate, primitive lattice choice is referred to as a **diamond lattice**. Either of these two unit cell choices (primitive or nonprimitive [= centered]) will, when repeated infinitely along two directions, produce the pattern of nodes in Fig. 7.5c.

A **hexagonal lattice** results when row number 1 is infinitely repeated by translations in direction x, with a translation distance of a, such that $a = b$ (or $a_1 = a_2$) and $\gamma = 60°$ (as in Fig. 7.5d)

A **square lattice** results when row number 1 is infinitely repeated by translations in direction x, with a translation distance of a, such that $a = b$ (or $a_1 = a_2$) and γ = 90° (Fig. 7.5e). Of the various choices of unit cells in Fig. 7.5, only one contains a central node, the *centered rectangular lattice*. All other choices contain only corner nodes and are *primitive lattices* (e.g., primitive oblique lattice, etc.).

The five different plane lattices (or nets) in Fig. 7.5 are intended to represent infinitely extending ordered patterns. The smallest units of repeat in these lattices are the *unit cells* (shaded in Fig. 7.5). They range in shape from a parallelogram (Fig. 7.5a), to *two types of rectangles* (Figs. 7.5b and c), to a *diamond shape* (Fig. 7.5c), to a *rhombus* (Fig. 7.5d), and a *square* (Fig. 7.5e). When selecting a unit cell in a two-dimensional pattern, generally the smallest possible unit cell should be chosen. In Fig. 7.5c there is a choice of two differently shaped and sized unit cells. The preferable choice, in this instance, however, is the rectangular (centered, and larger) unit cell because of the orthogonality of its shape and because the mirror lines inherent in the symmetry of the pattern are parallel to the axial directions of the unit cell.

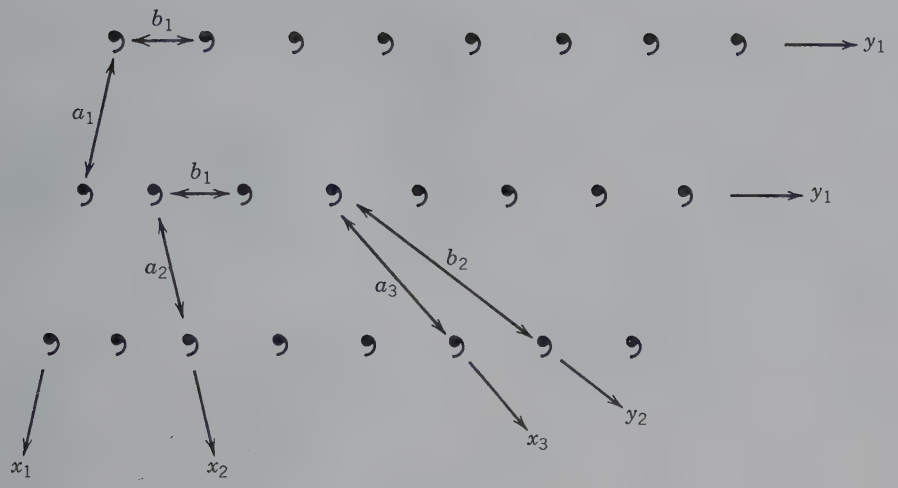

(a)

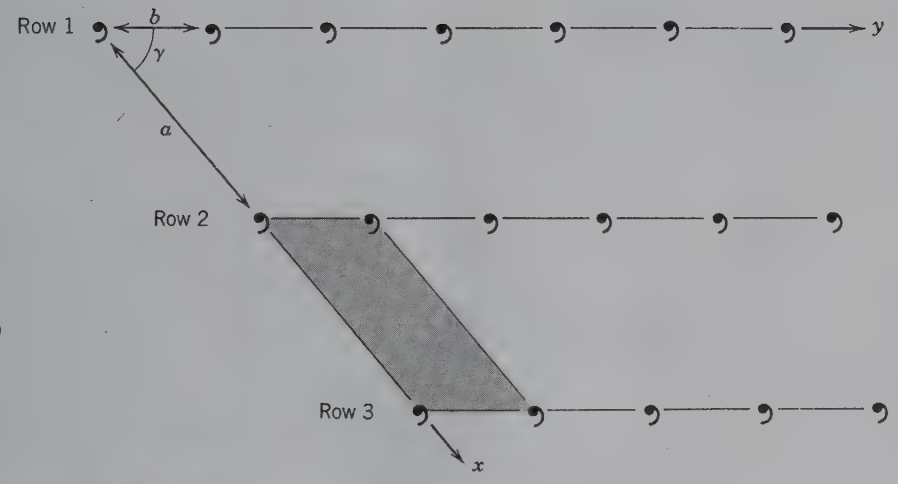

(b)

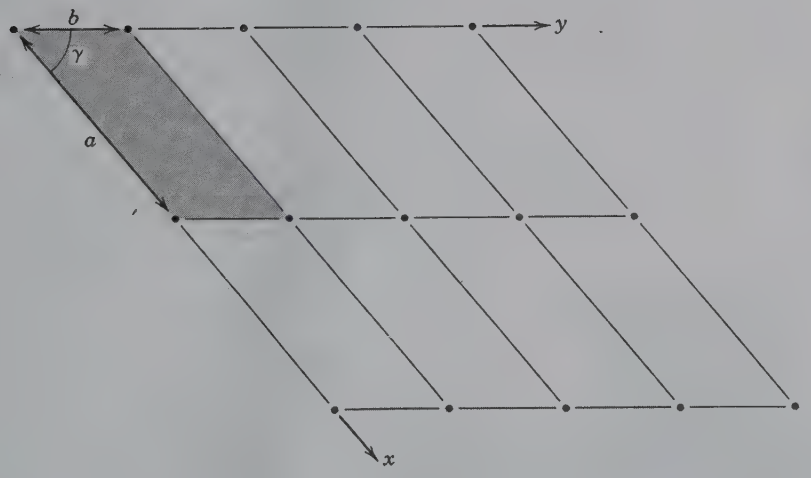

(c)

FIG. 7.4 (a) A two-dimensional, ordered array of motifs showing various different ways to generate the array by combining translation directions (x_1, x_2, x_3; y_1, y_2) and distances (a_1, a_2, a_3; b_1, b_2). These different choices all generate the same pattern. (b) Yet another choice of translation directions and translation distances. The angle between the two directions of x and y is γ. This arrangement represents an oblique ($\gamma \neq 90°$), two-dimensional (planar), and ordered array of motifs. (c) A planar lattice based on the array of motifs in (b). A lattice is, by definition, *infinitely extending*, but only finite portions are shown in illustrations. The shaded parallelogram in (b) represents the smallest unit of pattern and a unit cell in the lattice of (c).

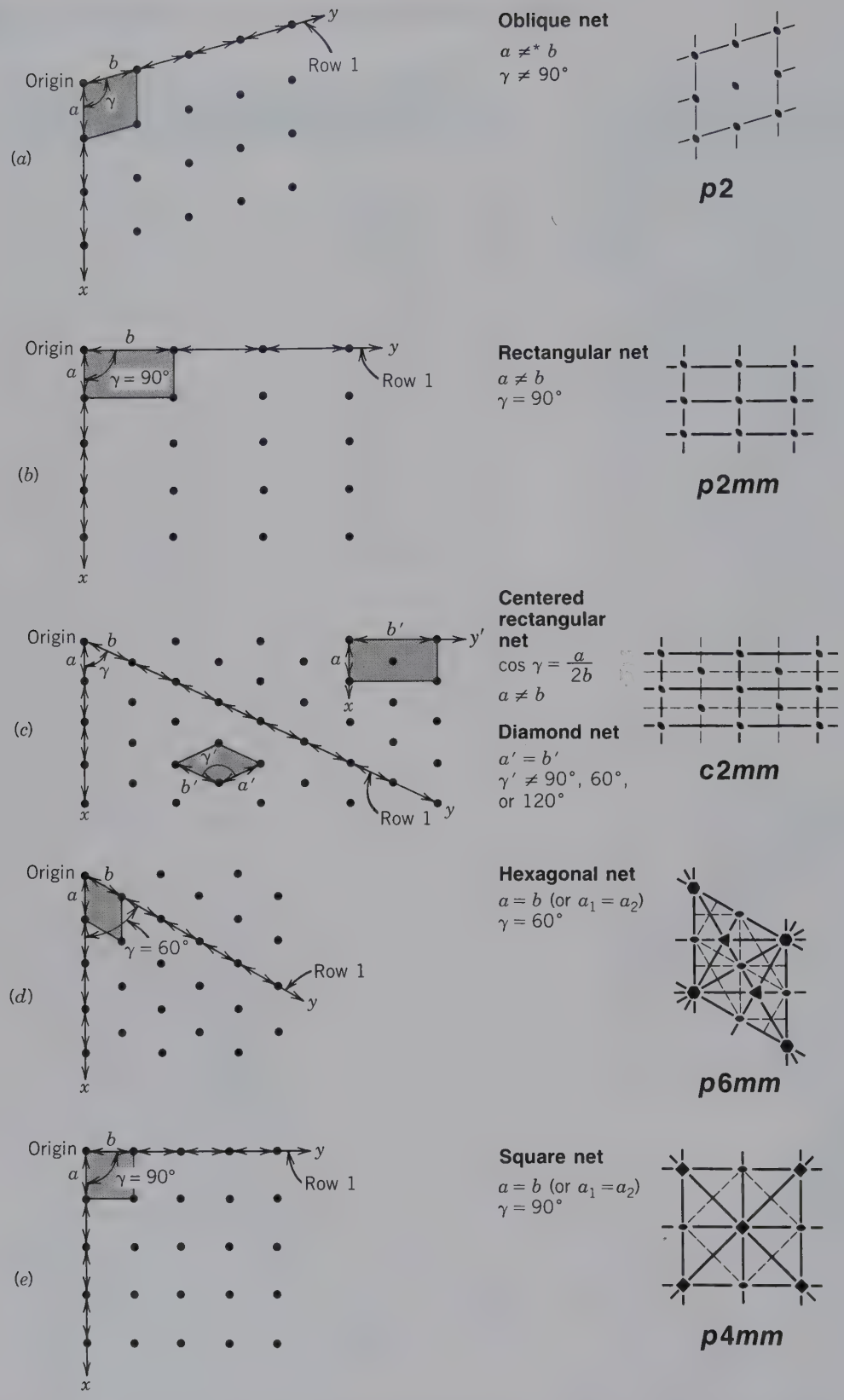

FIG. 7.5 Development of the five distinct plane lattices (or nets) by the infinite repeat of a row (along direction *y*, with specified translation distance *b*), along direction *x* with repeat distance *a*; γ is the angle between *x* and *y*. The total symmetry content of each of the unit cell choices is given in the right-hand column. Rotational axes are shown by standard symbols at nodes; mirrors by solid lines; and glide lines by dashed lines.

*The sign ≠ implies nonequality by reason of symmetry; accidental equality may occur.

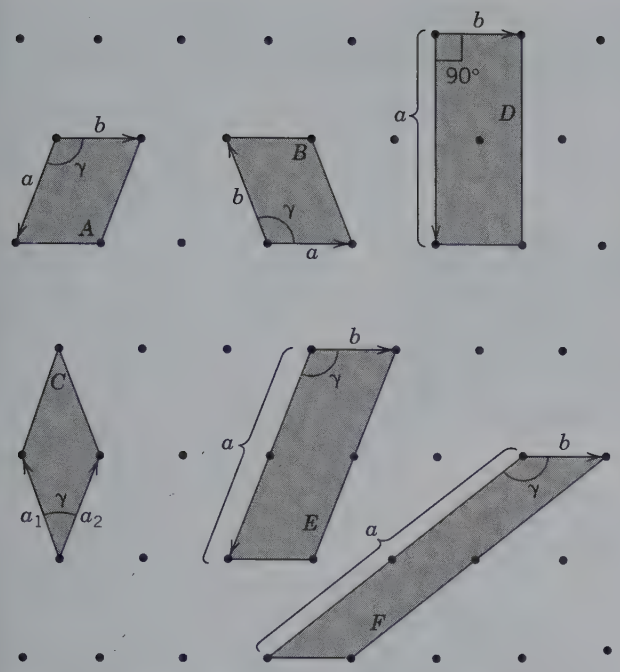

FIG. 7.6 A regular array of nodes that can be generated by the infinite repeat of various unit cell choices (labeled *A, B, C, D, E,* or *F*) along two vectors **a** and **b**.

This underscores the fact that one may be confronted with a number of choices for the unit cell in an ordered pattern. For example, Fig. 7.6 shows a regular array of nodes that was originally generated by the two vectorial directions **a** and **b** and angle, γ, as shown in the primitive, oblique unit cell marked *A*. Another unit cell choice, which through infinite repeat along two vectors in the plane of the page would have generated the same pattern, is unit cell *B*. The spacings and angle are the same as in *A* and it is an equivalent primitive, oblique unit cell. A third choice, designated as *C*, is also primitive and oblique but with $a_1 = a_2$ and with a different angle, γ. All the other choices, *D*, *E*, and *F*, are *nonprimitive* or *multiple* unit cells. This is because each contains, in addition to parts of each of the four corner nodes (a total of one node), one more node per unit cell. In *D* the additional node is centered (a *centered unit cell*). In *E* and *F*, it is made up of two half nodes in the center of two of the sides. Generally, the smallest unit cell (e.g., *A*, *B*, or *C*) or an orthogonal and centered unit cell (e.g., *D*) is the most appropriate choice.

Each unit cell, for each of the five different plane lattices (nets), also contains symmetry. The distribution of symmetry elements in one unit cell of each pattern (shaded in the left column) is shown on the right of Fig. 7.5. The locations of the various rotational symmetry axes (2, 3, 4, and 6), perpendicular to the page, are shown by the standard symbols. The locations of mirrors perpendicular to the page are shown by broad black lines. But remember, there are no mirrors or symmetry axes in the plane of the page (i.e., parallel to the page). In the lattices in Figs. 7.5d and e, the dashed lines represent *glide lines*, which are a combination of translation and reflection (and are discussed later in this chapter). The notation for symmetry contents is similar to that used earlier (e.g., 2 for A_2, *m* for mirror). However, each symmetry listing is preceded by a small letter: *p* (for primitive) or *c* (for centered) to indicate the lattice choice.

The concepts of symmetry and translation in the repetition of a motif are often seen in wallpaper designs (Fig. 7.7). Each motif in this design contains a two-fold rotation axis perpendicular to the page and two reflection lines (*m*) perpendicular to each other (planar point group symmetry *2mm*). The pattern of motifs can be described by a primitive, oblique unit cell with edges a_1 and *b*, but the most appropriate choice, in view of the *2mm* symmetry content of the motifs, would be a rectangular centered unit cell with edges a_2 and *b*. This is in keeping with the symmetry of the lattice and that of the motif. For three-dimensional patterns, several rules have been made to restrict the possible choices of unit cells (see page 159).

FIG. 7.7 Alternate unit cell choices for a wallpaper design. Edges are shown by solid lines (a_1, a_2, *b*); the dashed lines indicate other edges for unit cell choices. The motif of the wallpaper contains symmetry *2mm*. It is best to choose a unit cell consistent with this symmetry, which results in the rectangular (centered) unit cell.

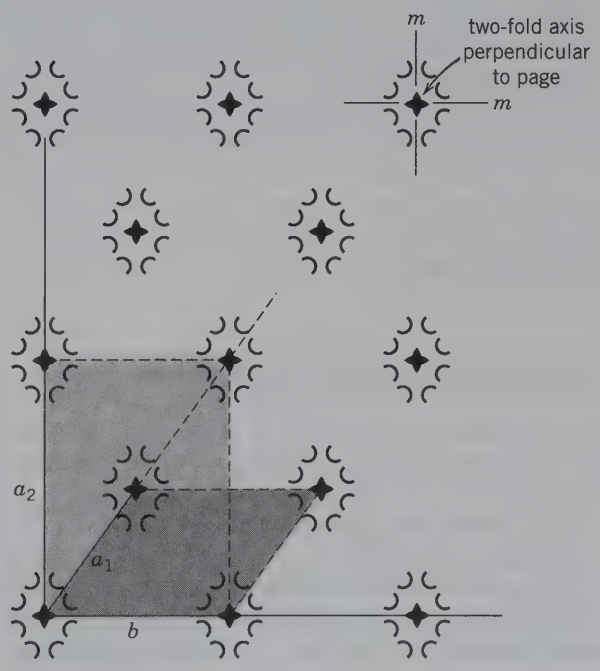

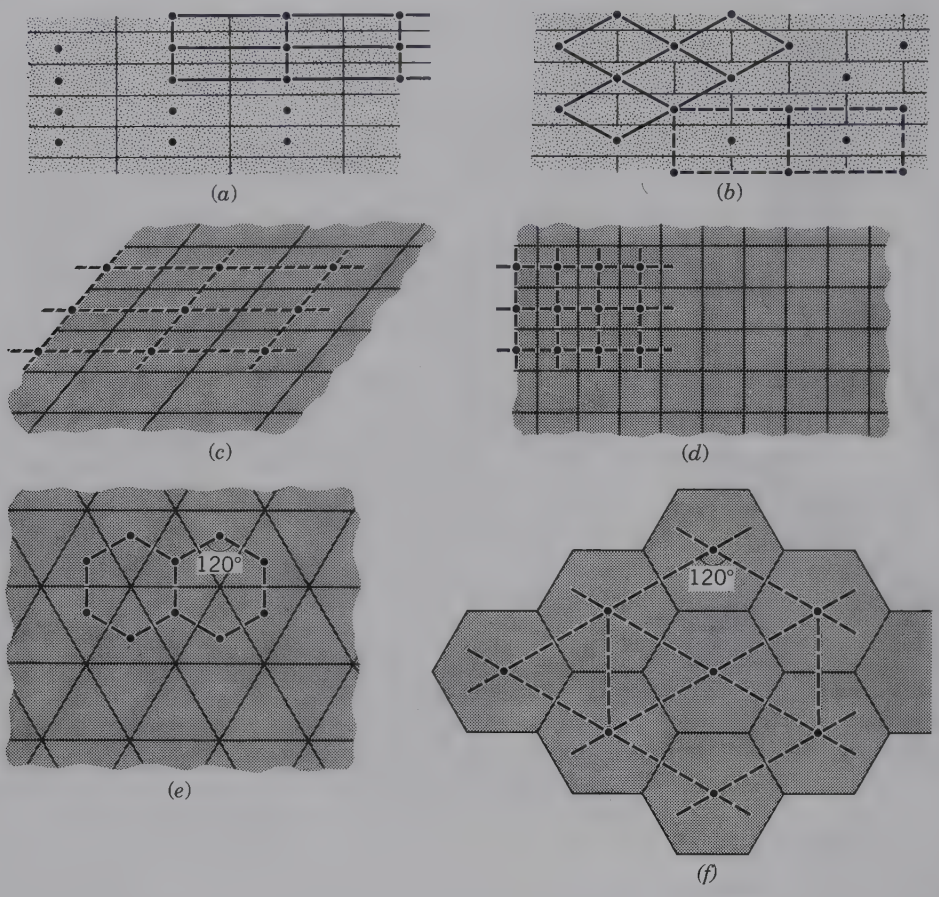

FIG. 7.8 (a) and (b) represent brick walls; (c) through (f) are possible arrangements of tiles. In each case, the original motifs (bricks or tiles) are, in part, replaced by lattice points (nodes). When these points are connected, the shape of the lattice becomes obvious. (a) a rectangular lattice; (b) a centered rectangular lattice, or a diamond lattice; (c) an oblique lattice; (d) a square lattice; (e) a hexagonal lattice; and (f) a hexagonal lattice (with a centering node) or a noncentered rhombus lattice.

Our daily surroundings are full of various types of two-dimensional ordered patterns (see Box 7.1). For example, brick or tiled walls can be regarded as the result of repeating a motif (e.g., a brick or a ceramic tile) along two different translation directions (t_1 and t_2) parallel to the wall. This aspect of crystallography is readily practiced when viewing tiled floors or walls in buildings. Figure 7.8 illustrates some common examples as well as their lattice types and unit cell choices. It reemphasizes the fact that the five plane lattices (nets) in Fig. 7.5 are the only possible ways to arrange motifs (points) periodically in two dimensions. These 5 two-dimensional nets represent the only shapes that can "tile" a planar surface with no gaps.

ROTATION ANGLE RESTRICTIONS

Five-fold rotational symmetry is not possible in minerals (as discussed in Chapter 6, page 116). The geometric restrictions on rotation axes *in ordered arrangements that also contain translation* are described using Fig. 7.9. If the motif units, represented by large nodes in Fig. 7.9, are part of an ordered arrangement, then the distances AB and BC must be equal. If the motif at B contains a rotation axis with the axis $\perp$ to the plane of the figure, then the translations require similar axes at A and C. In addition, if points D, E, F, and G are related to B by a rotation, then $BC = BD = BE = BF = BG = t$. This also means that the distance ED, which lies on a line parallel to AC, must be equal to AB or a multiple

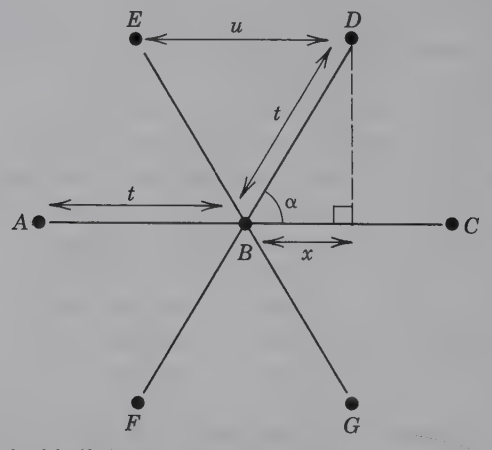

FIG. 7.9 Motifs (points) separated by translation (t) and a possible axis of rotation, perpendicular to the page, at each of the motif units. One axis of rotation at motif B is shown. See text for an explanation of distances and operations consistent with the ordered arrangements of points (nodes) shown here.

BOX 7.1 Patterns in Our Environment

Regular, planar patterns are all around us: in print, in designs of dresses and ties, in brick patterns in sidewalks, in tiling arrangements along walls, and in floors. All such designs are the result of a motif having been repeated infinitely along two (noncoincident) directions. Very interesting, regular patterns can also be observed in the plantings and plowing of farmer's fields, especially when these are viewed from an aircraft at relatively low altitude.

Examples of remarkable patterns, photographed by Alex MacLean, are available in the beautifully illustrated book *Look at the Land: Aerial Reflections on America*, 1993, by Alex MacLean, with text by Bill McKibben, Rizzoli International Publications, Inc., New York, New York. The jacket of this book reads: "Photographer and aviator Alex MacLean has spent twenty years traveling the length and breadth of America by air. With one hand navigating his plane and the other steadying his camera, he has skillfully captured in intensely colorful, unique photographs what can only be seen from above; the interconnectedness and extraordinary patterns of our natural and created environments." Here, two of these remarkable images are reproduced as black-and-white photographs.

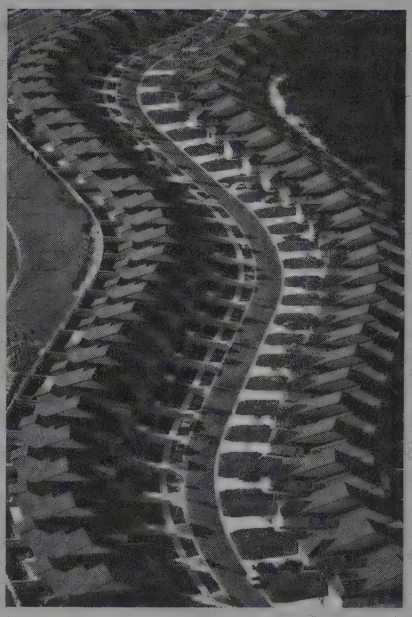

Sinuous rows of new tract housing in Palm City, Florida.

Boats and moored docks off Lincoln Park in Chicago creating a daisy pattern on Lake Michigan (both aerial photographs by Alex S. MacLean/ Landslides, used with permission).

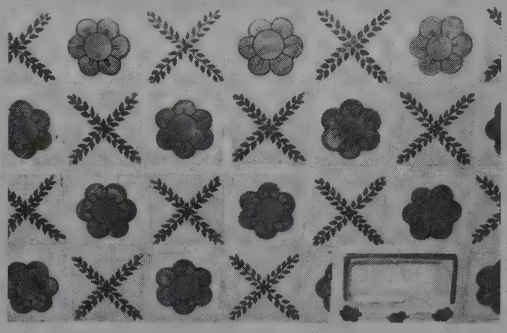

Mexican tiling, Santa Fe, New Mexico (photograph by C. Klein).

thereof. In other words, $ED = u = mt$, where m = integer. If the rotation by which A, F, G, C, D, and E are related, is through an angle α, the following geometric relations hold:

$$\cos\alpha = x/t \quad \text{and also} \quad x = \tfrac{1}{2}ED = \tfrac{1}{2}u$$
$$\therefore \cos\alpha = \tfrac{1}{2}u/t = u/2t$$
$$\therefore 2t\cos\alpha = u$$

Combining $u = mt$ and $u = 2t\cos\alpha$ gives

$$mt = 2t\cos\alpha \quad \text{or} \quad \cos\alpha = m/2$$

where m is an integer. This leads to restrictions on the solutions possible for the angle of rotation α.

For $m = 2$
$m/2 = 1$, $\alpha = 0°$ or $360°$ $(=A_1)$
For $m = 1$
$m/2 = 1/2$, $\alpha = 60°$ $(=A_6)$
For $m = 0$
$m/2 = 0°$, $\alpha = 90°$ $(=A_4)$
For $m = -1$
$m/2 = -1/2$, $\alpha = 120°$ $(=A_3)$
For $m = -2$
$m/2 = -1$, $\alpha = 180°$ $(=A_2)$

Any other integral values of m produce values of $\cos\alpha$ greater or less than ± 1, which is possible but mathematically meaningless. Other rotation angles produce

noninteger values of *m*. For example, a five-fold rotation axis would require an angle of rotation of 72°. This leads to a value for cos 72° = 0.30902. Such a number cannot equal *m*/2 in which *m* must be an integer. Therefore, a five-fold rotation axis is not possible in an ordered, crystalline structure. Five-fold symmetry is, however, common in objects in the biological world (e.g., in the distribution of petals in a geranium flower).

SYMMETRY CONTENT OF PLANAR MOTIFS

Two-dimensional motifs, as seen in printed cloth, in ceramic tiles, and elsewhere, can also display variable symmetry contents. However, because such motifs are printed on one side of a paper (with the other side generally blank), there are no symmetry elements that lie in the plane of the paper. That is, there are no mirror planes parallel to the paper, nor are there axes of rotational symmetry parallel to the plane of the paper. However, there may be symmetry elements perpendicular to the plane of the drawing. These are mirror lines (*m*) (in three-dimensional patterns, *m*s are referred to as mirror planes; in two-dimensional patterns they are known as mirror lines; their reflection operations are equivalent) and rotation axes (1, 2, 3, 4, and 6). Although one can create an independent motif unit with 5-, or 11-, or more-fold rotational axes, the symmetry content of motif units that are part of a repetitive and ordered crystalline array cannot contain such axes.

There are *only 10 possible symmetry contents for two-dimensional motifs* that, through regular translation, can be part of two-dimensional ordered patterns. These may contain mirror lines (*m*s) and rotation axes (1, 2, 3, 4, and 6) perpendicular to the plane of the pattern or illustration. The symmetry content of these 10 motifs is shown in Fig. 7.10. All of their symmetry elements relate to a central (stationary) point and are referred to as the **10 planar point groups.**

There are 10 because each of the 6 symmetry elements, 1, 2, 3, 4, 6, and *m*, can occur individually, and the other 4 consist of combinations of rotational symmetry and mirrors, as in 2*mm*, 3*m*, 4*mm*, and 6*mm*.

The notation used is the same as that discussed earlier for the Hermann–Mauguin (international) notation of point groups or crystal classes (Chapter 6). The numerals refer to rotations about a point. The *m*s in 2*mm* and 3*m* and the first *m* in 4*mm* and 6*mm* refer to reflection lines that are coincident with the axial directions. These lines are at right angles in orthogonal

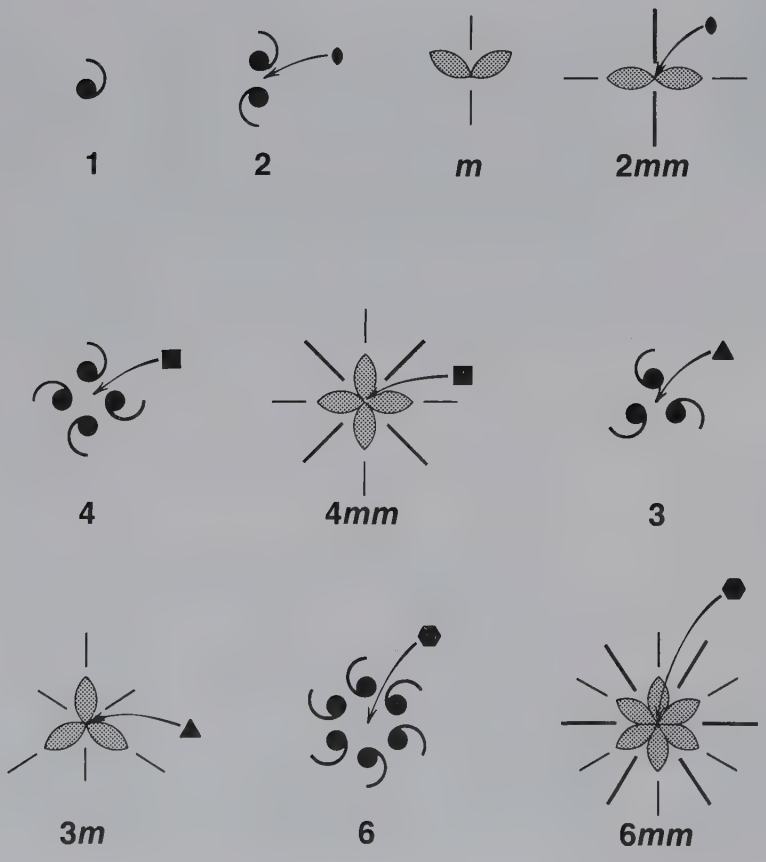

FIG. 7.10 The symmetry content of two-dimensional motifs, designated by Hermann-Mauguin symbols. Locations of mirror lines (*m*) are shown by solid lines and rotational axes by the standard symbols.

arrays but at 120° to each other in six-fold and three-fold patterns. Thus, in *4mm* there are two kinds of mirror lines; the first *m* refers to two reflection lines at right angles to each other (Fig. 7.10). The second *m* in *4mm* and *6mm* refers to intermediate reflection lines, which in *4mm* are at 45° to the first set of lines, and in *6mm* are at 30°. *The 10 planar point groups are the two-dimensional analogues to the 32 three-dimensional point groups (crystal classes)* discussed in Chapter 6. (These concepts are extensively illustrated in module III of the CD-ROM.)

SYMMETRY CONTENT OF PLANE LATTICES

Two-dimensional ordered arrays can be evaluated in terms of their lattice type (Fig. 7.5) and the symmetry of the motif (Fig. 7.10). Figure 7.11 shows some examples of the interaction of lattice type and motif distributions. Figure 7.11a is a primitive oblique unit cell based on a regular distribution of commas. Only a one-fold axis (1) is compatible with this pattern. Because the lattice is primitive (*p*) and contains only one-fold

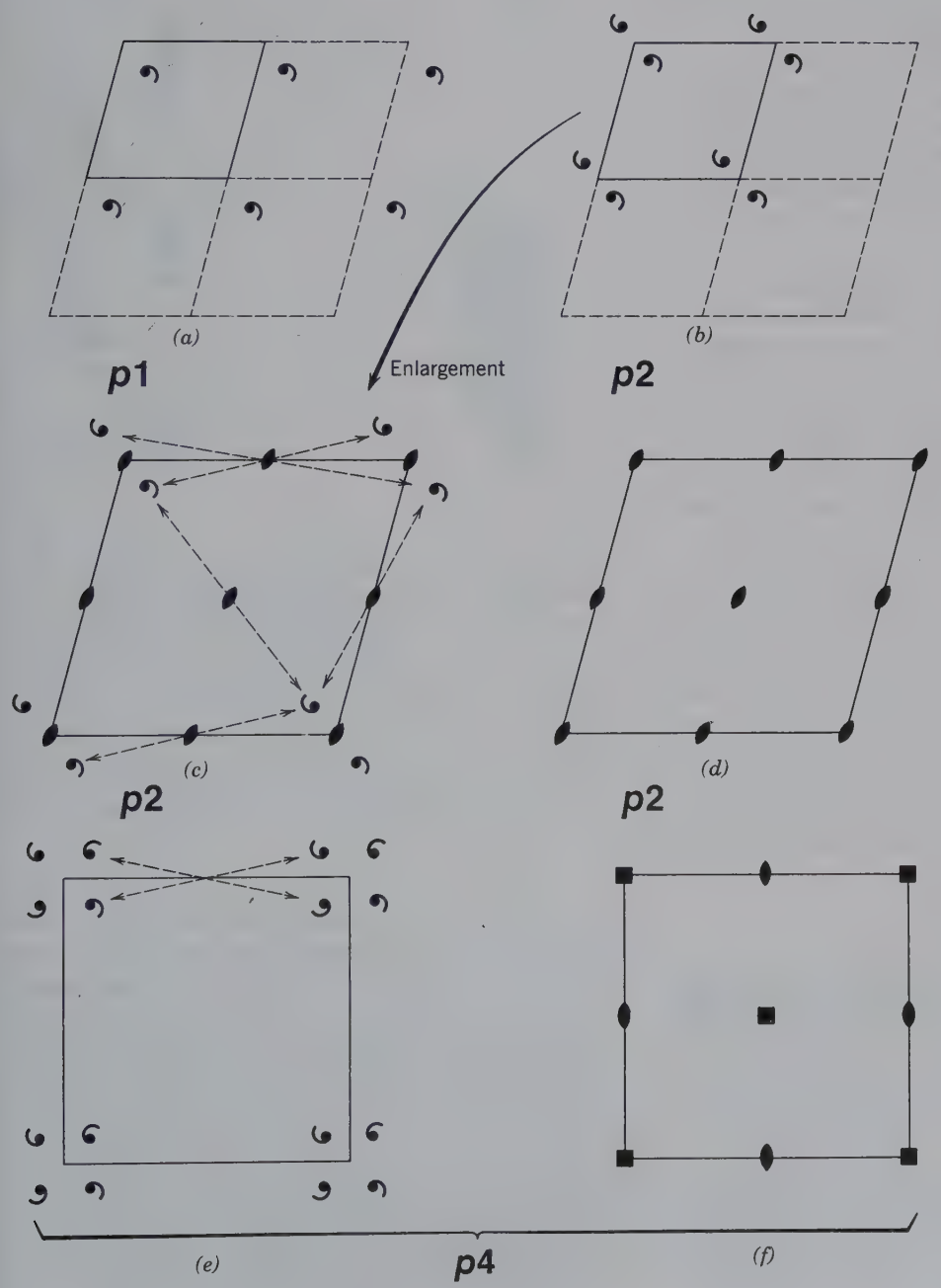

FIG. 7.11 Examples of rotational symmetry elements compatible with a primitive oblique lattice [(a) through (d)] and a primitive square lattice [(e) and (f)]. See text for explanation.

rotational symmetry (1), their combination is plane group *p*1. A repeat of two commas related by two-fold rotation, on the same lattice as in *a*, is shown in Fig. 7.11b. This is described as *p*2, a primitive lattice with two-fold symmetry. When the locations of all possible two-fold rotations are shown, Fig. 7.11c results. (This is an enlarged unit cell drawing of Fig. 7.11b). The two-fold rotations occur at the corner nodes, halfway along each of the cell edges, as well as at a location in the center of the cell. The dashed lines indicate the relationship between selected commas by such two-fold rotations. To represent the total symmetry content of e.g., *p*2, it is standard to eliminate the motif units (e.g., in *International Tables for Crystallography*, vol. A) and to simply show symmetry content (as in Fig. 7.11d).

Another example is a square lattice choice, as in Fig. 7.11e. This lattice contains points of four-fold rotation at the corner nodes and in the center, if the distribution of commas (as motifs) is carefully evaluated. In addition, there are two-fold rotations at the centers of the square's edges. The total symmetry content of *p*4 is shown in Fig. 7.11f.

A plane lattice is the result of translations in two different directions, therefore, combinations of mirror reflections (*m*) and translations (*t*) must be considered. Such a combination of reflection and translation (*m* + *t*) is referred to as a **glide operation**, with the symmetry element being a *glide reflection* (*g*). Figure 7.12a is an illustration of how a reflection line acts upon a regular row of nodes. This is quite different from what happens when a glide line (or glide reflection) is present. A glide reflection causes a motif to be reflected across a mirror and to be translated, by distance $\frac{1}{2}$ *t*, parallel to the reflection line (Figs. 7.12b, c, and d). The motif units are related by a glide line (or glide plane) that has a translation component of *t*/2, where *t* is the shortest translation paralleling the glide line.

Consideration of the ten two-dimensional (planar) point groups (Fig. 7.10) in conjunction with the five plane lattices (Fig. 7.5), and the possibility of glide reflections (*g*) in addition to (or in place of) possible mirror reflections (*m*), leads to the so-called two-dimensional **plane groups**.

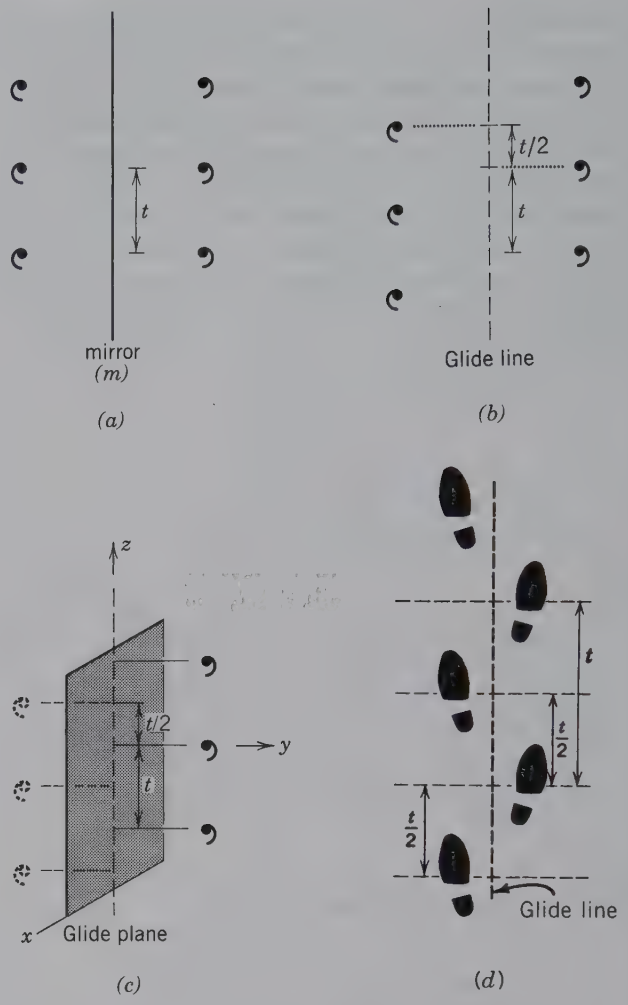

FIG. 7.12 Mirror symmetry and glide lines and planes. (a) A two-dimensional array of an asymmetric motif with a spacing of *t* related by a reflection line, or a mirror (*m*) perpendicular to the page. (b) A two-dimensional array of motifs that are related, across a glide line, by a glide component of *t*/2. (c) A three-dimensional illustration of a glide plane with glide component *t*/2. (In graphical illustrations, reflection lines and the traces of mirrors perpendicular to the page are shown by solid lines; glide lines and the traces of glide planes perpendicular to the page are shown by dashed lines.) (d) Human tracks showing the relationship of motifs (footprints) by a glide line. Glide component *t*/2.

TWO-DIMENSIONAL PLANE GROUPS

The infinite and regular repetition of motifs on a plane is described by two-dimensional **plane groups**. To evaluate the two-dimensional group requires determining the shape (oblique, rectangular, hexagonal, or square) and the possible multiplicity (*p* or *c*) of the plane lattice type (Fig. 7.5), as well as the compatibility of the translation-free point groups (1, 2, 3, 4, 6, *m*, 2*mm*, 3*m*, 4*mm*, and 6*mm*) with those lattice types (Fig. 7.10). Furthermore, the possible presence of glide reflections (*g*) in place of, or in addition to, possible mirror reflections (*m*) must be assessed and all of the possible combinations of lattice types with permissible symmetry elements must be considered. For an oblique cell, only *p*1 and *p*2 are appropriate (as in Figs. 7.11a and b). For a rectangular cell, the symmetry elements *m* and *g* are possible as well as the choice of a primitive (*p*) or a centered (*c*) cell. As an example, point group *m* might result in *pm*, *pg*, *cm*, and *cg* as possible two-dimensional plane groups (Fig. 7.13). Similarly, for 2*mm* we might consider *p*2*mm*, *c*2*mm*, *p*2*mg*, *p*2*gg*, *c*2*mg*, and *c*2*gg* as permissible two-dimensional plane group choices. Not all of the aforementioned combinations are, however, valid plane groups.

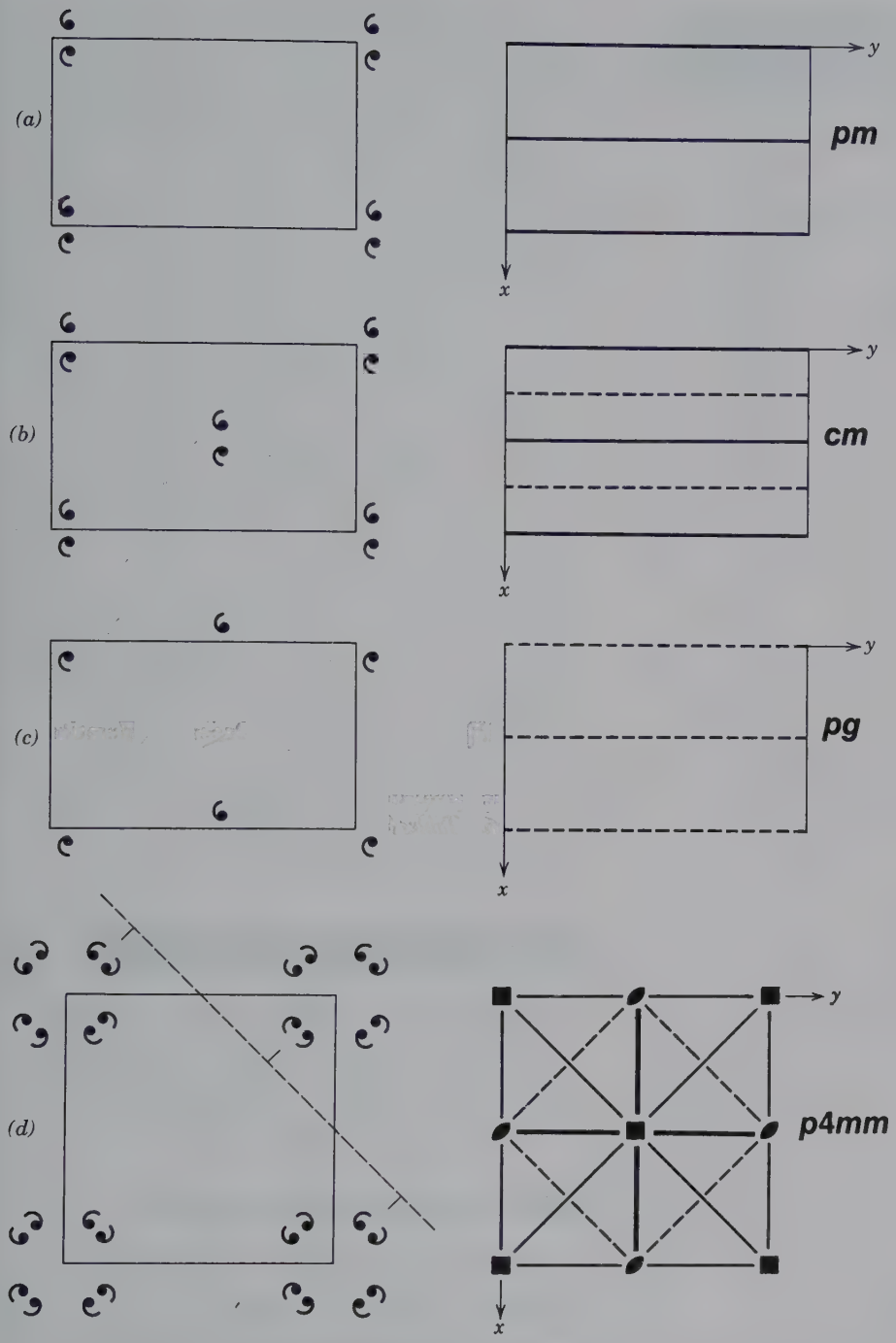

FIG. 7.13 Examples of mirror and glide symmetry compatible with a rectangular [(a) through (c)] and a square lattice (d). The left-hand column shows the shape of the unit cell and the distribution of the motifs with respect to the outline of the unit cell. In the right-hand-column only the distribution of the symmetry elements with respect to the unit cell outline is given. Crystallographic directions are indicated by axes *x* and *y*. Mirror lines (*m*) are shown by solid heavy lines and glide lines (*g*) by dashes. Rotation axes are shown by the standard symbols (see Figs. 6.12 and 6.24).

(a) A primitive rectangular cell with mirror lines parallel to the *y* axis.

(b) A centered rectangular cell. The combination of centering and mirror lines produces glide lines parallel to and interleaved with the mirrors.

(c) A primitive rectangular cell with glides parallel to the *y* axis.

(d) In the left-hand illustration, the location of one of four possible diagonal glide lines is shown on the basis of the distribution of motif clusters. In the right-hand column, the total symmetry of this square planar array consists of four-fold rotation axes at corners and the center of the cell; two-fold rotation axes at the centers of edges; mirror lines parallel to the two axes *x* and *y*; mirror lines in two diagonal positions; and glide lines interleaved with the diagonal mirror lines.

Table 7.1 Two-Dimensional Point Groups and Space Groups*

Lattice	Point Group	Plane Group
Oblique *p*	1	*p*1
	2	*p*2
Rectangular *p* and *c*	*m*	*p m* *p g* *c m*
	2*mm*	*p*2 *mm* *p*2 *mg* *p*2 *gg* *c*2 *mm*
Square *p*	4	*p*4
	4*m m*	*p*4 *mm* *p*4 *gm*
Hexagonal *p*	3	*p*3
	3*m*	*p*3 *m*1† *p*3 1*m*†
	6	*p*6
	6 *m m*	*p*6 *mm*

*From *International tables for X-ray crystallography*. 1969. v. 1, N. F. M. Henry and K. Lonsdale, eds.: Symmetry Groups, International Union of Crystallography, Kynoch Press, Birmingham, England.

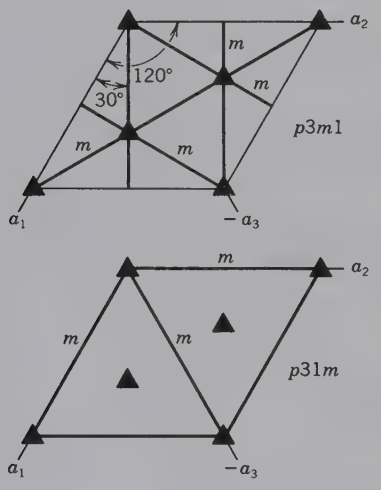

†There are two distinct groups for 3*m*—*p*3*m*1 and *p*31*m*. They have the same total symmetry content and shape. However, the conventional location of cell edges (as defined by three axes a_1, a_2, and a_3) differs by 30° in the two groups. In *p*3*m*1 the mirror lines are at 30° from the cell edges; in *p*31*m* the reflection lines coincide with the cell edges.

It turns out that there are only *17 possible two-dimensional plane groups* (see Table 7.1, Fig. 7.14). The table of all possible two-dimensional plane groups, including those compatible with point group symmetries *m* and 2*mm* (Table 7.1), shows that only 7 of the 10 aforementioned possibilities actually occur for those groups. The reason for this is that not all combinations lead to new or different plane groups. Furthermore, *the interaction of the symmetry of the motif (planar point group) with the symmetry of the various plane lattices affects the overall resultant symmetry content of the planar pattern.* The final pattern displays the symmetry of the lattice when the symmetry elements of the motif are aligned with the corresponding symmetry elements of the lattice. If the motif has less symmetry than the lattice, the pattern will express the motif's lesser degree of symmetry, with the symmetry elements of the motif aligned with the corresponding symmetry elements of the lattice. These 17 possible plane patterns are known as *plane groups* and are illustrated in Fig. 7.14. Illustrations that represent four of these plane groups are shown in Box 7.2. (Interactive graphical developments of 7 of the 17 possible plane groups are given in module III of the CD-ROM under the heading "2-Dimensional Order: Generation of Seven Plane Groups.") More detailed illustrations of each of these two-dimensional plane groups are given in *International Tables for X-ray Crystallography* 1: 57–72 (see reference at the end of this chapter.)

THREE-DIMENSIONAL ORDER III

The foundation is now built for understanding the regularity expressed by three-dimensional crystalline matter. For three-dimensional order, a third direction (vector) is needed to describe the distribution of nodes in a three-dimensional (space) lattice.

THREE-DIMENSIONAL LATTICES

Assessing the atomic structures of crystals requires the concept of a three-dimensional (3D) lattice. This can be constructed by adding one additional translation direction (vector) to the plane (2D) lattices in Fig. 7.5. This third vector must not lie in the plane of the two-dimensional nets. In 3D, vector space is referred to three non-coplanar axes, *x*, *y*, and *z*, which intersect at the origin. The unit cell vectors are denoted as **a**, **b**, and **c**, and the unit cell translations along *x*, *y*, and *z*, respectively, are noted as *a*, *b*, and *c* (Fig. 7.15). The *x*, *y*, and *z* coordinate axes are commonly referred to as the *a*, *b*, and *c* axes. The unit cell dimensions, as reported in mineral descriptions (see Chapters 15–19), are expressed as *a*, *b*, and *c*, in angstrom (Å) or nanometer (nm) units.

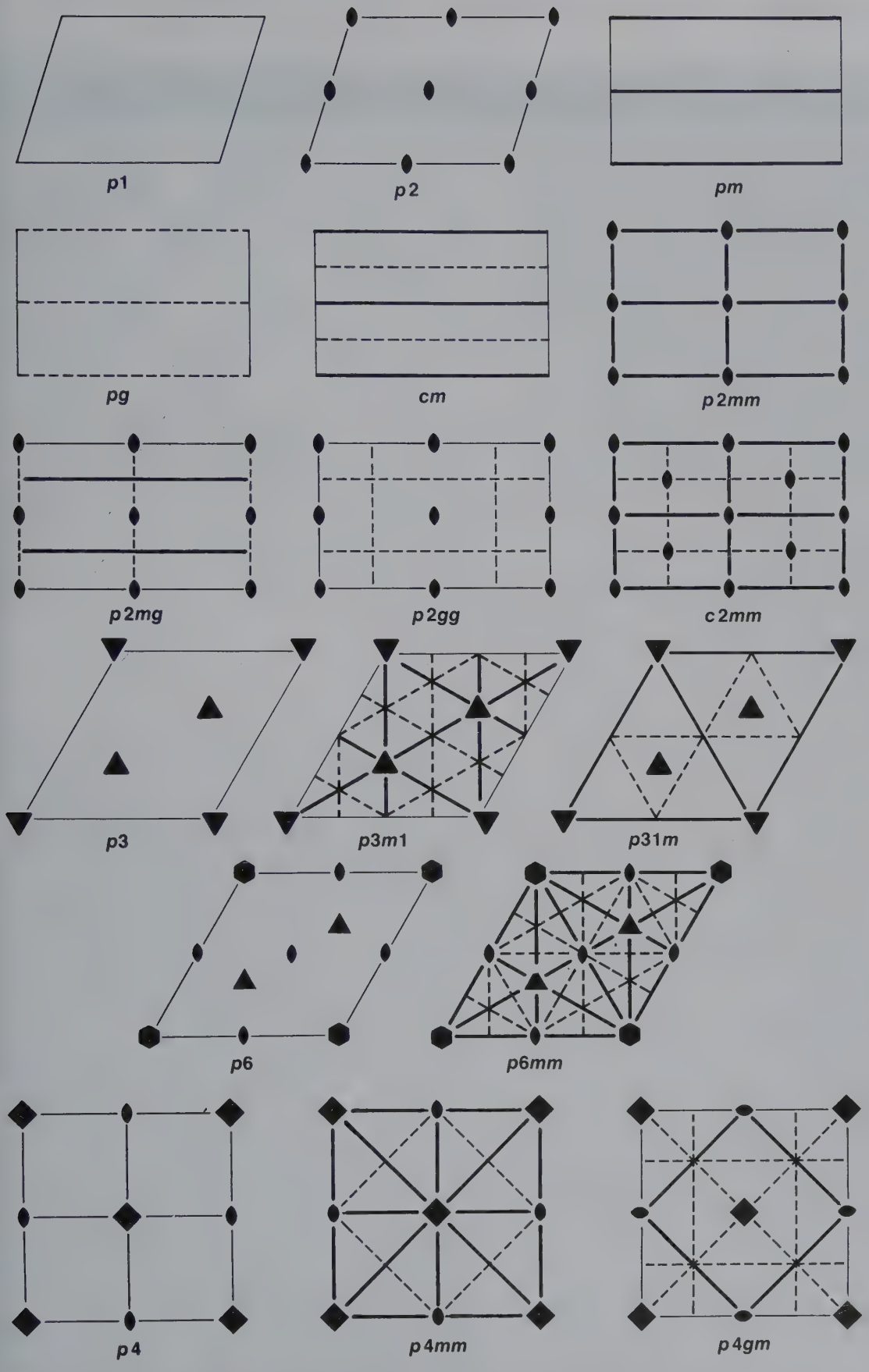

FIG. 7.14 Graphical representation of the symmetry content of the 17 plane groups. Heavy solid lines (*m*), dashed lines (*g*), and rotational symmetry axes are perpendicular to the page.

BOX 7.2 Periodic Drawings

Science and art often meet. Perhaps the most obvious example of symmetry in art is displayed by the intricate drawings of M. C. Escher, a Dutch graphic artist. His designs of fish, birds, horsemen and other objects cover space as two-dimensional tilings. The symmetry inherent in these two-dimensional drawings represents various patterns of the 17 two-dimensional plane groups. Many of these drawings have been compiled by Caroline H. MacGillavry in a book titled *Fantasy and Symmetry: The Periodic Drawings of M. C. Escher* (see references). Two of the Escher drawings from this book are shown. The following is a brief passage from the introduction to this book (page IX):

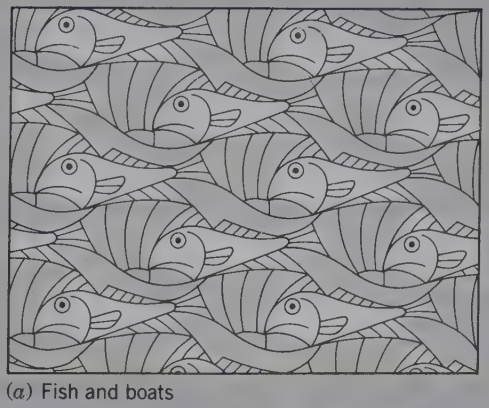

(*a*) Fish and boats

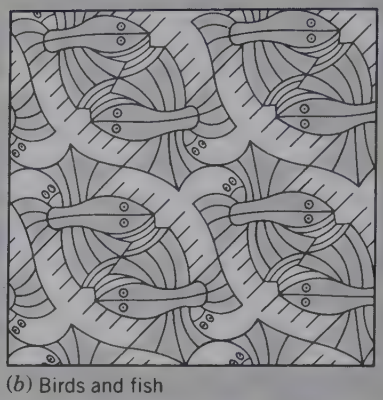

(*b*) Birds and fish

(*c*) The sailing ship *Bluenose*

(*d*) Canadian maple leaf

> It occurred to several scientists attending this meeting [Fifth International Congress of the International Union of Crystallography, held in Cambridge, England, in 1960] that Escher's periodic drawings [in an exhibition arranged for that same meeting by crystallographers J. D. H. and Gabrielle Donnay] would make excellent material for teaching the principles of symmetry. These patterns are complicated enough to illustrate clearly the basic concepts of translation and other symmetry, which are so often obscured in the clumsy arrays of little circles, pretending to be atoms, drawn on blackboard by teachers of crystallography classes. On the other hand, most of the designs do not present too great difficulties for the beginner in the field.

Any of the books on Escher are wonderful for exploring two-dimensional symmetry in tilings and in nature and for determining many aspects of crystal structures. The arrangements of motifs in the four illustrations represent 4 of the 17 possible two-dimensional plane groups (as listed in Table 7.1 and illustrated in Fig. 7.14). When color is added to these two-dimensional planar patterns, two-dimensional patterns result that can be interpreted as the projection of a three-dimensional pattern on the plane of the page (see, for example, Buseck, 1997).

(a) and (b) are redrawn from illustrations (plates 1a and 2, respectively) by M. C. Escher, as published by Caroline H. MacGillavry (see reference list); copyright © 2006 The M. C. Escher Company–Holland. All rights reserved. (c) and (d) are redrawn from François Brisse in his publication entitled "La Symétrie bidimensionelle et le Canada" (see reference list at the end of this chapter), which he prepared for the Twelfth Congress of the International Union of Crystallography, held in Ottawa, Canada, 1981. The two-dimensional plane groups represented by these illustrations are (a) *p*1, (b) *p*2, (c) *pg*, and (d) *p*4*gm*.

The best way to evaluate the shape and size of the unit cell, as well as the symmetry content of an infinitely extending periodic drawing, is to place a sheet of transparent paper over it. On this transparent overlay, substitute opaque circles (nodes) for the smallest motif, or a part of the motif (a motif unit). If symmetry is present, it is best to locate the nodes on the location of such symmetry elements (rotations, *m* or *g*). Once the nodes have been located, the lattice of the design can be seen by drawing lines between the nodes. Be sure to use the standard symbols for rotations perpendicular to the page (⬮, ▲, ■, ⬢) and for mirrors (solid lines) and glides (dashed lines). This will reveal the similarity of the two-dimensional plane group (as deduced from these four artistic illustrations) with the representations in Fig. 7.14 (see also Klein, 2008; Buseck, 1997; complete references at the end of this chapter; http://marie.epfe.ch/escher/).

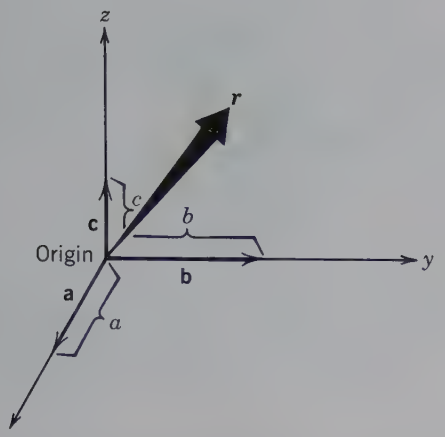

FIG. 7.15 (a) Schematic representation of vectors **a**, **b**, and **c**, along coordinate axis directions *x*, *y*, and *z*. Unit cell translations are given as *a*, *b*, *c*, along directions *x*, *y*, and *z*, respectively. A general vector, **r** , in this three-dimensional space can be expressed as a linear combination of **a**, **b**, **c**, such that $\mathbf{r} = x\mathbf{a} + y\mathbf{b} + z\mathbf{c}$, where *x*, *y*, and *z* are real numbers. The *x*, *y*, and *z* coordinate axes (associated with cell edges *a*, *b*, and *c*, respectively) are generally referred to as the *a*, *b*, and *c* axes.

In three-dimensional arrays, a considerable number of unit cell choices are possible. To reduce the number of choices, crystallographers have drawn up the following restrictions as to unit cell choice:

1. The edges of the unit cell should coincide, if possible, with symmetry axes of the lattice.
2. The edges should be related to each other by the symmetry of the lattice.
3. The smallest possible cell should be chosen in accordance with (1) and (2).

Any regular three-dimensional array of nodes can be outlined by a primitive lattice. However, it is frequently desirable and appropriate to choose a nonprimitive unit cell.

When the five planar nets (shown in Fig. 7.5) are stacked in various ways along a third direction (*z*), periodic arrays in three-dimensions result. These are referred to as **space lattices** and may be primitive or nonprimitive (Fig. 7.16). A **primitive space lattice** *is a parallelepiped with lattice points only at its corners.* If the unit cell is nonprimitive, additional nodes occur in several locations. (1) Nodes may be centered on a pair of opposite faces of the unit cell. When centered along the *a* (*x*) axial direction, it is called *A*-centered, along *b* (*y*) B-centered, and along *c* (*z*) C-centered. (2) If nodes are centered on *all* faces of the unit cell, this is referred to as *F* (for all face-centered). (3) When a node is present in the center of the unit cell, it is referred to as *I*, body-centered (*I* from the German word *innenzentriert*). These various types of unit cells are shown in Fig. 7.16 and the lattice types are referred to by their descriptive letters, *P*, *A*, *B*, *C*, *F*, or *I*.

There are two choices of unit cells in space lattices that are derived from stacking a hexagonal net (see Fig. 7.5d, Fig. 7.16, numbers 10, 11). A net, with two equal translations (a_1 and a_2) that make an angle of 120° with each other, produces a hexagonal space lattice (Fig. 7.16, number 10) when stacked along the third-dimension. A rhombohedral (*R*) unit cell is produced when the hexagonal net is stacked along the edge directions of a rhombohedron such that the translation directions are a_R and the angles between the three equivalent edges of the unit cell are α_R(Fig. 7.16, number 11).

Space lattices must also be compatible with the 32 nonidentical symmetry elements and combinations of symmetry elements (translation-free, as discussed in Chapter 6) that define the crystal classes (point groups) and crystal systems. *There are 14 lattices that are compatible with these 32 point groups.* These are termed **Bravais Lattices** and are illustrated in Fig. 7.16. These lattice types are unique, as was shown by Auguste Bravais (1811–1863), after whom they are named. *They represent the only possible ways in which nodes can be arranged periodically in three dimensions.* (Ten of the fourteen Bravais lattice types are developed through animations in module III of the CD-ROM under the heading "3-Dimensional Order: Generation of 10 Bravais Lattices.")

The various lattices can be arranged among the six crystal systems (refer to Chapter 6) and that is shown in Fig. 7.17. There is a primitive (*P*) lattice choice for each of the six crystal systems and centered lattices occur in five of them. For example, in the triclinic system, which includes the symmetries 1 and $\bar{1}$, the unit cell compatible with these symmetries has no constraints, and its shape is one of low symmetry. In contrast, the isometric system contains very high symmetry ($4/m\bar{3}2/m$, $\bar{4}32$, $43m$, $2/m\bar{3}$ and 23), which is reflected in the unit cell having the highest symmetry constraints. It should be noted that only one face-centered lattice (namely, *C*, in the orthorhombic system) is shown in Fig. 7.17. If the lattice had been chosen in such a way as to be *A*-centered or *B*-centered rather than *C*-centered, this would not introduce a new category of lattice type. The *A*-, *B*-, and *C*-centered lattices are symmetrically identical and can be converted into each other by an appropriate exchange of the crystallographic axes. Table 7.2 summarizes this discussion.

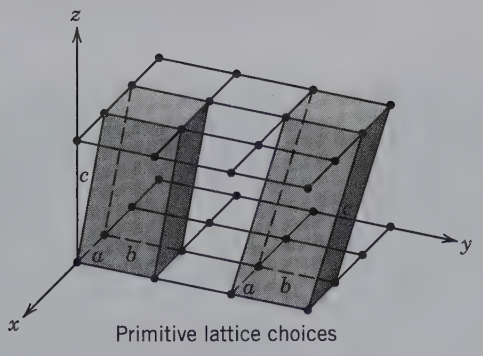

(1) Stacking of an oblique net (or plane lattice) at an arbitrary angle results in *primitive triclinic lattices.*

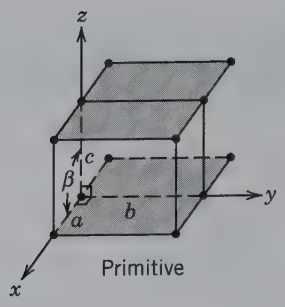

(2) Stacking of a primitive rectangular net in a vertical direction (z), with $x \wedge z$ angle (β) $\neq 90°$, leads to a *primitive monoclinic lattice.*

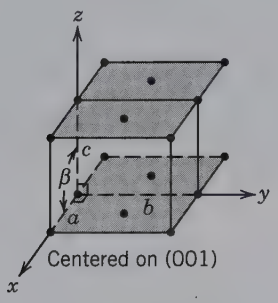

(3) Stacking of a centered rectangular net in a vertical direction (z), with $x \wedge z$ angle (β) $\neq 90°$, results in a *centered monoclinic lattice.*

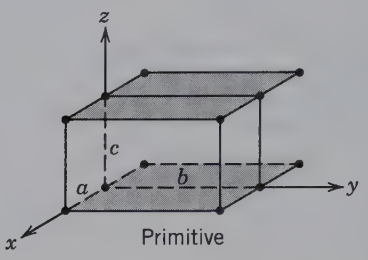

(4) Stacking of a primitive rectangular net in a vertical direction (z), with the $x \wedge z$ angle = 90°, leads to a *primitive orthorhombic lattice.*

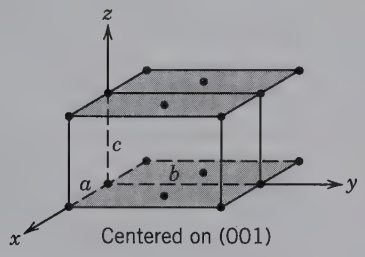

(5) Stacking of a centered rectangular net in a vertical direction (z), with the $x \wedge z$ angle = 90°, leads to a *centered orthorhombic lattice.*

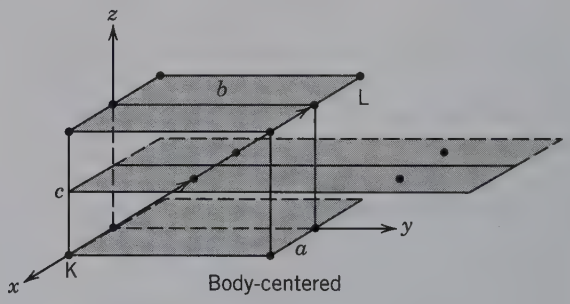

(6) Stacking of a primitive rectangular net along the direction between nodes K and L results in an orthorhombic lattice with a central node. This is an *orthorhombic body-centered lattice.*

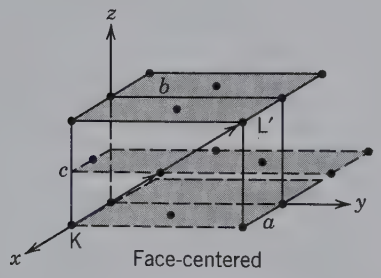

(7) Stacking of a centered rectangular net along the direction between nodes K and L′ (on the front face) leads to centering on all faces of the three-dimensional lattice. This is a *face-centered orthorhombic lattice.*

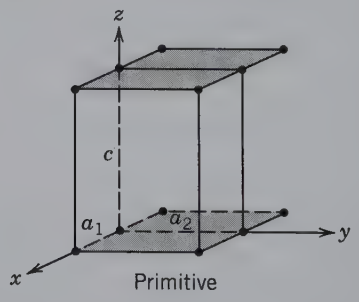

(8) Stacking of a square net along the z direction, with angle $x \wedge z = 90°$, and with the c translation $\neq a_1$ or a_2, results in a *primitive tetragonal lattice.*

FIG. 7.16 Stacking of the five nets (plane lattices; Fig. 7.5) in various ways in the third-dimension (as specifically noted below each illustration) leads to the 14 possible space lattices. *a*, *b*, and *c* represent unit cell dimensions along *x*, *y*, and *z* axes, respectively. These 14 lattice types are also known as the 14 Bravais lattices (see also Fig. 7.17).

(*continued*)

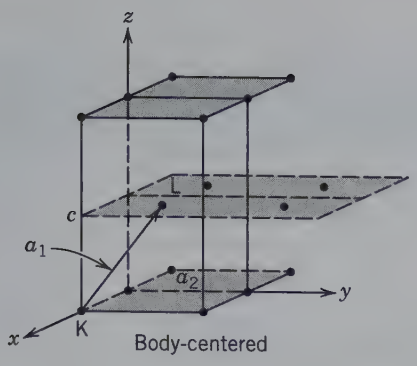

Body-centered

(9) Stacking of the same net as in (8) but now in a direction between nodes K and L results in a *body-centered tetragonal lattice.*

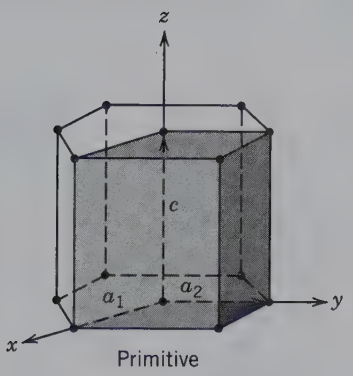

Primitive

(10) Stacking of a hexagonal net in a z direction such that angle $x \wedge z = 90°$, leads to a primitive hexagonal lattice. If this lattice choice is rotated three times about z, it results in a *c-centered hexagonal lattice.*

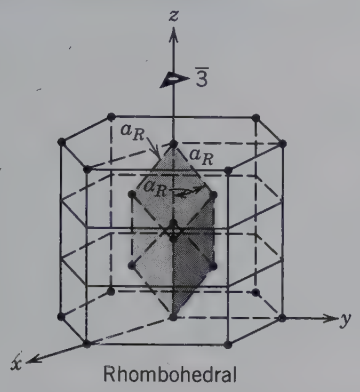

Rhombohedral

(11) A hexagonal net can also be stacked along the edge directions of a rhombohedron (a_R). This results in a *rhombohedral lattice,* the edge directions of which are symmetrical with respect to the $\bar{3}$ axis along the z direction.

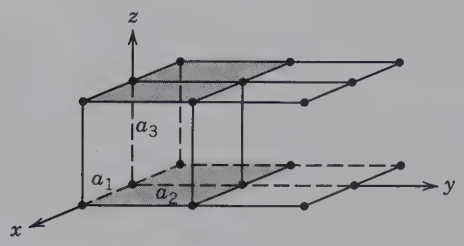

Primitive

(12) Stacking of a square net along the z direction with $x \wedge z$ angle = 90° and with c translation = a_1, and a_2, results in a *primitive isometric lattice.*

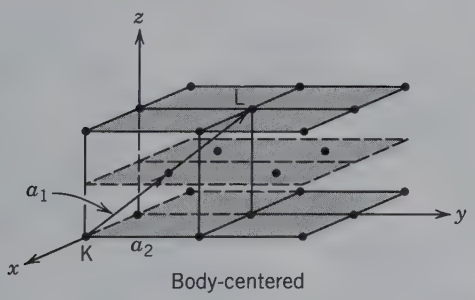

Body-centered

(13) Stacking of a square net along the direction between nodes K and L (a body diagonal) results in a *body-centered isometric lattice.*

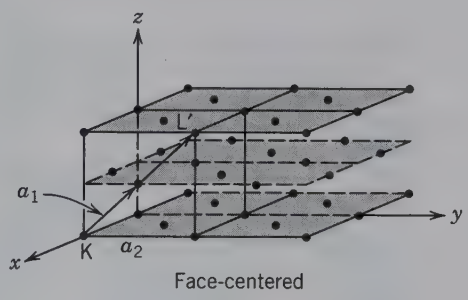

Face-centered

(14) Stacking of a square net along the direction between nodes K and L′ (along the front face), results in a *face-centered isometric lattice.*

FIG. 7.16 (*continued*)

The multiplicity of the cell (Table 7.2) differentiates the *primitive* and *nonprimitive* lattice choices. Recall that a primitive lattice has nodes only at the corners. Each corner node is shared between eight adjoining cells in 3D. For such a primitive lattice, there are eight corner nodes, of which 1/8th of each node contributes to the cell. That is, the unit cell has a multiplicity of $8 \times 1/8 = 1$. In a face-centered cell, each node on a face is shared between two adjoining cells. Therefore, the total node content of a side-centered cell is $8 \times 1/8 = 1$ (for corner nodes) + $2 \times \frac{1}{2} = 1$ (for face-centered nodes), resulting in a multiplicity of $1 + 1 = 2$. Any node in the interior of a cell, as in a body-centered choice, belongs only to its own cell. (See also the illustration that opens Chapter 4.)

In minerals, the shape and size of unit cells are most commonly determined by X-ray diffraction techniques (see Chapter 14). High-resolution transmission electron microscopy (HRTEM) is one analytical method that allows for the *direct observation* of

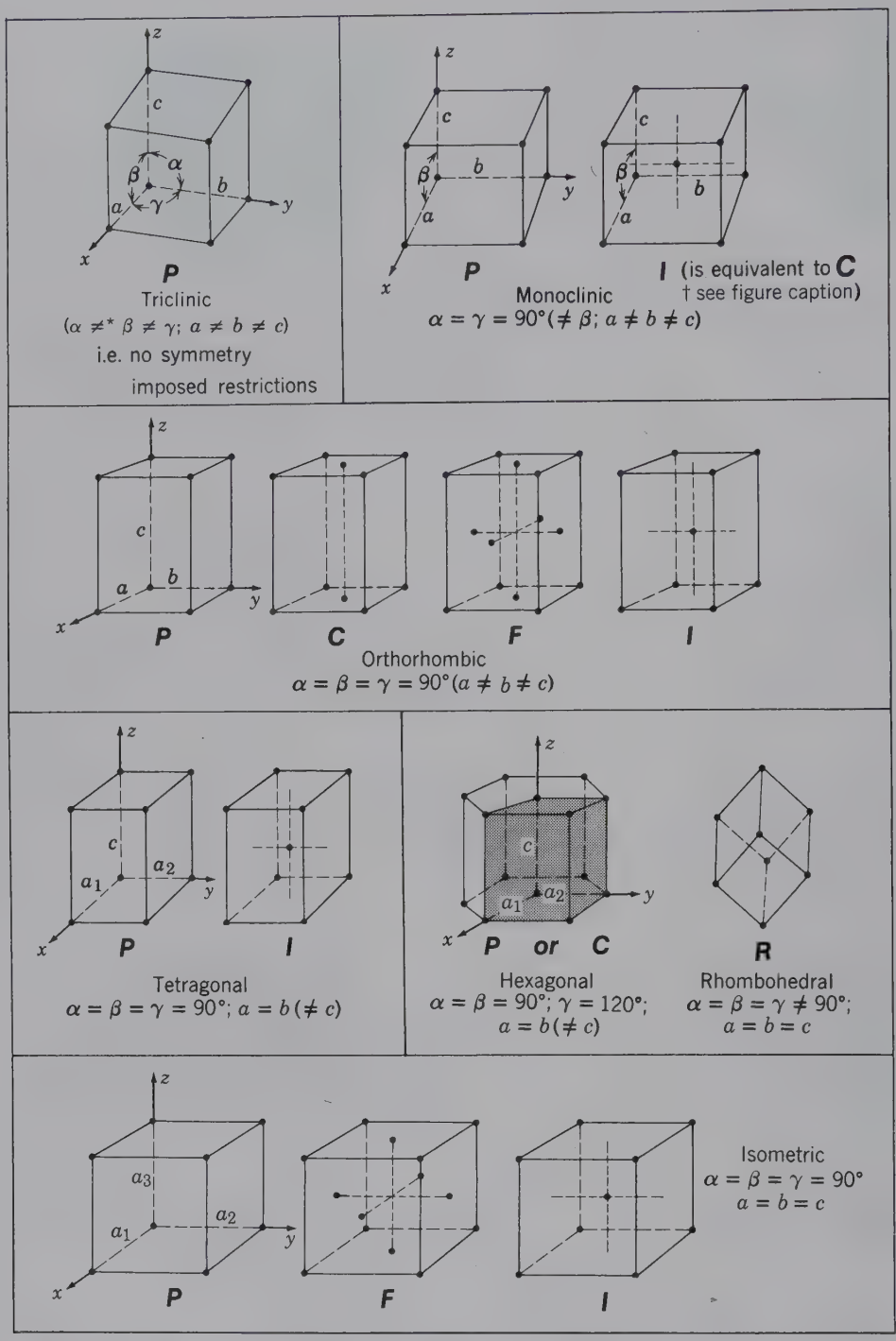

FIG. 7.17 The 14 unique types of space lattices, known as the Bravais lattices, arranged according to the crystal system. Axial lengths are indicated by *a*, *b*, and *c* and axial angles by α, β, and γ. Each lattice type has its own symmetry constraints on lengths of edges *a*, *b*, and *c* and angles between edges, α, β, and γ. In the notations, the nonequivalence of angles or edges that usually exist, but is not mandatory, is set off by parentheses.

*The sign ≠ implies nonequality by reason of symmetry; accidental equality may occur.

†In the monoclinic system, the unit cell can be described by a body-centered (*I*) or a *C* face–centered cell by a change in choice of the length of the *a* axis and the angle β. Vectorially these relations are: $a_I = c_C + a_C$; $b_I = b_C$; $c_I = -c_C$; and $\sin\beta_I = a_C \sin\beta_C$. Subscripts *I* and *C* refer to the unit cell types.

Table 7.2 Description of Space Lattice Types and Distribution of the 14 Bravais Lattices among the Six Crystal Systems

Name and Symbol	Location of Nonorigin Nodes	Multiplicity of Cell
Primitive (*P*)	.....	1
Side-centered (*A*)	Centered on A face (100)	2
(*B*)	Centered on B face (010)	2
(*C*)	Centered on C face (001)	2
Face-centered (*F*)	Centered on all faces	4
Body-centered (*I*)	An extra lattice point at the center of the cell	2
Rhombohedral (*R*)	A primitive rhombohedral cell	1

Primitive (*P*) in each of the six crystal systems	= 6
Body-centered (*I*) in monoclinic, orthorhombic, tetragonal, and isometric	= 4
Side-centered (*A* = *B* = *C*) in orthorhombic	= 1
Face-centered (*F*) in orthorhombic and isometric	= 2
Rhombohedral (*R*) in hexagonal	= 1
	Total = 14

projected images of crystal structures on photographic plates. Such a structure image is shown in Fig. 7.18 for the mineral cordierite. The dark parts of the photograph are areas of high electron density that outline the projected image of the structure and display the periodicity of the structure. The superimposed rectangle shows the *a* and *b* dimensions of the unit cell of cordierite.

A quantitative three-dimensional reconstruction of the location of the atoms (or ions), the chemical bond types and their orientations, and the overall internal symmetry of the structure is generally acquired by a

FIG. 7.18 High magnification structure image of an *a*–*b* section through the mineral cordierite, $(Mg, Fe)_2Al_4Si_5O_{18}{\cdot}nH_2O$. The rectangular *a*–*b* base of an orthorhombic unit cell is outlined and distances are given in angstroms. The insert shows the idealized structure of cordierite, as determined by X-ray diffraction techniques. The rings that appear in both images have a composition of $(Si,Al)_6O_{18}$. The scales of the idealized structure and the electron transmission image are identical. (From Buseck and Iijima. 1974. *American Mineralogist* 59: 1–22).

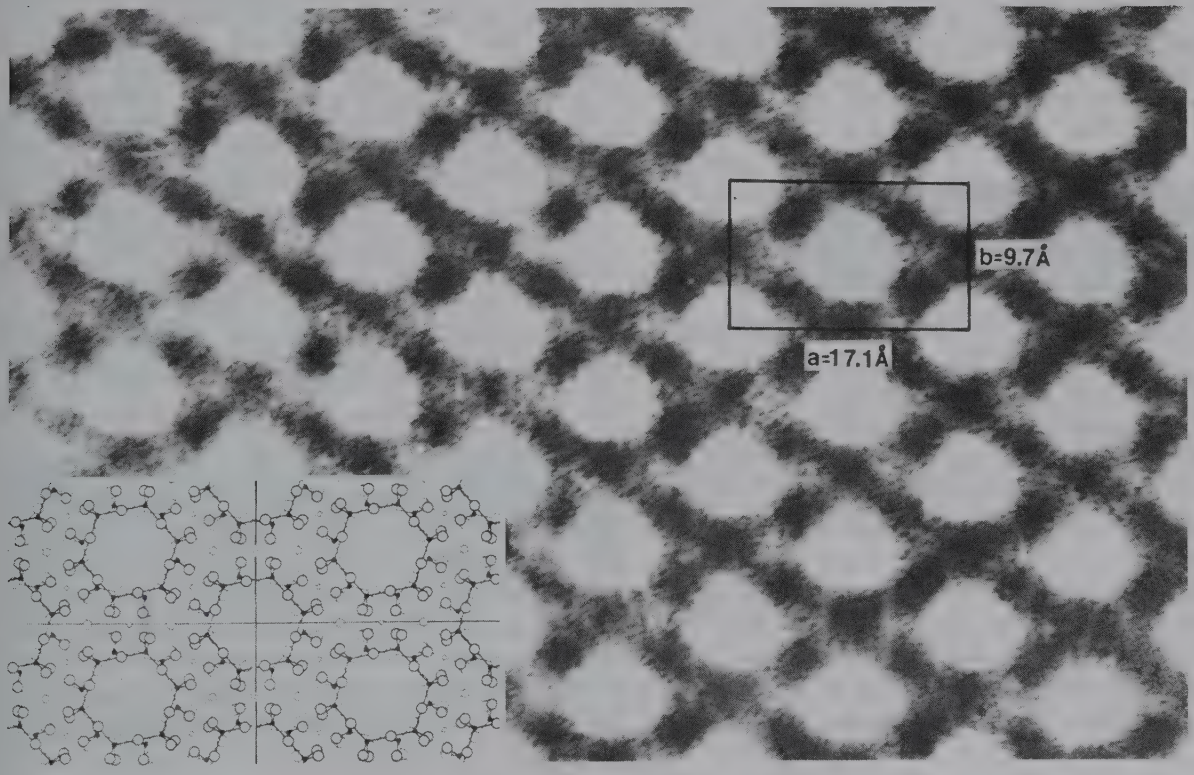

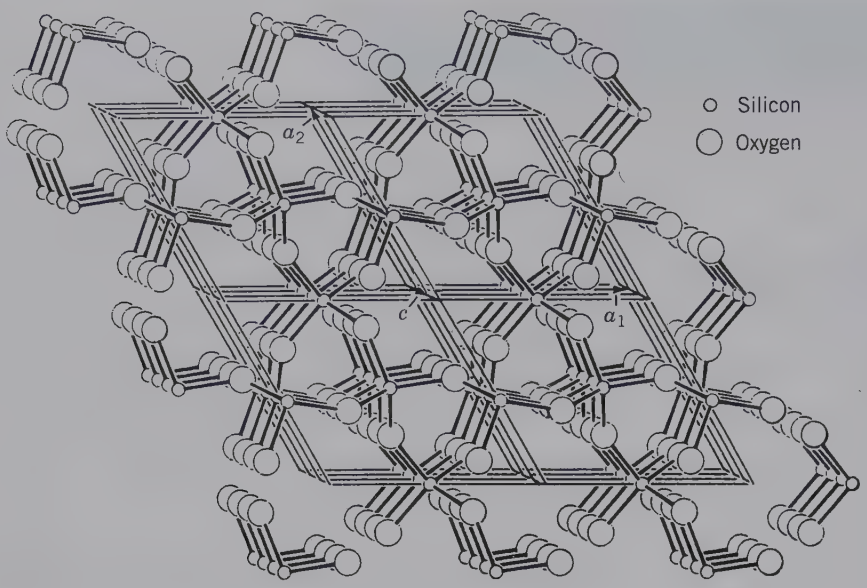

FIG. 7.19 A drawing of the structure of low (α) quartz, SiO_2, with the normally vertical *c* axis tilted at a small angle to better show the repeat distance *c* (of the unit cell) in this direction. The primitive hexagonal space lattice, outlined by the various parallelepipeds, shows that each unit cell (with edges a_1, a_2, and *c*) contains a complete and representative unit of the repeating pattern of the structure. (From Boisen, M. G. and G. V. Gibbs. 1990, *Mathematical Crystallography.* rev. ed. *Reviews in mineralogy* 15. Mineralogical Society of America, Washington, D.C.)

combination of X-ray, neutron, and electron diffraction techniques, and may be supplemented by a combination of spectroscopic methods (see Chapter 14). These methods, used singly or in combination, provide the structural information from which the appropriate three-dimensional (space) lattice can be derived. Figure 7.19 illustrates the appropriate lattice type and unit cell for the structure of low (α) quartz, SiO_2. This illustration also shows that the equivalent points in a lattice are generally not atomic positions. Rather, as in Fig. 7.19, they are geometric points in the structure that have the same angle and distance relationships to the Si and O atoms (and hence to the three-fold and two-fold axes of the structure).

SYMMETRY ELEMENTS IN 3D THAT INVOLVE TRANSLATION: SCREW AXES AND GLIDE PLANES

In our prior discussion of ordered three-dimensional arrays, as in the ordered structures of minerals, the focus has been on three non-coplanar vectorial directions of the lattice with specific spacings along them (these are commonly referred to as the *periodicity* of the structure). Now, those symmetry elements that combine a symmetry operation with translation, must also be considered.

The combination of a rotational operation with translation (*t*) parallel to the axis of rotation produces a **screw operation**. The combination of a mirror reflection with a translation component (*t*/2 or *t*/4) parallel to the mirror, results in a **glide operation**. The corresponding symmetry elements are **screw axes** and **glide planes**. (Animations of screw axis and glide operations are given in module III of the CD-ROM under the heading "3-Dimensional Order: Screw Axes and Glide Planes.")

Several screw axes are possible because the two-, three-, four-, and six-fold rotational operations can all be combined with a translation. (A one-fold rotation axis combined with a translation is equivalent to a translation only.) Rotation alone, through an angle (α) about an imaginary axis, generates a sequence of motifs along a circle. For a 90° rotation angle, a pattern with four motifs is generated, as shown in Fig. 7.20. In a four-fold *screw operation*, the three additional motifs are generated from the original motif in a three-dimensional, helical path (as in a screw motion; Fig. 7.20b). This means that four-fold screw operations rotate the motif through 90° angles while translating the motif parallel to the axis of rotation. Screw axes are said to be *isogonal* (from the Greek word meaning "same angle") with the equivalent rotational axes. All possible screw axes, isogonal with rotational axes, are illustrated in Fig. 7.21.

The screw axis symbols consist of the symbols for rotation axes (2, 3, 4, and 6) followed by a subscript that, which when inverted, represents the fraction of the translation (*t*) inherent in the operation (Table 7.3). For example, 2_1 means that $\frac{1}{2}\ t$ is the translation distance involved (where $\frac{1}{2}$ is obtained by placing the subscript over the main axis symbol, to derive the fraction). For a three-fold rotation, there are two possible screw axes, 3_1 and 3_2. The translation component in both screw axes is $1/3t$ but a convention allows for the

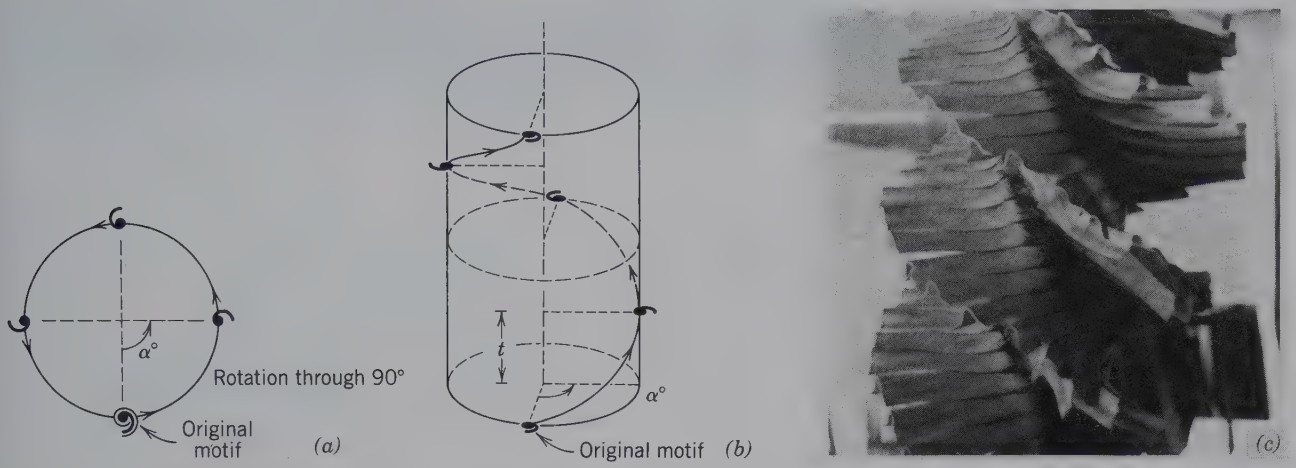

FIG. 7.20 Generation of patterns by four-fold rotation (a) and a combination of translation and rotation (b), which results in a screw motion (4_1). (c) Example of a many-fold screw axis in the vertical direction of a palm. The screw operation is shown by the trimmed remains of the leaves. The rotational symmetry is approximately 30. (Photographed by C. Klein in Darwin, Northern Territory, Australia.) As discussed on page 115, independent objects can have unlimited rotational symmetry, whereas such symmetry is limited to 1, 2, 3, 4, and 6 in ordered arrays.

distinction between the directions of the screw. When the ratio of the subscript to the number of the rotation axis (as 1/3 for 3_1) is less than $\frac{1}{2}$, the screw is considered to be *right-handed*. A right-handed screw is defined as one that advances away from the observer when rotated clockwise. When this ratio is more than $\frac{1}{2}$, it is *left-handed* (as in 3_2), and when the ratio is $\frac{1}{2}$ the screw is considered *neutral* in direction (the motif ends up at the same place irrespective of which direction rotation occurs; Fig. 7.21.) In other words, 3_1 and 3_2 are an *enantiomorphous pair of screw axes*, with 3_1 right-handed and 3_2 left-handed. Similarly, the following pairs are enantiomorphous: 4_1 and 4_3, 6_1 and 6_5, and 6_2 and 6_4 (Table 7.3). See Chapter 9 for further discussion of the representation of screw axes.

A regular pattern can also be generated by a combination of a mirror reflection and a translation ($m + t$). This is referred to as a **glide operation** or *glide reflection* (as shown in Figure 7.12c). In planar patterns (Figs. 7.13b and c), a glide line relates motifs on either side of the line with a periodicity of half the lattice translation.

Table 7.3 Nomenclature for Symmetry Operations Involving Translation

Name	Translational Symmetry Operations	Hermann–Mauguin Notation
Screw Axis	Rotation + Translation	2_1; 3_1, 3_2*; 4_1, 4_3; 4_2; 6_1, 6_5; 6_2, 6_4; 6_3
Glide Plane	Reflection + Translation	*a, b, c, d, n*

*Enantiomorphic pairs are grouped together.

In three-dimensional patterns, a wider variety of glide movements can occur and these are represented by **glide planes**. Recall that the internal order, as well as external morphology of crystals, is referenced to three axes, *a*, *b*, and *c* (Chapter 6). The *c* axis is vertical and the *a* and *b* axes lie in a plane that does not contain *c*. Specific glide directions can be identified in two- and three-dimensional patterns and expressed in terms of these axes. If the glide component ($t/2$) in a three-dimensional ordered arrangement is parallel to the *a* axis, it is referred to as an *a glide* and is represented by the symbol *a*. Similarly, if the glide component ($t/2$) is parallel to the *b* or *c* axes, the glide is referred to as a *b* or *c glide*, respectively. If the glide component is represented by $a/2 + b/2$, $a/2 + c/2$, $b/2 + c/2$, or $a/2 + b/2 + c/2$, it is referred to as a *diagonal glide* and is represented by the symbol *n*. If the glide component is represented by $a/4 + b/4$, $b/4 + c/4$, $a/4 + c/4$, or $a/4 + b/4 + c/4$, it is known as a *diamond glide* and is symbolized by the letter *d* (see Table 7.3). In the *diamond* (*d*) *glide*, the simultaneous translations are one-fourth of the cell edges, whereas for a *diagonal* (*n*) *glide* the translation components are equal to one-half of the cell edges. See Chapter 9 for further discussion of the representation of various glide operations.

SPACE GROUPS

All of the symmetry and translational operations that may be present in the internal ordered arrangement of a crystal have now been introduced. When the 14 possible

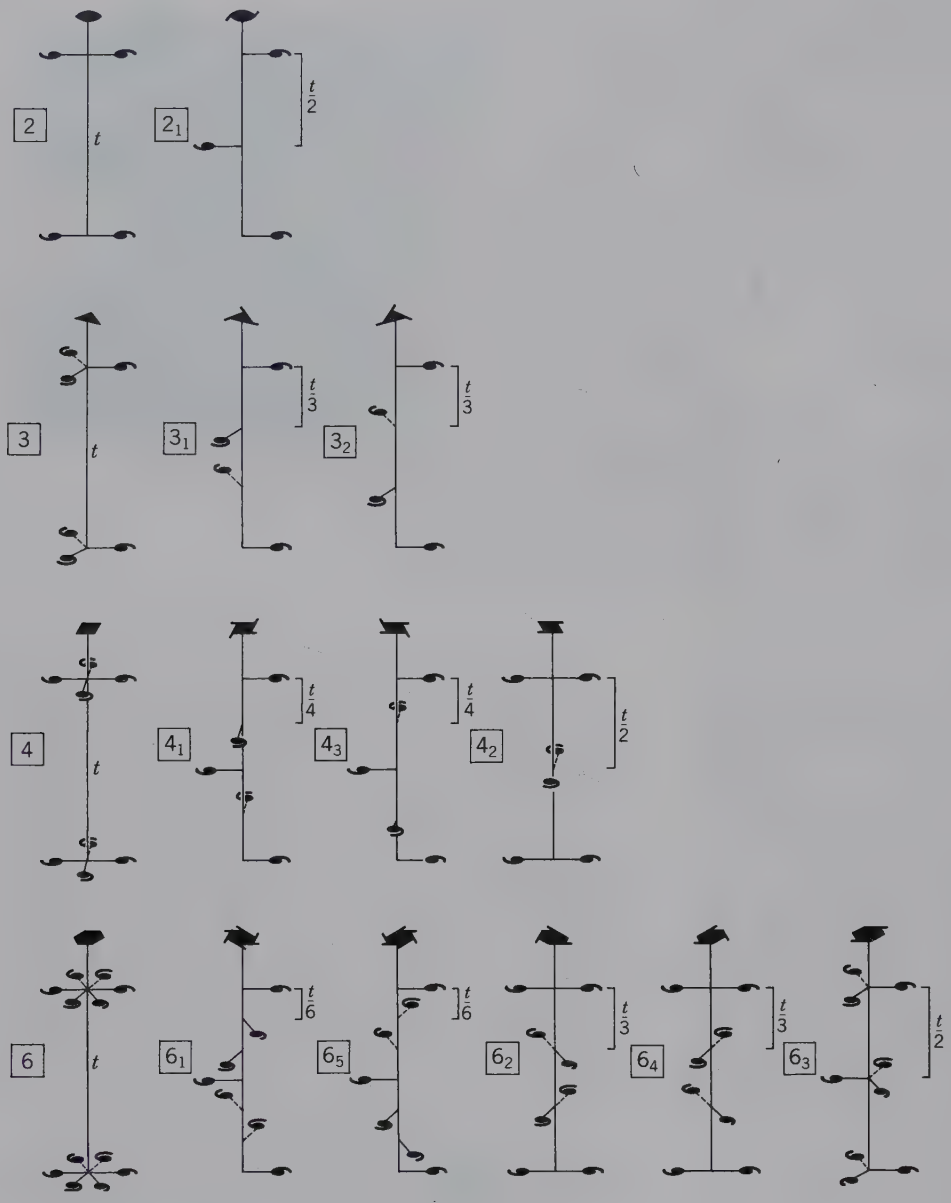

FIG. 7.21 Repetition of motif units by screw axes for four different rotational symmetries. The left column represents rotation axes, and the columns to the right represent isogonal screw axes. The symbols at the top of the rotation and screw axes are internationally accepted. For projections of these screw operations, see Fig. 9.40.

space lattice types (Bravais lattices) are combined with the symmetry inherent in the 32 crystal classes (the translation-free point groups), as well as the two symmetry operations that involve translation (screws and glides), the concept of **space groups** results. *Space groups represent the various ways in which motifs* (such as atoms in crystals) *can be arranged in space in a homogeneous array* (that is, each motif is equivalent to every other motif in the pattern). Surprisingly, there are only *230 space groups* (Table 7.4). The translation-free symmetry combinations are *point groups*, whereas *space groups* define symmetry and translations in space. If the translation components in the 230 space groups are ignored, the 32 point groups (as shown in Table 7.4) result.

In the late 1800s, three men of different nationalities and interests independently derived the number of unique patterns that could occur in three-dimensional periodic arrays. These were E. von Federov, a Russian crystallographer, Artur Schoenflies, a German mathematician, and William Barlow, a British amateur mineralogist. Their unanimous conclusion was that there are 230 such unique three-dimensional arrays; these are known as *230 space groups*.

Space groups have the following characteristics. (1) They are based on 1 of the 14 Bravais lattices that is compatible with a specific point group, and (2) they are isogonal with 1 of the 32 point groups. That is, the rotation (e.g., 6) and screw axes (e.g., 6_1, 6_5) have the same

Table 7.4 The 230 Space Groups, and the Isogonal 32 Crystal Classes (Point Groups). The Space Group Symbols Are, in general, Unabbreviated*

Crystal Class	Space Group
1	*P*1
$\bar{1}$	*P*$\bar{1}$
2	*P*2, *P*2$_1$, *C*2
m	*Pm*, *Pc*, *Cm*, *Cc*
2/*m*	*P*2/*m*, *P*2$_1$/*m*, *C*2/*m*, *P*2/*c*, *P*2$_1$/*c*, *C*2/*c*
222	*P*222, *P*222$_1$, *P*2$_1$2$_1$2, *P*2$_1$2$_1$2$_1$, *C*222$_1$, *C*222, *F*222, *I*222, *I*2$_1$2$_1$2$_1$
*mm*2	*Pmm*2, *Pmc*2$_1$, *Pcc*2, *Pma*2, *Pca*2$_1$, *Pnc*2, *Pmn*2$_1$, *Pba*2, *Pna*2$_1$, *Pnn*2, *Cmm*2, *Cmc*2$_1$, *Ccc*2, *Amm*2, *Abm*2, *Ama*2, *Aba*2, *Fmm*c, *Fdd*2, *Imm*2, *Iba*2, *Ima*2
2/*m*2/*m*2/*m*	*P*2/*m*2/*m*2/*m*, *P*2/*n*2/*n*2/*n*, *P*2/*c*2/*c*2/*m*, *P*2/*b*2/*a*2/*n*, *P*2$_1$/*m*2/*m*2/*a*, *P*2/*n*2$_1$/*n*2/*a*, *P*2/*m*2/*n*2$_1$/*a*, *P*2$_1$/*c*2/*c*2/*a*, *P*2$_1$/*b*2$_1$/*a*2/*m*, *P*2$_1$/*c*2$_1$/*c*2/*n*, *P*2/*b*2$_1$/*c*2$_1$/*m*, *P*2$_1$/*n*2$_1$/*n*2/*m*, *P*2$_1$/*m*2$_1$/*m*2/*n*, *P*2$_1$/*b*2/*c*2$_1$/*n*, *P*2$_1$/*b*2$_1$/*c*2$_1$/*a*, *P*2$_1$/*n*2$_1$/*m*2$_1$/*a*, *C*2/*m*2/*c*2/*m*, *C*2/*m*2/*c*2$_1$/*a*, *C*2/*m*2/*m*2/*m*, *C*2/*c*2/*c*2/*m*, *C*2/*m*2/*m*2/*a*, *C*2/*c*2/*c*2/*a*, *F*2/*m*2/*m*2/m, *F*2/*d*2/*d*2/*d*, *I*2/*m*2/*m*2/*m*, *I*2/*b*2/*a*2/*m*, 12/*b*2/*c*2/*a*, *I*2/*m*2/*m*2/*a*
4	*P*4, *P*4$_1$, *P*4$_2$, *P*4$_3$, *I*4, *I*4$_1$
$\bar{4}$	*P*$\bar{4}$, *I*$\bar{4}$
4/*m*	*P*4/*m*, *P*4$_2$/*m*, *P*4/*n*, *P*4$_2$/*n*, *I*4/*m*, *I*4$_1$/*a*
422	*P*422, *P*42$_1$2, *P*4$_1$22, *P*4$_1$2$_1$2, *P*4$_2$22, *P*4$_2$2$_1$2, *P*4$_3$22, *P*4$_3$2$_1$2, *I*422, *I*4$_1$22
4/*mm*	*P*4/*mm*, *P*4*bm*, *P*4$_2$*cm*, *P*4$_2$*nm*, *P*4*cc*, *P*4*nc*, *P*4$_2$*mc*, *P*4$_2$*bc*, *I*4*mm*, *I*4*cm*, *I*4$_1$*md*, *I*4$_1$*cd*
$\bar{4}$2*m*	*P*$\bar{4}$2*m*, *P*$\bar{4}$2*c*, *P*$\bar{4}$2$_1$*m*, *P*$\bar{4}$2$_1$*c*, *P*$\bar{4}$*m*2, *P*$\bar{4}$*c*2, *P*$\bar{4}$*b*2, *P*$\bar{4}$*n*2, *I*$\bar{4}$*m*2, *I*$\bar{4}$*c*2, *I*$\bar{4}$2*m*, *I*$\bar{4}$2*d*
4/*m*2/*m*2/*m*	*P*4/*m*2/*m*2/*m*, *P*4/*m*2/*c*2/*c*, *P*4/*n*2/*b*2/*m*, *P*4/*n*2/*n*2/*c*, *P*4/*m*2$_1$/*b*2/*m*, *P*4/*m*2$_1$/*n*2/*c*, *P*4/*n*2$_1$/*m*2/*m*, *P*4/*n*2$_1$/*c*2/*c*, *P*4$_1$/*m*2/*m*2/*c*, *P*4$_2$/*m*2/*c*2/*m*, *P*4$_2$/*n*2/*b*2/*c*, *P*4$_2$/*n*2/*n*2/*m*, *P*4$_2$/*m*2$_1$/*b*2/*c*, *P*4$_2$/*m*2$_1$/*n*2/*m*, *P*4$_1$/*n*2$_1$/*m*2/*c*, *P*4$_2$/*n*2$_1$/*c*2/*m*, *I*4/*m*2/*m*2/*m*, *I*4/*m*2/*c*2/*m*, *I*4$_1$/*a*2/*m*2/*d*, *I*4$_1$/*a*2/*c*2/*d*
3	*P*3, *P*3$_1$, *P*3$_2$, *R*3
$\bar{3}$	*P*$\bar{3}$, *R*$\bar{3}$
32	*P*312, *P*321, *P*3$_1$12, *P*3$_1$21, *P*3$_2$12, *P*3$_2$21, *R*32
3*m*	*P*3*m*1, *P*31*m*, *P*3*c*1, *P*31*c*, *R*3*m*, *R*3*c*
$\bar{3}$2/*m*	*P*$\bar{3}$1*m*, *P*$\bar{3}$1*c*, *P*$\bar{3}$*m*1, *P*$\bar{3}$*c*1, *R*$\bar{3}$*m*, *R*$\bar{3}$*c*
6	*P*6, *P*6$_1$, *P*6$_5$, *P*6$_2$, *P*6$_4$, *P*6$_3$
$\bar{6}$	*P*$\bar{6}$
6/*m*	*P*6/*m*, *P*6$_3$/*m*
622	*P*622, *P*6$_1$22, *P*6$_5$22, *P*6$_2$22, *P*6$_4$22, *P*6$_3$22
6*mm*	*P*6*mm*, *P*6*cc*, *P*6$_3$*cm*, *P*6$_3$*mc*
$\bar{6}$*m*2	*P*$\bar{6}$*m*2, *P*$\bar{6}$*c*2, *P*$\bar{6}$2*m*, *P*$\bar{6}$2*c*
6/*m*2/*m*2/*m*	*P*6/*m*2/*m*2/*m*, *P*6/*m*2/*c*2/*c*, *P*6$_3$/*m*2/*c*2/*m*, *P*6$_2$/*m*2/*m*2/*c*
23	*P*23, *F*23, *I*23, *P*2$_1$3, *I*2$_1$3
2/*m*$\bar{3}$	*P*2/*m*$\bar{3}$, *P*2/*n*$\bar{3}$, *F*2/*m*$\bar{3}$, *F*2/*d*$\bar{3}$, *I*2/*m*$\bar{3}$, *P*2$_1$/*a*$\bar{3}$, *I*2$_1$/*a*$\bar{3}$
432	*P*432, *P*4$_2$32, *F*432, *F*4$_1$32, *I*432, *P*4$_3$32, *P*4$_1$32, *I*4$_1$32
$\bar{4}$3*m*	*P*$\bar{4}$3*m*, *F*$\bar{4}$3*m*, *I*$\bar{4}$3*m*, *P*$\bar{4}$3*n*, *F*$\bar{4}$3*c*, *I*$\bar{4}$3*d*
4/*m*$\bar{3}$2/*m*	*P*4/*m*$\bar{3}$2/*m*, *P*4/*n*$\bar{3}$2/*n*, *P*4$_2$/*m*$\bar{3}$2/*n*, *P*4$_2$/*n*$\bar{3}$2/*m*, *F*4/*m*$\bar{3}$2/*m*, *F*4/*m*$\bar{3}$2/*c*, *F*4$_1$/*d*$\bar{3}$2/*m*, *F*4$_1$/*d*$\bar{3}$2/*c*, *I*4/*m*$\bar{3}$2/*m*, *I*4$_1$/*a*$\bar{3}$2/*d*

*From *International Tables for Crystallography*. 1983. v. A. T. Han, ed: *Space group symmetry*. International Union of Crystallography, Reidel Publ. Co., Boston, USA.

rotational angle (that is, 60° in a six-fold rotation or six-fold screw axis). This means that the screw axes 6_1, 6_2, 6_3, 6_4, and 6_5 are isogonal with the rotation axis 6. In other words, *the point group is the translation-free residue of a family of possible isogonal space groups*.

Symbols used for specific space groups are similar to those for point groups (discussed in Chapter 6) but with added translational components. A specific point group designation (translation-free) consists of a series of symmetry elements, as in 2/*m* 2/*m* 2/*m* (see Chapter 6). For each of the specific point group symmetry elements, there is a possible space group element. That is, instead of a mirror plane perpendicular to the first two-fold rotation axis and a mirror plane perpendicular to the second two-fold rotation axis, there may be glide planes in their places. If so, the mirror plane symbol (*m*) would be replaced by the symbol for the appropriate glide, such as 2/*b* 2/*a* 2/*m*. If there are screw axes present, the symbol for each screw axis would replace the corresponding translation-free rotational axis, such as $2_1/b$ $2_1/c$ $2_1/a$. Additionally, the space group symbol is preceded by a symbol that designates the general lattice type (*P*, *A*, *B*, *C*, *I*, *F*, or *R*). The full symbol for a space group that is isogonal with 2/*m* 2/*m* 2/*m* might be *I* 2/*b* 2/*a* 2/*m*. Another example of a space group isogonal with 2/*m* 2/*m* 2/*m* would be $P2_1/b\ 2_1/c\ 2_1/a$. This group contains screw axes with $\frac{1}{2}\,t$ in place of the two-fold rotation axes (for all isogonal groups for 2/*m* 2/*m* 2/*m* see Table 7.4).

By glancing at Table 7.4, one can see easily the isogonality between the column "Crystal Class" and the corresponding column "Space Group." This also illustrates the ease with which a space group symbol can be reduced to its isogonal point group (crystal class). Simply remove the translational components from the space group, and the point group becomes obvious. Lattice type, screw axes, and glide planes all contain translational elements. If these translational elements are removed and the translation-free equivalent operations are substituted for them, the point group, which is isogonal with the space group, will result. For example, the last space group in Table 7.4 is listed as $I4_1/a\bar{3}2/d$. Because lattice types are not reflected in translation-free symbols for crystal classes (point groups), the lattice type must be dropped. The remaining symbols must become translation-free as well. This means that *a* and *d* glides must be replaced by the translation-free mirrors, *m*. If screw axes are present, a similar process allows easy conversion from space group to point group. For the above space group, the screw axis (4_1) is replaced by the isogonal four-fold rotation axis (4). This leads to the point group notation $4/m\bar{3}2/m$ in the isometric system. The relationship between point and space group symmetries is one of the powerful aspects of the Hermann–Mauguin or (international) notation. It allows for the easy replacement of the space group notation into its isogonal and simpler point group notation. It should be remembered that *the presence of translations (as in lattices, or glide planes, or screw axes) cannot be detected morphologically because the translations involved are on the order of 1 to 10 Å.* (Various aspects of space groups are illustrated with animations in module III of the CD-ROM under the heading "3-Dimensional Order: Space Group Elements in Structures.")

In some cases, crystallographers use what are known as *abbreviated symbols*. In our discussion of point groups, the complete symbol, such as $2/m2/m2/m$ and $4/m2/m2/m$, is used. The abbreviated symbolism for these two point groups would be *mmm* and $4/mmm$, respectively (see also Table 9.1). The reason for the $2/m2/m2/m$ abbreviation is the understanding that the three mutually perpendicular mirror planes intersect each other along two-fold axes (see Chapter 6). Similar reasoning explains the abbreviation $4/mmm$. For reasons of clarity, only complete *point group symbols* are used. Abbreviated symbols are generally used in the literature. For example, a mineral with point group $4/m\bar{3}2/m$ may have its space group reported as $Fm3m$, because the presence of four-fold and two-fold rotation axes is implied. Such abbreviated symbols for space group notation are used in the five chapters on systematic mineralogy.

Another system of space group notation may be encountered in the literature, especially in older texts. This is known as the *Schoenflies notation*. Because this notation does not logically follow from the Hermann–Mauguin symbols, it is not developed here. References at the end of this chapter will enable you to find the Schoenflies system.

REFERENCES AND FURTHER READING

Bloss, F. D. 1994. *Crystallography and crystal chemistry: An introduction.* Reprint of the original text of 1971 by the Mineralogical Society of America, Washington, D.C.

Boisen, M. B., Jr., and G. V. Gibbs. 1990. Mathematical crystallography. *Reviews in Mineralogy* 15. Mineralogical Society of America, Washington, D. C.

Bragg, W. L., and G. F. Claringbull. 1965. *Crystal structures of minerals.* Cornell University Press, Ithaca, New York.

Brisse, F. 1981. La Symétrie bidimensionelle et le Canada. *Canadian Mineralogist* 19: 217–24 (all illustrations are in color).

Buseck, P. R. 1997. From 2D to 3D: I. Escher drawings, crystallography, crystal chemistry and crystal "defects." In *Teaching mineralogy.* Ed. J. Brady, D. Mogk, and D. Perkins, 213-228. Mineralogical Society of America, Washington D.C.

Escher, M. C. 1968. *The graphic works of M. C. Escher.* Hawthorn Books, New York.

Grunbaum, B. and G.C. Shephard. 1987. *Tilings and patterns.* W. H. Freeman and Company, New York, N.Y.

International Tables for Crystallography. 1983. Vol. A, *Space group symmetry.* Edited by T. Hahn. International Union of Crystallography, D. Reidel Publishing Company, Boston.

International Tables for X-ray Crystallography. 1969. Vol. 1, *Symmetry groups.* Edited by N. F. M. Henry and K. Lonsdale. International Union of Crystallography, Kynoch Press, Birmingham, England.

Klein, C. 2008. *Minerals and rocks: Exercises in crystal and mineral chemistry, crystallography, X-ray powder diffraction, mineral and rock identification, and ore mineralogy.* 3rd ed. Wiley, New York.

MacGillavry, C. H. 1976. *Fantasy and symmetry: The periodic drawings of M. C. Escher.* Harry N. Abrams, New York.

Phillips, F. C. 1971. *An introduction to crystallography.* Wiley, New York.

Schattschneider, D. 2004. *M. C. Escher: Visions of symmetry.* 2nd Ed. W. H. Freeman, New York.

Shubnikov, A. V., and V. A. Koptsik. 1974. *Symmetry in science and art.* Plenum Press, New York.

Stevens, P. S. 1991. *Handbook of regular patterns: An introduction to symmetry in two dimensions.* MIT Press, Cambridge, Massachusetts.

Selected Web Resources:

http://marie.epfl.ch/escher
http://www.kaagaard.dk/illusion/escher/escher.htm

CHAPTER 8

Crystal Projections

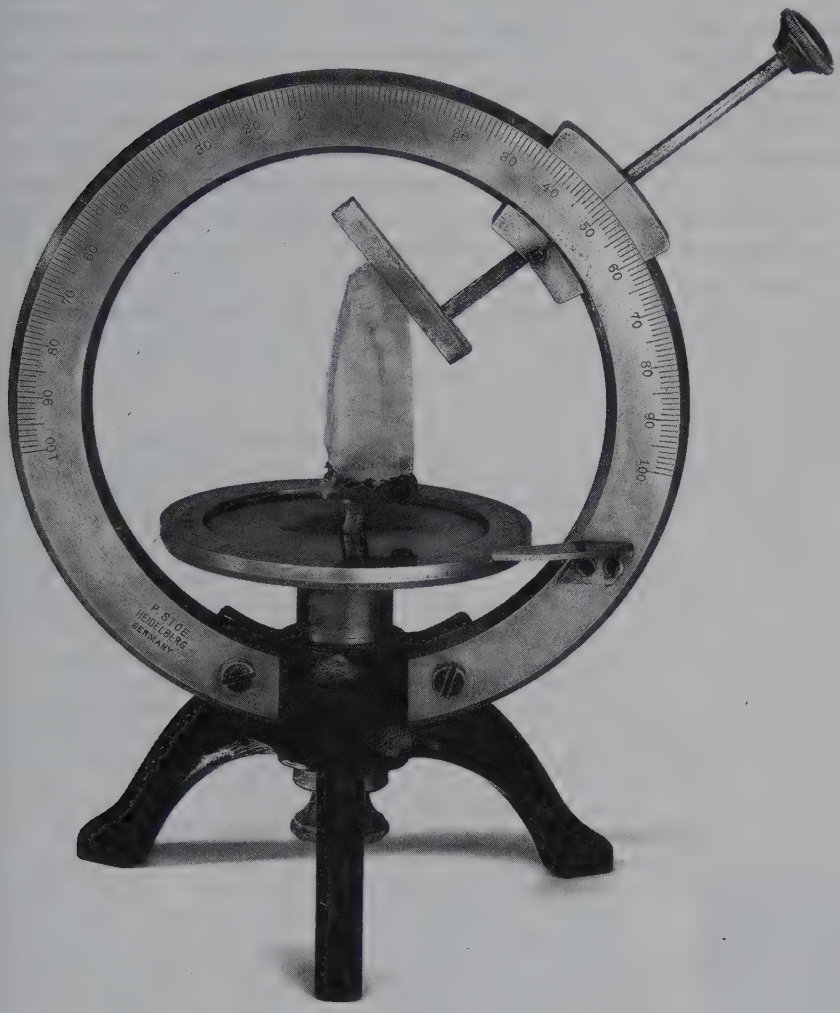

Antique, two-circle contact goniometer based on the 1896 design of Victor Goldschmidt. The horizontal circle allows for the measurement of ϕ angles, and the vertical circle of ρ angles. The crystal is quartz.

Crystals are three-dimensional objects that may exhibit a variety of symmetry elements in different parts of the crystal. Although drawings of crystals are used to display such features, one cannot manipulate these two-dimensional images to observe the crystals and their symmetry from another direction. Instead, crystallographic projections are used. These ingenious methods allow the complete symmetry of a three-dimensional crystal, and its point group, to be displayed in two-dimensions—without losing information. This chapter develops a widely used projection technique (i.e., stereographic projection) that allows for the graphical representation of point group symmetry, together with information about the distribution of faces (specifically face poles) on a crystal. These techniques also allow for the quantitative measurement of geometric aspects of crystals.

The crystal drawings used throughout this text are known as **clinographic projections**. They are a type of perspective drawing that yields a portrait-like picture of the crystal in two dimensions. This is the best means to convey the appearance of a crystal and generally serves much better for this purpose than a photograph.

A **crystal projection** is a much more quantitative method of representing a three-dimensional crystal on a two-dimensional planar surface. Different projections are used for different purposes, but each has some definite rules so that the projection bears a known and reproducible relationship to the crystal. A series of steps are presented that develop these projections to show how they can be used to represent the symmetry of crystals. These then allow for detailed graphical images of point groups.

SPHERICAL PROJECTION

Steno's law (see Chapter 6) states that "the angles between equivalent faces of the same substance are constant," regardless of whether the crystal faces are misshapen or ideal. Such angles are measured between the normals (perpendiculars) to the crystal faces. A graphical representation of these angles and the normals to the crystal faces will reveal the symmetry of the crystal and, consequently, its crystal class. Therefore, the size and shape of the various faces on a crystal are *not* important in the evaluation of its symmetry content. To evaluate the angular relationships, a **spherical projection** is first developed (Fig. 8.1).

Position a crystal with well-formed faces at the center of a sphere. Construct perpendiculars (poles) to

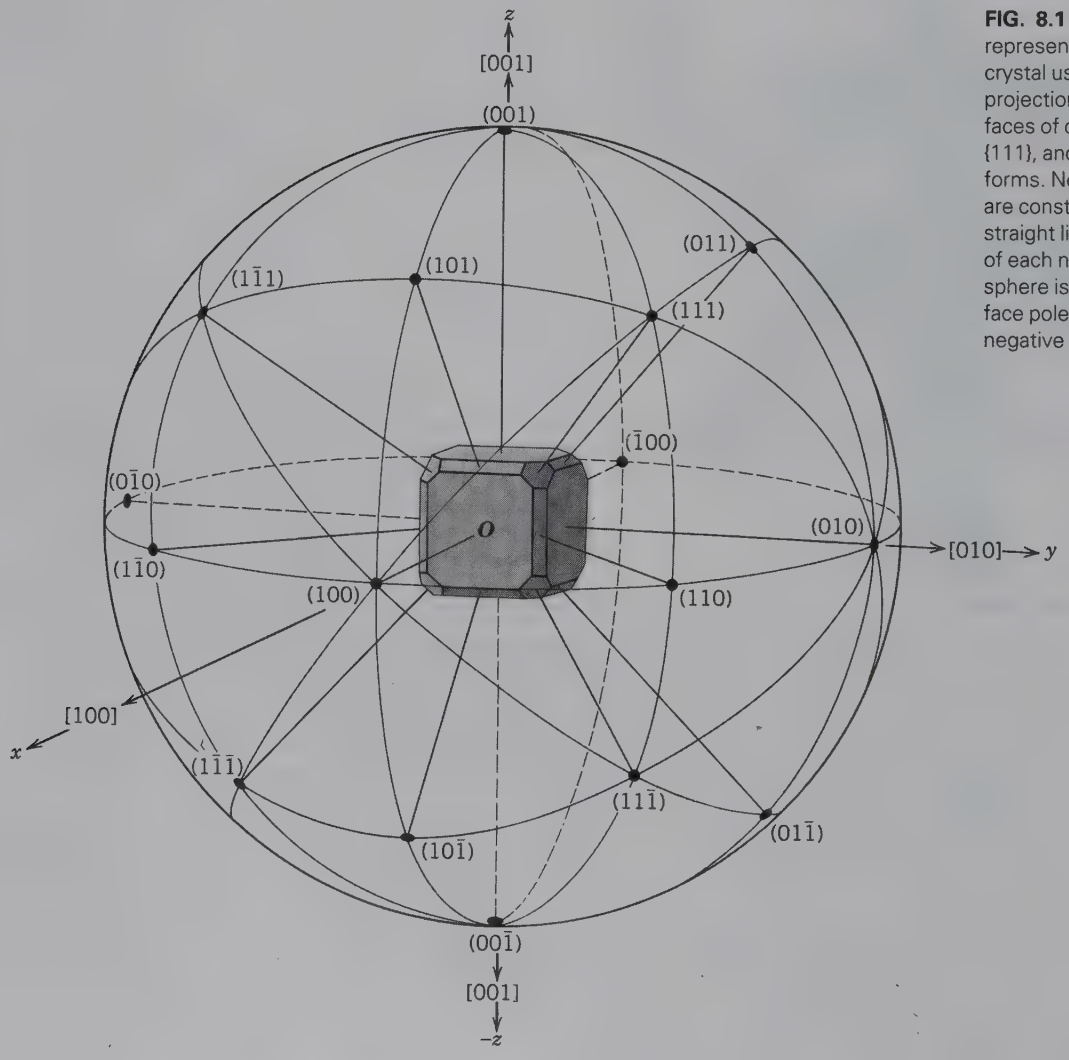

FIG. 8.1 Graphical representation of an isometric crystal using a spherical projection. This crystal displays faces of cubic {001}, octahedral {111}, and dodecahedral {011} forms. Normals to these faces are constructed and shown as straight lines. The intersection of each normal with the outer sphere is the location of the face pole. Dashed lines indicate negative crystal directions.

these faces so that they pierce the surrounding sphere (Fig. 8.1). These pierce points are the **face poles**. To visualize this, place a hollow crystal model, with well-formed faces, containing an intense point source of light, at the center of the sphere. This is shown for an isometric crystal in Fig. 8.1. A pinhole in each of the crystal faces will allow rays of light to emerge from the hole in a direction perpendicular to each face. These rays are shown as lines perpendicular to the faces in Fig. 8.1. These rays of light will fall on the inner surface of the sphere and mark bright spots. This resembles a planetarium in which the crystal model, with its internal light source and pinholes, is the projector, and the translucent sphere is the dome. When the position of each light spot on the sphere (shown as black dots in Fig. 8.1) is marked, the model may be removed but a permanent record of the *poles* to its faces is maintained. This is shown for the large cube faces {001}, the octahedral faces {111}, and the dodecahedral faces {011}. Each face pole is labeled by the Miller indices (*hkl*) for the crystal face. This is the *spherical projection*.

The position of each pole and its angular relationship to other poles is described using angular coordinates on the sphere. This is done by defining a coordinate system with north and south poles (N and S) and with an arbitrary point of origin on the equator (E). The location of any point on the sphere is specified by two spherical angular coordinates: a **polar angle**, ρ, measured from the north pole, and an **azimuth**, ϕ, measured from an east-west direction. These angular coordinates are similar to the location of points on the Earth's surface by longitude and latitude. For example, the angular coordinates 74°00′ west longitude, 40°45′ north latitude, locate a point in New York City (Fig. 8.2). This means that the angle, measured at the center of the Earth, between the plane of the equator and a line from the center of the Earth through that point in New York, is exactly 40°45′; and the angle between the Greenwich meridian and the meridian passing through the point in New York, measured west in the plane of the equator, is exactly 74°00′. These relations are shown in Fig. 8.2.

There is one major difference between locating points on a spherical projection and locating points on the Earth's surface. On Earth, the latitude is measured in degrees north or south from the equator, whereas

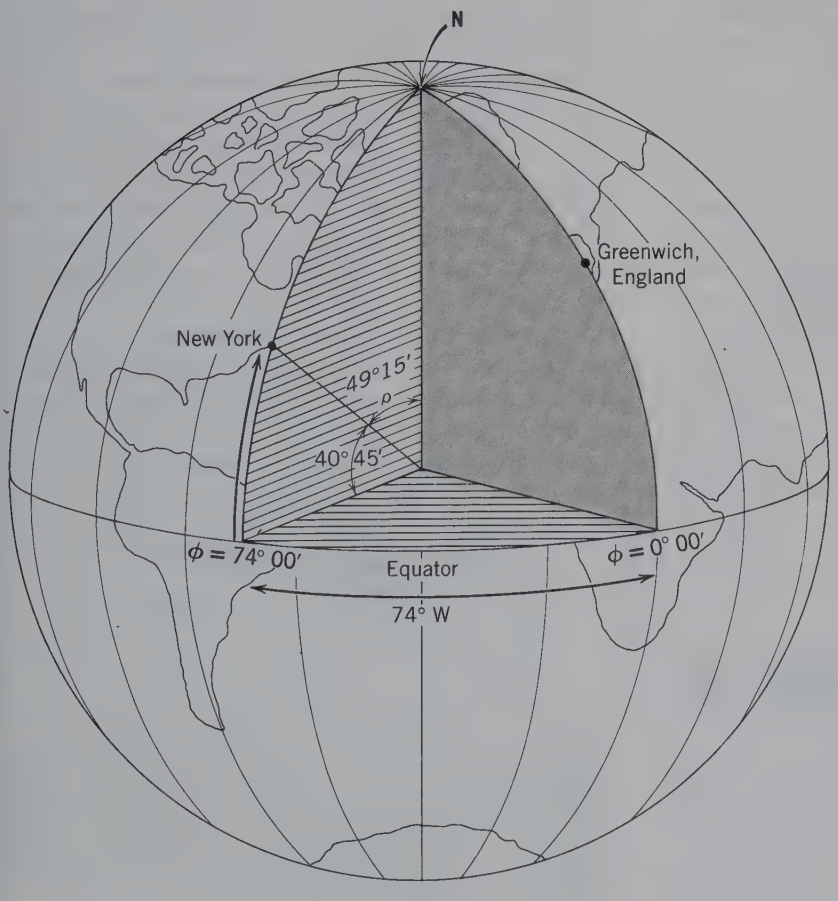

FIG. 8.2 Latitude and longitude as measured for New York City.

the *polar angle*, ρ, is measured in degrees from the *north pole*. The piercing point of a pole perpendicular to a top face, (001), on a crystal has a polar angle, ρ = 0°. Piercing points from vertical faces lie on the equator at ρ = 90°. Using this system, the ρ of New York City is 49°15′.

The *crystal longitude* (*azimuth*, ϕ) of a face pole in a spherical projection is measured in degrees up to 180°, clockwise and counterclockwise from a starting meridian, analogous to that of the Greenwich meridian of geography. To locate this starting meridian, the crystal is oriented with the (010) face (or *b* axis) to the right of the crystal. The meridian passing through the pole of this face is taken as zero. To determine the crystal longitude of any other crystal face, a meridian is passed through the pole of that face, and the angle between it and the zero meridian is measured in the plane of the equator. This angle, the *azimuth*, is designated by the Greek letter ϕ . With these two angular measurements (ϕ and ρ), a point is uniquely defined.

An additional feature of this projection allows for the assessment of geometric relationships between crystal faces. If any plane is passed through a sphere, it will intersect the surface of the sphere in a circle. The circles of maximum diameter are those formed by planes passing through the center and having a diameter equal to the diameter of the sphere. These are called **great circles**. In Fig. 8.1, all circles shown are great circles as all include the center of the sphere. All other circles formed by passing planes through the sphere are **small circles**. The meridians on the Earth are great circles, as is the equator. In contrast, the parallels of latitude are small circles.

To determine which crystal faces belong to a **zone**, simply evaluate which face poles lie along the same great circle. *All of the faces that belong to a zone lie along the same great circle of the projection.* In Fig. 8.1 faces (001), (101), (100), (10$\bar{1}$) and (00$\bar{1}$) lie in a zone with the zone axis [010]. The zone axis is always perpendicular to the plane containing the face poles; thus, all vertical circles have horizontal zone axes. Because the great circle, along which the poles of these faces lie, passes through the north and south poles of the projection, it is called a *vertical great circle*.

STEREOGRAPHIC PROJECTION

Because of its three-dimensional nature, the spherical projection is, however, difficult to use. A more useful approach is to collapse the three-dimensional representation onto a two-dimensional planar surface such that the angular relations of the faces are preserved in such a way as to reveal the true symmetry. This is done with the **stereographic projection**.

The *stereographic* projection is the projection of half of the *spherical* projection, usually the northern hemisphere, onto the equatorial plane of the sphere (shaded plane in Fig. 8.3). The *primitive* circle (the circle outlining the projection) is the equator. The northern hemisphere with face poles and the equatorial plane with the same face poles are shown in Fig. 8.3. If one were to view the poles of crystal faces located in the northern hemisphere (of the spherical projection) with the eye at the south pole, the intersections of the lines of sight with the equatorial plane will generate the poles on the stereographic projection. Therefore, a stereographic projection is constructed by drawing lines from the south pole to the face poles in the northern hemisphere. The stereographic projection points, which correspond to face poles, are where these lines intersect the equatorial plane (as in Fig. 8.3). This allows for the display of angular relations on a convenient two-dimensional plane. (Various animations that illustrate the principles of stereographic projection are provided in module II of the CD-ROM under the heading "Stereographic Projection.")

In practice, one wants to plot poles directly on a stereographic projection. Therefore, it is necessary to determine stereographic distances in relation to angles of the spherical projection. To develop these angular relations, envisage a vertical plane through the sphere, as shown in Fig. 8.4. This is the "zero meridian," or the plane containing the pole of (010). The north (N) and south (S) poles are those of the spherical projection and *O* is the center of the projected crystal (as in Figs. 8.1 and 8.3). Consider the face (011) shown on the primitive circle. *OD* is the perpendicular to the face (011), and *D* is the pole of this face on the spherical projection. The line from the south pole, *SD*, intersects the plane of the equator, *FG*, at the point *D′*. This is the stereographic pole of (011). The angle *NOD* is the angle ρ. In order to plot *D′* directly on the stereographic projection, the distance *OD′* is needed in terms of angle ρ.

Because ΔSOD is an isosceles triangle, $\angle ODS = \angle OSD$.
$\angle \hat{O}DS + \angle OSD = \angle NOD = \rho$
Therefore, $\angle OSD = \rho/2$. $OS = r$, the radius of the primitive circle of the projection.
$\tan \rho/2 = OD'/r$ or $OD' = r \tan \rho/2$

Therefore, the distance in a stereographic projection from the center to the pole of any face, is the tangent of one-half of ρ of that face multiplied by the radius (*r*) of the projection (Fig. 8.5). The distance obtained will have whatever units are used to measure the radius of the primitive circle of the projection.

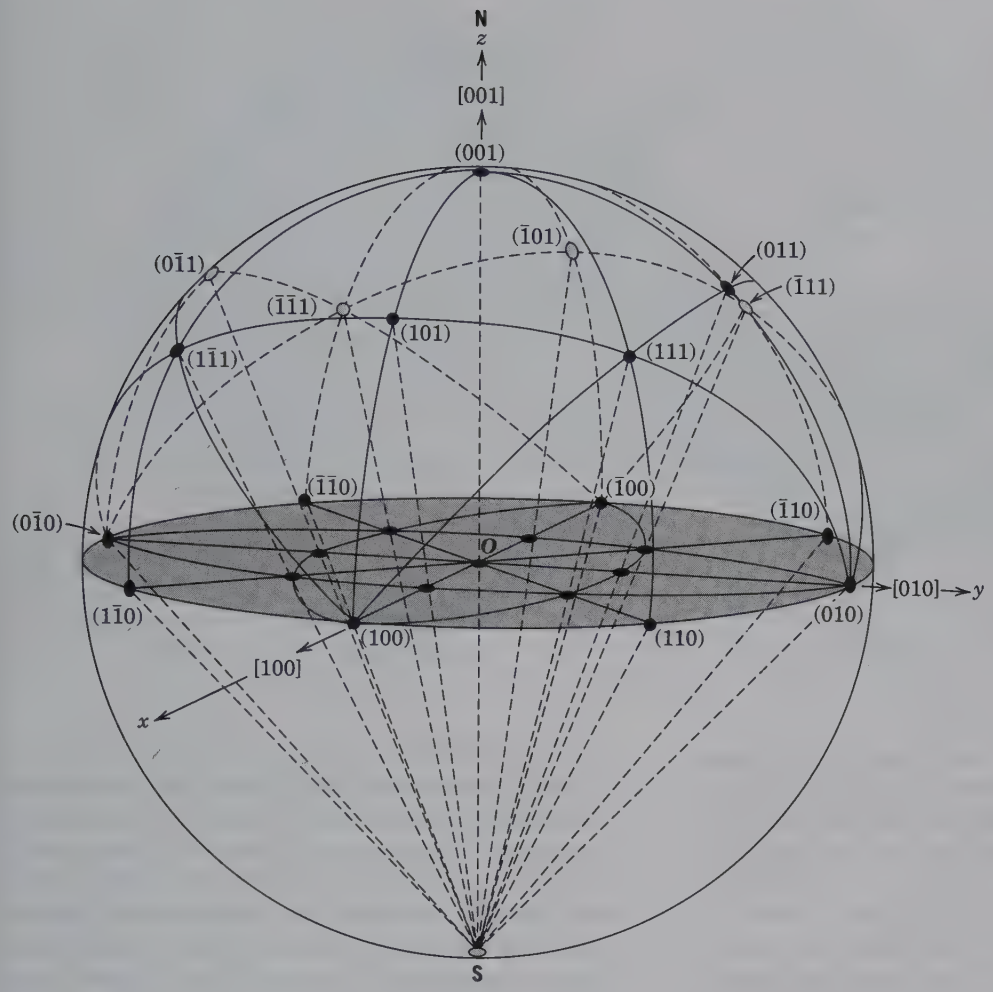

FIG. 8.3 Relationship of spherical and stereographic projections (for the crystal in Fig. 8.1). Face poles are shown only for the northern hemisphere with their corresponding piercing points projected down onto the stereographic projection—the shaded equatorial plane. *O* marks the center of the crystal as in Figs. 8.1 and 8.4. The dashed lines that connect the face poles to the south pole are used to locate their intersections with the equatorial plane. (After Wahlstrom, E. E. 1951. *Optical crystallography.* Wiley, New York.)

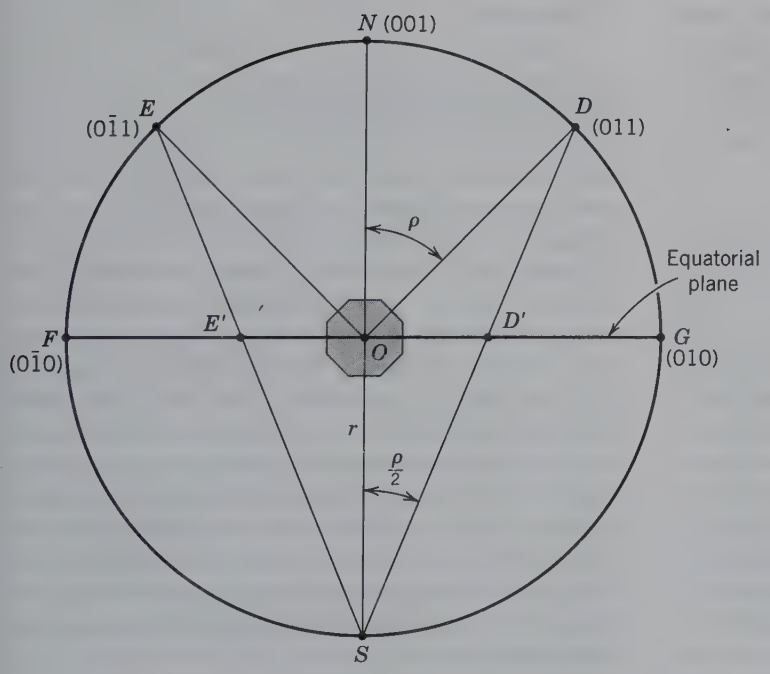

FIG. 8.4 Vertical section through the sphere of projection (as in Fig. 8.3) showing the relationship of spherical to stereographic poles. See the text for details.

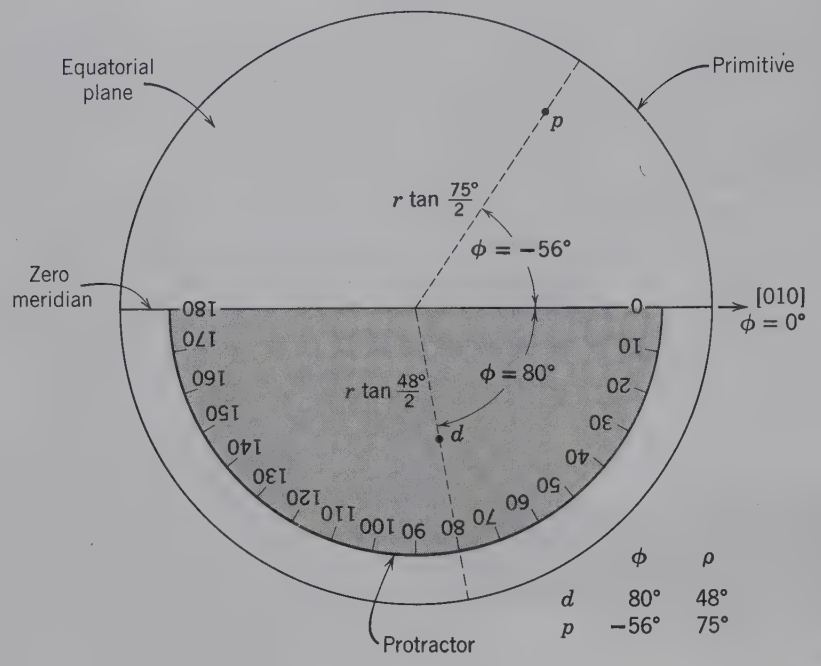

FIG. 8.5 Locating the ϕ and ρ angles of two poles for stereographic projection of crystal faces shown in Fig. 8.1. The "zero meridian" is the line bisecting the circle. The circle represents the shaded (equatorial) plane in Fig. 8.3.

It is also necessary to determine the pole's *longitude*, or ϕ angle. Because the angle is measured in the plane of the equator, which is also the plane of the stereographic projection, it can be marked off directly on the primitive circle by a circular protractor. First, fix the "zero meridian" by marking a point on the primitive circle to represent the pole of (010), and by drawing a straight line through this point and the center of the projection (Fig. 8.5). With the protractor edge along this line and the center point at the center of the projection, the ϕ angle is marked off. On a construction line, from the center of the projection through this point, lie all possible face poles having the specified ϕ angle. Positive ϕ angles are clockwise from (010); negative ϕ angles are counterclockwise, as shown in Fig. 8.5.

In order to plot the pole of a face with specific ϕ and ρ angles, it is further necessary to find the natural tangent of one-half of ρ, to multiply that by the radius (r) of the projection, and to mark the resulting distance along the ϕ line. Although any projection radius may be chosen, 10 cm is usually used. This is sufficiently large to give accuracy but not be unwieldy, and at the same time simplifies the calculation. With a 10-cm radius, it is only necessary to look up the natural tangent, move the decimal point one place to the right, and plot the result as centimeters from the center of the projection.

When the poles of crystal faces are plotted stereographically as explained previously, their symmetry relationships become apparent (Fig. 8.6). In the spherical projection, the loci of face poles lying in a crystal zone fall along a great circle. When projected stereographically, vertical great circles become diameters of the projection; all other great circles project as circular arcs that subtend the diameter. The limiting case of such great circles is the primitive of the projection, which is a great circle common to both the spherical and stereographic projections. The poles of vertical crystal faces lie on the primitive and, thus, are projected without angular distortion.

STEREOGRAPHIC NET AND THE MECHANICS OF PLOTTING

Both the measurement and plotting of angles on the stereographic projection are greatly simplified by using a template of the projected coordinate system; a **stereographic net**. This type of net is also called the Wulff net, named after G. V. Wulff, Russian crystallographer (1863–1925). Using this net, there is no need for a protractor or a calculator to plot points. The *stereographic net* is the result of a coordinate system on a sphere, with circles of equal longitude (great circles) and circles of equal latitude (small circles), having been projected onto a plane using the stereographic projection technique (as in Fig. 8.3). Both great and small circles are drawn on the net at intervals of 1° or 2°, as shown in Fig. 8.7. (This net has a radius of 5 cm and a net with radius of 10 cm is reproduced as an end paper at the back of this text.)

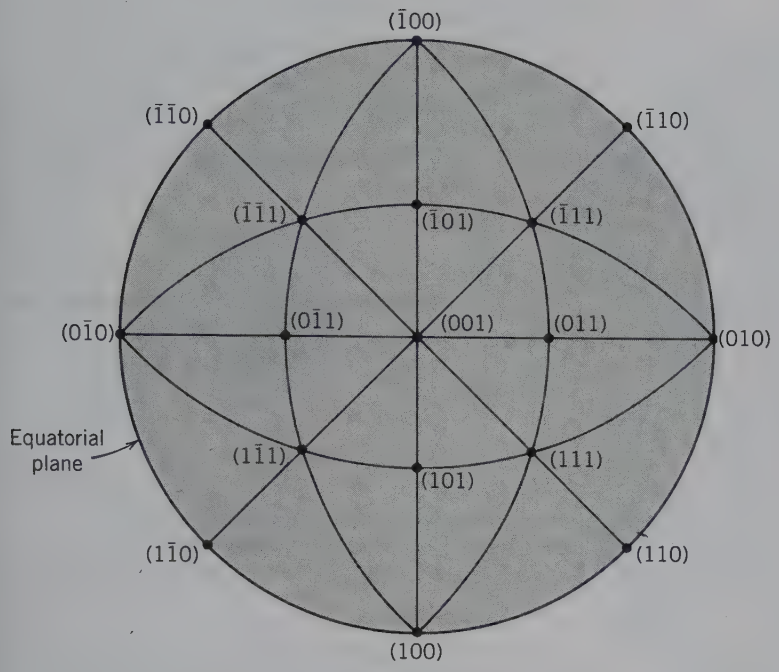

FIG. 8.6 Stereographic projection of crystal faces on an isometric crystal. This circular diagram is the same as the equatorial plane in Fig. 8.3. Extensive animations of the projection procedure are shown in module II of the CD-ROM under the heading "Crystallography: Stereographic Projection."

The basics of plotting on a stereonet are as follows. In practice, using a net with a 10-cm radius is most convenient. The 10-cm net at the back of this text can be photocopied and mounted on thin poster board to stabilize and preserve it. The actual points are typically plotted on a sheet of tracing paper over the net. Once mounted, the exact center of the net can be pierced from the back by a thumbtack. The sharp point of the thumbtack will function as the pivot about which the sheet of tracing paper, overlying the net, can be rotated (Fig. 8.8a). The user should trace the outer (primitive) circle onto the overlay and should also mark the E–W and N–S directions. The eastern end of the E–W line should be marked $\phi = 0°$, the southern end of the N–S line as $\phi = 90°$, and the northern end of this same line as $\phi = -90°$ (Fig. 8.8a). This allows the ϕ angles to be plotted directly along the primitive circle in a clockwise (+) or counterclockwise (−) direction.

The angle ρ can be located directly along the two vertical great circles, the N–S and E–W directions that intersect in the center of the projection. Only along these two directions are the divisions available for the direct plotting of ρ angles. The ρ angle of any face that projects at the center of the projection (at the location of the thumbtack) is equal to 0°. Any face that lies on the outside perimeter of the primitive circle has a $\rho = 90°$. Therefore, any ρ angle between 0° and 90° is plotted outward from the center of the projection along the E–W or N–S directions. If a combination of ϕ and ρ angles is such that the ϕ angle is neither 0° nor 90°, and the ρ is also neither 0° nor 90°, the transparent overlay must be rotated about the center until the ϕ direction of the specific plane coincides with either the N–S or E–W direction. Only then can the ρ angle of that plane be plotted.

For example, a crystal face has $\phi = 30°$ and $\rho = 60°$. Place the overlay such that it is aligned with the N–S and E–W directions (Fig. 8.8a). Because $\phi = 30°$, it is positive and the angle can be counted off in a clockwise direction 30° from the E–W line. Mark this point by a short line at $\phi = 30°$ on the circumference, the location of the ϕ angle of the pole to that plane (Fig. 8.8b). To determine the position of ρ, rotate the $\phi = 30°$ mark to be coincident with the E–W or N–S lines. Count 60° outward from the center of the stereonet along the coincident line; the $\rho = 60°$ is plotted directly using the graduations available on the underlying stereographic net (Fig. 8.8c). This is the location of the pole of a face with $\phi = 30°$, $\rho = 60°$.

Measuring Crystal Angles

Instead of measuring ϕ and ρ angles, one usually measures interfacial angles. To obtain a careful angular measurement, *goniometers* are used. For accurate work, a *reflecting goniometer* is required (see Fig. 1.13d for an antique example). A crystal mounted on this instrument can be rotated about a zone axis and will reflect a collimated beam of light from its faces through a telescope to the eye. The angle through which a crystal must be turned, in order to throw successive beams of

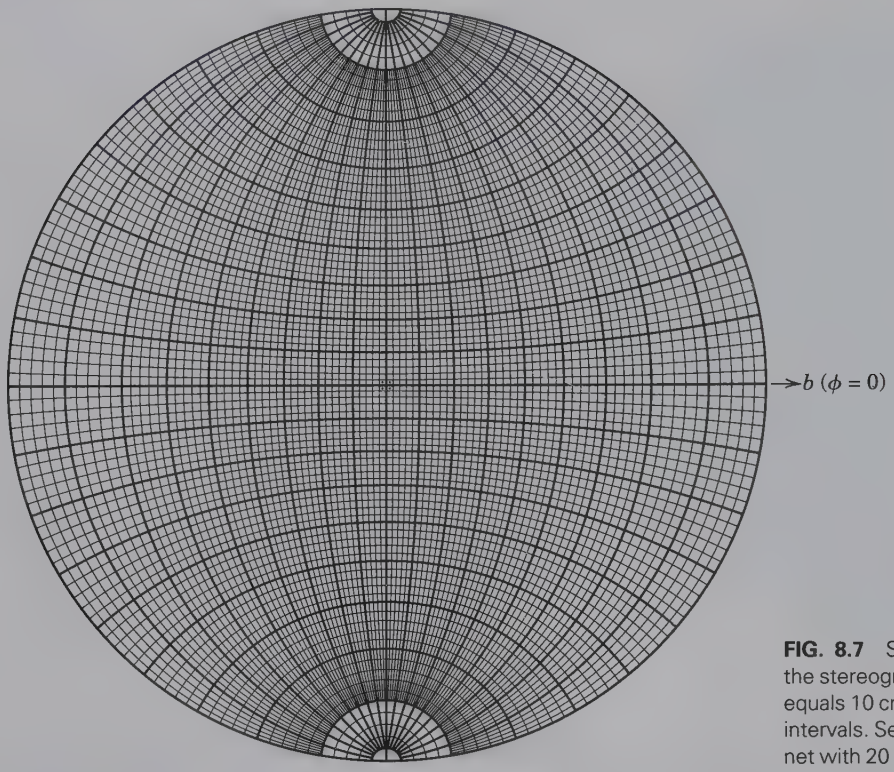

FIG. 8.7 Stereographic (Wulff) net used to simplify the stereographic plotting of crystal faces. Radius equals 10 cm with great and small circles at 2° intervals. See the back of this text for a stereographic net with 20 cm radius.

FIG. 8.8 (a) Illustration of the use of a stereographic net when mounted on a thin board, pierced in its center by a thumbtack from the back, and overlain by transparent paper. The primitive circle, as well as the locations of $\phi = 0°$, $\phi = 90°$, and $\phi = -90°$, must always be marked on the transparent overlay prior to plotting, to maintain proper orientation. (b) To project the pole of a plane with $\phi = 30°$ and $\rho = 60°$, the angle $\phi = 30°$ is plotted (x) on the primitive in a clockwise direction from $\phi = 0°$. (c) The direction of $\phi = 30°$ has been rotated to coincide with the E–W direction and the angle $\rho = 60°$ can be measured directly along the vertical great circle. The black dot is the pole of the crystal face with $\phi = 30°$, $\rho = 60°$.

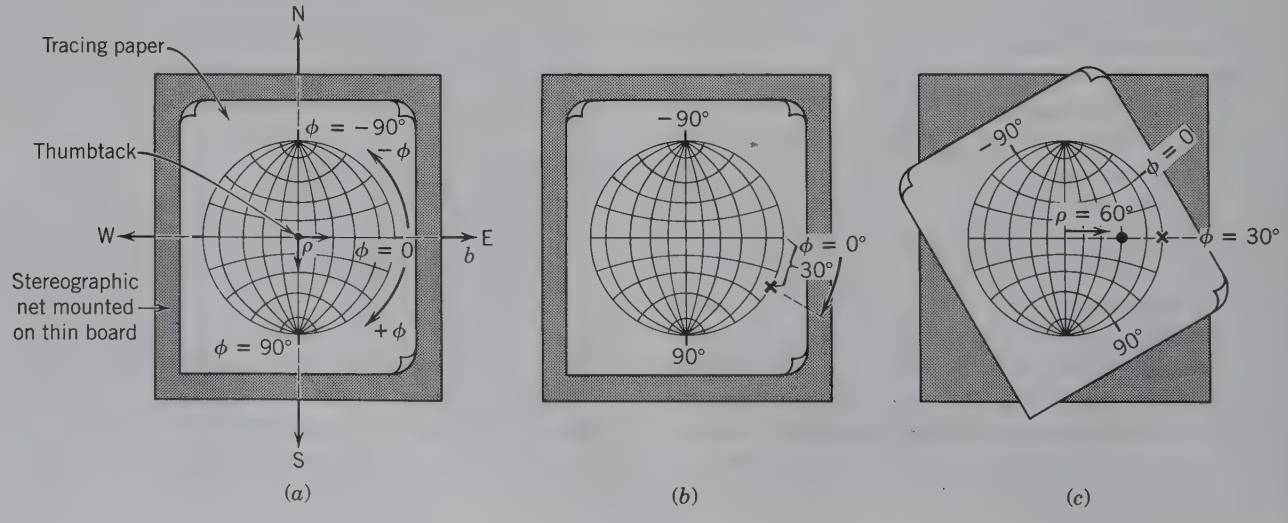

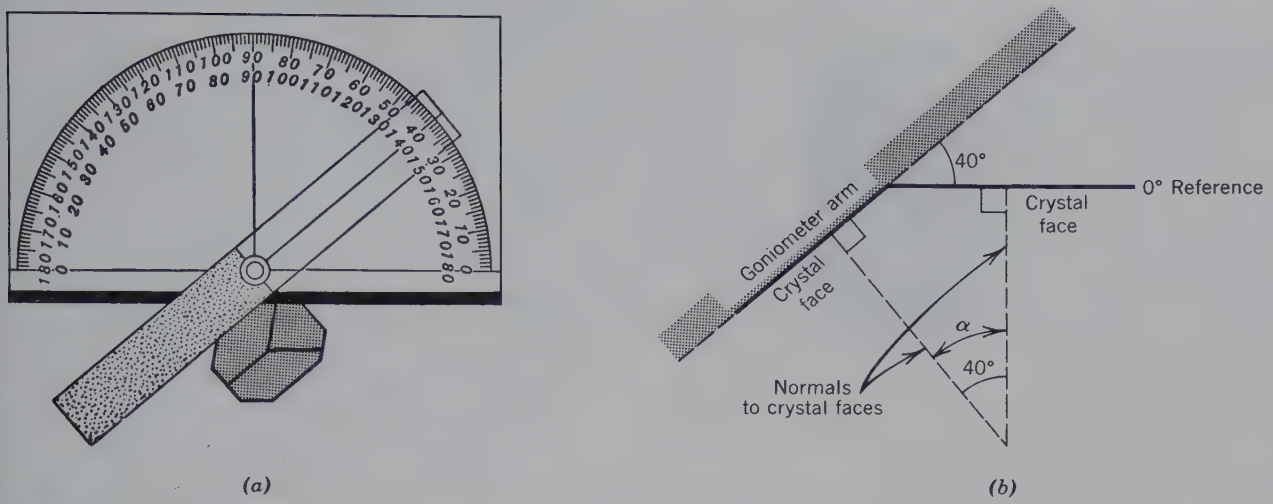

FIG. 8.9 Contact goniometer for measuring angles between crystal faces on hand specimen–sized crystals. (b) Schematic enlargement of (a) showing the measurement of the internal angle α, which would be ϕ or ρ depending on the orientation of the goniometer with respect to the crystal.

light from two adjacent faces into the telescope, determines the angle between the faces. A simpler instrument, used for approximate work and with larger crystals, is the *contact goniometer* (Fig. 8.9a). In using a contact goniometer, it is imperative that the plane determined by the two arms of the goniometer be exactly at right angles to the edge between the measured faces. It is clear from the construction in Fig. 8.9b that the angle between the poles to the crystal faces, the *internal angle*, is measured. Thus, in Fig. 8.9a the angle that one reads is 40°, not 140°.

Interfacial angles are commonly measured as angles with respect to (010) or (001) faces of the crystal (if the crystal shows the presence of these two forms). The interfacial angles measured with a contact goniometer, or the ϕ and ρ angles available in the literature, can be plotted directly with the aid of a stereographic net.

Examples follow for plotting of the face poles for two types of crystals: (1) for an orthorhombic crystal in which the three axial directions (*a*, *b*, and *c*) are at 90° to each other and (2) for a monoclinic crystal where two of the three crystallographic directions are nonorthogonal (≠ 90°).

PROJECTION OF AN ORTHORHOMBIC CRYSTAL

In this example, the crystal symmetry and interfacial angles for the mineral anglesite, $PbSO_4$, (Fig. 8.10a) are used. The angles ϕ and ρ for the crystal faces that lie in the positive quadrant are given (Fig. 8.10b).

To locate the poles of these faces on the stereographic projection, begin by orienting the stereonet: mark the N–S, E–W vertical circles and draw the primitive. Then, as in all projections, assign (010), face *b*. The pole of this face should be placed on the primitive at 0°. Next plot the ϕ angles. The interfacial angles $b \wedge n = 32\frac{1}{2}°$ and $b \wedge m = 52°$, can be plotted directly (count clockwise from 0°) as angles on the primitive. Because their ρ angles are 90° (and fall on the primitive), no further plotting is necessary. Face *c* is (001); it makes an angle of 90° with *b*, and its pole should be placed at the center of the projection (where ρ = 0°). Face *o* has a ϕ angle of 0° and is in a zone with faces *c* and *b*. Its ρ angle, $c \wedge o = 52°$, can be measured directly and plotted along the vertical great circle. Face *d* lies in a vertical zone at 90° to the zone *c*, *o*, *b* and has ϕ = 90°. Therefore, ρ, or $c \wedge d = 39\frac{1}{2}°$, can be plotted along the vertical circle of the net by counting from the center outward.

The pole of face *y* cannot be plotted directly, but the angles $b \wedge y = 45°$ and $c \wedge y = 57°$ can be used. To locate this pole, the projection is rotated 90° (to the N–S direction) so that *b* lies along the radii of the small circles of the net, and a tracing of the 45° circle is made (Fig. 8.10c). This small circle is the locus of all poles 45° from *b*. The locus of $c \wedge y = 57°$ is also a circle, 57° outward, centered on the pole of (001), the center of the stereographic projection. This circle is one of colatitude (or polar angle as in the spherical projection) and is most easily drawn with a compass, after the spread of the compass has been measured along, for example, the E–W direction of the stereographic net at ρ = 57°. Where the two circles intersect (where the 57° circle intersects the small circle of $b \wedge y = 45°$), marks the location of the pole of *y* (Fig. 8.10c).

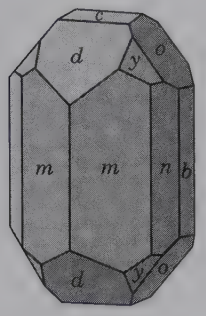

(a)

	φ	ρ
c(001)	— — —	0°
b(010)	0°	90°
n(110)	32½°	90°
m(210)	52°	90°
o(011)	0°	52°
d(101)	90°	39½°
y(111)		57°
y(111)	angle $b \wedge y = 45°$	

(b)

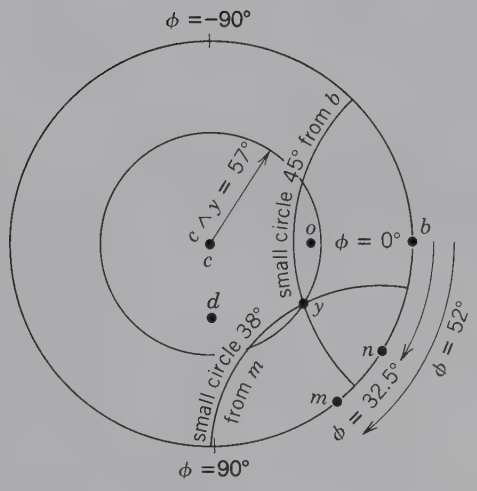

(c)

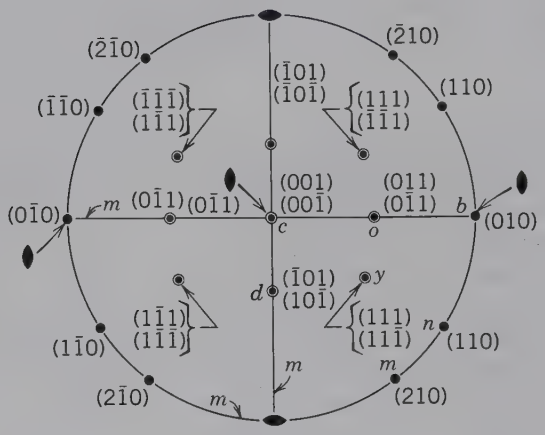

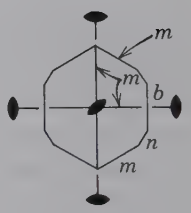

2/m 2/m 2/m

(d)

FIG. 8.10 (a) A crystal of the orthorhombic mineral anglesite with symmetry 2/*m*2/*m*2/*m*. Faces belonging to the same form are labeled with the same letter. (b) Listing of ϕ and ρ angles, as reported in the literature and originally measured by reflecting goniometer (see Fig. 1.13d), for the faces of the anglesite crystal shown in (a). (c) A stereographic projection of the faces in the positive quadrant of the mineral anglesite. (d) The location of all of the face poles, with their Miller indices, as well as the symmetry elements consistent with the location of these face poles. A horizontal cross section of the crystal in (a) is shown as well.

To check this position, measure the angle $m \wedge y = 38°$. This is most easily done by locating the pole to *m* at the $\phi = 90°$ position (southern end) of the stereographic net and reading the angular difference between *m* and *y* along one of the inclined great circles. Indeed, one can trace a small circle with *m* at $\phi = 90°$, which will intersect the pole of *y* (see Fig. 8.10c). Now that the pole of *y* is located, its ϕ and ρ angles can be read directly from the stereographic net. The ϕ value is 32.5° and the ρ value is 57° (Fig. 8.10c).

Figure 8.10d shows *all* of the faces plotted for the crystal of anglesite shown in Fig. 8.10a; not only those in the upper, positive quadrant of the stereographic projection (shown as solid dots), as in Fig. 8.10c, but all other faces as well (with those in the negative direction of *c* as open circles). The distribution of these face poles is consistent with the combination of symmetry elements 2/*m*2/*m*2/*m*. There are 3 two-fold axes at 90° to each other, as well as 3 mirror planes that intersect at the center of the stereographic projection. Two of these mirrors stand vertically as shown along the N–S and E–W directions. The third mirror is parallel to the page, in the plane of the primitive circle. Thus, a crystal's overall symmetry is expressed by the location of the poles to its crystal faces.

PROJECTION OF A MONOCLINIC CRYSTAL

The location of the crystallographic axes in a monoclinic crystal is somewhat less straightforward than in the orthorhombic case because not all of the crystallographic axes are at 90° to each other. In this text, the two-fold rotation axis in monoclinic crystals is located in a horizontal, E–W direction, as the *b* axis. This orientation is referred to as the "second setting" (in the "first setting" the two-fold axis is vertical). This means that a possible mirror plane (as in 2/*m*), which is perpendicular to the two-fold axis, stands vertically. If the monoclinic crystal shows an elongated habit, the direction of elongation is commonly chosen as parallel to the *c* axis. If there is a prominent sloping plane, such as face *c* in Fig. 8.11a, the *a* axis is taken as parallel to it and at right angles to *b*.

An example of a monoclinic crystal is that of diopside, $CaMgSi_2O_6$ (shown in Fig. 8.11a). It is oriented with the mirror plane vertical, the two-fold axis parallel to the *b* axis, (horizontal in an E–W direction) and *a* sloping down and forward. A vertical cross-section (Fig. 8.11c) shows the *c* axis parallel to the elongation of the crystal, and the *a* axis parallel to the sloping *c* faces (001) and $(00\bar{1})$. The relevant interfacial angles, measured on the crystal shown in Fig. 8.11a, are listed in Fig. 8.11b. The interfacial angle $c \wedge a$ [(001) ∧ (100)] = 74° is shown in the cross-section of the crystal (Fig. 8.11c). The nonorthogonal angle (β) between the two crystallographic axes *a* and *c* = 106°. In descriptions of monoclinic minerals in this text, the angle between the *a* and *c* crystallographic axes, known as the β angle, is taken as the angle that is not equal to 90°. Because of the presence of this nonorthogonal angle between the two axial directions of *a* and *c*, the location of one of these two axes will be different from what is observed in the stereographic projection of, for example, the orthorhombic crystal (Fig. 8.10). To help clarify this, the upper part of the diopside crystal is drawn and surrounded by the sphere of the spherical projection in Fig. 8.11d. This figure shows that the pole to (001) is not coincident with the piercing point of the (+) end of the *c* axis. Similarly, the pole of (100) is not coincident with the piercing point of the (+) end of the *a* axis. The *b* axis lies in the E–W great circle.

A cross-section parallel to the *a*–*c* (vertical) plane of the crystal in the spherical projection is shown in Fig. 8.11e. The angular relations shown here are identical to those of Fig. 8.11c. In this cross section it is important to note the inclined position of the *a* axis. Only the (−) end of the *a* axis is *above* the trace of the stereographic projection (the horizontal diameter of this figure); the (+) end of the *a* axis lies below it. When the ends of the *a* axis are projected onto the stereographic projection, the (−) end will project as indicated in Fig. 8.11e. Its piercing point will be located at 16° (106°–90°) inward from the primitive circle; its projected location is shown as an opaque dot (because it is in the northern hemisphere) in Fig. 8.11f. The (+) end of the *a* axis lies below the trace of the stereographic projection and must be projected upward. The point where it pierces the spherical projection is indicated as an open circle 16° inside of the primitive. This is also shown in Fig. 8.11f.

Once the *a* and *c* axes are located, the various face poles can be plotted. All those in the vertical zone (∥ *c* axis) can be located on the perimeter of the stereographic net; these are *b*, *m*, and *a*.

The interfacial angle $c \wedge a$ [(001) ∧ (100) = 74°] implies that the pole of the (001) face is 16° away from the piercing point of the *c* axis (90°–74°), in a southward direction along the N–S vertical great circle. This is shown in Fig. 8.11f. The only poles still to be located are those of the two inclined faces *u*, which are symmetrically oriented with respect to the *a*–*c* plane (the mirror plane). The interfacial angle $c \wedge u = 34°$. This angle can be plotted with respect to *c* (001) after the *c* pole has been moved to the E–W vertical great circle. The 34° angle between *c* and *u* can now be plotted because these two face poles lie in the same zone; that is, they both lie on the same great circle. In this case, the great circle passing through *c* and *u* is inclined by 16° from the vertical. Two such inclined great circles are shown with solid lines in Fig. 8.11f. Once both poles of the two *u* faces in the upper hemisphere are plotted, the $u \wedge u$ interfacial angle (as given in Fig. 8.11b) can be verified. The faces *b*, *u*, *u*, *b* lie in the same zone. As such, the poles to these four faces lie on the same (inclined) great circle. On this circle (solid in Fig. 8.11g), the interfacial angle of 48° can be measured (as was reported in Fig. 8.11b). The interfacial angle $c \wedge m = 79°$ can be verified in a similar manner: Faces *m*, *c*, *m* lie in the same zone; as such, their poles lie on the same inclined great circle.

All of the face poles of the diopside crystal are plotted in Fig. 8.11h, and a Miller index is assigned to each pole. The symmetry elements compatible with the distribution of the face poles are also shown. This turns out to be 2/*m* with the two-fold axis horizontal in an E–W direction and the mirror plane in a vertical position perpendicular to the two-fold axis. Once again, the total symmetry of the crystal has been highlighted. Stereographic projections allow for the representation of the angular positions of faces and the symmetry content of crystals on a two-dimensional page.

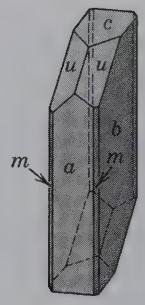

(a)

Interfacial Angles

ca, (001) ∧ (100) = 74°
mm, (110) ∧ (1$\bar{1}$0) = 93°
cu, (001) ∧ (111) = 34°
uu, (111) ∧ (1$\bar{1}$1) = 48°
cm, (001) ∧ (110) = 79°

(b)

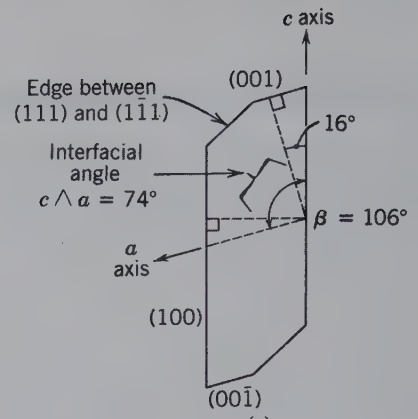

(c)

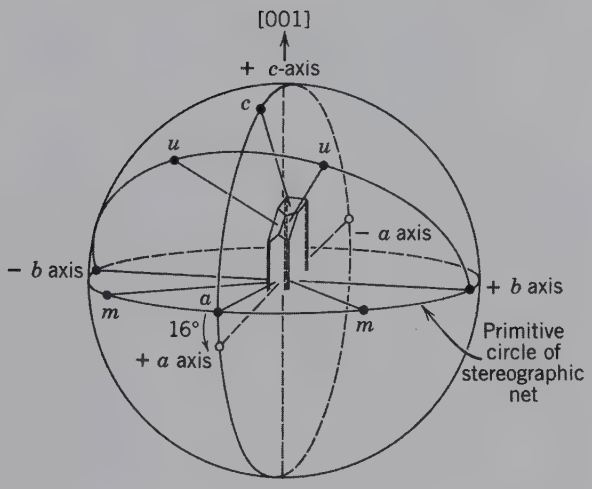

(d)

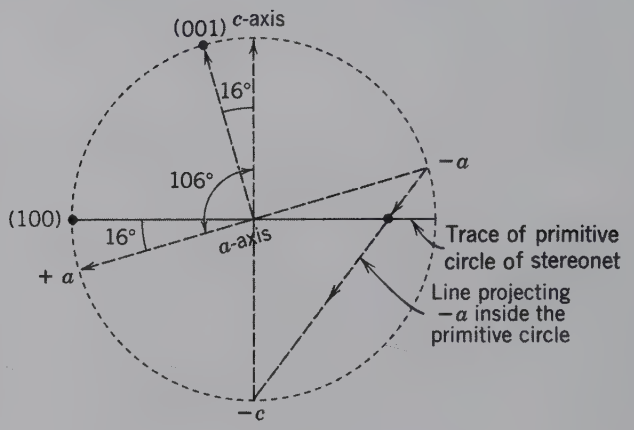

(e)

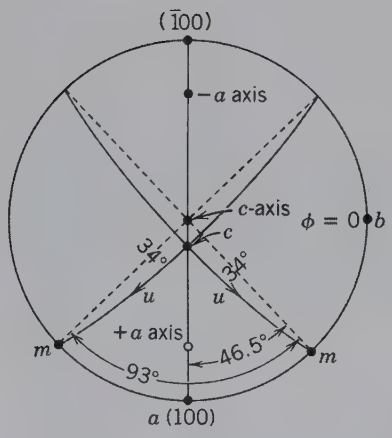

(f)

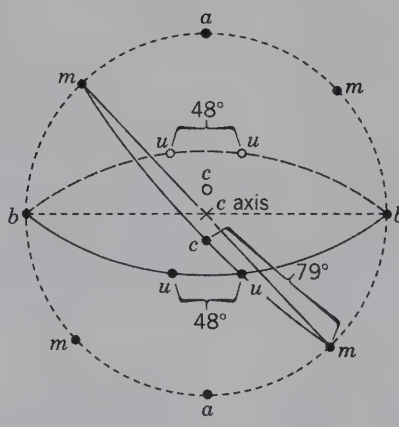

(g)

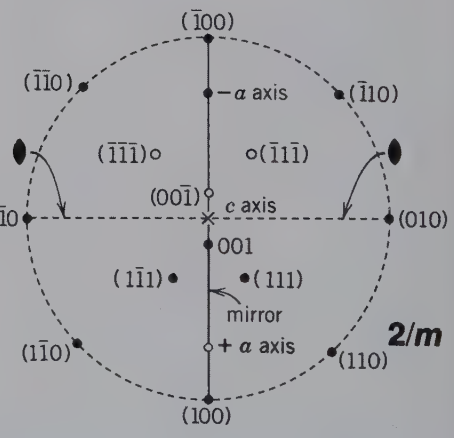

(h)

REFERENCES AND FURTHER READING

Bloss, F. D. 1994. *Crystallography and crystal chemistry: An introduction.* Reprint of the original text of 1971 by the Mineralogical Society of America, Washington, D.C.

Boisen, M. B., Jr., and G. V. Gibbs. 1990. *Mathematical crystallography. Reviews in Mineralogy* 15. Mineralogical Society of America, Washington, D.C.

Bragg, W. L., and G. F. Claringbull. 1965. *Crystal structures of minerals.* Cornell University Press, Ithaca, New York.

Buerger, M. J. 1978. *Elementary crystallography: An introduction to the fundamental geometric features of crystals.* Rev. ed. MIT Press, Cambridge, Massachusetts.

———, 1971. *Introduction to crystal geometry.* McGraw Hill, New York.

International tables for crystallography. 1983. Vol. A, *Space group symmetry.* Edited by T. Hahn. International Union of Crystallography, D. Reidel Publishing Company, Boston.

International tables for X-ray crystallography. 1969. Vol. 1, *Symmetry groups.* Edited by N. F. M. Henry and K. Lonsdale. International Union of Crystallography, Kynoch Press, Birmingham, England.

Klein, C. 2008. *Minerals and rocks: Exercises in crystal and mineral chemistry, crystallography, X-ray powder diffraction, mineral and rock identification, and ore mineralogy.* 3rd ed. Wiley, New York.

O'Keffe, M., and B. G. Hyde. 1996. *Crystal structures I: Patterns and symmetry.* Monograph. Mineralogical Society of America, Washington, D.C.

Wahlstrom, E. E. 1951. *Optical crystallography.* Wiley, New York.

FIG. 8.11 Plotting of face poles for a monoclinic crystal. (a) A crystal of the monoclinic mineral diopside. (b) Interfacial angles, as reported in the literature and originally measured by reflecting goniometer (see Fig. 1.13d), for the faces of the monoclinic crystal of diopside, shown in (a). (c) A vertical cross section through the diopside crystal showing the location of the *c* axis (parallel to the elongation of the crystal) and of the *a* axis [parallel to the (001) face]. The β angle of 106° and the interfacial angle $c \wedge a = 74°$ [between (001) and (100)] are shown. (d) The upper half of the diopside crystal centered within the sphere of the spherical projection. Note the location of the piercing points of the $+c$ and $+a$ axes as well as the poles of *c* (001), *a* (100) and the faces marked *m* [(110) and $(1\bar{1}0)$] and *u* [(111) and $1\bar{1}1$)]. (e) A vertical cross section through the sphere in (d); this section contains the *a* and *c* axes and the poles of (100) and (001). Note that the (+) end of the *a* axis lies below the equatorial plane of the stereographic projection (the primitive circle) and that the (−) end of *a* axis lies above it. Therefore, in projecting the piercing points of $-a$ and $+a$ from the sphere onto the stereographic projection, the "end points" of *a* move inward along the N–S direction (great circle) by 16° each. The $-a$ end projects from above (as a solid dot) and the $+a$ end projects from below (as an open circle). (f) Plotting of the poles of *b* [(010) at $\phi = 0°$], *a* at $\phi = 90°$, the two faces *m* with an interfacial angle = 93° (symmetrically on either side of *a*), and *c* (001) with an interfacial angle with $a = 74°$. The *c* axis is at the center of the projection and the − end of the *a* axis lies 16° inward from the pole to (100).

The interfacial angle $c \wedge u$ [$(001) \wedge (111)$] is listed as 34° in (b). With *c* and *u* on the same great circle, this 34° angle can be measured, symmetrically on either side of *c* (001). The projection shows that *m*, *u*, *c* lie on the same great circle and, consequently, in the same zone. (g) Here, all the face poles of the crystal in (a) are plotted. Those marked *u* and shown as black dots are for face poles in the upper part of the sphere, and those shown as open circles are for poles projected upward from the lower part of the sphere. The interfacial angles $u \wedge u$ [$(111) \wedge (1\bar{1}1)$] and $c \wedge m$ [$(001) \wedge (110)$] are shown along great circles as 48° and 79°, respectively (see listing in b). (h) The location of all of the face poles and their Miller indices, as well as the symmetry elements consistent with the distribution of these face poles.

CHAPTER 9

Selected Point Groups and Further Aspects of Space Groups

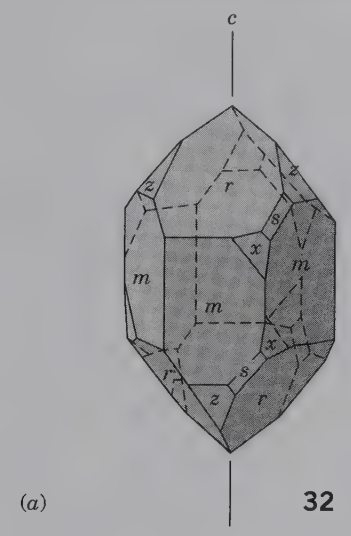

(a) **32**

(a). *External shape (morphology) of a right-handed quartz crystal. The small crystal face (marked x) is a trigonal trapezohedron. When it occurs at the top right of a larger prism face (marked m) the crystal is described as right-handed. The crystallographic* c *axis is vertical. The external symmetry (point group) is expressed as* ***32****.* (b). *Standard graphical representation of the lattice type as well as the internal symmetry elements of right-handed quartz. This graphic is the result of the projection of symmetry elements down the* c *axis of the crystal in* (a). *The space group notation for this is* ***P3$_1$21****. (Space group illustration from* International Tables for Crystallography. *1983. vol. A. T. Hahn, editor.)*

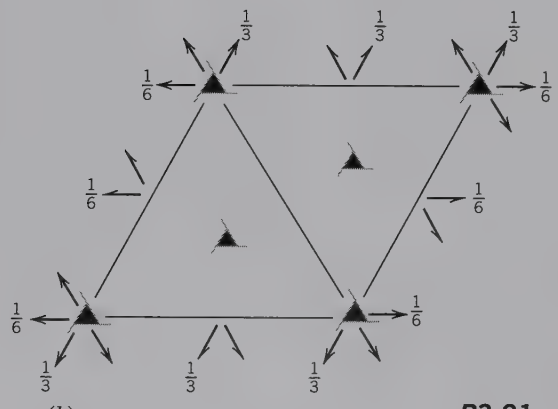

(b) ***P*3,21**

The external morphology of crystals ranges from very simple, as in the case of cubes of pyrite, to much more complex, as is commonly seen in crystals of quartz. The cube of pyrite consists of a single crystal form in the isometric system, whereas the many different faces of quartz belong to several forms in the hexagonal system. This chapter builds on the previously discussed concepts of morphological symmetry, describes in detail the various forms that occur in 19 of the most common crystal classes (or point groups), and explains how these forms combine to produce the external morphology observed in well-formed crystals. This chapter concludes with a further discussion of space groups and their two-dimensional representation.

Every crystal can be grouped into 1 of 32 crystal classes (or point groups) based on the symmetry inherent in the crystal. Common aspects of these 32 point groups allow them to be grouped into six crystal systems (as discussed in Chapter 6). The number of minerals (and synthetic crystalline compounds) falling within each of the six crystal systems is highly variable. A listing of 3,837 natural and synthetic crystalline compounds and their distribution among the 32 crystal classes is given by Bloss (1971, p. 28). For these compounds, the distribution is as follows:

Triclinic	2%
Monoclinic	21
Orthorhombic	20
Tetragonal	12
Hexagonal	19
Isometric	26

Within each of these six crystal systems, the largest number of mineral species is concentrated in the crystal class with the highest symmetry (referred to as the *holohedral* class, from the Greek word *holos* meaning whole or complete). The most symmetric classes in the six systems are: $\bar{1}$ in triclinic, $2/m$ in monoclinic, $2/m2/m2/m$ in orthorhombic, $4/m2/m2/m$ in tetragonal, $\bar{3}2/m$ in the hexagonal system (based on a rhombohedral lattice), $6/m2/m2/m$ in the hexagonal system (based on a hexagonal lattice), and $4/m\bar{3}2/m$ in the isometric system. (Animations for the following 19 point groups are given in module II of the CD-ROM under the heading "Crystallography: Crystal Classes.")

NINETEEN OF THE THIRTY-TWO POINT GROUPS

Nineteen of the most commonly occurring point groups (see Table 6.3) will now be described. These point groups are discussed according to crystal system, beginning with the least symmetric and progressing through to the most symmetric. For each, the relationship of the symmetry elements (as expressed by the Hermann–Mauguin notation) and the orientation of the crystallographic axes is reviewed (see Figs. 6.25 and 6.26).

Within each crystal system, the point groups are discussed in order of decreasing symmetry beginning with the most symmetric for that system. Each of the 32 point groups has a characteristic form, called the *general form*. This form consists of faces that cut each of the crystallographic axes at different lengths, and therefore, it has the Miller index of {*hkl*}. *An* (hkl) *face will not be parallel or perpendicular to a symmetry axis or plane, regardless of the crystal class* (see also Chapter 6). From these general forms, the name of the point group is derived. All other forms within the crystal class are *special forms*. Such forms consist of faces that are parallel or perpendicular to any of the symmetry elements in the crystal class. For most crystal classes, the general form contains a larger number of crystal faces than any of the special forms of that same class. Furthermore, there is the concept of the *open* versus the *closed form*. The two-faced form {111} for crystal class $\bar{1}$ is referred to as an *open form*, because it consists of two parallel faces that do not enclose space [see Figs. 6.36, (2) and 9.4]. In contrast, the eight-faced form {111} in crystal class $4/m\,\bar{3}2/m$ is a *closed form*, because the eight faces enclose space [see Figs. 6.30 and 6.36, (35)].

The symmetry of each crystal class is given by the unabbreviated Hermann–Mauguin notation but in the literature abbreviations are commonly used (Table 9.1). The symmetry of each class is graphically shown by means of a stereogram. In such a stereogram, faces in the northern and southern hemisphere are shown in order to portray the complete symmetry of each class. This is done by superimposing stereographic projections of the two hemispheres, with the poles in the northern hemisphere represented by solid points and those in the southern hemisphere by open circles (see Chapter 8). If a pole lies directly above another, it is represented by a solid point surrounded by a circle. A vertical face is represented by a single point on the primitive, for, although such a pole would appear on projections of both top and bottom of the crystal, it represents but one face. To display the total symmetry of these point groups in stereographic projections, standard graphical symbols are used for symmetry elements. These are shown in Table 9.2.

Forms are illustrated by crystal drawings. In order to properly identify a form, the crystal must be properly oriented. The crystal drawings in this text have a standardized orientation: The *c* axis is vertical, the *b* axis is east–west, and the *a* axis is toward the observer. The positions of these axes have been omitted in most crystal drawings. For example, Fig. 9.1a is a drawing of a crystal with a horizontal symmetry plane. Consequently, the stereogram of this crystal, Fig. 9.1b, shows

Table 9.1 Listing of the Equivalent Long and Abbreviated Forms of Six Crystal Classes

System	Long Form	Short Form
Orthorhombic	$2/m2/m2/m$	mmm
Tetragonal	$4/m2/m2/m$	$4/mmm$
Hexagonal	$\bar{3}2/m$	$\bar{3}m$
	$6/m2/m2/m$	$6/mmm$
Isometric	$2/m\bar{3}$	$m3$
	$4/m\bar{3}2/m$	$m3m$

Table 9.2 Graphical Symbols Used in Stereographic Illustrations

Axes of rotation	Written symbol	Graphical symbol
1-fold	1	none
2-fold	2	⬮
3-fold	3	▲
4-fold	4	■
6-fold	6	⬢
Axes of rotoinversion		
1-fold	$\bar{1}$	(equivalent to a center of symmetry or *i*, inversion)*
2-fold	$\bar{2}$	(equivalent to a mirror, *m*)
3-fold	$\bar{3}$	△
4-fold	$\bar{4}$	◧
6-fold	$\bar{6}$	⬣
Center of symmetry	*i*	
Mirror planes	*m* (horizontal, parallel to the plane of the page)	*m* none (see footnote)*
		solid line along primitive circle
	m (vertical, perpendicular to the plane of the page)	*m* *m* Both solid lines
	m absent, in both horizontal and vertical positions	
Crystallographic directions	*a*, *b*, *c*	- - - - *a*, *b*, or *c* broken lines labeled with the appropriate letter
		If *m* includes a crystallographic direction, a solid line is used—with *a*, *b*, or *c*

*A center of symmetry is shown in writing by the letter *i* for inversion, which is equivalent to $\bar{1}$. If a symmetry center occurs at the center of the sphere of projection, its presence is not shown by a symbol on the stereogram, but it can be detected from the arrangement of poles of equivalent faces (see also Fig. 6.24).

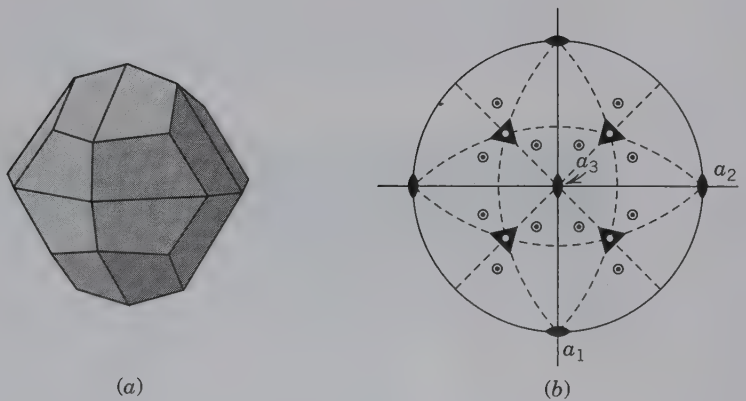

FIG. 9.1 Crystal with symmetry $2/m\bar{3}$. The stereogram shows a mirror plane at right angles to each of the two-fold rotation axes, and 4 three-fold axes of rotoinversion. The solid primitive circle denotes a horizontal mirror plane; faces at the bottom of the crystal lie directly below those at the top.

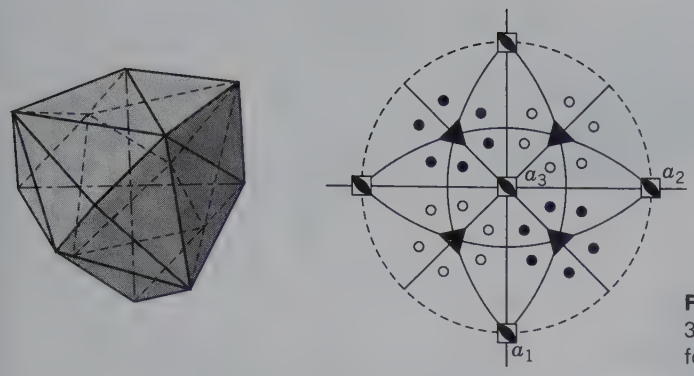

(*a*) (*b*)

FIG. 9.2 Crystal with symmetry $\bar{4}\,3m$. Stereogram shows 3 four-fold axes of rotoinversion, six mirror planes, and 4 three-fold rotation axes. The broken primitive circle indicates the lack of a horizontal mirror plane, and faces at the top of the crystal do not lie above those at the bottom.

all faces as solid points as well as surrounding circles to indicate corresponding faces at the top and bottom of the crystal. Figure 9.2a is a drawing of a crystal lacking a horizontal mirror plane. Its stereogram, Fig. 9.2b, has 12 solid points as poles of faces in the northern hemisphere and an additional 12 independent circles as poles of faces in the southern hemisphere. Locations of three-fold axes are given by the triangular symbols.

Although the geometrically perfect model is shown in each of the form illustrations, this ideal is rarely obtained in nature. Crystals may be malformed due to growth, and they usually display a combination of forms.

TRICLINIC SYSTEM

Crystallographic Axes. In the triclinic system the crystal forms are referred to three crystallographic axes of unequal lengths that make oblique angles with each other (Fig. 9.3). Three rules apply in the orientation of a triclinic crystal with respect to the position of the crystallographic axes:

1. The most pronounced zone should be vertical. The axis of this zone then becomes *c*.
2. {001} should slope forward and to the right.
3. Two forms in the vertical zone should be selected: one as {100}, the other as {010}.

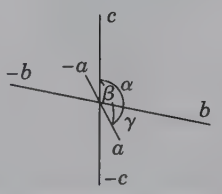

FIG. 9.3 Orientation of axes in the triclinic crystal system.

The directions of the *a* and *b* axes are determined by the intersections of {010} and {100}, respectively, with {001}. The *b* axis should be longer than the *a* axis, such that $c < a < b$. This is the convention when a new triclinic mineral is first described. The relative lengths of the three axes and the angles between them are established by X-ray diffraction techniques. The angles between the positive ends of *b* and *c*, *c* and *a*, and *a* and *b* are designated respectively as α, β, and γ (Fig. 9.3).

$\bar{1}$ II

Symmetry—*i*. The symmetry consists of a one-fold rotoinversion axis, which is equivalent to the center of symmetry, or inversion (*i*). This class is referred to as the **pinacoidal class** after its general {*hkl*} form. Fig. 9.4 illustrates a triclinic pinacoid (two-faced form) and its stereogram.

Forms. All the forms in this class are *pinacoids* and consist of two identical and parallel faces. Once a crystal is oriented, the Miller index of the pinacoid establishes its position.

$\bar{1}$

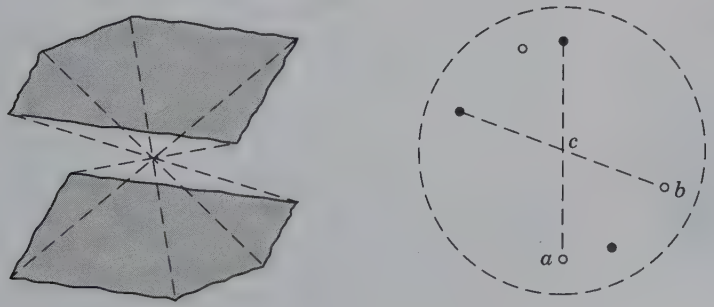

FIG. 9.4 Triclinic pinacoid (two-faced form) with stereogram showing location of faces and axes.

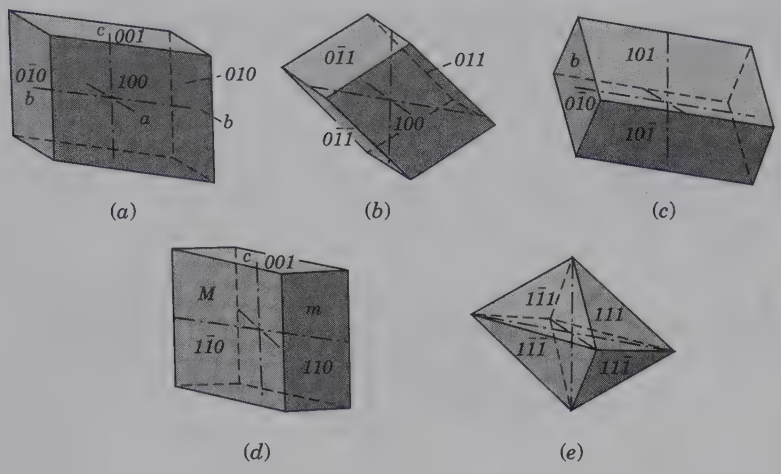

FIG. 9.5 Various combinations of triclinic pinacoids. (a) Front {100}, side {010}, and base {001}. (b) {011} positive, {0$\bar{1}$1} negative. (c) {101} positive, {10$\bar{1}$} negative. (d) {110} positive, {1$\bar{1}$0} negative. (e) Four different forms.

1. {100}, {010}, and {001} *Pinacoids*. Each of these pinacoids intersects one crystallographic axis and is parallel to the other two. The front or *a* pinacoid, {100}, intersects the *a* axis and is parallel to the other two; the side or *b* pinacoid, {010}, intersects only the *b* axis; the basal or *c* pinacoid, {001}, intersects only the *c* axis.
2. {0*kl*}, {*h*0*l*}, and {*hk*0} *Pinacoids*. The {0*kl*} form is parallel to *a* and can be positive {0*kl*}, or negative $\{0\bar{k}l\}$; the {*h*0*l*} form is parallel to *b*, {*h*0*l*} positive, and $\{\bar{h}0l\}$ negative; the {*hk*0} form is parallel to *c*, {*hk*0} positive, and $\{h\bar{k}0\}$ negative.
3. {*hkl*} *Pinacoids*. {*hkl*} positive right, $\{h\bar{k}l\}$ positive left, $\{\bar{h}kl\}$ negative right, $\{\bar{h}\bar{k}l\}$ negative left. Each of these two-faced forms can exist independently of the others.

Various combinations of these pinacoids are illustrated in Fig. 9.5. The distribution of forms in point groups of the triclinic system is listed in Table A3.1 of Appendix 3.

Among the minerals that crystallize in $\bar{1}$ are:

amblygonite	polyhalite
chalcanthite	rhodonite
microcline	turquoise
pectolite	ulexite
plagioclase feldspars	wollastonite

Of these minerals, microcline (see Plate VIII, no. 3), rhodonite, and chalcanthite are fairly common as well-formed crystals (Fig. 9.6).

FIG. 9.6 Triclinic crystals displaying various pinacoids. (a) Rhodonite. (b) Chalcanthite.

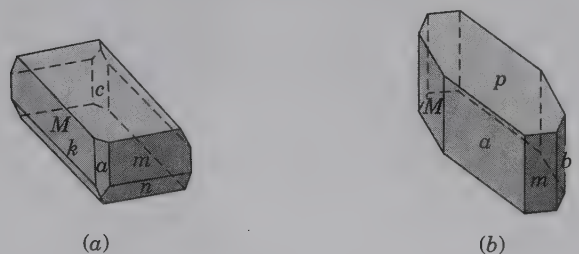

MONOCLINIC SYSTEM

Crystallographic Axes. Monoclinic crystals are referred to three axes of unequal lengths. The only restrictions in the angular relations are that $a \wedge b\ (= \gamma)$ and $c \wedge b\ (= \alpha) = 90°$. For most crystals, the angle between $+a$ and $+c\ (= \beta)$ is greater than 90°, although it can also be less than 90°. In some instances, β is extremely close to 90° (e.g., staurolite) such that the mineral appears orthorhombic based on morphology. Such crystals are referred to as *pseudo-orthorhombic*. The two-fold rotation axis, or the direction perpendicular to the mirror plane, is usually taken as the *b* axis; the *a* axis is inclined downward toward the front; and *c* is vertical. This is shown in Fig. 9.7 by crystallographic axes of the monoclinic mineral orthoclase, with $\beta = 116°01'$. This orientation, known as the "second setting," is traditional for mineralogists. (Some crystallographers orient monoclinic crystals according to the "first setting" in which the two-fold axis or the normal to the mirror plane is chosen as the *c* axis instead of the *b* axis. In this text, all monoclinic crystals are referenced to the "second setting.")

Although the direction of the *b* axis is fixed by symmetry, the directions for the *a* and *c* axes are matters of choice and depend on crystal habit and cleavage. If crystals show an elongated development (prismatic habit) parallel to a direction in the *a*–*c* plane, that direction often serves as the *c* axis. If there is a prominent sloping plane (or planes), such as planes *c* or *r* in the drawings of Fig. 9.10, the *a* axis may be taken as

FIG. 9.7 Orientation of axes in the monoclinic crystal system.

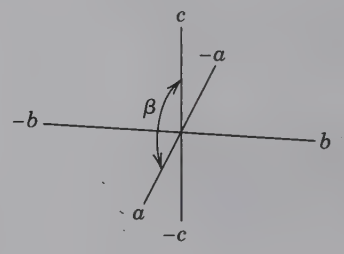

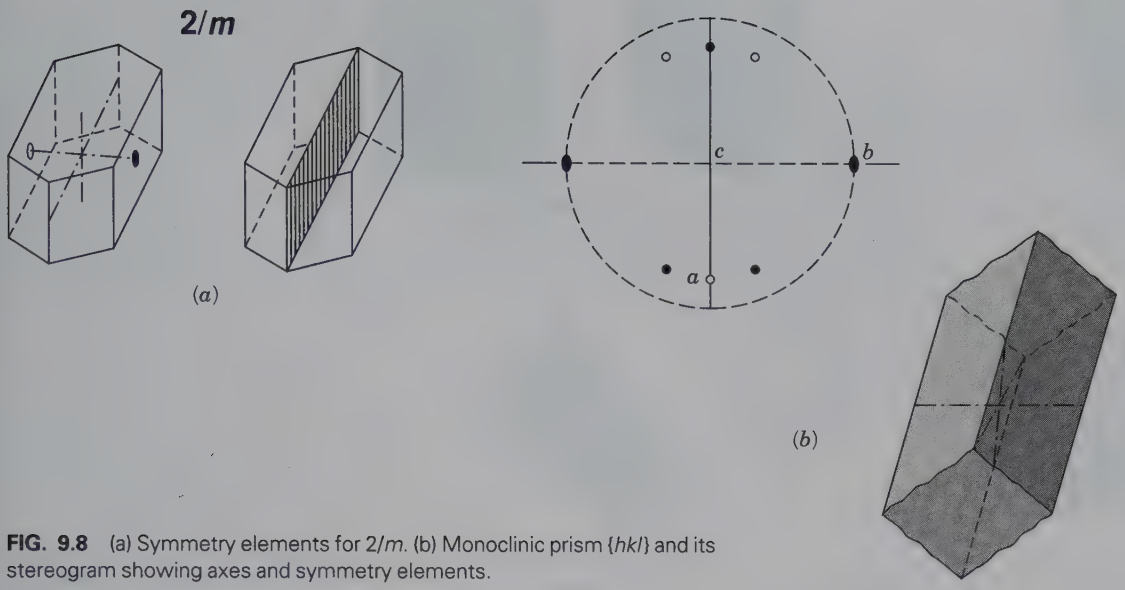

FIG. 9.8 (a) Symmetry elements for 2/*m*. (b) Monoclinic prism {*hkl*} and its stereogram showing axes and symmetry elements.

parallel to these. There may be several possibilities that are equally good, but in the description of a new mineral it is conventional to orient the crystals such that $c < a$.

Cleavage is also an important factor in orienting a monoclinic crystal. If there is good pinacoidal cleavage parallel to the *b* axis, as in orthoclase, it is usually taken as the basal cleavage. If there are two equivalent cleavage directions, as in the amphiboles and pyroxenes, they are usually taken to be vertical prismatic cleavages.

2/*m*

Symmetry—*i*, $1A_2$, $1m$. The axis of two-fold rotation is chosen as the *b* axis, and the *a* and *c* axes lie in the mirror plane, which is perpendicular to the *b* axis (Fig. 9.8*a*). The stereogram in Fig. 9.8b shows the symmetry of an {*hkl*} prism, the general form, and symmetry elements. Because the *a* axis slopes down and to the front, it lies below the equatorial plane; the positive end intersects the sphere of projection in the southern hemisphere and, therefore, projects inside the primitive circle (for further discussion see "Projection of a Monoclinic Crystal," in Chapter 8). This class is referred to as the **prismatic class**, because the general form {*hkl*} is a *prism*.

Forms. There are only two types of forms in this monoclinic class: *pinacoids* and *prisms*.

1. *Pinacoids* (two-faced forms). Front or *a* pinacoid, {100}, side or *b* pinacoid, {010}, and basal or *c* pinacoid, {001}. There are also {*h*0*l*} and $\{\bar{h}0l\}$ pinacoids; these two pinacoids are independent of each other, and the presence of one does not necessitate the presence of the other (Figs. 9.9 and 9.10).
2. *Prisms*. The four-faced prism {*hkl*} is the general form, but {0*kl*} and {*hk*0} are also prisms. The {0*kl*} prism intersects the *b* and *c* axes and is parallel to the *a* axis. The general form can occur as two independent prisms {*hkl*} and $\{\bar{h}kl\}$. Prisms are illustrated in Figs. 9.9 and 9.10.

The only form in this crystal class that is fixed by the choice of the *b* axis as the two-fold rotation axis, is the {010} pinacoid. The other forms may vary with the choice of the *a* and *c* axes. For instance, the {100} pinacoid, {001} pinacoid, and {*h*0*l*} pinacoids may be converted into each other by a rotation about the *b* axis. In the same manner, the prisms can be changed from one position to another. The distribution of forms in point groups of the monoclinic system is found in Table A3.1 of Appendix 3.

Many minerals crystallize in the monoclinic, prismatic class (see Plate VIII, no. 4). Some of the most common are:

azurite	kaolinite
borax	malachite
chlorite	mica (group)
clinoamphibole (group)	orpiment
clinopyroxene (group)	orthoclase
datolite	realgar
epidote	spodumene
gypsum	talc
heulandite	titanite

ORTHORHOMBIC SYSTEM

Crystallographic Axes. The crystal forms in the orthorhombic system are referred to three crystallographic axes of unequal lengths that make angles of 90° with each other (Fig. 9.11a). The relative lengths of the axes must be determined for each orthorhombic mineral. In orienting an orthorhombic crystal, the convention is to set the crystal such that $c < a < b$. In the past, this convention has not always been observed, and it is customary to conform to the orientation of the mineral given in the literature. One finds, therefore, that any one of the three axes may have been chosen as *c*. The longer of the other two is then taken as *b* and the shorter as *a*.

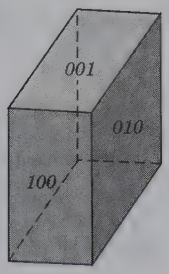

Pinacoids.
Front {100}, side {010}, and base {001}

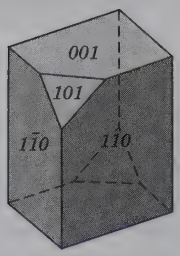

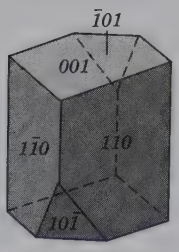

{101} or {10$\bar{1}$} pinacoids combined with {110} prism and a basal {001} pinacoid

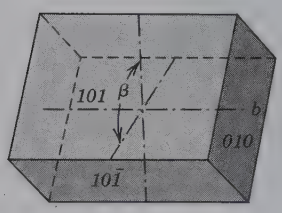

Combination of {101}, {10$\bar{1}$}, and {010} pinacoids

Combination of {011}, and {100} pinacoids

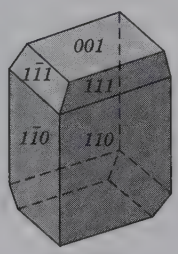

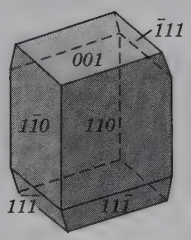

Combination of prism {111} (or {$\bar{1}$11}) and prism {110} and basal pinacoid {001}

FIG. 9.9 Commonly developed forms and form combinations in 2/*m*.

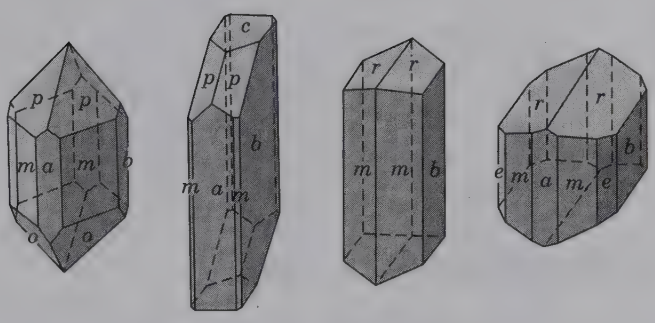

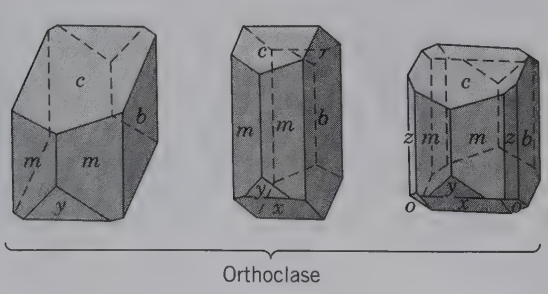

FIG. 9.10 Monoclinic crystals with 2/*m* symmetry. Forms: *a* {100}, *b* {010}, *c* {001}, *m* {110}, *p* {111}, *o* {$\bar{2}$21}, *r* {011}, *e* {120}, *x* {$\bar{1}$01}, *y* {$\bar{2}$01}, *z* {130}.

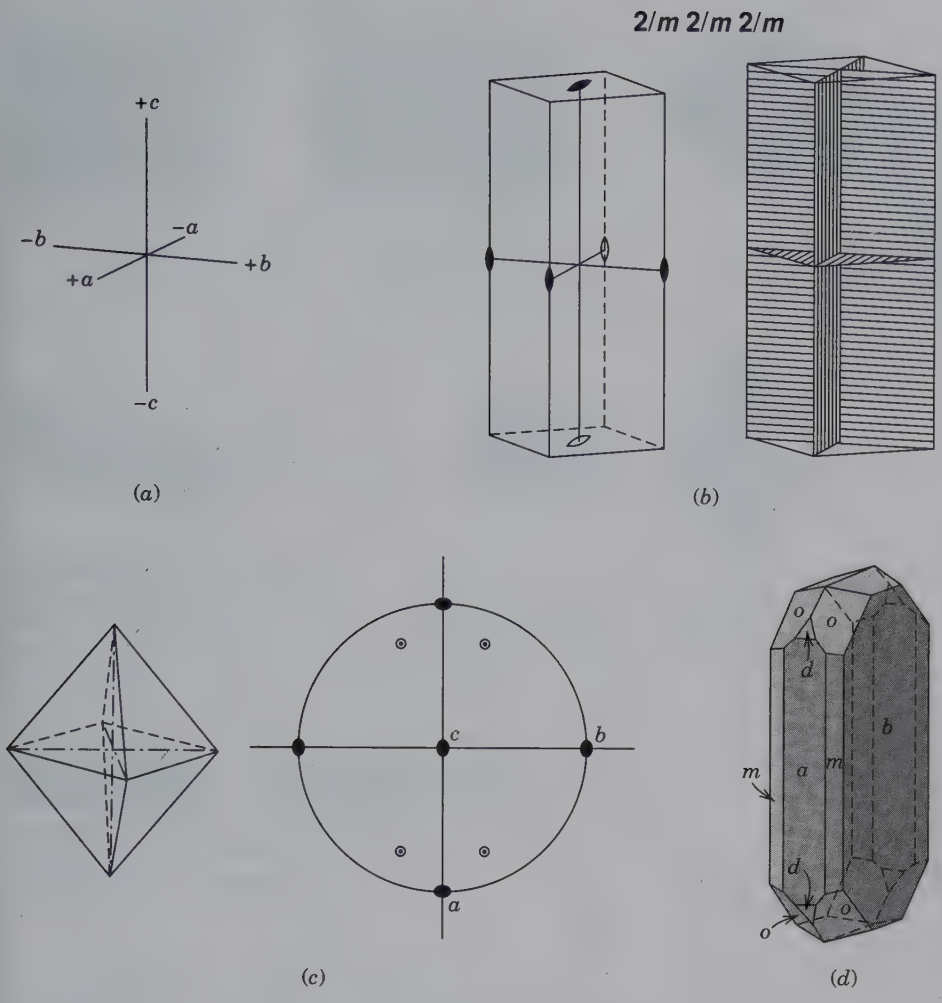

FIG. 9.11 (a) Orientation of axes in the orthorhombic crystal system. (b) Rotational axes and mirror planes in 2/*m*2/*m*2/*m*. (c) The rhombic dipyramid {*hkl*} and its stereogram. (d) A crystal of orthopyroxene showing the rhombic dipyramid, *o*, as well as several prisms.

Which of the three axes should be chosen as the vertical axis is based largely on the crystal habit of the mineral. If the crystals commonly show an elongation in one direction, this direction is usually chosen as the *c* axis (see topaz crystals in Fig. 9.12; Plate V, no. 3). If, on the other hand, the crystal shows a prominent pinacoid and is tabular, this pinacoid is usually taken as {001} with *c* normal to it (see barite and celestite crystals in Fig. 9.12). Cleavage also aids in orienting orthorhombic crystals. If, as in topaz, there is one pinacoidal cleavage, it is taken as {001}. If, as in barite, there are two equivalent cleavage directions, they are set vertical and their intersection edges determine *c*. After the orientation has been determined, the length of the axis chosen as *b* is taken as unity, and the relative lengths of *a* and *c* are given in terms of it. In the Hermann–Mauguin notation for the orthorhombic system, the symbols refer to the symmetry elements in the order *a*, *b*, *c*. For example, in the class *mm*2, the *a* and *b* axes lie in vertical mirror planes, and *c* is an axis of two-fold rotation.

2/m2/m2/m

Symmetry—*i*, $3A_2$, $3m$. The three axes of two-fold rotation coincide with the three crystallographic axes, and each axis has a perpendicular mirror plane (Fig. 9.11b). The general form is the *rhombic dipyramid* {*hkl*}, and this class is named the **rhombic-dipyramidal class** (Fig. 9.11*c*).

Forms. There are three types of forms in this class: pinacoids, prisms, and dipyramids.

1. *Pinacoid.* The pinacoid, consisting of two parallel faces, can occur in three different crystallographic orientations. These are: {100}, the front or *a* pinacoid, which intersects *a* and is parallel to *b* and *c*; {010}, the side or *b* pinacoid, which intersects *b* and is parallel to *a* and *c*; and {001}, the basal or *c* pinacoid, which intersects *c* and is parallel to *a* and *b* (Fig. 9.12).
2. *Rhombic Prisms.* Rhombic prisms consist of four faces that are parallel to one axis and intersect the other two. In the {0*kl*} prism, the faces are parallel to *a* but intersect *b* and *c*; in the {*h*0*l*} prism, the faces are parallel to *b* but intersect *a* and *c*; and in the {*hk*0} prism, the faces are parallel to *c* but intersect *a* and *b*. Examples of {011}, {101}, and {110} prisms are given in Fig. 9.12. Because all prisms intersect two axes and parallel the third, one prism can be transformed into another by a different choice of axes.
3. *Rhombic Dipyramid* {*hkl*}. A rhombic dipyramid (from the Greek word *di* meaning two) has eight triangular faces, each of which intersects all three crystallographic axes. The unit dipyramid {111} is illustrated in Fig. 9.12.

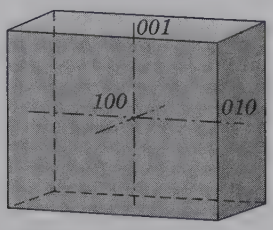

Pinacoids

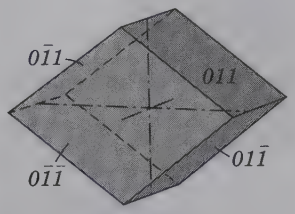

Rhombic prism {011} and pinacoid {100}

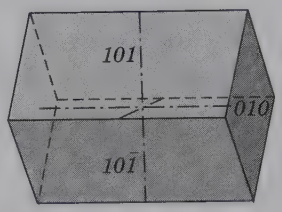

Prism {101} and pinacoid {010}

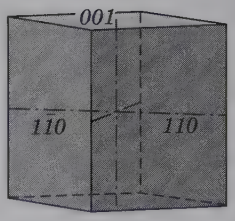

Prism {110} and pinacoid {001}

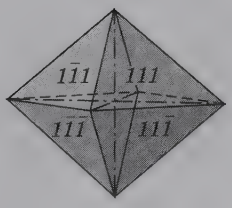

Rhombic dipyramid

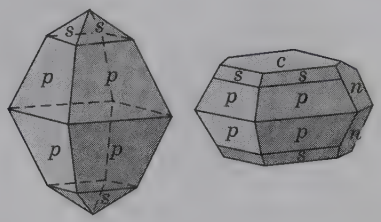

Sulfur crystals. Forms: *p* {111}, *s* {113}, both dipyramids. *n* {011}, prism, *c* {001}, basal pinacoid

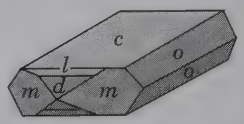

Celesite crystal. Forms: *c* {001}, *o* {011}, *d* {101}, *m* {210}, *l* {104}

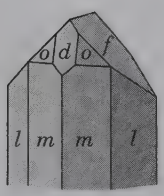

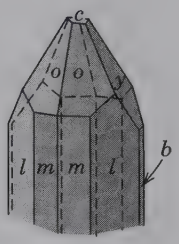

Topaz crystals. Forms: *c* {001}, *b* {010}, pinacoids. *f* {011}, *y* {021}, *d* {101}, *m* {110}, *l* {120}, prisms. *o* {111}, dipyramid

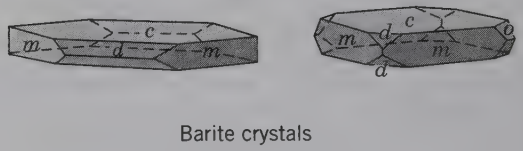

Barite crystals

FIG. 9.12 Commonly developed forms and form combinations in 2/*m*2/*m*2/*m*.

Combinations. Nearly all orthorhombic crystals consist of combinations of two or more forms because many forms are open forms. Characteristic combinations for various minerals are given in Fig. 9.12. The distribution of forms in point groups of the orthorhombic system is given in Table A3.1 of Appendix 3.

There are many mineral representatives in this class. Among the more common are the following:

andalusite (see Plate IV, no. 9)
anthophyllite (and other orthorhombic amphiboles)
aragonite (group)
barite (group)
brookite
chrysoberyl
columbite
cordierite
enstatite (and other orthopyroxenes)
goethite
marcasite
olivine
sillimanite
stibnite (see Plate II, no.3)
sulfur (see Plate I, no. 4)
topaz (see Plate V, no. 3)

*mm*2

Symmetry—2*m*, 1A$_2$. The two-fold rotation axis coincides with the *c* crystallographic axis. Two mirror planes at right angles to each other intersect in this axis. This class is referred to as the **rhombic-pyramidal class** after its general form, a *rhombic pyramid* {*hkl*} (Fig. 9.13).

Forms. Because of the absence of a horizontal mirror, the forms at the top and the bottom of the crystal are different. The rhombic dipyramid becomes two rhombic pyramids, {*hkl*} at the top, and $\{hk\bar{l}\}$ at the bottom. Similarly, {0*kl*} and {*h*0*l*} prisms do not exist, but each occurs as two domes. These domes have indices {0*kl*} and $\{0k\bar{l}\}$ as well as {*h*0*l*} and $\{h0\bar{l}\}$. There are also pedions, {001} and $\{00\bar{1}\}$, and {*hk*0} prisms. The distribution of forms in point groups of the orthorhombic system is found in Table A3.1 of Appendix 3.

Only a few minerals crystallize in this class—the most common representatives are hemimorphite, $Zn_4Si_2O_7(OH)_2{\cdot}H_2O$ (Fig. 9.13), and bertrandite, $Be_4Si_2O_7(OH)_2$.

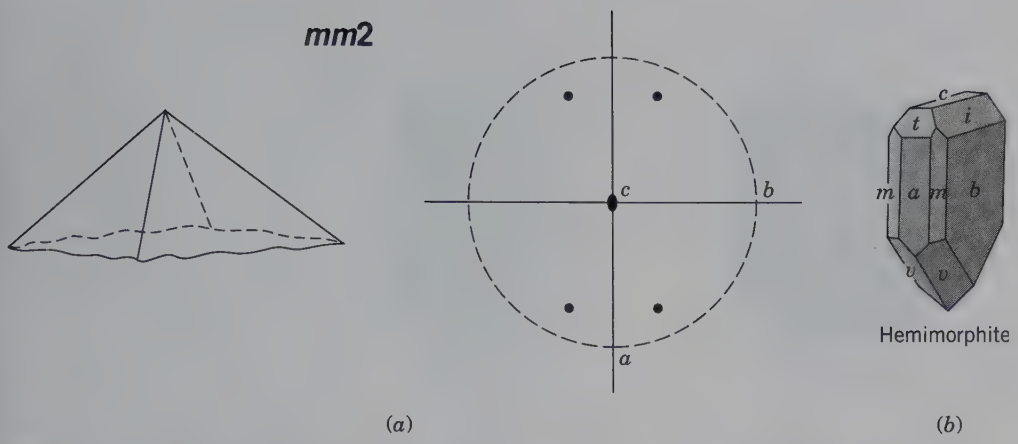

(a) (b)

FIG. 9.13 (a) Rhombic pyramid {*hkl*} and its stereogram. (b) A hemimorphite crystal showing a rhombic pyramid, *v*, at the lower end.

TETRAGONAL SYSTEM

Crystallographic Axes. The forms of the tetragonal system are referred to three crystallographic axes, all perpendicular to each other (Fig. 9.14). The two horizontal axes, *a*, are equal in length and interchangeable, but the vertical axis, *c*, is of a different length (it can be longer or shorter than *a* as in Figs. 9.14a,b). In the Hermann–Mauguin notation of the symmetry elements in the tetragonal system, the first part of the symbol (consisting of 4 or $\bar{4}$) refers to the *c* axis, and the second or third parts refer to the axial (a_1 and a_2) and diagonal symmetry elements, respectively.

4/*m*2/*m*2/*m*

Symmetry—*i*, $1A_4$, $4A_2$, $5m$. The four-fold rotation is the vertical *c* axis. There are four horizontal axes of two-fold symmetry, two of which coincide with the crystallographic axes (a_1 and a_2) and the others are at 45° to them. There are five mirror planes perpendicular to the symmetry axes. One of the horizontal symmetry axes lies in each of the vertical mirror planes (Fig. 9.15). The general form {*hkl*} is the *ditetragonal dipyramid* (Fig. 9.15) and this class is known as the **ditetragonal-dipyramidal class.**

Forms

1. *Basal Pinacoid* {001}. A two-faced form with faces perpendicular to the four-fold axis and parallel to the horizontal *m*. It often occurs in combination with various prisms (Fig. 9.16).

FIG. 9.14 Orientation of tetragonal crystal axes. (a) Crystallographic axes for the tetragonal mineral, zircon, with *c* less than *a*. (b) Crystallographic axes of a tetragonal mineral with *c* greater than *a*.

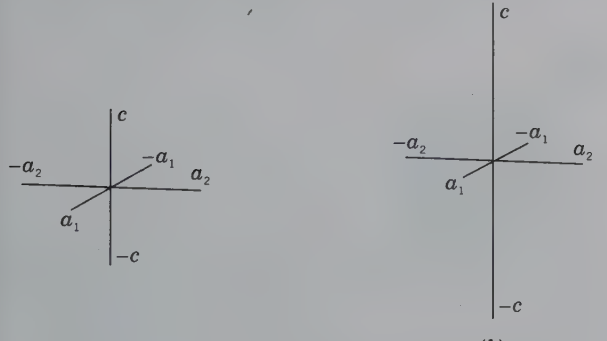

(a) (b)

FIG. 9.15 (a) Symmetry axes and planes for 4/*m*2/*m*2/*m*. (b) The ditetragonal dipyramid {*hkl*} and its stereogram.

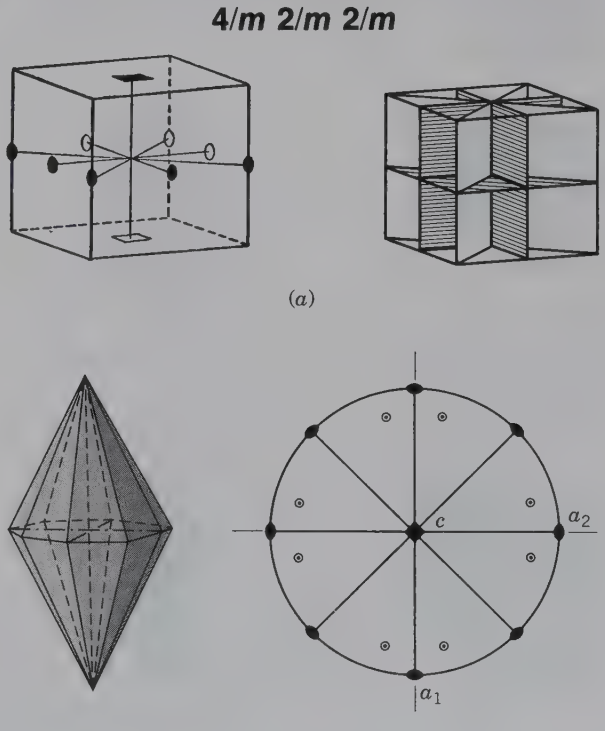

(a) (b)

Tetragonal Prisms

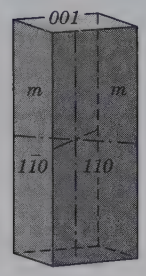

Prism {110} and pinacoid {001}

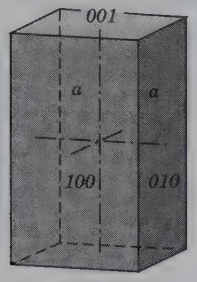

Prism {010} and pinacoid {001}

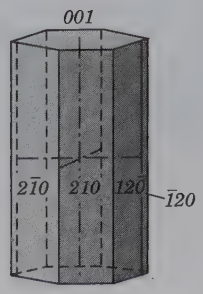

Prism {120} and pinacoid {001}

Tetragonal Dipyramids

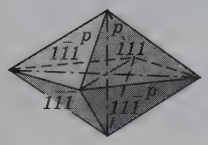

{111}

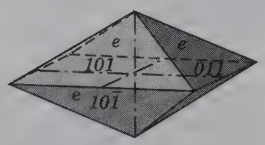

{011}

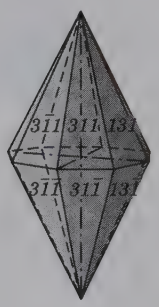

{131}

Tetragonal Crystals

Forms: e {011}, u {021}, c {001}, a {010}, m {110}, x {211}. In this illustration, the Miller indices for the forms are based on the knowledge of the orientation of the unit cell. If the forms were indexed on the basis of morphology, e would be {111}, a {110}, and u {221}.

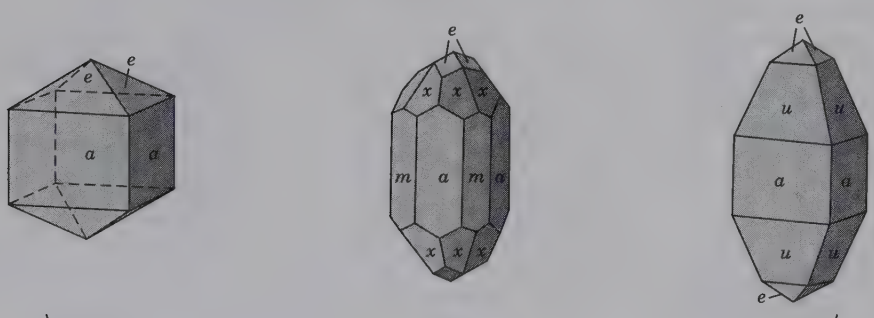

Zircon

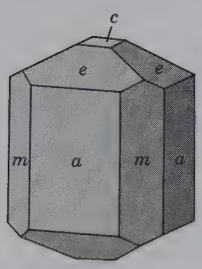

Vesuvianite

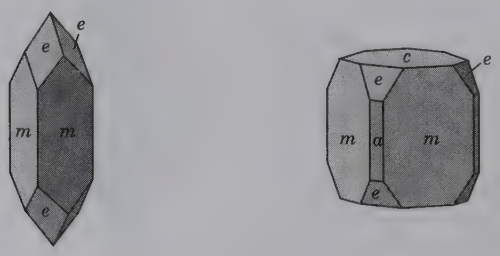

Apophyllite

FIG. 9.16 Commonly developed forms and form combinations in 4/*m*2/*m*2/*m*. Pinacoids, prisms, dipyramids, and combinations.

2. *Tetragonal Prisms* {010} and {110}. The {010} prism consists of four faces that are perpendicular to the two-fold axes of the first kind and parallel with the mirrors in the first 2/*m* in the symbol. The {110} prism has its faces perpendicular to the two-fold axes of the second kind and, thus, is parallel with the mirrors in the second 2/*m* in the symbol.
3. *Ditetragonal Prism* {*hk*0}. Consists of eight rectangular vertical faces, each of which intersects the two horizontal crystallographic axes unequally. There are various ditetragonal prisms, depending on their differing relations to the horizontal axes. A common form represented in Fig. 9.16 has the index {120}.
4. *Tetragonal Dipyramids* {*hhl*} and {0*kl*}. The {*hhl*} dipyramid has eight isosceles triangular faces, each of which intersects all three crystallographic axes, with equal intercepts on the two horizontal axes. There are various such dipyramids, depending on the inclination of their faces to *c*. The unit dipyramid {111} (Fig. 9.16), which intersects all the axes at their unit lengths, is most common. Indices of other similar dipyramids are {221}, {331}, {112}, {113}, and so on, or, in general, {*hhl*}. The {0*kl*} dipyramid is composed of eight isosceles triangular faces, each of which intersects one horizontal axis and the vertical axis, and is parallel to the second horizontal axis. There are several of these dipyramids with different intersections on the vertical axis. The most common is the unit dipyramid {011} (Fig. 9.16). Miller indices for other similar dipyramids are {021}, {031}, {012}, {013}, or, in general {0*kl*}.
5. *Ditetragonal Dipyramid* {*hkl*}. Composed of 16 triangular faces (8 intersecting $+c$ and 8 intersecting $-c$); each face intersects all three of the crystallographic axes, cutting the two horizontal axes at different lengths. There are various ditetragonal dipyramids, depending on the different intersections on the crystallographic axes. One of the most common is the dipyramid {131}, shown in Fig. 9.16.

Tetragonal Combinations. Characteristic combinations of forms in this class, as found on crystals of different minerals, are shown in Fig. 9.16. Prisms are terminated by pinacoids or dipyramids. The distribution of forms in point groups of the tetragonal system is found in Table A3.2 of Appendix 3.

Several common minerals crystallize in 4/*m*2/*m*2/*m*. Major representatives are rutile, TiO_2; anatase, TiO_2; cassiterite, SnO_2; apophyllite, $KCa_4Si_8O_{20}(OH,F)\cdot 8H_2O$; zircon, $ZrSiO_4$(see Plate IV, no.8); and vesuvianite, $Ca_{19}(Al,Mg,Fe)_{13}(Si_2O_7)_4(SiO_4)_{10}(O,OH,F)_{10}$.

$\bar{4}2m$

Symmetry—1 $\bar{A}_4$, 2A_2, 2*m*. The four-fold rotoinversion axis is chosen as the *c* axis and the axes of two-fold rotation as the two *a* axes. At 45° to the *a* axes are two vertical mirror planes intersecting in the vertical axis (Fig. 9.17a). This class is known as the **tetragonal-scalenohedral class**. A *tetragonal scalenohedron* {*hkl*} and its stereogram are illustrated in Figure 9.17b.

Forms

1. *Tetragonal Disphenoids*, {*hhl*} *positive*, $\{h\bar{h}l\}$ *negative* consist of four isosceles triangular faces that intersect all three of the crystallographic axes with equal intercepts on the two horizontal axes. These are the only important forms in this class. There may be different disphenoids, depending on their varying intersections with the vertical axis. Two different disphenoids and a combination of a positive and a negative disphenoid, are shown in Fig. 9.17c.

   The tetragonal disphenoid differs from the tetrahedron in the isometric system (to be discussed subsequently) in that its vertical crystallographic axis is not of the same length as the horizontal axes. The only common mineral in this class is chalcopyrite, crystals of which often show only the disphenoid {112}. This disphenoid closely resembles a tetrahedron, and it requires accurate measurements to confirm its tetragonal character.
2. *Tetragonal Scalenohedron* {*hkl*}. This form, Fig. 9.17b, if it were to occur by itself, is bounded by eight similar scalene triangles. It is a rare form and observed only in combination

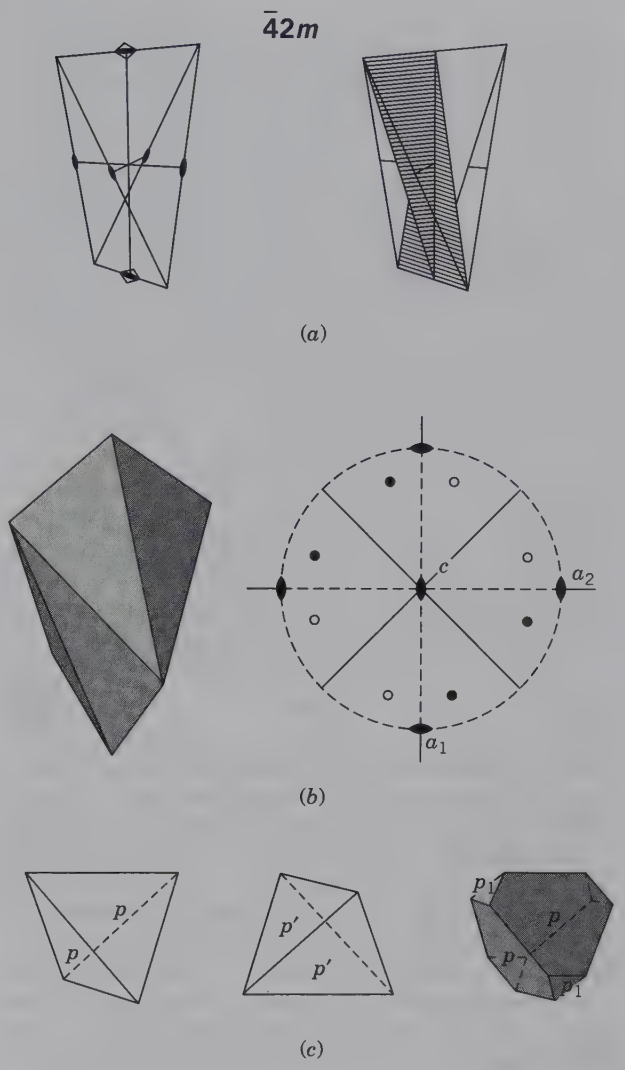

FIG. 9.17 (a) Symmetry axes and planes for $\bar{4}2m$. (b) The tetragonal scalenohedron {*hkl*} and its stereogram. (c) Tetragonal disphenoids {*hhl*} and $\{h\bar{h}l\}$ and a combination of the two forms.

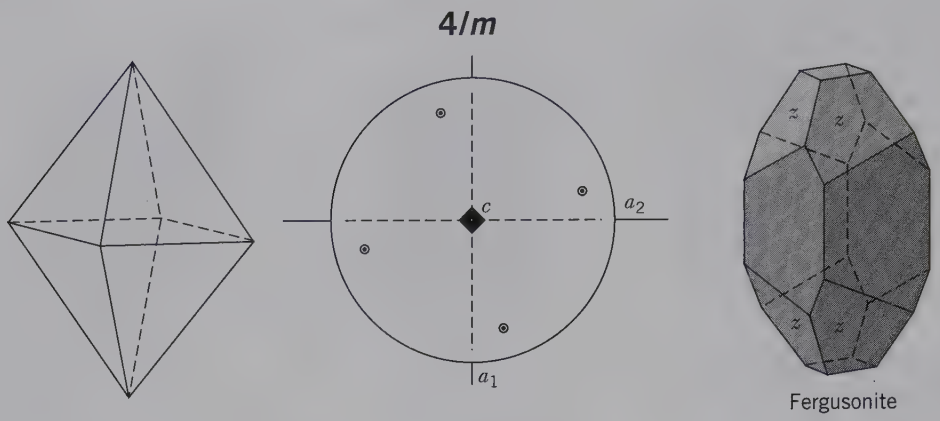

FIG. 9.18 Tetragonal dipyramid {*hkl*} and its stereogram. By itself this form appears to have higher symmetry. In the crystal of fergusonite, the presence of this form (*z*) reveals the true symmetry, 4/*m*.

with others. Other forms that may be present are pinacoid, tetragonal prisms, ditetragonal prisms, and tetragonal dipyramids.

Chalcopyrite, $CuFeS_2$, and stannite, Cu_2FeSnS_4, are the common minerals that crystallize in this class.

4/*m*

Symmetry—*i*, 1A$_4$, 1*m*. There is only the vertical four-fold rotation axis with a perpendicular symmetry plane. This class is known as the **tetragonal-dipyramidal class** after the general form {*hkl*}, a *tetragonal dipyramid* (Fig. 9.18).

Forms. The tetragonal dipyramid, {*hkl*}, is an eight-faced form having four upper faces directly above four lower faces. This form by itself appears to have higher symmetry, and it must be in combination with other forms to reveal the absence of vertical mirror planes. The pinacoid {001} and tetragonal prisms {*hk*0} may be present. The tetragonal prism {*hk*0} is equivalent to the four alternate faces of the ditetragonal prism and is present in those classes of the tetragonal system that have no vertical mirror planes or horizontal two-fold rotation axes.

Mineral representatives in this class are scheelite, $CaWO_4$; powellite, $CaMoO_4$; fergusonite, $YNbO_4$; and members of the scapolite series, $Na_4Al_3Si_9O_{24}Cl$ to $Ca_4Al_6Si_6O_{24}CO_3$. Figure 9.18 illustrates a crystal of fergusonite in which the tetragonal dipyramid *z* reveals the true symmetry of this class.

HEXAGONAL SYSTEM

All of the crystal classes in the hexagonal system can be based on a hexagonal lattice, whether their symbol begins with 6, $\bar{6}$, 3, or $\bar{3}$. The five classes beginning with 3 or $\bar{3}$ can also be based on a rhombohedral lattice.

Crystallographic Axes. The forms of the hexagonal system are referred to four crystallographic axes, designated a_1, a_2, and a_3; they lie in the horizontal plane and are of equal length with angles of 120° between the positive ends; the fourth axis, *c*, is vertical. When properly oriented, one horizontal crystallographic axis, a_2, is left to right, and the other two make 120° angles on either side of it (Fig. 9.19). The positive end of a_1 is to the front and left, the positive end of a_2 is to the right, and the positive end of a_3 is to the back and left. Figure 9.19b shows the four axes with the *c* axis vertical. Indices for any face of a hexagonal crystal require the use of four digits (the Bravais–Miller symbol). The numbers expressing the reciprocals of the intercepts of a face on the axes are given in the order a_1, a_2, a_3, *c*. Therefore, $(11\bar{2}1)$, which represents the intercepts $3a_1$, $3a_2$, $-3/2a_3$, $3c$, refers to a face that cuts the positive ends of the a_1 and a_2 axes at twice the distance it cuts the negative end of the a_3 axis; it cuts the *c* axis at the same relative number of units (3) as it cuts the a_1 and a_2 axes. The general Bravais–Miller form symbol is $[hki\bar{l}]$. The third digit of the index is the sum of the first two times -1; or, stated another way, $h + k + i = 0$ (see also Fig. 6.31, page 135).

In the Hermann–Mauguin notation, the first number refers to the principal axis of symmetry coincident with *c*. The second and third symbols, if present, refer respectively to symmetry elements parallel with and perpendicular to the crystallographic axes a_1, a_2, and a_3.

6/*m*2/*m*2/*m*

Symmetry—*i*, 1A$_6$, 6A$_2$, 7*m*. The vertical axis, *c*, is a six-fold rotation axis. There are six horizontal axes of two-fold rotation, three of which coincide with the crystallographic axes (a_1, a_2, and a_3); the other three lie midway between them. There are seven mirror planes, each perpendicular to one

FIG. 9.19 Hexagonal crystal axes. (a) Plan view, looking down the *c* axis. (b) Perspective view of the axes in the hexagonal system.

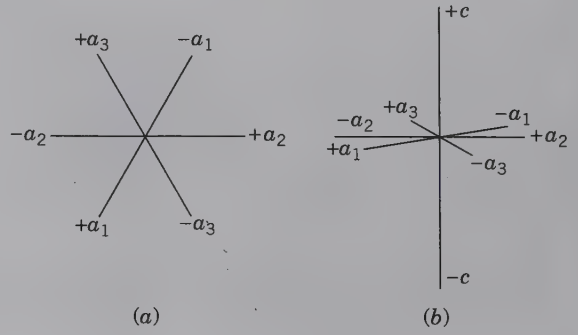

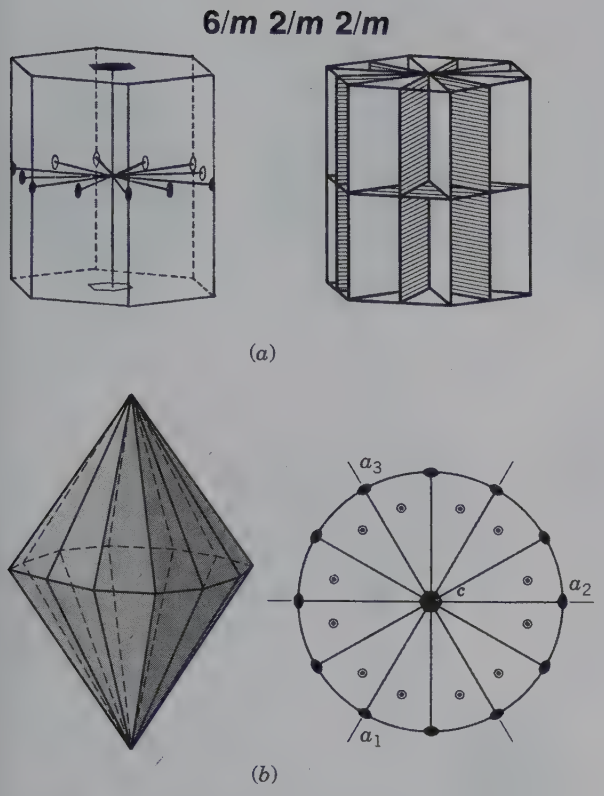

FIG. 9.20 (a) Symmetry axes and planes in 6/*m*2/*m*2/*m*. (b) The dihexagonal dipyramid and its stereogram.

of the symmetry axes (Fig. 9.20a). The general form is the *dihexagonal dipyramid*, and this class is known as the **dihexagonal-dipyramidal class**, after the general form $\{hk\bar{i}l\}$ (Fig. 9.20b).

Forms

1. *Pinacoid* {0001}. Composed of two parallel faces, perpendicular to the six-fold axis, and parallel with the horizontal *m*. It is commonly referred to as a basal pinacoid. It is shown in combination with various prisms in Fig. 9.21.
2. *Hexagonal Prisms* $\{10\bar{1}0\}$ and $\{11\bar{2}0\}$. The {1010} prism consists of six vertical faces, each of which intersects two of the horizontal crystallographic axes equally and is parallel to the third. The faces of this prism are parallel to the two-fold axes of the first kind. The $\{11\bar{2}0\}$ prism also has six vertical faces, but each of these intersects two of the horizontal axes equally and the intermediate horizontal axis at one-half this distance. These two types of hexagonal prisms are geometrically identical forms; the distinction between them is only in orientation (Fig. 9.21).
3. *Dihexagonal Prism* $\{hk\bar{i}0\}$. This form consists of 12 vertical faces, each of which intersects all three of the horizontal crystallographic axes at different lengths. There are various dihexagonal prisms, depending on their intercepts with the horizontal axes. A common dihexagonal prism with indices $\{21\bar{3}0\}$ is shown in Fig. 9.21.
4. *Hexagonal Dipyramids* $\{h0\bar{h}l\}$ and $\{hh(2\bar{h})l\}$. The $\{h0\bar{h}l\}$ hexagonal dipyramid consists of 12 isosceles triangular faces, each of which intersects two horizontal crystallographic axes equally, is parallel to the third, and intersects the vertical axis. Various hexagonal dipyramids are possible, depending on the inclination of the faces to the *c* axis. The unit form has the indices $\{10\bar{1}1\}$ (Fig. 9.21). The $\{hh(2\bar{h})l\}$ dipyramid is also composed of 12 isosceles triangular faces. Each face intersects two of the horizontal axes equally and the third (the intermediate horizontal axis) at one-half this distance; each face also intersects the vertical axis. Various such dipyramids are possible, depending on the inclination of the faces to c. A common form has the indices $\{11\bar{2}2\}$ (Fig. 9.21).
5. *Dihexagonal Dipyramid* $\{hk\bar{i}l\}$. This is composed of 24 triangular faces; 12 of which intersect $+c$ and 12 intersect $-c$. Each face is a scalene triangle that intersects all three of the horizontal axes differently and also intersects the vertical axis. A common form, $\{21\bar{3}1\}$, as well as various combinations of forms in this class are shown in Fig. 9.21.

The distribution of forms in point groups of the hexagonal system is listed in Table A3.3 of Appendix 3.

Beryl, $Be_3Al_2Si_6O_{18}$, and its gem variety aquamarine, are examples of a mineral representative in this class (see Plate V, no. 5). Other minerals are molybdenite, MoS_2; pyrrhotite, $Fe_{1-x}S$; and nickeline (synonymous with niccolite), NiAs.

6*mm*

Symmetry—1A$_6$, 6*m*. The six-fold rotation axis is chosen as the *c* axis, and six vertical mirror planes intersect in this axis. This class is known as the **dihexagonal-pyramidal class** after the $\{hk\bar{i}l\}$ general form, a *dihexagonal pyramid* (Fig. 9.22).

Forms. The forms of this class are similar to those of class 6/*m*2/*m*2/*m*, but because the horizontal mirror plane is missing, different forms appear at the top and bottom of the crystal. The dihexagonal pyramid is thus two forms: $\{hk\bar{i}l\}$ upper and $\{hk\bar{i}\bar{l}\}$ lower. The hexagonal-pyramidal forms are $\{h0\bar{h}l\}$ upper and $\{h0\bar{h}\bar{l}\}$ lower; and $\{h0(2\bar{h})l\}$ upper and $\{h0(2\bar{h})\bar{l}\}$ lower. The pinacoid cannot exist here, but instead there are two pedions {0001} and $\{000\bar{1}\}$. Hexagonal prisms and the dihexagonal prism may be present.

Wurtzite, ZnS; greenockite, CdS; and zincite, ZnO, are the most common mineral representatives in this class. Figure 9.22 shows a zincite crystal with a hexagonal prism terminated above by a hexagonal pyramid and below by a pedion.

622

Symmetry—1A$_6$, 6A$_2$. The symmetry axes are the same as those in class 6/*m*2/*m*2/*m* (Fig. 9.20a), but mirror planes and the center of symmetry are lacking. This class is referred to as the **hexagonal-trapezohedral class**, after its general form $\{hk\bar{i}l\}$.

Forms. The *hexagonal trapezohedrons*, $\{hk\bar{i}l\}$ *right* and $\{ih\bar{k}\bar{l}\}$ *left*, are enantiomorphic forms, each with 12 trapezium-shaped faces (Fig. 9.23). Other forms that may be present are the pinacoid, hexagonal prisms, dipyramids, and dihexagonal prisms. The distribution of forms in point groups of the hexagonal system is listed in Table A3.3 of Appendix 3.

High quartz, SiO_2, and kalsilite, $KAlSiO_4$, are the only mineral representatives in this class.

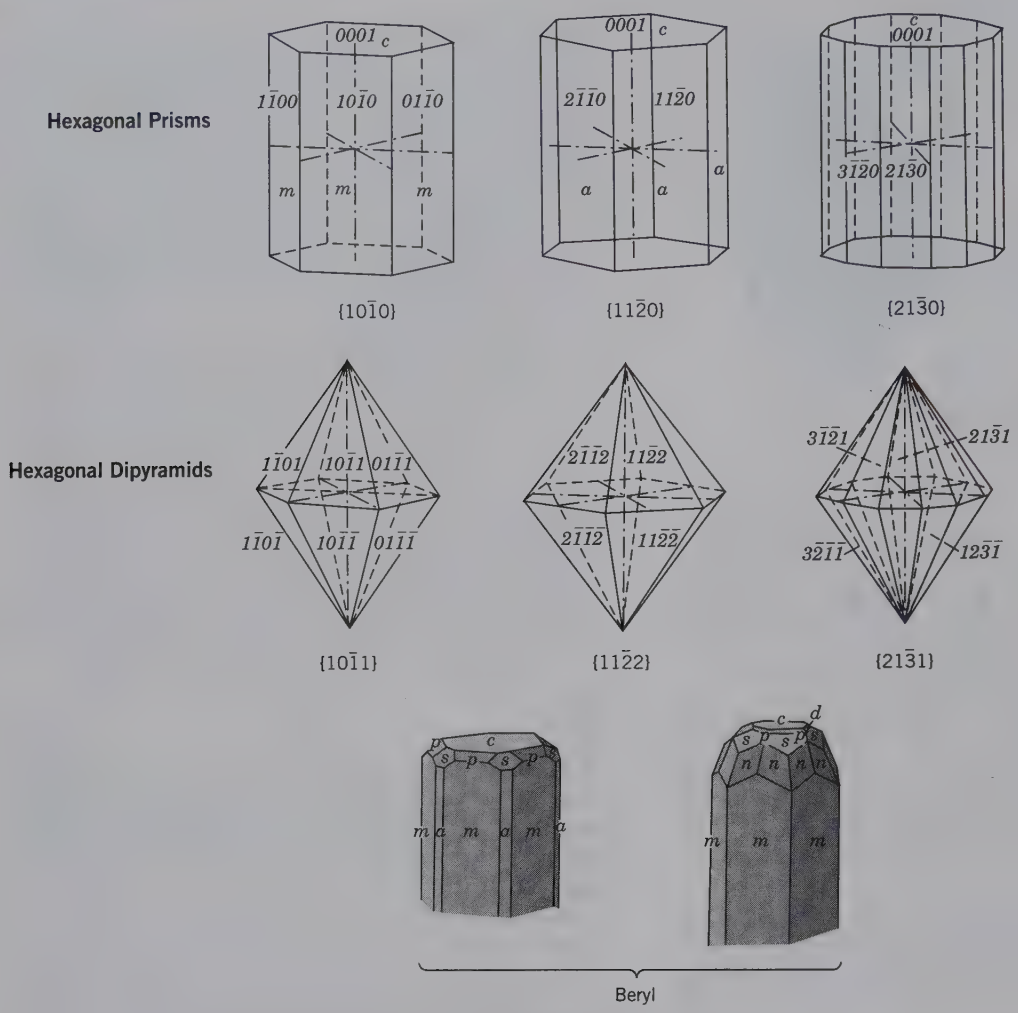

FIG. 9.21 Commonly developed forms and form combinations in 6/*m*2/*m*2/*m*.

6*mm*

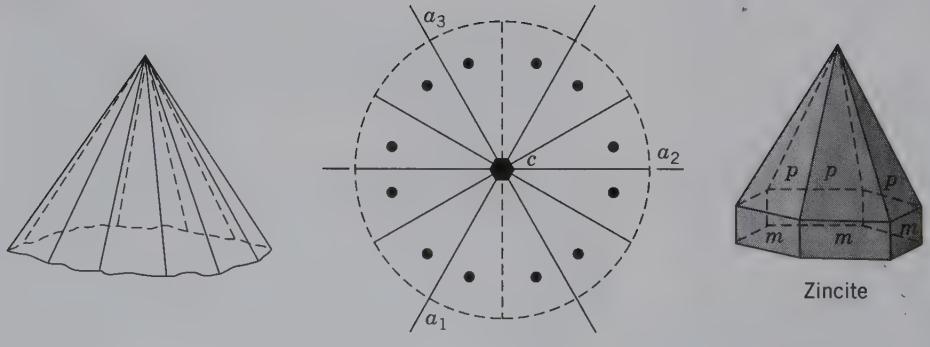

FIG. 9.22 Dihexagonal pyramid {*hkil*} and its stereogram. This pyramid (*p*) is shown in zincite crystals.

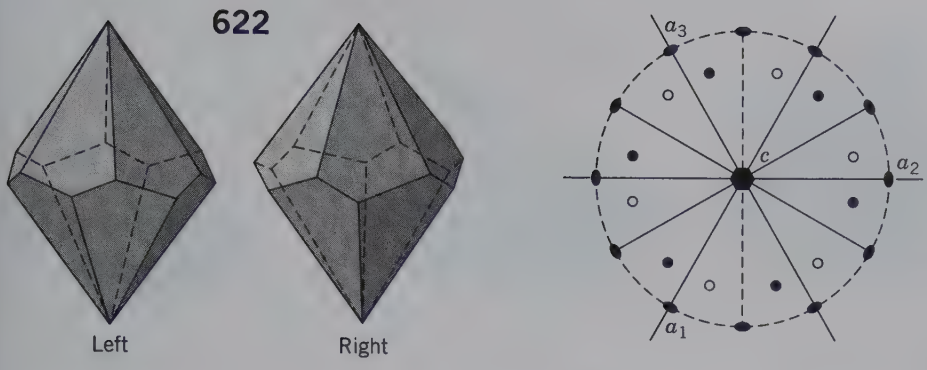

FIG. 9.23 Enantiomorphic, left- and right-handed hexagonal trapezohedrons, $\{ihk\bar{l}\}$ and $\{hki\bar{l}\}$ respectively. A stereogram of the left-handed form.

6/*m*

Symmetry—*i*, $1A_6$, $1m$. There is one vertical six-fold rotation axis with a symmetry plane perpendicular to it. This class is known as the **hexagonal-dipyramidal class** after its general form, a *hexagonal dipyramid* $\{hki\bar{l}\}$ (Fig. 9.24).

Forms. The general forms of this class are the *hexagonal dipyramids*, $\{hki\bar{l}\}$ positive, $\{khi\bar{l}\}$ negative. These forms consist of 12 faces, six above and six below, which correspond in position to one-half the faces of a dihexagonal dipyramid. Pinacoid and prisms may also be present (see Fig. 9.24). (See Table A3.3 of Appendix 3 for form combinations.)

The apatite group minerals, $Ca_5(PO_4)_3(OH, F, Cl)$, are the primary examples that crystallize in this class (see Plate IV, no. 4). The dipyramid revealing the symmetry of this class is rarely seen but is illustrated as face μ in Fig. 9.24.

$\bar{3}2/m$

Symmetry—$1\bar{A}_3$, $3A_2$, $3m$. The three-fold rotoinversion axis is the vertical axis and the 3 two-fold rotation axes are the three horizontal crystallographic axes (a_1, a_2, and a_3). Three vertical mirror planes bisect the angles between the horizontal axes (Figs. 9.25*a*). This class is known as the **hexagonal-scalenohedral class** after the general form, the *hexagonal scalenohedron* $\{hki\bar{l}\}$.

Forms

1. *Rhombohedron*, $\{h0\bar{h}l\}$ *positive*, $\{0h\bar{h}l\}$ *negative*. The rhombohedron is a form consisting of six rhomb-shaped faces, which correspond in their positions to the alternate faces of a hexagonal dipyramid $\{h0\bar{h}l\}$. The relation of these two forms to each other is shown in Fig. 9.25b. The rhombohedron may also be thought of as a cube deformed in the direction of one of the axes of three-fold rotoinversion (see Plate III, no. 6). The deformation may appear either as an elongation along the rotoinversion axis, producing an acute solid angle, or compression along the rotoinversion axis, producing an obtuse solid angle. Depending on the angle, the rhombohedron is known as acute or obtuse. Depending on the orientation, the rhombohedron may be positive or negative (Fig. 9.26). There are various rhombohedrons that differ from each other in the inclination of their faces to the *c* axis. The index symbol of the unit positive rhombohedron is $\{10\bar{1}1\}$ and of the unit negative rhombohedron $\{01\bar{1}1\}$.
2. *Scalenohedron*, $\{hki\bar{l}\}$ *positive*, $\{khi\bar{l}\}$ *negative*. This form consists of 12 scalene triangular faces (Fig. 9.25c) corresponding

FIG. 9.24 Hexagonal dipyramid $\{hki\bar{l}\}$ and its stereogram. This form by itself appears to have higher symmetry, but in combination with other forms reveals its low symmetry content. The form (μ) is the hexagonal dipyramid on the apatite crystal.

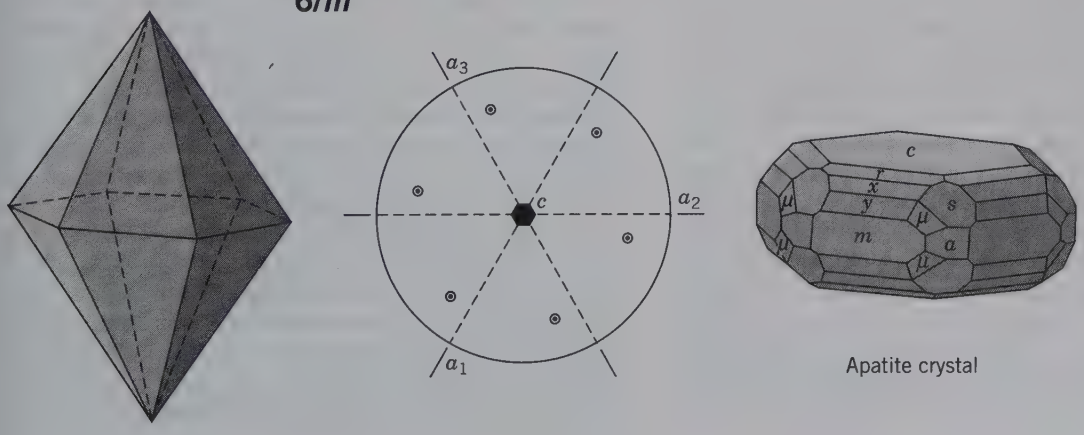

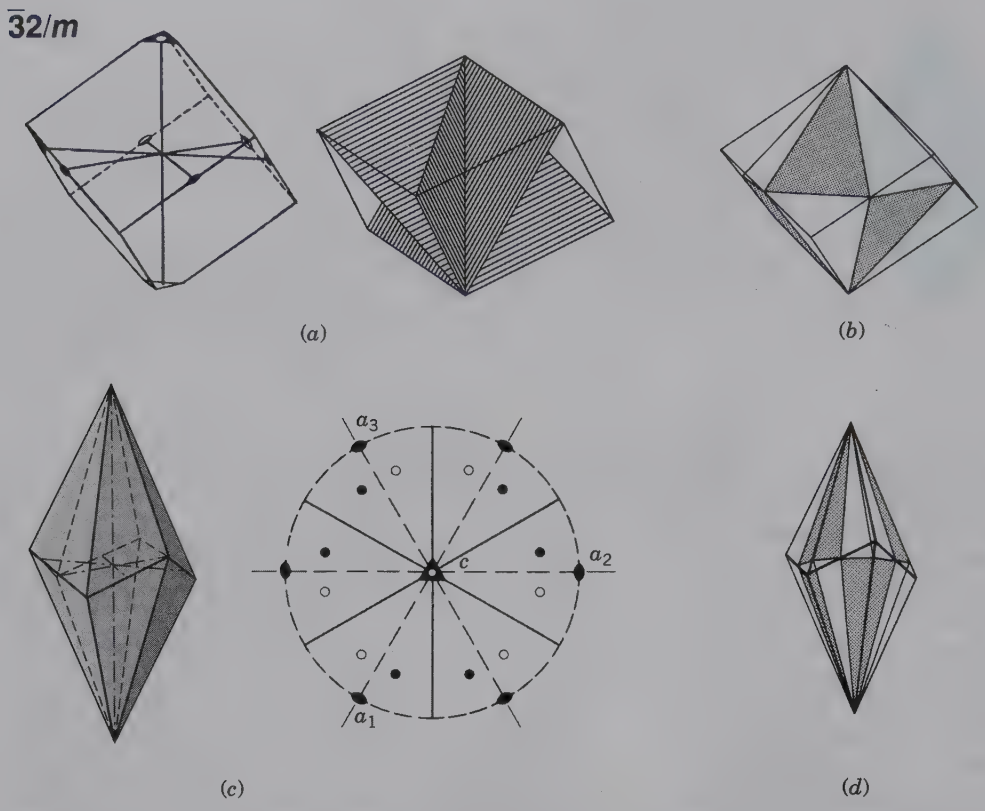

FIG. 9.25 (a) Symmetry axes and planes for $\bar{3}\,2/m$. (b) Relationship between the rhombohedron $\{h0\bar{h}l\}$ and a hexagonal dipyramid $\{hki\bar{l}\}$. (c) Hexagonal scalenohedron $\{hki\bar{l}\}$ and its stereogram. (d) Relationship between the scalenohedron (bold outline of faces) and a dihexagonal dipyramid (shaded faces).

in position to alternate *pairs* of faces of a dihexagonal dipyramid (Fig. 9.25d). The scalenohedron is differentiated from the dipyramid by the zigzag appearance of the middle edges. There are many different scalenohedrons; most frequently seen is $\{21\bar{3}1\}$ a common form on calcite; indicated by *v* in crystals in Fig. 9.26.

The rhombohedron and scalenohedron of this class may combine with forms found in classes of higher hexagonal symmetry. Consequently, they are found in combination with hexagonal prisms, dihexagonal prisms, hexagonal dipyramid, and pinacoid (see calcite, chabazite, and corundum crystals in Fig. 9.26). The distribution of forms in point groups of the hexagonal system is listed in Table A3.3 of Appendix 3.

Many common minerals crystallize in this class. Chief among them is calcite, $CaCO_3$, and the other members of the calcite group (Fig. 9.26). Additional minerals in this class include corundum, Al_2O_3; hematite, Fe_2O_3; brucite, $Mg(OH)_2$; nitratite, $NaNO_3$, synonymous with soda niter; arsenic, As; millerite, NiS; antimony, Sb; and bismuth, Bi.

3*m*

Symmetry—1A$_3$, 3*m*. The vertical axis is a three-fold rotation axis, and three mirror planes intersect in this axis (Fig. 9.27a). In the Hermann–Mauguin notation of this class, the 3 refers to the vertical *c* axis and the *m* refers to three planes perpendicular to the three horizontal axes a_1, a_2, and a_3. These three mirror planes intersect in the vertical three-fold axis. This class is known as the **ditrigonal pyramidal class**, after the general form, a *ditrigonal pyramid* $\{hki\bar{l}\}$. A ditrigonal pyramid $\{hki\bar{l}\}$ and its stereogram are shown in Fig. 9.27a.

Forms. The forms are similar to those of the class $\bar{3}2/m$ but with only half the number of faces. Because the two-fold rotation axes are absent, the faces at the top of the crystals belong to different forms from those at the bottom. There are four possible *ditrigonal pyramids*, with indices $\{hki\bar{l}\}$, $\{khi\bar{l}\}$, $\{hk\bar{i}l\}$, and $\{kh\bar{i}l\}$. Other forms that may be present are pedions, hexagonal prisms and pyramids, trigonal pyramids, trigonal prisms, and ditrigonal prisms. There are four possible trigonal pyramids with indices $\{h0\bar{h}l\}$, $\{0h\bar{h}l\}$, $\{0\bar{h}hl\}$, and $\{h0\bar{h}l\}$.

Tourmaline (Fig. 9.27b), photographed for the cover of this text, is the most common mineral crystallizing in this class. Its various forms are commonly displayed on large crystals, and the trigonal symmetry is also revealed in crystals that are sectioned perpendicular to the *c* axis (as on the cover). In addition, members of the proustite, Ag_3AsS_3 - pyrargyrite, Ag_3SbS_3, series and alunite, $KAl_3(SO_4)_2(OH)_6$, crystallize in this class.

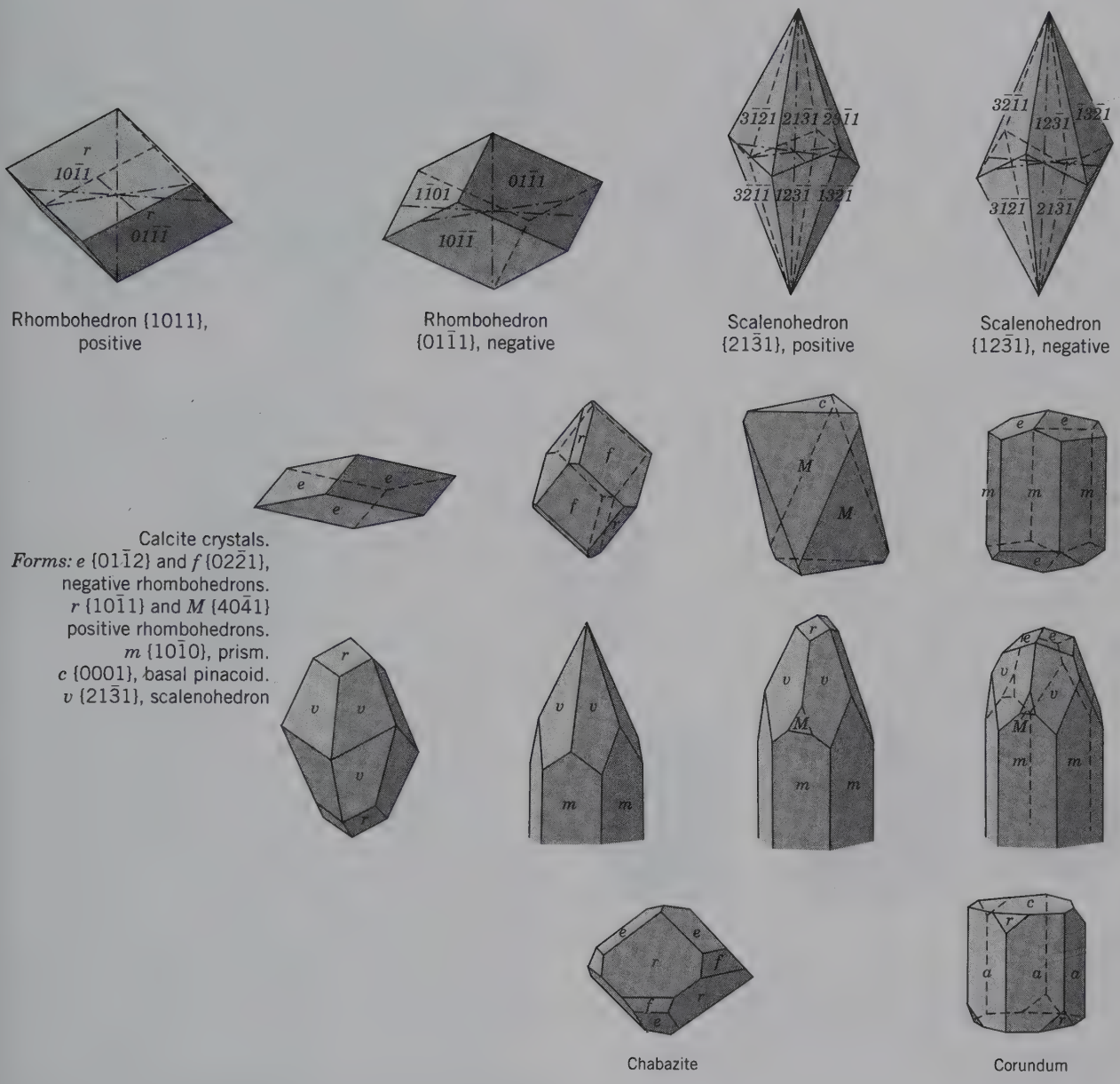

FIG. 9.26 Commonly developed forms and form combinations in $\bar{3}\,2/m$.

32

Symmetry—$1A_3$, $3A_2$. The vertical crystallographic axis is an axis of three-fold rotation and the three horizontal crystallographic axes are axes of two-fold rotation. The symmetry axes are similar to those in class $\bar{3}2/m$ but mirror planes are absent. The class is referred to as the **trigonal-trapezohedral class**, after the general $\{hk\bar{i}l\}$ form, the *trigonal trapezohedron* (Fig. 9.28). Both a positive left and a positive right trigonal trapezohedron can develop (Fig. 9.28a).

Forms. There are four *trigonal trapezohedrons*, each made up of six trapezium-shaped faces. Their Miller indices are $\{hk\bar{i}l\}$, $\{\bar{i}k\bar{h}l\}$, $\{kh\bar{i}l\}$ and $\{\bar{k}i\bar{h}l\}$. These forms can be grouped into two enantiomorphic pairs, each with a right and left form (Fig. 9.28a). Other forms that may be present are pinacoids, trigonal prisms, hexagonal prism, ditrigonal prisms, and rhombohedrons. The distribution of forms in point groups of the hexagonal system is given in Table A3.3 of Appendix 3.

The familiar, low-temperature quartz, SiO_2, is the most common mineral crystallizing in this class. Only rarely do we see small faces of the trigonal trapezohedron (x) on quartz crystals (in combination with prism faces), but when they are present, the crystals can be distinguished as right-handed or left-handed (Fig. 9.28b) based on the presence of this face.

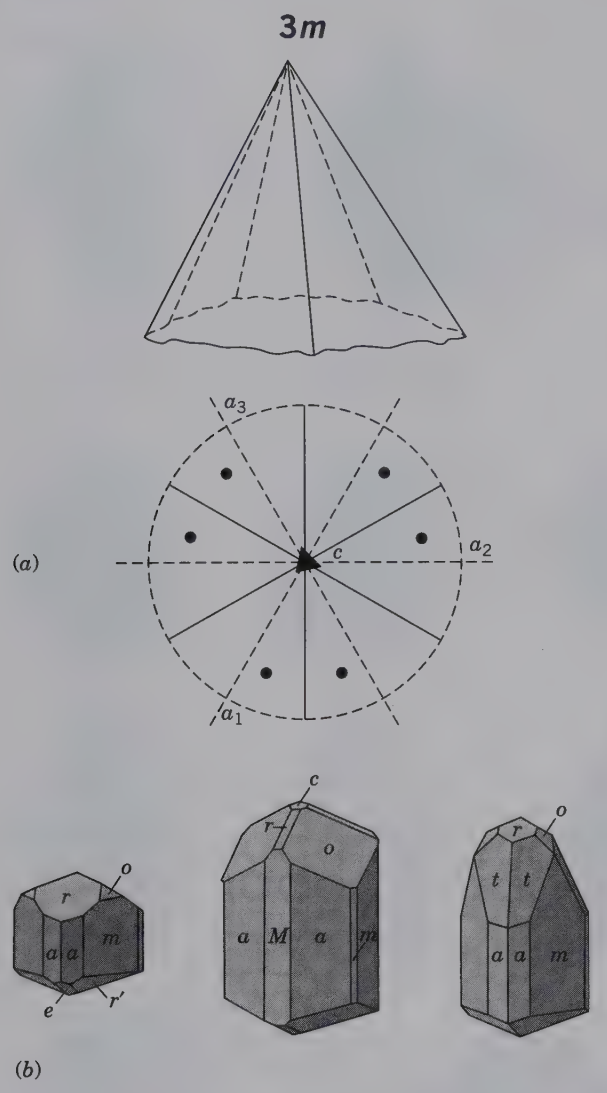

FIG. 9.27 (a) Ditrigonal pyramid $\{hki\bar{l}\}$ and its stereogram. In the conventional orientation of the symmetry elements of this crystal class, the mirror planes are perpendicular to a_1, a_2, and a_3. (b) Tourmaline crystals showing $3m$ symmetry with various combinations of forms.

With a prism face directly toward the observer and if the trigonal trapezohedral face, *x*, truncates the edge between the prism and the top rhombohedron at the right, it is right-handed; if at the left, it is left-handed. The faces marked *s* are trigonal pyramids (in Fig. 9.28b).

Cinnabar, HgS, and the rare mineral berlinite, $AlPO_4$, also crystallize in this class.

$\bar{3}$

Symmetry—$1\bar{A}_3$. The vertical axis is a three-fold axis of rotoinversion. This is equivalent to a three-fold rotation axis and a center of symmetry. This class is known as the **rhombohedral class**, after the general form, a *rhombohedron* $\{hki\bar{l}\}$ (Fig. 9.29).

Forms. The general forms of this class are four different *rhombohedrons*, each corresponding to six faces of the dihexagonal-dipyramid. If one of these appeared alone on a crystal, it would have the morphological symmetry of class $\bar{3}2/m$. It is only in combination with other forms that its true symmetry becomes apparent. The {0001} pinacoid and hexagonal prisms may be present. (See Table A3.3 of Appendix 3 for form combinations).

Dolomite, $CaMg(CO_3)_2$, is the most common mineral crystallizing in this class; other representatives are ilmenite, $FeTiO_3$; willemite, Zn_2SiO_4; and phenakite, Be_2SiO_4.

ISOMETRIC SYSTEM

Crystallographic Axes. The forms in classes of the isometric system are referred to three axes of equal length that make right angles with each other. Because the axes are identical, they are interchangeable and all are designated by the letter *a*. When properly oriented, a_1 is horizontal and oriented front (+) to back, a_2 is horizontal and right (+) to left (−), and a_3 is vertical (Fig. 9.30).

In the Hermann–Mauguin notation, the first number (4, $\bar{4}$ or 2) refers to the three crystallographic axes a_1, a_2, and a_3. If the number is 4 or $\bar{4}$, it means that there are 3 four-fold axes of rotation or rotoinversion coincident with the three crystallographic axes. If it is 2, there are 3 two-fold axes, coincident with the three crystallographic axes. The second number ($\bar{3}$ or 3) refers to the four diagonal directions of three-fold symmetry, between the corners of a cube (Fig. 9.31a). The third number or symbol (if present) refers to symmetry elements between the six pairs of opposing cube edges (Fig. 9.31a). If it is 2 (as in 432), there are 6 two-fold axes perpendicular to the edges; if it is *m* (as in $\bar{4}3m$), there are six mirror planes; if it is $2/m$ (as in $4/m\bar{3}2/m$) there are 6 two-fold axes with mirrors perpendicular to them.

Form Symbols. Although the symbol of any face of a crystal form might be used as the form symbol (because all faces on a form have the same relationship to the axes), it is conventional, when possible, to use one in which *h*, *k*, and *l* are all positive. In forms that have two or more faces with *h*, *k*, and *l* positive, the rule followed is to take the form symbol with $h < k < l$. For example, the form with a face symbol (123) also has faces with symbols (132), (213), (231), (312), and (321). Following the rule, {123} would be taken as the form symbol, for there $h < k < l$.

In giving the ϕ and ρ angles of a form, it is customary to give those for only one face; the others can be determined by knowing the symmetry. The face for which these coordinates are given is the one with the smallest ϕ and ρ values. This is the face of the form in which $h < k < l$.

$4/m\bar{3}2/m$

Symmetry—$3A_4$, $4\bar{A}_3$, $6A_2$, $9m$. The three crystallographic axes are axes of four-fold rotation. There are also four diagonal axes of three-fold rotoinversion; these axes emerge in the middle of each of the octants formed by the intersection of the crystallographic axes. There are six diagonal directions of two-fold rotation, each of which bisects one of

32

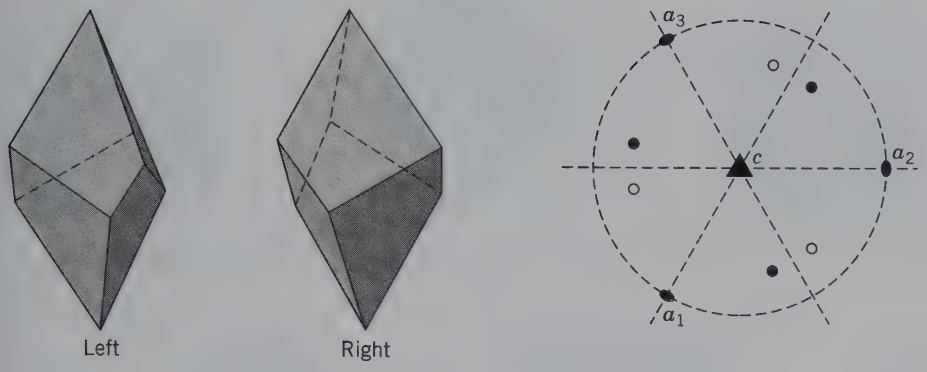

(*a*)

(*b*)

FIG. 9.28 (a) Trigonal trapezohedron $\{hki\bar{l}\}$, positive left- and positive right-handed forms, with a stereogram of the positive right form. (b) Left-handed and right-handed quartz crystals. The trigonal trapezohedral faces are marked by *x* and their placement determines the handedness of the crystal.

the angles between two of the crystallographic axes. There is also a center of symmetry because $\bar{3}$ is equivalent to $3 + i$. These symmetry elements are shown in Fig. 9.31a on a cube.

This class has nine mirror planes. Three of them are known as the axial planes, because each includes two crystallographic axes, and six are diagonal planes, because each bisects the angle between two of the axial planes (Fig. 9.31b). This combination of symmetry elements defines the highest symmetry possible in crystals. *Every crystal form and every combination of forms that belongs to this class must show its complete symmetry.* It is important to remember that in this class the three crystallographic axes are axes of four-fold rotation. Thus, one can easily locate the crystallographic axes and properly orient the crystal. The *hexoctahedron*, the general form $\{hkl\}$ from which the **hexoctahedral class** derives its name, is shown in Fig. 9.31c with a stereogram.

Forms. Illustrations of the most common forms and form combinations in this class are given in Figs. 9.32 and 9.33. Figures 6.36 (34) to (48) illustrate all 15 isometric forms.

1. *Cube* {001}. The cube is composed of six square faces that make 90° angles with each other. Each face intersects one of the crystallographic axes and is parallel to the other two.
2. *Octahedron* {111}. The octahedron is composed of eight equilateral triangular faces, each of which intersects all three of the crystallographic axes equally. When in combination with a cube, the octahedron can be recognized by its eight similar faces, each of which is equally inclined to the three crystallographic axes. Commonly, the faces of an octahedron truncate symmetrically the corners of a cube (Fig. 9.32)

FIG. 9.29 Rhombohedron $\{hki\bar{l}\}$ and its stereogram.

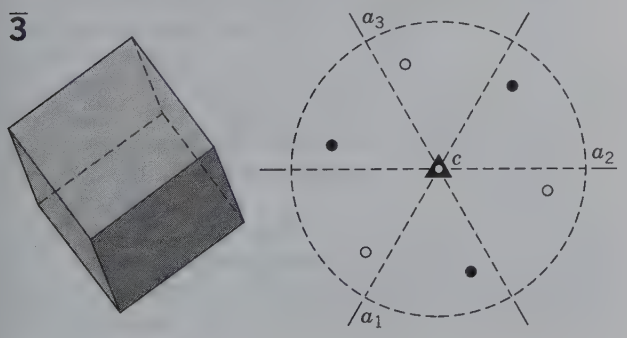

FIG. 9.30 Isometric crystal axes and their orientation.

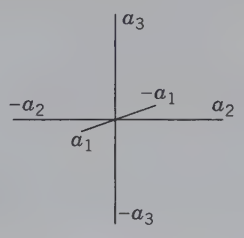

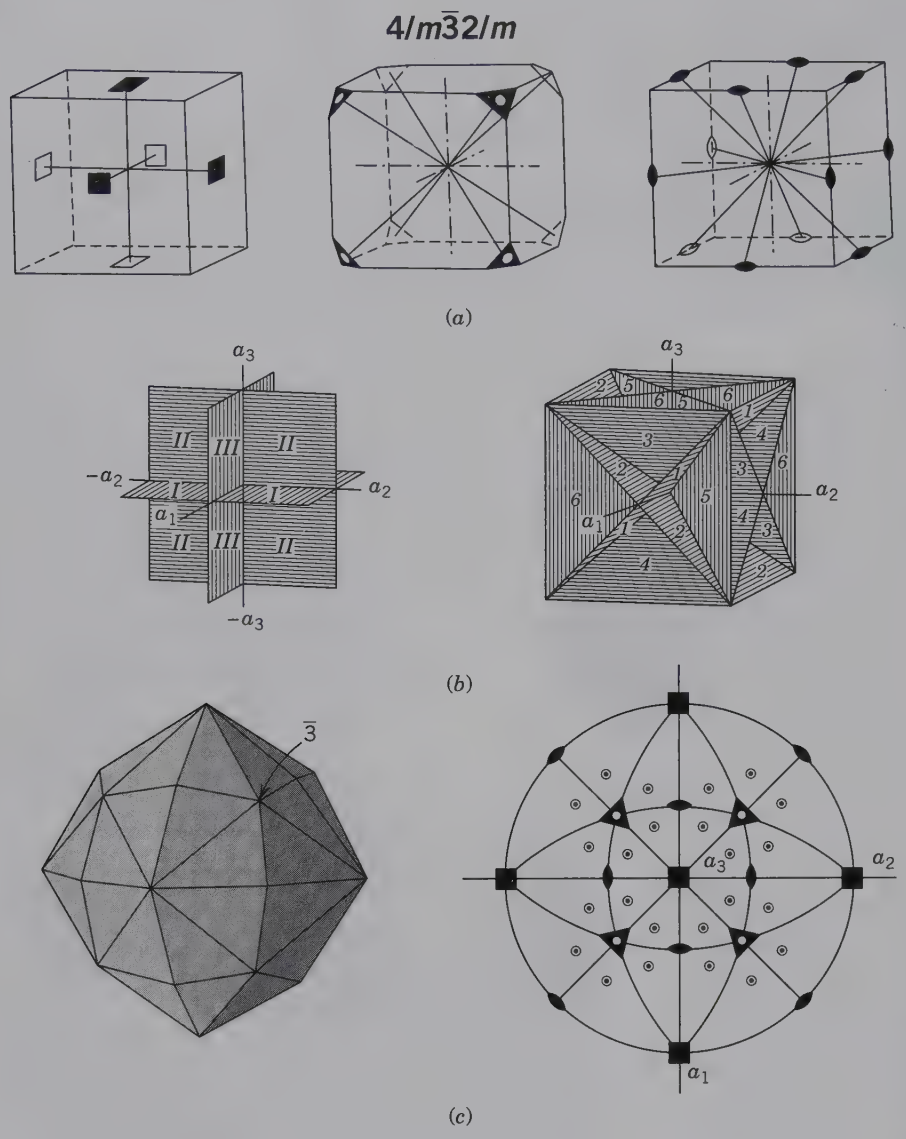

FIG. 9.31 (a) Symmetry axes, and (b) planes for $4/m\bar{3}\,2/m$, and (c) the hexoctahedron {*hkl*} and its stereogram. The location of one $\bar{3}$ is noted in the model.

3. *Dodecahedron* {011}. The dodecahedron is composed of 12 rhomb-shaped faces. Each face intersects two of the crystallographic axes equally and is parallel to the third. A dodecahedron may be the only form on a crystal or it may develop in combinations of a dodecahedron and a cube, of a dodecahedron and an octahedron, and of a cube, an octahedron, and a dodecahedron (see Fig. 9.32). The faces of a dodecahedron truncate the edges of both the cube and the octahedron.
4. *Tetrahexahedron* {0*kl*}. The tetrahexahedron is composed of 24 isosceles triangular faces, each of which intersects one axis at unity and the second at some multiple and is parallel to the third. Several tetrahexahedrons occur that differ from each other with respect to the inclination of their faces. The most common is {012}. The indices of other forms are {013}, {014}, {023}, and so on, or in general, {0*kl*}. To identify a tetrahexahedron, it is helpful to evaluate its name: *tetra* = 4, *hexa* = 6 (number of faces in a cube); each cube face is raised into four other triangular faces as in Fig. 9.32. A tetrahexahedron may also combine with a cube, with its edges all beveled by the faces of a tetrahexahedron (as in Fig. 9.32).
5. *Trapezohedron* {*hhl*}. The trapezohedron is composed of 24 trapezium-shaped faces, each of which intersects one of the crystallographic axes at unity and the other two at equal multiples. There are various trapezohedrons with their faces having different angles of inclination, but the most common is {112} (Fig. 9.33). Figure 9.33 shows the common trapezohedron *n* {112} truncating the edges of the dodecahedron. Both forms by themselves, and in combination, are common on the mineral garnet (see Plate IV, no. 7).
6. *Trisoctahedron* {*hll*}. The trisoctahedron is composed of 24 isosceles triangular faces, each of which intersects two of the crystallographic axes at unity and the third axis at some multiple. There are various trisoctahedrons, the

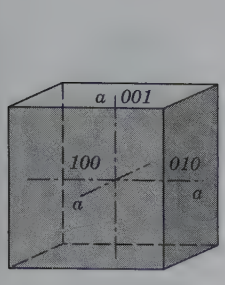

Cube {001}

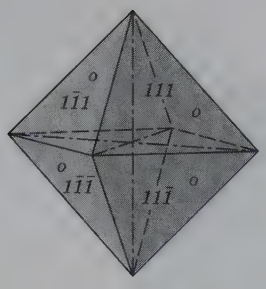

Octahedron {111}

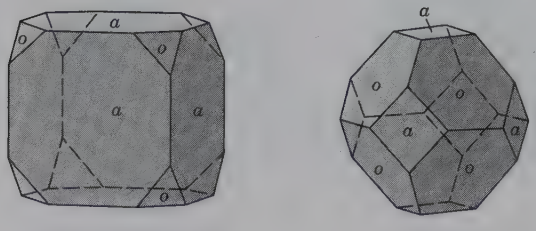

Cube and octahedron

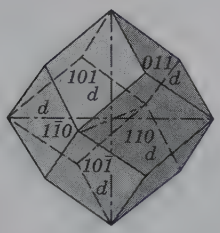

Dodecahedron {011}

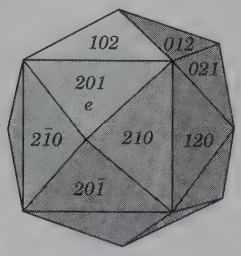

Tetrahexahedron {0*kl*}

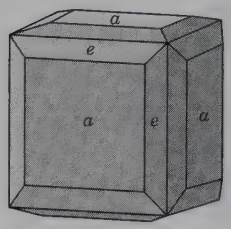

Cube and tetrahexahedron

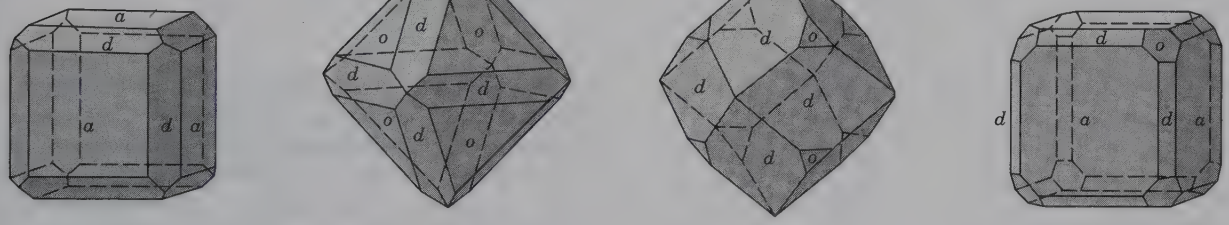

Combinations of cube and dodecahedron, octahedron and dodecahedron, and cube, octahedron, and dodecahedron

FIG. 9.32 Some of the commonly developed forms (closed forms) and form combinations in $4/m\,\bar{3}\,2/m$ (see also Fig. 9.33).

faces of which have different inclinations, but most common is {122} (Fig. 9.33). The trisoctahedron is a form that may be regarded as an octahedron (with 8 faces), in which each of these faces has been raised to accommodate three others (as in *tris*). Figure 9.33 shows a combination of an octahedron and trisoctahedron.

7. *Hexoctahedron* {*hkl*}. The hexoctahedron is composed of 48 triangular faces, each of which intersects all three crystallographic axes at different lengths. There are several hexoctahedrons that have varying ratios of axial intercepts. A common hexoctahedron has indices {123}. Other hexoctahedrons have indices {124}, {135}, and so on, or, in general, {*hkl*}. A hexoctahedron may be the only form on a crystal or it may occur in combination with other isometric forms (Fig. 9.33).

Determination of Indices of Forms. In determining the forms present on any crystal in this class, it is first necessary to locate the crystallographic axes (axes of four-fold symmetry). Once oriented by these axes, the forms can be evaluated by the number of faces, and by how many axes are intersected. The faces of the cube, dodecahedron, and octahedron are easily recognized because they intersect respectively one, two, and three axes at unit distances. The indices can be quickly obtained for faces of other forms that truncate symmetrically the edges between known faces. The algebraic sums of the *h*, *k*, and *l* indices of two faces give the indices of the face symmetrically truncating the edge between them. Thus, in Fig. 9.33 the algebraic sum of the two dodecahedron faces (101) and (011) is (112), or the indices of a face of a trapezohedron.

Occurrence of Isometric Forms in Class $4/m\bar{3}2/m$. The cube, octahedron, and dodecahedron are the most common isometric forms. The trapezohedron is frequently observed as the only form on a few minerals. The tetrahexahedron, trisoctahedron, and hexoctahedron, are rare and are ordinarily observed only as small truncations in combinations. The distribution of forms in point groups of the isometric system is listed in Table A3.4 of Appendix 3.

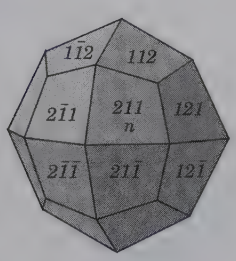

Trapezohedron
{*hhl*}

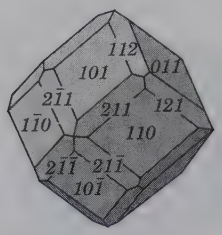

Dodecahedron and
trapezohedron in garnet

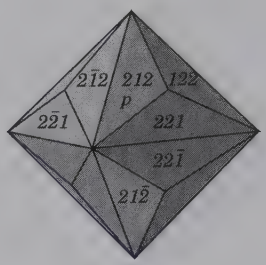

Trisoctahedron
{*hll*}

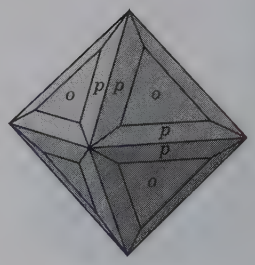

Octahedron and
trisoctahedron in diamond

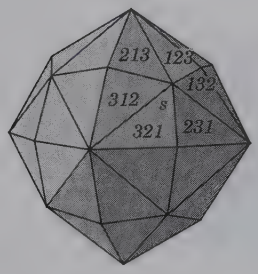

Hexoctahedron
{*hkl*}

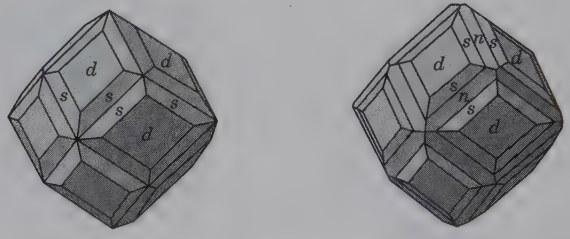

Dodecahedron and hexoctahedron. Dodecahedron,
trapezohedron, and hexoctahedron. Both crystals represent garnet

FIG. 9.33 Commonly developed forms and form combinations in $4/m\,\bar{3}\,2/m$ (see also Fig. 9.32).

Numerous minerals crystallize in this class. Some of the most common are:

analcime	gold
copper (see Plate I, no. 3)	halite
cuprite	silver
diamond (see Plate I, no. 5)	spinel group
fluorite (see Plate III, no. 5)	sylvite
galena (see Plate I, no. 8)	uraninite
garnet (see Plate IV, no.7)	lazurite

$\bar{4}3m$

Symmetry— $3\bar{A}_4$, $4A_3$, $6m$. The three crystallographic axes are axes of four-fold rotoinversion. The four diagonal axes are axes of three-fold rotation, and there are six diagonal mirror planes, the same planes shown in Fig. 9.31b for class $4/m\bar{3}2/m$. The location of all of these symmetry elements is shown in Fig. 9.34a. This class is known as the **hextetrahedral class** after the general form {*hkl*}, the *hextetrahedron* (Fig. 9.34c).

Forms

1. *Tetrahedron*, {111} *positive*, $\{1\bar{1}1\}$ *negative*. The tetrahedron is composed of four equilateral triangular faces, each of which intersects all the crystallographic axes at equal lengths. The tetrahedral form can be considered as derived from the octahedron in class $4/m\,\bar{3}\,2/m$ by the omission of the alternate faces and the extension of the others, as shown in Fig. 9.34b. The positive tetrahedron {111} is shown in Fig. 9.34a. If the other four faces of the octahedron in Fig. 9.34b had been extended, the tetrahedron resulting would have had a different orientation, resulting in the negative tetrahedron $\{1\bar{1}1\}$, as shown in Fig. 9.35. The positive and negative tetrahedrons are geometrically identical. Both must be recognized because they may occur together (as shown in Fig. 9.35). If the positive and negative tetrahedron are equally developed on the same crystal, the combination could not be distinguished from an octahedron unless, as commonly happens, the faces of the two forms show different lusters, etchings, or striations that would serve to differentiate them. Several forms and combinations of forms with the tetrahedron are possible (Fig. 9.35).
2. *Tristetrahedron*, {*hhl*} *positive*, $\{h\bar{h}l\}$ *negative*. These forms with 12 faces can be viewed as a tetrahedron, each face of which has been raised to accommodate three others (Fig. 9.35). The positive form may be made negative by a rotation of 90° about the vertical axis.
3. *Deltoid Dodecahedron* {*hll*} *positive*, $\{h\bar{l}l\}$ *negative*. This is a 12-faced form in which 3 four-sided faces occur in place of 1 face of the tetrahedron (Fig. 9.35).
4. *Hextetrahedron*, {*hkl*} *positive*, $\{h\bar{k}l\}$ *negative*. The hextetrahedron has 24 faces that can be viewed as a tetrahedron, each face of which has been raised to accommodate 6 others (Fig. 9.35).

Members of the tetrahedrite-tennantite series, $(Cu,Fe,Zn,Ag)_{12}Sb_4S_{13}$ to $(Cu,Fe,Zn,Ag)_{12}As_4S_{13}$, are the only common minerals that ordinarily show distinct hextetrahedral forms. Sphalerite, ZnS, occasionally exhibits them, but commonly its crystals are complex and distorted (see Plate I, no. 9.)

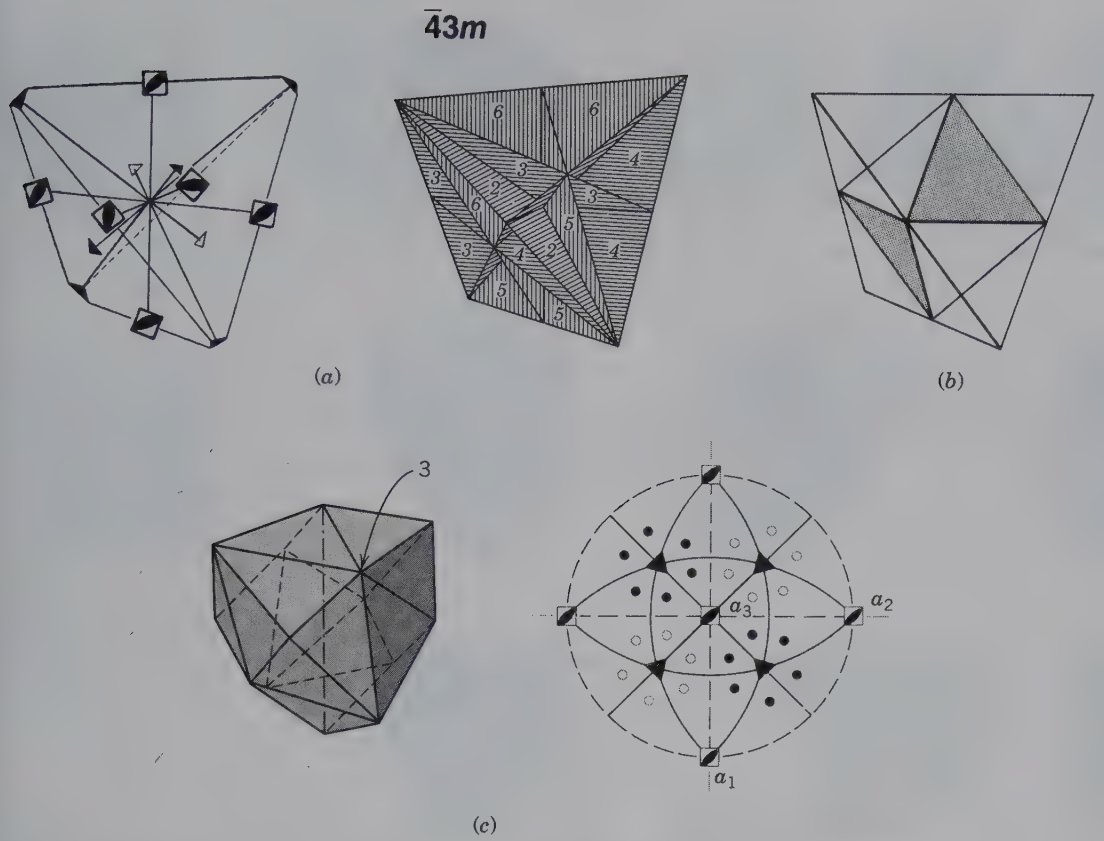

FIG. 9.34 (a) Symmetry axes and planes for $\bar{4}\,3m$. (b) Relation of octahedron (inset with shaded faces) and tetrahedron. (c) Hextetrahedron {*hkl*} and its stereogram. The 3 indicates the location of 1 three-fold axis in the model.

$2/m\bar{3}$

Symmetry—$3A_2$, $4\bar{A}_3$, $3m$. The three crystallographic axes are axes of two-fold rotation; the four diagonal axes, each of which emerges in the middle of an octant, are axes of three-fold rotoinversion; the three axial planes are mirror planes. This class has a center of symmetry because $\bar{3}$ is equivalent to $3 + i$. This class is known as the **diploidal class**, after the general form {*hkl*}, the positive *diploid* (Fig. 9.36).

Forms

1. *Pyritohedron*, {*h*0*l*} *positive*, {0*kl*} *negative*. This form consists of 12 pentagonal faces, each of which intersects one crystallographic axis at unity, intersects the second axis at some multiple of unity, and is parallel to the third. A rotation of 90° about a crystallographic axis brings the positive pyritohedron into the negative position. There are a number of pyritohedrons that differ from each other with respect to the inclination of their faces. The most common positive pyritohedron has indices {102} (Fig. 9.37). This figure also shows the corresponding negative pyritohedron.
2. *Diploid*, {*hkl*} *positive*, {*khl*} *negative*. The diploid is a rare form composed of 24 faces (see Fig. 9.36) that correspond to one-half of the faces of a hexoctahedron. The diploid may be pictured as having two faces built up on each face of the pyritohedron. As in the case of the pyritohedron, a rotation of 90° about one of the crystallographic axes brings the positive diploid into the negative position.

In addition to the pyritohedron and the diploid, the cube, dodecahedron, octahedron, trapezohedron, and trisoctahedron may be present in this class. On some crystals these forms may appear alone and may be so perfectly developed that they cannot be distinguished from the forms of class $4/m\bar{3}2/m$. This is often true of octahedra and cubes of pyrite. Usually, however, the presence of striation lines, or etch figures, display that they conform to the symmetry of class $2/m\bar{3}$. This is shown in Fig. 9.37 by a cube of pyrite with characteristic striations showing the lower symmetry (the striations are in three different directions). The pyritohedron may combine with forms of the hexoctahedral class, and may also occur in combination with cube and diploid {124} (Fig. 9.37). The distribution of forms in point groups of the isometric system is listed in Table A3.4 of Appendix 3.

The most common mineral crystallizing in this class is pyrite, FeS_2. Other rarer minerals are members of the skutterudite-nickel skutterudite series, $CoAs_{2-3}$ to $NiAs_{2-3}$; gersdorffite, NiAsS; and sperrylite, $PtAs_2$.

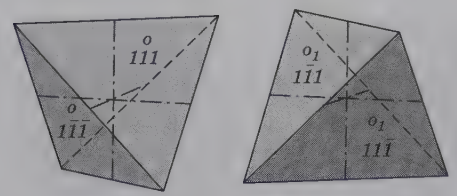

Tetrahedrons
positive {111} and negative {1$\bar{1}$1}

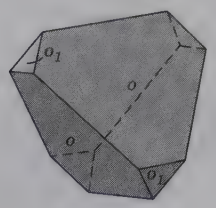

Combination (+) and (–)

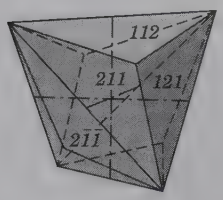

Tristetrahedron {*hhl*}

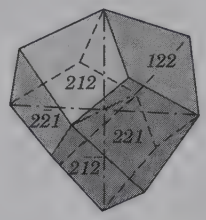

Deltoid dodecahedron {*hll*}

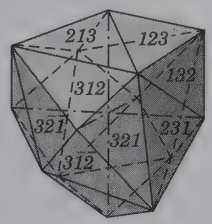

Positive hextetrahedron {*hkl*}

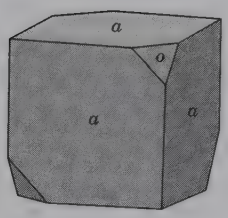

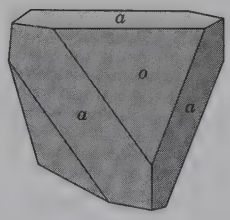

Combination of cube and tetrahedron

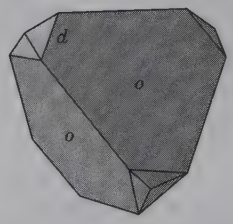

Tetrahedron and dodecahedron

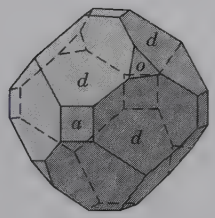

Dodecahedron, cube and tetrahedron

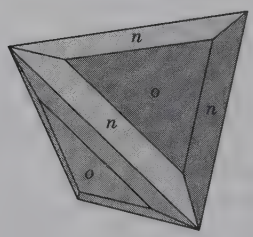

Tetrahedron and tristetrahedron

FIG. 9.35 Commonly developed forms and form combinations in $\bar{4}\,3m$.

FIG. 9.36 (a) Symmetry axes and planes for $2/m\,\bar{3}$ and (b) the diploid {*hkl*} and its stereogram. The $\bar{3}$ is the location of one $\bar{3}$ rotoinversion axis on the model.

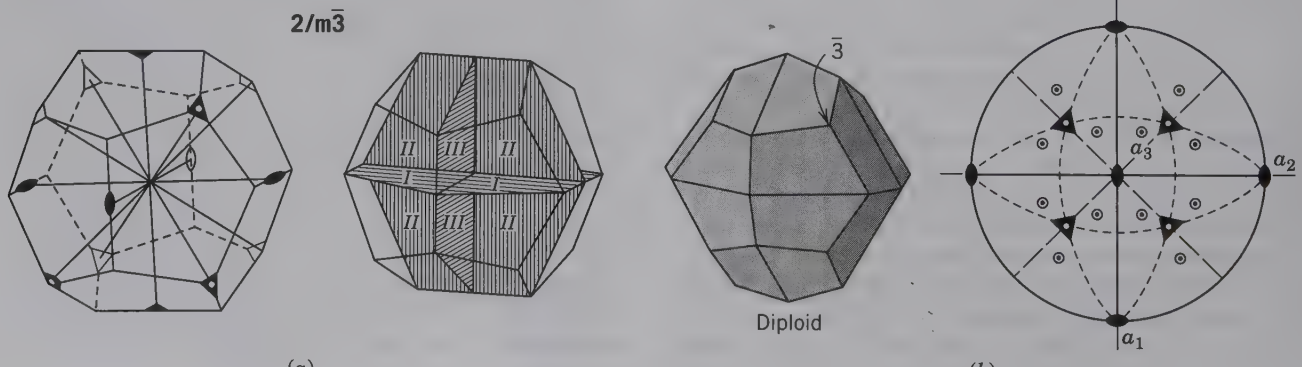

(*a*) (*b*)

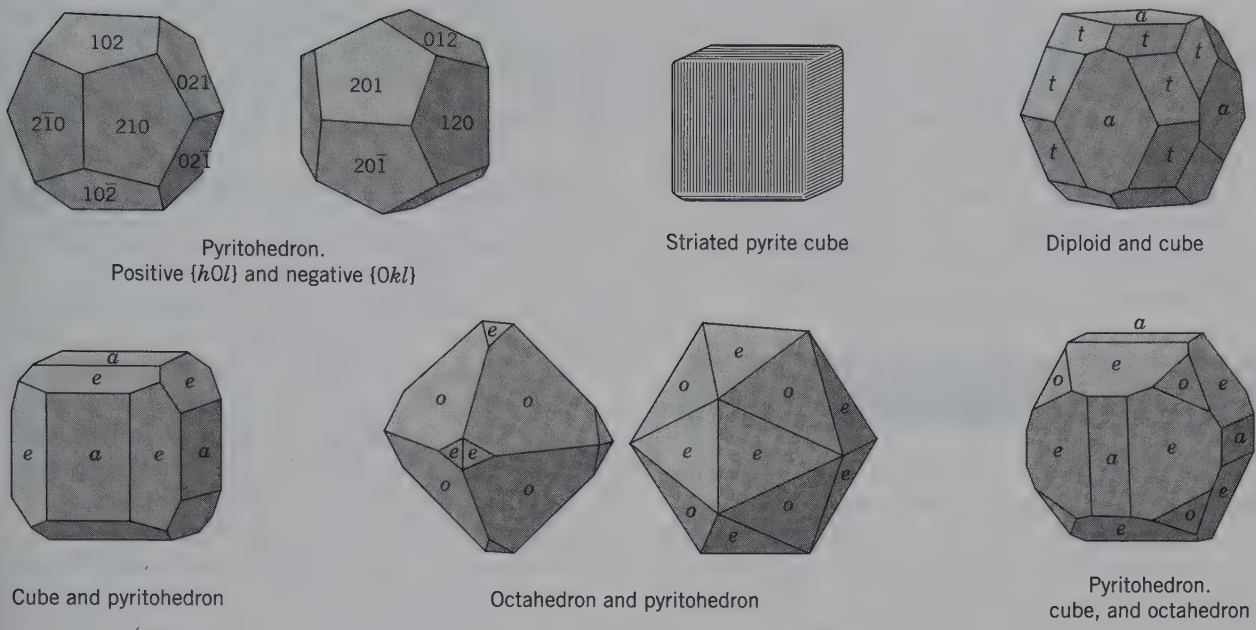

FIG. 9.37 Commonly developed forms and form combinations in $2/m\,\bar{3}$. The mineral pyrite occurs in these forms, especially that of the striated cube and the pyritohedron.

23

Symmetry—$3A_2$, $4A_3$. The three crystallographic axes are axes of two-fold rotation, and the four diagonal directions are axes of three-fold symmetry. This class is known as the **tetartoidal class** after the general form {*hkl*}, a *tetartoid* (Fig. 9.38).

Forms. There are four separate forms of the *tetartoid*: positive right {*hkl*}, positive left {*khl*}, negative right {$\bar{k}\bar{h}l$} and negative left, {$h\bar{k}\bar{l}$}. They comprise two enantiomorphic pairs, positive right and left, and negative right and left. Other forms that may be present in combination with the tetartoid are the cube, dodecahedron, pyritohedron, tetrahedron, and deltoid dodecahedron. Cobaltite, (Co,Fe)AsS, is the most common mineral representative crystallizing in this class.

CHARACTERISTICS OF ISOMETRIC CRYSTALS

Four three-fold symmetry axes are common to all isometric crystals. Symmetrically developed crystals are equidimensional in the three directions of the crystallographic axes. The crystals commonly show faces that are squares, equilateral triangles, or these shapes with truncated corners. All forms are *closed forms*. Crystals are characterized by a large number of similar faces; the smallest number of faces of any form in the hexoctahedral class is six. The distribution of forms in point groups of the isometric system is listed in Table A3.4 of Appendix 3.

FIG. 9.38 Enantiomorphic forms of the tetartoid. Positive left and positive right with a stereogram of the positive right {*hkl*} form. The 3 locates 1 of the three-fold axes on the positive right model.

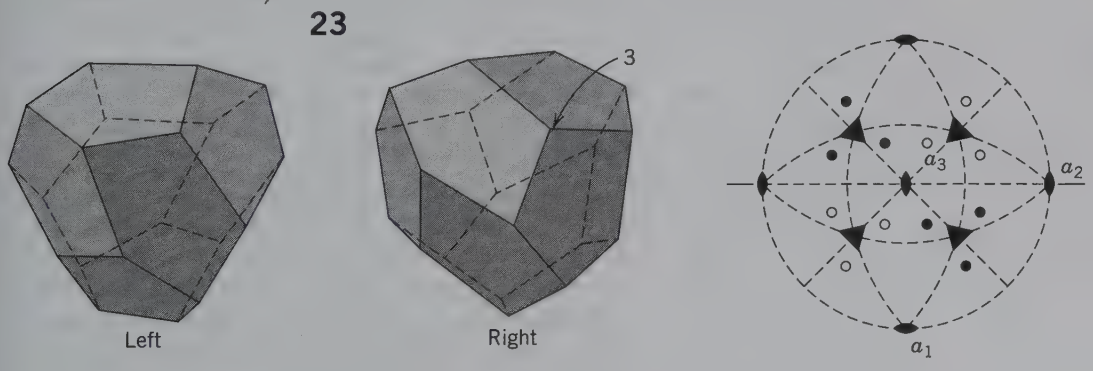

Interfacial angles of common crystal faces in the isometric system may be useful in the recognition of the most common forms. These are as follows:

Cube (100) ∧ cube (010) = 90°00′
Octahedron (111) ∧ octahedron ($\bar{1}11$) = 70°32′
Dodecahedron (011) ∧ dodecahedron (101) = 60°00′
Cube (100) ∧ octahedron (111) = 54°44′
Cube (100) ∧ dodecahedron (110) = 45°00′
Octahedron (111) ∧ dodecahedron (110) = 35°16′

REPRESENTATIONS OF SOME SPACE GROUPS

Space group notation is an elegant and powerful "shorthand" for the characterization and description of the internal structure of crystalline material. This section covers how three-dimensional space group elements are graphically represented in two-dimensions and the relationship of space group notation to morphology and structure. This draws on the concepts of three-dimensional lattices (the 14 Bravais lattice types, see Figs. 7.16 and 7.17), translational components of screw axes (Fig. 7.21) and glide planes and their relationship to morphological symmetry, and space group symbols. By understanding these concepts and the examples that follow, it should become possible to assess other space groups that are not specifically discussed here.

SPACE GROUP DERIVATION

To aid in the understanding of the 230 space groups introduced earlier (see Table 7.4), the various concepts involved in their derivation follow. Because the discussion of all 230 is a lengthy and complex task, only a few representative space groups that are common in rock-forming minerals, will be presented here as examples.

In the triclinic system, only two possible space groups can occur, namely, $P1$ and $P\bar{1}$. These are the combinations from the two possible point groups in the triclinic system, 1 and $\bar{1}$ (see Table 6.3), and the only possible lattice type, P (see Fig. 7.17). In contrast, in the monoclinic system, three point groups (2, m, and $2/m$) and two lattice types (P and I) must be considered. Here, one of the point groups (2) and the two possible lattice types P and I (I in the monoclinic system can be transposed into A, B, or C by a different choice of coordinate axes; see Fig. 7.17) is evaluated. The four possible space group notations are $P2$, $P2_1$, and $I2$, and $I2_1$. The arrangement of motifs (commas) about the two-fold rotation and two-fold screw axes in relation to a monoclinic unit cell is shown in Fig. 9.39. Of the four possible space groups, only three are unique because $I2$ and $I2_1$ are equivalent in their arrangement of symmetry elements, except for a change in the location of the origin chosen for the lattice. Therefore, the three unique space groups for the monoclinic point group 2 are $P2$, $P2_1$, and $I2$ (which is equivalent to $C2$). A more complete discussion of some additional space groups can be found in Buerger (1978).

ILLUSTRATIONS OF SPACE GROUPS

To understand illustrations of space groups requires that we first unlock the key to their symbols. The symbols used are those of the *International Tables for Crystallography* (1983, volume A), which are listed in Table 9.3 for all types of rotational symmetry. Figure 9.40 shows motif units related by both rotation and screw axes and their projection onto the plane of the page (projected from above the page). The fractions next to the motifs, in Fig. 9.40, represent the distance (t/n) the motif units lie above the plane of the page. For those that lie above the plane of the page, the fraction is preceded by a plus sign (+) (in the positive direction of z in an x, y, z coordinate system). For glide planes and mirrors, additional symbols are needed which depict these symmetry elements in graphical illustrations (Table 9.4). Three-dimensional views of various possible glide plane operations are shown in Fig. 9.41 and some of their two-dimensional projections are shown in Fig. 9.42.

Here, some general aspects of space group illustration are introduced. This is followed by discussion of four specific space groups. (Readers interested in systematic coverage of space groups should consult the standard references on the subject, three of which are profusely illustrated: *International Tables for X-ray Crystallography*, vols. 1 and A; *Elementary Crystallography*; and *Mathematical Crystallography*; complete references are given at the end of this chapter).

The coordinate axes (in Fig. 9.43) are oriented as follows. The a axis is toward the reader, the b to the right (in an E–W position), and the c axis is perpendicular to the page. The origins of the drawings are in the *upper left corner*. The motifs are represented by small circles with their heights indicated by + or − next to them: + means a distance upward (along c) from the page, and − means an equivalent distance in a downward direction. Motifs and symmetry operators can be accompanied by fractions (e.g., $\frac{1}{4}$, $\frac{1}{3}$, $\frac{1}{2}$), indicating a fractional distance (upward or downward, within the unit cell). The open circle (○) is considered a right-hand motif, whereas an open circle with a small comma inside (◉) is the left-hand equivalent. These two symbols are enantiomorphic and can be related by a mirror, glide, or inversion operation. The two types of circles are analogous to the enantiomorphic commas used in prior illustrations. The symbols for the various symmetry operators are given in Tables 9.3 and 9.4. An inversion point (center of symmetry) is noted by a very small circle. If its height is not given, it is assumed to be zero (equivalent to being in the

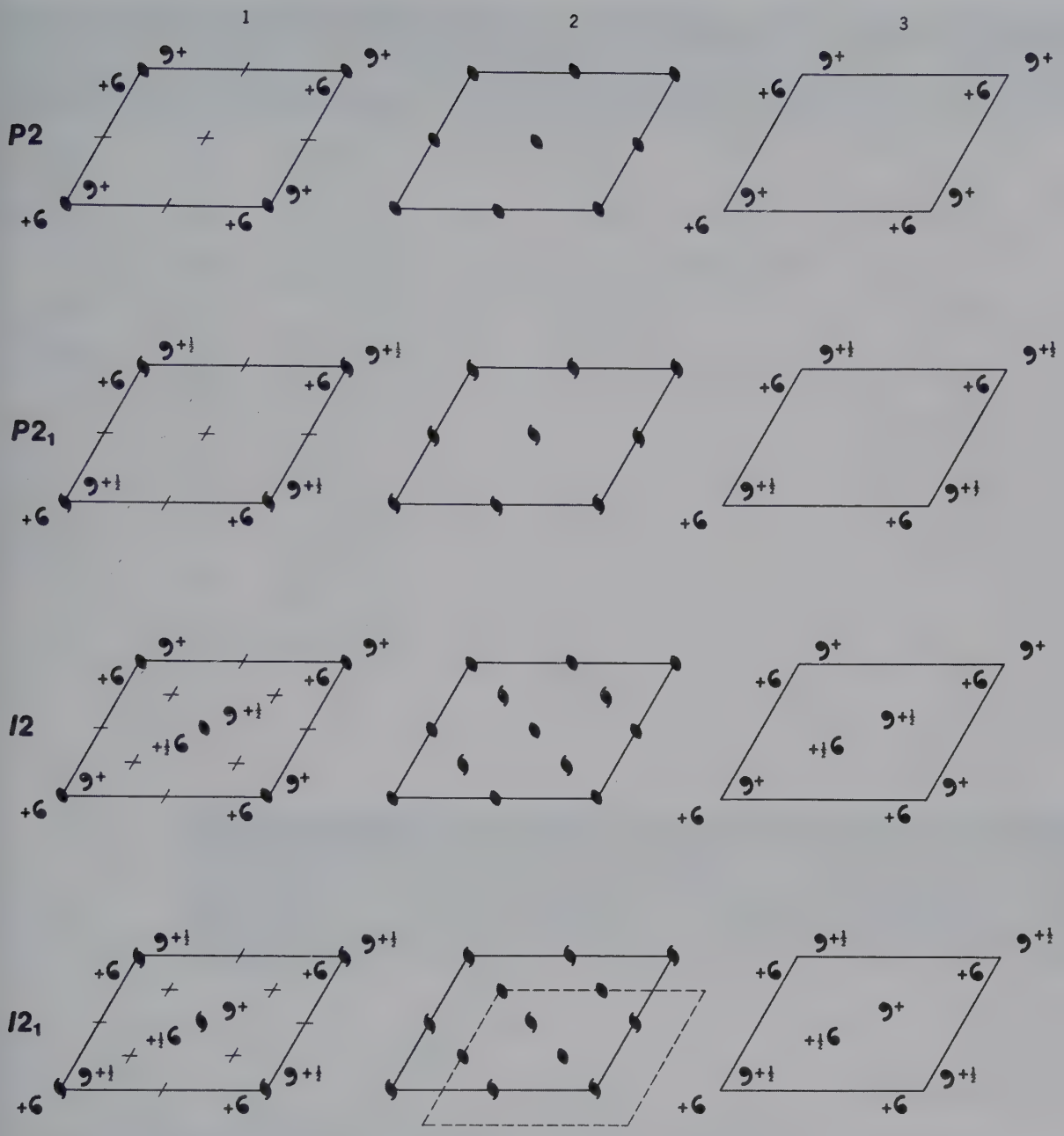

FIG. 9.39 Derivation of the monoclinic space groups $P2$, $P2_1$, $I2$, and $I2_1$. Column 1 depicts only the lattice type, the motif units, and the symmetry element specified for each lattice point (corners and centers). In the illustrations in column 1, additional symmetry elements are inherent in the unit cell at the points indicated by $\neq$. Column 2 depicts all the symmetry elements inherent in the pattern. Column 3 shows the arrangement of motif units only. For space group $I2_1$, the drawings demonstrate that the symmetry contained in the unit cell is equivalent to the symmetry in the unit cell for $I2$. Only a shift in origin of the unit cell is needed to obtain a symmetry pattern identical to that for $I2$ (column 2). The dashed unit cell indicates the actual shift necessary. In other words, $I2$ and $I2_1$ are identical and, therefore, only one of the two arrangements is unique. In Table 7.4 the space group $I2$ is listed as $C2$ because these two notations are equivalent (see figure caption to Fig. 7.17).

Table 9.3 Symbols for Symmetry Axes (All Graphical Symbols Are for Axes Normal to the Page, Unless Otherwise Noted)

Symbol	Symmetry Axis	Graphical Symbol	Type of Translation (If Present)	Symbol	G Symmetry Axis	raphical Symbol	Type of Translation (If Present)
$\frac{1}{1}$	one-fold rotation	None	None	4	four-fold rotation	■	None
$\bar{1}$	one-fold rotoinversion	°	None	4_1	four-fold screw (right-handed)	■	$\frac{1}{2}c$
2	two-fold rotation	⬮ → (parallel to paper)	None	4_2	four-fold screw (neutral)	■	$\frac{2}{4}c = \frac{1}{2}$
				4_3	four-fold screw (left-handed)	■	$\frac{3}{4}c$
2_1	two-fold screw	⬮	$\frac{1}{2}c$ $\frac{1}{2}a$ or $\frac{1}{2}b$	$\bar{4}$	four-fold rotoinversion	◪	None
				6	six-fold rotation	⬢	None
3	three-fold rotation	▲	None	6_1	six-fold screw (right-handed)	⬢	$\frac{1}{6}c$
3_1	three-fold screw (right-handed)	▲ 6	$\frac{1}{3}c$	$_2$	six-fold screw (right-handed)	⬢	$\frac{2}{6}c$
3_2	three-fold screw (left-handed)	▲ 6	$\frac{2}{3}c$	$_3$	six-fold screw (neutral)	⬢	$\frac{3}{6}c = \frac{1}{2}$
$\bar{3}$	three-fold rotoinversion	▲	None	6_4	six-fold screw (left-handed)	⬢	$\frac{4}{6}c$
				6_5	six-fold screw (left-handed)	⬢	$\frac{5}{6}c$
				$\bar{6}$	six-fold rotoinversion	◪	None

Table 9.4 Symbols for Mirror and Glide Planes*

Symbol	Symmetry Plane	Graphic Symbol: Normal to Plane of Projection	Graphic Symbol: Parallel to Plane of Projection†	Nature of Glide Translation
m	Mirror	———	120°	None
a, *b*	Axial glide plane	- - - - - - - - - -		*a*/2 along [100] or *b*/2 along [010]
c		.....	None	*c*/2 along the *c* axis
n	Diagonal glide plane	—·—·—·—·—		*a*/2 + *b*/2; *a*/2 + *c*/2; *b*/2 + *c*/2; or r *a*/2 + *b*/2 + *c*/2 (tetragonal and isometric)
d	Diamond glide plane	—·—·←·—·— —·—·—·→·—		*a*/4 + *b*/4; *b*/4 + *c*/4; *a*/4 + *c*/4; or r *a*/4 + *b*/4 + *c*/4 (tetragonal and isometric)

*From *International Tables for X-ray Crystallography*. 1969. v. 1, N. F. M. Henry and K. Lonsdale, Eds.; Birmingham, England: Symmetry Groups, International Union of Crystallography, Kynoch Press.

†When planes are parallel to the paper, heights other than zero are indicated by writing the *z* coordinate next to the symbol (e.g., $\frac{1}{4}$ or $\frac{3}{8}$). The arrows indicate the direction of the glide component.

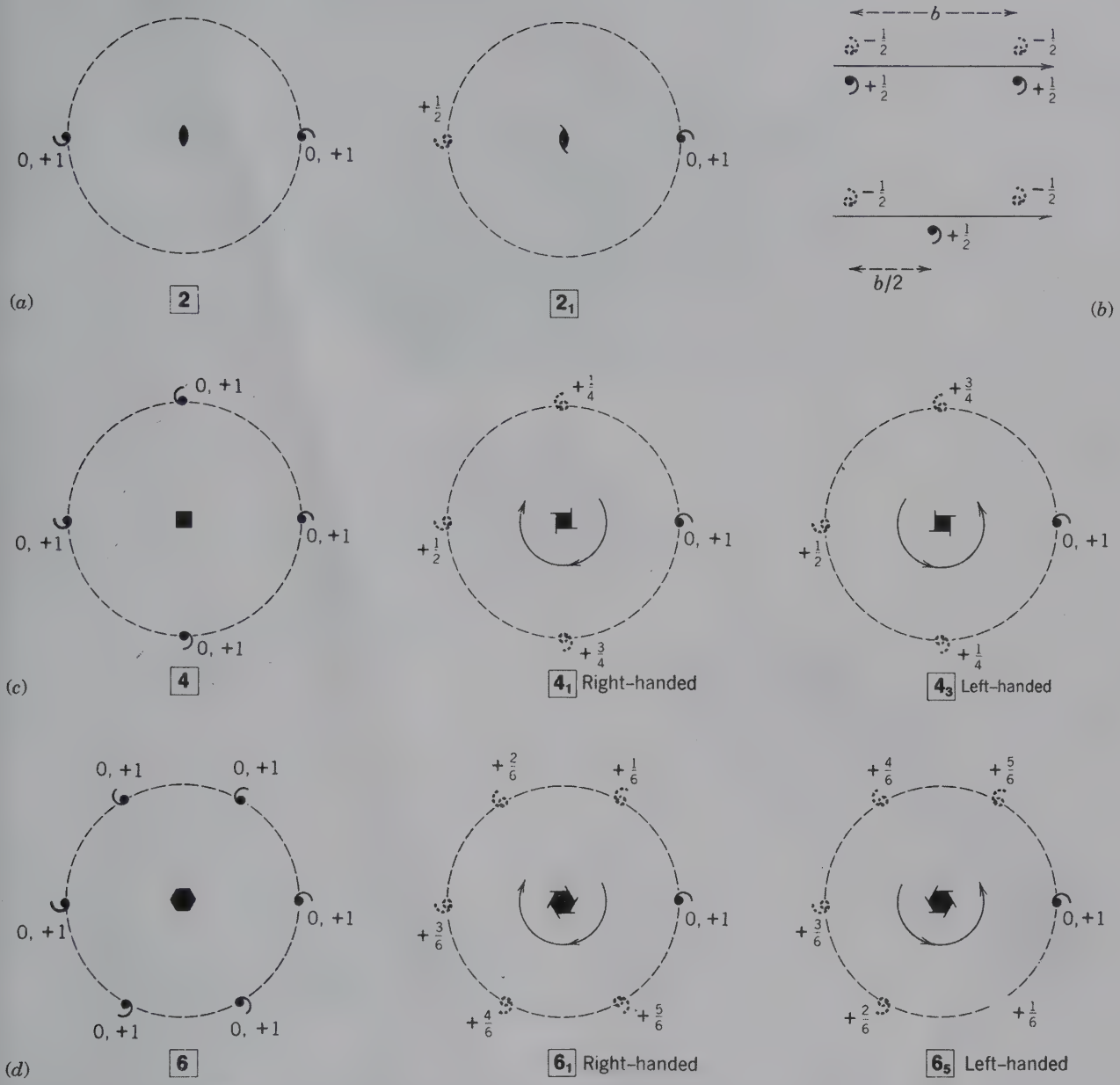

FIG. 9.40 Examples of several axes of rotation and some of their isogonal screw axes. The effect of these symmetry operations on motifs is shown as well. All diagrams are set such that the *a* and *b* axes (*x* and *y* directions) lie in the plane of the page. The height above the plane of the page, along the $+c$ axis (in the $+z$ direction), is indicated by a (+) sign. For example, 0 and +1 mean that the motif lies in the plane of the page (at zero height along the *c* axis) and is also repeated along the *c* axis by a unit lattice repeat to $+1c$. Fractions (e.g., $+\frac{1}{2}$, $+\frac{1}{3}$, $+\frac{1}{4}$) refer to heights above the page along the *c* axis (*z* direction). Motif units that do not lie in the plane of the page (but have been projected from above) are shown by a dashed comma design. (a) Two-fold rotation axis and isogonal screw axis. The circles show the effect of these axes on motifs when the axes are oriented perpendicular to the page. (b) These same axes when oriented parallel to the plane of the page (or, when they lie within the plane of the page). (c) Four-fold rotation axis and 2 enantiomorphic four-fold screw axes. The rotational directions of the screws ("handedness") are shown by the arrows. (d) Six-fold rotation axis and 2 enantiomorphic six-fold screw axes.

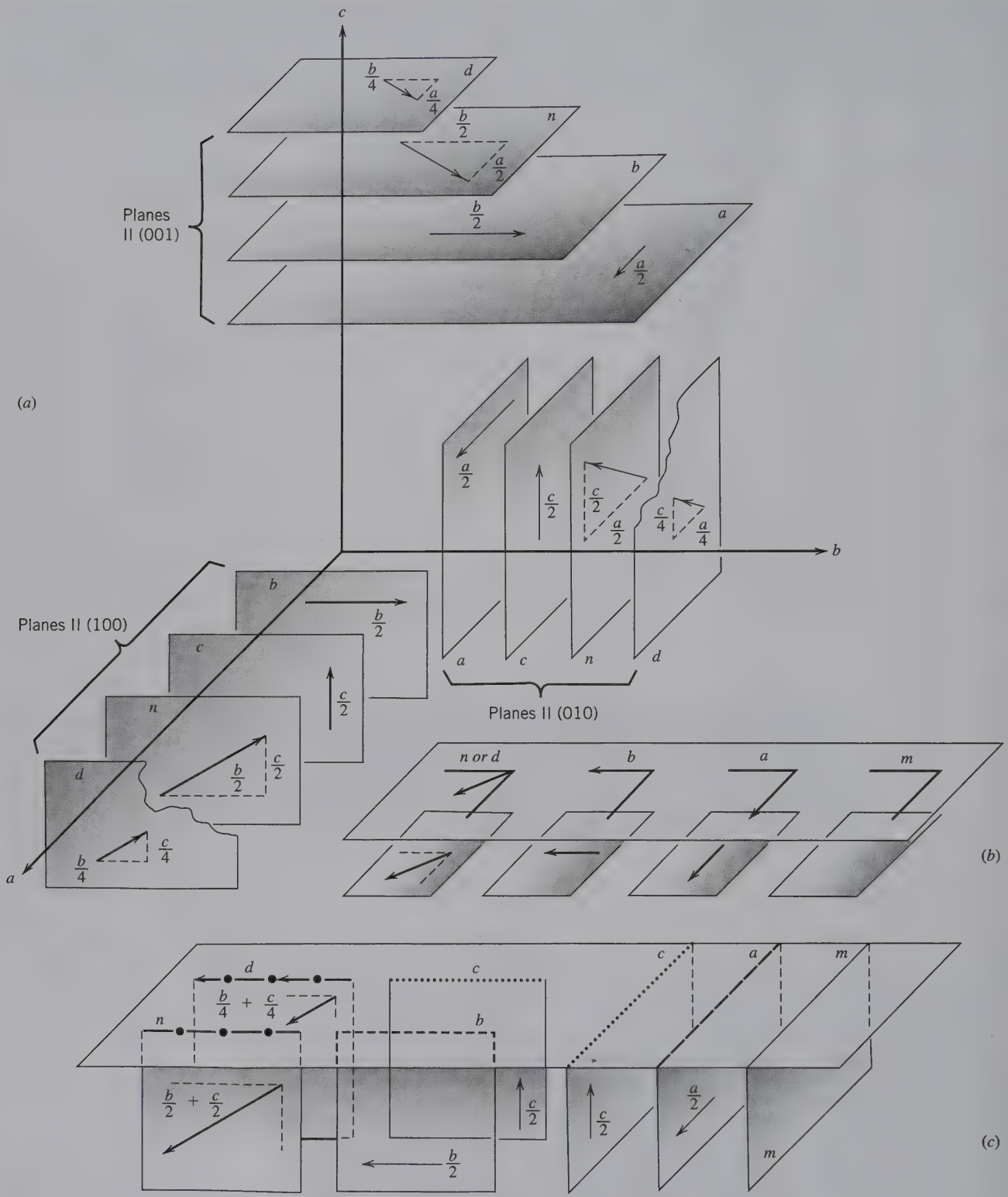

FIG. 9.41 (a) Sketch of the various glide planes and their translation components with reference to orthorhombic coordinate axes. (b) Symbols for glide and mirror planes when such planes are parallel to the plane of projection (001) or (0001). (c) Symbols for glide and mirror planes when such planes are perpendicular to the standard plane of projection. (Adapted from Bloss, F. D., 1971. *Crystallography and crystal chemistry: An introduction*. Figs. 7.9 and 7.11. 1994. Mineralogical Society of America. Reprinted by permission of the author.)

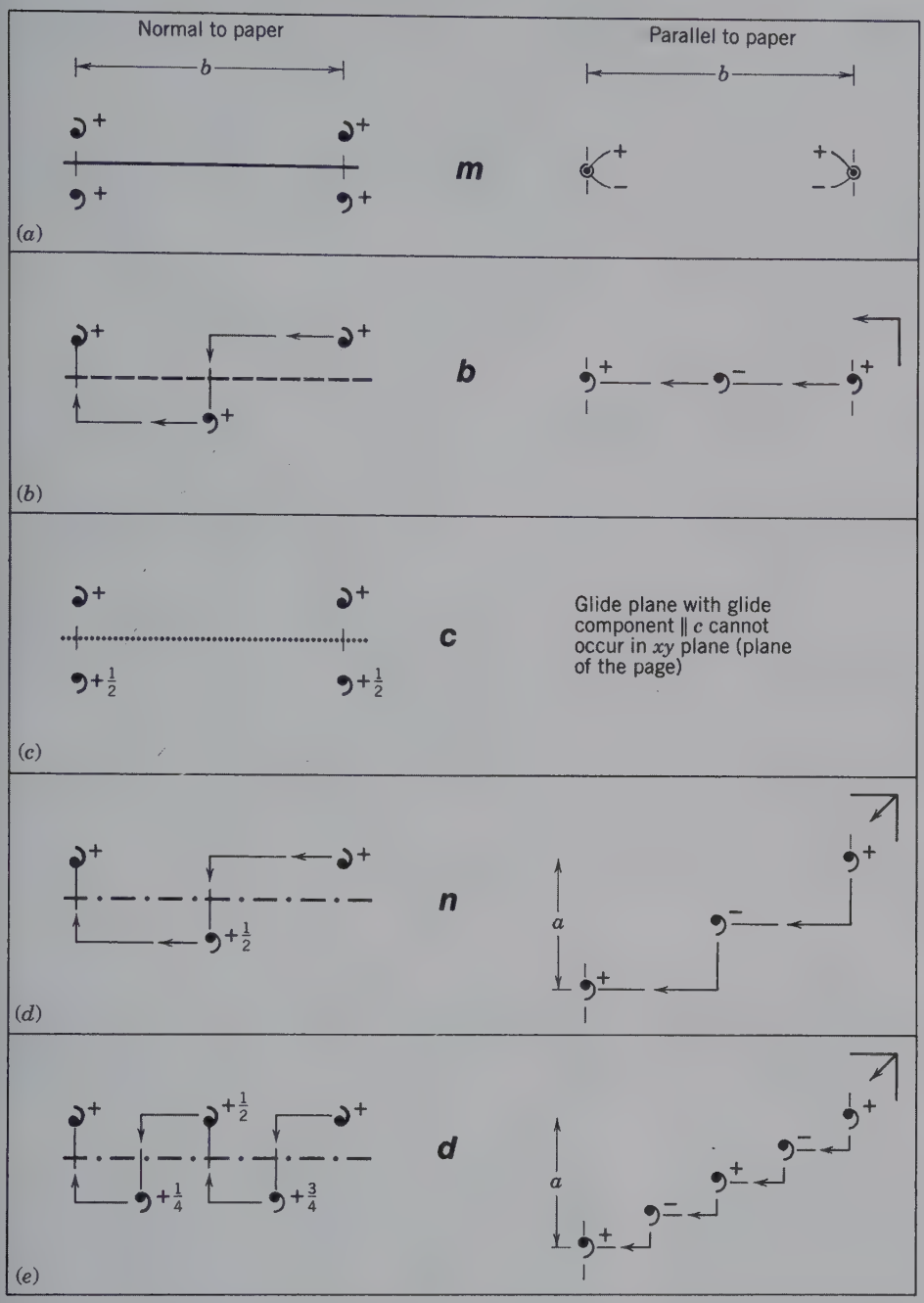

FIG. 9.42 Examples of symmetry planes and the distribution of motifs about them. In all drawings the plane of the paper is considered the *ab* plane. The location of a motif above the plane [in the (+) direction of *c*] is marked by +, or $+\frac{1}{4}$, $+\frac{1}{2}$, and so on. The (−) *c* direction is shown by (−) signs next to the motif. In the right-hand figure of (a) the motif units superimpose exactly; the upper motif is shown by •, the lower equivalent by a small circle about it. Note conventional symbols; see also Table 9.4. (a) A mirror plane. (b) A glide plane with a glide component parallel to the *b* axis (*b*/2). (c) A glide plane with a glide component parallel to the *c* axis (*c*/2). (d) A diagonal glide plane (*n*) with simultaneous glide components parallel to the *a* and *b* axes (*a*/2 + *b*/2). (e) A diamond glide plane (d) with simultaneous glide components parallel to the *a* and *b* axes (*a*/4 + *b*/4).

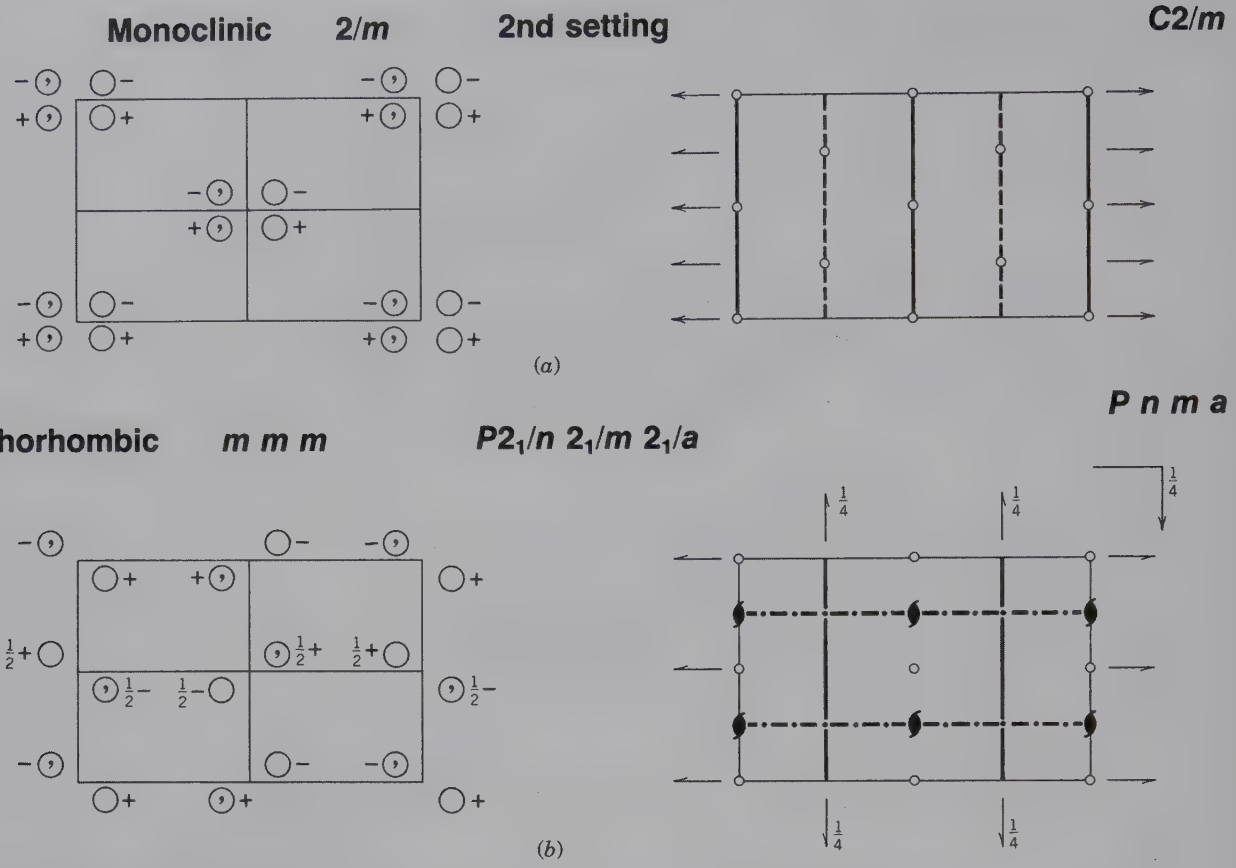

FIG. 9.43 Examples of illustrations of space groups. (Reproduced from *The International Tables for X-ray Crystallography*, vol. 1; see text for discussion.)

plane of the page). If a mirror exists parallel to the plane of projection (the plane of the page), the superimposed motifs are indicated by the small circle used for motifs, but now divided vertically down the middle (Ⓘ). This symbol is accompanied by + and − signs to indicate that one motif (above, +) superimposes with another below (−). The enantiomorphic relation, in such an occurrence, is shown by the small comma inside one half of the circle (ⓘ). The left-hand diagrams in Fig. 9.43 show the distribution of motifs in the unit cell of a three-dimensional periodic array, and the right-hand diagrams locate the various symmetry elements with respect to this unit cell.

The monoclinic space group $C2/m$ (Fig. 9.43a) is common in rock-forming minerals, such as clinoamphiboles and orthoclase. The space group illustration is oriented such that the y axis (equivalent to the b axis) is the two-fold axis in an east–west position (the second setting for this space group). The notation shows only two-fold rotation axes, but the right-hand side of Fig. 9.43a also shows two-fold screw axes interleaved with the two-fold rotation axes. Similarly, only *m*s are given in the space group symbol, but glide planes are interleaved with them. This is related to the choice of a c-centered lattice (C). In space groups with nonprimitive lattices, screw axes and glide planes are introduced because of centering. These new elements, however, are not noted in the symbols. Therefore, one should be alert to this in nonprimitive lattice types. The $C2/m$ diagrams also show the presence of mirrors and two-fold rotation axes at distances of one-half the appropriate cell lengths. These symmetry elements are parallel to other symmetry elements of the space group. Centers of symmetry (inversion) are indicated by small open circles for each unit cell.

Figure 9.43b illustrates the orthorhombic space group $P2_1/n2_1/m2_1/a$, which is isogonal with point group $2/m2/m2/m$, abbreviated as *mmm*. The analogous short symbol for the space group is *Pnma*. This space group notation is one of six possible choices each reflecting the different ways of orienting an orthorhombic unit cell with respect to the a, b, and c axes. The six equivalent permutations are *Pnma*, *Pbnm*, *Pmcn*, *Pnam*, *Pmnb*, and *Pcmn*. The structure of the common rock-forming mineral, olivine, is described in terms of space group *Pbnm*. The left-hand side of Fig. 9.43b shows the location of motifs, and the right-hand

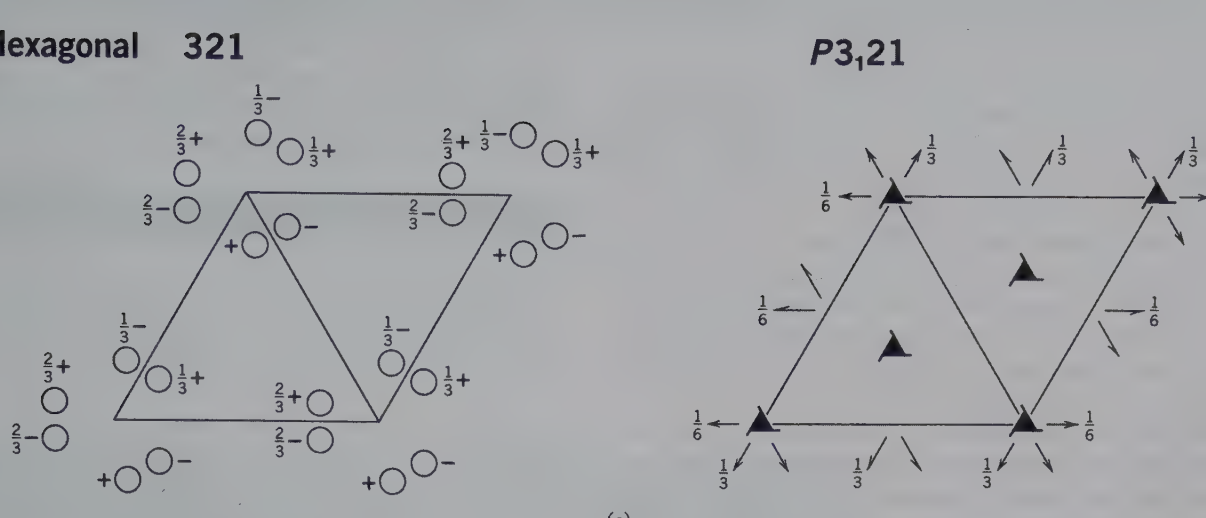

FIG. 9.43 *(continued)*

side illustrates the lattice type and the compatible symmetry elements. All two-fold rotation axes in the point group are represented by two-fold screw axes in the space group (each axial direction, *a*, *b*, and *c*, is coincident with 2_1 symmetry). The space group also contains a diagonal (*n*) glide perpendicular to the *a* axis (shown by the E–W dot-dash lines), *m*s perpendicular to the *b* axis (shown by the solid lines), and an *a* glide (shown by the graphical symbol for a plane parallel to the plane of the page; the arrow at the top right corner) but at one-fourth of the unit cell above the plane of projection.

The space group of the common form of quartz (low quartz) is illustrated in Fig. 9.43c. This is $P3_121$, which is one of a pair of enantiomorphic space groups, $P3_121$, and $P3_221$. These are isogonal with point group 321 (also referred to as 32). The unit cell is based on a primitive hexagonal outline. The location of motifs in the left-hand diagram reveals the three-fold screw axes at the four corners of the unit cell; two additional locations are present in the centers of the triangular halves of the unit cell (shown on the right of Fig. 9.43*c*). The locations of the two-fold rotation axes are coincident with the a_1, a_2, and a_3 axis directions. The last numeral in the notation, 1, refers to directions at 30° to the axial directions of the unit cell (the diagonal directions) and indicates that there is no symmetry in these directions.[1]

[1]The numeral *1* is commonly used in space group notation to signify the lack of symmetry in a specific direction. For example, point group 32 has, among others, isogonal space groups *P*312 and *P*321. The overall symmetry content is the same in both representations. In *P*312, however, there is no symmetry along the a_1, a_2, and a_3 axes, and the two-fold rotation axes lie in directions perpendicular to a_1, a_2, and a_3. In *P*321, the a_1, a_2, and a_3 axes are the directions of two-fold rotation and the directions perpendicular to a_1, a_2, and a_3 lack any symmetry. Other examples are: *P*3*m*1 and *P*31*m*; *P*32/*m*1 and *P*312/*m* (see footnote to Table 7.1).

This space group also contains two-fold screw axes that occur halfway along the cell translations and are parallel to the two-fold rotation axes. These are the result of combining a rotational axis with a nonparallel axial translation (e.g., the two-fold rotation axes that are not at 90° to the edges of the unit cell).

The tetragonal space group $P4_2/nnm$ (that of zircon) is illustrated in Fig. 9.43d. This space group is isogonal with point group $4/mmm$. The full (unabbreviated) symbols for space and point groups are $P4_2/n2/n2/m$ and $4/m2/m2/m$, respectively. The square lattice and inherently high symmetry content are clear in the illustrations. The four-fold rotation axes of the point group appear as alternating and parallel four-fold rotoinversion and four-fold screw axes (neutral as a result of 4_2). The n glide (in $4_2/n$) is parallel to the plane of the page at location $+1/4c$. The axial directions (a_1 and a_2) contain two-fold rotation axes and have vertical n glides parallel and perpendicular to the a_1 and a_2 axes (these locations are shown by the dot-dash lines). The diagonal directions (at 45° to the a_1 and a_2 axes) contain mirror planes as well as two-fold rotation axes with interleaved two-fold screw axes. Centers of symmetry are located at $+1/4c$.

These examples give an insight into the interpretation of these seemingly complex diagrams. Space groups illustrate the relationship of external morphology (point group symmetry) to internal structure and serve as a link between these two concepts. Detailed examples of the connection between morphology and structure are given in Appendix 4 for three minerals, clinopyroxene, beryl, and diamond. Various aspects of these same space groups are illustrated on the CD-ROM, module III, under the heading "3-Dimensional Order" and subsequent "Space group elements."

REFERENCES AND FURTHER READING

Bloss, F. D. 1994. *Crystallography and crystal chemistry: An introduction.* Reprint of the original text of 1971 by the Mineralogical Society of America, Washington, D.C.

Boisen, M. B., Jr., and G. V. Gibbs. 1990. *Mathematical crystallography. Reviews in Mineralogy* 15. Mineralogical Society of America, Washington, D.C.

Bragg, W. L., and G. F. Claringbull. 1965. *Crystal structures of minerals.* Cornell University Press, Ithaca, New York.

Buerger, M. J. 1978. *Elementary crystallography: An Introduction to the fundamental geometric features of crystals.* Rev. ed. MIT Press, Cambridge, Massachusetts.

———. 1971. *Introduction to crystal geometry.* McGraw Hill, New York.

Goldschmidt, V. 1913–23. *Atlas der Kristallformen* (9 volumes and 9 atlases). Universitätsbuchhandlung, Heidelberg.

International tables for crystallography. 1983. Vol. A, *Space group symmetry.* Edited by T. Hahn. International Union of Crystallography, D. Reidel Publishing Company, Boston.

International tables for X-ray crystallography. 1969. Vol. 1, *Symmetry groups.* Edited by N. F. M. Henry and K. Lonsdale. International Union of Crystallography, Kynoch Press, Birmingham, England.

Klein, C. 2008. *Minerals and rocks: Exercises in crystal and mineral chemistry, crystallography, X-ray powder diffraction, mineral and rock identification, and ore mineralogy.* 3rd ed. Wiley, New York.

O'Keffe, M., and B. G. Hyde. 1996. *Crystal structures I: Patterns and symmetry.* Monograph. Mineralogical Society of America, Washington, D.C.

CHAPTER 10

Crystal Growth and Defects; Twinning, Color, and Magnetism

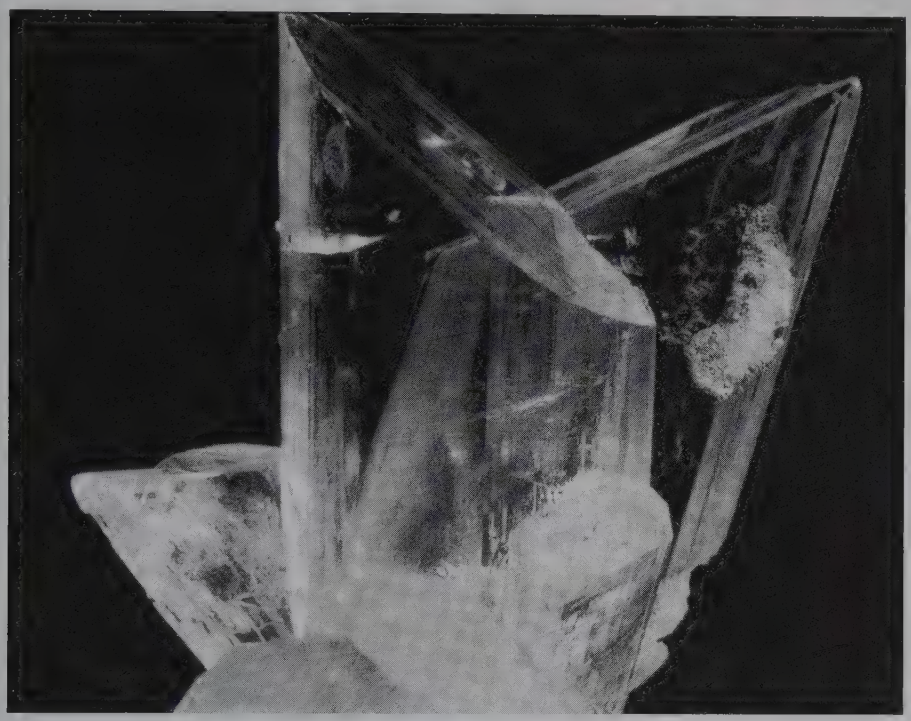

Clear, transparent, and colorless crystals of gypsum, $CaSO_4 \cdot 2H_2O$. These are tabular parallel to {010} with a basal pinacoid parallel to {001}. The spectacular external form of these two crystals is the result of their growth (from solutions) in an open space (a cavity in a rock sequence, commonly referred to as a vug) free from the competition of other, neighboring minerals that might have crowded their growth. From the Santa Eulalia mining district, Chihuahua, Mexico (Harvard Mineralogical Museum).

Inorganic crystals may form from solutions, melts, and vapors. The processes that cause atoms in these disordered states to reorganize in an ordered arrangement characteristic of a solid are fundamental to crystal nucleation and growth. Once nucleated, crystals grow by addition of new material to their outer surface in a regular and continuous pattern. This chapter provides a brief introduction to crystal nucleation and growth in perfect crystals. Such ideal crystals are rare in nature, and the various irregularities that may occur during growth are described. Twinning, one of the most obvious morphological expressions of a defect structure, follows. The origin of color and magnetism also are discussed in the context of crystal growth.

Mineral samples range in scale from nanometers to tens of meters in size and from weights in nanograms to thousands of kilograms. Yet, each of these specimens may display well-formed crystals. Mineralogic exhibits often highlight the more spectacular specimens, usually those with exceptional development of crystal faces and those that are large. The question that follows is, how do such well-formed crystals grow from small atomic clusters to large crystalline structures? To rephrase the same question in chemical terms, how are the chemical building blocks (atoms, ions, or ionic clusters) incorporated into a well-ordered crystalline pattern? And, why do certain crystal forms prevail at the expense of others? This chapter discusses some of the most basic aspects of crystal nucleation and growth, irregularities that occur in growing crystals, and physical properties related to growth.

CRYSTAL GROWTH

This first stage in the growth of a crystal is that of **nucleation**, which implies that growth can commence only after a **nucleus** (or *seed*) has formed. In most cases, the *nuclei* are the initial products of crystallization of minerals from solutions or melts. Atoms in the liquid state have a disordered and random distribution. During nucleation, the constituent atoms of a mineral must be in the same place at the same time, become organized, and then combine in the ordered pattern characteristic of the crystalline state. This occurs when the ordered crystalline state of the constituents represents a lower energy configuration than the disordered state of the liquid. The *nucleus* is the result of various ions (in the solution or melt) combining to form the initial regular structural pattern of a crystalline solid. The process of nucleation typically requires that some degree of supersaturation be attained in the solution. Supersaturation can be achieved by one of several mechanisms, such as changing concentration, temperature, and/or pressure.

As an example of nuclei forming from an aqueous solution consider sodium chloride, NaCl, dissolved in water (Fig. 10.1). During evaporation, the solution contains more and more Na^+ and Cl^- per unit volume. Ultimately, the water can no longer retain all of the Na^+ and Cl^- in solution, and solid NaCl begins to precipitate. If the evaporation of the solution is very slow, the ions of sodium and chlorine will cluster to form one or a few crystals with characteristic shapes, commonly sharing a crystallographic orientation. In contrast, if evaporation is rapid, many nuclei form resulting in small, randomly oriented crystals.

Crystals also nucleate from solution by lowering the temperature or the pressure to reach conditions of supersaturation. Hot water will dissolve slightly more salt (NaCl), for instance, than cold water. If a hot solution is allowed to cool, a temperature may be reached where the solution becomes sufficiently concentrated and NaCl will crystallize. A similar situation holds for pressure: the higher the pressure the more NaCl water can hold in solution. Thus, lowering the pressure of a saturated solution will result in supersaturation. Therefore, in general, *crystals may form from a solution by evaporation of the solvent and by changes in the temperature or pressure.*

A crystal is formed from a melt in much the same way as from a solution. The formation of igneous rocks from molten magmas, though more complicated, is similar to the freezing of water. Although it is not ordinarily considered in this way, water is fused ice. When the temperature is lowered sufficiently, the H_2O molecules, which were free to move in any direction in the liquid state, become fixed and arrange themselves in a definite order to build up a solid, crystalline mass. In magma, many ions and ionic groups exist in an uncombined state. Crystal nucleation and growth in a cooling magma are the result of two competing tendencies: (1) thermal vibrations that tend to destroy the nuclei of potential minerals, and (2) attractive forces that tend to aggregate atoms (and/or ions) into crystal structures. As the temperature falls, the temperature effect diminishes, which allows the attractive forces to dominate.

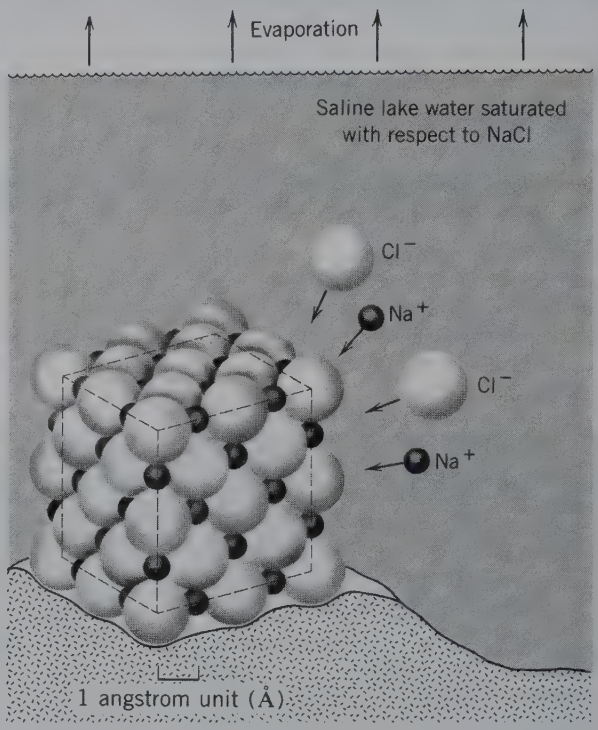

FIG. 10.1 Schematic representation of a *nucleus* of NaCl in an evaporating saline lake. The nucleus, as drawn, consists of only 125 regularly packed ions (Na^+ and Cl^-). Additional ions will accrete, in an ordered array, on the outside of the nucleus cube, thus, allowing it to grow to a larger crystal. The scale used for ionic size is the angstrom unit (1Å = 10^{-8} cm). A cubic crystal of NaCl, 1 cm along each edge, would contain approximately 10^{23} ions or atoms.

Although crystallization from a vapor is less common than from a solution or a melt, the underlying principles are similar. As the vapor is cooled, the dissociated atoms or molecules combine, eventually locking themselves into a crystalline solid. Familiar examples of this mode of crystallization are the formation of snowflakes from air saturated with water vapor and the formation of sulfur crystals at the base of fumaroles, or volcanic vents, from the condensation of sulfur-rich gas. All these processes create a supersaturated environment in which nucleation can occur.

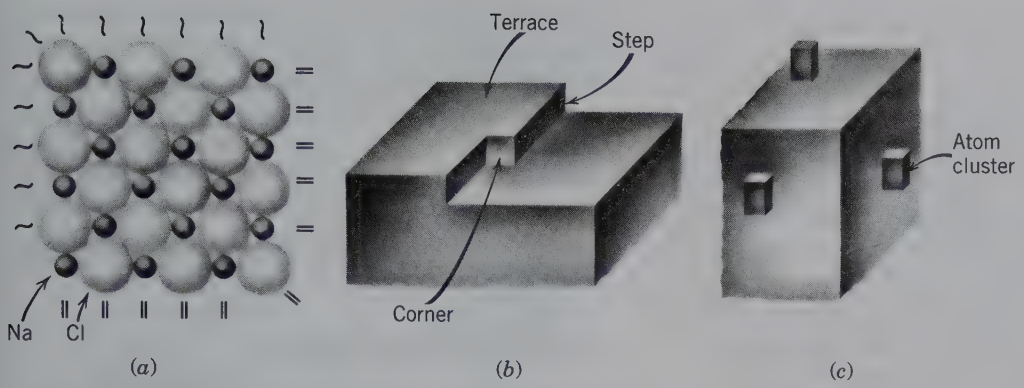

FIG. 10.2 (a) A section through a corner of an NaCl crystal showing well-bonded, closely packed ions in the internal part of the crystal and unsatisfied chemical bonds at the outer surfaces of the crystal (~ represents unsatisfied and = represents satisfied chemical bonds). (b) A crystal surface showing a submicroscopic step. Attachment of ions at the location of such a step lowers the energy of the crystal surface. This energy is the cumulative result of the unsatisfied bonds. (c) Submicroscopic clumps of atoms, shown as blocks, attached to the outer three surfaces of a crystal. Such blocks create steps for the attachment of new layers of ions on the outer surfaces of the crystal.

Consider now a more detailed example of nucleation. In an evaporating salt lake, the conditions might be appropriate for the random precipitation of nuclei of NaCl. This means that Na^+ and Cl^- ions in the lake water are combining with each other in a regular cubic array of alternating ions of Na^+ and Cl^- as required by the structure of NaCl (halite, or rock salt; Fig. 10.1). The formation of a single crystal of halite is generally preceded by the random formation of large numbers of potential nuclei. Most nuclei will not develop into larger crystals because in a solution saturated with respect to Na^+ and Cl^- ions, there is also a tendency for nuclei to be redissolved. Initially, these tiny crystals have a very large surface area compared to their volume. A large surface area implies that there are many atoms on the outer surface of the crystal with unsatisfied chemical bonds (each carrying electrical charges; Fig. 10.2a). Such a crystal (or mineral grain) needs to satisfy these bonds and is more soluble than a crystal (or mineral grain) with a large volume and small surface area, in which most of the atoms are internal with completely satisfied chemical bonds.

If a nucleus is to survive, it must grow rapidly enough to reduce its surface energy (expressed as the ratio of surface area to volume) and, consequently, its solubility. When a nucleus reaches a *critical size* through rapid deposition of further layers of ions, it will have a high chance of surviving and growing into a larger crystal. A simple but illustrative picture of crystal growth is one of enlargement of the nucleus by the ordered accretion of additional ions to its outer surfaces (Fig. 10.1). The outer solid surface of a nucleus (or crystal) in contact with a saturated solution represents a surface of unsatisfied chemical bonds (Fig. 10.2). The energy of such a surface is lowered when an atom attaches itself to it, and the amount of energy released by such an attachment depends on where the attachment occurs. For example, in Fig. 10.2b, the "step" location on the surface of the crystal is where it can lose much energy through the attachment by additional ions. This is because in ionically bonded crystals, as in halite (NaCl), the energy of attachment is greatest at the corners, intermediate at the edges, and least in the middle of faces (terraces). The greater attraction of atoms to the corners of ionic crystals commonly leads to rapid growth in these directions. In some types of crystals, which differ from NaCl because of their nonionic bonding, it is thought that atoms accrete on the outer surface as clumps of atoms. Such clumps, shown as blocks in Fig. 10.2c, provide the outer surface with steps along which a new outer layer of crystal can be constructed. (An animation of the growth process is given in module II of the CD-ROM under the heading "Crystal Growth.")

The rate of growth determines which faces will become prominent on a crystal; the *slowest growing faces* are manifest in a crystal's external morphology.

The growth rate is nonuniform in crystals and is intimately connected with the density of **lattice points** (or *nodes*) in a crystal plane. As was predicted by the Law of Bravais (discussed in Chapter 7), the faces most likely to form are parallel to lattice planes that have a high density of lattice points. The frequency with which a given face is observed is roughly proportional to the number of nodes it intersects in the lattice: the larger the number of nodes, the more common the

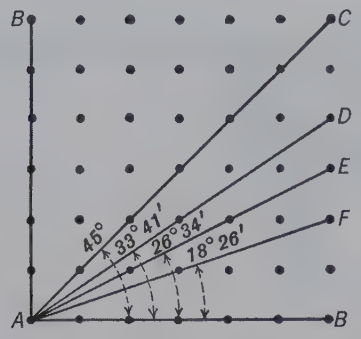

FIG. 10.3 This figure represents one layer of *lattice points* in a cubic lattice. Several lines, that include a greater or lesser number of *lattice points* (or nodes), are possible through the network. These lines represent the traces of possible crystal planes. The planes with the highest density of lattice points are typically the most common, such as *AB* and *AC*.

face, as is illustrated in Fig. 10.3. A plane intersecting *AB* in Fig. 10.3 has a much greater density of nodes than planes *AD*, *AE*, or *AF*. Calculations of the surface energy involved indicate that the energy of particles in a plane such as *AB*, in which there is a high density of nodes, is less than the energy of particles in less densely populated planes such as *AF*. Hence, the plane *AB* will be the most stable, *because in the process of crystallization, the configuration of lowest energy is that of maximum stability*. However, planes *AF*, *AD*, *AE*, and similar planes, will grow faster than *AB* because these are high-energy locations and fewer chemical units need to be added per unit area. In the growth of a crystal from a nucleus, the early forms that appear will be those of relatively high energy and rapid growth. Continued addition of material to these planes will build these faces outward while the less rapidly growing planes lag behind.

The differences in atomic environments (surface energies and, therefore, growth rates), are demonstrated by the cubic {001} and octahedral {111} packing of ions in the mineral halite, NaCl (Fig. 10.4). All of the cube faces {001} are composed of half Na^+ and half Cl^- ions [as shown by the front (100) plane]. These faces have low surface energy, little attraction for cations (or anions) in solution, and are slow to develop. Alternatively, the octahedral faces {111}, cutting the corners of the cube, have planes containing only Na^+ ions alternating with planes containing only Cl^- ions. Because the entire (111) face is made up of a layer of the same ions, resulting in a net positive or negative charge, it has high surface energy and each additional growth layer consists of either Na^+, or Cl^-. These oppositely charged ions are strongly attracted and bonded and, as a result, the octahedral faces {111} grow relatively fast. Thus, the edges and corners of a cube are built by addition of material, whereas little material is added to the cube faces. Crystal growth minimizes energy, causing the high energy faces to grow preferentially. As growth progresses, *the rapidly growing faces disappear, literally growing themselves out of existence*, building the slower-growing, more stable forms in the process. This is shown in Fig. 10.5. After the high-energy faces disappear (Fig. 10.5b, 1–3), growth is much slower, because addition of material is now entirely to the slower-growing, lowest-energy form (Fig. 10.5b, 4).

VECTORIAL PROPERTIES

Variable growth rates, due to the distinct atomic arrangements that underlie different crystal planes or crystallographic directions, serve as an example of **vectorial properties** exhibited by minerals. Because the magnitude of a property is dependent on direction, vectorial properties differ for different crystallographic directions. Other vectorial properties of crystals are hardness, conductivity for heat and electricity, thermal expansion, speed of light, solution rate, and diffraction of X-rays. Of these properties, some vary *discontinuously* with direction within the crystal while others vary *continuously* with direction.

Discontinuous vectorial properties pertain only to certain planes or directions within the crystal. There are no intermediate values of such properties connected

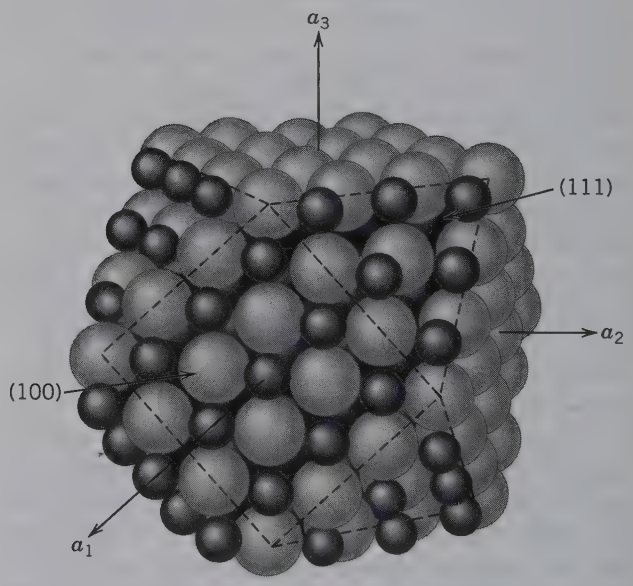

FIG. 10.4 Packing model of halite, NaCl, with cubo-octahedral outline, Na^+ small, Cl^- large. The cube faces {001}have sheets of equal numbers of Na^+ and Cl^- ions, whereas the octahedral faces (at the corners of the cube, {111}) consist of alternating planes of Na^+ and planes of Cl^- ions. Na^+ and Cl^- ions are both in 6-fold coordination in a face-centered lattice. This type of structure also is found in PbS; galena, MgO; and many other *AX* compounds.

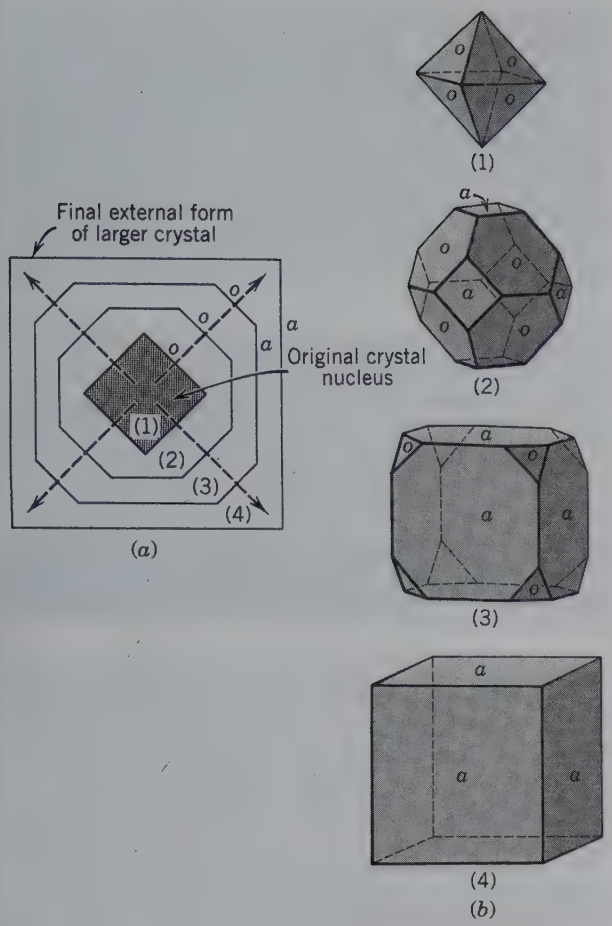

FIG. 10.5 (a) Schematic cross section of a crystal that grew from stage (1), a nucleus (with only *o*, octahedral faces), via stages (2) and (3) to the final form of (4), with only *a* (cube) faces. The arrows are growth vectors representing the direction of fastest crystal growth. Note that the faces perpendicular to these growth vectors (*o* faces) are finally eliminated in stage (4), growing themselves out of existence. (b) Illustration of the complete crystals (at the various stages 1 to 4), for which (a) provides the schematic cross section. The form consisting of *o* faces only is an octahedron, the one with *a* faces only is a cube, and the two intermediate forms are combinations of the octahedron and the cube in different stages of development. (See also CD-ROM module II, under "Crystal Growth.")

with intermediate crystallographic directions. These discontinuous vectorial properties include cleavage and rate of solution, in addition to the *rate of growth*. The vectorial nature of growth rate is exemplified by extremely fast growth that may result in the formation of **dendrites**, crystals with branches radiating from a central core (Fig. 10.6).

Differing growth velocities of specific faces on a crystal lead to the spectacular color zones observed in the mineral tourmaline when crystals are cut perpendicular to *c* (as shown on the cover of this textbook). The numerous oscillations in color reflect the changing chemical environment in which the tourmaline grew, the variation in growth velocities of faces, and the ease with which ions can be accommodated and diffused in the crystal. Certain faces accommodate ionic substitutions more readily than others. The tristar in the center of the crystal (see cover) reflects the rapid growth of the pyramidal faces (tourmaline belongs to point group $3m$) and the selective incorporation of specific color-causing chemical elements to these faces relative to the prismatic faces.

The *rate of solution* of a crystal in a chemical solvent is similarly a discontinuous vectorial process, and the solution of a crystal or any fragment of a single crystal may yield a more or less definite solution polyhedron. The vectorial nature of the rate of solution is seen by etch pits on a crystal surface. If a crystal is treated with a chemical solvent that attacks it, the faces are etched or pitted. The shape of these pits is regular and depends on the structure of the crystal, the face being etched, the presence of chemical substitutions and inclusions, and the nature of the solvent. Valuable information about the internal geometry of crystals may be obtained from a study of etch pits and etch pit morphology (see Fig. 6.35a).

Cleavage also is a discontinuous vectorial property and, like crystal form, reflects the internal structure. Cleavage always takes place along those planes across which the weakest bonding forces exist. Those planes are generally the most widely spaced and the least

FIG. 10.6 Dendrites of manganese oxide minerals on a bedding surface of limestone. Rapid growth in specific crystallographic orientations (edge growth) produces such a branching pattern. Specimen is 5 inches in width (photograph courtesy of D. Henry, Louisiana State University, Baton Rouge).

densely populated. Such planes are found in layered silicates, such as micas, and account for one direction of excellent cleavage {001}.

When properties vary continuously with direction within the crystal, they are termed **continuous vectorial properties**. These include, for example, hardness, electrical conductivity, thermal expansivity, and velocity of light.

The *hardness* of some crystals varies so greatly with crystallographic direction that the difference may be detected by simple scratch tests. An outstanding example is kyanite, Al_2SiO_5, a mineral that characteristically forms elongate bladed crystals. Kyanite can be scratched with an ordinary pocketknife in a direction parallel to the elongation, but it cannot be scratched by the knife perpendicular to the elongation. Some directions in a diamond crystal are harder than others. When diamond dust is used for cutting or grinding, a certain percentage of the grains always present the hardest surface and, hence, the dust is capable of cutting along planes in a crystal of lesser hardness. Vectorial hardness is measured by placing a perfect sphere of a crystal in a cylinder with abrasive and tumbling it for a long time. The softer portions of the crystal wear away more rapidly to produce a nonspherical shape. The resulting nonspherical solid serves as a hardness model for the substance being tested.

Ball bearings of synthetic ruby sound very attractive because the great hardness of ruby would slow wear and extend the life of the bearing. However, when heated, ruby expands differently along different crystallographic directions, and ruby ball bearings would rapidly become nonspherical with the rise of temperature from friction during operation. The *thermal expansion* diagram of ruby is an ellipsoid of revolution with a circular cross section. However, cylindrical roller bearings are practical if they are cut parallel to the crystal's three-fold axis. Most minerals have unequal coefficients of thermal expansion in different directions, leading to poor resistance to thermal shock and easy fracturing with heating or cooling. SiO_2 glass, which has an irregular internal structure as compared with crystalline quartz, is more resistant to thermal shock than the mineral quartz.

The directional character of *electrical conductivity* is of great importance in the manufacturing of silicon and germanium diodes, which are tiny bits of silicon and germanium crystals used to rectify alternating current. To obtain the optimal rectifying effect, the tiny piece of semimetal must be oriented crystallographically because the conduction of electricity through these crystals varies significantly with orientation.

The *velocity of light* in all transparent crystals, with the exception of those that are isotropic (see Chapter 13), varies continuously with crystallographic direction. Of all the vectorial properties of crystals, the optical parameters are the most easily determined quantitatively and are expressed as the index of refraction, or the ratio of the velocity of light in a vacuum to the velocity of light in the crystal. Each of these properties depends on the underlying crystal structure.

In this brief introduction to the subject of crystal growth and the resultant vectorial properties, it is implied that the addition of ions (or atoms or clumps of atoms) to the outside of a crystal occurs in a regular and continuous pattern. It also has been assumed that the resulting crystals are "perfect." However, crystals are rarely flawless, and natural as well as synthetic crystals commonly contain *imperfections*.

STRUCTURAL COMPLEXITIES AND DEFECTS

In almost all structural evaluations of crystalline material, it is assumed that repetitive, periodic order exists. However, specialized studies (e.g., TEM, HRTEM discussed in Chapter 14) have shown that atomic scale **structural defects** (or imperfections) are common in three-dimensional structures. Such imperfections affect growth rate, crystal morphology, and basic properties of crystalline materials, such as strength, conductivity, mechanical deformation, and color.

Imperfections in crystal structures are generally classified by the dimension of their geometry as **point defects, line defects**, or **plane defects**. These various types of defects are qualitatively illustrated in Fig. 10.7 by a photograph of a two-dimensional array of very small spheres that represents a two-dimensional model of a crystal. An almost perfectly ordered array of spheres is shown in Fig. 10.7a. These structurally perfect regions are interrupted by *point defects* or "holes," and are traversed by *linear defects* (Fig. 10.7b). Well-ordered blocks of the structure are separated by highly defective boundaries (Fig. 10.7c). These regions represent *domains* of slightly differing atomic orientation within a single crystal; as such, the single crystal is said to consist of a mosaic of slightly misoriented domains. Several defect structures are illustrated schematically in Fig. 10.8 and discussed subsequently.

POINT DEFECTS

Point defects represent holes or vacancies in the atomic structure that are typically absent in a regular (periodic) array. Because defects represent disorder, defects and vacant sites are more likely at higher temperatures. Specific examples of point defects are

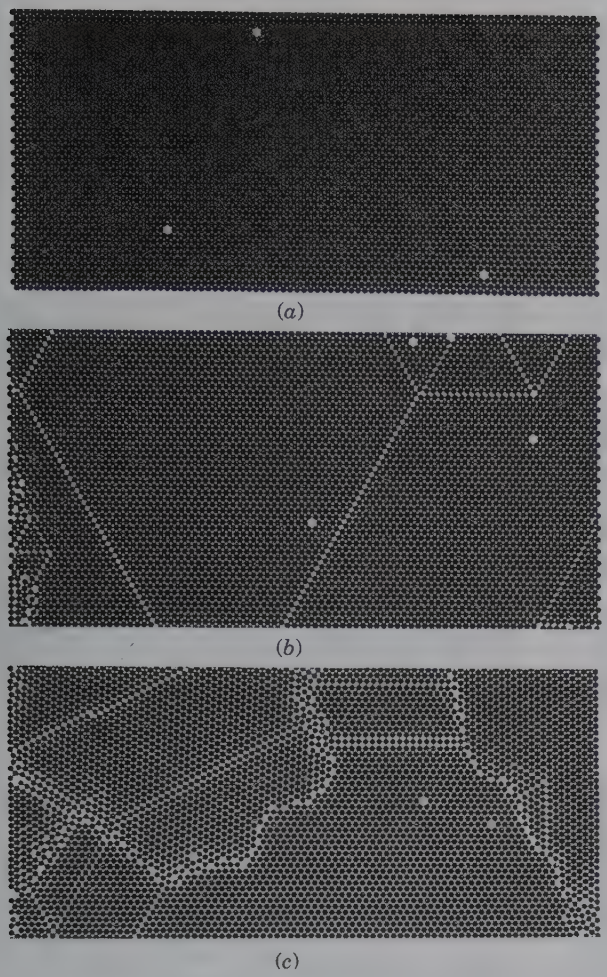

FIG. 10.7 A two-dimensional array of small spheres as a model for a crystal structure (6,000 high-precision, stainless-steel balls between two acrylic covers). (a) Regular, close packing of atoms with only three point defects in the pattern. (b) Point and line defects in the pattern. (c) A mosaic of domains separated by defective boundaries. (Photographs courtesy of Artorium, Inc., Montreal, Canada.)

Schottky defects and *Frenkel defects*. In a **Schottky defect**, some cations (or anions) are absent from their normal sites in the crystal structure. For a crystal with such defects to retain its electrical neutrality, the total charge on the cation vacancies (or defect) must equal that of the anion vacancies (or defect; Fig. 10.8a). A **Frenkel defect** represents the absence of a cation (or anion) from its proper structural site location and a mislocation of this same cation (or anion) in an interstitial site (Fig. 10.8b). This is more common for cations than anions because anions tend to be larger. Neither of these defects affects the stoichiometry of the mineral.

Another type of point defect is known as an **impurity defect**. Such defective points are the result of the addition of a foreign ion: (1) in an interstitial position in the crystal structure (Fig. 10.8c) or (2) in place of one or several of the normally present ions. *Impurity defects* will change the chemical composition of the original "perfect" crystal, but the amounts of impurities are generally so small (in the range of parts per million or parts per billion) that they may not be detected in routine chemical analyses. However, some properties, such as color, may be strongly affected by trace quantities of impurities.

LINE DEFECTS

Line defects involve concentrations of defects along linear features in a crystal structure. Such line defects are commonly known as **dislocations** because they create an offset in the crystal structure. There are two types: **edge dislocations** and **screw dislocations**. When a plane of atoms or ions in a crystal structure terminates in a line instead of continuing as would be required in a "perfect" crystal, it is said to contain an *edge dislocation* (Fig. 10.8d). The presence of line defects allows a crystal to deform under stress, by the slipping of these linear defects on an atomic scale throughout the structure. *Slip planes* in a crystal structure represent planes of atomic misfit and, therefore, of lesser coherence. *Screw dislocations* are structural defects arranged along a screw axis that normally is not present in the structure. Figure 10.8e shows that the upper atomic surface of the schematic structure resembles a spiral ramp, centered about a vertical dislocation line, which is equivalent to a screw axis direction. These spiral steps are of significance during crystal growth because new ions or atoms, which are added to the outside surface of a growing crystal, are easily incorporated along the ledge (see also Fig. 10.2).

PLANAR DEFECTS

Planar defects represent zones along which slightly misoriented blocks within a single crystal are joined. In ideally perfect crystals, the entire internal structure is regarded as a rigorously continuous and symmetrical repeat of unit cells. This implies short-range as well as long-range order. In less ideal (more real) crystals, blocks of structure may be slightly misoriented. Each block in the mosaic has short-range order, but the whole crystal lacks long-range order. This arrangement results in irregular zones or lines of edge dislocations spaced at irregular intervals (Fig. 10.8f). In a three-dimensional structure, these zones (or lines) will be irregular planar features along which ions (or atoms) have an irregular structural environment. These zones of irregularity are known also as *lineage structures*. The structures on either side of such lineages are slightly misoriented with respect to each other. When lineages

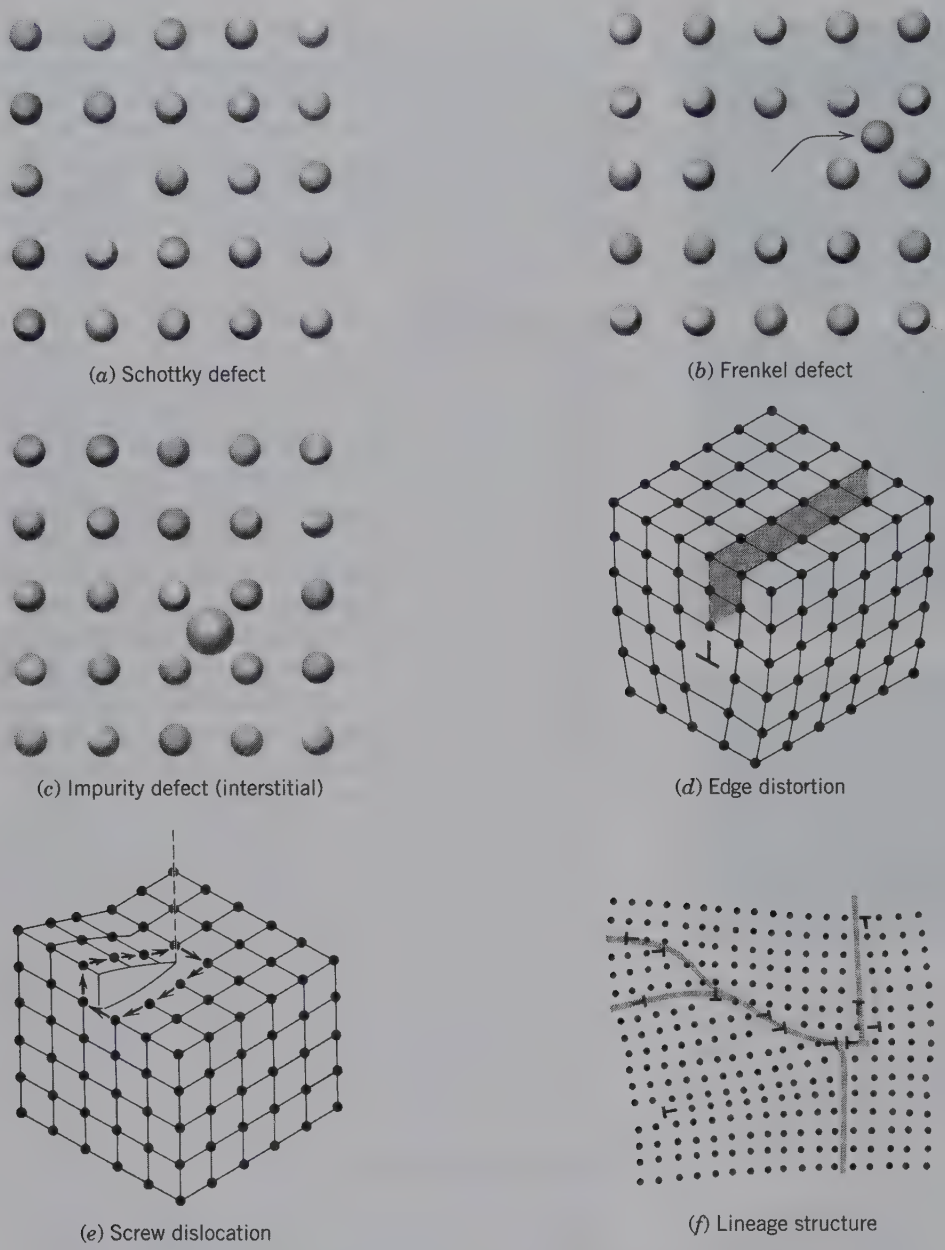

FIG. 10.8 Schematic representations of defects in crystal structures. (a) An ion (or atom) is missing from the structure. (b) An ion (or atom) is displaced from its normal site. (c) An interstitial impurity is randomly lodged in an otherwise regular structure. (d) A plane of atoms that stops along a dislocation line (the edge dislocation is shown by the graphical symbol ⊥). (e) A screw dislocation line (dashed) about which atomic planes wind in a helical form. (f) A crystal made of a mosaic of domains that differ only slightly in orientation. The irregular zones (which are planes in three dimensions) of defects are *lineage structures.*

are present, a continuous crystal structure must be viewed as comprising volumes of nearly perfect structure that occur in a mosaic of slightly misoriented domains.

Another planar defect is a **stacking fault** in which a regular sequence of layers (e.g., along the *c* axis of a structure) is interrupted by an improperly positioned layer. Stacking faults also occur when one of the layers required in a perfect crystal is missing. Examples of this are sequences of ions (or atoms) in hexagonal closest packing (*AB*, *AB*, *AB*, . . .) interrupted by a layer from a cubic closest packing sequence (*ABC*, *ABC*, *ABC*, . . .) (see Chapter 4 for a discussion on closest packing).

OTHER DEFECTS

Two other types of structural defects are exemplified by *omission solid solution* and *color centers*. Omission solid solution is discussed under "Compositional Variation in Minerals" (Chapter 5) and color centers under "Origin of Color" (later in this chapter).

MINERALOGIC EXAMPLES OF DEFECT STRUCTURES

Defects are best viewed at the atomic level by high resolution transmission electron microscopy (HRTEM, as shown in Fig. 10.9). Figure 10.9a is a structure image of crocidolite, a fibrous variety of the amphibole riebeckite,

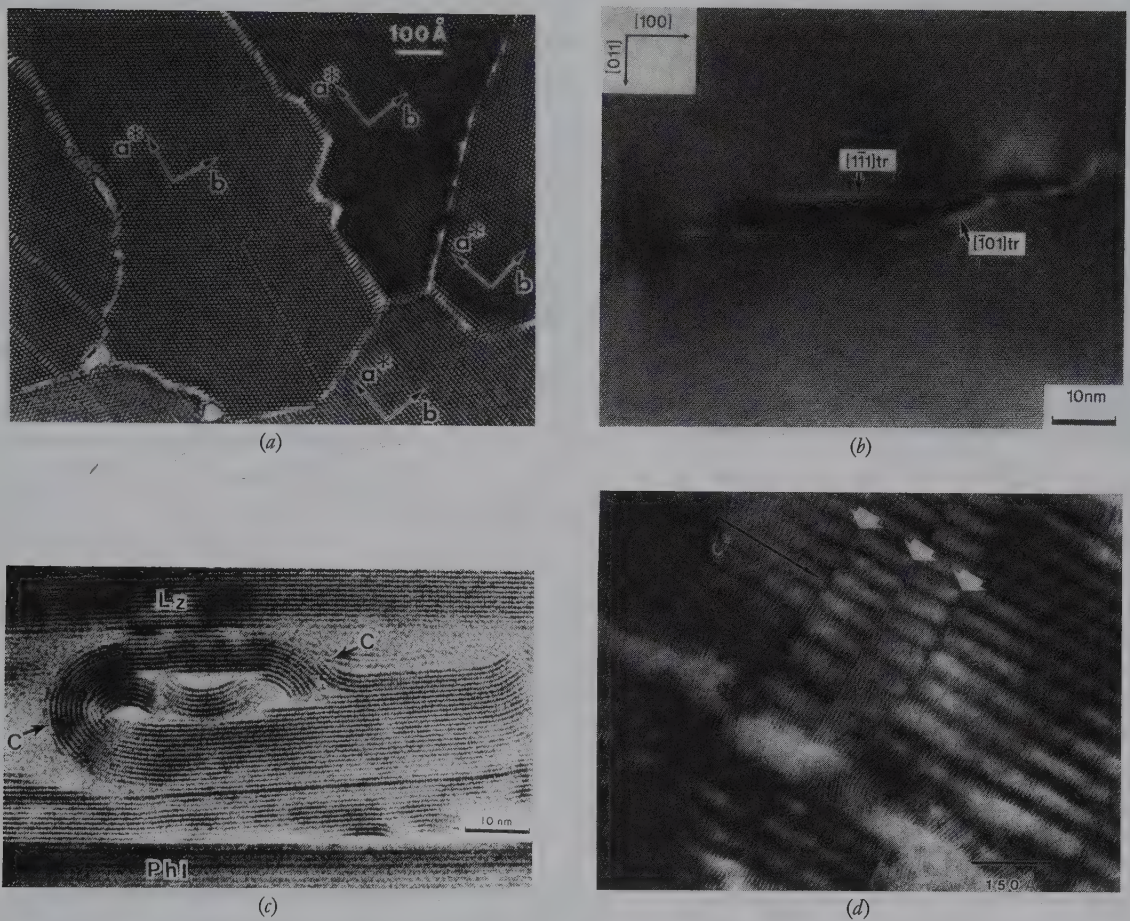

FIG. 10.9 Illustrations of structural complexities and defects. (a) HRTEM structure image of crocidolite, a fibrous variety of riebeckite, viewed down the *c* axis. The locations of the a^* and *b* directions are shown ($a^* = a \sin \beta$). Very slightly rotated domains (*subgrains*) are separated from each other along grain boundaries. The straight-line features inside several of the domains are errors in the widths of the structural chains of amphiboles. (From Ahn, J. H., and P. R. Buseck. 1991. Microstructures and fiber-formation mechanisms of crocidolite asbestos, *American Mineralogist* 76: 1467–78; see also Fig. 10.7.) (b) HRTEM structure image of a small dislocated region in an otherwise highly regular (ordered) matrix of grossular garnet. The central dislocated region is separated from the surrounding matrix by stacking faults. Crystallographic directions are shown as [011] and [100]. $[1\bar{1}1]$tr and $[\bar{1}01]$tr represent the traces of the $[1\bar{1}1]$ and $[\bar{1}01]$ directions, respectively. Both traces represent stacking faults. Scale is in nanometers. (From Allen, F. M., B. K. Smith, and P. R. Buseck. 1987. Direct observation of dissociated dislocations in garnet. *Science* 238: 1695–97; photo by J. Berry.) (c) HRTEM structure image of locally deformed (curled) serpentine (C) inside a matrix of well-layered lizardite (Lz), also a variety of serpentine. The curled region occurs along a cleavage fracture. Phl = phlogopite mica. Scale is in nanometers. (From Sharp, T. G., M. T. Otten, and P. R. Buseck. 1990. Serpentinization of phlogopite phenocrysts from a micaceous kimberlite. *Contributions to Mineralogy and Petrology* 104: 530–39.) (d) HRTEM image of modulations in antigorite, a variety of serpentine. The modulations are about 50 Å in length. The c^* direction = $c \sin \beta$. The short white arrows show defective boundaries, which may be out-of-phase or twin boundaries. (From Buseck, P. R., and J. M. Cowley. 1983. Modulated and intergrowth structures in minerals and electron microscope methods for their study, *American Mineralogist* 68: 18–40; photo by G. Spinnler.)

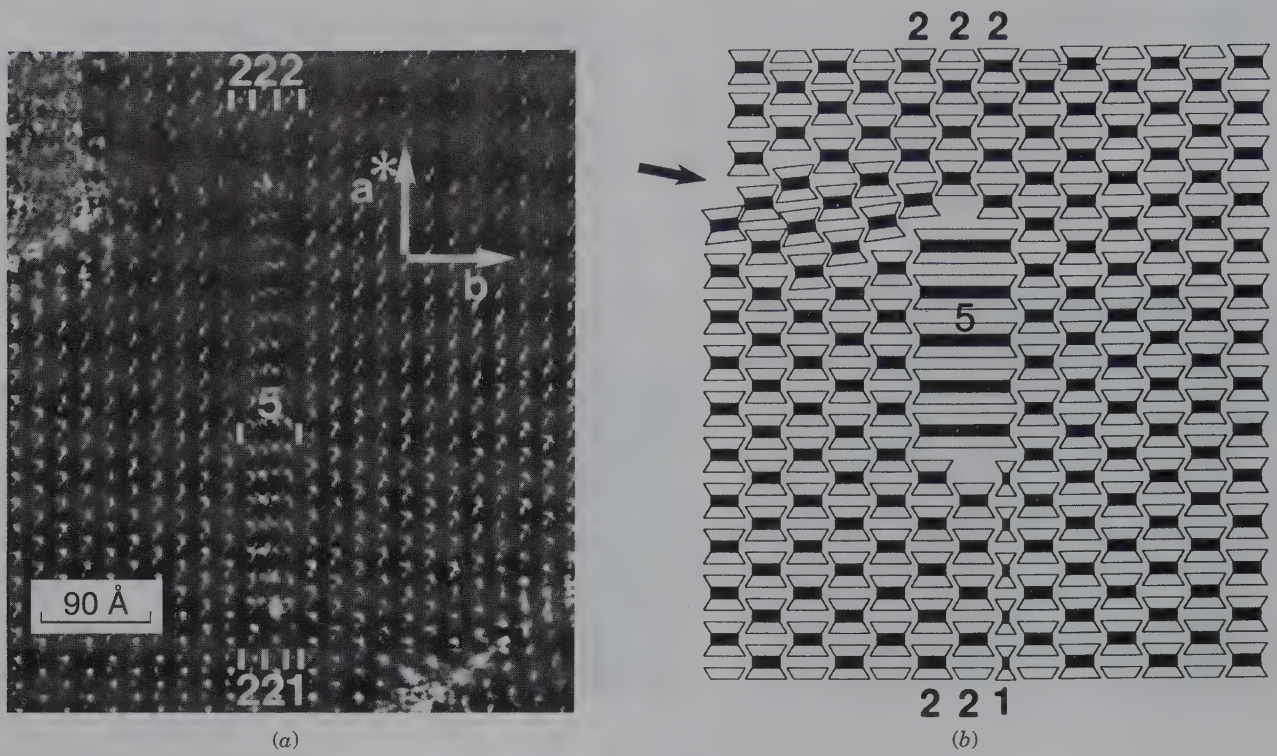

(a) (b)

FIG. 10.10 (a) HRTEM structure image of crocidolite, a fibrous amphibole, viewed down the *c* axis of the structure. Note the scale bar of 90 Å (1 angstrom = 0.1 nanometer). Most of the field is composed of a regular pattern, which is the structure image of adjoining double (2) chains in the amphibole structure (see also Fig. 18.22). However, the image also shows quintuple (5) and single (1) chain-width errors (these are marked by the appropriate numbers on the photograph). These defects appear as lines in the projected image, but represent continuous planar features in the three-dimensional structure. The a^* ($a^* = a \sin \beta$) and *b* directions are shown. (b) A schematic representation using I-beams to illustrate the complexities and defects observed in the structure image in (a). The arrow at the top left of the figure points toward a disrupted region caused by structural mismatch. Similar mismatch occurs just "north" and "south" of the quintuple (5) chain. The mismatch to the "south" of the quintuple chain has been accommodated by an orderly arrangement of two double (2) chain widths and one single (1) chain width. (*a* and *b* from Ahn, J. H., and P. R. Buseck. 1991. Microstructures and fiber-formation mechanisms of crocidolite asbestos, *American Mineralogist* 76: 1467–78.)

consisting of a mosaic of domains that show slightly different crystallographic orientations, separated by a lineage structure (planar defects) that represents grain boundaries. Stacking faults are shown in a structure image of grossular garnet (Fig. 10.9b) where a very small region (within the otherwise highly periodic and ordered garnet matrix) is dislocated and separated from the surrounding material by stacking faults. Misorientations are displayed in Fig. 10.9c that shows a deformed, curled region (*C*) in an otherwise well-layered matrix of lizardite (Lz), a variety of serpentine. Figure 10.9d depicts modulations and offsets of layers in the structure of antigorite, a variety of serpentine. Modulations in the antigorite structure are wave-like features that result from a small dimensional misfit that occurs between the tetrahedral and octahedral layers. This misfit is accommodated by a curling of the structural layers, similar to what happens when a telephone book is bent. A continuous curl results in the chrysotile structure (see Figs. 18.37 and 18.39).

Amphiboles display a variety of defects and structural complexities. Figure 10.10a shows several local defects, such as errors in the width of tetrahedral chains and misfits in the surrounding structure. Fig. 10.10b is a schematic interpretation of these same features.

INTERGROWTHS OF CRYSTALS

During the growth of a mineral, offsets to the atomic arrangement of the structure may occur that are *nonrandom*. This results in the development of relatively common intergrowth patterns of well-formed crystals (as well as anhedral grains). These intergrowths may be of minerals with different compositions, or they may be minerals of the same composition.

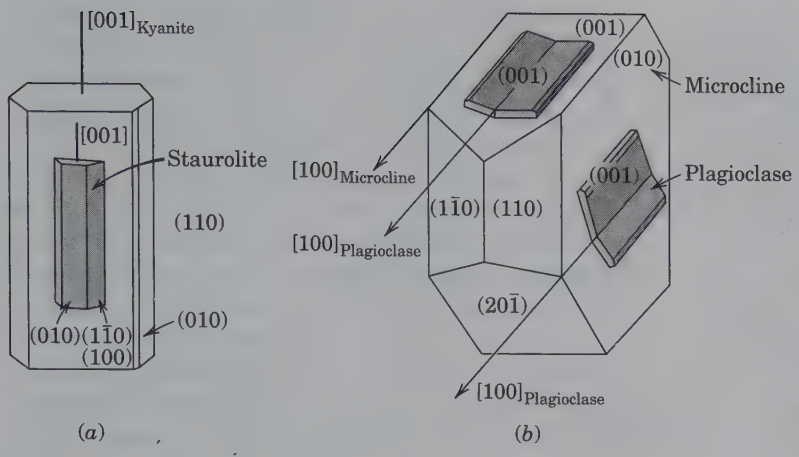

FIG. 10.11 Examples of epitaxis. (a) Parallel growth of staurolite, $Fe_{3-4}Al_{18}Si_8O_{48}H_{2-4}$, and kyanite, Al_2SiO_5. (b) Oligoclase, $NaAlSi_3O_8$ with about 13% substitution by $CaAl_2Si_2O_8$, overgrowths on microcline, $KAlSi_3O_8$. (This figure from Kern, R., and R. Gindt. 1958. *Bulletin Societé Française Min. Cryst.*, 81: 264.)

A type of non-random, crystallographically oriented growth of one crystalline substance on another of different composition, is known as **epitaxis**. Although the two compositionally distinct intergrown crystals will tend to have different structures (and unit cell sizes), there are planes in their internal structures where there is a good fit (or the least amount of misfit) between them. This similarity in substrate reduces the energy required for nucleation allowing for such preferential overgrowth.

As an example, staurolite (with monoclinic symmetry) may be observed with an overgrowth of kyanite (with triclinic symmetry) with the (010) plane of staurolite parallel to the (100) plane of kyanite (Fig. 10.11a). This occurs because the atomic spacing (and composition) of the (010) plane in staurolite is similar to that of the (100) plane in kyanite. The structure of staurolite is commonly described as consisting of layers of kyanite alternating with iron-hydroxide layers along (010) (see Chapter 19, page 495).

The epitaxial overgrowth of a plagioclase feldspar (oligoclase) on a crystal of microcline is illustrated in Fig. 10.11b. The common direction between the two different structures is identified by the forward-sloping arrows that are parallel to a crystallographic direction identified as [100]. The planes of attachment are (001) in plagioclase and (001) and (010) in microcline. These three planes have a good, but not perfect, fit between them in terms of the internal structure and atomic spacing for the two minerals involved.

Non-random intergrowths of the *same composition substance* are **parallel growths** (Fig. 10.12) and **twins** or **twinned crystals** (Fig. 10.13). An aggregate of similar crystals with their crystallographic axes and faces parallel to each other is called a **parallel growth**. Such aggregates, although they may at first appear to represent several crystals, are a single crystal because the internal atomic structure remains unchanged in orientation throughout the specimen. Parallel growth, as found in quartz and barite, is illustrated in Fig. 10.12.

TWINNING

Under certain conditions of growth, two or more crystals may form a rational, symmetrical intergrowth. Such a *crystallographically controlled intergrowth* is called a *twin*.

A **twin** *is a symmetrical intergrowth of two or more crystals of the same substance.*

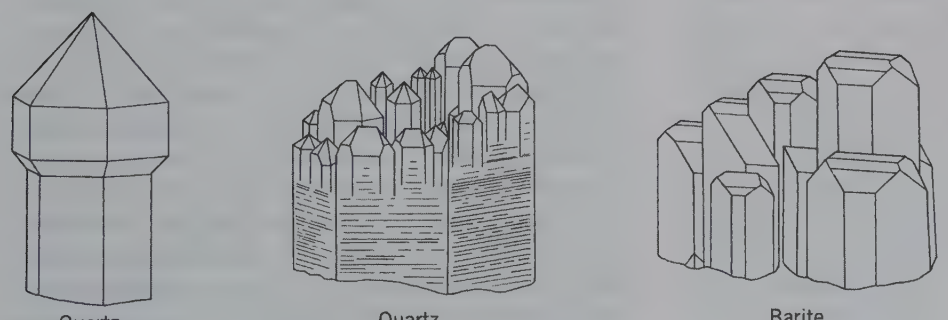

FIG. 10.12 Examples of parallel growth. (a) Overgrowth of a larger crystal of quartz on a smaller one, forming the shape of a scepter. (b) The termination of a large quartz crystal in a collection of smaller crystals, all in parallel orientation. (c) Parallel intergrowth of barite crystals.

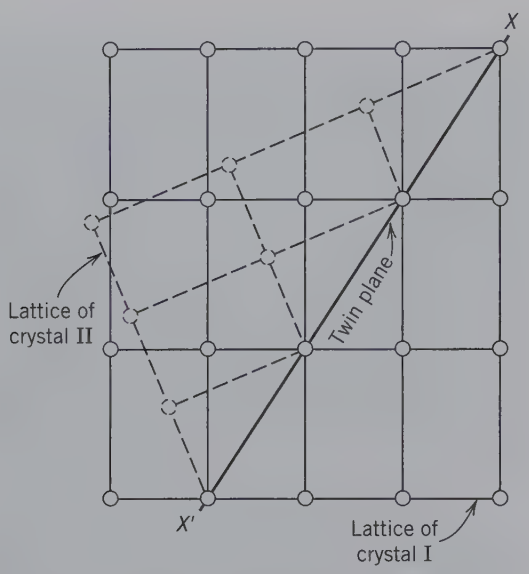

FIG. 10.13 Cross section through the orthorhombic lattice of an untwinned crystal (no. I). A twinned counterpart of I is shown by II in the inclined position. Along the line *XX'* atoms are compatible with either of two crystal orientations, as shown by the solid and dashed circles. If the inclined position is chosen, a twinned crystal results. Such a twin may be regarded as the result of a rotation of 180° about the line *XX'* or of a mirror reflection along *XX'*.

The lattice directions of one crystal in a twin bear a definite crystallographic relation to the lattice directions of the other crystal. Twinning can be considered a type of planar defect.

Growth twins are the result of an emplacement of atoms, or ions (or groups of atoms or ions) on the outside of a growing crystal in such a way that the regular arrangement of the original crystal structure (and, therefore, its lattice) is interrupted. For example, in Fig. 10.13, the line *XX'* may be considered the trace of an external face of a growing crystal. An ion or atom (or group of ions) would have the choice of attaching itself at structural sites that represent a continuation of the nodes in the lattice of crystal I or in nodes compatible with the lattice of crystal II. In the former case, the original structure is continued without interruption, but in the latter, a twinned relationship results. *Growth twinning*, therefore, reflects "accidents" (or nucleation errors) during free growth and is considered to be primary twinning. (Twinning that occurs after crystal growth is discussed in Chapter 12, page 275).

The two or more individual crystals of the twinned aggregate are related by a symmetry element that is absent in the original (untwinned) crystal. The new symmetry element, or **twin element**, brings one individual crystal into coincidence with another individual crystal in a twinned position. Twinning in the lower symmetry groups generally produces a resulting aggregate symmetry higher than that of each individual because the twin planes, or twin axis, are added symmetry elements. The presence of a twin is often visible by the occurrence of reentrant angles on the resulting crystal (see, for example, Figs. 10.20, 10.22 and 10.23).

The operations that relate a crystal to its twinned counterpart are symmetry operations: (1) reflection by a mirror plane, **twin plane**; (2) rotation about a crystal direction common to both, **twin axis**, with the angular rotation normally 180°; and (3) inversion about a point, **twin center**. The twin operation is known as a **twin law**, which states whether there is a center, an axis, or a plane of twinning. The twin law also states the crystallographic orientation for the twin axis or plane. A twin plane is identified by its Miller index [e.g., (010) or its form symbol for all equivalent planes {010}] and a twin axis direction is identified by a zone symbol (e.g., [001]). Various twin laws are discussed for the six crystal systems in the following section, "Common Twin Laws."

The surface on which two individuals are united is known as the **composition surface**. If this surface is a plane, it is called the **composition plane**, and its surface can be irregular or regular. The composition plane is commonly, but not invariably, the *twin plane*. If the twin law is simply a twin plane, the twin plane is always parallel to a possible crystal face but never parallel to a plane of symmetry. The twin plane is an additional symmetry element not present in the untwinned crystal. The twin axis is a zone axis or a direction perpendicular to a rational lattice plane; but it can never be an axis of even rotation (two-, four-, six-fold) if the twin rotation involved is 180°. In some crystals, a 90° rotation about a two-fold axis can be considered a twin operation. (Animations of the atomic aspects of twinning are given in module II of the CD-ROM under the heading "Twinning.")

TWIN CLASSIFICATION

Twinned crystals are classified as either *contact twins* or *penetration twins*. **Contact twins** have a *regular composition surface* separating the two individuals. The twin is defined by a twin plane such as in Fig. 10.14a. This plane is one of four possible and crystallographically equivalent directions in the octahedron {111} of the isometric system. Therefore, to describe all possible octahedral twin planes, the {111} form symbol is used instead of the notation (111) for a specific plane. A striking example of octahedral twin planes as observed in native copper is shown in Fig. 10.15. Other examples of contact twins are illustrated in Figs. 10.14b and 10.14c. **Penetration twins** are made up of interpenetrating individuals having an *irregular composition surface*, and the twin law is usually defined by a twin axis direction (e.g., [111] or [001]; Figs. 10.14d to f). (Several different

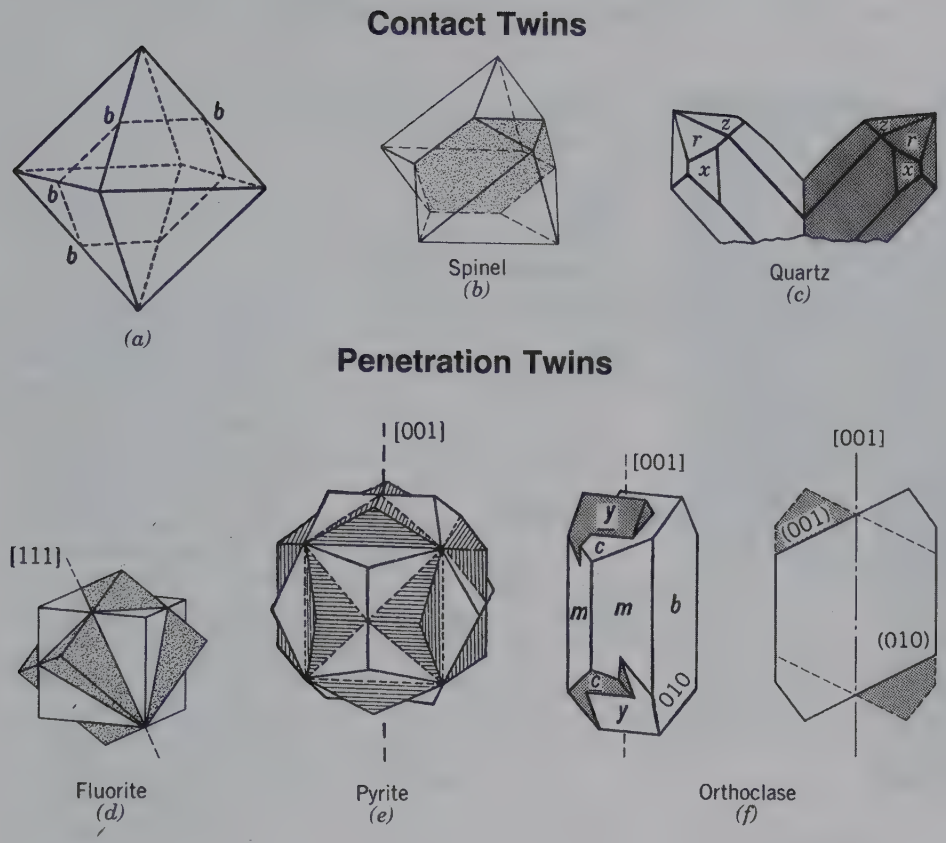

FIG. 10.14 (a) Octahedron with possible twin plane *b*–*b* ($\bar{1}\bar{1}1$). This is one of four octahedral directions in the form {111}. (b) Octahedral twinning {111} as shown by spinel. (c) Right- and left-handed quartz crystals twinned according to the ($11\bar{2}2$) *Japan twin law*. (d) Two interpenetrating cubes of fluorite twinned on [111] as the twin axis. (e) Two pyritohedral crystals (of pyrite) forming an *Iron Cross*, with twin axis [001]. (f) Orthoclase exhibiting the *Carlsbad twin law* in which two interpenetrating crystals are twinned by 180° rotation about the *c* axis, [001] direction. The schematic cross section, parallel to (010), reveals the presence of the two-fold twin axis along [001].

twins are illustrated, with animations, in module II of the CD-ROM under the heading "Twinning.")

Twinned crystals are further classified as **repeated**, or **multiple twins** that consist of three or more individual crystals twinned according to the same law. If all the composition surfaces are parallel, the resulting group is a **polysynthetic twin** (Figs. 10.16a, b, and c). When a large numbers of individuals in a polysynthetic twin are closely spaced, crystal faces or cleavages crossing the composition planes show striations because of the reversed positions of adjacent individuals. A highly diagnostic polysynthetic twin is albite twinning in the plagioclase feldspar series. The individual twin lamellae that can be seen by the naked eye are commonly quite thin, ranging from 0.1 to several millimeters in thickness (see Fig. 2.9b). This twin is evidenced by parallel lines or striations seen on cleavage faces (Figs. 10.16a and b; 10.17a and b). Polysynthetic twinning in a magnetite crystal is shown in Fig. 10.17c.

Striations, however, as seen on crystal faces, are by no means always the result of polysynthetic twinning. Figures 10.17d and e show striations that result from the intergrowths of two forms. Pyrite cubes (Fig. 10.17d) typically show striations that are the result of successive combinations of other faces or of another form, a pyritohedron, in narrow lines with the cube. The magnetite crystal, in Fig.10.17e, shows striations on the faces of a dodecahedron caused by the stepwise growth of octahedral faces with triangular outlines.

FIG. 10.15 Copper specimen displaying multiple spinel twins. Each crystal displays an approximate triangular outline. Specimen is from the Ray Mine, Pinal Co., Arizona, U.S.A., and is $7\frac{1}{2}$ inches tall. (Photograph courtesy of Stuart & Donna Wilensky, Wilensky Fine Minerals, Wurtsboro, NY.)

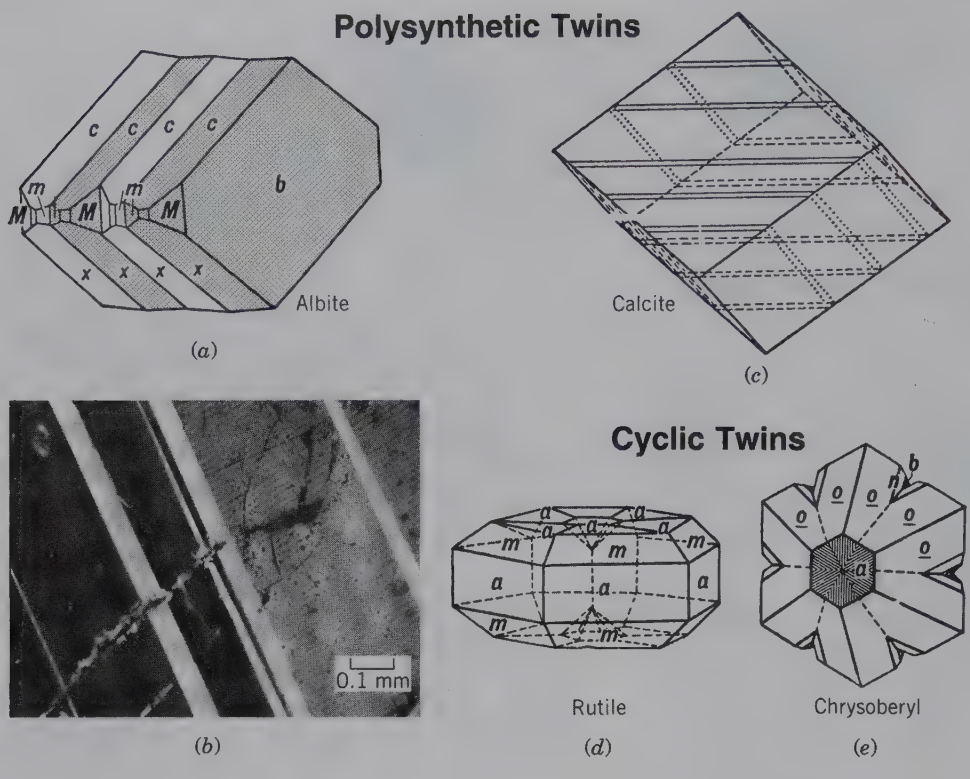

FIG. 10.16 (a) Albite polysynthetically twinned on {010}. (b) The same polysynthetic twinning as in (a) but as seen in a polarizing microscope. The dark and light lamellae in albite are related by reflection across (010). (c) Polysynthetic twinning in calcite on $\{\bar{1}012\}$, which is one of the three directions of the negative rhombohedron. (d) Cyclic twin in rutile with the twin planes parallel to faces of the form {011}. (e) Cyclic twin in chrysoberyl with the twin planes parallel to faces of the form {031}. Note the reentrant angles between individual crystals.

If successive composition planes are not parallel, a **cyclic twin** results (Figs. 10.16d and e, 16.28). Cyclic twins are common in the minerals aragonite and rutile.

Twinning is common in crystals, and the size of the individual twins can range from an almost atomic scale, with twin lamellae or twin domains on the order of tens to hundreds of angstroms in size, to such a large scale that the individuals are easily seen by the naked eye. It is generally necessary to do careful morphological measurements (mainly by reflecting goniometer

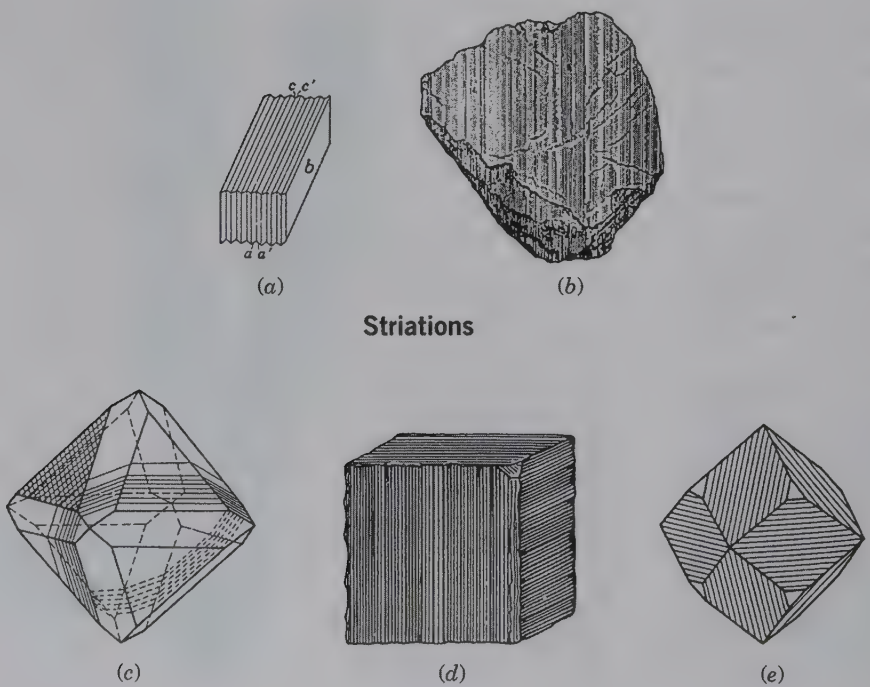

FIG. 10.17 Polysynthetic twinning and striations. (a) Albite polysynthetically twinned parallel to the vertical plane (010) marked *b*. (b) The appearance of albite twinning as striations or as parallel grooves across a cleavage surface or crystal face. (c) Octahedral crystal of magnetite with twinning lamellae appearing as striations on an octahedral face. (d) Striations on a cube of pyrite. (e) Striations on the faces of a dodecahedron of magnetite caused by the presence of octahedral faces, *o*. (From Klein, C. 2008. *Minerals and rocks: Exercises in crystal and mineral chemistry, crystallography, X-ray powder diffraction, mineral and rock identification, and ore mineralogy.* 3rd ed. Wiley, New York).

and/or X-ray precession methods) to distinguish a twin from a random intergrowth of crystals.

COMMON TWIN LAWS

The description of a **twin law** consists of stating the crystallographic orientation of the twin element, axis, or plane. The two twinned orientations of an orthorhombic lattice (shown in Fig. 10.13) are related by a mirror reflection or a 180° rotation along the direction *XX'*, which would represent a planar surface in a three-dimensional lattice. Along this direction, there is a perfect coincidence of lattice nodes (or atomic positions) of crystals I and II. In the illustration, the *XX'* direction (which would represent a planar surface in a three-dimensional lattice) is the contact between the two twinned crystals. The more nearly perfect the periodic atomic arrangement of a crystal is, the lower its internal energy will be. (Three-dimensional animations of the twin laws consistent with the two-dimensional drawing of Fig. 10.13 can be seen in module II of the CD-ROM under the heading "Twinning".)

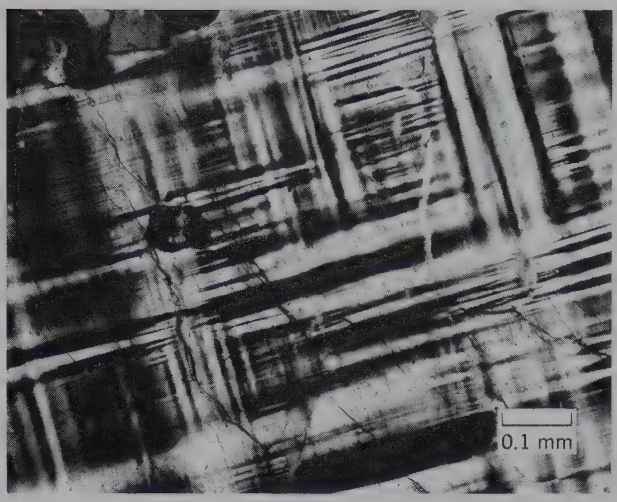

FIG. 10.18 Photomicrograph of tartan twinning in microcline. The specimen is viewed through a microscope with crossed polarizers. The section of the photograph is approximately parallel to (001). The twin laws represented are albite with twin and composition plane (010), and pericline with twin axis direction [010].

Triclinic System

The feldspars best illustrate twinning in the triclinic system. They are almost universally twinned according to the *albite law*, along the {010} twin plane, as shown in Figs. 10.17a and b. Another important type of twinning in triclinic feldspar is according to the *pericline law*, along [010], the twin axis. When albite and pericline twins are closely interwoven, as frequently occurs in microcline, a typical cross-hatched or "tartan" pattern can be seen under the polarizing microscope (Fig. 10.18). Triclinic feldspars also twin according to the same laws as monoclinic feldspars.

Monoclinic System

In the monoclinic system, twinning on {100} and {001} is most common. Figure 10.19 illustrates gypsum with {100} as the twin plane producing what is known as a *swallow-tail twin*. This same figure also shows three twin laws that occur in the mineral orthoclase. Two of these are contact twins: a *Manebach twin* with {001} as the twin plane, and a *Baveno twin* with {021} as the twin plane. The most common twin in orthoclase is the *Carlsbad twin*, an interpenetration twin in which the *c* axis, [001], is the twin element. In this case, the two individuals are united along an irregular surface roughly parallel to (010).

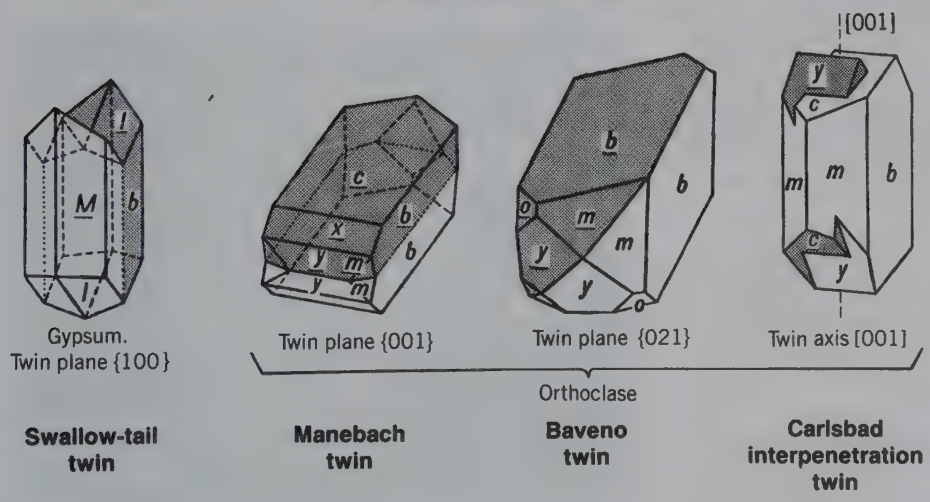

FIG. 10.19 Examples of common twin laws in monoclinic crystals.

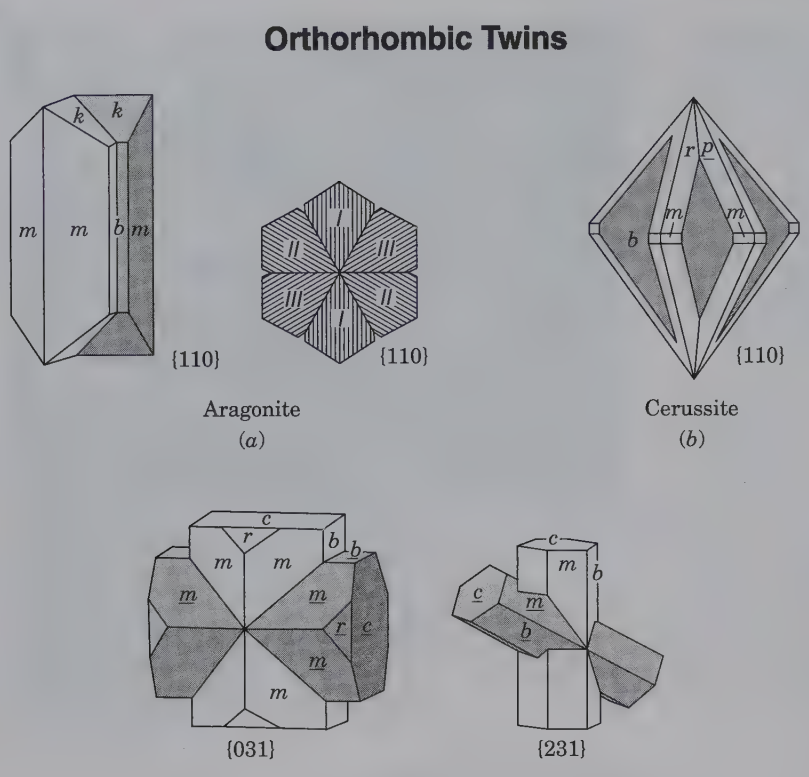

FIG. 10.20 Examples of common twins in orthorhombic crystals. (a) Contact and cyclic twinning on {110} in aragonite. (b) A cyclic twin on {110} in cerussite. (c) Staurolite twinned on {031} and {231}. The staurolite structure is actually monoclinic with $\beta \approx 90°$; therefore, it appears pseudo-orthorhombic. It is illustrated here because of its orthorhombic-looking morphology.

Orthorhombic System

In the orthorhombic system, the twin plane is most commonly parallel to a prism face. The contact twin of aragonite and the cyclic twins of aragonite and cerussite are all twinned on {110} (Figs. 10.20a and b). The pseudo-hexagonal appearance of the cyclically twinned aragonite results from the fact that $(110) \wedge (1\bar{1}0)$ is nearly 60°. The twinning of such a crystal is recognized by the presence of reentrant angles that occur between individual crystals (Figs. 10.20a and b). The mineral staurolite, which is monoclinic with a β angle close to 90°, is pseudo-orthorhombic and morphologically appears orthorhombic. It is commonly found displaying two types of penetration twins. In one, with {031} as the twin plane, a 90° cross results; in the other, with twin plane {231}, a 60° cross is formed (Fig. 10.20c).

Tetragonal System

The most common type of twin in the tetragonal system has {011} as the twin plane. Crystals of cassiterite and rutile, twinned according to this law, are shown in Fig. 10.21.

Hexagonal System

In the hexagonal system, the carbonates, especially calcite, serve as excellent examples of three twin laws. Several examples are shown in Fig. 10.22. The twin plane may be {0001}, with *c*, the twin axis (Fig. 10.22a), or it may be the positive rhombohedron $\{10\bar{1}1\}$. However, twinning on the negative rhombohedron $\{01\bar{1}2\}$ is most common (Figs. 10.22b and 10.23) and may yield contact twins or polysynthetic twins as the result of pressure. The ease of twinning according to this law can be demonstrated by the artificial twinning of a cleavage fragment of transparent calcite (Iceland spar) by the pressure of a knife blade (as shown in the far right crystal in Fig. 10.22b).

FIG. 10.21 Examples of common twin laws in tetragonal crystals.

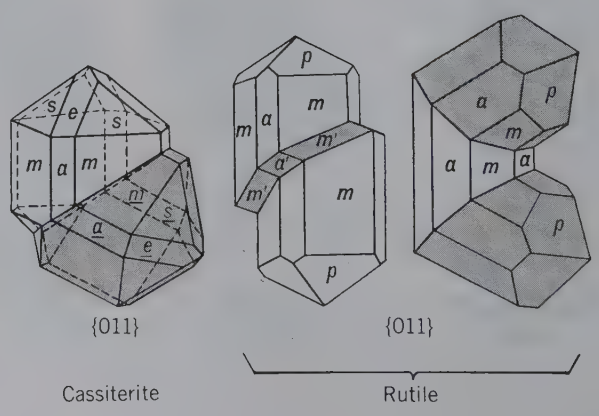

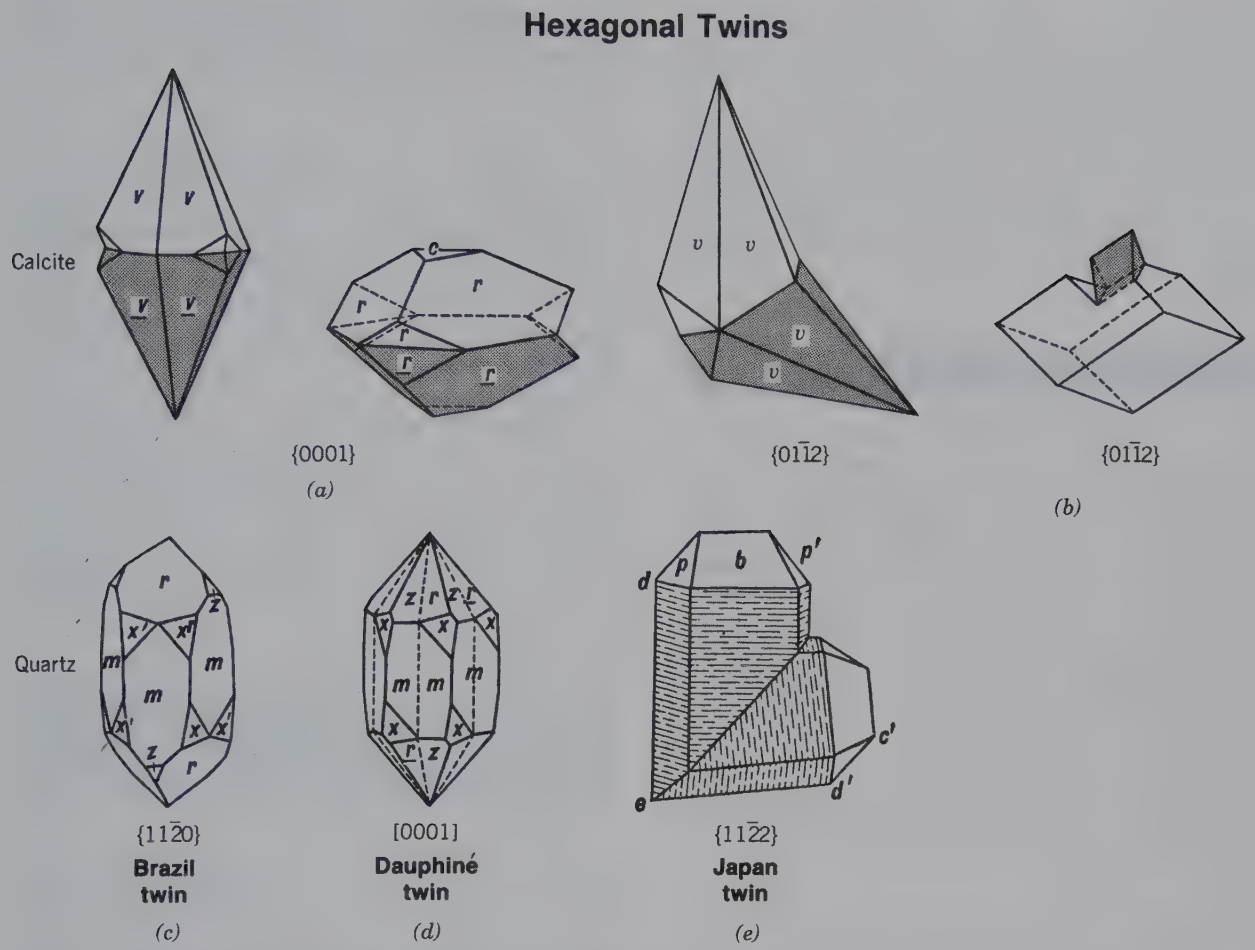

FIG. 10.22 Examples of twins in the hexagonal system. (a) and (b) Various twins in calcite. The calcite twin on the right is artificial and can be produced by pressure with a knife edge. (c) A *Brazil twin* in quartz. (d) A *Dauphiné twin* in quartz formed by rotation of 180° about the *c* axis, [0001]. (e) A *Japan twin* in quartz.

FIG. 10.23 Calcite displaying a "butterfly twin" and a prominent reentrant angle between individual crystals. Specimen is from Nanjing, China, and is $6\frac{1}{2}$ inches wide. (Photograph courtesy of Stuart & Donna Wilensky, Wilensky Fine Minerals, Wurtsboro, NY.)

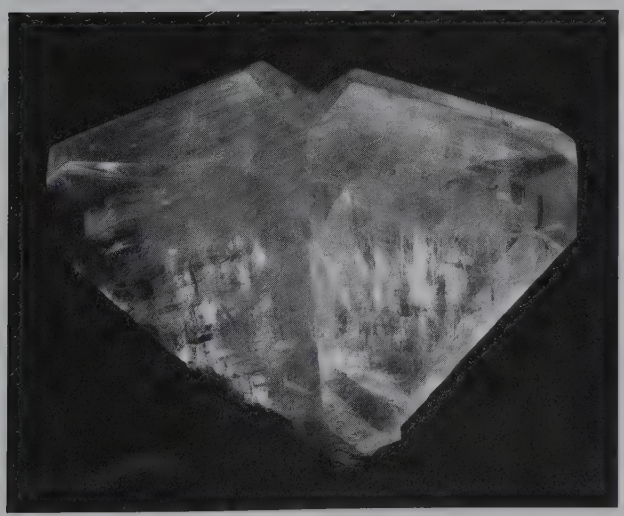

Quartz shows several types of twinning. Figure 10.22c illustrates the *Brazil law* with the twin plane parallel to $\{11\bar{2}0\}$. Here, right- and left-handed individuals have formed a penetration twin. Figure 10.22d shows a Dauphiné twin, which is a penetration twin with *c*, the twin axis. Such twins are composed either of two right-handed or two left-handed individuals. Figure 10.22e illustrates the *Japan law* with the twin plane $\{11\bar{2}\}$. The reentrant angles usually found on twinned crystals are not present in either Brazil or Dauphiné twins.

Isometric System

In the $4/m\bar{3}2/m$ class of the isometric system, the twin axis, with a few rare exceptions, is a three-fold symmetry axis, and the twin plane is parallel to a face of the octahedron. Figures 10.14a and b show an octahedron with plane *bb* as a possible twin plane, as well as an octahedron twinned according to this law, forming a contact twin. This type of twin is especially common in

spinel and is called a *spinel twin*. Figure 10.14d shows two cubes forming a penetration twin with the three-fold rotoinversion axis [111] as the twin axis.

In the class $2/m\bar{3}$, two pyritohedrons may form a penetration twin (Fig. 10.14e) with a 90° rotation about the twin axis [001]. This twin is known as the *iron cross*. The morphology expressed by twinned crystals can be highly diagnostic in the identification of a mineral species.

ORIGIN OF COLOR

Minerals possess many properties, of which color is usually the first and most easily observed. For many minerals, color serves as a distinguishing criterion; most people will recognize a number of the gem minerals and gemstones, shown in Plates IX to XII (Chapter 20), on the basis of their colors alone. However, in many minerals, color is one of the most changeable and unreliable diagnostic properties. This is due, in part, to the fact that the causes of color in many minerals are in response to structural irregularities.

Color is the response of the eye to the visible light range of the electromagnetic spectrum (Fig. 10.24). Visible light represents a range of wavelengths from about 350 to 750 nanometers (nm, 1 nm = 10 angstroms).

FIG. 10.24 A part of the electromagnetic spectrum, with three ways of numerically specifying the colors. The wavelength scale is in nanometers (nm; 1 nm = 10 Å); the wavenumber scale expresses the number of wavelengths per unit length (cm).

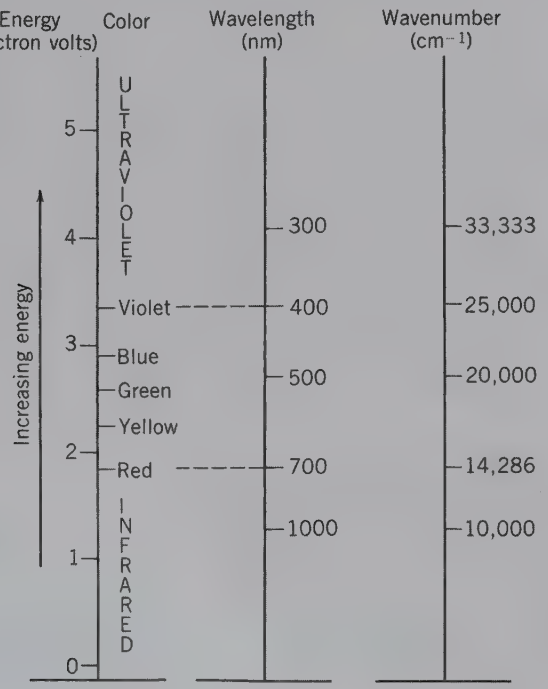

The energy of light, as of all electromagnetic radiation, can be expressed as follows:

$$E = h\nu = \frac{hc}{\lambda} = hc\bar{\nu}$$

where E denotes energy, h is Planck's constant, c is the speed of light (a constant), ν is frequency, λ is the wavelength, and $\bar{\nu}$ is the wavenumber. Wavenumber, $\bar{\nu}$, is the reciprocal of the wavelength and, because it is directly proportional to energy, is commonly used in analyses of color in minerals. The spectral range of visible light is defined in terms of energy, wavelength, and wavenumber scales in Fig. 10.24.

When white light strikes the surface of a mineral, it may be transmitted, scattered, reflected, refracted, or absorbed (see Fig. 2.5). The processes of scattering and reflection are part of the property perceived as the *luster* of a material (refer to Chapter 2). If light suffers no absorption, the mineral is colorless in reflected and transmitted light. In contrast, minerals are colored when certain wavelengths of light are absorbed.

> The perceived color results from the combination of those remaining wavelengths that are transmitted through the crystal and reach the eye.

To determine which wavelengths are absorbed by minerals (and which are transmitted), an instrument called a *spectrometer* is used to quantitatively measure absorption. The output of such an instrument is an *absorption spectrum*; an example for the mineral beryl is given in Fig. 10.25. The peaks in this pattern represent absorption of specific wavelengths of light, and are the result of the interaction of light at these wavelengths with ions, molecules, and bonds in the irradiated structure. The absorptions between 0.4 and 0.7 μm result from **chromophores**, or transition metal ions such as Fe^{3+} and Cr^{3+}, that cause the color (*chromophore* is derived from the Greek word meaning color-causing). In the infrared region between 1 and 4.5 μm, there are absorptions due to molecules, such as H_2O and CO_2, which are interstitial in the hexagonal channels of the beryl structure (see Fig. 5.8). Beyond 4.5 μm, the absorptions are the result of vibrations of the crystal lattice or the so-called lattice modes. Because these absorptions lie outside of the visible light range, they do not affect the perceived color.

As discussed in Chapter 3, the energies of electrons occur in discrete units, or *quanta*, and there are well-defined energy differences between these allowed energy levels. When electromagnetic radiation interacts with a material, those photons with wavelengths whose energies correspond exactly to the energy differences between the electronic levels will be absorbed

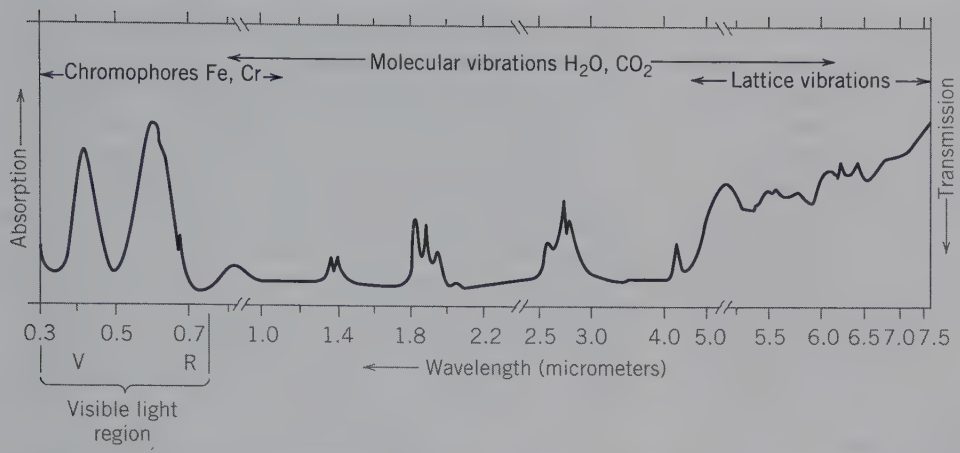

FIG. 10.25 The visible and infrared spectrum of beryl. Peaks correspond to absorption bands. Absorption in the visible region (0.1 to 0.8 μm) is caused by chromophores Fe and Cr; absorption in the 0.8 to 6.5 μm region results from molecular vibrations; and absorption above 4.5 μm is the result of lattice vibrations. 1 micrometer (μm) = 1000 nanometers (nm). V = violet, R = red. (After Wood, D. L., and K. Nassau. 1968. The characterization of beryl and emerald by visible and infrared absorption and spectroscopy, *The American Mineralogist* 53: 777–801.)

by exciting electrons from one level to a higher energy level. In colored minerals, the energy differences between these electron energy levels are in *the range of energy of visible light*. Thus, when white light shines on a mineral, certain wavelengths are absorbed, causing excitation of electrons between these levels. These wavelengths are, therefore, removed from the spectrum, and this is the underlying cause for color in minerals.

Color in minerals varies widely. Color can be used as a diagnostic property only when the element causing the color (a chromophore) is *essential to the mineral*. That is, the element must always be present in a specific quantity that results in all specimens of the same mineral having a constant color.

For example, almandine garnet, $Fe_3Al_2Si_3O_{12}$, is always dark red when pure and its color is a diagnostic feature. Elemental substitutions cause a range of colors in minerals. When color is due to such chemical substitutions (e.g., Mn substituting for Fe), typically color is not a diagnostic property. The reasons for this are discussed subsequently.

A variety of electronic and physical mechanisms cause minerals to be colored; only four are considered here (see Nausau, 1987 for other causes of color; see also Rossman, http://minerals.gps.caltech.edu/COLOR_Causes/index.htm). The *electronic processes* responsible for color in minerals can be classified as **crystal field transitions, molecular orbital (charge transfer) transitions**, and **color centers**. The *physical process* that causes minerals to be colored is the presence of **solid impurities** in the form of mechanical mixtures. The following discussion of these phenomena is based extensively on the publications of Loeffler and Burns (1976) and Nassau (1978, 1980).

CRYSTAL FIELD TRANSITIONS

Crystal field transitions are electronic transitions between partially filled 3*d* orbitals of the transition elements. These elements belong to the first transition series with electronic configurations of the general form: $1s^2\ 2s^2\ 2p^6\ 3s^2\ 3p^6\ 3d^{10-n}\ 4s^{1-2}$, with partially filled 3*d* orbitals (see Tables 3.5 and 3.6). Crystal field transitions are most common in minerals containing the transition elements: Ti, V, Cr, Mn, Fe, Co, Ni, and Cu. Of these elements, Fe is most abundant in the Earth's crust, and for that reason is a dominant cause of color in minerals. This is also related to the fact that Fe^{2+} readily substitutes for Mg^{2+}. Mg contributes no color to minerals but with the substitution of Fe, Mg-rich minerals become colored. The electrons in the partially filled 3*d* orbitals can be excited by quanta of energy from the visible spectrum; the electronic transitions absorb these wavelengths of light, thus, removing them from the spectrum. This absorption produces color. In contrast, ionic compounds made up of ions with a noble gas configuration are commonly colorless. This is because the energy gap between an occupied *p* orbital and the next available unoccupied orbital is considerably greater than the energy of visible light. Therefore, no specific wavelengths in the visible light range are absorbed, and the resulting mineral is colorless.

Crystal field theory describes electronic transitions between partially filled *d* orbitals. The negative charges of the coordinating anions (in a coordination

polyhedron) create an electrical field around the central transition metal ion. This is known as the *crystal field*, which has a specific symmetry and shape as a result of the number of anions, their distances from the cation, and their charges. The five 3*d* orbitals of a transition metal cation have the same energy in the absence of neighboring ions. They also have distinct probability distributions for the electrons (see Fig. 3.4*c*). Two of these orbitals, $d_{x^2-y^2}$ and d_{z^2} have their maximum electron densities along the *x*, *y*, and *z* coordinate axes, and are referred to as the e_g set. The other three orbitals, d_{xy}, d_{yz}, and d_{xz}, have their greatest electron density in directions between the coordinate axes. These are referred to as the t_{2g} set. When a transition element ion is surrounded by a spherically symmetrical cloud of negative charge, the electron orbitals all have the same energy. However, their overall energy levels will exceed those of the free ion because the spherical negative field will repel all electrons equally in these orbitals, which adds to their potential energy (Fig. 10.26, compare a and b).

When a transition metal ion is placed in a coordination site in a mineral, there will be a nonuniform crystal field interaction with the various *d* orbitals by the neighboring anions. If the coordination polyhedron about the cation is octahedral (Fig. 10.26c), the electrostatic repulsion between the anion orbitals and the centrally located cation orbitals raises the energy level of the $d_{x^2-y^2}$ and d_{z^2} orbitals (whose lobes of electron density are *along* the axes and directly toward the anions, see Fig. 3.4c) relative to the d_{xy}, d_{xz}, and d_{yz} orbitals (whose lobes of electron density are *between* the axes). This results in the six surrounding anions splitting the 3*d* energy levels of the central cation (Fig. 10.26d) and is known as **crystal field splitting**. In this illustration of crystal field splitting, an octahedral anion polyhedron is used. Minerals generally consist of several different coordination polyhedra (e.g., tetrahedra, octahedra) and in these differing polyhedra, the energy level splitting of the transition metals' 3*d* orbitals also will be different (see Dyar, 1997). These various energy levels cause different wavelengths of light to be absorbed and result in a range of mineral colors. In addition, any distortion of the coordination polyhedron about the central transition element will cause additional levels of splitting of 3*d* orbitals.

To illustrate this process, three well-known minerals and their gem varieties are considered: (1) peridot, a gem variety of olivine, with a yellow-green transmitted color (see Plate XI, no. 1); (2) chrysoberyl, with a characteristic pale yellow-green color (see Plate X, no. 8); and (3) almandine, a member of the garnet group, with a dark red transmitted color (see Plate XI, no. 2).

Peridot is gem-quality olivine, $(Mg, Fe)_2SiO_4$. The olivine crystal structure consists of independent SiO_4 tetrahedra linked to Mg^{2+} and Fe^{2+} in octahedral coordination (see Fig. 18.4). The Fe^{2+} ions are distributed among two slightly different octahedral sites (designated as *M1* and *M2*). If white light shines on a peridot and one measures the amount of light absorption as a function of wavelength, the optical spectrum shown in Fig. 10.27 is obtained. Wavelengths of light that correspond in energy exactly to the energy differences caused in the 3*d* orbitals by crystal field splitting, are

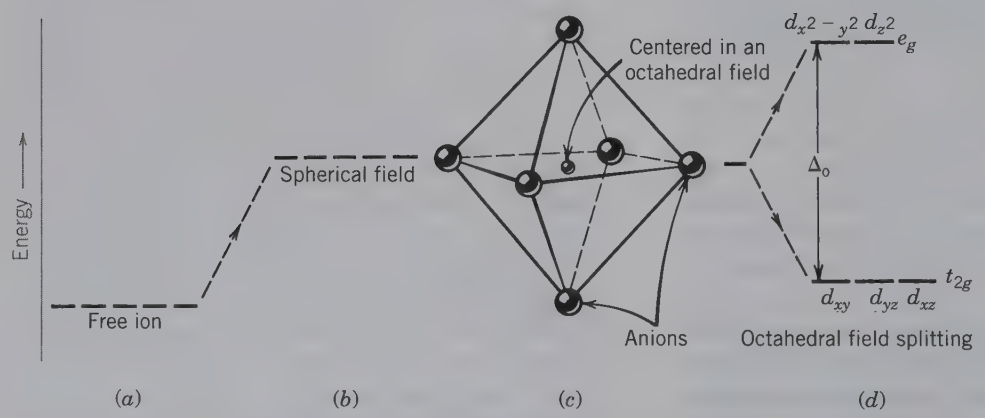

FIG. 10.26 Schematic representation of the energy levels of the five 3*d* orbitals in transition metals. (a) A free ion without surrounding neighbors, as in a gaseous state, is at the lowest relative energy. (b) The ion surrounded by a uniform and spherically distributed negative charge, at a higher energy state. (c) The transition metal ion surrounded by an octahedral field of negative charges (anions) experiences energy separation (or crystal field splitting, Δ_o) of the 3*d* orbitals, as shown in (d). The five 3*d* orbitals are separated into a higher-energy group (the e_g set) and a lower-energy group (the t_{2g} set). (Adapted from Loeffler, B. M., and R. G. Burns. 1976. Shedding light on the color of gems and minerals, *American Scientist* 64: 636–47.)

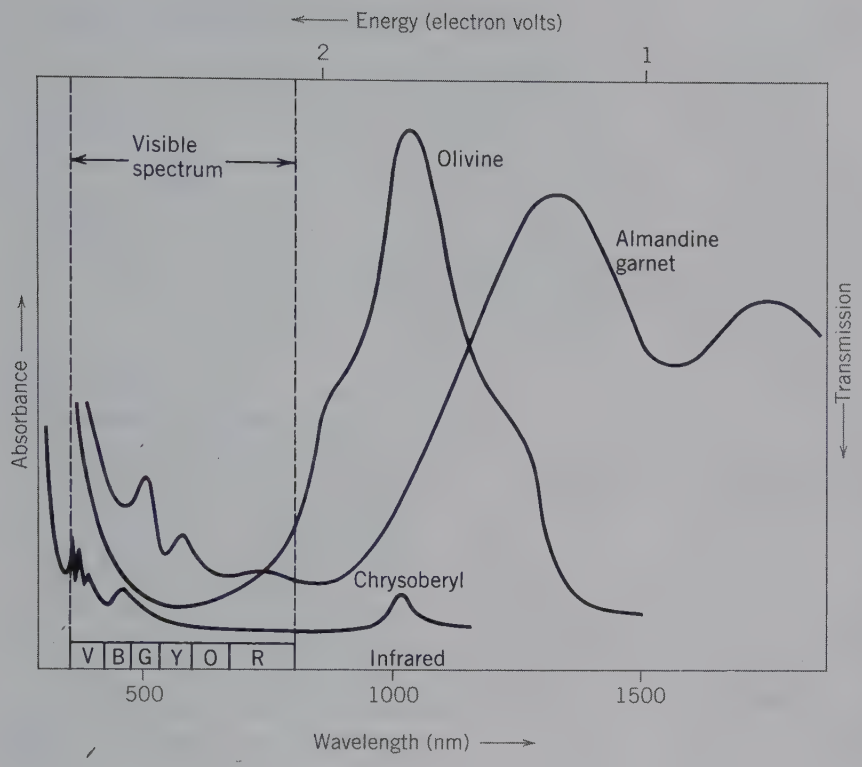

FIG. 10.27 Absorption spectra of two Fe^{2+}-bearing minerals, peridot, a gem variety of olivine, and almandine, a member of the garnet group. The spectrum of an Fe^{3+}-bearing mineral, chrysoberyl, is also shown. Those energies that are absorbed are removed from the visible light spectrum. (From Loeffler, B. M., and R. G. Burns. 1976, Shedding light on the color of gems and minerals, *American Scientist* 64: 636–47. Reprinted by permission of *American Scientist*, journal of Sigma Xi, The Scientific Research Society.)

absorbed. This absorbance in peridot takes place mainly in the infrared region and, consequently, has no impact on what we observe. There is some extension into the visible range. The absorption of the red and violet blue components of white light results in the yellow-green (transmitted) color of peridot. As such, Fe^{2+} in six-fold coordination produces a characteristic green transmitted color in minerals.

The oxidation state of the transition element also affects the transmitted color. In the mineral chrysoberyl, Al_2BeO_4, some Fe^{3+} may substitute for Al^{3+}. The crystal structure of chrysoberyl is very similar to that of peridot, with Al^{3+} (and small amounts of Fe^{3+}) in octahedral coordination. The optical absorption spectrum of chrysoberyl (Fig. 10.27) is, however, very different from that of peridot. Chrysoberyl absorbs only weakly in the violet and blue region of the spectrum, giving the characteristic pale yellow color of Fe^{3+}-containing chrysoberyl. The differences in the absorption spectra between peridot and chrysoberyl are the result of the differences in the electronic structures of Fe^{2+} and Fe^{3+}.

A change in coordination polyhedron about a transition element also affects the absorption spectrum and resultant transmitted color. In the structure of garnet (see Fig. 18.5), for example, independent SiO_4 tetrahedra are linked to trivalent cations in octahedral coordination and divalent cations in 8-fold coordination (distorted cubic coordination). In a common variety of garnet ($Fe_3Al_2Si_3O_{12}$, almandine), Fe^{2+} resides in the 8-fold site. The absorption spectrum of an almandine is given in Fig. 10.27. In this case, the main absorption peaks occur entirely outside the visible region, with lesser absorption in the region of violet-blue-green-yellow. The transmission color resulting from this is a deep red.

Two other minerals that occur as highly prized gems illustrate yet another factor contributing to color. These are (1) emerald, a grassy-green, Cr-containing variety of beryl, $Be_3Al_2Si_6O_{18}$ (see Plate IX, nos. 2 and 5), and (2) ruby, a blood-red, Cr-containing variety of corundum, Al_2O_3 (see Plate IX, nos. 4 and 7). In both minerals, small amounts of Cr^{3+} replace Al^{3+} in 6-fold sites (somewhat distorted octahedra). In beryl, a ring silicate (see Fig. 5.8), the six oxygens around Al^{3+} (or Cr^{3+}) are shared with SiO_4 and BeO_4 tetrahedra. In corundum, an oxide consisting of hexagonal closely packed layers of oxygen, Al^{3+} (or Cr^{3+}) occupies interstices between these layers. In the silicate structure of beryl there is a covalent component to the bonding, whereas in corundum the bonding is more ionic. This results in a weaker crystal field around the Cr^{3+} in beryl than in corundum, changing the energy (wavelength) required to excite electrons. These differences are clearly reflected in Fig. 10.28, which compares the absorption spectra of the two gems. Although the color of

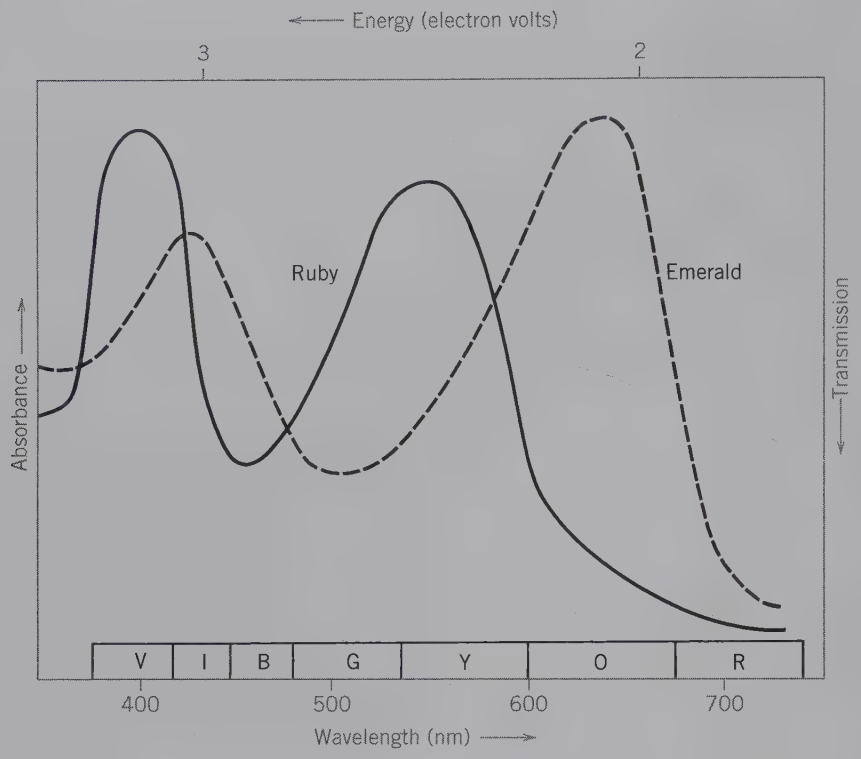

FIG. 10.28 Absorption spectra of emerald and ruby. In emerald, where the crystal field about Cr^{3+} is weaker, the absorption peaks are shifted to lower energy, producing transmission of green wavelengths. In ruby, the absorption peaks from Cr^{3+} are at higher energies, permitting transmission mainly in the blue and red regions. (From Loeffler, B. M., and R. G. Burns. 1976, Shedding light on the color of gems and minerals, *American Scientist* 64: 636–47. Reprinted by permission of *American Scientist*, journal of Sigma Xi, The Scientific Research Society.)

these two gems is caused by Cr^{3+}, their resulting colors are vastly different. In emerald, the absorption peaks are at a lower energy than in ruby. In emerald, the absorptions are in the violet and blue, in the yellow, and in the orange and red regions. This gives transmission in the green region resulting in the emerald-green color. In ruby, there is absorption in the violet, green, and yellow, with transmission in blue and red. The overall red color of ruby is further intensified by a characteristic red fluorescence. That is, not only does ruby absorb most wavelengths of white light such that red is transmitted, it also emits red light by fluorescence (see Chapter 2).

In summary, several factors that influence the transmitted color produced by crystal field interactions are:

1. the presence of a specific transition element,
2. its oxidation (valence) state, which determines the number of electrons in 3*d* orbitals,
3. the geometry of the site in which the transition metal resides, (octahedral, tetrahedral, etc.),
4. the strength of the crystal field (charges on anions, distortion of coordination polyhedra, etc.), and
5. the way in which the human eye interprets the pattern of transmitted wavelengths.

Table 10.1 is, in part, a summary of minerals whose color is the result of crystal field transitions.

Table 10.1 Examples of Common Minerals Whose Color Is Due to the Interaction of Transition Elements and Crystal Field Transitions*

Absorbing Ion	Mineral	Formula	Color
Cr^{3+}	Beryl (emerald)	$Be_3Al_2Si_6O_{18}$	Green
	Corundum (ruby)	Al_2O_3	Red
Mn^{3+}	Tourmaline (rubellite)	$Na(Li,Al)_3Al_6(BO_3)_3(Si_6O_{18})(OH)_4$	Pink
Mn^{2+}	Beryl (morganite)	$Be_3Al_2Si_6O_{18}$	Pink
	Spessartine garnet	$Mn_3Al_2(SiO_4)_3$	Yellow-orange
Fe^{3+}	Andradite garnet	$Ca_3Fe_2(SiO_4)_3$	Green
	Chrysoberyl	$BeAl_2O_4$	Yellow
Fe^{2+}	Olivine (peridot)	$(Mg,Fe)_2SiO_4$	Yellow-green
	Almandine garnet	$Fe_3Al_2(SiO_4)_3$	Dark red
Cu^{2+}	Turquoise	$CuAl_6(PO_4)_4(OH)_8{\cdot}4H_2O$	Light blue

*From Loeffler, B. M., and R. G. Burns. 1976. Shedding light on the color of gems and minerals, *American Scientist.* 64: 636–647. Many of the minerals listed in the table are illustrated in Plates IX through XII, Chapter 20.

MOLECULAR ORBITAL TRANSITIONS

Molecular orbital transitions, also known as charge-transfer transitions, occur in minerals when valence electrons transfer back and forth between ions in adjacent sites. This requires that each ion exists in more than one valence state. The electrons are contributed to **shared molecular orbitals** and as such are delocalized; that is, the valence electrons of a constituent atom are no longer in atomic orbitals centered on the atom. In such instances, crystal field theory does not apply, but instead *molecular orbital theory* best describes the observed spectra.

Examples of molecular orbital transitions are found in many minerals. Of these, $Fe^{2+} \rightarrow Fe^{3+}$ and $Fe^{2+} \rightarrow Ti^{4+}$ are the most common metal-metal charge transfer transitions. In the $Fe^{2+} \rightarrow Fe^{3+}$ charge transfer transition, an electron is transferred from Fe^{2+} (in site *A*, making it Fe^{3+}) to Fe^{3+} (in site *B*, making it Fe^{2+}) such that $Fe^{2+}_{(A)} + Fe^{3+}_{(B)} \rightleftharpoons Fe^{3+}_{(A)} + Fe^{2+}_{(B)}$. Energies of this reversible electron-hopping process generally correspond to wavelengths of visible light, and many minerals owe their intense blue color to such transitions. Examples are glaucophane (blue amphibole), crocidolite (blue fibrous amphibole), cordierite, kyanite (commonly blue), and sapphire (blue gem variety of corundum). The $Fe^{2+} \rightarrow Ti^{4+}$ charge transfer transition also is a large factor in the blue color of sapphire, Al_2O_3, which commonly contains small amounts of iron and titanium. Figure 10.29 shows the optical absorption spectrum of blue sapphire, in which the main absorbance peaks identified are due to $Fe^{2+} \rightarrow Ti^{4+}$, and $Fe^{2+} \rightarrow Fe^{3+}$ charge transfers. The main transmission of light is in the blue range of the visible spectrum (see Plate IX, nos. 3 and 6). Table 10.2 is, in part, a summary of some minerals whose color is the result of molecular orbital transitions.

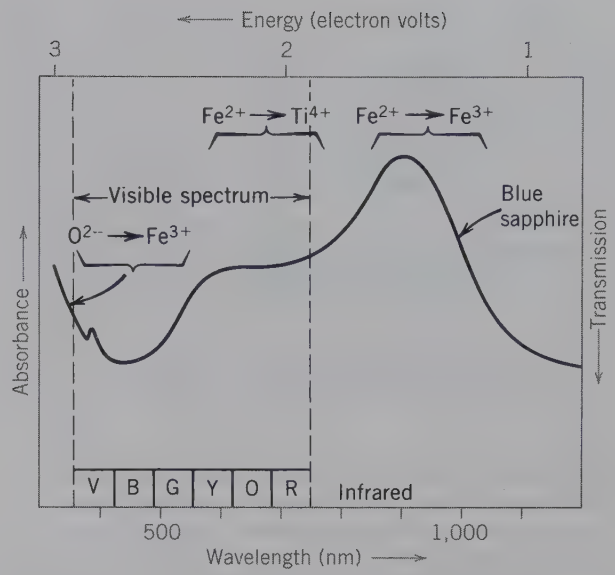

FIG. 10.29 Optical absorption spectrum of sapphire, blue gem corundum (see Plate IX, nos. 3 and 6, Chapter 20), and the molecular orbital transitions responsible for the absorption peaks ($Fe^{2+} \rightarrow Ti^{4+}$; $Fe^{2+} \rightarrow Fe^{3+}$; and $O^{2-} \rightarrow Fe^{3+}$ at the edge of the ultraviolet region). The only transmission in this spectrum is in the range of blue in the visible light spectrum. (From Loeffler, B. M., and R. G. Burns. 1976, Shedding light on the color of gems and minerals, *American Scientist* 64: 636–47. Reprinted by permission of *American Scientist*, journal of Sigma Xi, The Scientific Research Society.)

COLOR CENTERS

Color also can be caused by structural defects. This can be an excess electron that is unattached to any single atom and that is trapped at some structural defect, such as a missing ion or an interstitial impurity. A "hole," the absence of an electron, can have the same effect. These types of color-producing defects are known as **color centers**, or *F* centers (from the German word *Farbe* meaning color). The coloring mechanism in purple fluorite, CaF_2, is known to be the result of Frenkel defects (see Fig. 10.8b) in the fluorite structure. Such defects, in the network of F^- ions, are the result of (1) high-energy radiation (e.g., X-rays) that displaced the F^- from its usual position to another position in the structure, (2) the growth of fluorite in a chemical environment with an excess of calcium, or (3) removal of some F from the crystal by the

Table 10.2 Examples of Some Common Minerals Whose Color Is the Result of Charge Transfer Transitions, Described by Molecular Orbital Theory

Ion Pair	Mineral	Formula	Color
$Fe^{2+} \rightarrow Fe^{3+}$	Beryl (aquamarine)	$Be_3Al_2Si_6O_{18}$	Blue-yellow
$Fe^{2+} \rightarrow Fe^{3+}$	Cordierite	$(Mg,Fe)_2Al_4Si_5O_{18}{\cdot}nH_2O$	Blue
$Fe^{2+} \rightarrow Ti^{4+}$	Corundum (sapphire)	Al_2O_3	Blue
$Fe^{2+} \rightarrow Ti^{4+}$	Kyanite	Al_2SiO_5	Blue
$O^{2-} \rightarrow Cr^{6+}$	Crocoite	$PbCrO_4$	Orange
$O^{2-} \rightarrow Fe^{3+}$	Beryl (heliodore)	$Be_3Al_2Si_6O_{18}$	Yellow

*From Loeffler, B. M., and R. G. Burns. 1976. Shedding light on the color of gems and minerals, *American Scientist*. 64: 636–647.

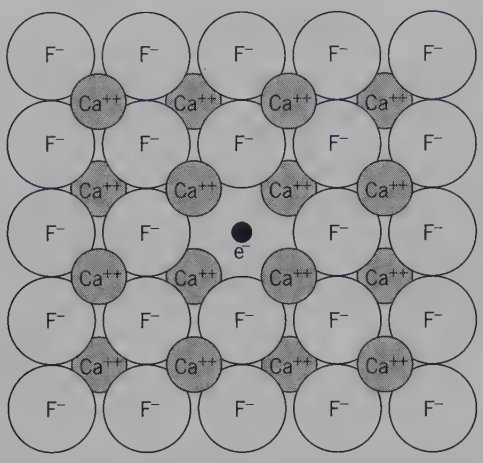

FIG. 10.30 Schematic illustration of the structure of fluorite, CaF_2, in which an electron fills a vacancy created by a fluorine ion that was removed. Here, a color center is the result of an electron taking the place of the dislodged ion. (Margaret C. Gladback, Estate of Mary E. and Dan Todd.)

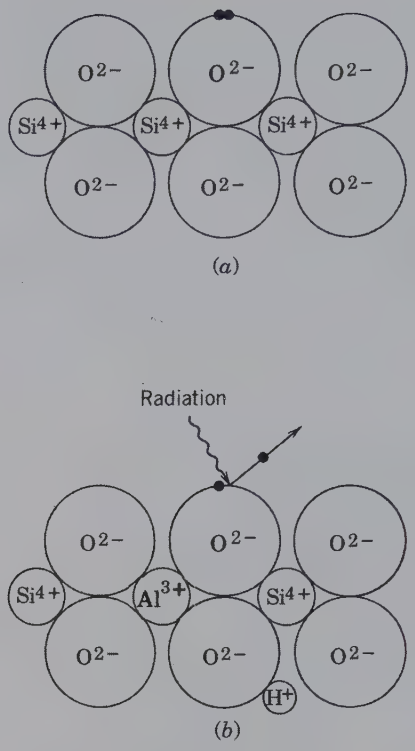

FIG. 10.31 Schematic illustration of the quartz structure. (a) The normal structure of pure SiO_2. (b) The structure with some ionic substitution of Al^{3+} for Si^{4+}, coupled with substitution of H^+ into the structure, in order to maintain electrical neutrality. Radiation ejects one of a pair of electrons from an O^{2-} and leaves a "hole" color center of smoky quartz. (After Nassau, K. 1978. The origins of color in minerals, *American Mineralogist* 63: 219–29.)

application of an electrical field. Because the overall structure must remain neutral, an electron usually occupies the empty position to produce an "*electron color center*," as in Fig. 10.30. Such an electron is not bound in place by a central nucleus, but by the electrical field (crystal field) of all of the surrounding ions. Within this field, it can occupy a ground state and various excited states similar to those of the transition elements described previously. The movement of electrons among these states can cause color and optical fluorescence. The original crystal structure of fluorite, without defects, can be restored by heating, thereby causing the color to fade.

The smoky color of some quartz crystals is attributed to the occurrence of a "*hole color center*." In such quartz, some Al^{3+} substitutes for Si^{4+} and this substitution is coupled with some interstitial Na^+ or H^+ ions in order to maintain electrical neutrality. When this type of quartz is exposed to an intense X-ray or gamma-ray beam for a few minutes, or when it has been exposed to low levels of radiation over geological periods, "hole color centers" are produced. The radiation expels one electron from a pair of electrons in an oxygen atom adjacent to an Al^{3+} ion, thereby leaving a single, unpaired electron in the orbital (illustrated schematically in Fig. 10.31). The missing electron is called a "hole," and the remaining unpaired electron has a set of excited states much like those of an excess electron, as described previously. Table 10.3 lists some mineral examples in which color is due to color centers.

PHYSICAL PROCESSES AS A CAUSE OF COLOR

An additional coloring agent in minerals is the **mechanical admixture** of impurities. These impurities give a variety of colors to otherwise colorless minerals. Quartz may be green because of the presence of finely dispersed chlorite; calcite may be black because it is colored by manganese oxide or graphite. Hematite is the most common pigmenting impurity, and it imparts its red color to many minerals including some feldspar,

Table 10.3 Examples of Minerals in Which the Coloration Is Due to Color Centers*

Mineral	Color
Amethyst, fluorite	Purple
Smoky quartz	Brown to black
Irradiated diamond	Green, yellow, brown, blue, pink
Natural and irradiated topaz	Blue
Halite	Blue and yellow

*From Nassau, K. 1978. The origins of color in minerals. *American Mineralogist.* 63: 219–229.

calcite, and the fine-grained variety of red quartz (jasper). Finely disseminated copper transforms white feldspar into a "sunstone" with brilliant copper color. Because these impurities are not found in all specimens of a specific mineral, the property of color cannot be used as a diagnostic tool.

ORIGIN OF MAGNETIC PROPERTIES

Some minerals behave like magnets, whereas most do not. Magnetic properties are the result of atomic properties that are specific to a number of elements. In Chapter 3, the three quantum numbers needed to specify the position of an electron in space were discussed. The *spin quantum number*, s, defines the spin of the electron (see Fig. 3.5), and is important to the development of magnetic properties. Because an electron can spin in only two directions, it has only two values, $\frac{1}{2}$ and $-\frac{1}{2}$. A spinning electron behaves as a small magnet and will produce a magnetic field while moving around its orbit (see Fig. 3.5). This is analogous to the production of a magnetic field by an electrical current moving through a coiled wire.

The spin of the electron is mainly responsible for the magnetic properties of atoms and molecules. The spinning electron can be regarded as a minute magnet (or *magnetic dipole*) with a **magnetic moment** that is defined as a Bohr magneton, $\mu_b = 9.27 \times 10^{-24}$ Am^2, which is a product of the electron charge (in units of amperes, A) and the area about which the electron spins (in units of m^2). Because two electrons in the same orbital must have opposing spins, with one having an up "↑" and the other a down "↓" orientation of its pole, this produces a zero net-magnetic moment. Such materials are known as **diamagnetic** because they experience no attraction for a magnet. They are slightly repelled by a magnetic field, which is a result of the behavior of the electron cloud of the atom and not of the electron spin. In these substances, there are the same number of electrons of each spin (↑ ↓), which cancels their magnetic effects. Many common minerals have no magnetic response; they are diamagnetic. They are composed of elements with core electron configurations of the inert gases, or with completely filled d orbitals (see Table 3.5). A few examples of the many common diamagnetic minerals are calcite, $CaCO_3$; albite, $NaAlSi_3O_8$; quartz, SiO_2; and apatite, $Ca_5(PO_4)_3(F, Cl, OH)$.

The most important elements that produce magnetic moments are those with unshared electrons (not involved in bonding) in $3d$ orbitals of the first transition series, including Ti, V, Cr, Mn, Fe, Co, Ni, and Cu ($Z = 22 - 29$; see periodic table at the back of this text or Table 3.5). Some of these elements, (Fe, Mn, Ti, and Cr), are very common mineral consitutents. The magnetic moments of these transition elements are the result of the spin of single, unpaired electrons and are proportional to the number of such electrons. The distribution of electrons in the five $3d$ orbitals is summarized in *Hund's rule: Electrons entering a subshell with more than one orbital will be distributed over the available orbitals with their spins in the same direction.* This means that in going from top to bottom in Table 10.4, electrons are first added to each orbital with their spins in the same direction and then doubled up until all orbitals are filled. This buildup continues until all electrons are paired, in all five $3d$ orbitals in Zn. The table shows that Fe^{3+} and Mn^{2+}, each with five unpaired electrons, are among the most magnetic ions.

Table 10.4 Transition Elements (Z 21 Through Z 30), Their Common Ions, Number of $3d$ Electrons, Electron Spin Directions, and Magnetic Moment (Expressed in Terms of Bohr Magnetons, μ_β)

Elements	Ions	Spin Directions and Number of $3d$ Electrons for the Ions						Magnetic Moment
Sc	Ti^{3+}, V^{4+}	↑					1	$1\mu_\beta$
Ti	Ti^{2+}, V^{3+}	↑	↑				2	$2\mu_\beta$
V	V^{2+}, Cr^{3+}, Mn^{4+}	↑	↑	↑			3	$3\mu_\beta$
Cr	Cr^{2+}, Mn^{3+}	↑	↑	↑	↑		4	$4\mu_\beta$
Mn	Mn^{2+}, Fe^{3+}	↑	↑	↑	↑	↑	5	$5\mu_\beta$
Fe	Fe^{2+}, Co^{3+}	↑↓	↑	↑	↑	↑	6	$4\mu_\beta$
Co	Co^{2+}	↑↓	↑↓	↑	↑	↑	7	$3\mu_\beta$
Ni	Ni^{2+}	↑↓	↑↓	↑↓	↑	↑	8	$2\mu_\beta$
Cu	Cu^{2+}	↑↓	↑↓	↑↓	↑↓	↑	9	$1\mu_\beta$
Zn	Zn^{2+}, Cu^+	↑↓	↑↓	↑↓	↑↓	↑↓	10	0

Although individual ions may be classified as more or less magnetic (as in Table 10.4), the question remains as to how such ions interact in crystal structures. If a structure has a *random arrangement of magnetic dipoles* (caused by specific constituent cations with unpaired spins, such as are listed in Table 10.4), it is said to be **paramagnetic**. When such a structure is placed into a magnetic field, the minute dipoles tend to align themselves with the external magnetic field. Thermal motion inside the structure, however, tends to randomize some of the dipole alignments. This results in only a small fraction of dipoles being aligned with the external magnetic field at any particular instant. As such, a paramagnetic material is drawn only weakly to an external magnetic field (shows low magnetic susceptibility). In addition, this imposed magnetization is not permanent. Examples of two common minerals that show paramagnetic behavior are olivine, $(Mg,Fe)_2SiO_4$, and augite, $(Ca,Na)(Mg,Fe,Al)(Si,Al)_2O_6$. Because of their different magnetic susceptibilities, minerals can be separated from each other by an electromagnet (as discussed in Chapter 2).

Another property related to paramagnetism is called **ferromagnetism**, which is observed in metallic iron. In a paramagnetic material, the magnetic dipoles are randomly oriented, but in a ferromagnetic substance, these become aligned because of "exchange forces" that result from overlap of the orbitals of nearest neighbor atoms or ions (for further discussion of the exchange forces, see O'Reilly, 1984). In a substance such as metallic iron, *domains* exist containing large numbers of paramagnetic atoms with their dipole moments well aligned. Ordinarily these domains are randomly oriented (Fig. 10.32a) so that their net magnetic effect is zero. When such a material is placed in a magnetic field, the domains become aligned with the external field (Fig. 10.32b), and it responds with strong magnetic attraction. This interaction is much stronger than normally experienced in paramagnetic materials. When the external magnetic field is removed from a paramagnetic substance, the magnetic domains randomize and no permanent magnetism remains. However, in a ferromagnetic material, the domains tend to remain in the orientation imposed by the external magnetic field even in the absence of the field. For example, a nail can be magnetized simply by running a permanent magnet over it; this process aligns ("poles") the magnetic domains in the nail fairly permanently. When a ferromagnetic material in which permanent magnetism has been induced is heated, the parallelism of the magnetic field is completely lost at the *Curie temperature*, above which it behaves paramagnetically. The Curie temperature for metallic iron is 770°C.

Another type of magnetism is known as **ferrimagnetism**, in which the ionic spin moments are antiparallel, instead of parallel as in ferromagnetism. In ferrimagnetic materials, the antiparallel spin moments are unequal, and as such there are permanent magnetic domains (Fig. 10.33a). Examples of ferrimagnetic minerals are members of the magnetite-ulvöspinel series,

FIG. 10.32 Magnetic domains in a ferromagnetic solid. (a) Random domains when unmagnetized. (b) Parallel alignment of domains as a result of an external magnetic field.

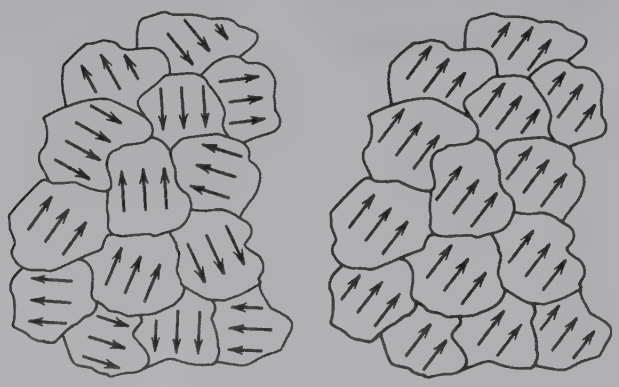

(a) (b)

FIG. 10.33 (a) Schematic illustration of the spin alignments of dipoles in ferrimagnetic and ferromagnetic materials. In ferrimagnetic solids, the ionic spins are antiparallel and their magnitudes are unequal. In ferromagnetic solids, all spins are parallel and aligned in the same direction. (b) Schematic representation of the spin directions in the tetrahedral and octahedral sites of magnetite, Fe_3O_4. A net magnetic moment is due to the noncancellation of the dipole moments of Fe^{2+} ions.

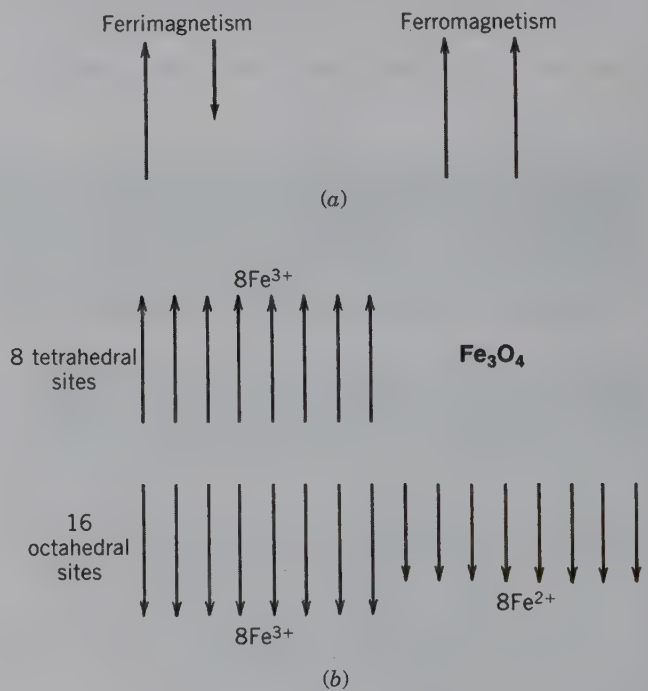

Fe_3O_4-Fe_2TiO_4 (see spinel group, page 372); hematite-ilmenite solid solution members, Fe_2O_3-$FeTiO_3$; and pyrrhotite, $Fe_{1-x}S$.

The distribution of magnetic dipoles in a ferrimagnetic material can be illustrated with reference to magnetite, a member of the spinel series. The formula of magnetite, Fe_3O_4, can be rewritten as $Fe^{3+}[Fe^{2+}Fe^{3+}]O_4$ in terms of a general XY_2O_4 formula for the spinel group. The spinel structure is based on cubic closest packing of oxygens with the cations in tetrahedral and octahedral interstices. The X cations occupy $\frac{1}{8}$ of the 64 (= 8) tetrahedral sites per unit cell of spinel and the Y cations occupy $\frac{1}{2}$ of the 32 (= 16) octahedral sites (per unit cell). The Fe^{3+} ions are distributed in two different lattice sites, but with opposing magnetic spin directions (Fig. 10.33b). The Fe^{2+} ions (with lesser magnetic moment; Table 10.4) are responsible for net unpaired spin and, thus, for the permanent magnetic domains in magnetite (Fig. 10.33b). This net magnetization is considerably less than if the magnetic moments of all the cations were parallel, as in magnetized native iron, which is ferromagnetic. The Curie temperature of magnetite is 580°C, above which the magnetic ordering completely disappears.

The permanent magnetism of *ferrimagnetic* minerals in various rock types allows for the study of the ancient geomagnetic field of the Earth, known as *paleomagnetism*. The study of the natural remanent magnetization of rocks can yield a record of the Earth's magnetic field through time. For example, as magnetite crystals in igneous rocks cool through the Curie temperature, the direction of the Earth's magnetic field is recorded in the orientation of the magnetic domains. This feature can be used to help reconstruct tectonic plate motion. *Lodestone*, a naturally occurring magnet of magnetite composition, is a ferrimagnetic substance in which all the net magnetic moments are strongly aligned ("poled"). The natural magnetism of lodestone is attributed to its having cooled from a melt (as part of an igneous rock) while under the influence of the Earth's magnetic field.

MINERALOIDS (NONCRYSTALLINE MINERALS)

The definition of a mineral includes ". . . *has a highly ordered atomic arrangement.*" There are, however, a number of noncrystalline, natural solids classed as amorphous. Figure 10.34a is a schematic illustration, on an atomic scale, of the amorphous state.

Amorphous materials include gel minerals and glasses. Gel minerals (mineraloids) are usually formed under conditions of low temperature and low pressure and commonly originate during weathering processes. They characteristically occur in mammillary, botryoidal, and stalactitic masses. The ability of amorphous materials to absorb disparate types of ionic species accounts for their typically wide variations in chemical composition. Common amorphous minerals are limonite, $FeO{\cdot}OH{\cdot}nH_2O$, and allophane, a hydrous aluminum silicate.

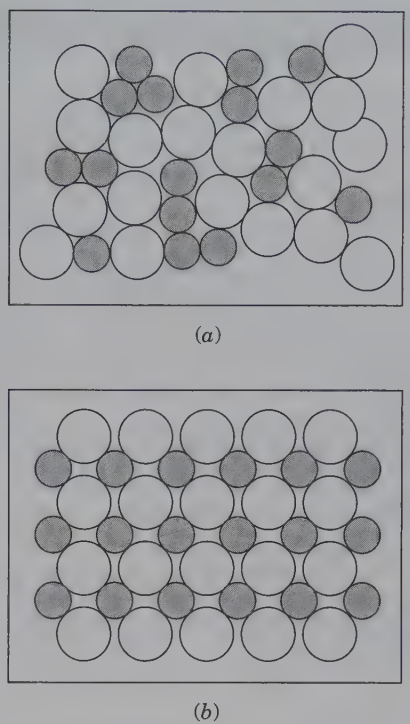

(*a*)

(*b*)

FIG. 10.34 Schematic illustration of the atomic arrangement in an amorphous alloy (a) and a crystalline alloy (b).

The structure of a silica-rich glass, such as volcanic glass, is said to have *short-range order* but lacks *long-range order* (Fig. 10.34b). The Si^{4+} and Al^{3+} ions in such a glass occur in tetrahedral coordination, as they do in crystalline compounds. In glasses, however, the tetrahedral coordination polyhedra do not repeat their pattern over more than a few angstrom units. In other words, *long-range order* characteristic of a periodic structure is absent, although *short-range order* (as shown by the presence of coordination tetrahedra) is present.

A well-known example of a partly amorphous material is opal. Its chemical composition can be represented as $SiO_2{\cdot}nH_2O$ with an average range of H_2O content from 4-to-9 weight percent. Opal was originally considered to be completely without internal structure; however, careful electron beam studies show that it contains an ordered arrangement of very small SiO_2 spheres (see Fig. 2.7).

REFERENCES AND FURTHER READING

Banerjee, S. K. 1991. Magnetic properties of Fe-Ti oxides. In *Oxide minerals: Petrologic and magnetic significance. Reviews in Mineralogy* 25. Mineralogical Society of America, Washington, D.C.

Buerger, M. J. 1945. The genesis of twin crystals. *American Mineralogist* 30: 469–82.

Burns, R.G. 1993. *Mineralogical applications of crystal field theory.* 2nd ed. Cambridge University Press, London.

Dyar, M.D. 1997. Color in minerals. In *Teaching mineralogy*, J. Brady, D. Mogk, D. Perkins, eds. Mineralogical Society of America, Washington D.C.

Fritsch, E., and G. Rossman. 1987. An update on color in gems. Part I. Introduction and colors caused by dispersed metal ions. *Gems and Gemology* 23:126–139.

Fritsch, E., and G. Rossman. 1987. An update on color in gems. Part II. Color casued by charge transfers and color centers. *Gems and Gemology* 24:3–15.

Goodman, C. H. L. 1973. *Crystal growth. Theories and techniques.* Plenum Press, New York.

Keffer, F. 1967. The magnetic properties of materials. *Scientific American* 217: 222–38.

Loeffler, B. M., and R. G. Burns. 1976. Shedding light on the color of gems and minerals. *American Scientist* 64: 636–47.

Nassau, K. 1978. The origins of color in minerals. *American Mineralogist* 63: 219–29.

———. 1980. *Gems made by man.* Chilton Book Co., Radnor, Pennsylvania. (Specifically, see Chapter 26, "The origin of color in gemstones.").

———. 1980. The causes of color. *Scientific American* 243: 124–56.

———. 1983. *The physics and chemistry of color: The fifteen causes of color.* J. Wiley, New York.

———. 1987. The fifteen causes of color: The physics and chemistry of color. *Color Research and Application*, 12:4–26.

O'Reilly, W. 1984. *Rock and mineral magnetism.* Blackie, London, England, distributed by Chapman and Hall, New York.

Putnis, A. 1992. *Introduction to mineral sciences.* Cambridge University Press, New York.

Rossman, G. 1981. Color in gems: The new technologies. *Gems and Gemology*, 17:60–71.

———. 1988. Optical Spectroscopy. In *Spectroscopic methods in mineralogy and Geology. Reviews in Mineralogy*, 18: 207–254. Mineralogical Society of America, Washington D.C.

Wood, D. L., and K. Nassau. 1968. The characterization of beryl and emerald by visible and infrared absorption spectroscopy. *American Mineralogist* 54: 777–801.

CHAPTER 11

Mineral Stability and Phase Diagrams

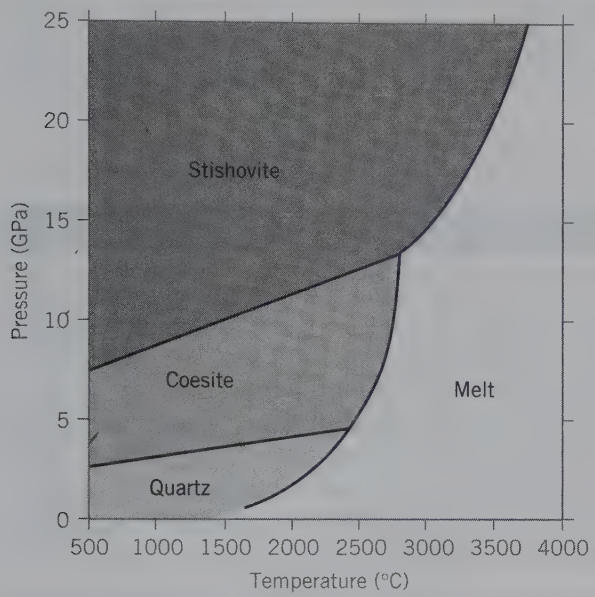

A stability diagram for various forms of SiO_2 in terms of temperature and pressure. Both scales extend to very high numbers, and this is generally considered a high-pressure phase diagram. Coesite and stishovite are high-pressure polymorphic forms of SiO_2, with stishovite having the densest structure. In stishovite Si is in 6-coordination (octahedral) instead of 4-coordination (tetrahedral), which is the case for all silicates that occur in the Earth's crust. The horizontal axis is scaled in terms of Gigapascals (Gpa) where 1 Gpa = 10 kilobars. A kilobar = 1,000 bars; 1 atmosphere = 1.01325 bars. (From Navrotsky, A. 1998. Thermodynamics of high-pressure phases. Ultra high-pressure mineralogy, *R.J. Hemley ed., Mineralogical Society of America,* Reviews in Mineralogy *37, 319–341.)*

Minerals originate over a wide array of externally imposed conditions, which include temperature, pressure, and the composition of the host material. Even in an environment with a limited number of chemical constituents, these chemical elements can unite to produce a multitude of minerals. How does one determine which mineral grows and persists under a specific set of external conditions? These factors require an introduction to the concepts of energy, equilibrium, and stability as well as the methods and diagrams that depict these relationships.

This chapter introduces *mineral reactions* and assesses some of these reactions in terms of quantitative evaluations of temperature and pressure, as shown in mineral *stability* (or *phase*) *diagrams*. This, by necessity, leads to a brief glimpse of the important and extensive subject of thermodynamics. Thermodynamics provides the underlying foundation for the determination of the stability of a system and the parameters required to depict these stability relations in graphical form. Such diagrams are used widely in the field of mineral science.

STABILITY, ACTIVATION ENERGY, AND EQUILIBRIUM

The concept of **stability** in a chemical system is related to the **energy** of the system (see discussion of Gibbs free energy later in this chapter). The low-energy state is the most stable state when one state is compared to other states in the same system. Stability can be intuitively appreciated by considering mechanical blocks in different positions on a surface (Fig. 11.1a). The block in Fig. 11.1a is barely stable as it stands on the beveled bottom edge. This position is the least stable of the three block positions because a slight nudge to the block in (a) will cause it to change to either position (b) or (c). This condition (in a) is referred to as being **metastable** with respect to the other two blocks (in b and c). It will not simply fall into another position unless some energy (a nudge) is added. A fundamental parameter of its stability is the location of its center of gravity (g); the block in (a) has the highest g position above the resting surface. The block in (b) is in a more stable condition because a reasonably large displacement (nudge) is required to change it to the position of the block in (c). It, too, is metastable with respect to (c). If only a small disturbance is applied to the block in (b), it will remain in the same orientation. Here, the center

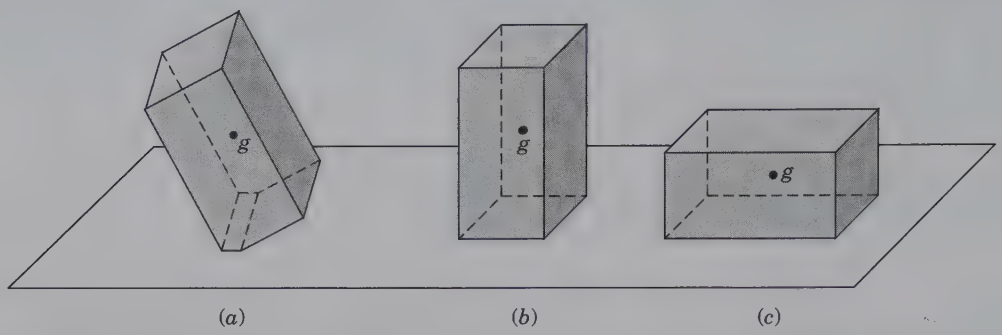

FIG. 11.1 Illustration of various degrees of stability for the same block in different orientations. (a) is less stable than (b) or (c) , or *metastable* with respect to (b) and (c). The most stable position is (c) with the lowest center of gravity (g).

of gravity (g) of block (b) is lower than that in (a) but considerably higher than that in (c). In (c) the orientation of the block is said to be **stable** because even after a reasonably large disturbance (or displacement), it will return to the orientation in which it is shown. The center of gravity (g) is now at the lowest position of the three orientations. Consequently, it represents the lowest (gravitational) energy configuration of the blocks, and it is the most *stable* of the three blocks.

The physical displacements (or disturbances) applied to the various blocks can be expressed in terms of energy. The amount of energy necessary to change the position of block (a) or (b) to that of block (c) is the **activation energy**. In a chemical system, the *activation energy* is the energy necessary to cause a chemical reaction to occur. For any process to proceed spontaneously requires that the system change from a higher- to a lower-energy configuration. In applying the concept of stability to minerals, one is generally concerned with differences in stability (i.e., differences in energy values) and not the absolute energy values.

The concept of *stability* is also related to time. If there is no change with time, the system is said to be at a *steady state* and the materials are said to be in **equilibrium**. In experimental studies, the experimentalist will conclude that the phases under investigation are in equilibrium when no further reaction takes place between them during a certain time interval. This may range from a few hours to several months, or even years, depending on the speed or sluggishness of the reactions studied and on the patience of the investigator. However, in rocks, where the constituent minerals have coexisted since their formation, perhaps several million years ago, one cannot always conclude unambiguously whether the mineral constituents are in equilibrium with each other or not. The minerals may be *metastable*, but there has been insufficient energy added to the system to drive them over the activation energy barrier to reach a more stable state.

INTRODUCTORY THERMODYNAMICS

To determine the stability, or energy, of a mineral (or an assemblage of minerals) is more complicated than measuring the gravitational energy associated with a mechanical block. **Thermodynamics** is the scientific method that allows the quantitative assessments of stability and phase equilibria. Only a very cursory introduction to thermodynamics is presented here, sufficient to aid in understanding the mineral stability diagrams that follow.

A fundamental and universal observation is that *all organizations of matter drive toward a minimal energy state* (or arrangement). Minerals and rocks tend toward the lowest energy state, which is the most stable state for their constituents.

The *first law of thermodynamics* states "the internal energy (E) of an isolated system is constant." A **system** is defined as any part of the universe being considered (e.g., it may be a hand specimen of a specific rock type, a specific mineral assemblage, or a specific chemical mixture ready for an experimental study). In a **closed system**, there is no addition or subtraction of material so that the mass remains constant, but there can be a loss or gain of energy. The change in *internal energy* (the differential of E, dE) of the system is the difference between heat (a form of energy, defined as Q) added to the system (expressed as dQ) and work (another form of energy, defined as W) done by the system (expressed as dW). The first law can be stated as:

$$dE = dQ - dW$$

Because work (W) = force × distance, and because force = pressure (P) × surface area, $W = P \times$ surface area × distance, or $W =$ pressure (P) × volume (V).

At constant pressure, and in the absence of other types of work (e.g., electrical, etc.), this results in $dW = PdV$. When this is substituted into the above equation, it yields the most familiar form of the first law of thermodynamics as:

$$dE = dQ - PdV.$$

The effect of this equation, in terms of heat and pressure, on a mineral can be qualitatively assessed. When heat energy is added to a mineral, the increase in internal energy (dE) of the mineral is proportional to, but less than, the heat added because part of the added energy is transformed into the work of thermal expansion of the mineral.

The *second law of thermodynamics* relates a change in thermal energy of a system (at constant pressure, P, and constant temperature, T) to a change in the degree of order (or disorder) in that system. *Entropy* (S) is a quantity that represents the degree of disorder or randomness in a system. The state of greatest *order* in a crystalline material is that at the lowest temperature. With increasing temperature, *disorder* of atoms in the structure becomes more prevalent. Relating this to entropy, *a rigorously ordered structure has lower entropy than a disordered structure*. For example, when heat is added to ice, some of the heat (energy) will convert ice to water. Water, because of its liquid state, is much less ordered than ice and will have a higher entropy. As a consequence of the second law,

$$\frac{dQ}{T} = dS$$

where dQ is the absorption of a quantity of heat. Because entropy is related to the amount of disorder (or randomness) in a system, there will be increases in entropy in the following reactions: solid → gas; solid → liquid; and liquid → vapor.

The *third law of thermodynamics* states that "at absolute zero (0 Kelvin, which is equivalent to −273.15°C), a crystalline structure approaches perfect order, and the entropy of such a perfect crystal is zero." This leads to the introduction of another important thermodynamic function, **Gibbs free energy, G,** as:

$$G = E + PV - TS$$

where E = internal energy, P = pressure, V = volume, T = temperature, and S = entropy. The Gibbs free energy term expresses the energy in excess of the internal energy; this is the excess energy needed to drive a chemical reaction. Units of energy are in joules or calories (where 1 calorie = 4.184 joules). When the Gibbs free energy equation is differentiated and combined with the equations for the first and second laws, the following equation results:

$$dG = VdP - SdT$$

This formulation of the Gibbs free energy expresses the stability of a chemical reaction. Using the above equation, the change in Gibbs free energy of a chemical reaction (dG_{rx}) can be formulated on the basis of the total free energies of the product (dG_p) and of the reactant (dG_r) minerals:

$$\Delta G_{rx} = \Delta G_p - \Delta G_r$$

If $\Delta G_{rx} < 0$ for a given temperature and pressure, the product assemblage is more stable and the reaction can proceed spontaneously. If $\Delta G_{rx} > 0$, the reaction direction is reversed, with the reactants more stable.

For a system in equilibrium, at constant P and T, the Gibbs free energy (G) is a minimum. At equilibrium, the Gibbs free energies of the reactant (r) and product (p) are equal, that is $G_r = G_p$, or $G_p - G_r = 0$ and $dG = 0$.

The above equation of Gibbs free energy can be differentiated with respect to T, at constant P, or with respect to P, at constant T. This results in two important relations that express the change in free energy (dG) with respect to pressure and temperature. These are:

$$\left(\frac{\partial G}{\partial P}\right)_T = V \qquad \text{where } V = \text{volume}$$

and

$$\left(\frac{\partial G}{\partial T}\right)_P = -S \qquad \text{where } S = \text{entropy}$$

The first of these expressions tells us that dense phases (i.e., those with small volumes) are favored at high pressures, and the second shows that high entropy states (with greater atomic disorder) are favored at high temperatures.

Basic aspects of the Gibbs free energy equation can be shown graphically as in Fig. 11.2. The equations given previously state that dG, a change in Gibbs free energy, is a function of only P (stated as dP) and of T (stated as dT). Because the three variables G, P, and T are interrelated, the function G can be represented graphically in terms of two variables, P and T. This is shown in Fig. 11.2a for two minerals (or phases) marked A and B. Each phase has its distinct G surface. Where the two G surfaces intersect, the two minerals (or phases) are in equilibrium because the condition of $G_A = G_B$ or $dG = 0$ is satisfied. Two cross-sections through the three-dimensional picture in a, show how mineral or phase stability is a function of T or P. Figure 11.2b shows a crossover of the entropy of B with respect to A (as a function of G and T at constant P). Because this diagram is at constant P, it is also known as an *isobaric* section. Figure 11.2c shows a crossover in the

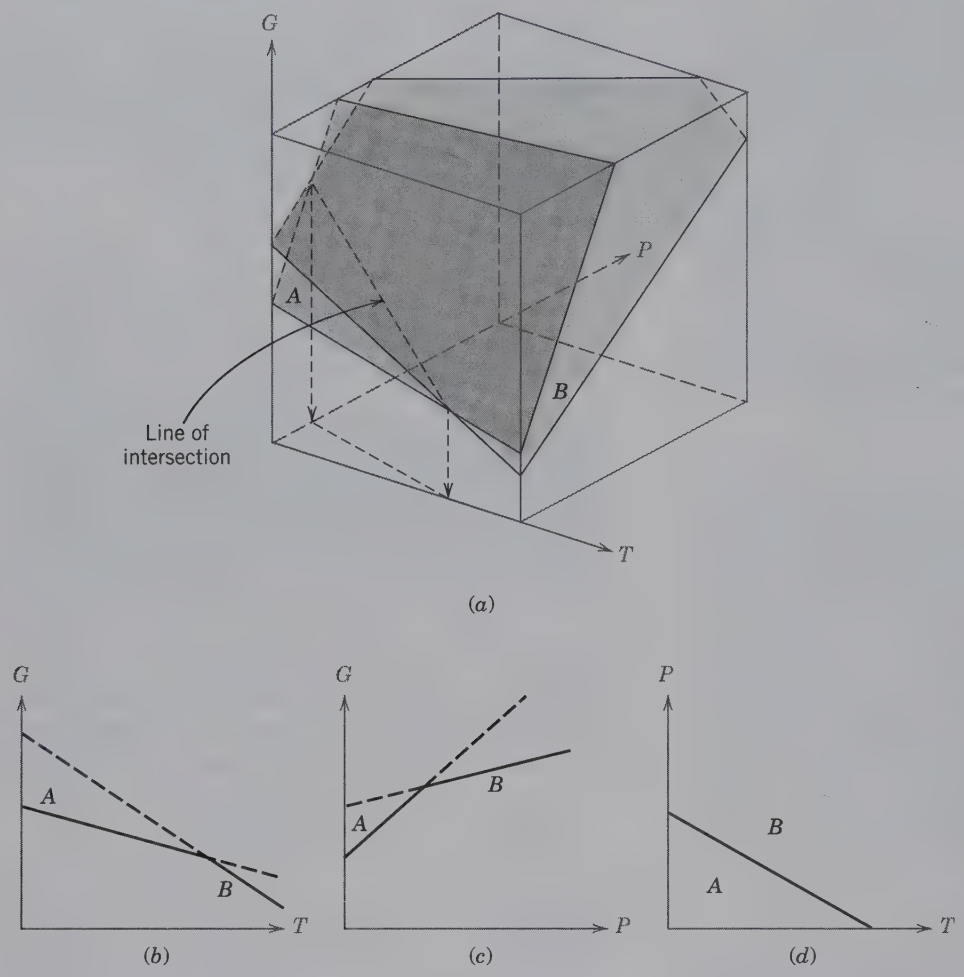

FIG. 11.2 (a) Three-dimensional representation of *G–T–P* space, with free energy surfaces for two minerals, *A* and *B*. Where the two surfaces intersect (along the line of intersection), the free energies of the two minerals are equal. Two sections through this space are shown: (b) a *G–T* section and (c) a *G–P* section. (d) is a projection of the line of intersection from (a) onto the *P–T* plane.

volume of *B* with respect to that of *A* (as a function of *G* and *P* at constant *T*). Because this diagram is at constant temperature, it is also known as an *isothermal* section. Mineral stability fields are more commonly shown on *P–T* diagrams, as in Fig. 11.2d. The standard *P–T* diagram is obtained from Fig. 11.2a by projection of the equilibrium curve (line of intersection), along which phases *A* and *B* coexist, onto the basal plane of *P–T*.

Figure 11.3, for the system H_2O, illustrates the *P–T* regions in which the specifically labeled state (e.g., ice, liquid, or vapor), has a free energy that is different from any of the other possible states. Along the curves (phase boundaries), the adjoining states have equal free energies and are in equilibrium.

One additional relationship, the **Clapeyron equation** allows for the determination of the *P–T* trajectory of equilibrium states on a *P–T* diagram as a function of entropy and volume changes. When ice and water are in equilibrium along a specific curve, as in Fig. 11.3, the changes in Gibbs free energy along the equilibrium curve must be equal. This allows us to equate two Gibbs free energy expressions (i.e., one for the reactant, ice, and one for the product, water). As such, the one equation must equal the other as follows:
For the reactant (*r*):

$$dG_r = V_r dP - S_r dT$$

and for the product (*p*):

$$dG_p = V_p dP - S_p dT$$

At equilibrium:

$$V_r dP - S_r dT = V_p dP - S_p dT$$

Rearrangement results in:

$$(V_p - V_r)dP = (S_p - S_r)dT$$

which results in:

$$\frac{dP}{dT} = \frac{\Delta S}{\Delta V}$$

the *Clapeyron equation*. In this equation, ΔS is the total entropy of the products minus the total entropy of the

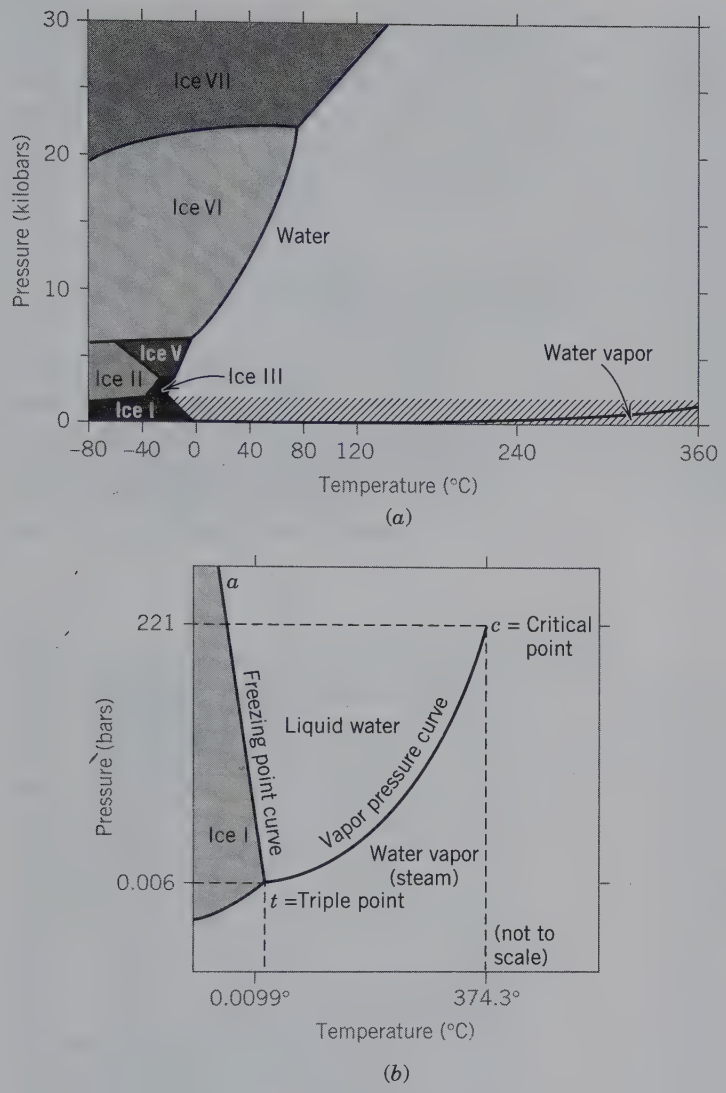

FIG. 11.3 (a) *P–T* diagram for H_2O. Six different structural types (polymorphs) of ice are indicated by I, II, III, V, VI, and VII. (After Bridgeman, P.W., 1937, *Journal of Chemical Physics* 5: 965, and *Phase Diagrams for Ceramists* © American Ceramic Society, Columbus, Ohio, 1964.) For clarity, the water/water vapor curve has been offset slightly toward higher pressure. The cross-hatched region in figure (a) is enlarged, but not to scale, in (b).

reactants. Similarly, ΔV is the total volume of the products minus the total volume of the reactants. As expressed on a *P–T* diagram, the slope of dP/dT is a function of both changes in entropy and volume of the system. These variables can be expressed on a variety of other diagrams to display the stable mineral phase or assemblage and to predict the reaction direction as a function of external conditions.

PHASE DIAGRAMS

The behavior of solids, liquids, and gases under variable external conditions, such as those of temperature and pressure, is expressed commonly on a **phase diagram** (or a *stability diagram*). A **phase** is a homogeneous substance with a well-defined set of physical and chemical properties. As such, the term *phase* can be used interchangeably with the term *mineral* but only if the mineral is a single composition and unzoned. For example, low quartz, SiO_2, is a low-temperature phase in the chemical system Si–O_2 (or SiO_2); kyanite, Al_2SiO_5, is a high-pressure phase in the chemical system Al_2O_3–SiO_2 (or Al_2SiO_5). A phase can be in a solid, liquid, or gaseous state, as in the case of H_2O, ice, water, and steam.

A specific phase diagram for the chemical system H_2O, shown in Fig. 11.3, is a **pressure-temperature stability diagram** (*P–T diagram*). It indicates the state (i.e., solid, liquid, or gas) at a specific set of *P–T* conditions. Regions of stability of a single phase are separated by the various curves in this diagram. Along the curves, two phases can *coexist stably, in equilibrium*, because their Gibbs free energies are equal. For example, ice and water coexist along the various *P–T* boundaries (freezing point curves) on the left side of the diagram. On the Earth's surface, this condition exists at the base

of glaciers or under the blade of an ice skater. A skater glides over the ice as the pressure on the blade melts the ice to produce liquid. At the point where all three curves meet, the three phases, ice, water, and steam, can coexist; this is known as the **triple point**, ***t***. Along the curve *t–c* (Fig. 11.3b), water and steam can coexist but with increasing *P* and *T*, the water phase becomes less dense (expands due to increasing temperature) and the steam phase more compressed (due to increasing *P*). At point ***c*** **(critical point)**, the properties of the two phases become identical, hence the phases are indistinguishable. This leads to a region of *supercritical* aqueous fluid (to the upper right of *c* in *P–T* space). In this region, fluid properties vary continuously. Fluids emanating from black smokers at mid-ocean ridges on the sea floor are typically at *P–T* conditions near the critical endpoint in the H_2O system.

Phase, or mineral stability, diagrams are useful in providing a visual image of what mineral or group of minerals is stable with respect to some other mineral or mineral assemblage, at a specific set of external (e.g., specified *P* and *T*) conditions. For example, in Fig. 11.3a, different structures of ice (labeled by I, II, etc.) are stable in different regions of the diagram (i.e., at different conditions of *P* and *T*). Each numbered ice field outlines the *P–T* space in which a specific structure of ice is stable. Ice VI has a much larger *P–T* region over which it is stable than, for example, ice III. It is also evident that ice VII is stable at the highest pressures and a range of low temperatures, whereas ice I is stable only over a range of relatively low *P* and *T* (essentially atmospheric) conditions. This leads to the conclusion that ice VII is unstable in the *P–T* space of ice I; the reverse statement is also true.

The phase diagrams for H_2O, as given in Fig. 11.3, were developed from the results of a large number of pressure-temperature experiments in the H_2O system and very careful characterization of the resultant reaction products. In addition, such diagrams can be calculated on the basis of the known thermodynamic parameters previously described.

Components

Phases in a chemical system are described by independent chemical species known as **components**; generally, a minimum number of chemical variables is chosen. Components can be actual minerals or they can be theoretical compositions. Whatever is chosen, *components are the chemical entities necessary to define the compositions of all the phases in a system*. For example, in the case of H_2O, the component H_2O can be chosen instead of defining the chemical system in terms of two components, H and O. In the system Al_2SiO_5 (andalusite-sillimanite-kyanite), Al_2SiO_5 is chosen as the component although three elements, Al, Si, and O, or two oxide components, Al_2O_3 and SiO_2, could have been selected to define the chemical system. To illustrate the stability fields of pyroxenes in the system $CaO\text{-}MgO\text{-}FeO\text{-}SiO_2$, the three compound components $CaSiO_3\text{-}MgSiO_3\text{-}FeSiO_3$ are normally chosen to define the chemical system (Fig. 11.11).

EXAMPLES OF MINERAL STABILITY (PHASE) DIAGRAMS

Several representative mineral stability diagrams illustrated here primarily represent conditions pertaining to the *solid state*. Diagrams used in igneous petrology involve a high-temperature melt, while others, used in sedimentary processes (such as in chemical sedimentation in the ocean), involve the representation of a fluid phase.

One-Component Diagrams

Some chemical systems can be described by a single chemical component, such as the four stability diagrams for various minerals in Fig. 11.4. These diagrams depict the stability fields of different structural arrangements of minerals in a specific chemical system as a function of *P* and *T*. The stability fields of diamond, graphite, carbon III, and melt are depicted for a one-component system, namely carbon (C). Diamond and graphite are the two common structural types of carbon (known as polymorphs, see Chapter 12 "Polymorphic Reactions"). Diamond has a large stability field in the high-pressure region of the diagram and diamond stability also extends to high temperature at certain pressures (up to about 4000°C at about 150 kilobars, kb). Diamond is not the stable form, however, at the surface of the Earth. Graphite is stable over a wide temperature range but only at relatively low pressures, such as those at the Earth's surface. Diamond has a much more densely packed structure than graphite, with a molecular volume that is about 36 percent smaller than that of graphite. As such, diamond is expected to be the high-pressure phase, as shown in the stability diagram. The reaction transforming diamond to graphite requires that chemical bonds in diamond be broken, and that the structure is reassembled to that of graphite. This requires large amounts of energy (activation energy), and because of this, diamond is persistent under conditions near the Earth's surface. Here, diamond is the metastable form of C, but diamonds can be considered to be "forever," even though thermodynamically the diagram shows that graphite is the stable mineral under atmospheric conditions. The conversion rate of diamond to graphite, at atmospheric conditions, is infinitely slow and cannot be detected.

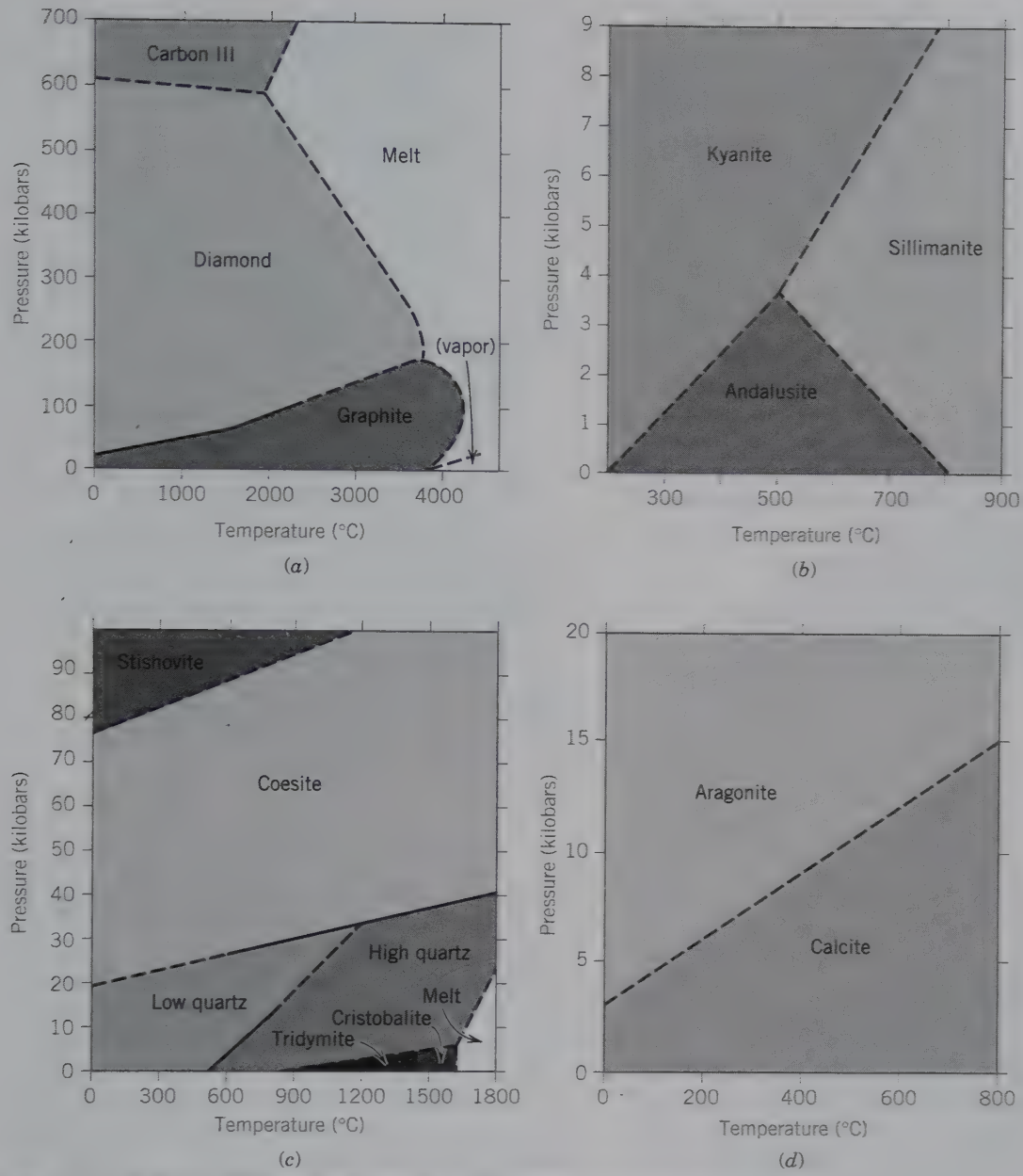

FIG. 11.4 Examples of mineral stability diagrams (*P–T* diagrams) for one-component systems. Each of these has been determined by experiments. When curves or lines are solid, their locations have been determined with certainty; when they are dashed, their location is less well-known. (a) The system C, based on experimental data from various sources. (b) The system Al_2SiO_5 as based on experimental results from Holdaway (1971). (c) The system SiO_2 from various sources. (d) The system $CaCO_3$. 1 kb = 1,000 bars; 1 bar = 0.987 atmosphere (atm).

Three different structural arrangements of Al_2SiO_5 are andalusite, sillimanite, and kyanite (Fig. 11.4b). This diagram is regarded as a one-component system because Al_2SiO_5 is the compound that represents the composition of all three minerals. Because kyanite occupies the high-pressure region of the *P–T* diagram, one would conclude kyanite to be the densest form (polymorph) of Al_2SiO_5. It also follows that kyanite has the tightest packing as shown by the densities and structural studies of the three Al_2SiO_5 polymorphs. The three structures may be represented as follows:

$Al^{[6]}Al^{[6]}SiO_5$ kyanite
$Al^{[5]}Al^{[6]}SiO_5$ andalusite
$Al^{[4]}Al^{[6]}SiO_5$ sillimanite

where the square brackets with superscripts denote the coordination polyhedron of Al ($Al^{[6]}$ = octahedral; $Al^{[5]}$ = irregular 5-fold; $Al^{[4]}$ = tetrahedral). In all of

these minerals, one-half of the total Al is in octahedral coordination; the other half of the Al ranges in coordination from 4 to 6. Kyanite, with the closest atomic packing of the three (largest **C.N.**), is stable at the highest pressures. Sillimanite, with four-fold coordination of Al, represents the highest temperature portion of the system where thermal expansion decreases the density of the atomic packing.

Kyanite, sillimanite, or andalusite can be found in metamorphic rocks at the Earth's surface of all geological ages, including those of the early Precambrian. This observation signifies that the activation energy necessary to transform a high-temperature or high-pressure phase into the lower *P–T* phase stable at atmospheric conditions is substantial and has not occurred. However, in many other metamorphic rocks that contain Al_2SiO_5 minerals, the following textural relations have been observed:

a center of kyanite rimmed by sillimanite
a center of sillimanite rimmed by kyanite
a center of sillimanite rimmed by andalusite
a center of andalusite rimmed by kyanite

The central mineral is the original, surrounded by growth of a later mineral as a rim representing a new equilibrium condition. Because the stability fields of such mineral pairs occupy different regions in a *P–T* stability diagram, the overgrowths in such a pair suggest a possible *P–T* trajectory (path) taken by the rock in which they are hosted. All of the previously mentioned textural occurrences delineate various *P–T* paths across the different equilibrium boundaries. An example of such *P–T* paths, interpreted in terms of various geologic processes, is shown in Fig. 11.5.

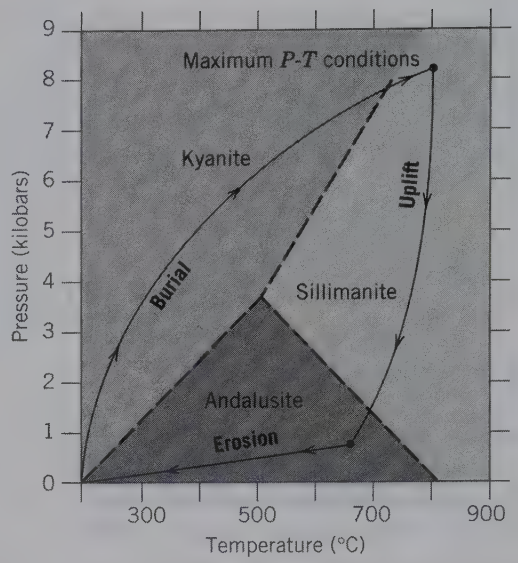

FIG. 11.5 The Al_2SiO_5 stability diagram with superimposed arrows showing the paths for various geologic processes. Material at the Earth's surface may originally have been buried to maximum *P–T* conditions of ~ 8 kb and 800°C. Subsequent to this, these metamorphic rocks may have been uplifted and eroded, returning the subducted material back to the Earth's surface. In addition to the evaluation of the textural reactions among the Al_2SiO_5 minerals, a geologist must assess the *P–T* conditions for other minerals in these same rocks, as well as the tectonic parameters of the region.

SiO_2 is chemically simple but its behavior as a function of *P* and *T* is quite complex (Fig. 11.4c). Low quartz is the form of SiO_2 found in plutonic, metamorphic, and sedimentary rocks and reflects formation at relatively low temperatures. Tridymite and cristobalite are found in high-temperature, volcanic assemblages of many geological ages. This means that these high-temperature minerals can exist metastably for long geologic time periods. In other volcanic occurrences, the original cristobalite or tridymite has converted to low quartz, but may preserve the crystal form of the original cristobalite or tridymite (these occurrences represent pseudomorphs of low quartz after higher-temperature SiO_2 polymorphs, see Chapter 12, Pseudomorphism, page 284). The high-pressure forms of SiO_2, coesite and stishovite, have been found in meteorite impact craters. Coesite also occurs as inclusions in diamonds and garnets from very high-pressure metamorphic rocks (e.g., from Parigi, Northern Italy, Chopin 1984; a complete reference is given at the end of this chapter). Coesite has been found in rocks that originated at a depth of about 170 to 200 km in the mantle, at pressures of approximately 60 to 70 kb (a pressure region in Figs. 11.4a and c where both diamond and coesite are stable). Coesite-diamond coexistences have also been reported from very high-pressure metamorphism of crustal rocks in eastern China (Shutong et al. 1992; a complete reference is given at the end of this chapter).

By far, the most common carbonate of sedimentary, metamorphic, or igneous rocks is calcite. The phase diagram in Fig. 11.4d suggests that the $CaCO_3$ formed at temperatures and pressures of the Earth's surface should be calcite. However, this is not always the case. Primary precipitation of $CaCO_3$ from seawater is commonly in the form of aragonite, producing aragonitic muds. Many organisms build their shells of aragonite, and the main constituent of pearls is aragonite. These observations imply that aragonite is formed and precipitated as a *metastable* mineral that, over time, will convert to calcite. This transformation can be very slow, as shown by the preservation of aragonite in reefs that are about 300 million years old. However, the aragonite-to-calcite reaction is more easily accomplished than the transformations from diamond to graphite or coesite to quartz. If energy is applied in the form of increased temperature, as a result of burial, aragonite will transform to calcite.

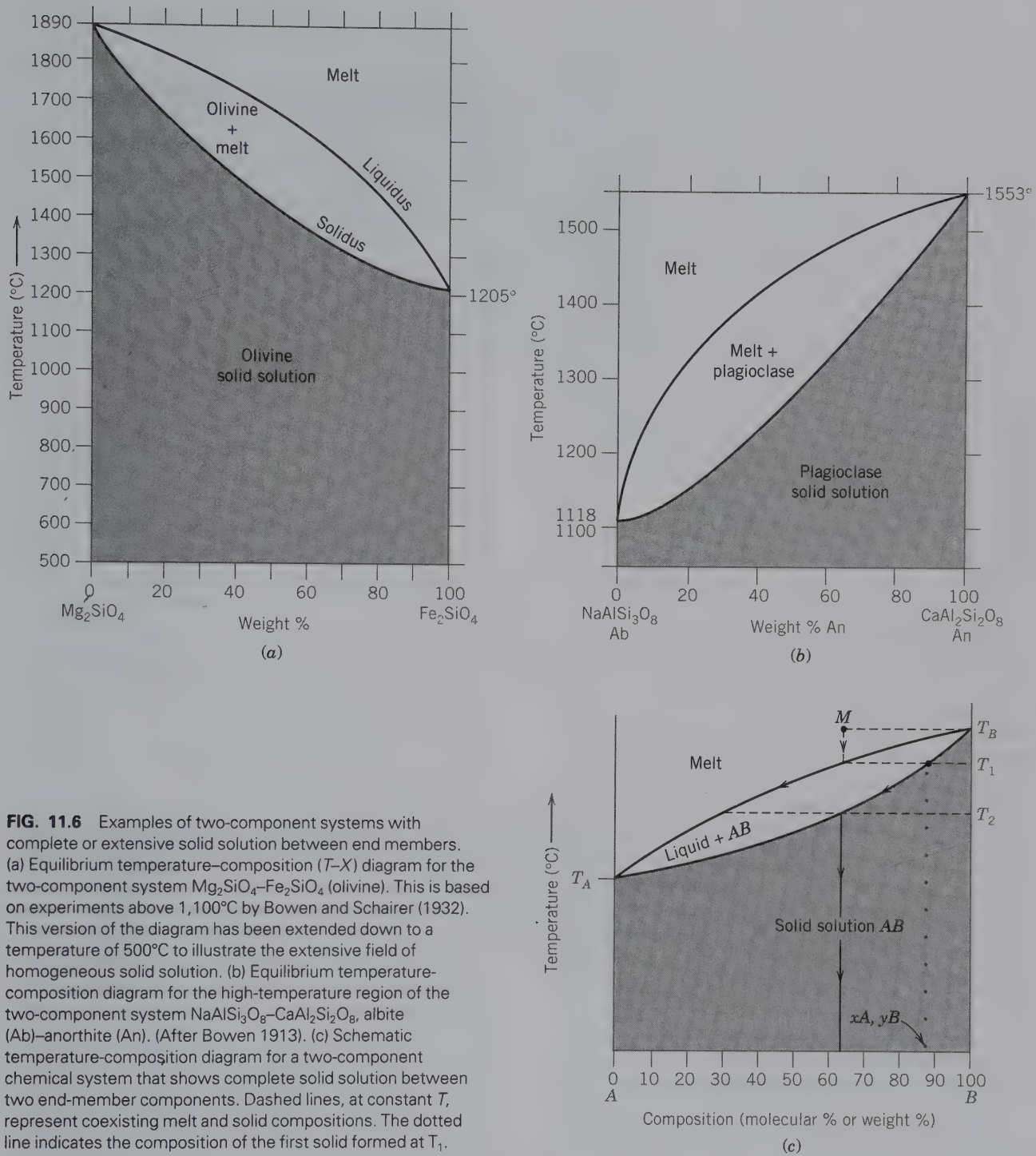

FIG. 11.6 Examples of two-component systems with complete or extensive solid solution between end members. (a) Equilibrium temperature–composition (*T–X*) diagram for the two-component system Mg_2SiO_4–Fe_2SiO_4 (olivine). This is based on experiments above 1,100°C by Bowen and Schairer (1932). This version of the diagram has been extended down to a temperature of 500°C to illustrate the extensive field of homogeneous solid solution. (b) Equilibrium temperature-composition diagram for the high-temperature region of the two-component system $NaAlSi_3O_8$–$CaAl_2Si_2O_8$, albite (Ab)–anorthite (An). (After Bowen 1913). (c) Schematic temperature-composition diagram for a two-component chemical system that shows complete solid solution between two end-member components. Dashed lines, at constant *T*, represent coexisting melt and solid compositions. The dotted line indicates the composition of the first solid formed at T_1.

Two-Component Diagrams

Typically, two-component stability diagrams are constructed to display compositional variability in a system as a function of temperature. The horizontal axis is a composition bar, and the vertical axis is temperature. In these diagrams, pressure is a constant. Such **temperature–composition (*T–X*) diagrams** exhibit very different features from *P–T* diagrams. They may depict (1) complete solid solution between two end-member compositions, (2) partial solid solution between two end-members as shown by the presence of a miscibility gap, or (3) no solid solution between two mineral species that can be represented along the two-component composition bar.

The following are examples of two-component *T–X* diagrams in which there is complete solid solution over the entire temperature range of the diagram: the olivine series, between Mg_2SiO_4 (forsterite) and Fe_2SiO_4 (fayalite), and the high-temperature region in the plagioclase feldspar series ($NaAlSi_3O_8$ to $CaAl_2Si_2O_8$). Both diagrams, depicted in Figs. 11.6a and b, are the result of experimental studies at 1 atmosphere pressure (= 1.01325 bars). These two diagrams are also known as **liquidus diagrams** because they involve a liquid phase, or melt. Such *liquidus diagrams* are used to predict the melting relations of igneous rock compositions, as well as the crystallization sequence of minerals from a melt. The upper curve in Fig. 11.6a is known as the **liquidus**, a line or surface along which compositions of melt are in equilibrium with a crystalline phase. The lower curve is known as the **solidus**, a line or surface along which compositions of a crystalline phase are in equilibrium with the melt. The region above the liquidus is liquid (melt); everything below the solidus is solid (minerals). The schematic diagram in Fig. 11.6c displays the crystallization behavior of solids from a melt in these types of melt diagrams. The pure end-member *A* (left side of diagram) melts at a temperature T_A and pure end member *B* melts at T_B. Intermediate compositions (*AB*), which consist of a single phase that is part of the solid solution series, melt through a range of temperatures intermediate between T_A and T_B. The temperature for the beginning of melting for a point on the solidus is found by drawing a horizontal line for the chosen composition point to the vertical *T* axis. A melt of composition *M* at temperature T_B will remain entirely liquid until it cools to T_1 (intersects the liquidus). At T_1 the melt will begin to crystallize a member of the solid solution series *AB* with specific composition *xA*, *yB*. These crystals are enriched in the *B* component with respect to the melt composition *M*, and their growth will deplete the melt in component *B*. The melt composition will, as a result of this depletion, move along the liquidus curve toward *A* as indicated by the upper arrow. As a result of the continual lowering of the temperature, the solid phase of original composition *xA*, *yB* will react with the melt in the direction of the lower arrow along the solidus.

As such, both the melt and crystalline products will increase in content of *A* with decreasing *T* and the ratio of solid to melt will increase. Finally, at T_2, the crystallized products have the composition of the original melt *M*, and the amount of melt in equilibrium with the crystals is zero. Because only a solid phase remains with continued lowering of the temperature, the composition of the crystalline product remains constant at the bulk composition *M* of the original melt. These observations apply to both diagrams, Figs. 11.6a and b.

Although the original equilibrium melting and crystallization experiments necessary to construct Fig. 11.6b indicated a complete solid solution series for plagioclase at high temperature, subsequent detailed single-crystal X-ray diffraction and transmission electron microscope studies have shown this is more complex at lower temperatures (further discussed in the section "Exsolution" in Chapter 12).

The two-component system for the alkali feldspars series ($NaAlSi_3O_8$-$KAlSi_3O_8$) is an example of solid solution that varies dramatically with temperature; that is, an almost complete range of solid solution exists at high temperatures whereas only limited solid solution occurs at lower temperatures (Fig. 11.7a). The lack of solid solution at lower temperatures is mainly the result of the large difference in ionic sizes of Na^+ (1.18 Å in 8-fold coordination) and K^+ (1.51 Å in 8-fold coordination; see Table 3.8). The mineral names listed inside the diagram are the names for different structural states of $NaAlSi_3O_8$ (monalbite = monoclinic albite; high, intermediate, and low albite) and of $KAlSi_3O_8$ (sanidine, orthoclase, and microcline). This diagram shows a region known as a **miscibility gap**. At high temperatures, there is a region of solid solution where a single phase occurs. However, at lower temperatures (the unshaded domal region of the diagram), homogeneous mineral compositions of the alkali feldspar series cannot exist and two feldspar phases form (see Chapter 12 "Exsolution" for further discussion).

The configuration of the diagram in Fig. 11.7a is altered substantially when H_2O (at high water pressure = P_{H_2O}) is added to the chemical system, as in Fig. 11.7b. A high aqueous-fluid pressure considerably lowers the melting temperatures, while increased pressure applied to the system raises the maximum temperature of the miscibility gap such that now the solidus and the miscibility gap intersect. Point *e*, the **eutectic point** (Fig. 11.7b, see further discussion next), is the lowest temperature point on the liquidus at which a unique melt of fixed composition is in equilibrium with two feldspar compositions (i.e., an Na-rich feldspar solid solution and a K-rich feldspar solid solution). The crystallization of a melt composition at *e*, therefore, allows for the direct crystallization from the liquid of coexisting albite and K-feldspar, without the need for unmixing to produce two phases as is shown in the anhydrous system of Fig. 11.7a. The coexistence of coarse-grained albite and K-feldspar is common in granites and pegmatites and reflects crystallization of both minerals from a melt. Perthitic intergrowths, however, represent exsolution in the solid state (see "Exsolution," Chapter 12).

When there is *no* solid solution between minerals in a two-component system, a different temperature-composition diagram results (Fig. 11.8). With decreas-

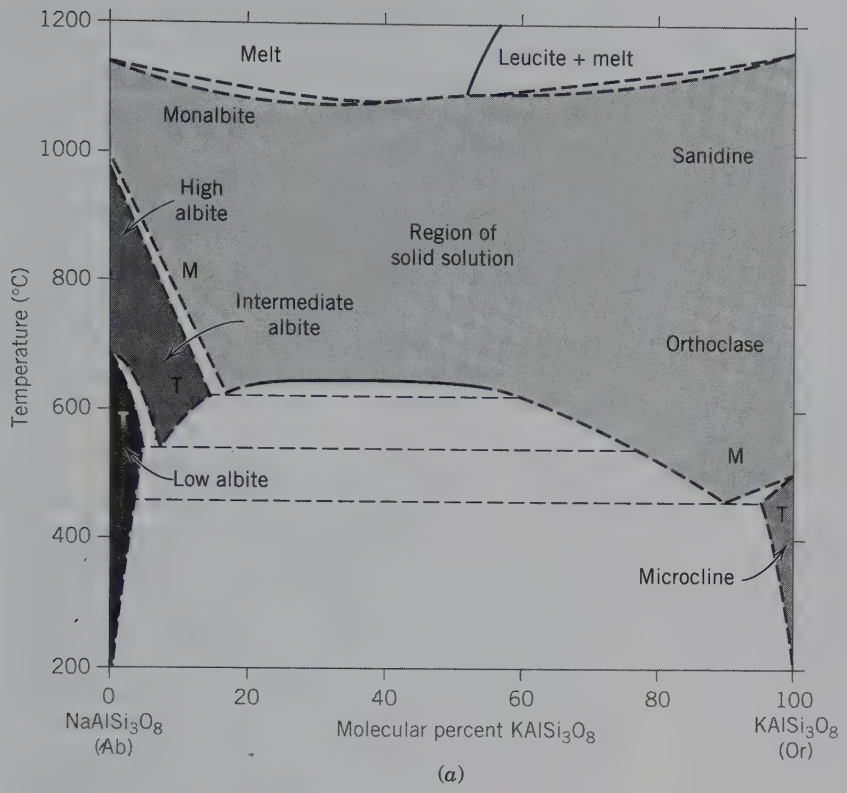

(a)

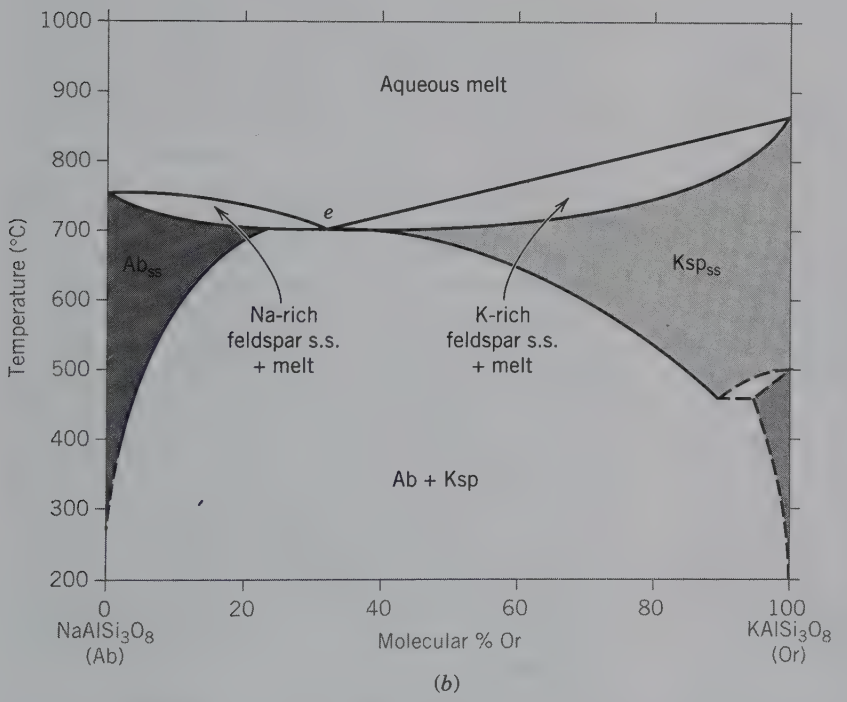

(b)

FIG. 11.7 (a) Schematic phase diagram for the system $NaAlSi_3O_8$ (Ab)–$KAlSi_3O_8$ (K-feldspar) showing a large miscibility gap at temperatures below ~ 650°C. *M* and *T* mean monoclinic and triclinic, respectively. (Modified with permission after Smith, J. V. and W. L. Brown. 1988. Feldspar minerals, v. 1, *Crystal structures, physical, chemical, and microtextural properties.* Springer-Verlag, New York, Fig. 1.2.) (b) Approximate and schematic phase diagram for the same chemical system, except for addition of H_2O to the melt, at P_{H_2O} = 5 kb. The solidus and the miscibility gap intersect at point *e*, the eutectic point; see text for discussion. s.s. = solid solution. (Modified after Morse, S. A., 1970. Alkali feldspars with water at 5 kb pressure, *Journal of Petrology* 11: 221–51.) Refer to Chapter 12 "Exsolution" for further discussion.

ing temperature, the melt changes composition (along the liquidus curve) until a temperature is reached where no further liquid is present (Fig. 11.8a). These two-component phase diagrams display *eutectic* relationships. Phases *A* and *B* are pure substances with no solid solution between them (Fig. 11.8a). For composition *A* the melting temperature is T_A. Similarly, for composition *B* the melting temperature is T_B, and the solid curves represent the liquidus. The addition of some of composition *B* to a melt of *A* lowers the temperature of the melt that can coexist with *A*, along the curve between T_A and *e* (*eutectic point*, which is the minimum

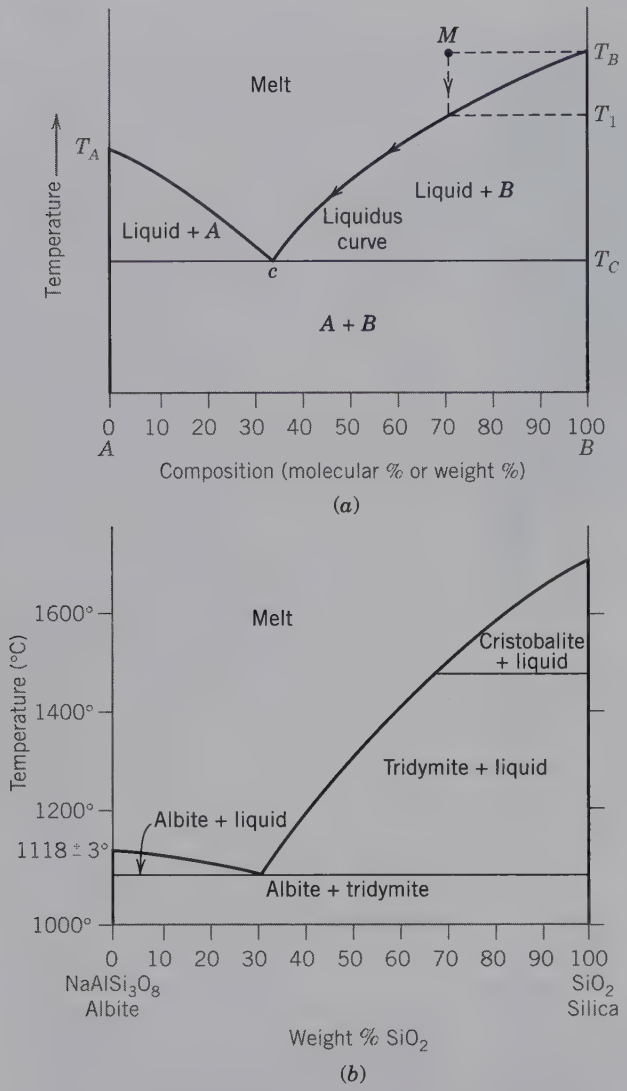

FIG. 11.8 (a) Schematic temperature-composition section showing eutectic crystallization of components *A* and *B*; both components are pure substances (no solid solution between them). (b) The system $NaAlSi_3O_8$ (Ab)–SiO_2. (After Schairer, J. F. and N. L. Bowen. 1956. *American Journal of Science* 254:161.)

temperature point of the liquid field). Similarly, the melting temperature of the melt that can coexist with *B* is lowered by the addition of some of *A*, as shown by the curve between T_B and *e*. The lowest temperature at which crystals and melt are in equilibrium is T_C, the temperature of the eutectic.

The crystallization sequence of a melt of composition *M* is shown by the arrow in the melt and the further arrows along the liquidus curve (Fig. 11.8a). When the original melt temperature (= T_B) is lowered, the melt will start to crystallize the pure substance *B* at T_1. As temperatures continue to fall, the crystallization of *B* from the melt will proceed following the *liquidus curve* (T_B to *e*). This continually increases the content of substance *A* in the melt. At the eutectic point (*e*), phase *A* will join *B* as a crystallization product. At this point, there is no further change in composition of the melt because both *A* and *B* crystallize from the melt in the same proportions as they are present in the melt. With continued crystallization, the melt will disappear and the final crystalline products will be *B* and *A* in the proportions represented by the original bulk composition *M*. Figure 11.8b illustrates the high-temperature portion of the system $NaAlSi_3O_8$-SiO_2 which also displays a eutectic melting relationship as discussed for Fig. 11.8a.

Three- or More-Component Diagrams

Because most igneous, metamorphic, and sedimentary rocks commonly consist of six to ten or more chemical components, one-component and two-component stability diagrams generally have only limited applicability to more complex naturally occurring mineral assemblages. However, easy graphical representation of multicomponent chemical systems is limited mainly to three-component, triangular diagrams as discussed in Chapter 5. Four-component systems with chemical components at each of the four corners of a tetrahedron also are used, but tetrahedral representations become graphically complex and are difficult to visualize.

Triangular phase diagrams are common in igneous petrology and are used to represent the experimentally studied melting relations of igneous rock compositions, as well as to depict the crystallization sequence from a melt. One such diagram is given in Fig. 11.9 in terms of three components; SiO_2, $KAlSiO_4$, and Mg_2SiO_4. Each of these components occupies one of the corners and mineral compositions are plotted in their appropriate positions (refer to Chapter 5 for details). The contours in this triangular diagram are known as **isotherms** (meaning equal temperature) and represent melting temperatures for specific compositions. The surface defined by these isotherms is the *liquidus surface*. The arrows along the boundaries of the various phase fields indicate crystallization paths that occur with decreasing temperature. As crystallization progresses, melt follows the path directly away from the crystallizing composition until a liquidus surface is intersected and it then follows decreasing temperature.

In the study of the mineralogy of mineral assemblages, triangular diagrams are commonly used to depict mineral stabilities below the liquidus and solidus surfaces—that is, in the **subsolidus** region. A schematic, composite liquidus-subsolidus diagram is shown in Fig. 11.10a for the triangular composition space of feldspar. The bottom triangle (in Fig. 11.10b)

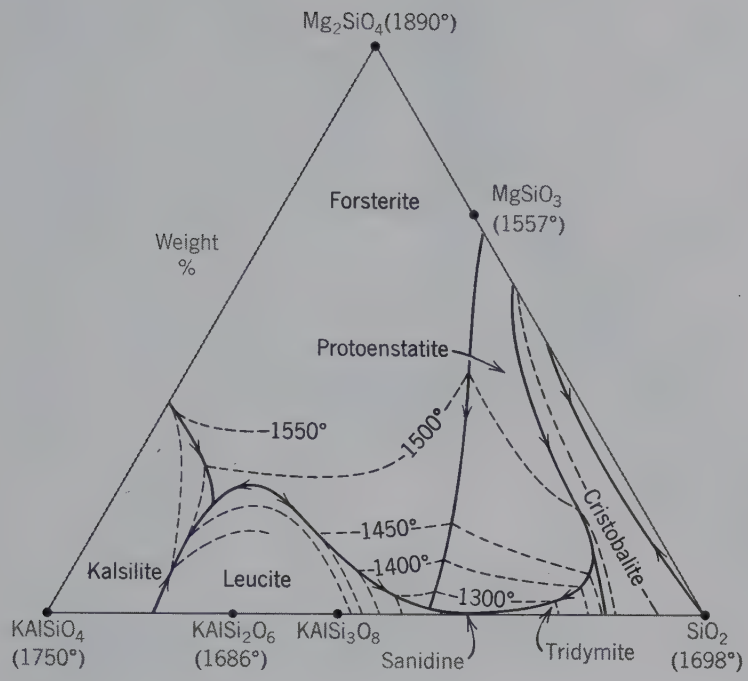

FIG. 11.9 Melting relations among minerals in the system SiO_2–$KAlSiO_4$–Mg_2SiO_4. Temperatures next to compositions refer to the melting temperatures of those compositions in °C. Protoenstatite instead of enstatite is produced in experiments of this type. The compositions of protoenstatite and enstatite are identical, but their structures differ in detail. (After Luth, W. C., 1967. *Journal of Petrology:* 373, reprinted by permission of Oxford University Press.)

is based on three major feldspar end-member compositions: $KAlSi_3O_8$–$NaAlSi_3O_8$–$CaAl_2Si_2O_8$ and is used to depict the compositional extent of solid solution in the feldspars as a function of temperature at constant P_{H_2O} = 1 kb. At the highest temperature (900°C), the feldspars show the most extensive solid solution as depicted by the curve and field shaded for 900°C on the diagram. At the lowest temperature studied, 650°C, there is the least extent of solid solution. Along the join from $KAlSi_3O_8$–$NaAlSi_3O_8$ (left side of triangle) there is a considerable break (gap) in the central part of the solid solution series at 650°C. In this gap, no solid solution occurs and this reflects the intersection of the miscibility gap in this system at about that temperature (Fig. 11.7a). This is also the $T - X$ section for $KAlSi_3O_8$–$NaAlSi_3O_8$, without H_2O present in the system. The plagioclase compositional field in Fig. 11.10b suggests that solid solution at 650°C is continuous between $NaAlSi_3O_8$–$CaAl_2Si_2O_8$. However, it is known that three miscibility gaps exist in this series, below about 800°C (Fig. 11.10a). These gaps are not reflected in the experimental results used for construction of Fig. 11.10b, because the chemical analytical techniques (used to determine compositions of experimental products) cannot resolve the extremely fine-scale compositional variations across the three gaps.

Another commonly used triangular diagram is one that represents the main compositional variation among members of a mineral group. The example shown in Fig. 11.11 is for the pyroxene group and is expressed in terms of three components, $CaSiO_3$, wollastonite, a pyroxenoid; $MgSiO_3$, enstatite; and $FeSiO_3$, ferrosilite. The compositional range between end members of various pyroxene series in igneous and metamorphic rocks is shown by shading. The compositional space between augite and pigeonite/orthopyroxene represents a region of immiscibility (discussed in Chapter 12, "Exsolution"). In this region, two coexisting pyroxenes crystallize instead of a single solid solution phase; such pyroxene occurrences are connected by tielines. This diagram is the result of the compilation and graphical plotting of thousands of pyroxene analyses from the published literature. Such a compilation of analyses from natural occurrences does not distinguish compositional regions that result from the analyses of high-temperature pyroxenes (as in basalt flows) from those for lower-temperature pyroxenes (as in andesites). Therefore, such a diagram is useful only as a graphical representation of the average extent of solid solution of common pyroxenes. Triangular composition diagrams similar to Fig. 11.11 are used commonly in the graphical representation of the composition of other mineral groups, such as members of the olivine and amphibole groups.

Three-component triangular diagrams also may be used to illustrate the common coexistence of possible mineral pairs or groups of three minerals. Such diagrams are known as **assemblage diagrams.** To identify the appropriate components for the diagram, the first step involves listing the minerals that compose the rock

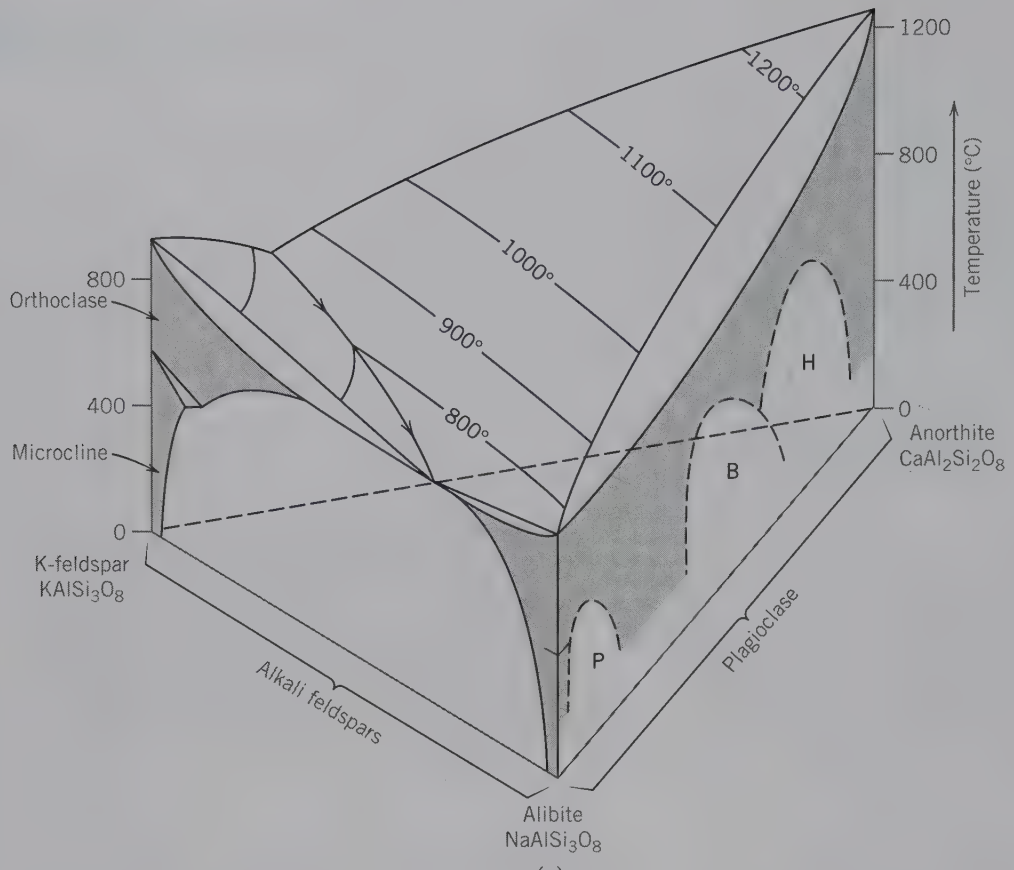

(a)

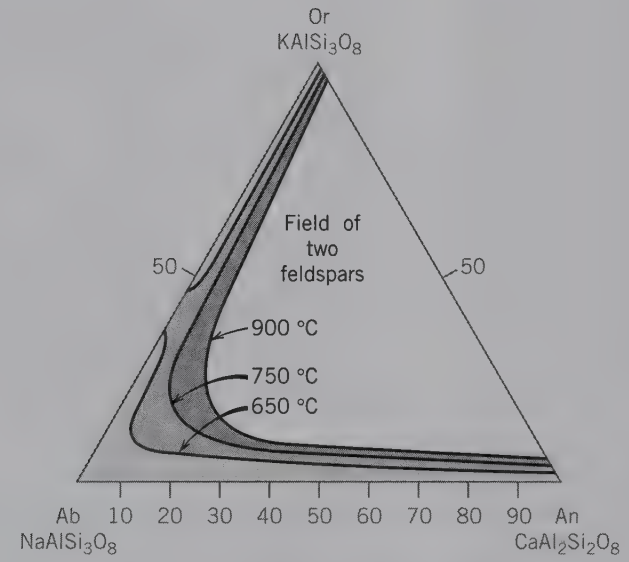

(b)

FIG. 11.10 (a) Highly schematic temperature-composition diagram for the three-component system $KAlSi_3O_8$ (K-feldspar)–$NaAlSi_3O_8$ (albite)–$CaAl_2Si_2O_8$ (anorthite), at $P_{H_2O} \sim 5$ kb. Details of the interior are complex and have been omitted. The upper, contoured surface of the diagram is the liquidus surface. The three intergrowth regions, as a result of miscibility gaps, in the lower temperature range of the plagioclase series are: P = peristerite, B = Bøggild intergrowth, H = Huttenlocher intergrowth. Solid solution is shown by shading. Compare the left front side of this diagram with more detailed information given in Fig. 11.7b. (Adapted from Ribbe, P. H., 1987. Feldspars. *McGraw-Hill Encyclopedia of Science and Technology*, 6th ed., v. 7, 45; reproduced with permission of McGraw-Hill.)
(b) Experimentally determined extent of solid solution plotted on the triangular base of the diagram in (a), at $P_{H_2O} = 1$ kb. (After Ribbe, P. H. 1975. The chemistry, structure, and nomenclature of feldspar. *Reviews in Mineralogy, Feldspar Mineralogy* 2: R1–R72, Fig. R1.)

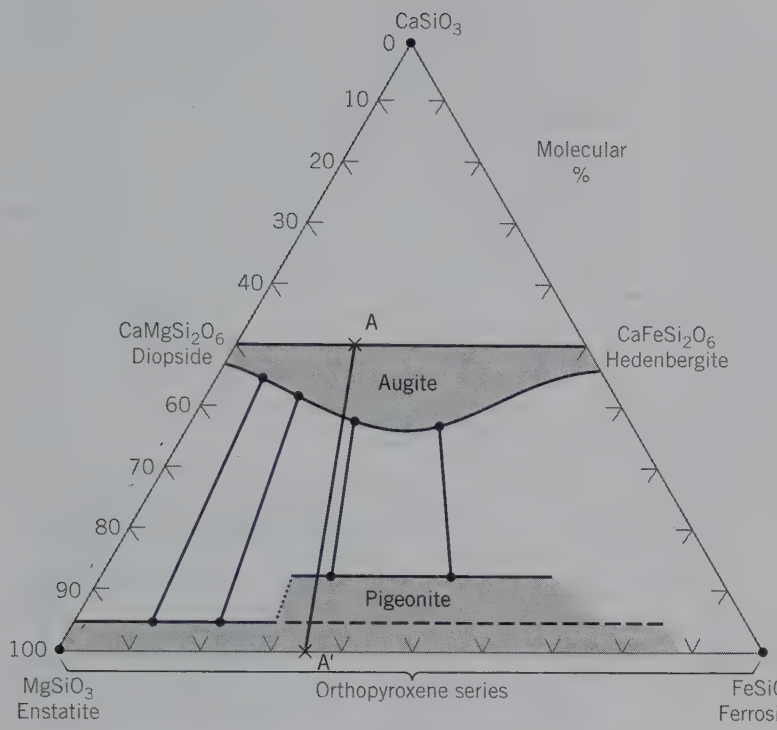

FIG. 11.11 (a)The extent of pyroxene solid solution in the system $CaSiO_3$–$MgSiO_3$–$FeSiO_3$. Representative tielines across the miscibility gap between augite and the more Mg-Fe-rich orthopyroxenes connect coexisting compositions. *AA'* locates the section across this diagram shown in Fig. 12.17.

under study. A granite may consist of orthoclase, albite, quartz, and biotite. The spatial relationships of the minerals (its texture) in this granite indicate that all four minerals formed as crystallization products at about the same elevated temperature. A petrologist, therefore, might conclude that orthoclase-albite-quartz-biotite is the main **mineral assemblage** of this granite. Although the term *assemblage* is commonly used to include all the minerals that compose a rock, it should be restricted to those minerals in a rock that appear to have been *in equilibrium*. As an example, the previously mentioned granite may be found to contain vugs (holes) in outcrop that are lined by several clay minerals, as well as some limonite. These minerals represent relatively low-temperature alteration products of the original higher-temperature granite. The high-temperature granitic assemblage consists of orthoclase-albite-quartz-biotite, and a separate, later formed, low-temperature assemblage consists of clays-limonite. In short, an assemblage consists of minerals that formed under the same, or very similar, conditions of pressure and temperature. *In practice, all minerals that coexist (physically touch each other) and show no alteration or rimming relations are considered to constitute the assemblage.* In a distinctly banded rock, the mineral assemblages in the various bands are typically very different from each other because the bands may represent major differences in bulk chemistries.

The evaluation of whether all minerals in a rock are in *equilibrium* with each other is generally not straightforward. If the texture does not show reaction rims or alterations, it is possible that the minerals are in equilibrium. Nevertheless, detailed chemical tests are needed to define the equilibrium assemblage without ambiguity. Similarly, the evaluation of equilibrium in an experimental study is not straightforward. However, in spite of the problems inherent in the assessment of the equilibrium of an assemblage, triangular mineral assemblage diagrams are used commonly to depict the observed pairs and groupings of three possible minerals in a specific chemical system.

Figure 11.12 shows commonly observed coexistences (as deduced from natural assemblage occurrences as well as synthetic studies) of minerals in the system SiO_2 (quartz, tridymite, cristobalite)–$NaAlSiO_4$(nepheline)–$KAlSiO_4$(kalsilite). This chemical system also includes the alkali fieldspar series and leucite, $KAlSi_2O_6$. The diagram shows that there is a complete solid solution between albite and orthoclase (the alkali feldspar series) and extensive solid solution in nepheline, kalsilite, and leucite. Because this diagram was determined experimentally and drawn for high-temperature conditions of about 1000°C, the SiO_2 phase expected at this temperature is tridymite (Fig. 11.4c). The assemblages depicted, therefore, are analogous to those found in high-temperature volcanic occurrences. *Tielines connect mineral compositions that represent equilibrium coexistences.* Triangles consist of three sets of tielines (outlining the triangle) depicting three-phase equilibrium coexistences. The diagram

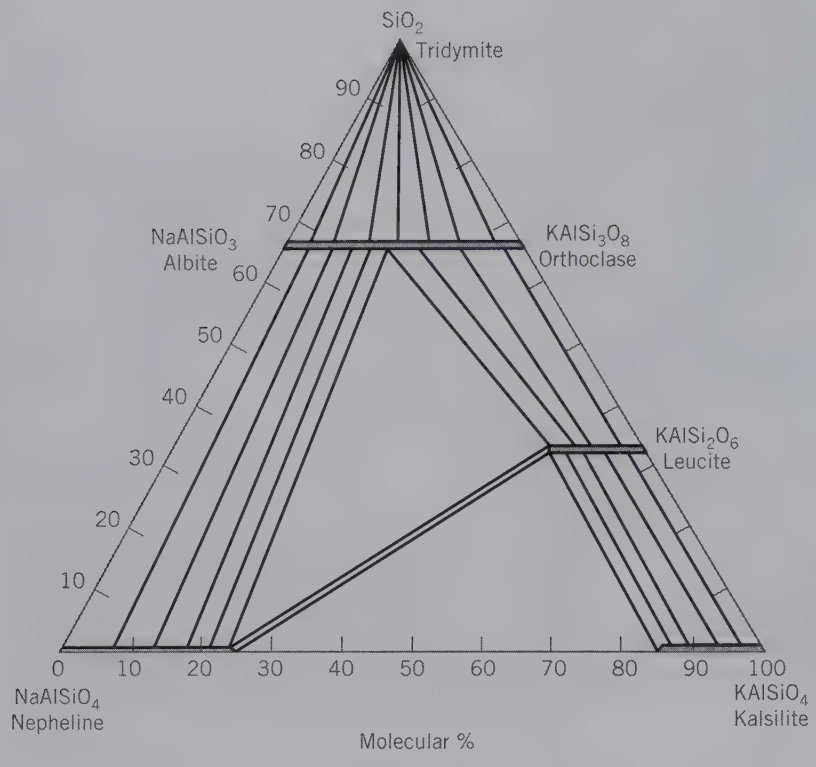

FIG. 11.12 The system SiO_2–$NaAlSiO_4$ (nepheline)–$KAlSiO_4$ (kalsilite) at ~1,000°C and 1 atm. *P*, as determined experimentally. The extent of solid solution for several phase regions is shown, as are tielines between coexisting pairs of minerals. Triangles represent three-phase coexistences. (Adapted from *Petrologic Phase Equilibria*, 21st ed., Fig. 4.39, by W. G. Ernst. Copyright © 1976 by W. H. Freeman and Company.)

illustrates that feldspathoids do not coexist with tridymite because of the intervening alkali feldspar series. This specific triangular diagram is of importance in igneous petrology because it outlines mineral compositions in SiO_2-rich and SiO_2-poor rocks. All assemblages above the albite-orthoclase series contain an SiO_2 phase, whereas all assemblages below the alkali feldspar series are free of SiO_2 minerals.

Another illustration of an assemblage diagram for carbonate minerals is shown in Fig. 11.13. This dia-

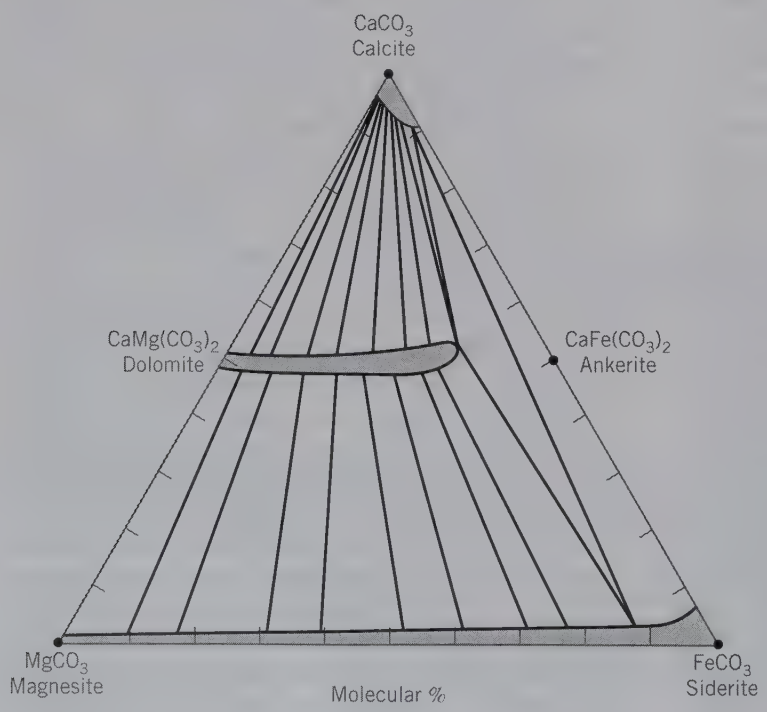

FIG. 11.13 (a) The system $CaCO_3$–$MgCO_3$–$FeCO_3$ showing extent of solid solution for phase regions and coexistences for natural assemblages metamorphosed to about 400°C (biotite zone of the greenschist facies). A three-phase assemblage is shown by a triangle. In this diagram, the extent of solid solution is based on experimental data as well as on analytical results of natural assemblages. The compositions of coexisting carbonates is based on electron microprobe analyses of carbonates over a wide compositional range in low- to medium-grade metamorphic rocks. The open regions across which tielines are drawn are miscibility gaps. Extent of solid solution is shaded. (Adapted from Anovitz, L. M., and E. J. Essene. 1987. Phase equilibria in the system $CaCO_3$–$MgCO_3$–$FeCO_3$. *Journal of Petrology* 28: 389–415.)

gram is based upon naturally occurring compositional ranges and coexistences of metamorphic carbonates at a temperature of about 400°C (the biotite zone of the greenschist facies; see Chapter 21). The shaded areas depict the very small solid solution region for calcite, $CaCO_3$, the extensive (but commonly not complete) series between dolomite, $CaMg(CO_3)_2$, and ankerite, $CaFe(CO_3)_2$, and the complete series between magnesite, $MgCO_3$, and siderite, $FeCO_3$. Tielines between coexisting pairs are shown, as well as one three-phase coexistence (siderite + dolomite + calcite).

Triangular assemblage diagrams are most commonly determined from experimental results, or from carefully studied and chemically analyzed natural assemblages. To delineate the extent of solid solution of any of the minerals in such diagrams, one of several chemical analytical techniques must be used (see Chapter 14). However, for mineral assemblages that represent a relatively simple chemical system, and where the minerals involved are relatively easily identifiable, mineral assemblage diagrams can be constructed on the basis of hand specimen study of a large suite of assemblages that relate to the system in question. In hand specimen study, no knowledge can be gained about solid solution; therefore, the mineral formula for each mineral is plotted as a point on the triangular diagram, without reference to any possible solid solution extent. Coexistences (and, as such, tielines) are based upon the visual observation of two or three minerals touching each other in the hand specimen. An example of such an assemblage diagram in the system Cu–Fe–S is shown in Fig. 11.14. Here, all minerals are represented as points on the diagram, reflecting the fact that any possible solid solution within any of the minerals was ignored.

To represent more complex chemical systems found in rocks, two components may be grouped at a specific corner on a triangular diagram (Fig. 11.15). Two assemblage diagrams, in which two oxide components have been grouped together in the right-hand corner, are illustrated in Fig. 11.15. Typically the components that are grouped together are those that display solid solution for each other. This allows for a more complete representation of the mineral compositions in this instance. In Fig. 11.15, the basalt assemblage may have crystallized at a constant and relatively low P (e.g., 1 to 2 kb) and a temperature of somewhere between 1000 and 1200°C. Here, the coexisting minerals are plagioclase + clinopyroxene + orthopyroxene. The chemically equivalent metamorphic assemblage (eclogite) formed at a much higher pressure, possibly over a range of 12 to 30 kb, and a temperature range of 400 to 800°C. It contains a variety of minerals including kyanite, grossular (garnet), omphacite (pyroxene), orthopyroxene, and/or pyrope (garnet). In other words, the two assemblage diagrams represent

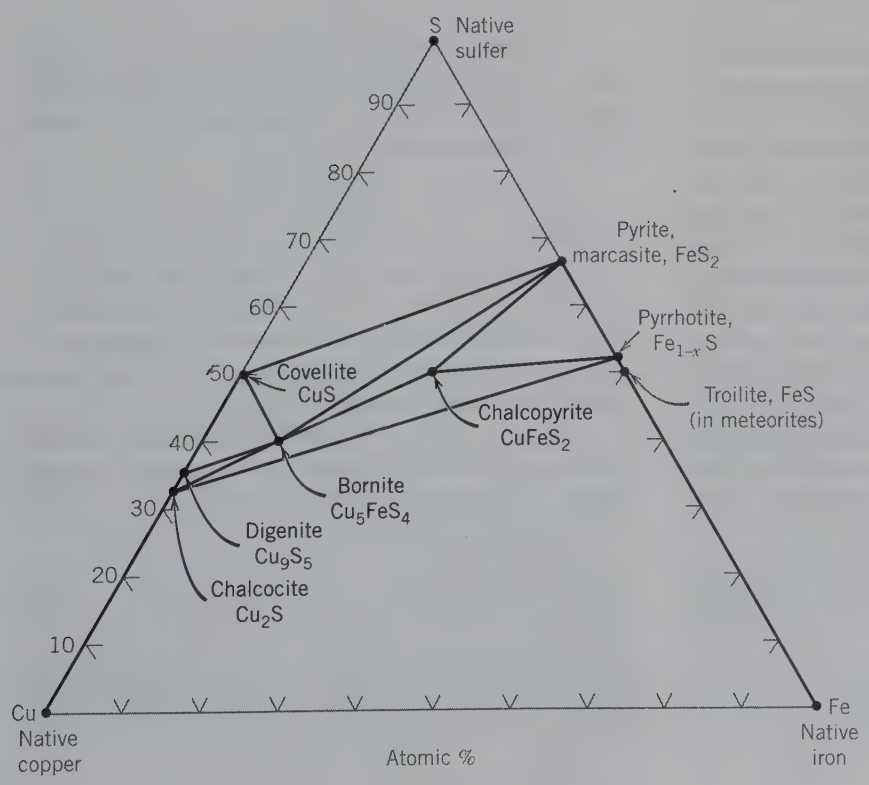

FIG. 11.14 Some of the most common sulfides represented in the Cu–Fe–S system. Two of these sulfides (e.g., bornite and chalcopyrite) show some solid solution of especially Cu and Fe; this is not shown in the diagram. Tielines connect commonly occurring pairs of minerals. Triangles indicate coexistences of three sulfides. The Fe–FeS coexistence is common in iron meteorites.

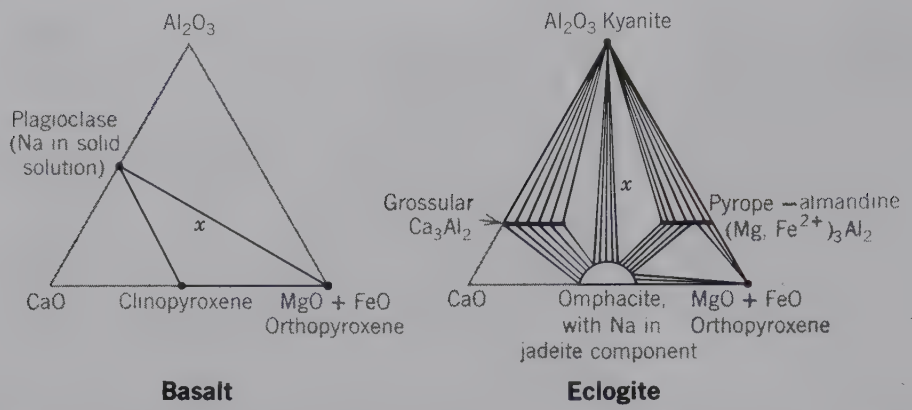

FIG. 11.15 Coexisting minerals in the system Al_2O_3–CaO–(MgO + FeO)–SiO_2–Na_2O. In *basalt*, a common assemblage is plagioclase-clinopyroxene-orthopyroxene, as shown by the triangle of connecting tielines (the *x* represents a possible bulk composition of basalt with this mineral assemblage). In *eclogite*, of the same bulk composition and marked by *x*, the assemblage kyanite-omphacite-pyrope (as a component in almandine) occurs. Composition bars and the omphacite field in the eclogite diagram outline approximate extents of solid solution. Eclogitic rocks may form in the mantle of the Earth from basaltic compositions.

distinctly different *P* and *T* conditions for identical bulk chemical compositions. In assemblage diagrams obtained from experimental studies, the temperatures and pressures can be closely controlled, and isobaric and isothermal phase diagrams can be obtained for much narrower ranges in *P* and *T* than is possible for natural rock or mineral systems.

Diagrams for Mineral Reactions Involving H_2O or CO_2

Pressure-temperature diagrams are used to delineate the stability field of a mineral that, along some *P–T* curve, gives way to another mineral by a chemical reaction. These chemical reactions may include only solid phases, as in the *P–T* diagrams discussed thus far involving structural changes (Figs. 11.4 and 11.5), or they may also include a fluid phase. Hydrous minerals are stable at lower temperatures than anhydrous minerals, and they give way to their anhydrous equivalents at higher temperatures. Such reactions can also be displayed on a *P–T* diagram. For example, in Fig. 11.16a, the stability region of anthophyllite, $Mg_7Si_8O_{22}(OH)_2$, occurs in the lower-temperature part of the diagram and gives way to its higher-temperature reaction products: enstatite, $MgSiO_3$; quartz, SiO_2; and fluid at about 800°C. This chemical system can be defined by MgO–SiO_2–H_2O. The curve delineates the boundary of two stability regions, between which the breakdown of Mg–amphibole occurs, according to

$$Mg_7Si_8O_{22}(OH)_2 \rightleftarrows 7MgSiO_3 + SiO_2 + H_2O\uparrow$$

The H_2O enters the fluid phase produced in the reaction.

A pressure-temperature diagram involving mineral stabilities as a function of CO_2 is shown in Fig. 11.16b. In the system CaO–CO_2, calcite is stable to high temperatures, even at relatively low CO_2 pressures (in Fig. 11.16b calcite is still stable at about 1000°C with P_{CO_2} of less than 10 bars). At temperatures to the right of that curve (at the far right of the diagram), calcite decomposes by the reaction:

$$CaCO_3 \rightleftarrows CaO + CO_2\uparrow$$

However, the addition of SiO_2 (quartz) to the system, resulting in the system CaO-SiO_2–CO_2, produces a large stability field for wollastonite, $CaSiO_3$, on account of the reaction:

$$CaCO_3 \rightleftarrows SiO_2 + CaSiO_3 + CO_2\uparrow$$

Consequently, $CaCO_3$ reacts at much lower temperatures in the presence of SiO_2 than in the simple system CaO–CO_2 (Fig. 11.16b). The diagrams shown in Fig. 11.16 are used in metamorphic petrology to evaluate mineral stabilities as a function of increasing temperature and pressure.

To evaluate the *P–T* conditions that metamorphic rocks may have undergone, composite *P–T* diagrams with stability curves for several minerals or mineral assemblages are used (Fig. 11.17). The stability curves for Al_2SiO_5 and for muscovite + quartz ⇄ K-feldspar + sillimanite + H_2O are especially relevant to metamorphic rocks with high Al_2O_3 contents relative to other components, such as CaO, MgO, and FeO. Shales with abundant clay minerals have relatively high Al_2O_3 contents, and during metamorphism, mineral

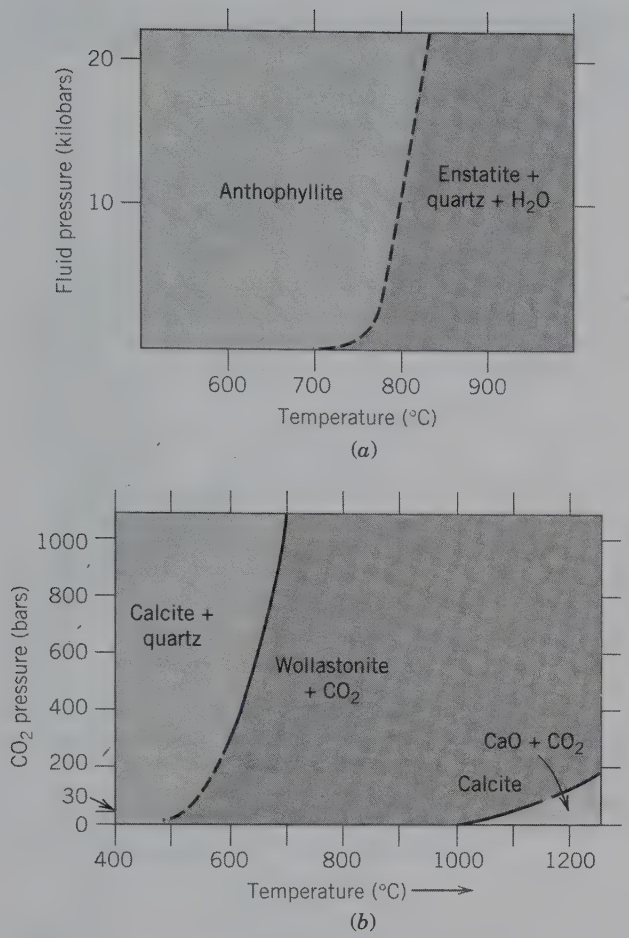

FIG. 11.16 (a) Schematic *P–T* diagram for the system $MgO–SiO_2–H_2O$. The stability fields of anthophyllite, $Mg_7Si_8O_{22}(OH)_2$, and reaction products, enstatite, $MgSiO_3$ + quartz + H_2O are shown. (After Greenwood, H. J. 1963. *Journal of Petrology* 4: 325.) (b) *P–T* diagram for the system $CaO–SiO_2–CO_2$, showing the stability fields of calcite in the presence of SiO_2, and without SiO_2 in the assemblage. (Modified from *Petrologic Phase Equilibria*, 21st ed. Fig. 6.14a, by W. G. Ernst. Copyright © 1976 by W. H. Freeman and Company. Reprinted by permission.)

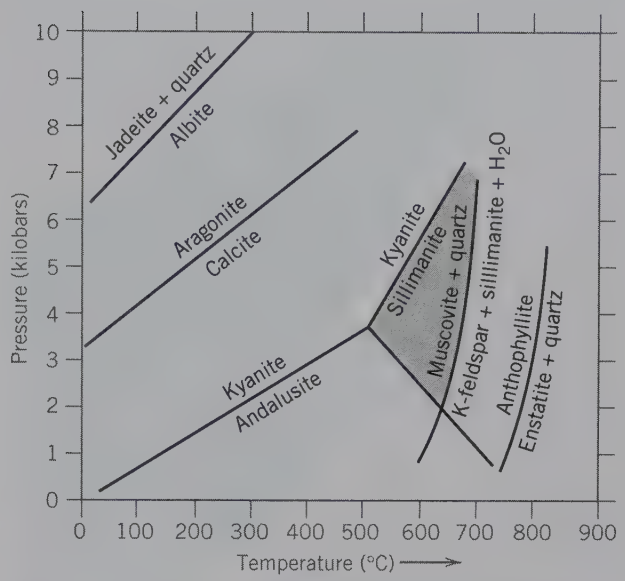

FIG. 11.17 Reaction curves for some common metamorphic minerals. Coexisting minerals are represented by the shaded area. See the text for details.

reactions take place in the shale. The metamorphic equivalents of shales may contain abundant sillimanite, muscovite, and quartz. Because many of these minerals have restricted stability fields, the *P–T* condition of the resulting rock can be estimated by the overlap in *P–T* stability regions (as shown by the shaded area in Fig. 11.17). In metamorphic rocks that may have undergone very high pressures, the original albite may have reacted to form jadeite + quartz, and any original calcite may have transformed to aragonite. The presence of jadeite + quartz, for example, would indicate a minimum pressure during metamorphism of about 10 kb at 300°C (see upper-left curve in Fig. 11.17).

Eh–pH Diagrams

Although mineral stability diagrams as previously discussed can be used to represent mineral assemblages that formed at low temperatures (essentially room temperature; 25°C) and low pressure (atmospheric pressure), it is often useful to express the stability fields of low temperature phases or minerals in terms of Eh (oxidation potential) and pH (the negative logarithm of the hydrogen ion concentration). Recall that acidic conditions have pH = 0–7, basic conditions have pH = 7–14, and neutral solutions have pH = 7 at 25°C, 1 bar. The construction of such diagrams, on the basis of thermodynamic parameters, is outlined in Garrels and Christ (1965; see the reference list at the end of this chapter). Using thermodynamic data for minerals and fluids, stability fields for various minerals can be calculated.

One such diagram (Fig. 11.18) displays the stability fields of some iron oxides and iron sulfides as calculated for atmospheric conditions (25°C, 1 atmosphere pressure). The large region of hematite stability is in an oxidizing region (high Eh) across a wide range of pH values. In hematite, Fe_2O_3, all iron is present in the oxidized, trivalent state (Fe^{3+}). Magnetite, on the other hand, is stable under more reducing conditions and a lower Eh. Magnetite, Fe_3O_4, which can be rewritten as $FeO{\cdot}Fe_2O_3$, consists of $1/3Fe^{2+}$ and $2/3Fe^{3+}$. The two sulfides, pyrite and pyrrhotite, occur under reducing conditions and pH values between 4 and 9. In both of these, the oxidation state of iron is Fe^{2+}. Along the boundaries that separate the various mineral fields, two

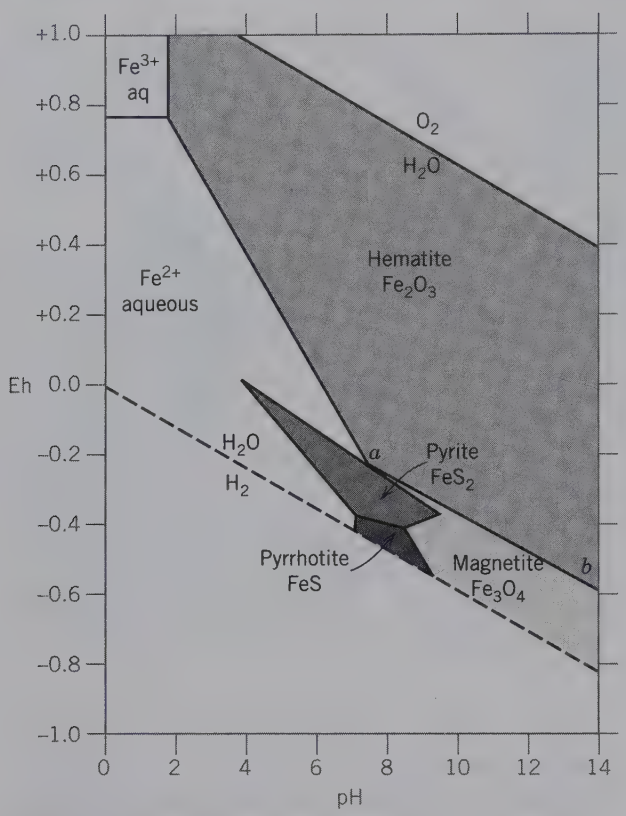

FIG. 11.18 Stability fields of iron oxides and iron sulfides in water at 25°C and 1 atm total pressure, with an activity of total dissolved sulfur = 10^{-6}. The pyrrhotite field is calculated on the basis of the formula FeS in this diagram; more correctly it would be $Fe_{1-x}S$. (Adapted from Garrels, R. M. and C. L. Christ. 1965. *Solutions, minerals, and equilibria.* Freeman, Cooper and Co., San Francisco, Fig. 7.20.)

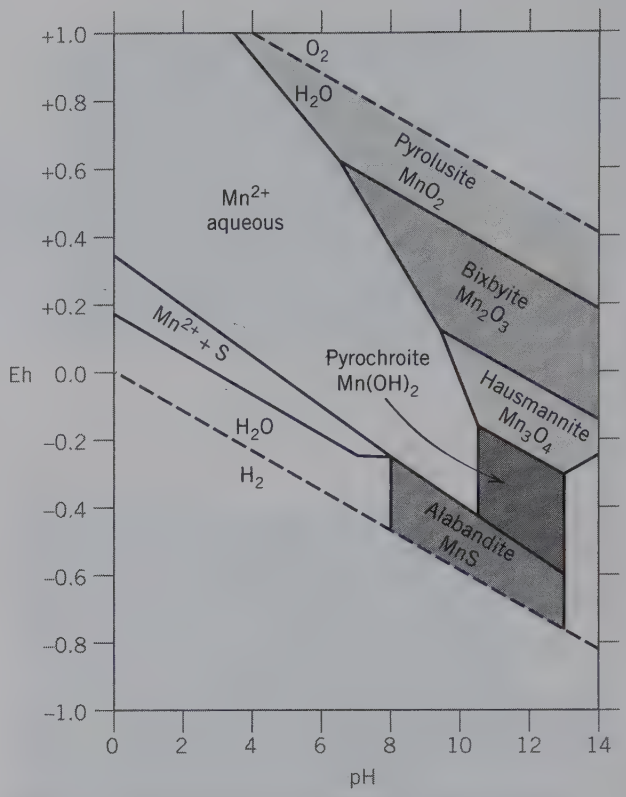

FIG. 11.19 Stability fields of manganese oxides, hydroxide, and sulfide in water at 25°C and 1 atm total pressure, with activity of total dissolved sulfur = 10^{-1}. (Adapted from Runnels, D. D. 1962. in H. H. Schmitt, ed., *Equilibrium diagrams for minerals at low temperatures and pressure.* Geology Club of Harvard, Cambridge, Massachusetts. 199)

of the minerals can coexist in equilibrium. For example, hematite and magnetite can coexist under conditions of variable pH and Eh (line *ab*, Fig. 11.18); indeed, hematite and magnetite occur together in Precambrian iron formations. On the basis of this assemblage, one may be able to evaluate the Eh and pH of the original sedimentary basin in which such Fe-rich minerals were deposited. Diagrams of this type are especially useful in evaluating some of the physical-chemical parameters that prevail during conditions of atmospheric weathering and of chemical sedimentation and alteration of water-laid sediments. The size of the fields for pyrite and pyrrhotite depends on the amount of sulfur in solution. If sulfur were lower and the CO_2 content high, there would be a stability field of siderite, $FeCO_3$, instead.

The stability fields of three manganese oxides, one manganese hydroxide, and one manganese sulfide are shown in Fig. 11.19 as a function of Eh-pH. Here, the most oxidized mineral is stable at the highest Eh values. Pyrolusite, MnO_2, is the most oxidized naturally occurring oxide, with all Mn in the Mn^{4+} state. Bixbyite, Mn_2O_3, with all Mn in the Mn^{3+} state, is stable over a slightly less highly oxidizing Eh range. Hausmannite, Mn_3O_4, which can be rewritten as $MnO{\cdot}Mn_2O_3$, contains $1/3Mn^{2+}$ and $2/3Mn^{3+}$. As a consequence, it is stable at Eh values below bixbyite. In $Mn(OH)_2$ and MnS, both of which show stability fields at the bottom of the Eh scale, Mn is present at Mn^{2+}. This type of diagram is useful not only in the prediction of what Mn-rich minerals may precipitate from an Mn-rich system at atmospheric conditions, but also for the interpretation of the conditions of formation of naturally occurring Mn compounds in manganese formations.

There are many other types of stability diagrams that can be used to portray mineral assemblages. Those discussed previously provide a small sample of the types of diagrams that are commonly used.

REFERENCES AND FURTHER READING

Bohlen, S. R., A. Montana, and D. M. Kerrick. 1991. Precise determinations of the equilibria kyanite ⇄ sillimanite and kyanite ⇄ andalusite and a revised triple point for Al_2SiO_5 polymorphs. *American Mineralogist* 76: 677–80.

Bowen, N. L. 1913. The melting phenomena of the plagioclase feldspars. *American Journal of Science* 34: 577–99.

Bowers, T. S., K. J. Jackson, and H. C. Helgeson. 1984. *Equilibrium activity diagrams for coexisting minerals and aqueous solutions at pressure and temperatures up to 5 kb and 600 °C.* Springer-Verlag, New York.

Brookins, D. G. 1988. *Eh-pH diagrams for geochemistry.* Springer-Verlag, New York.

Chatterjee, N. D. 1991. *Applied mineralogical thermodynamics.* Springer-Verlag, Berlin.

Chopin, C. 1984. Coesite and pure pyrope of the Western Alps: A first record and some consequences. *Contributions to Mineralogy and Petrology* 86: 107–18.

Denbigh, K. 1981. *The principles of chemical equilibrium.* 4th ed. Cambridge University Press, New York.

Ehlers, E. G. 1972. *The interpretations of geological phase diagrams.* W. H. Freeman, San Francisco.

Ernst, W. G. 1976. *Petrologic phase equilibria.* W. H. Freeman, San Francisco.

Garrels, R. M., and C. L. Christ. 1965. *Solutions, minerals, and equilibria.* Freeman, Cooper and Co., San Francisco.

Holdaway, M. J. 1971. Stability of andalusite and the aluminum silicate phase diagram. *American Journal of Science* 271: 97–131.

Kern, R., and A. Weisbrod. 1967. *Thermodynamics for geologists.* Freeman, Cooper and Co., San Francisco.

Liu, L., and W. A. Bassett. 1986. *Elements, oxides, silicates: High-pressure phases with implications for the Earth's interior.* Oxford University Press, New York.

Mitchell, R. H. 1986. *Kimberlites: Mineralogy, geochemistry and petrology.* Plenum Press, New York.

Nordstrom, D. K., and J. L. Munoz. 1994. *Geochemical thermodynamics.* 2nd ed. Blackwell Scientific Publications, Inc. Cambridge, Massachusetts.

Ottonello, G. 1997. *Principles of geochemistry.* Columbia University Press, New York.

Putnis, A. 1992. *Introduction to mineral sciences.* Cambridge University Press, New York.

Ribbe, P. H. 1975. The chemistry, structure, and nomenclature of feldspar. *Feldspar Mineralogy, Reviews in Mineralogy 2.* Mineralogical Society of America, Washington, D.C.

Shutong, X. A. I. Okay, J. Shouyuan, A. M. C. Sengör, S. Wen, L. Yican, and J. Laili. 1992. Diamond from the Dabie Shan metamorphic rocks and its implication for tectonic setting. *Science* 256:80–82.

Silica: Physical behavior, geochemistry, and materials applications. 1994. Edited by P. J. Heaney, C. T. Prewitt, and G. V. Gibbs. *Reviews in Mineralogy* 29, Mineralogical Society of America, Washington, D.C.

Smith, J. V., and W. L. Brown. 1988. *Feldspar minerals.* Vol. 1, *Crystal structures, physical, chemical, and microtextural properties.* Springer-Verlag, New York.

Ultrahigh-pressure mineralogy: Physics and chemistry of the Earth's deep interior. 1998. Edited by R. J. Hemley. *Reviews in Mineralogy* 34, Mineralogical Society of America, Washington, D.C.

CHAPTER 12

Post-Crystallization Processes in Minerals

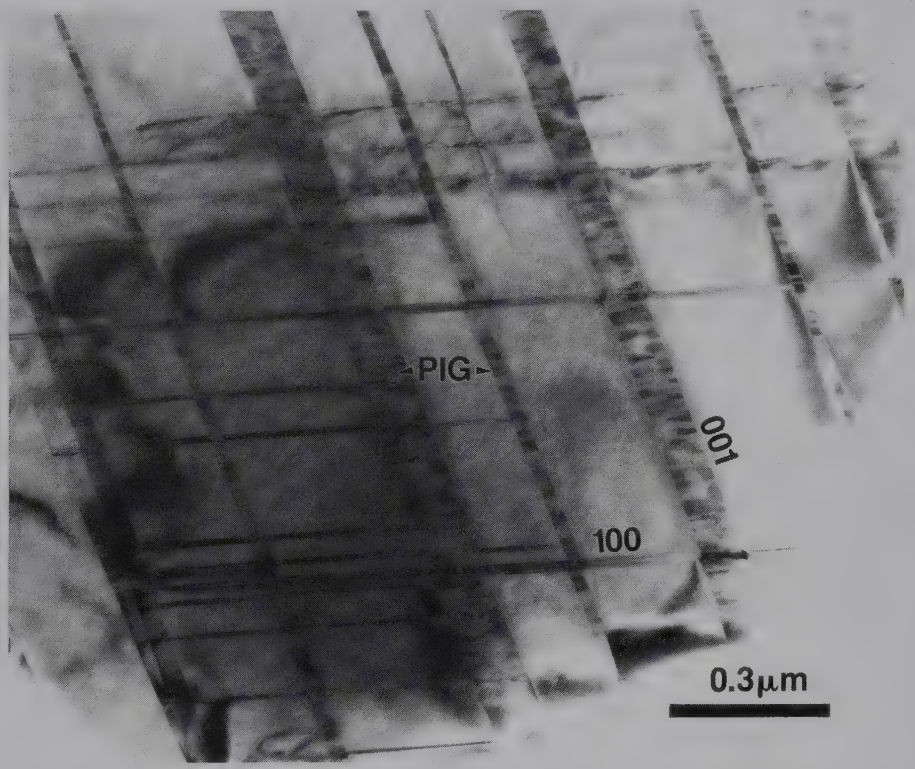

Exsolution texture in a pyroxene as shown by transmission electron microscopy (TEM). The matrix (the homogeneous, light-colored oblique blocks) are made up of augite (a monoclinic pyroxene with space groups $C^2/_c$) and the mottled lamellae are made up of pigeonite (a monoclinic pyroxene with space group $P^2/_c$). Subsequent to crystallization from a melt, already in the solid state (at a temperature of about 1100°C), none of this texture existed. The whole crystal at that temperature was homogeneous, without the grid pattern. This texture developed at about 950°C as a result of exsolution (a process involving diffusion) in the solid state. This is part of a silicate-rich meteorite (of basaltic composition), named Zagami, that was observed to have fallen on October 3, 1962, in Zagami Rock, Nigeria. Scale is in micrometers, μm. (Brearley, A. J. 1991. Subsolidus microstructures and cooling history of pyroxenes in the Zagami Shergottite, Abstract, Lunar and planetary science *XXII, Houston, Texas, 135–137. Photograph courtesy of Adrian Brearley, University of New Mexico, Albuquerque).*

Subsequent to crystal growth, dynamic processes may occur that alter previously formed minerals. In response to changes in external conditions, such as temperature, pressure, or chemical environment, the original stable mineral may undergo structural transformations in the solid state. In some minerals, self-irradiation destroys their periodic structure. These post-crystallization processes reflect the newly imposed conditions. This chapter focuses on these processes, their causal conditions, and the use of such features to interpret the geologic history of a mineral.

An important objective in the study of minerals is the deduction of the processes that they have undergone as a result of their geologic past. Such processes may have involved changes in temperature or pressure, or both, as well as changes in their chemical environments. For instance, in the discussion of solid solution in minerals (in Chapter 5), it was noted that an increase in temperature commonly leads to an increase in the extent of solid solution. Conversely, a decrease in temperature applied to a crystal structure may reduce the extent of solid solution that a structure can tolerate. This may lead to a process in which an initially homogeneous mineral separates into domains (or regions) that are different in composition from the original homogeneous mineral. Although almost all minerals show highly ordered internal atomic structures, some, due to internal "self irradiation" or external irradiation by radioactive elements, become partially or wholly amorphous. These post-crystallization changes will be discussed under the headings of polymorphic reactions, secondary twinning, exsolution, metamictization, and pseudomorphism.

POLYMORPHIC REACTIONS

Some chemical compounds can exist in more than one structural or atomic arrangement, even though their chemical composition does not change.

The ability of a specific chemical substance to occur with more than one type of structure (as a function of changes in temperature, pressure, or both) is known as **polymorphism** (from the Greek word meaning "many forms"). The various structures of such a chemical element or compound are known as **polymorphs.**

Examples of minerals and their polymorphs include diamond and graphite, which are both made of C, sillimanite-andalusite-kyanite, which are composed of Al_2SiO_5, and several others given in Table 12.1. The stability fields of polymorphs can be outlined in *P–T* diagrams, and these can be used to decipher the conditions under which they formed. The stability regions of various polymorphs, in terms of temperature (*T*) and pressure (*P*), for the chemical systems SiO_2 and H_2O are illustrated in Fig. 12.1. (Fig. 11.4 shows additional diagrams for other polymorphic systems.)

The reason why a constant chemical composition may have different structural arrangements is the tendency of a crystal structure to minimize its internal energy. Some structural configurations represent greater (or lesser) internal (structural) energies (*E*) than others. The relative internal energy of a specific polymorph is a function of temperature, pressure, or both. A higher internal energy, as a function of increasing temperature, is caused by higher frequencies of atomic vibrations. In some cases, there are abrupt differences in the relative internal energy levels of different polymorphs as a function of temperature (Fig. 12.2a). In Fig. 12.2a, the polymorphs are represented by three structures that are completely different from each other, and there is a discrete energy change in going from one form to the other. In contrast, the behavior displayed in Fig. 12.2b shows a continuous increase in the internal energy in going from one form to the next, as a function of increasing temperature. Pressure also can be a major driving force in polymorphic transformations. Increasing pressure favors the development of structural arrangements that result in an increase in the density of atomic packing [as reflected in increased density (*D*), or specific gravity (*G*)], and a decrease in molar volume (see Chapter 2). This is shown in Fig. 12.2c,

Table 12.1 Examples of Polymorphous Minerals

Composition	Mineral Name	Crystal System and Space Group	Hardness	Specific Gravity
C	Diamond	Isometric–$Fd3m$	10	3.52
	Graphite	Hexagonal–$P6_3/mmc$	1	2.23
FeS_2	Pyrite	Isometric–$Pa3$	6	5.02
	Marcasite	Orthorhombic–$Pnnm$	6	4.89
$CaCO_3$	Calcite	Rhombohedral–$R\bar{3}c$	3	2.71
	Aragonite	Orthorhombic–$Pnam$	$3\frac{1}{2}$	2.94
SiO_2	Low quartz	Hexagonal–$P3_121$	7	2.65
	High quartz	Hexagonal–$P6_222$		2.53
	High tridymite	Hexagonal–$P6_3/mmc$	7	2.20
	Low tridymite	Orthorhombic–$C222_1$		2.26
	High cristobalite	Isometric–$Fd3m$	$6\frac{1}{2}$	2.20
	Low cristobalite	Tetragonal–$P4_12_12$		2.32
	Coesite	Monoclinic–$C2/c$	$7\frac{1}{2}$	3.01
	Stishovite	Tetragonal–$P4_2/mnm$		4.30

Crystal systems and space group notation are discussed in Chapters 6 and 7, respectively.

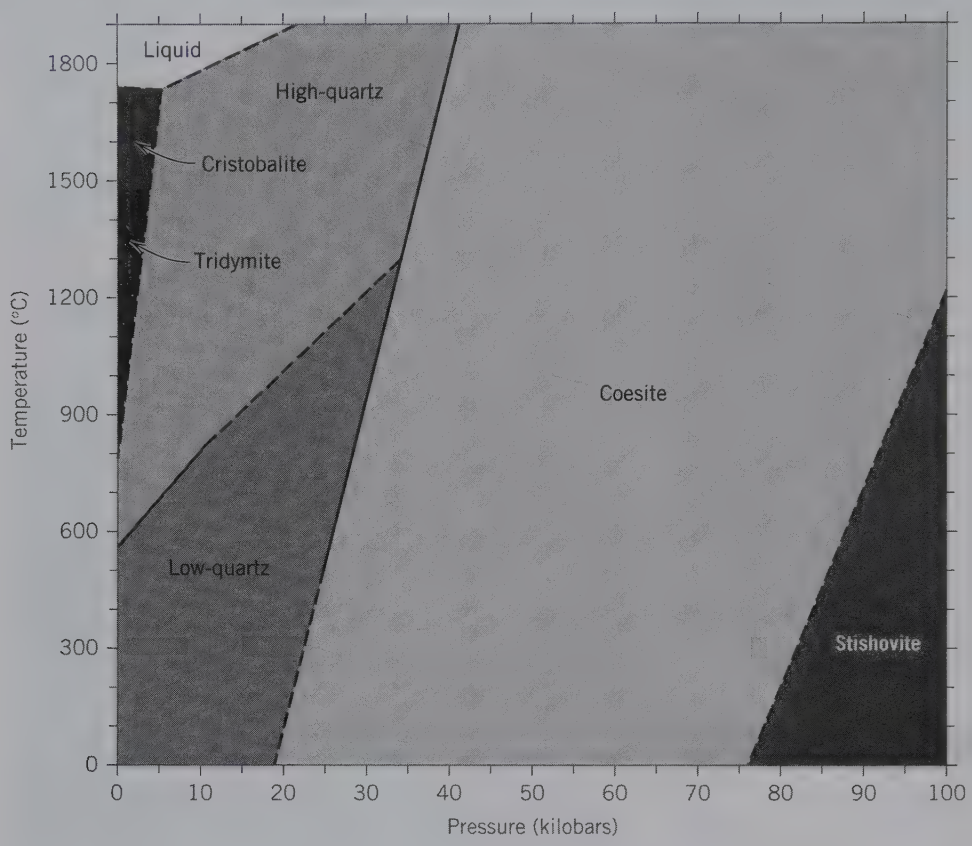

(*a*)

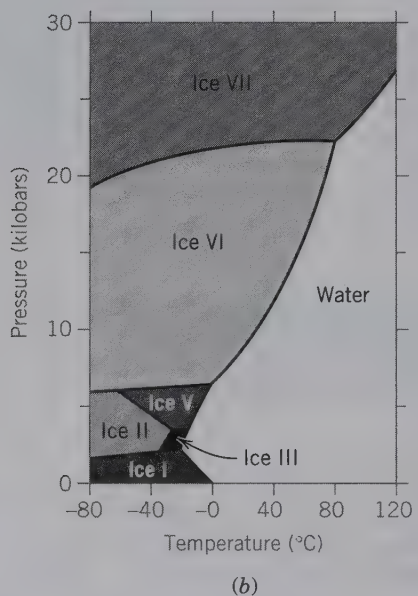

(*b*)

FIG. 12.1 (a) Stability relations of the SiO_2 polymorphs. Pressure is expressed in kilobars (kb) = 1,000 bars, where 1 bar = 0.987 atmosphere. (b) *P–T* diagram for H_2O. Six polymorphic types of ice are indicated by I, II, III, V, VI, and VII. (After Bridgman, P. W. 1935. *Journal of Chemical Physics* 5:965, and *Phase Diagrams for Ceramists*, copyright 1964 by the American Ceramic Society.)

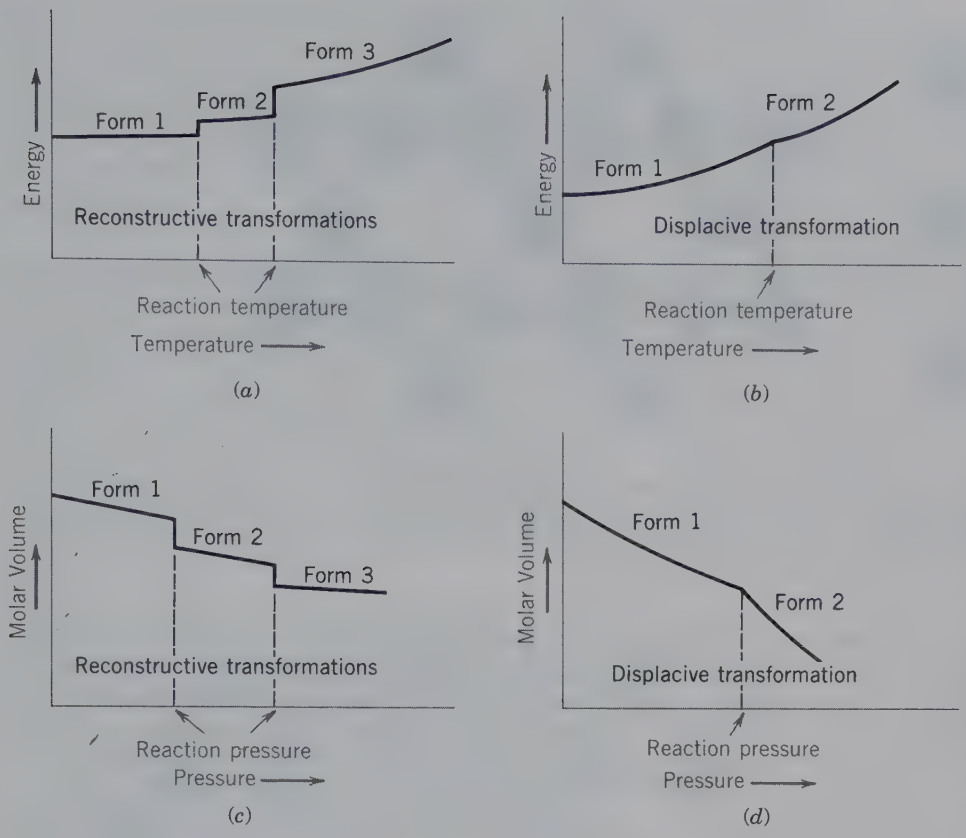

FIG. 12.2 Variation in internal energy (E) as a function of temperature for (a) three reconstructive polymorphs and (b) two displacive polymorphic forms. (Adapted from Buerger, M. J. 1961. Polymorphism and phase transformations, *Fortschritte Mineralogie* 39:9–14.) (c) Variation in molar volume as a function of pressure for three reconstructive polymorphs, and (d) for two displacive polymorphic forms.

where there are abrupt discontinuities in the molar volume values of three different structure types; in Fig. 12.2d, however, there are no discontinuities but the *slopes* of the molar volumes are discontinuous.

Three major types of mechanisms are recognized by which one polymorph of a mineral transforms into another. These are: **reconstructive, displacive**, and **order-disorder polymorphism**. (Each of these is illustrated with animations in module I of the CD-ROM under the heading "Polymorphism.")

RECONSTRUCTIVE POLYMORPHISM

A **reconstructive** polymorphic reaction involves the breaking of atomic bonds and a reassembly of the structural units into a different arrangement (Fig. 12.3). This type of transformation requires a large amount of energy, is not readily reversed, and proceeds sluggishly. Therefore, one polymorph may exist metastably in the stability field of another. An example of a reconstructive polymorphic reaction involves the change from tridymite or cristobalite to low quartz. All three are polymorphs of SiO_2. Cristobalite and tridymite are formed at high temperatures and relatively low pressures (Fig. 12.1a), such as in SiO_2-rich lava flows. Their high-temperature origin is manifest by their specific gravity values (ranging from 2.20 to 2.32 gm/cm^3), which are much lower than those of other SiO_2 polymorphs (Table 12.1). A high activation energy is needed to break bonds and transform the cristobalite (or tridymite) SiO_2 framework into the arrangement of the low quartz structure. Although cristobalite and tridymite are metastable under atmospheric conditions, both minerals are still abundantly present in very old terrestrial volcanic flows as well as in Precambrian lunar rocks.

The persistence of metastable minerals testifies to the fact that high energy is required to activate a reconstructive polymorphic transformation. Coesite and stishovite are forms of SiO_2 that are stable at high to very high pressures (Fig. 12.1a). Coesite and stishovite both occur in meteorite impact craters, such as Meteor Crater in Arizona, USA. Coesite is also found in kimberlites, which are high pressure host rocks for diamond and originate in the upper part of the Earth's mantle. High-pressure SiO_2 polymorphs are more densely packed and have higher specific gravities than other SiO_2 forms (Table 12.1). On an atomic level, stishovite is unusually densely packed for a silicate structure; here, Si is in 6-fold (octahedral) coordination, whereas all other SiO_2 polymorphs contain Si in tetrahedral coordination.

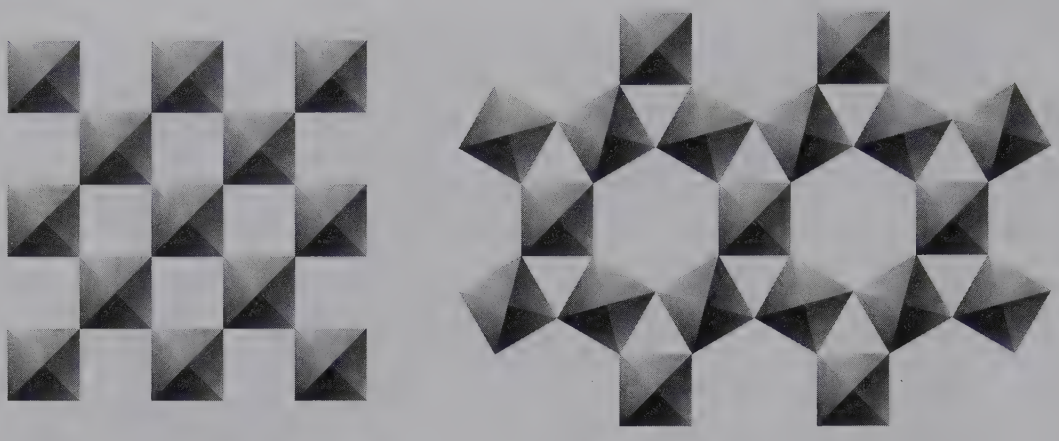

FIG. 12.3 Schematic representation of reconstructive polymorphism. The transformation of a hypothetical structure (a) made of octahedral coordination polyhedra to (b) requires the breaking of bonds and complete rearrangement of the octahedral units. (Adapted from Buerger, M. J. 1961. Polymorphism and phase transformations, *Fortschritte Mineralogie* 39:9–14.)

The three reconstructive polymorphs of Al_2SiO_5 (kyanite, sillimanite, and andalusite) reflect changes in coordination numbers of one of the chemical elements in the formula. As discussed in Chapter 11, one Al in the structural formula of each polymorph is in octahedral coordination whereas the coordination of the other Al is variable (4-, 5-, or 6-fold) and determines which polymorph is formed. Because the energy required for the transformation from one to the other of these three Al_2SiO_5 polymorphs is high, rocks in the Earth's crust commonly contain more than one Al_2SiO_5 polymorph.

The importance of variable pressure regimes in the formation of reconstructive polymorphs is also

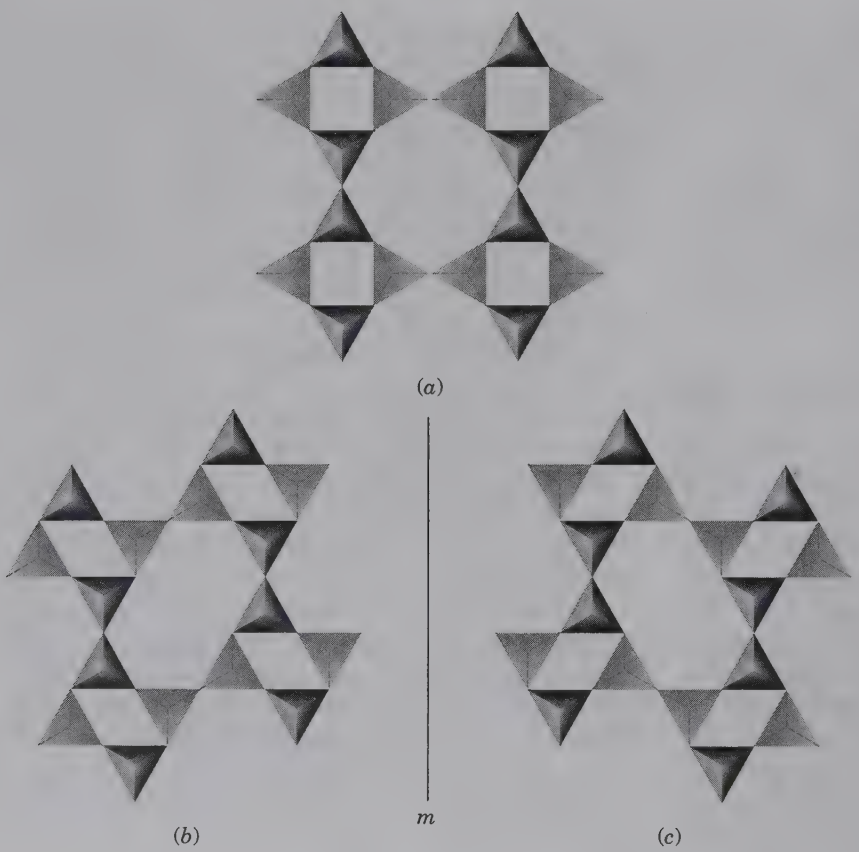

FIG. 12.4 Schematic representation of displacive polymorphism. (a) A hypothetical structure consisting of an infinite network of tetrahedra. It represents a fairly open atomic arrangement with relatively high symmetry. This would be the high-temperature polymorphic form. (b) The same infinite network of tetrahedra as shown in (a) but in a less symmetrical and somewhat collapsed (kinked) arrangement. This represents the lower temperature polymorph. The two oppositely kinked structures are mirror images of each other, with *m* representing the mirror.

seen in Fig. 12.1b. The stability fields of the various polymorphs of ice are strongly dependent on the pressure applied to the system H_2O. The differences between the structures of polymorphs for C, FeS_2, and $CaCO_3$ (Table 12.1) are such that extensive reworking and rearrangement of the structure is required for transformation.

DISPLACIVE POLYMORPHISM

In a **displacive** polymorphic transformation, only a slight displacement of atoms (or ions) and readjustment of bond angles ("kinking") between ions is needed. The structure is generally left completely intact and no bonds between ions are broken so that only a small amount of energy is required. This type of transformation occurs instantaneously and is easily reversible, that is, one polymorph can easily transform into another and vice versa.

Figure 12.4a is a schematic representation of a possible tetrahedral structure (with relatively high symmetry) kinking to produce two structural arrangements with lesser symmetry. These polymorphs may be related by a symmetry element, such as a twin plane (a mirror plane) as shown in Fig. 12.4b. A similar displacive transformation occurs when the high quartz form of SiO_2 is cooled to below 573°C (at atmospheric pressure; see also Fig. 12.1a) and instantaneously rearranges its structure to that of low quartz. The difference between the two forms of quartz is expressed by their space groups (high quartz, $P6_222$; low quartz, $P3_221$; for discussion of space groups, see Chapters 7 and 9) and shown in a basal projection of the SiO_2 framework for both forms (Fig. 12.5). The structural

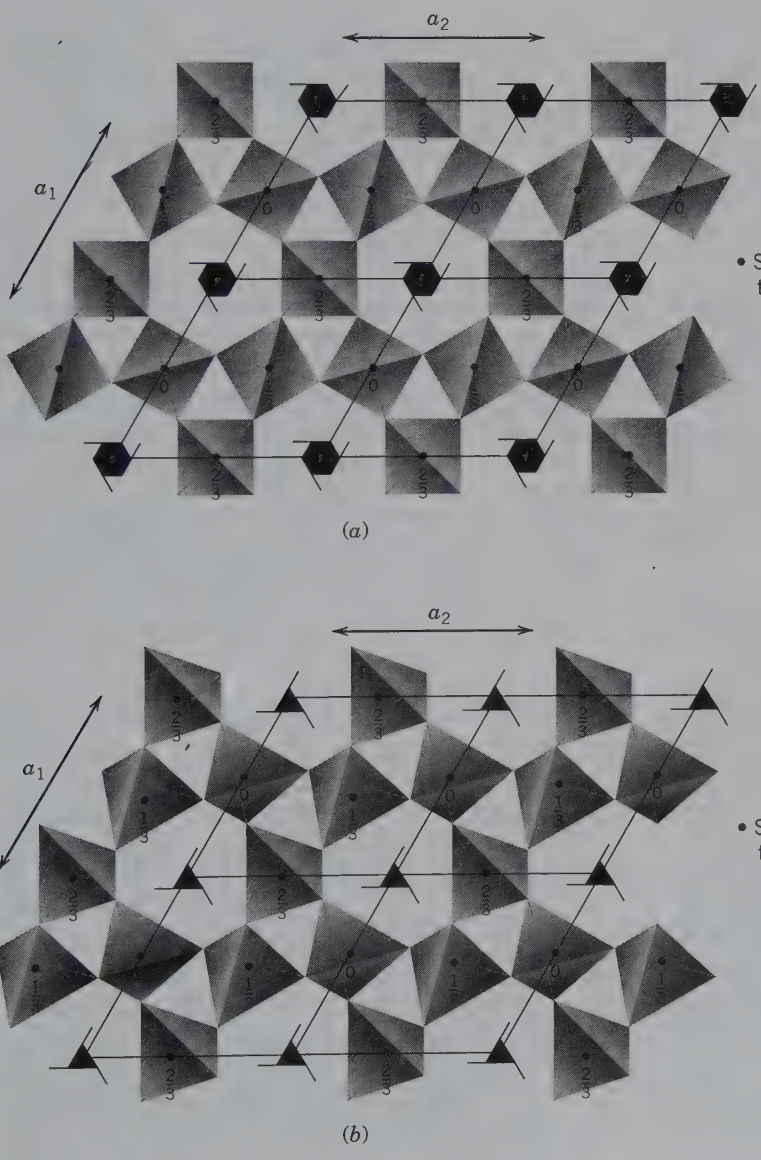

FIG. 12.5 (a) Projection of the tetrahedral SiO_2 framework of high quartz onto (0001). Four unit cells and the locations of six-fold screw axes (6_2) are shown. Fractional heights represent locations of centers (Si) of tetrahedra. (b) Projection of the tetrahedral SiO_2 framework of low quartz onto (0001). Four unit cells and the locations of three-fold screw axes (3_2) are shown. Fractional heights represent locations of centers (Si) of tetrahedra. These two figures illustrate a displacive transformation.

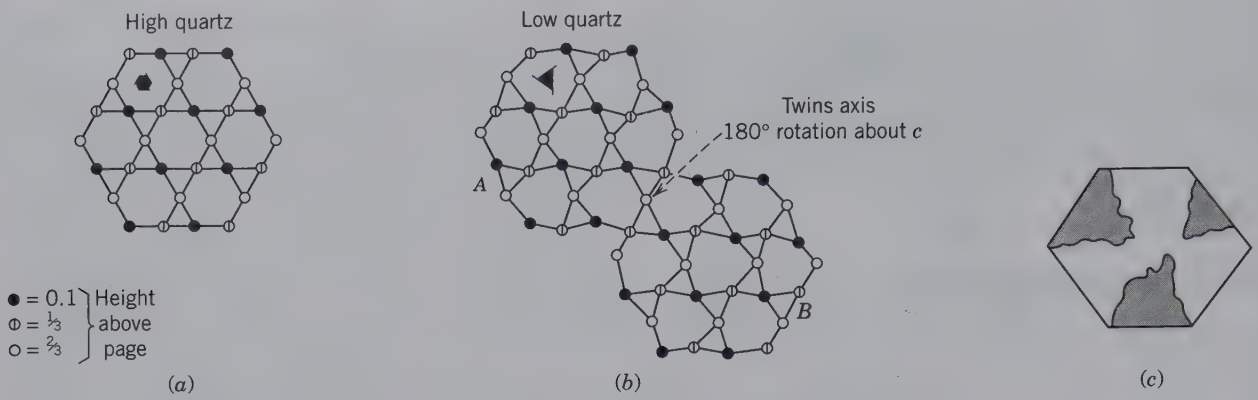

FIG. 12.6 (a) The distribution of silicon atoms in high quartz. The atomic positions are given in terms of thirds above the page. (b) A part of the low quartz structure (*A*) twinned with respect to another part (*B*) by a rotation axis of 180° perpendicular to the page. Note the presence of three-fold screw axes instead of six-fold screw axes as in high quartz. (c) The three-fold distribution of sectors of low quartz twinned according to the Dauphiné Law. The composition surfaces are generally irregular. This type of twin is visible only on sawed and etched basal sections of low quartz.

arrangement in the low-temperature form is slightly less symmetric and somewhat denser than in the high-temperature form. The transition from high to low quartz is the result of kinking or rotation of atomic bonds in the original high quartz structure.

Because the high-temperature form of quartz (high quartz) shows a higher symmetry (A_6) than the low-temperature form (A_3), twinning may result in the transition from high to low quartz. These *transformation twins* record the displacive transformation. They are known as *Dauphiné twins* (Fig. 12.6), and represent a megascopic expression of the presence of obversed and reversed units of structure in a low quartz crystal (see subsequent discussion entitled "Secondary Twinning").

ORDER-DISORDER POLYMORPHISM

A third type of polymorphism is referred to as an **order-disorder transformation**. Recall that *perfect order* in a mineral structure occurs only at absolute zero (0 Kelvin = −273.15°C). An increase in temperature disturbs a perfectly ordered structure, until at some high temperature, a totally disordered (random) state may occur (Fig. 12.7). As such, there is no definite transition point between perfect order and complete disorder; a continuum of structural states exists.

In a perfectly ordered crystal, the atoms are located in specific crystallographic sites of the structure. At high temperatures, close to but below the melting point of a mineral, atoms (or ions) tend to become disordered. Slow cooling of such a high temperature mineral allows the randomized ions (at high temperatures) to select specific sites in the structure and become more ordered as temperature decreases. Therefore, a mineral may exist in various states of disorder, of which a totally disordered and a perfectly ordered state are two extreme conditions. Figure 12.8a is a qualitative illustration of various degrees of disorder.

A more quantitative statement of order-disorder is shown in Fig. 12.8b. This shows a mineral of composition *AB* containing 50% of *A* and 50% of *B*, with *A* and *B* (both spheres) occupying two distinct sites. In a completely ordered state, atoms of *A* are arranged in a regular repeat with respect to *B* atoms (Fig. 12.8b-I). Atom *A* is always in structural site 1 and atom *B* in structural site 2. Two examples of intermediate disordered states for the atomic arrangement of such a mineral are shown in Figs. 12.8b-II and III. Here, the dis-

FIG. 12.7 The relationship of structural order and temperature. The higher the temperature the more disordered the distribution of atoms in specific structural sites. This would apply, for example, to the distribution of Al^{3+} versus Si^{4+} among tetrahedrally coordinated sites in the feldspar structure (see Fig. 12.9).

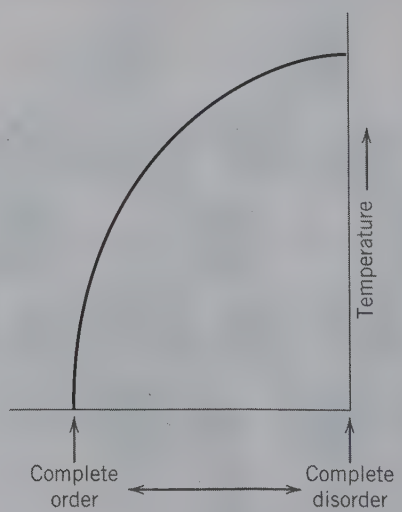

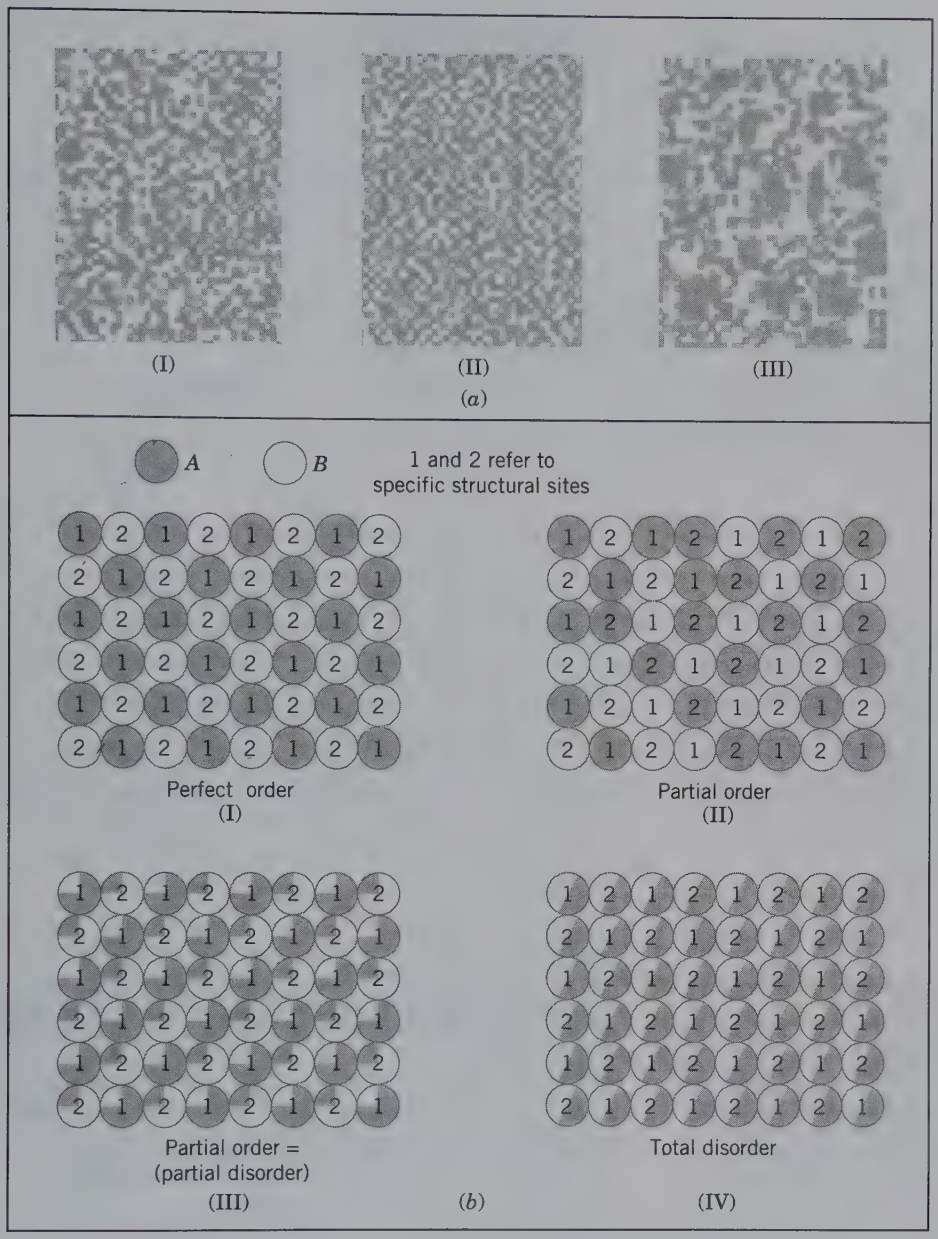

FIG. 12.8 (a) Distribution patterns of black-and-white squares. I: statistically random; II: somewhat less random, toward a chessboard-like pattern; III: more ordered with segregations of larger black-and-white domains. Shading represents percent occupancy by a constituent. (From Laves, F. reproduced in C. W. Correns. 1967. *Introduction to mineralogy.* Springer-Verlag, New York, 92. Original reference to Laves could not be located.) (b) Schematic illustration of order-disorder polymorphism in alloy *AB* (see the text for explanation).

tributions are not perfectly ordered but also not random. In Fig. 12.7b-II, the ratio $A:B$ is still 1:1, but the atoms A and B are in a partially disordered array. In Fig. 12.8b-III, out of every four No. 1 sites, three sites are occupied by A (on average) and one site is occupied by B (on average). The opposite holds for site No. 2. In other words, the probability ratio for site 1 being occupied by atoms of A rather than B is 3:1 (in Fig. 12.8b-III). A state of total disorder for the mineral AB is shown schematically in Fig. 12.8b-IV. Total disorder, on an atomic scale, implies equal probability of finding either A or B in a specific site in the structure (as shown by shading of half of the spheres). In other words, the probability of a given atomic site being occupied by one type of atom instead of another equals 1. This means that for a graphical representation, as in Fig. 12.8b-IV, each atomic position is indicated to represent A as well as B occupancy (in a statistical sense).

An example of order-disorder polymorphism in a mineral is shown by potassium feldspar ($KAlSi_3O_8$). This structure has four tetrahedral sites over which Al and Si are distributed. Al occupies a structural position identical with, and replacing Si in the mineral. The high-temperature form, sanidine, shows a disordered distribution of Al in the aluminosilicate framework. That is, there is an equal probability of finding the Al in any of the four tetrahedral sites (Fig. 12.9a). In contrast, the low-temperature form, microcline, shows an

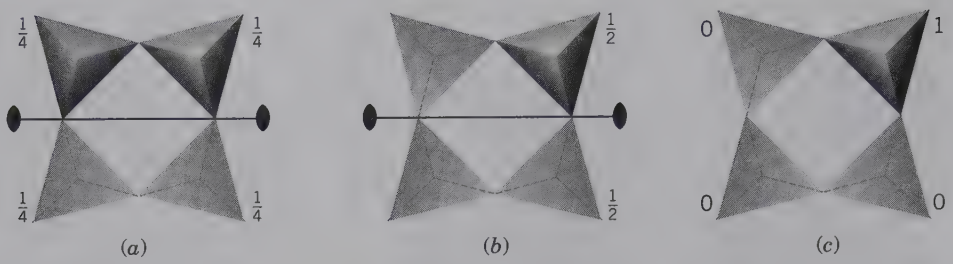

FIG. 12.9 Schematic representation of order-disorder of Al^{3+} and Si^{4+} in four linked tetrahedra that may be part of a tetrahedral framework structure (the composition of the ring is $AlSi_3O_8$.) (a) The probability of finding Al^{3+} is equal for all four tetrahedra, that is, $\frac{1}{4}$ Al is statistically distributed over the four tetrahedral sites (*total disorder*). This is compatible with a two-fold rotation axis as shown. (b) The Al-Si distribution is such that each of two tetrahedra (on average) contains $\frac{1}{4}$ Al, whereas the other two tetrahedra contain Si only. This *partial order* is still compatible with two-fold rotation symmetry. (c) All the Al (one Al^{3+} per ring) is concentrated in one tetrahedron. This is a state of *complete order*. The ring now has lost the two-fold rotation symmetry.

ordered distribution of Al in the aluminosilicate framework. Here, there is a 100% probability of finding the Al in only one of the four tetrahedral sites (Fig. 12.9c). States of intermediate order (also known as intermediate disorder) are present between that of high-temperature sanidine and low-temperature microcline (Fig. 12.9b). This type of transformation requires little energy and a more ordered structure tends to be more stable (less energetic) at lower temperature.

POLYTYPISM

A special kind of polymorphism, known as *polytypism*, occurs when two polymorphs differ only in the stacking of identical, two-dimensional sheets or layers. As a consequence, the unit cell dimensions parallel to the sheets will be identical in the two polytypes. However, the atomic spacings between the sheets (or layers) will be related to each other as multiples or submultiples.

Polytypism is a well-known feature of SiC, ZnS, the micas, and other layer silicates. The only difference between sphalerite, ZnS, and its polymorph wurtzite, ZnS, is that the S atoms in sphalerite are in cubic closest packing, whereas in wurtzite they are in hexagonal closest packed arrays. However, wurtzite shows extensive polytypism as reflected in *c* dimensions of the unit cell (the "thickness" of the basic ZnS layer is 3.12 Å). Examples of wurtzite polytypes and their *c* dimensions are 4*H*, 12.46 Å; 6*H*, 18.73 Å; 8*H*, 24.96 Å; and 10*H*, 31.20 Å (*H* refers to a hexagonal unit cell). The various Å dimensions show multiples of the basic unit along the *c* axis.

Micas and other layer silicates consist of infinitely extending tetrahedral silicate sheets [of composition $Si_2O_5(OH)$] that are stacked in various ways along the *c* axis. The inherent symmetry of such sheets is monoclinic. Because of the hexagonal symmetry about the (OH) group in the plan view of the $Si_2O_5(OH)$ tetrahedral sheets, there are six alternate directions (Fig. 12.10a) in which $Si_2O_5(OH)$ sheets can be stacked. These six directions can be represented by three vectors (1, 2, and 3, and opposite negative directions $\bar{1}$, $\bar{2}$, and $\bar{3}$) at 120° to each other. If the stacking of $Si_2O_5(OH)$ sheets is always in the same direction (Fig. 12.10b), the resulting structure will have monoclinic symmetry; this is referred to as the 1*M* (*M* = monoclinic) polytype with stacking sequence [1, 1, 1, . . .]. If the stacking sequence of $Si_2O_5(OH)$ sheets consists of alternating 1 and $\bar{1}$ directions (in opposing directions along the same vector), a structure results that is best described as orthorhombic. This stacking sequence can be expressed as [1, $\bar{1}$, 1, $\bar{1}$, . . .] and the polytype is known as 2*O* (*O* = orthorhombic). If the stacking sequence consists of two vectors at 60° to each other, that is [1, $\bar{2}$, 1, $\bar{2}$, . . .], another monoclinic polytype results; this is known as $2M_1$ (Fig. 12.10c). When stacking occurs along three vectors, such as in [1, 2, 3, . . .], a trigonal polytype, 3*T* (*T* = trigonal), results. (Extensive animations that illustrate these various polytype stackings are found in module I of the CD-ROM under the heading "Polytypism.")

Table 12.2 lists the stacking sequence, its rotation angle, the number of layer repeats, and the resulting repeat distance (along the vertical *c* axis), as well as the polytype symbol for six different stacking arrangements of sheet silicates. A polytype is represented by a *Ramsdell structure symbol* consisting of a number to indicate the number of layers in the repeating unit along the vertical (*c*) axis and letters to designate the resulting symmetry (*M* = monoclinic, *O* = orthorhombic, *T* = trigonal, *H* = hexagonal). Subscripts 1 and 2 are used to differentiate structures that have the same unit repeat and symmetry.

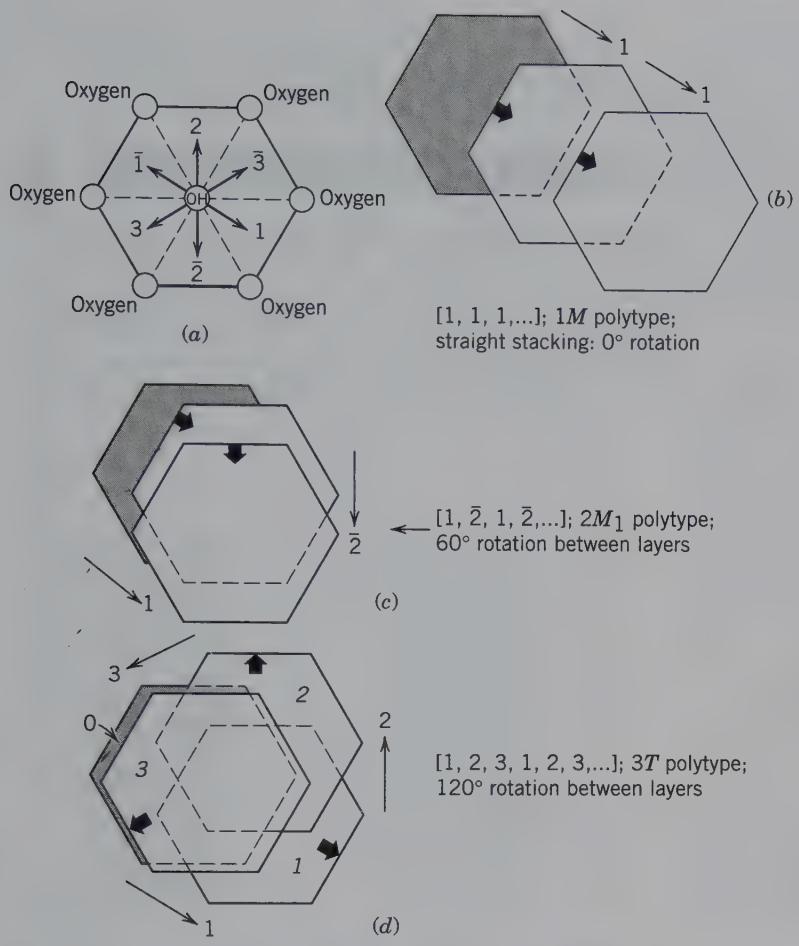

FIG. 12.10 Schematic illustration of some possible stacking polymorphs (*polytypes*) in mica. (a) Three vectorial directions for possible location of the (OH) group in an $Si_2O_5(OH)$ sheet that is stacked above or below the hexagonal ring shown. (b) Stacking of $Si_2O_5(OH)$ sheets in the same direction. (c) Stacking in two directions at 60° to each other. (d) Stacking in three directions at 120° to each other. Here, sheet 3 should lie directly above sheet 0 but is offset slightly for illustrative purposes.

SECONDARY TWINNING

Twinning also can occur in minerals in the solid state after growth of the crystals is complete (compare to twinning discussed in Chapter 10). **Transformation twinning** results when a crystal that formed at high temperature is cooled and, subsequently, rearranges its structure to a symmetry different from that of the high-temperature form (as in a polymorphic transition). For example, if high quartz is cooled below 573°C, it transforms to low quartz. The original high quartz structure (Fig. 12.6a) has a choice of two orientations, related by

Table 12.2 Aspects of Stacking in Sheet Silicates: the Vertical Dimension of the Layer in Such Structures is Approximately 10 Å.

Stacking sequence	[1, 1]	[1, $\bar{2}$]	[1, 2]	[1, $\bar{1}$]	[1, 2, 3]	[1, $\bar{3}$, 2, $\bar{1}$, 3, $\bar{2}$]
Layer rotation	0°	60°	120°	180°	120°	60°
Number of layers in the final repeat	1	2	2	2	3	6
Original layer thickness	10 Å	10 Å	10 Å	10 Å	10 Å	10 Å
Final repeat distance	10 Å	20 Å	20 Å	20 Å	30 Å	60 Å
Ramsdell symbol for polytype	1*M*	$2M_1$	$2M_2$	2*O*	3*T*	6*H*

(Based on Figure 6 in Hollocher, K. 1997. Building crystal structure ball models using pre-drilled templates: sheet structures, tridymite, and cristobalite. In *Teaching Mineralogy*, Mineralogical Society of America: 255–283.)

180° rotation, for the trigonal structural arrangement of low quartz (Fig. 12.6b; see also Figs. 12.4 and 12.5). The relationship of these two orientations is known as a *Dauphiné twin* and is expressed as a 180° rotation about the vertical *c* axis or about the direction identified as [0001]. If such a twin of low quartz is heated above 573°C, the Dauphiné twinning will disappear, and untwinned high quartz will form spontaneously. Figure 12.6c shows a basal section of low quartz with the three-fold distribution of the twinned orientations of low quartz.

Another example of transformation twinning is provided by $KAlSi_3O_8$, which occurs in three different structural forms: high-temperature sanidine (with monoclinic symmetry), lower-temperature orthoclase (also with monoclinic symmetry), and lowest-temperature microcline (with triclinic symmetry); refer back to "Polymorphism." Microcline invariably shows the microscopic twin pattern shown in Fig. 10.18, which is known as *microcline* or *"tartan" twinning*. The cross-hatched pattern consists of two types of twins, twinned according to the *albite* and *pericline* laws (see page 231) but is usually visible only between crossed polarizers of a microscope (see Chapter 13). This combination of twinned relations is a key feature in the symmetry change from monoclinic (as in sanidine) to triclinic (as in microcline). In this transition from a high temperature form, the mirror plane and the two-fold rotation axis are lost, leading to nucleation of triclinic "domains" that are related by twinning.

Deformation twinning is another type of *secondary twinning* and results when a crystal is deformed by the application of a mechanical stress. If the stress produces atomic slippage on a small scale, *gliding* (or *deformation*) *twins* may result (Fig. 12.11). If the movement of the atoms is large, slip or gliding may occur without twinning, which may finally lead to the rupture of the crystal. Deformation twinning is common in metals and is frequently present in metamorphosed limestones, as shown by the presence of polysynthetically twinned calcite (see Fig. 10.16c). Similarly, plagioclase feldspars from metamorphic terrains may show deformation twinning.

FIG. 12.11 Deformation twinning in an oblique lattice due to the application of mechanical stress as indicated by the arrows. Note that the amount of movement of the first layer above and parallel with the twin plane in (b) is less than that of the successive layers further removed from the twin plane.

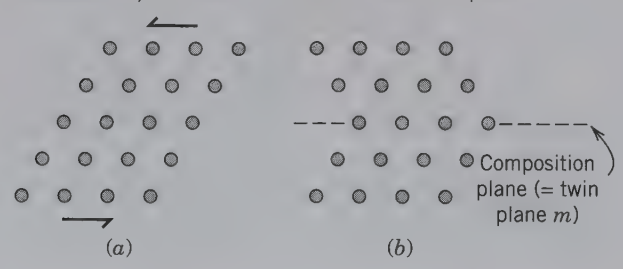

EXSOLUTION

Solid solution is a common phenomenon in many minerals (see Chapter 5) and its extent is a function of the size difference between substituting ions (or atoms) and the requirement of electrical neutrality. For ions (or atoms) that differ in size from each other by about 15%–30%, the amount of substitution is expected to be *limited* and, if their size difference is greater than 30%, it is *poor*. However, at elevated temperatures, mineral structures expand as the amplitudes of atomic vibrations increase. Previously distinct structural sites (at lower temperature) become more similar, and ultimately these sites become indistinguishable at high temperatures. This allows for greater substitution of ions with considerable size differences (e.g., in the *limited* to *poor* ranges) than could be incorporated at lower temperatures. This also allows for the interchange of ions between sites that were once distinct. This disorder produces an average chemical content that is the same for each structural site (Fig. 12.12a), which results in a homogeneous phase.

When an originally homogeneous high-temperature mineral containing ions of considerably different sizes cools, thermal vibrations decrease and the original structure becomes unstable (contains excess energy). This results in a structural reorganization in which exsolution occurs (Fig. 12.12b).

Exsolution is the process whereby an initially homogeneous solid solution separates into two (or possibly more) distinct crystalline minerals without the addition or removal of material to or from the system. This means that there is no change in the bulk composition.

Exsolution or "unmixing" of an originally homogeneous phase is analogous to the well-known phenomenon that occurs when a mixture of oil and vinegar (a vinaigrette) is made. The oil and vinegar are energetically shaken or stirred to produce a homogeneous, but cloudy, liquid suspension of very fine particles of both ingredients. When this mixture is allowed to rest, the original components will separate out (or unmix) and produce two clear liquids of the end members, oil and vinegar. A mineral undergoing exsolution behaves in a similar manner. Consider a homogeneous material containing elements *A* and *B* that have an equal probability of occurring in every site (Fig. 12.12a). During

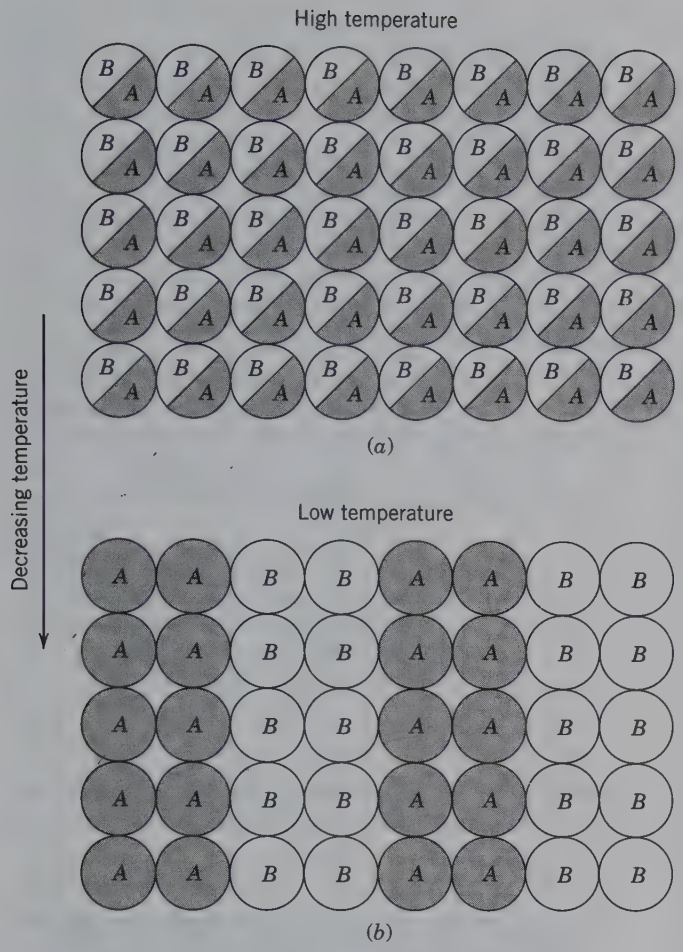

FIG. 12.12 (a) Schematic two-dimensional representation of elements *A* and *B* in a completely disordered array (at high temperature). (b) Separation of elements *A* and *B* to *A*-rich and *B*-rich regions = exsolution (at lower temperature).

exsolution, distinct regions of composition *A* and composition *B* are formed (Fig. 12.12b). In the case of minerals, exsolution generally, although not necessarily, occurs upon cooling.

The driving force for exsolution is the minimization of the free energy (*G*) in the crystal. Free energy (*G*) varies as a function of composition at constant *T*, as illustrated on a *G*–*X* diagram (Fig. 12.13, also refer to Chapter 11). For a limited solid solution at low temperatures, the free energy content of the homogeneous disordered compositional phase is much higher than that of the free energy of two exsolved minerals, whose compositions are marked as x_2 and x_3 on the compositional bar. As discussed in Chapter 11, Gibbs free energy (*G*) is defined as $G = E + PV - TS$, where E = internal energy, PV is a pressure-volume term (which for solids at 25°C and 1 bar is negligible compared to other thermodynamic quantities, see Chapter 11), and TS is a temperature-entropy term. *Exsolution* provides the mechanism for the decrease of the overall free energy of the crystal.

FIG. 12.13 Free energy (*G*)-composition curves illustrating the free energy changes during exsolution. The dashed line, which is tangential to the two minima in the free energy curves, gives the composition of the coexisting minerals at a specific temperature.

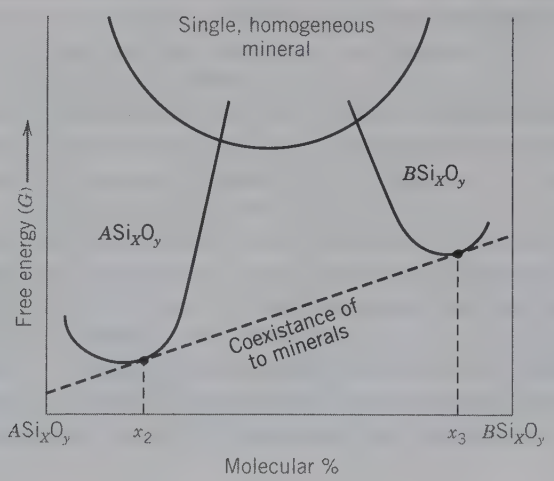

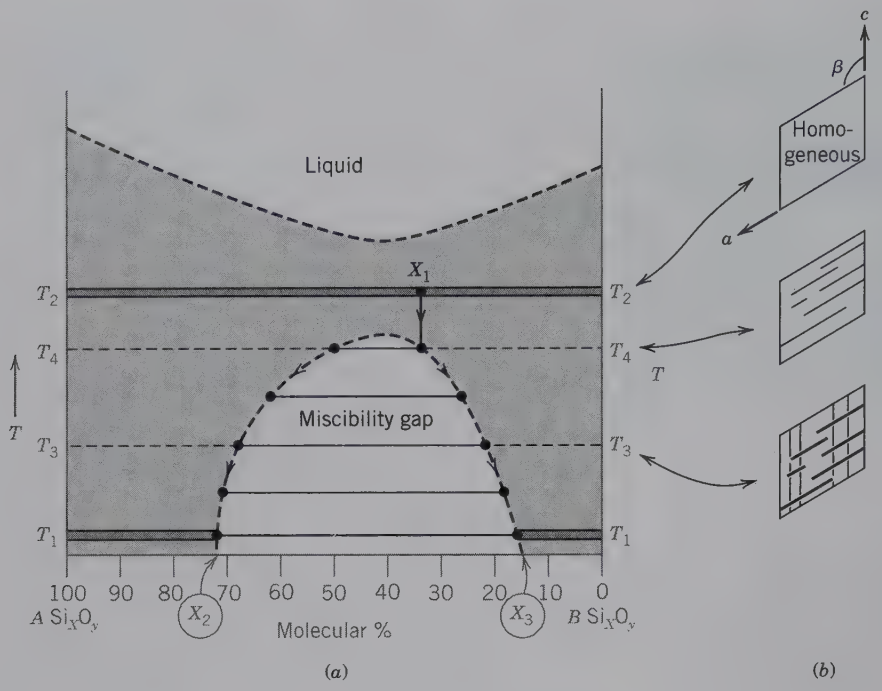

FIG. 12.14 (a) Schematic T–X (X = composition and is expressed as molecular or atomic %) diagram for hypothetical silicates ASi_xO_y and BSi_xO_y. At temperature T_2, a complete solid solution exists between the two end members. At lower temperatures, a miscibility gap occurs. The arrows along the edge of the gap indicate the change in compositions of the coexisting silicates with decreasing T. The process of exsolution is discussed in the text. (b) Cross-sections of mineral (with composition X_1 in Fig. 12.14a) illustrating the sequence of appearance of possible exsolution lamellae. (1) homogeneous, at T_2. (2) exsolution lamellae parallel to (001) at T_4. (3) additional set of exsolution lamellae parallel to (100) at T_3, and coarsened lamellae parallel to (001).

The products of exsolution are described with reference to a schematic temperature-composition (T–X) phase diagram in Fig. 12.14 (T–X phase diagrams are discussed in Chapter 11). The horizontal axis represents the compositional range between two possible silicates that are isostructural. The hypothetical silicates are monoclinic and are represented by the general formulas ASi_xO_y and BSi_xO_y (for pyroxene or amphibole groups, for example). The ionic sizes of A and B differ by about 25%. Based on data from laboratory experiments at low temperature, limited solid solution exists between the two end-members, as shown graphically by the low-temperature (T_1) composition bar (shaded region). At high temperature (T_2), data show the presence of a complete solid solution series (illustrated by shading in Fig. 12.14).

The region of reduced solid solution between T_2 and T_1 is outlined by the **miscibility gap** in the diagram (unshaded dome). This gap represents a region of immiscibility in temperature-composition space. For a specific composition (X_1), in the region above the miscibility gap at T_2, the structure of the silicate is in a high-energy state that allows accommodation of A and B (although these may differ by as much as 25% in ionic radius) in the same atomic sites. In other words, the A and B ions randomly occupy the various cationic sites in the structure (disorder; see Fig. 12.12a). Upon cooling of this mineral composition (X_1), the structure is unable to maintain a complete solid solution between A and B ions at temperature (T_4). Stresses in the structure resulting from the size discrepancy cause ions of A^+ to diffuse into regions with a preponderance of A^+; simultaneous B^+ ion diffusion results in silicate regions rich in B^+. This begins the process of *unmixing*; the original homogeneous mineral segregates into two chemically different minerals (Fig. 12.12b). The region of unmixing, represented by the miscibility gap, continually widens as the temperature is lowered from T_4 to T_1 and the structure becomes less tolerant of ionic size differences. For bulk compositions inside the region of immiscibility, two minerals of distinct composition coexist rather than one homogeneous phase. Under equilibrium conditions, the compositions of exsolution intergrowths that form as a result of decreasing temperature are shown by dots along the edge of the miscibility gap (solvus); coexisting compositional dots are joined by horizontal tielines.

On an atomic scale, the complex process of unmixing is one of atomic migration (diffusion). An increase in temperature (and an increase in kinetic energy) will increase the mobility of an atom (or ion) and its chances of breaking away from its neighbors and moving to a new position. This means that the diffusion rate is strongly dependent upon temperature. As the temperature is lowered, as in the unmixing process depicted in Fig. 12.14, the mobility of the atoms may become so limited that the original homogeneous mineral cannot split into the pure end-member compositions shown in

Fig. 12.12b. A composition may result that is a compromise between lowering the thermodynamic free energy of the system, and the decrease in the mobility of the atoms. The phase or assemblage of phases with the lowest free energy will be the most stable. In the exsolution process, the exsolved phases (the two or more minerals) have a much lower free energy than the original homogeneous, high-temperature and disordered composition (Fig. 12.13). Although the segregation of ions within the silicate structure (which began at T_4 in Fig. 12.14) is complex on an atomic level, it is due mainly to the inability of a single structure to house ions of disparate sizes in a random distribution when decreasing temperature lowers the energy of the crystal. (Illustrations of exsolution can be found in module I of the CD-ROM under the heading "Solid Solution Mechanisms: Exsolution.")

Exsolution typically produces fine **lamellae** of one or several minerals that are generally crystallographically oriented in the host phase (Fig. 12.15). Many of these exsolution features can be observed under a high-powered microscope when the scale of exsolution is about 1 μm (1 μm = 10^{-6} m). At the lowest temperature, T_1 (Fig. 12.14), it is typical to observe a coarse-grained, crystallographically well-oriented intergrowth of $(A,B)Si_xO_y$ lamellae with composition (X_2) in a host of $(B,A)Si_xO_y$ with specific composition (X_3). The schematic sequence of cross sections in Fig. 12.14b illustrates what may be seen under the microscope as a result of the exsolution processes depicted in Fig. 12.14a. An originally homogeneous crystal of composition X_1 develops sets of differently oriented exsolution lamellae between temperatures T_4 and T_3. These segregation (diffusion) processes all take place within the silicate structure in the solid state. The T–X diagram depicting this sequence of events (Fig. 12.14) is, therefore, in general referred to as a *subsolidus phase diagram*.

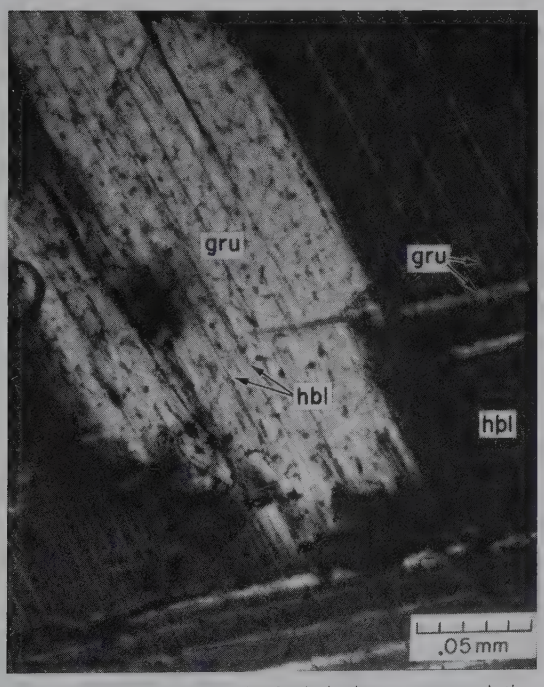

FIG. 12.15 Photomicrograph of relatively coarse exsolution lamellae of hornblende (hbl) in grunerite (gru) and grunerite lamellae in hornblende. The lamellae are oriented parallel to (001) and (100), respectively.

Although exsolution intergrowths are common in many mineral groups, the resulting textures are rarely visible in hand specimens. However, the alkali feldspars ($NaAlSi_3O_8$–$KAlSi_3O_8$) are an example where exsolution features may be seen with the naked eye. Na^+ (radius = 1.18 Å for **C.N.** = 8) and K^+ (radius = 1.51 Å for **C.N.** = 8; from Table 3.8) display complete solid solution (or miscibility) between the $NaAlSi_3O_8$ and $KAlSi_3O_8$ end members at high temperature, about 1000°C. However, at lower temperatures (about 600°C), Na-K have limited solid solution in the feldspar structure and exsolution results (see Fig. 11.7). In the alkali (Na-K) feldspar system, exsolution lamellae may be seen approximately parallel to {100}. Such coarse-grained intergrowths consist of Na-rich feldspar (typically white) lamellae exsolved from a K-rich host (salmon-colored); these are known as **perthite**. If exsolution is on such a scale that it can be resolved only microscopically, it is referred to as **microperthite** (see Fig. 19.77); and if X-ray diffraction techniques are needed to resolve extremely fine (submicroscopic) lamellae, the intergrowth is known as **cryptoperthite**.

The size of the exsolution lamellae is a good indicator of the cooling rate of the rock in which this intergrowth texture occurs. In slowly cooled rocks, more time is available for diffusion (and unmixing), and as a result, the exsolution texture may be coarser. In rocks that are cooled extremely quickly ("quenched"), the high-temperature, homogeneous, disordered mineral may be preserved, although in a metastable state. In a slightly slower but still rapidly cooling process, very fine exsolution textures may develop.

Exsolution phenomena and their resulting exsolution textures are common in many mineral systems: in the iron oxides, amphiboles, pyroxenes, and plagioclase feldspar series to name a few examples. An example of exsolution in amphiboles as viewed in a polarizing microscope is shown in Fig. 12.15. In amphiboles, the orientation of exsolved lamellae is commonly parallel to {001} and {100}. Examples of extremely fine ex-

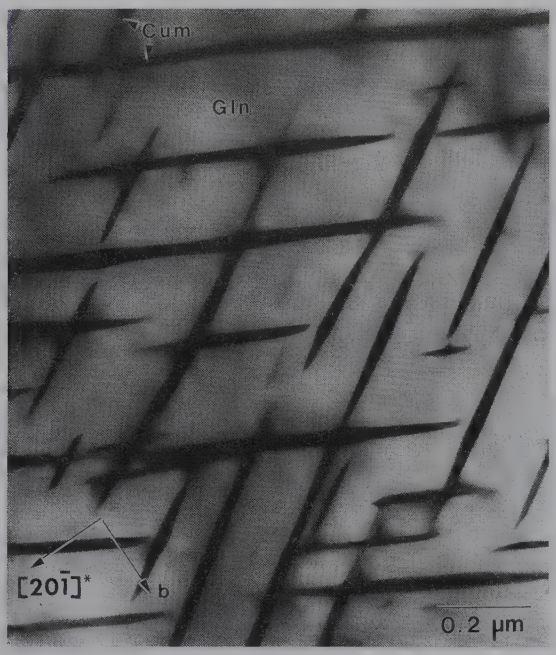

(*a*)

(*b*)

FIG. 12.16 (a) Bright-field transmission electron microscope (TEM) image of cummingtonite (cum) exsolution lamellae in a glaucophane (gln) host (both amphiboles). The narrow lamellae of cummingtonite occur in two symmetrically related orientations, nearly parallel to (28$\bar{1}$) and ($\overline{2}$8$\bar{1}$) of the glaucophane structure. These unusual orientations represent planes of best dimensional fit between the glaucophane and cummingtonite structures. This amphibole appeared perfectly homogeneous in the optical microscope and in the electron microprobe. (From Smelik, E. A. and D. R. Veblen. 1991. Exsolution of cummingtonite from glaucophane: A new direction for exsolution lamellae in clinoamphiboles. *American Mineralogist* 76: 971–84.) (b) HRTEM image showing a sodic pyroxene lamella (Napx) parallel to (100) in an augite matrix. (From Ottn, M. T. and P. R. Buseck. 1987. TEM study of the transformation of augite to sodic pyroxene in eclogitized ferrogabbro. *Contributions to Mineralogy and Petrology* 96: 529–38).

solution lamellae in amphiboles and pyroxenes are given in Fig. 12.16.

The pyroxene series exhibits exsolution as shown in the subsolidus section (Fig. 12.17; note that the solidus and/or liquidus surfaces are not even shown) across pyroxene compositional space as shown in Fig. 11.11. This temperature composition section shows the slight increase in solid solution at elevated temperatures in orthopyroxene, and the much larger solid solution field of augite at high temperatures. It also demonstrates that pigeonite is specifically a high-temperature phase region that must invert at about 1150°C to an orthopyroxene matrix with augite exsolution lamellae (due to the presence of the miscibility gap and the fact that the structure of pigeonite is different from that of orthopyroxene; see Fig. 12.17). Pigeonite occurs only in quickly cooled high-temperature basalts. If the basalt cooled slowly, the original pigeonite inverts to orthopyroxene with augite exsolution lamellae. See the opening photograph of this chapter for a TEM image of exsolution in the pyroxenes.

There are three broad miscibility gaps found within the plagioclase feldspar series (Fig. 12.18). The three regions have been named, in increasing An content, the *peristerite gap*, the *Bøggild intergrowth region*, and the *Huttenlocher intergrowth region*. These regions represent exsolution phenomena on an extremely fine scale. Exsolution lamellae are responsible for the *iridescence* (see Chapter 2) of plagioclase (called moonstone) as a result

FIG. 12.17 A temperature-composition section across the pyroxene compositional regions in the Wo (wollastonite)–En (enstatite)–Fs (ferrosilite) diagram; see Fig. 11.11. This section (labeled *A′A*) is at about $En_{65}Fs_{35}$ (see location as marked *A′A* in Fig. 11.11). A broad miscibility gap exists between orthopyroxene (opx) and augite (clinopyroxene = cpx) compositions. Pigeonite is stable only at high-temperature conditions.

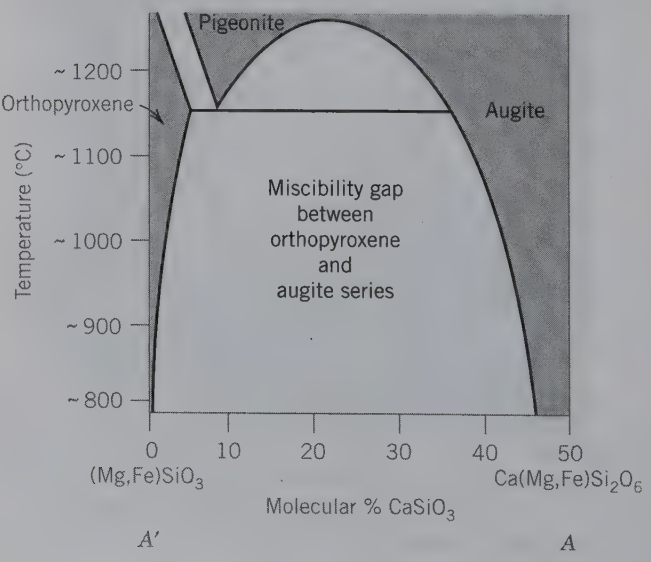

of the presence of closely spaced lamellae of An_0 and An_{25} composition (in the peristerite region, Fig. 12.18a; also referred to as the peristerite gap). Similarly, the *labradorescence* of labradorite (plagioclase) is caused by very fine exsolution lamellae of An_{47} to An_{58} composition as shown in Fig. 12.18a (see also Fig. 2.9) across the gap described as Bøggild intergrowth. A further miscibility gap occurs in the Huttenlocher region (Fig. 12.18a). A more detailed temperature-composition diagram, that incorporates the data in Fig. 12.18a as well as the high-temperature melting region for the plagioclase series, is given in Fig. 12.18b. This figure shows two major miscibility gaps at temperatures below about 800°C and an almost complete solid solution series above about 800°C, up to the solidus of the diagram. Sometimes, the composition of the exsolved plagioclase phases can be used to determine the original temperature of the host rock in which such plagioclase occurs.

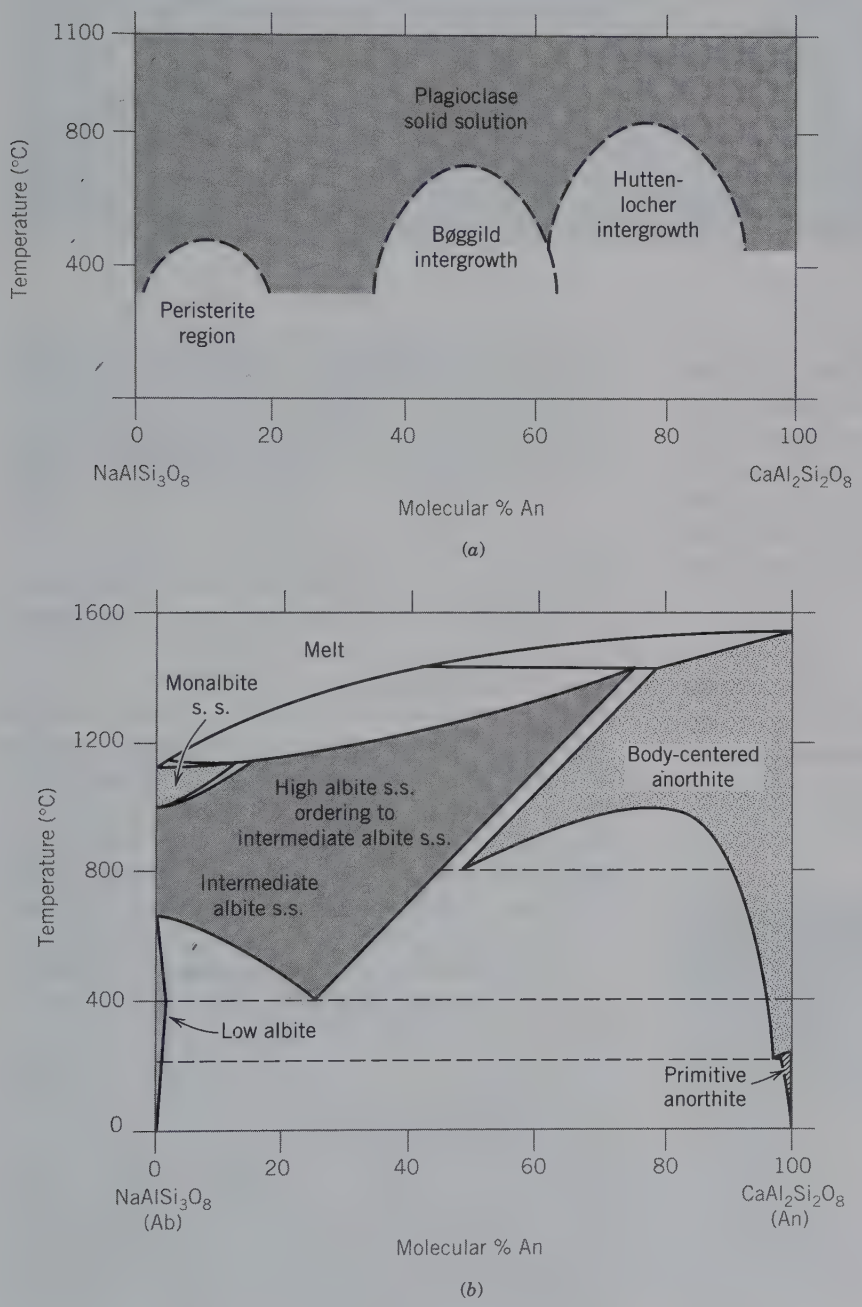

FIG. 12.18 (a) Approximate location of three miscibility gaps in the low-temperature region of the plagioclase feldspar series. (b) Schematic phase diagram for the plagioclase feldspar series showing a range of almost complete subsolidus solid solution at high temperatures, and the various miscibility regions at lower temperatures. (Simplified with permission after Smith, J. V. and W. L. Brown. 1988. Feldspar minerals, v. 1, *Crystal structures, physical, chemical, and microtextural properties*. Springer-Verlag, New York. Fig. 1.4, 828.)

RADIOACTIVITY AND METAMICITIZATION

During mineral formation, radioactive elements may be incorporated into the crystal structure. The nuclei of these elements are unstable and decay spontaneously to different kinds of nuclei, with the release of radioactive energy in the process. Examples of geologically important unstable nuclei are the following isotopes: ^{40}K, ^{87}Rb, ^{232}Th, ^{238}U, and ^{235}U (also see Table 12.3). In the decay process of such unstable nuclei, nuclear particles (including alpha or beta particles) are emitted, as are gamma rays. An *alpha particle* consists of two protons and two neutrons that are tightly bonded together. The alpha particle, which is identical with the nucleus of ^4He, is ejected from the unstable nucleus during alpha decay. In such decay, the atomic number, Z, of the nucleus decreases by two because of the removal of two protons and the mass number decreases by four. An example of such decay is:

$$^{238}_{92}U \rightarrow ^{234}_{90}Th + \alpha + \gamma + \text{energy}$$

A *beta particle* is a negatively charged particle with the mass of an electron that is emitted from the unstable parent nucleus. Nuclei do not contain electrons, and the origin of this electron must be regarded as the decay of a neutron into a proton, with the emission of the beta particle ($n = p + \beta^-$). By this process, the charge of the nucleus is increased by 1 and the parent nucleus becomes the nucleus of the next higher element in the periodic table:

$$^{87}_{37}Rb \rightarrow ^{87}_{38}Sr + \beta^- + \text{energy}$$

In the decay series of $^{238}U \rightarrow ^{206}Pb$, $^{235}U \rightarrow ^{207}Pb$, and $^{232}Th \rightarrow ^{208}Pb$, which form the basis for three independent methods of absolute age determination, several alpha and beta particles are produced in a sequence of intermediate radioactive products.

Table 12.3 Radioactive Isotopes Used in Radiometric Dating, Their Half-Lives, and Daughter Elements

Element	Isotope	Half-life* (in years)	Ultimate Daughter Elements†
Potassium	^{40}K	1.28×10^9 yr	^{40}Ca and ^{40}Ar
Rubidium	^{87}Rb	5×10^{11} yr	^{87}Sr
Thorium	^{232}Th	1.41×10^{10} yr	^{208}Pb and ^4He
Uranium	^{238}U	4.51×10^9 yr	^{206}Pb and ^4He
	^{235}U	7.1×10^8 yr	^{207}Pb and ^4He

*Half-life is the time required for one-half of the original number of radioactive atoms to decay

†The daughter elements are the new atoms formed at the expense of the distintegrated ones, the parent elements.

The process of disintegration can also occur by *electron capture*, in which an orbital electron is captured by the nucleus; this converts a proton to a neutron ($p + e^- = n$). The nuclear charge decreases by 1 without any significant change in mass. An example of this reaction is:

$$^{40}_{19}K + \text{orbital } e^- \rightarrow ^{40}_{18}Ar + \gamma + \text{energy}$$

In the previous equations, γ stands for high-energy electromagnetic radiation emitted by an excited nucleus as it drops into a less-excited state. Such emitted radiation is usually a byproduct of alpha and beta decay and electron capture. Gamma radiation is on the short wavelength side of X-radiation (Fig. 10.24).

Because radioactivity is a statistically random process, the probability that a nucleus will decay in a given time interval is expressed in terms of a decay constant, λ, the fraction of the radioactive nuclei present that will decay in a unit of time. The equation that expresses the decay is:

$$\frac{dP}{dt} = -\lambda P$$

where P is the number of parent atoms at time t and λ is the *disintegration* or *decay constant*, whose units are reciprocal time. The decay constants are now well known for many radioactive elements. Because these decay rates are constant, the measured amount of the daughter product (that is produced by decay) can be used to determine the time required to produce that quantity. This is basic to any radioactive "time clock," which provides radiometric (or absolute) ages of minerals and rocks.

In minerals with considerable amounts of U and Th, this radiation effect is readily measured and is, therefore, a diagnostic property in the characterization of radioactive minerals. Examples of radioactive minerals are uraninite, UO_2; thorianite, ThO_2; and autunite, $Ca(UO_2)_2(PO_4)_2 \cdot 10\text{–}12H_2O$. The radiation is most easily measured, in the laboratory and in the field, by a Geiger counter or scintillation counter. The presence of radiation can also be shown by placing unexposed film in an opaque wrapper against a radioactive specimen. The radiation will expose the film; this is known as *autoradiography* (Fig. 12.19).

METAMICT MINERALS

As a result of the production of energetic alpha particles (and the associated recoil energy these particles impart to the daughter nucleus), beta particles, and gamma radiation, and the changes in ionic size from parent to daughter elements, the crystal structure in which such processes occur is generally profoundly affected.

FIG. 12.19 Autoradiograph of a dendritic aggregate of uraninite, UO_2. Locality: Ruggles Pegmatite, Grafton Center, New Hampshire (Harvard Mineralogical Collection). (From Frondel, C. 1958. *Systematic mineralogy of uranium and thorium.* U.S. Geological Survey Bulletin no. 1064, 400.)

Minerals described as **metamict** originally formed as well-ordered, crystalline solids, but their crystal structure has been destroyed, to various degrees, by radiation from radioactive elements present in the original structure.

All metamict minerals are *radioactive*, and decay of a radioactive element can result in the complete destruction of the periodic structure around the radioactive element. For this reason, most U- and Th-rich minerals have undergone partial or complete destruction of their structures, leading to various stages of **metamictization** (the degree to which the original crystalline structure has been destroyed).

Usually this is caused by daughter elements of different sizes and charges from the parent element. However, the process is not well understood because some minerals containing less than 0.5% of these elements may be *metamict*, whereas other minerals containing high percentages of them may be crystalline.

The various stages of metamictization are determined by a combination of X-ray diffraction and high-resolution transmission electron microscopy (HRTEM) techniques. A well-ordered structure gives well-defined X-ray diffraction patterns, shows optical microscopic interference effects, and has ordered electron beam images (in electron diffraction and structural projections). As the original structure is damaged, the changes are reflected in the X-ray and electron diffraction and structural patterns. Several such stages of destruction of the original crystal structure of zircon, $ZrSiO_4$, owing to the presence of radioactive uranium and thorium, are shown in Fig. 12.20. Stage I(a) shows a well-ordered structure with well-established periodicities throughout; this is the unaltered structure. Stage I(b) shows incipient destruction of the structure and the appearance of some aperiodic domains (amorphous regions). Stage II shows increases in the volume percentage of aperiodic (amorphous) domains as a result of continued destruction of the periodic structure. In the final stage, III, all periodicities of the original structure are lacking, and the material is totally amorphous. The changes in the electron diffraction and X-ray diffraction patterns are the evidence on which the structural reconstructions are based. X-rays only diffract from crystalline structures, thus, the original sharp peak becomes a broad hump as the periodic structure is destroyed. Such destruction is shown in an HRTEM illustration of metamict domains in an otherwise crystalline matrix of olivine, $(Mg,Fe)_2SiO_4$, in Fig. 12.21. In this instance, the damage was artificially induced by high-voltage ion beam irradiation of the originally completely ordered, crystalline olivine.

The original nonmetamict mineral may have displayed good cleavage. The metamict product will, however, show no cleavage but instead will exhibit conchoidal fracture because the original strong bonds are broken. Many metamict minerals are bounded by crystal faces and are amorphous pseudomorphs (discussed later in this chapter) after an earlier crystalline mineral. When a metamict mineral is heated, its crystal structure may be reconstituted and its density increased.

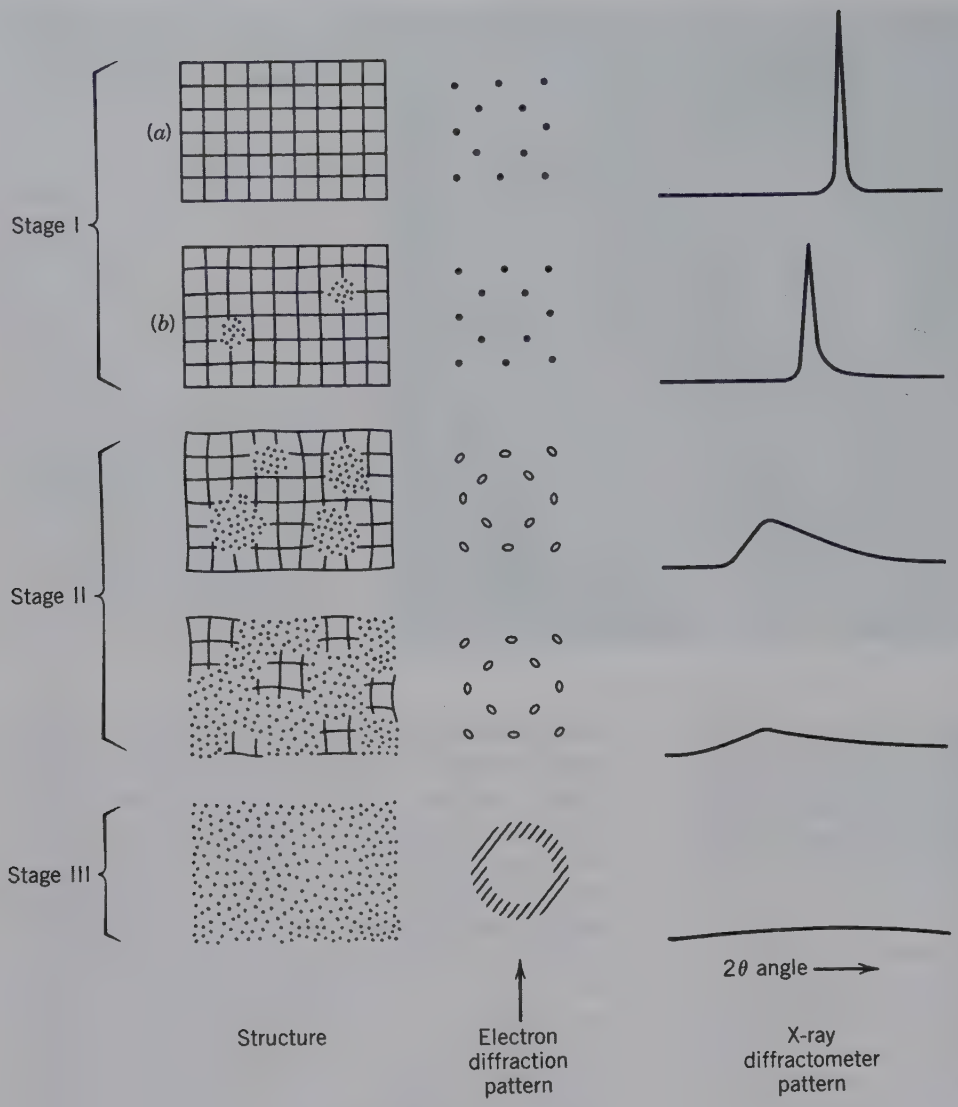

FIG. 12.20 Schematic representation of the progressive damage done to the structure of zircon as a result of radioactive decay. Electron diffraction patterns or X-ray diffraction patterns can be used, in addition to HRTEM, to establish the amount of structural damage. (After Murakimi, T., B. C. Chakoumakos, R. C. Ewing, G. R. Lumpkin, and W. J. Weber. 1991. Alpha-decay event damage in zircon. *American Mineralogist* 76: 1510–32.)

PSEUDOMORPHISM

In addition to the post-crystallization processes described previously, minerals can be completely replaced in the solid state or by the infiltration of fluids.

The *process of replacement in which a mineral retains the outward crystal form of another mineral species* is known as **pseudomorphism**.

If a crystal of a mineral is altered so that its internal structure or chemical composition is changed but its external form is preserved, it is called a **pseudomorph** (from the Greek word meaning "false form"). The chemical composition and structure of a pseudomorph belong to one mineral species, whereas the crystal form corresponds to another. For example, pyrite, FeS_2, commonly alters to limonite, $FeO{\cdot}OH{\cdot}nH_2O$, but during alteration all the external features of the pyrite are preserved. Such a crystal is described as a pseudomorph of *limonite after pyrite*. Pseudomorphs are defined according to the manner in which they were formed.

1. **Substitution**. In this type of pseudomorph, there is removal of the original material and a corresponding and simultaneous replacement of it by another, with no chemical reaction between the two. A common example of this is the substitution of silica for wood fiber to form petrified wood or fossilized pinecones (see Fig. 1.3). An exotic example of pseudomorphism is the replacement of a snail shell by emerald (Schwarz and Giuliani, 2002). Another

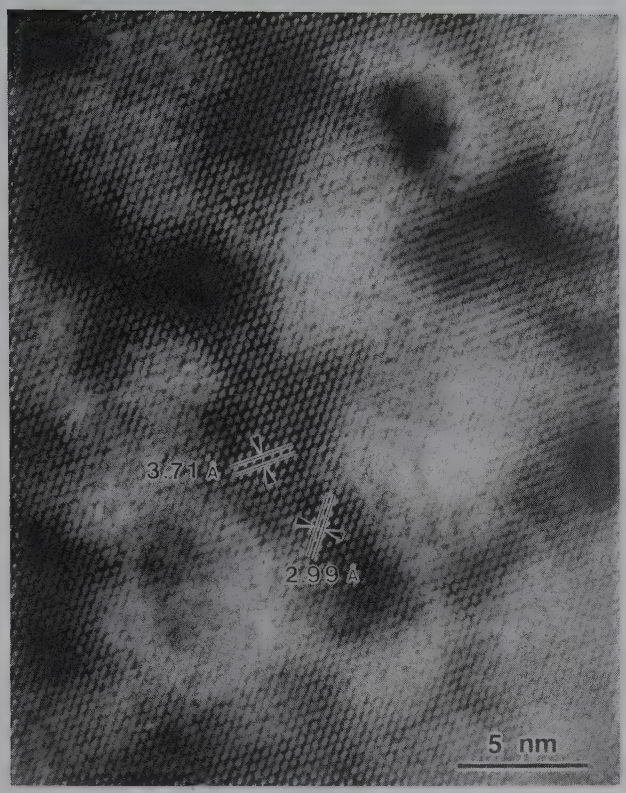

FIG. 12.21 High-resolution transmission electron microscope (HRTEM) structural image of radiation-induced metamict domains inside a well-crystallized host of olivine, $(Mg, Fe)_2SiO_4$. The damage was artificially produced by subjecting the original olivine crystal to a high-kilovoltage ion beam. Scale bar is in nanometers (nm): 1 nm = 10 Å. (From Wang, L. M., M. L. Miller, and R. C. Ewing. 1991. High-resolution TEM observation of displacement cascades in krypton-irradiated silicate minerals. *Proceedings of the 49th Annual Meeting of the Electron Microscopy Society of America*, EMSA, 910–11).

is the complete replacement of cyclic twins of aragonite by native copper.

2. **Encrustation**. In this type of pseudomorph, a crust of one mineral is deposited over crystals of another. Often the substrate over which the mineral originally grew is completely dissolved and removed. A common example of this is quartz encrusting cubes of fluorite (Fig. 12.22). Later, the fluorite may be removed entirely by dissolution, but its former presence is indicated by the cubic outline of the encrustation.
3. **Alteration**. In this type of pseudomorph, there has been a partial addition of new material and/or a partial removal of the original materials. The change of anhydrite, $CaSO_4$, to gypsum, $CaSO_4{\cdot}2H_2O$; the change of galena, PbS, to anglesite, $PbSO_4$; and the change of azurite, $Cu_3(CO_3)_2(OH)_2$, to malachite, $Cu_2CO_3(OH)_2$ (see Fig. 17.29), are examples of alteration pseudomorphs. Another example is a pseudomorph of muscovite, $KAl_2AlSi_3O_{10}(OH)_2$, after corundum, Al_2O_3. A core of the original unaltered mineral may be found in these pseudomorphs.

REFERENCES AND FURTHER READING

Bowen, N. L. 1913. The melting phenomena of the plagioclase feldspars. *American Journal of Science* 34: 577–99.

Ferry, J. M., (ed.) 1982. *Characterization of metamorphism through mineral equilibria. Reviews in Mineralogy* 10. Mineralogical Society of America, Washington, D.C.

Frondel, C. 1958. *Systematic mineralogy of uranium and thorium.* U.S. Geological Survey Bulletin no. 1064.

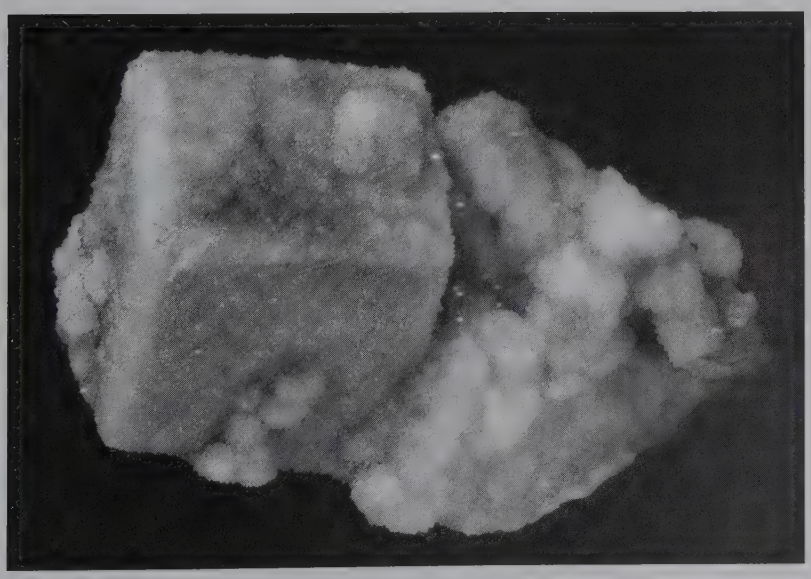

FIG. 12.22. Quartz pseudomorph after fluorite. Numerous small quartz crystals completely encrust the fluorite crystals preserving the cube {001} and dodecahedron {011} forms of fluorite. Specimen from Kwa Ndebele, Mphumelanga, Boekenhouthoek, Republic of South Africa. Sample is 9.4 cm high. (Photographs courtesy of Jeff Scovil, collection © Jeff Scovil.)

Heaney, P. J., C. T. Prewitt, and G. V. Gibbs (eds). 1994. *Silica: Physical behavior, geochemistry, and materials applications. Reviews in Mineralogy* 29, Mineralogical Society of America, Washington, D.C.

Holdaway, M. J. 1971. Stability of andalusite and the aluminum silicate phase diagram. *American Journal of Science* 271: 97–131.

Karato, S., and H.-R. Wenk (eds). 2002. Plastic deformation of minerals and rocks. *Reviews in Mineralogy and Geochemistry* 51. Mineralogical Society of America, Washington, D.C.

Putnis, A. 1992. *Introduction to mineral sciences.* Cambridge University Press, New York.

———, J. D. C. McConnell, 1980. *Principles of mineral behaviour.* Elsevier, New York, 257.

Ribbe, P. H. 1975. The chemistry, structure, and nomenclature of feldspar. *Feldspar Mineralogy, Reviews in Mineralogy* 2. Mineralogical Society of America, Washington, D.C.

Schwarz, D., and G. Giuliani. 2002. South America: Columbia. *extraLapis English No. 2: Emerald.* Lapis International, LLC. East Hampton, CT. 36–45.

Smith, J. V., and W. L. Brown. 1988. Feldspar minerals, 1, *Crystal structures, physical, chemical, and microtextural properties.* Springer-Verlag, New York.

CHAPTER 13

Optical Microscopy

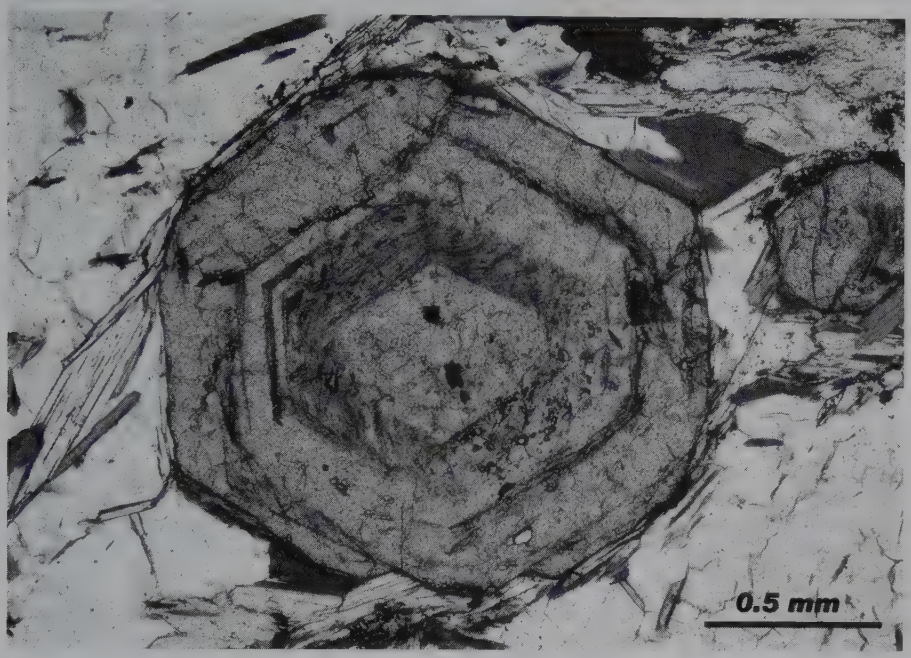

A 30 micrometer thick slice of an almandine-rich garnet as viewed through the microscope under plane polarized light. The euhedral cross-section was cut through a dodecahedral crystal and displays several concentric zones. These zones represent separate growth stages and are separated by inclusion-rich rims. (The complete assemblage is garnet-biotite-chlorite-muscovite-quartz-plagioclase-ilmenite-graphite.) This sample formed at temperatures near 550°C and at about 7 kb pressure (one kilobar = 1,000 bars; 1 atmosphere = 1.01325 bars) and is from the metamorphic Moine Series of Scotland. (Photograph courtesy of Darrell Henry, Louisiana State University, Baton Rouge.)

The optical properties of minerals, and those of other crystalline and amorphous materials, are highly diagnostic, and their quantitative evaluation commonly leads to the proper identification of an unknown. Small mineral fragments (that are purposely broken off from a larger hand specimen) or thinly sliced mineral specimens (known as "thin sections" with a thickness of about 30 μm) can be studied with a polarizing microscope to yield measurable optical data produced by the interaction of visible light with the transparent sample. Furthermore, optical studies allow direct observation of mineral intergrowths and textures on a microscopic scale. These features are used in the interpretation of mineral growth, deformation, reactions, subsequent alteration, and, ultimately, the geologic history of the sample.

Optical studies of crystalline solids make use of a petrographic microscope (discussed subsequently), in which minerals can be studied with polarized light. For this reason, a petrographic microscope is also referred to as a polarizing microscope. Most of the discussion that follows focuses on the study of translucent materials and transmitted-light optics, with a brief section covering reflected-light optics for the study of opaque minerals.

The materials that are studied commonly with a petrographic microscope include small crystal fragments or thin sections of crystalline materials (most commonly rocks). Mineral fragments are samples that were broken off from a larger hand specimen in order to acquire more information. Such are samples that could not be identified with certainty strictly on the basis of macroscopic properties assessed in hand specimen. For the study of mineral separates or unconsolidated materials, grain mounts consisting of loose fragments embedded in epoxy or immersed in oil are used. Thin sections are ~30 μm thick slices (the thickness of a human hair) of crystalline materials affixed to glass slides with transparent cement, with or without cover slips. On both types of samples (small crystal fragments or thin sections), various optical measurements can be made that aid in their unique identification. The most quantitative optical identification technique involves the measurement of one or more refractive indices (R.I.) and other parameters such as optic angle and

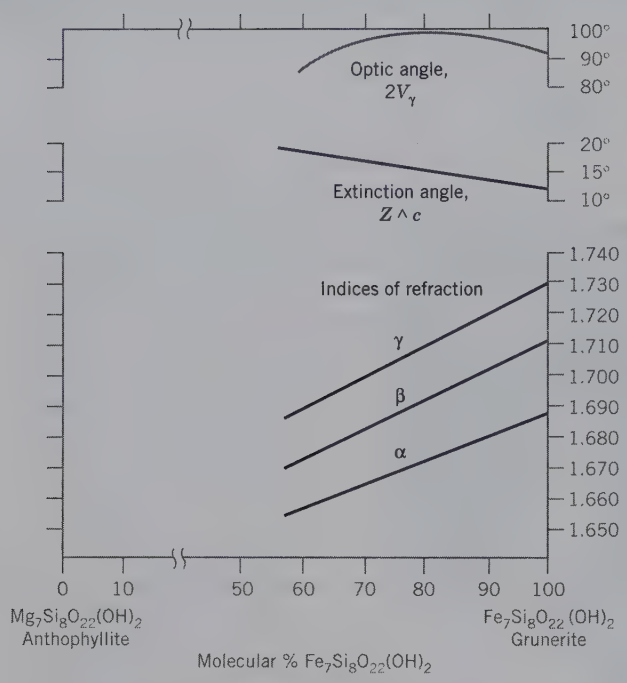

FIG. 13.1 Variation in several optical parameters as a function of changing chemical composition in the monoclinic amphibole series known as the cummingtonite–grunerite series. The $Mg_7Si_8O_{22}(OH)_2$ composition is orthorhombic and is called anthophyllite. (From Klein, C. 1964. Cummingtonite-grunerite series: Chemical, optical and X-ray study. *American Mineralogist* 49: 963–82.)

sign, color, and orientation of optical directions with respect to crystallographic axes. Such optical data can be compared with reference data in tables of optical parameters, most of which are arranged in terms of refractive index (see Table 22.3 in Chapter 22, and the references at the end of this chapter).

Optical techniques typically provide the quickest route to unambiguous mineral identification. Such identification may need to be supplemented with more sophisticated chemical tests or information from X-ray diffraction (see Chapter 14). If the unknown mineral that is being identified (through optical properties) is part of a relatively simple solid solution series, considerable information about its chemical composition can be obtained if a variation diagram (relating optical parameters to changing chemical composition) is available (Fig. 13.1). Microscopic observations also provide textural and spatial information about mineral constituents. Mineral reactions, frozen in time, can be seen optically and the evaluation of such reactions may aid in constraining their *P–T* history. Mineral grains used in geochronology are first located in the thin section and checked to assure that no mineral alteration exists. The optical technique of mineral identification is quick and reliable for those who have mastered the various optical concepts that underlie the measurements. Optical microscopy uses visible light as an energy source, which necessitates an understanding of phenomena associated with light.

NATURE OF LIGHT

Visible light, as a portion of the electromagnetic spectrum (see Fig. 10.24), has properties of both a wave and a particle (photon). To account for all the properties of light, it is necessary to consider two theories: the *wave theory* and the *corpuscular theory*. Here, the focus is on **wave theory** for explaining the optical behavior of light interacting with crystals. This theory assumes that visible light travels in a straight direction and vibrates at right angles to the direction of propagation. The wave motion is similar to that generated by dropping a pebble into still water, with waves moving out from the central point. The water merely rises and falls; it is only the wave front that moves forward. The **wavelength** (λ) of such a wave motion is the distance between successive crests (or troughs); the **amplitude** is the displacement on either side of the position of equilibrium; the **frequency** is the number of waves that pass a fixed point per unit time; and the **velocity** is the frequency multiplied by the wavelength. Similarly, light waves (Fig. 13.2) have length, amplitude, frequency, and velocity, but their transverse vibrations, perpendicular to the direction of propagation, take place in all possible directions. The relationship between wavelength (λ), velocity (c), and frequency (f) for any wave is:

$$c = f$$

Visible light occupies a very small portion of the electromagnetic spectrum (Fig. 10.24). The wavelength determines the color of light and ranges from slightly more than 700 nm at the red end to about 400 nm at the violet end. White light is composed of all wavelengths between these limits, and a prism can separate white light into its constituent components. Light of a single wavelength is termed **monochromatic**.

The frequency of monochromatic light remains constant as it enters another material. However, the wavelength and the velocity of the light do change as light passes through another material. Therefore, considering light passing from material A into material B, leads to the following relationship:

$$\frac{c_A}{c_B} = \frac{\lambda_A}{\lambda_B}$$

Consequently, the wavelength of light entering the new material changes in proportion to the change in velocity.

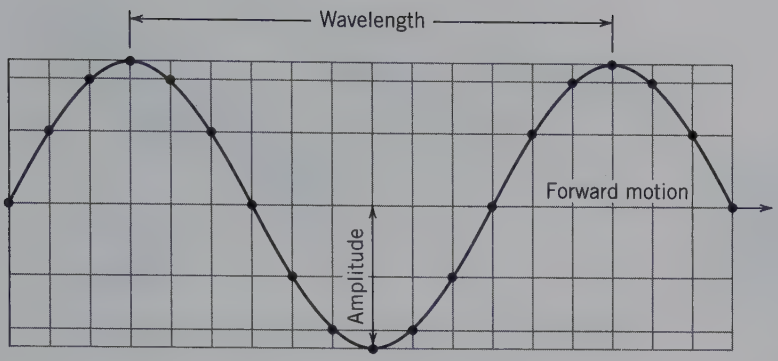

FIG. 13.2 Wave motion depicted by bold line.

REFLECTION AND REFRACTION

When a light ray passes from a low-density medium, such as air, into a denser medium, such as glass, part of it is reflected from the surface back into the air, and part enters the glass (Fig. 13.3). The **reflected** ray obeys the laws of reflection:

1. The angle of incidence (i) equals the angle of reflection (r'), where both angles are measured from the surface normal (Fig. 13.3).
2. The incident and reflected rays lie in the same plane.

The light that passes into the glass travels at a slower velocity than in air and no longer follows the path of the incident ray but is bent or *refracted*. The amount of bending depends on the obliquity of the incident ray and the relative velocities of light in the two media; the greater the angle of incidence and the greater the velocity difference, the greater the refraction. In other words, **refraction** is the change in direction of wave propagation as light passes from one medium into another, and is accompanied by a change in velocity.

REFRACTIVE INDEX AND SNELL'S LAW

When light passes from one material into another, it either speeds up or slows down as a function of the differing atomic structures of the two materials. Light travels at a velocity (c) of 3×10^{17} nm per second in a vacuum. In a denser material, light travels with a lesser velocity (c_m). The **refractive index** (***n*** or ***R.I.***) of a material may be defined as:

$$n = \frac{c}{c_m} \qquad \text{or} \qquad n = \frac{c_{air}}{c_{mineral}}$$

Here, c is typically the velocity of light in a vacuum (c) and c_m is the velocity of light in the material. For minerals, this ratio is typically the velocity of light in air (c_{air}; nearly the same as in a vacuum), relative to the velocity of light in a mineral ($c_{mineral}$). The resulting refractive index (n) of a transparent material will be at a value greater than 1.0 because c_m, for denser transparent materials, is always less than c. The higher the density of a transparent substance, the slower the light travels through it. High density (or specific gravity) correlates with high refractive index (Bloss, 1999).

If the light velocity in two materials is different, the direction of propagation changes according to **Snell's law**:

$$\frac{\sin i}{\sin r} = \frac{n_r}{n_i} = \frac{c_i}{c_r} \qquad \text{or} \qquad \sin r = \left(\frac{n_i}{n_r}\right) \sin i$$

where i = angle of incidence, r = angle of refraction, n_r and n_i are refractive indices (Fig. 13.3), and c_r and c_i are velocities of light. A light ray passing from a medium of low n into one of higher n (Fig. 13.3) is refracted toward the normal to the interface, and vice versa.

The velocity of light in glass is equal to frequency multiplied by wavelength; therefore, with fixed frequency, the longer the wavelength the greater the velocity. Red light with its longer wavelength has a greater velocity than violet light and because of the reciprocal relation between velocity and refractive index, n for red light is less than n for violet light (Fig. 13.4). Therefore, a crystal has different refractive indices for different wavelengths of light. This phenomenon is known as **dispersion** and because of it, only one wavelength of light, *monochromatic light*, is used for accurate determination of refractive index.

FIG. 13.3 Reflected and refracted light. i = angle of incidence, r' = angle of reflection, r = angle of refraction; density refers to the medium through which light is moving, n = refractive index, c = velocity.

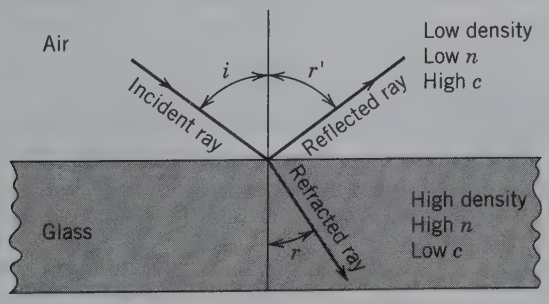

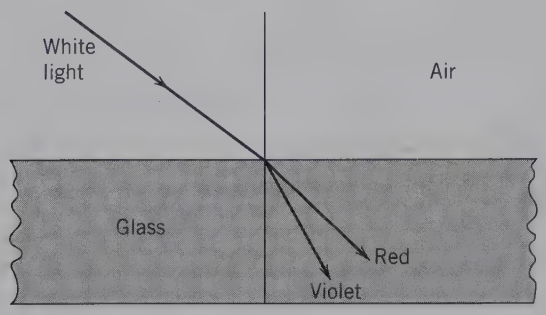

FIG. 13.4 Different wavelengths of white light are refracted at different angles in a medium. This is also known as *dispersion*.

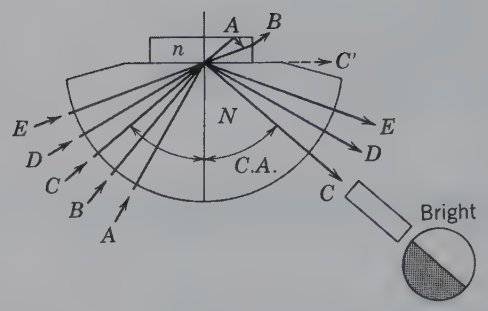

FIG. 13.6 Pulfrich refractometer and measurement of the critical angle *C.A.* $N = 1.90$, *C.A.* $= 50°$, $n = 1.455$.

Total Reflection and the Critical Angle

When light passes from a medium with a lower refractive index to a medium with a higher refractive index, it is refracted toward the normal (Fig. 13.3). When the conditions are reversed and the light moves from the higher to the lower index medium, it is refracted away from the normal as in Fig. 13.5. In Fig. 13.5, assume that lines *A*, *B*, *C*, and so forth represent light rays moving through glass and into air at point *O*. The greater the obliquity of the incident ray, the greater the angle of refraction. Ultimately, an angle of incidence is reached, as at ray *D*, for which the angle of refraction is 90°, and the ray then grazes the surface of the interface. The angle of incidence at which this takes place is known as the **critical angle**, which is the value of the angle required for $(n_i/n_r \sin i) = 1.0$. Rays such as *E* and *F*, striking the interface at a greater angle, are *totally reflected* back into the higher index medium.

The measurement of the *critical angle* is a quick and easy method of determining the refractive index of both liquids and solids. The instrument used for this measurement is a refractometer. A description of the Pulfrich refractometer illustrates the underlying principles. This instrument employs a polished hemisphere of high-refractive index glass (Fig. 13.6). A crystal face or polished surface of the mineral is placed on the equatorial plane of the hemisphere and, depending on the angle of incidence, light is either partly refracted through the unknown or totally reflected back through the hemisphere. If a telescope is placed in a position to receive the reflected rays, one can observe a sharp boundary between the portion of the field intensely illuminated by the totally reflected light and the remainder of the field. When the telescope is moved so that its cross hairs are precisely on the contact, the critical angle is read on a scale. Knowing this angle and the index of refraction of the hemisphere, *N*, one can calculate the index of refraction of the mineral: *n* (mineral) = sin (critical angle) × *N* (hemisphere).

FIG. 13.5 Light rays moving through glass and striking the glass–air interface at angle *C.A.* (critical angle). At greater angles, light is totally reflected.

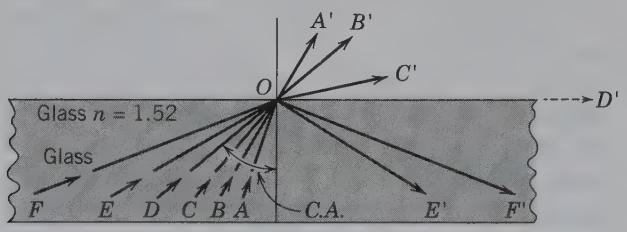

ISOTROPIC AND ANISOTROPIC CRYSTALS

For optical considerations, all transparent substances can be divided into two groups: **isotropic** and **anisotropic**. The isotropic group includes noncrystalline substances, such as gases, liquids, and glass, but it also includes crystals that belong to the isometric crystal system. In isometric crystals, light moves in all directions with *equal* velocity (*iso* from the Greek word meaning "equal".) Therefore, each *isotropic* substance has a single refractive index. In *anisotropic* substances, which include all crystals except those of the isometric system, the velocity of light varies with crystallographic direction, and, thus, there is more than one refractive index.

In general, light passing through an anisotropic crystal is broken into two polarized rays that travel at different velocities and vibrate in mutually perpendicular planes. Thus, for a given orientation, a crystal has two indices of refraction, one associated with each polarized ray. Anisotropic substances are further divided into uniaxial minerals characterized by two refractive indices *R.I.*s and biaxial mineral characterized by three *R.I.*s.

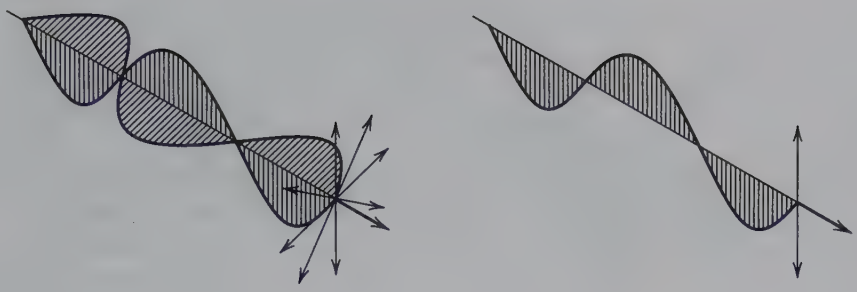

(a) (b)

FIG. 13.7 Plane polarized light. (a) Unpolarized light with light vibrating in all directions (shown by arrows) at right angles to the direction of propagation. (b) Plane polarized light consisting of waves confined to vibration in only one plane through the line of propagation.

POLARIZED LIGHT

Light can be considered a wave motion with vibrations occurring in all directions at right angles to the direction of propagation. When the wave motion is confined to vibrations in a single plane, the light is said to be **plane polarized** (Fig. 13.7). Two ways of polarizing light are by absorption and reflection.

Polarized Light by Absorption

The polarized rays in which light is divided in anisotropic crystals may be differentially absorbed. If one ray suffers nearly complete absorption and the other very little, the emerging light will be plane polarized. This phenomenon is well-illustrated schematically by tourmaline crystals (Fig. 13.8a). Light that passes through the crystal at right angles to [0001] emerges essentially plane polarized, with vibrations parallel to the *c* axis. The other ray, vibrating perpendicularly to it, is almost completely absorbed. When two tourmaline crystals are placed at right angles one above the other, the polarized ray emerging from one is absorbed by the other. Polarizing sheets, such as *Polaroid*®, are made by aligning crystals on an acetate base. These crystals absorb very little light in one vibration direction, but are highly absorptive in the other (Fig. 13.8b). The light transmitted by the sheet is, thus, plane polarized. Because these thin sheet are manufactured into larger sizes, polarizing plates are used extensively in optical equipment, including most polarizing microscopes.

FIG. 13.8 Polarized light by absorption. (a) Schematic illustration of two superimposed tourmaline crystals. (b) *Polaroid*® sheets. Arrows indicate directions of maximum transmission; directions of maximum absorption are at right angles.

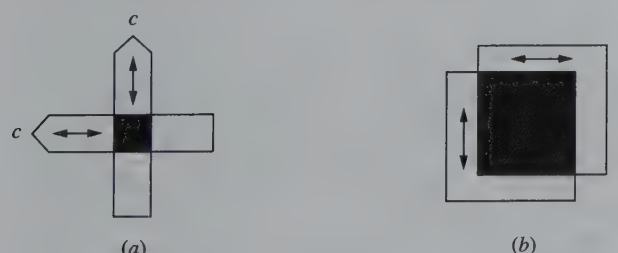

(a) (b)

Polarized Light by Reflection

Light reflected from a smooth, nonmetallic surface is partially polarized with the vibration directions parallel to the reflecting surface (Fig. 13.9). The extent of polarization depends on the angle of incidence and the index of refraction of the reflecting surface. The fact that reflected light is polarized can be easily demonstrated by viewing it through a polarizing filter. When the vibration direction of the filter is parallel to the reflecting surface, the light passes through the filter with only a slight reduction in intensity (Fig. 13.9a); when the filter is turned 90°, only a small percentage of the light reaches the eye (Fig. 13.9b). An example of this is the use of *Polaroid*® lenses in sunglasses. Much light that is reflected from the ground surface, as well as objects, is horizontally polarized. *Polaroid*® sunglasses are vertically polarized and, therefore, eliminate much reflected light (Fig. 13.9c).

THE POLARIZING MICROSCOPE

The polarizing microscope is the most important instrument for determining the optical properties of minerals; more information can be obtained easily and quickly with it than with more specialized devices. Several manufacturers each make a number of models of polarizing microscopes that vary in complexity of design, sophistication, and in price. A student model made by Nikon is illustrated in Fig. 13.10 with the essential parts located.

Although a polarizing microscope differs in detail from an ordinary compound microscope, its primary function is the same: to yield an enlarged image of an object placed on the **stage**. The *magnification* is produced by a combination of two sets of lenses: the *objective* and the *ocular*. The function of the **objective lens**, at the

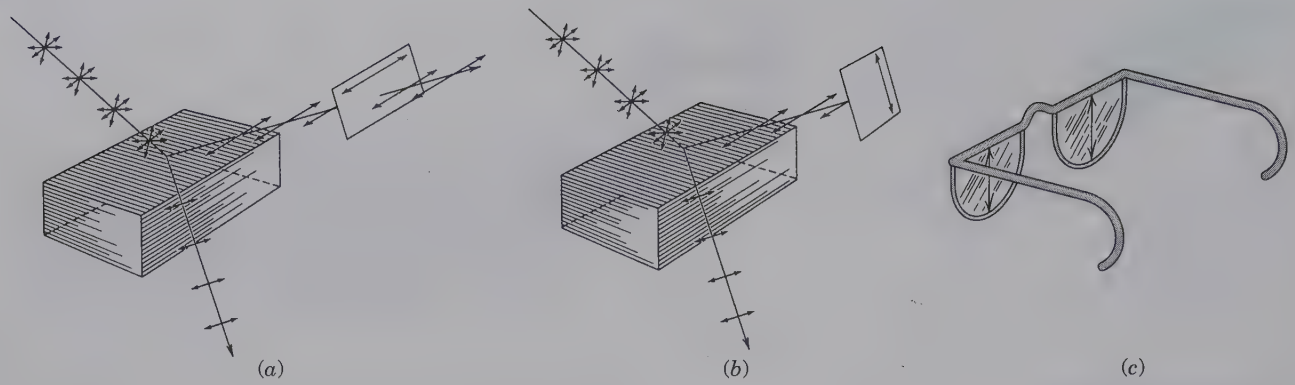

FIG. 13.9 Polarized light by reflection and refraction. (a) Polaroid filter transmits most reflected light. (b) Polaroid filter blocks reflected light. (c) Polaroid sunglasses that would block the reflected glare.

lower end of the microscope tube, is to produce an image that is sharp and clear. The **ocular** merely enlarges this image including any imperfection resulting from a poor quality objective. It is desirable to have three *objectives* for mineralogical work: low, medium, and high power. In Fig. 13.10, these are shown mounted on a revolving nosepiece and can be successively rotated into position. The magnification produced by an objective is usually indicated on its housing, such as 4× (low), 10× (medium), and 100× (high). Oculars also have different magnifications such as 5×, 7×, 10×. The total magnification of the image can be determined by multiplying the magnification of the objective by that of the ocular as: 50×10× = 500×. In routine work, the three objectives are frequently interchanged, but a single ocular usually suffices. The ocular assembly, which slips into the upper end of the microscope tube, carries cross hairs—one N–S (front–back) the other E–W. These enable one to locate, under high power, a particular mineral grain that has been brought to the center of the field under low power. They are also essential in aligning cleavage fragments for making angular measurements. A **condenser** is located below the stage. The upper lens of the condenser, used with high-powered objectives, makes the light *converge* strongly and can be rotated easily into or out of the optical system. The **iris diaphragm**, also located below the stage, can be opened or closed to control the depth of focus and to regulate the intensity of light striking the object.

FIG. 13.10 Polarizing microscope, Labophot-Pol, manufactured by Nikon. 1. Oculars. 2. Analyzer. 3. Slot for accessory plate. 4. Revolving nosepiece for objectives. 5. Objectives. 6. Rotating stage. 7. Lever for swinging in and out condenser lens. 8. Rotatable polarizer. 9. Vertical adjustment of stage, for focusing (knobs on both sides). 10. Field diaphragm. 11. Substage illuminator. 12. Intensity adjustment knob for illuminator. 13. On/off switch. (Courtesy of S & M Microscopes Inc., Colorado Springs, Colorado.)

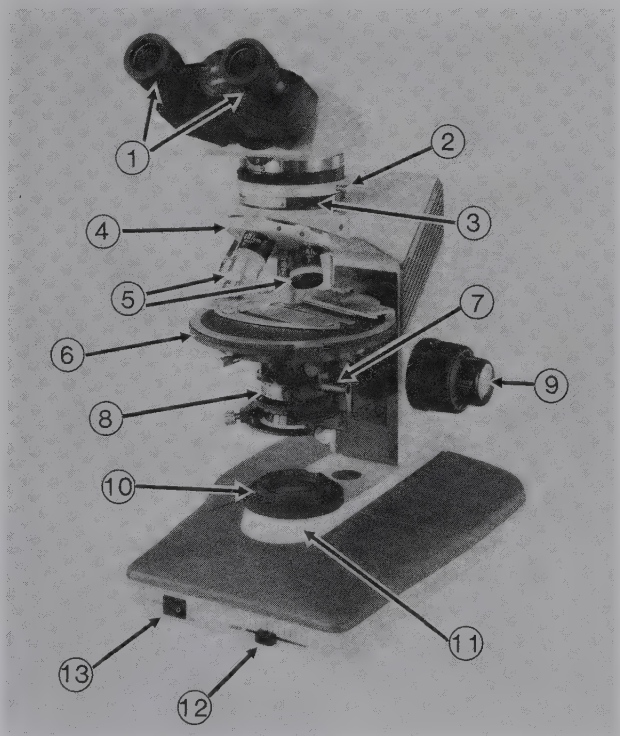

In addition to the lenses, condenser, and diaphragm mentioned previously that are common to all compound microscopes, the polarizing microscope has several other features. The **polarizer** below the stage is a polarizing plate that transmits plane polarized light vibrating in an N–S (front–back) direction. This is referred to as plane polarized light (or PPL). The **analyzer**, fitted in the tube above the stage, is a similar plate or prism that transmits light vibrating only in an E–W direction (at 90° to the lower polarizer). The polarizer and analyzer are collectively called **polars**. When both polars are in position, they are said to be crossed (or XPL), and, if no anisotropic crystal is between them, no light reaches the eye. The *polarizer remains fixed* but the *analyzer can be removed* from the optical path at will. The **Bertrand lens** is an accessory that is used to observe interference figures (see section

on "Interference"). In working with mineral grains, it is frequently necessary to change their orientation. This is accomplished by means of a rotating **stage**, whose axis of rotation is the same as the microscope axis.

Microscopic Examination of Minerals and Rocks

The polarizing microscope is also called the *petrographic* microscope because it is used in the study of rocks. In examining thin sections of rocks, the textural relationships are studied and certain optical properties can be determined. It is equally effective in working with powdered mineral fragments. On such loose grains, all the optical properties can be determined, and in most cases they sufficiently characterize a mineral to permit its identification.

The *immersion method* is used to determine the refractive indices of mineral grains. The optimal size of mineral grains for examination with a polarizing microscope is 0.3 mm to 2.0 mm, but larger or smaller sizes may be used. To prepare a mount for examination (1) place a few mineral grains on a glass slide, which is usually 40 mm × 27 mm; (2) immerse the grains in a drop of liquid of known refractive index; and (3) place a cover glass on top of the liquid.

A series of calibrated liquids ranging in refractive index from 1.41 to 1.77, with a difference of 0.01 or less between adjacent liquids, is used in this method. These liquids span the refractive index range of most of the common minerals. The immersion method is one of trial and error and involves comparing the refractive index of the unknown with that of a known liquid.

Isotropic Crystals and the Becke Line

Because light moves in all directions through an isotropic substance with equal velocities, there is no double refraction and only a single index of refraction. With a polarizing microscope, objects are always viewed in polarized light, which conventionally vibrates N–S. If the object is an isotropic mineral, the light passes through it and continues to vibrate in the same plane. These minerals do not reorient the light. If the analyzer is inserted, darkness results because this polar permits light to pass only if it is vibrating in an E–W direction. Darkness remains as the position of the crystal is changed by rotating the microscope stage. This characteristic distinguishes isotropic from anisotropic crystals.

The single refractive index, of an isotropic substance, is determined by first mounting crystal fragments using any liquid. If the mineral is a complete unknown, it is best to select a liquid near the middle of the *R.I.* range. When the grains are brought into sharp focus using a medium-power objective and plane polarized light, in all likelihood they will stand in **relief**, that is, they will be clearly discernible from the surrounding liquid. This is because the light is refracted as it passes from one medium to another of different refractive index. The greater the difference between the indices of refraction of mineral and liquid, the greater is the relief. **Relief** is a measure of the relative difference between the index of refraction of the mineral and that of the surrounding medium (a liquid or another mineral). Grains are characterized as having *low* or *high relief*, which can be used to estimate *n*. When the refractive indices of the crystal fragment and the surrounding liquid are the same, there is no refraction at the interface, and the grains are essentially invisible.

Relief shows that the index of refraction of the mineral is different from that of the liquid; but is it higher or lower? The answer to this important question can be found by means of the **Becke line** (Fig. 13.11). If the mineral grain moves out of focus by lowering the stage, a narrow line of light will form at its edge and move toward the medium of higher refractive index. Thus, if the Becke line moves into the mineral grain, the mineral has a higher refractive index than the surrounding liquid, and a new mount must be made using a liquid of higher refractive index. Several attempts may be needed before the correct *R.I.* liquid is identified. When there is no Becke line and the mineral grains are invisible in a given liquid, the index of refraction of the mineral is the same as that of the calibrated liquid. More frequently, however, the refractive index of the

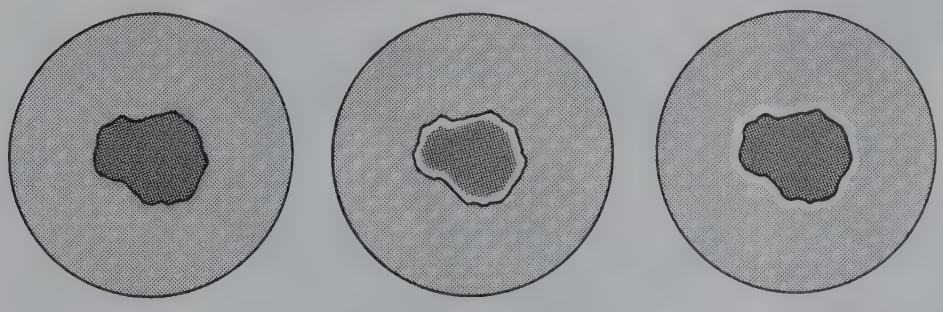

FIG. 13.11 The Becke Line. When the image moves out of focus by raising the microscope tube (or lowering the stage), the white line moves into the medium of higher refractive index. (a) In focus. (b) *n* of grain > *n* of liquid. (c) *n* of grain < *n* of liquid.

mineral is found to be greater than that of one liquid but less than that of its next higher neighbor. In such cases, it is necessary to interpolate between these values. If the Becke line moving into the mineral in the lower-index liquid is more intense than the line moving out of the mineral into the next higher-index liquid, it can be assumed that the refractive index of the mineral is closer to that of the higher liquid. In this way, it is usually possible to report a refractive index to $\pm$ 0.003.

Frequently, the Becke line can be sharpened by restricting the light by means of the substage diaphragm. Most liquids have a greater dispersion than minerals. Thus, if the refractive index of liquid and mineral are matched for a wavelength near the center of the spectrum, the mineral has a higher index than the liquid for red light but a lower index for violet light. This is evidenced, when observed in white light, by a reddish line moving into the grain while a bluish line moves out.

Aside from color, the single index of refraction is the only significant optical characteristic of isotropic minerals. It is, therefore, important in mineral identification to consider other properties such as cleavage, fracture, color, hardness, and specific gravity. Table 22.3 (Chapter 22) gives a listing of increasing refractive index for many minerals.

UNIAXIAL CRYSTALS

Light moves in all directions through an isotropic substance with equal velocity and vibrates in all directions at right angles to the directions of propagation. In hexagonal and tetragonal crystals, there is one and only one direction in which light moves in this way. Along this direction, light is not reoriented. This is parallel to the *c* axis, with vibrations in all directions in the basal plane (Fig. 13.12a). For this reason the *c* axis is called the **optic axis**, and hexagonal and tetragonal crystals are called optically **uniaxial**. This distinguishes them from orthorhombic, monoclinic, and triclinic crystals (refer to Chapter 6), which have two optic axes and are called **biaxial**.

When light moves in uniaxial crystals in any direction other than parallel to the *c* axis, it is split into two rays traveling with different velocities (Fig. 13.12b). One, the **ordinary ray (*O*)**, is reoriented to vibrate in the basal plane; the other, the **extraordinary ray (*E*)**, vibrates at right angles to it and, thus, in a plane that includes the *c* axis. Such a plane, of which there is an infinite number, is referred to as the *principal section*. The nature of these two rays can be explained as follows. Assume that the direction of the incident beam is varied to make all possible angles with the crystal axes, and that the distance traveled by the resulting rays in any instant can be measured. As such:

1. One ray, with waves always vibrating in the basal plane, travels the same distance in the same time. Its surface can be represented by a sphere, and because it acts much as ordinary light does, it is the *ordinary ray* (*O ray*).
2. The other ray, with waves vibrating in the plane that includes the *c* axis, travels different distances, in an equivalent time, depending on the orientation of the incident beam. If the varying distances of this

FIG. 13.12 (a) Calcite crystal with a triangular face cut perpendicular to the *c* axis. This means the viewer looks at the crystal parallel to the *c* axis (the optic axis). In this orientation, calcite shows no double refraction. (b) Calcite showing double refraction when viewed normal to a rhombohedral face. The double repetition of "calcite" at the top of the photograph is seen obliquely through a face cut on the specimen parallel to the (0001) face. See text for details. (Specimens from the Harvard Mineralogical Museum.)

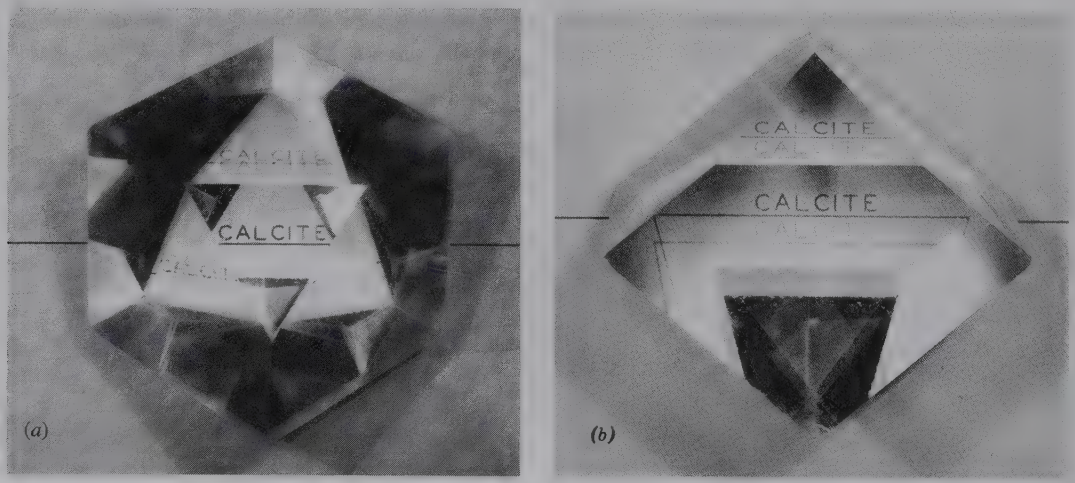

extraordinary ray (*E ray*) are plotted, they will outline an ellipsoid of revolution with the optic axis as the axis of revolution.

Uniaxial crystals are divided into two optical groups: positive and negative. They are *positive* if the *O* ray has the greater velocity, and *negative* if the *E* ray has the greater velocity. Cross sections of the ray velocity surfaces are shown in Fig. 13.13. In both positive and negative crystals, the *O* and *E* rays have the same velocity when traveling along the optic *c* axis. But the difference in their velocities becomes progressively greater as the direction of light propagation moves away from the optic axis, reaching a maximum at 90°.

Because the two rays have different velocities, there are two indices of refraction in uniaxial crystals. Each index is associated with a vibration direction. The index related to vibration along the ordinary ray is designated ω (omega), whereas that associated with the extraordinary ray is ϵ (epsilon) or ϵ′. In positive crystals, the *O* ray has a greater velocity than the *E* ray, and ω is less than ϵ. But in negative crystals with the *E* ray having the greater velocity, ω is greater than ϵ. The two principal indices of refraction of a uniaxial crystal are ω and ϵ and the difference between them is the **birefringence**.

The **uniaxial indicatrix** is a geometric figure that is helpful in visualizing the relation of the refractive indices and their vibration directions that are perpendicular to the direction of propagation of light through a crystal. For positive crystals, the indicatrix is a prolate spheroid of revolution (Fig. 13.14a); for negative crystals, it is an oblate spheroid of revolution (Fig. 13.14b). In their construction, the direction of radial lines is proportional to the refractive indices. First, consider light moving parallel to the optic axis. It is not doubly refracted but moves through the crystal as the ordinary ray with waves vibrating in all directions in the basal plane. This is why light moving parallel to the *c* axis of calcite (Fig. 13.12a) produces a single image. There is a single refractive index for all these vibrations, proportional to the radius of the equatorial circle of the indicatrix.

FIG. 13.13. Ray velocity surfaces of uniaxial crystals.

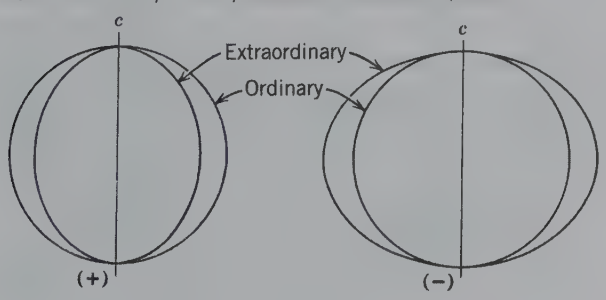

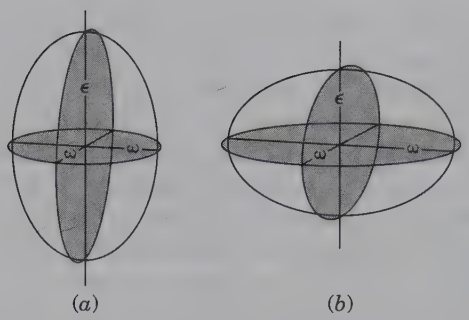

FIG. 13.14 Optical indicatrix, uniaxial crystals. (a) Positive. (b) Negative.

Now, consider light traveling perpendicular to the optic axis. It is **doubly refracted.** The waves of the ordinary ray vibrate, as always, in the basal plane and the associated refractive index, ω, is again an equatorial radius of the indicatrix. The vibration direction of waves of the extraordinary ray must be at right angles to both the vibration direction of the ordinary waves and the direction of propagation. Thus, in this special case, it is parallel to the optic axis. The axis of revolution of the indicatrix is then proportional to ϵ, the greatest index in (+) crystals and the least in (−) crystals. It can be seen that light moving through a crystal in a random direction gives rise to two rays: (1) the *O* ray with waves vibrating in the basal section, the associated index, ω; and (2) the *E* ray with waves vibrating in the principal section in a direction at right angles to propagation. The length of the radial line along this vibration direction is ϵ′, a refractive index lying between ω and ϵ.

A study of the indicatrix shows that (1) ω can be determined on *any* crystal grain, and only ω can be measured when light moves parallel to the optic axis; (2) ϵ can be measured only when light moves normal to the *c* axis; and (3) a randomly oriented grain yields, in addition to ω, an index intermediate to ω and ϵ, called ϵ′. The less the angle between the direction of light propagation and the normal to the optic axis, the closer is the value ϵ′ to true ϵ.

UNIAXIAL CRYSTALS BETWEEN CROSSED POLARS

Extinction

Because isotropic crystals remain dark in all positions between crossed polars, they can be distinguished from anisotropic crystals. However, there are special conditions under which uniaxial crystals present a dark field when viewed between crossed polars. One of these conditions is when light moves parallel to the optic axis. Moving in this direction, light from the polarizer passes through the crystal as through an isotropic substance and is completely cut out by the analyzer. The

other special condition is when the vibration direction of light from the polarizer coincides exactly with one of the vibration directions of the crystal. In this situation, light passes through the crystal as either the *O* ray or the *E* ray to be completely eliminated by the analyzer, and the crystal is said to be at **extinction**. As the crystal is rotated from this extinction position, it becomes progressively lighter and reaches a maximum brightness at 45°. There are four extinction positions in a 360° rotation, one every 90°.

Interference

As the crystal is rotated from one extinction position to another, it affects the behavior of polarized light. Figure 13.15 represents five positions of a tiny quartz crystal elongated on the *c* axis and lying on a prism face. It is assumed in the diagrams that light from the polarizer is moving upward, normal to the page, and vibrating in direction *P–P*. The vibration direction of the analyzer is *A–A*. The crystal in *a* is at an extinction position, and light moves through it as the *E* ray vibrating parallel to the *c* axis. At 90°, position *b*, the crystal is also at extinction with light moving through it as the *O* ray. When the crystal is turned as in *c*, *d*, and *e*, polarized light entering it is resolved into two components. One component moves through it as the *O* ray, vibrating in the basal plane; the other as the *E* ray, vibrating in the principal section. In *c*, most light is transmitted as the *E* ray, but in *e* it is transmitted mostly as the *O* ray. In *d*, the 45° position, the amounts of light transmitted by the two rays are equal.

When these rays from the crystal enter the analyzer, each is broken up into an *O* and an *E* ray conforming in vibration directions to those of the analyzer.

FIG. 13.15 Quartz crystal between crossed polars displaying the direction of the *O* and *E* rays.

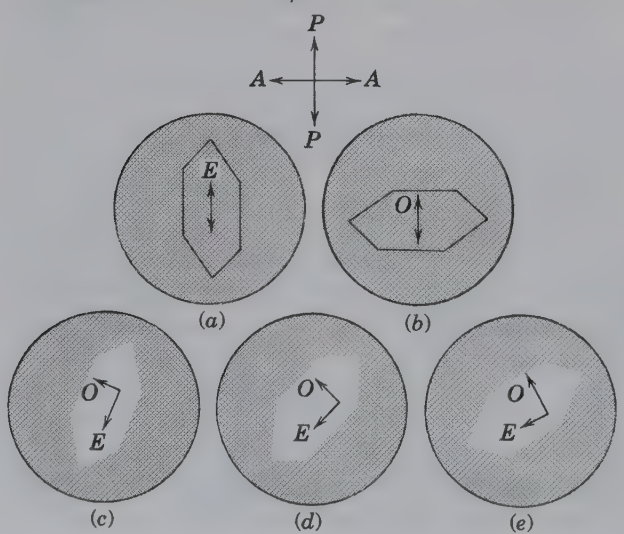

Only the components of the rays vibrating in an E–W direction are permitted to pass. During their passage through the crystal, the two rays travel with different velocities. When they emerge from the crystal, there is a phase difference between these because one is ahead of the other. The amount it is ahead depends both on the difference in velocities and on the thickness of crystal traversed. Because both rays vibrate in the same plane of the analyzer, they interfere. For monochromatic light, if one ray is an integral number ($n = 1, 2, 3$, etc.) of wavelengths ($n\,\lambda$) behind the other, it is said to be retarded [retardation (Δ) is expressed as $\Delta = n\,\lambda$, with $n = 1, 2, 3$, etc.]. Such interference conditions result in darkness. On the other hand, if the path difference is $\lambda/2$, $3\,\lambda/2$, or in general retardation, $\Delta = n + \frac{1}{2}\lambda$, the waves reinforce one another to produce maximum brightness.

Each wavelength has its own set of critical conditions when interference produces darkness. Consequently, when white light is used, "darkness" for one wavelength means its elimination from the spectrum and its complementary color appears. The colors produced are called **interference colors**. There are different *orders* of interference that depend on whether the color results from a path difference of $1\lambda, 2\lambda, 3\lambda, \ldots, n\lambda$.

These are called first-order, second-order, third-order, and so forth, interference colors, as indicated on the interference color plate that appears on the endpaper at the back of this text.

Interference colors depend on three factors: optical orientation, thickness, and **birefringence**, which is the difference between the two refractive indices (i.e., ω–ϵ for negative crystals and ϵ–ω for positive crystals). Birefringence is an inherent characteristic of a given mineral, as are its refractive indices. The colored chart of interference colors (at the back of this text) is a graphical representation of the relationship between retardation (Δ), birefringence, and crystal thickness. The chart displays the normal sequence from left to right of interference colors between crossed polars. Each color results from a specific retardation as expressed in nanometers (nm) along the bottom of the chart. Retardation, and the resulting color, are dependent on thickness. The thickness is given along the left or vertical scale, in micrometers (mm). Birefringence ($n_2 - n_1$) values are listed at the top of the chart with lines radiating from the lower-left corner representing values of equal birefringence as a function of thickness. In summary, the interference color chart is a graphical representation of the formula $\Delta = d\,(n_2 - n_1)$, which expresses the fact that retardation (Δ) is a function of crystal thickness (d) and birefringence ($n_2 - n_1$).

With a continuous change in direction of light, from parallel to perpendicular to the optic axis, there is

a continuous increase in interference colors. For a given orientation, the thicker the crystal and the greater its birefringence, the higher the order of interference color. If a crystal plate is of uniform thickness, as a cleavage flake may be or a grain in a rock thin section, it will show a single interference color. As seen in immersion liquids, grains commonly vary in thickness, and a variation in interference colors reflects this irregularity.

Accessory Plates

The gypsum plate, mica plate, and quartz wedge are accessory plates used with the polarizing microscope; their function is to produce interference of known amounts and, thus, predetermined colors. They are all constructed so that the fast ray (the vibration direction of the lesser refractive index) is parallel to the long dimension. The *gypsum plate* is made by cleaving a gypsum crystal to such a thickness that it produces a uniform red interference color in white light: *first-order red*. The *mica plate* is made with a thin mica flake, cleaved to a thickness such that it yields a path difference of a quarter of a wavelength for yellow light. Therefore, it is called the *quarter wave plate*. The *quartz wedge* is an elongated, wedge-shaped piece of quartz with the vibration direction of the fast ray (ω) parallel to its length and the slow ray (ϵ) across its length. As thicker portions of the wedge are placed in the optical path, the path difference of the rays passing through it also increases, producing a succession of interference colors. The number of orders depends on the wedge angle: the greater the angle, the more orders per unit of length.

UNIAXIAL CRYSTALS IN CONVERGENT POLARIZED LIGHT

Specific interference results in **interference figures**, seen when properly oriented crystal sections are examined in convergent polarized light. To see them, the polarizing microscope (usually used as an orthoscope) is converted to a conoscope by swinging in the upper substage condensing lens, so that the section can be observed in strongly converging light, using a high-power objective (100× works best). The interference figure then appears as an image just above the upper lens of the objective and can be seen between crossed polars by inserting a Bertrand lens and looking through the ocular (or by removing the ocular and looking down the microscope tube).

The principal interference figure of a uniaxial crystal, the optic axis figure (Fig. 13.16), is seen when the crystal is viewed parallel to the *c* axis. There is no double refraction for the central rays from the converging lens; the others, traversing the crystal in directions not parallel to the *c* axis, are resolved into *O* and *E* rays and have increasing path differences as the obliquity to the *c* axis increases. The interference of these rays produces concentric circles of interference colors. The center is black with no interference, but moving outward there is a progression from first-order to second-order to third-order, and so forth, interference colors. If the crystal section is of uniform thickness, no change will be noted as it is moved horizontally. If, however, the thickness varies, as in a wedge-shaped fragment, the positions of the colors change with horizontal movement. At the thin edge, there may be only first-order gray, but as the crystal is moved so the light path through it becomes greater, all the first-order colors may appear. With increasing crystal thickness, the path difference of the two rays may be great enough to yield second-, third-, and higher-order interference colors.

The reason for the black cross superimposed on the rings of interference colors is because these vibration directions are parallel or nearly parallel to the vibration directions of the polarizer and analyzer so that no light passes through them. Therefore, a dark cross results, as shown in Fig. 13.16a. The radial dashes in this drawing indicate the vibration directions of the *E* ray and those at right angles indicate the vibration directions of the *O* ray.

(*a*) (*b*) (*c*)

FIG. 13.16 Uniaxial optic axis interference figures. (a) Radial lines indicate vibration directions of the *E* ray; tangential lines indicate vibration directions of the *O* ray. (b) and (c) show isochromatic curves.

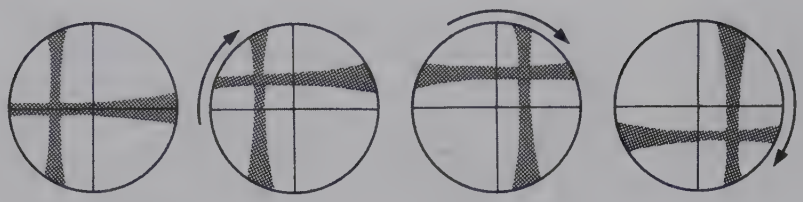

FIG. 13.17 Positions of an off-centered uniaxial optic axis figure on clockwise rotation of the microscope stage.

Fig. 13.16 illustrates a centered optic axis figure as obtained on a crystal plate whose *c* axis coincides with the axis of the microscope; as the stage is rotated, no movement of the figure is seen. If the optic axis of the crystal makes an angle with the axis of the microscope, the black cross is no longer symmetrically located in the field of view (Fig. 13.17). When the stage is rotated, the center of the cross moves in a circular path, but the bars of the cross remain parallel to the vibration directions of the polarizer and analyzer. Even if the inclination of the optic axis is so great that the center of the cross does not appear, on rotation of the crystal, the bars move across the field and maintain their parallelism to the vibration directions of the polars.

The **flash figure** is an interference figure produced by a uniaxial crystal when its optic axis is normal to the axis of the microscope; that is, a hexagonal or tetragonal crystal lying on a face in the prism zone. When the crystal is at an extinction position, the figure is an ill-defined cross occupying much of the field. On rotation of the stage, the cross breaks into two hyperbolas that rapidly leave the field in those quadrants containing the optic axis. The cross forms because the converging light is broken into *O* and *E* rays with vibration directions mostly parallel or nearly parallel to the vibration directions of the polarizer and analyzer. A centered flash figure indicates the vibration direction of the *E* ray, and assures one that a true value of ϵ can be obtained in plane polarized light in this direction.

DETERMINATION OF OPTIC SIGN

The mica plate, the gypsum plate, and the quartz wedge may be used with a uniaxial optic axis figure to determine the **optic sign**; that is, whether the crystal is positive or negative. They are inserted below the analyzer in a slot in the microscope tube and are positioned so that when the plates are in place, their vibration directions make angles of 45° with the vibration directions of the polars.

It was discussed previously, that in an optic axis interference figure, the *E* ray vibrates radially and the *O* ray tangentially. By use of an accessory plate in which vibration directions of the slow and fast rays are known, one can tell whether the *E* ray of the crystal is slower (positive crystals) or faster (negative crystals) than the *O* ray and, thus, determine the optic sign. For most equipment, the vibration of the slow ray is at right angles to the length of the plate and is marked on the metal carrier. However, the vibration directions should be checked before using an accessory. The principle in the use of all the plates is the same: to add or subtract from the path difference of the *O* and *E* rays of the crystal.

If the *mica plate* is superimposed on a uniaxial optic axis figure in which the ordinary ray is slow (negative crystal), the interference of the plate reinforces the interference colors in the SE and NW quadrants, causing them to shift slightly toward the center. At the same time, subtraction causes the colors in the NE and SW quadrants to shift slightly away from the center. The most marked effect produced by the mica plate is the formation of two black spots near the center of the black cross in the quadrants where subtraction occurs (Fig. 13.18).

The *gypsum plate* is usually used to determine the optic sign when low-order interference colors or no colors at all are seen in the optic axis figure. It has the effect of superimposing red of the first-order on the interference figure. If the figure shows several orders of interference colors, one should consider the color

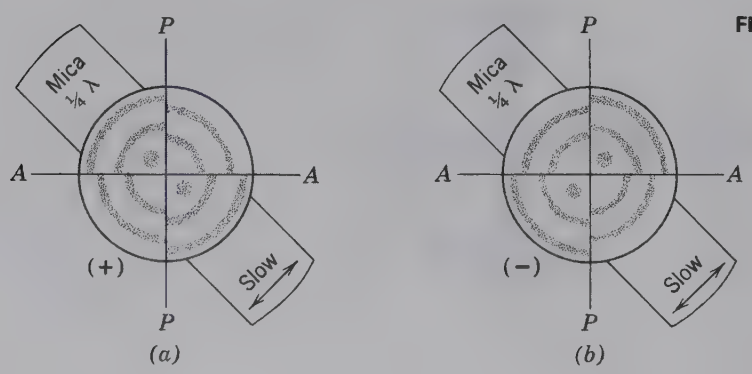

FIG. 13.18 Determination of optic sign with a mica plate.

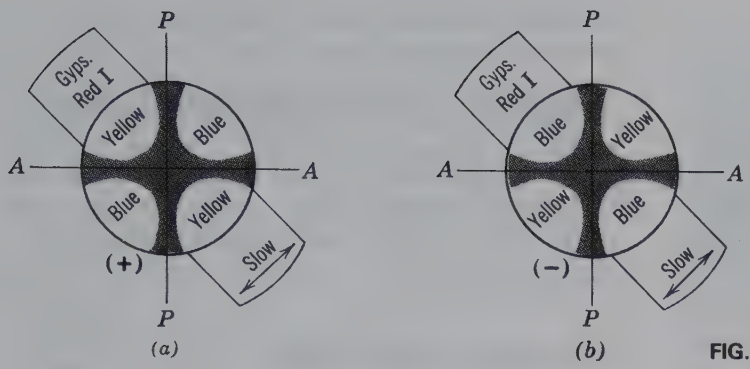

FIG. 13.19 Determination of optic sign with a gypsum plate.

effect on the grays of the first-order near the center. In the quadrants where there is addition, the red plus the gray gives blue; in the alternate quadrants the red minus the gray gives yellow. The arrangement of colors in positive crystals is: yellow SE–NW; blue NE–SW; and in negative crystals, yellow NE–SW, blue SE–NW. It is suggested that the reader insert the colors in Fig. 13.19.

The *quartz wedge* is most effective in determining optic sign when high-order interference colors are present in the optic axis figure. The wedge is usually inserted with the thin edge first. If its retardation is added to that of the crystal, the interference colors in two opposite quadrants will increase progressively as the wedge moves through the microscope tube. If the retardation is subtracted from that produced by the crystal, the order of colors will decrease. Thus, as the quartz wedge is slowly inserted over an optic axis figure of a negative crystal, the color bands in the SE–NW quadrants move toward the center and disappear. At the same time, the colors in the NE–SW quadrants move outward to the edge of the field. Similar phenomena are observed in a positive crystal, but the colors move in the opposite directions, that is, away from the center in the SE–NW quadrants and toward the center in the NE–SW quadrants.

SIGN OF ELONGATION

Hexagonal and tetragonal crystals are commonly elongated on the *c* axis or have prismatic cleavage that permits them to break into splintery fragments also elongated parallel to *c*. If such an orientation is known, one can determine the optic sign by turning the elongated grain to the 45° position and inserting the gypsum plate. If the interference colors rise (gray of mineral plus first-order red equals blue), the slow ray of the gypsum has been superimposed on the slow ray of the mineral. If this is also the direction of elongation, it means that the *E* ray is slow (ϵ is the higher refractive index) and the mineral has positive elongation and is optically positive. When the slow ray of the gypsum plate is parallel to the elongation of the mineral grain and the interference colors fall (gray of mineral minus first-order red equals yellow), the mineral has negative elongation and is optically negative (Fig. 13.20).

Very commonly, the interference colors of small grains are first-order grays. Thus, on superimposing red of the first order, addition gives a blue color and subtraction a yellow color.

ABSORPTION AND DICHROISM

In the previous discussion of polarized light, it was pointed out that in some tourmaline the absorption of one ray is nearly complete but for the other ray it is negligible. Although less striking, many crystals show a similar phenomenon; more light is absorbed in one vibration direction than in the other. In tourmaline where absorption of the *O* ray is greatest, it is expressed as, absorption: $O > E$ or $\omega > \epsilon$. In other crystals, certain wavelengths may be absorbed in one direction and the complementary colors are transmitted. Thus, the crystal has different colors in different vibration directions and is said to be *dichroic*. Dichroism is expressed by giving the colors, for example, *O* or ω = yellow, *E* or ϵ = pink. Absorption is independent of other properties and is considered a fundamental optical property of crystals as are refractive indices.

FIG. 13.20 Determination of sign of elongation with a gypsum plate. In diagrams Y = yellow, B = blue. (a) Positive elongation, (b) Negative elongation.

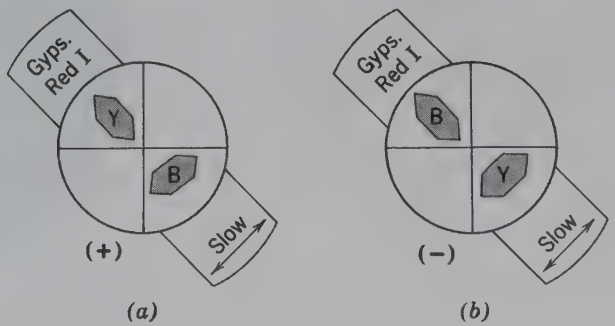

BIAXIAL CRYSTALS

Orthorhombic, monoclinic, and triclinic crystals are called optically biaxial because they have two directions in which light travels with zero birefringence (it is not reoriented). These minerals are characterized by three R.I.s. In uniaxial crystals, there is only one such direction and the minerals are characterized by two R.I.s.

Light moving through a biaxial crystal, except along an optic axis, travels as two rays with mutually perpendicular vibrations. The velocities of the rays differ from each other and change with changing crystallographic direction. The vibration directions of the fastest ray, *X*, and the slowest ray, *Z*, are at right angles to each other. The direction perpendicular to the plane defined by *X* and *Z* is designated as *Y*. For biaxial crystals, there are three indices of refraction resulting from rays vibrating in each of these principal optical directions. The numerical difference between the greatest and least refractive indices is the **birefringence**. Various letters and symbols have been used to designate the refractive indices, but the most generally accepted are the Greek letters as follows:

Index*		Direction	Ray Velocity
(alpha)	α lowest	*X*	highest
(beta)	β middle	*Y*	intermediate
(gamma)	γ highest	*Z*	lowest

*Other equivalent designations are: $\alpha = nX, n_x, N_x, N_p$; $\beta = nY, n_y, N_y, N_m$; $\gamma = nZ, n_z, N_z, N_g$.

THE BIAXIAL INDICATRIX

The biaxial indicatrix is a visualization of relative values of the three principal indices of refraction and is used in much the same manner as the uniaxial indicatrix. Its general shape (Fig. 13.21a) is that of a triaxial ellipsoid with its three axes mutually perpendicular optical directions *X*, *Y*, and *Z*. The lengths of the semiaxes are proportional to the refractive indices: α along *X*, β along *Y*, and γ along *Z*. Sections through this triaxial ellipsoid are all ellipses (Fig. 13.21b and c) except for two sections that are marked as **circular sections** (in Fig. 13.21c) with their radii noted as *S*.

FIG. 13.21 (a) Biaxial indicatrix in which the lengths of the three principal axes are the refractive indices α, β, γ, measured along the optical directions *X*, *Y*, and *Z*. (b) and (c) Principal sections through the biaxial indicatrix of a positive crystal. The section in (c) shows the location of the two circular sections with the optic axes perpendicular to them.

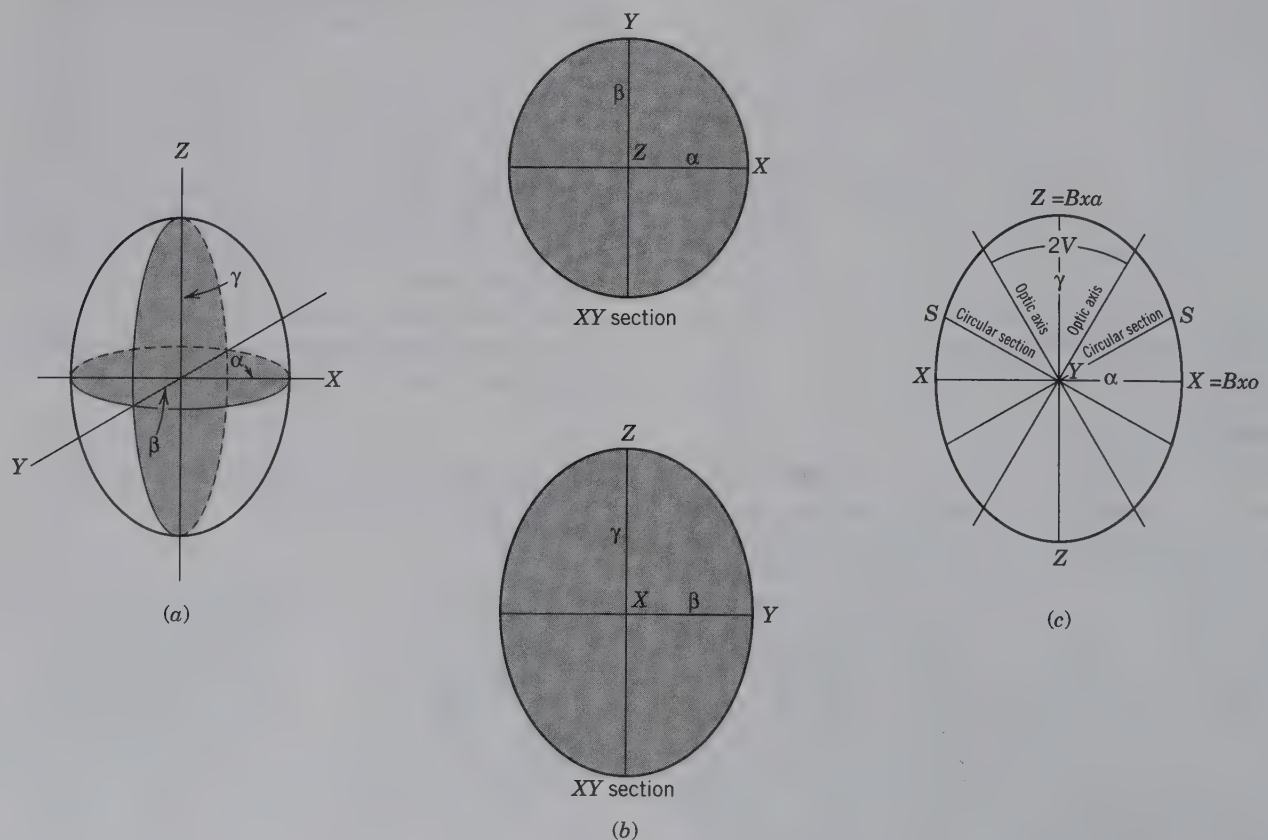

The two directions normal to these sections are the *optic axes*; and the XZ plane in which they lie is called the **optic plane**. The Y direction perpendicular to this plane is the **optic normal**. Light moving along the optic axes and vibrating in the circular sections shows no birefringence and gives the constant refractive index, β. The optic axis of a uniaxial crystal is analogous to these directions because light moving parallel to it also vibrates in a circular section with a constant refractive index.

With variation in refractive indices, there is a corresponding variation in the axial lengths of the biaxial indicatrix. Some crystals are nearly uniaxial, and in these, the intermediate index, β, is very close to either α or γ. If β is close to α, the circular sections make only a small angle with the XY plane and the optic axes make the same angle with the Z direction. This is angle V and the angle between the two optic axes, known as the **optic angle**, is $2V$. The optic angle is always acute and because, in this case, it is bisected by Z, Z is called the *acute bisectrix* (Bxa); X is the *obtuse bisectrix* (Bxo) because it bisects the obtuse angle between the optic axes. When Z is the Bxa, the crystal is optically positive.

If β is closer to γ than to α, the acute angle between the optic axes is bisected by X and the obtuse angle is bisected by Z. In this case, with X the Bxa, the crystal is negative. When β lies exactly halfway between α and γ, the optic angle is 90°.

The relation between the optic angle and the indices of refraction is expressed by formula (a). A close approximation to the optic angle can be made using formula (b).

$$\text{(a)}\quad \cos^2 V_x = \frac{\gamma^2(\beta^2 - \alpha^2)}{\beta^2(\gamma^2 - \alpha^2)}$$

$$\text{(b)}\quad \cos^2 V_x = \frac{\beta - \alpha}{\gamma - \alpha}$$

The error using the simplified formula increases with the increase of both birefringence and V and always yields values for V' less than true V. It should be noted that in using either formula, *half* the optic angle is calculated and is determined with X as the bisectrix. Thus, when $V < 45°$, the crystal is negative but when $V > 45°$, the crystal is positive.

Optical Orientation in Biaxial Crystals

The orientation of the optical indicatrix is one of the fundamental optical properties. It is given by expressing the relationship of X, Y, and Z optical directions to the crystallographic axes, a, b, and c.

In *orthorhombic crystals*, each of the crystallographic axes is coincident with one of the principal optical directions. For example, the optical orientation of anhydrite is $X = c$, $Y = b$, $Z = a$. Usually the optical directions coinciding with only two axes are given, for this completely fixes the position of the indicatrix.

It is difficult or impossible to determine the axial directions on microscopic grains of some minerals. To do so, one must use a fragment oriented by X-ray study or broken from a crystal with identified crystal faces. However, even in small particles, orientation can be expressed relative to cleavage. Powdered fragments tend to lie on cleavage faces, which in orthorhombic crystals are commonly pinacoidal or prismatic. For example, barite has {001} and {210} cleavages and most grains lie on faces of these forms. Those lying on {001} will be diamond shaped (Fig. 13.22a) and have **symmetrical extinction**. That is, the extinction position makes equal angles with the bounding cleavage faces. Fragments lying on {210} will have **parallel extinction** (Fig. 13.22*b*). Symmetrical and parallel extinction are characteristic of orthorhombic crystals.

Barite is positive (+), $X = c$, $Y = b$, $Z = a$. Thus, grains lying on {001} yield a centered Bxo figure, and one can determine β in the b direction and γ in the a direction. Grains showing parallel extinction do not give a centered interference figure, but α can be measured parallel to c.

In *monoclinic crystals*, one of the principal optical directions (X, Y, or Z) of the indicatrix coincides with the b axis; the other two lie in the a–c plane of the crystal. The orientation is given by stating which optical direction equals b and indicating the **extinction angle**, the angle between the c axis and one of the other optical

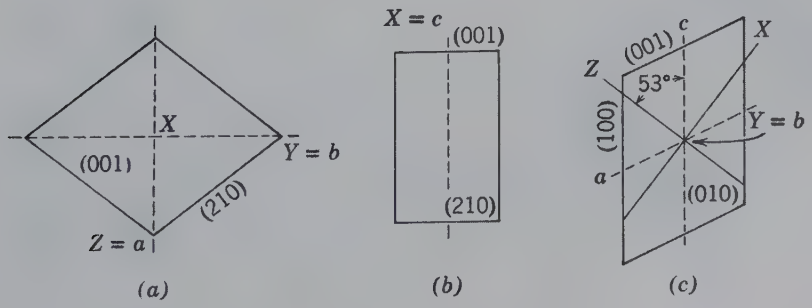

FIG. 13.22 Optical orientation. (a) Barite on {001} showing symmetrical extinction. (b) Barite on {210} showing parallel extinction. (c) Gypsum on {010} showing extinction angle.

directions. If the extinction lies between the + ends of the *a* and *c* axes, the angle is positive; between $+c$ and $-a$, the angle is negative. In gypsum $Y = b$ and $Z \wedge c = 53°$. Thus, a fragment lying on the {010} cleavage would yield an optic normal interference figure and α and γ could be determined; γ at the extinction position $+53°$; α at extinction position $-37°$ (Fig. 13.22c). A grain lying on the {100} cleavage would show parallel extinction and β could be measured at right angles to the trace of {010}. Crystal fragments lying on any other face in the [001] zone, as on {110}, will show an extinction angle, but the angle to be recorded, usually that of *maximum extinction*, is observed on {010}. Parallel extinction indicates the grain is lying on a face in the [010] zone and the index of the ray vibrating parallel to *b* can be measured.

In *triclinic crystals*, the optical indicatrix can occupy any position relative to the crystallographic axes. Thus, a complete optical orientation necessitates giving ϕ and ρ angles of the principal optical directions. In most cases, however, it suffices to give the extinction angles observed on grains lying on known cleavage faces.

BIAXIAL CRYSTALS IN CONVERGENT POLARIZED LIGHT

Biaxial interference figures are obtained and observed in the same manner as uniaxial figures, that is, with converging light, a high-power objective, and a Bertrand lens. Although interference figures can be observed on random sections of biaxial crystals, the most symmetrical and informative are obtained on sections normal to the optical directions *X*, *Y*, and *Z*, as well as to an optic axis.

The **acute bisectrix figure** is observed on a crystal plate cut normal to the acute bisectrix. If $2V$ is very small, there are four positions during a 360° rotation at which the figure resembles the uniaxial optic axis figure. That is, a black cross is surrounded by circular bands of interference colors. However, as the stage is turned, the black cross breaks into two hyperbolas that have a slight but maximum separation at a 45° rotation; and the color bands, known as *isochromatic curves*, assume an oval shape. The hyperbolas are called *isogyres* and the dark spots, called *melatopes*, at their vertices in the 45° position, result from light rays that traveled along the optic axes in the crystal. Thus, the separation of the isogyres increases with increasing optic angle, and the isochromatic curves are arranged symmetrically about the melatopes as shown in Fig. 13.23. When $2V$ exceeds 60°, the isogyres leave the field at the 45° position; the larger the optic angle, the faster they leave.

The portion of the interference figure occupied by the isogyres is dark, because here, light emerging from the section has vibration directions parallel to those of the polarizer and analyzer. Thus, the dark cross is present when the obtuse bisectrix and optic normal coincide with the vibration directions of the polars. The bar of the cross parallel to the optic plane is narrower and better defined than the other bar (Fig. 13.23). Because light travels along the optic axes with no birefringence, their points of emergence are dark in all positions of the figure.

The Apparent Optic Angle

The distance between the points of emergence of the optic axes is dependent not only on $2V$ but on β as well. The refractive index of crystals is β for light rays moving along the optic axes. These rays are refracted on leaving the crystal, giving an apparent optic angle, $2E$, greater than the real angle, $2V$ (Fig. 13.24). The higher the β refractive index, the greater is the refraction. Thus, if two crystals have the same $2V$, the one with the higher β index has the larger apparent angle, which results in the optic axes being farther apart as they emerge in the interference figure.

The **optic axis figure** is observed on mineral grains cut normal to an optic axis. Such grains are easy

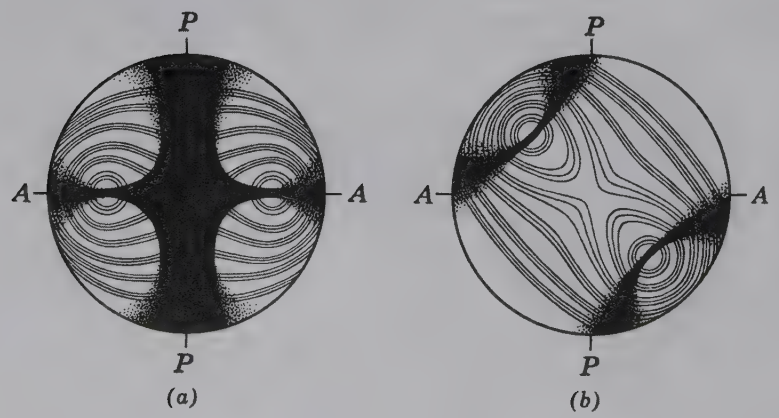

FIG. 13.23 Acute bisectrix interference figure. (a) Parallel position. (b) 45° position.

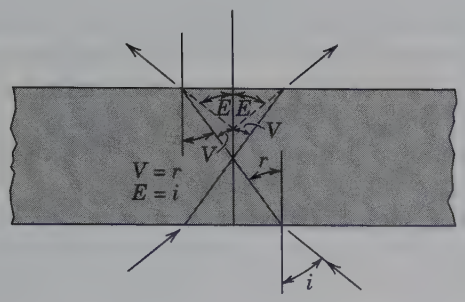

FIG. 13.24 Relation of $2V$ to $2E$.

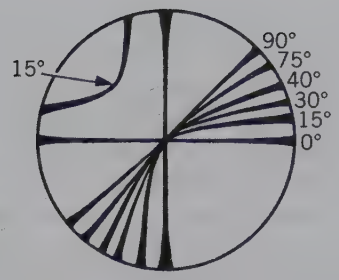

FIG. 13.25 Curvature of isogyre in an optic axis figure from 0° to 90° $2V$.

to select, for they remain essentially dark between crossed polars on complete rotation. The figure consists of a single isogyre, at the center of which is the emergence of the optic axis. When the optic plane is parallel to the vibration direction of either polar, the isogyre crosses the center of the field as a straight bar. As the stage rotates, it swings across the field forming a hyperbola in the 45° position. In this position, the figure can be pictured as half an acute bisectrix figure with the convex side of the isogyre pointing toward the acute bisectrix. As $2V$ increases, the curvature of the isogyre décreases, and when $2V = 90°$, the isogyre is straight (Fig. 13.25).

The **obtuse bisectrix figure** is obtained on a crystal section cut normal to the obtuse bisectrix. When the plane of the optic axes is parallel to the vibration direction of either polar, there is a black cross. Rotating the stage causes the cross to break into two isogyres that move rapidly out of the field in the direction of the acute bisectrix. Although not as informative as an acute bisectrix figure, a centered obtuse bisectrix figure indicates that an accurate determination of β and of either α or γ can be made on the mineral section producing it.

The **optic normal figure** is obtained on sections cut parallel to the plane of the optic axes and resembles the flash figure of a uniaxial crystal. When the X and Z optical directions are parallel to the vibration directions of the polars, the figure is a poorly defined cross. On slight rotation of the stage, it splits into hyperbolas that move rapidly out of the field in the quadrants containing the acute bisectrix. An optic normal figure is obtained on sections with maximum birefringence and indicates that α and β can be determined on this section.

DETERMINATION OF OPTIC SIGN OF BIAXIAL CRYSTALS

The optic sign of biaxial crystals can best be determined on acute bisectrix or optic axis figures with the aid of accessory plates. Let us assume that *a* in Fig. 13.26 represents an acute bisectrix figure of a negative crystal in the 45° position. By definition, X is the acute

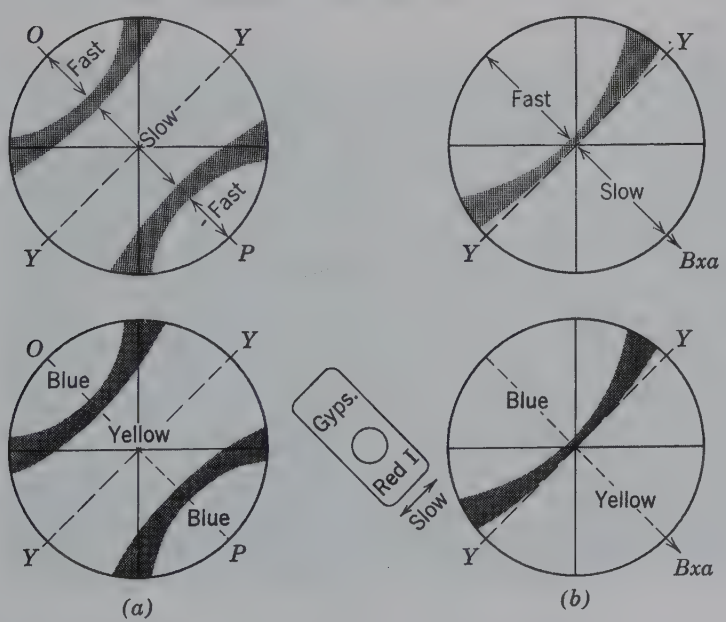

FIG. 13.26 Optic sign determination of a negative crystal with a gypsum plate. (a) Acute bisectrix figure. (b) Optic axis figure.

bisectrix and Z the obtuse bisectrix. *OP* is the trace of the optic plane and Y the vibration direction of β, at right angles. The velocity is constant for all rays moving along the optic axes, and for them the refractive index of the crystal is β including those vibrating in the optic plane. Consider the velocities of other rays, vibrating in the optic plane. In a negative crystal, those emerging between the isogyres of an acute bisectrix figure have a lesser velocity, and those emerging outside the isogyres have a greater velocity. If the gypsum plate is superimposed over such a figure, the slow ray of the plate combines with the fast ray of the crystal, and subtraction of interference colors produces a yellow color on the *convex* sides of the isogyres. On the *concave* sides of the isogyres, a blue color is produced by addition of the slow ray of the plate over the slow ray of the crystal. In a positive crystal, the reverse color effect is seen, for here Z is the acute bisectrix.

An optic axis figure in the 45° position can be used in a manner similar to that of the acute bisectrix figure in determining optic sign. Insertion of the gypsum plate yields for a (−) crystal: convex side yellow, concave side blue (Fig. 13.26b), and for a (+) crystal: convex side blue, concave side yellow.

The quartz wedge may be used to determine optic sign if several isochromatic bands are present. As the wedge is inserted, the colors move out in those portions of the figure where there is subtraction and move in where there is addition. In other words, in the areas that a gypsum plate would render blue, the colors move in; in those that it would render yellow, they move out.

When using the immersion technique, it is time-saving, particularly in working with biaxial minerals, to first match as closely as possible the refractive indices of the unknown with n of the liquid. An interference figure, then, in addition to the optic sign, will yield other useful information. Using a grain giving an optic axis figure, β can be compared with n of the liquid. On a grain yielding an acute bisectrix figure, β and either α or γ can be compared with the refractive index of the liquid. The indices of a grain showing highest interference colors are most likely to be close to α and γ. Therefore, in the same mount, one should check such a grain to estimate how far α and γ are from the refractive index of the liquid.

ABSORPTION AND PLEOCHROISM

The absorption of light in biaxial crystals may differ in the X, Y, and Z optical directions. If the difference is only in intensity and X has the greatest **absorption** and Z the least, it is expressed as $X > Y > Z$. If different wavelengths are selectively absorbed in different directions, the color of the mineral varies as a function of crystallographic orientation. It is said to be **pleochroic**, and the color of the transmitted light is given. Pleochroism can be observed only in plane polarized light. For example, for a member of the orthopyroxene series, the *pleochroism* may be stated as X = brownish red, Y = reddish yellow, Z = green. The term *pleochroism* is commonly used to denote all differential absorption of light in both uniaxial and biaxial crystals.

Other Properties

Additional optical observations may provide valuable information about a sample under study. These include cleavage, twinning, habit, extinction angle, mineral alteration, and/or metamict features. Cleavage is most easily observed in plane polarized light. The number of cleavage directions and the intersection angle between them commonly serve as distinguishing features for many minerals. For example, pyroxenes display two cleavages that are at 90° to each other whereas amphiboles display two cleavages that are at angles near 60°/120°. The presence of twinning is optically apparent, such as in feldspars that show both simple and polysynthetic twins (see Figs. 10.17 and 10.18). Crystal morphology that may be acicular, tabular, or euhedral, is easily determined. The relationship between the orientation of the indicatrix and the crystallographic axes is given by the extinction angle. Uniaxial and orthorhombic minerals have parallel extinction whereas monoclinic and triclinic crystals display inclined extinction. Minerals that incorporate radioactive elements stand out by the damage they inflict on host phases. This results in the development of a pleochroic halo in the surrounding minerals. Some minerals alter to distinct phases and such alteration features may be diagnostic.

OPTICAL PROPERTIES OF OPAQUE MINERALS

The discussion in this chapter has dealt entirely with the optical properties of *nonopaque* minerals. Opaque minerals also possess optical properties by which they are characterized. Specially built microscopes, or adaptations to polarizing microscopes, are used for viewing polished sections of these minerals in *reflected* light. An additional light source is needed, which is directed downward onto the surface of a polished sample. The light that is reflected from the sample's surface returns through the objective to the ocular (see Fig. 13.27 for an illustration of the light path in a reflecting light microscope). Reflected light microscopy requires the use of a highly polished (mirror) surface, such as on a thin

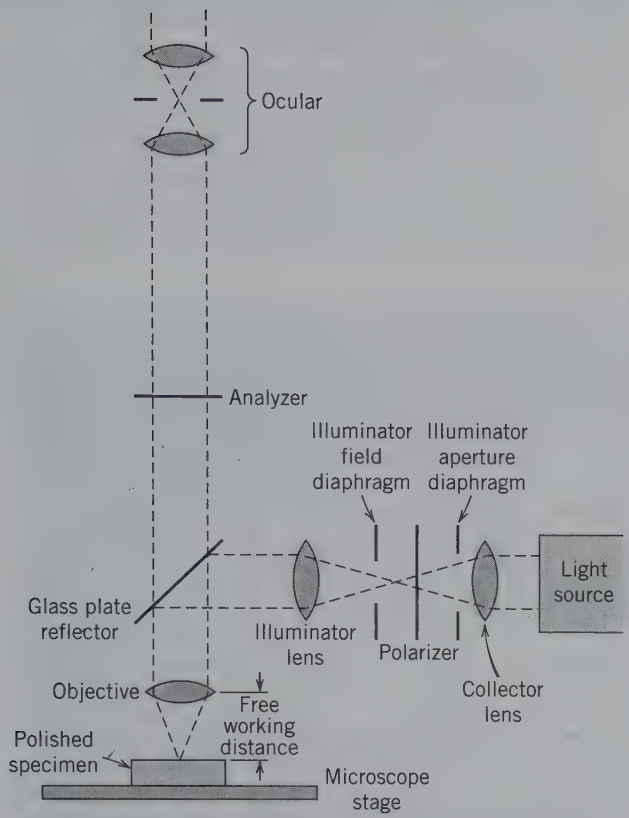

FIG. 13.27 Schematic cross section through a reflecting light microscope showing the light path and some of the components of the microscope.

section (without a cover slip) or on a polished mineral surface in an epoxy mount. Because most of the ore minerals are opaque, the techniques for polished section study with the *ore microscope* (or *reflecting light microscope*) have been developed and used mainly by those interested in economically important "ore" minerals (see Box 15.1).

In reflected light, colors, reflectivity, and bireflectance are diagnostic optical properties. Color is the first and frequently the most important property observed, and the skilled microscopist is able to distinguish one mineral from another by a subtle color difference. Commonly, these are shades of gray and/or yellow. Figure 13.28 illustrates the appearance of some opaque minerals in reflected light.

Reflectivity is an expression of the percentage of the incident light that is reflected from a mineral's surface. Using polarized light many nonisometric minerals show **bireflectance**, a property analogous to pleochroism in nonopaque minerals. That is, there is a change in brightness or color as the mineral is rotated on the microscope stage. Different minerals show this property in varying degrees. When viewed between crossed polars, nonisometric opaque minerals will show, as do nonopaque minerals, four positions of extinction in a 360° rotation. Isotropic minerals show neither bireflectance nor extinction positions and, thus, can be distinguished from anisotropic minerals.

The microscopic study of polished sections of opaque minerals gives important clues to the paragenesis and origin of mineral deposits. From the textural relationship of the minerals, one can determine their order of deposition and their subsequent replacement and exsolution phenomena. There is a large literature on ore microscopy, but even a brief discussion of the methods and techniques is beyond the scope of this text. Interested readers should refer to one of the many books on the subject given in the references at the end of the chapter.

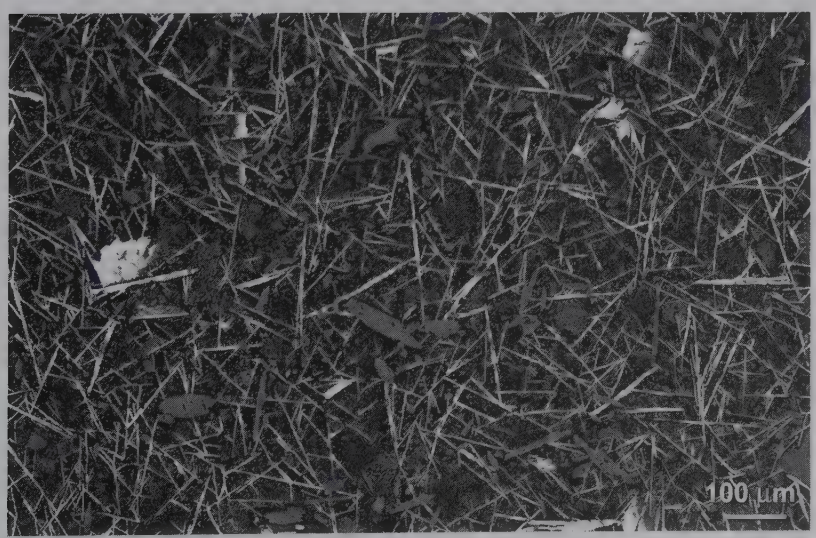

FIG. 13.28 Photomicrograph taken in reflected light of a polished section of minerals from the Salton Sea geothermal field, California, USA. The minerals are: chalcopyrite, white clumps; hematite, white acicular crystals; anhydrite, gray crystals; chlorite, dark gray matrix. Here, the spatial distribution of minerals is easily observed. (Photograph by B. Dutrow.)

REFERENCES AND FURTHER READING

Bloss, F. D. 1999. *Optical crystallography.* Monograph #5. Mineralogical Society of America, Washington, D.C.

Optical Microscopy: Nonopaque Minerals

Deer, W. A., R. A. Howie, and J. Zussman. 1992. *The rock-forming minerals.* 2nd ed. Longman Group UK Limited, London.

Ehlers, E. G. 1987. *Optical mineralogy.* Vol. 1, *Theory and techniques*; Vol. 2, *Mineral descriptions.* Blackwell Scientific Publications, Palo Alto, California.

Heinrich, E. W. 1965. *Microscopic identification of minerals.* McGraw-Hill, New York.

Humphries, D. W. 1992. *The preparation of thin sections of rocks, minerals, and ceramics.* Oxford University Press, Oxford.

Larsen, E. S., and H. Berman. 1934. *The microscopic determination of the nonopaque minerals.* 2nd ed. U.S. Geological Survey Bulletin no. 848. U. S. Government Printing Office, Washington, D.C.

MacKenzie, W. S., and C. Guilford. 1980. *Atlas of rock-forming minerals in thin section.* Wiley, New York.

Nesse, W. D. 1991. *Introduction to optical mineralogy.* 2nd ed. Oxford University Press, New York.

Phillips, W. R. 1971. *Minerals optics: Principles and techniques.* W. H. Freeman & Co. San Francisco.

Phillips, W. R., and D. T. Griffen. 1981. *Optical mineralogy: The nonopaque minerals.* W. H. Freeman & Co., San Francisco.

Shelley, D. 1985. *Optical mineralogy.* 2nd ed. Elsevier Science Publishers, New York.

Stoiber, R. E., and S. A. Morse, 1981. *Microscopic identification of crystals.* Rev. ed. Robert E. Krieger Publishing Co.

Vernon, R. H. 2004. *A practical guide to rock microstructures.* Cambridge University Press, Cambridge.

Wahlstrom, E. E. 1979. *Optical crystallography.* 5th ed. Wiley, New York.

Optical Microscopy: Opaque Minerals

Craig, J. R., and D. J. Vaughan. 1981. *Ore microscopy and ore petrology.* Wiley, New York.

Galopin, R., and N. F. M. Henry. 1972. *Microscopic study of opaque minerals.* McCrone Research Associates Ltd., London.

Ixer, R. A. 1990. *Atlas of opaque and ore minerals in their associations.* Van Nostrand Reinhold, New York.

Ramdohr, P. 1969. *The ore minerals and their intergrowths.* Pergamon Press, New York.

Uytenbogaardt, W., and E. A. J. Burke. 1971. *Tables for microscopic identification of ore minerals.* 2nd ed. Elsevier-North Holland, New York.

CHAPTER 14

Analytical and Imaging Methods in Mineral Science

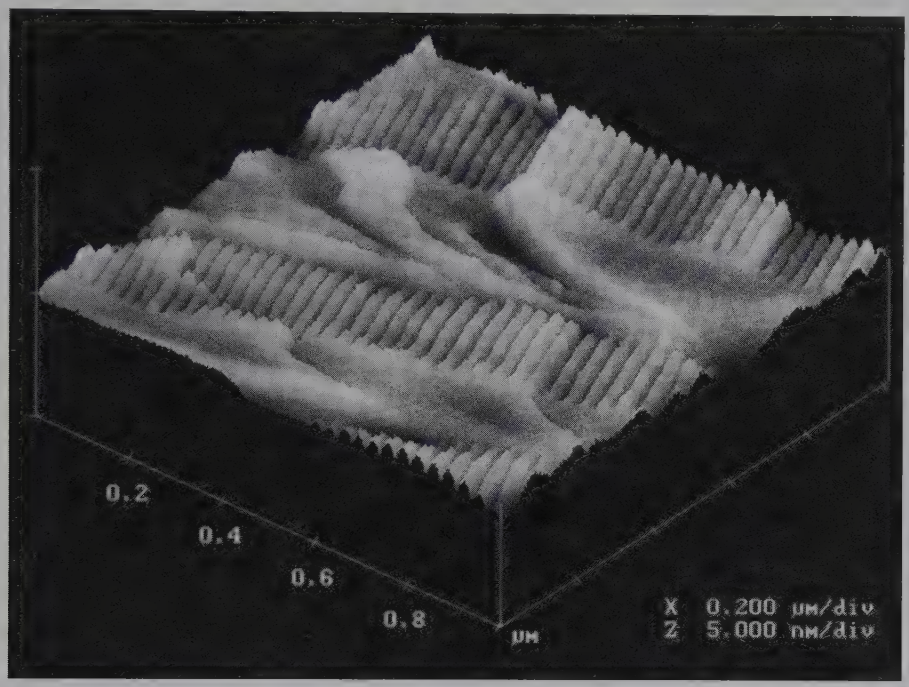

An extremely high-resolution image of a cleavage (001) surface of cryptoperthite (an extremely fine exsolution intergrowth of Na- and K-feldspar). This image was obtained by atomic force microscopy (AFM). The Na-rich lamellae, $NaAlSi_3O_8$, show closely spaced albite twins as expressed by the regularly spaced ridges. The K-rich lamellae (close to orthoclase, $KAlSi_3O_8$, in composition) have an essentially flat surface. The horizontal scales are expressed in increments of 0.2 μm (micrometers); the vertical scale is 5 nanometers (nm) per division (after Xu, H. 1997. Surface characters of twin domain and exsolution lamellae in a feldspar crystal: Atomic force microscopy study. Materials Research Bulletin, *32: 1121–27; photograph courtesy of Huifang Xu, University of Wisconsin, Madison).*

The evaluation of a range of physical and chemical properties of minerals is a basic aspect of mineral science studies. Recent advances in instrumentation provide a wide array of analytical techniques for the acquisition of qualitative and quantitative chemical data as well as structural information. Some techniques also reveal morphological features of crystals. The well-established methods that rely on data generated by high-energy electrons include scanning electron microscopy (SEM), transmission electron microscopy (TEM) and electron microprobe analysis (EMPA). X-ray diffraction (XRD) and X-ray fluorescence (XRF) use X-radiation to produce X-ray patterns that provide structural information and chemical data, respectively. Secondary ion mass spectrometry (SIMS) and atomic force microscopy (AFM) are more specialized techniques used to evaluate mineral composition and surface structure. Because X-ray powder diffraction equipment is widely available, this technique is treated in greater detail than other methods. This chapter provides an overview of these techniques and their applications to mineral studies.

Advanced mineralogic studies commonly involve imaging of the morphological features, the quantitative evaluation of chemical constituents, and determination of the crystal structure. As a follow up to hand-specimen physical property tests (discussed in Chapter 2) and optical methods (presented in Chapter 13), analytical and imaging tools provide high-quality data at scales ranging from the atomic level to that of bulk properties of the entire mineral. The analytical techniques covered here are grouped in terms of the energy source used to generate the data; X-rays, electrons, and other energy sources. Within each section, techniques are arranged such that those methods that provide qualitative data are discussed before those that produce more quantitative

information; some instruments provide both. For example, an electron microprobe can be fitted with a secondary electron detector to provide the investigator with excellent high-magnification images of crystal morphology as well as detailed chemical analyses.

TECHNIQUE OVERVIEW

Single-crystal X-ray diffraction techniques are most commonly used in the determination of crystal structures, unit cell sizes, atomic parameters, and bond distributions. Powder X-ray diffraction is a rapid and commonly available technique for mineral identification and can also provide information about unit cell sizes. X-ray fluorescence is a sensitive technique for obtaining chemical analyses of bulk samples including low-abundance elements. High-energy electrons, accelerated from 10 KeV to over 150 KeV, form the basis for numerous electron beam methods. The scanning electron microscope (SEM) provides images of crystal morphology at the micrometer level. Transmission electron microscopes (TEMs) allow for the direct imaging of crystal structures, defects in the structures, and extremely fine-grained intergrowths of different minerals or mineral reactions that are not visible using lower-resolution techniques, such as optical microscopy. Electron diffraction results (as part of TEM techniques) commonly complement structural data obtained from X-ray single crystal experiments. The high-resolution transmission electron microscope (HRTEM) mode allows for the projection of structures on a two-dimensional image with a resolution of about 1.5 Å. Atomic force microscopy (AFM) allows for the characterization of surfaces of minerals on an atomic or near-atomic scale. However, the overviews presented here are inadequate for a thorough understanding of all of the underlying concepts and additional references are given.

Several analytical techniques are specifically designed to obtain *quantitative* chemical data whereas others are best used for *qualitative* data. A **qualitative** analysis involves the detection and identification of all the chemical constituents of a compound ("What is present?"). A **quantitative** analysis involves the determination of the weight percentages (or parts per million composition) of all elements in a compound ("How much of each is present?"). A preliminary *qualitative* analysis is commonly helpful in deciding on the methods to be followed in a subsequent *quantitative* analysis.

Prior to 1947, quantitative chemical analyses of minerals were obtained mainly by "wet" analytical techniques, in which the mineral was dissolved by some appropriate acid. Subsequently, each constituent element was precipitated out of solution and weighed, with results reported as weight percentage of the oxides. Since 1960, the majority of quantitative analyses have been made by instrumental techniques, such as electron microprobe analysis (EMPA) for *in situ* chemical analyses of areas as small as 1 micrometer in diameter (1 $\mu m = 10^{-6} m$) and/or X-ray fluorescence analysis (XRF) for chemistry of bulk samples. Secondary ion mass spectrometry (SIMS) uses a focused ion beam to excavate ions from a mineral surface and analyzes their mass and charge with a mass spectrometer. Each of these techniques has its own specific sample preparation requirements and has well-established detection limits, precision, and accuracy values and error ranges. The results of any chemical analysis are generally presented in a table of weight percentages of the elements or oxide components in the mineral analyzed.

TECHNIQUES THAT USE X-RAYS

X-RAY DIFFRACTION TECHNIQUES (XRD)

Since the discovery of X-rays by Wilhelm Conrad Roentgen in 1895, and the first application of an X-ray experiment to the study of crystalline material in 1912 by Max von Laue (see Chapter 1), X-ray diffraction techniques have been fundamental to *crystal structure analysis*. Current knowledge of the location of atoms, their sizes, and their bonding in crystal structures, as well as a structure's space group symmetry and chemical composition and size of its unit cell, has been derived largely from single crystal X-ray diffraction studies. X-ray crystallography is a science that is pursued by researchers with a broad knowledge base in mathematics, physics, chemistry, and computational methods.

This section briefly introduces X-rays and their diffraction effects, followed by a short overview of crystal structure analysis, using *single-crystal techniques* and an introduction to the *X-ray powder diffraction method*, which is routinely used in mineral identification. This quick and inexpensive identification method is especially powerful in the study of minerals (and other materials) that are too fine-grained to be evaluated by optical microscopy. Examples of such materials are members of the clay mineral and zeolite groups. Powder diffraction equipment is generally available in many geology and chemistry departments, as well as industrial laboratories, and is widely used for the study of minerals.

X-ray Spectra

Electromagnetic waves form a continuous series ranging in wavelength from long radio waves with wavelengths of the order of thousands of meters to cosmic

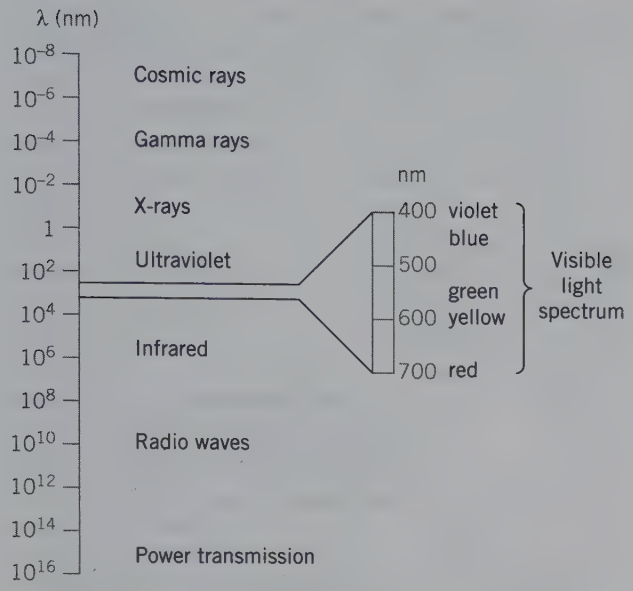

FIG. 14.1 The electromagnetic spectrum with the visible region expanded. Wavelength (λ) values are expressed in nm (nanometers), where 1 nm = 10 Å = 10^{-9} meters.

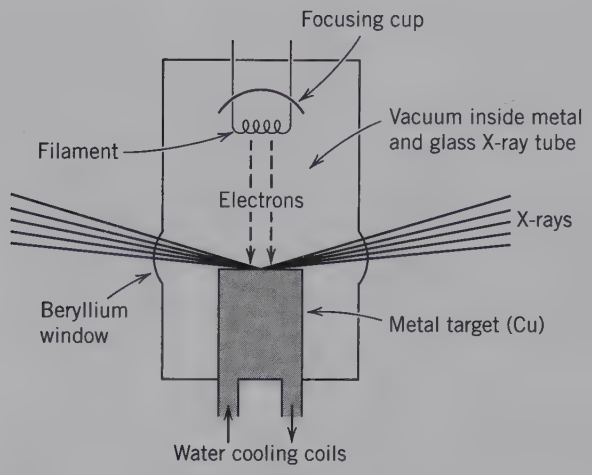

FIG. 14.2 Schematic representation of a sealed vacuum X-ray tube. The tungsten filament is heated to very high temperature, making electrons boil off. The differential voltage between the filament and the target metal accelerates the electrons toward the target. When the electrons strike the target, X-rays are produced that leave the X-ray tube housing through beryllium windows.

radiation whose wavelengths are of the order of 10^{-12} meters (see Figs. 10.24 and 14.1). All forms of electromagnetic radiation have certain properties in common, such as propagation along straight lines at a speed of 300,000 km per second in a vacuum, reflection, refraction according to Snell's law (in Chapter 13), diffraction at edges and by slits or gratings, and a relation between energy and wavelength given by the Einstein equation:

$$E = h\nu = hc/\lambda$$

where E is energy, ν is frequency, c is velocity of propagation, λ is wavelength, and h is Planck's constant. This equation shows that the shorter the wavelength the greater its energy, thus, the greater its powers of penetration. X-rays occupy only a small portion of the electromagnetic spectrum, with wavelengths ranging between slightly more than 100 Å and 0.02 Å (Fig. 14.1). X-rays used in the investigation of crystals have wavelengths on the order of 1 Å, similar in magnitude to the size of a unit cell. Visible light has wavelengths between 7,200 and 4,000 Å (720–400 nm), more than 1,000 times as great; therefore, it is less penetrative and less energetic than X-radiation.

When electrons moving at high velocity strike the atoms of any element, X-rays are produced. This is the case in an X-ray tube where electrons bombard a target material (Fig. 14.2). These X-rays result in two types of X-ray spectra: **continuous** and **characteristic** (Fig. 14.3).

A high vacuum exists in an X-ray tube. The tube is fitted with a tungsten filament as a cathode that provides the source of electrons. The anode consists of a single metal, such as Mo, Cu, or Fe, and acts as the target for the electrons. When the filament is heated by passage of a current, electrons are emitted that are accelerated toward the target anode by a high voltage applied across the tube. X-rays are generated when the source electrons impact the target (anode). The wavelength of the X-rays depends on the metal of the target and on the applied voltage. No X-rays are produced until the voltage reaches a minimum value dependent on the target material. At that voltage, a **continuous spectrum** is generated. With increasing accelerating potential, the intensity of all wavelengths increases, and the minimum wavelength of the continuous spectrum decreases (Fig. 14.3a). The *continuous spectrum*, also referred to as *white radiation*, is caused by the stepwise loss of energy of bombarding electrons in series of encounters with atoms of the target material. When an electron is instantaneously stopped, it loses all its energy at once, and the X-radiation emitted is that of the shortest wavelength (Fig. 14.3a). The stepwise energy losses from a stream of electrons produce a continuous range of wavelengths that can be plotted as a continuous function of intensity against wavelength (Fig. 14.3a). The curves begin at the short wavelength limit, rise to a maximum, and extend toward infinity at very low intensity levels.

If the voltage across the X-ray tube is increased to a critical level, which is dependent on the element of the

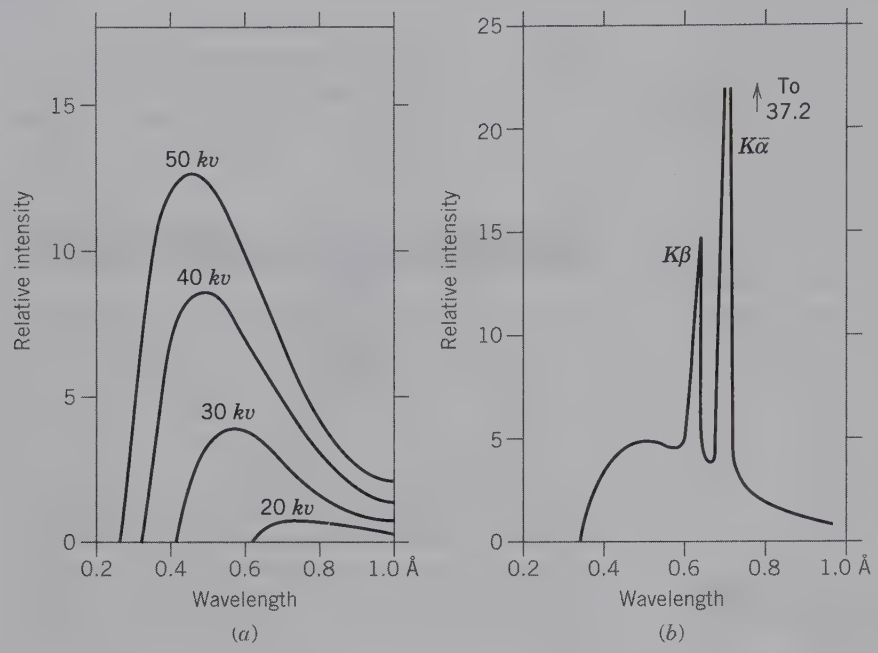

FIG. 14.3 X-ray spectra. (a) Distribution of intensity with wavelength in the continuous X-ray spectrum of tungsten at various voltages. (b) Intensity curve showing characteristic wavelengths superimposed on the continuous X-ray spectrum of molybdenum. (After Ulrey, C. T. 1918. An experimental investigation of the energy in the continuous X-ray spectra of certain elements. *Physics Reviews* 11: 401–10.)

target, a *line spectrum* of **characteristic radiation** specific to the target material becomes superimposed on the continuous spectrum. This characteristic radiation, many times more intense than the continuous spectrum, consists of several isolated, discrete wavelengths, as shown in Fig. 14.3b by *K*β and *K*α peaks.

The characteristic X-ray spectrum is produced when the bombarding electrons have sufficient energy to dislodge inner shell electrons in atoms of the target material. When these inner electrons are expelled, they leave vacancies that are filled by electrons from surrounding electron shells. The electron transitions, from outer to inner shells, are accompanied by the emission of X-radiation with specific energy (wavelength). Electrons falling from the *L*- to the *K*-shell produce $K\overline{\alpha}$ radiation, and those from the *M*- to the *K*-shell cause *K*β radiation (Fig. 14.4). The *K*β peak can be eliminated by an appropriate filter to yield essentially a single X-ray wavelength. By analogy to monochromatic light, this is called **monochromatic X-radiation**. The $K\overline{\alpha}$ radiation consists of the weighted average of two peaks, $K\alpha_1$ and $K\alpha_2$, which are very close together in wavelength.

The wavelengths of the characteristic X-radiation emitted by various metals have been accurately determined. The $K\overline{\alpha}$ wavelengths of the most commonly used anode metals are:

	Å		Å
Molybdenum	0.7107	Cobalt	1.7902
Copper	1.5418	Iron	1.9373
		Chromium	2.2909

FIG. 14.4 Schematic illustration of the production of *K* and *L* characteristic spectra as a result of electrons cascading from upper to lower energy levels in the atomic structure. X-ray emission lines are labeled with a capital letter representing the shell whose vacancy is being filled. The Greek letter is α if the electron that fills the vacancy originates in the next highest shell, β if the electron comes from two shells up, and so on. The Arabic numeral subscripts indicate specific subshells (1 for *s*, 2 for *p*) for the origin of the electron that fills the vacancy.

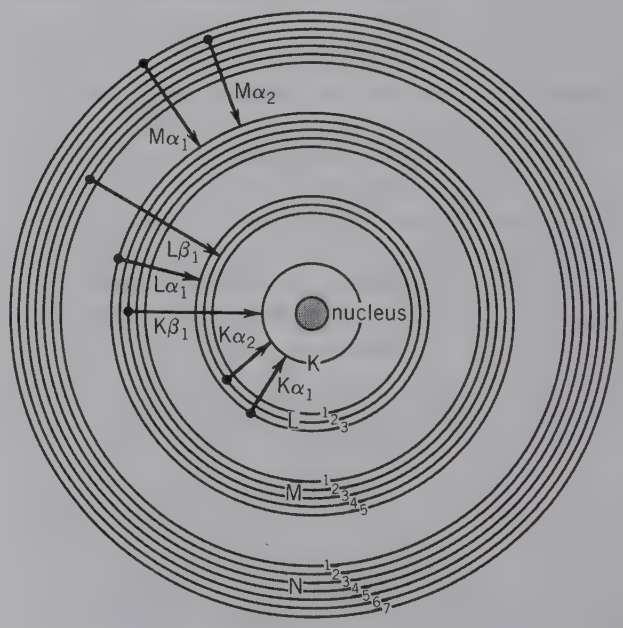

Diffraction Effects and the Bragg Equation

Minerals consist of an ordered three-dimensional structure with characteristic periodicities along the crystallographic axes. When an X-ray beam strikes such a three-dimensional orderly arrangement, it causes electrons in its path to vibrate with a frequency of the incident X-radiation. These vibrating electrons absorb some of the X-ray energy and, acting as a source for new wave fronts, emit (scatter) this energy as X-radiation of the same frequency and wavelength. In general, the scattered waves interfere destructively, but in some specific directions, they reinforce one another (interfere constructively), to produce a cooperative scattering effect known as **diffraction**.

In a row of regularly spaced atoms that is bombarded by X-rays, every atom can be considered the center of radiating, spherical wave shells (Fig. 14.5). When the scattered waves interfere constructively, they produce wave fronts that are *in phase*, and diffraction will occur. Figure 14.6 illustrates that rays 1 and 2 will be in phase only when distance AB represents an integral number of wavelengths; in other words, when $AB = n\lambda = c \cos \phi$ (where n represents whole numbers, such as $0, 1, 2, 3, \ldots, n$). For a specific value of $n\lambda$, ϕ is constant, and the locus of all possible diffracted rays will be represented by a cone with the row of scattering points as the central axis. Because the scattered rays will be in phase for the same angle ϕ on the other side of the incident beam, there will be another similar but inverted cone on that side (Fig. 14.7). The two cones with $n = 1$ would have ϕ (as in Fig. 14.7) as the angle between the cone axis and the outer surface of the cone. When $n = 0$, the cone becomes a plane that includes the incident beam. The greater the value of n, the larger is the value of $\cos \phi$; the smaller the angle ϕ, the narrower the cone. All have the same axis, however, and all have their vertices at the same point, the intersection of the incident beam and the row of atoms.

In a three-dimensional lattice there are three axial directions, each with its characteristic periodicity of scattering points and each capable of generating its own series of nested cones with characteristic apical angles. Diffraction cones from any three noncoplanar rows of scattering atoms may or may not intersect each other, but only when all three intersect in a common line is there a diffracted beam (Fig. 14.8). This direction (shown by the arrow in Fig. 14.8) represents the

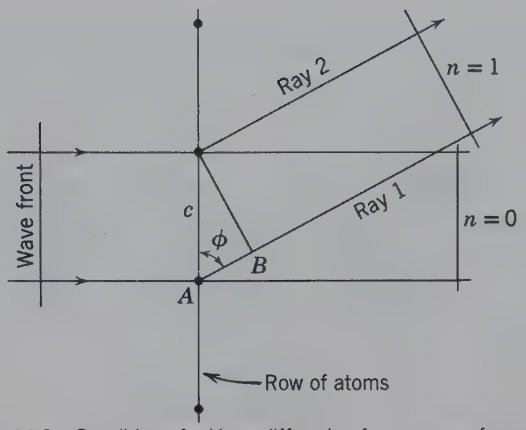

FIG. 14.6 Conditions for X-ray diffraction from a row of atoms.

FIG. 14.5 Scattering of X-rays by a row of equally spaced, identical atoms.

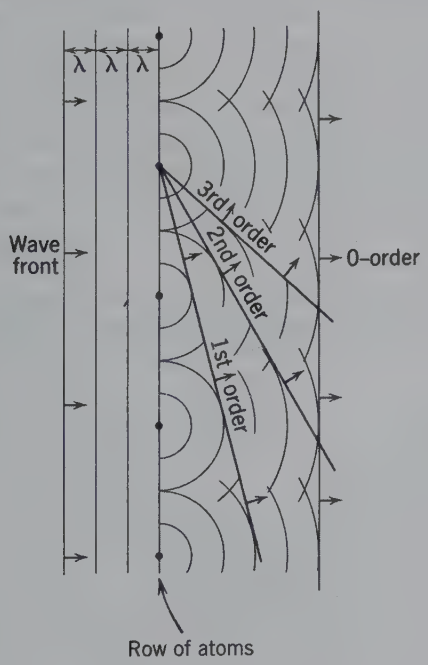

FIG. 14.7 Diffraction cones from a row of atoms.

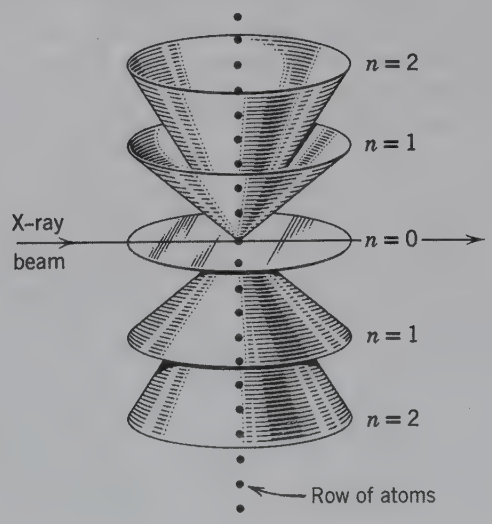

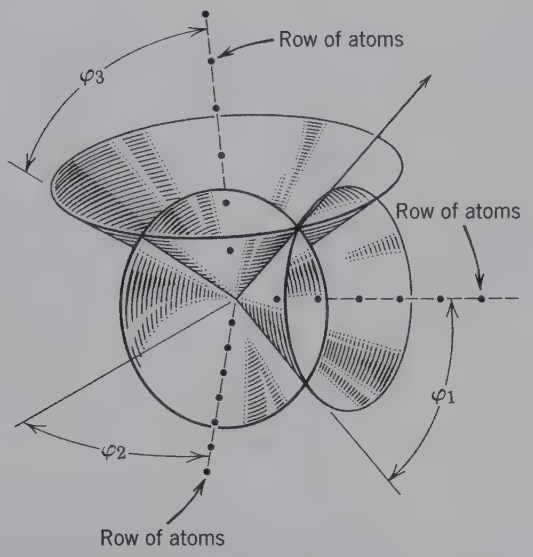

FIG. 14.8 Diffraction cones from three noncoplanar rows of scattering atoms, intersecting in a common line.

direction of the diffracted beam, which can be recorded on a film or registered electronically. The geometry of the three intersecting cones in Fig. 14.8 can be expressed by three independent equations (the Laue equations) in which the three cone angles (ϕ_1, ϕ_2, and ϕ_3) define a common direction along the path of the arrow (the common intersection of the three cones). In order to produce a diffraction effect (a spot on a photographic plate or film), these three geometric equations must be simultaneously satisfied. The three equations are named after Max von Laue, who originally formulated them.

Shortly after the publication of these equations, W. L. Bragg pointed out that although X-rays are indeed diffracted by crystals, the diffracted X-rays act as though they were reflected from planes within the crystal. Unlike the reflection of light, however, X-rays are not "reflected" continuously from a given crystal plane. Using a given wavelength, λ, Bragg showed that a "reflection" takes place from a family of parallel planes only under certain conditions. These conditions must satisfy the equation: $n\lambda = 2d \sin \theta$, where n is an integer (1, 2, 3, . . . , n), λ is the wavelength, d is the distance between successive parallel planes, and θ is the angle of incidence and "reflection" of the X-ray beam from the given atomic plane. This equation, known as **Bragg's law**, expresses in a simpler manner the simultaneous fulfillment of the three Laue equations.

As was discussed under "Crystal Growth," (Chapter 10) the faces that are most likely to appear on crystals are those parallel to atomic planes with the greatest density of lattice nodes. Parallel to each face is a family of equally spaced identical planes. When an X-ray beam strikes a crystal, it penetrates it, and the resulting diffraction effect is not from a single plane but from an almost infinite number of parallel planes (inside the structure), each contributing a small bit to the total diffraction maximum. In order for the diffraction effect ("reflection") to be of sufficient intensity to be recorded, the individual "reflections" must be *in phase* with one another. The following conditions necessary for reinforcement were demonstrated by W. L. Bragg.

In Fig. 14.9, the lines p, p_1, and p_2 represent the traces of a family of atomic planes with spacing d. X-rays striking the outer plane pp would be reflected at the incident angle θ, whatever the value of θ. However, to reinforce one another in order to give a "reflection" that can be recorded, all "reflected" rays must be *in phase*. The path of the waves along *DEF* "reflected" at *E* is longer than the path of the waves along *ABC* "reflected" at *B*. If the two sets of waves are to be *in phase*, the path difference of *ABC* and *DEF* must be a whole number of wavelengths ($n\lambda$). In Fig. 14.9, *BG* and *BH* are drawn perpendicular to *AB* and *BC*, respectively, so that $AB = DG$ and $BC = HF$. To satisfy the condition that the two waves be in phase, $GE + EH$ must be equal to an integral number of wavelengths. *BE* is perpendicular to the lines p and p_1 and is equal to the interplanar spacing d. In ΔGBE, $d \sin \theta = GE$; and, in ΔHBE, $d \sin \theta = EH$. Thus, for in phase "reflection," $GE + EH = 2d \sin \theta = n\lambda$. This equation,

$$n\lambda = 2d \sin \theta$$

is the **Bragg equation**. For a given interplanar spacing (d) and a given λ, "reflections" (diffraction maxima) occur only at those angles of θ that satisfy the equation.

Suppose for example, a monochromatic X-ray beam is parallel to a cleavage plate of halite, and the plate is supported in such a way that it can be rotated about an axis at right angles to the X-ray beam. As the halite is slowly rotated, there is no "reflection" until the incident beam makes an angle θ that satisfies the Bragg

FIG. 14.9 Geometry of X-ray "reflection" from equally spaced planes (p, p_1, p_2) in a crystal structure with spacing d between them.

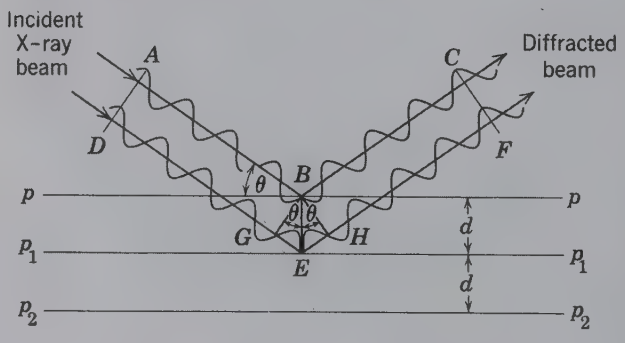

equation, with $n = 1$. On continued rotation, there are additional "reflections" only when the equation is satisfied at certain θ angles with $n = 2, 3, \ldots$. These are known as the first-, second-, third-order, etc., "reflections." These "reflections" are the diffraction effects that occur when the three diffraction cones about three noncoplanar rows of atoms intersect in a common direction (Fig. 14.8). This diffraction process is the basis for single crystal and powder X-ray techniques.

Single-Crystal X-ray Diffraction and Structure Analysis

Single-crystal X-ray diffraction, as the name implies, is the interaction of an X-ray beam with a very small single-crystal (about 1 mm in size or smaller) of a mineral (or other crystalline substance). The interaction of the X-ray beam and the crystalline structure produces X-ray diffraction effects that can be recorded on film or measured by an electronic device, such as an X-ray counter (or detector). Until 1970, almost all X-ray diffraction studies involved film methods that consisted of a crystal positioned in an X-ray beam at a fixed distance from a film wrapped in a light-tight envelope. Figure 14.10a shows this arrangement for the *Laue method* in which the crystal is stationary and the X-ray beam is unfiltered (meaning that it contains X-rays represented by $K\beta$ radiation as well as the continuum in addition to the $K\alpha$ radiation). Although the Laue method is now mainly of historic interest, it is mentioned here because the resulting diffraction effects, as recorded on a flat film, display the symmetry of the crystal as long as one of the crystallographic axes of the crystal is aligned parallel with the X-ray beam. Figure 14.10b illustrates the four-fold symmetry arrangement of X-ray diffraction spots (about the center of the film) for the tetragonal mineral vesuvianite. Here, the X-ray beam was parallel to the *c* axis, the four-fold axis in vesuvianite.

In other single-crystal film methods, the film is generally not stationary, and furthermore, the film may not be contained in a flat but instead in a cylindrical housing. The most commonly used single-crystal method in which a flat film and a single crystal move in a complex gyratory motion, is known as the *precession method*. An example of an X-ray single-crystal precession photograph of vesuvianite is shown in Fig. 14.11.

Although enormous numbers of crystal structures have been solved on the basis of data obtained on film using single-crystal camera techniques, the modern approach to data acquisition is by a *single-crystal diffractometer*. In such instrumentation (see also "X-ray

FIG. 14.10 (a) Obtaining a Laue photograph with a stationary crystal. (b) Laue photograph of vesuvianite with point group symmetry 4/*m*2/*m*2/*m*. The photograph was taken along the four-fold rotation axis (*c* axis) of vesuvianite, thus, revealing four-fold symmetry and mirrors in the arrangement of diffraction spots. The axial directions, a_1 and a_2, were inked onto the photograph after it had been developed.

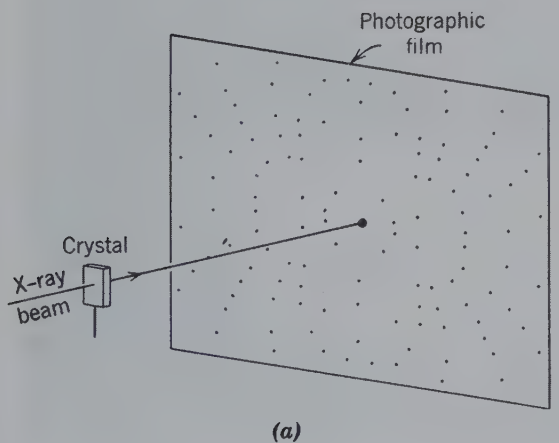

(a)

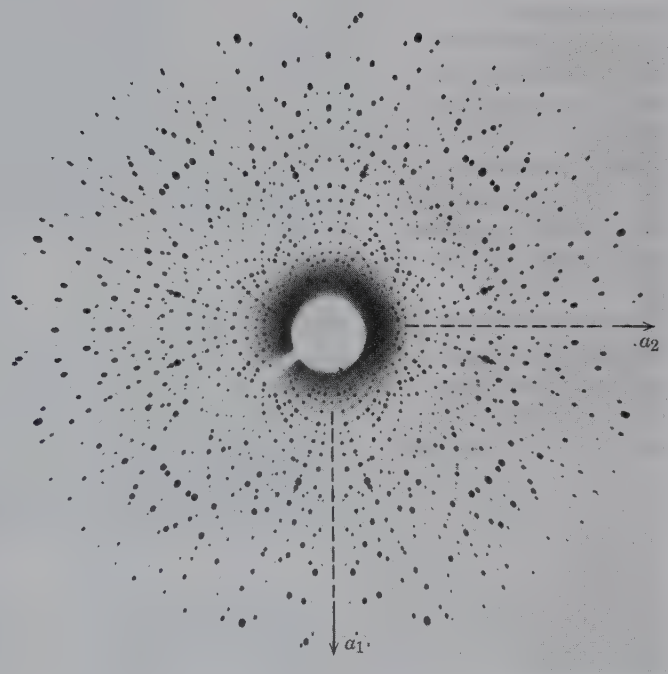

(b)

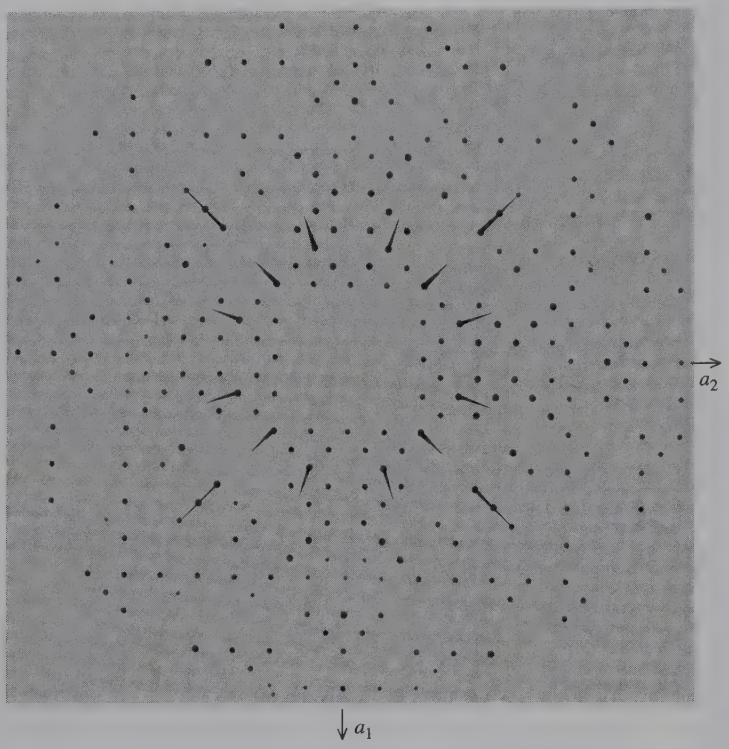

FIG. 14.11 Precession photograph of vesuvianite, with point group symmetry 4/*m*2/*m*2/*m*. The photo was taken along the four-fold rotation *c* axis, thus, revealing the four-fold symmetry about the axis, as well as the mirror planes. Compare with Fig. 14.10b.

Powder Diffraction and Mineral Identification" later in this chapter), the intensity of X-ray diffraction maxima is not evaluated from the intensity of a spot on an X-ray film, but instead is measured by an X-ray counter (or detector). Such detectors greatly improve the accuracy of X-ray intensity measurements over those obtained by film techniques. In addition, automated detectors can measure large numbers of X-ray effects with high accuracy. The most commonly used automated technique in X-ray structure analysis is the *four-circle diffractometer*. The name four-circle arises from its possession of four arcs that are used to orient the single crystal so as to bring desired (atomic) planes into diffraction positions. An automated four-circle diffractometer is shown in Fig. 14.12.

The Determination of Crystal Structures

The orderly arrangement of atoms in a crystal is known as the **crystal structure**. Crystal structure analysis provides information on the location of all the atoms, bond positions and bond types, space group symmetry, and the chemical content and size of the unit cell.

The first steps in determining the atomic structure of a crystal are the measurement of its unit cell size and the evaluation of its space group. The systematic measurement of the geometric distribution of diffracted X-ray beams on single crystal X-ray photographs in one or more crystallographic orientations (precession photographs are most convenient) yields information about the geometry of that crystal's unit cell, specifically the lengths of the unit cell edges and the angles between them. Information about the space group and the crystal structure (i.e., the symmetry of the atomic arrangement and the coordinates of atoms within the unit cell) is contained in the intensities of the diffracted beams, which are measured either from X-ray single crystal photographs, or more commonly with quantum counting detectors on single-crystal diffractometers. The diffracted beams are identified by Bragg indices, *hkl*, associated with the lattice planes of the same indices.

The relationship between the intensity (I) of the diffracted beam associated with lattice planes having Bragg diffraction indices *hkl* and coordinates $x_j y_j z_j$ of atom j in the unit cell is

$$I = k\left[\sum_j f_j e^{i2\pi(hx_j+ky_j+lz_j)}\right]^2 = kF_{hkl}^2$$

where k is a term containing several physical constants and experimental factors, including a scale factor; f_j is the scattering factor of atom j (which depends on atomic number and scattering angle and includes corrections for atomic thermal motion); and the summation is over all atoms in the unit cell. The summation is termed the **structure factor**, F_{hkl}, and its value depends on the kinds of atoms in the unit cell and their positions.

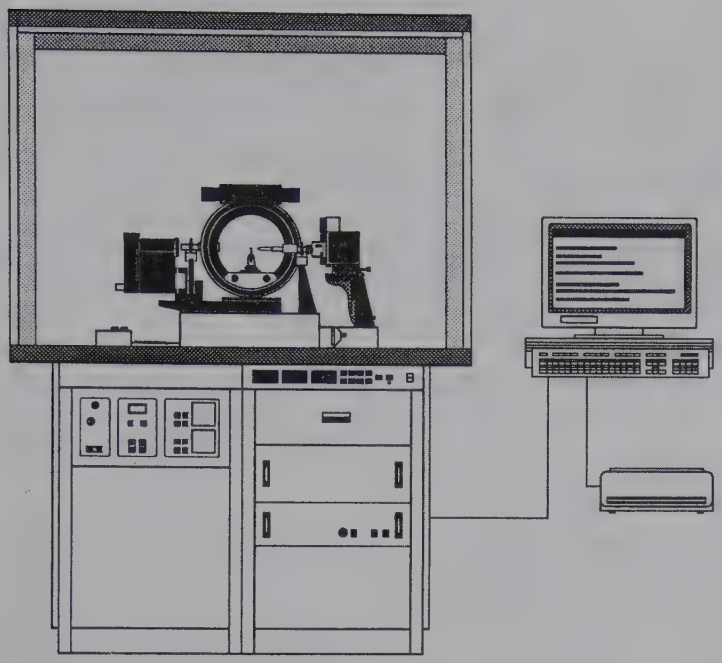

(*a*)

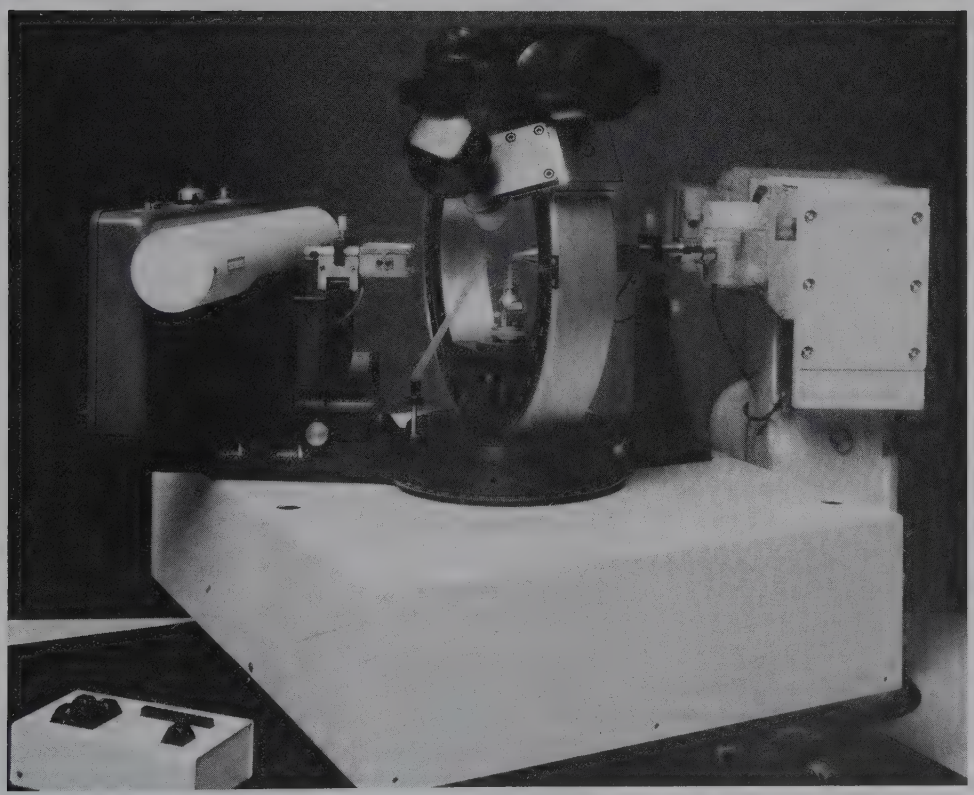

(*b*)

FIG. 14.12 (a) Schematic illustration of the P4 single-crystal X-ray diffractometer manufactured by Siemens Industrial Automation. (b) Close-up of the four-circle goniometer for controlling the orientation of the single crystal (in the center of the photograph). To the right is the X-ray tube, and to the left is the X-ray detector, a scintillation counter. (Courtesy of Siemens Industrial Automation, Inc., Madison, Wisconsin.)

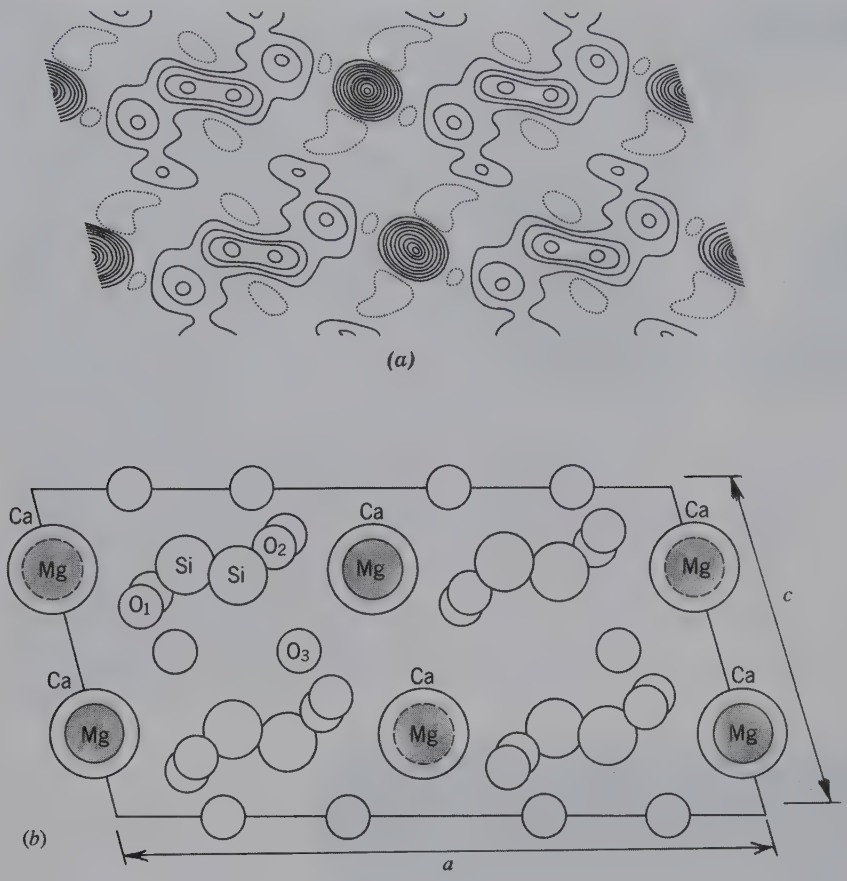

FIG. 14.13 (a) The summation of Fourier series for diopside, $CaMgSi_2O_6$, projected on (010). The distribution of scattering matter is indicated by contour lines drawn through points of equal density in the projection. (b) The atomic positions of diopside (with space group $C2/c$) projected on (010), as derived from the distribution in (a). (Redrawn after Bragg, W. L. 1929. *Zeitschrift für Kristallographie* 70:488.)

Because the intensities of diffracted beams are related to F^2_{hkl} rather than F_{hkl}, the atomic coordinates cannot be extracted directly from measured intensities. Current methods, by which these intensities can be made to yield atomic positions, are based either on using Fourier techniques or so-called direct methods. Fourier techniques are very powerful, particularly when the positions of a small number of heavy atoms are known. Direct methods are essentially statistical in nature and have become extremely successful as computing power has increased. An illustration of a now-classical electron density map (and the structure derived from it) by W. L. Bragg in 1929 is given in Fig. 14.13. Once the atom positions are known crudely, they can be refined to high precision, using least-squares analysis on many measured F^2_{hkl}. This procedure can yield amplitudes of atomic thermal vibration as well as site occupancies of substituting atomic species in minerals that are members of a solid solution series. Accurate interatomic distances (bond lengths) can then be calculated from refined atomic coordinates. In recent years, highly accurate electron density maps, calculated as a Fourier series in which the structure factors are the Fourier coefficients, have yielded information about bonding and the spatial distribution of valence electrons. Examples of such detailed electron density maps are given in "Molecules as models for bonding in silicates," by G. V. Gibbs (1982).

To illustrate the chemical and physical interrelationships in the derivation of a simple crystal structure, sodium chloride (NaCl) is used. The external morphology of halite is consistent with isometric symmetry (point group: $4/m\bar{3}2/m$). X-ray diffraction data indicate that the unit cell has an edge dimension (a) of 5.64 Å. A chemical analysis yields 39.4 weight percent Na and 60.6 weight percent Cl. Division of these weight percentage figures by the appropriate atomic weights yields an atomic ratio for Na:Cl or 1:1, which is expressed as NaCl. The density of halite is 2.165 g/cm^3.

If the density (D) and the volume (V) of the unit cell (a^3) are known, then the number of formula units per unit cell (Z) can be calculated from $D = (Z \times M)/(N \times V)$, where M is molecular weight and N is Avogadro's number (6.02338×10^{23}).

The number of formula units per unit cell for halite is four, which means that the unit cell contains four NaCl units, or four Na^+ and four Cl^- ions. It is now possible to assess the structural arrangement of the ions in

NaCl. The radius ratio of Na^+ to Cl^- would predict a coordination of six about each of the ions. A reasonable, and correct, interpretation of the crystal structure is given in Fig. 4.17.

Supplementing structure analyses based on diffraction phenomena (these are X-ray, neutron, and electron diffraction techniques), a variety of spectroscopic methods (that provide information about the local environments or ionization states of certain atomic species) are used. Spectroscopic techniques include infrared, optical, Mössbauer, and resonance techniques, such as nuclear magnetic resonance (NMR). Thus, a complete structural picture of a mineral at the atomic level usually requires information obtained by both diffraction and spectroscopy.

X-ray Powder Diffraction and Mineral Identification

The relative rarity of well-formed crystals and the difficulty of achieving the precise orientation required by single-crystal methods led to the discovery of the **powder method** of X-ray investigation. In X-ray diffraction studies of powders, the original specimen is prepared by grinding it to a fine powder, which is bonded with an amorphous material into a small spindle (for powder film methods) or spread uniformly over the surface of a glass slide. If sufficient powder is available, it can be packed into a special rectangular sample holder (for powder diffractometer techniques). The *powder mount* consists ideally of crystalline particles in completely random orientation. To ensure randomness of orientation of these tiny particles with respect to the impinging X-ray beam, the spindle mount (used in film cameras) is generally rotated in the path of the beam during exposure.

When a beam of monochromatic X-rays strikes the mount, all possible diffractions take place simultaneously. If the orientation of the crystalline particles in the mount is truly random, for each family of atomic planes with its characteristic interplanar spacing (d), there are many particles whose orientation is such that they make the proper angle with the incident beam to satisfy the *Bragg law*: $n\lambda = 2d \sin \theta$. The diffraction maxima from a given set of planes form cones with the incident beam as axis and the internal angle 4θ. Any set of atomic planes yields a series of nested cones corresponding to "reflections" of the first, second, third, and higher orders ($n = 1, 2, 3, \ldots$). Different families of planes with different interplanar spacings will satisfy the Bragg law at appropriate values of θ for different integral values of n, thus, giving rise to separate sets of nested cones of "reflected" rays.

If the rays forming these cones are permitted to fall on a flat photographic plate at right angles to the incident beam, a series of concentric circles will result (Fig. 14.14). However, only "reflections" with small values of the angle 2θ can be recorded in this manner. In order to record all the possible diffraction cones that may occur in three dimensions (Figs. 14.7 and 14.8), a film method is used in which the film is wrapped around the inside of a cylindrical camera. This camera is known as a *powder camera* in which the film fits snugly to the inner curve of the camera (Fig. 14.15a). This type of mounting is known as the *Straumanis method.* Figure 14.15b shows the circular film strip with two holes cut into it, one to allow the X-ray beam to enter the camera and the other for a lead-lined beam catcher. Although this powder camera method has been used extensively for mineral identification, the X-ray *powder diffractometer* is the instrumental method currently used most often. This powerful analytical tool uses essentially monochromatic X-radiation and a finely powdered sample, as does the powder film method, but records the information about the "reflections" as electronic counts (X-ray counts) that are stored and graphically displayed on a computer screen.

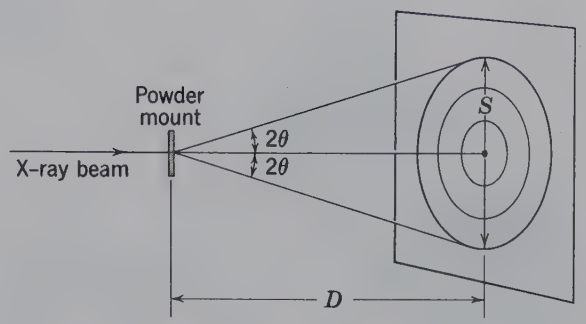

FIG. 14.14 X-ray diffraction from a powder mount recorded on a flat photographic plate inside a light-tight envelope.

The instrument is constructed such that when the sample is in place, it rotates in the path of a collimated X-ray beam while an X-ray detector, mounted on an arm, rotates about the sample to collect the diffracted X-ray signals (Fig. 14.16). When the instrument is set at zero position, the X-ray beam is parallel to the base of the sample holder and passes directly into the X-ray detector. The slide mount and the X-ray counter are driven by a motor through separate gear trains so that, while the sample rotates through the angle θ, the detector rotates through 2θ.

If the specimen has been properly prepared, there will be thousands of tiny crystalline particles in random orientation. As in powder photography, all possible "reflections" from atomic planes take place simultaneously. Instead of recording all of them on a film at one time, however, the X-ray detector maintains the appropriate geometrical relationship to receive each diffraction maximum separately.

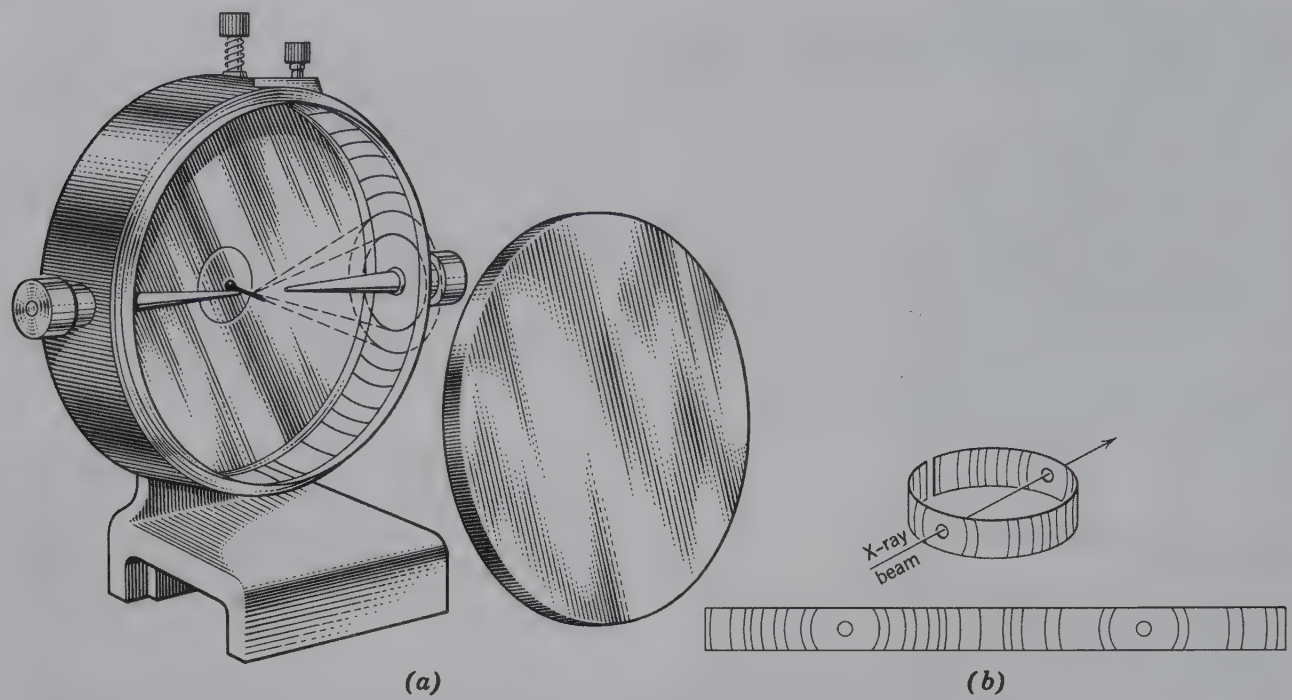

FIG. 14.15 (a) Metal powder diffraction camera with a powder spindle in the center and film strip against the inner cylindrical wall of the camera. (b) Circular film strip with curved lines that represent the conical "reflections" produced inside the camera.

In operation, the sample, the X-ray detector, and the recording device are activated simultaneously. If an atomic plane has an interplanar spacing (d) such that a reflection occurs at $\theta = 20°$, there is no evidence of this reflection until the counting tube has been rotated through 2θ, or 40°. At this point, the diffracted beam enters the X-ray detector, causing it to respond. The pulse generated is amplified and causes an electronic response on a vertical scale that represents peak height. The angle 2θ at which the diffraction occurs is read on a horizontal scale. The heights of the peaks are directly proportional to the intensities of the diffraction effects.

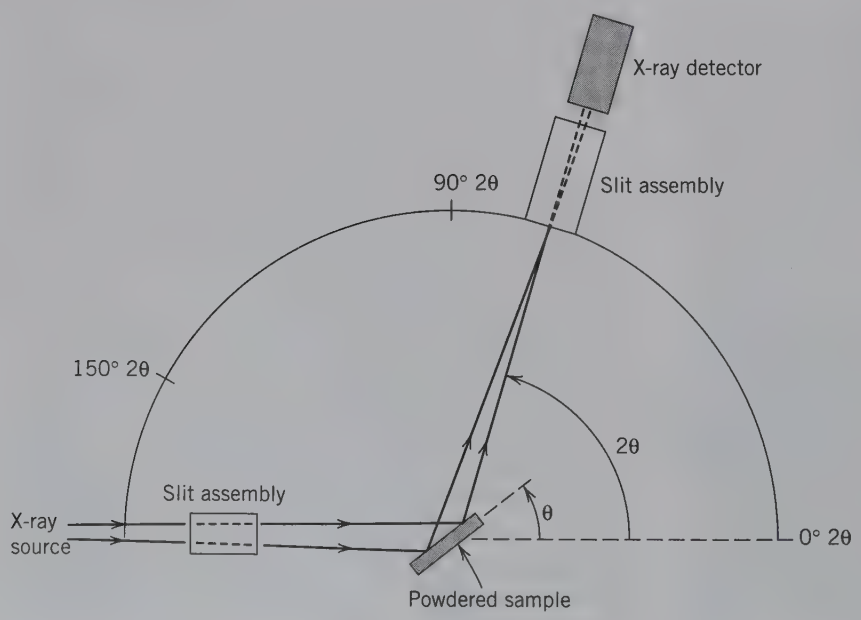

FIG. 14.16 Schematic illustration of the essential components of a powder X-ray diffractometer. In such an instrument the sample holder rotates at $\theta°$ while the detector arm rotates $2\theta°$.

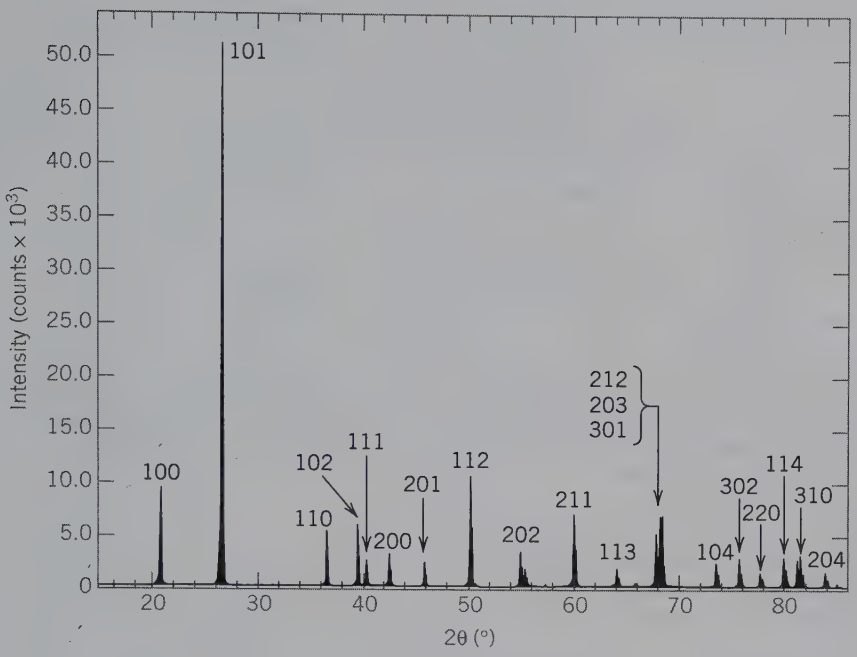

FIG. 14.17 X-ray powder diffractometer tracing for a finely powdered sample of low quartz. Peaks are indexed with the appropriate *hkl* responsible for the "reflection."

An example of a diffractometer tracing for low quartz is given in Fig. 14.17. The 2θ positions of the diffraction peaks in such a tracing can be read off directly or they can be tabulated as 2θ positions by an online computer. The interplanar spacings giving rise to them are calculated using the equation $n\lambda = 2d \sin \theta$.

Once a diffractometer tracing has been obtained and the various diffraction peaks have been tabulated in a sequence of decreasing interplanar spacings (d), together with their relative intensities (I, with the strongest peak represented by 100 and all the other peaks scaled with respect to 100), the investigator can begin the mineral identification process. Through a computer search technique (searching for comparable or identical diffraction patterns on the basis of the strongest lines or the largest interplanar spacings), the diffraction pattern of an unknown can be compared with records stored in the Powder Diffraction File (PDF) published by the International Center for Diffraction Data (ICDD). (This database is available in electronic format from the ICDD.)

The PDF is the world's largest and most complete collection of X-ray powder diffraction patterns, containing more than 217,000 calculated and experimental patterns for natural and synthetic crystalline materials compiled by the ICDD since 1941. Each pattern includes a table of interplanar (d) spacings, relative intensities (I), and Miller indices, as well as additional information, such as chemical formula, compound name, mineral name, structural formula, crystal system, physical data, experimental parameters, and references. An example printout for low quartz from this file is shown in Fig. 14.18. Entries are indexed to allow for topical searches of inorganics, organics, minerals, metals and alloys, pharmaceuticals, zeolites, and many others. By this automated search procedure, a completely unknown substance can be identified in a short time using a very small volume of sample.

The powder method is of wider usefulness, however, and there are several other valuable applications. Variations in chemical composition of a known substance involve the substitution of ions, generally of a somewhat different size, in specific sites in a crystal structure. As a result of this substitution, the unit cell dimensions, and, consequently, the interplanar spacings, are slightly changed. Commensurate with the changes in interplanar spacing, the positions of the lines in the powder diffractogram shift accordingly. By measuring these small shifts in position of the lines in powder patterns of substances of known structure, changes in chemical composition may be accurately detected. Figure 14.19 illustrates a variation diagram that correlates unit cell dimensions (b and unit cell volume, V) and changes in the position of a specific diffraction maximum (1,11,0) with composition for members of the cummingtonite-grunerite (amphibole) series.

Further, the relative proportions of two or more known minerals in a mixture may be determined by the comparison of the intensities of the same peaks in diffractometer patterns of prepared control samples of

PDF#33-=1161 (Deleted Card): QM = Star (+); d = Diffractometer, I = Diffractometer — PDF Card

Quartz, syn
SiO2

Radiation = CuKa1 — Lambda = 1.540598 — Filter =
Calibration = Internal (Si) — d-Cutoff = — I/Ic (RIR) = 3.6
Ref = Natl. Bur. Stand. (U.S.) Mongr. 25, 18 61 (1981)

Hexagonal—(Unknown), P3221(154) — Z = 3 — mp =
Cell = 4.9134 × 5.4053 — Pearson = hP9 (O2 Si)
Censity (c) = 2.649 Density (m) = 2.656 Mwt = 60.08 Vol. = 113.01 — F(30) = 76.8 (.0126,31)
Ref = Ibid.

NOTE: Sample from the Glass Section at NBS, Gaithersburg, MD, USA, ground single-crystals of optical quality. To replace 5-490 and validated by calculated pattern. Plus 6 additional reflections to 0.9089. Pattern taken at 25 C. Pattern reviewed by Hozler, J., McCarthy, G., North Dakota State Univ., Fargo, ND, USA, ICDD Grant-in-Aid (1990). Agrees well with experimental and calculated patterns. Deleted by 46-1045, higher F#N, more complete, LRB 1/95.
Color: Colorless

Strong Line: 3.34/X 4.26/2 1.82/1 1.54/1 2.46/1 2.28/1 1.37/1 1.38/1 2.13/1 2.24/1
39 Lines, Wavelength to Compute Theta = 1.54056A (Cu), 1%-Type = (Unknown)

#	d(A)	I(f)	h	k	l	2-Theta	Theta	1/(2d)	#	d(A)	I(f)	h	k	l	2-Theta	Theta	1/(2d)
1	4.2570	22.0	1	0	0	20.850	10.425	0.1175	21	1.2285	1.0	2	2	0	77.660	38.830	0.4070
2	3.3420	100.0	1	0	1	26.651	13.326	0.1495	22	1.1999	2.0	2	1	3	79.875	39.938	0.4167
3	2.4570	8.0	1	1	0	36.541	18.271	0.2035	23	1.1978	1.0	2	2	1	80.044	40.022	0.4174
4	2.2820	8.0	1	0	2	39.455	19.727	0.2191	24	1.1843	3.0	1	1	4	81.145	40.572	0.4222
5	2.2370	4.0	1	1	1	40.283	20.141	0.2235	25	1.1804	3.0	3	1	0	81.470	40.735	0.4236
6	2.1270	6.0	2	0	0	42.464	21.232	0.2351	26	1.1532	1.0	3	1	1	83.818	41.909	0.4336
7	1.9792	4.0	2	0	1	45.808	22.904	0.2526	27	1.1405	1.0	2	0	4	84.969	42.484	0.4384
8	1.8179	14.0	1	1	2	50.139	25.070	0.2750	28	1.1143	1.0	3	0	3	87.451	43.731	0.4487
9	1.8021	1.0	0	0	3	50.610	25.305	0.2775	29	1.0813	2.0	3	1	2	90.855	45.428	0.4624
10	1.6719	4.0	2	0	2	54.867	27.434	0.2991	30	1.0635	1.0	4	0	0	92.819	46.410	0.4701
11	1.6591	2.0	1	0	3	55.327	27.663	0.3014	31	1.0476	1.0	1	0	5	94.662	47.331	0.4773
12	1.6082	1.0	2	1	0	57.236	28.618	0.3109	32	1.0438	1.0	4	0	1	95.115	47.558	0.4790
13	1.5418	9.0	2	1	1	59.947	29.973	0.3243	33	1.0347	1.0	2	1	4	96.223	48.112	0.4832
14	1.4536	1.0	1	1	3	63.999	32.000	0.3440	34	1.0150	1.0	2	2	3	98.734	49.367	0.4926
15	1.4189	1.0	3	0	0	65.759	32.879	0.3524	35	0.9898	1.0	4	0	2	102.195	51.098	0.5052
16	1.3820	6.0	2	1	2	67.748	33.874	0.3618	36	0.9873	1.0	3	1	3	102.556	51.278	0.5064
17	1.3752	7.0	2	0	3	68.128	34.064	0.3636	37	0.9783	1.0	3	0	4	103.880	51.940	0.5111
18	1.3718	8.0	3	0	1	68.321	34.160	0.3645	38	0.9762	1.0	3	2	0	104.195	52.098	0.5122
19	1.2880	2.0	1	0	4	73.460	36.730	0.3882	39	0.9636	1.0	2	0	5	106.141	53.071	0.5189
20	1.2558	2.0	3	0	2	75.668	37.834	0.3982									

FIG. 14.18 Example of the printout for SiO_2, low quartz, as obtained from the powder diffraction file (PDF-2) licensed by the International Center for Diffraction Data (JCPDS), 12 Campus Boulevard, Newton Square, PA., 19073-3273; copyright © JCDPS-ICDD, 1999. The printout was obtained using Jade 5.0 from Materials Data Inc. (MDI).

known composition. This is commonly applied to the study of fine-grained materials, such as clay minerals. For X-ray diffraction patterns of clay minerals, oriented powders are used that maximize reflection from specific and characteristic *hkl*s (mainly the 00*l* peaks). However, relating the intensity of a diffraction peak to the abundance of the material is not straightforward, and numerous factors must be taken into account (refer to Moore and Reynolds, 1997 for details).

An X-ray powder diffraction technique, the *Rietveld refinement method*, allows for the extraction of structural information from powdered instead of single-crystal specimens. This is an especially important development for the determination of crystal structures of minerals that are typically finely crystalline and are not found in well-developed single crystals. Examples of such finely crystalline or poorly ordered minerals are clay minerals, manganese and iron oxides and hydroxides,

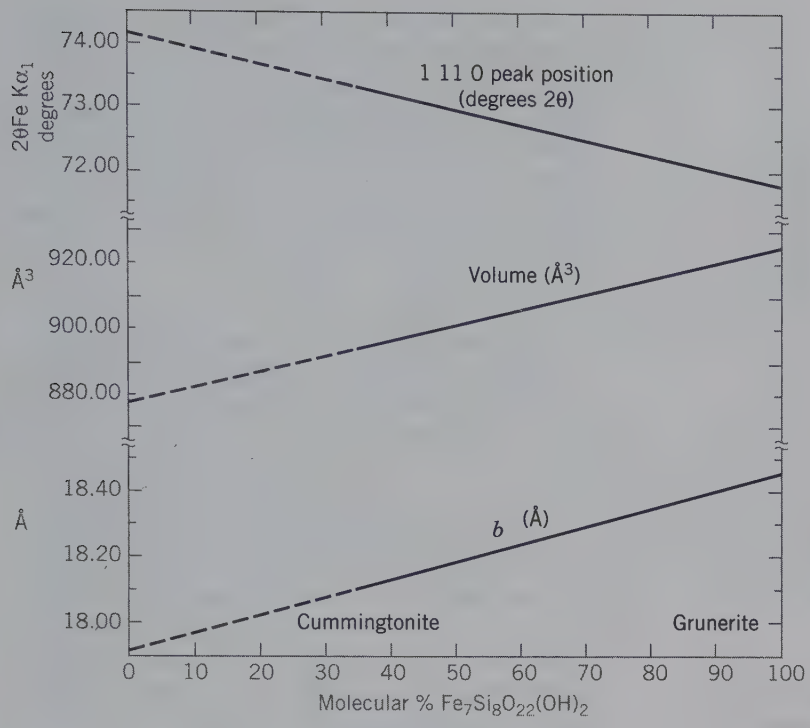

FIG. 14.19 Variation of *b* and *V* (volume) of the unit cell and the position of the 1,11,0 peak as a function of composition in the monoclinic cummingtonite–grunerite series with composition ranging from $Fe_2Mg_5Si_8O_{22}(OH)_2$ to $Fe_7Si_8O_{22}(OH)_2$. (After Klein, C., and D. R. Waldbaum. 1967. X-ray crystallographic properties of the cummingtonite-grunerite series. *Journal of Geology* 75:379–92).

and some zeolites. There are three basic requirements of the Rietveld refinement:

1. Availability of accurate powder diffraction intensity data measured at specific intervals of 2θ.
2. A basic understanding ("starting model") of the actual crystal structure of the material that is being studied.
3. A quantitative understanding of shapes, width, and any systematic errors in the positions of X-ray peaks in the powder pattern.

For further discussion of the Rietveld method, see Post and Bish (1989; see the reference list for complete reference).

Several exercises using X-ray powder diffraction film and diffractometer techniques are given in Klein (2008).

X-RAY FLUORESCENCE ANALYSIS (XRF)

This analytical technique, also known as **X-ray emission spectrography**, is used in most research laboratories that study the chemistry of inorganic substances. It is widely used by petrologists to acquire bulk chemical compositions of rocks including the abundance of rare earth elements. It is also routinely used in a wide range of industrial applications. Examples of such applications are in the mining industry (for quality control of the product shipped to the consumer), in the glass and ceramics industry, in the manufacture of metals and alloys, and in environmental-protection and pollution-control applications.

The analysis sample, in this technique, is ground to a fine powder and subsequently compressed into a circular pellet, or into a disc with the admixture of a binder. The pellet or disc of sample is irradiated (for a short period of time) with polychromatic X-rays generated in a high-intensity X-ray tube (Fig. 14.1 for the λ range of X-rays). These incident X-rays from the X-ray tube are, to a considerable extent, absorbed according to Beer's Law:

$$\log \frac{I_o}{I} = K_d \Delta d$$

where I_0 is the incident X-ray intensity, I is the intensity of the X-ray beam that was not absorbed in the sample, K_d is a proportionality constant, and Δd is the thickness of the sample. The X-ray energy that is absorbed in the sample results in the generation of an *X-ray emission spectrum that is characteristic* for each element in the sample. In the process of the absorption of X-ray energy in the sample, electrons are dislodged from the innermost shells (*K*, *L*, *M*; as discussed earlier for X-ray diffraction). An expelled electron (from, e.g., the *K*-shell) must be replaced, and it is highly probable that the vacancy will be filled from the next outer shell (the *L*-shell) rather than from a more remote shell. This creates a new vacancy, which is filled from the next shell, and so on. Electrons that "fall into" inner electron shells move

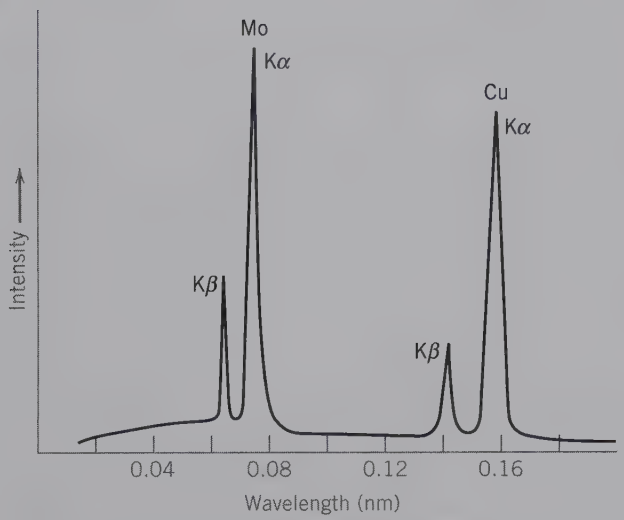

FIG. 14.20 Characteristic K-spectra for the elements Mo and Cu, superimposed on a continuous spectrum. This continuous spectrum is considered part of the background X-ray intensity in analytical techniques.

from higher- to lower-energy levels and as a result emit energy in the form of characteristic X-radiation (Fig. 14.4). The groupings of spectral lines are classified as *K*-, *L*-, or *M*-spectra in terms of the patterns in which the outer electrons fall into the lower-energy states. These generated characteristic X-rays are known as *secondary X-rays* and the emission phenomenon is called **X-ray fluorescence**. Each element has characteristic spectral lines with specific wavelengths superimposed on a low-intensity continuous background spectrum. Examples of two characteristic K-spectra for two different elements are given in Fig. 14.20.

The generated (fluorescence or secondary) X-ray spectrum may contain a very large number of spectral lines in a sample that consists of more than one or two elements. Such a spectrum must be resolved into its spectral-line components; all lines can be identified by wavelengths (in nm or Å) and these can be related to specific chemical elements responsible for their production. This is achieved with an X-ray spectrometer consisting of a diffracting crystal (with known spacing between atomic planes) and an X-ray detector. The crystal will diffract the various λ values of the impinging X-rays according to the Bragg equation:

$$n\lambda = 2d \sin \theta$$

where n is generally a small number, ranging from 1 to 2 or 3 (the "order of diffraction"), λ is the wavelength of a specific spectral line, d is the distance between a specific set of atomic planes in the diffracting crystal, and λ is the angle over which the X-ray is "reflected" by the crystal.

The intensity and position of each spectral line diffracted by the crystal in the spectrometer is recorded by an electronic X-ray counting device (generally a scintillation counter or flow proportional counter). This is traced on a recorder or presented on a high-resolution visual display terminal. A schematic diagram of the major components that constitute an X-ray fluorescence analyzer is given in Fig. 14.21.

Qualitative X-ray fluorescence analysis involves identification of the various spectral lines with the elements responsible for them (Fig. 14.22). Quantitative analysis is more involved because each X-ray intensity must be quantitatively compared with that of a standard (of known composition) of the same elemental makeup. Both peak and background intensities near the peak are counted to permit estimation of peak heights. Quantitative correction procedures are done online in an extremely short time.

X-ray fluorescence analysis can be used for the quantitative determination of major elements (those in the one to many tens of percent range). The size of the

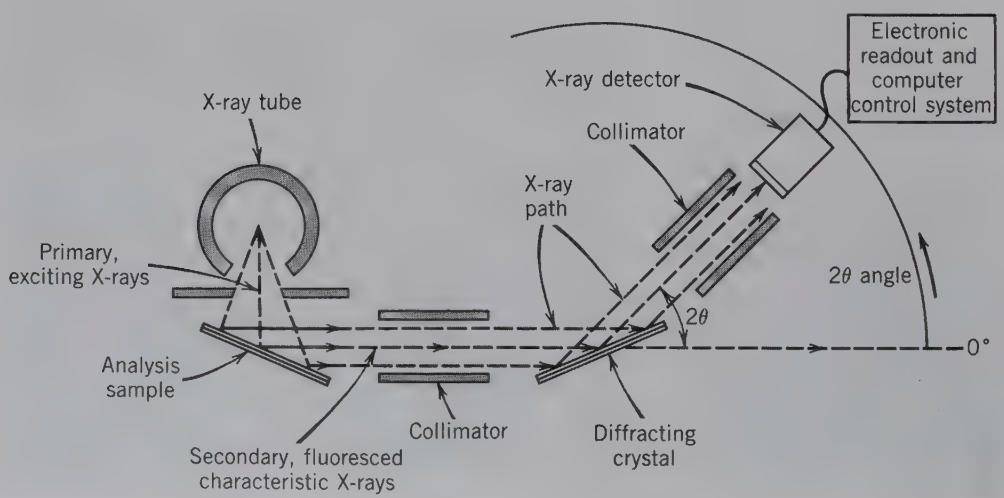

FIG. 14.21 Schematic illustration of the major components in an X-ray fluorescence analyzer.

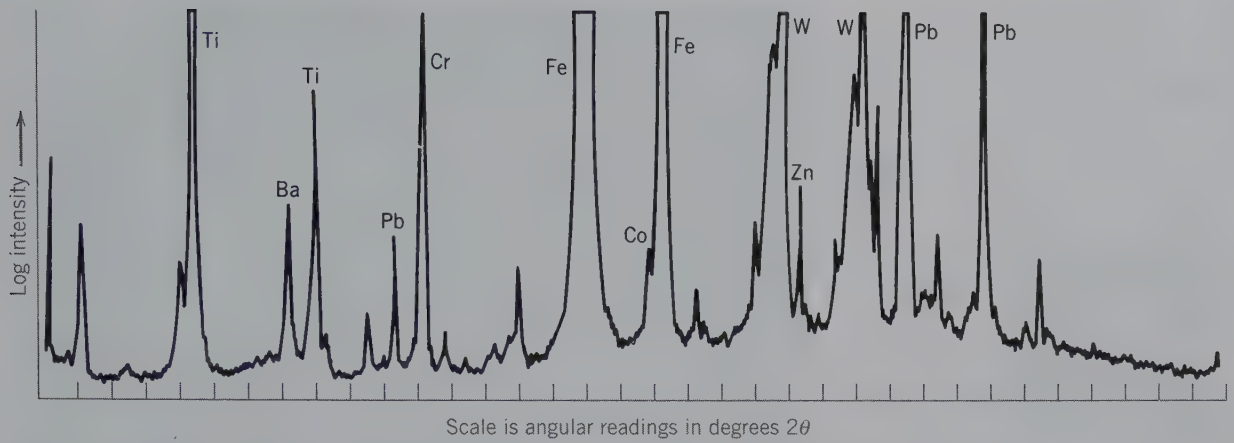

FIG. 14.22 Chart recording of the X-ray fluorescence spectrum obtained of elements present in a genuine bank note. The elements responsible for specific peaks are identified. The W peaks are due to the X-ray tube used with a W target; they are not part of the chemical composition of the bank note. The horizontal scale is in angles of 2θ, expressed as degrees. (From Liebhafsky, H. A., H. G. Pfeiffer, E. H. Winslow, and P. D. Zemany. 1960. *X-ray absorption and emission in analytical chemistry.* Wiley: New York.)

X-ray beam allows larger samples to be analyzed (than with electron beams) and provides better statistics. XRF is also very sensitive to accurate determinations of trace element components (e.g., Y, Zr, Sr, Rb, in the ppm range) because of near-zero background.

ELECTRON BEAM TECHNIQUES

SCANNING ELECTRON MICROSCOPY (SEM)

The **scanning electron microscope** is primarily used to obtain information on the morphology and surface features of materials at micrometer scales including direct observation of crystal intergrowths, textures, or reaction relationships (Fig. 14.23). To acquire such images, the SEM has an electron optical column in which a finely focused electron beam can be scanned over a specified area of the specimen, either small particles mounted on a stub or a polished mineral section. Resolution in an SEM ranges from about 50 to 25Å (5 to 2.5 nm). The electron column in an SEM is similar to that shown in Fig. 14.24 for an electron microprobe. In an electron microprobe, the electron beam is generally focused in a stationary mode, on a specific mineral grain; in the SEM, however, a high intensity electron beam is scanned across it.

The impact of an electron beam on the surface of a solid sample causes various types of radiation signals that are recorded by detectors above the specimen. These signals include secondary electrons (SE), backscattered electrons (BSE), X-rays, cathodoluminescence (CL) radiation (this is the emission of electromagnetic radiation in the ultraviolet, visible, or infrared

FIG. 14.23 Scanning electron microscope (SEM) photograph, using secondary electrons, of fibrous hollandite, $BaMn_8O_{16}$. (Photograph courtesy of M. Spilde, Institute of Meteoritics, University of New Mexico, Albuquerque.)

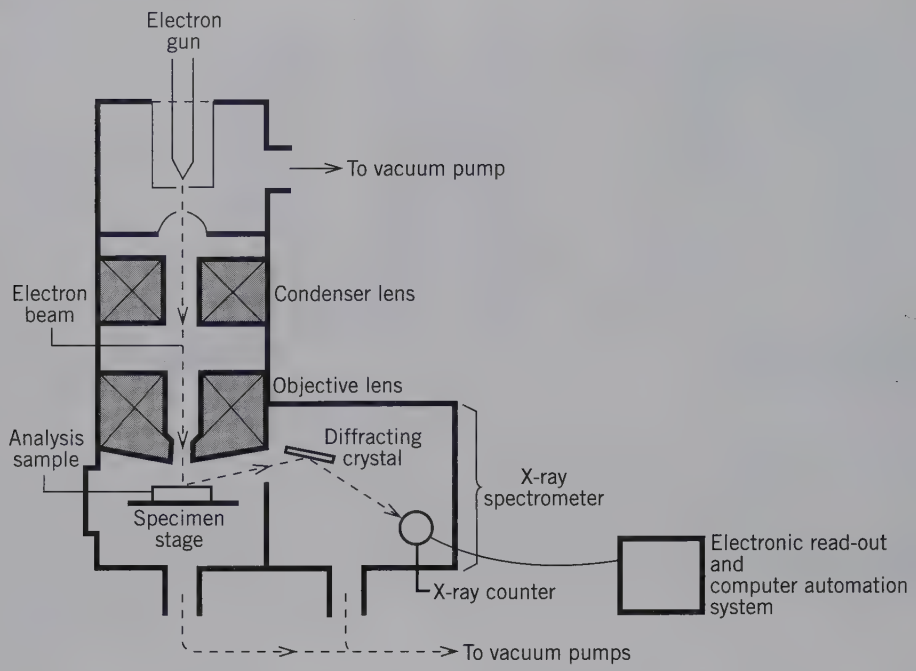

FIG. 14.24 Schematic cross section through the electron optical column and X-ray spectrometer of an electron microprobe.

wavelengths during electron bombardment), and electrons absorbed by the specimen (also known as *specimen current*). Typically an SEM is fitted with numerous detectors (e.g., SE, BSE, and CL) to measure these signals. An illustration of the location of a backscatter electron detector with respect to the electron beam is given in Fig. 14.25. The intensity of the signal detected in a backscatter electron detector is related to the average atomic number of the specimen, its crystallographic orientation, and surface topography; consequently, a polished sample surface is required for best results. Because BSE is a function of the mean atomic weight of the sample, such features as chemical zoning or reaction fronts in a crystal can be observed (Fig. 14.26). Figure 14.23 is an SEM photo (using secondary electrons) of a fibrous mineral illustrating its morphological details (see also Fig. 2.1). An important feature of the SEM is its large depth of field (when in the secondary electron mode), which results in very high definition images.

FIG. 14.25 Schematic drawing of a finely focused electron beam impinging on a material surface producing backscattered electrons (as well as other signals) inside the electron column of a scanning electron microscope (SEM). A backscatter electron detector (or secondary electron detector) is shown.

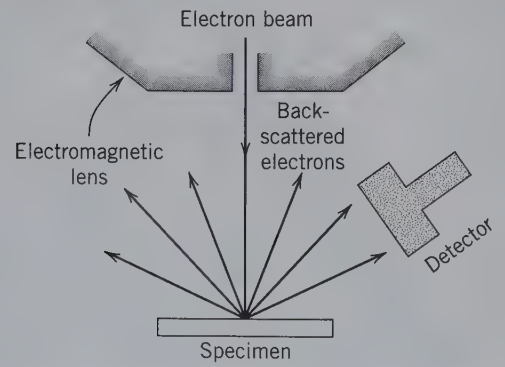

Many SEM installations have an energy-dispersive X-ray detection system (EDS), which allows for the spectral analysis of X-rays generated from the specimen directly under the electron beam. This provides *qualitative* chemical information that is generally sufficient for identification of an unknown. Because most specimens studied by SEM have a rough (unpolished) surface, the chemical data obtained are generally not of the same high quality as those obtained by electron microprobe analysis (EMPA, discussed subsequently). Nonetheless, an SEM has many applications in mineralogy, and when combined with EDS, it allows for topographic, crystallographic, and compositional information that can be obtained rapidly and simultaneously from the same area. In comparison to a TEM, much larger areas of a sample can be examined in the SEM technique.

TRANSMISSION ELECTRON MICROSCOPY (TEM)

A transmission electron microscope (TEM) consists of a finely focused electron beam that impinges on a very thin foil of the material under investigation and can be

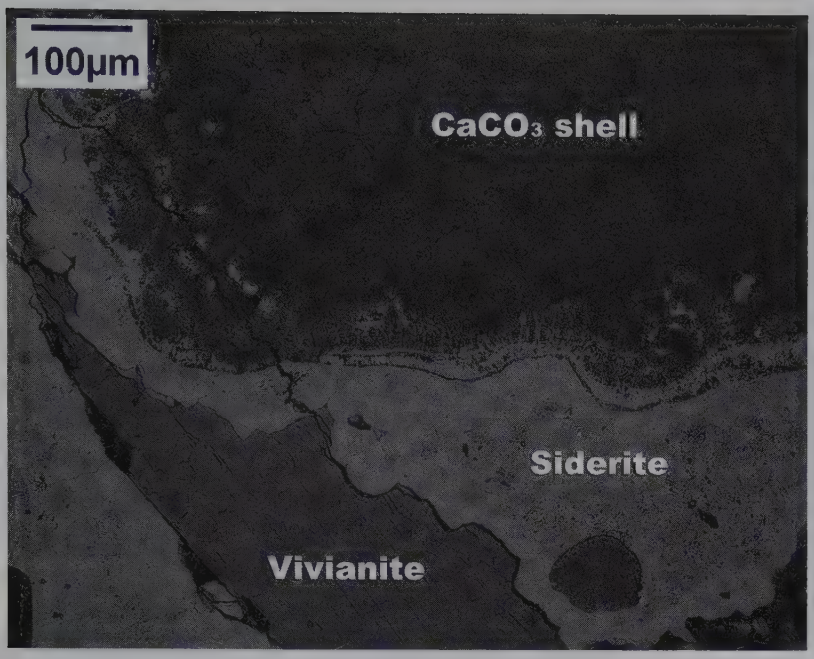

FIG. 14.26. Backscattered electron (BSE) image showing textural features of minerals replacing a mollusk, $CaCO_3$, shell. A large crystal of vivianite, $Fe_3^{2+}(PO_4)_2 \cdot 8H_2O$, originally replaced the shell. A siderite-rich mud (light) then replaced the vivianite, as shown by the scalloped edges, and the $CaCO_3$ shell while maintaining the shell's texture. Siderite fibers have grown perpendicular to the shell border, and suggest replacement of the $CaCO_3$ crystals. Specimen is from the Kerch Iron-Ore Deposits, Ukraine. (Photograph courtesy of C. Armstrong, LSU; see also Armstrong, C., Dutrow, B. and Henry, D. J., 2005. Geological Society of America Abstracts with Program 37: 300).

used to display electron diffraction patterns and high-resolution transmission electron microscope (HRTEM) images. A schematic drawing of the electron column in a TEM with its electromagnetic lenses is shown in Fig. 14.27. The thin foil of the material to be investigated is produced by ion bombardment or sputter-etching methods for nonconducting materials or by ultramicrotomy. For metals and conducting materials, foil preparation is done by electrochemical methods.

The thin foil, which is on the order of a few nanometers thick so that the electron beam can be transmitted through the material, is held in place with a sample holder centered in the electron beam.

Instruments allow for textural, crystallographic, and chemical evaluation from areas as small as a square nanometer (10Å × 10Å) and from features that are as little as 0.14 nm (1.4Å) apart. By comparison, most minerals have crystal structures whose basic unit cells are greater than 0.4 nm^2 (4$Å^2$).

The TEM technique is especially powerful in elucidating structural features that range in size from 100 to 10,000 Å, which cannot be directly evaluated by X-ray diffraction techniques. The structures of most minerals have been determined by single-crystal X-ray diffraction techniques. Such structure analyses, based on the averaged information obtained from many thousands of unit cells (all of which are assumed to be identical), locate accurately the positions of atoms in the unit cell on a scale of 1 to 100 Å. The TEM technique provides complementary data. TEM studies allow for

FIG. 14.27 Schematic cross section through the column of a transmission electron microscope, showing the electron beam path for structural imaging. The four lenses are electromagnetic lenses.

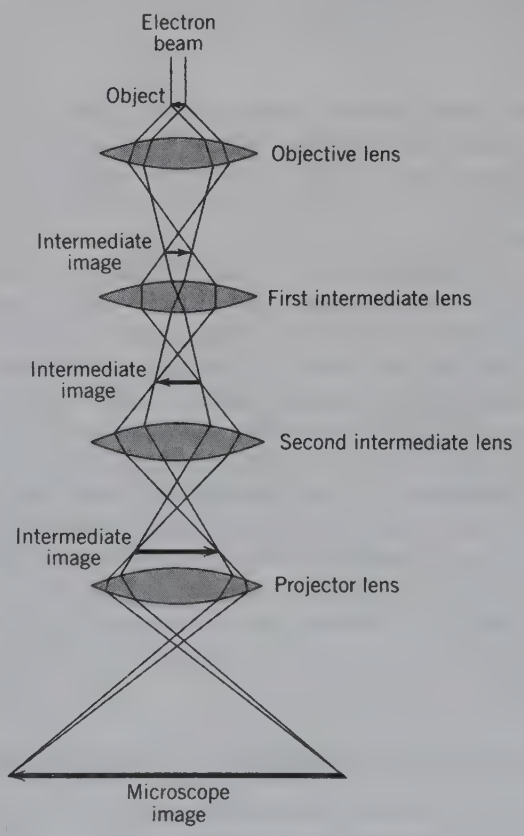

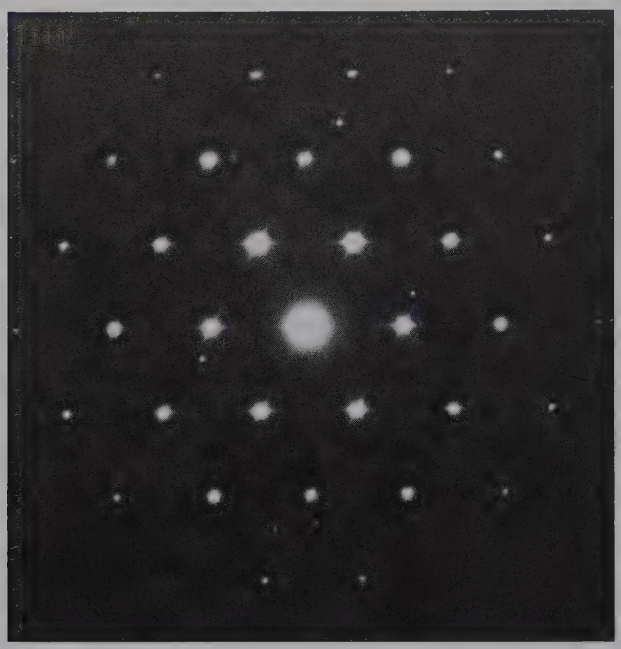

FIG. 14.28 Electron diffraction pattern from an isometric spinel grain with the [111] axis of the grain perpendicular to the page (i.e., parallel to the electron beam). The [111] axis is the $\bar{3}$ axis at the corner of a cube. Compare this electron diffraction photo with a very similar single-crystal X-ray diffraction photo in Fig. 14.11. (After Brearley, A. J., D. C. Rubie, and E. Ito. 1992. Mechanisms of transformations between the α, β, and γ polymorphs of Mg_2SiO_4 at 15 GPa, *Physics and Chemistry of Minerals* 18: 343–58; photograph courtesy of A. J. Brearley.)

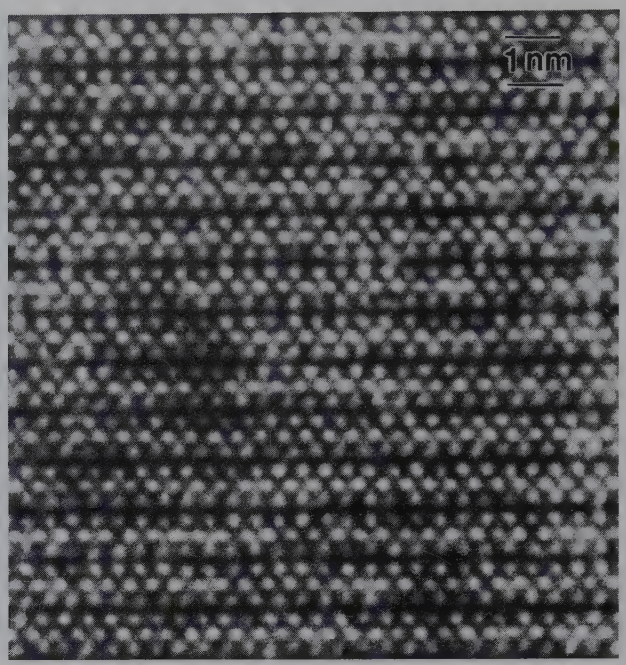

FIG. 14.29 HRTEM image of biotite with the *c* crystallographic axis almost vertical in an N–S direction on the page. Bright (light-colored) regions represent relatively low electron density within the structure. Perfect {0001} cleavage is shown by the whitest, linear, horizontal features. The dark horizontal lines represent Fe and Mg located in octahedral sheets (high-electron density means darkness). Magnification approximately 10 million times. (After Xu, H., and D. R. Veblen. 1995. Periodic and nonperiodic stacking in biotite from the Bingham Canyon Porphyry Copper Deposit, Utah, *Clays and Clay Minerals* 43: 159–73; photograph courtesy of Huifang Xu.)

phase identification of extremely small particles (such as the identification of asbestiform minerals) or intergrowths, of exsolution patterns in minerals, of polytype stackings, and defect structures (described in Chapters 10 and 12).

An example of an electron diffraction pattern is given in Fig. 14.28. Such patterns can be indexed with Miller indices (similar to the indexing of X-ray diffraction patterns) to provide information about crystal symmetry; distances among indexed diffraction maxima provide information about unit cell size. This, in turn, allows for phase identification. An example of an image obtained by TEM in the HRTEM mode is given in Fig. 14.29 (see also Fig. 1.16). This shows the image of structural features of mica at a resolution of about 0.1 nm (1 Å). Similar HRTEM images are used throughout this text to illustrate defect structures and exsolution features (see e.g., Figs. 10.9,10.10, 21.9, 21.15 and 21.16).

ELECTRON MICROPROBE ANALYSIS (EMPA)

The advent of the electron microprobe (EMP) in the 1960s revolutionized chemical analysis of minerals. Instead of obtaining the average bulk chemical composition of a finely ground powder, the EMP quantitatively measures the *in situ* chemical composition from a ~1–3 μm volume of a mineral. Thus, fine-scale chemical zoning and chemical heterogeneities can be detected. These high-resolution chemical data provide the input necessary for algorithms used to determine other parameters, such as the pressure and temperature during the growth history of a mineral.

Electron microprobe analyses are now routinely used for *quantitative* chemical analyses that are far more precise and accurate than data obtained with EDS. Commonly, such data are used to determine the exact stoichiometry of a mineral (such as those presented in Chapter 5). As the name implies, this is a *microanalytical* technique because it allows for the quantitative analysis of a minute volume of material. EMPA can detect small chemical differences (< 0.01 wt. %) across spatial domains with sizes on the order of 1–3 μm.

EMPA uses a finely focused beam of electrons as an energy source. A heated tungsten filament emits free electrons (inside the high vacuum of the electron

gun of the instrument; Fig. 14.24) that are accelerated down the column as a consequence of an energy potential difference of 10–20 KeV between the filament and sample target. These electrons (as charged particles) can be focused into a very fine beam through a set of electromagnetic lenses between the electron source (the filament) and the sample to be analyzed (Fig. 14.24). Because electrons in the beam impinge upon the sample at high velocity, they penetrate the sample to a depth that is about three times greater than the diameter of the beam (Fig. 14.30). Therefore, the chemical analysis is actually from a very small volume of material. This minimal analysis volume ranges from about 10 to 20 μm^3, which in weight is approximately 10^{-11} grams (for a silicate material).

In this very small analysis volume, the incident higher-energy electrons displace inner-shell electrons of the constituent atoms of the sample. Outer-shell electrons fill these inner-shell vacancies, releasing energy by the emission of X-rays of a wavelength characteristic of each element (see Figs. 14.4 and 14.20). These wavelengths can be identified by crystal spectrometers (detecting distinct wavelengths) or by an energy dispersive X-ray spectrometer (detecting a range of energies). A *qualitative* electron microprobe analysis is relatively quick and easy to perform by obtaining the various elemental signatures. A *quantitative* analysis involves complex correction procedures that address various interactions between the generated X-rays and their travel path through the sample before detection by the spectrometer and is based on standards used for comparison of the measured quantities. These matrix corrections are performed by a computer that is online with the instrument.

Because EMPA involves a finely focused electron beam that can cause considerable heating of the sample analysis area, and because a minute analysis volume is involved, the sample preparation procedure is critical for obtaining accurate analyses. Most commonly, the sample to be analyzed is a highly polished sample (or polished thin section) of a mineral, rock, or other solid material. The polished surface is accurately located under the finely focused electron beam by a precise and, generally, computer-controlled stage mechanism. This permits location of grains, or analysis area, as small as 1 μm in diameter, as viewed in the field of a high-powered optical (transmitted and reflected light) microscope built into the electron beam column.

Generally, chemical elements from boron (B) to uranium (U) are analyzed by this technique. The minimum detection limit for most elements analyzed by the electron microprobe technique is not as good as that for X-ray fluorescence because of the presence of a continuum (background) spectrum. However, the ability to obtain a quantitative chemical analysis on a minute volume of material (or a specific mineral grain) is the main reason for the widespread use of this technique in studies of minerals, rocks, ceramics, alloys, and other materials.

As in an SEM, the electron beam in an electron microprobe can be moved at high speed across a small area of the specimen. Such a rastered beam can generate linear and areal scans of X-rays, cathodoluminescence radiation (i.e., the emission of electromagnetic radiation in the ultraviolet, visible, or infrared wavelengths during electron bombardment), and secondary and backscattered electrons. An EDS or a wavelength dispersive spectrometer (WDS) records the X-ray radiation generated over the small area scanned. Figure 14.31 is an example of Mn zonation in calcite as *qualitatively* expressed by cathodoluminescence. A *quantitative* line traverse across this zoned calcite is shown in the lower half of the photograph. The graph consists of a horizontal distance bar with quantitative weight percentage data for Mn and Fe along the vertical axis. These quantitative data were produced with a stationary electron beam positioned at specific points along a traverse; at each analysis point, X-ray signals resulted that were converted to weight percentage values of Mn and Fe through the complex matrix corrections mentioned previously. Each of these chemical data points allows for a quantitative assessment of the changing conditions during the growth of the calcite.

FIG. 14.30 Schematic representation of the small volume irradiated by electrons incident upon the polished surface of a sample in an EMPA instrument. Characteristic X-rays generated are dispersed and analyzed by a spectrometer (with a diffracting crystal, as in X-ray fluorescence) or an energy-dispersive analysis system (see Fig. 14.24 for a schematic cross section of the instrument).

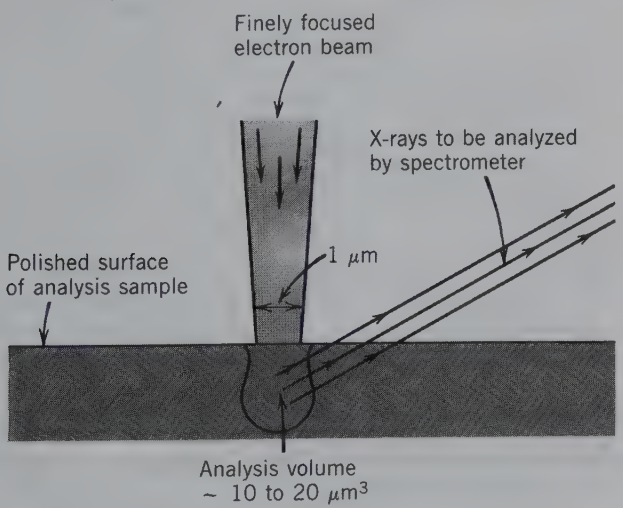

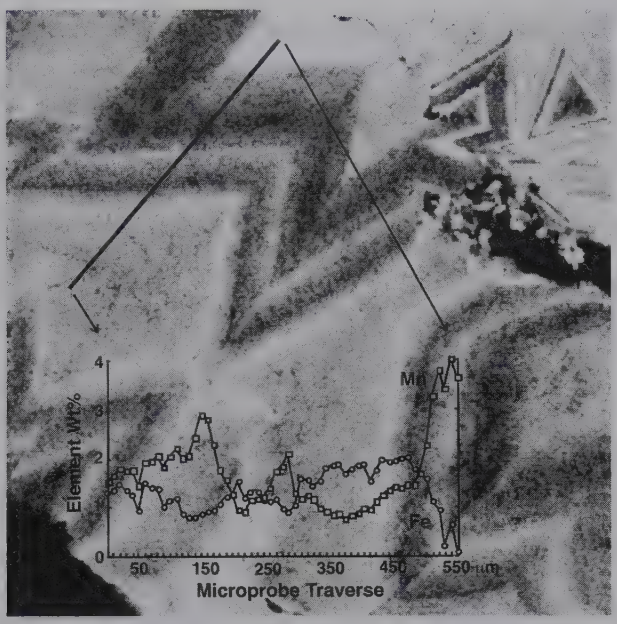

FIG. 14.31 A polished section of calcite that shows clearly defined zoning as outlined by cathodoluminescence under an electron beam that was rastered over the surface of the specimen. The total area scanned and photographed is 1,000 × 1,000 mm. Zones with high luminescence (bright regions) are enriched in manganese content compared to the darker regions. A quantitative line traverse, along the inclined line in the upper-left corner, shows the variation in Fe and Mn in weight percentage. (After Denniston, R. F., C. K. Shearer, G. D. Layne, and D. T. Vaniman. 1997. SIMS analyses of minor and trace element distributions in fracture calcite from Yucca Mountain, Nevada, USA. *Geochimica et Cosmochimica Acta* 61: 1803–18.)

ADDITIONAL TECHNIQUES

SECONDARY ION MASS SPECTROMETRY (SIMS)

This technique offers very high-sensitivity quantitative elemental analysis, *in situ*, with detection limits in the parts per million (ppm) to parts per billion (ppb) range. Most chemical elements from H to U, as well as their isotopes, can be analyzed. While the detection levels are lower than for EMPA, the lateral resolution of this surface analytical technique is approximately 5 μm, larger than for EMPA.

The instrumentation employs a focused beam of ions that impinges on the solid surface of the sample. The atoms on the surface of the sample are extracted as secondary ions and analyzed with respect to mass (using a mass spectrometer). This collision process (Fig. 14.32) causes atoms at or near the surface of the sample to escape due to the energy received from the ion beam. In this process, particles are ejected as atoms or molecules in a neutral, excited, or ionized state, but only the ionized species can be used in SIMS analysis.

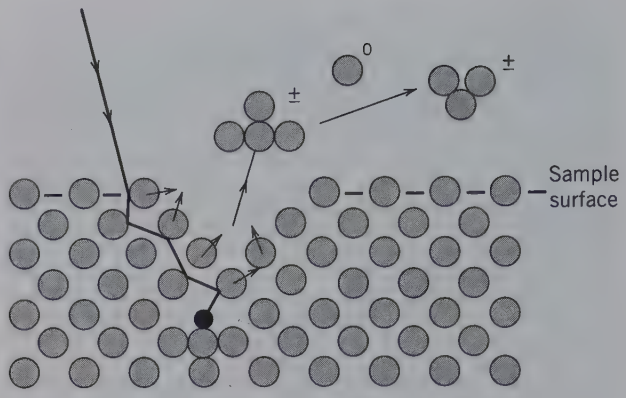

FIG. 14.32 Schematic illustration of the sputtering process showing emission of secondary particles induced by a collision cascade of primary particles. (After MacRae, N. 1995. Secondary-ion mass spectrometry. *The Canadian Mineralogist* 33: 219–36.)

The instrument consists of a source of bombarding primary ions (commonly O^- or Cs^+) that are focused onto the specimen sample by lens systems. In most of the instruments used for mineralogical analysis, the secondary ions (produced by sputtering at the sample surface) are extracted and are focused into a double focusing *mass spectrometer* that separates ions on the basis of energy and mass. Mass spectrometry is extremely sensitive and can detect mass differences among isotopes of the same element. Figure 14.33 shows the general layout of the instrumentation.

Although the instrument can be used to determine the concentration of any chemical element (especially those that occur at very low levels), it is commonly applied to the determination of the abundance and distri-

FIG. 14.33 Schematic diagram of an ion microprobe. (Illustration courtesy of C. Shearer, Institute of Meteoritics, University of New Mexico, Albuquerque.)

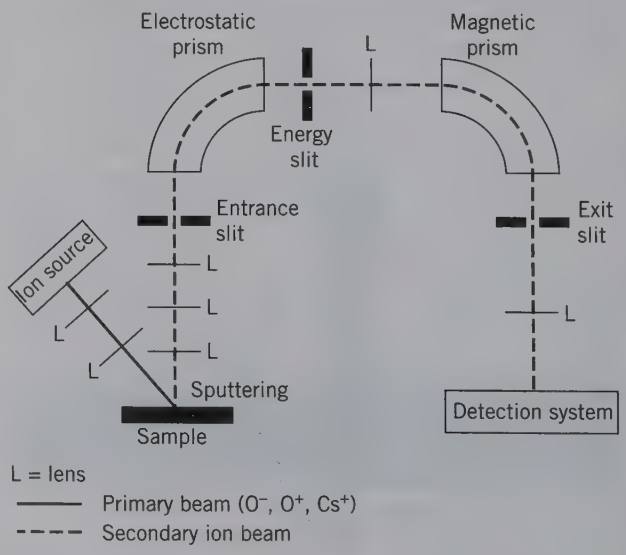

bution of light elements (e.g., H, Li, and B that cannot be detected with EMPA), of the rare earth elements (REE) and of isotopes. Light elements affect the stoichiometry of a mineral and may provide information on the conditions of a mineral's formation. REEs are commonly used as petrogenetic indicators (petrogenesis is that part of petrology that deals with the origin and formation of rocks). In geologic samples, REE abundances are typically below the detection levels of electron microprobe analysis. The SIMS technique also allows collecting isotopic compositions for use in absolute age dating and for diffusion studies of minerals.

An ion microprobe known as the SHRIMP, for Sensitive High-Resolution Ion Microprobe, has the unique capability of accurate microprobe analysis for U and Pb on a microscale (area of analysis is about 20 μm). This technique has been especially successful in the U and Pb analyses of individual portions of zircon grains for age dating many of the oldest rock types (about four billion years old) in the Precambrian.

ATOMIC FORCE MICROSCOPY (AFM)

A different approach to the study of mineral surfaces is provided by atomic force microscopy (AFM). This high-resolution imaging technique allows for the study of surface morphology and structure at the *atomic scale*. Atomic force microscopy was developed as an outgrowth of work on the scanning tunneling microscope (STM), which is applied to electrically conductive materials, such as metals as well as semiconductors like sulfides. In the STM analytical method, an atomically sharp, conducting voltage-biased tip is brought close to the surface of the conducting material. Electrons tunnel from the material to the tip, or from the tip to the material. The spatial variation in current is a reflection of the surface at an atomic or near-atomic scale. Atomic force microscopy produces similar-scale images for insulators.

The atomic force microscope makes use of the interatomic forces between atoms forming the surface of the sample under study and the atoms forming the end of a sharp probe tip attached to a cantilever-type spring (Fig. 14.34). The application of a small tracking force keeps the tip in contact with the surface. Any force acting on the probe tip deflects the cantilever, and such deflection reflects the atomic topography of the sample surface. The tip displacement is proportional to the force between the surface and the tip. The resultant bending of the cantilever can be measured optically by laser interferometry or beam deflection. One important advantage of AFM is that material can commonly be imaged "as is" with essentially no sample preparation.

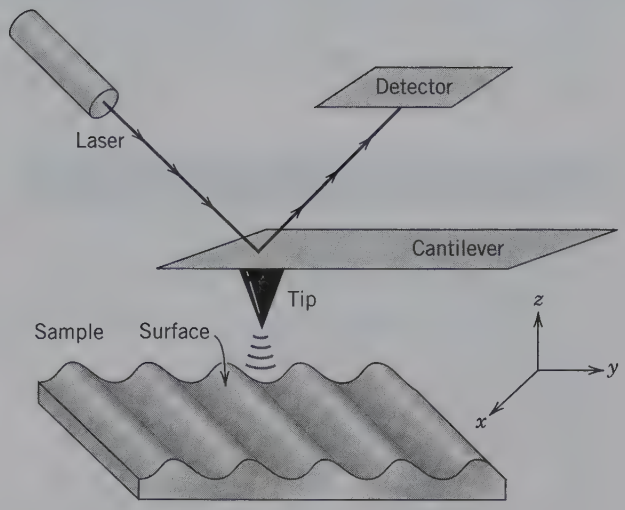

FIG. 14.34 Schematic illustration of some of the components in an atomic force microscope (AFM). (Diagram courtesy of Huifang Xu, Department of Geology and Geophysics, University of Wisconsin, Madison.)

Figure 14.35 is an AFM image of an octahedral sheet in lizardite, one of three polymorphs of serpentine. The resolution (as shown by the rectangular axes) is on the order of 0.1 nm (1Å). An AFM image is also shown at the start of this chapter. Such high-resolution images

FIG. 14.35 An AFM image of the atomic structure of an octahedral sheet that forms the surface of the sheet silicate lizardite, one of three polymorphs of serpentine, $Mg_3Si_2O_5(OH)_4$. Hydroxyl groups (pale gray) are arranged in triangles and are bonded to magnesium ions (medium gray). Black areas are empty sites. The scales are shown in increments of 0.4 nm (4 Å). (After Wicks, F. J., K. Kjoller, R. K. Eby, F. C. Hawthorne, G. S. Henderson, and G. A. Vrdoljak. 1993. Imaging the internal atomic structure of layer silicates using the atomic force microscope. *The Canadian Mineralogist* 31: 541–50; photograph courtesy of F. J. Wicks.)

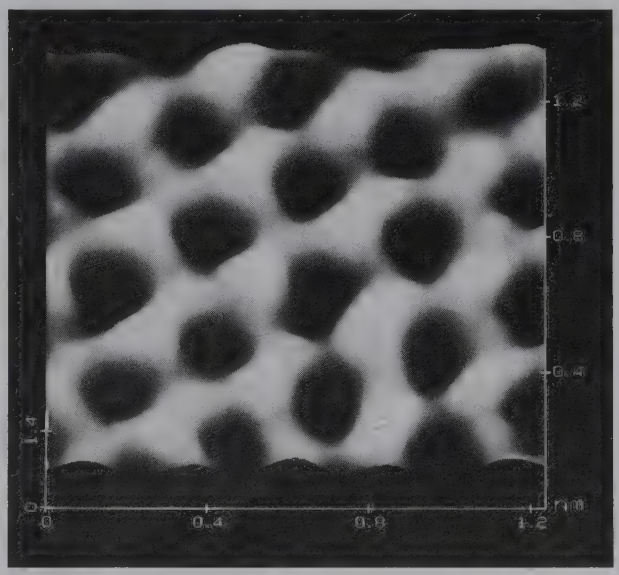

allow scientists to evaluate processes such as crystallization, dissolution, adsorption, and alteration at the atomic scale.

REFERENCES AND FURTHER READING

X-ray Diffraction

Azaroff, L. V. 1968. *Elements of X-ray crystallography.* McGraw-Hill, New York.

Azaroff, L. V., and M. J. Buerger. 1958. *The powder method in X-ray crystallography.* McGraw-Hill, New York.

Bragg, W. L. 1949. *The crystalline state: A general survey.* G. Bell and Sons, Ltd., London.

Buerger, M. J. 1964. *The precession method in X-ray crystallography.* Wiley, New York.

Cullity, B. D. 1978. *Elements of X-ray diffraction.* 2nd ed. Addison-Wesley, Reading, Massachusetts.

Gibbs, G. V. 1982. Molecules as models for bonding in silicates. *American Mineralogist* 67: 421–451.

Klein, C. 2008. *Minerals and rocks: Exercises in crystal and mineral chemistry, crystallography, X-ray powder diffraction, mineral and rock identification, and Ore Mineralogy.* 3rd ed. Wiley, New York.

Klug, H. P., and L. E. Alexander. 1974. *X-ray diffraction procedures for polycrystalline and amorphous materials.* 2nd ed. Wiley, New York.

Moore, D. M., and R. C. Reynolds, Jr. 1997. *X-ray diffraction and the identification and analysis of clay minerals.* 2nd ed. Oxford University Press, New York.

Nuffield, E. W. 1966. *X-ray diffraction methods.* Wiley, New York.

Post, J. E., and D. L. Bish. 1989. Rietveld refinement of crystal structures using X-ray powder diffraction data. *Modern powder diffraction*, edited by D. L. Bish and J. E. Post. *Reviews in Mineralogy* 20: 277–308. Mineralogical Society of America, Washington, D.C.

Scanning Electron Microscopy and Electron Microprobe Analysis

Goldstein, J. I., D. E. Newbury, P. Echlin, D. C. Joy, A. D. Romig Jr., C. E. Lyman, C. Fiori, and E. Lifshin. 1992. *Scanning electron microscopy and X-ray microanalysis, a text for biologists, material scientists, and geologists.* 2nd ed. Plenum Press, New York.

Electron Microscopy

Buseck, P. R., and S. Iijima. 1974. High resolution electron microscopy of silicates. *American Mineralogist* 59: 1–24.

Electron microscopy in mineralogy. 1976. Coordinating ed. H. R. Wenk. Springer-Verlag, New York.

Hirsch, P., A. Howie, R. B. Nicholson, D. W. Pashley, and M. J. Whelan. 1977. *Electron microscopy of thin crystals.* Robert E. Krieger Publishing Co., Malabar, Florida.

Veblen, D. R. 1985. Direct imaging of complex structures and defects in silicates. *Annual Review of Earth and Planetary Sciences* 13: 119–46.

Chemical and X-ray Fluorescence Analysis

Laitenen, H. A., and S. Harris. 1975. *Chemical Analysis.* 2nd ed. McGraw-Hill, New York.

Liebhafsky, H. A., H. G. Pfeiffer, E. H. Winslow, and P. D. Zemany. 1960. *X-ray absorption and emission in analytical chemistry.* Wiley, New York.

Skoog, D. A., and J. L. Leary. 1992. *Principles of instrumental analysis.* 4th ed. Saunders College Publishing, New York.

Strobel, H. A., and W. R. Heineman. 1989. *Chemical instrumentation: A systematic approach.* 3rd ed. Wiley, New York.

Sylvester, P. ed. 2001. *Laser-ablation-ICPMS in the earth sciences.* Mineralogical Association of Canada, Ottawa, Ontario, Canada.

Willard, H. H., L. M. Merritt, J. A. Dean, and F. A. Settle. 1981. *Instrumental methods of analysis.* 6th ed. D. Van Nostrand Co., New York.

Ion Microprobe Analysis

Reed, S. J. B. 1989. Ion microprobe analysis—A review of geological applications. *Mineralogical Magazine* 53: 3–24.

Sykes, D. E. 1989. Dynamic secondary ion mass spectrometry. *Methods of surface analysis.* Edited by J. M. Walls. Cambridge University Press, New York.

Atomic Force Microscopy

Binnig, G., C. F. Quate, and C. Gerber. 1986. Atomic force microscopy. *Physical Review Letters* 56: 930–33.

Hochella, M. F., Jr., C. M. Eggleston, V. B. Elings, and M. S. Thompson. 1990. Atomic structure and morphology of the albite {010} surface: An atomic force microprobe and diffraction study. *American Mineralogist* 75: 723–30.

Wicks, F. J., K. Kjoller, R. K. Eby, F. C. Hawthorne, G. S. Henderson, and G. A. Vrdoljak. 1993. Imaging the internal atomic structure of layer silicates using the atomic force microscope. *The Canadian Mineralogist* 31: 541–50.

Additional References

Microbeam techniques in the earth sciences. 1995. Edited by F. C. Hawthorne and R. F. Martin. *The Canadian Mineralogist* 33, part 2: 201–508.

Spectroscopic methods in mineralogy and geology. 1988. Edited by F. C. Hawthorne. *Reviews in Mineralogy* 18. Mineralogical Society of America, Washington, D. C.

Zolensky, M. E., C. Pieters, B. Clark, and J. J. Papike. 2000. Small is beautiful: The analysis of nanogram-sized astromaterials. *Meteorites and Planetary Science* 35: 9–29.

CHAPTER 15

Crystal Chemistry and Systematic Descriptions of Native Elements, Sulfides, and Sulfosalts

Chalcopyrite, Cu_5FeS_4, as disphenoid crystals that are tetrahedral in aspect. The white crystals are quartz, SiO_2, with well-developed prisms and terminating rhombohedrons. (From St. Agnes, Cornwall, England (Harvard Mineralogical Museum.)

This chapter and the four subsequent chapters discuss the crystal chemistry and systematic descriptions of the common minerals and those rarer ones of most economic importance. These five chapters treat in detail about 200 mineral species, which is a relatively small number compared with the 4,155 minerals that are recognized.[1] The names and chemical compositions of related minerals are also given. Of the 4,155 recognized mineral species, 90 are native elements and 624 are sulfides and sulfosalts combined. This first chapter provides information on a considerable number of minerals that are of economic importance.

The systematic description of all minerals[2] follows a common scheme of presentation. The headings used and the data given under each are as follows:

Crystallography. Under this heading is given the following crystallographic information:

The crystal system and symbol of the crystal class.

Crystallographic features usually observed by visual inspection, such as habit, twinning, and crystal forms.

[1]All numerical data regarding mineral species are courtesy of J. A. Mandarino, Toronto, Ontario, Canada.

[2]Mineral names are given in boldface capitals (e.g., **GOLD**) or lowercase (e.g., **Acanthite**). Those in boldface capitals are considered most common or important.

Other pertinent data are listed without subheadings. For example, consider the following data for cerussite:

Pmcn (space group), $a = 5.15$, $b = 8.47$, $c = 6.11$ Å (unit cell dimensions), $Z = 4$ (formula units per unit cell).

ds: 3.59(10), 3.50(4), 3.07(2), 2.49(3), 2.08(3) (strongest X-ray lines in angstrom units with relative intensities in parentheses). This explanation in parentheses is omitted in subsequent descriptions.

Physical Properties. The physical properties *cleavage*, **H** (hardness), **G** (specific gravity), *luster*, *color*, and *optics* (brief summary of optical data) are listed.

Composition and Structure. The chemical composition is given. Commonly, it includes the percentage of elements or oxides, as well as the elements that substitute for those given in the chemical formula. The most important aspects of the crystal structure are briefly described.

Diagnostic Features. The outstanding properties and tests that aid one in recognizing the mineral and distinguishing it from others.

Occurrence. A brief statement of the mode of occurrence and characteristic mineral associations is given. The localities where a mineral is or has been found in notable amount or quality are mentioned. For minerals found abundantly the world over, emphasis is on North American localities.

Use. For a mineral of economic value, there is a brief statement of its uses.

Similar Species. The similarity of the species listed to the mineral whose description precedes it may be on the basis of either chemical composition or crystal structure.

MINERAL CLASSIFICATION

Chemical composition has been the basis for the classification of minerals since the middle of the nineteenth century. According to this scheme, minerals are divided into classes depending on the dominant anion or anionic group (e.g., oxides, halides, sulfides, silicates, etc.). There are a number of reasons why this criterion is a valid basis for the broad framework of mineral classification. First, minerals having the same anion or anionic group dominant in their composition have unmistakable family resemblances, in general stronger and more clearly marked than those shared by minerals containing the same dominant cation. Thus, the carbonates resemble each other more closely than do the minerals of copper. Second, minerals related by the same anion tend to occur together or in the same or similar geological environment. Thus, the sulfides occur in close mutual association in deposits of vein or replacement type, whereas the silicates make up the great bulk of the rocks of the Earth's crust. Third, such a scheme of mineral classification is consistent with the current chemical practice in naming and classifying inorganic compounds.

However, early in the study of minerals it was recognized that chemistry alone does not adequately characterize a mineral. A full appreciation of the nature of minerals was to wait until X-rays were used to determine internal structures. It is now clear that mineral classification must be based on **chemical composition** and **internal structure**, because these together represent the essence of a mineral and determine its physical properties. Crystallochemical principles were first used by W. L. Bragg and V. M. Goldschmidt for silicate minerals. This large mineral group was divided into subclasses partially on the basis of chemical composition but principally in terms of internal structure. Within the silicate class, therefore, framework, chain and sheet silicate (etc.) **subclasses** exist on the basis of the structural linkage of SiO_4 tetrahedra. Such structural principles in combination with chemical composition provide a logical classification. It is this scheme of classification that is used in the subsequent sections on systematic mineralogy.

The broadest divisions of the classification used in this book (as based on C. Palache, H. Berman, and C. Frondel, *Dana's System of Mineralogy*, 7th ed., and H. Strunz and E. H. Nickel, *Strunz Mineralogical Tables*, 9th ed.; see references) are as follows:

Native elements Sulfides Sulfosalts	Chapter 15
Oxides (a) Simple and multiple (b) Hydroxides	Chapter 16
Halides Carbonates Nitrates Borates Phosphates Sulfates Tungstates	Chapter 17
Silicates	Chapters 18 and 19

These classes are subdivided into **families** on the basis of chemical types, and the family in turn may be divided into **groups** on the basis of structural similarity. A group is made up of **species**, which may form **series** with each other. Species have the same structure but different chemistries. A **species** may be subdivided into chemical **varieties** by adjectival modifiers that reflect the presence of unusual amounts of chemical con-

stituents. The following are some examples of such modifiers:

aluminian	: Al-rich
calcian	: Ca-rich
chromian	: Cr-rich
ferroan	: Fe^{2+}-rich
ferrian	: Fe^{3+}-rich
magnesian	: Mg-rich
manganoan	: Mn-rich

These are used in the minerals manganoan aegirine, ferrian diopside, and magnesian augite, for example.

In each of the classes, the mineral with the highest ratio of metal to nonmetal is given first followed by those containing progressively less metal. Because a relatively small number of minerals is described in this text, often only one member of a group or family is represented, and, thus, a rigorous adherence to division and subdivision is impractical.

Minerals are grouped into several additional classes. Although new minerals are discovered every year, Table 15.1 provides a list of all minerals recognized by 2006 organized by class (data from J. Mandarino, March, 2006). This provides a quick overview of the rarity or abundance of mineral species in the various classes.

Table 15.1 Chemical Classes Represented in Mandarino Database*

Chemical Class	Number
Acetates	3
Antimonates	13
Antimonites	8
Arsenates	256
Arsenites	29
Borates	135
Carbides	7
Carbonates	234
Chromates	18
Citrates	1
Formates	2
Germanates	3
Halides	150
Iodates	11
Molybdates	24
Native elements, alloys	90
Nitrates	15
Nitrides	5
Organics	18
Oxalates	17
Oxides and hydroxides	411
Phosphates	438
Phosphides	3
Selenates	2
Selenites	21
Silicates	1,139
Sulfates	301
Sulfides, selenides, tellurides, sulfosalts	624
Sulfites	4
Tellurates	21
Tellurites	33
Tungstates	18
Vanadates	69
Vanadium oxysalts	32
Total	4,155

*Data kindly provided by J. A. Mandarino, Toronto, Ontario, Canada; March 2006.

CRYSTAL CHEMISTRY OF NATIVE ELEMENTS, SULFIDES, AND SULFOSALTS

NATIVE ELEMENTS

With the exception of the free gases of the atmosphere, only about 20 elements are found in the native state. These elements can be divided into (1) **metals**; (2) **semimetals**; (3) **nonmetals**. The more common **native metals**, which display very simple structures, constitute three groups: the *gold group* (space group: $Fm3m$), gold, silver, copper, and lead, all of which are isostructural; the *platinum group* (space group: $Fm3m$), platinum, palladium, iridium and osmium, all of which are isostructural; and the *iron group*, iron and nickel-iron, of which pure Fe as well as kamacite have space group $Im3m$ and the more Ni-rich variety of nickel-iron (taenite) $Fm3m$.

Metals		Semimetals	
Gold group		Arsenic group	
Gold	Au	(Arsenic	As)
Silver	Ag	(Bismuth	Bi)
Copper	Cu	Nonmetals	
Platinum group		Sulfur	S
Platinum	Pt	Diamond	C
Iron group		Graphite	C
Iron	Fe		
(Kamacite	Fe, Ni)		
(Taenite	Fe, Ni)		

In addition, mercury, tantalum, tin, and zinc have been found. The **native semimetals** form two isostructural groups: arsenic, antimony, and bismuth (space group $R3m$), and the less common selenium and tellurium (space group $P3_121$). The important **nonmetals** are sulfur and carbon in the form of diamond and graphite.

NATIVE METALS

Our knowledge of the properties and usefulness of metals arose from the chance discovery of nuggets and masses of gold group minerals. Many relatively advanced early cultures were restricted in their use of metal to that found in the native state.

The elements of the **gold group** belong to the same group in the periodic table of elements and, hence, their atoms have somewhat similar chemical properties; all are sufficiently inert to occur in an elemental state in nature. When uncombined with other elements, the atoms of these metals are united into crystal structures by the rather weak metallic bond. The minerals are isostructural and are built on the face-centered cubic lattice with atoms in 12-coordination (see Fig. 15.1a). Complete solid solution takes place between gold and silver, as these two elements have the same atomic radii (1.44 Å). Copper, because of its smaller atomic radius (1.28 Å), exhibits only limited solid solution in gold and silver. Conversely, native copper carries only traces of gold and silver in solid solution.

The similar properties of the members of this group arise from their common structure. All are rather soft, malleable, ductile, and sectile. All are excellent conductors of heat and electricity, display metallic luster and hackly fracture, and have rather low melting points. These are properties conferred by the metallic bond. All are isometric hexoctahedral and have high densities resulting from the cubic closest packing of their structures.

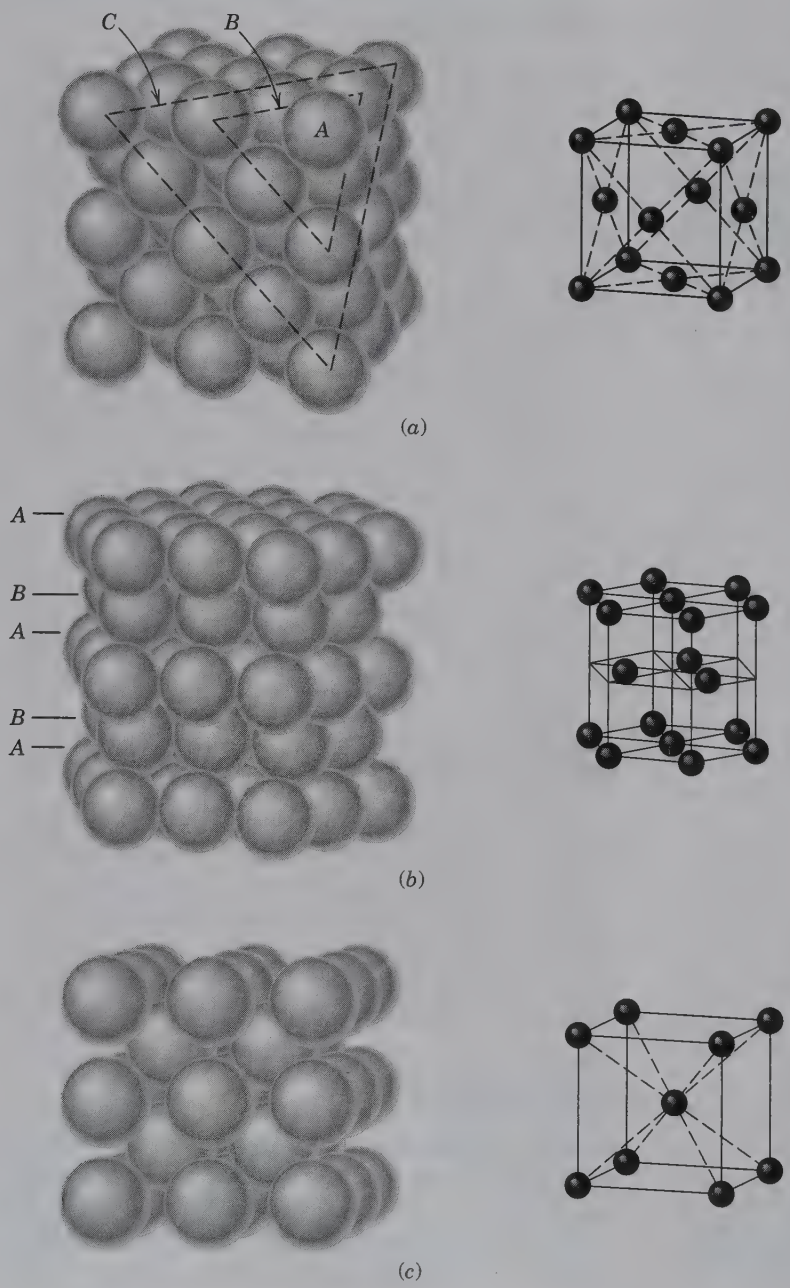

FIG. 15.1 (a) Close-packed model of cubic closest packing (*ABCABC . . .*) of equal spheres as shown by Cu, Au, Pt, and many other metals. Each metal atom is surrounded by 12 closest neighbors (see also Figs. 4.1 and 4.2). Close-packed layers are parallel to {111}. The face-centered cubic lattice (*F*) compatible with this packing sequence is illustrated on the right. (b) Close-packed model of hexagonal closest packing (*ABAB . . .*) of equal spheres as shown by Mg, Zn, and Cd. Each metal atom is surrounded by 12 closest neighbors (see also Figs. 4.1 and 4.2). This type of stacking leads to a hexagonal (*H*) lattice, as illustrated on the right. (c) Close-packed model of body-centered cubic packing of equal spheres, as shown by Fe. Each sphere is surrounded by 8 closest neighbors. This packing is not as close as that exhibited by CCP and HCP. The body-centered (*I*) lattice compatible with this packing model is illustrated on the right

Different properties exhibited by the minerals of this group arise from the properties of the atoms of the individual elements. Thus, the yellow of gold, the red of copper, and the white of silver are atomic properties. The specific gravities likewise depend on atomic properties and show a rough proportionality to the atomic weights.

Although only platinum is discussed here, the *platinum group* also includes the rarer minerals palladium, platiniridium, and iridosmine. The last two are, respectively, alloys of iridium and platinum and iridium and osmium, with hexagonally close-packed structures and space group $P6_3/mmc$. Platinum and iridium, however, have cubic closest packed structures, similar to metals of the gold group, with space group $Fm\bar{3}m$. The platinum metals are harder and have higher melting points than metals of the gold group.

Members of the **iron group** metals are isometric and include pure iron (Fe), which occurs only rarely on the Earth's surface, and two species of nickel-iron (*kamacite* and *taenite*), which are common in meteorites. Iron and nickel have almost identical atomic radii (1.26 Å and 1.25 Å, respectively), and thus nickel can and usually does substitute for some of the iron. Pure iron and kamacite, which contains up to about 5.5 weight percent Ni, show cubic close packing with space group $Im\bar{3}m$. Taenite, which shows a range in Ni content from 27 to 65 weight percent, is cubic closest packed with space group $Fm\bar{3}m$ (see Figs. 15.1a and 15.1c). These two minerals are characteristic of iron meteorites and it is suggested that Fe–Ni alloys of this type constitute a large part of the Earth's core.

Native Semimetals

The semimetals arsenic, antimony, and bismuth belong to an isostructural group with space group $R\bar{3}m$. Their structures, unlike those of the metals, cannot be represented as a simple packing of spheres, because each atom is somewhat closer to three of its neighbors than to the remainder of the surrounding atoms. In Fig. 15.2a, which represents the structure of arsenic (or antimony), the spheres intersect each other along the flat circular areas. The bonding between the four closest atoms, forming pyramidal groups (see Fig. 15.2b), is due to the covalent nature of these bonds. This covalency is related to the position of these semimetals in group V of the periodic table toward the electronegative end of a row. The relatively strong bonding to four closest neighbors results in a layered structure, as shown in Fig. 15.2b. These layers are parallel to {0001}, and the weak bonding between them gives rise to a good cleavage. Members of this group have similar physical properties. They are rather brittle and much poorer conductors of heat and electricity than the native metals. These properties reflect a bond type intermediate between metallic and covalent. Hence, it is stronger and more directional than pure metallic bonding in its properties and this leads to lower symmetry.

Because native arsenic and bismuth as minerals are uncommon, there are no detailed descriptions of these species.

Native Nonmetals

The structure of the nonmetals, sulfur, diamond, and graphite are very different from those of the metals and semimetals. *Sulfur* ordinarily occurs in orthorhombic

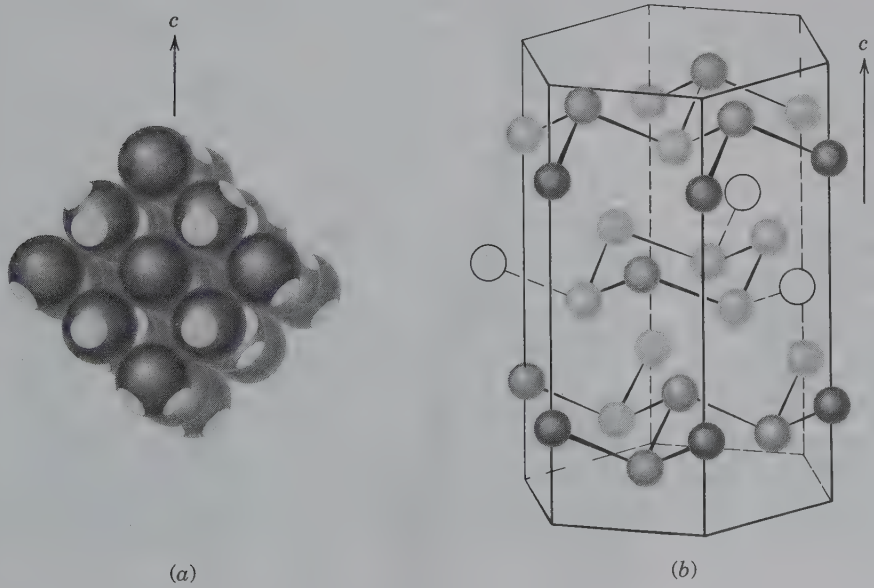

FIG. 15.2 (a) Close-packed model of the structures of As and Sb. Flat areas represent overlap between adjoining atoms. (b) Expanded view of the structure of As or Sb, showing corrugated layers of covalently bonded groups, parallel to {0001}.

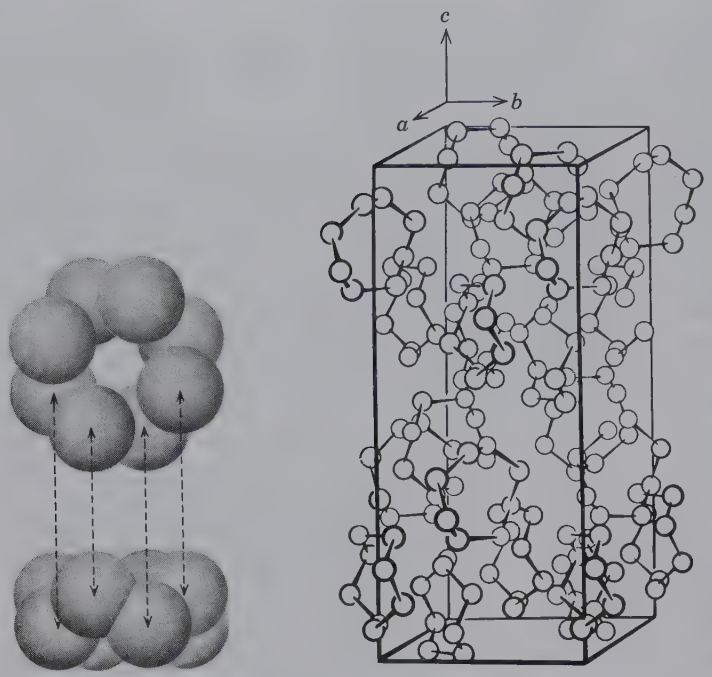

FIG. 15.3 (a) S_8 rings in orthorhombic sulfur as seen parallel (below) and perpendicular to the rings (above). (b) Unit cell of the structure of sulfur, showing the arrangement of S_8 rings.

crystal form (with space group *Fddd*) in nature; two monoclinic polymorphs are very rare in nature but are commonly produced synthetically. The orthorhombic structure of S is stable at atmospheric pressure below 95.5°C, and a monoclinic polymorph is stable from 95.5 to 119°C. This monoclinic polymorph melts above 119°C. The unit cell of the orthorhombic form of sulfur contains a very large number of S atoms, 128. The sulfur atoms are arranged in puckered rings of eight atoms that form closely bonded S_8 molecules (see Fig. 15.3a). These rings are bonded to each other by van der Waals forces, with a relatively large spacing between the rings (see Fig. 15.3b); 16 of such rings are present in the unit cell. Small amounts of selenium (atomic radius 1.16 Å) may substitute for S (atomic radius 1.04 Å) in the structure.

The structures of the two carbon polymorphs, *diamond* and *graphite*, are shown in Figs. 15.4a and b. Diamond has an exceptionally close-knit and strongly bonded structure in which each carbon atom is bound by powerful and highly directive covalent bonds to four carbon neighbors at the apices of a regular tetrahedron. The resulting structure, although strongly bonded, is not closed packed, and only 34% of the available space is filled. The presence of rather widely spaced sheets of carbon atoms parallel to {111} (see Fig. 15.4a) accounts for prominent octahedral cleavage in diamond. The {111} sheets are planes of maximum atomic population.

The structure of graphite, illustrated in Fig. 15.4b, consists of six-membered rings in which each carbon atom has three near neighbors arranged at the corners of an equilateral triangle. Three of the four valence electrons in each carbon atom may be considered to be locked up in tight covalent bonds with three close carbon neighbors in the plane of the sheet. The fourth is free to wander over the surface of the sheet, creating a dispersed electrical charge that is responsible for its relatively high electrical conductivity. In contrast, diamond, in which all four valence electrons are locked up in covalent bonds, is among the best electrical insulators.

The sheets composing the graphite crystal are stacked in such a way that alternate sheets are in identical positions, with the intervening sheet translated a distance of one-half the periodicity in the plane of the sheets (see Fig. 15.4b). The distance between sheets is much greater than one atomic diameter, and van der Waals bonding forces perpendicular to the sheets are very weak. The wide separation and weak bonding give rise to the perfect basal cleavage and easy gliding parallel to the sheets. Because of this open structure, only about 21% of the available space in graphite is filled, and the specific gravity is proportionately less than that of diamond. See modules III and IV on the CD-ROM for various illustrations of the structures of diamond and graphite.

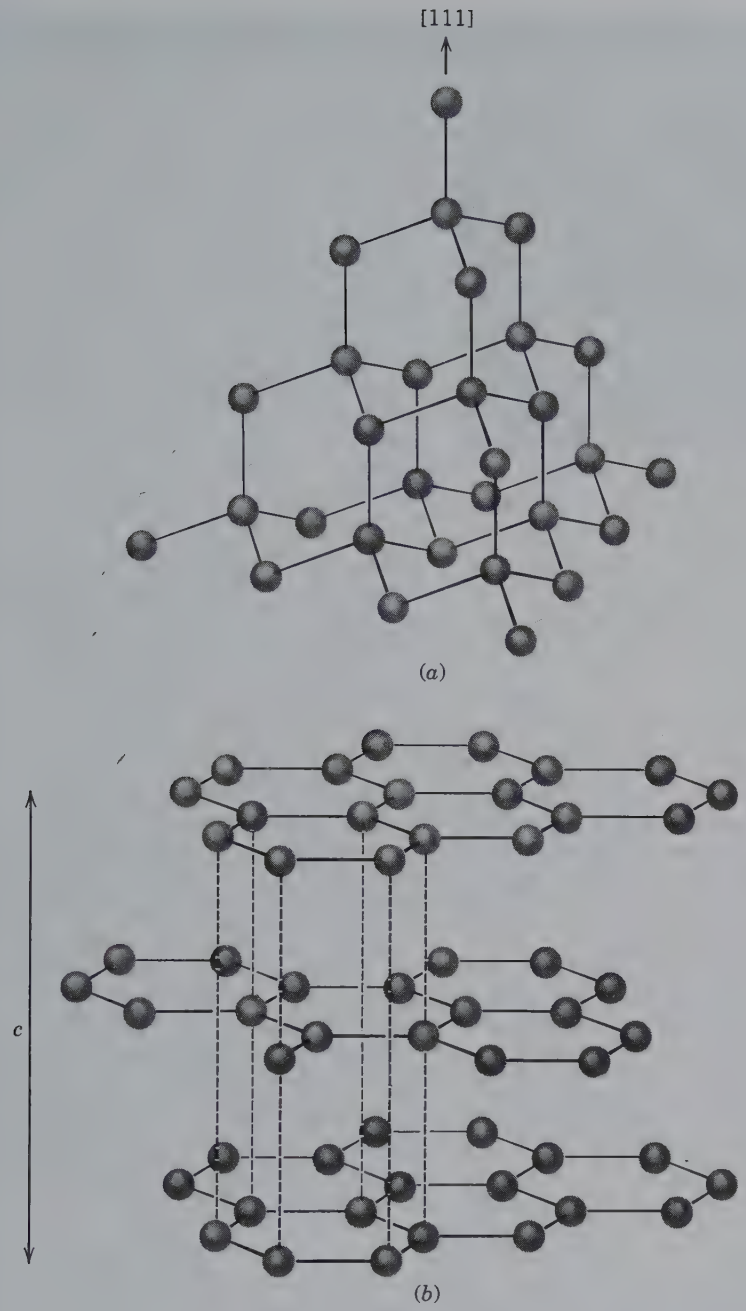

FIG. 15.4 (a) Partial representation of the structure of diamond. The horizontal plane is (111). (b) The structure of graphite with sheets // {0001}. Dashed vertical lines link atoms in successive sheets; these lines do not represent bonds.

SULFIDES

The sulfides form an important class of minerals that includes a majority of the ore minerals. (An **ore** is a naturally occurring material from which a mineral or minerals of economic value can be extracted at a reasonable profit. An ore mineral is that part of an ore deposit, usually metallic, that is economically desirable (see Box 15.1). In contrast, **gangue** is the valueless material associated with the ore). With them are classed the similar but rarer sulfarsenides, arsenides, selenides, and tellurides.

Most of the sulfide minerals are opaque with distinctive colors and characteristically colored streaks. Those that are nonopaque, such as cinnabar, realgar, and orpiment, have distinctive colors, extremely high refractive indices and transmit light only on thin edges.

The general formula for the sulfides is given as X_mZ_n in which X represents the metallic elements and Z the nonmetallic element. The general order of listing of the various minerals is in a decreasing ratio of $X:Z$.

BOX 15.1 ECONOMIC GEOLOGY

From aluminum in soda cans to copper in all electrical devices to zinc in duct tape, humanity depends on chemical elements extracted from minerals in the Earth. Because of the critical role that earth materials play in the survival of nations, their technological advances, and their standard of living, an entire discipline of geology, **economic geology**, is devoted to the study of economically important minerals. (Refer to Chapter 1 for average annual mineral use in the United States.)

Although these valuable commodities span the range from base metal deposits to nonmetallic minerals to coal, oil, and water, the field of economic geology focuses primarily on metallic mineral deposits. When a metal is sufficiently concentrated so that it can be mined and extracted at a profit, it is referred to as an **ore**. Ore, therefore, is an *economic term* that has no specific geologic significance. Minerals associated with ores that cannot be avoided during mining but have no value are termed **gangue**. For example, sphalerite, ZnS, commonly occurs with quartz, SiO_2. Sphalerite is an ore mineral from which Zn is extracted whereas quartz is the gangue mineral. Ore minerals are generally native metals, sulfides, and oxides (see list that follows). Only under exceptional geologic circumstances are ore minerals sufficiently concentrated to develop ore deposits. To enable economic geologists to discover new deposits, the ore-forming processes and the physicochemical environments in which ores are deposited must be understood. Because minerals commonly retain a record of these processes, economic geologists must have a strong foundation in mineral science.

Mineral deposits are divided into two broad categories: resources and reserves. A **resource** is that total amount of a geologic material, both discovered and undiscovered (but that can be reasonably inferred to exist), that may have future potential for economic recovery. In contrast, a **reserve** is a small part of a resource that has been discovered and can be profitably, legally, and technically extracted using contemporary mining and production practices. With technological advances or fluctuations in commodity markets, resources may reach the status of reserves. Because economic minerals are generated on geologic time scales, all metals must be considered nonrenewable resources. These valuable commodities are found worldwide, but are not distributed evenly among nations. Wars have been fought to secure such deposits, and in the time of war, specific deposits may be critically necessary, as was the case in World War II for Pb—used for munitions.

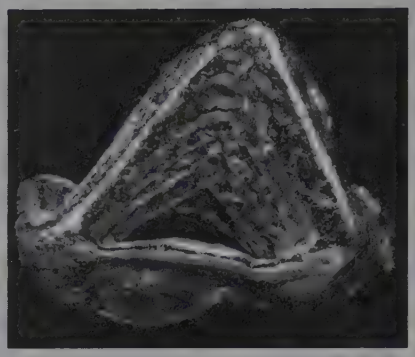

Gold crystal displaying a skeletal octahedron. Specimen is 7 mm on an edge and from Icabaru, Bolivar, Venezuela. (Photo courtesy of Dr. Carl Francis, Harvard Mineralogical Museum #119638)

Gold is a well-known ore mineral that has long been treasured for its beauty and durability, but it is also a valuable long-term commodity. It is estimated that 150,000 tons of gold have been mined over the ages*. About 15% of this gold is estimated to have been lost or used in dissipative processes. Of the amount remaining, about 25% is held as official stocks, and 75% is held privately as bullion, coin, and jewelry. In 2004, the United States Geological Survey estimated world gold reserves of 42,000 t (where t is a metric ton). The Republic of South Africa is the largest world producer of gold with about 14% of the world total, followed by the United States, Australia, and China. Currently, the world market supply of gold bullion is nearly 3,900 t/yr. (One gram per metric ton = one part per million). The average amount of gold in an ore is about 5 gm gold/t of rock (Kesler, 1996) where 1t is about $1m^3$rock. Therefore, a single gold ring weighing 20 gm would require four tons of ore to be processed and would generate a waste pile of about 12 m^3 (assuming a three-fold increase in volume of rock with pulverizing).

10-oz gold bars known as gold bullion. Bullion is legal tender minted by national governments and is of declared gold content but without a declared face value (Butterman and Amey, 2005). Bullion is sold at a premium value over the price of the actual amount of contained gold. These, as well as large gold bars, are housed in vaults of many national banks as well as investment houses (Photograph from the Wiley research department.)

Extraction of metals alters the landscape, and the need for more mineral resources drives exploration into increasingly remote regions. Increased mining and consumption of precious earth resources, therefore, must be balanced with environmental degradation associated with the extraction of materials.

Some important ore minerals include: Argentite, Ag_2S; Bornite, Cu_5FeS_4; Cassiterite, SnO_2; Chromite, $MgCr_2O_4$; Cinnabar, HgS; Copper, Cu; Ferrotantalite, $FeTa_2O_6$; Galena, PbS; Gold, Au; Hematite, Fe_2O_3; Ilmenite, $FeTiO_3$; Molybdenite, MoS_2; Scheelite, $CaWO_4$, Sphalerite, ZnS; Uraninite, UO_2; Wolframite, $FeWO_4$.

**Data source:* U.S. Geological Survey, *Mineral Commodity Summaries,* January 2005. Butterman, W. C., and E. B. Amey, III. 2005. *Mineral commodity profiles—gold.* U.S. Geological Survey, Open-File Report 02-303.

Kesler, S. E., 1996. *Mineral resources, economics, and the environment.* MacMillan, New York.

The sulfides can be divided into small groups of similar structures but it is difficult to make broad generalizations about their structure. Regular octahedral or tetrahedral coordination about sulfur is found in many simple sulfides such as in galena, PbS, (with an NaCl-type structure), and in sphalerite, ZnS (see Fig. 15.5a). In more complex sulfides, as well as sulfosalts, distorted coordination polyhedra may be found (see tetrahedrite, Fig. 15.5c). Many of the sulfides have ionic and covalent bonding, whereas others, displaying most of the properties of metals, have metallic bonding characteristics. The structures and some aspects of the crystal chemistry of a few of the most common sulfides (e.g., sphalerite, chalcopyrite, pyrite, marcasite, and covellite) are discussed.

ZnS occurs in two polymorphic forms: the sphalerite-type (Fig. 15.5a) and the wurtzite-type structures (Fig. 15.6). In both the sphalerite and wurtzite structures Zn is surrounded by four sulfurs in tetrahedral coordination, but in sphalerite, the Zn atoms are arranged in a face-centered cubic lattice, whereas in wurtzite they are approximately in positions of hexagonal closest packing. The atomic arrangement in sphalerite is like that in diamond (see Fig. 15.4a) in which the carbon has been replaced by equal amounts of Zn and S. Greenockite, CdS, a relatively rare sulfide, is isostructural with ZnS and occurs in both the sphalerite and wurtzite type structures. Natural sphalerite shows extensive Fe^{2+} and very limited Cd^{2+} substitution for Zn (see Table 5.4).

FIG. 15.5 The sphalerite structure and derivatives. (a) Sphalerite, ZnS. Compare this illustration with Fig. 4.19a. (b) Chalcopyrite, $CuFeS_2$. (c) Tetrahedrite, $Cu_{12}Sb_4S_{13}$. (After Wuensch, B.J. 1974. *Sulfide mineralogy, Reviews in Mineralogy* 1, Mineralogical Society of America, Washington, D.C.)

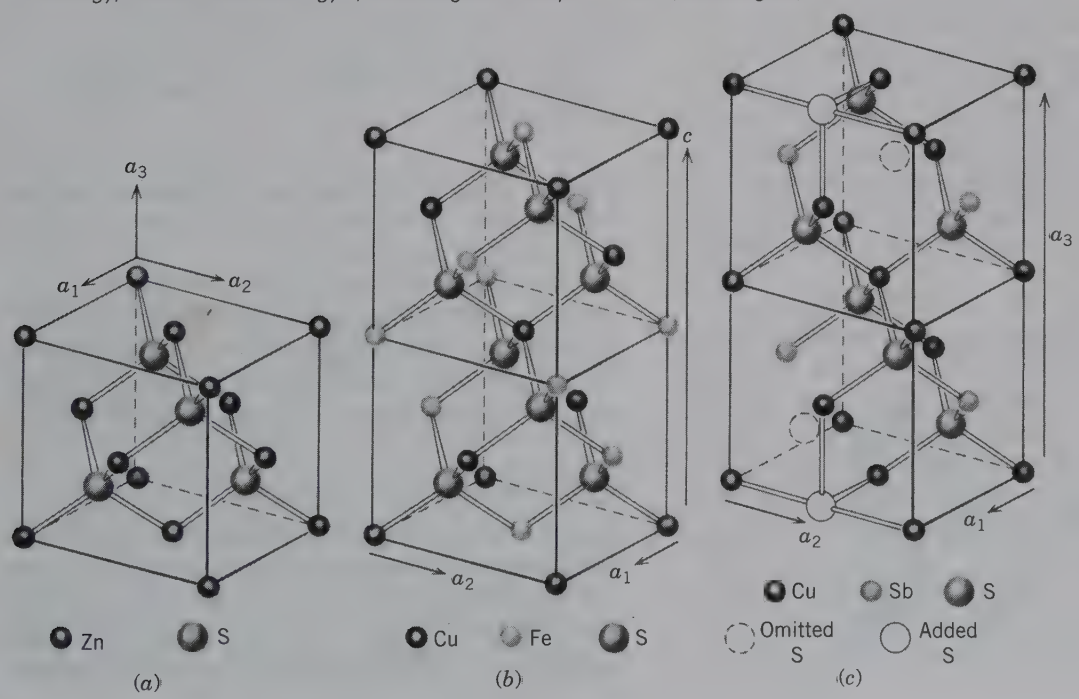

Sulfides, Sulfarsenides, and Arsenides			
Acanthite (Argentite)	Ag_2S	Cinnabar	HgS
Chalcocite	Cu_2S	Realgar	AsS
Bornite	Cu_5FeS_4	Orpiment	As_2S_3
Galena	PbS	Stibnite	Sb_2S_3
Sphalerite	ZnS	Pyrite	FeS_2
Chalcopyrite	$CuFeS_2$	Marcasite	FeS_2
Pyrrhotite	$Fe_{1-x}S$	Molybdenite	MoS_2
Nickeline	NiAs	Cobaltite	CoAsS
Millerite	NiS	Arsenopyrite	FeAsS
Pentlandite	$(Fe, Ni)_9S_8$	Skutterudite	$CoAs_3$
Covellite	CuS		

Chalcopyrite, $CuFeS_2$, has a structure (Fig. 15.5b) that can be derived from the sphalerite structure by regularly substituting Cu and Fe ions for Zn in sphalerite; this leads to a doubling of the unit cell. Stannite, Cu_2FeSnS_4, has a structure based on sphalerite in which layers of ordered Fe and Sn alternate with layers of Cu (chalcopyrite can be rewritten as $Cu_2Fe_2S_4$; this illustrates chemically the close similarity to Cu_2FeSnS_4).

Covellite, CuS, is an example of a chemically simple substance with a rather complex structure (see Fig. 15.7) in which part of the Cu is tetrahedrally coordinated by four S, and part coordinated by three S in the form of a triangle. The structure can, therefore, be viewed as made of sheets of CuS_3 triangles, between double layers of CuS_4 tetrahedra; covalent sulfur-sulfur bonds link the layers.

Pyrite, FeS_2, has a cubic structure as shown in Fig. 15.8a. The structure contains covalently bonded S_2 pairs, which occupy the position of Cl in the NaCl structure type. The pyrite structure may be considered as derived from the NaCl structure in which Fe is found in the Na positions of NaCl (Fig. 4.17). Another polymorphic form of FeS_2 is marcasite (Fig. 15.8b) with an orthorhombic structure. This structure, as pyrite, contains closely spaced S_2 pairs. The stability fields of the two polymorphs, pyrite and marcasite, remain unclear. From geological occurrences one would conclude that marcasite occurs over a range of low to medium temperature in sedimentary rocks and metalliferous veins. Pyrite, however, occurs also as a magmatic (high T) constituent.

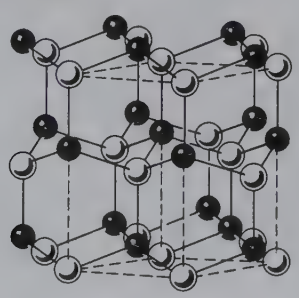

FIG. 15.6 The wurtzite type polymorph of ZnS. See Fig. 15.5a for the sphalerite polymorph.

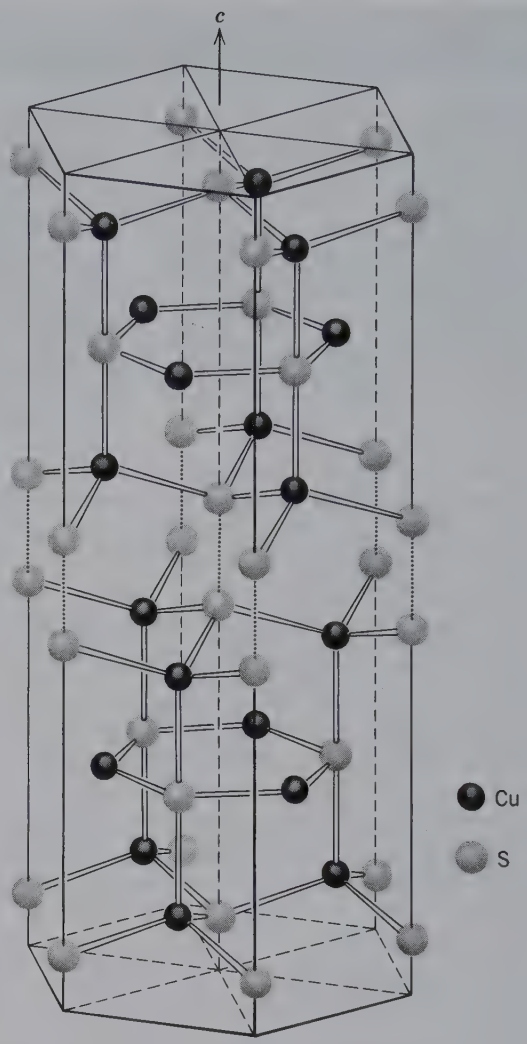

FIG. 15.7 Structure of covellite, CuS. The dotted lines indicate covalent S-S bonds. (After Wuensch, B. J., 1974. *Sulfide Mineralogy, Reviews in Mineralogy* 1, Mineralogical Society of America, Washington, D.C.)

The structure of arsenopyrite, FeAsS, can be derived from the marcasite (FeS_2 or FeSS) structure (see Fig. 15.8c) in which one S per unit formula is replaced by As. The general coordination of the atoms in marcasite and FeAsS is approximately the same in both structures.

SULFOSALTS

The term **sulfosalt** was originally proposed to indicate that a compound was a salt of one of a series of acids in which sulfur had replaced the oxygen of an ordinary acid. Because such acids are purely hypothetical, it is somewhat misleading to endeavor to explain this class

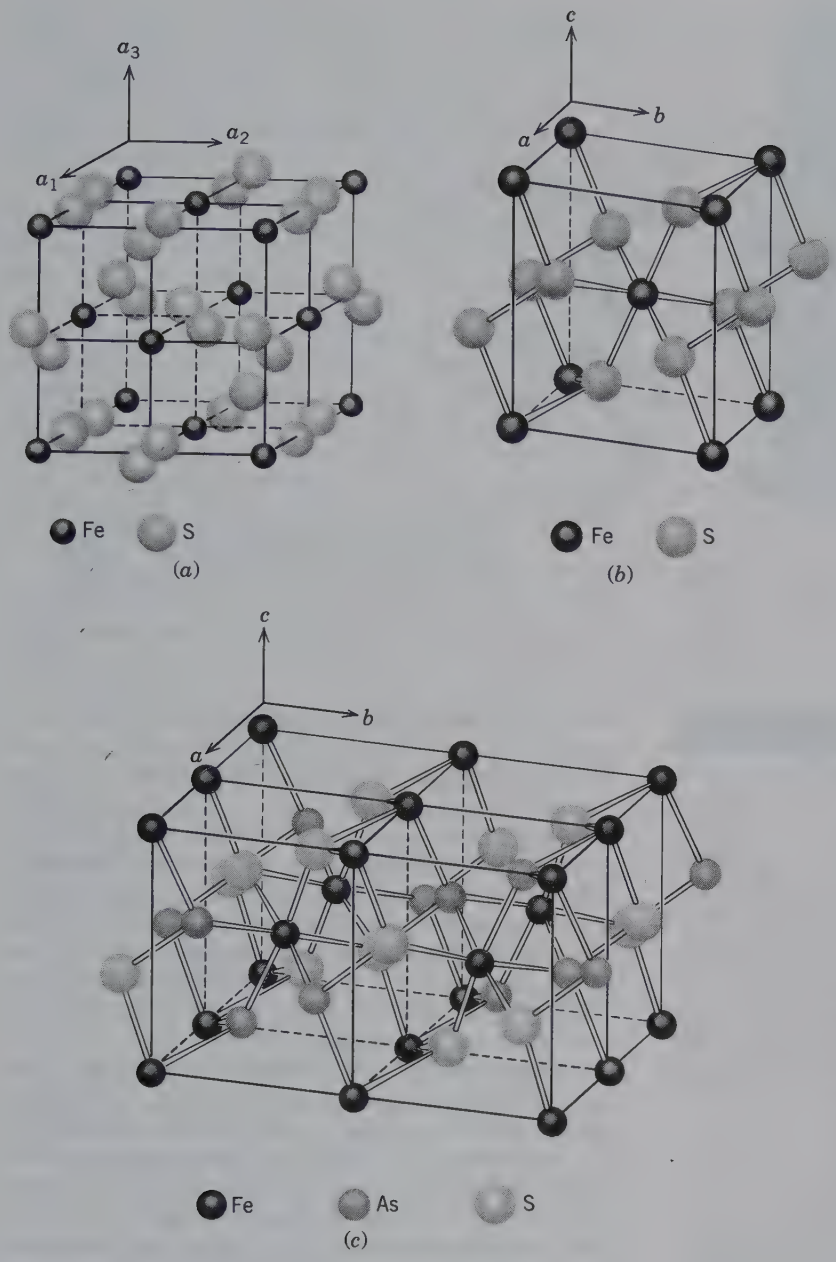

FIG. 15.8 (a) The structure of pyrite, as based on NaCl type structure (compare with Fig. 4.10a). Note the closely spaced sulfurs in S_2 groups. (b) The structure of marcasite, showing coordination of ions to closest neighbors. (c) The structure of arsenopyrite, FeAsS, a derivative of the marcasite structure type. (b and c after Wuensch, B.J. 1974. *Sulfide Mineralogy, Reviews in Mineralogy* 1, Mineralogical Society of America, Washington, D.C.)

of minerals in such a manner. Nevertheless, the term sulfosalt has been retained for indicating a certain type of unoxidized sulfur mineral that is structurally distinct from a sulfide.

The sulfosalts comprise a diverse and relatively large group of minerals with about 100 species. They differ from sulfides, sulfarsenides, and arsenides in that As, Sb, and rarely Bi play a role more or less like that of metals in the structure; in sulfarsenides and arsenides the semimetals take the place of sulfur in the structure. For example, in arsenopyrite, FeAsS (Fig. 15.8c), the As is substituted for S in a marcasite type of structure. In enargite, Cu_3AsS_4, on the other hand, As enters the metal position of the wurtzite type of structure and is coordinated to four neighboring S ions (see Fig. 15.9). Sulfosalts may be considered double sulfides. As such, enargite, Cu_3AsS_4, may be considered $3Cu_2S{\cdot}As_2S_5$.

The sulfosalts usually occur as minor minerals in hydrothermal veins associated with the more common sulfides. With only rare exceptions, they are compounds containing silver, copper, or lead but only a very few are abundant enough to have served as ores of these metals. Mention is made next of only five of the more important sulfosalts.

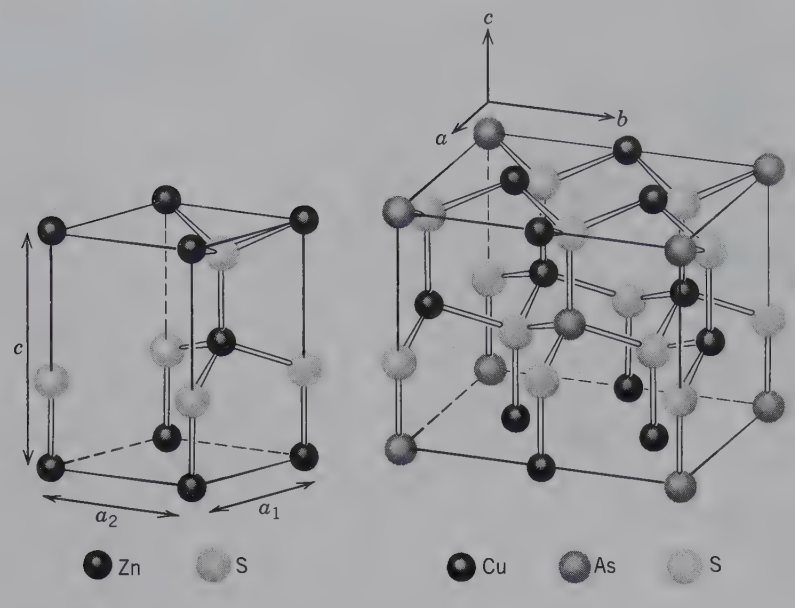

FIG. 15.9 (a) Wurtzite structure type of ZnS. (b) Enargite, Cu_3AsS_4, an orthorhombic derivative of the wurtzite structure. (After Wuensch, B. J. 1974. *Sulfide Mineralogy, Reviews in Mineralogy* 1, Mineralogical Society of America, Washington, D.C.)

SYSTEMATIC DESCRIPTIONS

NATIVE METALS

GOLD—Au

Crystallography. Isometric; $4/m\bar{3}2/m$. Crystals are commonly octahedral (Fig. 15.10a, see also Box 15.1), rarely showing the faces of the dodecahedron, cube, and trapezohedron {113}. Often in arborescent crystal groups with crystals elongated in the direction of a three-fold symmetry axis, or flattened parallel to an octahedron face. Crystals are irregularly formed, passing into filiform, reticulated, and dendritic shapes (Fig. 15.10b). Seldom shows crystal forms; usually in irregular plates, scales, or masses.

$Fm3m$; $a = 4.079$ Å; $Z = 4$. *ds*: 2.36(10), 2.04(7), 1.443(6), 1.229(8), 0.785(5).

Physical Properties. **H** $2\frac{1}{2}$–3, **G** 19.3 when pure. The presence of other metals decreases the specific gravity, which may be as low as 15. *Fracture* is hackly. Very malleable and ductile. Opaque. *Color* is various shades of yellow, depending on the purity becoming paler with increase of silver (see Plate I, no. 1).

FIG. 15.10 (a) Distorted gold octahedron. (b) Dendritic gold.

Composition and Structure. A complete solid solution series exists between Au and Ag, and most gold contains some Ag. California gold carries 10% to 15% Ag. When Ag is present in amounts of 20% or greater, the alloy is known as *electrum*. Small amounts of Cu and Fe may be present, as well as traces of Bi, Pb, Sn, Zn, and the platinum metals. The purity or *fineness* of gold is expressed in parts per 1,000. Most gold contains about 10% of other metals and has a fineness of 900. The structure of gold is based on cubic closest packing of Au atoms (see Fig. 15.1a).

Diagnostic Features. Gold is distinguished from the yellow sulfides pyrite and chalcopyrite and from yellow flakes of altered micas by its sectility and its high specific gravity.

Occurrence. Gold has an average abundance of 0.004 ppm in the Earth's crust, and is, therefore, a rare element. It occurs in nature, widely distributed in small amounts. It is found most commonly in veins that have a genetic relation to silicic types of igneous rocks. Most gold occurs as the native metal. For a listing of some other, rare gold minerals, see "Similar Species."

The chief sources of gold are hydrothermal gold-quartz veins where, together with pyrite and other sulfides, gold was deposited from ascending mineral-bearing solutions. Gold is also recovered as a byproduct from sulfide deposits mined essentially for the base metals. The gold is merely mechanically mixed with the sulfides and is not in chemical substitution. In most of the veins, gold is so finely disseminated and uniformly distributed that its presence in the ore can only be detected by microscopic techniques.

When gold-bearing veins are weathered, the gold liberated either remains in the soil mantle as an eluvial deposit, or is washed into the neighboring streams to form a placer deposit. Because of its high specific gravity, gold works its way

through the lighter sands and gravels to lodge behind irregularities or to be caught in crevices in the bedrock. The rounded or flattened nuggets of placer gold can be removed by panning, a process of washing away all but the heavy concentrate from which the gold can be easily separated. On a larger scale, gold-bearing sand is washed through sluices where the gold collects behind crossbars or riffles and amalgamates with mercury placed behind the riffles. Most placer mining is today carried on with dredges, some of which are gigantic and can extract the gold from thousands of cubic yards or gravel a day.

Of the estimated world production of gold in 2004 about 14% came from the Republic of South Africa. The principal sources of South African gold are the Precambrian Witwatersrand conglomerate "the Rand," in the Transvaal and similar conglomerates in the Orange Free State. The "reefs" in these conglomerates in which the gold is concentrated are thought to be fossil placers. Other major gold producers are the United States, Australia, Russia, and Canada.

The most important gold-producing states in the United States, in decreasing importance are Alaska, Nevada, Utah, Arizona, and Montana. The gold from Utah and Arizona is essentially a byproduct of copper mining. For 100 years following the discovery of gold in the streams of California in 1848, that state was the leading producer. The most important gold-producing districts were those of the Mother Lode, gold-quartz veins along the western slope of the Sierra Nevada.

Use. Most of the existing gold is owned by various countries as bullion and is used for international settlements. An increasing amount in the form of medallions and small bars is used for investment purposes. Other uses are in jewelry, scientific instruments, electroplating, gold leaf, and dental appliances (see Box 15.1).

Similar Species. In addition to native gold there are 19 relatively rare to extremely uncommon minerals in which gold combines with other elements. The majority of these are tellurides. The most prominent examples are: *calaverite*, $AuTe_2$, associated with other tellurides at Cripple Creek, Colorado, and at Kalgoorlie, Western Australia; and *sylvanite*, $(Au,Ag)Te_2$, also found at Cripple Creek, Colorado, and at Kalgoorlie, Western Australia. Others are *krennerite*, $(Au,Ag)Te_2$; *petzite*, Ag_3AuTe_2; *kostovite*, $CuAuTe_4$; *montbrayite*, $(Au,Sb)_2Te_3$; and *muthmannite*, (Ag,Au)Te. Other compounds are: *uytenbogaardtite*, Ag_3AuS_3; *fischesserite*, Ag_3AuSe_2; and *nagyagite*, $Pb_5Au(Te,Sb)_4S_{5\text{-}8}$. For a complete listing of gold-containing minerals see Wilson (1982) or refer to an on-line database. References are given at the end of the Chapter.

SILVER—Ag

Crystallography. Isometric; $4/m\bar{3}2/m$. Crystals are commonly malformed and in branching, arborescent, or reticulated groups. Found usually in irregular masses, plates, and scales; in places as coarse or fine wire (Fig. 15.11).

Fm3m; $a = 4.09$ Å, $Z = 4$. *ds*: 2.34(10), 1.439(6), 1.228(8), 0.936(7), 0.934(8).

Physical Properties. **H** $2\frac{1}{2}$–3. **G** 10.5 when pure, 10 to 12 when impure. *Fracture* is hackly. Malleable and ductile.

FIG. 15.11 Silver, Kongsberg, Norway

Luster metallic. *Color* and *streak* are silver-white, often tarnished to brown or gray-black (see Plate I, no. 2).

Composition and Structure. Native silver commonly contains alloyed Au, Hg, and Cu, more rarely traces of Pt, Sb, and Bi. *Amalgam* is a solid solution of Ag and Hg. The structure of silver is based on cubic closest packing of Ag atoms (see Fig. 15.1a).

Diagnostic Features. Silver can be distinguished by its malleability, color on a fresh surface, and high specific gravity.

Occurrence. Native silver is widely distributed in small amounts in the oxidized zone of ore deposits. However, native silver in larger deposits is the result of deposition from primary hydrothermal solutions. There are three types of primary deposits: (1) Associated with sulfides, zeolites, calcite, barite, fluorite, and quartz as typified by the occurrence in Kongsberg, Norway. Mines at this locality were worked for several hundred years and produced magnificent specimens of wire silver (Fig. 15.11). (2) With arsenides and sulfides of cobalt, nickel, and silver and with native bismuth. Such was the type at the old silver mines at Freiberg and Schneeberg in Saxony, Germany, and at Cobalt, Ontario. (3) With uraninite and cobalt-nickel minerals. Deposits at Jáchymov (Joachimsthal), Czech Republic, and at Great Bear Lake, Northwest Territories, Canada, are of this type.

In the United States, small amounts of primary native silver are associated with native copper on the Keweenaw Peninsula, Michigan. This has been the best U.S. source of crystallized silver. Elsewhere in the United States native silver is largely secondary. Most of the world's supply comes from silver sulfides and sulfosalts. Large producers of silver are Peru, China, Mexico, Australia, and the United States, with Mexico a very important producer historically.

Use. An ore of silver, although most of the world's supply comes from other minerals such as *acanthite*, Ag_2S, *proustite*, Ag_3AsS_3 and *pyrargyite*, Ag_3SbS_3. Silver has many uses, chief of which are in photographic film emulsions, plating, brazing alloys, tableware, electronic equipment and in

rear-window defrosters in cars. Because of declining production and increased price, silver in coinage has been largely replaced by other metals, such as nickel and copper.

COPPER—Cu

Crystallography. Isometric; $4/m\bar{3}2/m$. Tetrahexahedron faces are common, as well as the cube, dodecahedron, and octahedron. Crystals are usually malformed and in branching and arborescent groups (Figs. 15.12a and b). Usually occurs in irregular masses, plates, and scales, and in twisted and wire-like forms.

Fm3m; $a = 3.615$ Å; $Z = 4$. *ds*: 2.09(10), 1.81(10), 1.28(10), 1.09(10), 1.05(8).

Physical Properties. **H** $2\frac{1}{2}$–3. **G** 8.9. Highly ductile and malleable. *Fracture* hackly. *Luster* metallic. *Color* copper-red on fresh surface, usually dark with dull luster because of tarnish (see Plate I, no. 3).

Composition and Structure. Native copper often contains small amounts of Ag, Bi, Hg, As, and Sb. The structure of copper is based on cubic closest packing of Cu atoms (see Fig. 15.1a).

Diagnostic Features. Native copper can be recognized by its red color on fresh surfaces, hackly fracture, high specific gravity, and malleability.

Occurrence. Small amounts of native copper have been found at many localities in the oxidized zones of copper deposits associated with cuprite, malachite, and azurite.

Most primary deposits of native copper are associated with basaltic lavas, where deposition of copper resulted from the reaction of hydrothermal solutions with iron oxide minerals. The only major deposit of this type is on the Keneenaw Peninsula, Michigan, on the southern shore of Lake Superior. The rocks of the area are composed of Precambrian basic lava flows interbedded with conglomerates. The series, exposed for 100 miles along the length of the peninsula, dips to the northwest beneath Lake Superior to emerge on Isle Royale 50 miles away. Some copper is found in veins cutting these rocks, but it occurs principally either in the lava flows filling cavities or in the conglomerates filling interstices or replacing pebbles. Associated minerals are prehnite, datolite, epidote, calcite, and zeolites. Small amounts of native silver are present. Michigan copper had long been used by the American Indians, but it was not until 1840 that its source was located. Exploitation began shortly thereafter, and during the next 75 years, there was active mining through the length of the Keweenaw Peninsula. Most of the copper in the district was in small irregular grains, but notable large masses were found; one found in 1857 weighed 520 tons.

Sporadic occurrences of copper similar to the Lake Superior district have been found in the sandstone areas of the eastern United States, notably in New Jersey, and in the glacial drift overlying a similar area in Connecticut. In Bolivia at Corocoro, southwest of La Paz, there is a noted occurrence in sandstone. There are also superb specimens of native copper pseudomorphs after aragonite from Corocoro. Native copper, sometimes as fine crystal groups, occurs in small amounts associated with the oxidized copper ores of Ajo, Bisbee, and Ray, Arizona, and the Chino Mine, Santa Rita, New Mexico.

Use. A minor ore of copper; copper sulfides are today the principal ores of the metal. The greatest use of copper is for electrical purposes, mostly as wire. It is also extensively used in alloys, such as brass (copper and zinc), bronze (copper and tin with some zinc), and German silver (copper, zinc, and nickel). These and many other minor uses make copper second only to iron as a metal essential to modern civilization.

PLATINUM—Pt

Crystallography. Isometric; $4/m\bar{3}2/m$. Cubic crystals are rare and commonly malformed. Usually found in small grains and scales. In some places it occurs in irregular masses and nuggets of larger size.

Fm3m; $a = 3.923$ Å; $Z = 4$. *ds*: 2.27(9), 1.956(8), 1.384(8), 1.180(10).

Physical Properties. **H** 4–$4\frac{1}{2}$ (unusually high for a metal). **G** 21.45 when pure, 14 to 19 when native. Malleable

(*a*) (*b*)

FIG. 15.12 (a) Dendritic copper, Broken Hill, New South Wales, Australia. (b) Native copper, Keweenaw Peninsula, Michigan. (Harvard Mineralogical Museum.)

and ductile. *Color* steel-gray, with bright luster. Magnetic when rich in iron.

Composition and Structure. Platinum is usually alloyed with several percent Fe and with smaller amounts of Ir, Os, Rh, Pd; also Cu, Au, Ni. The structure of platinum is based on cubic closest packing of atoms (see Fig. 15.1a).

Diagnostic Features. Determined by its high specific gravity, malleability, and steel-gray color.

Occurrence. Most platinum occurs as the native metal in ultrabasic rocks, especially dunites, associated with olivine, chromite, pyroxene, and magnetite. It has been mined extensively in placers, which are usually close to the platinum-bearing igneous parent rock.

Platinum was first discovered in Colombia, South America. It was taken to Europe in 1735, where it received the name *platina* from the word *plata* (Spanish for silver) because of its resemblance to silver. A small amount of platinum is still produced in Colombia from placers in two districts near the Pacific Coast. In 1822, platinum was discovered in placers on the Upper Tura River on the eastern slope of the Ural Mountains in a large district surrounding Nizhniy Tagil, Russia. From that time until 1934, most of the world's supply of platinum came from placers of that district, which centered around the town of Nizhniy Tagil. In 1934, because of the large amount of platinum recovered from the copper-nickel ore of Sudbury, Ontario, Canada, that area became the leading producer. In 1954, the Republic of South Africa moved into first place. Part of the South African production is a byproduct from gold mining on the Rand, but the primary source is the Merensky Reef in the ultrabasic rocks of the Bushveld igneous complex. The Merensky Reef is a horizon of this layered intrusive about 12 inches thick and extending for many miles with a uniform platinum content of about one-half ounce per ton of ore. The chief mining operations are near Rustenburg in the Transvaal. It is estimated that today about half of the world's platinum-group metals comes from Russia. In the United States, small amounts are produced as a byproduct of copper mining. In Canada, most of the platinum comes from *sperrylite*, $PtAs_2$, which occurs in the copper–nickel ore in Sudbury, Ontario.

Use. Many of the uses of platinum depend on its high melting point (1755°C), resistance to chemical attack, and superior hardness. But its major use is as catalysts to control automobile exhaust emissions and in the chemical and petroleum industries. It is also used in dentistry, surgical instruments, jewelry, and electrical equipment.

Similar Species. *Iridium*; *iridosmine*, an alloy of iridium and osmium; and *palladium* are rare minerals of the platinum group associated with platinum.

Iron—Fe

Crystallography. Isometric; $4/m\bar{3}2/m$. Crystals are rare. Terrestrial: in blebs and large masses; meteoritic (*kamacite*): in plates and lamellar masses, and in regular intergrowth with nickel-iron (*taenite*).

Ordinary iron (α-Fe and kamacite) body-centered cubic, $Im3m$, a = 2.86 Å; Z = 2. *ds*: 2.02(9), 1.168(10), 1.430(7), 1.012(7). Nickel-iron (taenite), face-centered cubic, $Fm3m$, a = 3.56 Å, Z = 4. *ds*: 2.06(10), 1.073(4), 1.78(3), 1.27(2).

Physical Properties. (α-Fe). *Cleavage* {001} poor. **H** $4\frac{1}{2}$. **G** 7.3–7.9. *Fracture* hackly. Malleable. Opaque. *Luster* metallic. *Color* steel-gray to black. Strongly magnetic.

Composition and Structure. α-Fe always contains some Ni and frequently small amounts of Co, Cu, Mn, S, C. *Kamacite* contains approximately 5.5 weight percent Ni. *Taenite* is highly variable in Ni content and ranges from about 27 to 65 weight percent Ni. The structures of α-Fe and kamacite are based on body-centered cubic packing of atoms (see Fig. 15.1c), whereas the structure of taenite is based on face-centered cubic packing (see Fig. 15.1a).

Diagnostic Features. Iron can be recognized by its strong magnetism, its malleability, and the oxide coating usually on its surface.

Occurrence. Occurs sparingly as terrestrial iron but commonly in meteorites. Iron in the elemental (native) state is highly unstable in the oxidizing conditions in rocks of the upper crust and in the Earth's atmosphere. Iron is normally present as Fe^{2+} or Fe^{3+} in oxides such as magnetite, Fe_3O_4, or hematite, Fe_2O_3, or as the hydroxide, goethite, FeO·OH. Terrestrial iron is regarded as a primary magmatic constituent or a secondary product formed by the reduction of iron compounds by assimilated carbonaceous material. The most important locality is Disko Island, Greenland, where fragments ranging from small grains to masses of many tons are included in basalts. Masses of nickel-iron have been found in Josephine and Jackson counties, Oregon.

Iron meteorites are composed largely of a regular intergrowth of *kamacite* and *taenite*. Evidence of the intergrowth, the Widmanstätten pattern (Fig. 1.2), is seen on polished and etched surfaces of such meteorites. Stony-iron meteorites consist of mixtures of silicates, kamacite, taenite, and troilite (FeS) (Fig. 5.6).

NATIVE NONMETALS

SULFUR—S

Crystallography. Orthorhombic; $2/m2/m2/m$. Pyramidal habit common (Fig. 15.13a), often with two dipyramids, prism {011}, and base in combination (Figs. 15.13b and 15.14). Commonly found in irregular masses imperfectly crystallized. Also massive, reniform, stalactitic, as incrustations, earthy.

$Fddd$; a = 10.47, b = 12.87, c = 24.49 Å; Z = 128. *ds*: 7.76(4), 5.75(5), 3.90(10), 3.48(4), 3.24(6).

FIG. 15.13 Sulfur crystals.

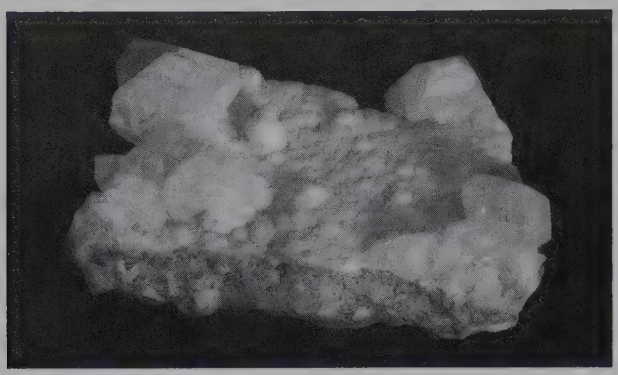

FIG. 15.14. Sulfur crystals on a background of fine-grained, white aragonite, Cinciana, Sicily, Italy (Harvard Mineralogical Museum).

Physical Properties. *Fracture* conchoidal to uneven. Brittle. **H** $1\frac{1}{2}$–$2\frac{1}{2}$. **G** 2.05–2.09. *Luster* resinous. *Color* sulfur-yellow, varying with impurities to yellow shades of green, gray, and red. Transparent to translucent (see Plate I, no. 4). *Optics*: (+); $\alpha = 1.957$, $\beta = 2.037$, $\gamma = 2.245$, $2V = 69°$.

Sulfur is a poor conductor of heat. When a crystal is held in the hand close to the ear, it will be heard to crack. This is due to the expansion of the surface layers because of the heat from the hand, while the interior, because of the slow heat conductivity, is unaffected. Crystals of sulfur should, therefore, be handled with care.

Composition and Structure. Native sulfur may contain small amounts of selenium in substitution for S. The structure of the orthorhombic polymorph is given in Fig. 15.3. This structure consists of covalently bonded S_8 groups in the shape of puckered rings. These discrete and compact S_8 rings are relatively loosely bound to each other by van der Waals bonds. The unit cell of sulfur contains 128 atoms of sulfur distributed among 16 S_8 rings. Sulfur melts at 119°C to a liquid in which the covalently bonded S_8 rings retain their identity up to 160°C. The monoclinic polymorphs (α and β sulfur) are very rare in nature.

Diagnostic Features. Sulfur can be identified by its yellow color and the ease with which it burns; it ignites in a candle flame. The absence of a good cleavage distinguishes it from orpiment.

Occurrence. Sulfur often occurs at or near the crater rims of active or extinct volcanoes, where it has been derived from the gases given off in fumaroles. These may furnish sulfur as a direct sublimation product or by the incomplete oxidation of hydrogen sulfide gas. It is also formed from sulfates, by the action of sulfur-forming bacteria. Sulfur may be found in veins associated with metallic sulfides and formed by the oxidation of the sulfides. It is most commonly found in Tertiary sedimentary rocks associated with anhydrite, gypsum, and limestone; often in clay rocks; frequently with bituminous deposits. The large deposits near Girgenti, Sicily, are world famous for the fine crystals associated with celestite, gypsum, calcite, aragonite. Sulfur is also found associated with the volcanoes of Mexico, Hawaii, Japan, Argentina, and at Ollague, Chile, where it is mined at an elevation of 19,000 feet.

In the United States, the most productive deposits are in Texas and Louisiana, where sulfur is associated with anhydrite, gypsum, and calcite in the cap rock of salt domes. There are 10 to 12 producing localities, but the largest are Boling Dome in Texas and Grand Ecaille, Plaquemines Parish, Louisiana. Sulfur is also recovered from salt domes in Mexico and offshore in the waters of the Gulf of Mexico. Sulfur is obtained from these deposits by the Frasch method. Superheated water is pumped down to the sulfur horizon, where it melts the sulfur; compressed air then forces the sulfur to the surface.

About half of the world's sulfur is produced as the native element; the remainder is recovered as a byproduct in smelting sulfide ores, from sour natural gas, and from pyrite.

Use. Sulfur is used primarily for the manufacture of sulfur compounds, such as sulfuric acid (H_2SO_4) and hydrogen sulfide (H_2S). Large quantities of elemental sulfur are used in insecticides, synthetic fertilizers, and the vulcanization of rubber. Sulfur compounds are used in the manufacture of soaps, textiles, leather, paper, paints, dyes, and in the refining of petroleum.

DIAMOND—C

Crystallography. Isometric; $4/m\bar{3}2/m$. Crystals usually octahedral but may be cubic or dodecahedral. Curved faces, especially of the octahedron (see Fig. 15.15) and hexoctahedron are frequently observed (Figs. 15.16a and b; see Plate I, no. 5 and also Plate IX, no. 1, in Chapter 20). Crystals may be flattened on {111}. Twins on {111} (spinel law) are common, usually flattened parallel to the twin plane (Fig. 15.16c). *Bort*, a variety of diamond, has rounded forms and rough exterior resulting from a radial or cryptocrystalline aggregate. The term is also applied to badly colored or flawed diamonds without gem value.

$Fd\bar{3}m$; $a = 3.567$ Å; $Z = 8$. *ds*: 2.06(10) 1.26(8), 1.072(7), 0.813(6), 0.721(9).

Physical Properties. *Cleavage* {111} perfect. **H** 10 (hardest known mineral). **G** 3.52. *Luster* adamantine; uncut crystals have a characteristic greasy appearance. The very high refractive index, 2.42, and the strong dispersion of light account for the brilliancy and "fire" of the cut diamond. *Color* usually pale yellow or colorless; also shades of pale pink to red, orange, green, blue, and brown. Deeper shades are rare. *Carbonado* or *carbon* is black or grayish-black bort. It is noncleavable, opaque, and less brittle than crystals.

Composition and Structure. The composition is pure carbon. The structure of diamond is illustrated in Figs. 15.4a and A4.3. (Many aspects of the diamond structure are illustrated with animations on the CD-ROM, module III, under the heading "Three-dimensional Order; Space Group Elements in Structures.") Figure 15.4a shows that each carbon is surrounded by four neighboring carbon atoms in tetrahedral coordination. This is the result of covalent bonding in which four valence electrons in each carbon fill the bonding orbitals of the four neighboring carbon atoms by electron sharing. Every carbon atom is linked in this way to

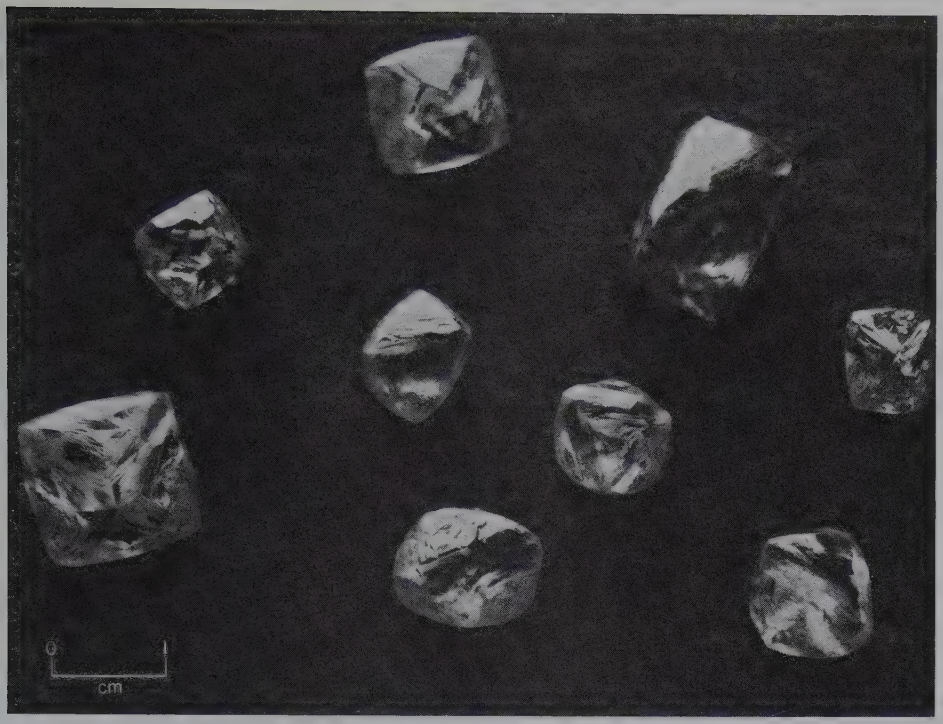

FIG. 15.15 Diamond crystals all showing a pronounced octahedral habit. (Courtesy of the Diamond Information Center, New York)

four others, forming a continuous network. Refer to Appendix 4 Fig. A4.3c to see the face-centered arrangement of the carbon atoms in a cubic unit cell. Figure A4.3d shows the location of some of the symmetry elements in the unit cell of diamond. Figure A4.3e illustrates the many complexities of the diamond space group, $F4_1/d\bar{3}2/m$ (which is abbreviated to $Fd3m$).

Diamond, as is to be expected from its high specific gravity and fairly close packing, is the high-pressure polymorph (see Box 15.2). At low pressures or temperatures it is unstable with respect to graphite and may be converted to graphite at moderate temperatures. The reason that diamond and graphite can coexist at room temperatures and pressures is because the reconstructive polymorphic reaction between the two minerals is very sluggish. In order to permit the change from graphite to diamond, extremely high temperature, that is, high activation energy, is needed to cause the carbon atoms in the graphite structure to break loose by thermal agitation, and to make them available for building the diamond structure. Such temperatures also increase the pressure required to bring about the polymorphic reaction (see Box 15.2).

Diagnostic Features. Diamond is distinguished from minerals that it resembles by its great hardness, adamantine luster, and cleavage.

Occurrence. Diamonds have been discovered on every continent but in only a few localities in notable amounts. Most commonly, diamond is found in alluvial deposits, where it accumulates because of its inert chemical nature, its great hardness, and its fairly high specific gravity. In several countries in Africa and North America, and in China, Venezuela, Australia, India, and Siberia, diamonds have been found *in situ*. The rock in which they occur is called *kimberlite*, after the type locality of Kimberley, South Africa. Kimberlites are a group of volatile-rich (mainly CO_2), potassic ultrabasic rocks with a range of megacryst compositions set in a fine-grained groundmass (a megacryst is a megascopically visible crystal that stands out from the finer groundmass, but

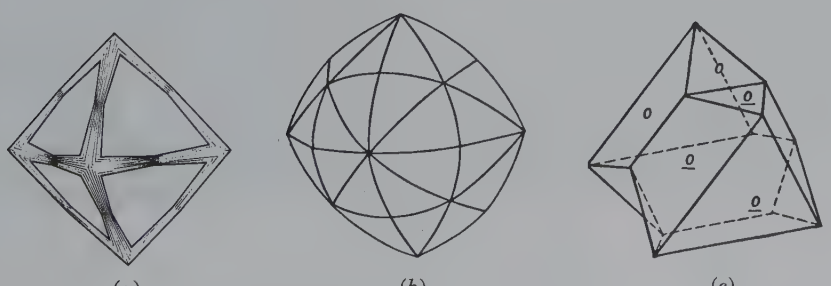

FIG. 15.16 Diamond crystals.

BOX 15.2 DIAMOND SYNTHESIS

The synthesis of diamond is based on the stability fields of the various carbon polymorphs as shown in the accompanying pressure-temperature phase diagram for carbon (based on experimental data from various sources). There are three major problems associated with the synthesis of diamond. First, in order to achieve the dense, strongly bonded structure of diamond (it is the hardest material known to man), extremely high pressure must be achieved in the laboratory. Second, even when such high pressure is achieved, a very high temperature is necessary to permit the carbon atoms to diffuse for the conversion from other forms of carbon to diamond (the *P-T* region used for diamond growth is shaded in the diagram with a white edge). Third, most of the synthetic diamonds produced are in small grains and growth of large single crystals suitable for gemstones presents yet further problems.

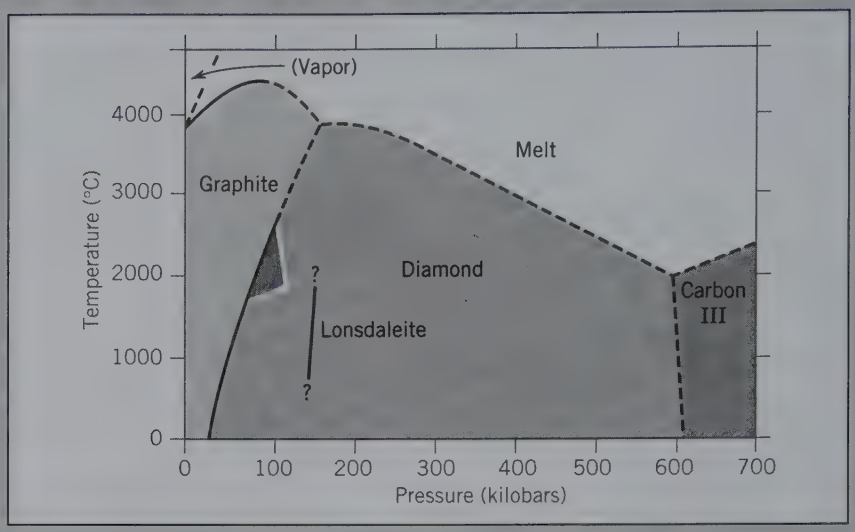

The first synthetic diamonds were made in 1953 by Dr. Erik Lundblad in the research laboratories of ASEA in Sweden. These resulted from experimental conditions of about 2700°C at about 76 kilobars using an apparatus that simultaneously exerted very high pressures and withstood extremely high temperatures. The ASEA technique was not patented at that time because the synthesis mechanism was not yet fully understood. In 1955, General Electric began the synthetic manufacture of small diamonds. World production of synthetic diamonds is now on the order of 559 million carats (one carat = 200 milligrams; a unit weight in gemstones), or about three and one-half times the production of diamond mined from the Earth. The synthetic material, which is identical to natural diamonds, offers the prospect of an assured and unlimited supply of diamonds. In recent years experimental techniques have produced diamond as large as 11.1 ct. of good quality; however, the synthetic process is still too costly to be competitive with high-quality larger diamonds of natural origin but stones that are in the 1- to 2-carat range are being sold for 10% to 30% less than comparable natural diamonds.

The success of diamond synthesis encouraged experimentation with boron nitride, BN, whose structure is similar to that of graphite. At very high pressures and temperatures (on the order of 85 kilobars and 2400°C) it transforms, similar to the graphite-diamond transition to cubic boron nitride (with the trade name of *Borazon*). This is extremely strong and hard, second only to diamond. It is manufactured in considerable quantities and is used mainly as an abrasive. This synthesis illustrates the application of crystal chemical concepts first evolved and tested in minerals.

After the initial synthesis of diamond, scientists at General Electric continued experimentation. In 1967, they produced a hexagonal transparent polymorph of carbon with specific gravity and refractive indices close to those of diamond. Almost simultaneously a hexagonal diamond was found in meteoritic material from the Cañon Diablo, Arizona, meteorite crater. The name *lonsdaleite* is given to this naturally occurring hexagonal polymorph of diamond. Lonsdaleite is also found closely intergrown with polycrystalline diamond, *carbonado* in *yakutiite,* named after its occurrence in alluvial deposits of northern Yakutia, Siberia. It is likely that yakutiite is the result of a meteorite impact.

Much recent research involves the synthesis of gem-quality diamond from chemical vapor deposition (CVD). Carbon is transformed into plasma and precipitated as microscopic diamonds onto substrates, such as glass and silicon. These thin films provide protective coatings (e.g., to windows in military aircraft) and are used in semiconductors. Because diamond is stable to high temperatures, research now centers on diamond computer chips.

whether it formed in the same kimberlite magma is uncertain). The megacryst assemblage may consist of ilmenite, pyrope garnet, olivine, clinopyroxene, phlogopite, enstatite, and chromite. The matrix mineralogy is complex and includes olivine, phlogopite, perovskite, spinel, and diopside. Although these intrusive bodies vary in size and shape, many are roughly circular with a pipelike shape and are referred to as "*kimberlite* " or "*diamond pipes*." In the deepest mines, (e.g., in Kimberley, South Africa), the diameter of the pipes decreased with depth and mining stopped at a depth of 3,500 feet, although the pipes continued. At the surface, the kimberlite is weathered to a soft yellow rock, "yellow ground," that in depth gives way to a harder "blue ground." The ratio of diamonds to barren rock varies from one pipe to another. In the Kimberley mine it was 1 : 8,000,000, but in some it may be as high as 1 : 30,000,000.

Diamonds were first found in India, which remained virtually their only source until they were discovered in Brazil in 1725. The early diamonds came from stream gravels in southern and central India, and it is estimated that 12 million carats were produced from this area (one carat weighs 0.2 g). Today the Indian production is only a few hundred carats a year.

Following their discovery in stream gravels in the state of Minas Gerais, Brazil, diamonds were also found in the states of Bahia, Goias, and Mato Grosso. Brazil's production today is chiefly from stream gravels. Extensive upland deposits of diamond-bearing gravels and clays are also worked. The black carbonado comes only from Bahia, Brazil.

In 1866 diamonds were discovered in the gravels of the Vaal River, South Africa, and in 1871 in the "yellow ground" of several pipes located near the present city of Kimberley. Although some diamonds are still recovered from gravels, the principal South African production is from kimberlite pipes. The deposits were originally worked as open pits, but as they deepened, underground methods were adopted. The world's largest and most productive diamond mine is the Premier, 24 miles east of Pretoria, South Africa. Since mining began there in 1903, nearly 30 million carats or six tons of diamonds have been produced. It was at the Premier Mine in 1905 that the world's largest diamond, the Cullinan, weighing 3,106 carats, was found. Prospecting for diamonds has located in South Africa over 700 kimberlite pipes, dikes, and sills, most of which are barren. As recently as 1966, the Finsch Mine, 80 miles west of Kimberley, came into production. Even more recently diamonds have been found in kimberlite in Botswana and in northern South Africa, close to the border with Zimbabwe. The most productive pipe of all was found in about 1979 in Western Australia, and is now known as the Argyle Mine. This pipe consists of *lamproite*. Lamproite is a rock name that describes highly potassic and somewhat aluminum-poor igneous rocks with the following range of minerals: phlogopite, K-rich soda tremolite (also known as richterite), leucite, sanidine, diopside, and a variety of rare K-rich, Ba-rich, Ti-rich, and Zr-rich oxides and silicates.

In Cape Province, South Africa, on the desert coast just south of the mouth of the Orange River, terrace deposits containing high-quality stones were discovered in 1927; previously, in 1908, diamonds were found near Luderitz on the coast of Namibia. Elsewhere in Africa diamonds, mostly alluvial, have been found in a dozen different countries. The principal producers are Democratic Republic of the Congo, Botswana, Angola, Ghana, Sierra Leone, the Central African Republic, and Tanzania. Botswana and the Congo are by far the largest African producers. Russia is also a major producer of diamonds from both pipes and placers. Important kimberlite localities in Russia are Mir kimberlite, Mirny, and Udachnaya kimberlite, Udachnaya, both in Yakutia; and Pomorskaya kimberlite, Arkhangelsk, Onega Peninsula, White Sea. Important alluvial deposits with diamonds in rivers and associated placers are found in the Urals and in Yakutia.

The world's main diamond producers, listed for 2004, with their natural rough diamond production recorded in millions of carats are

Russia	35.6
Botswana	31.1
Congo (Kinshasa)	28.0
Australia	20.8
South Africa	14.5
Canada	12.3

(Data from *U.S. Geological Survey Minerals Yearbook—2004*, Diamond Industrial, Table 5. Report by D. W. Olson).

For a discussion of diamond synthesis see Box 15.2.

After 30 years of searching for the source of diamonds found further south in North American glacial deposits, in 1991, diamonds were discovered in the Northwest Territories (the Barrens), Canada. The Ekati mine opened in 1998, and two more mines are now in operation producing high-quality diamonds, which accounts for an industry worth more than $2.0 billion.

Diamonds have been found sparingly in various parts of the United States. Small stones have occasionally been discovered in the stream sands along the eastern slope of the Appalachian Mountains in Virginia south to Georgia. Diamonds have also been reported from the gold sands of northern California and southern Oregon, and sporadic occurrences have been noted in the glacial drift in Wisconsin, Michigan, and Ohio. In 1906 diamonds were found in a lamproite pipe near Murfreesboro, Pike County, Arkansas. This locality, resembling the diamond pipes of South Africa, has yielded about 40,000 stones but is at present unproductive. In 1951 the old mine workings were opened to tourists who, for a fee, were permitted to look for diamonds. This area is now a state park.

Use. *In industry*, fragments of diamond crystals are used to cut glass. The fine powder is employed in grinding and polishing diamonds and other gemstones. Wheels are impregnated with diamond powder for cutting rocks and other hard materials. Steel bits are set with diamonds, especially the cryptocrystalline variety, *carbonado*, for diamond drilling in exploratory mining work. Diamond is also used in wire drawing and in tools for the truing of grinding wheels.

The diamond is also one of the most highly prized *gemstones*. Its value depends on its hardness, its brilliancy, which

results from its high index of refraction, and its "fire," resulting from its strong dispersion. In general, the most valuable are those flawless stones that are colorless or possess a "blue-white" color. A faint straw-yellow color, which diamond often shows, detracts from its value. Diamonds colored deep shades of yellow, red, green, or blue, known as *fancy* stones, are greatly prized and bring very high prices. Diamonds can be colored deep shades of green by irradiation with high-energy nuclear particles, neutrons, deuterons, and alpha particles, and blue by exposing them to fast-moving electrons. A stone colored green by irradiation can be made a deep yellow by proper heat treatment. These artificially colored stones are difficult to distinguish from those of natural color. See Chapter 20 for further discussion and illustrations of gem diamonds.

Name. The name diamond is a corruption of the Greek word *adamas*, meaning *invincible*. The luster term, *adamantine*, which describes the very high luster of minerals with a high index of refraction, such as of diamond and cerussite, is derived from *adamas*.

Similar Species. For a discussion of materials that are marketed as gem diamond imitations see Chapter 20 and specifically Table 20.2.

GRAPHITE—C

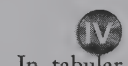

Crystallography. Hexagonal; $6/m2/m2m$. In tabular crystals of hexagonal outline with prominent basal plane. Distinct faces of other forms very rare. Triangular markings on the base are the result of gliding along an $\{hh\bar{2}h\bar{l}\}$ pyramid. Usually in foliated or scaly masses, but may be radiated or granular. A photograph of two polymorphs of carbon, diamond, and graphite, is given in Fig. 15.17.

$P6_3/mmc$; $a = 2.46$, $c = 6.74$ Å; $Z = 4$. *ds*: 3.36(10), 2.03(5), 1.675(8), 1.232(3), 1.158(5).

Physical Properties. *Cleavage* {0001} perfect. **H** 1–2 (readily marks paper and soils the fingers). **G** 2.23. *Luster* metallic, sometimes dull earthy. *Color* and streak, black. Greasy feel. Folia flexible but not elastic (see Plate I, no. 6).

FIG. 15.17 The two polymorphs of carbon: fibrous graphite from Buckingham, Quebec, Canada, and an octahedral diamond from the Republic of South Africa (Harvard Mineralogical Museum).

Composition and Structure. Carbon. Some graphite impure with iron oxide, clay, or other minerals. The structure is illustrated in Fig. 15.4b.

Diagnostic Features. Graphite is recognized by its color, hardness, foliated nature, and greasy feel. Distinguished from molybdenite by its black color (molybdenite has a blue tone), and black streak on unglazed porcelain.

Occurrence. Graphite most commonly occurs in metamorphic rocks, such as recrystallized limestones, schists, and gneisses. It may be found as large, crystalline plates or disseminated in small flakes in sufficient amount to form a considerable proportion of the rock. In these cases, it has probably been derived from carbonaceous material of organic origin that has been converted into graphite during metamorphism. Metamorphosed coal beds may be partially converted into graphite, as in the graphite coals of Rhode Island and in the coal fields of Sonora, Mexico. Graphite also occurs in hydrothermal veins associated with quartz, biotite, orthoclase, tourmaline, apatite, pyrite, and titanite, as in the deposits of Ticonderoga, New York. The graphite in these veins may have been formed from hydrocarbons introduced into them during the metamorphism of the region and derived from the surrounding carbon-bearing rocks. Graphite occurs occasionally as an original constituent of igneous rocks as in the basalts of Ovifak, Greenland, in a nepheline syenite in India, and in a graphite pegmatite in Maine. It is also found in some iron meteorites as graphite nodules.

The principal countries producing natural graphite are: China, Russia, North and South Korea, India, and Mexico.

Synthesis. Graphite is manufactured on a large scale in electrical furnaces using anthracite coal or petroleum coke as the raw materials. The use of artificial graphite in the United States is considerably in excess of that of the natural mineral.

Use. Used in the manufacture of refractory crucibles for the steel, brass, and bronze industries. Flake graphite for crucibles comes mostly from Sri Lanka and Madagascar. Mixed with oil, graphite is used as a lubricant, and mixed with fine clay, it forms the "lead" of pencils. It is used in the manufacture of protective paint for structural steel and is used in foundry facings, batteries, electrodes, generator brushes, and in electrotyping.

Name. Derived from the Greek word meaning *to write*, in allusion to its use in pencils.

SULFIDES, SULFARSENIDES, AND ARSENIDES

Acanthite—Ag_2S

Crystallography. Monoclinic, $2/m$ below 173°C; isometric, $4/m\bar{3}2/m$ above 173°C. Crystals, twinned pseudomorphs after the high-temperature form, commonly show the cube, octahedron, and dodecahedron and frequently are arranged in branching or reticulated groups. Most commonly massive or as a coating. Historically, acanthite has been referred to as argentite.

$P2_1/n$; $a = 4.23$, $b = 6.93$, $c = 7.86$ Å, $\beta = 99°35'$; $Z = 4$. *ds*: 2.60(10), 2.45(8), 2.38(5), 2.22(3), 2.09(4).

Physical Properties. **H** 2 –$2\frac{1}{2}$. **G** 7.3. Very sectile; can be cut with a knife, like lead. *Luster* metallic. *Color* black. *Streak* black, shining. Opaque. Bright on fresh surface but on exposure becomes dull black.

Composition and Structure. Ag 87.1, S 12.9%. Ag_2S has space group $P2_1/n$ below 173°C, and space group $Im\bar{3}m$ above 173°C. On cooling Ag_2S from above 173°C the structure twins pervasively to produce apparently cubic crystals of twinned acanthite, known to mineralogists as *argentite*. However, it seems that acanthite is the only stable form of Ag_2S at ordinary temperatures.

Diagnostic Features. Acanthite can be distinguished by its color, sectility, and high specific gravity.

Occurrence. Acanthite is an important primary silver mineral found in veins associated with native silver, the ruby silvers, polybasite, stephanite, galena, and sphalerite. It may also be of secondary origin. It is found in microscopic inclusions in argentiferous galena. Acanthite is an important ore in the silver mines of Guanajuato and elsewhere in Mexico. Formerly important European localities are Freiberg, Saxony, Germany; Jáchymov (Joachimsthal), Baňská Štiavnica (Schemnitz), and Kremnitz, Czech Republic, and Kongsberg, Norway. In the United States it has been an important ore mineral in Nevada, notably at the Comstock Lode and at Tonopah. It is also found in the silver districts of Colorado, and in Montana at Butte associated with copper ores.

Use. An important ore of silver.

Name. The name *acanthite* comes from the Greek word meaning *thorn*, in allusion to the shape of the crystals. The name *argentite* comes from the Latin *argentum*, meaning silver.

CHALCOCITE—Cu_2S

Crystallography. Monoclinic, pseudo-orthorhombic; $2/m$ or m, (below 105°C); above 105°C, hexagonal. Crystals are uncommon, usually small and tabular with hexagonal outline; striated parallel to the *a* axis (Fig. 15.18). Commonly fine-grained and massive.

$P2_1/c$ or Pc; $a = 11.82$, $b = 27.05$, $c = 13.43$Å, $\beta = 90°$; $Z = 96$. *ds*: 3.39(3), 2.40(7), 1.969(8), 1.870(10), 1.695(4).

Physical Properties. *Cleavage* {110} poor. *Fracture* conchoidal. **H** $2\frac{1}{2}$–3. **G** 5.5–5.8. *Luster* metallic. Imperfectly sectile. *Color* shining lead-gray, tarnishing to dull black on exposure. *Streak* grayish-black. Some chalcocite is soft and sooty.

FIG. 15.18 Chalcocite crystals.

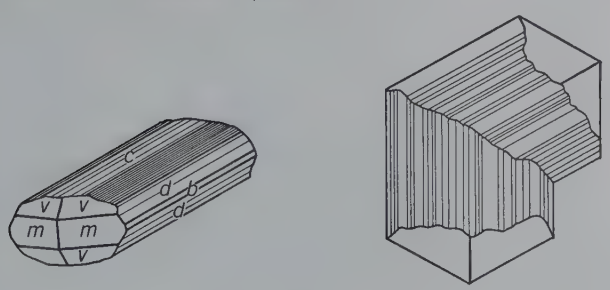

Composition and Structure. Cu 79.8, S 20.2%. May contain small amounts of Ag and Fe. Below 105°C the structure is based on hexagonal closest packing of sulfur atoms with a monoclinic space group. Above 105°C it inverts to high chalcocite with space group $P6_3/mmc$.

Diagnostic Features. Chalcocite is distinguished by its lead-gray color and sectility.

Occurrence. Chalcocite is one of the most important copper-ore minerals. Fine crystals are rare but have been found in Cornwall, England, and Bristol, Connecticut. Chalcocite may occur as a primary mineral in veins with bornite, chalcopyrite, enargite, and pyrite. But its principal occurrence is as a supergene mineral in enriched zones of sulfide deposits. Under surface conditions, the primary copper sulfides are oxidized; the soluble sulfates formed move downward, reacting with the primary minerals to form chalcocite and, thus, enrich the ore in copper. The water table is the lower limit of the zone of oxidation, and here a "chalcocite blanket" may form (see Box 15.3). Many famous copper mines owe their greatness to this process of secondary enrichment, as: Rio Tinto, Spain; Ely, Nevada; Morenci, Miami, and Bisbee, Arizona; and Butte, Montana.

Much of the world's copper is today produced from what is called porphyry copper deposits. In these deposits, primary copper minerals disseminated through the rock, usually a porphyry, have been altered, at least in part, to chalcocite and thus enriched to form a workable ore body. The amount of copper in such deposits is small, rarely greater than 1% or 2% and may be as low as 0.40%.

Use. An important copper ore.

Name. From the Greek word *chalkos* meaning *copper*.

Similar Species. *Digenite*, Cu_9S_5, is blue to black, associated with chalcocite. *Djurleite*, $Cu_{31}S_{16}$, a black to dark gray mineral, occurs in many of the large porphyry copper deposits of the Western Cordillera, U.S.A.

BORNITE—Cu_5FeS_4

Crystallography. Tetragonal. $\bar{4}2m$, below 228°C; isometric, $4/m\bar{3}2/m$, above 228°C. The most common form is tetragonal. Rarely in rough pseudocubic and less commonly dodecahedral and octahedral crystals. Usually massive.

$P\bar{4}2_1c$; $a = 10.94$, $c = 21.88$ Å; $Z = 16$. *ds*: 3.31(4), 3.18(6), 2.74(5), 2.50(4), 1.94(10).

$Fm\bar{3}m$; $a = 5.50$ Å; $Z = 1$. *ds*: 3.17(5), 2.75(5), 1.94(10), 1.66(1).

Physical Properties. **H** 3. **G** 5.06–5.08. *Luster* metallic. *Color* brownish-bronze on fresh fracture but quickly tarnishing to variegated purples and blues (called *peacock ore*; see Plate I, no. 7) and finally to almost black on exposure. *Streak* grayish-black.

Composition and Structure. Cu 63.3, Fe 11.2, S 25.5% for stoichiometric Cu_5FeS_4. Shows extensive solid solution within the Cu-Fe-S system. Its stoichiometric composition in terms of Cu-Fe-S is shown in the diagram in Box 15.4, with the compositions of other common sulfides in this system. The structure of the high *T* polymorph of bornite is relatively

BOX 15.3 VEINS AND VEIN MINERALIZATION

Although ore and mineral deposits can be of igneous, metamorphic, or sedimentary origin a large number of mineral deposits exist as tabular or lenticular bodies known as *veins*. They represent former fractures or fluid pathways now filled with minerals.

Vein mineralization is generally the result of what is known as deposition from *hydrothermal solutions*. This term refers to heated or hot magmatic fluids rich in water as well as heated aqueous solutions that have no demonstrable magmatic affiliations. An example of relatively high-temperature vein mineralization in and adjacent to granitic intrusions occurs in Cornwall, England. The mineral assemblage in such veins consists of quartz-mica-tourmaline-wolframite-stannite-cassiterite-molybdenite. In many mining districts, however, there is no apparent relationship between the ore veins and possible igneous activity.

Associated with the economically useful minerals (*ore minerals*) are minerals of no commercial value (*gangue*). Careful assemblage studies, involving both ore and gangue mineralizations, together with the study of very small inclusions of remaining hydrothermal fluid (fluid inclusions) in mineral grains allow for the division of hydrothermal ore deposits in terms of temperature of origin: low (50°–150°C), intermediate (150°–400°C), and high temperature (400°–600°C).

The *primary* or hypogene ore minerals may alter near the surface to secondary or *supergene* minerals. The primary sulfide minerals, such as pyrite, chalcopyrite, galena, and sphalerite, are particularly subject to such alteration. Under the influence of low-temperature and oxygenated meteoric waters, sphalerite (ZnS) alters to hemimorphite, $Zn_4(Si_2O_7)(OH)_2 \cdot H_2O$, and smithsonite, $ZnCO_3$; galena, PbS to anglesite, $PbSO_4$, and cerussite, $PbCO_3$; copper sulfides, such as chalcopyrite and bornite to covellite, chalcocite, native copper, cuprite, malachite, and azurite. The circulating surface waters dissolve primary minerals at near-surface conditions, producing a barren and leached zone (see the schematic cross-section of a vein that was originally rich in primary Cu-sulfides; the leached zone is the result of original pyrite, as well as other sulfides, having been oxidized producing goethite and/or limonite). These waters fre-

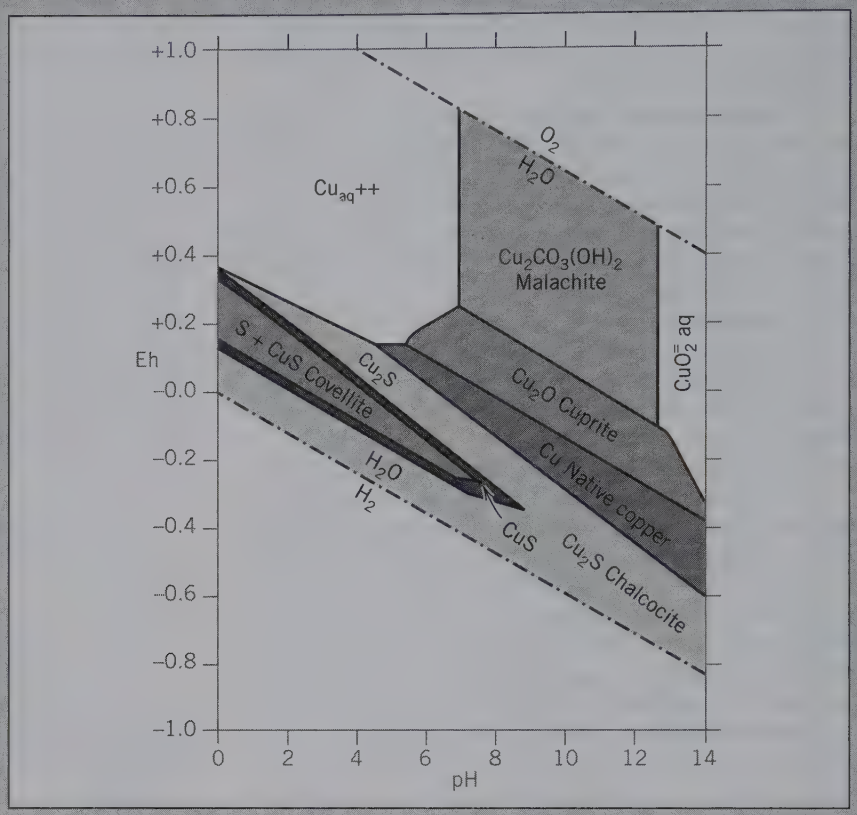

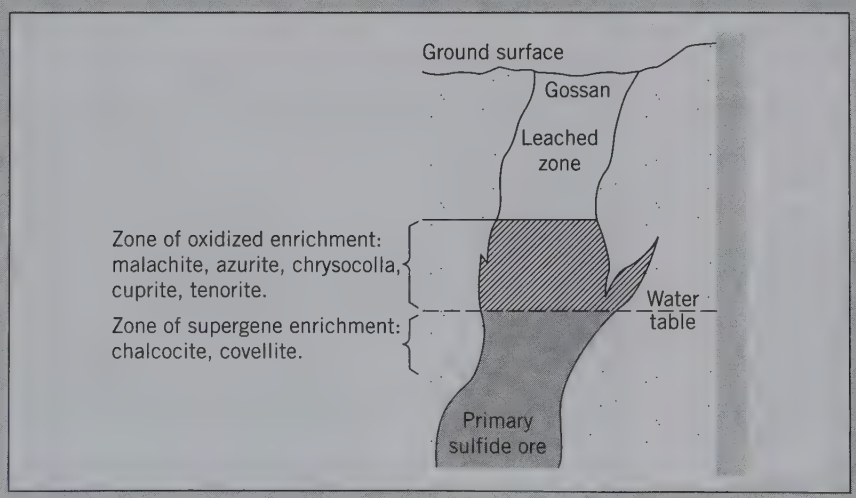

quently redeposit part of the soluble species below and close to the groundwater table, producing *secondary enrichment zones*. This process of *supergene enrichment* is especially important in ore formation because metals leached from the oxidized upper parts of mineral deposits may be redeposited at depth. Because all such chemical processes take place at essentially atmospheric conditions (about 25°C and 1 atmosphere pressure) Eh-pH stability diagrams for appropriate chemical systems can be used to illustrate conditions in supergene deposits. Such a diagram is shown at the right for the system Cu-H_2O-O_2-S-CO_2 at 25° and 1 atmosphere total pressure. (Adapted from Anderson, J., in Garrels, R. M., and Christ, C. L. 1965. *Solutions, minerals, and equilibria*, Freeman, Cooper, and Co., San Francisco, Fig. 7.27b on p. 240; see same book for construction of such diagrams.)

complex with sulfur atoms in a face-centered cubic lattice and the Cu and Fe atoms in tetrahedral coordination to S. The structure of the low temperature form is derived from the high *T* form with the addition of defects. This defect structure gives rise to large variations in Cu, Fe, and S contents.

Diagnostic Features. Bornite is distinguished by its characteristic bronze color on the fresh fracture and by the purple tarnish.

Alteration. Bornite alters readily to chalcocite and covellite.

Occurrence. Bornite is a widely occurring copper ore usually found associated with other sulfides (chalcocite, chalcopyrite, covellite, pyrrhotite and pyrite; see diagram in Box 15.4) in hypogene deposits. It is less frequently found as a supergene mineral, in the upper, enriched zone of copper veins. It occurs disseminated in basic rocks, in contact metamorphic deposits, in replacement deposits, and in pegmatites. It is not as important an ore of copper as chalcocite and chalcopyrite.

Good crystals of bornite have been found associated with crystals of chalcocite at Bristol, Connecticut, and in Cornwall, England. Found in large masses in Chile, Peru, Bolivia, and Mexico. In the United States, it has been an ore mineral at the Magma Mine, Arizona; Butte, Montana; Engels Mine, Plumas County, California; Halifax County, Virginia; and Superior, Arizona.

Use. An ore of copper.

Name. Bornite was named after the Austrian mineralogist Ignatius von Born (1742–1791).

GALENA—PbS

Crystallography. Isometric; $4/m\bar{3}2/m$. The most common form is the cube, sometimes truncated by the octahedron (Figs. 15.19 and 15.20). Dodecahedron and triscotahedron rare.

$Fm3m$; $a = 5.936$ Å; $Z = 4$. *ds*: 3.44(9), 2.97(10), 2.10(10), 1.780(9), 1.324(10).

Physical Properties. *Cleavage* perfect {001}. **H** $2\frac{1}{2}$. **G** 7.4–7.6. *Luster* bright metallic. *Color* and *streak* lead-gray (see Plate I, no. 8).

Composition and Structure. Pb 86.6, S 13.4%. Silver is usually present as admixtures of silver minerals, such as acanthite or tetrahedrite but also in solid solution. Inclusions probably also account for the small amounts of Zn, Cd, Sb, As, and Bi that may be present. Selenium may substitute for sulfur and a complete series of PbS–PbSe has been reported. Galena has an NaCl type of structure with Pb in place of Na and S in place of Cl.

Diagnostic Features. Galena can be easily recognized by its good cleavage, high specific gravity, softness, and lead-gray streak.

Alteration. By oxidation galena is converted into anglesite, $PbSO_4$, and cerussite, $PbCO_3$.

Occurrence. Galena is a common metallic sulfide, found in veins associated with sphalerite, pyrite, marcasite, chalcopyrite, cerussite, anglesite, dolomite, calcite, quartz, barite, and fluorite. When found in hydrothermal veins, galena is frequently associated with silver minerals; it often contains silver and so becomes an important silver ore. A large part of the supply of lead comes as a secondary product from ores mined chiefly for their silver. In a second type of deposit typified by the lead–zinc ores of the Mississippi Valley, galena, associated with sphalerite, is found in veins, open space filling, or replacement bodies in limestones. These are low-temperature deposits, located at shallow depths, and usually contain little silver. Galena is also found in contact metamorphic deposits, in pegmatites, and as disseminations in sedimentary rocks.

Famous world localities are Freiberg, Saxony, and the Harz Mountains, Germany; Příbram, Czech Republic; Derbyshire and Cumbria, England; Sullivan Mine, British Colombia; and Broken Hill, Australia.

In the past, many districts in the United States were significant lead producers, but today only three are of importance. Chief of these is in southeast Missouri, which yields nearly 90% of the domestic production. Here, galena is disseminated through limestone. A small production comes from the Coeur d'Alene district, Idaho, where galena is the primary

FIG. 15.19 Galena crystals.

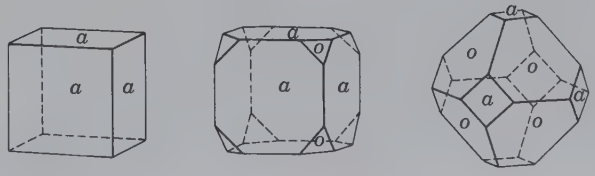

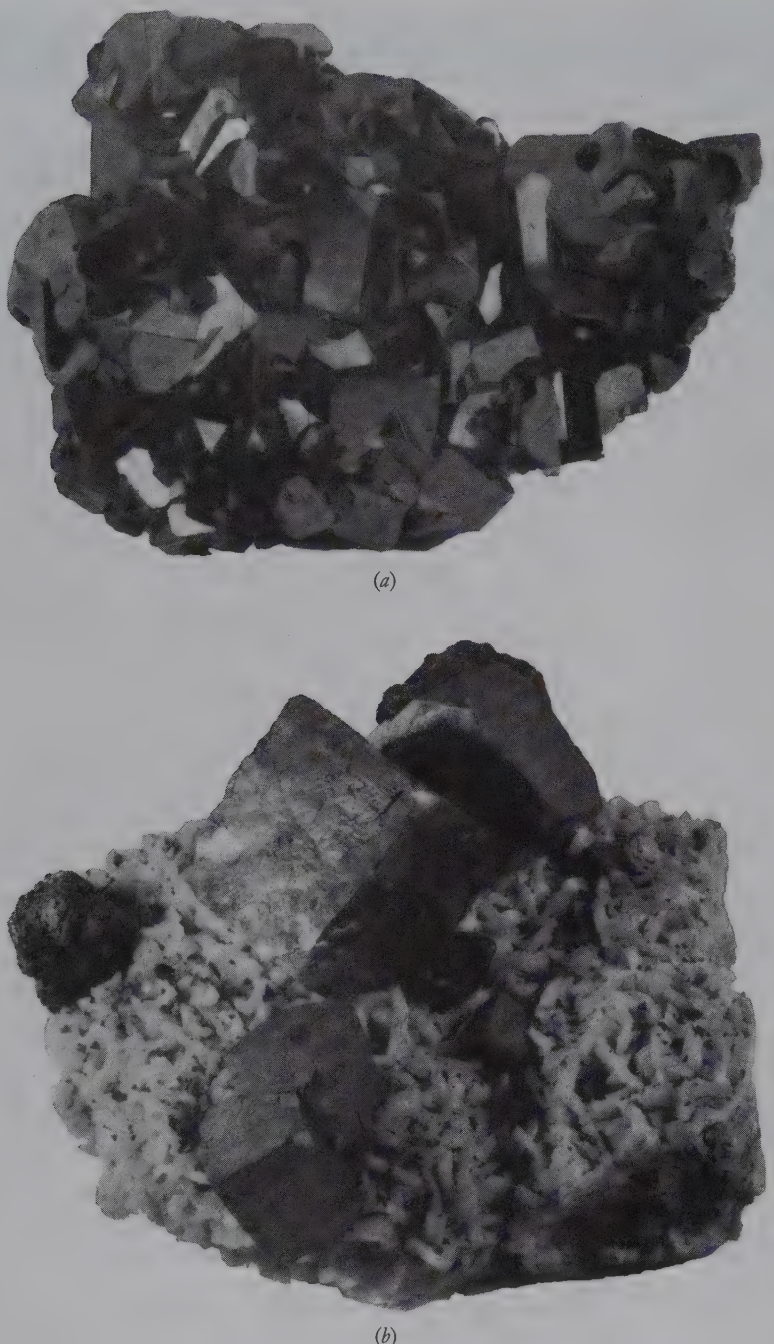

(*a*)

(*b*)

FIG. 15.20 (a) Galena crystals, Wellington Mine, Breckenridge, Colorado. (b) Galena on sphalerite and dolomite crystals, Jasper County, Missouri, U.S.A. (both specimens from the Harvard Mineralogical Museum.)

ore mineral in the lead–silver veins, and from Colorado, where lead is recovered mostly as a byproduct from the mining of silver and gold ores. Formerly, the tristate district of Missouri, Kansas, and Oklahoma was an important lead producer. In this region galena, associated with sphalerite, occurred in irregular veins and pockets in limestone and chert. Because the minerals could grow into open spaces, the tristate district is famous for its many beautifully crystallized specimens of galena, sphalerite, marcasite, chalcopyrite, calcite, and dolomite.

Use. Practically the only source of lead and an important ore of silver. The largest use of lead is in storage batteries, but nearly as much is consumed in making metal products, such as pipe, sheets, and shot. Lead is converted into the oxides (*litharge*, PbO, and *minium*, Pb_3O_4) used in making glass and in giving a glaze to earthenware, and into white lead (the basic carbonate), the principal ingredient of many paints. However, this latter use is diminished because of the poisonous nature of lead-based paints. Diminished also is its use in gasoline antiknock additives because of environmental restrictions. Lead is a principal metal of several alloys as solder (lead and tin), type metal (lead and antimony), and low-melting alloys (lead, bismuth, and tin). Lead is used as shielding around radioactive materials.

BOX 15.4 Sulfide Minerals as Ores and as Mining-Related Contaminants

In sulfide ore-mineral assemblages pyrite is commonly the most abundant sulfide. Chalcopyrite is generally the next most common sulfide species and represents the most important copper mineral. Bornite is commonly associated with pyrite and chalcopyrite. Chalcocite, and to a lesser degree, covellite may occur as primary constituents in some ore deposits (Most commonly these two Cu-sulfides occur in supergene enriched sulfide deposits; see Box 15.3.) Other sulfides that may be present are pyrrhotite, molybdenite (MoS_2), galena (PbS), and sphalerite (ZnS). The triangular diagram in this box shows some of the most common sulfides that can be represented in the Cu-Fe-S system. Many of these sulfides (e.g., bornite and chalcopyrite) naturally exhibit some solid solution of especially Cu and Fe; this is not shown in the diagram. *Tielines* (the bold lines in the diagram) are a graphical representation for the common occurrence of two or more minerals in a mineral assemblage. The Fe-FeS (troilite) coexistence is common in iron meteorites. Triangles indicate coexistences of three sulfides.

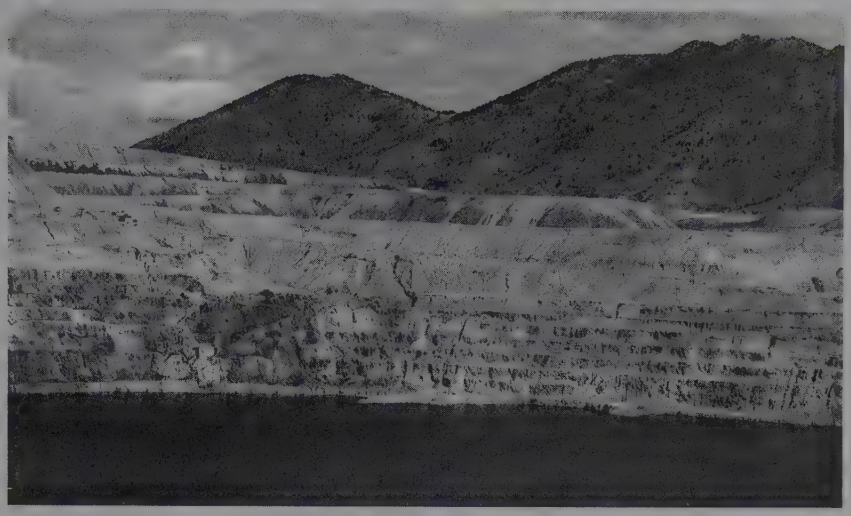

In the mining process, the sulfide ore minerals are extracted from the various rock types in which they occur. This produces commonly very large accumulations of waste rock that become essentially permanent deposits in the area surrounding the mining operation. This also happens in the coal mining industry where pyrite is a common minor constituent of the coal beds. These waste dumps are exposed to natural precipitation and oxygen from the atmosphere, which together cause the slow dissolution of the sulfides and the subsequent production of acidic sulfate- and metal-rich waters; this is known as acid mine drainage (AMD). A key reaction in this process is:

$$\underset{\text{pyrite}}{FeS_2} + \underset{\text{aqueous}}{7/2\ O_2} + \underset{\text{liquid}}{H_2O} \rightarrow \underset{\text{aqueous}}{Fe^{2+}} + \underset{\text{aqueous}}{2(SO_4)^{2-}} + \underset{\text{aqueous}}{2H^+}$$

The dissolved Fe^{2+}, $(SO_4)^{2-}$, and H^+ represent an increase in the total dissolved solids and acidity of the water. The increasing acidity of the water results in a decrease in pH. One such example is shown here: the tailings pile and highly acid lake waters at Butte, Montana, USA.

This same process is intensified if the mining company applies methods of waste rock leaching in which the waste dumps are naturally and artificially leached by meteoric as well as irrigation water so as to recover any metals that are still in the waste rock. Depending on the local hydrologic conditions these acidic, metal-rich solutions may enter nearby streams, rivers, and lakes as well as the groundwater system. Such pollution is common in many sulfide and coal-mining areas and may be contained with very expensive and complex remediation procedures.

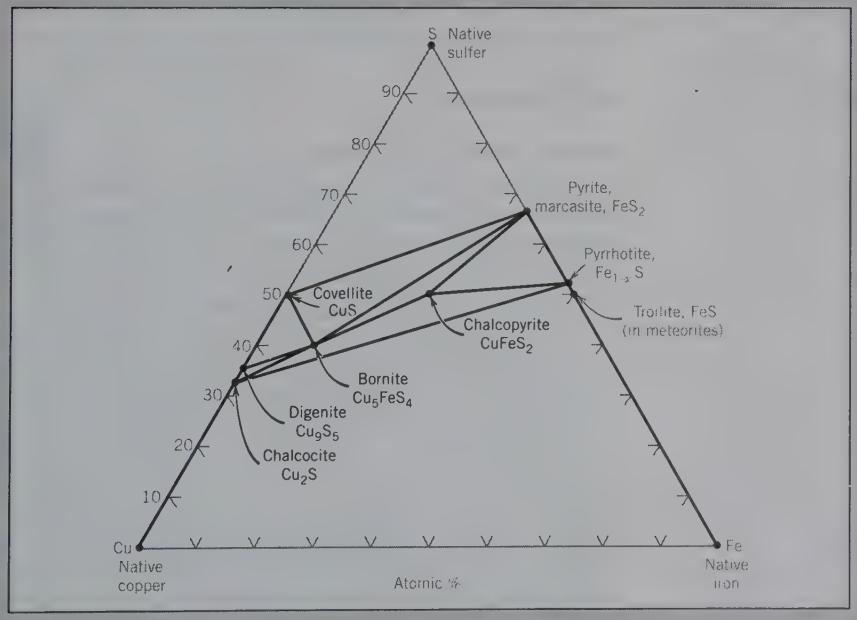

Name. The name galena is derived from the Latin word *galena*, a name originally given to lead ore.

Similar Species. *Altaite*, PbTe, and *alabandite*, MnS, like galena, have an NaCl type of structure.

SPHALERITE—ZnS

Crystallography. Isometric; $\bar{4}3m$. Tetrahedron, dodecahedron, and cube common forms (Fig. 15.21), but the crystals, frequently highly complex and usually distorted or in rounded aggregates, often show polysynthetic twinning on {111}. Usually found in cleavable masses, coarse to fine granular. Compact, botryoidal, cryptocrystalline.

$F\bar{4}3m$; $a = 5.41$ Å; $Z = 4$. *ds*: 3.12(10), 1.910(8), 1.631(7), 1.240(4), 1.106(5).

Physical Properties. *Cleavage*, {011} perfect but some sphalerite is too fine grained to show cleavage. **H** $3\frac{1}{2}$–4. **G** 3.9–4.1. *Luster* nonmetallic and resinous to submetallic; also adamantine. *Color* colorless when pure, and green when nearly so (see Plate I, no. 9). Commonly yellow, brown to black, darkening with increase in iron (called blackjack). Also red (ruby zinc). Transparent to translucent. *Streak* white to yellow and brown. *Optics*: $n = 2.37$.

Composition and Structure. Zn 67, S 33% when pure. Nearly always contains some Fe, with the amount of Fe dependent on the temperature and chemistry of the environment. If Fe is in excess, as indicated by association with pyrrhotite, the amount of FeS in sphalerite can reach 50 mole percent (see also Table 5.4). If sphalerite and pyrrhotite crystallize together, the amount of iron is an indication of the temperature of formation, and sphalerite can be used as a geological thermometer. Mn and Cd are usually present in small amounts in solid solution (see Table 5.4).

The structure of sphalerite is similar to that of diamond with one half of the carbon atoms replaced by Zn and the other half by S (see Figs. 4.19 and 15.5a). Sphalerite is considered the low-temperature cubic polymorph of ZnS, and wurtzite the high-temperature polymorph stable above 1020°C at 1 atmosphere pressure. The *wurtzite* polymorph (space group $P6_3mc$), with Zn atoms in hexagonal closest packing (see Fig. 15.6), shows a very large number of stacking sequences, referred to as wurtzite *polytypes*, which differ in the length of their *c* axes. For example the 4*H* polytype has a *c* axis of 12.46 Å and the 8 *H* polytype a *c* axis of 24.96 Å (*H* = hexagonal).

Diagnostic Features. Sphalerite can be recognized by its striking resinous luster and perfect cleavage. The dark varieties (blackjack) can be distinguished by the yellow-brown streak, always lighter than the massive mineral.

Occurrence. Sphalerite, the most important ore mineral of zinc, is extremely common. Its occurrence and mode of origin are similar to those of galena, with which it is commonly found. In the shallow seated lead–zinc deposits of the tristate district of Missouri, Kansas, and Oklahoma (now largely exhausted), these minerals are associated with marcasite, chalcopyrite, calcite, and dolomite. Sphalerite with only minor galena occurs in hydrothermal veins and replacement deposits associated with pyrrhotite, pyrite, and magnetite. Sphalerite is also found in veins of igneous rocks and in contact metamorphic deposits.

Zinc is mined in significant amounts in more than 40 countries. Although in a few places the ore minerals are hemimorphite and smithsonite and, at Franklin and Sterling Hill, New Jersey, willemite, zincite, and franklinite, most of the world's zinc comes from sphalerite. The principal producing countries are: Canada, China, United States, Australia, Peru, Mexico, and Japan. In the United States, nearly 99% of the zinc is produced from Alaska, Missouri, and Montana. Elmwood, Tennessee, produces some outstanding specimen material.

Use. The most important ore of zinc. The chief uses for metallic zinc, or *spelter*, are in galvanizing iron; making brass, an alloy of copper and zinc; in electric batteries; and as sheet zinc. Zinc oxide, or zinc white, is used extensively for making paint. Zinc chloride is used as a preservative for wood. Zinc sulfate is used in dyeing and in medicine. Sphalerite also serves as the most important source of cadmium, indium, gallium, and germanium.

Name. Sphalerite comes from the Greek word meaning *treacherous*. It was called blende because, although often resembling galena, it yielded no lead; from the German word meaning *blind* or *deceiving*.

Similar Species. *Greenockite*, CdS, a rare mineral mined as a source of cadmium, is isostructural in two polymorphic forms with sphalerite and wurtzite. Cadmium is recovered from greenockite associated with zinc minerals, especially sphalerite.

CHALCOPYRITE—$CuFeS_2$

Crystallography. Tetragonal; $\bar{4}2m$. Commonly tetrahedral in aspect with the disphenoid *p* {112} dominant (see photograph that opens this chapter and Fig. 15.22). Other forms shown in Fig. 15.22 are rare. Usually massive.

$I\bar{4}2d$; $a = 5.25$, $c = 10.32$ Å; $Z = 4$. *ds*: 3.03(10), 1.855(10), 1.586(10), 1.205(8), 1.074(8).

Physical Properties. **H** $3\frac{1}{2}$–4. **G** 4.1–4.3. *Luster* metallic. *Color* brass-yellow; often tarnished to bronze or iridescent. *Streak* greenish-black. Brittle.

Composition and Structure. Cu 34.6, Fe 30.4, S 35.0%. It deviates very little from ideal $CuFeS_2$. See diagram in Box 15.4 for chalcopyrite composition in the Cu–Fe–S system. Its structure can be regarded as a derivative of the sphalerite structure in which half the Zn is replaced by Cu and the other half by Fe. This leads to a doubling of the unit cell (see Fig. 15.5b).

FIG. 15.21 Sphalerite crystals.

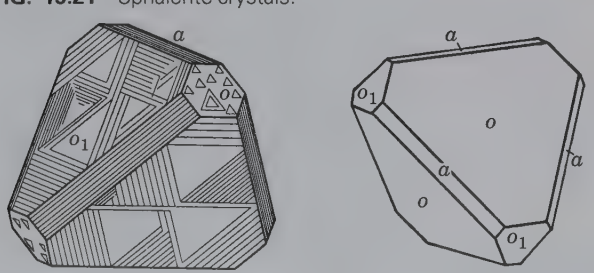

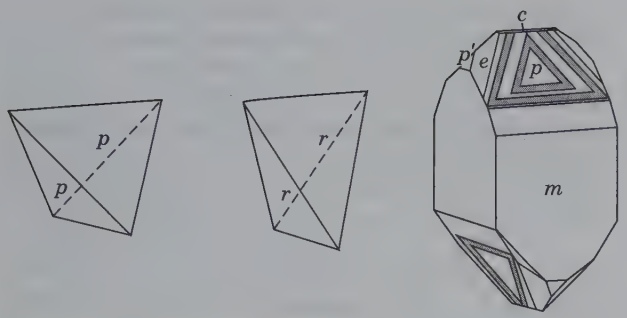

FIG. 15.22 Chalcopyrite crystals.

Diagnostic Features. Recognized by its brass-yellow color (see Plate II, no. 1) and greenish-black streak. Distinguished from pyrite by being softer than steel and from gold by being brittle. Known as *fool's gold*, a term also applied to pyrite.

Occurrence. Chalcopyrite is the most widely occurring copper mineral and one of the most important sources of that metal. Most sulfide ores contain some chalcopyrite, but the most important economically are the hydrothermal vein (see Box 15.4) and replacement deposits. In the low-temperature deposits as in the tristate district, it occurs as small crystals associated with galena, sphalerite, and dolomite. Associated with pyrrhotite and pentlandite, it is the chief copper mineral in the ores of Sudbury, Ontario, and similar high-temperature deposits. Chalcopyrite is the principal primary copper mineral in the "porphyry-copper" deposits. Also occurs as an original constituent of igneous rocks; in pegmatite dikes; in contact metamorphic deposits; and disseminated in schistose rocks. It may contain gold or silver and become an ore of those metals—often in subordinate amount with large bodies of pyrite, making them serve as low-grade copper ores.

A few of the localities and countries in which chalcopyrite is the chief ore of copper are Cornwall, England; Falun, Sweden; Baňská Štiavnica (Schemnitz) and Horní Slavkov (Schlaggenwald), Czech Republic; Freiberg, Saxony, Germany; Rio Tinto, Spain; South Africa; Zambia; and Chile. Found widely in the United States but usually with other copper minerals in equal or greater amount; found at Butte, Montana; Bingham, Utah; Jerome, Arizona; Ducktown, Tennessee; and various districts in California, Colorado, and New Mexico. In Canada, the most important occurrences of chalcopyrite are at Sudbury, Ontario, and in the Rouyn-Noranda district, Quebec.

Alteration. Chalcopyrite is the principal source of copper for the secondary minerals malachite, azurite, covellite, chalcocite, and cuprite. Concentrations of copper in the zone of supergene enrichment are often the result of such alteration and removal of copper in solution with its subsequent deposition (see Box 15.3).

Use. Important ore of copper.

Name. Derived from the Greek word *chalkos*, meaning *copper*, and from *pyrites*.

Similar Species. *Stannite*, Cu_2FeSnS_4, tetragonal, is a rare mineral and a minor ore of tin. The crystal structure of stannite can be derived from that of chalcopyrite by substitution of Fe and Sn in place of part of the Cu in chalcopyrite, see page 340.

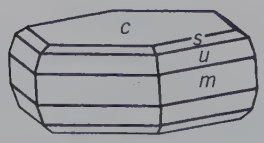

FIG. 15.23 Pyrrhotite crystal.

PYRRHOTITE—$Fe_{1-x}S$

Crystallography. Monoclinic; $2/m$, for low-temperature form, stable below about 250°C; hexagonal, $6/m2/m2/m$, for high-temperature forms. Hexagonal crystals, usually tabular but in some cases pyramidal (Fig. 15.23), indicate formation as the high-temperature polymorph.

$A2/a$; $a = 12.78$, $b = 6.86$, $c = 11.90$Å, $\beta = 117°17'$; $Z = 4$. No specific *d*s are given here because there are several monoclinic forms.

$C6/mmc$; $a = 3.44$, $c = 5.73$ Å; $Z = 2$. *d*s: 2.97(6), 2.63(8), 1.06(10), 1.718(6), 1.045(8).

Physical Properties. **H** 4. **G** 4.58–4.65. *Luster* metallic. *Color* brownish-bronze (see Plate II, no. 2). *Streak* black. Magnetic, but varying in intensity; the greater the amount of iron, the lesser the magnetism. Opaque.

Composition and Structure. Most pyrrhotites have a deficiency of iron with respect to sulfur, as indicated by the formula $Fe_{1-x}S$, with x between 0 and 0.2. This is referred to as omission solid solution (see page 99 and Fig. 5.9). A complete solid solution series from FeS (with 50 atomic percent Fe) to pyrrhotite, with 44.9 atomic percent Fe, exists in the high-temperature part of the pyrrhotite stability field (from its melting point, at 1190°C, to about 400°C). This phase field has hexagonal symmetry. At lower temperatures (see Fig. 15.24), the pyrrhotite phase field narrows and the single, hexagonal solid solution field of pyrrhotite gives way to several hexagonal and monoclinic types. The monoclinic pyrrhotite compositions center at about Fe_7S_8. The monoclinic variety is stable from 0° to 254°C, where it inverts to the hexagonal type (see Fig. 15.24).

The structure of pyrrhotite is a complex derivative of the NiAs structure type. The sulfur atoms are arranged in approximate hexagonal closest packing. A large number of ordered structures exist for this nonstoichiometric sulfide. Several hexagonal structure types are stable over various temperature ranges in the field labeled "hexagonal varieties of pyrrhotite" in Fig. 15.24. The monoclinic structure is stable only below 254°C. The structural relations within the various polymorphs are complex. The mineral *troilite* is essentially FeS in composition.

Diagnostic Features. Recognized usually by its massive nature, bronze color, and magnetism.

Occurrence. Pyrrhotite is commonly associated with basic igneous rocks, particularly norites. It occurs in them as disseminated grains or, as at Sudbury, Ontario, as large masses associated with pentlandite, chalcopyrite, or other sulfides. At

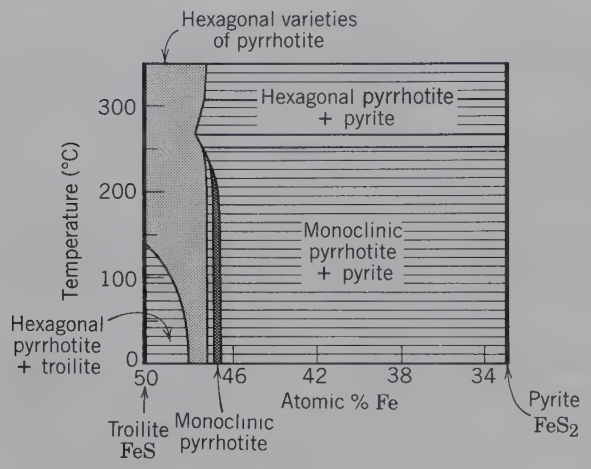

FIG. 15.24 The stability field of pyrrhotite, $Fe_{1-x}S$, in a temperature–composition section for the join FeS–FeS_2. The stability field of monoclinic pyrrhotite is fairly narrow and centers on Fe_7S_8. Its maximum temperature limit is 254°C. The hexagonal pyrrhotite field is narrow at 0° but widens all the way to the FeS axis at 140°C. The extent of solid solution is shown by shading. (Simplified after Kissin, S. A. 1974. *Sulfide Mineralogy, Reviews in Mineralogy* 1, Mineralogical Society of America, Washington, D.C., CS–25.)

Sudbury vast tonnages of pyrrhotite are mined principally for the copper, nickel, and platinum that are extracted from associated minerals. Pyrrhotite is also found in contact metamorphic deposits, in vein deposits, and in pegmatites.

Large quantities are known in Finland, Norway, Sweden, and Russia. Fine crystals are found in Santa Eulalia, Chihuahua, Mexico; in the Morro Velho gold mine, Nova Lima, Minas Gerais, Brazil; and in Trepča, Serbia. In the United States considerable amounts are found at Ducktown, Tennessee.

Use. It is mined for its associated nickel, copper, and platinum. At Sudbury, Ontario, it is also a source of sulfur and an ore of iron.

Name. The name pyrrhotite comes from the Greek word meaning *reddish*.

Similar Species. *Troilite*, FeS, common in iron meteorites.

Nickeline—NiAs

Crystallography. Hexagonal; $6/m2/m2/m$. Rarely in tabular crystals. Usually massive, reniform with columnar structure.

$C6/mmc$; $a = 3.61$, $c = 5.02$ Å; $Z = 2$. *ds*: 2.66(10), 1.961(9), 1.811(8), 1.328(3), 1.071(4).

Physical Properties. **H** 5 –$5\frac{1}{2}$. **G** 7.78. *Luster* metallic. *Color* pale copper-red (called *copper nickel*), with gray to blackish tarnish. *Streak* brownish-black. Opaque.

Composition and Structure. Ni 43.9, As 56.1%. Usually a little Fe, Co, and S. As frequently replaced in part by Sb. The structure of NiAs is based on hexagonal closest packing of arsenic atoms giving a sequence *ABABAB*. . . . The nickel atoms are coordinated to six closest As atoms.

Diagnostic Features. Characterized by its copper-red color. Gives nickel test with dimethylglyoxime.

Alteration. Quickly alters to *annabergite* (green nickel bloom, $Ni_3(AsO_4)_2 \cdot 8H_2O$) in moist atmosphere.

Occurrence. Nickeline with other nickel arsenides and sulfides, pyrrhotite, and chalcopyrite, frequently occurs in, or is associated with, norites. Also found in vein deposits with cobalt and silver minerals.

Found in Germany in the silver mines of Saxony, the Harz Mountains, in Hessen–Nassau; and at Cobalt, Ontario.

Use. A minor ore of nickel.

Name. The first name of this mineral, *kupfernickel*, gave the name *nickel* to the metal. It is now called nickeline, after its nickel content.

Similar Species. *Breithauptite*, NiSb, is isostructural with nickeline with similar occurrence and association. Breithauptite has a distinctive light copper-red color on fresh fracture.

Millerite—NiS

Crystallography. Hexagonal; $\bar{3}2/m$ (low-temperature polymorph stable below 379°C). Usually in hairlike tufts and radiating groups of slender to capillary crystals, Fig. 15.25. In velvety incrustations. Rarely in coarse, cleavable masses.

$R3m$; $a = 9.62$, $c = 3.16$ Å; $Z = 9$. *ds*: 4.77(8), 2.75(10), 2.50(6), 2.22(6), 1.859(10).

Physical Properties. *Cleavage*, $\{10\bar{1}1\}$, $\{01\bar{1}2\}$ good. **H** 3 –$3\frac{1}{2}$. **G** 5.5 ± 0.2. *Luster* metallic. *Color* pale brass-yellow; with a greenish tinge when in fine hairlike masses. *Streak* black, somewhat greenish.

Composition and Structure. Ni 64.7, S 35.3%. The low-temperature form, stable below 379°C, shows little if any solid solution. Ni and S are both in 5-coordination in the low-temperature form. The high-temperature form (stable above 379°C) has an NiAs type of structure and exhibits considerable metal deficiency, $Ni_{1-x}S$, similar to pyrrhotite.

Diagnostic Features. Characterized by its capillary crystals and distinguished from minerals of similar color by nickel tests.

FIG. 15.25 Millerite in a calcite-lined vug, Keokuk, Iowa (Harvard Mineralogical Museum.)

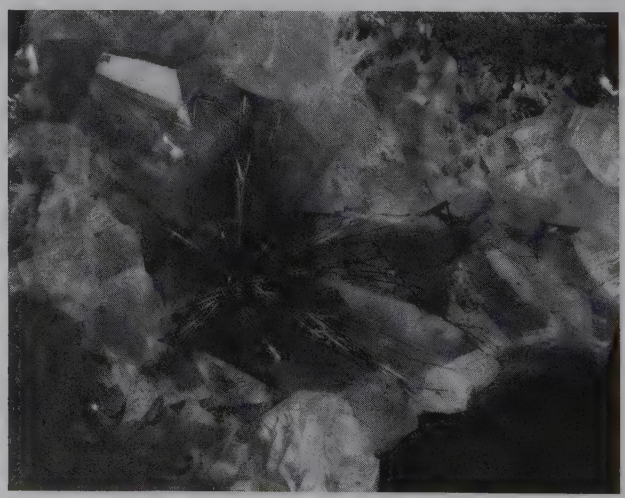

Occurrence. Millerite forms as a low-temperature mineral often in cavities and as an alteration of other nickel minerals, or as crystal inclusions in other minerals.

In the United States, it is found with hematite and ankerite at Antwerp, New York; in vugs and geodes in limestone in Harrodsburg, Indiana; Keokuk, Iowa; and Milwaukee, Wisconsin. In coarse, cleavable masses it is a major ore mineral at the Marbridge Mine, Lamotte Township, Quebec.

Use. A subordinate ore of nickel.

Name. In honor of the mineralogist, W. H. Miller (1801–1880), who first studied the crystals.

Pentlandite—$(Fe,Ni)_9S_8$

Crystallography. Isometric; $4/m\bar{3}2/m$. Massive, usually in granular aggregates with octahedral parting.

$Fm3m$; $a = 10.07$ Å; $Z = 4$. *ds*: 5.84(2), 3.04(6), 2.92(2), 2.31(3), 1.78(10).

Physical Properties. Parting on {111}. **H** $3\frac{1}{2}$–4. **G** 4.6–5.0. Brittle. *Luster* metallic. *Color* yellowish-bronze. *Streak* light bronze-brown. Opaque. Nonmagnetic.

Composition and Structure. $(Fe,Ni)_9S_8$. Usually the ratio of Fe:Ni is close to 1:1. Commonly contains small amounts of Co. A rather complicated face-centered cubic structure with the metal atoms in octahedral as well as tetrahedral coordination with sulfur, see Fig. 15.26. Pure $(Fe,Ni)_9S_8$, without Co, is stable up to 610°C in the Fe–Ni–S system. Pentlandite with as much as 40.8 weight percent Co is stable up to 746°C. Pentlandite commonly occurs as exsolution lamellae within pyrrhotite.

Diagnostic Features. Pentlandite closely resembles pyrrhotite in appearance but can be distinguished from it by octahedral parting and lack of magnetism. Gives nickel test with dimethyglyoxime.

Occurrence. Pentlandite usually occurs in basic igneous rocks where it is commonly associated with other nickel minerals and pyrrhotite, and chalcopyrite, and has probably accumulated by magmatic segregation.

Found at widely separated localities in small amounts, but its chief occurrences are in Canada where, associated with pyrrhotite, it is the principal source of nickel at Sudbury, Ontario, and the Lynn Lake area, Manitoba. It is also an important ore mineral in similar deposits in the Petsamo district of Karelia in Russia and in the Kimbalda area of Western Australia.

Use. The principal ore of nickel. The chief use of nickel is in steel. Nickel steel contains $2\frac{1}{2}$–$3\frac{1}{2}$ nickel, which greatly increases the strength and toughness of the alloy, so that lighter machines can be made without loss of strength. Nickel is also an essential constituent of stainless steel (see Box 16.1). The manufacture of Monel metal (68% Ni, 32% Cu) and Nichrome (38–85% Ni) consumes a large amount of the nickel produced. Other alloys are German silver (Ni, Zn, and Cu); metal for coinage—the 5-cent coin of the United States is 25% Ni and 75% Cu; low-expansion metals for watch springs; and other instruments. Nickel is used in plating; although chromium now largely replaces it for the surface layer, nickel is used for a thicker underlayer.

Name. After J. B. Pentland, who first noted the mineral.

Covellite—CuS

Crystallography. Hexagonal; $6/m2/m2/m$. Rarely in tabular hexagonal crystals. Usually massive as coatings or disseminations through other copper minerals.

$P6_3/mmc$; $a = 3.80$, $c = 16.36$ Å; $Z = 6$. *ds*: 3.06(4), 2.83(6), 2.73(10), 1.899(8), 1.740(5).

Physical Properties. *Cleavage* {0001} perfect giving flexible plates. **H** $1\frac{1}{2}$–2. **G** 4.6–4.76. *Luster* metallic. *Color* indigo-blue or darker. *Streak* lead-gray to black. Often iridescent. Opaque.

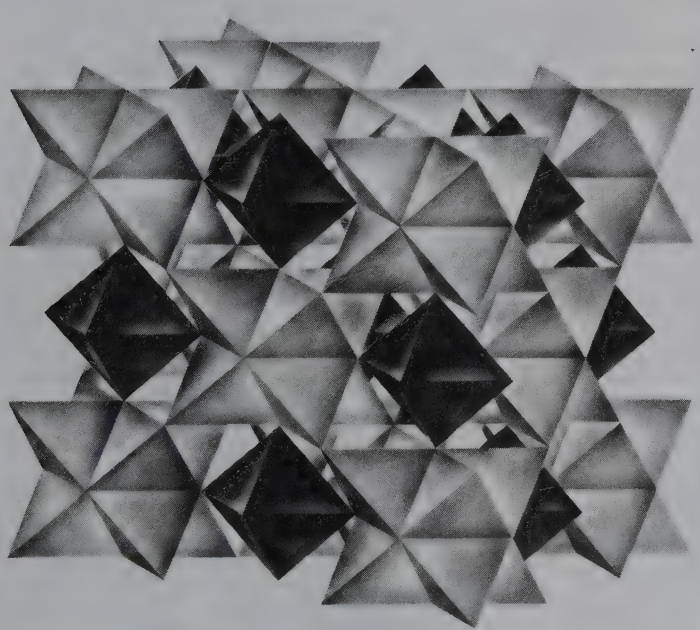

FIG. 15.26 The structure of pentlandite, $(Fe,Ni)_9S_8$, which consists of Fe and Ni in octahedral and tetrahedral coordination with S. The starlike clusters consist of eight linked $(Fe,Ni)S_4$ tetrahedra. The sulfur atoms are in cubic closest packing.

Composition and Structure. Cu 66.4, S 33.6%. A small amount of Fe may be present. Covellite has a rather complex structure (see Fig. 15.7). One type of Cu atom is in tetrahedral coordination with S, with the tetrahedra sharing corners to form layers. A second type of Cu is in trigonal coordination with S to build planar layers. The excellent {0001} cleavage is parallel to this layer structure. Covellite is stable up to 507°C, its temperature of decomposition.

Diagnostic Features. Characterized by the indigo-blue color, micaceous cleavage yielding flexible plates, and association with other copper sulfides.

Occurrence. Covellite is not an abundant mineral but is found in most copper deposits as a supergene mineral, usually as a coating, in the zone of sulfide enrichment (see Box 15.3). It is associated with other copper minerals, principally chalcocite, chalcopyrite, bornite, and enargite, and is derived from them by alteration. Primary covellite is known but uncommon.

Found at Bor, Serbia, and Leogang, Austria. In large iridescent crystals from the Calabona Mine, Alghero, Sardinia, Italy. In the United States covellite is found in appreciable amounts and excellent crystals at Butte, Montana, and Summitville, Colorado. Formerly found at Kennecott, Alaska.

Use. A minor ore of copper.

Name. In honor of N. Covelli (1790–1829), the discoverer of the Vesuvian covellite.

CINNABAR—HgS

Crystallography. Hexagonal; 32 (low-temperature polymorph stable below approximately 344°C). High-temperature form, known as *metacinnabar*, isometric; $\bar{4}3m$. Crystals of cinnabar usually rhombohedral, often in penetration twins. Trapezohedral faces are rare. Usually fine granular, massive; also earthy, as incrustations and disseminations through the rock. Metacinnabar crystals are tetrahedral, with rough faces; usually massive.

$P3_121$ or $P3_221$; $a = 4.146$, $c = 9.497$ Å; $Z = 3$. *ds*: 3.37(10), 3.16(8), 2.87(10), 2.07(8), 1.980(8).

$F\bar{4}3m$; $a = 5.852$Å; $Z = 4$. *ds*: 3.38(10), 2.93(3), 2.07(5), 1.764(4).

Physical Properties. *Cleavage* $\{10\bar{1}0\}$ perfect. **H** $2\frac{1}{2}$. **G** 8.10. *Luster* adamantine when pure to dull earthy when impure. *Color* vermilion-red when pure to brownish-red when impure. *Streak* scarlet. Transparent to translucent. *Metacinnabar* has a metallic luster and grayish-black color. *Hepatic cinnabar* is an inflammable liver-brown variety of cinnabar with bituminous impurities; usually granular or compact, sometimes with a brownish streak.

Composition and Structure. Hg 86.2, S 13.8%, with small variations in Hg content. Traces of Se and Te may replace S. Frequently impure from admixture of clay, iron oxide, bitumen. The structure of cinnabar, which is different from that of any other sulfide, is based on infinite spiral Hg–S–Hg chains which extend along the *c* axis; it can be represented by one of two enantiomorphic space groups (see previous). *Metacinnabar*, isometric, is stable above about 344°C. Some Hg deficiency is found in this polymorph and its composition may be represented as $Hg_{1-x}S$, with x ranging from 0 to 0.08.

Diagnostic Features. Recognized by its red color and scarlet streak, high specific gravity, and cleavage.

Occurrence. Cinnabar is the most important ore of mercury but is found in quantity at comparatively few localities. Occurs as impregnations and as vein fillings near recent volcanic rocks and hot springs and evidently deposited near the surface from solutions which were probably alkaline. Associated with pyrite, marcasite, stibnite, and sulfides or copper in a gangue of opal, chalcedony, quartz, barite, calcite, and fluorite.

The important localities for the occurrence of cinnabar are at Almaden, Spain; Idria, Slovenia; and in superb twinned crystals in the provinces of Kweichow and Hunan, China. In the United States deposits are in California at New Idria, and New Almaden.

Use. The only important source of mercury. The principal uses of mercury are in electrical apparatus, industrial control instruments, electrolytic preparation of chlorine and caustic soda, and in mildew proofing of paint. Other lesser but important uses are in dental preparations, scientific instruments, drugs, catalysts, and in agriculture. Formerly a major use of mercury was in the amalgamation process for recovering gold and silver from their ores, but amalgamation has been essentially abandoned in favor of other methods of extraction.

Name. The name *cinnabar* is supposed to have come from India, where it is applied to a red resin.

Realgar—AsS

Crystallography. Monoclinic; $2/m$. Found in short, vertically striated, prismatic crystals (Fig. 15.27). Frequently coarse to fine granular and often earthy and as an incrustation.

$P2_1/n$; $a = 9.29$, $b = 13.53$, $c = 6.57$ Å; $\beta = 106°33'$, $Z = 16$. *ds*: 5.40(10), 3.19(9), 2.94(8), 2.73(8), 2.49(5).

Physical Properties. *Cleavage* {010} good. **H** $1\frac{1}{2}$–2. **G** 3.48. Sectile. *Luster* resinous. *Color* and *streak* red to orange. Translucent to transparent.

Composition and Structure. As 70.1, S 29.9%. The realgar structure contains ringlike groups of As_4S_4, somewhat similar to the rings of S_8 in native sulfur. Each As is bonded covalently to another arsenic as well as to two sulfur atoms.

Diagnostic Features. Realgar is distinguished by its red color, resinous luster, orange-red streak, and almost invariable association with orpiment.

Alteration. On long exposure to light, disintegrates to a reddish-yellow powder.

FIG. 15.27 Realgar.

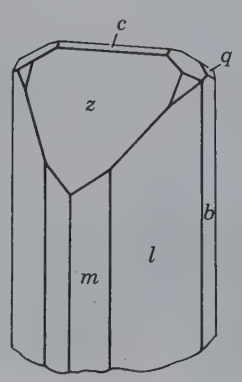

Occurrence. Realgar is found in veins of lead, silver, and gold ores associated with orpiment, other arsenic minerals, and stibnite. It also occurs as a volcanic sublimation product and as a deposit from hot springs.

Found in good crystals at Nagyág, Romania; Binenthal, Switzerland; and Allchar, Macedonia. In the United States realgar is found at Mercur, Utah; at Manhattan, Nevada; and deposited from the geyser waters in the Norris Geyser Basin, Yellowstone National Park.

Use. Realgar was used in fireworks to give a brilliant white light when mixed with saltpeter and ignited. Today, artificial arsenic sulfide is used for this purpose. It was formerly used as a pigment.

Name. The name is derived from the Arabic phrase, *Rahj al ghar*, meaning *powder of the mine*.

Orpiment—As_2S_3

Crystallography. Monoclinic; $2/m$. Crystals small tabular or short prismatic (Fig. 15.28), and rarely distinct; many pseudo-orthorhombic. Usually in foliated or columnar masses.

$P2_1/n$; $a = 11.49$, $b = 9.59$, $c = 4.25$ Å; $\beta = 90°27'$; $Z = 4$. *ds*: 4.78(10), 2.785(4), 2.707(6), 2.446(6), 2.085(4).

Physical Properties. *Cleavage* {010} perfect; cleavage laminae flexible but not elastic. Sectile. **H** $1\frac{1}{2}$–2. **G** 3.49. *Luster* resinous, pearly on cleavage face. *Color* lemon-yellow. *Streak* pale yellow. Translucent.

Composition and Structure. As 61, S 39%. Contains up to 2.7% Sb. In the structure of orpiment trigonal pyramids of AsS_3 can be recognized that share corners to form six-membered rings. These rings are linked to produce a corrugated As_2S_3 layer structure. The bonds within the layers are essentially covalent, whereas those between the layers are van der Waals in nature. The perfect {010} cleavage is parallel to these layers.

Diagnostic Features. Characterized by its yellow color and foliated structure. Distinguished from sulfur by its perfect cleavage.

Occurrence. Orpiment is a rare mineral, associated usually with realgar and formed under similar conditions. Found in good crystals at several localities in Romania and the Czech Republic. In the United States it occurs at Mercur, Utah, and at Manhattan, Nevada. Deposited with realgar from geyser waters in the Norris Geyser Basin, Yellowstone National Park.

Use. Used in dyeing and in a preparation for the removal of hair from skins. Artificial arsenic sulfide is largely used in place of the mineral. Both realgar and orpiment were formerly used as pigments, but this use has been discontinued because of their poisonous nature.

Name. Derived from the Latin word, *auripigmentum*, meaning "golden paint," in allusion to its color and because the substance was supposed to contain gold.

STIBNITE—Sb_2S_3

Crystallography. Orthorhombic; $2/m2/m2/m$. Slender prismatic habit, prism zone vertically striated. Crystals often steeply terminated (Figs. 15.29 and 15.30) and sometimes curved or bent (Fig. 15.30). Often in radiating crystal groups or in bladed forms with prominent cleavage. Massive, coarse to fine granular.

Pbnm; $a = 11.22$, $b = 11.30$, $c = 3.84$ Å; $Z = 4$. *ds*: 5.07(4), 3.58(10), 2.76(3), 2.52(4), 1.933(5).

Physical Properties. *Cleavage* {010} perfect, showing striations parallel to [100]. **H** 2. **G** 4.52–4.62. *Luster* metallic, splendent on cleavage surfaces. *Color* and *streak* lead-gray to black. Opaque (see Plate II, no. 3).

Composition and Structure. Sb 71.4, S 28.6%. May contain small amounts of Au, Ag, Fe, Pb, and Cu. The structure of stibnite is composed if zigzag chains of closely bonded Sb and S atoms that are parallel to the *c* axis. Sb–S distances in the chains range from 2.5Å to 3.1Å; these represent covalent linking. Distances between adjoining bands are larger, ranging from 3.2 to 3.6 Å (see Fig. 15.31). The long, striated prisms (//*c*) of stibnite are parallel to these structural chains. The excellent {010} cleavage occurs between Sb–S chains.

Diagnostic Features. Characterized by its easy fusibility, bladed habit, perfect cleavage in one direction, lead-gray color, and soft black streak. Fusible in a candle flame.

Occurrence. Stibnite is found in low-temperature hydrothermal veins or replacement deposits and in hot spring deposits. It is associated with other antimony minerals that have formed as the product of its decomposition, and with galena, cinnabar, sphalerite, barite, realgar, orpiment, and gold.

There are numerous localities in Romania for well-crystallized stibnite, but the finest crystals have come from the province of Iyo, Island of Shikoku, Japan. The world's most important producing district is in the province of Hunan, China. Found in quantity at only a few localities in the United States, notably Manhattan, Nevada.

FIG. 15.28 Orpiment.

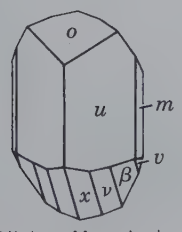

Allchar, Macedonia

FIG. 15.29 Stibnite.

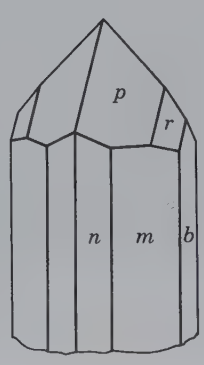

FIG. 15.30 Cluster of stibnite crystals, and a single, curved crystal, Ischinokowa, Japan (Harvard Mineralogical Museum).

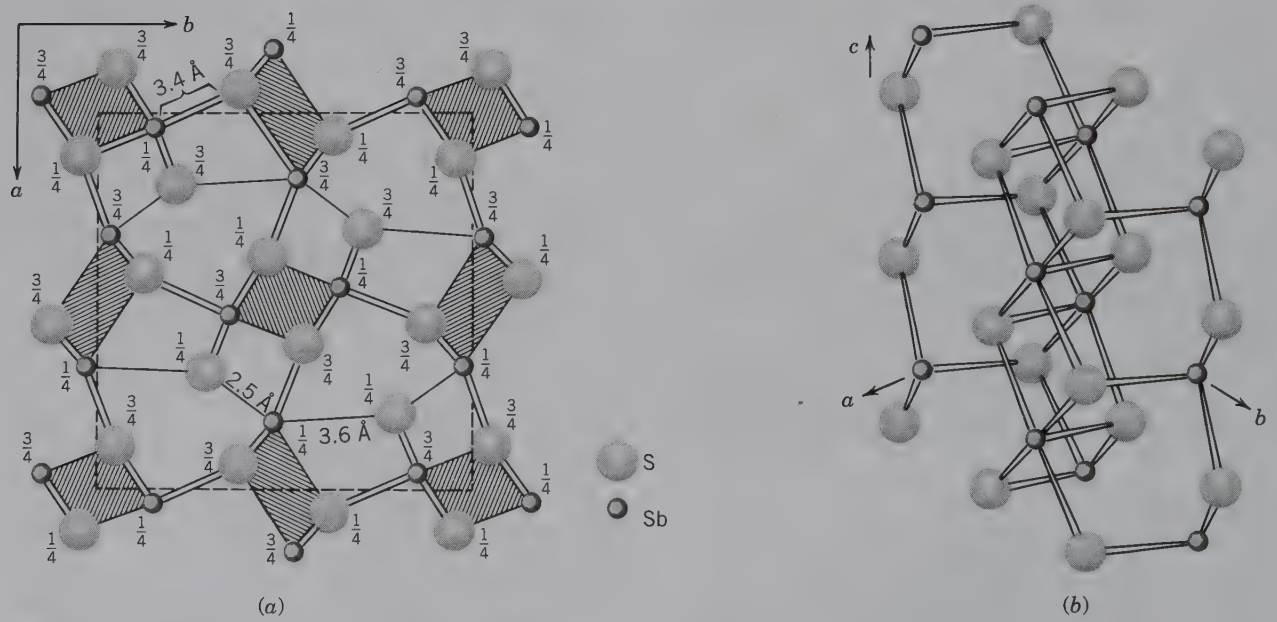

FIG. 15.31 (a) The structure of stibnite, Sb_2S_3, projected on (001). The heights of the atoms are indicated by fractions along the *c* axis. The regions with the lined patterns represent the projections of zigzag chains parallel to the *c* axis. The interatomic distances within the chains are shown as ranging between 2.5 and 3.1 Å; those between chains range from 3.4 to 3.6 Å. (Redrawn after Hellner, E. and G. Leineweber. 1956. Über komplex zusammengesetzte sulfidische Erze. *Zeitschrift für Kristallographie* 107: 105–154.) (b) Representation of one of the zigzag chains in the structure of stibnite.

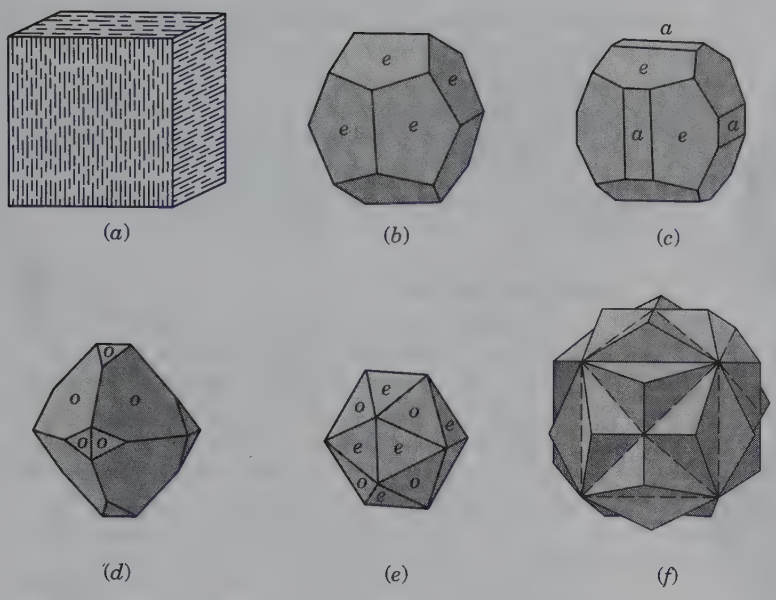

FIG. 15.32 Pyrite crystals. (a) Striated cube. (b) Pyritohedron {210}; (c) Cube and pyritohedron. (d) and (e) Octahedron and pyritohedron. (f) Twinned pyritohedrons, *iron cross*.

Use. The primary ore of antimony but much of the metal is produced as a byproduct from smelting lead ores. Antimony trioxide is used as a pigment and for making glass.

Name. The name *stibnite* comes from an old Greek word that was applied to the mineral.

Similar Species. *Bismuthinite*, Bi_2S_3, is a rare mineral isostructural with stibnite and with similar physical properties.

PYRITE—FeS_2

Crystallography. Isometric; $2/m\bar{3}$. Frequently in crystals (Figs. 15.32, 15.33, and 15.34). The most common forms are the cube, the faces of which are usually striated, the pyritohedron, and the octahedron. Figure 15.32f shows a penetration twin, known as the *iron cross* with [001] the twin axis. Also massive, granular, reniform, globular, and stalactitic.

$Pa3$; a = 5.42 Å; Z = 4. *d*s: 2.70(7), 2.42(6), 2.21(5), 1.917(4), 1.632(10).

Physical Properties. *Fracture* conchoidal. Brittle. **H** 6–6½ (unusually hard for a sulfide). **G** 5.02. *Luster* metallic, splendent. *Color* pale brass-yellow, see Plate II, no. 4; may be darker because of tarnish. *Streak* greenish or brownish-black. Opaque. Paramagnetic.

Composition and Structure. Fe 46.6, S 53.4%. May contain small amounts of Ni and Co. Some analyses show considerable Ni, and a complete solid solution series exists between pyrite and *bravoite*, $(Fe,Ni)S_2$. Frequently carries minute quantities of Au and Cu as microscopic impurities. The structure of pyrite can be considered as a modified NaCl type of structure with Fe in the Na and S_2 in the Cl positions (Fig. 15.8a). FeS_2 occurs in two polymorphs, pyrite and *marcasite*.

Diagnostic Features. Distinguished from chalcopyrite by its paler color and greater hardness, from gold by its brittleness and hardness, and from marcasite by its deeper color and crystal form.

FIG. 15.33 Pyrite cube with quartz. Specimen is from Daye, Hubei, China, and is 6.5 cm high. (Photographs courtesy of Jeff Scovil, collection © Jeff Scovil.)

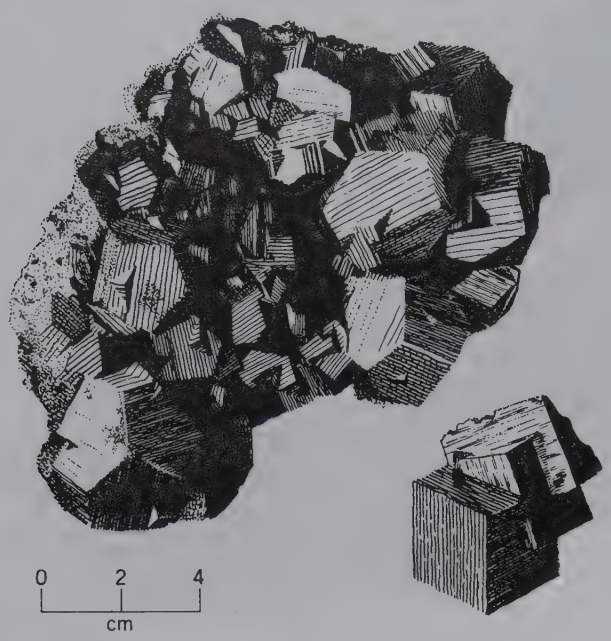

FIG. 15.34 Pyrite (Harvard Mineralogical Museum).

Alteration. Pyrite is easily altered to oxides of iron, usually limonite. In general, however, it is much more stable than marcasite. Pseudomorphic crystals of limonite after pyrite are common. Pyrite veins are usually capped by a cellular deposit of limonite, termed *gossan* (see Box 15.3). Rocks that contain pyrite are unsuitable for structural purposes because the ready oxidation of pyrite would serve both to disintegrate the rock and to stain it with iron oxide.

Occurrence. Pyrite is the most common and widespread of the sulfide minerals and the worldwide occurrences of fine crystals are too many to enumerate. A few of the notable localities of crystals in the United States are: Chester, Vermont; Leadville and Central City, Colorado; and Bingham, Utah. Fine crystals are found in La Libertad and Huanzala, Peru and in China (Fig. 15.33). Sculptural groups of crystals occur at Ambasaguas and Navajun, Spain.

Pyrite has formed at both high and low temperatures, but the largest masses probably at high temperature. It occurs as magmatic segregations, as an accessory mineral in igneous rocks, and in contact metamorphic deposits and hydrothermal veins. Pyrite is a common mineral in sedimentary rocks, being both primary and secondary. It is associated with many minerals but found most frequently with chalcopyrite, sphalerite, and galena.

Large and extensively developed deposits occur at Rio Tinto and elsewhere in Spain and also in Portugal. Important deposits of pyrite in the United States are in Virginia, where it occurs in large lenticular masses that conform in position to the foliation of the enclosing schists; in St. Lawrence County, New York; at the David Mine, near Charlemont, Massachusetts; and in various places in California, Colorado, and Arizona.

Use. Pyrite is often mined for the gold or copper associated with it. Because of the large amount of sulfur present in the mineral, it is used as an iron ore only in those countries where oxide ores are not available. Its chief use is a source of sulfur for sulfuric acid and *copperas* (ferrous sulfate). Copperas is used in dyeing, in the manufacture of inks, as a preservative of wood, and as a disinfectant. Pyrite may be cut as a gemstone which is sold under the name of its polymorph, marcasite.

Name. The name *pyrite* is from a Greek word meaning *fire*, in allusion to the brilliant sparks emitted when struck by steel.

MARCASITE—FeS_2

Crystallography. Orthorhombic; *2/m2/m2/m*. Crystals commonly tabular {010}; less commonly prismatic [001] (Fig. 15.35). Often twinned, giving cockscomb and spear-shaped groups (Figs. 15.36 and 15.37). Usually in radiating forms. Often stalactitic, having an inner core with radiating structure and covered with irregular crystal groups. Also globular and reniform.

Pmnn; $a = 4.45$, $b = 5.42$, $c = 3.39$ Å; $Z = 2$. *ds*: 2.70(10), 2.41(6), 2.32(6), 1.911(5), 1.755(9).

Physical Properties. H $6-\frac{1}{2}$. G 4.89. *Luster* metallic. *Color* pale bronze-yellow to almost white on fresh fracture; hence, called *white iron pyrites*. Yellow to brown tarnish. *Streak* grayish-black. Opaque.

Composition and Structure. Of constant composition, FeS_2, dimorphous with pyrite. The marcasite structure is shown in Fig. 15.8b. The configuration of nearest neighbor atoms is the same as in pyrite. The stability relationships of pyrite and marcasite are still unclear. Experimental evidence indicates that marcasite is metastable relative to pyrite and pyrrhotite above about 157°C. Geological occurrences of marcasite indicate a lower temperature stability range than for pyrite which may occur in magmatic segregations.

Diagnostic Features. Usually recognized and distinguished from pyrite by its pale yellow color, its crystals, or its fibrous habit.

Alteration. Marcasite usually disintegrates more easily than pyrite with the formation of ferrous sulfate and sulfuric acid. The white powder that forms on marcasite is *melanterite*, $FeSO_4 \cdot 7H_2O$.

Occurrence. Marcasite is found in metalliferous veins, frequently with lead and zinc ores. It is less stable than pyrite, being easily decomposed, and is much less common. It is deposited at low temperatures from acid solutions and is commonly formed under surface conditions as a supergene mineral. Flattened spheres of marcasite commonly occur in black shales and are referred to as "pyrite suns." Marcasite most

FIG. 15.35 Marcasite crystals.

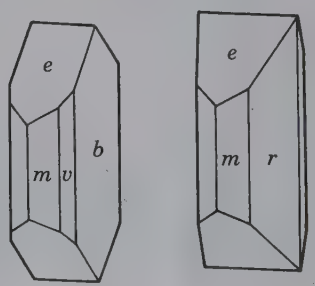

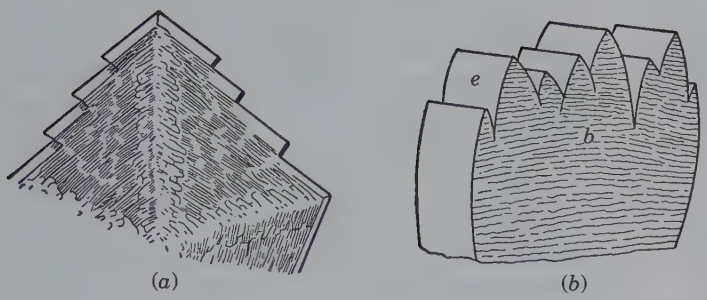

FIG. 15.36 (a) Spear-shaped, twinned and (b) "cockscomb" marcasite.

frequently occurs as replacement deposits in limestone, and often in concretions embedded in clays, marls, and shales.

Found abundantly in clay near Carlsbad and elsewhere in the Czech Republic; in the chalk marl of Folkestone and Dover, England. In the United States, marcasite is found with zinc and lead deposits of the Joplin, Missouri, district; at Mineral Point, Wisconsin; and at Galena, Illinois.

Use. Marcasite is used to a slight extent as a source of sulfur.

Name. Derived from an Arabic word, at one time applied generally to pyrite.

MOLYBDENITE—MoS_2

Crystallography. Hexagonal; *6/m2/m2/m*. Crystals in hexagonal plates or short, slightly tapering prisms. Commonly foliated, massive, or in scales.

$P6_3/mmc$; $a = 3.16$, $c = 12.32$ Å; $Z = 2$. *ds*: 6.28(10), 2.28(9), 1.824(6), 1.578(4), 1.530(4).

Physical Properties. *Cleavage* {0001} perfect, laminae flexible but not elastic. Sectile. **H** 1 –$1\frac{1}{2}$. **G** 4.62–4.73. Greasy feel. *Luster* metallic. *Color* lead-gray (see Plate II, no. 5). *Streak* grayish-black. Opaque.

FIG. 15.37 Spear-shaped twins of marcasite in limestone. Folkstone, England (Harvard Mineralogical Museum).

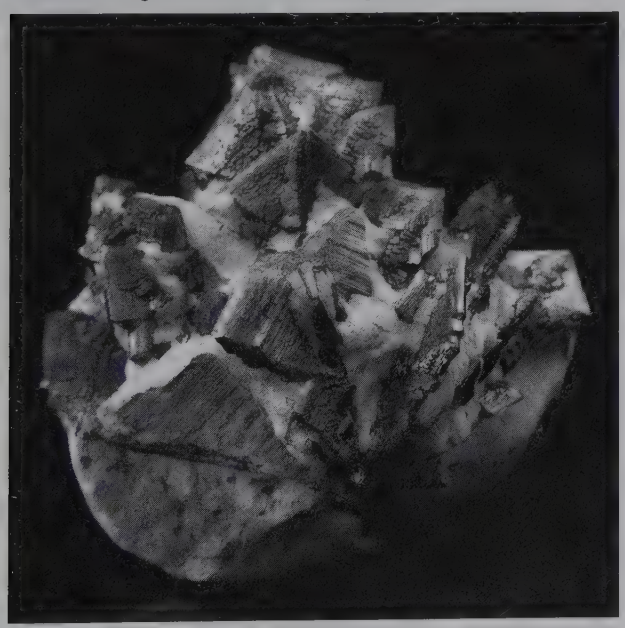

Composition and Structure. Mo 59.9, S 40.1%, of essentially constant composition. In the structure of molybdenite a sheet of Mo atoms is sandwiched between two sheets of S atoms, the three sheets together forming a layered structure. The bond strengths within the layer are much stronger than between the layers, giving rise to the excellent {0001} cleavage. MoS_2 occurs as two polytypes of which one is hexagonal (*2H*) and the other rhombohedral (*3R*).

Diagnostic Features. Resembles graphite but is distinguished from it by higher specific gravity; by a blue tone to its color, whereas graphite has a brown tinge. On unglazed porcelain, it gives a grayish-black streak, graphite a black streak.

Alteration. Molybdenite alters to yellow *ferrimolybdite*, $Fe_2(MoO_4)_3{\cdot}8H_2O$.

Occurrence. Molybdenite forms as an accessory mineral in certain granites; in pegmatites and aplites; also associated with porphyry copper deposits. Commonly in high-temperature vein deposits associated with cassiterite, scheelite, wolframite, and fluorite. Also in contact metamorphic deposits with calcium silicates, scheelite, and chalcopyrite.

Exceptionally good crystals are found at Kingsgate, New South Wales, Australia. In the United States, molybdenite is found in many localities; examples are Okanogan County, Washington, and Questa, New Mexico. From various pegmatites in Ontario, Canada. The bulk of the world's supply comes from Climax, Colorado, where molybdenite occurs in quartz veinlets in silicified granite with fluorite and topaz. Much molybdenum is produced at Bingham Canyon, Utah, as a byproduct of the copper mining.

Use. The principal ore of molybdenum.

Name. The name *molybdenite* comes from the Greek word *molybdos* meaning *lead*.

COBALTITE—CoAsS

Crystallography. Orthorhombic; *mm2*. Pseudoisometric with forms that appear isometric, that is, cubes and pyritohedrons with the faces striated as in pyrite. Also granular.

$Pca2_1$; $a = 5.58$, $b = 5.58$, $c = 5.58$ Å; $Z = 4$. *ds*: 2.77(8), 2.49(10), 2.27(9), 1.680(10), 1.490(8).

Physical Properties. *Cleavage* pseudocubic, perfect. Brittle. **H** $5\frac{1}{2}$. **G** 6.33. *Luster* metallic. *Color* silver-white, inclined to red. *Streak* grayish-black.

Composition and Structure. Usually contains considerable Fe (maximum about 10%) and lesser amounts of Ni. *Gersdorffite*, NiAsS, and cobaltite form a complete solid solution series, but intermediate compositions are rare. The

structure of cobaltite is closely related to that of pyrite (Fig. 15.8a) in which half the S_2 pairs are replaced by As. Such a substitution causes a lowering of the symmetry of the structure of cobaltite as compared to that of pyrite. Natural cobaltites have a somewhat disordered distribution of As and S in the structure.

Diagnostic Features. Although in crystal form cobaltite resembles pyrite, it can be distinguished by its silver color and cleavage.

Occurrence. Cobaltite is usually found in high-temperature deposits, as disseminations in metamorphosed rocks, or in vein deposits with other cobalt and nickel minerals. Notable occurrences of cobaltite are at Tunaberg, Sweden, and Cobalt, Ontario. The largest producer of cobalt today is Democratic Republic of Congo, where oxidized cobalt and copper ores are associated.

Use. An ore of cobalt.

Name. In allusion to its chemistry.

ARSENOPYRITE—FeAsS

Crystallography. Monoclinic; $2/m$, pseudoorthorhombic. Crystals are commonly prismatic elongated on c and less commonly on b (Fig. 15.38). Twinning on {100} and {001} produces pseudo-orthorhombic crystals; on {110} generates contact or penetration twins; may be repeated, as in marcasite.

$P2_1$; $a = 5.74$, $b = 5.67$, $c = 5.78$ Å, $\beta = 112°17'$; $Z = 4$. *ds*: 2.68(10), 2.44(9), 2.418(9), 2.412(9), 1.814(9).

Physical Properties. *Cleavage* {101} poor. **H** $5\frac{1}{2}$–6. **G** 6.07. *Luster* metallic. *Color* silver-white. *Streak* black. Opaque.

Composition and Structure. Close to FeAsS with some variation in As and S contents ranging from $FeAs_{0.9}S_{1.1}$ to $FeAs_{1.1}S_{0.9}$. Cobalt may replace part of the Fe and a series extends to *glaucodot*, (Co,Fe)AsS. The structure of arsenopyrite is a derivative of the marcasite structure type (see Fig. 15.8b) in which one-half of the S is replaced by As.

Diagnostic Features. Distinguished from marcasite by its silver-white color. Its crystal form distinguishes it from skutterudite.

Occurrence. Arsenopyrite is the most common mineral containing arsenic. It occurs with tin and tungsten ores in high-temperature hydrothermal deposits, associated with silver and copper ores, galena, sphalerite, pyrite, chalcopyrite. Frequently associated with gold. Often found sparingly in pegmatites, in contact metamorphic deposits, disseminated in crystalline limestones.

FIG. 15.38 Arsenopyrite crystals.

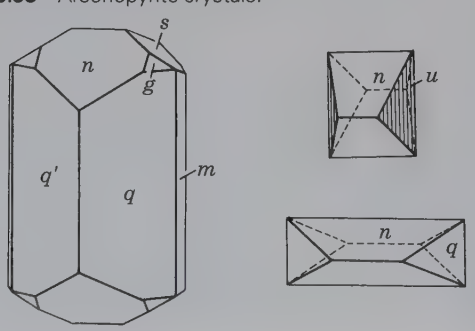

Arsenopyrite is a widespread mineral and is found in considerable abundance in many localities, as at Freiberg and Munzig, Saxony, Germany; with tin ores in Cornwall, England; from Tavistock, Devonshire; in various places in Bolivia. In the United States, it is associated with gold at Lead, South Dakota. Large quantities occur at Deloro, Ontario.

Use. The principal source of arsenic. Most of the arsenic produced is recovered in the form of the oxide, as a byproduct in the smelting of arsenical ores for copper, gold, lead, and silver. Metallic arsenic is used in some alloys, particularly with lead in shot metal. Arsenic is used chiefly, however, in the form of white arsenic or arsenious oxide in medicine, insecticides, preservatives, pigments, and glass. Arsenic sulfides are used in paints and fireworks.

Name. Arsenopyrite is a contraction of the older term *arsenical pyrites*.

SKUTTERUDITE—$CoAs_{2-3}$

Crystallography. Isometric; $2/m\bar{3}$. Common crystal forms are cube and octahedron, more rarely dodecahedron and pyritohedron. Usually massive, dense to granular.

$Im3$; $a = 8.21$–8.29 Å; $Z = 8$; *ds*: 2.61(10), 2.20(8), 1.841(9), 1.681(7), 1.616(9).

Physical Properties. **H** $5\frac{1}{2}$–6. **G** 6.5 ± 0.4. Brittle. *Luster* metallic. *Color* tin-white to silver-gray. *Streak* black. Opaque.

Composition and Structure. Essentially $(Co,Ni)As_3$ but Fe usually substitutes for some Ni or Co. The high nickel varieties are called *nickel skutterudite*, $(Ni,Co)As_3$. A remarkable feature of the structure of skutterudite is the square grouping of As as As_4. The unit cell contains 8(Co + Ni) atoms and six As_4 groups which leads to the formula $(Co,Ni)As_3$. *Smaltite*, $(Co,Ni)As_{3-x}$ and *chloanthite*, $(Co,Ni)As_{3-x}$ (with $x = 0.5 - 1.0$) have skutterudite-like structures but a deficiency of As.

Diagnostic Features. Tin-white to silver-gray color. Chemical tests may be necessary for identification.

Occurrence. Skutterudite is usually found with cobaltite and nickeline in veins formed at moderate temperature. Native silver, bismuth, arsenopyrite, and calcite are also commonly associated with it.

Notable localities are Skutterud, Norway; Annaberg and Schneeberg, in Saxony, Germany; and Cobalt, Ontario, where skutterudite is associated with silver ores. Well-crystallized material is found near Bou Azzer, Morocco.

Use. An ore of cobalt and nickel. Cobalt is primarily used in alloys for making permanent magnets and high-speed tool steel. Cobalt oxide is used as blue pigment in pottery and glassware.

Name. Skutterudite from the locality, Skutterud, Norway.

Similar Species. *Linnaeite*, Co_3S_4, associated with cobalt and nickel minerals.

SULFOSALTS

Enargite—Cu_3AsS_4

Crystallography. Orthorhombic; $mm2$. Crystals elongated parallel to c and vertically striated, also tabular parallel to {001}. Columnar, bladed, massive.

$Pnm2_1$; $a = 6.41$, $b = 7.42$, $c = 6.15$ Å; $Z = 2$. *ds*: 3.22(10), 2.87(8), 1.859(9), 1.731(6), 1.590(5).

Physical Properties. *Cleavage* {110} perfect, {100} and {010} distinct. **H** 3. **G** 4.45. *Luster* metallic. *Color* and *streak* grayish-black to iron-black. Opaque.

Composition and Structure. In Cu_3AsS_4: Cu 48.3, As 19.1, S 32.6%. Sb substitutes for As up to 6% by weight, and some Fe and Zn are usually present. The structure of enargite can be regarded as a derivative of the wurtzite structure (Fig. 15.9), in which $\frac{3}{4}$ of Zn is replaced by Cu and $\frac{1}{4}$ of Zn by As. In chemical terms Zn_4S_4 becomes Cu_3AsS_4. The low-temperature polymorph of Cu_3AsS_4 (stable below 320°C) is *luzonite* with a tetragonal structure ($I\bar{4}m$). *Famatinite*, Cu_3SbS_4, the antimony analogue of enargite is isostructural with luzonite. Extensive solid solution exists in famatinite toward luzonite, and famatinite toward enargite.

Diagnostic Features. Characterized by its color and cleavage. Distinguished from stibnite by a test for Cu.

Occurrence. Enargite is a comparatively rare mineral, found in vein and replacement deposits formed at moderate temperatures associated with pyrite, sphalerite, bornite, galena, tetrahedrite, covellite, and chalcocite.

Notable localities: Morococha, Quiruvilca, and Cerro de Pasco, Peru; also from Chile and Argentina; Island of Luzon, Phillippines. In the United States it was an important ore mineral at Butte, Montana, and to a lesser extent in the Tintic district, Utah. Occurs in the silver mines of the San Juan Mountains, Colorado.

Use. An ore of copper.

Name. From the Greek word *enarges* meaning *distinct*, in allusion to the cleavage.

Pyrargyrite—Ag_3SbS_3, Proustite—Ag_3AsS_3

These minerals are known as the *ruby silvers* and in places have been important ores. They are isostructural with similar crystals forms, physical properties, and occurrences but there is little solid solution between them. Ruby red, hexagonal ($3m$) prismatic crystals make attractive mineral specimens.

Tetrahedrite—$Cu_{12}Sb_4S_{13}$, Tennantite—$Cu_{12}As_4S_{13}$

These two isostructural minerals form a complete solid solution series. They are so similar in crystallographic and physical properties that it is impossible to distinguish them by inspection. They are isometric, $\bar{4}3m$, and frequently occur in tetrahedral crystals (Fig. 15.39). Fe, Zn, and less commonly Ag, Pb, and Hg may substitute for Cu. The argentiferous variety, *freibergite*, may contain 18% Ag and thus become a silver ore.

FIG. 15.39 Tetrahedrite crystals.

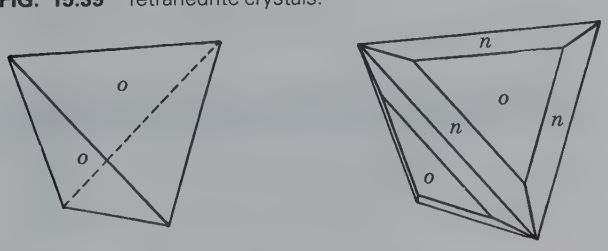

REFERENCES AND FURTHER READING

Anthony, J. W., R. A. Bideaux, K. W. Bladh, and M. C. Nichols. 1990. *Handbook of mineralogy.* Vol. 1, *Elements, sulfides, sulfosalts.* Mineral Data Publications, Tucson, Arizona.

Blackburn, W. H., and W. H. Dennen. 1997. Encyclopedia of mineral names. *The Canadian Mineralogist*, Special publication 1.

Bragg, L., and G. F. Claringbull. 1965. *Crystal structures of minerals.* G. Bell and Sons, Ltd. London.

Cabri, L. J. 1972. The mineralogy of the platinum-group elements. *Minerals Science and Engineering* 4: 3–29.

Deer, W. A., R. A. Howie, and J. Zussman. 1962. *Rock forming minerals.* Vol. 5: *Non-Silicates.* Wiley: New York.

———. 1992. *An introduction to the rock forming minerals.* 2nd ed. Wiley: New York.

Gaines, R. B., H. W. C. Skinner, E. E. Foord, B. Mason, and A. Rosenzweig. 1997. *Dana's new mineralogy.* Wiley: New York.

Gilbert, J. M., and C. F. Park. Jr. 1986. *The geology of ore deposits.* W. J. Freeman and Co., New York.

Harlow, G. E. 1998. *The nature of diamonds.* Cambridge University Press, Cambridge, England.

Mandarino, J. A., and M. E. Back. 2004. *Fleisher's glossary of mineral species.* The Mineralogical Record Inc., Tuczon, Arizona.

Nickel, E. H., and M. C. Nichols. 1991. *Mineral reference manual.* Van Nostrand Reinhold: New York.

Palache, C., H. Berman, and C. Frondel. 1944. *The system of mineralogy.* 7th ed. Vol. 1, *Elements, sulfides, sulfosalts, oxides.* Wiley: New York.

Strunz, H., and Nickel, E. H. 2001. *Strunz Mineralogical Tables.* 9th ed E. Schweizerbart'sche Verlagsbuchhandlung, Stuttgart.

Sulfide mineralogy. 1974 *Reviews in Mineralogy.* Vol. 1. Mineralogical Society of America. Washington, D.C.

Vaughan, D. J., and J. R. Craig. 1978. *Mineral chemistry of metal sulfides.* Cambridge University Press: New York.

Wilks, J., and E. Wilks. 1991. *Properties and applications of diamond.* Butterworth-Heinemann Ltd.: Oxford.

Wilson, W. E. 1982. The gold-containing minerals: A review. *Mineralogical Record* 13: 389–400.

Web Resources

http://webmineral.com/strunz.shtml
http://webmineral.com
http:/www.mindat.org
http://minerals.usgs.gov/minerals/pubs/commodity for the *U.S. Geological Survey, Mineral Commodity Summaries*, January 2005.

CHAPTER 16

Crystal Chemistry and Systematic Descriptions of Oxides, Hydroxides, and Halides

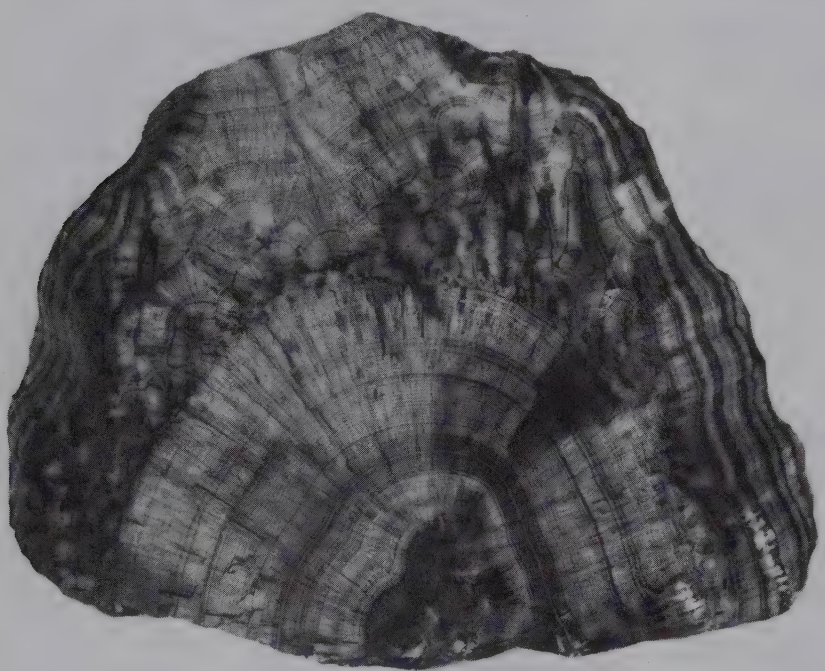

Goethite, α FeO(OH), with a radiating fibrous texture. From an iron ore mine near Negaunce, Michigan (Harvard Mineralogical Museum).

This chapter provides an overview of the crystal chemistry of the most common and/or important oxides, hydroxides, and halides. That is followed by their systematic descriptions. There are 411 known oxides and hydroxides and 150 known halides. Of these, 16 oxides, 6 hydroxides, and 6 halides are covered in detail. Oxides are characterized by oxygen as the anion, hydroxides by the $(OH)^-$ molecules, and halides by a halogen. Each group includes important ore minerals.

The *oxides* are a group of minerals that are relatively hard, dense, and refractory and generally occur as accessory minerals in igneous and metamorphic rocks and as resistant detrital grains in sediments. The *hydroxides* tend to be lower in hardness and density and are found mainly as secondary alteration or weathering products. The *halides* comprise about 150 chemically related minerals with diverse structure types and of diverse geological origins.

CRYSTAL CHEMISTRY OF OXIDES

The oxide minerals include those natural compounds in which oxygen is combined with one or more metals.

They are here grouped as simple oxides and multiple oxides. The simple oxides, compounds of one metal and oxygen, are of several types with different X:O ratios (the ratio of metal to oxygen) as X_2O, XO, X_2O_3. Although not described on the following pages, ice, H_2O (see Fig. 3.26d and also the structure illustration at the very beginning of Chapter 3), is a simple oxide of the X_2O type in which hydrogen is the cation. The most common of all oxides, SiO_2, is not considered here, but instead is treated in Chapters 18 and 19 with the silicates because the structure of quartz and its polymorphs is most closely related to that of other Si–O compounds. The multiple oxides, XY_2O_4, have two nonequivalent metal atom sites (A and B). Within the oxide class are several minerals of economic importance. These include the ores of iron (hematite, magnetite, and goethite), chromium (chromite), manganese (pyrolusite), as well as manganite, and romanechite, tin (cassiterite), and uranium (uraninite).

The bond type in oxide structures is generally strongly ionic, in contrast to the sulfide structures with ionic, covalent, as well as metallic bonding. One of the first structure determinations reported by Sir Lawrence Bragg in 1916 was that of cuprite, Cu_2O, in which the oxygen atoms are arranged at the corners and center of tetrahedral groups. The Cu atoms lie halfway between the oxygens (see Fig. 16.1) within the tetrahedral groups. The oxide mineral structures that will be discussed in this section are listed in the table below.

***X_2O* and *XO* types**			
Cuprite	Cu_2O		
Periclase	MgO		
(Zincite	ZnO)		
***X_2O_3* type**		***XY_2O_4* type**	
Hematite Group		Spinel Group	
Corundum	Al_2O_3	Spinel	$MgAl_2O_4$
Hematite	Fe_2O_3	Gahnite	$ZnAl_2O_4$
Ilmenite	$FeTiO_3$	Magnetite	Fe_3O_4
		Franklinite	(Zn,Fe,Mn)-$(Fe,Mn)_2O_4$
		Chromite	$FeCr_2O_4$
***XO_2* type (excluding SiO_2)**			
Rutile Group			
Rutile	TiO_2	Chrysoberyl	$BeAl_2O_4$
Pyrolusite	MnO_2	Ferrocolumbite	(Fe,Mn)-$(Nb,Ta)_2O_6$
Cassiterite	SnO_2		
Uraninite	UO_2		

The structures of the *hematite group* are based on hexagonal closest packing of oxygens with the cations in octahedral coordination between them (see Fig. 16.2a as well as various animations of the corundum, Al_2O_3, structure in module III of the CD-ROM under the title of "Three-dimensional Order: Space Group Elements in Structures"). As can be seen in a basal projection of this structure, only $\frac{2}{3}$ of the octahedral spaces are occupied by Fe^{3+} or Al^{3+}. The presence of $\frac{1}{3}$ oxygen octahedra without central Al^{3+} or Fe^{3+} ions is related to the electrostatic valency (e.v.) or bond strength of the Al^{3+}–O^{2-} and Fe^{3+}–O^{2-} bonds. Because Al^{3+} is surrounded by six oxygens, the e.v. of each of the six Al–O bonds = $\frac{1}{2}$. Each oxygen is shared between four octahedra, which means that four bonds of e.v. = $\frac{1}{2}$ can radiate from an oxygen position. In the (0001) plane, as in Fig. 16.2a, this allows for only *two* Al–O bonds from each oxygen, as shown by the geometry of two octahedra sharing one oxygen corner. A vertical section through the corundum (or hematite) structure (Fig. 16.2b) shows the arrangement of the Al^{3+} (or Fe^{3+}) ions and of the omitted cations as well. In the vertical stacking of octahedra, each octahedron shares a face between two adjoining layers. The cations, Al^{3+} or Fe^{3+}, within the octahedra that share faces will tend to move away from the shared face because of the repulsive forces between them. The corundum and hematite structures have space group $R\bar{3}m$. The ilmenite structure, in which Fe and Ti are arranged in alternating Fe–O and Ti–O layers (Fig. 16.2c), has a lower symmetry (space group $R\bar{3}$) because of the ordered Fe and Ti substitution for Al^{3+} (as in corundum) or Fe^{3+} (as in hematite).

The structure of periclase, MgO, is identical to that of NaCl with cubic space group $Fm3m$. In a section parallel to {111} this structure appears similar (see Fig. 16.3) to that of members of the *hematite group*. In this section a "layer" of octahedra is fully occupied. With Mg in 6-coordination, the e.v. of each of the Mg–O bonds is $\frac{1}{3}$. This allows for six bonds, each with

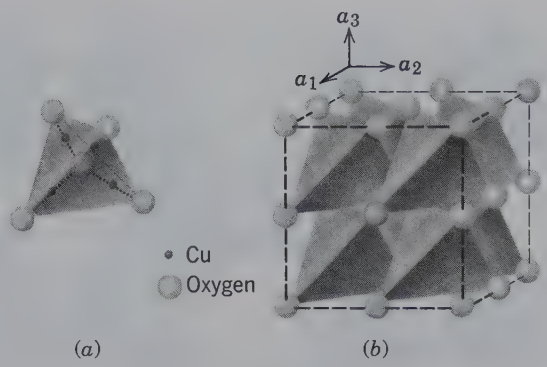

FIG. 16.1 Structure of cuprite. (a) Oxygen atoms at the corners and the center of a tetrahedral group; Cu halfway between two oxygens. (b) Oxygens in a cubic lattice, as shown in a polyhedral representation of the cuprite structure.

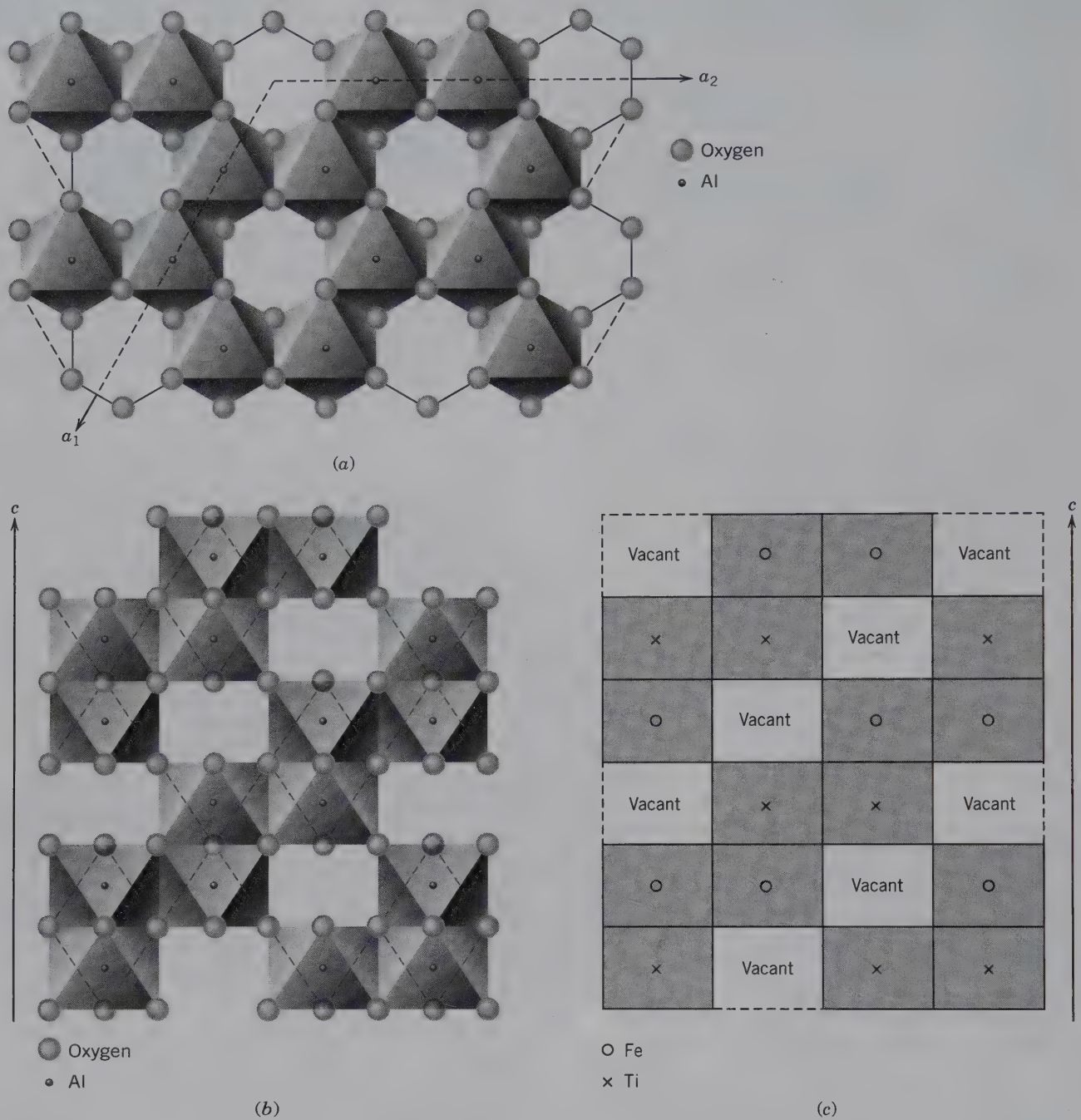

FIG. 16.2 Structures of the hematite group. (a) Basal sheet of octahedra in corundum, Al_2O_3, or hematite, Fe_2O_3, with one octahedron vacant for every two octahedra with Al or Fe^{3+} in center. (b) Vertical section through the corundum structure showing the locations of filled and empty octahedra. (c) Schematic vertical cross section through the ilmenite structure. This representation is the same as in Fig. 16.2b with oxygen positions and octahedral outlines eliminated; only cation locations are shown.

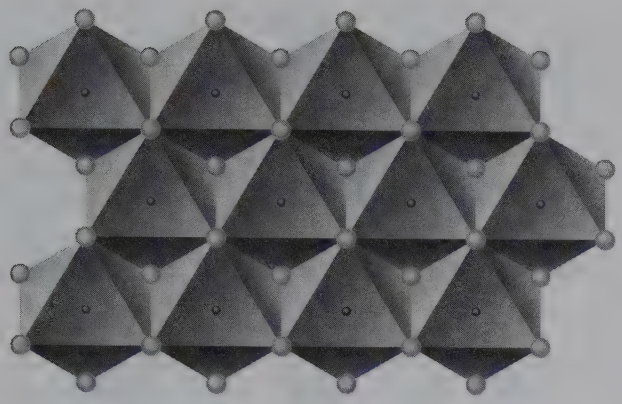

FIG. 16.3 Structure of periclase, MgO, as seen parallel to (111). Compare this with Fig. 16.2a as well as with Fig. 16.7, of brucite.

e.v. $= \frac{1}{3}$, to radiate from every oxygen ion in the structure. Each oxygen is shared between six Mg–O octahedra, and not between just four Al–O (or Fe–O) octahedra as in the structures of the *hematite group*. The MgO type of structure, therefore, shows no cation vacancies.

The structures of XO_2-type oxides to be considered fall into two structure types. One is the structure typified by *rutile*, in which the cation is in 6-coordination with oxygen. The radius ratio, $R_X:R_O$, in this structure lies approximately between the limits of 0.732 and 0.414 (see Table 16.1). The other has the *fluorite* structure (see Fig. 16.11), in which each oxygen has four cation neighbors arranged about it at the apices of a more or less regular tetrahedron, whereas each cation has eight oxygens surrounding it at the corners of a cube. The oxides of 4-valent uranium, thorium, and cerium, of interest because of their connection with nuclear chemistry, have this structure. In general, all dioxides with radius ratios close to the limits for 8-coordination (0.732–1) are expected to have this structure and to be isometric hexoctahedral (see Table 16.1).

Table 16.1 Radius Ratios in XO_2 Type Oxides ($R_{oxygen} = 1.36$ Å)

R_x	[C.N.]	R_x/R_O	Ion	Mineral	Structure Type
0.53	[6]	0.39	Mn^{4+}	Pyrolusite	Rutile
0.61	[6]	0.45	Ti^{4+}	Rutile	Rutile
0.69	[6]	0.51	Sn^{4+}	Cassiterite	Rutile
0.97	[8]	0.71	Ce^{4+}	Cerianite	Fluorite
1.00	[8]	0.74	U^{4+}	Uraninite	Fluorite
1.05	[8]	0.77	Th^{4+}	Thorianite	Fluorite

The members of the *rutile group* are isostructural with space group $P4_2/mnm$. (Rutile has two polymorphs, anatase and brookite, with slightly different structures.) In the rutile structure (see Figs. 16.4 and 4.21) Ti^{4+} is located at the center of oxygen octahedra, the edges of which are shared forming chains parallel to the *c* axis. These chains are cross-linked by the sharing of octahedral corners (see Fig. 16.4b). Each oxygen is linked to three titanium ions and the e.v. of each of

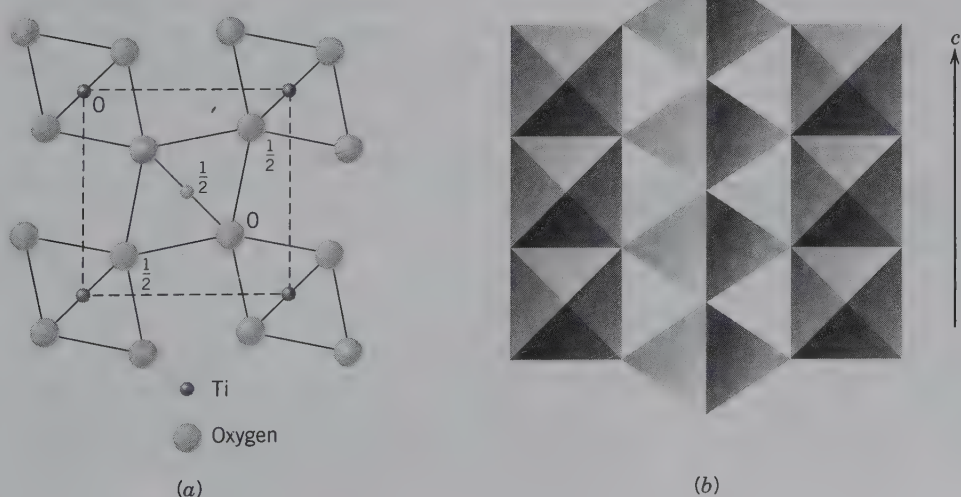

FIG. 16.4 Structure of rutile. (a) Projection on (001) showing location of Ti and O atoms and the outline of the unit cell (dashed lines). (b) Projection on (110) showing chains of octahedra parallel to *c*. Compare these illustrations with Fig. 4.21.

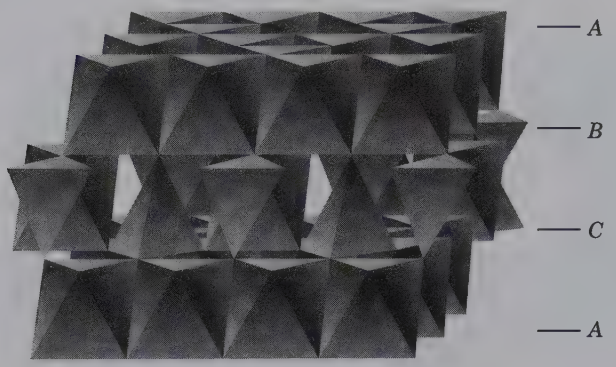

FIG. 16.5 The spinel (AB_2O_4) structure ($F4_1/d\bar{3}2/m = Fd3m$) with alternating layers parallel to {111} of octahedral and octahedral-tetrahedral polyhedra, as based upon approximate cubic closest packing. (From Waychunas, G. A., 1991. Crystal chemistry of oxides and hydroxides. *Oxide Minerals. Reviews in Mineralogy* 25. Mineralogical Society of America, Washington, D.C.)

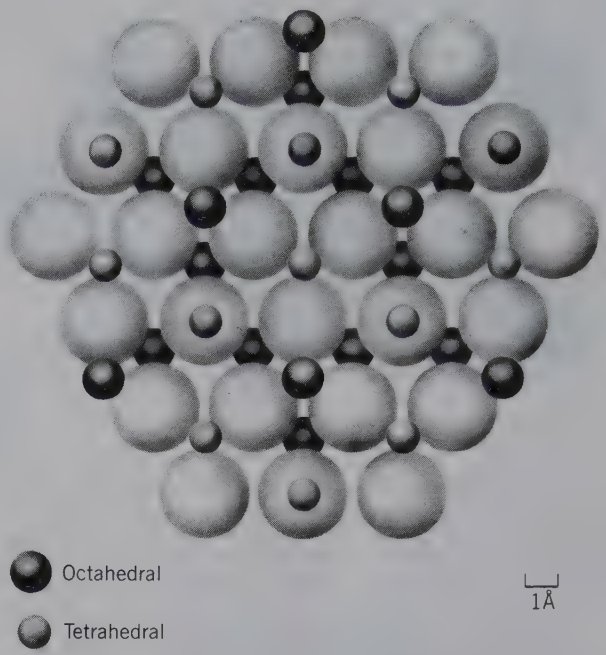

FIG. 16.6 An oxygen layer in the spinel structure, projected onto the (111) plane. See Fig. 16.5 for the position of such planes in the structure. The large circles are oxygen in approximate cubic closest packing. The cation layers on either side of the oxygen layer are shown as well. (Redrawn after Lindsley, D. H. 1976. The crystal chemistry and structure of oxide minerals as exemplified by the Fe-Ti oxides. *Oxide Minerals, Reviews in Mineralogy* 3. Mineralogical Society of America, Washington, D.C.)

the Ti–O bonds = $\frac{2}{3}$. The prismatic habit of minerals of the rutile group is a reflection of the chainlike arrangement of octahedra.

The minerals of the *spinel group*, with the general formula XY_2O_4, are based on an arrangement of oxygens in approximate cubic closest packing along (111) planes in the structure (see Fig. 16.5). Several end members are listed in Table 16.2. The cations that are interstitial to the oxygen framework are in octahedral and tetrahedral coordination polyhedra with oxygen. In a unit cell of spinel, with edge length of approximately 8 Å, there are 32 possible octahedral sites and 64 possible tetrahedral sites; of these, 16 octahedral and 8 tetrahedral sites are occupied by cations. Occupied octahedra are joined along edges to form rows and planes parallel to {111} of the structure and occupied tetrahedra, with their apices along $\bar{3}$ axes, provide cross-links between layers of octahedra (see Fig. 16.5). A plan view of an oxygen layer parallel to (111), and its coordination with cations, is given in Fig. 16.6.

The general chemical formula of the spinel group is XY_2O_4 (or $X_8Y_{16}O_{32}$ per unit cell), where X and Y are various cations with variable valence. In magnetite, $X = Fe^{2+}$ and $Y = Fe^{3+}$, whereas in ulvöspinel, $X = Ti^{4+}$, and $Y = Fe^{2+}$. There are two types of spinel structures, and these are referred to as the "normal spinel" and the "inverse spinel" structures. In the normal spinel structure, the eight X cations occupy the 8 tetrahedral sites and the Y cations occupy the 16 octahedral sites, giving the formula $X_8Y_{16}O_{32}$ (which is equivalent to XY_2O_4). In the inverse spinel structure 8 of the 16 Y cations occupy the eight tetrahedral sites, resulting in the formula $Y(YX)O_4$ (see Table 16.2). Most naturally occurring spinels have cation distributions between the normal and inverse structure types.

Table 16.2 End Members of the Spinel Group (XY_2O_4)

Normal Spinel Structure		Inverse Spinel Structure	
Spinel	$MgAl_2^{3+}O_4$	Magnetite	$Fe^{3+}(Fe^{2+}Fe^{3+})O_4$
Hercynite	$FeAl_2^{3+}O_4$	Magnesioferrite	$Fe^{3+}(Mg^{2+}Fe^{3+})O_4$
Gahnite	$ZnAl_2^{3+}O_4$	Jacobsite	$Fe^{3+}(Mn^{2+}Fe^{3+})O_4$
Galaxite	$MnAl_2^{3+}O_4$	Ulvöspinel	$Fe^{2+}(Fe^{2+}Ti^{4+})O_4$
Franklinite	$ZnFe_2^{3+}O_4$		
Chromite	$Fe^{2+}Cr_2^{3+}O_4$		
Magnesiochromite	$Mg^{2+}Cr_2^{3+}O_4$		

The coordination polyhedra about the various cations in spinel are not what might be predicted on the basis of the ionic sizes of the cations. Because Mg^{2+} is larger than Al^{3+}, Mg is expected to occur in octahedral and Al in tetrahedral coordination with oxygen. In the normal spinel structure, however, the general concepts of radius ratio do not apply. Rather, the larger cation is in the smaller polyhedron, and vice versa. Crystal field stabilization energies (Chapter 10) are the cause of this deviation.

The spinel structure has a coordination scheme similar to that of the silicates of the olivine series (discussed in Chapter 18). The composition of members of the forsterite-fayalite series with a total solid solution series from Mg_2SiO_4 to Fe_2SiO_4 can be represented as $X_2^{2+}Y^{4+}O_4$. Although this is not the same as $X^{2+}Y_2^{3+}O_4$ as in spinel, the total cation charge is identical. The spinel structure is, however, about 12% denser than the olivine structure for the same composition. This observation has led petrologists to suggest that olivine, which is thought to be abundant in the mantle, is converted to spinel-type structures at great depth. Two of the high-pressure olivine polymorphs are known as *ringwoodite* and *wadsleyite*, respectively. In 1969, an olivine, *ringwoodite*, from a stony meteorite, was found to have a spinel structure. This same olivine composition $(Fe_{0.7}Mg_{0.3})_2SiO_4$ had been previously synthesized as a spinel in the laboratory of A. E. Ringwood, Australian National University, Canberra, Australia.

CRYSTAL CHEMISTRY OF HYDROXIDES

The hydroxide minerals considered in this section are:

Brucite	$Mg(OH)_2$
Manganite	$MnO(OH)$
Romanechite	$(Ba,H_2O)_2(Mn^{4+},Mn^{3+})_5O_{10}$
Goethite Group	
Diaspore	α AlO(OH)
Goethite	α FeO(OH)
Bauxite—mixture of diaspore, gibbsite, and boehmite	

All minerals in this group are characterized by the presence of the hydroxyl $(OH)^-$ group, or H_2O molecules. The $(OH)^-$ groups cause the bond strengths in these structures generally to be much weaker than in the oxides.

The structure of *brucite* (see Fig. 16.7) consists of Mg^{2+} octahedrally coordinated to $(OH)^-$, with the octahedra sharing edges to form a layer. Because each $(OH)^-$ group is shared between three adjoining octahedra, the Mg^{2+} to $(OH)^-$ bond strengths have an e.v. $= \frac{1}{3}$. With three such bonds $(3 \times \frac{1}{3} = 1)$, the $(OH)^-$ group is neutralized. For this reason, the layers in the brucite structure are held together by only weak bonds (compare Fig. 16.7 with Fig. 16.3). The structure of *gibbsite*, $Al(OH)_3$, is similar to that of brucite except that, because of charge requirements, $\frac{1}{3}$ of the octahedrally coordinated cation positions are vacant (see Fig. 16.2a). A basal structural layer in corundum (as in Fig. 16.2) is structurally equivalent to the Al–OH sheets in gibbsite. The brucite structure type is referred to as *trioctahedral* (each $(OH)^-$ group is surrounded by three occupied octahedral positions) and the gibbsite structure type as *dioctahedral* (only two out of three octahedrally coordinated cation sites are filled). Such trioctahedral and dioctahedral layers are essential building units of the phyllosilicates (see page 457).

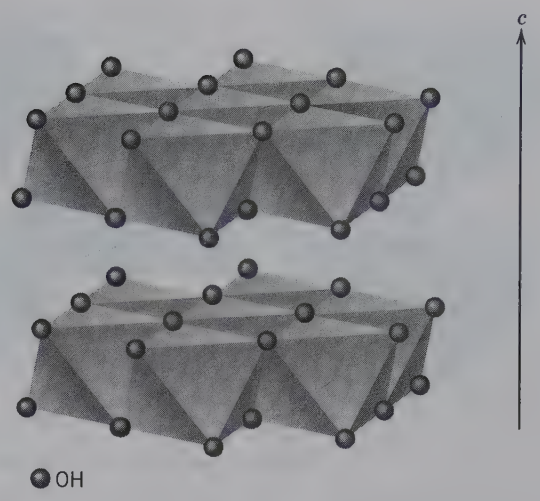

FIG. 16.7 Structure of brucite, composed of parallel layers of Mg^{2+} in octahedral coordination with $(OH)^-$. Large spacing along the *c* axis is caused by weak bonding between adjacent layers.

The structure of *diaspore* (αAlO(OH); space group *Pbnm*) is shown in Fig. 16.8. Oxygen and $(OH)^-$ groups are arranged in hexagonal closest packing with Al^{3+} in octahedral coordination between them. A chainlike pattern is produced by $Al(O,OH)_6$ octahedra extending along the *c* axis. The octahedra in each chain share edges, and the chains are joined to each other by adjoining apical oxygens. *Goethite*, αFeO(OH), is isostructural with diaspore. Both compositions, AlO(OH) and FeO(OH), occur in nature in two crystal forms, γAlO(OH), *boehmite*, and γFeO(OH), *lepidochrocite*, both with space group *Amam*. They show a somewhat different linkage of the octahedrally coordinated cations from that found in diaspore or goethite as seen in Fig. 16.9. The octahedra are linked by their apices to form chains; the chains, in turn, are joined by the

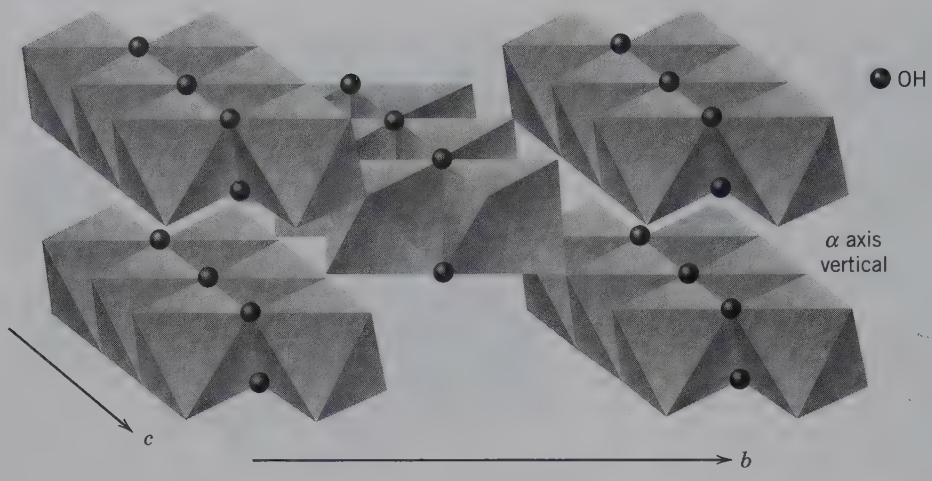

FIG. 16.8 The structure of diaspore, αAlO(OH), and goethite, αFeO(OH). The double chains of $AlO_3(OH)_3$ or $FeO_3(OH)_3$ octahedra run parallel to the *c* axis. Only (OH) groups are indicated; all unmarked apices of octahedra represent oxygen.

sharing of octahedral edges, which result in corrugated sheets parallel to {010}. The sheets are weakly held together by hydrogen bonds between pairs of oxygens. Such bonding is represented as $(OH)^-$ groups in Fig. 16.9.

CRYSTAL CHEMISTRY OF HALIDES

The chemical class of halides is characterized by the dominance of the electronegative halogen ions, Cl^-, Br^-, F^-, and I^-. These ions are large, have a charge of only −1, and are easily polarized. When they combine with relatively large, weakly polarized cations of low valence, both cations and anions behave as almost perfectly spherical bodies. The packing of these spherical units leads to structures of the highest possible symmetry (point group $4/m\bar{3}2/m$).

The structure of NaCl, shown in Figs. 16.10 and 4.17, was the first to be determined by X-ray diffraction techniques by W. H. and W. L. Bragg in 1913. The arrangement of the ions in the structure showed unambiguously that no molecules exist in the NaCl structure. Each cation and each anion is surrounded by six closest neighbors in octahedral coordination. Many halides of the *XZ* type crystallize with the NaCl structure (see Fig. 4.17); some mineral examples are, *sylvite*, KCl, *carobbiite*, KF and *chlorargyrite*, AgCl. Some *XZ* sulfides and oxides that have the NaCl-type structure are *galena*, PbS, *alabandite*, MnS, and *periclase*, MgO.

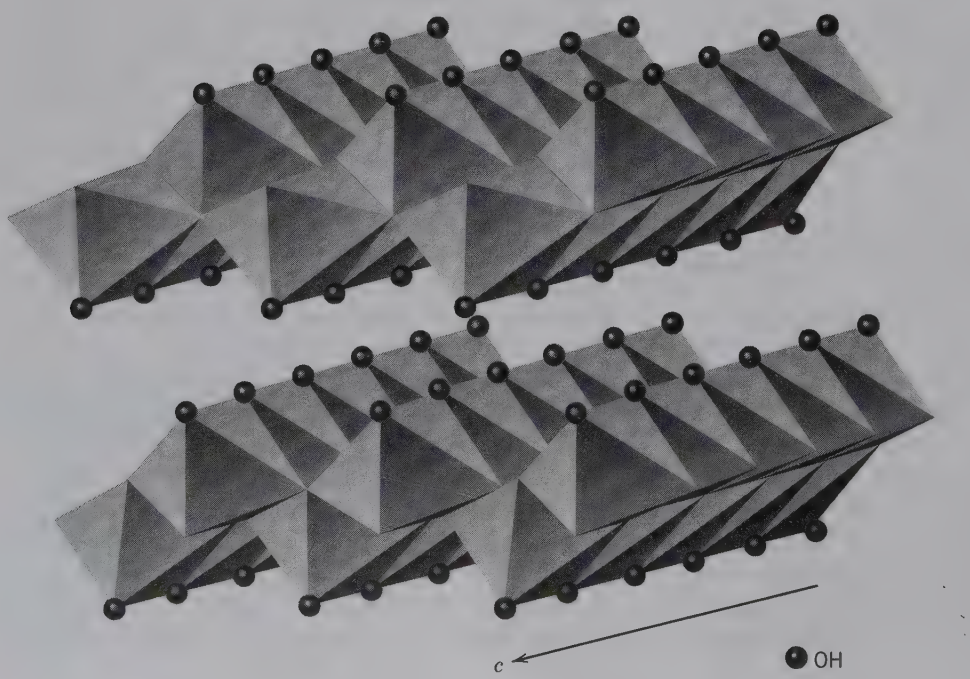

FIG. 16.9 The structure of boehmite, γAlO(OH) and lepidocrocite, γFeO(OH), showing the arrangement of $AlO_4(OH)_2$ or $FeO_4(OH)_2$ octahedra. The corrugated sheets are parallel to (010). Only (OH) groups are indicated; all unmarked apices of octahedra represent oxygen.

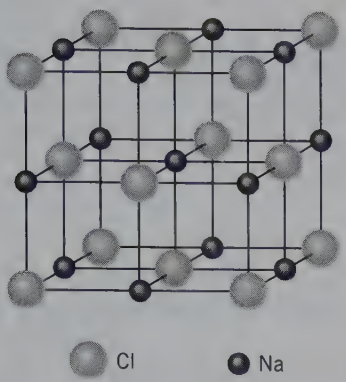

FIG. 16.10 The structure of halite. Compare this illustration with Fig. 4.17.

Several alkali halides, such as CsCl, CsBr, and CsI, none of which is naturally occurring, do not have the NaCl type structure but crystallize with a geometric arrangement of eight closest neighbors (cubic coordination) around the cation as well as the anion. This is known as the CsCl-structure type (see Fig. 4.18). The radius ratio (R_X:R_Z) is the primary factor in determining which of the two structure types is adopted by a given alkali halide of the *XZ* type.

The structures of several of the XZ_2 halides are identical to that of fluorite, CaF_2 (see Fig. 16.11), in which the Ca^{2+} ions are arranged at the corners and face centers of a cubic unit cell. F^- ions are tetrahedrally coordinated to four Ca^{2+}. Each Ca^{2+} is coordinated to eight F^-, which surround it at the corners of a cube. The radius ratio ($R_{Ca^{2+}}$:R_{F^-} = 0.752) leads to 8-coordination for Ca. Several oxides, such as *uraninite*, UO_2, and *thorianite*, ThO_2, have a fluorite-type structure.

Because the weak electrostatic charges are distributed over the entire surface of the nearly spherical ions, the halides are the most perfect examples of pure ionic bonding. The isometric halides all have relatively low hardness and moderate to high melting points and are poor conductors of heat and electricity in the solid state. Any conduction of electricity that takes place does so by electrolysis—that is, by transport of charges by ions rather than by electrons. As the temperature increases and ions are liberated by thermal disorder, electrical conductivity increases rapidly, becoming excellent in the molten state. Commercial methods take advantage of this conductivity in the preparation of sodium and chlorine by electrolysis of molten sodium chloride.

FIG. 16.11 The structure of fluorite. Compare this illustration with Fig. 4.20.

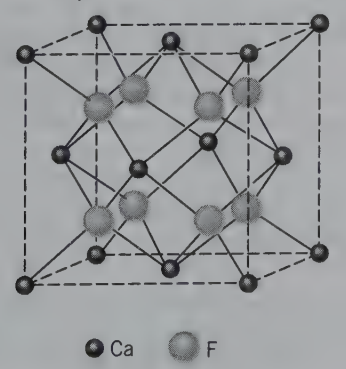

When the halogen ions are combined with smaller and more strongly polarizing cations than those of the alkali metals, structures of lower symmetry result, and the bond has more covalent properties. In such structures, water or hydroxyl may enter as essential constituents, as in the mineral atacamite. Although there are 150 halide species, only 6 are considered in detail.

SYSTEMATIC DESCRIPTIONS

OXIDES

Cuprite—Cu_2O

Crystallography. Isometric; $4/m\bar{3}2/m$. Commonly occurs in crystals showing the cube, octahedron, and dodecahedron, frequently in combination (Fig. 16.12). Sometimes in elongated capillary crystals, known as "plush copper" or *chalcotrichite*.

*Pn*3*m*; a = 4.27 Å; Z = 2. *ds*: 2.46(10), 2.13(6), 1.506(5), 1.284(4), 0.978(3).

Physical Properties. H $3\frac{1}{2}$–4. G 6.1. *Luster* metallic-adamantine in clear crystallized varieties. *Color* red of various shades; ruby-red in transparent crystals, called "ruby copper." *Streak* brownish-red.

Composition and Structure. Cu 88.8, O 11.2%. Usually pure, but FeO may be present as an impurity. The structure, as based on O atoms at the corners and centers of tetrahedral groups, is shown in Fig. 16.1.

Diagnostic Features. Usually distinguished by its red color, and from other red minerals by its crystal form, high luster, streak, and association with limonite.

Occurrence. Cuprite is a supergene copper mineral and in places an important copper ore. It is found in the upper oxidized portions of copper veins, associated with limonite and secondary copper minerals, such as native copper, chalcocite, malachite, azurite, and chrysocolla (see Box 15.3).

FIG. 16.12 Cuprite crystals.

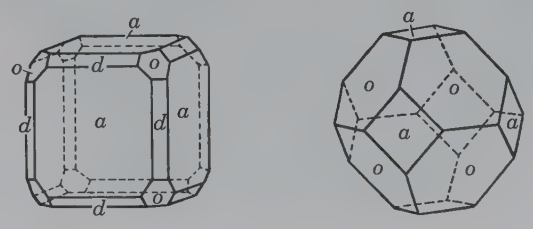

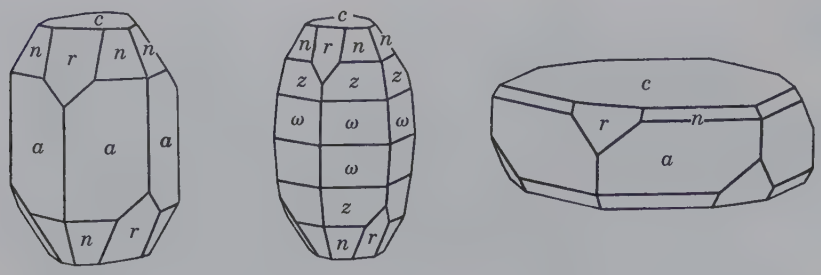

FIG. 16.13 Corundum crystals.

Noteworthy countries where cuprite is an ore are Chile, Bolivia, Australia, and Congo. Fine crystals have been found at Cornwall, England; Chessy, France; and the Onganja Mine and Tsumeb, Namibia. Found in the United States in excellent crystals in the copper deposits at Bisbee, Arizona, and Chino at Santa Rita, New Mexico. Also found at Clifton and Morenci, Arizona.

Use. A minor ore of copper.

Name. Derived from the Latin word *cuprum*, meaning *copper*.

Similar Species. *Tenorite*, CuO, is a black supergene mineral.

Zincite—ZnO

Crystallography. Hexagonal; *6mm*. Crystals are rare, terminated at one end by faces of a steep pyramid and the other by a pedion. Usually massive with platy or granular appearance.

$P6_3mc$; $a = 3.25$, $c = 5.19$ Å; $Z = 2$. *ds*: 2.83(7), 2.62(5), 2.49(10), 1.634(6), 1.486(6).

Physical Properties. *Cleavage* $\{10\bar{1}0\}$ perfect; {0001} parting. **H** 4. **G** 5.68. *Luster* subadamantine. *Color* deep red to orange-yellow. *Streak* orange-yellow. Translucent. *Optics*: (+) $\omega = 2.013$, $\epsilon = 2.029$.

Composition and Structure. Zn 80.3, O 19.7%. Mn^{2+} often present and probably colors the mineral; pure ZnO is white. The structure of zincite is similar to that of wurtzite (see Fig. 15.6). Zn is in hexagonal closest packing and each oxygen lies within a tetrahedral group of four Zn ions.

Diagnostic Features. Distinguished by its red color, orange-yellow streak, and the association with franklinite and willemite.

Occurrence. Zincite is confined almost exclusively to the zinc deposits at Franklin and Sterling Hill, New Jersey, where it is associated with franklinite and willemite in calcite, often in an intimate mixture. Reported only in small amounts from other localities.

Use. An ore of zinc, particularly used for the production of zinc white (zinc oxide).

Similar Species. *Periclase*, MgO, is another oxide of *X*O composition. The structure of MgO is of the NaCl type with space group $Fm3m$. Continuous octahedral sheets can be identified in the structure parallel to {111}, see Fig. 16.3. It is found in contact metamorphosed Mg-rich limestones by the reaction: $CaMg(CO_3)_2 \rightarrow CaCO_3 + MgO + CO_2$.

HEMATITE GROUP, X_2O_3[1]

CORUNDUM—Al_2O_3

Crystallography. Hexagonal; $\bar{3}2/m$. Crystals are commonly tabular on {0001} or prismatic $\{11\bar{2}0\}$. Often tapering hexagonal dipyramids (Fig. 16.13), rounded into barrel shapes with deep horizontal striations. May show rhombohedral faces. Usually poorly crystallized or massive; coarse or fine granular. Polysynthetic twinning is common on $\{10\bar{1}1\}$ and {0001}.

$R\bar{3}c$; $a = 4.76$, $c = 12.98$ Å; $Z = 6$. *ds*: 2.54(6), 2.08(9), 1.738(5), 1.599(10), 1.374(7).

Physical Properties. Parting on {0001} and $\{10\bar{1}1\}$, the latter giving nearly cubic angles; more rarely prismatic parting. **H** 9. Corundum may alter to mica, and care should be taken to obtain a fresh surface for a hardness test. **G** 4.02. *Luster* adamantine to vitreous to dull. Transparent to translucent. *Color* usually some shade of brown, pink, or blue, but may be colorless or any color. Colors may vary in a single crystal. *Ruby* is red gem corundum, see Plate II, no. 6; *sapphire* is gem corundum of any other color. Rubies and sapphires having a stellate opalescence when viewed in the direction of the *c* crystal axis are termed *star ruby* or *star sapphire* (see Fig. 2.10). *Emery* is a black granular corundum intimately mixed with magnetite, hematite, or hercynite. *Optics*: (−), $\omega = 1.769$, $\epsilon = 1.760$.

Composition and Structure. Al 52.9, O 47.1%. Rubies contain trace amounts of Cr (ppm) as a coloring agent and sapphires are blue due to trace amounts of Fe and Ti (see pages 238 and 239). The structure of corundum (Fig. 16.2) consists of oxygen in hexagonal closest packing and Al in octahedral coordination. Two-thirds of the octahedra are occupied by Al and $\frac{1}{3}$ are vacant (see also discussion on page 369).

Diagnostic Features. Characterized by its great hardness, high luster, specific gravity, and parting. Infusible.

Occurrence. Corundum is found in silica-deficient, aluminum-rich rocks, most commonly metamorphosed bauxites. Also found as an accessory mineral in some metamorphic rocks, such as recrystallized limestone, mica-schist, gneiss; in igneous rocks, such as syenites and nepheline syenites; and in large masses in the zone separating peridotites from adjacent country rocks. It is disseminated in small crystals through certain lamprophyric dikes and is found in large crystals in Si-poor pegmatites. Found frequently in crystals and rolled pebbles in detrital soil and stream sands, where it

[1]The long-established morphological unit with *c* one-half the length of *c* of the unit cell is retained here for members of this group; the indices of forms of these minerals are expressed accordingly.

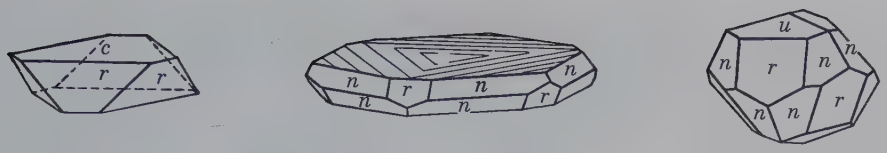

(*a*) (*b*) (*c*) **FIG. 16.14** Hematite crystals.

has been preserved through its hardness and chemical inertness. Associated minerals are commonly chlorite, micas, magnetite, spinel, kyanite, and diaspore.

The finest rubies have come from Myanmar; the most important locality is near Mogok, 90 miles north of Mandala. Some stones are found here in the metamorphosed limestone that underlies the area, but most of them have been recovered from the overlying soil and associated stream gravels. Recently rubies of fine quality occurring *in situ* have been mined in southern Kenya. Darker, poorer quality rubies have been found in alluvial deposits near Bangkok, Thailand, and at Battambang, Cambodia. In Sri Lanka, rubies of relatively inferior grade, associated with more abundant sapphires and other gemstones, are recovered from stream gravels. In the United States, a few rubies have been found associated with the large corundum deposits of North Carolina.

Sapphires are found in the alluvial deposits of Thailand, Sri Lanka, Madagascar and Cambodia associated with rubies. The stones from Cambodia of a cornflower-blue color are most highly prized. Sapphires occur in Kashmir, India, and are found over an extensive area in central Queensland, Australia. In the United States, small sapphires of fine color are found in various localities in Montana. They were first discovered in the river sands east of Helena during placer operations for gold, and later found embedded in the rock of a lamprophyre dike at Yogo Gulch.

Common abrasive corundum has in the past been mined in many countries, but today Zimbabwe, Russia, and India are the only significant producers. At one time it was extensively mined in North Carolina, where it occurs in large masses at the edges of intruded olivine rock (dunite), and in Craigmont, Ontario, where, as a primary constituent of nepheline syenite, corundum makes up more than 10% of the rock mass.

Emery is found in large quantities on Cape Emeri on the island of Naxos, Greece, where mining continues today as it has for many centuries. In the United States, emery was mined at Chester, Massachusetts, and at Peekskill, New York.

Synthesis. Synthetic corundum is manufactured from bauxite on a large scale. This material, together with other manufactured abrasives, notably silicon carbide, has largely taken the place of natural corundum as an abrasive.

Synthetic rubies and sapphires, colored with small amounts of Cr and Ti, are synthesized by fusing alumina powder in an oxy-hydrogen flame, which on cooling forms single crystal *boules*. This, the Verneuil process, has been in use since 1902. In 1947, Linde Air Products of the United States succeeded in synthesizing star rubies and star sapphires. This was accomplished by introducing titanium, which, during proper heat treatment, exsolves as oriented rutile needles to produce the star. The synthetic gems rival the natural stones in beauty, and it is difficult for the untrained person to distinguish them (see also Chapter 20).

Use. As a gemstone and abrasive. The deep red ruby is one of the most valuable of gems, second only to emerald. The blue sapphire is also valuable, and stones of other colors command high prices (for color illustrations see Plate IX in Chapter 20). Stones of gem quality are used as watch jewels and as bearings in scientific instruments. Corundum is used as an abrasive, either ground from the pure massive mineral or in its impure form as emery.

Name. Probably from Kauruntaka, the Indian name for the mineral.

HEMATITE—Fe_2O_3

Crystallography. Hexagonal; $\bar{3}2/m$. Crystals are usually thick to thin tabular on {0001}, basal planes often show triangular markings, and the edges of the plates may be beveled with rhombohedral forms (Fig. 16.14b). Thin plates may be grouped in rosettes (*iron roses*) (Fig. 16.15). More rarely crystals are distinctly rhombohedral, often with nearly cubic angles, and may be polysynthetically twinned on {0001} and $\{10\bar{1}1\}$. Also in botryoidal to reniform shapes with radiating structure, *kidney ore* (see Fig. 2.4). May also be micaceous and foliated, *specular*, see Plate II, no. 7. May also occur with *oölitic* texture, composed of small spheres. Usually earthy; called *martite* when in octahedral pseudomorphs after magnetite.

$R\bar{3}c$; $a = 5.04$, $c = 13.76$ Å; $Z = 6$. *d*s: 2.69(10), 2.52(8), 2.21(4), 1.843(6), 1.697(7).

Physical Properties. *Parting* on $\{10\bar{1}1\}$ with nearly cubic angles, also on {0001}. **H** $5\frac{1}{2}$–$6\frac{1}{2}$, **G** 5.26 for crystals. *Luster* metallic in crystals and dull in earthy varieties. *Color* red to reddish-brown to black. Red earthy variety is known as

FIG. 16.15 Hematite, iron rose. St. Gotthard, Switzerland. (Harvard Mineralogical Museum.)

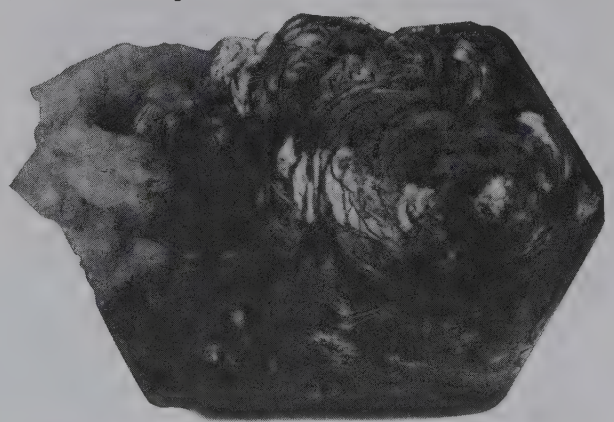

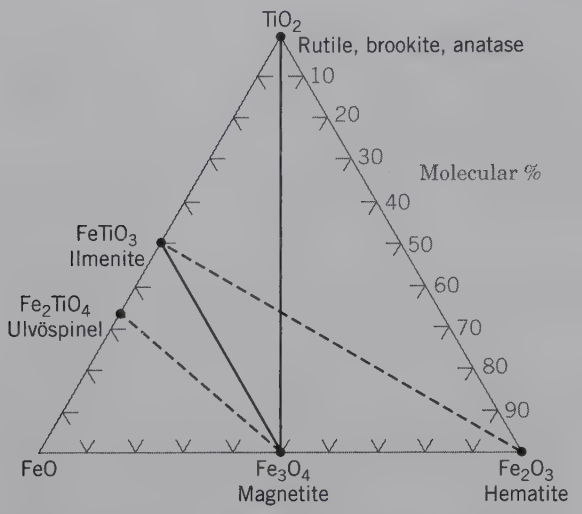

FIG. 16.16 Compositions of naturally occurring oxide minerals in the system FeO-Fe_2O_3-TiO_2. Solid lines (tielines) indicate common geological coexistences at relatively low temperatures. Dashed lines indicate complete solid solution between end members. Hematite-ilmenite is a complete series above 950°C. Magnetite-ulvöspinel is a complete series above about 600°C. Magnetite commonly contains ilmenite lamellae. It is possible that such intergrowths result from the oxidation of members of the magnetite-ulvöspinel series. Compare with Fig. 16.26.

red ocher, platy and metallic variety as *specularite*. *Streak* light to dark red, which becomes black on heating. Translucent.

Composition and Structure. Fe 70, O 30%; essentially a pure substance at ordinary temperatures, although small amounts of Mn and Ti have been reported. Forms a complete solid solution series with ilmenite above 950°C (see Figs. 16.16 and 16.26). The structure is similar to that of corundum (see Fig. 16.2 and page 370).

Diagnostic Features. Distinguished by its characteristic red streak.

Occurrence. Hematite is widely distributed in rocks of all ages and forms the most abundant and important ore of iron. It may occur as a sublimation product from volcanic activity. Occurs in contact metamorphic deposits and as an accessory mineral in feldspathic igneous rocks, such as granite. Found from microscopic scales to enormous masses in regionally metamorphosed rocks where it may have originated by the oxidation of siderite, or magnetite. It is found in red sandstones as the cementing material that binds the quartz grains together. The quantity of hematite in a deposit that can be mined economically must be measured in tens of millions of tons. Such major accumulations are largely sedimentary in origin and many of them, through leaching of associated silica by meteoric waters, have been enriched to high-grade (direct shipping) ores (over 50% Fe). It may form in irregular masses and beds as the result of the weathering and oxidation of iron-bearing rocks. The oölitic ores are of sedimentary origin and may occur in beds of considerable size.

Noteworthy localities for hematite crystals are on the island of Elba, Italy; St. Gotthard, Switzerland, in "iron roses"; in the lavas of Vesuvius, Italy; at Cleator Moor, Cumbria, England; and in Minas Gerais, Brazil.

In the United States, the columnar and earthy varieties are found in enormous bedded, Precambrian deposits that have furnished a large proportion of the iron ore of the world. The chief iron ore districts of the United States are grouped around the southern and northwestern shores of Lake Superior in Michigan, Wisconsin, and Minnesota. The primary districts, referred to as iron ranges, are, from east to west, the Marquette in northern Michigan; the Menominee in Michigan to the southwest of the Marquette; the Penokee-Gogebic in northern Wisconsin. In Minnesota the Mesabi, northwest of Duluth; the Vermilion, near the Canadian boundary; and the Cuyuna, southwest of the Mesabi. The iron ore of these different ranges varies from the hard specular variety to the soft, red earthy type. Of the several ranges the Mesabi is the largest, and since 1892 has yielded over 2.5 billion tons of high-grade ore, over twice the total production of all the other ranges.

Oölitic hematite is found in the United States in the rocks of the Clinton formation, which extends from central New York south along the line of the Appalachian Mountains to central Alabama. The most important deposits lie in eastern Tennessee and northern Alabama, near Birmingham. Hematite has been found at Iron Mountain and Pilot Knob in southeastern Missouri. Deposits of considerable importance are located in Wyoming in Laramie and Carbon counties.

Although the production of iron ore within the United States remains considerable, the rich deposits have been largely worked out. In the future, much of the iron must come from low-grade deposits or must be imported. The low-grade, silica-rich iron-formation from which the high-grade deposits have been derived is known as *taconite*, which contains about 25% iron. The iron reserves in taconite are far greater than were the original reserves of high-grade ore.

Exploration outside the United States has been successful in locating several ore bodies with many hundreds of millions of tons of high-grade ore. These are notably in Venezuela, Brazil, Canada, and Australia. Brazil's iron mountain, Itabira, is estimated to have 15 billion tons of very pure hematite. In 1947, Cerro Bolivar in Venezuela was discovered as an extremely rich deposit of hematite, and by 1954 ore was being shipped from there to the United States. In Canada major Precambrian iron ore deposits have been located in the Labrador Trough close to the boundary between Quebec and Labrador. A 350-mile railroad built into this previously inaccessible area began in 1954 to deliver iron ore to Seven Islands, a major port on the St. Lawrence River. Large Australian deposits are located in the Precambrian rocks of the Hamersley Range, Western Australia. The main producers of iron ore are China, Brazil, Australia, India, Russia, Ukraine, and the United States (see also Box 16.1).

Use. Most important ore of iron for steel manufacture. Also used in pigments, red ocher, and as polishing powder. Black crystals may be cut as gems.

Name. Derived from the Greek word *haimatos* meaning *blood*, in allusion to the color of the powdered mineral.

Similar Species. *Maghemite*, γFe_2O_3, dimorphous with hematite. Formed by weathering or low-temperature oxidation of spinels containing ferrous iron, commonly magnetite.

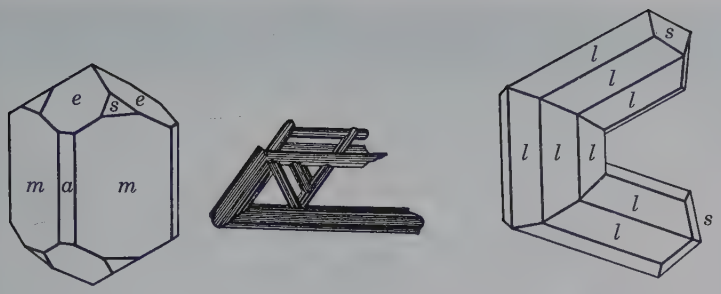

FIG. 16.17 Rutile crystals.

ILMENITE—$FeTiO_3$

Crystallography. Hexagonal; $\bar{3}$. Crystals are usually thick tabular with prominent basal planes and small rhombohedral truncations. Often in thin plates. Usually massive, compact; also in grains or as sand.

$R\bar{3}$; $a = 5.09$, $c = 14.06$ Å; $Z = 6$. *ds*: 2.75(10), 2.54(7), 1.867(5), 1.726(8), 1.507(4).

Physical Properties. **H** $5\frac{1}{2}$–6. **G** 4.7. *Luster* metallic to submetallic. *Color* iron-black. *Streak* black to brownish-red. May be magnetic without heating. Opaque.

Composition and Structure. Fe 36.8, Ti 31.6, O 31.6% for stoichiometric $FeTiO_3$. The formula is more realistically expressed as (Fe, Mg, Mn)TiO_3 with limited Mg and Mn substitution. Ilmenite may contain Fe_2O_3 (less than 6 weight percent) at ordinary temperatures. However, a complete solid solution exists between Fe_2O_3 and $FeTiO_3$ above 950°C (see Figs. 16.16 and 16.26). Related species are *geikielite*, $MgTiO_3$, and *pyrophanite*, $MnTiO_3$. The structure of ilmenite is similar to that of corundum (Figs. 16.2b and c) with Fe and Ti ordered in alternate octahedrally coordinated layers perpendicular to the *c* axis (see Fig. 16.2c).

Diagnostic Features. Ilmenite can be distinguished from hematite by its streak and from magnetite by its lack of strong magnetism.

Occurrence. Ilmenite is a common accessory mineral in igneous and metamorphic rocks. It may be present in large masses in gabbros, diorites, and anorthosites as a product of magmatic segregation intimately associated with magnetite. It is also found in some pegmatites and vein deposits. As a constituent of black sands it is associated with magnetite, rutile, zircon, and monazite.

Found in large quantities at Krägerö and other localities in Norway; in Finland; and in crystals at Miask in the Ilmen Mountains, Russia. A large percentage of the production of ilmenite is recovered from beach sands, notably in Australia, Republic of South Africa, India, China, Norway, Ukraine, and, in the United States from Florida. Until recently, ilmenite was actively mined at Tahawas, New York. A large ilmenite-hematite deposit is mined at Allard Lake, Quebec, Canada. The world production of ilmenite is about 4 million tons.

Use. The major source of titanium. It is used principally in the manufacture of titanium dioxide for paint pigments, replacing lead compounds. As the metal and in alloys, because of its high strength-to-weight ratio and high resistance to corrosion, titanium is used for aircraft and space vehicle construction in both frames and engines.

Name. From the Ilmen Mountains, Russia.

Similar Species. *Perovskite*, $CaTiO_3$, a pseudoisometric titanium mineral found usually in nepheline syenites and carbonatites. *Pseudobrookite*, Fe_2TiO_5, and solid solutions toward *ferropseudobrookite*, $FeTi_2O_5$ (see Fig. 16.26), occur in igneous rocks, in kimberlites, and in meteorite-impacted basalts.

RUTILE GROUP, XO_2

RUTILE–TiO_2

Crystallography. Tetragonal; $4/m2/m2/m$. Usually in prismatic crystals with dipyramid terminations common and vertically striated prism faces. Frequently in elbow twins, often repeated (Figs. 16.17 and 16.18) with twin plane {011}. Crystals frequently slender acicular. Also compact, massive.

$P4_2/mnm$; $a = 4.59$, $c = 2.96$ Å; $Z = 2$. *ds*: 3.24(10), 2.49(5), 2.18(3), 1.687(7), 1.354(4).

Physical Properties. *Cleavage* {110} distinct. **H** 6–$6\frac{1}{2}$. **G** 4.18–4.25. *Luster* adamantine to submetallic. *Color* red, reddish-brown to black, see Plate II, no. 8. *Streak* pale brown. Usually subtranslucent, may be transparent. *Optics*: (+) $\omega = 2.612$, $\epsilon = 2.899$. High dispersion.

FIG. 16.18 Rutile. Cyclic twin, Parksburg, Chester County, Pennsylvania. Elbow twin, Pfitch, Austria (Harvard Mineralogical Museum).

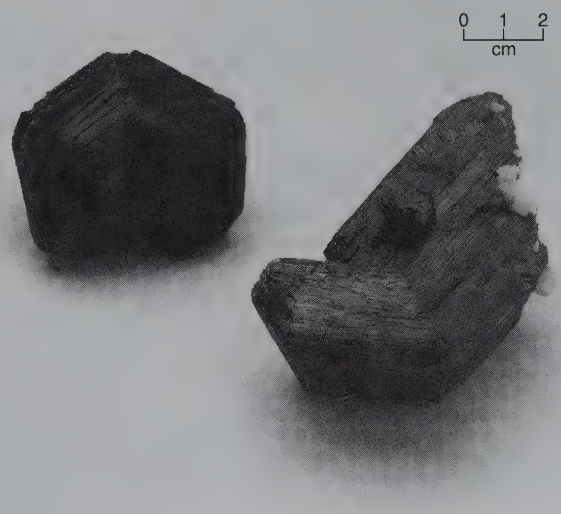

BOX 16.1 Ore Minerals for the Steel Industry

Iron is the mainstay of modern civilization. It is used in an enormous range of applications—among them, in transportation (automobiles, trains, and ships), in construction, in industrial machines, in containers (e.g., oil drums), and in household appliances. The major iron ore minerals are **hematite**, **magnetite**, and **goethite**. They are found in large quantities in iron ore deposits that have formed as a result of the leaching of silica (SiO_2) that is normally a major component of the banded iron-formations (BIF) in which such ore deposits are hosted. Supergene enrichment and oxidation processes (see Box 15.3) concentrate the iron minerals into richer ore types. Some of the main iron-producing countries are China, Australia, and Brazil.

The BIFs in which the iron ore deposits are hosted are all Precambrian, ranging from 3.8 billion to about 1.8 billion years in age. Their abundance peaks at about 2.5 billion years ago with a much smaller reoccurrence between 0.8 and 0.6 billion years ago (see diagram). Most BIFs have similar bulk chemistries (large amounts of Fe and Si) and consist of magnetite, hematite, Fe-silicates, Fe-carbonates (such as siderite), and chert (see photograph). These are chemical sedimentary sequences that are the result of precipitation from ocean systems in which deep ocean hydrothermal input (of Fe^{2+} and Si) mixed with seawater. Such upwelling, Fe-enriched waters appear to have been reducing, or anaerobic, or even anoxic (so as to allow for the transport of Fe^{2+} in solution), with the atmosphere gradually changing from originally reducing to slightly oxidizing in the early Proterozoic (2.5 billion to 570 million years ago).

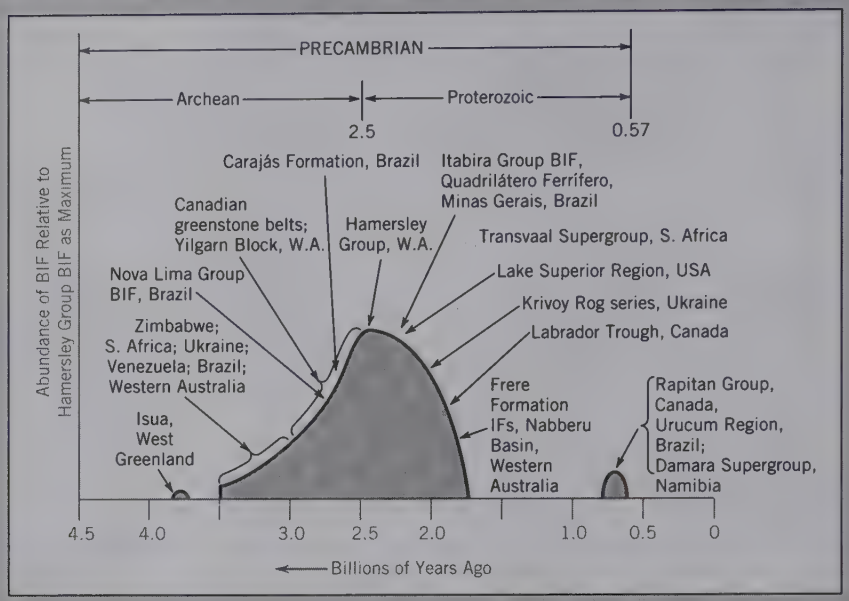

Highly schematic diagram showing the relative abundance of Precambrian BIFs versus geologic time with several of the major BIFs or major BIF regions identified by name. The maximum at 2.5 billion years ago is represented by the BIFs in the Hamersley Basin of Western Australia. (From Klein, C. 2005. Some Precambrian iron-formations (BIFS) from around the world: Their age, geological setting, mineralogy, metamorphism, and origin. American Mineralogist *90: 1473–99).*

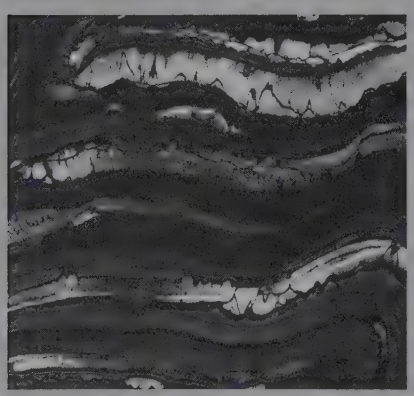

Photograph of a polished hand specimen of banded iron-formation (BIF) that displays alternating thin bands of hematite (dark), chert (gray), and tiger's eye (light). Specimen is from the Hamersley Range in Western Australia. Field of view is about 10 cm (Photograph by B. Dutrow.)

In addition to iron, other chemical elements are commonly used in alloying to yield special steels with specific properties. These include manganese, chromium, nickel, niobium, molybdenum, tungsten, vanadium, and cobalt.

Common manganese ore minerals are **pyrolusite**, **manganite**, and **romanechite** (formerly known as **psilomelane**). The largest reserves of manganese ore are in the Kalahari manganese field of South Africa, of early Proterozoic age. This area holds 81% of the world's known land-based reserves.

The only chromium ore mineral is **chromite**. Chromite is a rock-forming mineral that occurs as magmatic segregations in ultrabasic rocks such as peridotites. Two major chromite-producing regions are the Precambrian Bushveld igneous complex of South Africa and the Great Dike of Zimbabwe.

The most common nickel ore mineral is **pentlandite**, $(Fe,Ni)_9S_8$, which is always associated with pyrrhotite and chalcopyrite. Major nickel-producing districts are in Sudbury, Ontario, Canada, and in the southwestern part of Western Australia.

Composition and Structure. Ti 60, O 40%. Although rutile is essentially TiO_2, some analyses report considerable amounts of Fe^{2+}, Fe^{3+}, Nb, and Ta. When Fe^{2+} substitutes for Ti^{4+}, electrical neutrality is maintained by twice as much Nb^{5+} and Ta^{5+} entering the structure. This leads to the formulation: $Fe_x(Nb,Ta)_{2X}Ti_{1-3X}O_2$. The structure of rutile is given in Figs. 16.4 and 4.21 and described on page 371. TiO_2 occurs in two additional, relatively rare polymorphs, tetragonal *anatase* (space group $I4_1/amd$) and orthorhombic *brookite* (space group *Pbca*). In anatase TiO_6 octahedra share four edges, in brookite the octahedra share three edges, whereas in rutile they share only two edges. The stability fields of the three polymorphs are still not well-defined. Rutile is generally considered to be a high *T* polymorph of TiO_2 and occurs in rocks that formed over a wide range of *P* and *T*. Its large stability range may suggest that the polymorph in which only two edges are shared between adjoining octahedra is the most stable structure.

Diagnostic Features. Characterized by its peculiar adamantine luster and red color. Lower specific gravity distinguishes it from cassiterite.

Occurrence. Rutile is found in granites, granite pegmatites, gneisses, mica schists, metamorphic limestone, and dolomite. It may be present as an accessory mineral in the rock or in quartz veins traversing it. Often occurs as slender crystals inside quartz and micas. In quartz, referred to as rutilated quartz, blades radiate from a hematite core. When in clear quartz, it is prized as gem material (see Fig. 19.73). Is found in considerable quantities in black sands associated with ilmenite, magnetite, zircon, and monazite.

Notable European localities are: Krägerö, Norway; Yrieix, near Limoges, France; in Switzerland; and the Tyrol. Rutilated quartz specimens come from Minas Gerais, Brazil. Rutile from beach sands of northern New South Wales and southern Queensland makes Australia the largest producer of rutile. In the United States, remarkable crystals have come from Graves Mountain, Lincoln County, Georgia. Rutile is found in Alexander County, North Carolina, and at Magnet Cove, Arkansas. It has been mined in Amherst and Nelson counties, Virginia, and derived in commercial quantities from the black sands of northeastern Florida.

Synthesis. Single crystals of rutile have been manufactured by the Verneuil process (see page 568). With the proper heat treatment they can be made transparent and nearly colorless, quite different from the natural mineral. Because of its high refractive index and dispersion, this synthetic material makes a beautiful cut gemstone with only a slight yellow tinge. It is sold under a variety of names, some of the better known are *titania*, *kenya gem*, and *miridis*.

Use. Most of the rutile produced is used as a coating of welding rods. Some titanium derived from rutile is used in alloys; for electrodes in arc lights; to give a yellow color to porcelain and false teeth. Manufactured oxide is used as a paint pigment (see ilmenite).

Name. From the Latin word *rutilus*, red, an allusion to the color.

Similar Species. *Stishovite*, a very high-pressure polymorph of SiO_2, isostructural with rutile, is found rarely in meteorite impact craters. This dense form of SiO_2 is the only example of Si in 6-coordination rather than its common tetrahedral coordination. *Leucoxene*, a fine-grained, yellow to brown alteration product of minerals high in Ti (ilmenite, perovskite, titanite), consists mainly of rutile, less commonly anatase.

PYROLUSITE—MnO_2

Crystallography. Tetragonal; $4/m2/m2/m$. Rarely in well-developed crystals. Usually in radiating fibers or columns. Also granular massive; often in reniform coatings and dendritic shapes (Fig. 16.19) finely intergrown with other Mn-oxides and hydroxides. Frequently forms pseudomorphs after manganite.

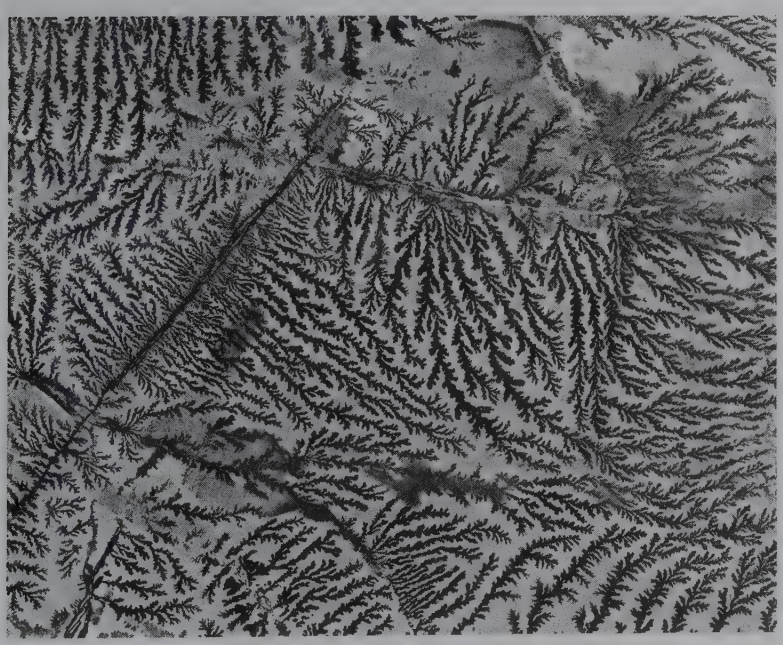

FIG. 16.19 Dendrites of manganese oxide minerals on limestone. Sardinia, Italy (Harvard Mineralogical Museum).

$P4_2/mnm$; a = 4.39, c = 2.86 Å; Z = 2. *ds*: 3.11(10), 2.40(5), 2.11(4), 1.623(7), 1.303(3).

Physical Properties. *Cleavage* {110} perfect. **H** 1–2 (often soiling the fingers). For coarsely crystalline *polianite* the hardness is 6–6½. **G** 4.75. *Luster* metallic. *Color* and *streak* iron-black, see Plate II, no. 9. *Fracture* splintery. Opaque.

Composition and Structure. Mn 63.2, O 36.8%. Commonly contains some H_2O. The structure is the same as that of rutile (see Fig. 16.4) with Mn in 6-coordination with oxygen.

Diagnostic Features. Characterized by and distinguished from other manganese minerals by its black streak and low hardness.

Occurrence. Manganese is present in small amounts in most crystalline rocks. When dissolved from these rocks, it may be redeposited as various minerals, but primarily as pyrolusite. Nodular deposits of pyrolusite are found in bogs, on lake bottoms, and on the floors of seas and oceans. Nests and beds of manganese ores are found enclosed in residual clays, derived from the decay of manganiferous limestones. Also found in veins with quartz and various metallic minerals.

Pyrolusite is the most common manganese ore and is widespread in its occurrence. The chief manganese-producing countries are Russia, Republic of South Africa, Brazil, China, and India. Current production in the United States is negligible.

Use. Most important manganese ore. Manganese is used with iron in the manufacture of *spiegeleisen* and *ferromanganese*, employed in making steel (see also Box 16.1). This is its principal use, for about 13.2 pounds of manganese are consumed in the production of one ton of steel. Also used in various alloys with copper, zinc, aluminum, tin, and lead. Pyrolusite is used as an oxidizer in the manufacture of chlorine, bromine, and oxygen; as a disinfectant in potassium permanganate; as a drier in paints; as a decolorizer of glass; and in electric dry-cells and batteries. Manganese is also used as a coloring material in bricks, pottery, and glass.

Name. *Pyrolusite* is derived from two Greek words, *pyros* meaning *fire* and *louo* meaning *to wash*, because it is used to free glass through its oxidizing effect of the colors due to iron.

Similar Species. *Alabandite*, MnS, is comparatively rare, associated with other sulfides in veins. *Wad* is the name given to manganese ore composed of an impure mixture of hydrous manganese oxides.

CASSITERITE—SnO_2

Crystallography. Tetragonal; $4/m2/m2/m$. The common forms are the prisms {110} and {010} and the dipyramids {111} are {011} (Fig. 16.20a). Frequently in elbow-shaped twins with a characteristic notch, giving rise to the miner's term *visor tin* (Figs. 16.20b and 16.21); the twin plane is {011}. Usually massive granular; often in reniform shapes with radiating fibrous appearance, *wood tin*.

$P4_2/mnm$; a = 4.73, c = 3.18 Å; Z = 2. *ds*: 2.36(8), 2.64(7), 1.762(10), 1.672(4), 1.212(5).

Physical Properties. *Cleavage* {010} imperfect. **H** 6–7. **G** 6.8–7.1 (unusually high for a nonmetallic mineral). *Luster*

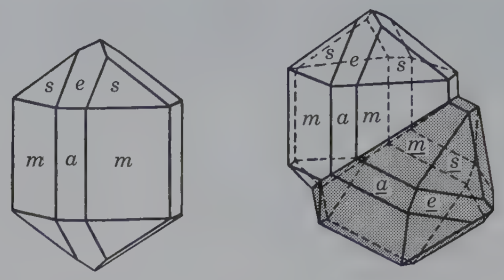

FIG. 16.20 Cassiterite crystals.

adamantine to submetallic and dull. *Color* usually brown or black; rarely yellow or white. *Streak* white. Translucent, rarely transparent. *Optics*: (+); ω = 1.997, ε = 2.093.

Composition and Structure. Close to SnO_2 with Sn 78.6, O 21.4%. Small amounts of Fe^{3+} may be present and lesser amounts of Nb and Ta substitute for Sn. The structure is that of rutile (see Fig. 16.4 and page 371).

Diagnostic Features. Recognized by high specific gravity, adamantine luster, and light streak.

Occurrence. Cassiterite is widely distributed in small amounts but is produced on a commercial scale in only a few localities. It has been noted as an original constituent of igneous rocks and pegmatites, but it is more commonly found

FIG. 16.21 Twinned crystal of cassiterite. Horní Slavkov (Schlaggenwald), Czech Republic (Harvard Mineralogical Museum).

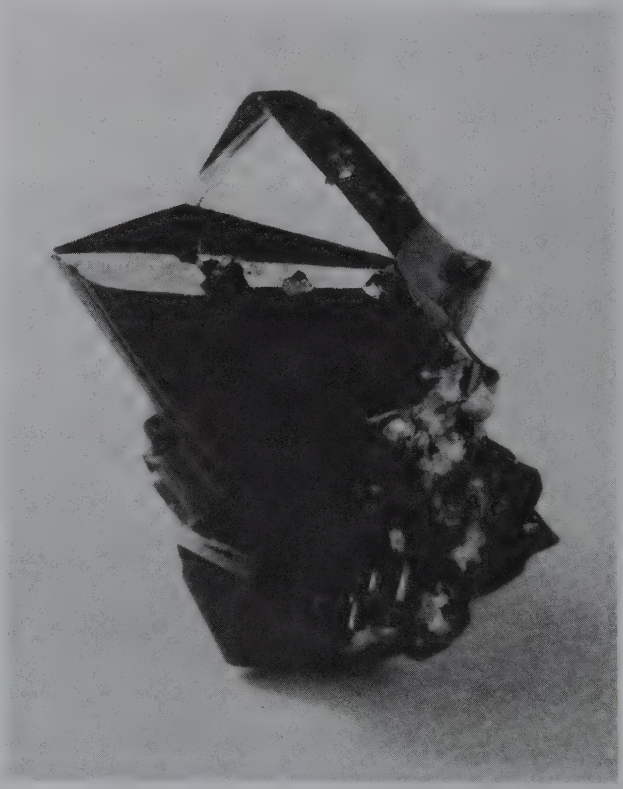

in high-temperature hydrothermal veins in or near granitic rocks. Tin veins usually have minerals that contain fluorine or boron, such as tourmaline, topaz, fluorite, and apatite, and the minerals in the adjacent rocks are commonly much altered. Frequently associated with wolframite, molybdenite and arsenopyrite. Cassiterite is commonly found in the form of rolled pebbles in placer deposits, *stream tin*.

Most of the world's supply of tin comes from alluvial deposits chiefly in Malaysia, Russia, Indonesia, and Thailand. Bolivia is the only country where a significant production comes from vein deposits; but in the past, the mines of Cornwall, England, were major producers. Fine specimens originate from Horní Slavkov (Schlaggenwald), Czech Republic, from Cornwall, England, and from Araca, Bolivia. In the United States, cassiterite is not found in sufficient quantities to warrant mining but is present in small amounts in numerous pegmatites. *Wood tin* is found in rhyolites in New Mexico and Mexico.

Use. Principal ore of tin. The primary use of tin was in the manufacture of *tin plate* and *tern plate* for food containers. Tern plate is made by applying a coating of tin and lead instead of pure tin. Presently, aluminum, glass, paper, plastic, and tin-free steel are replacing tin-plated containers. Tin is also used with lead in solders, in babbitt metal with antimony and copper, and in bronze and bell-metal with copper. "Phosphor bronze" contains 89% Cu, 10% Sn, and 1% P. Synthetic tin oxide is a polishing powder.

Name. From the Greek word *kassiteros* meaning *tin*.

Similar Species. *Stannite*, Cu_2FeSnS_4, is structurally similar to chalocopyrite and sphalerite. It is a minor ore of tin.

URANINITE—UO_2

Crystallography. Isometric; $4/m\bar{3}2/m$. The rare crystals are usually octahedral with subordinate cube and dodecahedron faces. More commonly as the variety *pitchblende*: massive or botryoidal with a banded structure.

$Fm3m$; $a = 5.46$ Å; $Z = 4$. *ds*: 3.15(7), 1.926(6), 1.647(10), 1.255(5), 1.114(5).

Physical Properties. H $5\frac{1}{2}$. **G** 7.5–9.7 for crystals; 6.5–9 for pitchblende. The specific gravity decreases with oxidation of U^{4+} to U^{6+}. *Luster* submetallic to pitchlike, dull. *Color* black. *Streak* brownish-black.

Composition and Structure. Uraninite is always partially oxidized, and, thus, the actual composition lies between UO_2 and U_3O_8 ($= U^{4+}O_2 + 2U^{6+}O_3$). Th can substitute for U and a complete series between uraninite and *thorianite*, ThO_2, has been prepared synthetically. In addition to Th, analyses usually show the presence of small amounts of Pb, Ra, Ce, Y, He, and Ac. The lead occurs as one of two stable isotopes (^{206}Pb and ^{207}Pb) that result from the radioactive decay of uranium. For example: $^{238}U \rightarrow {}^{206}Pb + 8{}^{4}He$ and $^{235}U \rightarrow {}^{207}Pb + 7{}^{4}He$. Thorium decays as follows: $^{232}Th \rightarrow {}^{208}Pb + 6{}^{4}He$. In addition to ionized helium atoms (α particles), electrons (β particles) are emitted during the decay process. Because the radioactive disintegration proceeds at a uniform and known rate, the accumulation of both helium and lead can be used as a measure of the time elapsed since the mineral crystallized. For example, for the decay of ^{238}U, the *half-life*, *T*, which is the time needed to reduce the number of ^{238}U atoms by one-half, is 4.51×10^9 years (see Table 12.3). Both lead-uranium and helium-uranium ratios have been used by geologists to determine the age of rocks (see also page 282).

It was in uraninite that helium was first discovered on Earth, having been previously noted in the sun's spectrum. Also, radium was discovered in uraninite. The structures of uraninite and thorianite are like that of fluorite (Fig. 16.11) in which the metal atom is at the center of eight oxygens at the corner of a cube, with each oxygen at the center of a tetrahedral group of metal atoms.

Diagnostic Features. Characterized chiefly by its pitchy luster, high specific gravity, color, and streak. Because of its radioactivity, uraninite, as well as other uranium compounds, can be detected in small amounts by Geiger and scintillation counters.

Occurrence. Uraninite occurs as a primary constituent of granitic rocks and pegmatites. It also is found in high-temperature hydrothermal veins associated with cassiterite, chalcopyrite, pyrite, and arsenopyrite as at Cornwall, England; or in medium-temperature veins with native silver and Co-Ni-As minerals as at Horní Slavkov (Joachimsthal), Czech Republic, and Great Bear Lake, Canada. The world's most productive uranium mine during and immediately following World War II was the Shinkolobwe Mine in Congo. Here, uraninite and secondary uranium minerals are in vein deposits associated with cobalt and copper minerals. The ores also carry significant amounts of Mo, W, Au, and Pt.

Wilberforce, Ontario, has been a famous Canadian locality, but the present major Canadian sources are the mines at Great Bear Lake, the Beaverlodge region, Saskatchewan; and the Blind River area, Ontario. At Blind River, uraninite occurs as detrital grains in a Precambrian quartz conglomerate. In the same type of deposit, it is found in the gold-bearing Witwatersrand conglomerates, Republic of South Africa.

In the United States, uraninite was found long ago in isolated crystals in pegmatites at Middletown, Glastonbury, and Branchville, Connecticut, and the mica mines of Mitchell County, North Carolina. Following World War II, exploration has located many workable deposits of uraninite and associated uranium minerals on the Colorado Plateau in Arizona, Colorado, New Mexico, and Utah.

Use. Uraninite is the primary ore of uranium although other minerals are important sources of the element such as *carnotite* (page 433), *tyuyamunite* (page 433), *torbernite* (page 433), and *autunite* (page 432).

Uranium is important because of its susceptibility to nuclear fission, a process by which the nuclei of uranium atoms are split apart with the generation of tremendous amounts of energy. This energy, first demonstrated in the atomic bomb, is now produced by nuclear-power reactors for generating electricity.

Uraninite is also the source of radium but contains it in very small amounts. Roughly 750 tons of ore must be mined in order to furnish 12 tons of concentrates; chemical treatment of these concentrates yields about 1 gram of a radium

salt. In the form of various compounds uranium has a limited use in coloring glass and porcelain, in photography, and as a chemical reagent.

Name. Uraninite in allusion to the composition.

Similar Species. *Thorianite*, ThO_2, is dark gray to black with submetallic luster. Found chiefly in pegmatites and as water-worn crystals in stream gravels. *Cerianite*, $(Ce,Th)O_2$, an extremely rare mineral, has, as does thorianite, the fluorite structure.

SPINEL GROUP, XY_2O_4

The minerals of the *spinel group* show extensive solid solution between the various end-member compositions listed in Table 16.2. There is, for example, extensive solid solution between magnetite, Fe_3O_4, ulvöspinel, Fe_2TiO_4, and a synthetic end-member composition, Mg_2TiO_4 (a magnesian titanate with inverse spinel structure). Furthermore, there are substitutions between chromite, $FeCr_2O_4$, and magnesiochromite, $MgCr_2O_4$; between spinel, $MgAl_2O_4$, and hercynite, $FeAl_2O_4$, and so on. The complexity of the chemical substitutions in this group makes it very difficult to use triangular composition diagrams for expression of the various solid solutions' extents; instead, a "spinel prism" is used for such chemical representations. Figure 16.22 shows three such prisms: (a) for the compositional space between normal spinels at the base of the prism and inverse spinels, with (Fe^{2+} + Ti^{4+}) substitutions, at the top edge; (b) for the compositional space between normal spinels at the base of the prism and inverse spinels, with Fe^{3+} substitutions, along the upper edge; and (c) the general nomenclature for compositions in this prism.

SPINEL—$MgAl_2O_4$

Crystallography. Isometric; $4/m\bar{3}2/m$. Usually in octahedral crystals or in twinned octahedra (spinel twins) (Figs. 16.23a and b). Dodecahedron may be present as small truncations (Fig. 16.23c), but other forms are rare. Also massive and as irregular grains.

Fd3m; a = 8.10 Å; Z = 8. *ds*: 2.44(9), 2.02(9), 1.552(9), 1.427(10), 1.053(10).

Physical Properties. **H** 8. **G** 3.5–4.1. **G** 3.55 for the composition as given. Nonmetallic. *Luster* vitreous. *Color* various: white, yellow, red, lavender, blue, green, brown, black. *Streak* white. Usually translucent, may be clear and transparent. *Optics*: n = 1.718.

Composition and Structure. MgO 28.2, Al_2O_3 71.8%. Fe^{2+}, Zn, and less commonly Mn^{2+} substitute for Mg in all proportions. Fe^{3+} and Cr may substitute in part for Al. The clear red, nearly pure magnesium spinel is known as *ruby spinel*. *Ferroan spinel*, intermediate between spinel and hercynite,

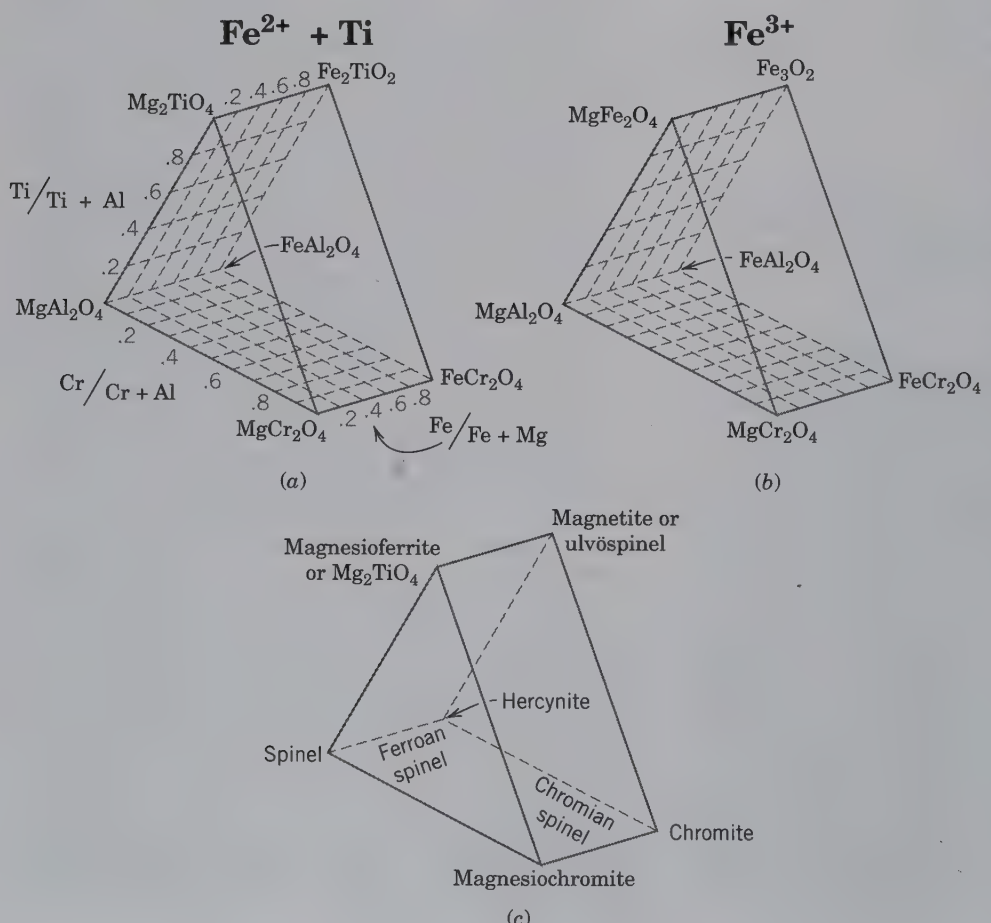

FIG. 16.22 End-member compositions in the spinel group as represented in a spinel prism. (a) Compositions in this space range from those of normal spinels (in the base of the prism) to those with [Fe^{2+} (or Mg^{2+}) + Ti] end-members along the upper edge (these are inverse spinels). (b) Compositions in this space range from those of the normal spinels (in the base) to those with Fe^{3+}-rich end members along the upper edge (these are inverse spinels). (c) Nomenclature for members of the spinel group as based on the chemical compositions represented in (a) and (b).

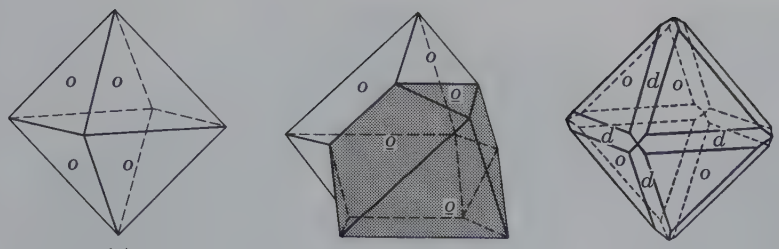

FIG. 16.23 Spinel crystals.

$FeAl_2O_4$, is dark green to black, and *chromian spinel*, intermediate between hercynite and *chromite*, $FeCr_2O_4$, is yellowish to greenish-brown (see Fig. 16.22 for compositional definitions). The structure of spinel is illustrated in Figs. 16.5 and 16.6 and discussed on page 372.

Diagnostic Features. Recognized by its hardness (8), its octahedral crystals, and its vitreous luster. The iron spinel can be distinguished from magnetite by its nonmagnetic character and white streak.

Occurrence. Spinel is a common high-temperature mineral occurring in contact metamorphosed limestones and metamorphic clay-rich rocks poor in SiO_2. Occurs also as an accessory mineral in many dark igneous rocks. In contact metamorphic rocks, it is associated with phlogopite, pyrrhotite, chondrodite, and graphite. Found frequently as rolled pebbles in stream sands, where it has been preserved because of its resistant physical and chemical properties. The ruby spinels are found in this way, often associated with gem corundum, in the sands of Sri Lanka, Thailand, Upper Myanmar, and Madagascar. Ordinary spinel is found in various localities in New York and New Jersey.

Use. When transparent and finely colored, spinel is used as a gem (see Plate X, no. 10, Chapter 20). Usually red and known as *ruby spinel* or *balas ruby*. Some stones are blue. The largest cut stone known weighs about 80 carats. The stones are usually comparatively inexpensive.

Synthesis. Synthetic spinel has been made by the Verneuil process (see corundum) in various colors rivaling the natural stones in beauty. Synthetic spinel is also used as a refractory.

Similar Species. *Hercynite*, $FeAl_2O_4$, is associated with corundum in some emery; also found with andalusite, sillimanite, and garnet in metamorphic rocks. *Ferroan galaxite*, $(Fe^{2+},Mn)Al_2O_4$, an Fe^{2+}-rich variety of *galaxite*, $MnAl_2O_4$, occurs sporadically in nature.

Gahnite—$ZnAl_2O_4$

Crystallography. Isometric; $4/m\bar{3}2/m$. Commonly octahedral with faces striated parallel to the edge between the dodecahedron and octahedron. Less frequently showing well-developed dodecahedrons and cubes.

Fd3m; $a = 8.12$ Å; $Z = 8$. *ds*: 2.85(7), 2.44(10), 1.65(4), 1.48(6), 1.232 (8).

Physical Properties. **H** $7\frac{1}{2}$–8. **G** 4.55. *Luster* vitreous. *Color* dark green. *Streak* grayish. Translucent. *Optics*: $n = 1.80$.

Composition and Structure. Fe^{2+}, Mn^{2+}, Co^{2+}, and Ni^{2+} may substitute for Zn; and Fe^{3+} for Al. Structure is that of spinel (see Figs. 16.5 and 16.6 and page 372).

Diagnostic Features. Characterized by crystal form (striated octahedrons) and hardness.

Occurrence. Gahnite is a rare mineral. It occurs in granite pegmatites, in zinc deposits, and also as a metamorphic mineral in metabauxites and in marbles. Found in large crystals at Bodenmais, Bavaria, Germany; in a talc schist near Falun, Sweden. In the United States, it is found at Charlemont, Massachusetts, and Franklin, New Jersey.

Name. After the Swedish chemist J. G. Gahn, the discoverer of manganese.

MAGNETITE—Fe_3O_4

Crystallography. Isometric; $4/m\bar{3}2/m$. Magnetite is frequently in octahedral crystals (Figs. 16.24a and 16.25), more rarely in dodecahedrons (Fig. 16.24b). Dodecahedra may be striated parallel to the intersection with the octahedron (Fig. 16.24c). Other forms are rare. Usually granular massive, coarse-, or fine-grained.

Fd3m; $a = 8.40$ Å; $Z = 8$. *ds*: 2.96(6), 2.53(10), 1.611(8), 1.481(9), 1.094(8).

Physical Properties. Octahedral parting on some specimens. **H** 6. **G** 5.18. *Luster* metallic. *Color* iron-black, see

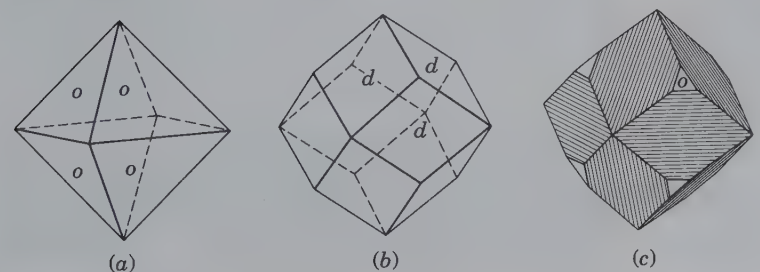

FIG. 16.24 Magnetite crystals.

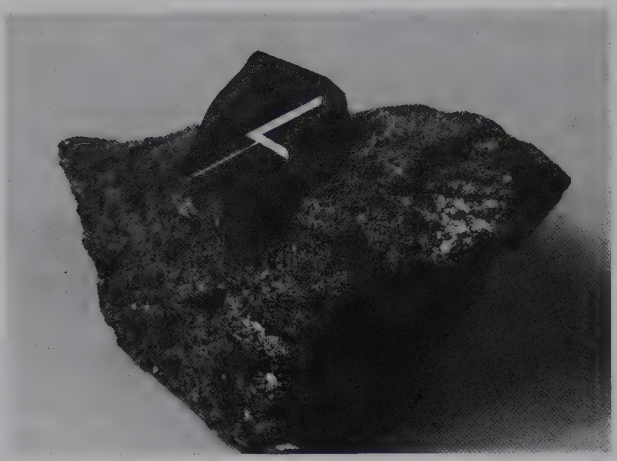

FIG. 16.25 Octahedral magnetite crystal. Binnenthal, Switzerland (Harvard Mineralogical Museum).

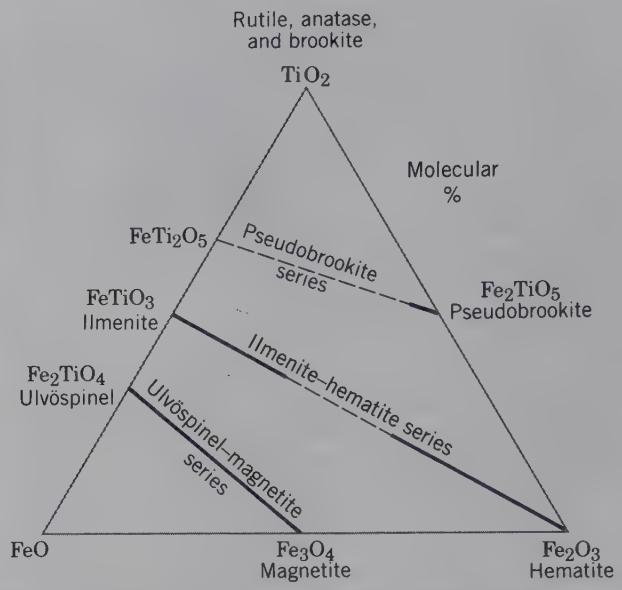

FIG. 16.26 Solid solution series and their extent among oxides in the system TiO_2-FeO-Fe_2O_3. The extent of solid solution between end-member compositions is shown by solid bars, for mineral assemblages synthesized in the laboratory at about 600°C. At higher temperatures, the extent of solid solution will increase considerably in, for example, the ilmenite-hematite and pseudobrookite series. Lack of solid solution at about 600°C is shown by dashed lines. Compare with Fig. 16.16. (Compiled from Haggerty, S. E. 1976. Oxidation of opaque mineral oxides in basalts, and opaque mineral oxides in terrestrial igneous rocks. *Oxide Minerals, Reviews in Mineralogy*. Mineralogical Society of America, Washington, D.C.)

Plate III, no 1. *Streak* black. Strongly magnetic; may act as a natural magnet, known as *lodestone*. Opaque.

Composition and Structure. Fe 72.4, O 27.6%. The composition of most magnetite corresponds closely to Fe_3O_4. However, analyses may show considerable percentages of Mg and Mn^{2+} substituting for Fe^{2+} and Al, Cr, Mn^{3+}, and Ti^{4+} substituting for Fe^{3+}. Above 600°C a complete solid solution series is possible between magnetite and *ulvöspinel*, Fe_2TiO_4 (see Figs. 16.16 and 16.26). The structure of magnetite is that of an *inverse spinel* (see page 372), which can be expressed by rewriting the formula as $Fe^{3+}(Fe^{2+},Fe^{3+})_2O_4$ (see Table 16.2, p. 372).

Diagnostic Features. Characterized chiefly by its strong magnetism, its black color, and its hardness (6). Can be distinguished from magnetic franklinite by streak.

Occurrence. Magnetite is a common mineral found disseminated as an accessory through most igneous rocks. Through magmatic segregation, magnetite may become one of the chief constituents of the rock and form large ore bodies. Such bodies are often highly titaniferous. Commonly associated with metamorphic rocks and may occur as large beds and lenses. It is a common constituent of sedimentary and metamorphic banded Precambrian iron-formations. In such occurrences, it is of chemical, sedimentary origin. Found in the black sands of the seashore. Occurs as thin plates and dendritic growths between plates of mica. Often intimately associated with corundum, forming *emery*.

The largest magnetite deposits in the world are in northern Sweden at Kiruna and Gellivare associated with apatite and are believed to have formed by magmatic segregation. Other important deposits are in Norway, Romania, and Ukraine. The most powerful natural magnets are found in Siberia, in the Harz Mountains, on the Island of Elba, and in the Bushveld igneous complex, Republic of South Africa. The extensive Precambrian iron deposits in the Lake Superior region and in the Labrador Trough, Canada, contain considerable magnetite as an ore mineral.

The Precambrian iron-formations of the Lake Superior region, containing about 25% iron, mostly in the form of magnetite, were a major source of iron in the United States. This low-grade ore, *taconite*, has been actively mined and the magnetite separated magnetically from the waste material. Found as lodestone and in crystals at Magnet Cove, Arkansas.

Use. An important iron ore (see also Box 16.1).

Name. Probably derived from the locality Magnesia, bordering on Macedonia. A fable told by Pliny ascribes its name to a shepherd named Magnes, who first discovered the mineral on Mount Ida by noting that the nails of his shoes and the iron ferrule of his staff adhered to the ground.

Similar Species. *Magnesioferrite*, $Fe^{3+}(Mg,Fe^{3+})_2O_4$ (or $MgFe_2O_4$) with an inverse spinel structure, is a rare mineral found primarily in fumaroles. *Jacobsite*, $Fe^{3+}(Mn,Fe^{3+})_2O_4$ (or $MnFe_2O_4$), an inverse spinel and a rare mineral found at Långban, Sweden. *Ulvöspinel*, $Fe^{3+}(Ti,Fe^{2+})_2O_4$ (or Fe_2TiO_4), also with an inverse spinel structure, is not uncommonly present as exsolution blebs and lamellae within magnetite (see also Table 16.2). *Maghemite*, γFe_2O_3, dimorphous with hematite. Formed by weathering or low-temperature oxidation of spinels containing ferrous iron, commonly magnetite. *Martite*, hematite pseudomorphous after magnetite.

Franklinite—(Zn,Fe,Mn)(Fe,Mn)$_2$O$_4$

Crystallography. Isometric; $4/m\bar{3}2/m$. Crystals are octahedral (see Fig. 16.27) with dodecahedral truncations; commonly rounded. Also massive, coarse, or fine granular, in rounded grains.

FIG. 16.27 Franklinite. Franklin, New Jersey (Harvard Mineralogical Museum).

Fd3m; $a = 8.42$ Å; $Z = 8$. *ds*: 2.51(10), 1.610(10), 1.480(9), 1.278(6), 1.091(6).

Physical Properties. **H** 6. **G** 5.15. *Luster* metallic. *Color* iron-black. *Streak* reddish-brown to dark brown. Slightly magnetic.

Composition and Structure. Dominantly $ZnFe_2O_4$ but always with some substitution of Fe^{2+} and Mn^{2+} for Zn, and Mn^{3+} for Fe^{3+}. Analyses show a wide range in the proportions of the various elements. The structure of franklinite is that of a normal spinel (see page 372 and Figs. 16.5 and 16.6).

Diagnostic Features. Resembles magnetite but is only slightly magnetic and has a dark brown streak. Usually identified by its characteristic association with willemite and zincite.

Occurrence. Franklinite, with only minor exceptions, is confined to the zinc deposits at Franklin, New Jersey, where, enclosed in a granular limestone, it is associated with zincite and willemite.

Use. As an ore of zinc and manganese. The zinc is converted into zinc white, ZnO, and the residue is smelted to form an alloy of iron and manganese, *spiegeleisen*, used in the manufacture of steel.

Name. From Franklin, New Jersey.

CHROMITE—$FeCr_2O_4$

Crystallography. Isometric; $4/m\bar{3}2/m$. Habit octahedral, but crystals are small and rare. Commonly massive, granular to compact.

Fd3m; $a = 8.36$ Å; $Z = 8$. *ds*: 4.83(4), 2.51(10), 2.08(5), 1.602(6), 1.473(8).

Physical Properties. **H** $5\frac{1}{2}$. **G** 4.6. *Luster* metallic to submetallic; frequently pitchy. *Color* iron-black to brownish-black. *Streak* dark brown. Subtranslucent. *Optics*: $n = 2.16$.

Composition and Structure. For $FeCr_2O_4$, FeO 32.0, Cr_2O_3 68.0%. Some Mg is always present substituting for Fe^{2+} and some Al and Fe^{3+} may substitute for chromium. There is extensive solid solution between chromite and magnesiochromite, $MgCr_2O_4$. The structure of chromite is that of a normal spinel (see page 372 and Figs. 16.5 and 16.6).

Diagnostic Features. The submetallic luster usually distinguishes chromite. Often appears granular, with bright green alteration (Cr-oxide).

Occurrence. Chromite is a common constituent of peridotites and other ultrabasic rocks and of serpentines derived from them. One of the first minerals to separate from a cooling magma; large chromite ore deposits are thought to have been derived by such magmatic differentiation. For example, the Bushveld igneous complex of South Africa and the Great Dike of Zimbabwe contain many seams of chromite enclosed in pyroxenites. Associated with olivine, serpentine, and corundum.

The important countries for its production are Republic of South Africa, Turkey, Kazakhstan, and India. Chromite is found only sparingly in the United States, but in the past, Pennsylvania, Maryland, North Carolina, Wyoming, California, Alaska, and Oregon were small producers. During World War II, bands of low-grade chromite were mined in the Stillwater igneous complex, Montana.

Use. The only ore of chromium. Chromite ores are grouped into three categories—metallurgical, refractory, and chemical—on the basis of their chrome content and their Cr/Fe ratio. As a metal, chromium is used as a ferroalloy to give steel the combined properties of high hardness, great toughness, and resistance to chemical attack. Chromium is a major constituent in stainless steel (see Box 16.1). *Nichrome*, an alloy of Ni and Cr, is used for resistance in electrical heating equipment. Chromium is widely used in plating plumbing fixtures, automobile accessories, and so forth.

Because of its refractory character, chromite is made into bricks for the linings of metallurgical furnaces. The bricks are usually made of crude chromite and coal tar but sometimes of chromite with kaolin, bauxite, or other minerals. Chromium

is a constituent of certain green, yellow, orange, and red pigments and in $K_2Cr_2O_7$ and $Na_2Cr_2O_7$, which are used as mordants to fix dyes.

Similar Species. *Magnesiochromite*, $MgCr_2O_4$, is similar to chromite in both occurrence and appearance.

Name. Named in allusion to the composition.

Chrysoberyl—$BeAl_2O_4$

Crystallography. Orthorhombic; *2/m2/m2/m*. Usually in crystals tabular on {001}, the faces of which are striated parallel to [100]. Commonly twinned on {130}, giving pseudohexagonal appearance (Fig. 16.28a and b).

Pmnb; $a = 5.47$, $b = 9.39$, $c = 4.42$ Å; $Z = 4$. *d*s: 3.24(8). 2.33(8), 2.57(8), 2.08(10), 1.61(10).

Physical Properties. *Cleavage* {110}. **H** $8\frac{1}{2}$. **G** 3.65–3.8 *Luster* vitreous. *Color* various shades of green, brown, yellow; may be red by transmitted light. *Optics*: (+), $\alpha = 1.746$, $\beta = 1.748$, $\gamma = 1.756$; $2V = 45°$; $X = c$, $Y = b$.

Alexandrite is a gem variety, emerald-green in daylight, but red to purple by transmitted light and usually red by artificial light. *Cat's eye*, or *cymophane*, is a chatoyant variety that, when cut as an oval or round *cabochon gem*, shows a narrow band of light on its surface. The effect results from minute tubelike cavities or needlelike inclusions parallel to the *c* axis.

Composition and Structure. BeO 19.8, Al_2O_3 80.2%. Be 7.1%. From its formula, $BeAl_2O_4$, it would appear that chrysoberyl is a member of the spinel group. However, because of the small size of Be^{2+}, chrysoberyl has a structure of lower symmetry. It consists of oxygen atoms in hexagonal closest packing with Be in 4-coordination with O and Al in 6-coordination with O. Morphologically and structurally chrysoberyl is very similar to olivine $(Mg,Fe)_2SiO_4$. Be is in the same coordination as Si, and Al in the same coordination as Fe^{2+} or Mg. The hexagonal closest packed arrangement of O in chrysoberyl leads to a pseudohexagonal lattice, angles, and twinning.

Diagnostic Features. Characterized by its high hardness, its yellowish to emerald-green color, and its twin crystals.

Occurrence. Chrysoberyl is a rare mineral. It occurs in granitic rocks, pegmatites, and mica schists rich in Be. Frequently in river sands and gravels. The outstanding alluvial gem deposits are found in Brazil and Sri Lanka; the *alexandrite* variety comes from the Ural Mountains and Brazil. In the United States, chrysoberyl of gem quality is rare, but it has been found in Oxford County and elsewhere in Maine; Haddam, Connecticut; and Greenfield, New York. Recently found in Colorado.

Use. As a gemstone. The ordinary yellowish-green stones are inexpensive; the varieties alexandrite and cat's eye are highly prized gems (see Chapter 20).

Name. *Chrysoberyl* means *golden beryl*. *Cymophane* is derived from two Greek words meaning *wave* and *to appear*, in allusion to the chatoyant effect. *Alexandrite* was named in honor of Alexander II of Russia.

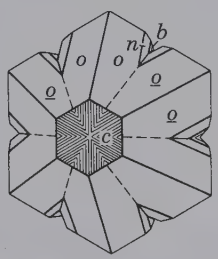

(*a*)

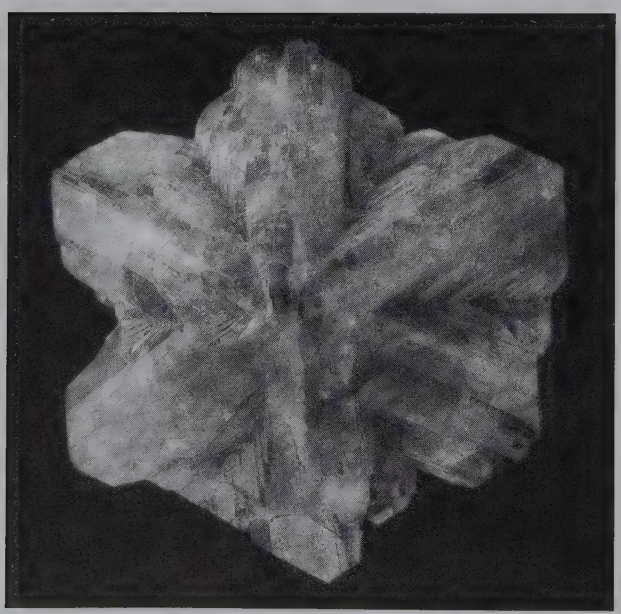

(*b*)

FIG. 16.28 (a) Cyclic twin of chrysoberyl. (b) Chrysoberyl, cyclic twin. From Minas Gerais, Brazil. Specimen is 4.6 cm high. (Photographs courtesy of Jeff Scovil, collection © Jeff Scovil.)

Ferrocolumbite–Ferrotantalite—$(Fe,Mn)Nb_2O_6$–$(Fe,Mn)Ta_2O_6$

Crystallography. Orthorhombic; *2/m2/m2/m*. Commonly in crystals. The habit is short prismatic or thin tabular on {010}; often in square shapes because of prominent development of {100} and {010} (Fig. 16.29). Also in heart-shaped twins, twinned on {201}.

Pcan; $a = 5.74$, $b = 14.27$, $c = 5.09$ Å; $Z = 4$. *d*s for ferrocolumbite: 3.66(7), 2.97(10), 1.767(6), 1.735(7), 1.712(8).

Physical Properties. *Cleavage* {010} good. **H** 6. **G** 5.2–7.9, varying with the composition, increasing with rise in percentage of Ta_2O_5 (Fig. 16.30). *Luster* submetallic. *Color* iron-black, frequently iridescent. *Streak* dark red to black. Subtranslucent.

Composition and Structure. A complete solid solution exists from *ferrocolumbite*, $(Fe,Mn)Nb_2O_6$, to *ferrotantalite*, $(Fe,Mn)Ta_2O_6$. Often contains small amounts of Sn and W. A variety known as *manganotantalite* is essentially tantalite with Mn^{2+} substituting for most of the Fe^{2+}. In the structure octahedral chains of $(Mn,Fe)O_6$ and $(Ta,Nb)O_6$ exist in which octahedra join through sharing of edges. The chains are linked to each other by common apices.

Diagnostic Features. Recognized usually by its black color with lighter-colored streak, and high specific gravity.

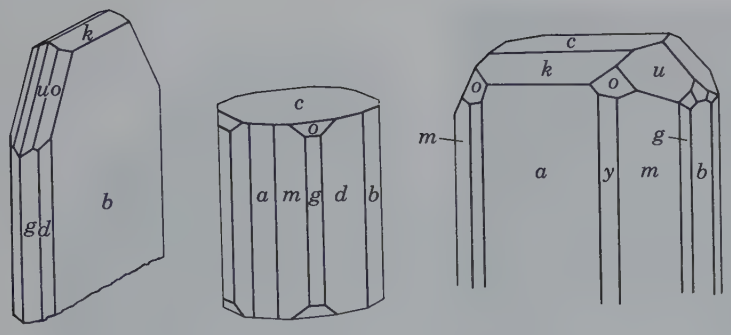

FIG. 16.29 Ferrocolumbite-ferrotantalite crystals.

Distinguished from wolframite by lower specific gravity and less distinct cleavage.

Occurrence. The minerals occur in granitic rocks and pegmatites, associated with quartz, feldspar, mica, tourmaline, beryl, spodumene, cassiterite, wolframite, microlite, and monazite.

Notable localities for their occurrence are Bernie Lake, Manitoba, Canada; Congo; Nigeria; Brazil; near Moss, Norway; Bodenmais, Bavaria, Germany; Ilmen Mountains, Russia. Western Australia (*manganotantalite*); and Madagascar. In the United States, it is found at Standish, Maine; Haddam, Middletown, and Branchville, Connecticut; in Amelia County, Virginia; Mitchell County, North Carolina; Black Hills, South Dakota; and near Canon City, Colorado.

Use. Source of tantalum and niobium. Because of its resistance to acid corrosion, tantalum is employed in chemical equipment, in surgery for skull plates and sutures, also in some tool steels and in electronic tubes. Niobium has its chief use in alloys in weldable high-speed steels, stainless steels, and alloys resistant to high temperatures, such as used in the gas turbine of the aircraft industry.

Name. *Columbite* from Columbia, a name for America, where the original specimen was obtained. *Tantalite* from the mythical Tantalus in allusion to the difficulty in dissolving in acid.

Similar Species. *Microlite*, $Ca_2Ta_2O_6(O,OH,F)$, is found in pegmatites; *pyrochlore*, $(Ca,Na)_2(Nb,Ta)_2O_6(O,OH,F)$, and *fergusonite*, $YNbO_4$, an oxide of niobium, tantalum, and rare earths (represented by *Y* in the fergusonite formula) are found associated with alkalic rocks.

FIG. 16.30 Ferrocolumbite-ferrotantalite. Variation of specific gravity with composition.

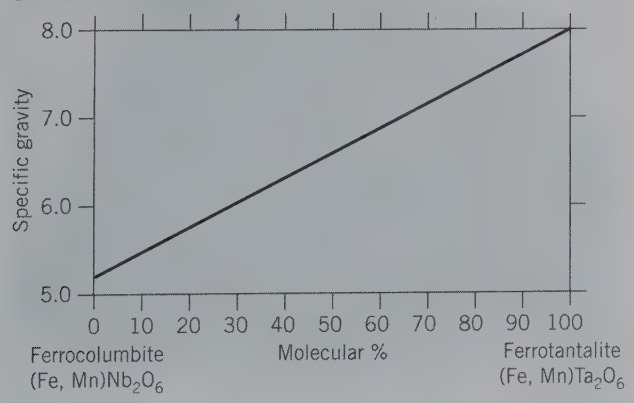

HYDROXIDES

Brucite—$Mg(OH)_2$

Crystallography. Hexagonal; $\bar{3}2/m$. Crystals are usually tabular on {0001} and may show small rhombohedral truncations. Commonly foliated (Fig. 16.31), massive.

$C\bar{3}m$; $a = 3.13$, $c = 4.74$ Å; $Z = 1$. *ds*: 4.74(8), 2.37(10), 1.793(10), 1.372(7), 1.189(9).

Physical Properties. *Cleavage* {0001} perfect. Folia flexible but not elastic. Sectile. **H** $2\frac{1}{2}$. **G** 2.39. *Luster* on base pearly, elsewhere vitreous to waxy. *Color* white, gray, light green. Transparent to translucent. *Optics*: (+), $\omega = 1.566$, $\epsilon = 1.581$.

Composition and Structure. For $Mg(OH)_2$: MgO 69.0, H_2O 31.0%. Fe^{2+} and Mn^{2+} may substitute for Mg. The structure is illustrated in Fig. 16.7. The perfect {0001} cleavage is parallel to the octahedral sheets. Upon heating, brucite transforms into periclase (MgO).

Diagnostic Features. Recognized by its foliated nature, light color, and pearly luster on cleavage face. Distinguished from talc by its greater hardness and lack of greasy feel, and from mica by being inelastic.

Occurrence. Brucite is found associated with serpentine, dolomite, magnesite, and chromite; as an alteration product of periclase and magnesium silicates, especially serpentine. It is also found in recrystallized limestone.

Notable localities for its occurrence are at Unst, one of the Shetland Islands, Scotland, and Aosta, Italy. In the United States, it is found at Tilly Foster Iron Mine, Brewster, New York; at Wood's Mine, Texas, Pennsylvania; and in Gabbs, Nevada.

Use. Brucite is used as a raw material for magnesia refractories and is a minor source of metallic magnesium.

Name. In honor of the early American mineralogist Archibald Bruce.

Similar Species. *Gibbsite*, $Al(OH)_3$, one of the three hydroxides of Al that are the main constituents of bauxite. The structure of gibbsite is like that of brucite, with one-third of the octahedral cation positions vacant (compare with Fig. 16.2a).

FIG. 16.31 Brucite crystals. Wood's Mine, Texas, Pennsylvania (Harvard Mineralogical Museum).

MANGANITE—MnO(OH)

Crystallography. Monoclinic; $2/m$ (pseudo-orthorhombic). Crystals are usually prismatic parallel to c and vertically striated (Figs. 16.32 and 16.33). Often columnar to coarse fibrous. Twinned on {011} as both contact and penetration twins.

$B2_1/d$; $a = 8.84$, $b = 5.23$, $c = 5.74$ Å, $\beta = 90°$; $Z = 8$. *d*s: 3.38(10), 2.62(9), 2.41(6), 2.26(7), 1.661(9).

Physical Properties. *Cleavage* {010} perfect, {110} and {001} good. **H** 4. **G** 4.3. *Luster* metallic. *Color* steel-gray to iron-black, see Plate III, no. 2. *Streak* dark brown. Opaque.

Composition and Structure. Mn 62.4, O 27.3, H_2O 10.3%. The structure consists of hexagonal closest packing of oxygen and $(OH)^-$ groups with Mn^{3+} in octahedral coordination with O^{2-} and $(OH)^-$. In this respect the structure is similar to that of diaspore (see Fig. 16.8); however the distribution of the cations is quite different.

Diagnostic Features. Recognized chiefly by its black color and prismatic crystals. Hardness (4) and brown streak distinguish it from pyrolusite.

Occurrence. Manganite is found associated with other manganese oxides in deposits formed by meteoric waters. Found often in low-temperature hydrothermal veins associated with barite, siderite, and calcite. It frequently alters to pyrolusite.

Occurs at Ilfeld, Harz Mountains, Germany, in fine crystals; also at Ilmenau, Thuringia, Germany, and Cornwall, England. In the United States, it is found at Negaunee, Michigan. It is also found in Nova Scotia, Canada.

Use. A minor ore of manganese.

Name. Named in allusion to the composition.

FIG. 16.32 Manganite.

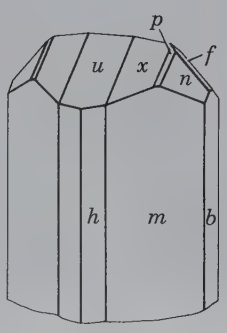

Romanechite—$(Ba,H_2O)_2(Mn^{4+},Mn^{3+})_5O_{10}$

Crystallography. Monoclinic, $2/m$. Massive, botryoidal, stalactitic (Fig. 16.34). Appears amorphous.

$P222$; $a = 9.45$, $b = 13.90$, $c = 5.72$; $Z = 2$. *d*s: 3.46(7), 2.87(7), 2.41(7), 2.190(10), 1.820(7).

Physical Properties. **H** 5–6. **G** 3.7–4.7. *Luster* submetallic. *Color* black. *Streak* brownish-black. Opaque.

FIG. 16.33 Manganite. Ilfeld, Germany (Harvard Mineralogical Museum).

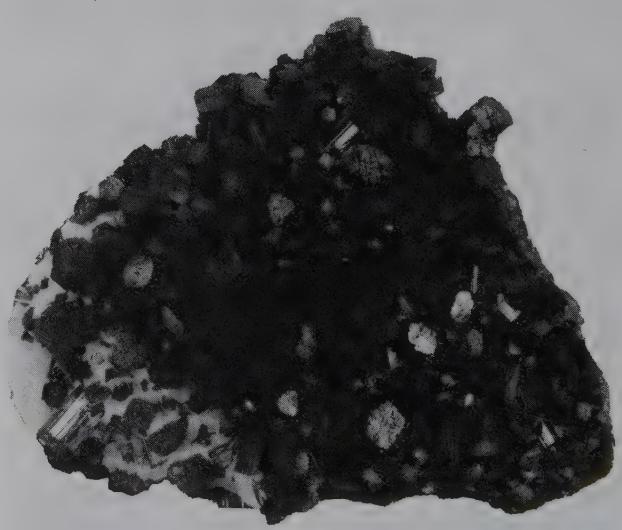

FIG. 16.34 Romanechite. Ironwood, Michigan (Harvard Mineralogical Museum).

Composition and Structure. Small amounts of Mg, Ca, Ni, Co, Cu, and Si may be present. The structure is somewhat similar to that of rutile (Fig. 16.4) with complex chains of MnO,OH octrahedra and large channels between adjoining chains. Both Ba and adsorbed H_2O are located in these channels. Upon heating to about 600°C, romanechite transforms into *hollandite*, $Ba_2Mn_8O_{16}$ (see Fig. 14.23).

Diagnostic Features. Distinguished from the other manganese oxides by its greater hardness and botryoidal form, and from limonite by its black streak.

Occurrence. Romanechite is a secondary mineral, often forms dendrites (Fig. 16.19); it occurs usually with pyrolusite, and its origin and associations are similar to those of that mineral.

Use. An ore of manganese. (See pyrolusite.)

Similar Species. Many of the hard botryoidal masses formerly called *psilomelane* are now known to be a mixture of several manganese oxides of which romanechite is a major constituent. Some of the other minerals commonly present in the mixture are *cryptomelane*, KMn_8O_{16}, *manjiroite*, $(Na,K)Mn_8O_{16}{\cdot}nH_2O$, and *todorokite* $(Mn,Ca,Mg)Mn_3O_7{\cdot}H_2O$. The presence of these and other minerals accounts for the oxides of Na, K, Ca, Co, Cu, Al, and Fe reported in chemical analyses of psilomelane.

Name. From the locality at Romanèche, France.

Diaspore—αAlO(OH)

Crystallography. Orthorhombic; $2/m2/m2/m$. Usually in thin crystals, tabular parallel to {010}; sometimes elongated on [001]. Bladed, foliated, massive, disseminated.

Pbnm; $a = 4.41$, $b = 9.40$, $c = 2.84$ Å; $Z = 4$. *d*s: 3.98(10), 2.31(8), 2.12(7), 2.07(7), 1.629(8).

Physical Properties. *Cleavage* {010} perfect. **H** $6\frac{1}{2}$–7. **G** 3.35–3.45. *Luster* vitreous except on cleavage face, where it is pearly. *Color* white, gray, yellowish, greenish. Transparent to translucent. *Optics*: (+), $\alpha = 1.702$, $\beta = 1.722$, $\gamma = 1.750$; $2V = 85°$; $X = c$, $Y = b$; $r < v$.

Composition and Structure. Al_2O_3 85, H_2O 15%. The structure is illustrated in Fig. 16.8 and consists of Al in 6-coordination with oxygen and OH^- forming $AlO_3(OH)_3$ octahedra. The structure of *boehmite*, γAlO(OH), is shown in Fig. 16.9.

Diagnostic Features. Characterized by its good cleavage, its bladed habit, and its high hardness.

Occurrence. Diaspore is commonly associated with corundum in emery rock, in dolomite, and in chlorite schist. In a fine-grained massive form, it is a major constituent of much bauxite.

Notable localities are Mugla, Turkey; the island of Naxos, Greece; and Postmasburg, South Africa. In the United States, it is found in Chester County, Pennsylvania; at Chester, Massachusetts; and with alunite, forming rock masses at Mt. Robinson, Rosite Hills, Colorado. It is found abundantly in the bauxite and aluminous clays of Arkansas, Missouri, and elsewhere in the United States.

Use. As a refractory.

Name. Derived from a Greek word meaning *to scatter*, in allusion to its decrepitation when heated.

GOETHITE—αFeO(OH)

Crystallography. Orthorhombic; $2/m2/m2/m$. Rarely in distinct prismatic, vertically striated crystals. Often flattened parallel to {010}. In acicular crystals. Also massive, reniform, stalactitic, in radiating fibrous aggregates (see photograph at the very beginning of this chapter). Foliated. The so-called *bog ore* is generally loose and porous.

Pbnm; $a = 4.65$, $b = 10.02$, $c = 3.04$ Å; $Z = 4$. *d*s: 4.21(10), 2.69(8), 2.44(7), 2.18(4), 1.719(5).

Physical Properties. *Cleavage* {010} perfect. **H** 5–$5\frac{1}{2}$. **G** 4.37; may be as low as 3.3 for impure material. *Luster* adamantine to dull, silky in certain fine, scaly, or fibrous varieties. *Color* yellowish-brown to dark brown, see Plate III, no. 3. *Streak* yellowish-brown. Subtranslucent.

Composition and Structure. Fe 62.9, O 27.0, H_2O 10.1%. Mn is often present in amounts up to 5%. The massive varieties often contain adsorbed or capillary H_2O. Goethite is isostructural with diaspore (see Fig. 16.8). *Lepidocrosite*, γFeO(OH), a polymorph of goethite, is a platy mineral and is often associated with goethite; it is isostructural with boehmite (see Fig. 16.9).

Diagnostic Features. Distinguished from hematite by its streak.

Occurrence. Goethite is one of the most common minerals and is typically formed under oxidizing conditions as a weathering product of iron-bearing minerals. It also forms as a direct inorganic or biogenic precipitate from water and is widespread as a deposit in bogs and springs. Goethite forms the gossan or "iron hat" over metalliferous veins (see Box 15.3). Large quantities of goethite have been found as residual lateritic mantles resulting from the weathering of serpentine.

Goethite in some localities constitutes an important ore of iron. It is the principal constituent of the valuable minette ores of Alsace-Lorraine, France. Other notable European

localities are: Eiserfeld in Westphalia, Germany; Příbram, Bohemia, Czech Republic; and Cornwall, England. Large deposits of iron-rich laterites composed essentially of goethite are found in the Mayari and Moa districts of Cuba.

In the United States, goethite is common in the Lake Superior hematite deposits and has been obtained in fine specimens at Negaunee, near Marquette, Michigan. Goethite is found in iron-bearing limestones along the Appalachian Mountains, from western Massachusetts as far south as Alabama. Such deposits are particularly important in Alabama, Georgia, Virginia, and Tennessee. Finely crystallized material occurs with smoky quartz and microcline in Colorado at Florissant and in the Pikes Peak region.

Use. An ore of iron (see also Box 16.1).

Name. In honor of Goethe, the German poet and philosopher.

Similar Species. *Limonite*, $FeO{\cdot}OH{\cdot}nH_2O$, is used mainly as a field term to refer to natural hydrous iron oxides of uncertain identity.

BAUXITE[2]—A Mixture of Diaspore, Gibbsite, and Boehmite

Crystallography. A mixture of minerals. Pisolitic, in round concretionary grains (Fig. 16.35); also massive, earthy, claylike.

Physical Properties. **H** 1–3. **G** 2–2.55. *Luster* dull to earthy. *Color* white, gray, yellow, red. Translucent.

Composition. A mixture of hydrous aluminum oxides in varying proportions. Some bauxites closely approach the composition of *gibbsite*, $Al(OH)_3$ (see brucite, "Similar Species"), but most are a mixture and usually contain some Fe. As a result, bauxite is not a mineral and should be used only as a rock name. The principal constituents of the rock bauxite are *gibbsite*, see Fig. 16.36; *boehmite*, $\gamma AlO(OH)$ (see Fig. 16.9), and *diaspore*, $\alpha AlO(OH)$ (see Fig. 16.8), any one of which may be dominant.

Diagnostic Features. Can usually be recognized by its pisolitic character.

Occurrence. Bauxite is of supergene origin, commonly produced under subtropical to tropical climatic conditions by prolonged weathering and leaching of silica from aluminum-bearing rocks. Also may be derived from the weathering of clay-bearing limestones. It has apparently originated as a colloidal precipitate. It may occur in place as a direct derivative of the original rock, or it may have been transported and deposited in a sedimentary formation. In the tropics deposits known as *laterites*, consisting largely of hydrous aluminum and ferric oxides, are found in the residual soils. These vary widely in composition and purity, but many are valuable as sources of aluminum and iron.

Bauxite occurs over a large area in the south of France, an important district being at Baux, near Arles, France. The principal world producers are Australia, Guinea, Brazil, Jamaica, and China. Other major producing countries are India, Russia, Kazakhstan, and Venezuela. In the United States, the chief deposits are found in Arkansas, Georgia, and Alabama. In Arkansas, bauxite has formed by the alteration of a nepheline syenite.

Use. The ore of aluminum. Eighty-five percent of the bauxite produced is consumed as aluminum ore. Because of its low density and great strength, aluminum has been

FIG. 16.35 Pisolitic bauxite. Bauxite, Arkansas.

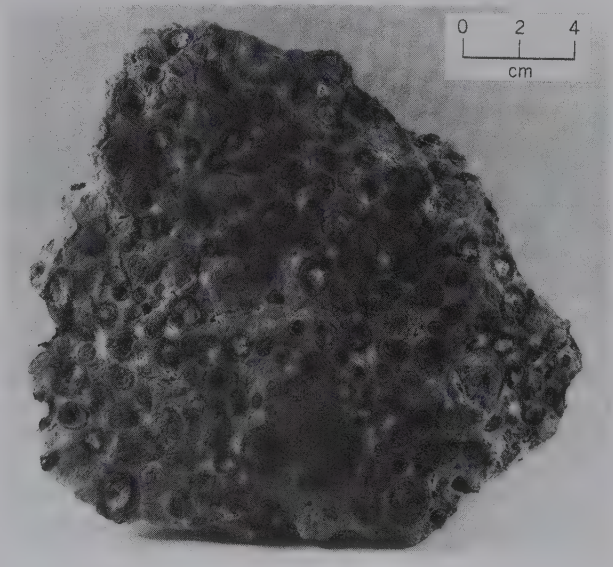

FIG. 16.36 Scanning electron micrograph of very small prismatic crystals of gibbsite (monoclinic) in bauxite from Surinam, South America (Courtesy of H. H. Murray, Indiana University).

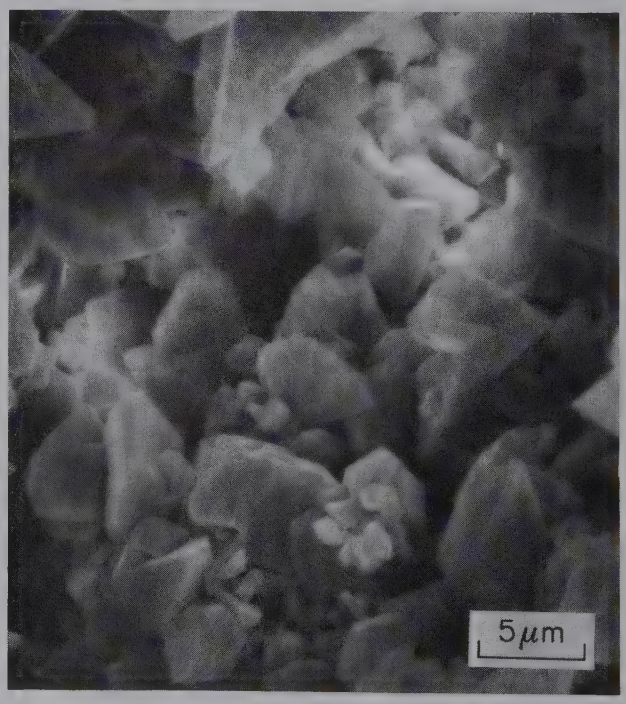

[2]Although bauxite is not a mineral species, it is described here because of its importance as the ore of aluminum.

adapted to many uses. Sheets, tubes, and castings of aluminum are used in automobiles, airplanes, and railway cars, where light weight is desirable. It is manufactured into cooking utensils, food containers, household appliances, and furniture. Aluminum is replacing copper to some extent in electrical transmission lines. Aluminum is alloyed with copper, magnesium, zinc, nickel, silicon, silver, and tin. Other uses are in paint, aluminum foil, and numerous salts.

The second largest use of bauxite is in the manufacture of Al_2O_3, which is used as an abrasive. It is also manufactured into aluminous refractories. Synthetic alumina is also used as the principal ingredient in heat-resistant porcelain, such as spark plugs.

Name. From its occurrence at Baux, France.

HALIDES

HALITE—NaCl

Crystallography. Isometric; $4/m\bar{3}2/m$. Habit cubic, see Plate III, no. 4; other forms are very rare. Some crystals hopper-shaped (Fig. 16.37). Found in crystals or granular crystalline masses showing cubic cleavage, known as *rock salt*. Also massive, granular to compact.

Fm3m; $a = 5.640$ Å; $Z = 4$. *ds*: 2.82(10), 1.99(4), 1.628(2), 1.261(2), 0.892(1).

Physical Properties. *Cleavage* {001} perfect. **H** $2\frac{1}{2}$. **G** 2.16. *Luster* transparent to translucent to greasy. *Color* colorless or white, or when impure may have shades of yellow, red, blue, purple. Salty taste. *Optics*: $n = 1.544$.

Composition and Structure. Na 39.3, Cl 60.7%. Commonly contains impurities, such as calcium and magnesium sulfates and calcium and magnesium chlorides. The structure of halite is illustrated in Figs. 16.10 and 4.17. This structure exists in a large number of *XZ* compounds with a radius ratio of between 0.41 and 0.73.

FIG. 16.37 Halite, hopper-shaped crystals.

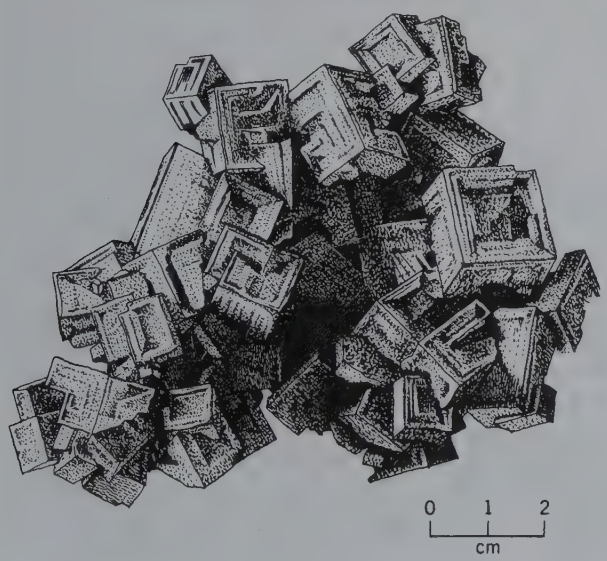

Diagnostic Features. Characterized by its cubic cleavage and taste, and distinguished from sylvite by its less bitter taste.

Occurrence. Halite is a common mineral, occurring in extensive beds and irregular masses, precipitated by evaporation with gypsum, sylvite, anhydrite, and calcite. Halite is dissolved in the waters of salt springs, salt lakes, and the ocean. It is a major salt in playa deposits of enclosed basins.

The deposits of salt have been formed by the gradual evaporation and ultimate drying up of enclosed bodies of salt water (see Box 16.2). The salt beds formed in this way may have subsequently been covered by other sedimentary deposits and gradually buried beneath the rock strata formed on them. Salt beds range between a few feet to over 200 feet in thickness, and it is estimated that some are buried beneath as much as 35,000 feet of overlying strata.

Extensive bedded deposits of salt are widely distributed throughout the world and are mined in over 110 countries. Important production comes from China, India, Australia, France, Canada and Mexico.

The United States is the world's largest producer; salt in commercial amounts is, or has been, produced in every state, either from rock-salt deposits or by evaporation of saline waters. Thick beds of rock salt extend from New York State through Ontario, Canada, and into Michigan. Salt is recovered from these beds at many localities. Notable deposits are also found in Ohio, Kansas, and New Mexico, and in Canada—in Nova Scotia and Saskatchewan. Salt is obtained by the evaporation of sea waters in California and Texas and from the waters of the Great Salt Lake in Utah.

Salt is also produced from *salt domes*, nearly vertical pipelike masses of salt that have risen upward to the surface from an underlying salt bed because salt is less dense than overlying rocks. Anhydrite, gypsum, and native sulfur are commonly associated with salt domes. Geophysical prospecting for frequently associated petroleum has located several hundred salt domes along the Gulf Coast of Louisiana and Texas and far out into the Gulf itself. Here, salt was deposited in a Jurassic-age rift basin to a thickness of over 1,500 m. Structures caused by these domes are traps for oil and gas. Salt domes are also found in Germany, Romania, Spain, and Iran. In Iran, in an area of complete aridity, salt that has punched its way to the surface is not dissolved but moves down slope as a salt glacier.

Use. Halite finds its greatest use in the chemical industry where it is the source of sodium and chlorine for the manufacture of hydrochloric acid and a large number of sodium compounds.

Salt is used extensively in the natural state in tanning hides, in fertilizers, in stock feeds, in salting icy highways, and as a weed killer. In addition to its familiar functions in the home, salt enters into the preparation of foods of many kinds, such as the preservation of butter, cheese, fish, and meat.

Name. Halite comes from the Greek word *halos* meaning *salt*.

BOX 16.2 Evaporite Minerals

When a restricted body of seawater or the waters of saline lakes evaporate, the elements in solution (see table) are precipitated in what are known as *evaporites*. More than 80 minerals (excluding clastic material) have been recorded in evaporites, and most of these are chlorides, sulfates, carbonates, and borates. Only about 11 rank as major constituents (see table). Upon evaporation, the general sequence of precipitation is this: some *calcite* (when the original volume of seawater is reduced by evaporation to about one-half), *gypsum* or *anhydrite* (with the volume reduced to one-fifth of the original), *halite* (with the volume reduced to one-tenth of the original), and finally *sulfates* and *chlorides* of Mg and K. If all the salt in a 1,000-foot (305 m) column of seawater were precipitated, it would form 0.5 feet (0.15 m) of calcium sulfate, 11.8 feet (3.6 m) of NaCl, and 2.6 feet (0.8 m) of K- and Mg-bearing salts, producing a total salt column of 15 feet (4.6 m) thick.

The photograph shows the fine and regular banding of calcite (darker bands in the photograph) alternating with gypsum (lighter bands) in the upper Permian Castile Evaporite sequence of West Texas and New Mexico. Seasonal changes in temperature and/or ionic concentration in the evaporating body of water result in regular cycles of mineral precipitation, and each couplet is concluded to represent a *varve*, which is an annual layer of sedimentation resulting from evaporation (Anderson, R.Y., W. E. Dean, Jr., D. W. Kirkland, and H. Snider, 1972, Permian Castile varved evaporite sequence. *Geological Society of America Bulletin* 83: 59–86).

Major Ionic Constituents of Seawater and Most Common Minerals in Evaporite Sequences*

	Normal Seawater (Ion Concentration as Parts per million)	Common Minerals in Marine Evaporites
K^{+}	380	Halite—NaCl
Na^{+}	10,556	Sylvite—KCl
Ca^{+2}	400	Carnallite—$KMgCl_3 \cdot 6H_2O$
Mg^{+2}	1,272	Anhydrite—$CaSO_4$
Cl^{-1}	18,980	Gypsum—$CaSO_4 \cdot 2H_2O$
$(SO_4)^{-2}$	2,649	Langbeinite—$K_2Mg_2(SO_4)_3$
$(HCO_3)^{-1}$	140	Polyhalite—$K_2Ca_2Mg(SO_4)_4 \cdot 2H_2O$
Total	34,387	Kieserite—$MgSO_4 \cdot H_2O$
		Calcite—$CaCO_3$
		Magnesite—$MgCO_3$
		Dolomite—$CaMg(CO_3)_2$

*After Stewart, F. H. 1963. *Marine Evaporites*. U.S. Geological Survey Professional Paper no. 440-Y

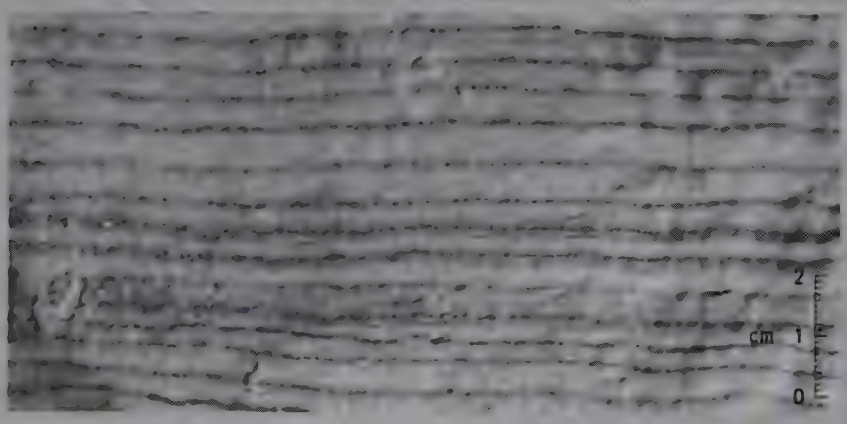

Finely varved outcrop specimen showing alternating bands of calcite (dark on account of enclosed organic matter) and gypsum (light). Diamond drill cores show that several hundred feet below the outcrop surface the original anhydrite has not yet been transformed (hydrated) to gypsum.

In natural deposits, the less-soluble minerals that precipitate early in the evaporation sequence tend to show increased abundance. Hence, gypsum and anhydrite are by far the most abundant evaporate minerals and commonly form massive beds. The deposition of calcium sulfate as gypsum or anhydrite depends on the temperature and salinity of the brine; anhydrite is formed at higher salt concentrations and at higher temperatures than gypsum. Halite forms about 95% of the chloride minerals in an evaporite sequence, but the more soluble salts are commonly missing in natural deposits. When present, thick and extensive beds of rock salt overlie the gypsum-anhydrite zone of marine evaporites.

Commercially, the amount of salt consumed as sodium chloride is relatively small compared to the amount used to produce chemicals, such as sodium hydroxide, chlorine, and chlorides. Common salt is also extracted from seawater in shallow impoundments where the modern climate allows evaporation, as in Western Australia, Mexico, Bahamas, India, Brazil, and Spain. Deposits of the more soluble salts such as sylvite, carnallite, and polyhalite are rare, because the deposition from brine may be interrupted or the salts may be redissolved. Nevertheless, large deposits (particularly of sylvite) have formed in places and are mined extensively as the chief source of potassium. Potassium is the third most common component of most chemical fertilizers (NPK: nitrogen, phosphorus, and potassium; see also Box 17.1).

SYLVITE—KCl

Crystallography. Isometric; $4/m\bar{3}2/m$. Cube and octahedron frequently in combination. Usually in granular crystalline masses showing cubic cleavage; compact.

Fm3m; $a = 6.293$ Å; $Z = 4$. *ds*: 3.15(10), 2.22(6), 1.816(2), 1.407(2), 1.282(4).

Physical Properties. *Cleavage* {001} perfect. **H** 2. **G** 1.99. Transparent when pure. *Color* colorless or white; also shades of blue, yellow, or red from impurities. Readily soluble in water. Salty taste but more bitter than halite. *Optics*: $n = 1.490$.

Composition and Structure. K 52.4, Cl 47.6%. May contain admixed NaCl. Sylvite has the NaCl structure (see Fig. 16.10) but because of the difference in the ionic radii of Na^+ (1.02 Å) and K^+ (1.38 Å) there is little solid solution between KCl and NaCl.

Diagnostic Features. Distinguished from halite by its more bitter taste.

Occurrence. Sylvite has the same origin, mode of occurrence, and associations as halite but is much rarer. It remains in solution after the precipitation of halite and is one of the last salts to be precipitated (see Box 16.2).

It is found in quantity and frequently well crystallized, associated with the salt deposits at Stassfurt, Germany. In the United States, it is found in large amounts in the Permian salt deposits near Carlsbad, New Mexico, and in western Texas. More recently, deposits have been located in Utah. The most important world reserves are in Saskatchewan, Canada, where extensive bedded deposits have been found at depths greater than 3,000 feet.

Use. It is the chief source of potassium compounds, which are principally used as fertilizers. (see Box 17.1).

Name. Potassium chloride is the *sal digestivus Sylvii* of early chemistry, whence the name for the species.

Other Potassium Salts. Several other potassium minerals are commonly associated with sylvite and are found in Germany and Texas in sufficient amount to make them valuable as sources of potassium salts. These are *carnallite*, $KMgCl_3 \cdot 6H_2O$, a usually massive to granular, generally light-colored mineral; *kainite*, $KMg(Cl,SO_4) \cdot 2\frac{3}{4}H_2O$; and *polyhalite*, $K_2Ca_2Mg(SO_4)_4 \cdot 2H_2O$.

Chlorargyrite—AgCl

Crystallography. Isometric; $4/m\bar{3}2/m$. Habit cubic, but crystals are rare. Usually massive, resembling wax; often in plates and crusts.

Fm3m; $a = 5.55$ Å; $Z = 4$. *ds*: 3.20(5), 2.80(10), 1.97(5), 1.67(2), 1.61(2).

Physical Properties. **H** 2–3. **G** 5.5 ±. Sectile, can be cut with a knife; hornlike appearance, hence the name *horn silver*. Transparent to translucent. *Color* pearl-gray to colorless. Rapidly darkens to violet-brown on exposure to light. *Optics*: $n = 2.07$.

Composition and Structure. Ag 75.3, Cl 24.7%. A complete solid solution series exists between AgCl and *bromargyrite*, AgBr. Small amounts of F may be present in substitution for Cl or Br. Some specimens contain Hg. Chlorargyrite is isostructural with NaCl (see Fig. 16.10).

Diagnostic Features. Distinguished chiefly by its waxlike appearance and its sectility.

Occurrence. Chlorargyite is an important supergene ore of silver found in the upper, enriched zone of silver deposits. It is found associated with native silver, cerussite, and secondary minerals in general.

Notable amounts have been found at Broken Hill, Australia; and in Peru, Chile, Bolivia, and Mexico. In the United States chlorargyrite was an important mineral in the mines at Leadville and elsewhere in Colorado, at the Comstock Lode in Nevada, and in crystals at the Poorman's Lode in Idaho.

Use. A silver ore.

Name. Chlorargyrite, from its composition.

Similar Species. Other closely related minerals that are less common but form under similar conditions, are *bromargyrite* AgBr, and *iodian bromargyrite*, Ag(Cl,Br,I), isostructural with chlorargyrite; and *iodargyrite*, AgI, which is hexagonal.

Cryolite—Na_3AlF_6

Crystallography. Monoclinic; $2/m$. Prominent forms are {001} and {110}. Crystals are rare, usually cubic in aspect, and in parallel groupings growing out of massive material. Usually massive.

$P2_1/n$; $a = 5.47$, $b = 5.62$, $c = 7.82$ Å, $\beta = 90°11'$; $Z = 2$. *ds*: 4.47(2), 3.87(2), 2.75(7), 2.33(4), 1.939(10).

Physical Properties. Parting on {110} and {001} produces cubical forms. **H** $2\frac{1}{2}$. **G** 2.95–3.0. *Luster* vitreous to greasy. *Color* colorless to snow-white. Transparent to translucent. *Optics*: (+), $\alpha = 1.338$, $\beta = 1.338$, $\gamma = 1.339$; $2V = 43°$; $X = b$, $Z \wedge c = -44°$, $r < v$. The low refractive index, near that of water, gives the mineral the appearance of watery snow or paraffin, and causes the powdered mineral to almost disappear when immersed in water.

Composition and Structure. Na 32.8, Al 12.8, F 54.4%. In the structure of cryolite Al is octahedrally coordinated to six F^-. The Na^+ ions are also surrounded by six F^- ions, but in a somewhat less regular pattern. At high temperature (above 550°C), cryolite transforms to an isometric form with space group *Fm3m*.

Diagnostic Features. Characterized by pseudocubic parting, white color, and peculiar luster; and for the Greenland cryolite, the association of siderite, galena, and chalcopyrite.

Occurrence. The only important deposit of cryolite is at Ivigtut, on the west coast of Greenland. Here, in a large mass in granite, it is associated with siderite, galena, sphalerite, and chalcopyrite; and less commonly quartz, wolframite, fluorite, cassiterite, molybdenite, arsenopyrite, columbite. It is found at Miask, Russia; in the United States, at the base of Pikes Peak, Colorado; and in crystals in Montreal, Quebec, Canada.

Use. Cryolite is used for the manufacture of sodium salts, of certain kinds of glass and porcelain, and as a flux for cleansing metal surfaces. Early on, it was used as a source of aluminum. When bauxite became the ore of aluminum, cryolite was used as a flux in the electrolytic process. Today, with the essential exhaustion of the Ivigtut deposit, the sodium aluminum fluoride used in the aluminum industry is manufactured from fluorite.

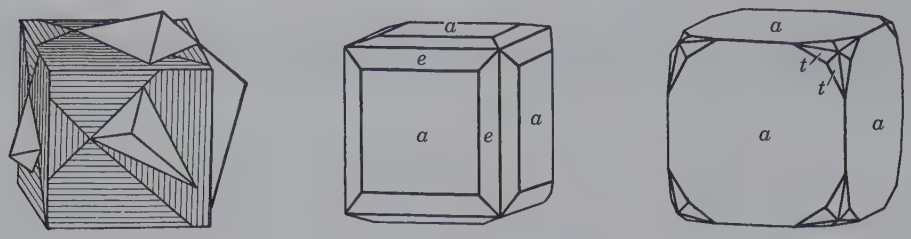

(a) (b) (c)

FIG. 16.38 Fluorite. (a) Penetration twin. (b) Cube and tetrahexahedron. (c) Cube and hexoctahedron.

Name. Name is derived from two Greek words, *kryos* meaning *frost* and *lithos* meaning *stone*, in allusion to its icy appearance.

FLUORITE—CaF_2

Crystallography. Isometric; $4/m\bar{3}2/m$. Usually in cubes, often as penetration twins twinned on [111] (Fig. 16.38a and 16.39). Other forms are rare, but examples of all forms of the hexoctahedral class have been observed; the tetrahexahedron (Fig. 16.38b) and hexoctahedron (Fig. 16.38c) are characteristic. Usually in crystals or in cleavable masses. Also massive; coarse or fine granular; columnar.

Fm3m; $a = 5.46$ Å; $Z = 4$. *d*s: 3.15(9), 1.931(10), 1.647(4), 1.366(1), 1.115(2).

Physical Properties. *Cleavage* {111} perfect, see Plate III, no. 5. **H** 4. **G** 3.18. Transparent to translucent. *Luster* vitreous. *Color* varies widely; most commonly light green (see Plate XII, no. 1, Chapter 20), yellow, bluish-green, or purple; also colorless, white, rose, blue, brown. The color in some fluorite results from the presence of a hydrocarbon, in others from Frenkel defects. A single crystal may show bands of varying colors; the massive variety is also often banded in color. The phenomenon of fluorescence (see page 26) received its name because early on it was observed in some varieties of fluorite. *Optics*: $n = 1.433$.

Composition and Structure. Ca 51.3, F 48.7%. The rare earths, particularly Y and Ce, may substitute for Ca. The fluorite structure is shown in Figs. 16.11 and 4.20.

Diagnostic Features. Determined usually by its cubic crystals and octahedral cleavage; also vitreous luster and usually fine coloring, and by the fact that it can be scratched with a knife.

Occurrence. Fluorite is a common and widely distributed mineral. Usually found in hydrothermal veins in which it may be the primary mineral or as a gangue mineral with metallic ores, especially those of lead and silver. Common in vugs in dolomites and limestone and has been observed also as a minor accessory mineral in various igneous rocks and pegmatites. Associated with many different minerals, as calcite, dolomite, gypsum, celestite, barite, quartz, galena, sphalerite, cassiterite, topaz, tourmaline, wolframite, and apatite.

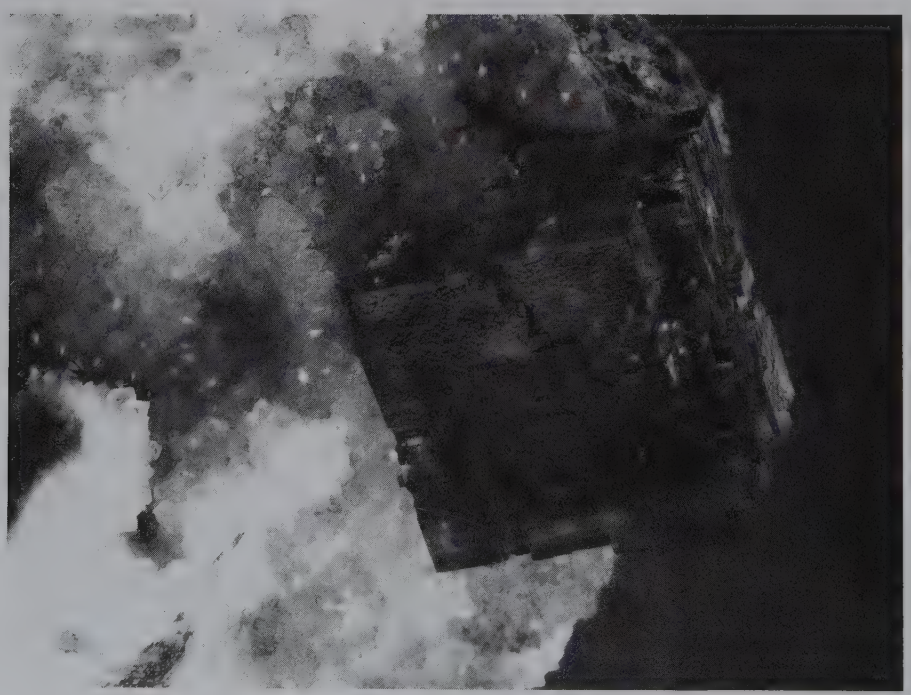

FIG. 16.39 Fluorite cube, displaying growth steps, on quartz. From La Collada, Asturias, Spain. Specimen is 2.4 cm high. (Photos courtesy of Jeff Scovil, collection © Jeff Scovil.)

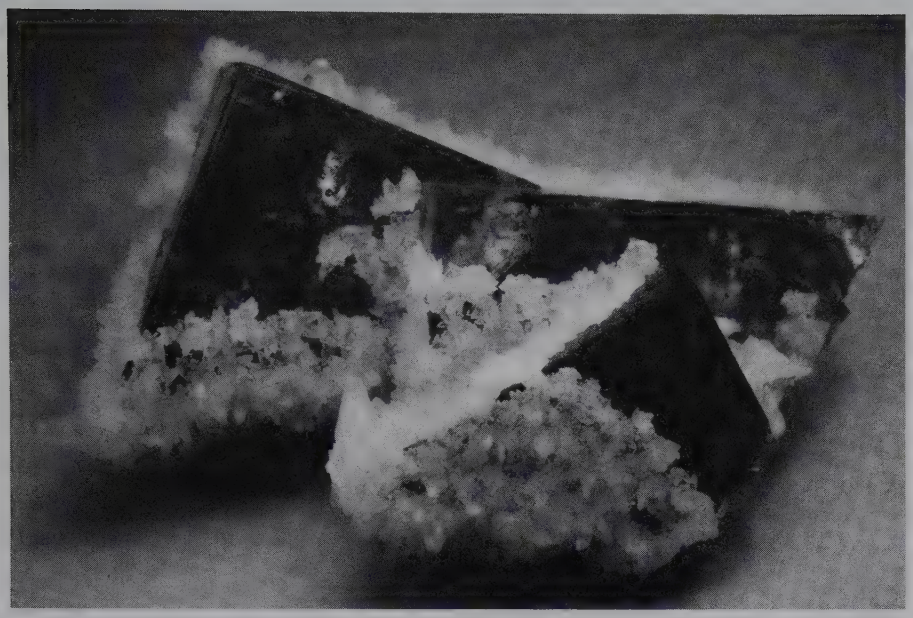

FIG. 16.40 Yellow fluorite cubes coated by white quartz crystals. Cave-in-Rock, Harding County, Illinois (Harvard Mineralogical Museum).

Fluorite is found in quantity in England, chiefly from Cumbria, Derbyshire, and Durham; the first two localities are famous for their magnificent crystallized specimens. Found commonly in the mines of Saxony, Germany. Fine specimens come from the Alps. The large producers of commercial fluorite (fluorspar) are: Mongolia, Russia, Republic of South Africa, China, Spain, and Mexico. Compared with these countries, the production in the United States is small, but there are significant amounts mined in southern Illinois near Rosiclare and Cave-in-Rock. Much of the fluorite at Cave-in-Rock is in coarse crystalline aggregates lining flat, open spaces, and thus the locality is the source of many beautifully crystallized specimens (Fig. 16.40). Fluorite is also mined in small amounts in Nevada, Texas, and Utah.

Use. The bulk of the fluorite produced is used in the chemical industry (over 50%), mainly in the preparation of hydrofluoric acid, and as a flux in the making of steel (over 40%). Other uses are in the manufacture of glass, fiberglass, pottery, and enamel. Formerly used extensively as an ornamental material and for carving vases and dishes. Small amounts of fluorite are used for lenses and prisms in various optical systems, but most of the optical material is now made synthetically.

Name. From the Latin *fluere*, meaning to flow, because it melts more easily than other minerals with which it was (in the form of cut stones) confused.

Atacamite—$Cu_2Cl(OH)_3$

Crystallography. Orthorhombic; $2/m2/m2/m$. Commonly found in slender prismatic crystals with vertical striations. Also tabular parallel to {010}. Usually in confused crystalline aggregates; fibrous; granular.

Pnam; $a = 6.02, b = 9.15, c = 6.85$ Å; $Z = 4$. *d*s: 5.48(10), 5.03(7), 2.84(5), 2.78(5), 2.76(6).

Physical Properties. *Cleavage* {010} perfect. **H** $3-3\frac{1}{2}$. **G** 3.75–3.77. *Luster* adamantine to vitreous. *Color* various shades of green. Transparent to translucent. *Optics*: (−), $\alpha = 1.831, \beta = 1.861, \gamma = 1.880$; $2V = 75°$; $r < v$. $X = b, Y = a$.

Composition and Structure. Cu 14.88, CuO 55.87, Cl 16.60, H_2O 12.65%. In the structure of atacamite part of the Cu atoms is in 6-coordination with five (OH) groups and one Cl. The remaining Cu is in 6-coordination with four (OH) groups and two Cl.

Diagnostic Features. Characterized by its green color and granular crystalline aggregates. Distinguished from malachite by its lack of effervescence in acid.

Occurrence. Atacamite is a comparatively rare copper mineral. Found originally as sand in the province of Atacama in Chile. Occurs in arid regions as a supergene mineral in the oxidized zone of copper deposits. It is associated with other secondary minerals in various localities in Chile, especially Chuquicamata, and in some of the copper districts of South Australia. In the United States, occurs sparingly in the copper districts of Arizona.

Use. A minor ore of copper.

Name. From the province of Atacama, Chile.

REFERENCES AND FURTHER READING

Anthony, J. W., R. A. Bideaux, K. W. Bladh, and M. C. Nichols. 1997. *Handbook of mineralogy*. Vol. 3, *Halides, hydroxides, oxides*. Mineral Data Publications, Tucson, Arizona.

Bragg, L., and G. F. Claringbull. 1965. *Crystal structures of minerals*. G. Bell and Sons, Ltd., London.

Evans, R. C. 1966. *An introduction to crystal chemistry*. 2nd ed. Cambridge University Press: Cambridge, England.

Mandarino, J. H., and M. E. Back. 2004. *Fleischer's glossary of mineral species 2004*. The Mineralogical Record, Inc., Tucson.

Oxide minerals. 1976. *Reviews in Mineralogy* 3. Mineralogical Society of America, Washington, D.C.

Oxide minerals: Petrologic and magnetic significance. 1991. *Reviews in Mineralogy* 25. Edited by D. H. Lindsley. Mineralogical Society of America, Washington, D.C.

Palache, C., H. Berman, and C. Frondel. 1944 and 1951. *The system of mineralogy.* 7th ed. Vols. 1 and 2. Wiley, New York.

U.S. Geological Survey, *Mineral Commodity Summaries*, 2005. Available at *http://minerals.usgs.gov/minerals/pubs/commodity.*

CHAPTER 17

Crystal Chemistry and Systematic Descriptions of Carbonates, Nitrates, Borates, Sulfates, Chromates, Tungstates, Molybdates, Phosphates, Arsenates, and Vanadates

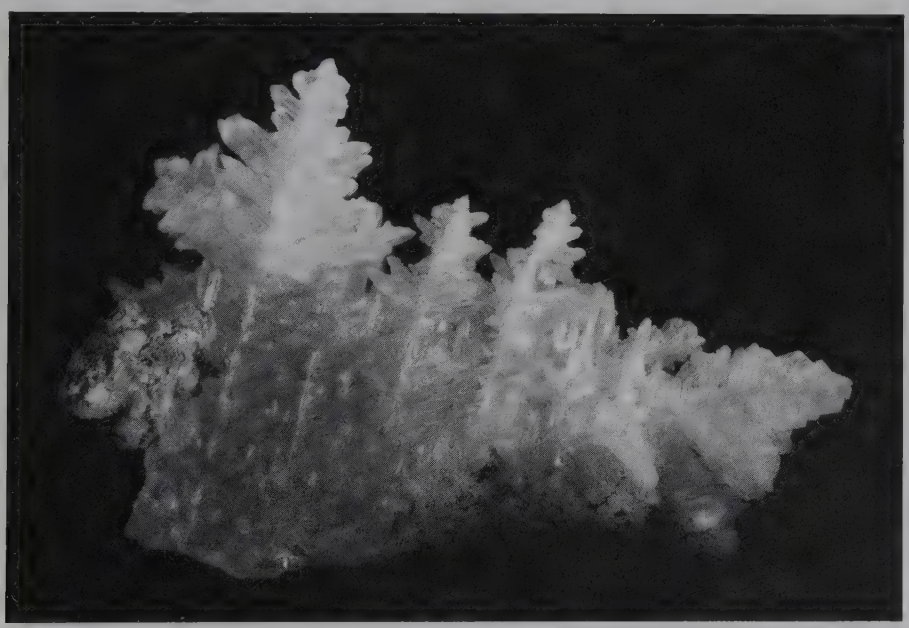

Cerussite, $PbCO_3$, in crystals that cross each other at 60° angles, forming what is known as a reticulated pattern. From Tsumeb, Namibia (Harvard Mineralogical Museum).

Carbonates, nitrates, borates, sulfates, chromates, tungstates, molybdates, phosphates, arsenates, and vanadates together number 1508 species, but most are uncommon minerals and only a few are considered here. The five largest groups are: phosphates with 438 species, sulfates with 301 species, arsenates with 256 species, carbonates with 234 species, and borates with 135 species. Many of these minerals are described as industrial minerals. They are those minerals that have a direct industrial application owing to their distinct physical properties or chemical composition. Specifically excluded from industrial minerals are the ore minerals because their primary function is the production of metals. Examples of the use of industrial minerals in products are: abrasives, cements, ceramics, drilling fluids, electronics, fluxes, glass, pigments, and wallboard.

These chemically diverse minerals are treated together because most of them contain *anionic complexes*, that are strongly bonded units in their structures. Examples of anionic complexes are: $(CO_3)^{2-}$ in carbonates, $(NO_3)^{-}$ in nitrates, $(PO_4)^{3-}$ in phosphates, $(SO_4)^{2-}$ in sulfates, $(CrO_4)^{2-}$ in chromates, $(WO_4)^{2-}$ in tungstates, and $(AsO_4)^{3-}$ in arsenates. The bond strengths within such anionic complexes are always stronger than those between the anionic complex and other ions of the structure; these compounds are therefore referred to as *anisodesmic* (see page 75). For example, in the carbonates, radius ratio considerations predict three closest oxygen neighbors about carbon. This arrangement is triangular with carbon at the center and oxygen at each of the corners of the triangle (see Fig. 17.1); the (NO_3) group is also triangular. The e.v. of the bonds between carbon (C^{4+}) and each of the three closest oxygens is: $\frac{\text{valence}}{\text{C.N.}} = \frac{4}{3} = 1\frac{1}{3}$. This means that each oxygen (O^{2-}) has a residual charge of e.v. $= \frac{2}{3}$ for bonding other ions in the carbonate structure. Figure 17.1 illustrates the anisodesmic character of structures with tetrahedral (PO_4) and (SO_4) anionic groups as well. Borates with triangular (BO_3) groups and silicates with tetrahedral (SiO_4) groups are examples of *mesodesmic* bonding (see page 76).

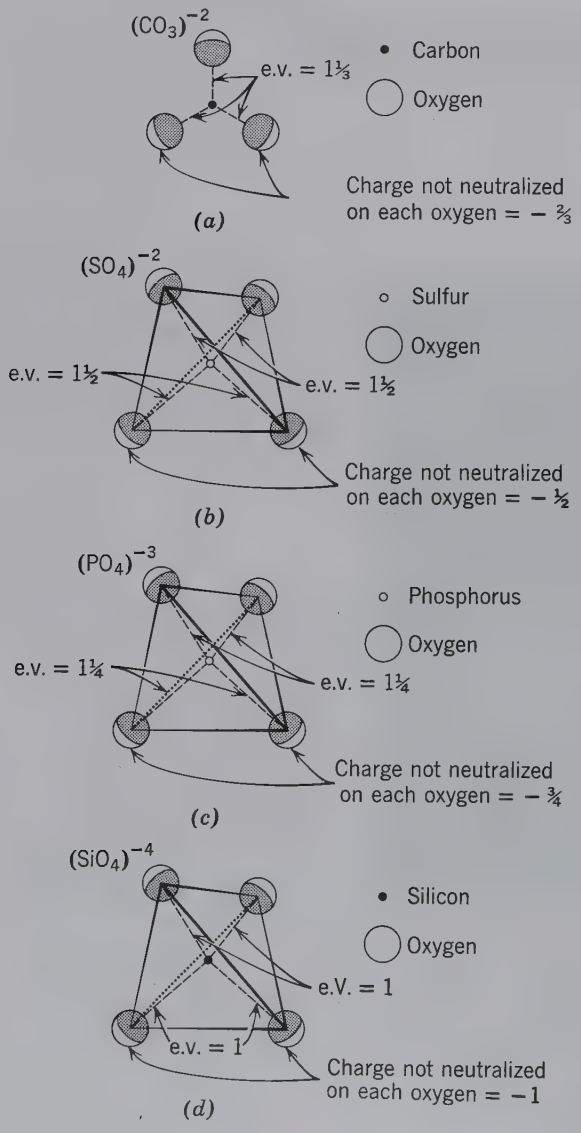

FIG. 17.1 (a), (b), (c) Examples of anionic complexes, their bond strengths between the central cation and oxygen, and the residual charges on the oxygens. (d) The tetrahedral (SiO_4) group in which the e.v.s between oxygen and the central cation are the same as the residual charge on the oxygen (= 1).

CRYSTAL CHEMISTRY OF CARBONATES

The anionic $(CO_3)^{2-}$ complexes of carbonates are strongly bonded units and do not share oxygens with each other (the residual e.v. of $\frac{2}{3}$ does not allow this). The triangular carbonate groups are the basic building units of all carbonate minerals and are largely responsible for the properties peculiar to the group.

Although the bond between the central carbon and its coordinated oxygens in the (CO_3) group is strong, it is not as strong as the covalent bond in CO_2. In the presence of hydrogen ion, the carbonate group becomes unstable and breaks down to yield CO_2 and water, according to $2H^+ + CO_3 \rightarrow H_2O + CO_2$. This reaction causes the familiar "fizz" with acid, which is widely used in the identification of carbonates.

The important anhydrous carbonates fall into three structurally different groups: the *calcite group*, the *aragonite group*, and the *dolomite group*. Aside from the minerals in these groups, the hydrous copper carbonates, azurite and malachite, are the other important carbonates.

Calcite Group (Hexagonal; $R\bar{3}c$)	
Calcite	$CaCO_3$
Magnesite	$MgCO_3$
Siderite	$FeCO_3$
Rhodochrosite	$MnCO_3$
Smithsonite	$ZnCO_3$

Aragonite Group (Orthorhombic; *Pmcn*)	
Aragonite	$CaCO_3$
Witherite	$BaCO_3$
Strontianite	$SrCO_3$
Cerussite	$PbCO_3$

Dolomite Group (Hexagonal; $R\bar{3}$)	
Dolomite	$CaMg(CO_3)_2$
Ankerite	$CaFe(CO_3)_2$

Monoclinic Carbonates with (OH)	
Malachite	$Cu_2CO_3(OH)_2$
Azurite	$Cu_3(CO_3)_2(OH)_2$

CALCITE GROUP

The above five members of the calcite group are isostructural with space groups $R\bar{3}c$. This group is characterized by cations with ionic radii less than 1 Å. The structure of calcite, one of the earliest to be analyzed by X-rays by W. L. Bragg in 1914 (see Fig. 17.2a), is a derivative of the NaCl structure in which triangular (CO_3) groups replace the spherical Cl, and Ca is in place of Na. The triangular shape of the (CO_3) groups causes the resulting structure to be rhombohedral instead of isometric as in NaCl. The (CO_3) groups lie in planes at right angles to the 3-fold (*c*) axis (Fig. 17.2a) and the Ca ions, in alternate planes, are in 6-coordination with oxygens of the (CO_3) groups.

FIG. 17.2 (a) Structure of calcite, $CaCO_3$. (b) The relation of the steep, true unit cell to the cleavage rhombohedron, which is face-centered. A hexagonal cell (rhomb-based prism) is also shown.

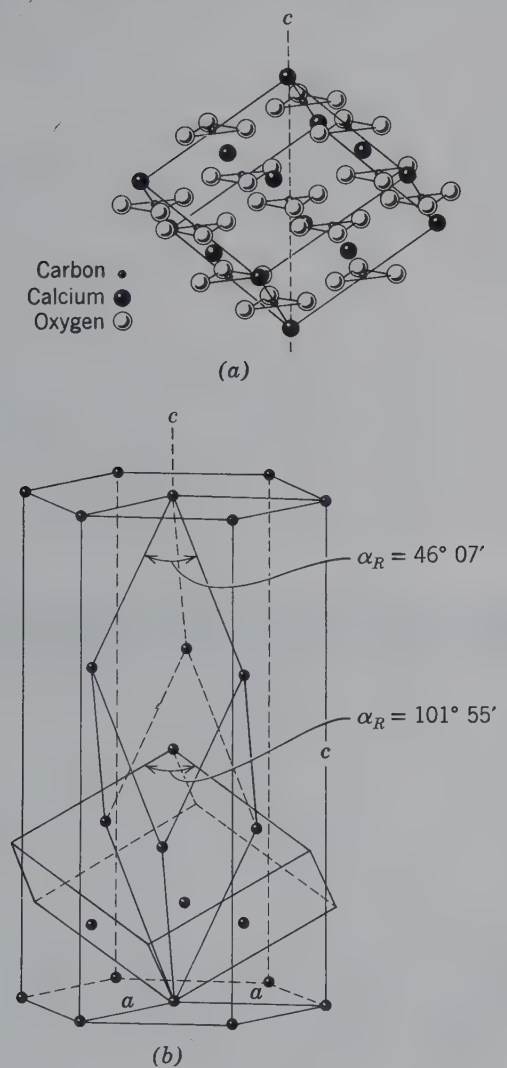

Each oxygen is coordinated to two Ca ions as well as to a carbon ion at the center of the (CO_3) group.

Calcite shows perfect rhombohedral cleavage to which, traditionally, the indices of $\{10\bar{1}1\}$ have been assigned. In the morphological descriptions and indexing of forms of the calcite and dolomite group minerals, this convention has been preserved. However, X-ray structural determinations have shown that this rhombohedron does not correspond to the correct unit cell, and that the simplest unit cell is a much steeper rhombohedron (Fig. 17.2b). Therefore, the structural axial ratios differ from the morphological. The radius ratio of Ca:O (= 0.714) in $CaCO_3$ is so close to the limiting value between 6- and 8-coordination (0.732) that $CaCO_3$ occurs in two structure types: *calcite*, with 6-coordination of Ca to O and *aragonite*, with 9-coordination of Ca to O.

ARAGONITE GROUP

When the (CO_3) group is combined with large divalent cations (ionic radii greater than 1.0 Å), the radius ratios generally do not permit stable 6-coordination and orthorhombic structures result. This is the *aragonite structure type* (Fig. 17.3 and Table 4.2, p. 68) with space group *Pmcn*. $CaCO_3$ occurs in both the *calcite* and *aragonite structure types* because although Ca is somewhat large for 6-coordination (calcite), it is relatively small, at room temperature, for 9-coordination (aragonite); calcite is the stable form of $CaCO_3$ at room temperature (see Fig. 17.4). Carbonates with larger cations, such as $BaCO_3$, $SrCO_3$, and $PbCO_3$, however, have the aragonite structure, stable at room temperature. In the aragonite structure, the (CO_3) groups as in calcite, lie perpendicular to the *c* axis, but in two structural planes.

FIG. 17.3 The structure of aragonite, $CaCO_3$, as projected on (100). Oxygens that would normally superimpose have been made visible by some displacement. Numbers represent heights of atomic positions above the plane of origin, marked with respect to *a*. Dashed rectangle outlines the unit cell. Ca–O bonds are also shown.

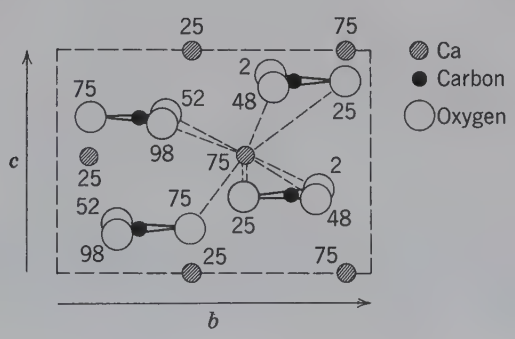

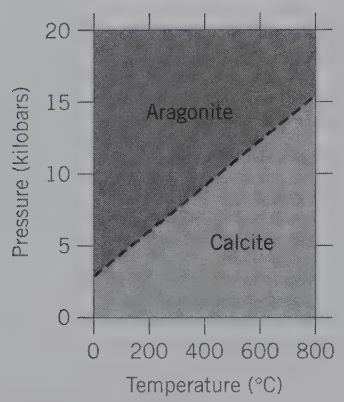

FIG. 17.4 The approximate location of the experimentally determined stability fields of calcite and aragonite.

The (CO_3) triangular groups of one plane point in opposite directions to those of the other. In calcite all (CO_3) groups lie in a single structural plane and point in the same direction (Fig. 17.2a). Each Ca is surrounded by nine closest oxygens. The cations are in approximate hexagonal closest packing, which gives rise to marked pseudohexagonal symmetry. This is reflected in both the crystal angles and in the cyclical twinning, which is characteristic of all members of the group.

Solid solution within the aragonite group is more limited than in the calcite group. Ca and Ba, respectively the smallest and largest ions in the group, form an ordered compound *barytocalcite*, $BaCa(CO_3)_2$, analogous to dolomite, $CaMg(CO_3)_2$, in the system $CaCO_3$–$MgCO_3$. The differences in physical properties of the minerals of the aragonite group are conferred largely by the cations. Thus, the specific gravity is roughly proportional to the atomic weight of the metal ions (Table 2.5).

DOLOMITE GROUP

The dolomite group includes *dolomite*, $CaMg(CO_3)_2$, *ankerite*, $CaFe(CO_3)_2$, and *kutnahorite*, $CaMn(CO_3)_2$. These three carbonates are isostructural with space group $R\bar{3}$. The structure of dolomite is similar to that of calcite but with Ca and Mg layers alternating along the *c* axis. The large difference in size of the Ca^{2+} and Mg^{2+} ions (33%) causes *cation ordering* with the two cations in specific, and separate levels in the structure. With the nonequivalence of Ca and Mg layers, the two-fold rotation axes of calcite do not exist, and the symmetry is reduced to that of the rhombohedral class, $\bar{3}$. The composition of dolomite is intermediate between $CaCO_3$ and $MgCO_3$ with Ca : Mg = 1 : 1. The occurrence of this ordered compound, however, does not imply that solid solution exists between $CaCO_3$ and $MgCO_3$ (see Fig. 17.5). In the dolomite structure, especially at low temperatures, each of the two divalent cations occupies a structurally distinct position. At higher temperatures (above 700°C), dolomite

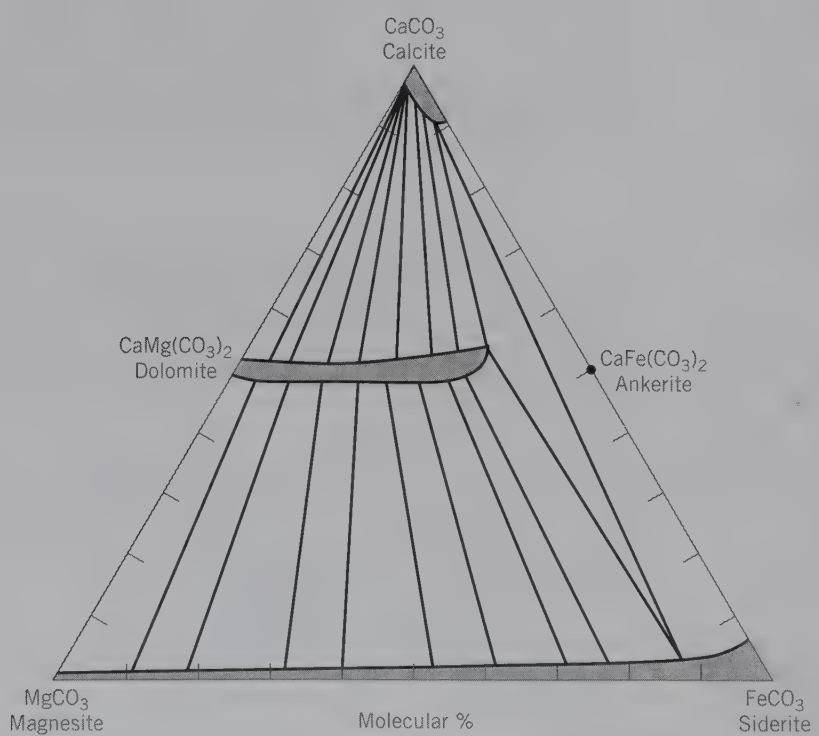

FIG. 17.5 Carbonates and their solid solution in the system CaO–MgO–FeO–CO_2. The extent of solid solution in this diagram is based upon chemical analyses of carbonates in metamorphic rocks that have been metamorphosed to about 400°C (biotite zone of the greenschist facies). Tielines connect commonly coexisting carbonate species. Calcite-dolomite coexistences are common in Mg-containing limestones; ankerite-siderite coexistences are found in banded iron-formations. (Adapted from Anovitz, L. M. and E. J. Essence. 1987. Phase equilibria in the system $CaCO_3$–$MgCO_3$–$FeCO_3$. *Journal of Petrology* 28, 389–415.)

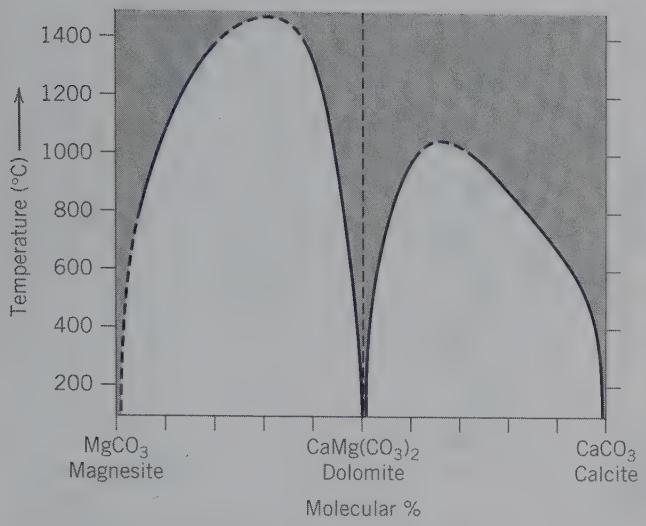

FIG. 17.6 T–X diagram of $CaCO_3$–$MgCO_3$ system at high CO_2 pressures that stabilize carbonates. Vertical dashed line is ideal dolomite composition. Solid solution is shown by shading. (Adapted from Anovitz, L. M. and E. J. Essene. 1987. Phase equilibria in the system $CaCO_3$–$MgCO_3$–$FeCO_3$. *Journal of Petrology* 28:389–415.)

shows small deviations from the composition with Ca : Mg = 1 : 1 as shown in Fig. 17.6. This diagram also shows that at elevated temperatures calcite coexisting with dolomite becomes more magnesian. Similarly dolomite in dolomite–calcite pairs becomes more calcic. At temperatures above about 1000° to 1100°C, a complete solid solution exists between calcite and dolomite, but not between dolomite and magnesite. The compositions of coexisting dolomite and calcite have been used for an estimate of temperatures of crystallization of rocks containing both carbonates, using the temperature scale in Fig. 17.6.

CRYSTAL CHEMISTRY OF NITRATES

The minerals in this group are structurally similar to the carbonates with planar, triangular $(NO_3)^-$ groups, much like the $(CO_3)^{2-}$ group. Like C in the (CO_3) group, the highly charged and highly polarizing N^{5+} ion binds its three coordinated oxygens into a close-knit group in which the strength of the oxygen-nitrogen bond (e.v. = $1\frac{2}{3}$) is greater than any other possible bond in the structure. Because of the greater strength of this N–O bond as compared with the C–O bond, nitrates are less readily decomposed by acids than carbonates. There are 15 nitrate minerals but, with the exception of nitratite and niter, they are very rare.

CRYSTAL CHEMISTRY OF BORATES

Within the borate group of minerals $(BO_3)^{3-}$ complexes are capable of polymerization (similar to the polymerization of SiO_4 tetrahedral groups in the silicates) in the form of chains, sheets, and isolated multiple groups (Fig. 17.7). This is possible because the small B^{3+} ion, which generally coordinates three oxygens in a triangular group, has bond strengths to each O with an e.v. = 1; this is exactly half the bonding energy of the oxygen ion. This permits a single oxygen to be shared between two boron ions linking the (BO_3) triangles into expanded structural units (double triangles, triple rings, sheets, and chains). Because the triangular coordination of (BO_3) is close to the upper stability limit of 3-coordination, boron is found also in 4-coordination in tetrahedral groups. In addition to (BO_3) and (BO_4) groups, natural borates may contain complex ionic groups, such as $[B_3O_3(OH)_5]^{2-}$ (Fig. 17.7e), that consist of one triangle and two tetrahedra. In the structure of *colemanite*, $CaB_3O_4(OH)_3{\cdot}H_2O$, complex infinite chains of tetrahedra and triangles occur, and in *borax*, $Na_2B_4O_5(OH)_4{\cdot}8H_2O$, a complex ion, $[B_4O_5(OH)_4]^{2-}$ consisting of two tetrahedra and two triangles is found (Fig. 17.7f). Borates can be classified on the basis of the structural anionic linking (or lack thereof) as insular (independent single or double (BO_3) or (BO_4) groups), chain, sheet, and framework structures.

Although it is possible to construct a three-dimensional boxwork made up of (BO_3) triangles only and having the composition B_2O_3, such a configuration has a very low stability and disorders readily, yielding a glass. Because of the tendency to form somewhat disordered networks of (BO_3) triangles, boron is regarded as a "network-former" in glass manufacture and is used in the preparation of special glasses of light weight and high transparency to energetic radiation.

CRYSTAL CHEMISTRY OF SULFATES

In the structures of sulfide minerals, sulfur occurs as the large, divalent sulfide anion. This ion results from the filling by captured electrons of the two vacancies in the outer, or valance, electron shell. The six electrons normally present in this shell may be lost, giving rise to a small, highly charged and highly polarizing positive S^{6+} ion (radius = 0.12 Å). It occurs in tetrahedral coordination with surrounding oxygens. The sulfur to oxygen bond in such an ionic group is very strong (e.v. = $1\frac{1}{2}$; see Fig. 17.1b) and covalent in its properties and produces tightly bound groups that do not share oxygens.

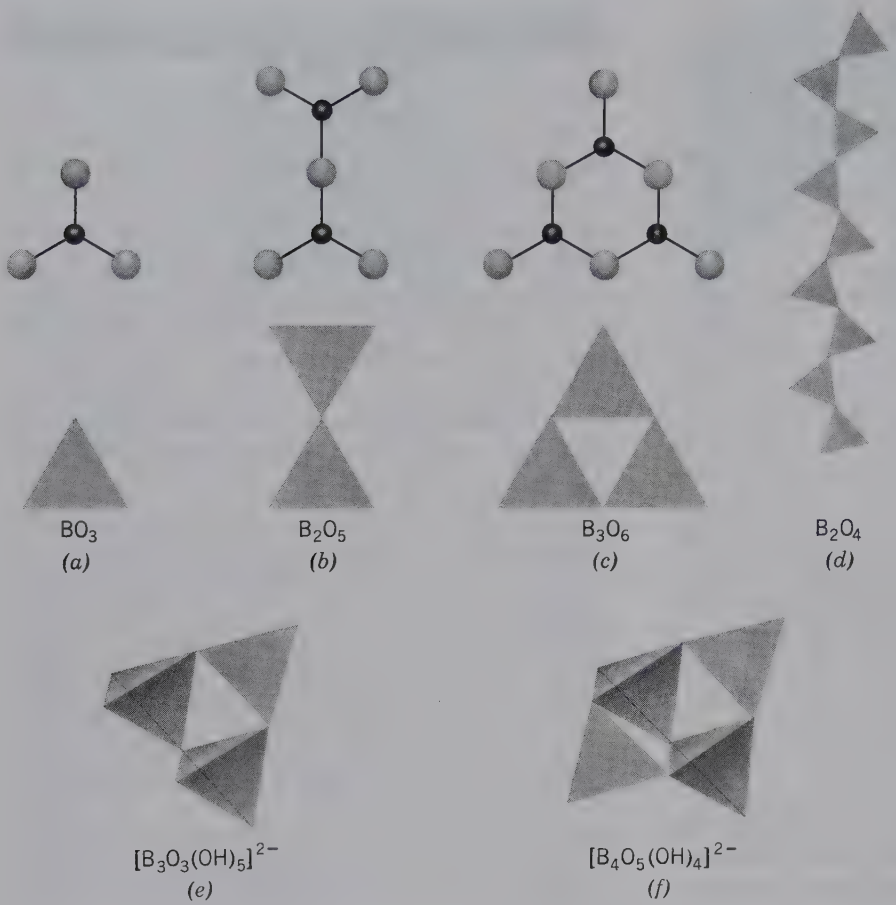

FIG. 17.7 Independent BO_3 triangles (a), multiple groups (b) and (c), and chains (d) in borates. Also complex triple and quadruple groups (e) and (f). The triple group in (e) consists of two $BO_2(OH)_2$ tetrahedra and a BO_2OH triangle. The group in (f) contains two BO_3OH tetrahedra and two BO_2OH triangles; this type of group is present in the structure of borax (see Fig. 17.35).

These anionic $(SO_4)^{2-}$ groups are the fundamental structure units of the sulfate minerals.

The most important and common of the anhydrous sulfates are members of the *barite group* (space group *Pnma*), with large divalent cations coordinated with the sulfate ion. Part of the structure of *barite*, $BaSO_4$, is illustrated in Fig. 17.8. Each barium ion is coordinated to 12 oxygen ions belonging to seven different (SO_4) groups. The barite type structure is also found in manganates (with MnO_4 tetrahedral groups) and chromates (with CrO_4 tetrahedral groups) which contain large cations.

Anhydrite, $CaSO_4$, because of the smaller size of Ca^{2+} compared to Ba^{2+}, has a different structure from that of barite (see Fig. 17.9). Each Ca^{2+} is coordinated to eight

FIG. 17.8 The structure of barite, $BaSO_4$, as projected on (010). The dashed lines outline the unit cell. The oxygen atoms, which would normally superimpose, have been displaced from their positions in this projection.

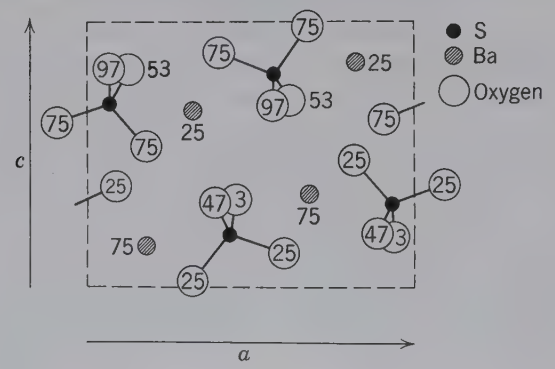

FIG. 17.9 The structure of anhydrite, $CaSO_4$.

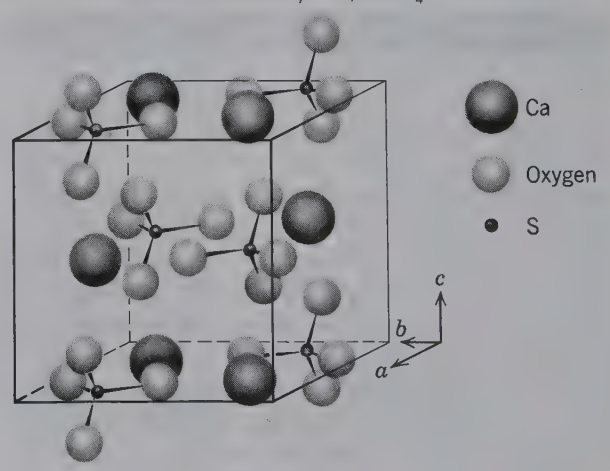

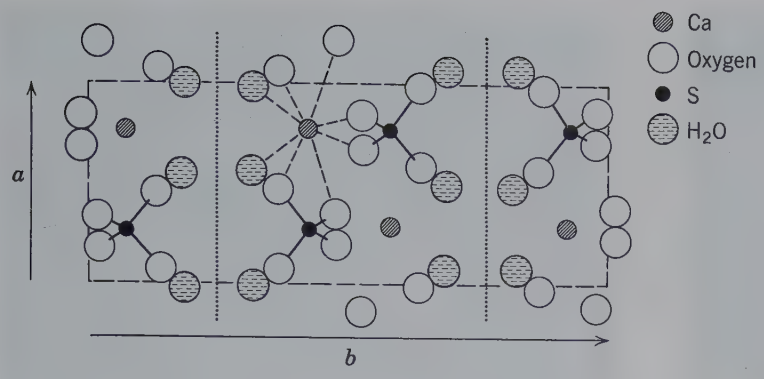

FIG. 17.10 The structure of gypsum, $CaSO_4 \cdot 2H_2O$, projected on (001). Perfect (010) cleavage is indicated by dotted lines. Dashed lines outline unit cell. The 8-coordination (six oxygens and two water molecules) is indicated for one Ca^{2+}.

nearest neighbor oxygens from the tetrahedral (SO_4) groups.

Of the hydrous sulfates, *gypsum*, $CaSO_4 \cdot 2H_2O$, is the most important and abundant. The structure of gypsum is illustrated in Fig. 17.10. Gypsum is monoclinic with space group *C2/c*. The structure consists of layers parallel to {010} of $(SO_4)^{2-}$ groups strongly bonded to Ca^{2+}. Successive layers of this type are separated by sheets of H_2O molecules. The bonds between H_2O molecules in neighboring sheets are weak, which explains the excellent {010} cleavage in gypsum. Loss of the water molecules causes collapse of the structure and transformation into a metastable polymorph of anhydrite ($\gamma CaSO_4$) with a large decrease in specific volume and loss of perfect cleavage.

CRYSTAL CHEMISTRY OF TUNGSTATES AND MOLYBDATES

W^{6+} and Mo^{6+} are considerably larger than S^{6+} and P^{5+}. Hence, when these ions enter into ionic groups with oxygen, the four coordinated oxygen ions do not occupy the apices of a regular tetrahedron, as is the case in the sulfates and phosphates, but form a somewhat flattened grouping of square outline. Although W (at. wt. 184) has a much greater atomic weight than Mo (96), both belong to the same family of the periodic table and, because of the lanthanide contraction, have the same ionic radii. As a result, each may substitute for the other in the anionic complex. In nature, however, geochemical differentiation often separates these elements, and it is not uncommon to find primary tungstates almost free of Mo and vice versa. In secondary minerals, the two elements are more commonly in solid solution with each other.

The minerals of this chemical class fall mainly into two isostructural groups. The *wolframite group* contains compounds with fairly small divalent cations such as Fe^{2+}, Mn^{2+}, Mg, Ni, and Co in 6-coordination with (MoO_4). Complete solid solution occurs between Fe^{2+} and Mn^{2+} in the minerals of this group.

The *scheelite group* contains compounds of larger ions such as Ca^{2+} and Pb^{2+} in 8-coordination with $(WO_4)^{2-}$ and $(MoO_4)^{2-}$ groups. The structure of scheelite (see Fig. 17.11) is close to that of anhydrite and zircon, $ZrSiO_4$, but differs from these in the manner of linking of the CaO_8 polyhedra. The (WO_4) tetrahedra are somewhat flattened along the *c* axis and join edges with CaO_8. W and Mo may substitute for each other, forming a partial series between *scheelite*, $CaWO_4$, and *powellite*, $CaMoO_4$; and *stolzite*, $PbWO_4$, and *wulfenite*, $PbMoO_4$. The substitution of Ca and Pb for one another forms partial series between scheelite and stolzite and between powellite and wulfenite.

FIG. 17.11 Structure of scheelite, $CaWO_4$.

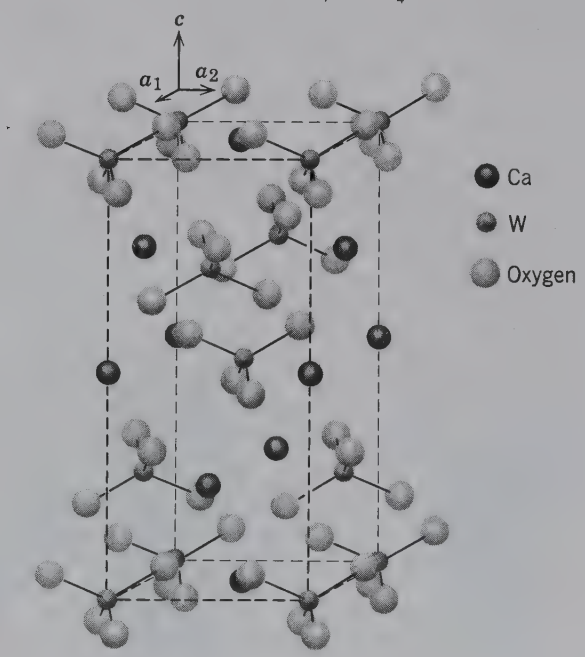

CRYSTAL CHEMISTRY OF PHOSPHATES, ARSENATES, AND VANADATES

P^{5+} is only slightly larger than S^{6+} and, like sulfur, forms a tetrahedral anionic $(PO_4)^{3-}$ group with oxygen (see Fig. 17.1). All phosphates contain this phosphate anionic complex as the fundamental building unit. Similar tetrahedral units, $(AsO_4)^{3-}$ and $(VO_4)^{3-}$ occur in arsenates and vanadates. P^{5+}, As^{5+}, and V^{5+} may substitute for each other in the anionic groups. This type of substitution is best shown in the pyromorphite series of the apatite group. *Pyromorphite*, $Pb_5(PO_4)_3Cl$, *mimetite*, $Pb_4(AsO_4)_3Cl$, and *vanadinite*, $Pb_5(VO_4)_3Cl$, are isostructural, and all gradations of composition between the end members exist.

The structure of *apatite*, $Ca_5(PO_4)_3(OH,F,Cl)$, which is the most important and abundant phosphate, is illustrated in Fig. 17.12. The oxygens of the (PO_4) groups are linked to Ca in two different structural sites. In one site Ca is in irregular 9-coordination, and in the other in irregular 8-coordination. Each fluorine (or Cl or OH) lies in a triangle with three calciums. Apatite shows extensive solid solution with respect to anions as well as cations. (PO_4) may be substituted for by (AsO_4) or (VO_4), but also in part by tetrahedral (CO_3OH) groups, giving rise to *carbonate–apatite*, $Ca_5F(PO_4,CO_3OH)_3$. Small amounts of (SiO_4) and (SO_4) may also be present in substitution for (PO_4); these types of substitution must be coupled with other cation substitutions in apatite in order to retain the electrical neutrality of the structure. F may be replaced by (OH) or Cl producing *hydroxylapatite*, $Ca_5(PO_4)_3(OH)$ and *chlorapatite*, $Ca_5(PO_4)_3Cl$. Mn^{2+} and Sr^{2+} may substitute for Ca. These varied ionic substitutions are typical of the phosphates, which generally have rather complicated structures.

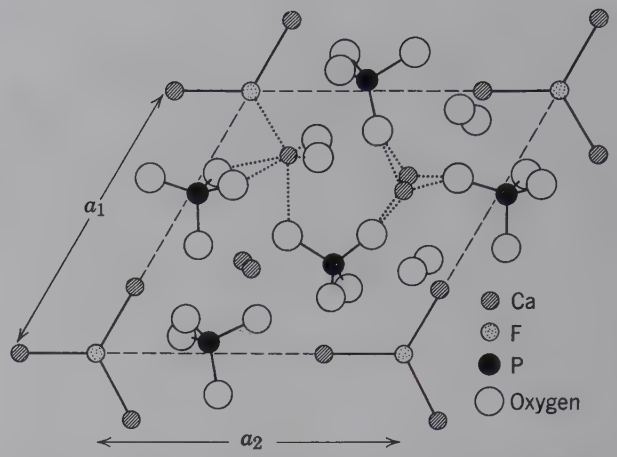

FIG. 17.12 Structure of fluorapatite, $Ca_5(PO_4)_3F$, projected on the (0001) plane. The dashed parallelogram outlines the base of the unit cell. The tetrahedral (PO_4) groups, triangular coordination of F to Ca, and examples of the two types of coordination about Ca are shown.

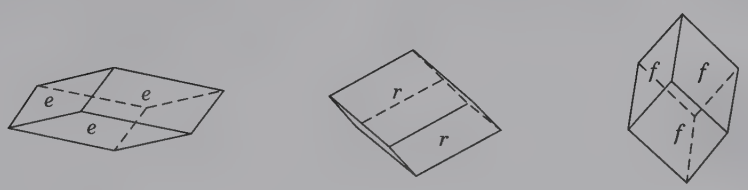

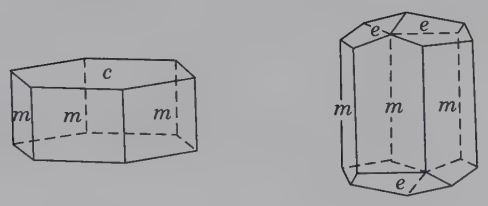

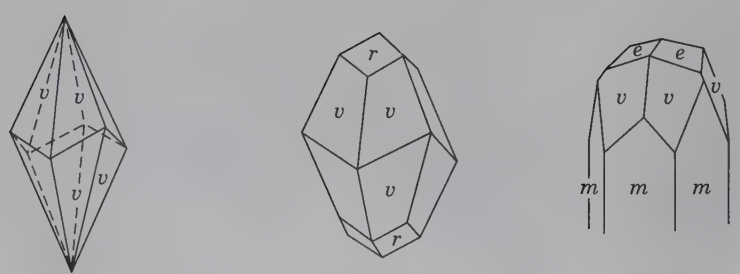

FIG. 17.13 Calcite crystals. Forms. $c\{0001\}$, $m\{10\bar{1}0\}$, $e\{01\bar{1}2\}$, $r\{10\bar{1}1\}$, $f\{02\bar{2}1\}$, $v\{21\bar{3}1\}$.

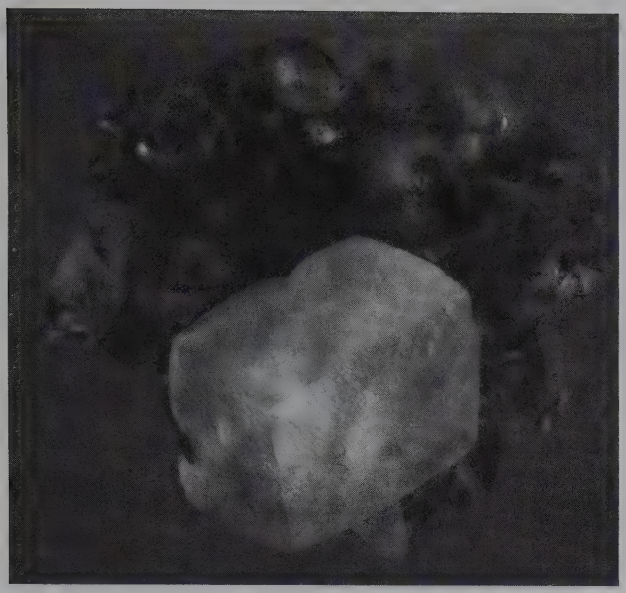

FIG. 17.14 Calcite rhombohedron, displaying growth steps, on amethyst. From Rio Grande do Sul, Brazil. Specimen is 8 cm high (Photographs courtesy of Jeff Scovil, collection © Jeff Scovil).

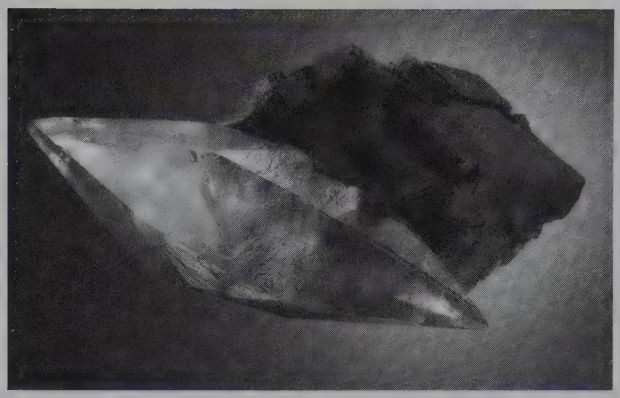

FIG. 17.15 Calcite scalenohedron on fluorite. Note the growth steps on and cubic crystal form of fluorite. From St. Louis Level, Annabel Lee Mine, Hardin County, Illinois, USA. Specimen is 10 cm long (Photographs courtesy of Jeff Scovil, collection © Jeff Scovil).

SYSTEMATIC DESCRIPTIONS

CARBONATES

Of the 234 carbonates known only 13 are described on the following pages.

CALCITE—$CaCO_3$

Crystallography. Hexagonal; $\bar{3}2/m$. Crystals are extremely varied in habit and often highly complex. More than 300 different forms have been described (Figs. 17.13 and 17.14). Three important habits exist: (1) prismatic, in long or short prisms, in which the prism faces are prominent, with base or rhombohedral terminations; (2) rhombohedral, in which rhombohedral forms predominate (Fig. 17.14); the unit (cleavage) form *r* is not common; (3) scalenohedral, in which scalenohedrons predominate (Fig. 17.15), often with prism faces and rhombohedral truncations. The most common scalenohedron is $\{21\bar{3}1\}$. All possible combinations and variations of these types are found.

Twinning with the twin plane, $\{01\bar{1}2\}$, very common (Fig. 17.16a); often produces twinning lamellae that may, as in marble, be of secondary origin. This twinning may be produced artificially (see page 276). Twins with {0001}, the twin plane common (Fig. 17.16b). Calcite is usually in crystals or in coarse- to fine-grained aggregates. Also fine-grained to compact, earthy, and stalactitic.

$R\bar{3}c$. Hexagonal cell, $a = 4.99$, $c = 17.06$ Å; $Z = 6$; rhombohedral cell, $a = 6.37$ Å, α (rhombohedral angle) = 46°05′; $Z = 2$. *ds*: 3.04(10), 2.29(2), 2.10(2), 1.913(2), 1.875(2).

Physical Properties. *Cleavage* $\{10\bar{1}1\}$ perfect (cleavage angle = 74°55′). Parting along twin lamellae on $\{01\bar{1}2\}$ **H** 3 on cleavage, $2\frac{1}{2}$ on base. **G** 2.71. *Luster* vitreous to earthy. *Color* usually white to colorless, but may be variously tinted, gray, red, green, blue, yellow; also when impure, brown to black. Transparent to translucent. The chemically pure and optically clear, colorless variety is known as *Iceland spar* because of its occurrence in Iceland, see Plate III, no. 6. *Optics:* (−); $\omega = 1.658$, $\epsilon = 1.486$.

Composition and Structure. Most calcites tend to be relatively close to pure $CaCO_3$ with CaO 56.0 and CO_2 44.0%. Mn^{2+}, Fe^{2+}, and Mg may substitute for Ca and a complete solid solution series extends to rhodochrosite, $MnCO_3$, above 550°C; a very partial series, with up to 5 weight percent FeO in calcite, exists between calcite and siderite, $FeCO_3$. Some inorganic calcites may contain from 0 to about 2 weight percent MgO. Calcites in the hard parts of living organisms, however, show a range of $MgCO_3$ of 2 to 16 molecular percent. See Fig. 17.5 for solid solution series in the system CaO–MgO–FeO–CO_2. The structure of calcite is shown in Fig. 17.2a and discussed on page 40.

Diagnostic Features. Fragments effervesce readily in cold dilute HCl. Characterized by its hardness (3),

FIG. 17.16 Twinned calcite crystals. Twin planes: (a) $\{01\bar{1}2\}$. (b) {0001}.

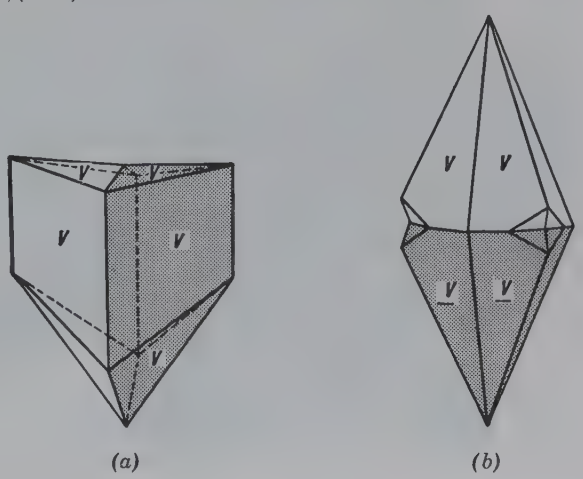

rhombohedral cleavage, light color, vitreous luster. Distinguished from dolomite by the fact that coarse fragments of calcite effervesce freely in cold HCl and distinguished from aragonite by lower specific gravity, rhombohedral cleavage, and crystal forms.

Occurrence. As a *rock-forming mineral*: Calcite is one of the most common widespread minerals. It occurs in extensive sedimentary rock masses in which it is the predominant mineral; in *limestones*, it is essentially the only mineral present. Metamorphosed limestones are *marbles*. *Chalk* is a fine-grained powdery deposit of calcium carbonate. Calcite is an important constituent of calcareous marls and calcareous sandstones. Limestone has, in large part, been formed by the deposition on a sea bottom of great thicknesses of calcareous material in the form of shells and skeletons of marine animals. A smaller proportion of these rocks has been formed directly by precipitation of calcium carbonate.

As cave deposits, and so on: Waters carrying calcium carbonate in solution and evaporating in limestone caves often deposit calcite as stalactites, stalagmites, and incrustations. Such deposits, usually semitranslucent and of light yellow colors, are often beautiful and spectacular. An example is Carlsbad Caverns, New Mexico. Both hot and cold calcareous spring water may form cellular deposits of calcite known as *travertine*, or *tufa*, around their mouths, or around vegetation. The deposit at Mammoth Hot Springs, Yellowstone Park, is more spectacular than most, but of similar origin. *Onyx marble* is banded calcite and/or aragonite used for decorative purposes. Because much of this material comes from Baja California, Mexico, it is also called *Mexican onyx*.

Siliceous calcites: Calcite crystals may enclose considerable amounts of quartz sand (up to 60%) and form what are known as sandstone crystals. Such occurrences are found at Fontainebleau, France (Fontainebleau limestone), and in the Badlands, South Dakota.

Calcite occurs as a primary mineral in some igneous rocks, such as carbonatites and nepheline syenites. One such occurrence is near Magnet Cove, Arkansas. It is a late crystallization product in the cavities in lavas. It is also a common mineral in hydrothermal veins associated with sulfide ores.

It is impossible to specify all the important districts for the occurrence of calcite in its various forms. Some of the more notable classic localities in which finely crystallized calcite is found are as follows: Andreasberg in the Harz Mountains, Germany; in Cumbria (Fig. 17.17), and Lancashire, England; Iceland; and Guanajuato, Mexico. In the United States, at Joplin, Missouri, and the Lake Superior copper district.

Use. The most important use for calcite is for the manufacture of cements and lime for mortars. Limestone is the chief raw material, which when heated to about 900°C forms *quicklime*, CaO, by the reaction: $CaCO_3 \rightarrow CaO + CO_2\uparrow$. The CaO, when mixed with water, forms one or several CaO-hydrates (slaked lime), swells, gives off heat, and hardens or, as commonly termed, *sets*. Quicklime when mixed with sand forms common mortar.

Limestone is used in the manufacture of cements. The type known as *Portland cement* is most widely produced. It is composed of about 75% calcium carbonate (limestone) with the remainder essentially silica and alumina. Small amounts of magnesium carbonate and iron oxide are also present. In some limestone, known as *cement rocks*, the correct proportions of silica and alumina are present as impurities. In others, these oxides are contributed by clay or shale mixed with the limestone before "burning." When water is mixed with cement, hydrous calcium silicates and calcium aluminates are formed.

Limestone is a raw material for the chemical industry, and finely crushed is used as a soil conditioner, for whiting and whitewash. The largest quantities are used as a flux for smelting various metallic ores, as an aggregate in concrete, as road material, and as an agent for flue gas desulfurization. A fine-grained limestone is used in lithography.

Calcite in several forms is used in the building industry. Limestone and marble as dimension stone are used both for

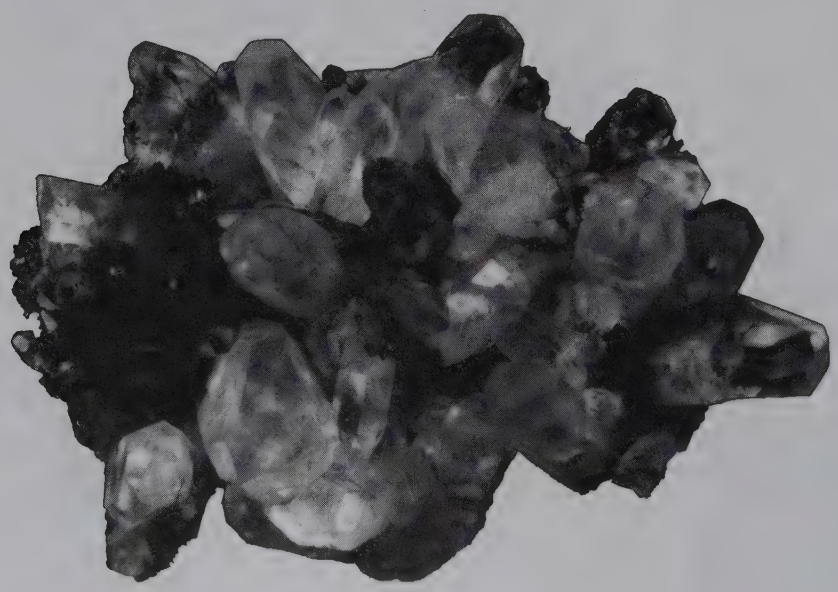

FIG. 17.17 Group of calcite crystals. Cumbria, England (Harvard Mineralogical Museum).

construction purposes and for decorative exterior facings. Polished slabs of travertine and Mexican onyx are commonly used as ornamental stone for interiors. Indiana is the primary source of building limestone (the Salem limestone) in the United States, with the most productive quarries in Lawrence and Monroe counties. Many of the federal buildings in Washington, D.C., have been constructed from this limestone. The most important marble quarries are in Vermont, New York, Georgia, and Tennessee.

Iceland spar, named for its occurrence in Iceland, is valuable for various optical instruments; its best known use was in the form of the Nicol prism to produce polarized light, prior to the use of Polaroid plates.

Name. From the Latin word *calx*, meaning *burnt lime*.

Magnesite—$MgCO_3$

Crystallography. Hexagonal; $\bar{3}2/m$. Crystals are rhombohedral, {10$\bar{1}$1}, but rare. Usually cryptocrystalline in white, compact, earthy masses, less frequently in cleavable granular masses, coarse to fine.

$R\bar{3}c$. Hexagonal cell, $a = 4.63$, $c = 15.02$ Å; $Z = 6$; rhombohedral cell, $a = 5.62$ Å, α (rhombohedral angle) = 48°10′, $Z = 2$. *d*s: 2.74(10), 2.50(2), 2.10(4), 1.939(1), 1.700(3).

Physical Properties. *Cleavage* {10$\bar{1}$1} perfect. **H** $3\frac{1}{2}$–5. **G** 3.0–3.2. *Luster* vitreous. *Color* white, gray, yellow, brown. Transparent to translucent. *Optics:* (−); $\omega = 1.700$, $\epsilon = 1.509$.

Composition and Structure. MgO 47.8, CO_2 52.2%. Fe^{2+} substitutes for Mg and a complete series extends to siderite (see Figs. 17.5 and 17.6). Small amounts of Ca and Mn may be present. Magnesite is isostructural with calcite (see Fig. 17.2).

Diagnostic Features. Cleavable varieties are distinguished from dolomite by higher specific gravity and absence of abundant calcium. The white massive variety resembles chert and is distinguished from it by lower hardness. Scarcely acted upon by cold HCl, but dissolves with effervescence in hot HCl.

Occurrence. Magnesite commonly occurs in veins and irregular masses derived from the alteration of Mg-rich metamorphic and igneous rocks (serpentinites and peridotites) through the action of fluids containing carbonic acid. Such magnesites are compact, cryptocrystalline, and often contain opaline silica. Beds of cleavable magnesite are (1) of metamorphic origin associated with talc schists, chlorite schists, and mica schists, and (2) of sedimentary origin, formed as a primary precipitate or as a replacement of limestones by Mg-containing solutions, dolomite being formed as an intermediate product.

Notable deposits of sedimentary magnesite are in China; at Satka in the Ural Mountains, Russia; and at Styria, Austria. The most famous deposit of the cryptocrystalline type is on the Island of Euboea, Greece. The best crystals originate from veins in Oberdorf, Austria, and Bahia, Brazil.

In the United States, the compact variety is found in irregular masses in serpentine in the Coast Range, California. The sedimentary type is mined at Chewelah in Stevens County, Washington, and in the Paradise Range, Nye County, Nevada. There are numerous minor localities in the eastern United States in which magnesite is associated with serpentine, talc, or dolomite rocks.

Use. Dead-burned magnesite, MgO, that is, magnesite that has been calcined at a high temperature and contains less than 1% CO_2, is used in manufacturing bricks for furnace linings. Magnesite is the source of magnesia for industrial chemicals. It has also been used as an ore of metallic Mg, but at present the entire production of Mg comes from brines and seawater.

Name. Magnesite is named in allusion to the composition.

SIDERITE—$FeCO_3$

Crystallography. Hexagonal; $\bar{3}2/m$. Crystals are usually unit rhombohedrons, frequently with curved faces. In globular concretions. Usually cleavable granular. May be botryoidal, compact, and earthy.

$R\bar{3}c$. Hexagonal cell, $a = 4.72$, $c = 15.45$ Å; $Z = 6$; rhombohedral cell, $a = 5.83$ Å, $\alpha = 47°45'$, $Z = 2$. *d*s: 3.59(6), 2.79(10), 2.13(6), 1.963(6), 1.73(8).

Physical Properties. *Cleavage* {10$\bar{1}$1} perfect. **H** $3\frac{1}{2}$–4. **G** 3.96 for pure $FeCO_3$, but decreases with presence of Mn^{2+} and Mg. *Luster* vitreous. *Color* usually light to dark brown. *Streak* white. Transparent to translucent. *Optics:* (−); $\omega = 1.875$, $\epsilon = 1.633$.

Composition and Structure. For pure $FeCO_3$, FeO 62.1, CO_2 37.9%. Fe 48.2%. Mn^{2+} and Mg substitute for Fe^{2+} and complete series extend to rhodochrosite and magnesite (see Figs. 17.5 and 17.6). The substitution of Ca for Fe^{2+} is limited due to the large difference in size of the two ions. Siderite is isostructural with calcite (see Fig. 17.2 and page 400).

Diagnostic Features. Distinguished from other carbonates by its color and high specific gravity, and from sphalerite by its rhombohedral cleavage and streak. Soluble in hot HCl with effervescence.

Alteration. Pseudomorphs of limonite after siderite are common.

Occurrence. Siderite is frequently found as *clay ironstone*, impure by admixture with clay materials, in concretions with concentric layers. As *black-band ore* it is found, contaminated by carbonaceous material, in extensive stratified formations lying in shales and commonly associated with coal measures. These ores have been mined extensively in Great Britain in the past, but at present are mined only in North Staffordshire and Scotland. Clay ironstone is also abundant in the coal measures of western Pennsylvania and eastern Ohio, but it is not used to any great extent as an ore. Siderite is also formed by the replacement action of Fe-rich solutions upon limestones. If such occurrences are extensive, they may be of economic value. The most notable deposit of this type is in Styria, Austria, where siderite is mined on a large scale. Siderite is a common vein mineral associated with various metallic ores containing silver minerals, pyrite, chalcopyrite, tetrahedrite, and galena. When siderite predominates in such veins, it may be mined, as in southern Westphalia, Germany. Siderite is also a common constituent of banded Precambrian iron deposits, as in the Lake Superior region. A famous classic locality is Cornwall, England. Modern localities are the Morro Velho Gold Mine, Nova Lima, Brazil, and Llallagua, Bolivia.

Use. An ore of iron. Important in Great Britain and Austria, but unimportant elsewhere.

Name. From the Greek word meaning *iron*. The name *spherosiderite* of the concretionary variety was shortened to *siderite* to apply to the entire species. *Chalybite*, used by some mineralogists, was derived from the Chalybes, ancient iron workers, who lived by the Black Sea.

Rhodochrosite—$MnCO_3$

Crystallography. Hexagonal; $\bar{3}2/m$. Only rarely in crystals of the unit rhombohedron; frequently with curved faces. Usually cleavable, massive; granular to compact.

$R\bar{3}c$. Hexagonal cell, $a = 4.78$, $c = 15.67$ Å; $Z = 6$; rhombohedral cell, $a = 5.85$ Å, $\alpha = 47°46'$, $Z = 2$. *ds*: 3.66(4), 2.84(10), 2.17(3), 1.770(3), 1.763(3).

Physical Properties. *Cleavage* $\{10\bar{1}1\}$ perfect. **H** $3\frac{1}{2}$–4. **G** 3.5–3.7. *Luster* vitreous. *Color* usually some shade of rose-red, see Plate III, no. 7; may be light pink to dark brown. *Streak* white. Transparent to translucent. *Optics:* (−); $\omega = 1.816$, $\epsilon = 1.597$.

Composition and Structure. For pure $MnCO_3$, MnO 61.7, CO_2 38.3%. Fe^{2+} substitutes for Mn^{2+} forming a complete solid solution series between rhodochrosite and siderite (see Fig. 17.18). Ca^{2+} shows some substitution for Mn^{2+}. The occurrence of *kutnahorite*, $CaMn(CO_3)_2$, with an ordered structure of the dolomite type, suggests that only limited solid solution occurs, at ordinary temperatures, between $CaCO_3$ and $MnCO_3$. Mg may also substitute for Mn but the $MnCO_3$–$MgCO_3$ series is incomplete. Considerable amounts of Zn may substitute for Mn (see smithsonite). Rhodochrosite is isostructural with calcite (see Fig. 17.2 and page 400).

Diagnostic Features. Characterized by its pink color and rhombohedral cleavage; the hardness (4) distinguishes it from rhodonite, $MnSiO_3$, with hardness of 6. Infusible. Soluble in hot HCl with effervescence.

Occurrence. Rhodochrosite is a comparatively rare mineral, occurring in hydrothermal veins with ores of silver, lead, and copper, and with other manganese minerals. Beautiful banded rhodochrosite is mined for ornamental and decorative purposes at Capillitas, Catamarca, Argentina (see Fig. 17.19). Excellent crystals are found in the Kalahari manganese region of Cape Province, Republic of South Africa, and at Pasto Bueno, Peru. In the United States, it is found at Butte, Montana, where it has been mined as a manganese ore. In good crystals at Alicante, Lake County; Alma Park County; and elsewhere in Colorado.

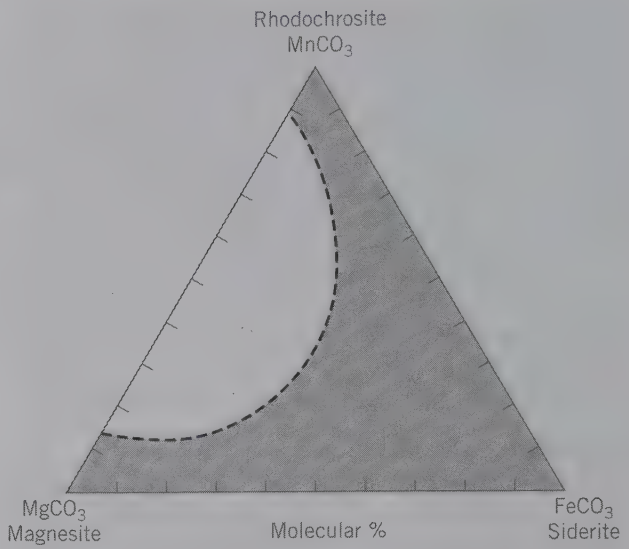

FIG. 17.18 The approximate extent of solid solution for carbonates in the three-component system $MgCO_3$–$FeCO_3$–$MnCO_3$. The lack of solid solution between $MnCO_3$ and $MgCO_3$ may be the result of a considerable difference in the size of the cationic radii, or it may reflect a lack of carbonate-rich rock types that bridge the gap between $MnCO_3$ and $MgCO_3$. (From Essene, E. J. 1983. Solid solutions and solvi among metamorphic carbonates with applications to geologic thermobarometry, *Carbonates: Mineralogy and Chemistry. Reviews in Mineralogy* 11, 77–96.)

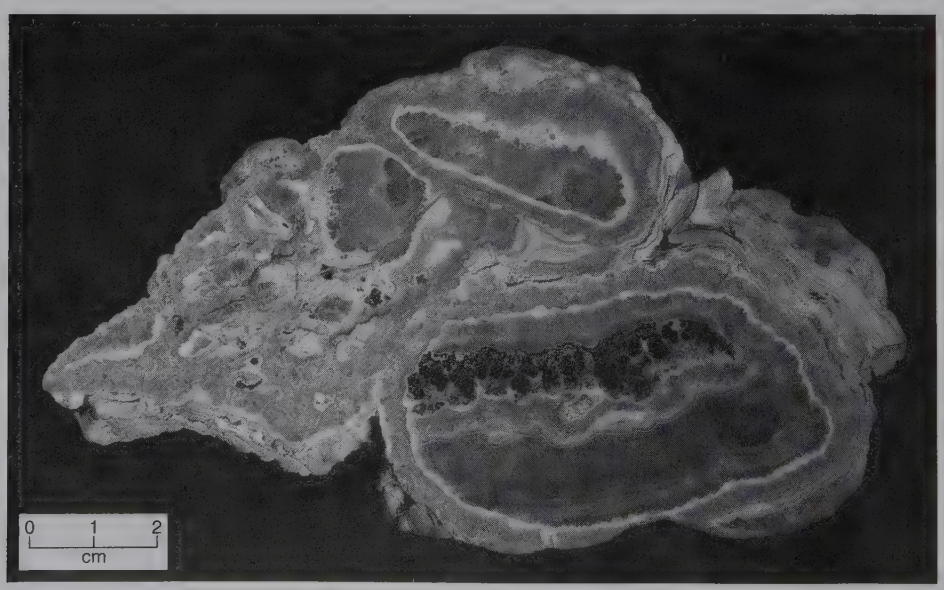

FIG. 17.19 Rhodochrosite, Capillitas, Catamarca, Argentina (Harvard Mineralogical Museum).

Use. A minor ore of manganese. Small amounts used for ornamental purposes.

Name. Derived from two Greek words meaning *rose* and *color*, in allusion to its rose-pink color.

Smithsonite—$ZnCO_3$

Crystallography. Hexagonal; $\bar{3}2/m$. Rarely in small rhombohedral or scalenohedral crystals. Usually reniform, botryoidal (Fig. 17.20), or stalactitic, and in crystaline incrustations or in honeycombed masses known as *dry-bone ore*. Also granular to earthy.

$R\bar{3}c$. Hexagonal cell, $a = 4.66$, $c = 15.02$ Å; $Z = 6$; rhombohedral cell, $a = 5.63$ Å, $\alpha = 48°20'$, $Z = 2$. *ds*: 2.75(10), 3.55(5), 2.33(3), 1.946(3), 1.703(4).

Physical Properties. *Cleavage* $\{10\bar{1}1\}$ perfect. **H** 4–4½. **G** 4.30–4.45. *Luster* vitreous to waxy. *Color* usually dirty brown. May be colorless, white, green, blue, or pink. The yellow variety contains Cd and is known as *turkey-fat ore*. *Streak* white. Translucent. *Optics:* (−); $\omega = 1.850$, $\epsilon = 1.623$.

Composition and Structure. For pure $ZnCO_3$, ZnO 64.8, CO_2 35.2%. Considerable Fe^{2+} may substitute for Zn, but there appears to be a gap in the $ZnCO_3$–$FeCO_3$ series. Mn^{2+} is generally present in only a few percent, but the occurrence of a zincian rhodochrosite with Zn:Mn = 1:1.2 suggests there may be a complete series between $ZnCO_3$ and $MnCO_3$. Ca and Mg are present in amounts of only a few weight percent. Small amounts of Co are found in a pink, and small amounts of Cu in a blue-green variety of smithsonite. Smithsonite is isostructural with calcite (see Fig. 17.2 and page 400).

Diagnostic Features. Soluble in cold HCl with effervescence. Distinguished by its effervescence in acids, tests for zinc, its hardness, and its high specific gravity.

Occurrence. Smithsonite is a zinc ore of supergene origin, usually found with zinc deposits in limestones. Associated with sphalerite, galena, hemimorphite, cerussite, calcite, and limonite. Often found in pseudomorphs after calcite. Smithsonite is found in places in translucent green or greenish-blue material, which is used for ornamental purposes. Laurium, Greece, is noted for this ornamental smithsonite, and Sardinia, Italy, for yellow stalactites with concentric banding. Fine crystallized specimens have come from the Broken Hill Mine, Zambia, and from Tsumeb, Namibia. In the United States smithsonite occurs as an ore in the zinc deposits of Leadville, Colorado; Arkansas and Wisconsin. Fine greenish-blue material has been found at the Kelly mine, Magdalena district, New Mexico (Fig. 17.20).

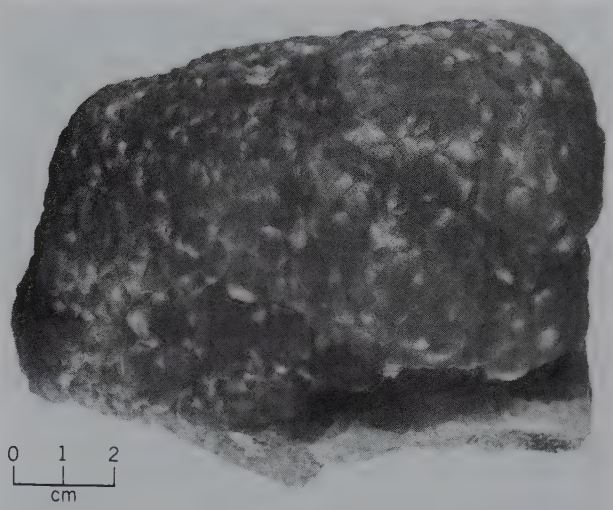

FIG. 17.20 Smithsonite. Kelly Mine near Socorro, New Mexico (Harvard Mineralogical Museum).

Use. An ore of zinc. A minor use is for ornamental purposes.

Name. Named in honor of James Smithson (1754–1829), who founded the Smithsonian Institution in Washington, D.C. English mineralogists formerly called the mineral *calamine*.

Similar Species. *Hydrozincite*, $Zn_5(CO_3)_2(OH)_6$, occurs as a secondary mineral in zinc deposits.

ARAGONITE—$CaCO_3$

Crystallography. Orthorhombic; $2/m2/m2/m$. Three habits of crystallization are common. (1) Acicular pyramidal; consisting of a vertical prism terminated by a combination of a very steep dipyramid and {110} prism (Fig. 17.21a). Usually in radiating groups of large to very small crystals (see Plate III, no. 8). (2) Tabular; consisting of prominent {010} modified by {110} and a low prism, *k*{011} (Fig. 17.21b); often twinned on {110} (Fig. 17.21c). (3) In pseudohexagonal twins (Figs. 17.21d and 17.22) showing a hexagonal-like prism terminated by a basal plane. These are formed by an intergrowth of three individuals twinned on {110} with {001}

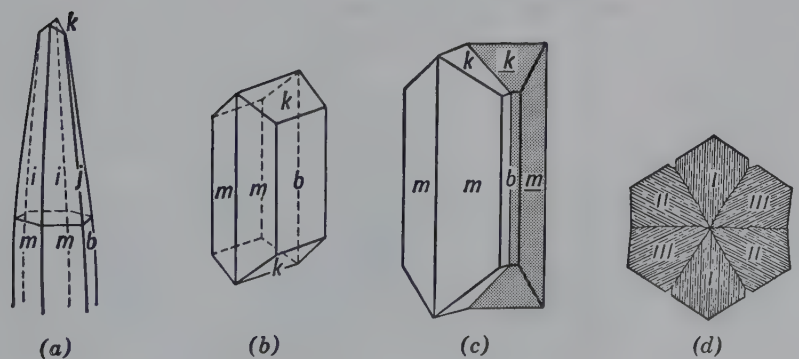

FIG. 17.21 (a) and (b) Aragonite crystals. (c) and (d) Aragonite twins on {110} with a repeated twin producing a pseudohexagonal outline as in (d).

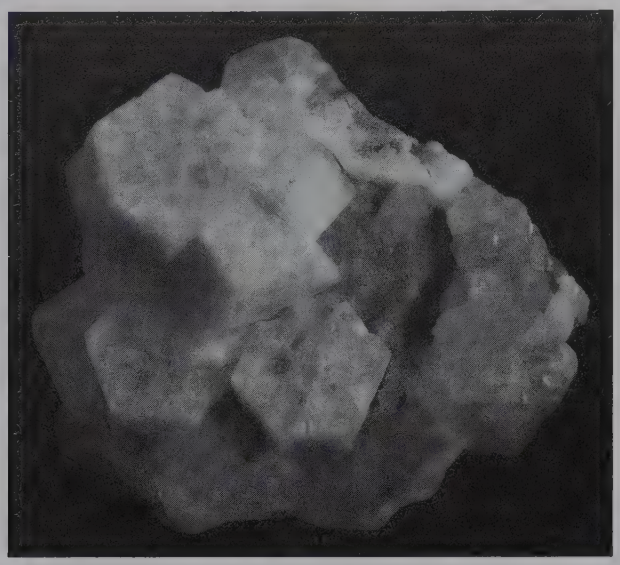

FIG. 17.22 Aragonite in cyclic twins (white) on surface of sulfur crystals (very light grey). Cyona Mine, Racalmuto, Agrigento, Italy (Harvard Mineralogical Museum).

planes in common. The cyclic twins are distinguished from true hexagonal forms by noting that the basal surface is striated in three different directions and that, because the prism angle of the simple crystals is not exactly 60°, the composite prism faces for the twin will often show slight *reentrant* angles. Also found in reniform, columnar, and stalactitic aggregates.

Pmcn; $a = 4.96$, $b = 7.97$, $c = 5.74$ Å; $Z = 4$. *ds*: 3.04(9), 2.71(6), 2.36(7), 1.975(10), 1.880(8).

Physical Properties. *Cleavage* {010} distinct, {110} poor. *Luster* vitreous. *Color* colorless, white, pale yellow, and variously tinted. *Streak* white. Transparent to translucent. **H** $3\frac{1}{2}$–4. **G** 2.94 (harder and higher specific gravity than calcite). *Optics:* (−); $\alpha = 1.530$, $\beta = 1.680$, $\gamma = 1.685$; $2V = 18°$; $X = c$, $Y = a$. $r < v$ weak.

Composition, Structure, and Synthesis. Most aragonite is relatively pure $CaCO_3$. Small amounts of Sr and Pb substitute for Ca. The structure of aragonite is given in Fig. 17.3 and discussed on page 401. Calcite can be transformed into the aragonite structure by extensive grinding with a mortar and pestle. This structural transformation can be determined only by X-ray diffraction techniques. The phase diagram for the polymorphs of $CaCO_3$ is given in Fig. 17.4. Aragonite, with a somewhat denser structure than calcite, is stable on the high P, low T side of the reaction curve. If the temperature of metamorphism in a metamorphic terrane can be arrived at independently, this curve allows for the estimation of a maximum or minimum pressure of metamorphism in calcite- or aragonite-bearing rocks.

Diagnostic Features. Effervesces in cold HCl. Distinguished from calcite by its higher specific gravity and lack of rhombohedral cleavage. Cleavage fragments of columnar calcite are terminated by a cross-cleavage that is lacking in aragonite. Distinguished from witherite and strontianite by lower specific gravity.

Alteration. Pseudomorphs of calcite after aragonite are common. $CaCO_3$ secreted by mollusks as aragonite is usually changed to calcite on the outside of the shell (see also Fig. 14.26).

Occurrence. Aragonite is less stable than calcite under atmospheric conditions and much less common. It is precipitated in a narrow range of physicochemical conditions represented by low temperature, near-surface deposits. Experiments have shown that carbonated waters containing calcium more often deposit aragonite when they are warm and calcite when they are cold. The pearly layer of many shells and the pearl itself is aragonite. Aragonite is deposited by hot springs; found associated with beds of gypsum and deposits of iron ore where it may occur in forms resembling coral, and is called *flos ferri*. It is found as fibrous crusts on serpentine and in amygdaloidal cavities in basalt. The occurrence of aragonite in some metamorphic rocks as in the Franciscan Formation in California and in blueschists of New Zealand is the result of recrystallization at high pressures and relatively low temperature.

Notable localities for the various crystalline types are as follows: pseudohexagonal twinned crystals are found in Aragon, Spain; and at Girgenti, Sicily, Italy, associated with native sulfur. Prismatic crystals were found at Dognácska, Slovakia. The acicular type is found at Alston Moor and Cleator Moor, Cumbria, England. Flos ferri is found in the iron mines of Styria, Austria. Some *onyx marble* from Baja California, Mexico, is aragonite. In the United States, pseudohexagonal twins are found at Lake Arthur, New Mexico. Flos ferri occurs in the Organ Mountains, New Mexico, and at Bisbee, Arizona.

Name. From Aragon, Spain, where the pseudohexagonal twins were first recognized.

Witherite—$BaCO_3$

Crystallography. Orthorhombic; *2/m2/m2/m*. Crystals are always twinned on {110} forming pseudohexagonal dipyramids by the intergrowth of three individuals (Fig. 17.23). Crystals often deeply striated horizontally and by a series of reentrant angles have the appearance of one pyramid capping another. Also botryoidal to globular; columnar or granular.

Pmcn; $a = 5.31$, $b = 8.90$, $c = 6.43$ Å; $Z = 4$. *ds*: 3.72(10), 2.63(6), 2.14(5), 2.03(5), 1.94(5).

FIG. 17.23 Witherite.

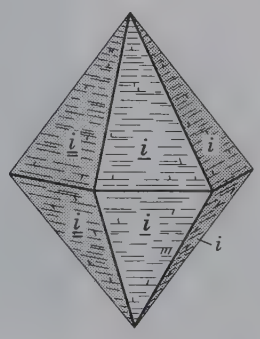

Physical Properties. *Cleavage* {010} distinct, {110} poor. **H** $3\frac{1}{2}$–4. **G** 4.31. *Luster* vitreous. *Color* colorless, white, gray. Translucent. *Optics:* (−), $\alpha = 1.529$, $\beta = 1.676$, $\gamma = 1.677$; $2V = 16°$; $X = c$, $Y = b$; $r > v$ weak.

Composition and Structure. BaO 77.7, CO_2 22.3%. Small amounts of Sr and Ca may substitute for Ba. Witherite is isostructural with aragonite (see Fig. 17.3 and page 401).

Diagnostic Features. Soluble in cold HCl with effervescence. Witherite is characterized by high specific gravity. It is distinguished from barite by its effervescence in acid.

Occurrence. Witherite is a comparatively rare mineral, most frequently found in veins associated with galena. Found in England in fine crystals near Hexham in Northumberland and Alston Moor in Cumbria. In the United States, found with fluorite at the Minerva Mine, Cave-in-Rock, Illinois.

Use. A minor source of barium.

Name. In honor of D. W. Withering (1741–1799), who discovered and first analyzed the mineral.

Strontianite—$SrCO_3$

Crystallography. Orthorhombic; *2/m2/m2/m*. Crystals are usually acicular, radiating like type 1 under aragonite. Twinning on {110} frequent, giving pseudohexagonal appearance. Also columnar, fibrous, and granular.

Pmcn; $a = 5.11$, $b = 8.41$, $c = 6.03$ Å; $Z = 4$. *ds*: 3.47(10), 2.42(5), 2.02(7), 1.876(5), 1.794(7).

Physical Properties. *Cleavage* {110} good. **H** $3\frac{1}{2}$–4. **G** 3.78. *Luster* vitreous. *Color* white, gray, yellow, green. Transparent to translucent. *Streak* white. *Optics:* (−), $\alpha = 1.520$, $\beta = 1.667$, $\gamma = 1.669$; $2V = 7°$; $X = c$, $Y = b$. $r < v$ weak.

Composition and Structure. SrO 70.2, CO_2 29.8% for pure $SrCO_3$. Ca may be present in substitution for Sr to a maximum of about 25 atomic percent. Strontianite is isostructural with aragonite (see Fig. 17.3 and page 400).

Diagnostic Features. Characterized by high specific gravity and effervescence in HCl. Can be distinguished from celestite by poorer cleavage and effervescence in acid.

Occurrence. Strontianite is a low-temperature hydrothermal mineral associated with barite, celestite, and calcite in veins in limestone or marl, and less frequently in igneous rocks and as a gangue mineral in sulfide veins. Occurs in commercial deposits in Westphalia, Germany; Spain; Mexico; and England. Fine specimens are found in Oberdorf, Austria. Uncommon in the United States; found with fluorite at Cave-in-Rock, Illinois.

Use. Source of strontium. Strontium has no great commercial application; used in fireworks, red flares, military rockets, in the separation of sugar from molasses, and in various strontium compounds.

Name. From Strontian in Argyllshire, Scotland, where it was originally found.

Cerussite—$PbCO_3$

Crystallography. Orthorhombic; *2/m2/m2/m*. Crystals of varied habit are common and show many forms. Often tabular on {010} (Fig. 17.24a). May form reticulated groups with the plates crossing each other at 60° angles, see photograph at the very beginning of this chapter; frequently in

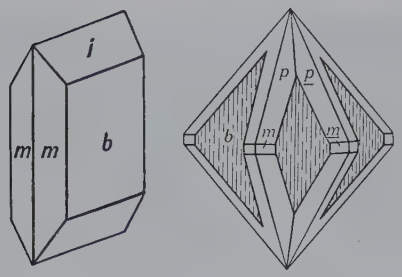

(a) (b)

FIG. 17.24 Cerussite.

pseudohexagonal twins with deep reentrant angles in the vertical zone (Fig. 17.24b). Also in granular crystalline aggregates; fibrous; compact; porous network of tabular crystals.

Pmcn; $a = 5.19$, $b = 8.44$, $c = 6.15$ Å; $Z = 4$. *ds*: 3.59(10), 3.50(4), 3.07(2), 2.49(3), 2.08(3).

Physical Properties. *Cleavage* {110} good, {021} fair. **H** 3–$3\frac{1}{2}$. **G** 6.58. *Luster* adamantine. *Color* colorless, white, or gray. *Streak* white. Transparent to subtranslucent. *Optics:* (−); $\alpha = 1.804$, $\beta = 2.077$, $\gamma = 2.079$; $2V = 9°$, $X = c$, $Y = b$, $r > v$.

Composition and Structure. Most cerussite is very close in composition to $PbCO_3$, with PbO 83.5 and CO_2 16.5%. It is isostructural with aragonite (see Fig. 17.3 and page 400).

Diagnostic Features. Recognized by its high specific gravity, white color, and adamantine luster. Crystal form and effervescence in nitric acid serve to distinguish it from anglesite.

Occurrence. Cerussite is an important and widely distributed supergene lead ore formed by the action of carbonated waters on galena. Associated with the primary minerals galena and sphalerite, and various secondary minerals, such as anglesite, pyromorphite, smithsonite, and limonite.

Notable localities for its occurrence are Mežica (Mies), Slovenia; on the island of Sardinia, Italy; at Tsumeb, Namibia; Touissit, Morocco; and Broken Hill, New South Wales, Australia. In the United States, it is found in various districts in Arizona; from the Organ Mountains, New Mexico; and in the Coeur d'Alene district in Idaho.

Use. An important ore of lead.

Name. From the Latin word meaning *white lead*.

Similar Species. *Phosgenite*, $Pb_2CO_3Cl_2$ (tetragonal), is a rare carbonate.

DOLOMITE—$CaMg(CO_3)_2$; Ankerite—$CaFe(CO_3)_2$

Crystallography. For *dolomite*. Hexagonal; $\bar{3}$. Crystals are usually the unit rhombohedron (Figs. 17.25a and 17.26), more rarely a steep rhombohedron and base (Fig. 17.25c). Faces are often curved, some so acutely as to form "saddle-shaped" crystals (Figs. 17.25b, 17.27, and Plate III, no. 9). Other forms are rare. In coarse, granular, cleavable masses to fine-grained and compact. Twinning on {0001} common; lamellar twinning on $\{02\bar{2}1\}$. *Ankerite* generally does not occur in well-formed crystals. When it does, the crystals are similar to those of dolomite.

$R\bar{3}$; $a = 4.84$, $c = 15.95$ Å; $Z = 3$. *ds*: 2.88(10), 2.19(4), 2.01(3), 1.800(1), 1.780(1).

(a) (b) (c) **FIG. 17.25** Dolomite.

FIG. 17.26 Dolomite, penetration twins. Eugui, Navarra, Spain. Specimen is 6.5 cm high (Photographs courtesy of Jeff Scovil, collection © Jeff Scovil).

Physical Properties. *Cleavage* $\{10\bar{1}1\}$ perfect. **H** $3\frac{1}{2}$–4. **G** 2.85. *Luster* vitreous; pearly in some varieties, *pearl spar*. *Color* commonly some shade of pink, flesh color; may be colorless, white, gray, green, brown, or black. *Streak* white. Transparent to translucent. *Optics:* (−); $\omega = 1.681$, $\epsilon = 1.500$. With increasing substitution of Fe (toward ankerite composition) **G** and indices of refraction increase. Ankerite is typically yellowish-white but, due to oxidation of the iron, may appear yellowish-brown.

Composition and Structure. *Dolomite:* CaO 30.4, MgO 21.7, CO_2 47.9%. *Ankerite:* CaO 25.9, FeO 33.3, CO_2 40.8%. Naturally occurring dolomite deviates somewhat from Ca:Mg = 1:1 (see Fig. 17.6) with the Ca:Mg ratio ranging from 58:42 to $47\frac{1}{2}$:$52\frac{1}{2}$. A complete solid solution series extends to *ankerite* and there is also a complete solid solution toward *kutnahorite*, $CaMn(CO_3)_2$ (see Fig. 17.28). Members of the dolomite group are isostructural. The structure of dolomite is discussed on page 402.

Diagnostic Features. For *dolomite*. In cold, dilute HCl large fragments are slowly attacked but are soluble with effervescence only in hot HCl; the powdered mineral is readily soluble in cold acid. Crystals commonly occur in curved rhombohedra and a flesh-pink color is also characteristic. The massive variety is distinguished from limestone by the less vigorous reaction with HCl. *Ankerite* is similar to dolomite in its physical and chemical properties except for its color, which ranges from yellow-brown to brown.

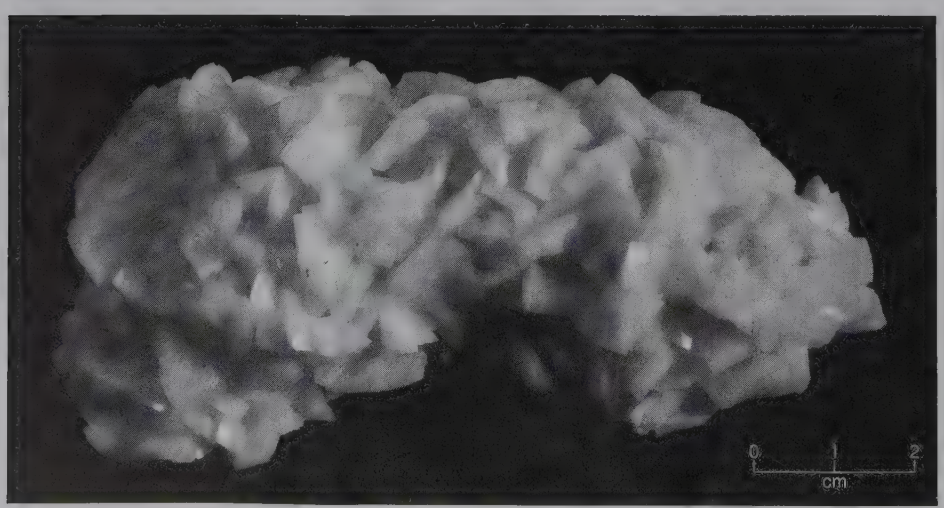

FIG. 17.27 Dolomite, St. Eustace. Quebec, Canada (Harvard Mineralogical Museum).

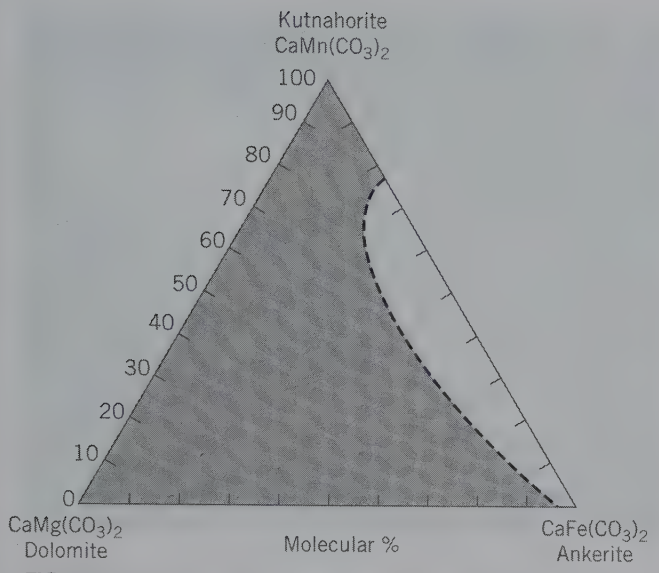

FIG. 17.28 The approximate extent of solid solution between $CaMn(CO_3)_2$–$CaMg(CO_3)_2$–$CaFe(CO_3)_2$. (From Essene, E. J. 1983. Solid solutions and solvi among metamorphic carbonates with applications to geologic thermobarometry. *Carbonates: Mineralogy and Chemistry. Reviews in Mineralogy* 11, 77–96.)

Occurrence. *Dolomite* is found in many parts of the world chiefly as extensive sedimentary strata, and the metamorphosed equivalent, dolomitic marble. Dolomite as a rock mass is generally thought to be secondary in origin, formed from ordinary limestone by the replacement of some of the Ca by Mg. The replacement may be only partial and, thus, most dolomite rocks (*dolostones*) are mixtures of dolomite and calcite. The mineral occurs also as a hydrothermal vein mineral, in lead and zinc veins that traverse limestone, associated with fluorite, calcite, barite, and siderite. *Ankerite* is a common carbonate in Precambrian iron-formations.

Dolomite is abundant in the Dolomite region of southern Tyrol, Italy; in crystals from the Binnenthal, Switzerland; Traversella in Piedmont, Italy; northern England; and Guanajuato, Mexico. In the United States, it is found as masses of sedimentary rock and gray to pink saddle-shaped crystals in vugs of rocks of many of the middle-western states, especially in the Joplin, Missouri, district.

Use of Dolomite. As a building and ornamental stone. For the manufacture of certain cements. For the manufacture of magnesia used in the preparation of refractory linings of the converters in the basic steel process. Dolomite is a potential ore of metallic Mg.

Name. *Dolomite* in honor of the French chemist, Dolomieu (1750–1801). *Ankerite* after M. J. Anker (1772–1843), Austrian mineralogist.

Similar Species. *Kutnahorite*, $CaMn(CO_3)_2$, is isostructural with dolomite.

Malachite—$Cu_2CO_3(OH)_2$

Crystallography. Monoclinic; $2/m$. Crystals are slender prismatic but seldom distinct. Crystals may be pseudomorphous after azurite (Fig. 17.29). Usually in radiating fibers forming botryoidal or stalactitic masses (Fig. 17.30). Commonly granular or earthy.

$P2_1/a$; $a = 9.48$, $b = 12.03$, $c = 3.21$ Å, $\beta = 98°44'$; $Z = 4$. *d*s: 6.00(6), 5.06(8), 3.69(9), 2.86(10), 2.52(6).

Physical Properties. *Cleavage* {201} perfect but rarely seen. **H** $3\frac{1}{2}$–4. **G** 3.9–4.03. *Luster* adamantine to vitreous in crystals; often silky in fibrous varieties; dull in earthy type. *Color* bright green, see Plate IV, no. 1. *Streak* pale green. Translucent. *Optics:* (−), $\alpha = 1.655$, $\beta = 1.875$, $\gamma = 1.909$;

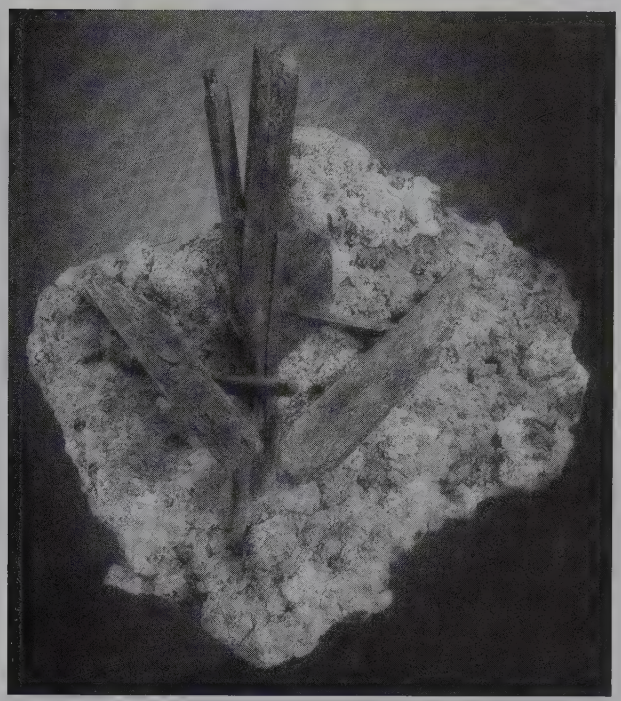

FIG. 17.29 Pseudomorphs of malachite after azurite. From Bisbee, Cochise County, Arizona. Specimen is 7.3 cm high (Photographs courtesy of Jeff Scovil, collection © Jeff Scovil).

FIG. 17.30 Malachite, cut and polished.

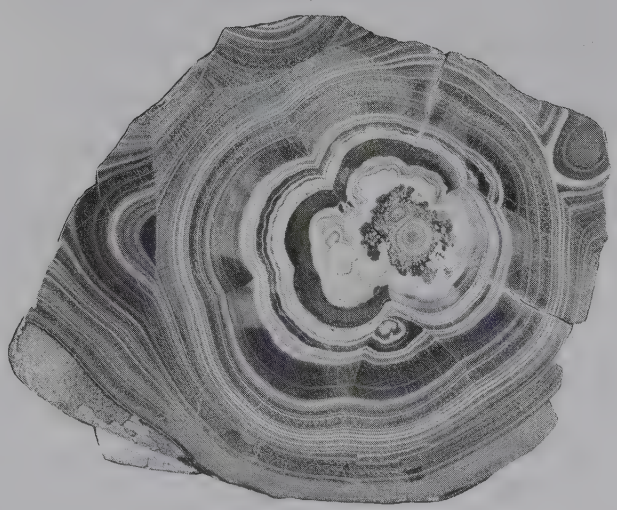

$2V = 43°$; $Y = b$, $Z \wedge c = 24°$; pleochroism: X colorless, Y yellow green, Z deep green.

Composition and Structure. CuO 71.9, CO_2 19.9, H_2O 8.2%. Cu 57.4%. Cu^{2+} is octahedrally coordinated by O^{2-} and $(OH)^-$ in $CuO_2(OH)_4$ and $CuO_4(OH)_2$ octahedra. These octahedra are linked along the edges forming chains that run parallel to the c axis. The chains are cross-linked by triangular $(CO_3)^{2-}$ groups.

Diagnostic Features. Soluble in HCl with effervescence, yielding a green solution. Recognized by its bright green color and botryoidal forms, and distinguished from other green copper minerals by its effervescence in acid.

Occurrence. Malachite is a widely distributed supergene copper mineral found in the oxidized portions of copper veins associated with azurite, cuprite, native copper, iron oxides. It usually occurs in copper deposits associated with limestone.

Notable localities for its occurrence are at Nizhniy Tagil in the Ural Mountains, Russia; pseudomorphous after cuprite at Chessy, near Lyons, France, and associated with azurite; from Tsumeb, Namibia; Katanga, Democratic Republic of Congo; and Broken Hill, New South Wales, Australia. In the United States, formerly an important copper ore in the southwestern copper districts; at Bisbee, Morenci, and other localities in Arizona.

Use. A minor ore of copper. It is used extensively as an ornamental and gem mineral. In the nineteenth century Russia was the primary source, but today most of the material comes from Congo.

Name. Derived from the Greek word *malache* meaning *mallows*, in allusion to its green color.

Azurite—$Cu_3(CO_3)_2(OH)_2$

Crystallography. Monoclinic; $2/m$. Habit varies (Fig. 17.31); crystals are frequently complex and malformed. Also in radiating spherical groups.

$P2_1c$; $a = 4.97$, $b = 5.84$, $c = 10.29$ Å, $\beta = 92°24'$; $Z = 2$. *ds*: 5.15(7), 3.66(4), 3.53(10), 2.52(6), 2.34(3).

Physical Properties. *Cleavage* {011} perfect, {100} fair. **H** $3\frac{1}{2}$–4. **G** 3.77. *Luster* vitreous. *Color* intense azure-blue, see Plate IV, no. 1. *Streak* light blue. Transparent to translucent. *Optics:* (+), $\alpha = 1.730$, $\beta = 1.758$, $\gamma = 1.838$; $2V = 67°$; $X = b$, $Z \wedge c = -13°$; pleochroic in blue $Z > Y > X$; $r > V$.

FIG. 17.31 Azurite crystals.

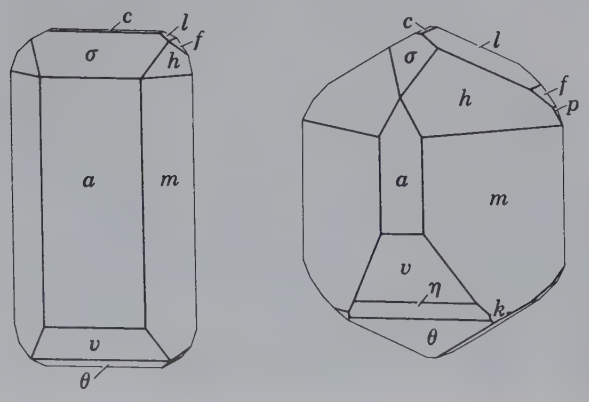

Composition and Structure. CuO 69.2, CO_2 25.6, H_2O 5.2%. Cu 55.3%. The structure of azurite contains Cu^{2+} ions in square, coplanar groups with $2O^{2-}$ and $2(OH)^-$. These square groups are linked into chains parallel to the b axis. Each $(OH)^-$ group is shared by 3 Cu^{2+} and each oxygen of the triangular (CO_3) group is bonded to one copper.

Diagnostic Features. Characterized chiefly by its azure-blue color and effervescence in HCl.

Alteration. Pseudomorphs of malachite after azurite commonly observed (Fig. 17.29); less common after cuprite.

Occurrence. Azurite is less common than malachite but has the same origin and associations. It was found in fine crystals at Chessy, near Lyons, France; Tsumeb, Namibia; Touissit, Morocco; and Broken Hill, New South Wales, Australia. In the United States at the Copper Queen and other mines, Bisbee and Morenci, Arizona. Widely distributed with copper ores.

Use. A minor ore of copper.

Name. Named in allusion to its color.

Rare Hydrous Carbonates. *Aurichalcite*, $(Zn,Cu)_5(CO_3)_2(OH)_3$ pale green to turquoise-blue in orthorhombic acicular crystals. *Gaylussite*, $Na_2Ca(CO_3)_2 \cdot 5H_2O$, monoclinic and *trona*, $Na_3(CO_3)(HCO_3) \cdot 2H_2O$, monoclinic, are both found in saline-lake deposits.

Nitrates

NITRATITE—$NaNO_3$. In nitratite $(NO_3)^-$ groups combine in one-to-one proportion with monovalent Na^+ in 6-coordination forming a structure analogous to that of calcite (see Fig. 17.2). Nitratite and calcite are isostructural with the same crystallography and cleavage. Because of the lesser cationic charge, nitratite is softer (**H** 1–2) and melts at a low temperature and, because of the lower atomic weight of sodium, has a lower specific gravity (**G** 2.29). Nitratite is soluble in water and is found only in arid regions. The most notable occurrence is in northern Chile where it is recovered as a source of nitrogen.

NITER (Saltpeter)—KNO_3. Niter is isostructural with aragonite (see Fig. 17.3) with similar crystallography and analogous pseudohexagonal twinning on {110}. Like nitratite it fuses easily and is soluble in water. Niter is less common than nitratite but has been recovered from the soils in several countries as a source of nitrogen for fertilizer.

BORATES

Of the 135 borate minerals known, only the 4 most common are considered here:

Kernite $Na_2B_4O_6(OH)_2 \cdot 3H_2O$
Borax $Na_2B_4O_5(OH)_4 \cdot 8H_2O$
Ulexite $NaCaB_5O_6(OH)_6 \cdot 5H_2O$
Colemanite $CaB_3O_4(OH)_3 \cdot H_2O$

Kernite—$Na_2B_4O_6(OH)_2 \cdot 3H_2O$

Crystallography. Monoclinic; $2/m$. Rarely in crystals; usually in coarse, cleavable aggregates.

$P2/a$; $a = 15.68$, $b = 9.09$, $c = 7.02$ Å; $\beta = 108°52'$; $Z = 4$. *ds*: 7.41(10), 6.63(8), 3.70(3), 3.25(2), 2.88(2).

FIG. 17.32 Kernite showing typically excellent {100} and {001} cleavage. Scale = 1 cm. From Boron, Kern County, California.

Physical Properties. *Cleavage* {001} and {100} perfect. Cleavage fragments are elongated parallel to the *b* crystallographic axis, see Fig. 17.32. The angle between the cleavages: (001) $\wedge$ (100) = 71°8′. **H** 3. **G** 1.95. *Luster* vitreous to pearly. *Color* colorless to white; colorless specimens become chalky white on long exposure to the air owing to a surface film of *tincalconite*, $Na_2B_4O_5(OH)_4{\cdot}3H_2O$. *Optics:* (−); $\alpha = 1.454$, $\beta = 1.472$, $\gamma = 1.488$; $2V = 70°$. $Z = b$, $X \wedge c = 71°$. $r > v$.

Composition and Structure. Na_2O 22.7, B_2O_3 51.0, H_2O 26.3%. The structure of kernite contains complex chains, parallel to the *b* axis, of composition $[B_4O_6(OH)_2]^{2-}$. These chains consist of BO_4 tetrahedra, joined at the vertices (as in the pyroxenes of the silicates) with remaining vertices connected to BO_3 triangles. The chains are linked to each other by Na^+ (in 5-coordination) and hydroxyl–oxygen bonds.

Diagnostic Features. Characterized by long, splintery cleavage fragments and low specific gravity. Slowly soluble in cold water.

Occurrence. The original locality and principal occurrence of kernite is in the Mohave Desert at Boron, California. Here, associated with borax, colemanite, and ulexite in a bedded series of Tertiary clays, it is present by the million tons. This deposit of sodium borates is 4 miles long, 1 mile wide, and as much as 250 feet thick, and lies from 150 to 1,000 feet beneath the surface. The kernite occurs near the bottom of the deposit and is suggested to have formed from borax by recrystallization caused by increased temperature and pressure. Kernite is also found associated with borax at Tincalayu, Argentina.

Use. Boron compounds are used in the manufacture of glass, especially in glass wool for insulation purposes. They are also used in soap, in porcelain enamels for coating metal surfaces, and in the preparation of fertilizers and herbicides.

Name. From Kern County, California, where the mineral is found.

Borax—$Na_2B_4O_5(OH)_4{\cdot}8H_2O$

Crystallography. Monoclinic; *2/m*. Commonly in prismatic crystals (Fig. 17.33). Also as massive, cellular material or encrustations.

C2/c; $a = 11.86$, $b = 10.67$, $c = 12.20$ Å; $\beta = 106°$; $Z = 4$. *ds*: 5.7(2), 4.86(5), 3.96(4), 2.84(5), 2.57(10).

Physical Properties. *Cleavage* {100} perfect. **H** 2–2½. **G** 1.7 ±. *Luster* vitreous. *Color* colorless or white. Translucent. Sweetish-alkaline taste. Clear crystals effloresce and turn white with the formation of *tincalconite*, $Na_2B_4O_5(OH)_4{\cdot}3H_2O$, see Fig. 17.34. *Optics:* (−); $\alpha = 1.447$, $\beta = 1.469$, $\gamma = 1.472$; $2V = 40°$. $X = b$, $Z \wedge c = -56°$. $r > v$.

Composition and Structure. Na_2O 16.2, B_2O_3 36.6, H_2O 47.2%. The structure of borax is shown in Fig. 17.35. It consists of $[BO_3OH]$ tetrahedra and $[BO_2OH]$ triangles that are joined parallel to the *c* crystallographic axis. The Na^+ is in 6-coordination with H_2O molecules, producing $Na(H_2O)_6$ octahedra that have common edges, forming ribbons parallel to the *c* crystallographic axis. The boron groups are linked to the Na-H_2O ribbons by van der Waals and hydrogen bonding.

Diagnostic Features. Characterized by its crystals and tests for boron. Readily soluble in water.

Occurrence. Borax is the most widespread of the borate minerals. It is formed on the evaporation of enclosed lakes and as an efflorescence on the surface in arid regions.

FIG. 17.33 Borax.

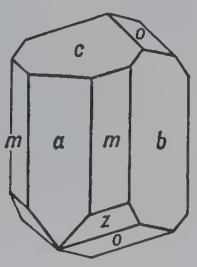

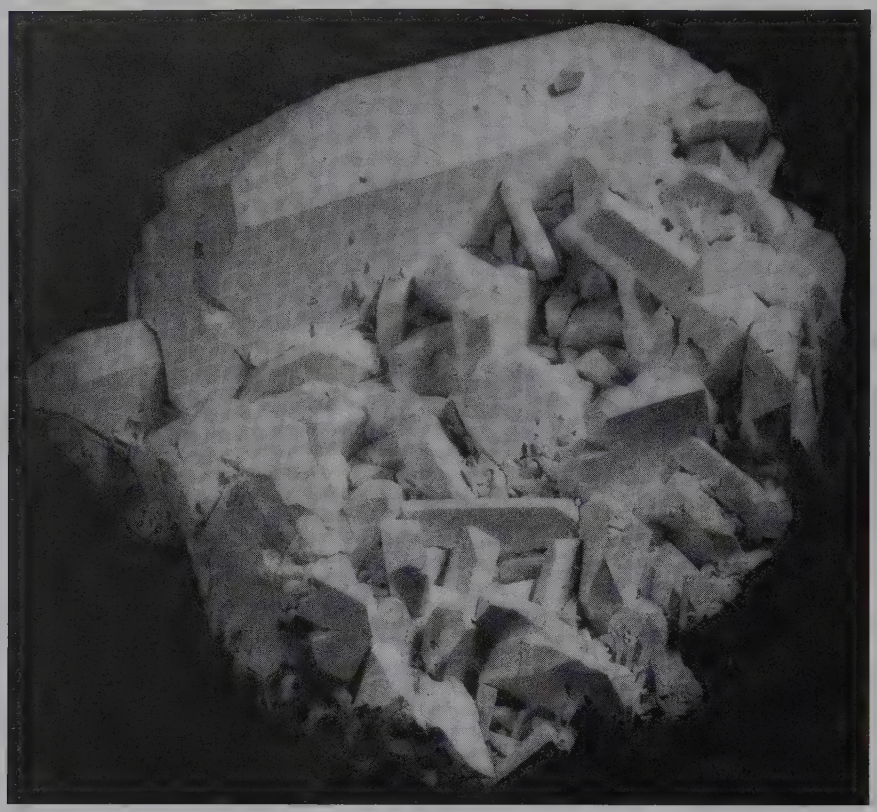

FIG. 17.34 Borax crystals, altered to white, chalky tincalconite. Baker Mine, Kramer borate district, California. (Courtesy of Richard C. Erd, U.S. Geological Survey.)

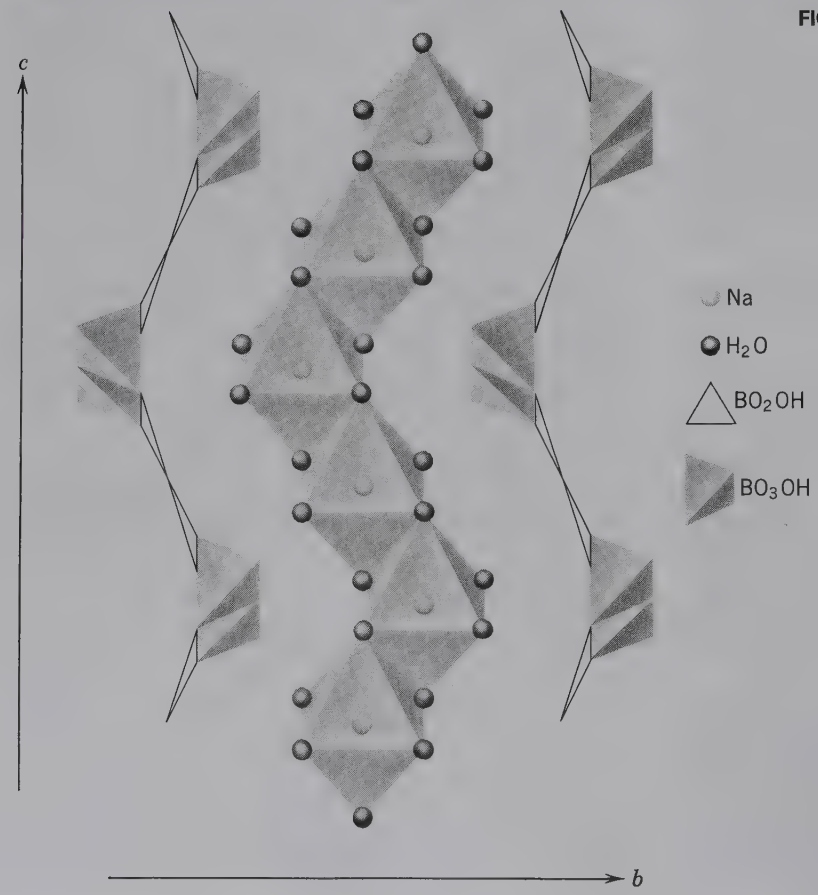

FIG. 17.35 The structure of borax as seen on (100).

Deposits in Tibet furnished the first borax, under the name of *tincal*, to reach western civilization. In the United States, it was first found in Lake County, California, and later in the desert region of southeastern California, in Death Valley, Inyo County, and in San Bernardino County. Associated with kernite, it is the principal mineral mined from the bedded deposits at Boron, California. It is also obtained commercially from the brines of Searles Lake at Trona, California.

Although the United States is the largest producer of borax, the world's most extensive deposits of borate minerals are in Turkey, notably in the Kirka area. Associated with other borates, borax is mined in the Andes Mountains in contiguous parts of Argentina, Bolivia, and Chile. Minerals commonly associated with borax are halite, gypsum, ulexite, colemanite, and various rare borates.

Use. Although boron is obtained from several minerals, it is usually converted to borax, the principal commercial product. There are many uses of borax. Its greatest use is in the manufacture of glass fibers for insulation and textiles. It is also used in soaps and detergents; as an antiseptic and preservative; in medicine; as a solvent for metallic oxides in soldering and welding; and as a flux in various smelting and laboratory operations. Elemental boron is used as a deoxidizer and alloy in nonferrous metals; and as a neutron absorber in shields for atomic reactors. Boron is used in rocket fuels and as an additive in motor fuel. Boron carbide, harder than corundum, is used as an abrasive.

Name. Borax comes from an Arabic name for the substance.

Ulexite—$NaCaB_5O_6(OH)_6{\cdot}5H_2O$

Crystallography. Triclinic; 1. Usually in rounded masses of loose texture, consisting of fine fibers that are acicular or capillary crystals, "cottonballs." Rarely in closely packed parallel fibers showing fiber-optical properties and called "television rock" (see Fig. 1.6).

$P\bar{1}$; $a = 8.73$, $b = 12.75$, $c = 6.70$ Å; $\alpha = 90°16'$, $\beta = 109°8'$, $\gamma = 105°7'$; $Z = 2$. *ds*: 12.3(10), 7.89(7), 6.60(7), 4.19(7), 2.67(7).

Physical Properties. *Cleavage* {010} perfect. **H** $2\frac{1}{2}$; the aggregate has an apparent hardness of 1. **G** 1.96. *Luster* silky. *Color* white. Tasteless. *Optics:* (+); $\alpha = 1.491$, $\beta = 1.504$, $\gamma = 1.520$; $2V = 73°$.

Composition and Structure. Na_2O 7.7, CaO 13.8, $B_2O_3$43.0, H_2O 35.5%. The structure contains large anionic groups of composition $[B_5O_6(OH)_6]^{3-}$. Each Ca^{2+} cation is surrounded by an irregular polyhedron of five oxygens, three (OH) groups, and two H_2O molecules. Each Na^+ cation is octahedrally coordinated by (OH) groups and H_2O molecules. Neighboring octahedra share edges to make continuous chains parallel to *c*.

Diagnostic Features. The soft "cottonballs" with silky luster are characteristic of ulexite.

Occurrence. Ulexite crystallizes in arid regions from brines that have concentrated in enclosed basins, as in playa lakes. Usually associated with borax. It occurs abundantly in the dry basins of northern Chile and in Argentina. In the United States, it has been found abundantly in certain enclosed basins of Nevada and California and with colemanite in bedded Tertiary deposits.

Use. A source of borax.

Name. In honor of the German chemist, G. L. Ulex (1811–1883), who discovered the mineral.

Colemanite—$CaB_3O_4(OH)_3{\cdot}H_2O$

Crystallography. Monoclinic; *2/m*. Commonly in short prismatic crystals, highly modified (Fig. 17.36). Cleavable massive to granular and compact.

$P2_1/a$; $a = 8.74$, $b = 11.26$, $c = 6.10$ Å, $\beta = 110°7'$; $Z = 4$. *ds*: 5.64(5), 4.00(4), 3.85(5), 3.13(10), 2.55(5).

Physical Properties. *Cleavage* {010} perfect. **H** 4–$4\frac{1}{2}$. **G** 2.42. *Luster* vitreous. *Color* colorless to white. Transparent to translucent. *Optics:* (+); $\alpha = 1.586$, $\beta = 1.592$, $\gamma = 1.614$; $2V = 55°$; $X = b$, $Z \wedge c = 84°$. $r > v$.

Composition and Structure. CaO 27.2, B_2O_3 50.9, H_2O 21.9%. The structure contains infinite chains with composition $[B_3O_4(OH)_2]^{2-}$ that are parallel to the *a* axis. The chains contain BO_3 triangles and $BO_2(OH)_2$ and $BO_3(OH)$ tetrahedra. Interspersed between the chains are Ca ions and H_2O molecules.

Diagnostic Features. Characterized by one direction of highly perfect cleavage and exfoliation on heating.

Occurrence. Colemanite deposits are interstratified with lake bed deposits of Tertiary age. Ulexite and borax are usually associated, and colemanite is believed to have originated by their alteration. Found in California in Los Angeles, Ventura, San Bernardino, and Inyo counties, and in Nevada in the Muddy Mountains and White Basin, Clark County. Also occurs extensively in Argentina and Turkey.

Use. A source of borax that, at the time of the discovery of kernite, yielded over half of the world's supply.

Name. In honor of William T. Coleman, merchant of San Francisco, who marketed the product of the colemanite mines.

Similar Species. Other borates, locally abundant, are *boracite*, $Mg_3ClB_7O_{13}$; *hydroboracite*, $CaMgB_6O_8(OH)_6{\cdot}3H_2O$ and *inyoite*, $CaB_3O_3(OH)_5{\cdot}4H_2O$.

Sinhalite, $Mg(Al,Fe)BO_4$ is a rare gem mineral found in the gravels of Sri Lanka and Myanmar. Before its description as a new mineral in 1952, cut stones had been misidentified as brown peridot.

FIG. 17.36 Colemanite.

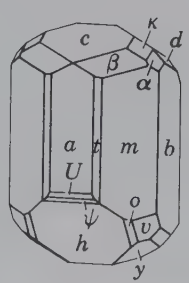

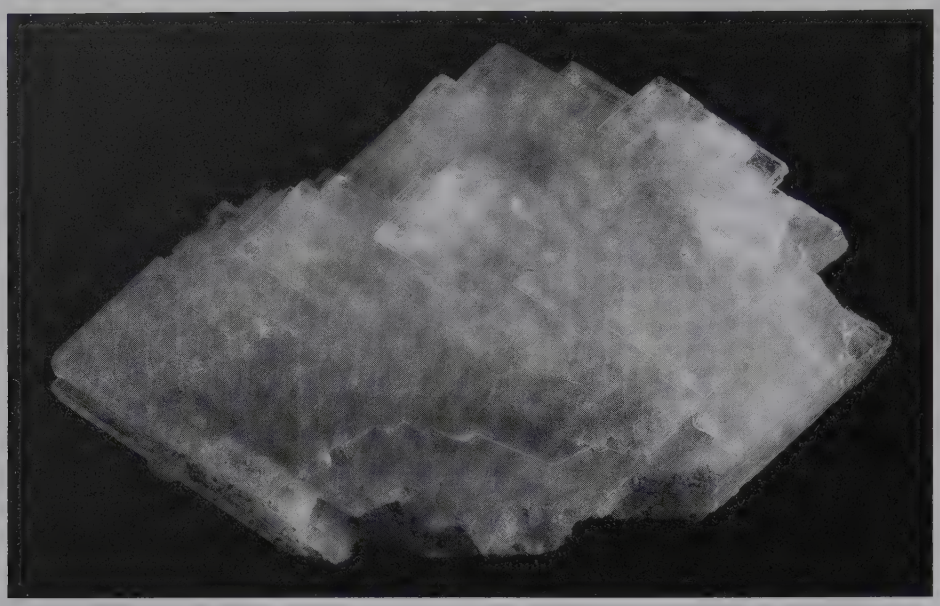

FIG. 17.37 Barite, Kalahari Manganese Field, Northern Cape Province, South Africa (Harvard Mineralogical Museum).

SULFATES AND CHROMATES

Although 319 minerals belong to these two classes only a few of them are common.

Anhydrous Sulfates and Chromate	
Barite group	
Barite	$BaSO_4$
Celestite	$SrSO_4$
Anglesite	$PbSO_4$
Anhydrite	$CaSO_4$
Crocoite	$PbCrO_4$
Hydrous and Basic Sulfates	
Gypsum	$CaSO_4 \cdot 2H_2O$
Antlerite	$Cu_3SO_4(OH)_4$
Alunite	$KAl_3(SO_4)_2(OH)_6$

BARITE GROUP

The sulfates of Ba, Sr, and Pb form an isostructural group with space group *Pnma*. They have closely related crystal constants and similar habits. The members of the group are: *barite*, *celestite*, and *anglesite*.

Barite—$BaSO_4$

Crystallography. Orthorhombic; *2/m2/m2/m*. Crystals are usually tabular on {001}; often diamond-shaped (Fig. 17.37). Both {0*kl*} and {*h*0*l*} prisms are usually present, either beveling the corners of the diamond-shaped crystals or the edges of the tables and forming rectangular prismatic crystals elongated parallel to either *a* or *b* (Fig. 17.38). Crystals may be very complex. Frequently in divergent groups of tabular crystals forming "crested barite" or "barite roses," see Fig. 17.39 and Plate IV, no. 2. Also coarsely laminated; granular, earthy.

Pnma; $a = 8.87$, $b = 5.45$, $c = 7.14$ Å; $Z = 4$. *d*s: 3.90(6), 3.44(10), 3.32(7), 3.10(10), 2.12(8).

Physical Properties. *Cleavage* {001} perfect, {210} less perfect. **H** 3–3½. **G** 4.5 (heavy for a nonmetallic mineral). *Luster* vitreous; on some specimens pearly on base. *Color* colorless, white, and light shades of blue, yellow, red (see Plate XII, no. 11, Chapter 20). *Streak* white. Transparent to translucent. *Optics:* (+); $\alpha = 1.636$, $\beta = 1.637$, $\gamma = 1.648$; $2V = 37°$. $X = c$, $Y = b$. $r < v$.

Composition and Structure. BaO 65.7, SO_3 34.3% for pure barite. Sr substitutes for Ba and a complete solid solution series extends to celestite, but most material is near one end or the other of the series. A small amount of Pb may substitute for Ba. The structure of barite is illustrated in Fig. 17.8 and discussed on page 404.

Diagnostic Features. Recognized by its high specific gravity and characteristic cleavage and crystals.

Occurrence. Barite is a common mineral of wide distribution. It occurs as a gangue mineral in hydrothermal veins, associated with ores of silver, lead, copper, cobalt, manganese, and antimony. It is found in veins in limestone with calcite, or as residual masses in clay overlying limestone. Also in sandstone with copper ores. In places acts as a cement in sandstone. Deposited occasionally as a sinter by waters from hot springs.

Notable localities for the occurrence of barite crystals are in Westmoreland, and Cumbria, England; Baia Sprie

FIG. 17.38 Barite crystals.

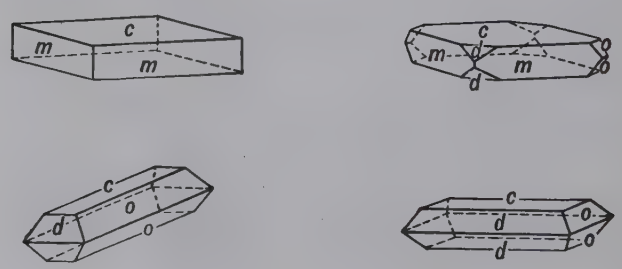

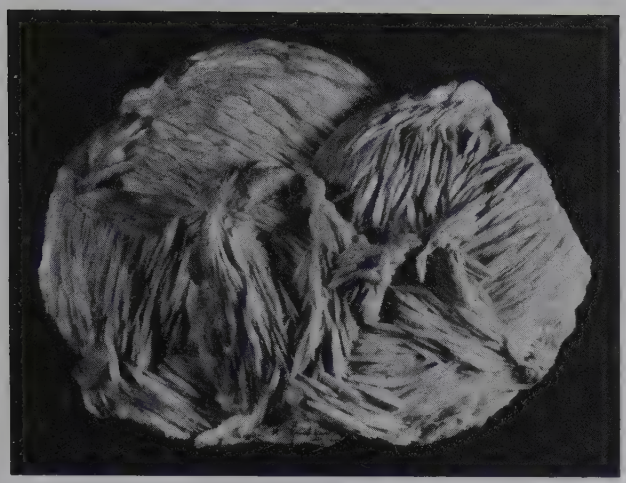

FIG. 17.39 Crested barite. Cumbria, England (Harvard Mineralogical Museum).

(Felsöbánya) and other localities, Romania; and Saxony, Germany. Massive barite, occurring usually as veins, nests, and irregular bodies in limestones, has been quarried in the United States in Georgia, Tennessee, Missouri, and Arkansas. Barite roses are mined in Oklahoma.

Use. More than 80% of the barite produced is used in oil- and gas-well drilling as an additive to make "heavy mud" to support drill rods, and to help prevent blowing out of gas. Barite is the primary source of Ba for chemicals. A major use of barium is in *lithopone*, a combination of barium sulfide and zinc sulfate that forms an intimate mixture of zinc sulfide and barium sulfate. Lithopone is used in the paint industry and to a lesser extent in floor coverings and textiles. Precipitated barium sulfate, "blanc fixe," is employed as a filler in paper and cloth, in cosmetics, as a paint pigment, and for barium meals in radiology.

Name. From the Greek word *barys* meaning *heavy*, an allusion to its high specific gravity.

Celestite—$SrSO_4$

Crystallography. Orthorhombic; *2/m2/m2/m*. Crystals usually more blocky than those of barite. Commonly tabular parallel to {001} or prismatic parallel to *a* or *b* with prominent development of {0*kl*} and {*h*0*l*} prisms. Crystals elongated parallel to *a* are frequently terminated by nearly equal development of faces of *d*{101} and *m*{210} (Fig. 17.40). Also radiating fibrous; granular.

Pnma; $a = 8.38$, $b = 5.37$, $c = 6.85$ Å; $Z = 4$. *d*s: 3.30(10), 3.18(6), 2.97(10), 2.73(6), 2.04(6).

Physical Properties. *Cleavage* {001} perfect, {210} good. **H** 3–3½. **G** 3.95–3.97. *Luster* adamantine to vitreous to pearly. *Color* colorless, white, gray, often faintly blue or red. Transparent to translucent. *Optics:* (+); $\alpha = 1.622$, $\beta = 1.624$, $\gamma = 1.631$; $2V = 50°$; $X = c$, $Y = b$.

Composition and Structure. SrO 56.4, SO_3 43.6% for pure celestite. Ba substitutes for Sr and a complete solid solution series exists between celestite and barite. At ordinary temperatures only a limited series exists between anhydrite, $CaSO_4$, and $SrSO_4$. Celestite is isostructural with barite (see Fig. 17.8).

Diagnostic Features. Commonly, crystals appear icy, gray-blue with adamantine luster. Differentiated from barite by more blocky crystal forms, by lower specific gravity, and by chemical test for strontium.

Occurrence. Celestite is found usually disseminated through limestone or sandstone, or in nests and lining cavities in rocks with sufficient Sr. Associated with calcite, dolomite, gypsum, halite, sulfur, fluorite. Also found as a gangue mineral in lead veins.

Notable localities for its occurrence are with the sulfur deposits of Silicy; and Yate, Gloucestershire, England. Spectacular crystals are from Sakoany, near Majunga, Madagascar. Found in the United States at Clay Center, Ohio, and elsewhere in northwestern and southeastern Michigan; Lampasas, Texas; and with colemanite in Inyo County, California.

Use. Used in the preparation of strontium nitrate for fireworks and tracer bullets, and with other strontium salts used in the refining of beet sugar.

Name. Derived from the Latin *caelestis* meaning *heavenly*, in allusion to the faint blue color of the first specimens described.

Anglesite—$PbSO_4$

Crystallography. Orthorhombic; *2/m2/m2/m*. Frequently in crystals with habit often similar to that of barite but more varied. Crystals may be prismatic parallel to any one of the crystal axes and frequently show many forms, with a complex development (Fig. 17.41). Also massive, granular to compact. Frequently earthy, in concentric layers that may have an unaltered core of galena.

Pnma; $a = 8.47$, $b = 5.39$, $c = 6.94$ Å; $Z = 4$. *d*s: 4.26(9), 3.81(6), 3.33(9), 3.22(7), 3.00(10).

Physical Properties. *Cleavage* {001} good, {210} imperfect. Fracture conchoidal. **H** 3.0. **G** 6.2–6.4 (unusually high for a non-metallic). *Luster* adamantine when in crystals, dull when massive. *Color* colorless, white, gray, pale shades of yellow. May be colored dark gray by impurities. Transparent

FIG. 17.40 Celestite crystals.

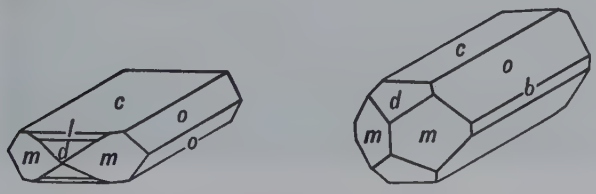

FIG. 17.41 Anglesite.

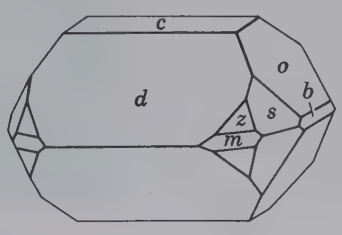

to translucent. *Optics:* (+); $\alpha = 1.877$, $\beta = 1.883$, $\gamma = 1.894$; $2V = 75°$; $X = c$, $Y = b$. $r < v$.

Composition and Structure. PbO 73.6, SO_3 26.4%. Anglesite is isostructural with barite (see Fig. 17.8 and page 404).

Diagnostic Features. Recognized by its high specific gravity, its adamantine luster, and frequently by its association with galena. Distinguished from cerussite in that it will not effervesce in nitric acid.

Occurrence. Anglesite is a common supergene mineral found in the oxidized portions of lead deposits. It is formed through the oxidation of galena, either directly, as is shown by concentric layers of anglesite surrounding a core of galena, or by solution and subsequent deposition and recrystallization. Anglesite is commonly associated with galena, cerussite, sphalerite, smithsonite, hemimorphite, and iron oxides.

Notable localities for its occurrence are Monte Poni, Sardinia, Italy; Island of Anglesey, Wales; Derbyshire, England; and Leadhills, Scotland. It can also be found in Sidi-Amorben-Salem, Tunisia; Tsumeb, Namibia; Broken Hill, New South Wales, and Dundas, Tasmania, Australia; and Touissit, Morocco. In addition, it is found in crystals embedded in sulfur at Los Lamentos, Chihuahua, Mexico. In the United States, it is in Phoenixville, Pennsylvania; Tintic district, Utah; and Coeur d'Alene district, Idaho.

Use. A minor ore of lead.

Name. Named from the original locality on the Island of Anglesey, Wales.

Anhydrite—$CaSO_4$

Crystallography. Orthorhombic. *2/m2/m2/m.* Crystals are rare; when observed are thick tabular on {010}, {100}, or {001} (see Fig. 17.42), also prismatic parallel to *b*. Usually massive or in crystalline masses resembling an isometric mineral with cubic cleavage. Also fibrous, granular, massive.

Amma; $a = 6.95$, $b = 6.96$, $c = 6.21$ Å; $Z = 4$. *ds*: 3.50(10), 2.85(3), 2.33(2), 2.08(2), 1.869(2).

Physical Properties. *Cleavage* {010} perfect, {100} nearly perfect, {001} good. **H** 3–3½. **G** 2.89–2.98. *Luster* vitreous to pearly on cleavage. *Color* colorless to gray to bluish or violet. Also may be white or tinged with rose, brown, or red. *Optics:* (+); $\alpha = 1.570$, $\beta = 1.575$, $\gamma = 1.614$; $2V = 44°$; $X = b$, $Y = a$; $r < v$.

Composition and Structure. CaO 41.2, SO_3 58.8%. The structure illustrated in Fig. 17.9 is very different from the barite type. In anhydrite, Ca is in 8-coordination with oxygen from SO_4 groups, whereas in barite, Ba is in 12-coordination with oxygen. A metastable polymorph of anhydrite ($\gamma CaSO_4$) is hexagonal and is formed as the result of slow dehydration of gypsum (see Fig. 17.45).

FIG. 17.42 Anhydrite.

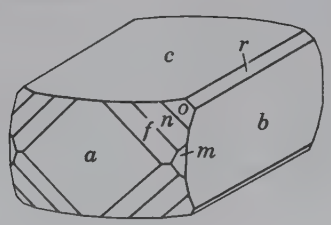

Diagnostic Features. Anhydrite is characterized by its three cleavages at right angles. It is distinguished from calcite by its higher specific gravity and from gypsum by its greater hardness. Some massive varieties are difficult to recognize but often appear "sugary," and one should test for sulfate.

Alteration. Anhydrite by hydration, at lower temperatures, changes to gypsum with an increase in volume, and in places large masses have been altered in this way.

Occurrence. Anhydrite occurs in similar settings as gypsum and is often associated with gypsum but is not nearly as common. Found in beds associated with salt deposits in the cap rock of salt domes, and in limestones. Found in some amygdaloidal cavities in basalt.

Notable localities are: Wieliczka, Poland; Aussee, Styria, and Hall near Innsbruck, Tyrol, Austria; and Bex, Switzerland. In the United States, found in Lockport, New York; West Paterson, New Jersey; New Mexico; and Texas. Found in large beds in Nova Scotia.

Use. Ground anhydrite is used as a soil conditioner and to a minor extent as a setting retardant in Portland cement. In Great Britain and Germany, it has been used as a source of sulfur for the production of sulfuric acid.

Name. Anhydrite is from the Greek word meaning *without water*, in contrast to the more common hydrous calcium sulfate, gypsum.

Crocoite—$PbCrO_4$

Crystallography. Monoclinic; *2/m.* Commonly in slender prismatic crystals, vertically striated, and columnar aggregates. Also granular.

$P2_1/n$; $a = 7.11$, $b = 7.41$, $c = 6.81$ Å, $\beta = 102°33'$; $Z = 4$. *ds*: 4.96(3), 3.28(10), 2.85(3), 2.33(2), 2.08(2), 1.869(2).

Physical Properties. *Cleavage* {110} imperfect. **H** 2½–3. **G** 5.9–6.1. *Luster* adamantine. *Color* bright hyacinth-red to orange-red. *Streak* orange-yellow. Translucent.

Composition and Structure. PbO 68.9, CrO_3 31.1%. *Crocoite* is isostructural with *monazite*, $CePO_4$, with Pb in 9-coordination with oxygen, linking six CrO_4 tetrahedra.

Diagnostic Features. Crocoite is characterized by its color, high luster, and high specific gravity. It may be confused with wulfenite, $PbMoO_4$, but can be distinguished from it by its redder color, lower specific gravity, and crystal form.

Occurrence. Crocoite is a rare mineral found in the oxidized zones of lead deposits in regions where lead veins have traversed rocks containing chromite. Associated with pyromorphite, cerussite, and wulfenite. Notable localities are: Dundas, Tasmania and Beresovsk near Sverdlovsk, Ural Mountains, Russia. In the United States, it is found in small quantities in the Vulture district, Arizona.

Use. Not abundant enough to be of commercial value, but of historic interest, because the element chromium was first discovered in crocoite.

Name. From the Greek word meaning *saffron*, in allusion to the color.

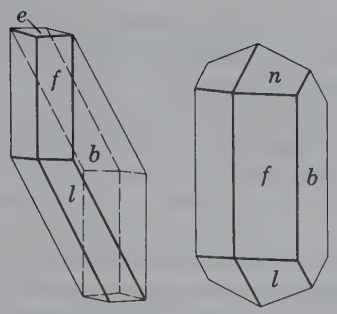

(a)

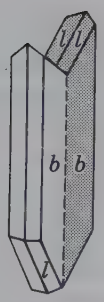

(b)

FIG. 17.43 (a) Gypsum crystals. (b) Gypsum twin.

GYPSUM—$CaSO_4 \cdot 2H_2O$

Crystallography. Monoclinic; $2/m$. Crystals are of simple habit (Figs. 17.43a and 17.44); tabular on {010}; diamond-shaped, with edges beveled by {120} and {$\bar{1}$11}. Other forms are rare. Twinning is common, on {100} (Fig. 17.43b), often resulting in swallowtail twins.

$C2/c$; $a = 6.28$, $b = 15.15$, $c = 5.67$ Å, $\beta = 114°12'$; $Z = 4$. *ds*: 7.56(10), 4.27(5), 3.06(6), 2.87(2), 2.68(3).

Physical Properties. *Cleavage* {010} perfect yielding thin folia; {100}, with conchoidal surface; {011}, with fibrous fracture. **H** 2. **G** 2.32. *Luster* usually vitreous; also pearly and silky. *Color* colorless, white, gray; various shades of yellow, red, brown, from impurities. Transparent to translucent, see Plate IV, no. 3.

Satin spar is a fibrous gypsum with silky luster. *Alabaster* is the fine-grained massive variety, often colored. *Selenite* is a variety that is colorless and transparent and yields cleavage folia. *Optics:* (+); $\alpha = 1.520$, $\beta = 1.523$, $\gamma = 1.530$; $2V = 58°$. $Y = b$, $X \wedge c = -37°$; $r > v$.

Composition and Structure. CaO 32.6, SO_3 46.5, H_2O 20.9%. As the result of dehydration of gypsum, $CaSO_4 \cdot 2H_2O$, several phases may form. These are: γ $CaSO_4$, when all H_2O is lost and a metastable phase $CaSO_4 \cdot \frac{1}{2}H_2O$. During the dehydration process the first $1\frac{1}{2}$ molecules of H_2O in gypsum are lost relatively continuously between 0° and about 65°C (see Fig. 17.45) perhaps with only slight changes in the gypsum structure. At about 70°C the remaining $\frac{1}{2}H_2O$ molecule in $CaSO_4 \cdot \frac{1}{2}H_2O$ is still retained relatively strongly, but at about 95°C this is lost and the structure transforms to that of a polymorph of anhydrite. The structure of gypsum is given in Fig. 17.10 and discussed on page 405.

Diagnostic Features. Characterized by its softness and its three unequal cleavages.

Occurrence. Gypsum is a common mineral widely distributed in sedimentary rocks, often as thick beds. If frequently occurs interstratified with limestones and shales and is usually found as a layer underlying beds of rock salt, having been deposited as one of the first minerals to crystallize on the evaporation of saltwaters (see Box 16.2). May recrystallize in veins, forming *satin spar*. Occurs also as lenticular bodies or

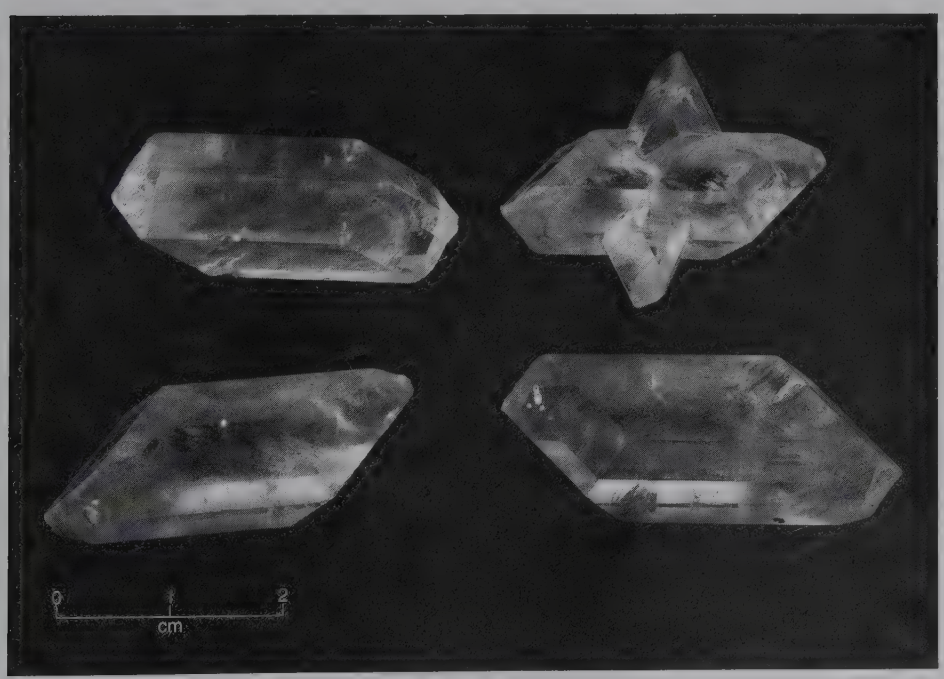

FIG. 17.44 Gypsum crystals. Ellsworth, Ohio (Harvard Mineralogical Museum).

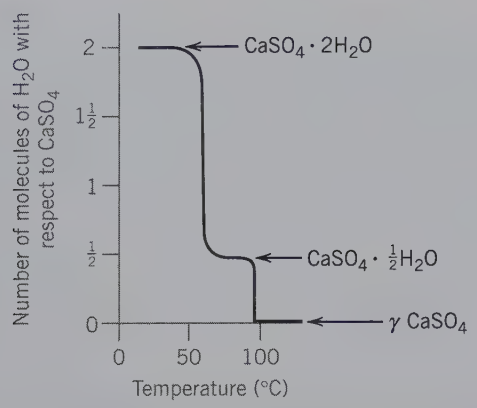

FIG. 17.45 Dehydration curve of gypsum showing formation of metastable $CaSO_4 \cdot \frac{1}{2}H_2O$ at about 65°C. At about 100°C the γ polymorph of $CaSO_4$ is formed.

scattered crystals in clays and shales. Frequently formed by the alteration of anhydrite, and under these circumstances may show folding because of increased volume. Found in volcanic regions, especially where limestones interact with sulfur vapors. Also common as a gangue mineral in metallic veins. Associated with many different minerals, the more common being halite, anhydrite, dolomite, calcite, sulfur, pyrite, and quartz.

Gypsum is the most common sulfate, and extensive deposits are found in many localities throughout the world. The principal world producers are the United States, Canada, Spain, Thailand, and Iran. In the United States, commercial deposits are found in many states, but the chief producers are located in California, Iowa, New York, Texas, and Oklahoma. Gypsum is found in large deposits in Arizona and New Mexico where it forms windblown "sand dunes," such as White Sands, New Mexico. Spectacular crystals originate from several mines in Mexico, especially Naica and Chihuahua.

Use. Gypsum is used chiefly for the production of gypsumboard or wallboard. In the manufacture of plaster of Paris, the gypsum is ground and then heated until about 75% of the water has been driven off, producing the substance $CaSO_4 \cdot H_2O$. This material, when mixed with water, slowly absorbs the water, crystallizes and, thus, hardens, or *sets*. Plaster of Paris is used extensively for *staff*, the material from which temporary exposition buildings are built, for gypsum lath, wallboard, and for molds and casts of all kinds. Gypsum is employed in making *adamant plaster* for interior use. Serves as a soil conditioner, *land plaster*, for fertilizer. Uncalcined gypsum is used as a retarder in Portland cement. Satin spar and alabaster are cut and polished for various ornamental purposes but are restricted in their use because of their softness.

Name. From the Greek name for the mineral, applied especially to the calcined mineral.

Antlerite—$Cu_3SO_4(OH)_4$

Crystallography. Orthorhombic; *2/m2/m2/m*. Crystals are usually tabular on {010} (Fig. 17.46b). May be in slender prismatic crystals vertically striated. Also in parallel aggregates, reniform, massive.

Pnam; $a = 8.24, b = 11.99, c = 6.03$ Å; $Z = 4$. *ds*: 4.86(10), 3.60(8), 3.40(3), 2.68(6), 2.57(6).

Physical Properties. *Cleavage* {010} perfect. **H** $3\frac{1}{2}$–4. **G** 3.9±. *Luster* vitreous. *Color* emerald to blackish-green. *Streak* pale green. Transparent to translucent. *Optics:* (+); $\alpha = 1.726$, $\beta = 1.738$, $\gamma = 1.789$; $2V = 53°$; $X = b$, $Y = a$; pleochroism X yellow-green, Y blue-green, Z green.

Composition and Structure. CuO 67.3, SO_3 22.5, H_2O 10.2%. The structure of antlerite contains Cu in two types of octahedral coordination: $CuO(OH)_5$ and $CuO_3(OH)_3$. These octahedra are linked with the SO_4 tetrahedra.

Diagnostic Features. Antlerite is characterized by its green color, {010} cleavage, and association. Lack of effervescence in HCl distinguishes it from malachite. It is commonly associated with atacamite and brochantite, and one must use optical or chemical properties to distinguish it from these minerals.

Occurrence. Antlerite is found in the oxidized portions of copper veins, especially in arid regions. It was formerly considered a rare mineral, but in 1925 it was recognized as the primary ore mineral at Chuquicamata, Chile, the world's largest copper mine. It may form directly as a secondary mineral on chalcocite, or the copper may go into solution and later be deposited as antlerite, filling fractures. In the United States, it is found at Bisbee, Arizona.

Use. An ore of copper.

Name. From the Antler Mine, Arizona, from which locality it was originally described.

Similar Species. *Brochantite*, $Cu_4SO_4(OH)_6$, is similar in all its properties to antlerite, but, although more widespread, it is nowhere abundant. Until the antlerite find in 1925, it was considered to be the primary ore mineral at Chuquicamata, Chile. Another rare hydrous copper sulfate is *chalcanthite*, $CuSO_4 \cdot 5H_2O$, which occurs abundantly at Chuquicamata and other arid areas in Chile. *Epsomite*, $MgSO_4 \cdot 7H_2O$, occurs as an efflorescence on the rocks in mine workings and on the walls of caves. *Melanterite*, $FeSO_4 \cdot 7H_2O$, is also a secondary mineral found as an efflorescence on mine timbers.

FIG. 17.46 Antlerite crystals.

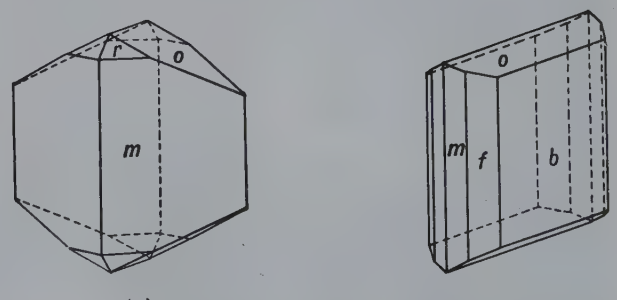

(a) (b)

Alunite—$KAl_3(SO_4)_2(OH)_6$

Crystallography. Hexagonal; $3m$. Crystals are usually a combination of positive and negative trigonal pyramids resembling rhombohedrons with nearly cubic angles (90°50′). May be tabular on {0001}. Commonly massive or disseminated.

$R3m$; $a = 6.97$, $c = 17.38$ Å; $Z = 3$. *ds*: 4.94(5), 2.98(10), 2.29(5), 1.89(6), 1.74(5).

Physical Properties. *Cleavage* {0001} imperfect. **H** 4. **G** 2.6–2.8. *Luster* vitreous to pearly in crystals, earthy in massive material. *Color* white, gray, or reddish. Transparent to translucent. *Optics:* (+); $\omega = 1.572$, $\epsilon = 1.592$.

Composition and Structure. K_2O 11.4, Al_2O_3 37.0, SO_3 38.6, H_2O 13.0%. Na may replace K at least up to Na:K = 7:4. When Na exceeds K in the mineral it is called *natroalunite*, $(Na,K)Al_3(SO_4)_2(OH)_6$. In the structure of alunite K and Al are in 6-coordination with respect to O and (OH). The SO_4 groups share some of their oxygens with the K-containing octahedra.

Diagnostic Features. Alunite is usually massive and difficult to distinguish from rocks such as limestone, and other massive minerals, such as anhydrite, dolomite, and granular magnesite.

Occurrence. Alunite, also called *alumstone*, is usually formed by sulfuric acid solutions acting on rocks rich in potash feldspar, and in some places large masses have thus been formed. It is found in smaller amounts about volcanic fumaroles. In the United States, it is found at Red Mountain in the San Juan district, Colorado; Goldfield, Nevada; and Marysvale, Utah.

Use. In the production of alum. At Marysvale, Utah, alunite has been mined to recover potassium and aluminum.

Name. From the Latin word meaning *alum*.

Similar Species. *Jarosite*, $KFe_3(SO_4)_2(OH)_6$, the Fe^{3+} analogue of alunite, is a secondary mineral found as crusts and coatings on ferruginous ores.

TUNGSTATES AND MOLYBDATES

The tungstates and molybdates comprise a group of 42 minerals, of which we will discuss only 3: *wolframite*, *scheelite*, and *wulfenite*.

Wolframite—$(Fe,Mn)WO_4$

Crystallography. Monoclinic; $2/m$. Crystals are commonly tabular parallel to {100} (Fig. 17.47) giving bladed habit, with faces striated parallel to *c*. In bladed, lamellar, or columnar aggregates. Massive granular.

$P2/c$; $a = 4.79$, $b = 5.74$, $c = 4.99$ Å; $\beta = 90°28'$; $Z = 2$. *ds*: 4.76(5), 3.74(5), 2.95(10), 2.48(6), 1.716(5). Cell parameters are slightly less for *ferberite*, $FeWO_4$, and greater for *hübnerite*, $MnWO_4$.

Physical Properties. *Cleavage* {010} perfect. **H** 4–4½. **G** 7.0–7.5, higher with higher Fe content. *Luster* submetallic to resinous. *Color* black in ferberite to brown in hübnerite. *Streak* from nearly black to brown.

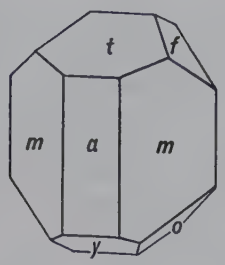

FIG. 17.47 Wolframite.

Composition and Structure. Fe^{2+} and Mn^{2+} substitute for each other in a complete solid solution series between *ferberite*, $FeWO_4$, and *hübnerite*, $MnWO_4$. The percentage of WO_3 is 76.3 in ferberite and 76.6 in hübnerite. The structure of wolframite consists of distorted tetrahedral (WO_4) groups and octahedral $(Fe,Mn)O_6$ groups. From the interatomic distances around W, it is suggested that W is in distorted octahedral coordination.

Diagnostic Features. The dark color, one direction of perfect cleavage, and high specific gravity serve to distinguish wolframite from other minerals.

Occurrence. Wolframite is a comparatively rare mineral found usually in pegmatites and high-temperature quartz veins associated with granites. More rarely in sulfide veins. Minerals commonly associated include cassiterite, scheelite, bismuth, quartz, pyrite, galena, sphalerite, and arsenopyrite. In some veins, wolframite may be the only metallic mineral present.

Found in fine crystals from Baia Sprie (Felsöbánya), Romania and from Horní Slavkov (Schlaggenwald), Czech Republic, and in the various tin districts of Saxony, Germany, and Cornwall, England. Important producing countries are China, Russia, Korea, Thailand, Bolivia, and Australia. Wolframite occurs in the United States in the Black Hills, South Dakota. Ferberite has been mined extensively in Boulder County, Colorado. Hübernite is found near Silverton, Colorado; Mammoth district, Nevada; and Black Hills, South Dakota. More than 90% of the world's estimated tungsten resources are outside the United States, with almost 60% in southeastern China.

Use. Primary ore of tungsten. Tungsten is used as hardening metal in the manufacture of high-speed tool steel, valves, springs, chisels, files, and so on. Its high melting point (3410°C) requires a special chemical process for reduction of the metal, which is produced in the form of a powder. By powder-metallurgy, pure metal products, such as lamp filaments, are fabricated. A large use for tungsten is in the manufacture of carbides, harder than any natural abrasives (other than diamond), used for cutting tools, rock bits, and hard facings. Sodium tungstate is used in fireproofing cloth and as a mordant in dyeing.

Name. Wolframite is derived from an old word of German origin. Feberite is after M. R. Ferber (1805–1875), German amateur mineralogist; hübnerite is after A. Hübner, German metallurgist.

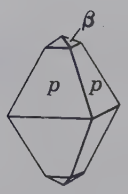

FIG. 17.48 Scheelite.

Scheelite—$CaWO_4$

Crystallography. Tetragonal; $4/m$. Crystals are usually simple dipyramids, {011} (Fig. 17.48). The dipyramid, {112}, closely resembles the octahedron in angles. Also massive granular.

$I4/a$; $a = 5.25$, $c = 11.40$ Å; $Z = 4$. *ds*: 4.77(7), 3.11(10), 1.94(8), 1.596(9), 1.558(7).

Physical Properties. *Cleavage* {101}, distinct. **H** $4\frac{1}{2}$–5. **G** 5.9–6.1 (unusually high for a nonmetallic mineral). *Luster* vitreous to adamantine. *Color* white, yellow, green, brown. Translucent; some specimens transparent (see Plate XII, no. 14, Chapter 20). Most scheelite will fluoresce with bluish-white color in short ultraviolet radiation. *Optics:* (+); $\omega = 1.920$, $\epsilon = 1.934$.

Composition and Structure. CaO 19.4, WO_3 80.6%. Mo can substitute for W and a partial series extends to *powellite*, $CaMoO_4$. The structure of scheelite (Fig. 17.11) consists of flattened (WO_4) tetrahedra and CaO_8 polyhedra.

Diagnostic Features. Recognized by its high specific gravity, crystal form, and fluorescence in short ultraviolet light. The test for tungsten may be necessary for positive identification.

Occurrence. Scheelite is found in granite pegmatites, contact metamorphic deposits, and high-temperature hydrothermal veins associated with granitic rocks. Associated with cassiterite, topaz, fluorite, apatite, molybdenite, and wolframite. Occurs with tin in deposits of Bohemia, Czech Republic, Saxony, Germany, and Cornwall, England; and in quantity in New South Wales and Queensland, Australia. In the United States, scheelite is mined near Mill City and Mina, Nevada; near Atolia, San Bernardino County, California; and in lesser amounts in Arizona, Utah, Montana, and Colorado.

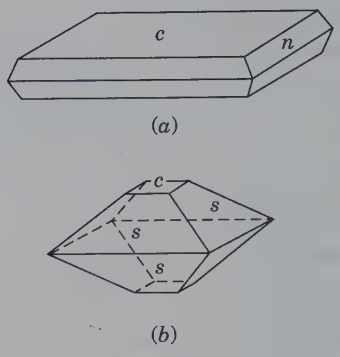

FIG. 17.49 Wulfenite crystals.

Use. An ore of tungsten. Wolframite furnishes most of the world's supply of tungsten, but scheelite is more important in the United States. Transparent crystals may be cut as faceted gems.

Name. After K. W. Scheele (1742–1786), the discoverer of tungsten.

Wulfenite—$PbMoO_4$

Crystallography. Tetragonal; 4 or $4/m$. Crystals are usually square, tabular in habit with prominent {001}; Figs. 17.49a and 17.50. Some crystals are very thin. More rarely pyramidal (Fig. 17.49b). Some crystals may be twinned on {001} giving them a dipyramidal habit.

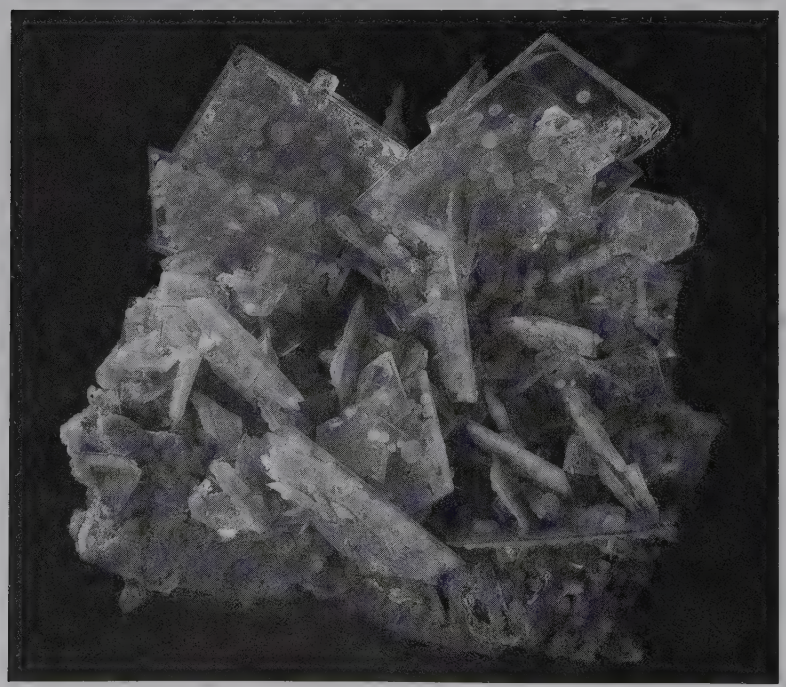

FIG. 17.50 Wulfenite crystals wtih mimetite. From the San Francisco Mine, Cucurpe, Sonora, Mexico. Specimen is about 10 cm wide (photograph courtesy of Stuart and Donna Wilensky, Wilensky Fine Minerals, Wurtsboro, New York.)

$I4_1/a$; $a = 5.42$, $c = 12.10$ Å; $Z = 4$. *ds*: 3.24(10), 3.03(2), 2.72(2), 2.02(3), 1.653(3).

Physical Properties. *Cleavage* {011} distinct. **H** 3. **G** 6.8 ±. *Luster* vitreous to adamantine. *Color* yellow, orange, red, gray, white. *Streak* white. Transparent to subtranslucent. Piezoelectricity suggests symmetry 4 rather than $4/m$ as determined from structure. *Optics:* (−); $\omega = 2.404$, $\epsilon = 2.283$.

Composition and Structure. PbO 60.8, MoO_3 39.2%. Ca may substitute for Pb, indicating at least a partial series to *powellite*, $Ca(Mo,W)O_4$. Wulfenite is isostructural with scheelite (see Fig. 17.11).

Diagnostic Features. Wulfenite is characterized by its square tabular crystals, orange to yellow color, high luster, and association with other lead minerals. Distinguished from crocoite by crystal form and test for Mo.

Occurrence. Wulfenite is found in the oxidized portions of lead veins with other secondary lead minerals, especially cerussite, vanadinite, and pyromorphite. Found in the United States in several places in the Southwest. Found in beautiful crystals at the Red Cloud, Glove, and Mammoth mines in Arizona; also at the Bennett mine in New Mexico; and in Mežica (Mies) and Črna pri Prevaljah (Schwartzenbach), Slovenia.

Use. A minor source of molybdenum. Molybdenite, MoS_2, is the chief ore.

Name. After X. F. Wulfen, Austrian mineralogist.

PHOSPHATES, ARSENATES AND VANADATES

This mineral group, composed mostly of phosphates, is very large (with 763 known species, Table 15.1) but most of its members are rare. Of the list of phosphates, arsenates, and vanadates given here, only apatite is considered common.

Triphylite—	$Li(Fe,Mn)PO_4$
Lithiophilite	$Li(Mn,Fe)PO_4$
Monazite	$(Ce,La,Y,Th)PO_4$
Apatite Group	
Apatite	$Ca_5(PO_4)_3(F,Cl,OH)$
Pyromorphite	$Pb_5(PO_4)_3Cl$
Vanadinite	$Pb_5(VO_4)_3Cl$
Erythrite	$Co_3(AsO_4)_2{\cdot}8H_2O$
Amblygonite	$LiAlPO_4F$
Lazulite—	$(Mg,Fe)Al_2(PO_4)_2(OH)_2$
Scorzalite	$(Fe,Mg)Al_2(PO_4)_2(OH)_2$
Wavellite	$Al_3(PO_4)_2(OH)_3{\cdot}5H_2O$
Turquoise	$CuAl_6(PO_4)_4(OH)_8{\cdot}4H_2O$
Autunite	$Ca(UO_2)_2(PO_4)_2{\cdot}10\text{–}12H_2O$
Carnotite	$K_2(UO_2)_2(VO_4)_2{\cdot}3H_2O$

Triphylite—$Li(Fe,Mn)PO_4$ Lithiophilite—$Li(Mn,Fe)PO_4$

Crystallography. Orthorhombic; $2/m2/m2/m$. Crystals are rare. Commonly in cleavable masses. Also compact.

Pmcn. For triphylite: $a = 6.01$, $b = 4.86$, $c = 10.36$ Å; $Z = 4$. *ds*: 4.29(8), 3.51(9), 3.03(9), 2.54(10), 1.75(5).

Physical Properties. *Cleavage* {001} nearly perfect, {010} imperfect. **H** $4\frac{1}{2}$–5. **G** 3.42–3.56 increasing with Fe content. *Luster* vitreous to resinous. *Color* bluish-gray in triphylite to salmon-pink or clove-brown in lithiophilite. May be stained black by manganese oxide. Translucent. *Optics:* (+); $\alpha = 1.669\text{–}1.694$, $\beta = 1.673\text{–}1.695$, $\gamma = 1.682\text{–}1.700$; $2V = 0°\text{–}55°$, $X = c$, $Y = a$, $Z = b$. Indices increase with Fe content.

Composition and Structure. A complete Fe^{2+}-Mn^{2+} series exists between two essentially pure end members. In the structure of members of this series Li and (Mn,Fe) are in 6-coordination. These octahedra are linked along their edges into zigzag chains that are connected by (PO_4) tetrahedra.

Diagnostic Features. Characterized by two cleavages at right angles, resinous luster, and association.

Occurrence. Triphylite and lithiophilite are pegmatite minerals associated with other phosphates, spodumene, and beryl. Notable localities are in Bavaria, Germany, and Finland. Lithiophilite is found at several localities in Argentina. In the United States, triphylite is found in large crystals at the Palermo Mine, North Grothon, New Hampshire, and elsewhere in New England, and in the Black Hills, South Dakota. Lithiophilite is found at Branchville, Connecticut.

Name. Triphylite from the Greek words meaning *three* and *family* in allusion to containing three cations. Lithiophilite from the Greek words meaning *lithium* and *friend*.

Monazite—$(Ce,La,Y,Th)PO_4$

Crystallography. Monoclinic; $2/m$. Crystals are rare and usually small, often flattened on {100}, or elongated on *b*. Usually in granular masses, frequently as sand.

$P2_1/n$; $a = 6.79$, $b = 7.01$, $c = 6.46$ Å; $\beta = 103°38'$; $Z = 4$. *ds*: 4.17(3), 3.30(5), 3.09(10), 2.99(2), 2.87(7).

Physical Properties. *Cleavage* {100} poor. Parting {001}. **H** 5–$5\frac{1}{2}$. **G** 4.6–5.4. *Luster* resinous. *Color* yellowish to reddish-brown. Translucent. *Optics:* (+); $\alpha = 1.785\text{–}1.800$, $\beta = 1.787\text{–}1.801$, $\gamma = 1.840\text{–}1.850$; $2V = 10°\text{–}20°$; $X = b$, $Z \wedge c = 2°\text{–}6°$.

Composition and Structure. A phosphate of the rare-earth metals essentially $(Ce,La,Y,Th)PO_4$. Th content ranges from a few to 20% ThO_2. Si is often present up to several percent SiO_2. The Si has been ascribed to admixture of *thorite*, $ThSiO_4$, but may be in part due to substitution of (SiO_4) for (PO_4). In the structure of monazite the rare earths are in 9-coordination with oxygen, linking six PO_4 tetrahedra. It is isostructural with *crocoite*, $PbCrO_4$ (see page 422).

Diagnostic Features. Radioactive. Large specimens may be distinguished from zircon by crystal form and lower hardness, and from titanite by crystal form and higher specific gravity. On doubtful specimens a test for phosphate is necessary.

Occurrence. Monazite as an accessory in granites, aplites, pegmatites, and most metamorphic rocks, and as rolled grains in the sands derived from the decomposition of such rocks. It is concentrated in sands because of its resistance to chemical attack and its high specific gravity, and is associated with other resistant and heavy minerals, such as magnetite, ilmenite, rutile, and zircon.

The bulk of the world's supply of monazite comes from beach sands in Brazil, India, and Australia. A dikelike body of massive granular monazite was mined near Van Rhynsdorp, Cape Province, South Africa. Found in the United States in North Carolina, both in gneisses and in the stream sands; and in the beach sands of Florida.

Use. Monazite is the primary source of thorium oxide, which it contains in amounts varying between 1% and 20%; commercial monazite usually contains between 3% and 9%. Thorium oxide is used in the manufacture of mantles for incandescent gas lights.

Thorium is a radioactive element and is receiving considerable attention as a source of atomic energy. A commercial thorium-fueled reactor is in operation at Fort St. Vrain, Colorado. In geology, monazite is used for radiometric age dating.

Name. The name *monazite* is derived from the Greek word *monachos* meaning *solitary*, in allusion to the rarity of the mineral.

APATITE GROUP

APATITE—$Ca_5(PO_4)_3(F,Cl,OH)$

Crystallography. Hexagonal; *6/m*. Commonly occurs in crystals of long prismatic habit, see Fig. 17.51; some short prismatic or tabular. Usually terminated by prominent dipyramid, $\{10\bar{1}1\}$ and frequently a basal plane. Some crystals show faces of a hexagonal dipyramid (μ, Fig. 17.52c), which reveals the true symmetry. Also in massive granular to compact masses.

$P6_3/m$; $a = 9.39$, $c = 6.89$ Å; $Z = 2$. *ds*: 2.80(10), 2.77(4), 2.70(6), 1.84(6), 1.745(3).

Physical Properties. *Cleavage* {0001} poor. **H** 5 (can just be scratched by a knife). **G** 3.15–3.20. *Luster* vitreous to subresinous. *Color* usually some shade of green or brown; also blue, violet, colorless, see Plate IV, no. 4. Transparent to translucent. *Optics:* (−); ω = 1.633, ε = 1.630 (fluorapatite).

Composition and Structure. $Ca_5(PO_4)_3F$, *fluorapatite* is most common; more rarely $Ca_5(PO_4)_3Cl$, *chlorapatite*, and $Ca_5(PO_4)_3(OH)$, *hydroxylapatite*. F, Cl, and OH can substitute for each other, giving complete series. (CO_3, OH) may substitute for (PO_4) giving *carbonate-apatite*. The (PO_4) group can be partially replaced by (SO_4) as well as (SiO_4). The P^{5+} to S^{6+} replacement is compensated by the coupled substitution of Ca^{2+} by Na^+. Furthermore, the P^{5+} to S^{6+} replacement may be balanced by substitution of Si^{4+} for P^{5+}. Mn and Sr can substitute in part for Ca. The structure of apatite is illustrated in Fig. 17.12.

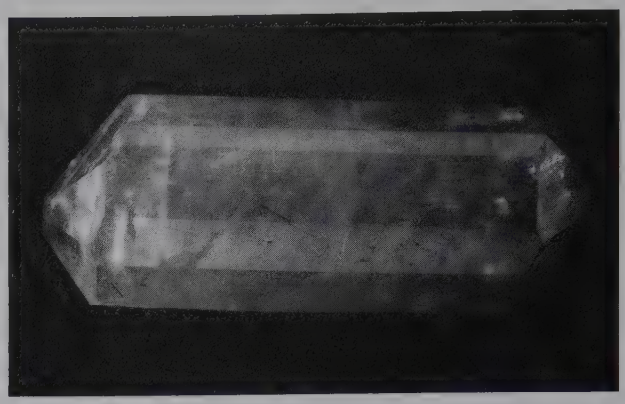

FIG. 17.51 Fluorapatite displaying prism, dipyramids and a pinacoid. From Imilchil, Morocco. Specimen is 4.7 cm high (Photographs courtesy of Jeff Scovil, collection © Jeff Scovil).

Collophane. The name collophane has been given to the massive, cryptocrystalline types of apatite that constitute the bulk of phosphate rock and fossil bone. X-ray study shows that collophane is essentially apatite and does not warrant designation as a separate species. In its physical appearance, collophane is usually dense and massive with a concretionary or colloform structure. It is usually impure and contains small amounts of calcium carbonate.

Diagnostic Features. Apatite is usually recognized by its crystals, color, and hardness. Distinguished from beryl by the prominent pyramidal terminations of its crystals and by its being softer than a knife blade.

Occurrence. Apatite is widely disseminated as an accessory mineral in all rocks—igneous, sedimentary, and metamorphic. It is also found in pegmatites and other veins, probably of hydrothermal origin. Found in titaniferous magnetite bodies. Occasionally concentrated into large deposits or veins associated with alkalic rocks. Phosphate materials of bones and teeth are members of the apatite group.

Apatite occurs in large amounts along the southern coast of Norway, between Langesund and Arendal, where it is found in veins and pockets associated with gabbro. It is distributed through the magnetite iron ore at Kiruna, Sweden, and Tahawas, New York. In Ontario and Quebec, Canada, large apatite crystals were formerly mined. The world's largest deposit of apatite is located on the Kola Peninsula, near Kirovsk, Karelia, Russia. Here, apatite in granular aggregates intimately associated with nepheline and titanite, is found in a great lens between two types of alkalic rocks.

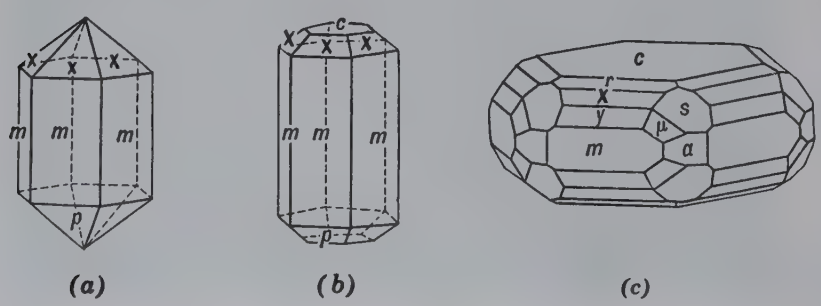

FIG. 17.52 Apatite crystals.

BOX 17.1 The Source of Chemicals in Fertilizers

Containers for chemical fertilizers prominently display three numbers that represent the weight percentages of three major components: nitrogen, phosphorus, and potassium–(**NPK**). Other components, such as S, Mg, and Fe, are generally present in smaller amounts and are listed in a table that is in smaller type.

The nitrogen component in fertilizers is obtained from ammonia, NH_3, and nitrate (NO_3^-) salts. Most of the ammonia is produced by the fractional distillation of liquid air. The four major producers of ammonia are Russia, China, the United States, and India.

The phosphorus component in fertilizers is derived from sedimentary phosphate rock (also known as phosphorite). About 90% of the world's production of phosphate is consumed in chemical fertilizers. The mineral that is mined is **apatite**, $Ca_5(PO_4)_3(F, Cl, OH)$. Apatite occurs in igneous as well as sedimentary rocks. Apatite of igneous origin is commonly close to $Ca_5(PO_4)_3(OH, F)$ in composition, whereas sedimentary apatite, also known as carbonate-apatite, is closer to $Ca_5(PO_4, CO_3, OH)_3(F,OH)$. The sedimentary deposits contain apatite in nodular or compact masses. The apatite is derived from a variety of sources, including marine invertebrates that secrete shells of calcium phosphate and the bones and excrement of vertebrates. Sedimentary deposition of phosphate continues today. Typical phosphorite beds contain about 30% P_2O_5. The United States is the world's largest exporter of phosphate rock, whereas Morocco may have the largest reserves of phosphate raw materials. Major U.S.-producing regions are along the eastern coastline (South Carolina, Georgia, and Florida) and in the Phosphoria Formation in Idaho.

Potash is the third component in most chemical fertilizers. This is mined from potash-bearing salt deposits that have resulted from the evaporation of seawater (see Box 16.2). The most important potassium minerals are **sylvite**, KCl, **carnallite**, and **langbeinite** (see Box 16.2 for compositions). A mixture of KCl and NaCl, known as *sylvinite*, is the highest-grade potash ore. The largest high-grade sylvinite ore reserves are found in Saskatchewan, Canada. Russia ranks second with about 32% of the world's potash reserves in several sedimentary basins.

FERTILIZER 16-8-8	%
Total nitrogen (N)	16.00
Available phosphoric acid (P_2O_5)	8.00
Soluble potash (K_2O)	8.00
Sulfur	14.00

Sulfur is a common additional component of chemical fertilizers. Only about 10% of sulfur production is shipped in international markets as elemental sulfur. Most is recovered or converted to sulfuric acid, H_2SO_4. Sulfuric acid is not only an important basic industrial chemical, but the largest use of sulfuric acid is in the chemical process of converting phosphate rock into components of chemical fertilizers. The four largest world producers of sulfur are the United States, Russia, Canada, and China. Most of the world's production is from *salt domes*. These are largely subsurface geologic structures that consist of a vertical cylinder of salt embedded in horizontal or inclined strata. Salt domes along the coast of the Gulf of Mexico contain abundant sulfur, as well as NaCl and potash. Sulfur is also recovered (ultimately as sulfuric acid) as a byproduct from natural gas and crude oil, and from sulfide ores in which a common constituent is pyrite, FeS_2.

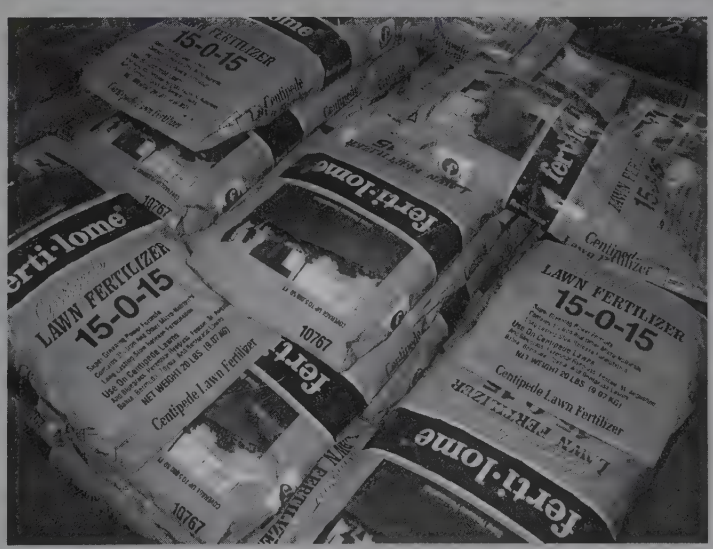

Finely crystallized apatite in pegmatites and veins occurs at various localities in the Tyrol, Austria; in Switzerland; in Panasquiera, Portugal; and Jumilla, Spain. In the United States at Auburn, Maine; St. Lawrence County, New York; Alexander County, North Carolina; and San Diego County, California.

The variety collophane is an important constituent of the rock *phosphorite* or *phosphate rock*. Bone is calcium phosphate, and large bodies of phosphorite are derived from the accumulation of animal remains as well as from chemical precipitation from seawater. Commercial deposits of phosphorite are found in northern France, Belgium, Spain, and especially in northern Africa in Tunisia, Algeria, and Morocco. In the United States, high-grade phosphate deposits are found in Tennessee and in Wyoming and Idaho. Deposits of "pebble" phosphate are found at intervals all along the Atlantic coast from North Carolina to Florida. The most productive deposits in the United States are in Florida.

Use. Crystallized apatite has been used extensively as a source of phosphate for fertilizer, but today only the deposits on the Kola Peninsula are of importance and phosphorite deposits supply most of the phosphate for fertilizer (see Box 17.1). The calcium phosphate is treated with sulfuric acid and changed to superphosphate to render it more soluble in the dilute acids that exist in the soil. Transparent varieties of apatite of fine color are occasionally used for gems (see Plate XII, no. 8 Chapter 20). The mineral is too soft, however, to allow its extensive use for this purpose.

Name. From the Greek word *apate* meaning *deceipt*, because the gem varieties were confused with other minerals.

Pyromorphite—$Pb_5(PO_4)_3Cl$

Crystallography. Hexagonal; $6/m$. Crystals are usually prismatic with basal plane (Fig. 17.53). Rarely shows pyramid truncations. Often in rounded barrel-shaped forms. Sometimes cavernous, the crystals being hollow prisms. Also in parallel groups. Frequently globular, reniform, fibrous, and granular.

$P6_3/m$; $a = 9.97$, $c = 7.32$ Å; $Z = 2$. *d*s: 4.31(6), 4.09(9), 2.95(10), 2.05(8), 1.94(7).

Physical Properties. **H** $3\frac{1}{2}$–4. **G** 7.04. *Luster* resinous to adamantine. *Color* usually various shades of green, brown, yellow; rarely orange-yellow, gray, white. *Streak* white. Subtransparent to translucent. *Tenacity* brittle. *Optics:* (−), $\omega = 2.058$, $\epsilon = 2.048$.

FIG. 17.53 Pyromorphite.

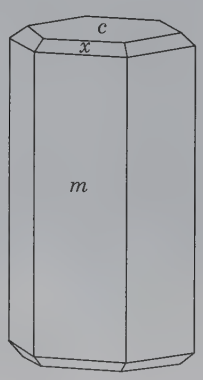

Composition and Structure. For pure $Pb_5(PO_4)_3Cl$, PbO 82.2, P_2O_5 15.7, Cl 2.6%. (AsO_4) substitutes for (PO_4) and a complete series extends to *mimetite*, $Pb_5(AsO_4)_3Cl$. Ca may substitute in part for Pb. Isostructural with apatite (see Fig. 17.12).

Diagnostic Features. Pyromorphite is characterized by its crystal form, high luster, and high specific gravity.

Occurrence. Pyromorphite is a supergene mineral found in the oxidized portions of lead veins, associated with other oxidized lead and zinc minerals.

Notable localities for its occurrence are the lead mines at Ems in Nassau and at Zschopau, Saxony, Germany; Příbram, Czech Republic; Beresovsk, Ural Mountains; in Cumbria, England and at Leadhills, Scotland. In the United States, it is found at Phoenixville, Pennsylvania, and the Cœur d'Alene district, Idaho.

Use. A subordinate ore of lead.

Name. Derived from two Greek words meaning *fire* and *form*, in allusion to the apparent crystalline form it assumes on cooling from fusion.

Similar Species. *Mimetite*, $Pb_5(AsO_4)_3Cl$, is isostructural with pyromorphite and is similar in appearance, occurrence, and most of its physical and chemical properties.

Vanadinite—$Pb_5(VO_4)_3Cl$

Crystallography. Hexagonal; $6/m$. Most commonly occurs in prismatic crystals with {10$\bar{1}$0} and {0001}. May have small pyramidal faces, rarely the hexagonal dipyramid. In rounded crystals; in some cases cavernous. Also in globular forms. As incrustations.

$P6_3/m$; $a = 10.33$, $c = 7.35$ Å; $Z = 2$. *d*s: 4.47(3), 4.22(4), 3.38(6), 3.07(9), 2.99(10).

Physical Properties. **H** 3. **G** 6.9. *Luster* resinous to adamantine. *Color* ruby-red, orange-red, brown, yellow. *Streak* brownish-yellow. Transparent to translucent. *Optics:* (−); $\omega = 2.25$–2.42, $\epsilon = 2.20$–2.35. Indices lowered by substitution of As or P for V.

Composition. PbO 78.7, V_2O_5 19.4, Cl 2.5%. PO_4 and AsO_4 substitute in small amounts for VO_4. In the variety *endlichite*, intermediate between vanadinite and mimetite, the proportion of V_2O_5 to As_2O_5 is nearly 1 : 1. Small amounts of Ca, Zn, and Cu substitute for Pb. Vanadinite is isostructural with apatite (see Fig. 17.12).

Diagnostic Features. Characterized by crystal form, high luster, and high specific gravity; distinguished from pyromorphite and mimetite by color.

Occurrence. Vanadinite is a rare secondary mineral found in the oxidized portion of lead veins associated with other secondary lead minerals. Found in fine crystals near Oudjda, Morocco, and Grootfontein, Namibia. In the United States, it occurs in various districts in Arizona and New Mexico.

Use. Source of vanadium and minor ore of lead. Vanadium is obtained chiefly from other ores, such as *patronite*, VS_4; the vanadate *carnotite*, $K_2(UO_2)_2(VO_4)_2 \cdot 3H_2O$; and a vanadium mica, *roscoelite*, $KV_2(AlSi_3O_{10})(OH)_2$. Vanadium is used chiefly as a steel-hardening metal. Metavanadic acid, HVO_3, is a yellow pigment, known as vanadium bronze. Vanadium oxide is a mordant in dyeing.

Name. In allusion to the composition.

Erythrite—$Co_3(AsO_4)_2 \cdot 8H_2O$

Crystallography. Monoclinic; *2/m*. Crystals are prismatic and vertically striated. Usually as crusts in globular, radial, and reniform shapes. Also powdery and earthy.

C2/m; $a = 10.20$, $b = 13.37$, $c = 4.74$ Å; $\beta = 105°$; $Z = 2$. *ds*: 6.65(10), 3.34(1), 3.22(1), 2.70(1), 2.32(1).

Physical Properties. *Cleavage* {010} perfect. **H** $1\frac{1}{2}$–$2\frac{1}{2}$. **G** 3.06. *Luster* adamantine to vitreous, pearly on cleavage. *Color* crimson to pink. Translucent. *Optics:* (−); $\alpha = 1.626$, $\beta = 1.661$, $\gamma = 1.699$; $2V = 90° \pm$; $X = b$, $Z \wedge c = 31°$; $r > v$. Pleochroism *X* pink, *Y* violet, *Z* red.

Composition and Structure. CoO 37.5, As_2O_5 38.4, H_2O 24.1%. Ni substitutes for Co to form a complete series to *annabergite*, $Ni_3(AsO_4)_2 \cdot 8H_2O$. *Annabergite*, or *nickel bloom*, is light green in color. The structure of erythrite is of a layer type with strong bonds between (AsO_4) tetrahedra and $Co(O,H_2O)$ octahedra that are linked by common vertices. The layers parallel to (010) are held together by weak residual bonds.

Diagnostic Features. The association of erythrite with other cobalt minerals and its pink color are usually sufficient to distinguish it from all other minerals.

Occurrence. Erythrite is a rare secondary mineral. In pink crusts known as *cobalt bloom* it occurs as an alteration product of cobalt arsenides. It is rarely present in large amounts and usually forms as crusts or fine aggregates filling cracks. Notable localities are at Schneeberg, Saxony, Germany, and Bon Azzer, Morocco.

Use. Although erythrite has no economic importance, it is used by the prospector as a guide to other cobalt minerals and associated native silver.

Name. From the Greek word *erythros*, meaning *red*.

Similar Species. *Vivianite*, $Fe_3(PO_4)_2 \cdot 8H_2O$, a secondary mineral formed from weathering of Fe–Mn ore deposits, also found in pegmatites containing phosphate minerals, in sediments, and in recent alluvial deposits. Found as incrustations on, or replacements of, fossils.

Amblygonite—$LiAlFPO_4$

Crystallography. Triclinic: $\bar{1}$. Usually occurs in coarse, cleavable masses. Crystals are rare, equant, and usually rough when large. Frequently twinned on {$\bar{1}\bar{1}\bar{1}$}.

$P\bar{1}$; $a = 5.19$, $b = 7.12$, $c = 5.04$ Å; $\alpha = 112°02'$, $\beta = 97°50'$, $\gamma = 68°8'$; $Z = 2$. *ds*: 4.64(10), 3.15(10), 2.93(10), 2.39(5), 2.11(4).

Physical Properties. *Cleavage* {100} perfect, {110} good, {$0\bar{1}1$} distinct. **H** 6. **G** 3.0–3.1. *Luster* vitreous, pearly on {100} cleavage. *Color* white to pale green or blue, rarely yellow (see Plate XII, no. 4, Chapter 20). Translucent. *Optics:* usually (−); $\alpha = 1.58$–1.60, $\beta = 1.50$–1.62, $\gamma = 1.60$–1.63; $2V = 50$–$90°$; $r > v$. Indices increase with increase in (OH) in substitution for F.

Composition and Structure. Li_2O 10.1, Al_2O_3 34.4, F 12.9, P_2O_5 47.9%. Na substitutes for Li; (OH) substitutes for F and probably forms a complete series. When OH > F, the mineral is known as *montebrasite*. In the structure of amblygonite, AlO_6 octahedra and PO_4 tetrahedra are linked by vertices; Li is in 5-coordination and lies between PO_4 tetrahedra and the nearest Al octahedra. The structure is fairly compact as reflected in the relatively high density.

Diagnostic Features. Cleavage fragments may be confused with feldspar, but are distinguished by cleavage angles.

Occurrence. Amblygonite is a rare mineral found in granite pegmatites with spodumene, tourmaline, lepidolite, and apatite. Found at Montebras, France. In the United States, it occurs at Hebron, Paris, Auburn, and Peru, Maine; Portland, Connecticut, and the Black Hills, South Dakota.

Use. A source of lithium.

Name. From the two Greek words *amblys*, meaning *blunt*, and *gonia*, meaning *angle*, in allusion to the angle between the cleavages.

Similar Species. *Beryllonite*, $NaBePO_4$, colorless and *brazilianite*, $NaAl_3(PO_4)_2(OH)_4$, colorless to yellow, are rare gem minerals found in pegmatites.

Lazulite—$(Mg,Fe)Al_2(PO_4)_2(OH)_2$; Scorzalite—$(Fe,Mg)Al_2(PO_4)_2(OH)_2$

Crystallography. Monoclinic; *2/m*. Crystals showing steep {*hkl*} prisms are rare. Usually massive, granular to compact.

$P2_1/c$; $a = 7.12$, $b = 7.26$, $c = 7.24$ Å; $\beta = 118°55'$; $Z = 2$. *ds*: 6.15(8), 3.23(8), 3.20(7), 3.14(10), 3.07(10).

Physical Properties. *Cleavage* {110} indistinct. **H** 5–$5\frac{1}{2}$. **G** 3.0–3.1. *Luster* vitreous. *Color* azure-blue. Translucent. *Optics:* (−); $\alpha = 1.604$–1.639, $\beta = 1.626$–1.670, $\gamma = 1.637$–1.680, $2V = 60°$; $Y = b$, $X \wedge c = 10°$; $r < v$. Absorption $X < Y < Z$. Indices increase with increasing Fe^{2+} content.

Composition and Structure. Probably a complete solid solution series exists from lazulite to scorzalite with the substitution of Fe^{2+} for Mg. In the structure $(Mg,Fe)(O,OH)_6$ octahedra are linked by edges and faces with $Al(O,OH)_6$ octahedra to form groups. These groups are joined to each other and to PO_4 tetrahedra.

Diagnostic Features. If crystals are lacking, lazulite is difficult to distinguish from other blue minerals without optical or chemical tests.

Occurrence. The members of the lazulite–scorzalite series are rare minerals found in high-grade metamorphic rocks and in pegmatites. They are usually associated with kyanite, andalusite, corundum, rutile, sillimanite, and garnet. Notable localities are Salzburg, Austria; Krieglach, Styria; and Horrsjoberg, Sweden. In the United States, they are found with corundum on Crowder's Mountain, Gaston County, North Carolina; with rutile on Graves Mountain, Lincoln County, Georgia; and with andalusite in the White Mountains, Inyo County, California.

Use. A minor gemstone.

Name. Lazulite derived from an Arabic word meaning *heaven*, in allusion to the color of the mineral. Scorzalite after E. P. Scorza, Brazilian mineralogist.

Wavellite—$Al_3(PO_4)_2(OH)_3 \cdot 5H_2O$

Crystallography. Orthorhombic; *2/m2/m2/m*. Single crystals rare. Usually in radiating, spherulitic (Fig. 17.54) and globular aggregates.

Pcmn; $a = 9.62$, $b = 17.34$, $c = 6.99$ Å; $Z = 4$. *ds*: 8.39(10), 5.64(6), 3.44(8), 3.20(8), 2.56(8).

FIG. 17.54 Wavellite. Hot Springs, Arkansas (Harvard Mineralogical Museum).

Physical Properties. *Cleavage* {110} and {101} good. **H** $3\frac{1}{2}$–4. **G** 2.36. *Luster* vitreous. *Color* white, yellow, green, and brown. Translucent. *Optics:* (+); $\alpha = 1.525$, $\beta = 1.535$, $\gamma = 1.550$; $2V = 70°$. $X = b$, $Y = a$; $r > v$.

Composition and Structure. Al_2O_3 38.0, P_2O_5 35.2, H_2O 26.8%. F may substitute for OH. Details of the structure are uncertain. $Al(O,OH)_6$ octahedra are linked by common vertices to PO_4 tetrahedra.

Diagnostic Features. Almost invariably found in radiating globular aggregates.

Occurrence. Wavellite is a secondary mineral found in small amounts in crevices in aluminous, low-grade metamorphic rocks, and in limonite and phosphorite deposits. Although it occurs in many localities, only rarely is it found in quantity. It is abundant in the tin veins of Llallagua, Bolivia. In the United States, wavellite occurs in a number of localities in Arkansas.

Name. After Dr. William Wavel, who discovered the mineral.

Turquoise—$CuAl_6(PO_4)_4(OH)_8 \cdot 4H_2O$

Crystallography. Triclinic; $\bar{1}$. Rarely in minute crystals, usually cryptocrystalline. Massive compact, reniform, stalactitic. In thin seams, incrustations, and disseminated grains.

$P\bar{1}$; $a = 7.48$, $b = 9.95$, $c = 7.69$; $\alpha = 111°39'$, $\beta = 115°23'$, $\gamma = 69°26'$; $Z = 1$. *ds*: 6.16(7), 4.80(6), 3.68(10), 3.44(7), 3.28(7).

Physical Properties. *Cleavage* {001} perfect, {010} good (rarely seen). **H** 6. **G** 2.6–2.8. *Luster* waxlike. *Color* blue, bluish-green, green (see Plates IV, no. 5 and XI, no. 7). Transmits light on thin edges. *Optics:* (+); $\alpha = 1.61$, $\beta = 1.62$, $\gamma = 1.65$; $2V = 40°$; $r < v$ strong.

Composition and Structure. Fe^{3+} substitutes for Al and a complete series exists between turquoise and *chalcosiderite*, $CuFe_6^{3+}(PO_4)_4(OH)_8 \cdot 4H_2O$. The structure consists of PO_4 tetrahedra and (Al,Fe^{3+}) octahedra linked by common vertices. Fairly large holes in the structure contain Cu which is coordinated to 4(OH) and 2 H_2O molecules.

Diagnostic Features. Turquoise can be recognized by its color. It is harder than chrysocolla, the only common mineral that it resembles. Much imitation material is marketed (see Chapter 20).

Occurrence. Turquoise is a secondary mineral usually found as small veins and stringers associated with silicic volcanic rocks in arid regions. The famous Persian deposits are found in trachyte near Nishapur in the province of Khorasan, Iran. In the United States, it is found in an altered trachytic rock in the Los Cerillos Mountains, near Santa Fe, and elsewhere in New Mexico. Turquoise is also found in Arizona, Nevada, and California. Small crystals have been found at Lunch Station, Virginia.

Use. As a gemstone. It is always cut in round or oval forms. Much cut turquoise is veined with the various gangue materials, and such stones are sold under the name of *turquoise matrix*.

Name. Turquoise is French and means *Turkish*, the original stones having come into Europe from the Persian locality through Turkey.

Similar Species. *Variscite*, $Al(PO_4) \cdot 2H_2O$, is a massive, greenish mineral somewhat resembling turquoise and used as a gem material. It has been found in nodules in a large deposit at Fairfield, Utah.

Autunite—$Ca(UO_2)_2(PO_4)_2 \cdot 10–12H_2O$

Crystallography. Tetragonal; $4/m2/m2/m$. Crystals are tabular on {001}; subparallel growths are common; also foliated and scaly aggregates.

$I4/mmm$; $a = 7.00$, $c = 20.67$ Å; $Z = 2$. *ds*: 10.33(10), 4.96(8), 3.59(7), 3.49(7), 3.33(7).

Physical Properties. *Cleavage* {001} perfect. **H** 2–$2\frac{1}{2}$. **G** 3.1–3.2. *Luster* vitreous, pearly on {001}. *Color* lemon yellow to pale green. *Streak* yellow. In ultraviolet light, fluoresces strongly yellow-green. *Optics:* (−); $\omega = 1.577$, $\epsilon = 1.553$. Pleochroism *E* pale yellow, *O* dark yellow.

Composition and Structure. Small amounts of Ba and Mg may substitute for Ca. The H_2O content apparently ranges from 10 to 12 H_2O. On drying and slight heating, autunite passes reversibly to *meta-autunite* I (a tetragonal phase with $6\frac{1}{2}$–$2\frac{1}{2}$ H_2O). On continued heating to about 80°C, this passes irreversibly to *meta-autunite* II (an orthorhombic phase with 0–6 H_2O). Neither meta-I nor the meta-II hydrate occurs as a primary phase in nature. The structure of autunite consists of (PO_4) tetrahedra and $(UO_2)O_4$ polyhedra, which are joined into tetragonal corrugated layers of composition $UO_2(PO_4)$ parallel to {001}. These layers are held together by weak hydrogen bonds to H_2O molecules.

Diagnostic Features. Autunite is characterized by yellow-green tetragonal plates and strong fluorescence in ultraviolet light. Radioactive.

Occurrence. Autunite is a secondary mineral found chiefly in the zone of oxidation and weathering derived from

the alteration of uraninite or other uranium minerals. Notable localities are near Autun, France; Sabugal and Vizeu, Portugal; Johanngeorgenstadt district and Falkenstein, Germany; Cornwall, England; and the Katanga district of Congo. In the United States, autunite is found in many pegmatites, notably at the Ruggles Mine, Grafton Center, New Hampshire; Black Hills, South Dakota; and Spruce Pine, Mitchell County, North Carolina. The finest specimens have come from the Daybreak Mine near Spokane, Washington.

Use. An ore of uranium (see uraninite, page 383).

Name. From Autun, France.

Similar Species. *Torbernite*, $Cu(UO_2)_2(PO_4)_2 \cdot 8–12H_2O$, is isostructural with autunite and has similar properties, but there is no evidence of a solid solution series. Color green, nonfluorescent. Associated with autunite.

Carnotite—$K_2(UO_2)_2(VO_4)_2 \cdot 3H_2O$

Crystallography. Monoclinic; $2/m$. Only rarely in imperfect microscopic crystals flattened on {001} or elongated on b. Usually found as a powder or as loosely coherent aggregates; disseminated.

$P2_1a$; $a = 10.47$, $b = 8.41$, $c = 6.91$ Å; $\beta = 103°40'$; $Z = 2$. *ds*: 6.56(10), 4.25(3), 3.53(5), 3.25(3), 3.12(7).

Physical Properties. *Cleavage* {001} perfect. *Hardness* unknown, but soft. **G** 4.7–5. *Luster* dull or earthy. *Color* bright yellow to greenish-yellow. *Optics:* (−); $\alpha = 1.75$, $\beta = 1.93$, $\gamma = 1.95$; $2V = 40°\pm$, $Y = b$, $X = c$. $r < v$. Indices increase with loss of water.

Composition and Structure. The water content varies with the humidity at ordinary temperatures; the $3H_2O$ is for fully hydrated material. Small amounts of Ca, Ba, Mg, Fe, and Na have been reported. The structure of carnotite consists of a layer pattern that is the result of strong bonds between the (VO_4) groups and the $UO_2(O_5)$ polyhedra. These layers, of composition $(UO_2)_2(VO_4)_2$, are held together by hydroxyl–hydrogen bonds to water molecules and also by K, Ca, and Ba between the layers.

Diagnostic Features. Carnotite is characterized by its yellow color, powdery nature, radioactivity, and occurrence. Unlike many secondary uranium minerals, carnotite will not fluoresce in ultraviolet light.

Occurrence. Carnotite is of secondary origin, and its formation is usually ascribed to the action of surface waters on preexisting uranium and vanadium minerals. It has a strong pigmenting power and when present in a sandstone in amounts even less than 1% will color the rock yellow. It is found principally in the plateau region of southwestern Colorado and in adjoining districts of Utah, where it occurs disseminated in a cross-bedded sandstone. Concentrations of relatively pure carnotite are found around petrified tree trunks.

Use. Carnotite is an ore of vanadium and, in the United States, a principal ore of uranium.

Name. After Marie-Adolphe Carnot (1839–1920), French mining engineer and chemist.

Similar Species. *Tyuyamunite*, $Ca(UO_2)_2(VO_4)_2 \cdot 5–8\frac{1}{2}H_2O$, is the calcium analogue of carnotite and similar in physical properties except for a slightly more greenish color and yellow-green fluorescence. It is found in almost all carnotite deposits. Named for Tyuya Muyum, southeastern Turkistan, where it is mined as a uranium ore.

REFERENCES AND FURTHER READING

Anthony, J. W., R. A. Bideaux, K. W. Bladh, and M. C. Nichols. *Handbook of Mineralogy*, Vol. IV, *Arsenates, Phosphates, Vanadates*. Mineral Data Publications, Tucson, Arizona.

Aristarain, L. F., and C. S. Hurlbut Jr. 1972. Boron minerals and deposits. *Mineralogical Record* 3:165–72, 213–20.

Boron mineralogy, petrology and geochemistry, 1996. *Reviews in Mineralogy*, 33. Mineralogical Society of America, Washington, D.C.

Carbonates. 1983. *Reviews in Mineralogy* 11. Mineralogical Society of America, Washington, D.C.

Carr, D. C., ed. 1994. *Industrial minerals and rocks*. Society for Mining, Metallurgy, and Exploration, Littleton, Colorado.

Chang, L. L. Y., R. A. Howie, and J. Zussman. 1996. *Rock-forming minerals* 5B. Nonsilicates. Longman Group Limited.

Gaines, R. B., H. C. W. Skinner, E. E. Foord, B. Mason, and A. Rosenzweig. 1997. *Dana's new mineralogy*. Wiley, New York.

Morgan, V., and R. C. Erd. 1969. Minerals of the Kramer borate district, California. *Mineral Information Service* (California Division of Mines and Geology) 22: 143–53, 165–72.

Palache, C., H. Berman, and C. Frondel. 1951. *The system of mineralogy*. 7th ed. Vol. 2. Wiley, New York.

Phosphates—geochemical, geobiological, and materials importance. 2002. *Reviews in Mineralogy and Geochemistry* 48. Mineralogical Society of America, Washington D.C.

Phosphate, potash, and sulfur—A special issue. 1979. *Economic Geology* 74: 191–496.

Strunz, H. and E. H. Nickel, 2001, *Strunz Mineralogical Tables*, 9th ed. Schweizerbart'sche Verlagsbuchhandlung, Stuttgart.

U.S. Geological Survey, *Mineral Commodity Summaries*, 2005. Available at http://minerals.usgs.gov/minerals/pubs/mcs.

CHAPTER 18

Crystal Chemistry of Rock-Forming Silicates

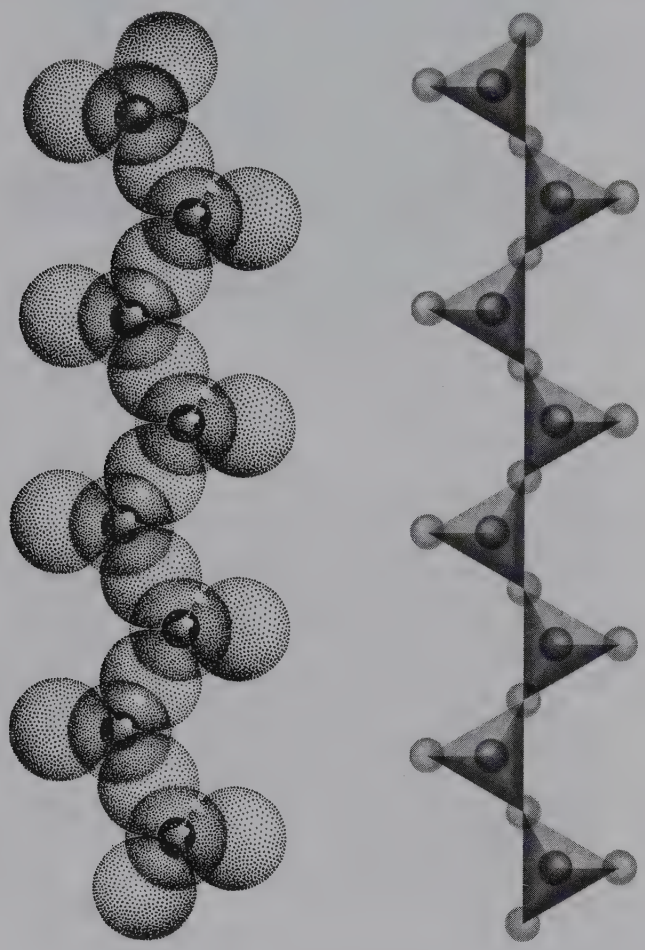

(a) (b)

Chains of SiO_4 tetrahedra as occur in the structure of pyroxenes. (a) The representation of such a chain in terms of large, close-packed spheres of oxygen and smaller silicon spheres. This illustration was created by a graphic artist for the seventeenth edition of the Manual of Mineralogy, *by C. S. Hurlbut, Jr., published by John Wiley and Sons in 1959. (b) The same chain but now in tetrahedral units, with only the oxygens shown. This is a modern-day computer-generated rendition of the image in (a).*

The silicate mineral class is of great importance because about 27% of the known minerals and nearly 40% of the common minerals are silicates. With few exceptions all the igneous rock-forming minerals are silicates, and they constitute well over 90% of the Earth's crust (see Fig. 18.1). In addition, most metamorphic rocks are composed primarily of silicate minerals. Rock-forming minerals are those minerals that make up the major components of a rock, and they are used in the classification of rock types (discussed more fully in Chapter 21). The more important rock-forming silicate minerals include olivine, garnet, pyroxenes, amphiboles, micas, clay minerals, feldspars, and quartz. Other rock-forming minerals are calcite and dolomite dominant in sedimentary rocks.

When the average weight percentages of the eight most common elements in the Earth's crust are recalculated on the basis of atomic percent (see Fig. 5.2), out of every 100 atoms, 62.5 are O, 21.2 are Si, and 6.5 are Al. Fe, Mg, Ca, Na, and K each account for about 2 to 3 more atoms. With the possible exception of Ti, all other elements are present in insignificant amounts in the Earth's crust (see Fig. 5.2). When the atomic percentages of the 8 most abundant elements are recalculated in terms of volume percentages (see Fig. 5.2, last column) the Earth's crust can be regarded as a packing of oxygen ions, with interstitial

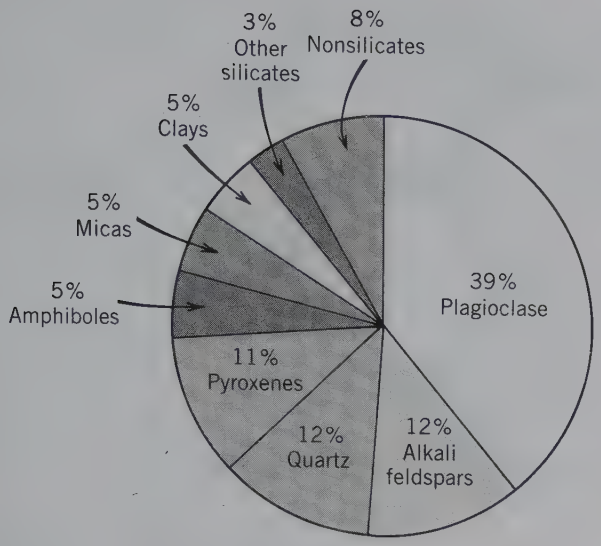

FIG. 18.1 Estimated volume percentages for the common minerals in the Earth's crust, inclusive of continental and oceanic crust. Ninety-two percent are silicates. (From Ronov, A. B. and A. A. Yaroshevsky. 1969. Chemical composition of the Earth's crust. American Geophysical Union Monograph no. 13, 50.)

metal ions, such as Si^{4+}, Al^{3+}, Fe^{2+}, Ca^{2+}, Na^{+}, K^{+}, and so forth.

The dominant minerals of the crust are silicates, with oxides and other oxygen compounds, such as carbonates, in subordinate amounts. Of the different assemblages of silicate minerals that characterize igneous, sedimentary, and metamorphic rocks, ore veins, pegmatites, weathered rocks, and soils, each has the potential to yield information about the environment in which the rock was formed.

A further compelling reason to study the silicates is that the soil from which our food is ultimately extracted is made up, in large part, of silicates. The brick, stone, concrete, and glass used in the construction of our buildings either are silicates or are largely derived from silicates. With the exploration of the solar system, our studies of the silicates increase in importance because the moon and the four terrestrial planets of our solar system have rocky crusts made of silicates and oxides much like those of Earth.

The fundamental structural unit of all silicates consists of four O^{2-} at the apices of a regular tetrahedron surrounding and coordinated by one Si^{4+} at the center (Figs. 17.1d and 18.2). The powerful bond that unites the oxygen and silicon ions is the cement that holds the Earth's crust together. This bond may be estimated by use of Pauling's electronegativity concept (see Fig. 3.21) as 50% ionic and 50% covalent. Although the bond arises in part from the attraction of oppositely charged ions, it also involves sharing of electrons and interpenetration of the electronic clouds of

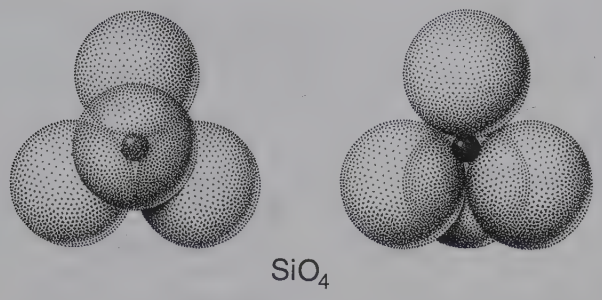

FIG. 18.2 Close packing representation of an SiO_4 tetrahedron.

the ions involved. The bond is strongly localized in the vicinity of these shared electrons.

Although electron sharing is present in the Si–O bond, the total bonding energy of Si^{4+} is distributed equally among its four closest oxygen neighbors. Hence, the strength of any single Si–O bond is equal to one-half the total bonding energy available in the oxygen ion. Each O^{2-} has, therefore, the potential of bonding to another silicon ion and entering into another tetrahedral group, thus, uniting the tetrahedral groups through the shared (or **bridging**) oxygen. Such linking of tetrahedra is often referred to as **polymerization**, and the capacity for polymerization is the origin of the great variety of silicate structures. In no case, however, are three or even two oxygens shared between two adjacent tetrahedra in nature. Such sharing would place two highly charged Si^{4+} ions close together, and the repulsion between them would destabilize the structure.

The sharing of oxygens may involve one, two, three, or all four of the oxygen ions in the tetrahedron, giving rise to a diversity of structural configurations. Figure 18.3 illustrates the various ways in which SiO_4 tetrahedra can be combined. Silicates with independent tetrahedral SiO_4 groups (in which the tetrahedra are not linked to each other) are known as *nesosilicates* (from the Greek word *nesos*, meaning *island*) or *orthosilicates* (from the Greek word *orthos*, meaning *normal*). Silicates in which two SiO_4 groups are linked, giving rise to Si_2O_7 groups are classed as *sorosilicates* (from the Greek word *soros*, meaning *heap*) or *disilicates* (in reference to the double tetrahedral groupings). If more than two tetrahedra are linked, closed ring-like structures are formed of a general composition Si_xO_{3x}. Four-fold tetrahedral rings have composition Si_4O_{12}. This group is known as the *ring silicates*, or the *cyclosilicates* (from the Greek word *kyklos*, meaning *circle*). Tetrahedra may also be joined to form infinite single chains with a unit composition Si_2O_6 (or SiO_3). Infinite double chains give a

Class	Arrangement of SiO_4 tetrahedra (central Si^{4+} not shown)	Unit composition	Mineral example
Nesosilicates	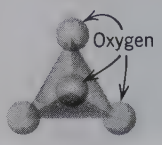	$(SiO_4)^{4-}$	Olivine, $(Mg, Fe)_2SiO_4$
Sorosilicates		$(Si_2O_7)^{6-}$	Hemimorphite, $Zn_4Si_2O_7(OH)\cdot H_2O$
Cyclosilicates	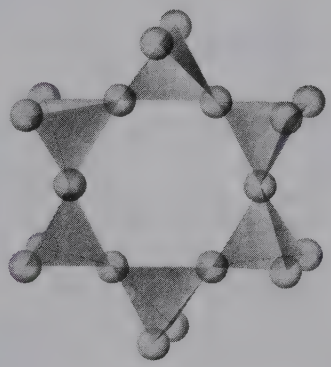	$(Si_6O_{18})^{12-}$	Beryl, $Be_3Al_2Si_6O_{18}$
Inosilicates (single chain)	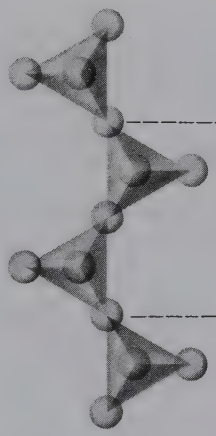	$(Si_2O_6)^{4-}$	Pyroxene e.g., Enstatite, $MgSiO_3$

FIG. 18.3 Silicate classification.

ratio of Si:O = 4:11, resulting in Si_4O_{11} (or Si_8O_{22}). Both of these types of *chain silicates* are also known as *inosilicates* (from the Greek word *inos*, meaning *thread*). When three of the oxygens of a tetrahedron are shared between adjoining tetrahedra, infinitely extending flat sheets are formed of unit composition Si_2O_5. Such *sheet silicates* are also referred to as *phyllosilicates* (from the Greek word *phyllon*, meaning *leaf*). When all four oxygens of a SiO_4 tetrahedron are shared by adjoining tetrahedra, a three-dimensional network of unit composition SiO_2 results. These *framework silicates* are also known as *tectosilicates* (from the Greek word *tecton*, meaning *builder*).

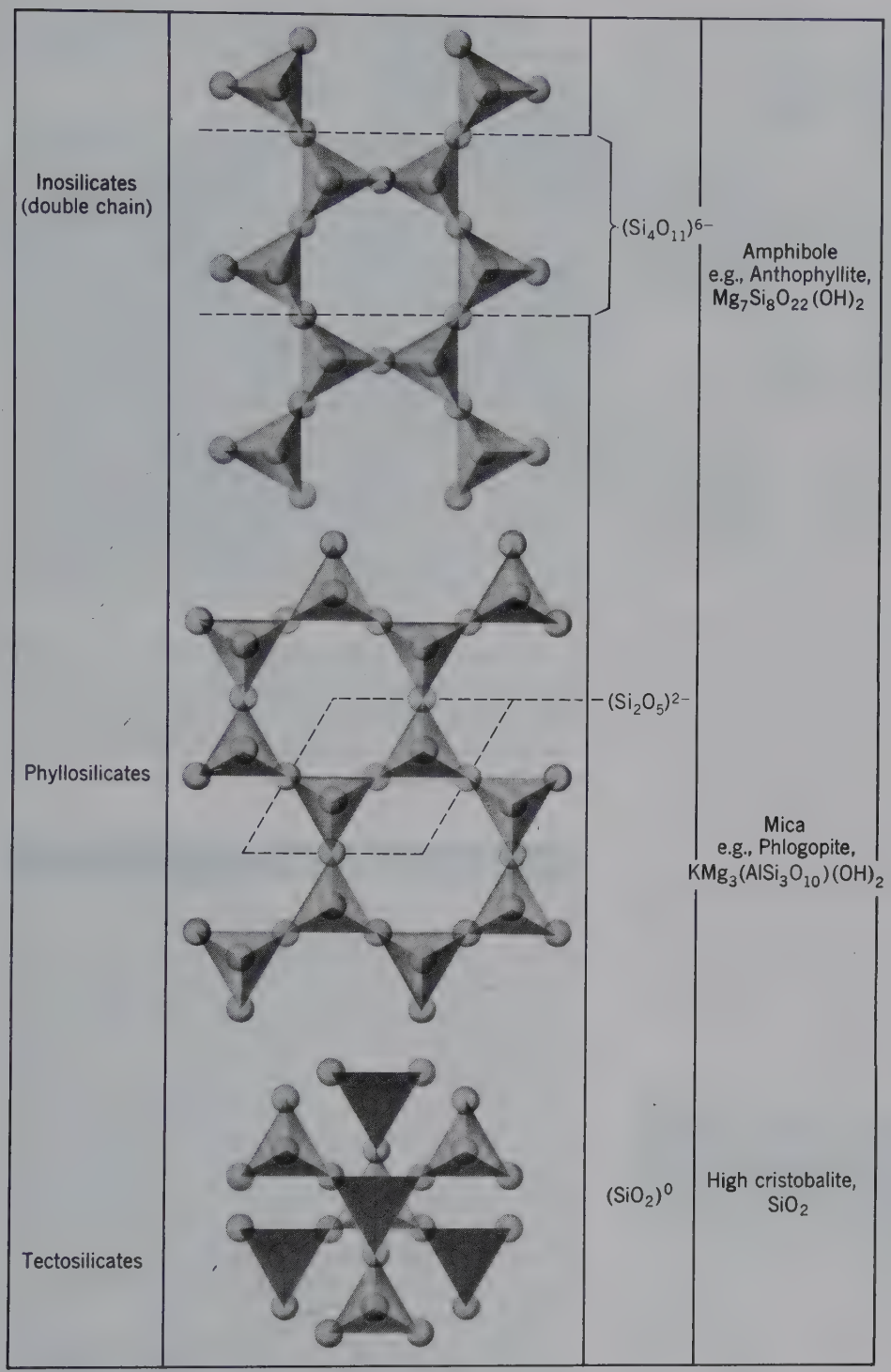

FIG. 18.3 *(continued)*

In the subsequent treatment of silicates, the previously mentioned structural classification (as illustrated in Fig. 18.3) of silicates is used. There are, however, alternate classifications, such as those proposed by Liebau (1985) and Zoltai (1960).

Next to O and Si, the most important constituent of the crust is Al. Al^{3+} has a radius of 0.39 Å and the radius ratio Al:O = 0.286, corresponding to 4-coordination with oxygen. This radius ratio is sufficiently close to the upper limit for 4-coordination so that 6-coordination is also possible. It is this capacity for playing a double role in silicate minerals that gives Al^{3+} its significance in the crystal chemistry of the silicates. When Al coordinates four Os

arranged at the apices of a regular tetrahedron, the resultant grouping occupies approximately the same space as a silicon–oxygen tetrahedron and may link with silicon tetrahedra in polymerized groupings. On the other hand, Al^{3+} in 6-coordination serves to link the tetrahedral groupings through simple ionic bonds, weaker than those that unite the ions in the tetrahedra. It is, thus, possible to have Al in silicate structures both in the tetrahedral sites, substituting for Si, and in the octahedral sites with 6-coordination, involved in solid solution with elements, such as Mg^{2+} and Fe^{2+}.

Mg^{2+}, Fe^{2+}, Fe^{3+}, Mn^{2+}, Al^{3+}, and Ti^{4+} all tend to occur in silicate structures in 6-coordination with oxygen (see Table 18.1). Although divalent, trivalent, and tetravalant ions are included here, all have about the same space requirements and about the same radius ratio relations with oxygen, and tend to occupy the same type of atomic site. Solid solution relations between ions of different charge are possible through the mechanism of coupled substitution (see page 98).

The larger and more weakly charged cations, Ca^{2+} and Na^{+}, of ionic radii 1.12 Å and 1.16 Å, respectively, generally enter sites having 8-coordination with respect to oxygen. Although the sizes of these two ions are very similar, their charges are different. This charge difference is compensated for by a coupled substitution. For example, in the plagioclase feldspars, $(Na^{+}+Si^{4+})$ substitutes for $(Ca^{2+}+Al^{3+})$ to maintain electrical neutrality.

The largest ions common in silicate structure are those of K^{+}, Rb^{+}, Ba^{2+}, and the rarer alkalis and alkali earths. These ions generally do not substitute for Na^{+} or Ca^{2+} and are found in high-coordination-number sites of unique type. Hence, solid solution between these ions and the other common ions is limited.

Table 18.1 Coordination of Common Elements in Silicates, Arranged in Decreasing Ionic Size*

	Ion	Coordination Number with Oxygen		Ionic Radius Å
X	K^{+}	8–12		1.51[8]–1.64[12]
X	Na^{+}	8–6	cubic to octahedral	1.18[8]–1.02[6]
	Ca^{2+}	8–6		1.12[8]–1.00[6]
Y	Mn^{2+}	6	octahedral	0.83[6]
	Fe^{2+}	6		0.78[6]
	Mg^{2+}	6		0.72[6]
	Fe^{3+}	6		0.65[6]
	Ti^{4+}	6		0.61[6]
	Al^{3+}	6		0.54[6]
Z	Al^{3+}	4	tetrahedral	0.39[4]
	Si^{4+}	4		0.26[4]

*See Table 3.8 for a listing of ionic radii.

Ionic substitution is generally common and extensive between elements that are grouped together in Table 18.1.

A general formula for all silicates is:

$$X_mY_n(Z_pO_q)W_r,$$

where *X* represents large, weakly charged cations in 8- or higher coordination with oxygen; *Y* represents medium-sized, two to four valent ions in 6-coordination; *Z* represents small, highly charged ions in tetrahedral coordination; *O* is oxygen; and *W* represents additional anionic groups, such as $(OH)^{-}$ or anions such as Cl^{-} or F^{-}. The ratio $p:q$ depends on the degree of polymerization of the silicate framework, and the other subscript variables, *m*, *n*, and *r*, depend on electrical neutrality. Any common silicate may be expressed by substitution in this general formula.

The subsequent discussion of individual silicates is based on subclasses that reflect their internal structure (neso-, soro-, cyclosilicates, etc.) and their chemical composition. Such a scheme is the basis of *Strunz Mineralogical Tables* (2001).

NESOSILICATES

In nesosilicates the SiO_4 tetrahedra are isolated (Fig. 18.3). These are bound to each other by ionic bonds from interstitial cations. Their structures depend primarily on the size and charge of the interstitial cations. The atomic packing of the nesosilicate structure is generally dense, causing the minerals of this group to have relatively high specific gravity and hardness. Because the SiO_4 tetrahedra are independent, bond strengths are about equal in all directions. Therefore, the crystal habit of the nesosilicates is generally equidimensional and pronounced cleavage directions are absent. Although Al^{3+} substitutes commonly for Si in silicates, the amount of Al substitution in SiO_4 tetrahedra in nesosilicates is generally low.

Common members, in high-temperature igneous rocks, of the nesosilicate group are *forsterite*, Mg_2SiO_4, and *fayalite*, Fe_2SiO_4, end-members of the $(Mg,Fe)_2SiO_4$ olivine series. The structure of olivine, which is shown in Fig. 18.4, consists of layers parallel to {100}. These layers consist of octahedra cross-linked by independent SiO_4 tetrahedra. The octahedrally coordinated sites are known as *M1* and *M2* with *M1* distorted and *M2* somewhat larger and more regular. In the $(Mg,Fe)_2SiO_4$ olivines, Mg and Fe^{2+} occupy the *M1* and *M2* sites

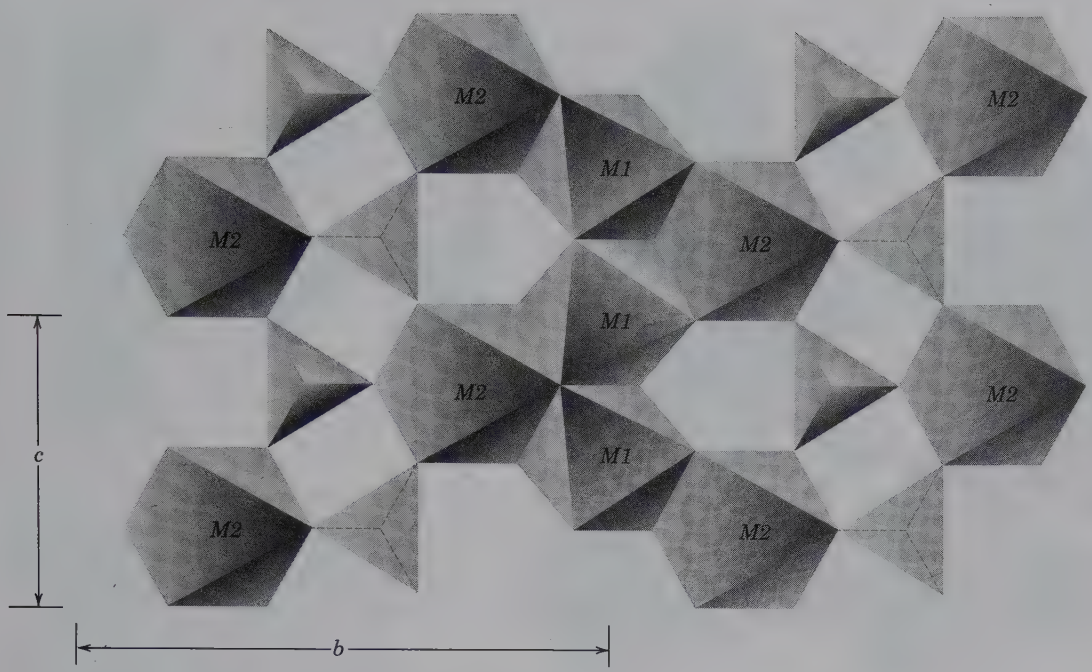

FIG. 18.4 Portion of the structure of olivine projected on (100). *M1* and *M2* are octahedral sites. The *M1* site is most distorted and the *M2* site is somewhat more regular. Extensive edge sharing among the polyhedra causes these distortions because shared edges are shortened as cations repel each other; see also page 76. (Redrawn after Papike, J. J., and M. Cameron. 1976. Crystal chemistry of silicate minerals of geophysical interest. *Reviews of Geophysics and Space Physics* 14: 37–80).

without any specific preference for either site. In the calcic olivines, however (e.g., *monticellite*, $CaMgSiO_4$), Ca enters into the *M2* site and Mg into *M1*.

Garnets are another group of common nesosilicate minerals, especially in metamorphic rocks. Their structural formula is represented as $A_3B_2(SiO_4)_3$, where *A* and *B* refer respectively to 8- and 6-coordinated cationic sites. The *A* sites are occupied by large divalent cations, whereas the *B* sites house smaller trivalent cations. Because of these size considerations, there is a well-defined division of the garnets into those with Ca and those with interchangeable divalent ions, such as Mg^{2+}, Fe^{2+}, Mn^{2+} in the *A* site. Similarly, because of the limited substitution possible in the *B* sites, there is a separation of garnets into Al^{3+}, Fe^{3+}, and Cr^{3+} bearing. These two trends give rise to two series of garnets: *pyralspite* (Ca absent in *A*; *B* = Al) and *ugrandite* (*A* = Ca).

Pyralspite		Ugrandite	
*Pyr*ope	$Mg_3Al_2Si_3O_{12}$	*U*varovite	$Ca_3Cr_2Si_3O_{12}$
*Al*mandine	$Fe_3Al_2Si_3O_{12}$	*Gr*ossular	$Ca_3Al_2Si_3O_{12}$
*Sp*essartine	$Mn_3Al_2Si_3O_{12}$	*And*radite	$Ca_3Fe_2^{3+}Si_3O_{12}$

This classification is an excellent mnemonic aid for the names and formulas. Another grouping on the basis of the ions in the *B* site yields three unequal groups:

Aluminum Garnets	Ferri-Garnet	Chrome-Garnet
Pyrope	Andradite	Uvarovite
Almandine		
Spessartine		
Grossular		

Hydroxyl, as tetrahedral $(OH)_4$ groups, may substitute to a limited extent for SiO_4 tetrahedra in hydrogarnets, such as *hydrogrossular*, $Ca_3Al_2Si_2O_8(SiO_4)_{1-m}(OH)_{4m}$, with *m* ranging from 0 to 1. Ti^{4+} may enter into the *B* sites concomitant with replacement of Ca by Na in the *A* sites, producing the black *melanite*.

The structure of garnet, illustrated in Fig. 18.5, consists of alternating SiO_4 tetrahedra and BO_6 octahedra that share corners to form a continuous three-dimensional network. The *A* sites are surrounded by eight oxygens in irregular coordination polyhedra.

The aluminosilicates of the nesosilicate group, *kyanite*, *sillimanite*, and *andalusite*, are commonly found in medium- to high-grade metamorphic rocks of Al-rich bulk composition. These three minerals are polymorphs of Al_2SiO_5, which may be stated structurally as $Al^{[4-6]}Al^{[6]}SiO_5$ (digits in square brackets indicate coordination number). Chains of edge-sharing octahedra, parallel to the *c* axis, are characertistic of all three structures.

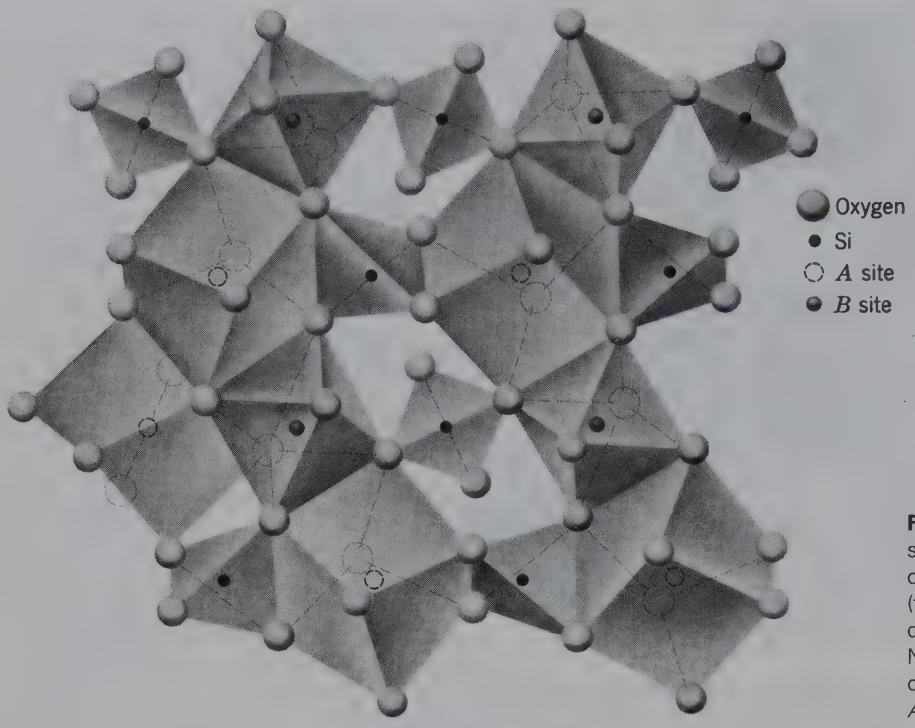

FIG. 18.5 Portion of the garnet structure projected on (001). Tetrahedra, octahedra and 8 coordination polyhedra (triangular dodecahedra, drawn as distorted cubes) are shown. (After Novak, G. A., and G. V. Gibbs. 1971. The crystal chemistry of the silicate garnets, *American Mineralogist* 56: 791–825.)

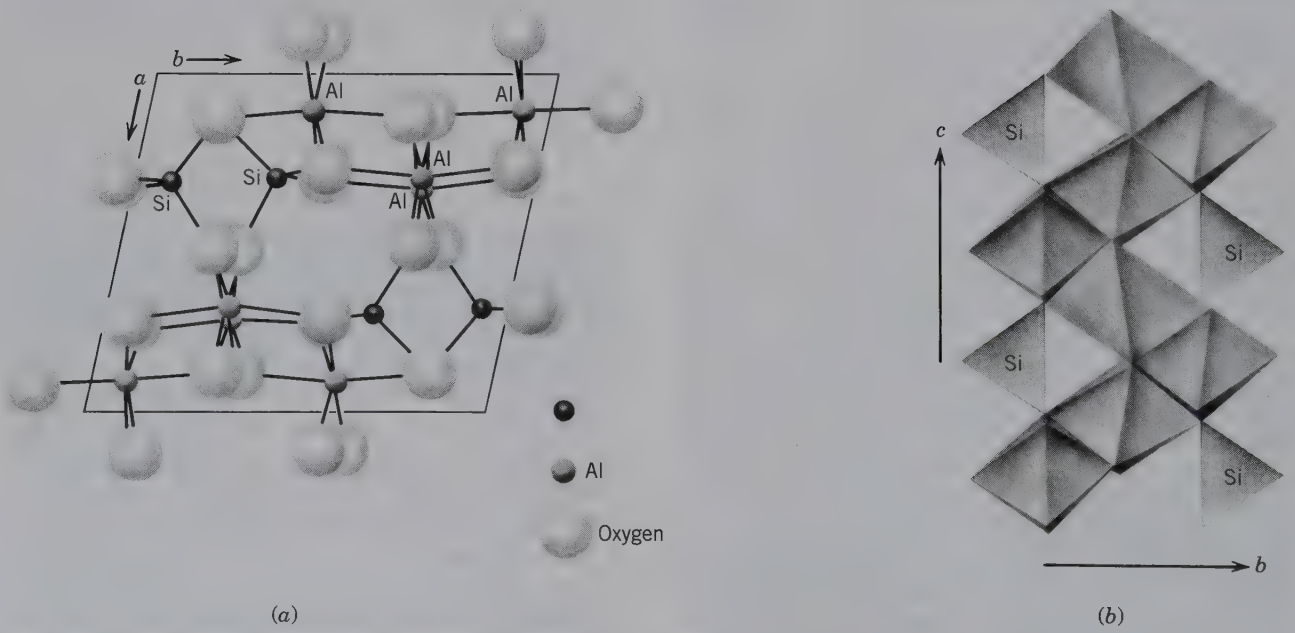

(a) (b)

FIG. 18.6 The structure of kyanite. (a) Projected on (001) and (b) showing zigzag chains of edge-sharing Al octahedra parallel to the *c* axis. (Redrawn after Burnham, C. W., 1963. Refinement of the crystal structure of kyanite. *Zeitschrift für Kristallographie* 118: 337–360; and Winter, J. K. and S. Ghose. 1979. Thermal expansion and high-temperature crystal chemistry of the Al_2SiO_5 polymorphs. *American Mineralogist* 64: 573–86; see also *Orthosilicates, Reviews in Mineralogy* 1980, Mineralogical Society of America, Washington, D.C.)

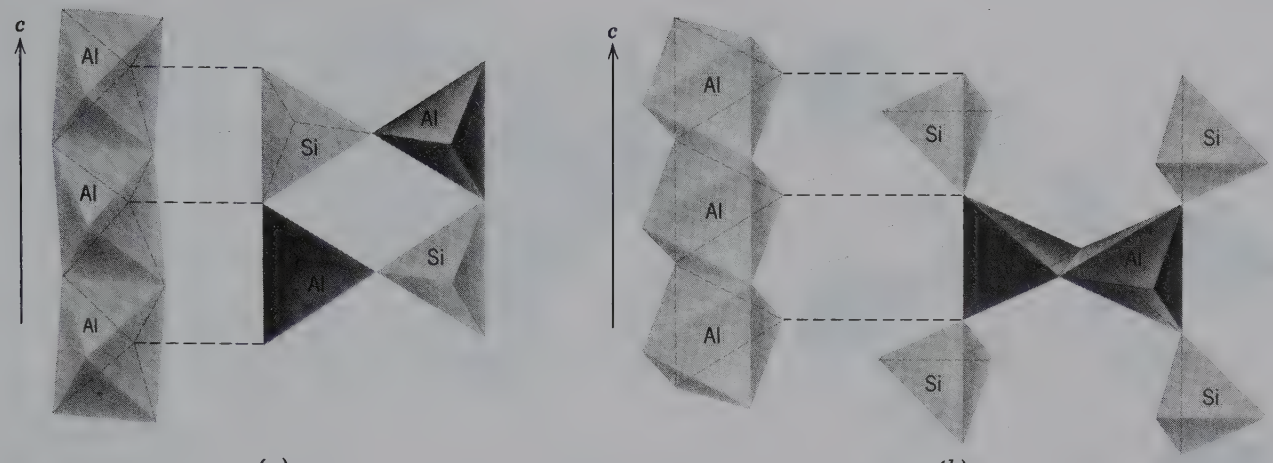

FIG. 18.7 (a) Projection of the sillimanite structure showing octahedral Al-chains parallel to the *c* axis. (Redrawn after Burnham, C. W. 1963. Refinement of the crystal structure of sillimanite. *Zeitschrift für Kristallographie:* 127–148.) (b) Projection of the andalusite structure showing octahedral chains parallel to the *c* axis, and the presence of AlO_5 polyhedra between SiO_4 tetrahedra. (Redrawn after Burnham, C. W. and M. J. Buerger. 1961. Refinement of the crystal structure of andalusite, *Zeitschrift für Kristallographie*: 269–290.)

In *kyanite*, $Al^{[6]}Al^{[6]}SiO_5$, the triclinic polymorph with space group $P\bar{1}$, all of the Al is octahedrally coordinated. It occurs as octahedral chains parallel to *c*, and as isolated Al octahedra (see Fig. 18.6). In *sillimanite*, $Al^{[5]}Al^{[6]}SiO_5$, an orthorhombic polymorph, with space group *Pbnm*, the octahedrally coordinated Al is found in octahedral chains (see Fig. 18.7a) and adjacent tetrahedral chains consist of alternating tetrahedral AlO_4 and SiO_4 groups. In *andalusite*, another orthorhombic polymorph with space group *Pbnm*, half the Al is found in octahedral chains and the other half occurs in 5-coordinated polyhedra (see Fig. 18.7b), which are linked by SiO_4 tetrahedra. The stability fields for these three polymorphs are shown in Fig. 19.13.

SOROSILICATES

The sorosilicates are characterized by isolated, double tetrahedral groups formed by two SiO_4 tetrahedra sharing a single apical oxygen (Fig. 18.8). The resulting ratio of silicon to oxygen is 2 : 7. More than 70 minerals are known in this group, but most of them are rare. The table below lists six species, of which members of the *epidote group* and *vesuvianite* are most important.

Hemimorphite	$Zn_4(Si_2O_7)(OH)_2{\cdot}H_2O$
Lawsonite	$CaAl_2(Si_2O_7)(OH)_2{\cdot}H_2O$
Epidote group	
Clinozoisite	$Ca_2Al_3O(SiO_4)(Si_2O_7)(OH)$
Epidote	$Ca_2(Fe^{3+},Al)Al_2O(SiO_4)(Si_2O_7)(OH)$
Allanite	$X_2Y_3O(SiO_4)(Si_2O_7)(OH)$
Vesuvianite	$Ca_{19}(Al,Fe,Mg)_{13}(Si_2O_7)_4(SiO_4)_{10}(O,OH,F)_{10}$

The structure of epidote (Fig. 18.9) contains both independent SiO_4 tetrahedra as well as Si_2O_7 groups. Chains of AlO_6 and $AlO_4(OH)_2$ octahedra, which share edges, run parallel to the *b* axis. (Similar octahedral chains are also present in the three polymorphs of Al_2SiO_5.) An additional octahedral position occurs outside the chains; this site is occupied by Al in clinozoisite and by Fe^{3+} and Al in epidote. The chains are linked by independent SiO_4 and Si_2O_7 groups. Ca is in irregular 8-coordination with oxygen. The site in which Ca^{2+} is housed may in part be filled by Na^+. The octahedral site outside the chains contains, in addition to Al, Fe^{3+}, Mn^{3+} and more rarely Mn^{2+}.

All members of the epidote group are isostructural and form monoclinic crystals characteristically elongate on *b*. Orthorhombic *zoisite* has a structure that may be derived from that of its monoclinic polymorph, *clinozoisite*, by a twinlike doubling of the cell along the

FIG. 18.8 Close-packed representation of an Si_2O_7 group.

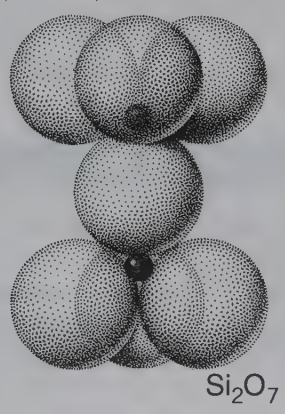

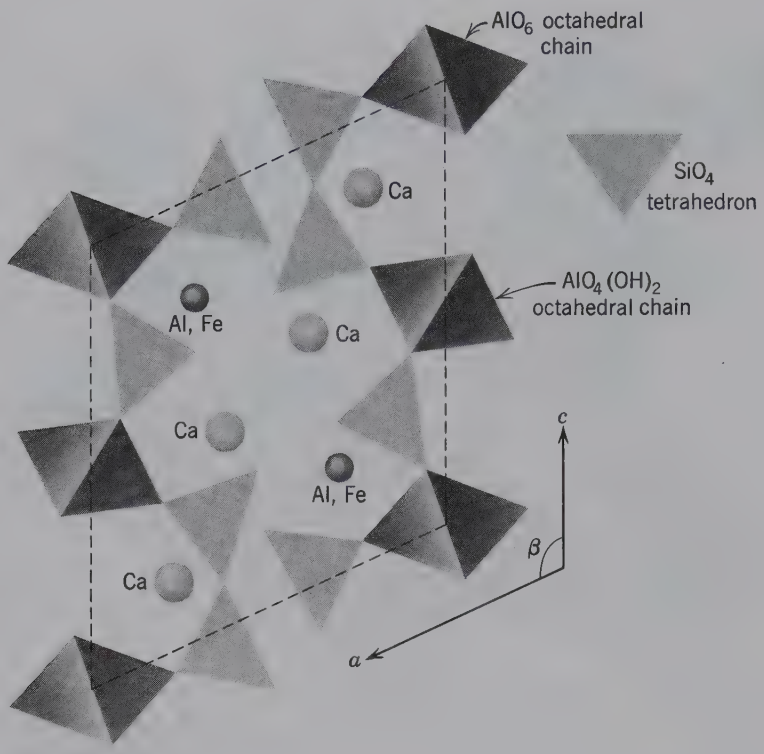

FIG. 18.9 Schematic representation of the structure of epidote, projected on (010). Dashed lines outline unit cell.

a axis, such that *a* of zoisite = 2 *a* sin β of clinozoisite (or epidote) (see Fig. 18.10). The structure of clinozoisite is the same as that of epidote, with all octahedral positions occupied by Al. *Allanite* is derived from the epidote structure by replacing some of the Ca^{2+} by rare earth elements and adjusting the electrostatic charge balance by replacing some of the Fe^{3+} by Fe^{2+}. As a result of the similar structures of epidote group minerals, the various ionic substitutions provide the major variables. These are:

	Ions in Ca Site	Ions in Al Site Outside Chains
Clinozoisite	Ca^{2+}	Al^{3+}
Epidote	Ca^{2+}	Fe^{3+},Al^{3+}
Piemontite	Ca^{2+}	Mn^{3+},Fe^{3+},Al^{3+}
Allanite	Ca^{2+},Ce^{3+},La^{3+}, Na^{+}	Fe^{3+},Fe^{2+},Mg^{2+}, Al^{3+}

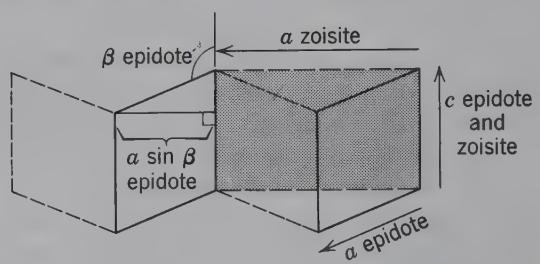

FIG. 18.10 Relation between unit cells of monoclinic epidote and orthorhombic zoisite, as projected on (010). The monoclinic unit cell outlined in solid can be related to its dashed equivalent by a mirror reflection (twinning). The orthorhombic unit cell is shown by shading.

CYCLOSILICATES

The cyclosilicates contain rings of linked SiO_4 tetrahedra having a ratio of Si:O = 1:3. Three possible closed cyclic configurations of this kind may exist, as shown in Fig. 18.11. The simplest is the Si_3O_9 ring, represented among minerals only by the rare titanosilicate *benitoite*, $BaTiSi_3O_9$. The Si_4O_{12} ring occurs only in a few very rare silicates. An example is *papagoite*, $Ca_2Cu_2Al_2Si_4O_{12}(OH)_6$. The Si_6O_{18} ring is the basic framework of the common and important minerals, *beryl*, $Be_3Al_2Si_6O_{18}$, and *tourmaline*. In the structure of beryl, Si_6O_{18} rings are arranged in layers parallel to {0001}. See Figs. 18.12a and b as well as several interactive illustrations of the beryl structure in module III of the CD-ROM under the heading "3-dimensional Order: Space Group Elements in Structures." Sheets of Be and Al ions lie between the layers of rings. Be in 4-coordination and Al in 6-coordination tie the layers together horizontally and vertically. The silicon-

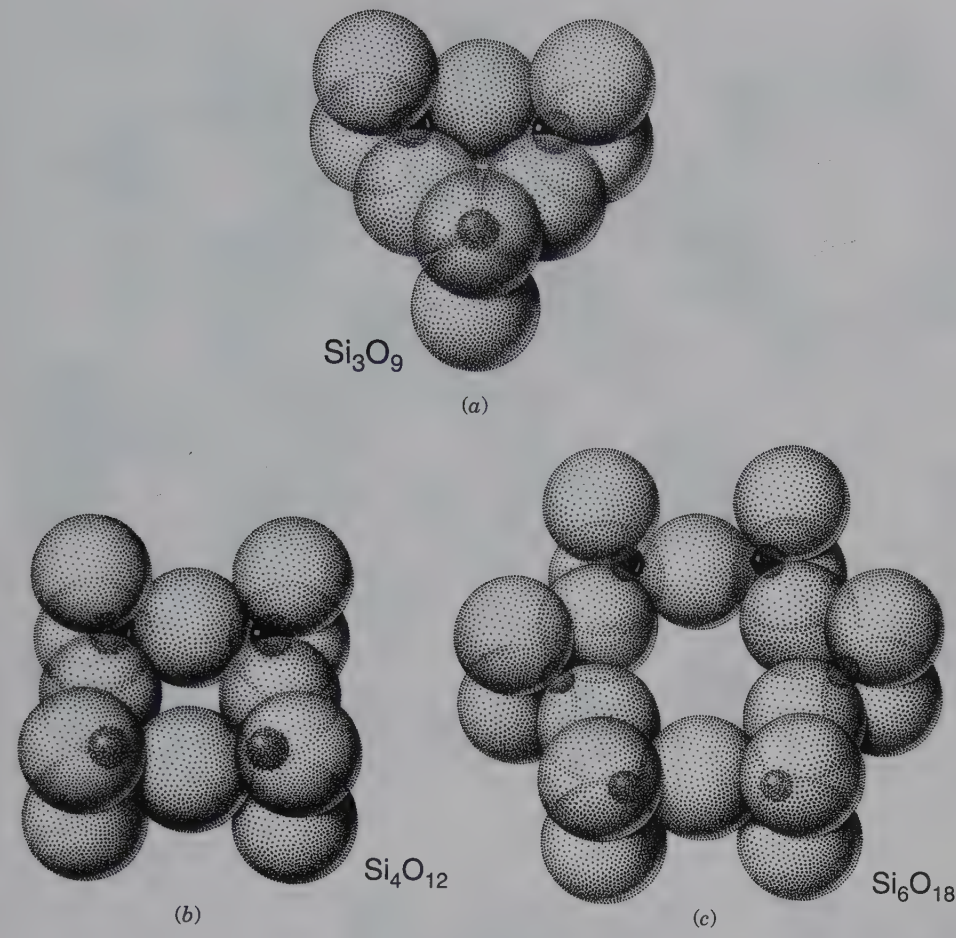

FIG. 18.11 Close-packed representation of ring structures in the cyclosilicates.

oxygen rings are so arranged as to be nonpolar; that is, a mirror plane passes through the tetrahedra in the plane of the ring (Fig. 18.12b). Rings are positioned one above the other in the basal sheets so that the central holes correspond, forming prominent channels parallel to the *c* axis. In these channels a wide variety of ions, neutral atoms, and molecules, can be housed such as $(OH)^-$, H_2O, F^-, He, and ions of Rb^+, Cs^+, Na^+, and K^+. With monovalent alkalis, such as Na^+ in the channels, the overall charge of the structure is neutralized by the substitution 2 alkalis$^{+1} \leftrightarrows Be^{2+}$, or by 3 alkalis^{+1} + 1$Al^{3+} \leftrightarrows$ 3 Be^{2+}. Additional coupled substitutions in beryl are: $Al^{3+} \rightleftarrows Be^{2+} + R^+$, $Si^{4+} \rightleftarrows Be^{2+} + 2R^+$, $Be^{2+} \rightleftarrows Li^+ + R^+$ and $Si^{4+} \rightleftarrows Al^{3+} + R^+$, where *R* represents Na^+, K^+, Rb^+, or Cs^+. Although beryl is here included as a member of the cyclosilicates on the basis of the Si_6O_{18} rings, consideration of the presence of the BeO_4 tetrahedra (see Fig. 18.12b) as an equally essential part of the structure reveals an overall three-dimensional network for this structure. For this reason, beryl also can be classified as a member of the framework (or tecto) silicates. For further discussion of the beryl structure and space group, see Fig. A4.2 in Appendix 4 and related text.

Cordierite, $(Mg,Fe)_2Al_4Si_5O_{18}{\cdot}nH_2O$, has a high-temperature polymorph, *indialite*, which is isostructural with beryl in which the Al is randomly distributed in the $(Si,Al)_6O_{18}$ rings. The common, lower-temperature form, *cordierite*, is orthorhombic (pseudohexagonal) in which two of the tetrahedra in the six-fold ring are occupied by Al, producing an ordered structure (see Fig. 18.13). Al occupies the Be sites and Mg and Fe^{2+} the octahedral Al sites of the beryl structure. H_2O molecules may reside in the channels of the structure. Gibbs (1966) points out that cordierite should be classified with the tectosilicates rather than the cyclosilicates because Al- and Si-tetrahedra are in perfect alternation in all directions of the structure except for two SiO_4 tetrahedra that share a common oxygen in the six-membered ring.

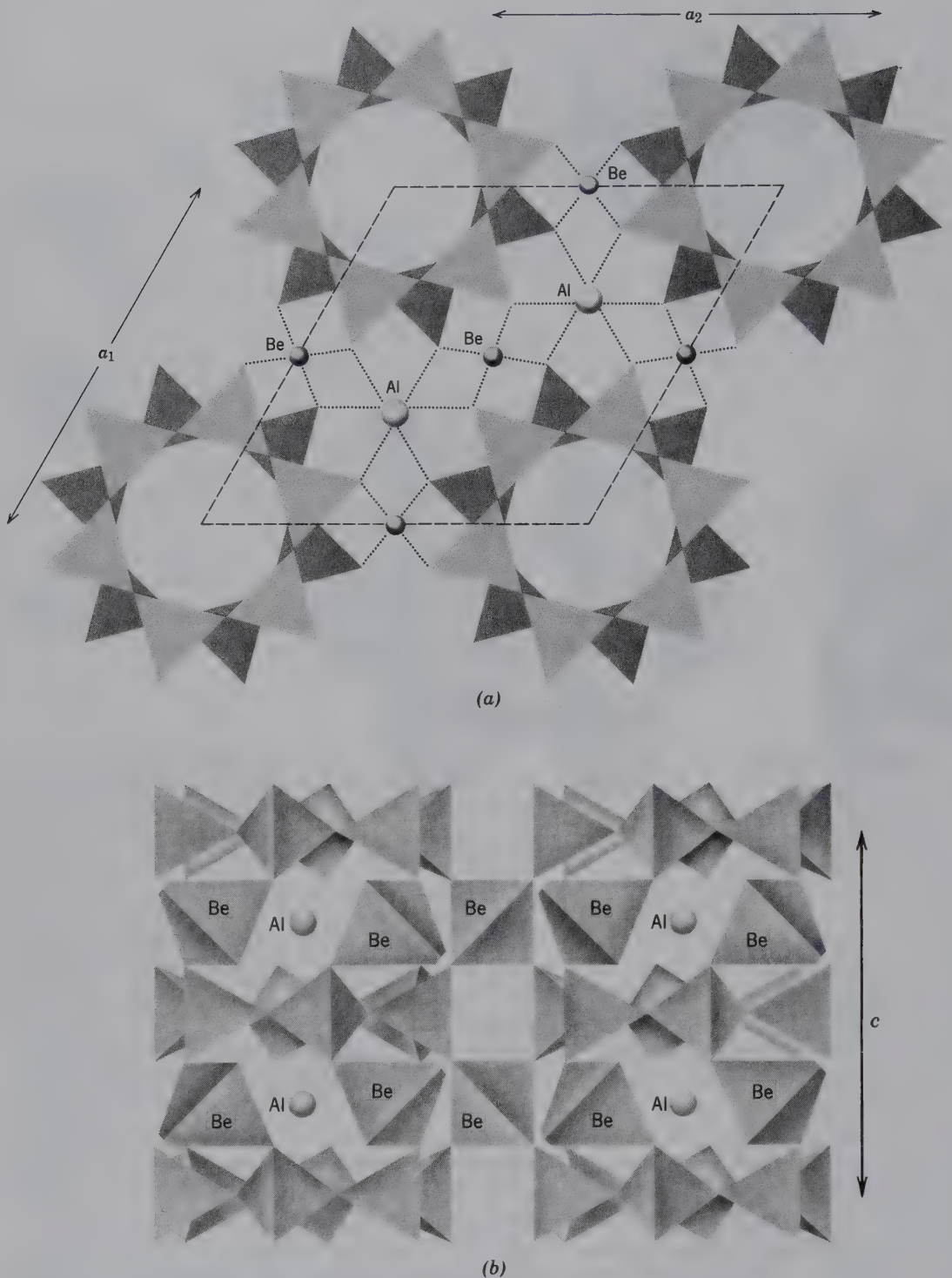

FIG. 18.12 The structure of beryl. (a) Projected onto (0001). Dashed lines outline the unit cell. (b) View of the beryl structure with *c* axis vertical.

Tourmaline is an acentric rhombohedral ($R3m$) borosilicate with a general chemical formula of $XY_3Z_6(T_6O_{18})(BO_3)_3V_3W$. (The letters indicate different structural sites, each of which can be occupied by a variety of chemical elements as given in the table that follows. These structural sites are labeled in Fig. 18.14b.) The structure of *tourmaline* is characterized by six-membered tetrahedral rings (T sites: Si_6O_{18}) whose apical oxygens all point toward the negative end of the *c* crystallographic axis (Figs. 18.14a and b).

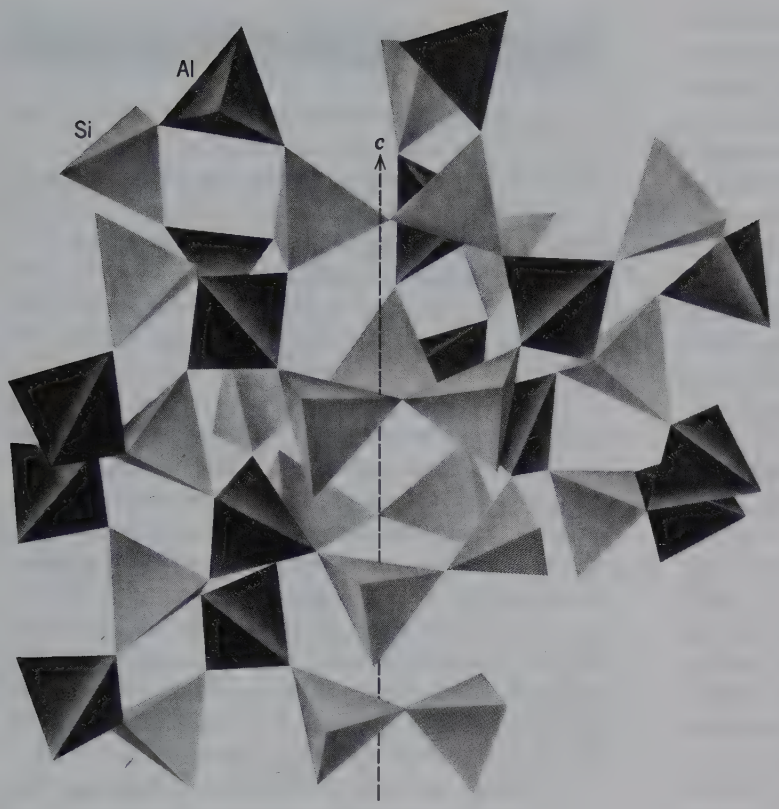

FIG. 18.13 Idealized drawing of the ($Al_4Si_5O_{18}$) framework in low cordierite. The octahedral coordination of Mg and Fe^{2+} is not shown. (After Gibbs, G.V. 1966. The polymorphism of cordierite I: The crystal structure of low cordierite. *American Mineralogist* 51: 1068–1087.)

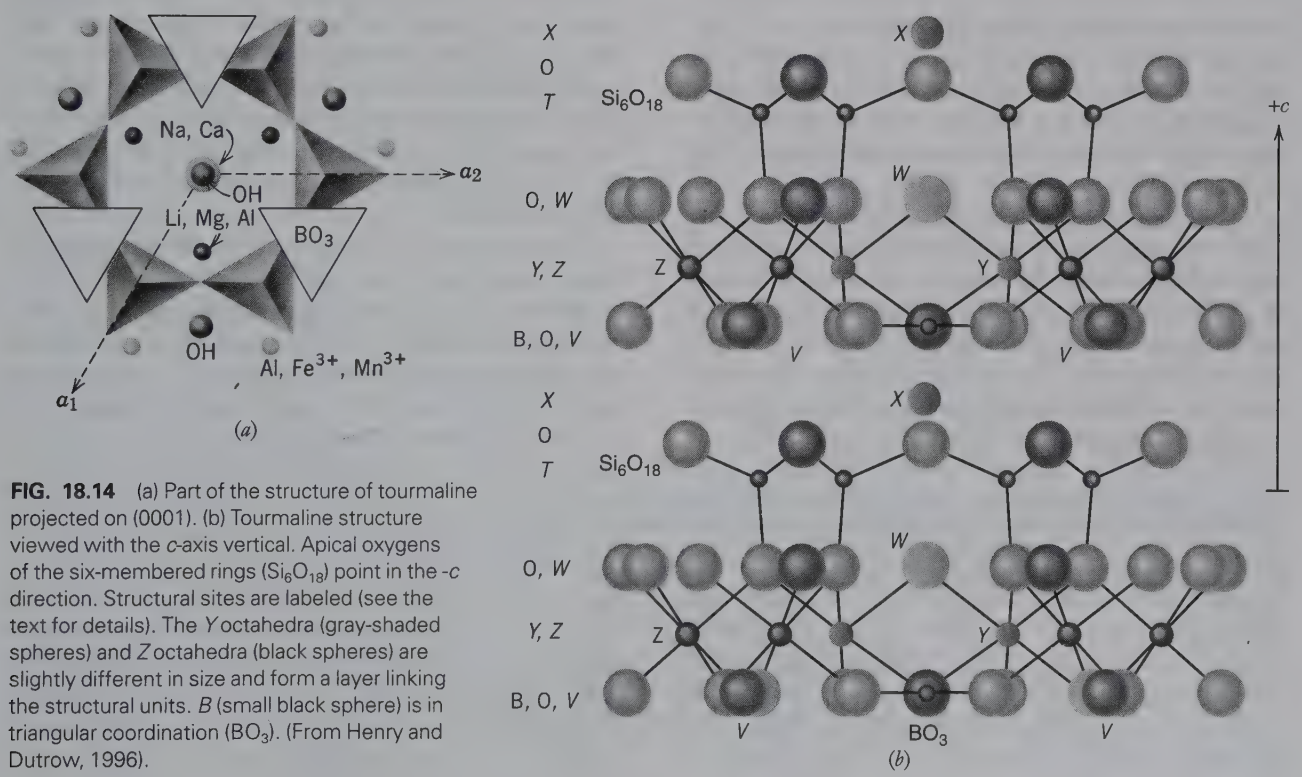

FIG. 18.14 (a) Part of the structure of tourmaline projected on (0001). (b) Tourmaline structure viewed with the *c*-axis vertical. Apical oxygens of the six-membered rings (Si_6O_{18}) point in the -*c* direction. Structural sites are labeled (see the text for details). The *Y* octahedra (gray-shaded spheres) and *Z* octahedra (black spheres) are slightly different in size and form a layer linking the structural units. *B* (small black sphere) is in triangular coordination (BO_3). (From Henry and Dutrow, 1996).

This produces a polar (acentric) structure because the net strength of the bonds on one side of the rings is unequal to the strength of bonds extending in the other direction. Distinct polar properties in tourmaline are manifest in its crystal habits and in its piezoelectric and pyroelectric nature. *T* sites are occupied primarily by Si^{4+}, with minor Al^{3+} and B^{3+}. Alternating over the tetrahedra are triangular BO_3 groups that lie parallel to the (0001) plane (Fig. 18.14a). Planar rings of tetrahedra are linked by two types of octahedra, *Z* and *Y*, that share edges to form brucite-like fragments. The *Z* octahedron is relatively small, somewhat distorted, and occupied predominantly by trivalent cations (Al^{3+}, Fe^{3+}) but can also contain Mg^{2+}. *Z*-site cations serve as links among structural fragments along a three-fold screw axis. The *Y* site is a regular octahedral site occupied primarily by (Fe^{2+}, Mg^{2+}, Li^{+}, Al^{3+}, Mn^{2+}). The *X* site is a 9-coordinated site, located along the three-fold axis of symmetry, commonly occupied by Na^{+}, Ca^{2+}, or can be largely vacant, ❑ (Fig. 18.14b). There are 31 anions in the structural formula. The *V* site contains OH^{-} and O^{2-}. The *W* site is located along the three-fold axis central to the pseudo-hexagonal ring of tetrahedra, and can contain OH^{-}, O^{2-} or F^{-}.

Chemical variability in tourmaline is extensive. Both simple and coupled ionic substitutions occur in tourmaline, of which the most common are: $Fe^{2+} \rightleftarrows Mg^{2+}$; $Na^{+} + Al^{3+} \rightleftarrows Ca^{2+} + Mg^{2+}$; $Li^{+} + Al^{3+} \rightleftarrows 2Fe^{2+}$. This chemical variability leads to a large number of tourmaline species. End members are determined by the site occupancy, commonly in more than one site. When the site occupancy of a specific element attains 50%, the mineral name changes to another species. A selection of such end-members is given below together with the primary element(s) occupying the various sites.

Although there has been a tendency to correlate color with composition in tourmaline, this correlation does not always hold. In most tourmaline, the color is caused by transition elements that occur as impurities in the structure (refer to Chapter 10). For example, uvite and dravite are both brown; rossmanite and liddicoatite are commonly colorless. Schorl is black, as are foitite and buergerite (not listed).

INOSILICATES

SiO_4 tetrahedra may link into chains by sharing oxygens (Fig. 18.3). Simple chains may be joined side-by-side by further sharing of oxygens in alternate tetrahedra to form bands or double chains (Fig. 18.3). In the simple chain structure, two of the four oxygens in each SiO_4 tetrahedron are shared, giving a ratio of Si:O = 1:3. In the band structure, half of the tetrahedra share three oxygens and the other half share two oxygens, yielding a ratio of Si:O = 4:11.

Included in the inosilicates are two important rock-forming groups of minerals: the *pyroxenes* as single chain members and the *amphiboles* as double chain members. Many similarities exist between the two groups in crystallographic, physical, and chemical properties. Although most pyroxenes and amphiboles are monoclinic, both groups have orthorhombic members. In both, the repeat distance along the chains, the *c* dimension of the unit cell, is approximately 5.2 Å. The *a* cell dimensions are also analogous but, because of the double chain, the *b* dimension of amphiboles is roughly twice that of the corresponding pyroxenes.

The same cations are present in both groups, but the amphiboles are characterized by the presence of (OH), which is lacking in pyroxenes. Although the color, luster, and hardness of analogous species are similar, the (OH) in amphiboles gives them, in general, slightly lower specific gravity and refractive indices than their pyroxene counterparts. The crystals have somewhat different habits. Pyroxenes commonly occur in blocky prisms, whereas amphiboles tend to form more elongated crystals, often acicular. Their cleavages have different angles and can be directly related to the underlying chain structure (see Figs. 18.17, 18.18, 18.23 and 18.24).

Pyroxenes are anhydrous and crystallize at higher temperatures than their amphibole analogues. Pyroxenes form early in a cooling igneous melt and occur also in high-temperature metamorphic rocks rich in Mg and Fe. If water is present in the melt or as a metamorphic fluid, the early-formed pyroxene may react with the liquid at lower temperatures to form amphi-

Common Species	(*X*)	(Y_3)	(Z_6)	T_6O_{18}	$(BO_3)_3$	V_3	*W*
Elbaite	Na	$Li_{1.5}Al_{1.5}$	Al_6	Si_6O_{18}	$(BO_3)_3$	$(OH)_3$	(OH)
Schorl	Na	$Fe^{2+}{}_3$	Al_6	Si_6O_{18}	$(BO_3)_3$	$(OH)_3$	(OH)
Dravite	Na	Mg_3	Al_6	Si_6O_{18}	$(BO_3)_3$	$(OH)_3$	(OH)
Liddicoatite	Ca	Li_2Al	Al_6	Si_6O_{18}	$(BO_3)_3$	$(OH)_3$	F
Uvite	Ca	Mg_3	$MgAl_5$	Si_6O_{18}	$(BO_3)_3$	$(OH)_3$	F
Rossmanite	❑*	$LiAl_2$	Al_6	Si_6O_{18}	$(BO_3)_3$	$(OH)_3$	(OH)
Foitite	❑	$Fe^{2}_{2} + {}_2Al$	Al_6	Si_6O_{18}	$(BO_3)_3$	$(OH)_3$	(OH)

*❑ = vacancy.

bole. Under prograde metamorphic conditions amphiboles dehydrate to form pyroxenes, and under retrograde metamorphic conditions pyroxenes hydrate to amphiboles (see Fig. 19.38).

PYROXENE GROUP

The chemical composition of pyroxenes can be expressed by a general formula as XYZ_2O_6, where X represents Na^+, Ca^{2+}, Mn^{2+}, Fe^{2+}, Mg^{2+}, and Li^+ in the *M2* crystallographic site; Y represents Mn^{2+}, Fe^{2+}, Mg^{2+}, Fe^{3+}, Al^{3+}, Cr^{3+}, and Ti^{4+} in the *M1* site; and Z represents Si^{4+} and Al^{3+} in the tetrahedral sites of the chain. (X cations, in general, are larger than the Y cations, in accordance with the cation size requirements of the sites *M2* and *M1*.) The pyroxenes can be divided into several groups, the most common of which can be represented as part of the chemical system $CaSiO_3$ (wollastonite, a pyroxenoid)–$MgSiO_3$(enstatite)–$FeSiO_3$ (ferrosilite). The lower one-half of the triangular diagram, forming a quadrilateral, includes members of the series *diopside*, $CaMgSi_2O_6$, *hedenbergite*, $CaFeSi_2O_6$, and of the series *enstatite-ferrosilite* (see Fig. 18.15a). Only the names for end-member compositions of the common pyroxenes are shown in Fig. 18.15a. The end-member names, as shown in Fig. 18.15a, apply from the end-member composition to the 50 molecular percentage point (the halfway point) in the diopside-hedenbergite and enstatite-ferrosilite series. If chemical analyses are available for intermediate compositions, they are expressed in terms of molecular percentages of the end members (see Fig. 18.15b). For example, pure enstatite can be stated as En_{100}. A member of the two-component orthopyroxene series composed of 80 molecular percent enstatite and 20 molecular percent ferrosilite can be listed as En_{80}. Similarly, the compositions of the two-component diopside–hedenbergite series can be expressed by molecular percentages that appear as subscripts to Di and Hed (e.g., $Di_{50}Hed_{50}$). Any more general chemical composition in the quadrilateral of Fig. 18.15b can be expressed in terms of molecular percentages of the three end members, Wo (for wollastonite), En (for enstatite), and Fs (for ferrosilite). An example, shown in Fig. 18.15b, would be $Wo_{50}En_{25}Fs_{25}$. Table 5.6 illustrates the recalculation of a pyroxene analysis in terms of Wo-En-Fs end-member components, and Fig. 5.12 (and related text) explains the procedure for plotting chemical compositions on triangular diagrams.

Compositionally *augite* is closely related to members of the diopside–hedenbergite series but with some substitution of, for example, Na for Ca in *M2*, Al for Mg (or Fe^{2+}) in *M1*, and Al for Si. *Pigeonite* represents a field of Mg–Fe solid solutions with a Ca-content slightly larger than in the *enstatite–ferrosilite* series, the composition field of the orthopyroxenes. Sodium-containing pyroxenes are *aegirine*, $NaFe^{3+}Si_2O_6$, and *jadeite*, $NaAlSi_2O_6$. Aegirine and augite represent a complete solid solution series as shown by members of intermediate composition, *aegirine–augite*. *Omphacite* represents a solid solution series between augite and jadeite. *Spodumene*, $LiAlSi_2O_6$, is a relatively rare pyroxene found in Li-rich pegmatites. Na- and Li-rich pyroxenes are referred to as *non-quad pyroxenes* because these compositions do not plot on the Ca–Fe–Mg quadrilateral.

The pyroxene structure is based on single SiO_3 chains that run parallel to the *c* axis. Figure 18.16 illustrates this tetrahedral chain as well as the double octahedral chain to which it is bonded. See also Fig. 18.3 and several interactive illustrations of the clinopyroxene structure in module III of the CD-ROM under the heading: "Three-dimensional Order: Space Group Elements in Structures." The structure contains two types of cation sites, labeled *M1* and *M2*. The *M1* site is a relatively regular octahedron, but in the monoclinic pyroxenes, the *M2* site is an irregular polyhedron of 8-coordination (in orthorhombic pyroxenes with Mg in the *M2* site, this polyhedron is closer to a regular octahedron). Figure 18.17a shows the pyroxene structure and the distribution of cation sites as seen in a direction parallel to the *c* axis. The cations in the *M1* sites are all coordinated by oxygens of two opposing SiO_3 chains, and, as such, produce a tetrahedral–octahedral–tetrahedral (*t–o–t*) strip. The coordination of cations in the *M2* position, however, is such that several of these *t–o–t* strips are cross-linked. These *t–o–t* strips are often schematically represented as in Fig. 18.17b; this, in turn, shows the relationship of the *t–o–t* strips to the cleavage angles in pyroxenes. Figure 11.18 is a direct structure image of the features shown in Fig. 18.17.

The majority of pyroxenes can be assigned to one of three space groups, two monoclinic ($C2/c$ and $P2_1/c$) and one orthorhombic (*Pbca*) (see Fig. 18.15b). The $C2/c$ structure is found in most of the common clinopyroxenes, such as diopside, $CaMgSi_2O_6$, jadeite, $NaAlSi_2O_6$, and augite. This structure is illustrated in Fig. 18.16. See Fig. A4.1 in Appendix 4 for an illustration of a clinopyroxene with $C2/c$ space group. The *M1* site is generally occupied by cations that are smaller than those of the *M2* site. For example, in the diopside–hedenbergite series, $CaMgSi_2O_6$–$CaFeSi_2O_6$, the *M1* site is occupied by Mg and Fe^{2+} in random distribution, whereas the *M2* is occupied solely by the larger Ca^{2+} ion, in 8-coordination. The *M2* site, however, can also house Mn^{2+}, Fe^{2+}, Mg, or Li, in which case the coordination is six-fold. The $P2_1/c$ space group is found in pigeonite (see Fig. 18.15), which may be represented

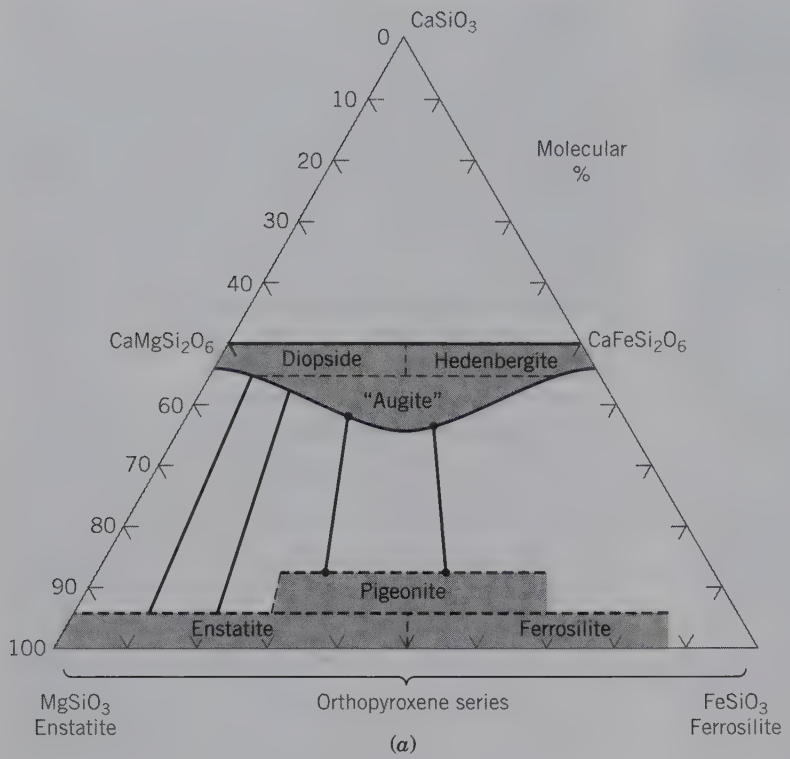

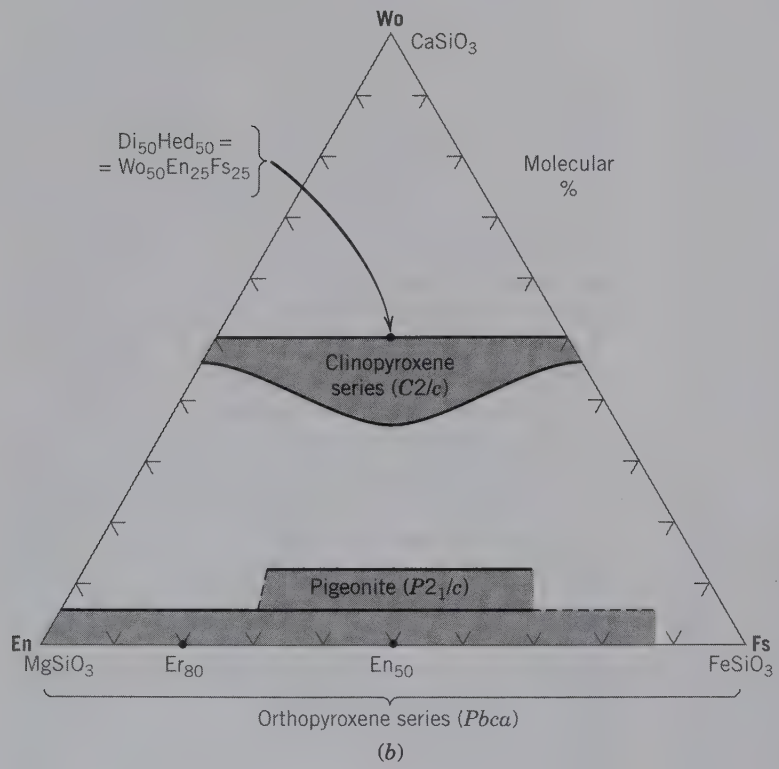

FIG. 18.15 (a) Pyroxene compositions in the system $CaSiO_3$–$MgSiO_3$–$FeSiO_3$. General compositional fields are outlined. Representative tielines across the miscibility gap between augite and more Mg–Fe-rich pyroxenes are shown. The "augite" field is labeled with quotation marks because all augite compositions contain considerable Al, which is not considered in this triangular composition diagram. (b) Nomenclature of pyroxenes in the system Wo (wollastonite), En (enstatite), and Fs (ferrosilite) as derived from chemical compositional information. Members of the orthopyroxene series range from En_{100} to En_0 (which is equivalent to Fs_0 to Fs_{100}). Any other, more general compositions are expressed in molecular percentages of Wo, En, and Fs (e.g., $Wo_{50}En_{25}Fs_{25}$). The space groups of the various solid solution series are shown.

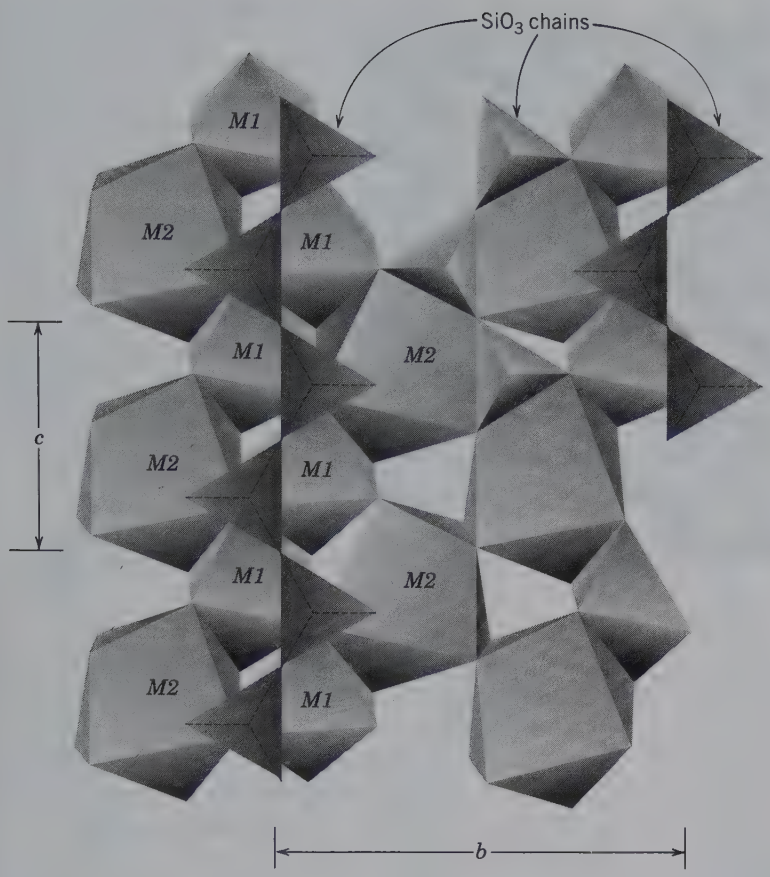

FIG. 18.16 The structure of jadeite, $NaAlSi_2O_6$, a monoclinic pyroxene in an approximate projection onto (100). The *M2* site is occupied by Na^+, the *M1* site by Al^{3+}. (After Prewitt, C. T. and C. W. Burnham. 1966. The crystal structure of jadeite, $NaAlSi_2O_6$. *American Mineralogist* 51: 956–75.)

FIG. 18.17 (a) Schematic projection of the monoclinic pyroxene structure on a plane perpendicular to the *c* axis. (b) Control of cleavage angles by *t–o–t* strips (also referred to as "I-beams") in the pyroxene structure, as compared with naturally occurring pyroxene cleavage.

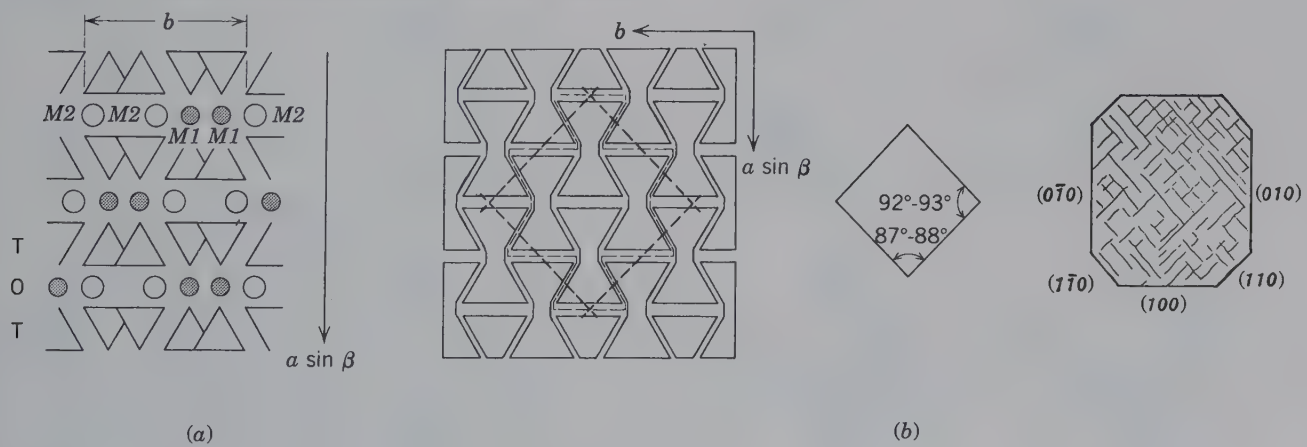

(*a*) (*b*)

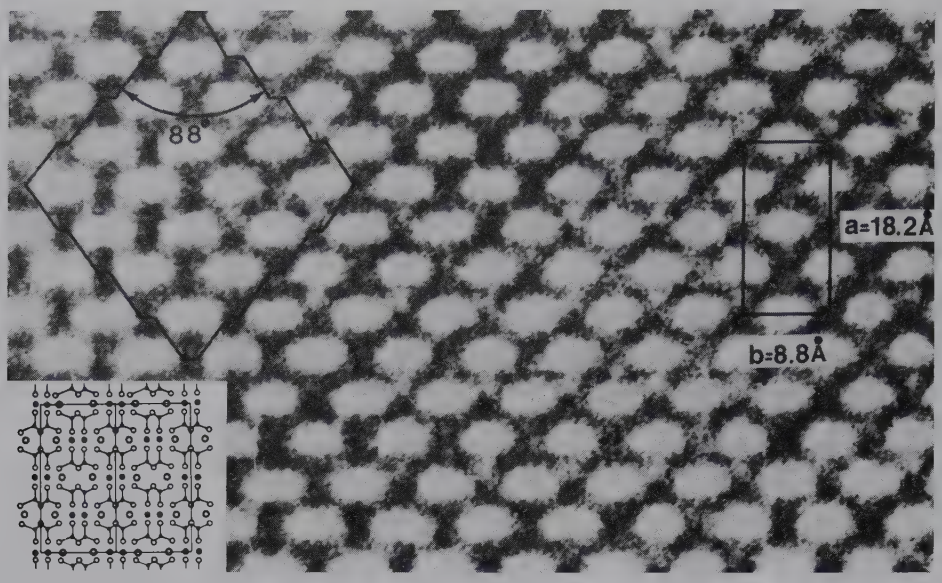

FIG. 18.18 High-resolution transmission electron microscope (HRTEM) image of an *a–b* section of enstatite. The white regions correspond to areas between *M2* sites in the structure. A unit cell and cleavage surfaces are outlined. The insert shows the enstatite structure at the same scale as the structure image. (From Buseck, P. R. and S. Iijima. 1974. High resolution electron microscopy of silicates. *American Mineralogist* 59: 1–21.)

as $Ca_{0.25}(Mg,Fe)_{1.75}Si_2O_6$ in which the *M2* site is occupied by all the Ca in the formula as well as additional Mg and Fe so as to make the composition of the site $[Ca_{0.25}(Fe + Mg)_{0.75}]$. The *M2* site, as present in the clinopyroxenes with space group *C2/c*, is too large to accommodate these smaller cations so that *M2* is somewhat smaller in pigeonite (hence, this site has irregular 7-coordination) due to a slight shift in the pigeonite structure as compared with the more regular diopside type structure. The orthorhombic *Pbca* structure is that found in the orthopyroxene series, which contains virtually no Ca. The Mg and Fe^{2+} ions are distributed among *M1* and *M2* with the larger cation (Fe^{2+}) showing strong preference for the somewhat larger and distorted *M2* site. The coordination of both the *M1* and *M2* sites in orthopyroxenes is six-fold.

The unit cells of the orthorhombic pyroxenes are related to the monoclinic unit cells by a twinlike mirror across {100} accompanied by an approximate doubling of the *a* cell dimension (e.g., *a* of enstatite $\approx 2\,a \sin \beta$ of diopside; see Fig. 18.19a). Figures 18.19b and c show schematically the development of monoclinic and orthorhombic pyroxene structures built up from *t–o–t* strips. The compositions represented by the orthopyroxene series may in rare occurrences be found in a monoclinic form, known as the *clinoenstatite–clinoferrosilite series*.

FIG. 18.19 (a) Relationship between unit cells of clinopyroxene (e.g., diopside) and orthopyroxene (e.g., enstatite) as projected on (010). The monoclinic unit cell outlined by shading can be related to the larger orthorhombic unit cell by a mirror reflection (compare with Fig. 18.25). (b) Schematic representation of a possible monoclinic pyroxene (looking down the *c* axis) with the *t–o–t* strips (or "I-beams") represented by strike and dip symbols; *g*s indicate glide planes (with a translation component parallel to *c*). (c) Schematic representation of a possible orthorhombic pyroxene; *m*s represent mirrors. (b and c after J. B. Thompson, Jr., Harvard University, pers. comm.)

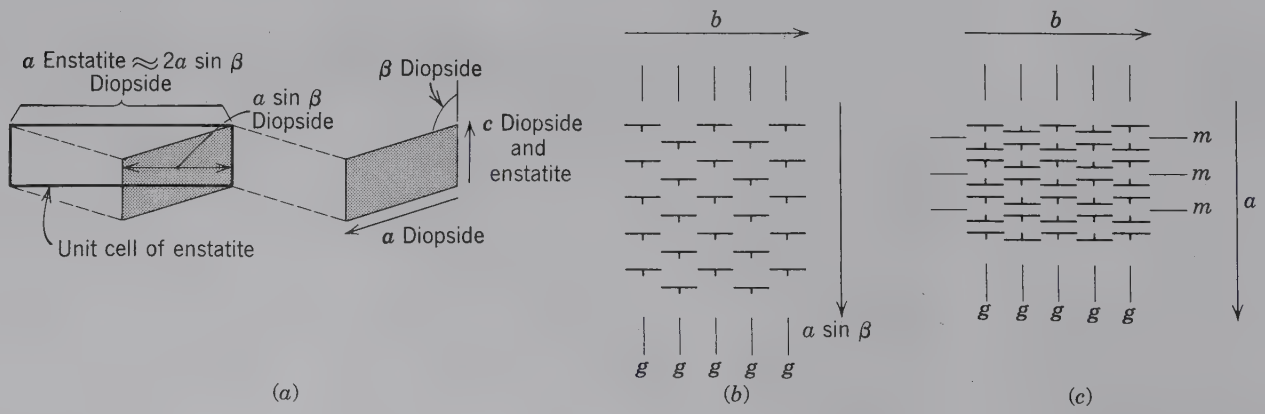

PYROXENOID GROUP

There are a number of silicate minerals, in addition to the pyroxenes, that have a ratio of Si:O = 1:3. However, their structures are not identical to those of the pyroxenes. Both pyroxene and pyroxenoid structures contain octahedrally coordinated cations between SiO_3 chains. In pyroxenoids, the geometry of the chains is not of the simple, infinitely extending type with a repeat distance of about 5.2 Å along the direction of the chain (see Fig. 18.20). Instead, pyroxenoid chains are kinked and exhibit a longer repeat distance. In wollastonite, $CaSiO_3$, the smallest repeat of the chain consists of three twisted tetrahedra with a repeat distance of 7.1 Å (see also Fig. 19.43) and in rhodonite, $MnSiO_3$, the unit repeat is built of five twisted tetrahedra with a repeat distance of 12.5 Å. Because of the lower symmetry of the chains (as compared with the pyroxene chain), the structures of pyroxenoids are triclinic. The chain

FIG. 18.20 SiO_3 chains in pyroxene (a) and pyroxenoids. (b) Wollastonite. (c) Rhodonite. (d) Pyroxmangite. (After Liebau, F. 1959. Über die Kristallstruktur des Pyroxmangits (Mn, Fe, Ca, Mg) SiO_3, *Acta Crystallographica* 12: 177–181.)

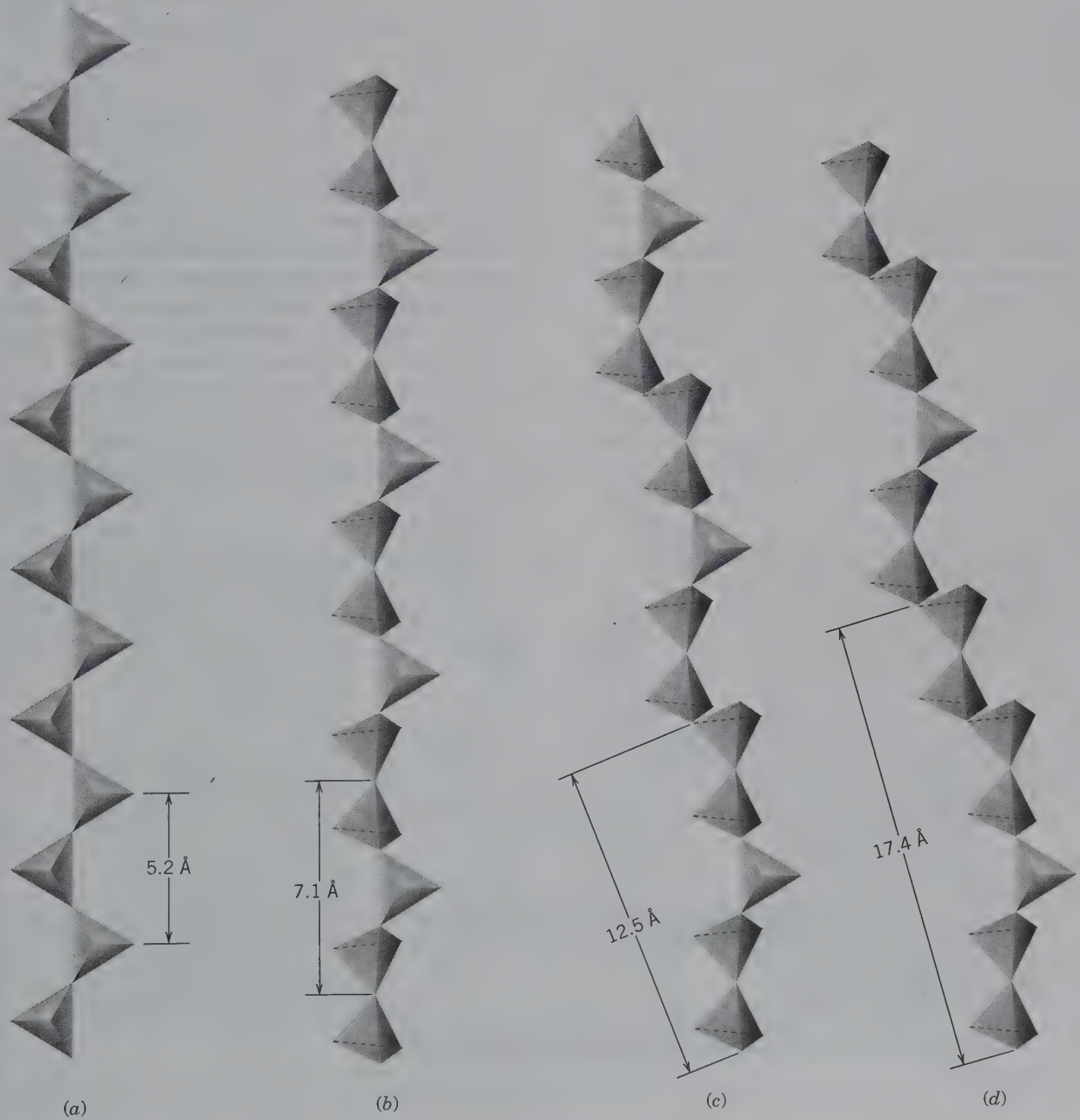

structure in the pyroxenoids is expressed by their generally splintery cleavages and sometime fibrous habit.

AMPHIBOLE GROUP

The chemical composition of members of the amphibole group can be expressed by the general formula $W_{0-1}X_2Y_5Z_8O_{22}(OH,F)_2$, where W represents Na^+ and K^+ in the A site, X denotes Ca^{2+}, Na^+, Mn^{2+}, Fe^{2+}, Mg^{2+}, and Li^+ in the *M4* sites, Y represents Mn^{2+}, Fe^{2+}, Mg^{2+}, Fe^{3+}, Al^{3+}, and Ti^{4+} in the *M1*, *M2*, and *M3* sites, and Z refers to Si^{4+} and Al^{3+} in the tetrahedral sites. Essentially complete ionic substitution takes place between Na^+ and Ca^{2+} and among Mg^{2+}, Fe^{2+}, and Mn^{2+}. There is limited substitution between Fe^{3+} and Al^{3+} and between Ti^{4+} and other Y-type ions; and partial substitution of Al for Si in the tetrahedral sites of the double chains. Partial substitution of F^- and O^{2-} for OH in the hydroxyl sites is also common. Several common series of the amphibole group are represented compositionally in the chemical system $Mg_7Si_8O_{22}(OH)_2$ (anthophyllite)–$Fe_7Si_8O_{22}(OH)_2$ (grunerite)–"$Ca_7Si_8O_{22}(OH)_2$," a hypothetical end member composition, as in Fig. 18.21. This illustration is very similar to the Wo–En–Fs diagram for the pyroxene group (Fig. 18.15). A complete series exists from *tremolite*, $Ca_2Mg_5Si_8O_{22}(OH)_2$, to *ferroactinolite*, $Ca_2Fe_5Si_8O_{22}(OH)_2$. The commonly occurring *actinolite* composition is a generally Mg-rich member of the tremolite–ferroactinolite series. The compositional range from $Mg_7Si_8O_{22}(OH)_2$ to about $Fe_2Mg_5Si_8O_{22}(OH)_2$ is represented by the orthorhombic species, *anthophyllite*. The *cummingtonite–grunerite* series is monoclinic and extends from about $Fe_2Mg_5Si_8O_{22}(OH)_2$ to $Fe_7Si_8O_{22}(OH)_2$. Miscibility gaps are present between anthophyllite and the tremolite–actinolite series, as well as between the members of the cummingtonite–grunerite series and the calcic amphiboles. These gaps are reflected in the common occurrence of anthophyllite–tremolite and grunerite–actinolite pairs, as well as exsolution textures between members of the Mg–Fe and the Ca-containing amphiboles of Fig. 18.21. No Ca-amphibole compositions are possible above the 2/7th line (representing two Ca out of a total of seven $X + Y$ cations) because Ca can be housed only in the two *M4* sites of the amphibole structure. *Hornblende* may be regarded as a tremolite–ferroactinolite type composition with additional partial substitution of Na in the *A* and *M4* sites, Mn, Fe^{3+}, and Ti^{4+} for Y cations, and Al for Si in the tetrahedral sites, leading to a very complex general formula. Sodium-containing amphiboles are represented by members of the *glaucophane*, $Na_2Mg_3Al_2Si_8O_{22}(OH)_2$,–*riebeckite*, $Na_2Fe_3^{2+}Fe_2^{3+}Si_8O_{22}(OH)_2$, series. *Arfvedsonite*, $NaNa_2Fe_4^{2+}Fe^{3+}Si_8O_{22}(OH)_2$, contains additional Na in the *A* site of the structure. Table 18.2 compares the composition of some of the common members of the pyroxene and amphibole groups, and Table 5.7 illustrates the recalculation of an amphibole analysis.

The amphibole structure is based on double Si_4O_{11} chains parallel to the *c* axis. Figure 18.22 illustrates this chain as well as the octahedral strip to which it is bonded. See also Fig. 18.3 and an interactive animation of the amphibole structure in module I of the CD-ROM under the heading "Solid Solution Mechanisms: Substitutional Solid Solution in Amphiboles." The structure contains several cation sites, labeled *A*, *M4*, *M3*, *M2*, *M1*, as well as the tetrahedral sites in the chains. The *A* site has 10- to 12-coordination with oxygen and (OH) and houses mainly Na, and at times small amounts of K. The *M4* site has 6- to 8-coordination and houses X type cations (see Table 18.2). The *M1*, *M2*, and *M3* octahedra accommodate Y type cations and share edges to form octahedral bands par-

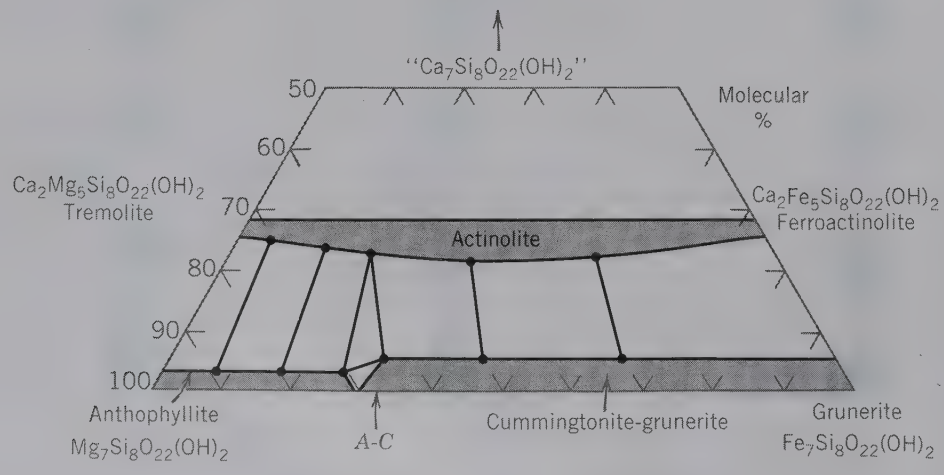

FIG. 18.21 Amphibole compositions in the system $Mg_7Si_8O_{22}(OH)_2$–$Fe_7Si_8O_{22}(OH)_2$–"$Ca_7Si_8O_{22}(OH)_2$". General compositional fields are outlined. Representative tielines across miscibility gaps are shown. Compare with Fig. 18.15. The composition marked *A–C* refers to an anthophyllite-cummingtonite intergrowth illustrated in Fig. 18.25b.

Table 18.2 Ions in Common Pyroxenes and Amphiboles

Pyroxenes			Amphiboles			
Atomic Sites		Name	Atomic Sites			Name
M2	*M1*		*A*	*M4*	(*M1* + *M2* + *M3*)	
Mg	Mg	Enstatite	□*	Mg	Mg	Anthophyllite
Fe	Mg	other members of the orthopyroxene series	□	Fe	Mg	Cummingtonite
			□	Fe	Fe	Grunerite
Ca	Mg	Diopside	□	Ca	Mg	Tremolite
Ca	Fe	Hedenbergite	□	Ca	Fe	Ferroactinolite
Ca	Mn	Johannsenite				
Ca, Na	Mg, Fe, Mn, Al, Fe^{3+}, Ti	Augite	□	Ca, Na	Mg, Fe^{2+}, Mn, Al, Fe^{3+}, Ti	Hornblende
Na	Al	Jadeite	□	Na	Mg, Al	Glaucophane
Na	Fe^{3+}	Aegirine	□	Na	Fe^{2+}, Fe^{3+}	Riebeckite
			Na	Na	Fe^{2+}, Fe^{3+}	Afrvedsonite
Li	Al	Spodumene	□	Li	Mg, Fe^{3+}, Al, Fe^{2+}	Holmquistite

*□ represents a vacant atomic site.

allel to *c*. *M1* and *M3* are coordinated by four oxygens and two (OH, F) groups, whereas *M2* is coordinated by six oxygens. Figure 18.23a shows the monoclinic amphibole structure and the distribution of cation sites as seen in a direction parallel to the *c* axis. The *t–o–t* strips (Fig. 18.23b) are approximately twice as wide (in the *b* direction) as the equivalent *t–o–t* strips in pyroxenes (see Fig. 18.17b) because of the doubling of the chain width in amphiboles. This wider geometry causes the typical 56° and 124° cleavage angles as shown in Fig. 18.23b. Figure 18.24 is a direct structure image of the features shown in Fig. 18.23a.

FIG. 18.22 Crystal structure of a monoclinic (*C2/m*) amphibole projected down the *a* axis. (OH) groups are located in the center of the large holes of the rings in the chains. *M1*, *M2*, and *M3* sites house *Y* cations and are 6-coordinated. The *M4* site houses larger *X* cations in 6- to 8-coordination. The ion in the *A* site, between the backs of double chains is 10- to 12-coordinated. (After Papike, J. J., et al. 1969. Mineralogical Society of America Special Paper no. 2, 120.)

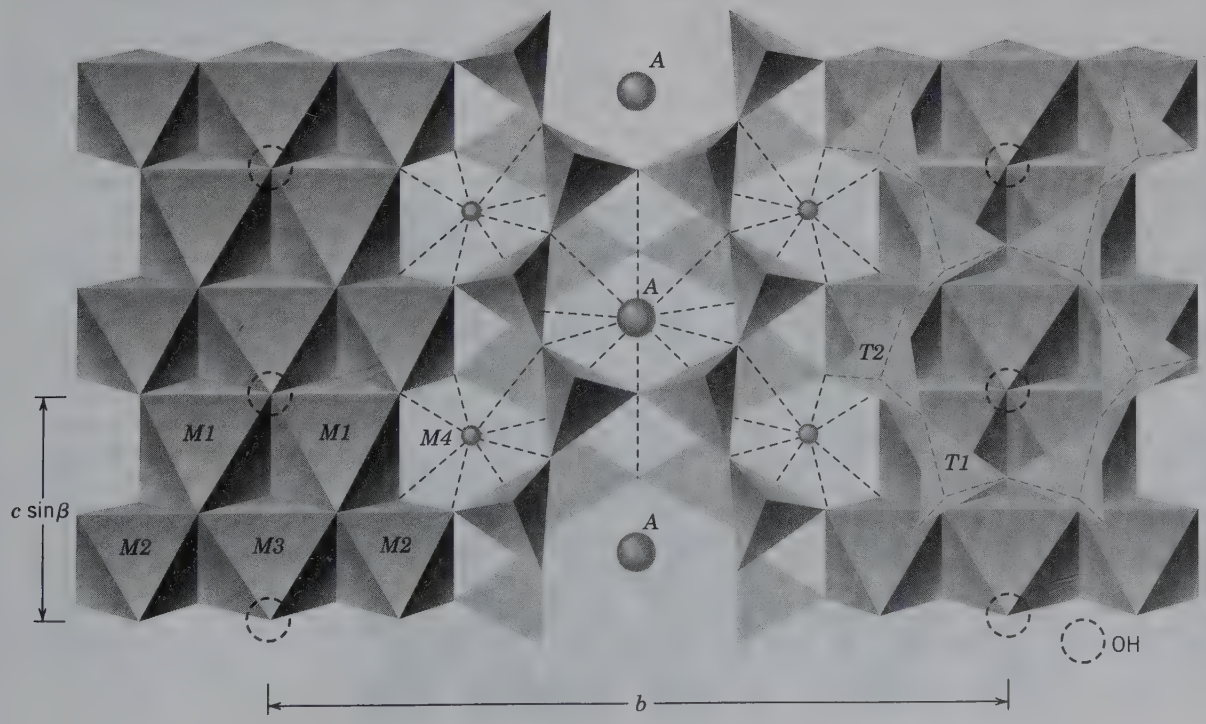

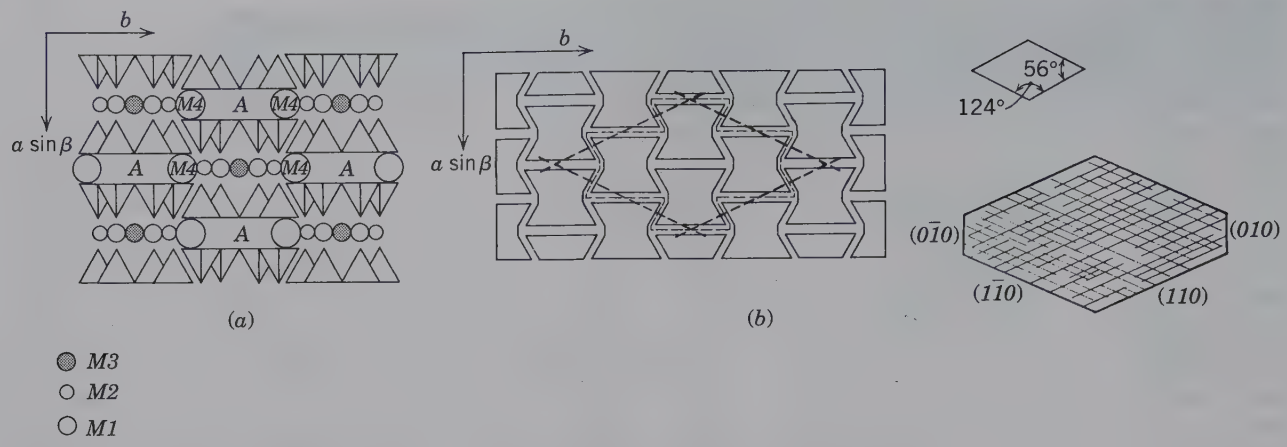

FIG. 18.23 (a) Schematic projection of the monoclinic amphibole structure on a plane perpendicular to the *c* axis (after Colville et al. 1966. *American Mineralogist* 51: 1739). Compare with Fig. 18.17a. (b) Control of cleavage angles by *t–o–t* strips (also referred to as "I-beams") in the amphibole structure, as compared with naturally occurring cleavage angles.

The majority of amphiboles can be assigned to one of three space groups, two monoclinic ($C2/m$ and $P2_1/m$) and one orthorhombic (*Pnma*). The $C2/m$ structure is found in all of the common clinoamphiboles, such as tremolite, $Ca_2Mg_5Si_8O_{22}(OH)_2$, and hornblende. This type of structure is illustrated in Fig. 18.22. The $P2_1/m$ space group is found in some Mg-rich cummingtonites, close to $(Mg, Fe)_2Mg_5Si_8O_{22}(OH)_2$ in composition, and results because the *M4* site is somewhat collapsed to house the relatively small Mg and Fe^{2+} ions. The orthorhombic *Pnma* structure is found in members of the anthophyllite, $Mg_7Si_8O_{22}(OH)_2$ to $Fe_2Mg_5Si_8O_{22}(OH)_2$, series and in gedrite, an Al and Na-containing anthophyllite, and in holmquistite. The presence of small cations in *M4*, *M3*, *M2*, and *M1* leads to an orthorhombic rather than a monoclinic structure. The unit cells of orthorhombic amphiboles are related to the monoclinic unit cells by a twinlike mirror across (100) accompanied by an approximate doubling of the *a* cell dimension (e.g., *a* of anthophyllite $\approx 2\,a \sin\beta$ of cummingtonite). This is illustrated schematically and also with a high-resolution transmission electron microscope (HRTEM) image in Fig. 18.25. This relationship between the structures of clinoamphiboles and orthoamphiboles is identical to that for clinopyroxenes and orthopyroxenes (see Fig. 18.19a).

The presence of (OH) groups in the structure of amphiboles causes a decrease in their thermal stabilities compared to those of the more refractory pyroxenes. This causes amphiboles to decompose to anhydrous minerals (often pyroxenes) at elevated temperatures below the melting point (see Figs. 19.38 and 19.51).

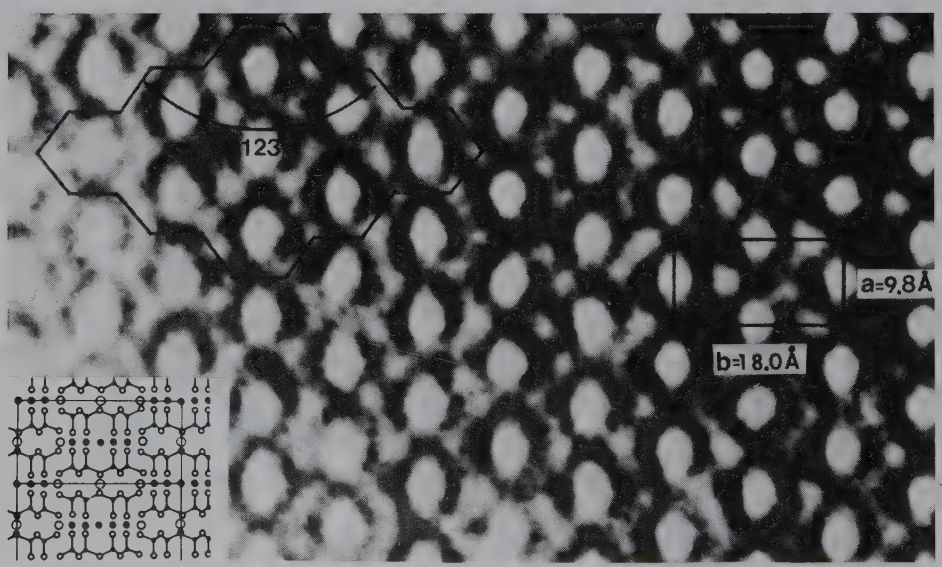

FIG. 18.24 HRTEM image of an *a–b* section of hornblende. The white regions correspond to the *A* sites. A unit cell and cleavage surfaces are outlined. The insert shows the hornblende structure at the same scale as the structure image. (From Buseck, P. R. and S. Iijima. 1974. High-resolution electron microscopy of silicates. *American Mineralogist* 59: 1–21.)

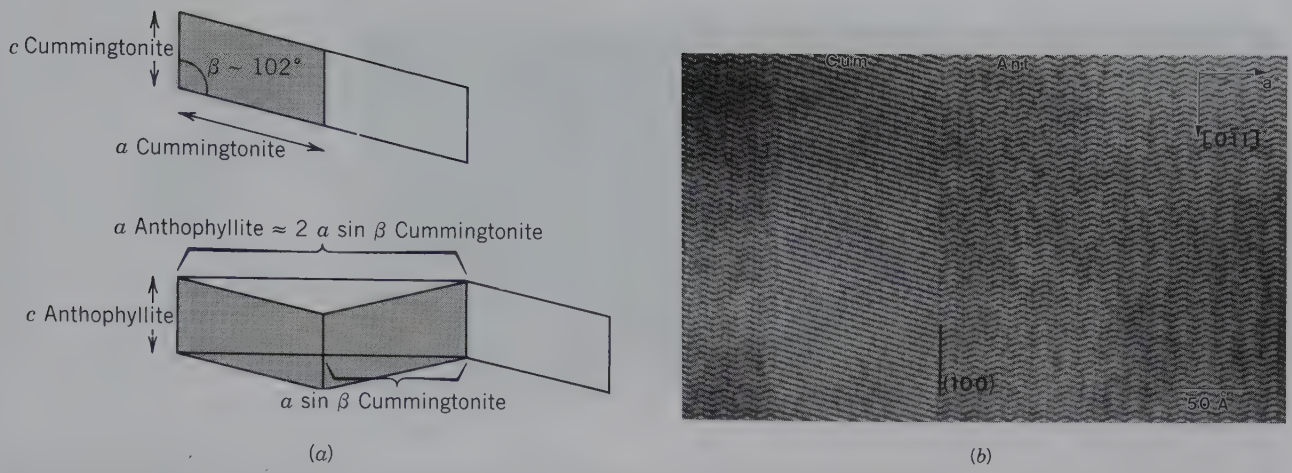

FIG. 18.25 (a) Relationship between unit cells of clinoamphiboles (e.g., cummingtonite or tremolite) and orthoamphibole (anthophyllite). The monoclinic unit cell (outlined by shading) can be repeated by a mirror reflection, which results in a zigzag pattern. This repeat pattern is described by the larger orthorhombic unit cell outline. This relationship is identical in the pyroxenes (see Fig. 18.19). (b) HRTEM image provides a direct picture of the relationships shown in (a). A cummingtonite (Cum) lamella (about 140 Å thick) is set in a matrix of anthophyllite (Ant). The stacking of the unit cells in cummingtonite is consistently in the same direction. However, the stacking of the unit cells in anthophyllite is the result of a mirror reflection parallel to (100), resulting in the zigzag pattern. Both amphiboles have approximately the same composition: $Na_{0.1}Fe_{2.2}Mg_{4.5}Al_{0.1}Si_8O_{22}(OH)_2$. In other words, the structure image is one of two polymorphs. The value of (Mg/(Mg + Fe) × 100%) for this formula is 67%, which plots it at the 67% molecular percentage point along the bottom edge of the triangle in Fig. 18.21, marked *A–C*. (Micrograph courtesy of Eugene A. Smelnik, Princeton University.)

In 1977, Veblen et al. reported several new structures that are closely related to amphiboles. These are referred to as *biopyriboles*, a term derived from *bio*tite (mica), *pyro*xene, and amph*ibole*. This collective term reflects the close architectural connection between numbers of the pyroxene, amphibole, and layer silicate groups. Two of the structures discovered, *jimthompsonite*, $(Mg,Fe)_{10}Si_{12}O_{32}(OH)_4$, and *chesterite*, $(Mg,Fe)_{17}Si_{20}O_{54}(OH)_6$, have chain widths and chain repeat sequences that can be interpreted in terms of single chain repeats (SiO_3 chains as in pyroxenes), double chain repeats ($Si_4O_{11}(OH)$ chains as in amphiboles), and triple chain repeats. These triple chain repeats are wider than those known in pyroxenes and amphiboles, and their increased width is suggestive of mica structures with infinitely extending sheets. Schematic illustrations of the pyroxene, amphibole, and new biopyribole structures are given in Fig. 18.26 in terms of I-beams. A direct image of some of these same structures, by HRTEM, is given in Fig. 18.27.

The new ordered structure types were found in a fine intergrowth with anthophyllite, and are considered

FIG. 18.26 Schematic illustration of "I-beams" projected onto the (001) plane in orthopyroxene, orthoamphibole, jimthompsonite, and chesterite. The digits mean: 1—single chain width as in pyroxene, 2—double chain width as in amphibole, and 3—triple chain width. (Redrawn after Veblen, D. R., P. R. Buseck, and C. W. Burnham. 1977. Asbestiform chain silicates: New minerals and structural groups. *Science* 198: 359–65.)

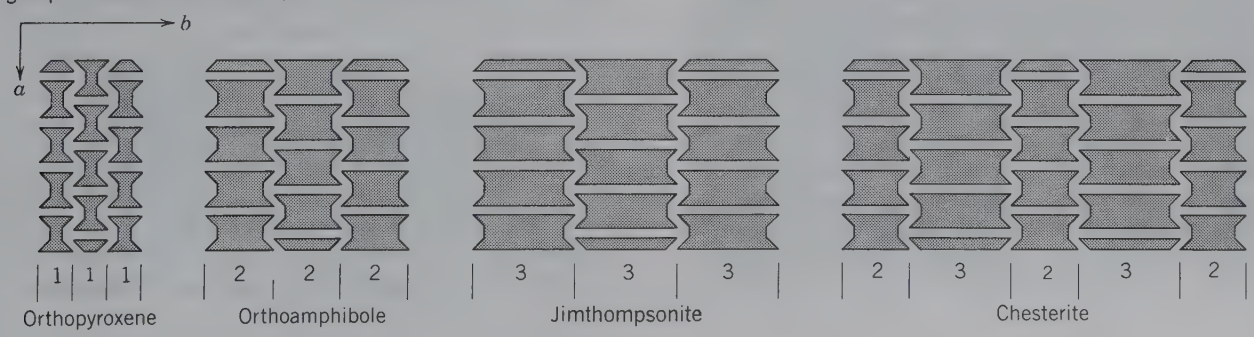

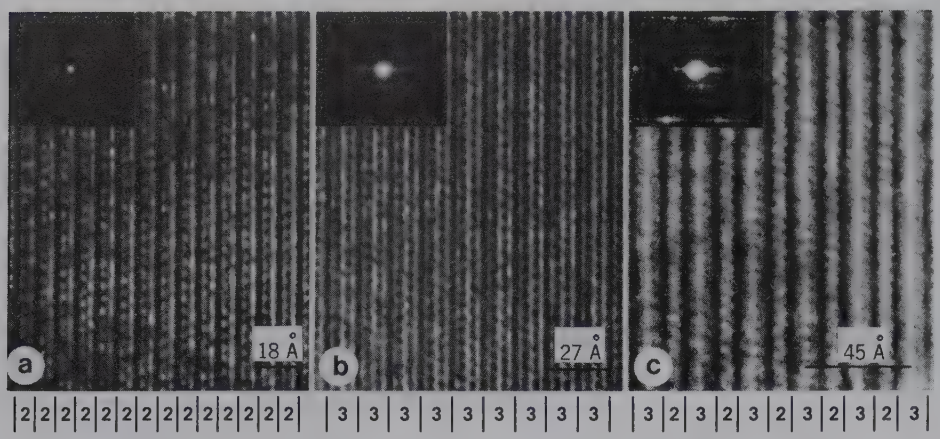

FIG. 18.27 HRTEM images of (a) anthophyllite, (b) jimthompsonite, and (c) chesterite. In each image, the c axis of the mineral is coincident with the vertical striping. In anthophyllite, the 2s locate double Si_4O_{11} chains. In jimthompsonite, the 3s refer to triple chains, and in chesterite the alternating 2s and 3s refer to alternating double and triple chains. The inset in each image is an electron diffraction pattern; this is used mainly by the microscopist for crystallographic orientation. (From Veblen, D. R., P. R. Buseck, and C. W. Burnham. 1977. Asbestiform chain silicates: New minerals and structural groups. *Science* 198: 359–65; copyright © 1977 by the AAAS. See also Veblen, D. R. 1981. Non-classical pyriboles and polysomatic reactions. *Amphiboles and other hydrous pyriboles, Reviews in Mineralogy* 9A, Mineralogical Society of America, 189–236.)

FIG. 18.28 HRTEM image of a disordered chain silicate, with chains of variable width aligned perpendicular to the plane of the photograph. The black regions represent the chains, and the white spots represent regions of low electron density between chains. The 2, 3, and 4 refer to double, triple, and quadruple chains, respectively. The precursor of this silicate material was an amphibole with double chains only. (From Buseck, P. R. and D. R. Veblen. 1978. Trace elements, crystal defects, and high resolution microscopy. *Geochimica et Cosmochimica Acta* 42: 669–78; see also Buseck, P. R. 1983. Electron microscopy of minerals. *American Scientist* 71: 175–85.) Compare this illustration with Fig. 10.10.

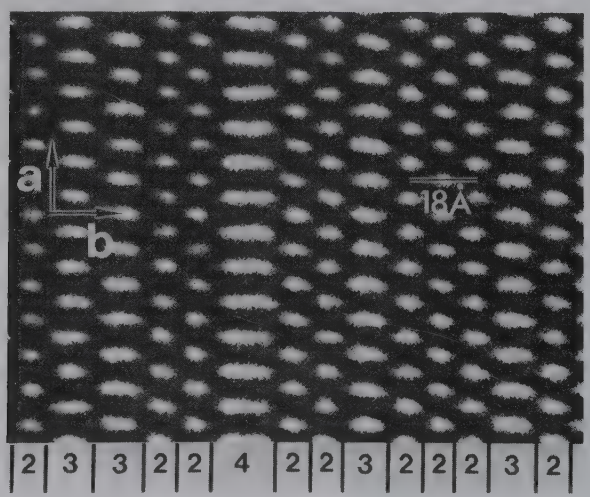

low-temperature alteration (and hydration) products of original enstatite and anthophyllite. They appear to be intermediate stages of structural development between pyroxenes (anhydrous, high-temperature minerals) and phyllosilicates (hydrous, lower-temperature minerals; see also Fig. 18.43). Many of the intermediate reaction products, however, turn out to be disordered rather than ordered structures. Figure 18.28 is an example of a random intergrowth of double, triple, and quadruple chain widths in a material whose precursor was an amphibole, with only double chain widths, prior to alteration. Solid state reactions, possibly as a result of low-temperature metamorphism, facilitated the wide chain construction.

PHYLLOSILICATES

As the derivation of the name of this important group implies (from the Greek word *phyllon* meaning *leaf*), most of its many members have a platy or flaky habit and one prominent cleavage. They are generally soft, of relatively low specific gravity, and may show flexibility or even elasticity of the cleavage lamellae. All these characterizing peculiarities arise from the dominance in the structure of the infinitely extended sheet of SiO_4 tetrahedra. In this sheet (see Fig. 18.3), three of the four oxygens in each SiO_4 tetrahedron are shared with neighboring tetrahedra, leading to a ratio of Si:O = 2:5. Each sheet, if undistorted, has sixfold symmetry.

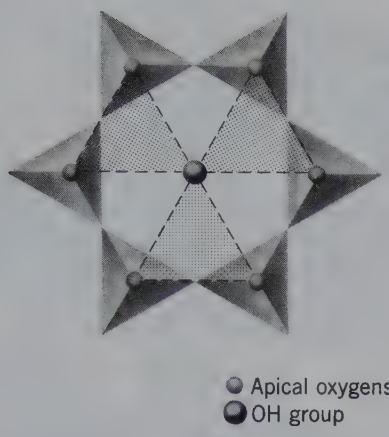

FIG. 18.29 Undistorted, hexagonal ring in an Si_2O_5 sheet showing the location of apical oxygens and (OH) group. In an ideal sheet structure the size of the triangles (outlined by shading) is the same as the size of triangular faces of XO_6 octahedra.

Most of the members of the phyllosilicates are hydroxyl bearing, with the (OH) group located in the center of the six-fold rings of tetrahedra, at the same height as the unshared apical oxygens in the SiO_4 tetrahedra (see Fig. 18.29). When ions, external to the Si_2O_5 sheet, are bonded to the sheets, they are coordinated to two oxygens and one OH, as shown in Fig. 18.29. The size of the triangle between two oxygens and one (OH) is just about the same as (but not identical to, see page 462) the triangular face of an XO_6 octahedron (with X commonly Mg or Al). This means that it is possible to bond to a regular net of apical oxygens and (OH) groups of $(Si_2O_5OH)^{3-}$ composition a sheet of regular octahedra, in which each octahedron is tilted onto one of its triangular sides (Fig. 18.30). When such tetrahedral and octahedral sheets are joined, the general geometry of the layered *lizardite* or *kaolinite* structures results (Fig. 18.31a).

The cations in the octahedral sheet may be divalent or trivalent. When the cations are divalent, for example, Mg or Fe^{2+}, the sheet will have the geometry of that of brucite (Fig. 16.7) in which each cation site is occupied. In such a sheet, six bonds, each with e.v. $= \frac{2}{6} = \frac{1}{3}$, originate from the Mg^{2+} ion. Three such bonds radiate from each oxygen, or (OH) group, thus, neutralizing one-half the charge of the oxygen but all of the OH. A sheet in which each oxygen or (OH) group is surrounded by three cations, as in the brucite, $Mg(OH)_2$, structure, is known as *trioctahedral*. When the cations in the octahedral sheet are trivalent, charge balance is maintained when one out of every three cations sites is unoccupied (see Fig. 18.31b). This is the case in gibbsite, $Al(OH)_3$, and corundum structures (Fig. 16.2; see page 370). Such a sheet structure in which each oxygen or (OH) group is surrounded only by two cations is known as *dioctahedral*. On the basis of the chemistry and geometry of the octahedral sheets, the phyllosilicates are divided into two major groups: *trioctahedral* and *dioctahedral*. (See the various interactive stacking animations in module I of the CD-ROM under the heading "Architecture of Layer Silicates.")

FIG. 18.30 Infinitely extending sheet of XO_6 octahedra. All octahedra lie on triangular faces.

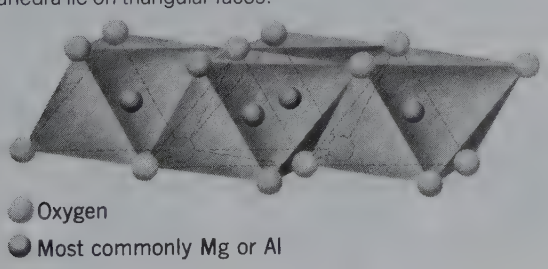

The geometries of an average Si_2O_5 sheet and a sheet of XO_6 octahedra are generally compatible, such that one can be bonded to the other. In terms of the chemistries of the octahedral and tetrahedral sheets, brucite, $Mg(OH)_2$, consists of two (OH) planes between which Mg is coordinated in octahedra. This is stated symbolically as $Mg_3\frac{(OH)_3}{(OH)_3}$. If two of the (OH) groups on one side of a brucite sheet are replaced by two apical oxygens of an Si_2O_5 sheet, $Mg_3\frac{Si_2O_5(OH)}{(OH)_3}$ results. This means that the $(OH)_3$-rich side of the sheet does not incorporate an Si_2O_5 sheet as shown in Fig. 18.31a. This is known as the *lizardite*, $Mg_3Si_2O_5(OH)_4$, structure. The equivalent structure with a dioctahedral sheet is *kaolinite*, $Al_2Si_2O_5(OH)_4$. In short, the antigorite and kaolinite structures are built of one tetrahedral ("*t*") and one octahedral ("*o*") sheet, giving *t–o* layers (see Fig. 18.34). Such *t–o* layers are electrically neutral and are bonded to one another by weak van der Waals bonds. In the lizardite and kaolinite structures, only one side of the octahedral sheet is coordinated to a tetrahedral sheet. However, other members of the phyllosilicate group are derived by joining tetrahedral sheets on both sides of the *o* sheet. This leads to *t–o–t* type layers (Fig. 18.32) as in *talc*, $Mg_3Si_4O_{10}(OH)_2$, and *pyrophyllite*, $Al_2Si_4O_{10}(OH)_2$. Begin with brucite, $Mg_3\frac{(OH)_3}{(OH)_3}$, and replace two (OH) groups in both the upper and lower (OH) planes by two oxygens of Si_2O_5 sheets, which results in $Mg_3\frac{Si_2O_5(OH)}{Si_2O_5(OH)}$ or $Mg_3Si_4O_{10}(OH)_2$, talc. Similarly, gibbsite, $Al_2\frac{(OH)_3}{(OH)_3}$, would result in $Al_2\frac{Si_2O_5(OH)}{Si_2O_5(OH)}$ by replacement of two out of three (OH) groups in the (OH)

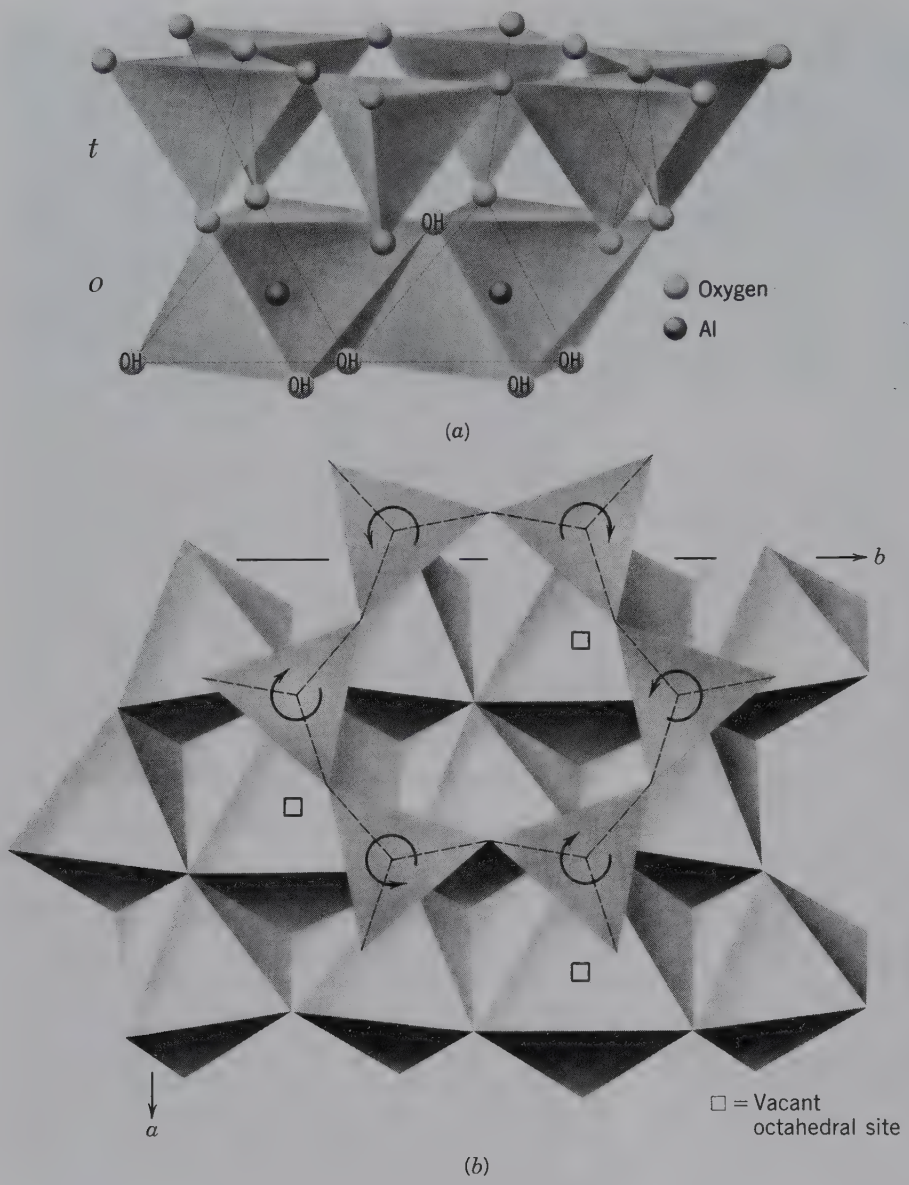

FIG. 18.31 (a) Diagrammatic sketch of the structure of kaolinite with a tetrahedral sheet bonded on one side by an octahedral sheet. (From Grim, R. E. 1968. *Clay Mineralogy.* McGraw-Hill Book Co, New York). (b) Plan view of the structure of muscovite in which the overall dimensions of an octahedral sheet are somewhat smaller than those of an idealized tetrahedral sheet. To accommodate this slight misfit, the SiO_4 tetrahedra in the tetrahedral sheet are rotated (in opposite directions as shown by the arrows) about axes normal to the sheet. This changes the shape of the six-membered tetrahedral rings from hexagonal to trigonal. The octahedra marked with a square are vacant (see discussion of dioctahedral micas). (From Bailey, S. W. 1984. Crystal structure of the true micas. *Micas, Reviews in Mineralogy* 13: 13–60, Mineralogical Society of America, Washington, D.C.)

planes by oxygens of Si_2O_5 sheets; this leads to pyrophyllite, $Al_2Si_4O_{10}(OH)_2$ (see Figs. 18.32 and 18.34). The *t–o–t* layers are electrically neutral and form stable structural units that are joined to each other by van der Waals bonds. Because this is a very weak bond, such structures have excellent cleavage, easy gliding, and greasy feel, as found in the minerals talc and pyrophyllite.

Other phyllosilicate structures are developed when Al is substituted for some of the Si in the tetrahedral sites of the Si_2O_5 sheets. Because Al is trivalent, whereas Si is tetravalent, each substitution of this kind causes a free electrical charge to appear on the surface of the *t–o–t* layer. If Al substitutes for every fourth Si, a charge of significant magnitude is produced to bind univalent cations (*interlayer cations*), in regular 12-coordination to *t–o–t* layers (see Fig. 18.34). By virtue of these *t–o–t*-interlayer cation bonds, the structure is more firmly held together, the ease of gliding is diminished, the hardness is increased, and the slippery feel is lost. The resulting mineral structures are those of the true *micas* (see Figs. 18.31b, 18.33, and 18.34). In the trioctahedral group of micas, the univalent interlayer cation is K^+; in the dioctahedral group, the cation can be K^+, as in muscovite, or Na^+, as in paragonite. In the micas, *one* of the aluminums belongs in the tetrahedral sheet and the formulae are written accordingly. Thus,

Trioctahedral	$KMg_3(AlSi_3O_{10})(OH)_2$	Phlogopite
Dioctahedral	$KAl_2(AlSi_3O_{10})(OH)_2$	Muscovite

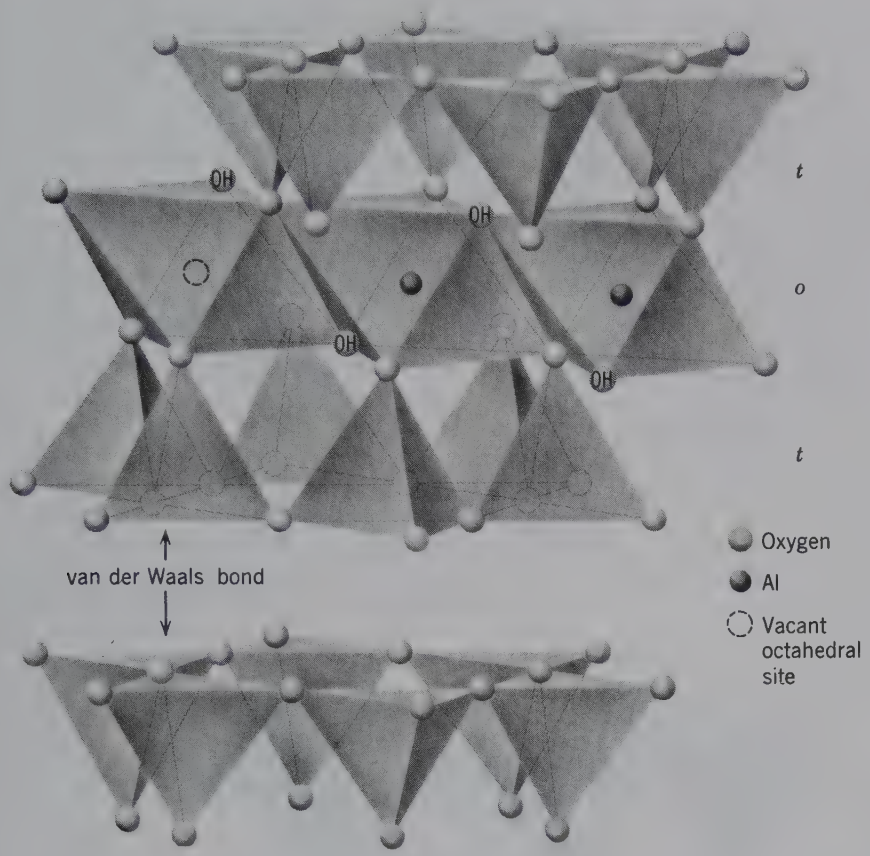

FIG. 18.32 Diagrammatic sketch of a *t–o–t* type layer as in pyrophyllite (after Grim, 1968).

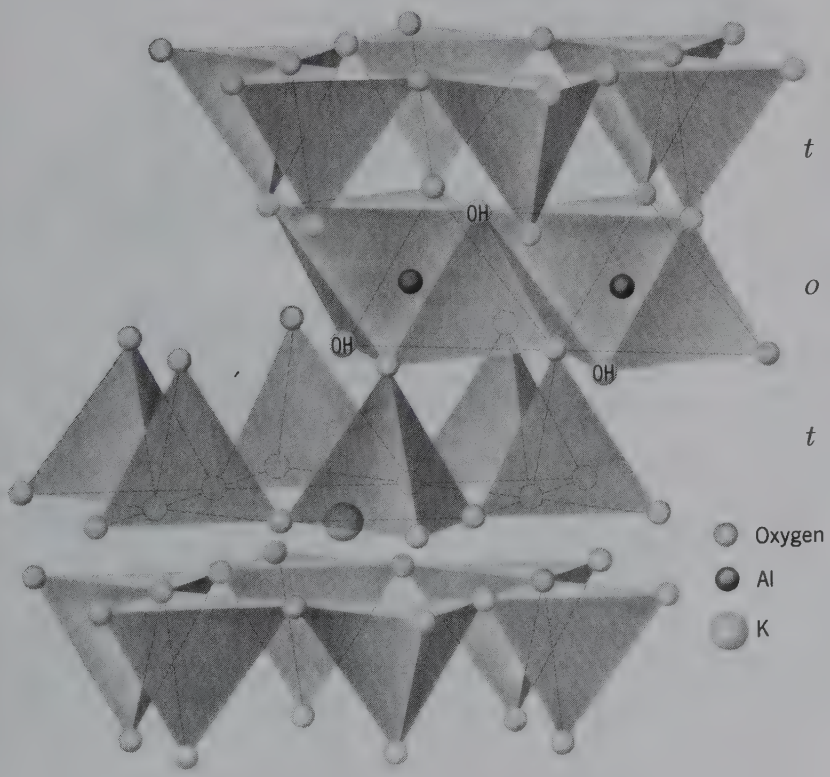

FIG. 18.33 Diagrammatic sketch of the muscovite structure (after Grim, 1968).

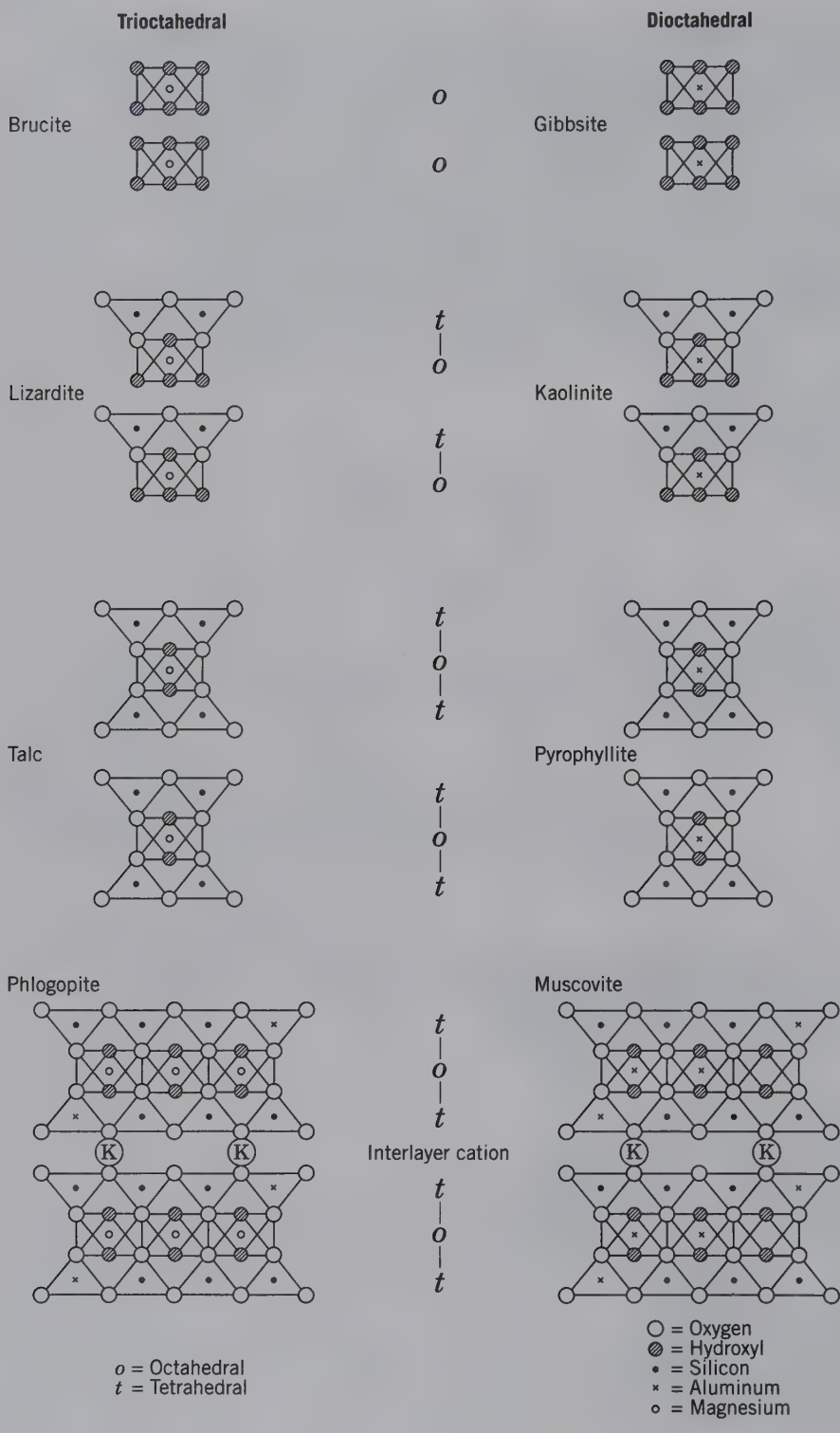

FIG. 18.34 Schematic development of some of the phyllosilicate structures (compare with Fig. 19.65).

If half the Si in the tetrahedral sites of the Si_2O_5 sheets is replaced by Al, two charges per *t–o–t* layer become available for binding an interlayer cation. Such ions as Ca^{2+}, and, to a smaller extent, Ba^{2+}, may enter between two layers of the mica structure (see Fig. 19.65). The interlayer cations are held by stronger ionic bonds and the quality of the cleavage is diminished, the hardness increased, the flexibility of the layers is almost lost, and the density is increased. The resulting minerals are the *brittle micas*, typified by

Trioctahedral	$CaMg_3(Al_2Si_2O_{10})(OH)_2$	Clintonite
Dioctahedral	$CaAl_2(Al_2Si_2O_{10})(OH)_2$	Margarite

There is little solid solution between members of the dioctahedral and trioctahedral groups, although there may be extensive and substantially complete ionic substitution of Fe^{2+} for Mg, of Fe^{3+} for Al, and of Ca for Na in appropriate sites. Ba may replace K, Cr may substitute for Al, and F may replace OH to a limited extent. Mn, Ti, and Cs are rarer constituents of some micas. The lithium micas are structurally distinct from muscovite and biotite because of the small lithium ion.

Additional members of the phyllosilicate group can be developed. The important group of *chlorites* may be viewed as consisting of two sheets of talc (or pyrophyllite) separated by a brucite- (or gibbsite-) like octahedral sheet (see Figs. 18.35 and 19.65). This leads to a formula such as $Mg_3Si_4O_{10}(OH)_2{\cdot}Mg_3(OH)_6$. However, in most chlorites, Al, Fe^{2+}, and Fe^{3+} substitute for Mg in octahedral sites both in the talc and brucite-like sheets, and Al substitutes for Si in the tetrahedral sites. A more general chlorite formula would be:

$$(Mg,Fe^{2+},Fe^{3+},Al)_3(Al,Si)_4O_{10}(OH)_2\text{-}(Mg,Fe^{2+},Fe^{3+},Al)_3(OH)_6$$

The various members of the chorite group differ from one another in amounts of substitution and the manner

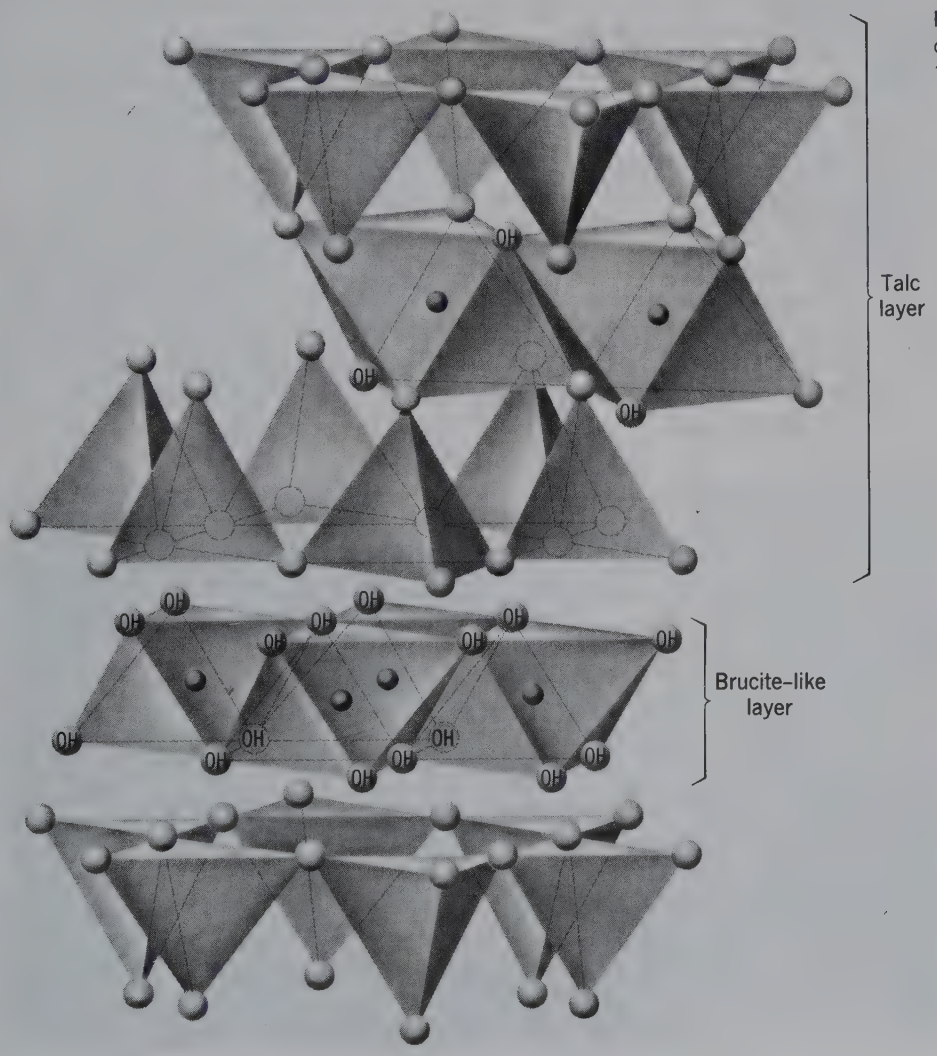

FIG. 18.35 Diagrammatic sketch of the structure of chlorite (after Grim, 1968).

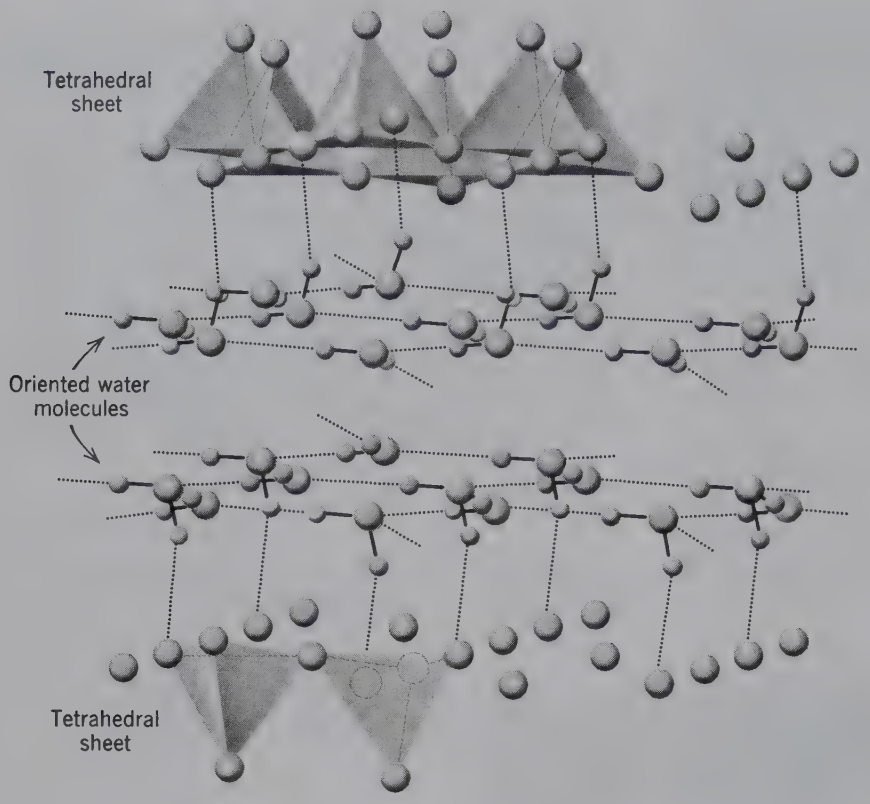

FIG. 18.36 Diagrammatic sketch of the vermiculite structure, showing layers of water (after Grim, 1968).

in which the successive octahedral and tetrahedral layers are stacked along the *c* axis.

The *vermiculite* minerals may be derived from the talc structure by interlamination of water molecules in definite sheets 4.98 Å thick, which is about the thickness of two water molecules (see Fig. 18.36). An example of a specific vermiculite formula would be $Mg_3(Si,Al)_4O_{10}(OH)_2{\cdot}4.5H_2O[Mg]_{0.35}$ in which [Mg] represents exchangeable ions in the structure. The presence of exchangeable ions located between layers of H_2O molecules, and the ability of the structure to retain variable amounts of H_2O, are of great importance in agriculture. When the vermiculite structure is saturated with H_2O, the basal spacing is approximately 14.8 Å. This water can be gradually extracted as shown by a discontinuous collapse sequence along the *c* axis, leading to a basal spacing of about 9.0 Å for a vermiculite without interlayer water. The structure of the *smectite* group is derived from the pyrophyllite structure by insertion of sheets of molecular water containing exchangeable cations between the pyrophyllite *t–o–t* layers, leading to a structure that is essentially identical to that of vermiculite. The members of the vermiculite and montmorillonite groups exhibit an unrivaled capacity for swelling when wetted because of their ability to incorporate large amounts of interlayer water (see also Box 19.3).

If occasional random substitution of aluminum for silicon in the tetrahedral sites of pyrophyllite sheets takes place, there may not be enough of an aggregate charge on the *t–o–t* layers to produce an ordered mica structure with all possible interlayer cation sites filled. Locally, however, occasional cation sites may be occupied, leading to properties intermediate between those of clays and micas. Introduction of some molecular water may further complicate this picture. K-rich minerals of this type, intermediate between montmorillonite clays and the true micas, are referred to as *alkali-deficient* micas, of which *illite* is an example.

It was suggested that there is a good geometric fit between an octahedral brucite sheet and a tetrahedral Si_2O_5 sheet (see Figs. 18.34 and 19.65). In detail, however, there is a considerable mismatch between a brucite sheet and an undistorted Si_2O_5 sheet with hexagonal rings. The misfit is due to the fact that the edges of an $Mg(OH)_6$ octahedron in the brucite sheet are somewhat greater than the distances between apical oxygens in the Si_2O_5 or $(Si,Al)_2O_5$ sheet; this means that the geometry shown in Fig. 18.29 is an oversimplification. In the case of the *serpentine minerals*, *antigorite* and *chrysotile*, both $Mg_3Si_2O_5(OH)_4$, this misfit is compensated for by a bending (stretching of the distance between apical oxygens) of the tetrahedral sheet to provide a better fit with the adjoining octahedral

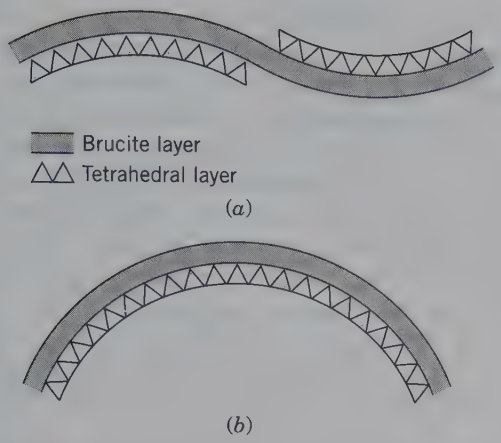

FIG. 18.37 (a) Diágrammatic sketch of the antigorite structure as viewed along the *b* axis, showing curved *t* and *o* sheets. (b) Highly schematic representation of the possible curvature in the chrysotile structure.

brucite sheet (see Fig. 18.37). In the variety *antigorite*, the bending is not continuous but occurs as corrugations. In the fibrous variety, *chrysotile*, the mismatch is resolved by a continuous bending of the structure into cylindrical tubes (see Figs. 18.38 and 18.39). These high-magnification electron micrographs reveal the existence of tubelike structures for the layers that occur in essentially parallel sheets in the kaolinite group.

In order to join the *t* sheet to a brucite *o* layer, or to an *o–t* sequence so as to produce *t–o* or *t–o–t* type layers, the octahedral sheet is staggered with respect to the tetrahedral sheets (see any of the phyllosilicate illustrations). This stagger reduces the symmetry of the overall

FIG. 18.38 Electron micrograph showing tubular fibers of chrysotile from Globe, Arizona. Magnification 35,000×. (After Hagy, B. and G. T. Gaust. 1956. Serpentines: Natural mixtures of chrysotile and antigorite. *American Mineralogist* 41: 817–38.)

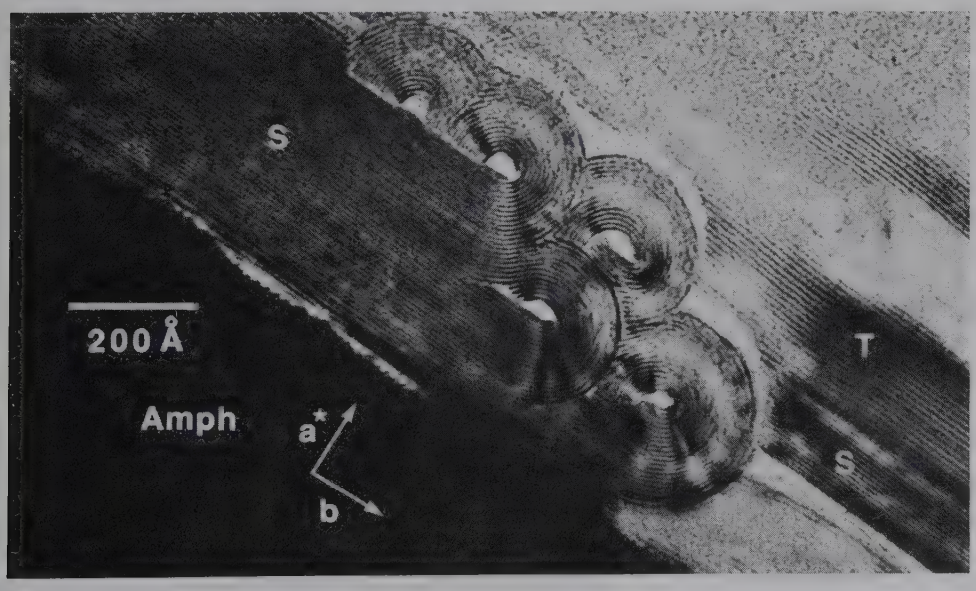

FIG. 18.39 HRTEM image of an intergrowth of planar and coiled structures in serpentine. The planar serpentine (S) is seen ending in rolls of *chrysotile*. Talc (T) is interlayered with the planar serpentine, *lizardite*. The two types of serpentine are formed against grains of amphibole (Amph). (From Veblen, D. R. and P. R. Buseck. 1979. Serpentine minerals: Intergrowths and new combination structures. *Science* 206: 1398–1400; copyright © 1979 by the AAAS. See also Buseck, P. R., 1983. Electron microscopy of minerals. *American Scientist* 71: 175–85.)

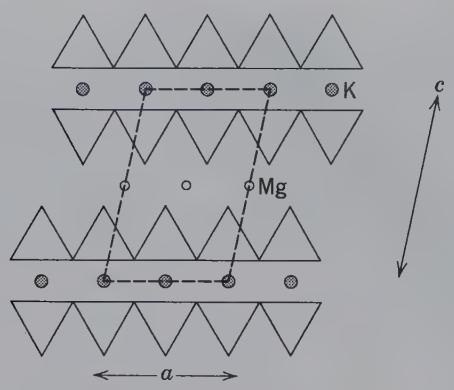

FIG. 18.40 Schematic projection along the *b* axis of the mica structure. Note stagger of *t* and *o* sheets with respect to each other. Unit cell is outlined by dashed lines.

structure to monoclinic (see Fig. 18.40), even though the tetrahedral sheets contain hexagonal holes. Most of the phyllosilicates, therefore, have monoclinic structures, some are triclinic, and a few orthorhombic or trigonal.

Because of the hexagonal to trigonal symmetry about the (OH) group in the $Si_2O_5(OH)$ tetrahedral sheets, there are three alternate directions (see Fig. 18.41) in which $Si_2O_5(OH)$ sheets can be stacked. These three directions can be represented by three vectors (1, 2, and 3; and negative directions $\bar{1}$, $\bar{2}$, and $\bar{3}$) at 120° to each other. If the stacking of $Si_2O_5(OH)$ sheets is always in the same direction (see Fig. 18.41b and Chapter 12 "Polytypism" and module I of the CD-ROM for various stacking polytype sequences under the heading "Polytypism"), the resulting structure will have monoclinic symmetry, with space group $C2/m$; this is referred to as the $1M$ (M = monoclinic) *polytype* with stacking sequence [1]. If the stacking sequence of $Si_2O_5(OH)$ sheets consists of alternating 1 and $\bar{1}$ directions (in opposing directions along the same vector), a structure results, which is best described as orthorhombic with space group $Ccm2_1$. This stacking sequence can be expressed as $\{1\bar{1}\}$ and the polytype is known as $2O$ (O = orthorhombic). If the stacking sequence consists of two vectors at 60° to each other, that

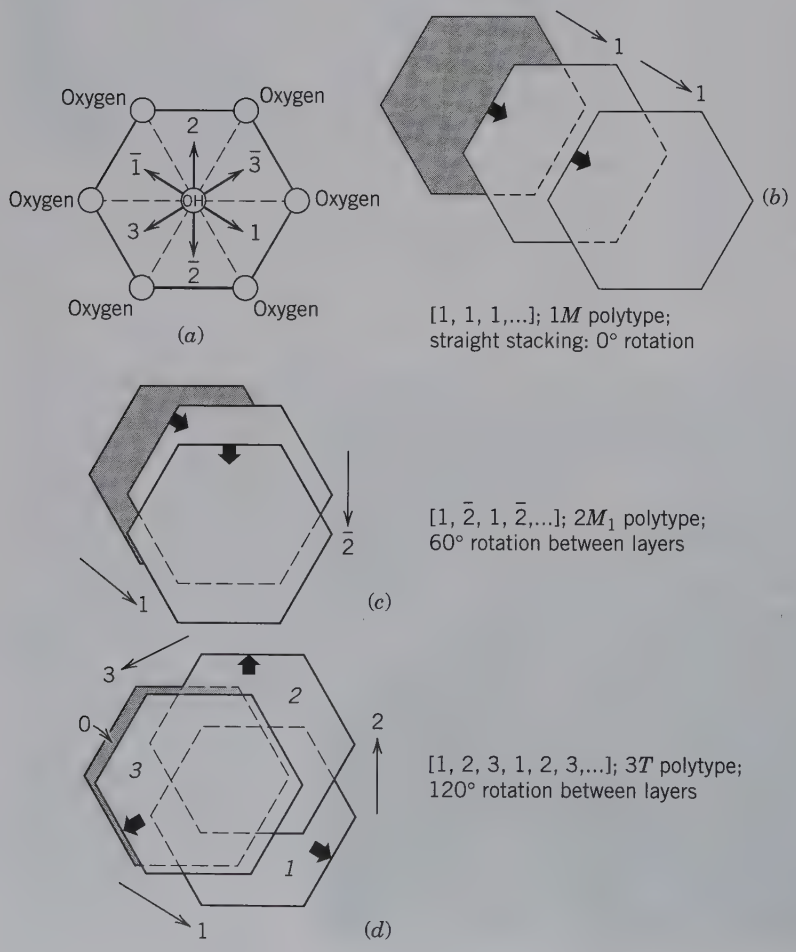

FIG. 18.41 Schematic illustration of some possible stacking polymorphs (*polytypes*) in mica. (a) Three vectorial directions for possible location of the (OH) group in an $Si_2O_5(OH)$ sheet, which is stacked above or below the hexagonal ring shown. (b) Stacking of $Si_2O_5(OH)$ sheets in the same direction. (c) Stacking in two directions at 60° to each other. (d) Stacking in three directions at 120° to each other. Here, sheet *3* should lie directly above sheet *o* but is offset slightly for illustrative purposes.

is $\{1\bar{2}\}$, another monoclinic polytype results; this is known as $2M_1$ with space group $C2/c$ (see Fig. 18.41c). When all three vectors come into play, such as in [123], a trigonal polytype, $3T$ (T = trigonal), results, which is compatible with either of two enantiomorphic space groups: $P3_112$ or $P3_212$. Additional *polytype* stacking sequences are possible, but most micas that commonly show *polytypism* belong to $1M$ ($C2/m$), $2M_1(C2/c)$, or $3T(P3_112)$ polytypes. Polytypism (see also page 274) is found in many layer silicates, among them serpentine, mica, and chlorite. Figure 18.42a illustrates two different polytypes for planar serpentine structures, and Fig. 18.42b shows two different polytypes of mica.

The importance of the phyllosilicates lies in part in the fact that the products of rock weathering, and hence the constituents of soils, are mostly of this structural type. The release and retention of plant nutrients, the stockpiling of water in the soil from wet to dry seasons, and the accessibility of the soil to atmospheric gases and organisms depend in large part on the properties of the sheet silicates.

Geologically, the phyllosilicates are of great significance. The micas are the primary minerals of schists and are widespread in igneous rocks. They form at lower temperatures than amphiboles or pyroxenes and frequently are formed as replacements of earlier minerals as a result

FIG. 18.42 (a) Two different polytypes (different stackings of *t–o* sheets along the *c* crystallographic axis) for planar serpentine.

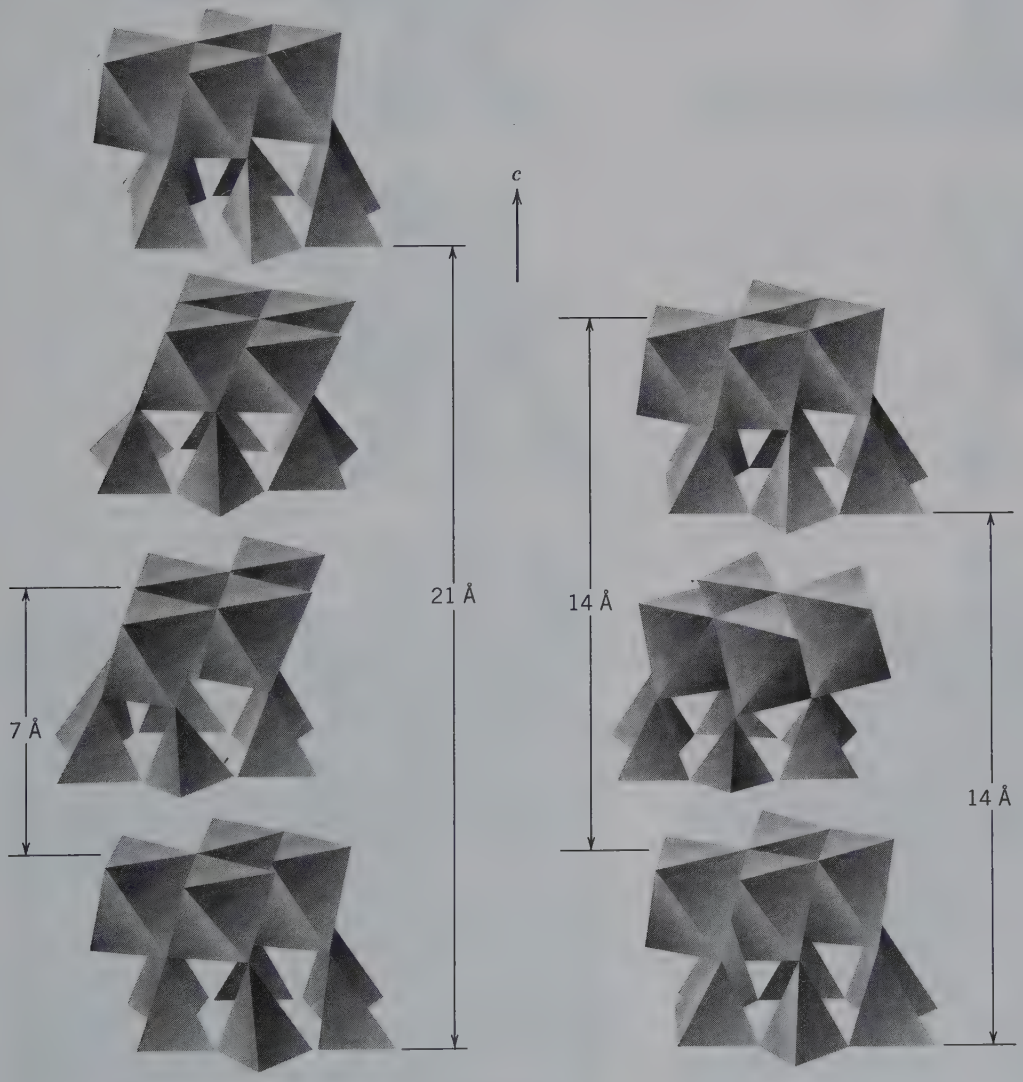

(*a*)

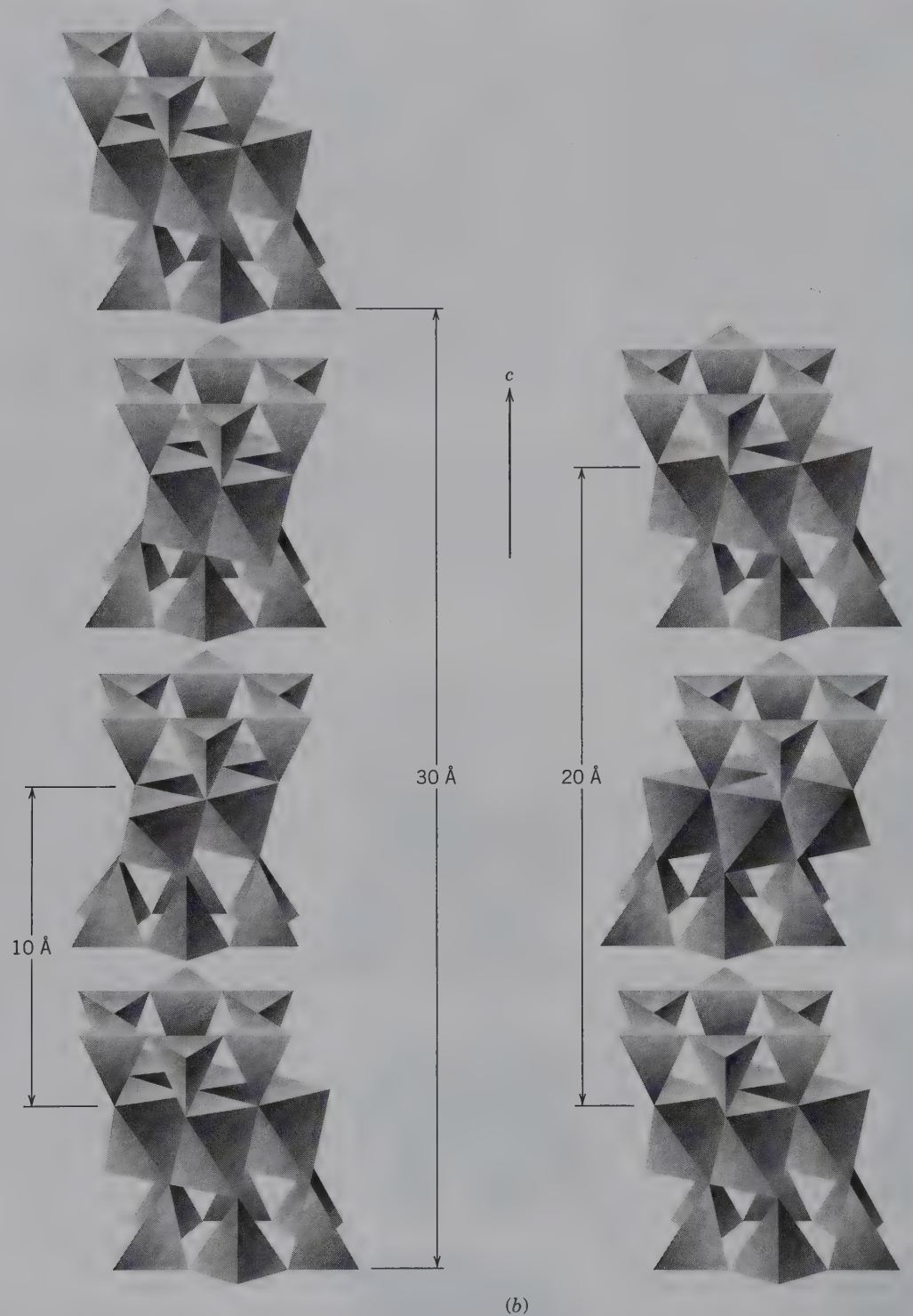

(*b*)

FIG. 18.42 (*continued*) (b) Two different polytypes for mica. (a and b from Bailey, S. W. 1988. X-ray diffraction identification of the polytypes of mica, serpentine, and chlorite. *Clays and Clay Minerals* 36: 193–213.)

of hydrothermal alteration. The chemical changes and structural transformations that take place in such alteration reactions are complex. Figure 18.43 is a schematic representation of the various reaction paths an originally high-temperature pyroxene (of igneous origin) might take during lower-temperature reactions (such as alteration by hydrothermal solutions). The lower-temperature end products, marked on the far right of the diagram, are layer silicates. The intermediate reaction products are mainly amphiboles, but also various pyri-

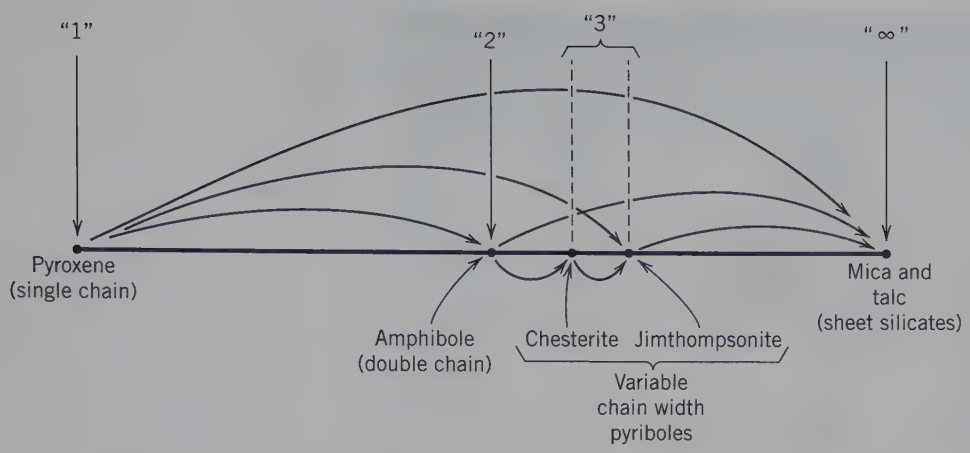

FIG. 18.43 The many possible reaction paths that lead from a high-temperature pyroxene to lower-temperature sheet silicates. Chesterite, and jimthompsonite are pyriboles. "1," "2," and "3" refer to chain width: "1" in pyroxenes, "2" in amphiboles, and "3" in biopyriboles with variable chain widths; "∞" means infinite chain width, resulting in sheets (see also Figs. 18.26 and 18.27). (From Veblen, D. R. and P. R. Buseck. 1981. Hydrous pyriboles and sheet silicates in pyroxenes and uralites: Intergrowth microstructures and reaction mechanisms. *American Mineralogist* 66: 1107–1134.)

boles (see Figs. 18.26 and 18.27 and related text). Figure 18.44 gives two high-resolution transmission electron microscope (HRTEM) structure images for igneous pyroxenes from the Palisades Sill, New Jersey. Figure 18.44a shows the presence of a triple chain pyribole between a relict (unaltered) augite and sheet silicate which is mainly talc. The pyribole material appears to be an intermediate product in the reaction sequence: pyroxene → triple chain silicate → talc (see Fig. 18.43). In Fig. 18.44b talc appears to have directly replaced orthopyroxene along a fracture.

TECTOSILICATES

Approximately 64% of the rocky crust of the Earth is made up of minerals built about a three-dimensional framework of linked SiO_4 tetrahedra (see Fig. 18.1). These minerals belong to the *tectosilicate* class in which all the oxygen ions in each SiO_4 tetrahedron are bridging oxygens that are shared with neighboring tetrahedra. This results in a stable, strongly bonded structure in which the ratio of Si : O is 1 : 2 (Fig. 18.3).

FIG. 18.44 HRTEM images of altered pyroxenes. (a) A complex intergrowth of high-temperature pyroxene (Px), and alteration products of talc and triple-chain silicate ("3" = pyribole). (b) Direct replacement of original orthopyroxene (Opx) by later talc along a fracture. (From Veblen, D. R. and P. R. Buseck. 1981. Hydrous pyriboles and sheet silicates in pyroxenes and uralites: Intergrowth microstructures and reaction mechanisms. *American Mineralogist* 66: 1107–1134.)

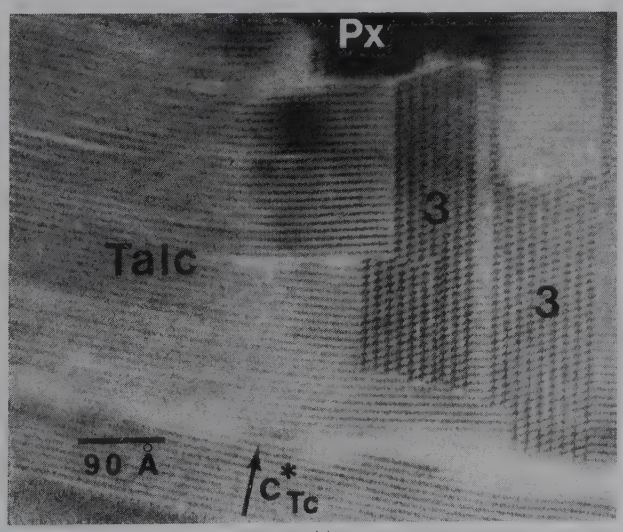

(*a*)

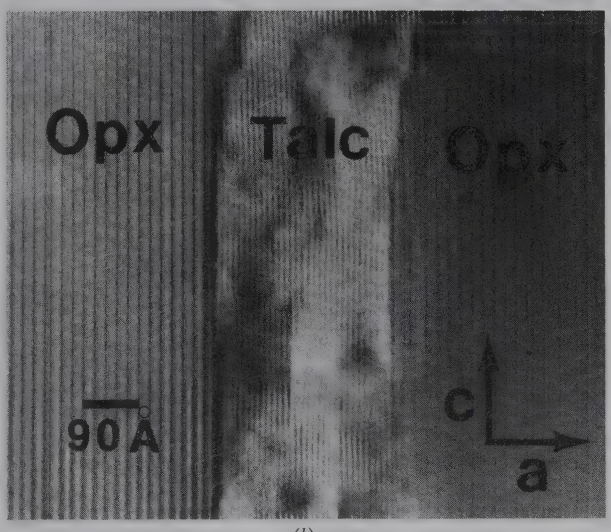

(*b*)

Table 18.3 Polymorphs of SiO_2

Name	Symmetry	Space Group	Specific Gravity	Refractive Index (Mean)
Stishovite*	Tetragonal	$P4_2/mnm$	4.35	1.81
Coesite	Monoclinic	$C2/c$	3.01	1.59
Low (α) quartz	Hexagonal	$P3_221$ (or $P3_121$)	2.65	1.55
High (β) quartz	Hexagonal	$P6_222$(or $P6_422$)	2.53	1.54
Keatite (synth.)	Tetragonal	$P4_12_12$ (or $P4_32_12$)	2.50	1.52
Low (α) tridymite	Monoclinic or Orthorhombic	$C2/c$ (or Cc) $C222_1$	2.26	1.47
High (β) tridymite	Hexagonal	$P6_3/mmc$	2.22	1.47
Low (α) cristobalite	Tetragonal	$P4_12_12$ (or $P4_32_12$)	2.32	1.48
High (β) cristobalite	Isometric	$Fd3m$	2.20	1.48

*Only polymorph with Si in octahedral coordination with oxygen.

SiO_2 GROUP

An SiO_2 framework that does not contain other cations is electrically neutral. There are at least nine different ways in which such a framework can be built. These modes of geometrical arrangement correspond to nine known polymorphs of SiO_2, one of which is synthetic (see Table 18.3). Each of these polymorphs has its own space group, cell dimensions, characteristic morphology, and lattice energy. Which polymorph is stable is determined primarily by energy considerations; the higher-temperature forms with great lattice energy possess the more expanded structures that are reflected in lower specific gravity and refractive index. In addition to the nine polymorphs of SiO_2 there are two related and essentially amorphous substances, *lechatelierite*, a high silica glass of variable composition, and *opal*, $SiO_2 \cdot nH_2O$, with a locally ordered structure of silica spheres and highly variable H_2O content. At low temperatures in sedimentary basins, amorphous silica (opal-A) transforms to macrocrystalline low (α) quartz through a series of intermediate disordered phases: opal-A → opal CT (cristobalite-tridymite) → chalcedony → α-quartz (Heaney, 1994). These phases are widely distributed in the oil-bearing rocks of the Monterey Formation in California.

The principal, naturally occurring SiO_2 polymorphs fall into three structural categories: *low quartz*, with the lowest symmetry and the most compact structure; *low tridymite*, with higher symmetry and a more open structure; and *low cristobalite*, with the highest symmetry and the most expanded structure of the three polymorphs. These polymorphs are related to each other by reconstructive transformations, a process that requires considerable energy (refer to p. 269). The sluggishness and energy requirements of reconstructive transformations allow the phases to exist metastably for long periods of time. The temperatures of reconstructive inversions vary widely, depending chiefly on the rate and direction of temperature change. Each of the three structure types mentioned previously has also a high–low inversion, as shown by the existence of high and low quartz, high and low tridymite, and high and low cristobalite (see Table 18.3). These transformations are displacive; they take place quickly and reversibly at a fairly constant and sharply defined temperature of inversion and may be repeated over and over again without physical disintegration of the crystal. The nearly instant high → low inversions take place with the release of a fairly constant amount of energy; very near the same temperature the low → high inversions take place with the absorption of energy (see Table 18.4). The structures of several SiO_2 polymorphs are illustrated in Fig. 18.45 (see Fig. 12.5 for high and low quartz structures).

Table 18.4 Inversion Temperatures for Displacive Transformations in Some SiO_2 Polymorphs

High *T* Polymorph	Minimum Crystallization *T* for Stable Form at 1 Atmosphere *P*	Inversion to Low *T* Form at 1 Atmosphere *P*
High cristobalite	1470°C	~268°C
High tridymite	870°C	~120°–140°C
High quartz	574°C	573°C

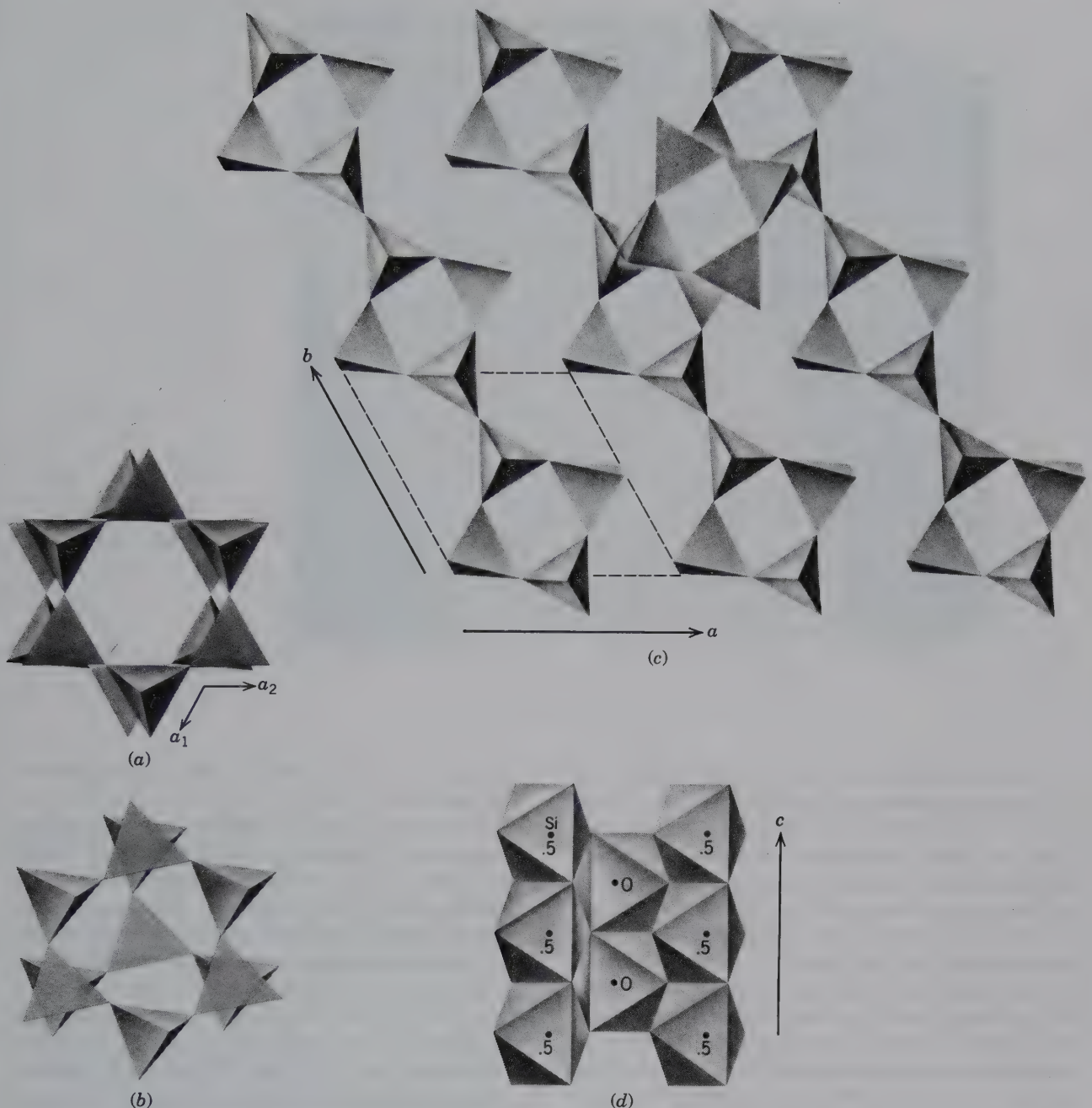

FIG. 18.45 Structures of some polymorphs of SiO_2 (see Fig. 12.5 for illustration of low and high quartz structures). (a) Tetrahedral layers in high tridymite projected onto (0001). (b) Portion of the high cristobalite structure projected onto (111). (c) Coesite structure showing four-membered tetrahedral rings that lie parallel to (001). (d) Structure of stishovite, with Si in octahedral coordination with oxygen, projected on (100) (a, b, c, and d after Papike, J. J. and M. Cameron. 1976. Crystal chemistry of silicate minerals of geophysical interest. *Reviews of Geophysics and Space Physics* 14: 37–80.)

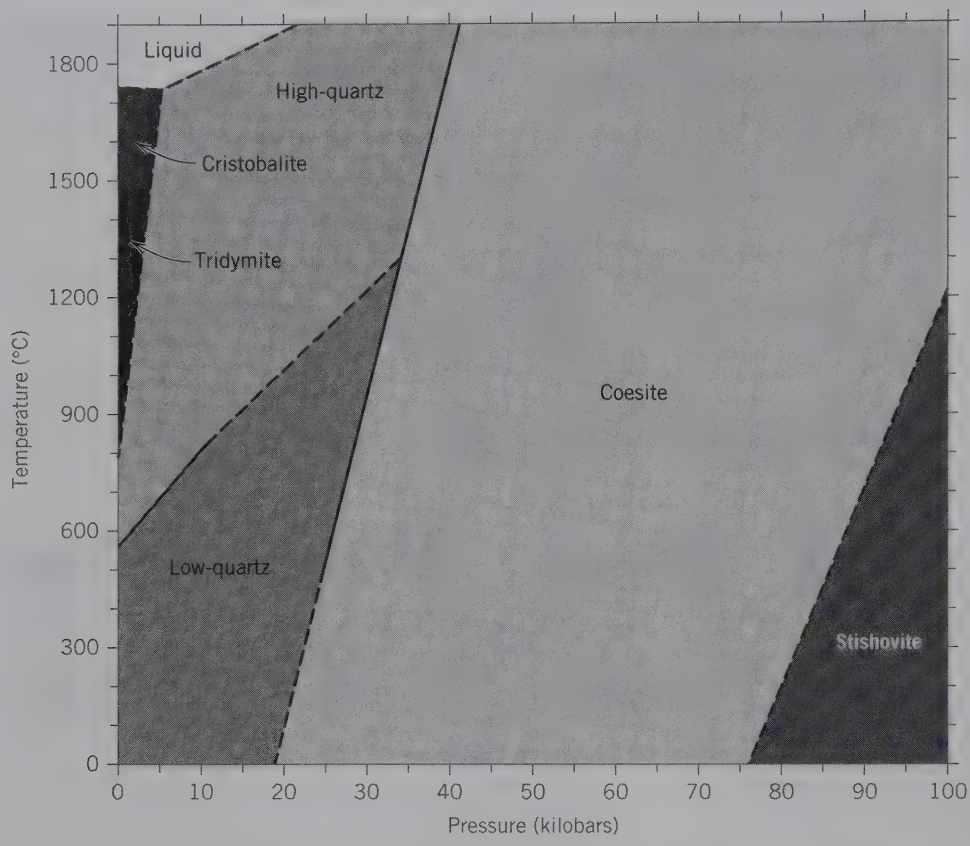

FIG. 18.46 Stability relations of the SiO_2 polymorphs.

The low-temperature form of each of the displacive polymorphic pairs has a lower symmetry than the higher-temperature form (see Table 18.3), but this symmetry change is less than in the reconstructive transformations. The effect of increased pressure is to raise all inversion temperatures and for any temperature to favor the crystallization of the polymorph most economical of space (Fig. 18.46).

The most dense of the silica polymorphs are *coesite* and *stishovite*. *Coesite* was synthesized in 1953 and *stishovite*, which is isostructural with rutile, TiO_2, in 1961 and it was not until later that they were found in nature. They have both been identified in small amounts at Meteor Crater, Arizona. Their formation is attributed to the high pressure and high temperature resulting from the impact of a meteorite. *Coesite* has been found in ultrahigh pressure metamorphic rocks that form at P over ~30kb (see Fig. 11.4c and related text). *Keatite* has not been found in nature.

FELDSPAR GROUP

When Al^{3+} substitutes for Si^{4+} in the framework structure, a coupled substitution is required to maintain charge balance. Consequently, large monovalent or divalent cation can enter the SiO_2 framework to produce feldspar.

The compositions of the majority of common feldspars can be expressed in terms of the system $KAlSi_3O_8$ (orthoclase; Or)–$NaAlSi_3O_8$ (albite; Ab)–$CaAl_2Si_2O_8$ (anorthite; An). The members of the series between $KAlSi_3O_8$ and $NaAlSi_3O_8$ are known as the *alkali feldspars* and the members in the series between $NaAlSi_3O_8$ and $CaAl_2Si_2O_8$ as the *plagioclase feldspars*. Members of both of these feldspar groups are given specific names, between specific compositions, as shown in Fig. 18.47. The chemical compositions of feldspars in this ternary system are generally expressed in terms of molecular percentages or Or, Ab, and An; for example, $Or_{20}Ab_{75}An_5$. Barium feldspars, such as *celsian*, $BaAl_2Si_2O_8$, and *hyalophane*, $(K,Ba)(Al,Si)_2Si_2O_8$, are relatively rare. All feldspars show good cleavages in two directions which make an angle of 90°, or close to 90°, with each other. Their hardness is about 6, and specific gravity ranges from 2.55 to 2.76 (excluding the Ba feldspars).

The unambiguous characterization of a feldspar requires a knowledge of the chemical composition and of the structural state of the species. The structural state, which refers to the Al and Si distribution in tetrahedral sites of the framework structure, is a function of

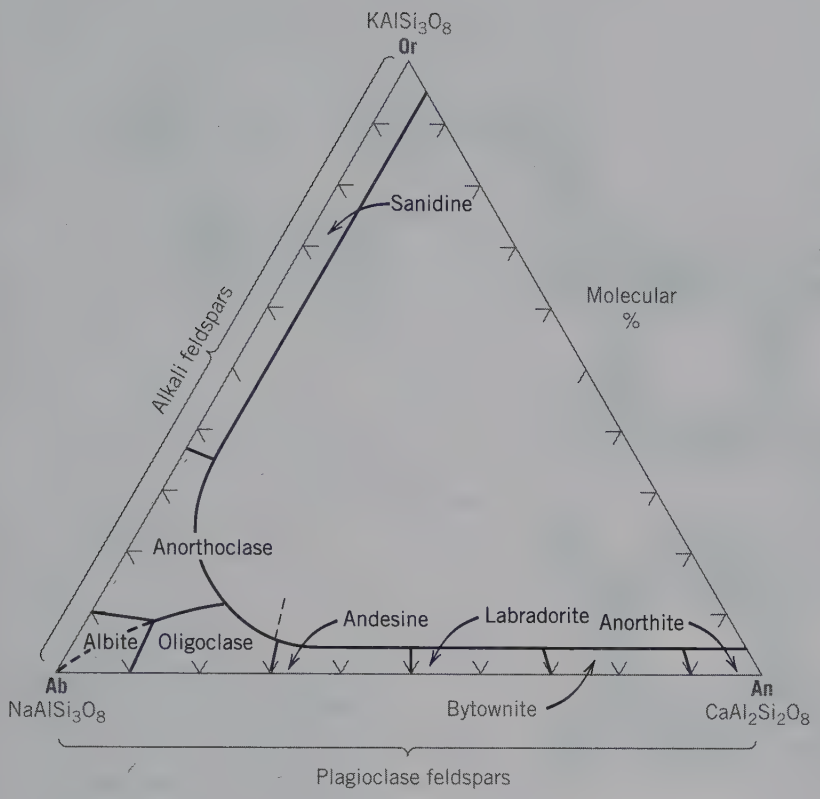

FIG. 18.47 Nomenclature for the plagioclase feldspar series and the high-temperature alkali feldspars. (After Deer, W. A., R. A. Howie, and J. Zussman. 1963, *Rock-Forming Minerals* 4. Wiley, New York, 2.)

the crystallization temperature and subsequent thermal history of a feldspar. In general, feldspars that cooled rapidly after crystallization at high temperature show a disordered Al–Si distribution (high structural state) as discussed in Chapter 12, p. 273. Those that cooled very slowly from high temperatures or those that crystallized at low temperatures generally show an ordered Al–Si distribution (low structural state).

Structure

The feldspar structure, similar to the structures of the various polymorphs of SiO_2, consists of an infinite network of SiO_4 as well as AlO_4 tetrahedra. The feldspar structure can be considered a "stuffed" derivative of the SiO_2 structures, by incorporation of Al into the tetrahedral network, and concomitant housing of Na^+ (or K^+ or Ca^{2+}) in available voids. When only one Si^{4+} (per feldspar formula unit) is substituted by Al^{3+}, the structure can be neutralized by incorporating one K^+ or one Na^+. Similarly when two Si^{4+} (per feldspar formula unit) are substituted for by Al^{3+}, the electrostatic charge of the network can be balanced by a divalent cation, such as Ca^{2+}, as follows:

$$Si_4O_8 \text{ framework} \rightarrow Na(AlSi_3O_8) \rightarrow Ca(Al_2Si_2O_8)$$

In the plagioclase structures, the amount of tetrahedral Al varies in proportion to the relative amounts of Ca^{2+} and Na^+ so as to maintain electrical neutrality; the more Ca^{2+}, the greater the amount of Al^{3+}.

The general architecture of the feldspar structure is illustrated by the high-temperature polymorph of $KAlSi_3O_8$, *sanidine*, with space group *C2/m* (see Fig. 18.48). In this structure, the Al–Si distribution is completely disordered, meaning that the Al and Si ions are randomly distributed among the two crystallographically distinct tetrahedral sites, *T1* and *T2*. The K^+ ions, bonded to the nine nearest oxygens in large interstices, occupy special positions on mirror planes perpendicular to the *b* axis. The Si–Al tetrahedral framework consists of four-membered rings of tetrahedra that are linked into chains (of a double crankshaft type) parallel to the *a* axis (see Fig. 18.49). The square, blocky outline of these chains, imparted by the four-membered rings, is responsible for the right-angled cleavage and pseudotetragonal habit characteristic of feldspar. The structure of *microcline*, a low-temperature polymorph of $KAlSi_3O_8$, has triclinic symmetry (space group *C*1) and lacks the mirror planes and rotation axes of sanidine as shown in Fig. 18.48. In other words, its structure is less symmetric and the K^+ ions are no longer located in special positions.

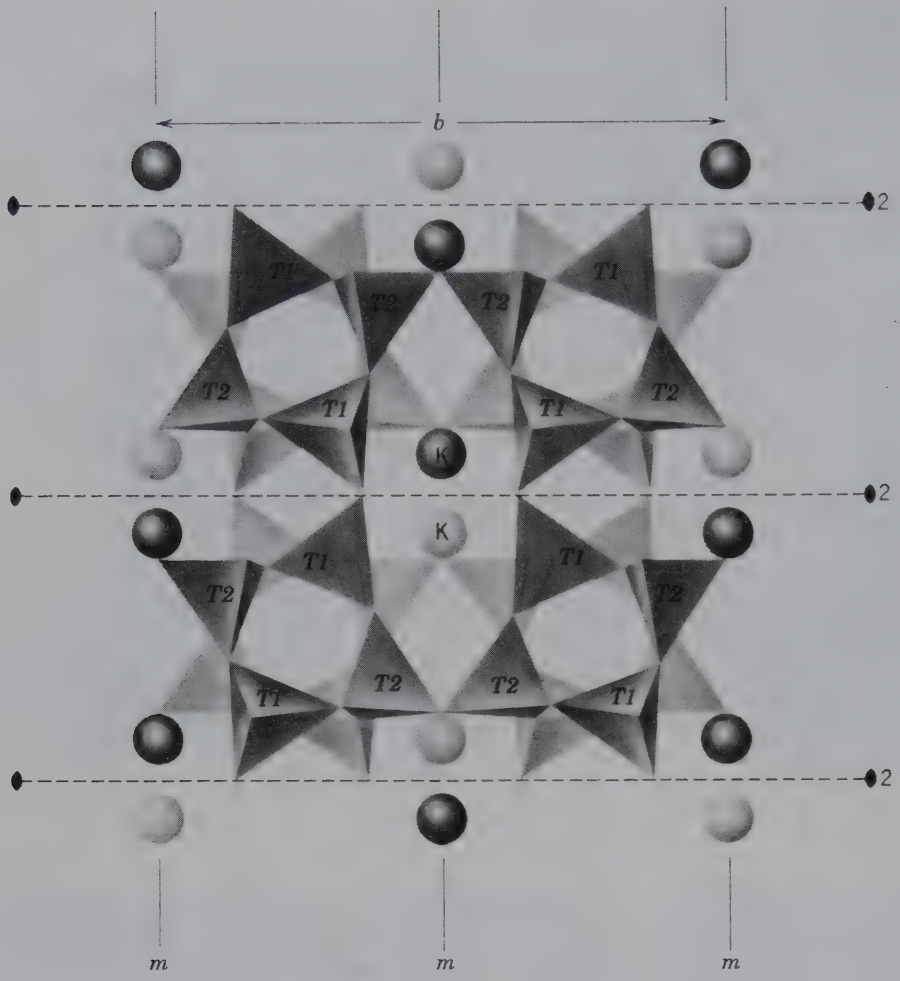

FIG. 18.48 The structure of high sanidine, $KAlSi_3O_8$, projected on $(\bar{2}01)$. Mirror planes (m) and two-fold rotation axes (2) are shown. Other symmetry elements such as glide planes and two-fold screw axes are also present, but their location is not shown here. (After Papike, J. J. and M. Cameron. 1976. Crystal chemistry of silicate minerals of geophysical interest. *Reviews of Geophysics and Space Physics* 14: 66.)

The Al–Si distribution is completely ordered in what is known as low-temperature or maximum microcline (maximum refers to maximum *triclinicity*, which results from the complete order). The tetrahedra that contain Al in this structure can be unambiguously located, whereas in sanidine the Al–Si distribution is completely random. *Orthoclase* represents a polymorph of $KAlSi_3O_8$ in which the Al–Si distribution is between the total randomness found in sanidine and the total order of microcline. Orthoclase, with space group $C2/m$, crystallizes at intermediate temperatures (see Fig. 18.50). Unambiguous distinction between the three structurally different K-feldspars, sanidine, orthoclase, and microcline, is based on careful measurements of unit cell dimensions and/or optical parameters, such as 2V and/or extinction angle $b \wedge Z$. Their descriptions (in Chapter 19) will be based on generally recognizable characteristics in hand specimens, therefore, the terms *orthoclase* and *microcline* are used loosely. However, the definitions of the three types of K-feldspar as used in the literature are based on parameters that can be obtained only by X-ray and optical techniques (see Smith and Brown, 1988, or Smith 1974). Such measurements allow for the definition of maximum microcline, and high, intermediate, and low orthoclase, and provide the investigator with information about the state of order or disorder of the Al–Si distribution in the feldspar structure.

The question of whether a specific, originally high-temperature feldspar retains its high-temperature (disordered) structure type or whether it will transform (upon cooling) to a lower temperature (more ordered) structural state is much influenced by the cooling rate of the process. Figure 18.51 is a schematic illustration of the various cooling paths for a potassium feldspar, as a function of temperature and cooling rate.

Microcline is particularly characteristic of slowly cooled, deep-seated rocks and pegmatites, orthoclase of intrusive rocks formed at intermediate temperatures and sanidine of quickly cooled, extrusive, high-temperature lavas.

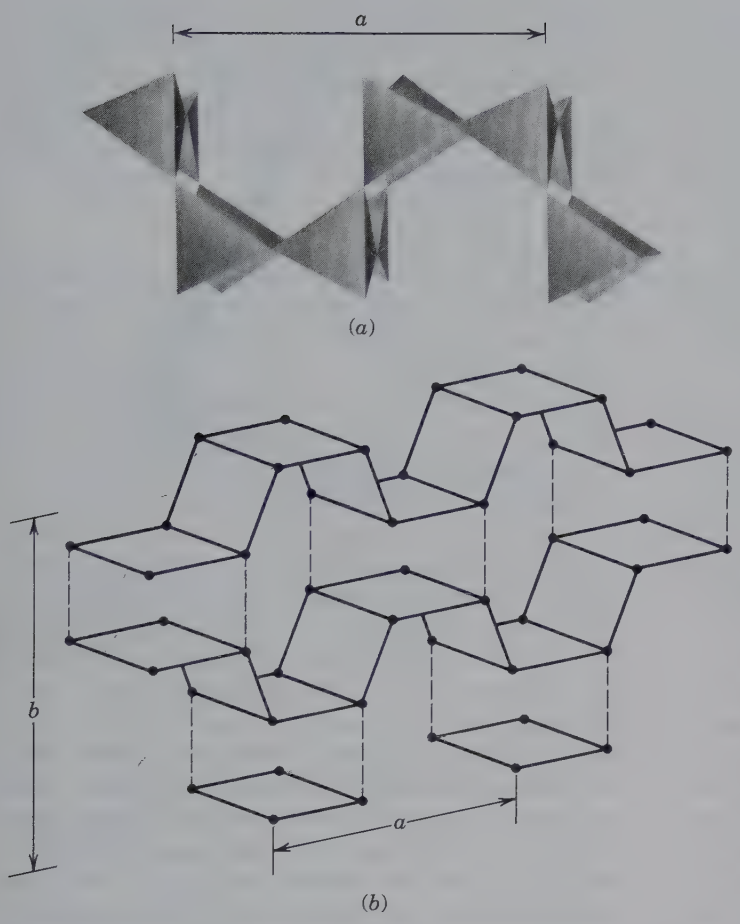

FIG. 18.49 (a) The four-membered rings in Fig. 18.48 are linked to form crankshaft-like chains that run parallel to the *a* axis. (After Papike, J. J., and M. Cameron. 1976. Crystal chemistry of silicate minerals of geophysical interest. *Reviews of Geophysics and Space Physics* 14: 67.) (b) Schematic representation of the location and orientation of the four-membered crankshaft-like chains in the feldspar structure. Black dots are locations of Si. Dashed lines locate bonds between adjoining $(Si, Al)O_4$ tetrahedra. (Modified with permission after Ribbe, P. 1987. Feldspar. *McGraw-Hill Encyclopedia of Science and Technology*, 6th ed., v. 7, 38–47, New York, McGraw-Hill Book Co., copyright 1987. Reproduced with permission of The McGraw-Hill Companies.)

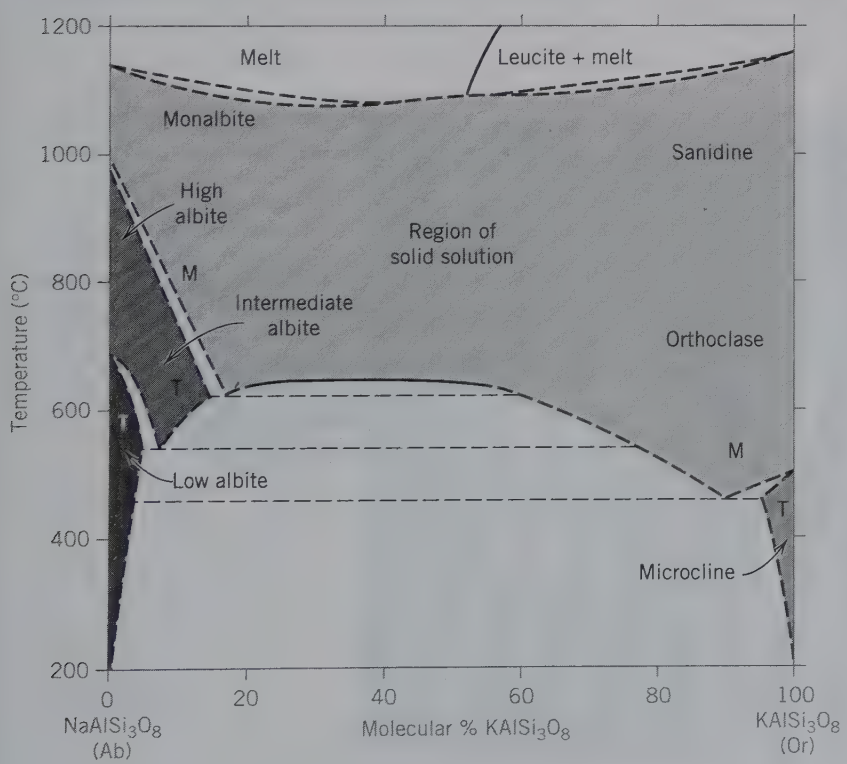

FIG. 18.50 Schematic phase diagram for the system $NaAlSi_3O_8$ (Ab)–$KAlSi_3O_8$ (Kspar) showing a large miscibility gap at temperatures below approximately 650°C. *M* and *T* mean monoclinic and triclinic, respectively. Compare with Fig. 11.7. (Modified with permission after Smith, J. V., and W. L. Brown. 1988. *Feldspar minerals* 1. Springer Verlag, New York., Fig. 1.2.)

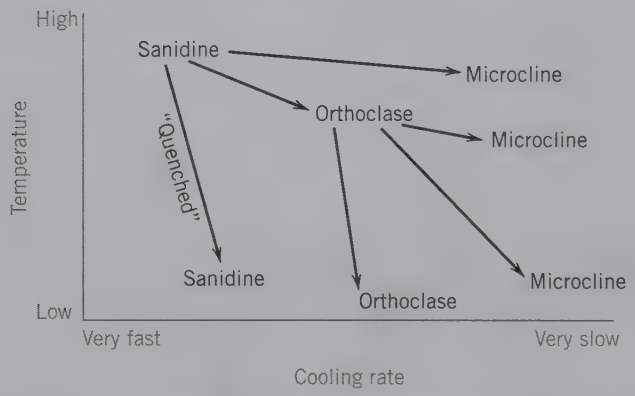

FIG. 18.51 The various possible temperature-cooling rate paths that an originally high-temperature K-feldspar (sanidine) can follow. The path marked *quenched* depicts a path in which the original high-temperature sanidine is cooled so rapidly that all characteristics of the high-temperature state are preserved in the final cooled product. (Modified with permission from Putnis, A., and J. D. C. McConnell. 1980. *Principles of mineral behavior.* Oxford, England. Blackwell Scientific Publications, Oxford, England, Fig. 7.8, reprinted with permission.)

The general structure of members of the plagioclase series is very similar to that of microcline. The Na end member, *albite*, is generally triclinic (space group $C\bar{1}$) with a low albite form that shows a highly ordered Al–Si distribution and a high albite form with a highly disordered Al-Si distribution. A monoclinic variety of albite occurs at very high temperature and is known as *monalbite*. The Ca end member, *anorthite*, is also triclinic with space group $P\bar{1}$ at room temperature, and perfect Al-Si ordering in the structure. At elevated temperatures the structure of anorthite becomes body-centered with space group $I\bar{1}$. The general stability fields of the various forms of feldspar are shown in Figs. 18.50, 18.54, and 18.56.

Composition

The alkali feldspar series ($NaAlSi_3O_8$ to $KAlSi_3O_8$) shows complete solid solution only at high temperatures (see Fig. 18.50). For example, members of the sanidine–high albite series are stable at elevated temperatures but at lower temperature, two separate phases, low albite and microcline, become stable. As can be seen from Fig. 18.50, the compositional ranges of low albite and microcline are very small. If a homogeneous feldspar, of composition $Or_{50}Ab_{50}$, in which the Na^+ and K^+ ions are randomly distributed, is allowed to cool slowly, segregation of Na^+ and K^+ ions will result because the size requirements of the surrounding structure become more stringent. The Na^+ will diffuse to form Na-rich regions and the K^+ will segregate into K-rich regions in the structure, causing the originally homogeneous feldspar to become a heterogeneous intergrowth. The separation most commonly results in thin layers of albite in a host crystal of K feldspar. Such intergrowths are known as *perthites*, and are the result of *exsolution* (see Fig. 12.14 and discussion on page 276). In the alkali feldspar series the orientation of the exsolution lamellae is roughly paral-

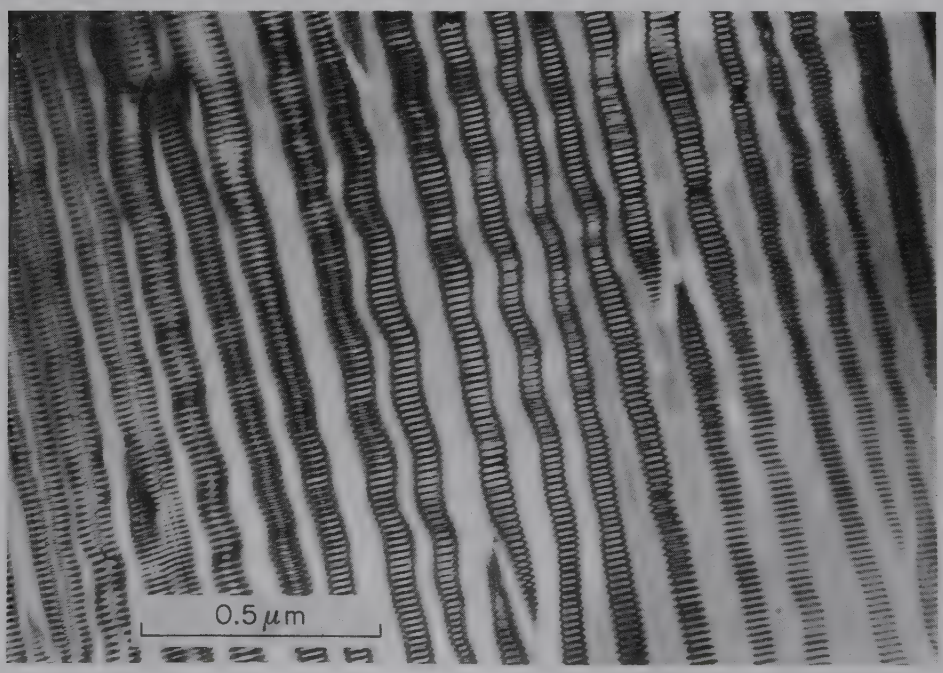

FIG. 18.52 Microstructure in an alkali feldspar of composition 57.3 weight percent Or. The Na-rich lamellae are twinned according to the albite law. This very high magnification photograph was taken with a transmission electron microscope. (From Champness, P. E., and G. W. Lorimer. 1976. Exsolution in silicates. *Electron Microscopy in Mineralogy*, H. R. Wenk, ed., Springer-Verlag, New York.)

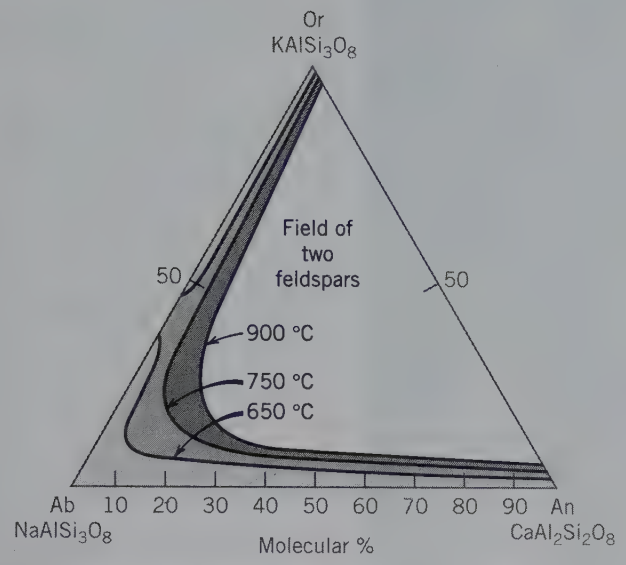

FIG. 18.53 Experimentally determined extent of solid solution in the system Or–Ab–An at P_{H_2O} = 1 kilobar. (After Ribbe, P. H., 1975. *Feldspar mineralogy, Reviews in Mineralogy* 2, Mineralogical Society of America, Washington, D.C., Figure R-1.)

lel to {100}. When these intergrowths are visible to the naked eye, they are known as *macroperthite*, when visible only by optical microscope they are referred to as *microperthite*, and when detectable only by X-ray or electron microscope techniques, they are called *cryptoperthite* (see Fig. 18.52). More rarely, the host mineral is a plagioclase feldspar and the lamellae are of $KAlSi_3O_8$ composition; this is called *antiperthite*.

Only very limited solid solution occurs between $KAlSi_3O_8$ and $CaAl_2Si_2O_8$ (see Fig. 18.53). Essentially complete solid solution, however, exists at elevated temperatures in the plagioclase series ($NaAlSi_3O_8$ to $CaAl_2Si_2O_8$) (see Fig. 18.54). The general formula of a feldspar in this series may be written as: $Na_{1-x}Ca_x(Si_{3-x}Al_{1+x})O_8$, where x ranges from 0 to 1. The structural interpretation of the region of essentially complete solid solution is complicated because of the varying ratio of Al/Si from albite, $NaAlSi_3O_8$, to anorthite, $CaAl_2Si_2O_8$. Three types of exsolution textures found in the plagioclase series are not visible to the naked eye, but may be detected because of iridescence. *Peristerite* intergrowths occur in the range An_2 to An_{15} (see Fig. 18.55). *Bøggild intergrowths* occur in some plagioclase with composition between An_{47} and An_{58}; their presence is indicated by the play of colors in labradorite (Plate VIII, no. 5). A third intergrowth occurs in the An_{60} to An_{85} region and is known as *Huttenlocher intergrowths*. These discontinuities in the solid solution series between Ab and An are on a very fine scale, however, and most properties, such as specific gravity or refractive index, show a generally linear change with chemical composition. Thus, determination of a suitable property with sufficient precision permits a close approximation of the chemical composition in the plagioclase series. Figure 18.56 is a simplified representation of the three-component feldspar system ($KAlSi_3O_8$—K-spar; $NaAlSi_3O_8$—albite; $CaAl_2Si_2O_8$—anorthite) showing the major miscibility gaps, and melting temperatures at water pressure of about five kilobars (compare with Fig. 11.7).

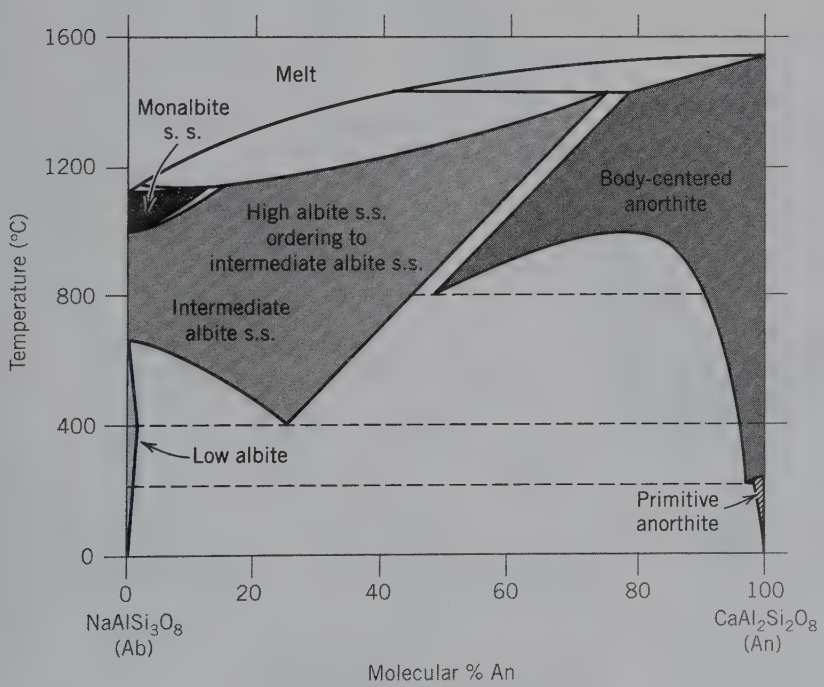

FIG. 18.54 Schematic phase diagram for the plagioclase feldspar series showing a range of almost complete solid solution at high temperatures, and two broad miscibility regions at lower temperatures. (Simplified with permission after Smith, J. V., and W. L. Brown. 1988. *Feldspar minerals* 1. Springer Verlag, New York, Figure 1.4.)

FIG. 18.55 Microstructure in the peristerite region of the plagioclase series (between An_2 and An_{15}), showing sharply defined, very fine lamellae approximately parallel to $(0\bar{4}1)$. These lamellae act as a diffraction grating for white light, producing the delicate bluish sheen of moonstone. This photograph was taken with a transmission electron microscope. (From Champness, P. E., and G. W. Lorimer. 1976. Exsolution in silicates. *Electron Microscopy in Mineralogy*, H. R. Wenk, ed., Springer-Verlag, New York, chapter 4.1.)

FIG. 18.56 Highly schematic temperature-composition diagram for the three-component system $KAlSi_3O_8$ (K-feldspar)–$NaAlSi_3O_8$ (albite)–$CaAl_2Si_2O_8$ (anorthite), at water pressure of about 5 kilobars. Details of the interior are complex and have been omitted. The upper, contoured surface of the diagram is the liquidus surface. The three intergrowth regions, as a result of miscibility gaps, in the lower temperature range of the plagioclase series are: *P* = peristerite, *B* = Bøggild intergrowth, *H* = Huttenlocher intergrowth. Solid solution is shown by shading. Compare the two vertical sides of this diagram with more detailed information given in Figs. 18.50 and 18.54. (Adapted with permission from Ribbe, P. H. 1987. Feldspars. *McGraw-Hill Encyclopedia of Science and Tech*, 6th ed., v. 7. McGraw-Hill Book Co., New York; copyright 1987. Reproduced with the permission of The McGraw-Hill Companies.)

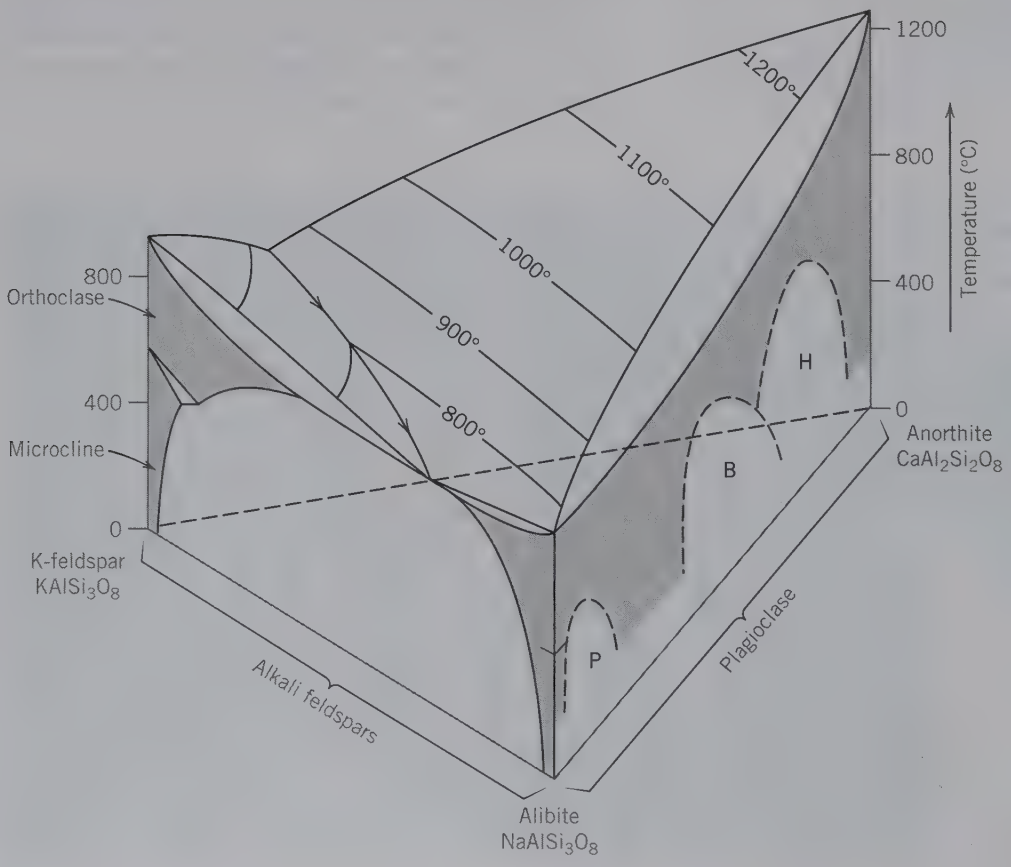

FELDSPATHOID GROUP

The feldspathoids are anhydrous framework silicates that are chemically similar to the feldspars. The primary chemical difference between feldspathoids and feldspars is that feldspathoids contain one-third less silica than alkali feldspar. They tend to form from melts rich in alkalis (Na and K) and poor in SiO_2 (see Fig. 18.57). The structures of the feldspathoids are closely related to those of the feldspars and silica minerals. However, several feldspathoids show the development of somewhat larger structural cavities (than feldspar or silica minerals) as a result of four- and six-membered tetrahedral linkages. This open architecture of the feldspathoid structures, when compared to the feldspars, is expressed in their lower specific gravity:

G range for feldspars: 2.54–2.75
G range for feldspathoids: 2.15–2.50

Examples of the aluminosilicate frameworks in the feldspathoids are given in Figs. 18.58 to 18.60. The structure of *leucite*, $KAlSi_2O_6$, has tetragonal symmetry (space group $I4_1/a$) at low to intermediate temperatures; at approximately 605°C it inverts to a cubic structure with space group $Ia3d$. In the low-temperature form the Al and Si tetrahedra share corners to form four- and six-membered rings (see Fig. 18.58). The K^+ ions are in 12-coordination with oxygen in large cavities in the structure. The structure of *nepheline*, $(Na,K)AlSiO_4$ (space group $P6_3$), is considered a derivative of the high tridymite structure with Al replacing Si in half the tetrahedra and Na and K in interstitial voids. The Si and Al are ordered in specific tetrahedral sites of the structure; the *T1* and *T4* sites are Al-rich, the *T2* and *T3* sites Si-rich. One-fourth of

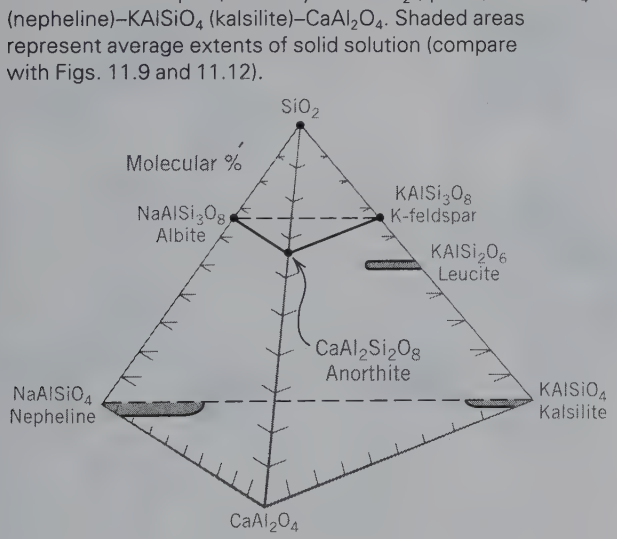

FIG. 18.57 Feldspathoid compositions, as compared to those of the feldspars, in the system SiO_2 (quartz)–$NaAlSiO_4$ (nepheline)–$KAlSiO_4$ (kalsilite)–$CaAl_2O_4$. Shaded areas represent average extents of solid solution (compare with Figs. 11.9 and 11.12).

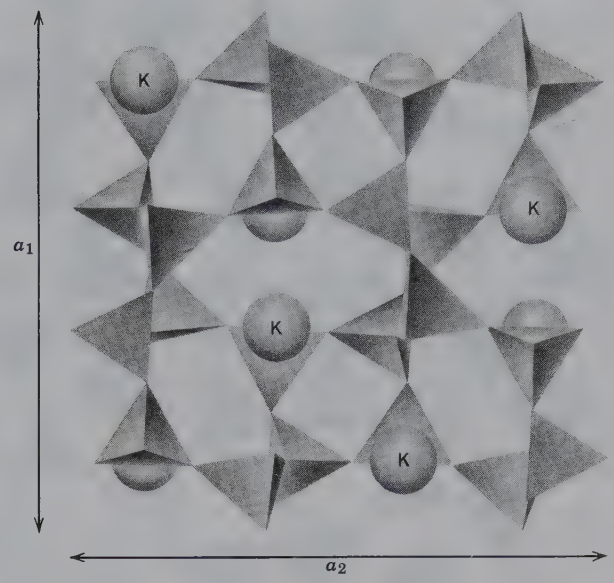

FIG. 18.58 Portion of the leucite structure projected down the *c* axis. (After Papike, J. J., and M. Cameron. 1976. Crystal chemistry of silicate minerals of geophysical interest. *Reviews of Geophysics and Space Physics* 14: 74.)

the interstitial sites, which are filled by K, are nearly hexagonal in geometry (see Fig. 18.59). The other three-fourths of the sites are irregular in configuration and are occupied by Na. The structure of *sodalite*, $Na_8(AlSiO_4)_6Cl_2$ (see Fig. 18.60), has large cavities occupied by Na^+ and Cl^-. The structural framework consists of corner-sharing, alternating SiO_4 and AlO_4 tetrahedra. The cagelike cavities result from the linking of 6 four-membered and 8 six-membered tetrahedral rings. The six-membered rings form channelways parallel to the cube diagonals of the structure. The large central cavities are occupied by Cl^-, which are tetrahedrally coordinated by Na^+.

Some of the members of the feldspathoid group contain unusual anions. *Sodalite* contains Cl and cancrinite incorporates CO_3. *Nosean* houses SO_4 and *lazurite* SO_4, S, and Cl ions. These large anionic groups and anions are located in large interstices of the structure.

ZEOLITE GROUP

The zeolites form a large group of hydrous silicates that show close similarities in composition, association, and mode of occurrence. They are framework aluminosilicates with Na, Ca, and K, and highly variable amounts of H_2O in the generally large voids of the framework. Many of them fuse readily with marked intumescence (a swelling up which results when water is expelled during heating), hence the name *zeolite*, from two Greek words meaning *to boil* and *stone*. Traditionally, the zeolites have been thought of as well-crystallized minerals found in

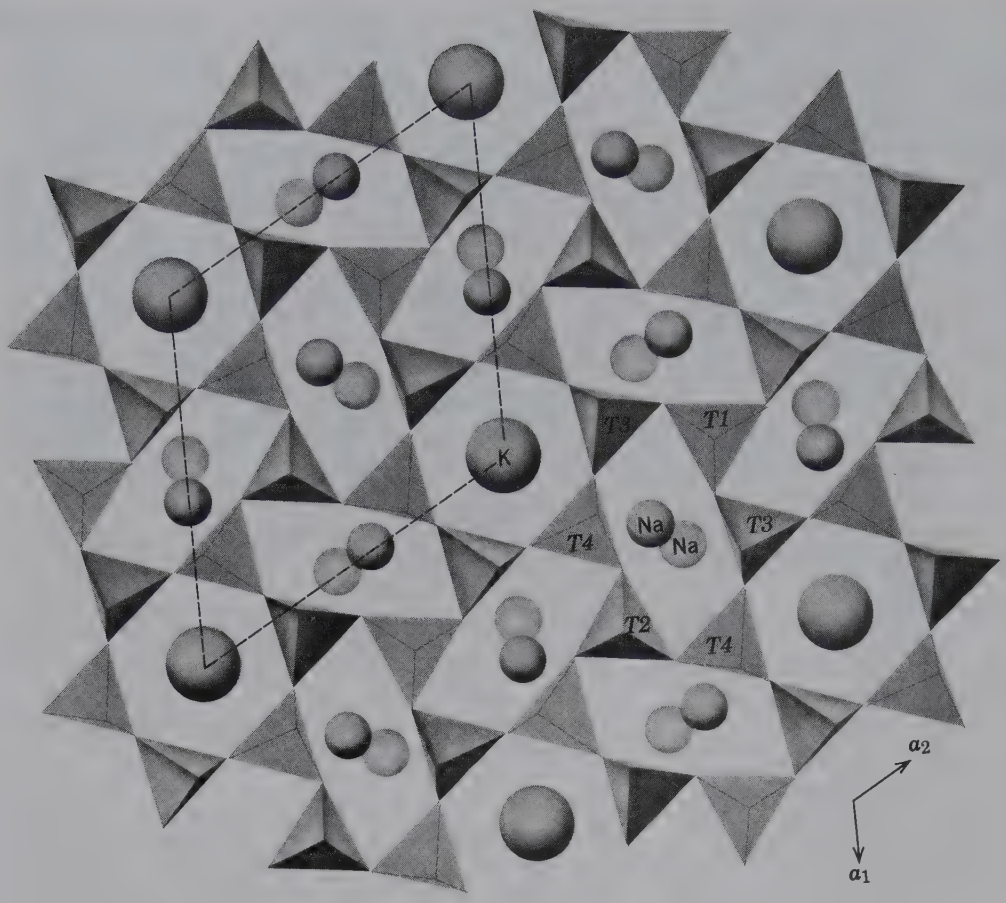

FIG. 18.59 Projection of the nepheline structure onto (0001). Dashed lines outline unit cell. *T1*, *T2*, *T3*, and *T4* refer to crystallographically distinct tetrahedral sites. (After Papike, J. J., and M. Cameron. 1976. Crystal chemistry of silicate minerals of geophysical interest. *Reviews of Geophysics and Space Physics* 14: 56.)

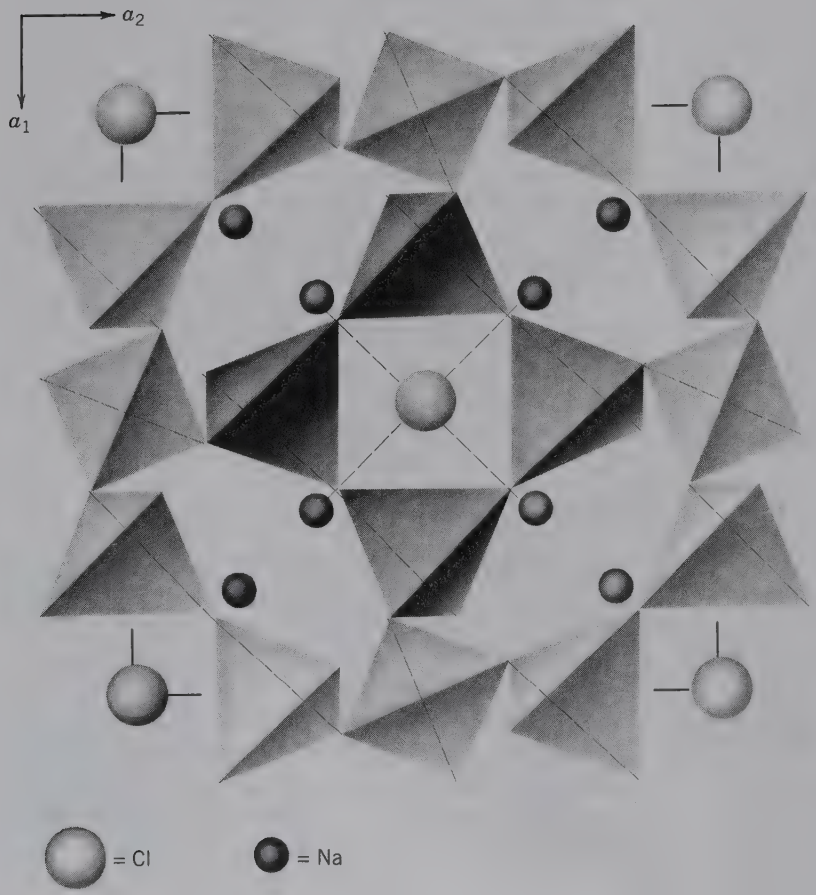

FIG. 18.60 The structure of sodalite, $Na_8(AlSiO_4)_6Cl_2$. This can be visualized as a cubic unit cell with a four-membered tetrahedral ring on each cube face, and a six-membered tetrahedral ring around each corner of the cube. (From Papike, J. J. 1988. Chemistry of the rock-forming silicates: Multiple chain, sheet, and framework structures. *Reviews of Geophysics* 26: 407–44.)

cavities and veins in basic igneous rocks. More recently, large deposits of zeolites have been found in the western United States and in Tanzania as alterations of volcanic tuff and volcanic glass. Such zeolites are the diagenetic alteration products of silicic tuffs in Cenozoic lacustrine deposits, especially those that were deposited in highly saline and alkaline waters. The occurrence of zeolites in various rock types is used to define the low-grade regional metamorphic zone known as the *zeolite facies*.

Physical properties, such as hardness (**H**) and specific gravity (**G**) of members of the zeolite group show a pronounced decrease, when compared to those of the silica minerals, feldspars, and feldspathoids:

	H	G
Quartz	7	2.65
Feldspars	6	2.54–2.75
Feldspathoids	5–6	2.15–2.50
Zeolites	$3\frac{1}{2}$–$5\frac{1}{2}$	2.00–2.40

The zeolites, like the feldspars and feldspathoids, are built of frameworks of AlO_4 and SiO_4 tetrahedra; the zeolite frameworks, however, are very open with large interconnecting spaces or channels. The zeolites can be divided into those with a fibrous habit and an underlying chain structure (Fig. 18.61), those with a platy habit and an underlying sheet structure, and

FIG. 18.61 (a) Chains of AlO_4 and SiO_4 tetrahedra as found in natrolite and other fibrous zeolites. (b) The structural framework of natrolite projected on (001). The Na^+ ions (small black spheres) are located near the channel centers and are related to each other by a 2_1 screw axis in the [001] channel center. H_2O molecules (lighter spheres) are located nearer to the channel edges (From Armbruster, T. and M. Gunter, 2001. Crystal Structures of Natural Zeolites, in Natural Zeolites: Occurrences, properties, applications. D. L. Bish and D. W. Ming, Eds. *Reviews in Mineralogy & Geochemistry*, v. 45, pp. 1–68. Mineralogical Society of America, Washington, D.C.)

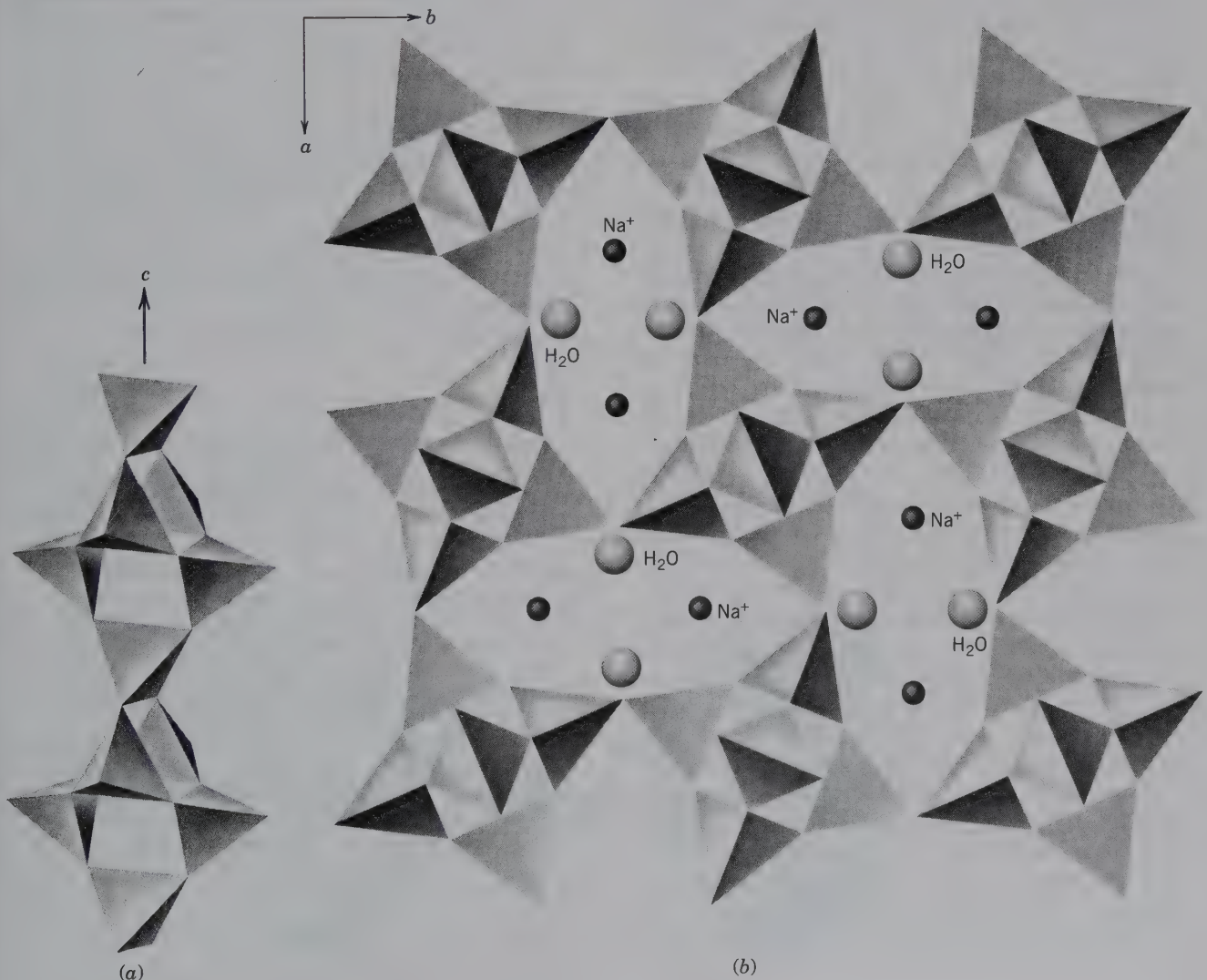

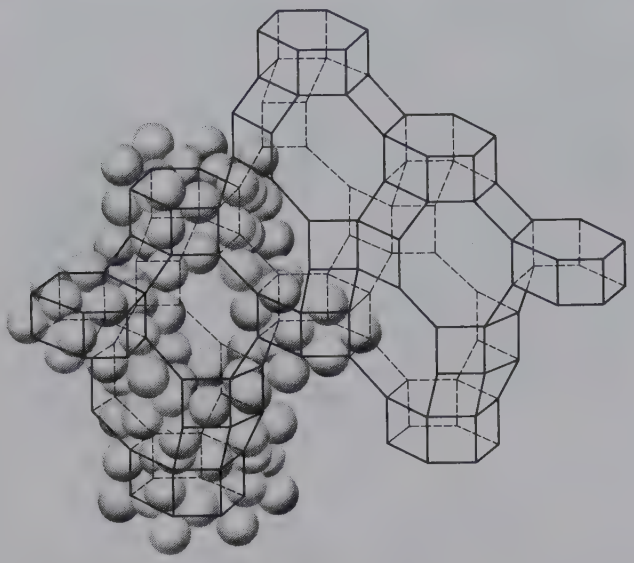

FIG. 18.62 Schematic representation of the structure of chabazite. Si and Al (not shown) occupy the corners of the framework outlined by the lines. The spheres represent oxygen in close packing. Each framework unit contains a cavity which is connected to adjacent cavities by channels. The channel-diameter in chabazite is 3.9 Å. (From Breck, D. W., and J. V. Smith. 1959. Molecular sieves. *Scientific American* 200, no. 1: 88. All rights reserved.)

those with an equant habit and an underlying framework structure (Fig. 18.62).

Much of the industrial interest in zeolites derives from the spacious channels and the water molecules and variable amounts of Na^+, Ca^{2+}, and K^+ that are housed in the channels. The water molecules are weakly tied by hydrogen bonding to anionic framework atoms. When a zeolite is heated, the water in the channelways is given off easily and continuously as the temperature rises, leaving the structure intact. This phenomenon of continuous water loss as a function of increasing temperature is illustrated in Fig. 18.63 for several common, natural zeolites. The formulas in Fig. 18.63 show the large and variable numbers of water molecules per formula unit. The thermal gravimetric analysis (TGA) curves show a continuous loss of water with increasing temperature and also illustrate the fact that 80% to 90% of all the water is lost from the structure below about 350°C. This relatively low-temperature water loss occurs via the channels of the structures without collapse of the framework. Collapse and overall destruction of the framework (known as decrepitation) commonly occurs at temperatures above 600°C. Such water-loss behavior is in sharp contrast to that observed in silicates with (OH) groups in which (OH) is an integral part of their structures (e.g., amphiboles

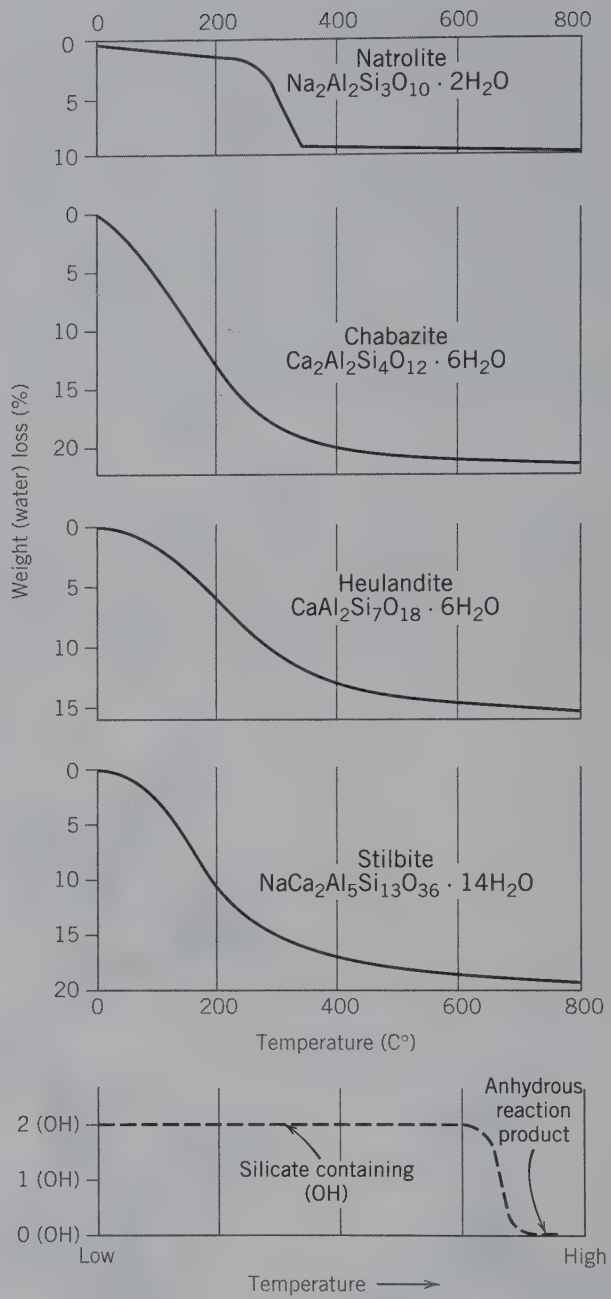

FIG. 18.63 Thermal gravimetric analysis (TGA) curves for four selected zeolites. In each of these four curves there is a continuous water loss with increasing temperature. In every case about 80% to 90% of the water in these structures is lost by about 350°C. The zeolite formulas used here are simplified over those given in Chapter 19. (From Gottardi, G., and E. Galli. 1985. *Natural Zeolites*. Springer-Verlag, New York, with permission.) The schematic curve at the bottom illustrates the behavior of silicates with (OH) groups (e.g., amphiboles, micas) and the abrupt loss of this (OH) at some high temperature, at which the original (OH)-containing structure is destroyed and converts to an anhydrous reaction product + H_2O.

and micas). Such (OH) groups are generally lost over a very small temperature range at high temperatures. As the result of such loss, new, commonly anhydrous minerals form (see the schematic curve at the bottom of Fig. 18.63). Dehydration behavior similar to that of zeolites, but at much lower temperature than for (OH)-containing silicates, is shown by gypsum, $CaSO_4 \cdot 2H_2O$ (see Fig. 17.45), which converts initially (at about 65°C) to $CaSO_4 \cdot \frac{1}{2}H_2O$ and at about 100°C to the γ polymorph of $CaSO_4$.

The dehydrated zeolite structure can be completely rehydrated when it is immersed in water. In industrial applications, the property of rehydration allows zeolites to be used as desiccants, such as in the removal of water from gaseous hydrocarbons and petroleum. Zeolites in their dehydrated state can absorb other molecules as well, as long as the overall size of the zeolite channels is large enough to accommodate such molecules. Molecules too large to pass through the channels are excluded, giving rise to the "molecular sieving" property of most zeolites. For example, a specific zeolite with channel diameters of about 4.5 Å is able to filter normal hydrocarbons, such as octane and pentane (with effective cross-sectional diameters of about 4.3 Å), but will exclude branch chain hydrocarbons, such as isooctane and isopentane (with effective cross-sectional diameters of 5.0 Å or larger). This sieving property is illustrated in Fig. 18.64.

Zeolites, in addition to their commercial use as molecular sieves, are also much exploited on account of their cation exchange properties (see Box 19.6). The cations (such as Na^+, K^+, and Ca^{2+}) are loosely bonded to the tetrahedral framework and can be removed or exchanged easily by washing with a strong solution of another ion. This ability for cation exchange is the basis for water softeners, in which "hard" water (with high Ca^{2+} concentrations) is made "soft" by exchanging the Ca^{2+} (in the water) with Na^{2+} (supplied by a natural or synthetic zeolite, e.g., $Na_2Al_2Si_3O_{10} \cdot 2H_2O$). "Hard" water, that is, water containing many calcium ions in solution, is passed through a tank filled with Na-rich zeolite grains. The Ca^{2+} ions replace the Na^+ ions in the zeolite, forming $CaAl_2Si_3O_{10} \cdot 2H_2O$, contributing Na^+ ions to the solution. Water containing sodium does not form scum and is said to be "soft." When the zeolite in the tank has become saturated with calcium, a strong NaCl brine is passed through the tank. The high concentration of sodium ions forces the reaction to go in the reverse direction, and the $Na_2Al_2Si_3O_{10} \cdot 2H_2O$ is reconstituted, with calcium going into solution. By base exchange many ions, including silver, may be substituted for the alkali-metal cations in the zeolite structure. These cation exchange properties are used in removing harmful ions from radioactive waste, or ammonia from sewage and agricultural waste.

Because of the great demand for various zeolites used in commercial applications, such as in catalytic cracking (cracking is the molecular weight reduction process by which the heavier components of crude oil are converted to lighter, more volatile materials, such as those used in gasoline), there is a large industrial production (through laboratory synthesis) of zeolites. The first synthetic zeolites were produced in the 1950s by the Linde Division of the Union Carbide Corporation. Such syntheses have produced many structures

FIG. 18.64 Schematic illustration of how a zeolite sieve separates a straight chain hydrocarbon (e.g., octane) from a branching chain hydrocarbon (e.g., isooctane). These two organic compounds have almost identical properties and, thus, are very hard to separate by other methods. Isooctane has the higher "antiknock" rating. (From Flanigen, E. M., and F. A. Mumpton. 1977. Commercial properties of natural zeolites. *Mineralogy and Geology of Natural Zeolites, Reviews in Mineralogy* 4, Mineralogical Society America, 165–75.)

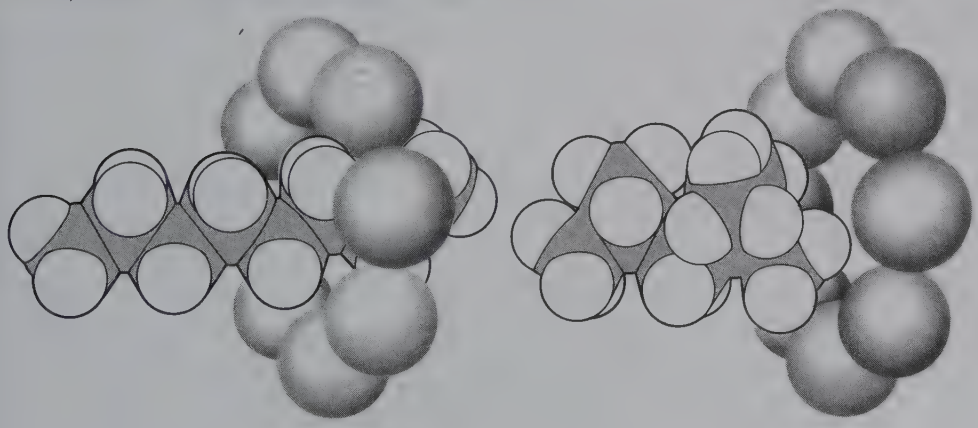

and compositions that have no natural counterpart. The number of naturally occurring zeolites is about 52, and only a few of these are found in sufficient quantity and purity to be used as a commercial product. Synthetic zeolite production now occurs on a large scale with a production of more than 1.39 million tons per year. Very specific zeolite structures (with unique channel diameters and/or cation exchange properties) are being produced for unique industrial applications (see Box 19.6).

REFERENCES AND FURTHER READING

Anthony, J. W., R. A. Bideaux, K. W. Bladh, and M. C. Nichols. 1995. *Handbook of mineralogy.* Vol. 2, *Silica, silicates.* Mineral Data Publications. Tucson, Arizona.

Armbruster, T. and H. Gunter, 2001. Crystal Structures of Natural Zeolites in *Natural Zeolites: Occurrences, properties, applications.* D. L. Bish and D. W. Ming, eds. *Reviews in Mineralogy and Geochemistry*, v. 45, pp. 1–68. Mineralogical Society of America, Washington, D.C.

The Al_2SiO_5 polymorphs. 1990. *Reviews in Mineralogy* 22. Mineralogical Society of America, Washington, D.C.

Amphiboles. 1981. *Reviews in Mineralogy* 9A. Mineralogical Society of America, Washington, D.C.

Breck, D. W. 1974. *Zeolite molecular sieves.* Wiley, New York.

Buseck, P. R. 1983. Electron microscopy of minerals. *American Scientist* 71: 175–85.

Buseck, P. R., and S. Iijima. 1974. High resolution electron microscopy of silicates. *American Mineralogist* 59: 1–22.

Darragh, P. J., A. J. Gaskin, and J. V. Sanders. 1976. Opals. *Scientific American* 234, 4: 84–95.

Deer, W. A., R. A. Howie, and J. Zussman. 1962 and 1963. *Rock-forming minerals*, v. 1–4. Wiley, New York.

———. 1978. *Single-chain silicates*, v. 2A. 1982, *Orthosilicates*, v. 1A; 1986; *Disilicates and ring silicates* v. 1B; *Double-chain silicates*, v. 2B. For vols. 2A, 1A, and 1B. Wiley, New York. For vol. 2B, The Geological Society, London.

———. 1992. *An introduction to the rock-forming minerals.* 2nd ed. Wiley, New York.

Feldspar mineralogy. 1983. *Reviews in Mineralogy* 2. Mineralogical Society of America, Washington, D.C.

Frondel, C. 1962. *The system of mineralogy* 3. *Silica Minerals.* Wiley, New York.

Gibbs, G. V. 1966. The polymorphism of cordierite I: The crystal structure of low cordierite. *American Mineralogist:* 1068–88.

Gottardi, G., and E. Galli. *Natural zeolites.*Springer-Verlag, New York.

Grim, R. E. 1968. *Clay mineralogy.* 2nd ed. McGraw-Hill, New York.

Hawthorne, F. C. 1983. The crystal chemistry of amphiboles. *Canadian Mineralogist* 21: 173–480.

Heaney, P. J. 1994. Structure and chemistry of the low-pressure silica polymorphs. P. J. Heaney and G. V. Gibbs, eds. *Silica: Physical Behavior, geochemistry and materials applications.* 1994. *Reviews in Mineralogy.* Mineralogical Society of America, Washington, D.C.

Henry, D. J., and B. Dutrow. 1996. Metamorphic tourmaline and its petrologic applications. E. S. Grew and L. M. Anovitz, eds. *Boron: Mineralogy, Petrology and Geochemistry.* 503–58. *Reviews in Mineralogy.* Mineralogical Society of America, Washington, D.C.

Hydrous phyllosilicates. 1988. *Reviews in Mineralogy* 19. Mineralogical Society of America, Washington, D.C.

Liebau, F. 1985. *Structural chemistry of silicates: Structure, bonding, and classification.* Springer-Verlag, New York.

Micas. 1984. *Reviews in Mineralogy* 13. Mineralogical Society of America, Washington, D.C.

Natural Zeolites: Occurrence, properties, applications. 2001. D. L. Bish, D. W. Ming, eds. *Reviews in Mineralogy and Geochemistry* 45. Mineralogical Society of America, Washington, D.C.

Orthosilicates. 1980. *Reviews in Mineralogy* 5. Mineralogical Society of America, Washington, D.C.

Papike, J. J., and M. Cameron. 1976. Crystal chemistry of silicate minerals of geophysical interest. *Reviews of Geophysics and Space Physics* 14: 37–80.

Putnis, A. 1992. *Introduction to mineral sciences.* Cambridge University Press, New York.

Pyroxenes. 1980. *Reviews in Mineralogy* 7. Mineralogical Society of America, Washington, D.C.

Smith, J. V. 1974. *Feldspar minerals*, vols. 1, 2. Springer-Verlag, New York.

Smith, J. V., and W. L. Brown. 1988. *Feldspar minerals.* Vol. 1, *Crystal structures, physical, chemical, and microtextural properties.* Springer-Verlag, New York.

Smyth, J. R., and D. L. Bish. 1988. *Crystal structures and cation sites for the rock-forming minerals.* Allen and Unwin, Boston.

Strunz, H., and E. H. Nickel, 2001, *Strunz Mineralogical Tables.* 9th ed. Schweizerbart'sche Verlagsbuchhandel, Stuttgart.

Veblen, D. R., P. R. Buseck, and C. W. Burnham. 1977. Asbestiform chain silicates: new minerals and structural groups. *Science* 198: 359–65.

Wenk, H. R., ed. 1976. *Electron microscopy in mineralogy.* Springer-Verlag, New York.

Zoltai, T. 1960. Classification of silicates and other minerals, with tetrahedral structures. *American Mineralogist* 45: 960–73.

CHAPTER 19

Systematic Descriptions of Rock-Forming Silicates

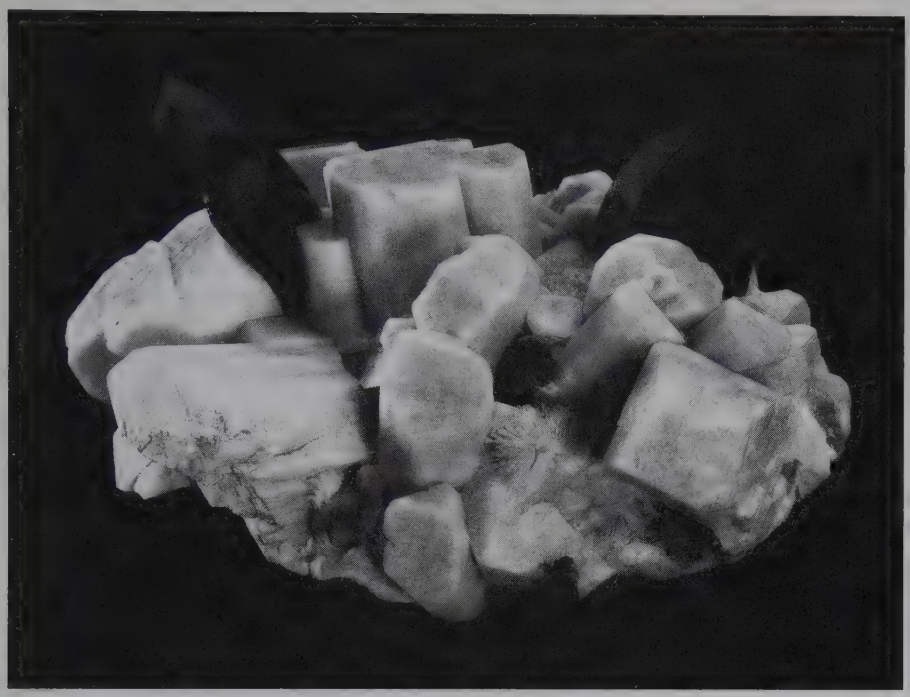

Smoky quartz and amazonite (green variety of microcline) crystals. From Crystal Peak, Colorado (Harvard Mineralogical Museum).

This chapter contains 75 systematic silicate mineral entries. This number is very small compared with that of 1,139 which represents the total number of silicates that are known. The small number is a reflection of the fact that only relatively few silicates are common as rock-forming minerals. The remaining 1,000 or so silicates range from uncommon to very rare. Another reason for the small number of systematic entries in this chapter is that several major silicate groups are treated under one mineral heading, such as olivine and garnet. In such instances, a number of separately named mineral species are described under one mineral group name. Such a group may show considerable to extensive solid solution with two or more end-member compositions (with specific species names given to such end-member compositions). Of the 75 entries, 28 of the mineral names are printed in lowercase (instead of boldface capitals) because these are considered to be less common or important. The silicate mineral group includes a considerable number of industrial minerals.

NESOSILICATES

The following minerals in the nesosilicate group will be discussed in detail:

Phenacite Group			
Phenacite	Be_2SiO_4		
Willemite	Zn_2SiO_4		
Olivine Group			
Forsterite	Mg_2SiO_4		
Fayalite	Fe_2SiO_4		
Garnet Group $A_3B_2(SiO_4)_3$			
Pyrope	Mg_3Al_2	Uvarovite	Ca_3Cr_2
Almandine	Fe_3Al_2	Grossular	Ca_3Al_2
Spessartine	Mn_3Al_2	Andradite	$Ca_3Fe^{3+}_2$
Zircon Group			
Zircon	$ZrSiO_4$		
Al_2SiO_5 Group			
Andalusite, Sillimanite, Kyanite	Al_2SiO_5		
Topaz	$Al_2SiO_4(F,OH)_2$		
Staurolite	$Fe_{3-4}Al_{18}Si_8O_{48}H_{2-4}$		
Humite Group			
Chondrodite	$Mg_5(SiO_4)_2(OH,F)_2$		
Datolite	$CaB(SiO_4)(OH)$		
Titanite	$CaTiO(SiO_4)$		
Chloritoid	$(Fe,Mg)_2Al_4O_2(SiO_4)_2(OH)_4$		

Phenacite Group

Phenacite—Be_2SiO_4

Crystallography. Hexagonal; $\bar{3}$. Crystals are usually flat rhombohedral or short prismatic. Often with complex development. Frequently twinned on $\{10\bar{1}0\}$.

$R\bar{3}$; $a = 12.45$, $c = 8.23$ Å; $Z = 18$. *ds*: 3.58(6), 2.51(8), 2.35(6), 2.18(8), 1.258(10).

Physical Properties. *Cleavage* $\{11\bar{2}0\}$ imperfect. **H** $7\frac{1}{2}$–8. **G** 2.97–3.00. *Luster* vitreous. *Color* colorless, white. Transparent to translucent. *Optics*: (+); $\omega = 1.654$, $\epsilon = 1.670$.

Composition and Structure. BeO 45.6, SiO_2 54.4%. The structure consists of SiO_4 and BeO_4 tetrahedra with each oxygen linked to two Be and one Si at the corners of an equilateral triangle.

Diagnostic Features. Characterized by its crystal form and great hardness.

Occurrence. Phenacite is a rare pegmatite mineral associated with topaz, chrysoberyl, beryl, and apatite. Fine crystals are found at the emerald mines in the Ural Mountains, Russia, and in Minas Gerais, Brazil. In the United States found at Mount Antero, Colorado.

Use. Occasionally cut as a gemstone.

Name. From the Greek word *phenakos* meaning a *deceiver*, in allusion to its resemblance to quartz.

Willemite—Zn_2SiO_4

Crystallography. Hexagonal; $\bar{3}$. In hexagonal prisms with rhombohedral terminations. Usually massive to granular. Rarely in crystals.

$R\bar{3}$; $a = 13.96$, $c = 9.34$ Å; $Z = 18$. *ds*: 2.84(8), 2.63(9), 2.32(8), 1.849(8), 1.423(10).

Physical Properties. *Cleavage* {0001} good. **H** $5\frac{1}{2}$. **G** 3.9–4.2. *Luster* vitreous to resinous. *Color* yellow-green, flesh-red, and brown; white when pure. Transparent to translucent. Most willemite from Franklin, New Jersey, fluoresces under ultraviolet light. *Optics*: (+); $\omega = 1.691$, $\epsilon = 1.719$.

Composition and Structure. ZnO 73.0, SiO_2 27.0%. Mn^{2+} often replaces a considerable part of the Zn (manganiferous variety called *troostite*); Fe^{2+} may also be present in small amount. Willemite is isostructural with phenacite, with SiO_4 and ZnO_4 tetrahedra. Because Zn^{2+} (radius = 0.60 Å) is much larger than Be^{2+} (radius = 0.27 Å) the structure of willemite is expanded over that of phenacite.

Diagnostic Features. Recognized by its association with other zinc-bearing minerals, such as franklinite and zincite.

Occurrence. Willemite is found in marble and may be the result of a metamorphism of earlier hemimorphite or smithsonite. It is also found sparingly as a secondary mineral in the oxidized zone of zinc deposits.

Found at Altenberg, near Moresnet, Belgium; Tsumeb, Namibia. The most important locality is in the United States at Franklin, New Jersey, where willemite occurs associated with franklinite and zincite and as grains embedded in calcite. It has also been found at the Merritt mine, New Mexico, and Tiger, Arizona.

Use. A valuable zinc ore at Franklin, New Jersey. Occasionally used as a gem.

Name. In honor of the King of the Netherlands, Willem I (1553–1584).

OLIVINE GROUP

The composition of most olivines can be represented in the system CaO–MgO–FeO–SiO_2 (Fig. 19.1). The most common series in this system is from *forsterite*, Mg_2SiO_4, to *fayalite*, Fe_2SiO_4. Relatively rare olivines occur also along the *monticellite*, $CaMgSiO_4$, to *kirschsteinite*, $CaFe^{2+}SiO_4$, join. Very little, if any, solid solution exists between these two series. Mn^{2+} may substitute for Fe^{2+}, forming a relatively rare series between fayalite and *tephroite*, Mn_2SiO_4. The structure of olivine, with similar *M1* and *M2* octahedral sites, and independent SiO_4 tetrahedra, is shown in Fig. 18.4.

Members of the forsterite–fayalite series are common as primary crystallization products in Mg-rich, silica-poor melts (magmas). *Dunites* and *peridotites* are > 90% olivine and olivine plus pyroxene rocks, respectively. Olivine concentrations in igneous rocks may result from their accumulation due to gravity settling during melt crystallization. Members of the forsterite–fayalite

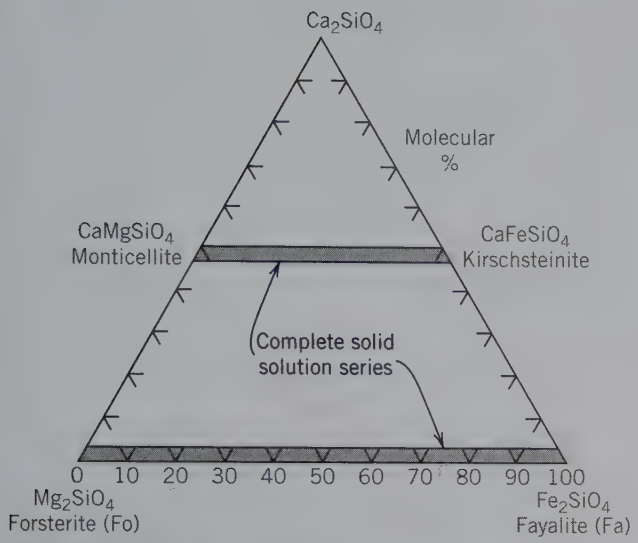

FIG. 19.1 Olivine compositions in the system Ca_2SiO_4-Mg_2SiO_4-Fe_2SiO_4.

series are highly refractory, as can be seen from Fig. 19.2 (forsterite melting point = 1890°C and fayalite melting point = 1205°C). This diagram represents a complete solid solution series (see Fig. 11.6 and related discussion). When a melt with composition x (50 weight percent Fe_2SiO_4) is cooled to the liquidus curve, olivine crystals of composition x_1 will start to form. The liquid, as a result of the Mg-rich olivine crystallization, will become more Fe-rich, as shown by the upper arrow. This, in turn, will cause a more Fe-rich olivine to crystallize, as shown by x_2, until finally all melt crystallizes. At this point, under equilibrium conditions, the final composition to crystallize is of composition x_3, which is the same as the original x. Chemical zoning in olivines

FIG. 19.2 Temperature-composition diagram for the system Mg_2SiO_4-Fe_2SiO_4 at atmospheric pressure (see also Fig. 11.6 and related discussion).

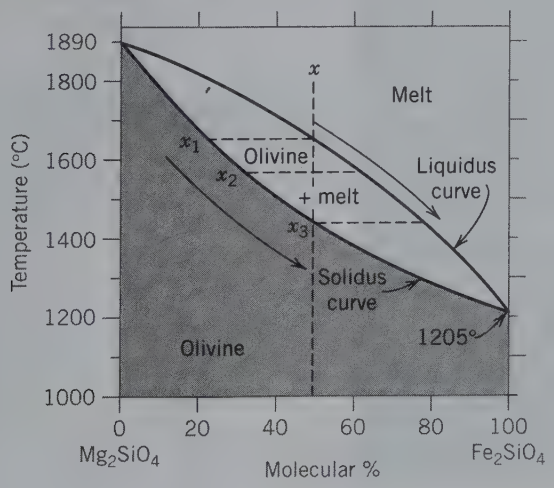

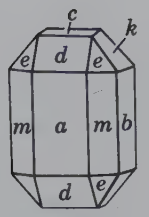

FIG. 19.3 Olivine.

with Mg-rich cores and more Fe-rich rims is found in high-temperature igneous rocks. Such rimming is the result of nonequilibrium crystallization in the direction of the arrows in Fig. 19.2.

OLIVINE—$(Mg,Fe)_2SiO_4$

Crystallography. Orthorhombic; *2/m2/m2/m*. Crystals are usually a combination of the three prisms, the three pinacoids, and a dipyramid. Often flattened parallel to either {100} or {010} (see Fig. 19.3). Usually appears as embedded grains or in granular masses.

Pbnm; $Z = 4$. Mg_2SiO_4: $a = 4.75$, $b = 10.20$, $c = 5.98$ Å. Fe_2SiO_4: $a = 4.82$, $b = 10.48$, $c = 6.09$ Å. *d*s for common olivine: 4.29(10), 2.41(8), 2.24(7), 1.734(8), 1.498(7). d_{130} can be used to determine compositions in this series (see Fig. 19.4a).

Physical Properties. *Fracture* conchoidal. **H** $6\frac{1}{2}$–7. **G** 3.27–4.37, increasing with increase in Fe content (see Fig. 19.4b). *Luster* vitreous. *Color* pale yellow-green to olive-green in forsterite, see Plate IV, no. 6; darker, brownish-green with increasing Fe^{2+}. Transparent to translucent. *Optics*: forsterite (+), others (−). For $Mg_{1.6}Fe_{0.4}SiO_4$: $\alpha = 1.674$, $\beta = 1.692$, $\gamma = 1.712$, $2V = 87°$; $X = b$, $Z = a$ (see Fig. 19.4b).

Composition and Structure. A complete solid solution exists from *forsterite*, Mg_2SiO_4, to *fayalite*, Fe_2SiO_4 (see Fig. 19.1). The more common olivines are richer in Mg than in Fe^{2+}. An example of the recalculation of an olivine analysis is given in Table 5.5. Compositions intermediate to the end members, forsterite (Fo) and fayalite (Fa), are commonly expressed as Fo_xFa_y, for example, $Fo_{60}Fa_{40}$, which is shortened to Fo_{60}. The structure of olivine is given in Fig. 18.4 and discussed on page 438. An HRTEM structure image is given in Fig. 19.5. Under very high pressures, the olivine structure transforms to one of two different high-pressure polymorphs of the spinel structure known as wadsleyite and ringwoodite, respectively (see Fig. 19.6). Olivine is thought to be abundant in the upper mantle and occurs as the perovskite structure at great depths (see Fig. 5.4 and related text).

Diagnostic Features. Distinguished usually by its glassy luster, conchoidal fracture, green color, and granular nature.

Occurrence. Olivine is a common rock-forming mineral, varying in amount from that of an accessory to that of a main constituent. It is found principally in Mg-rich igneous rocks, such as gabbro, peridotite, and basalt, coexisting with plagioclase and pyroxenes. The rock, *dunite*, is made up of > 90% olivine. Forsterite is not stable in the presence of free

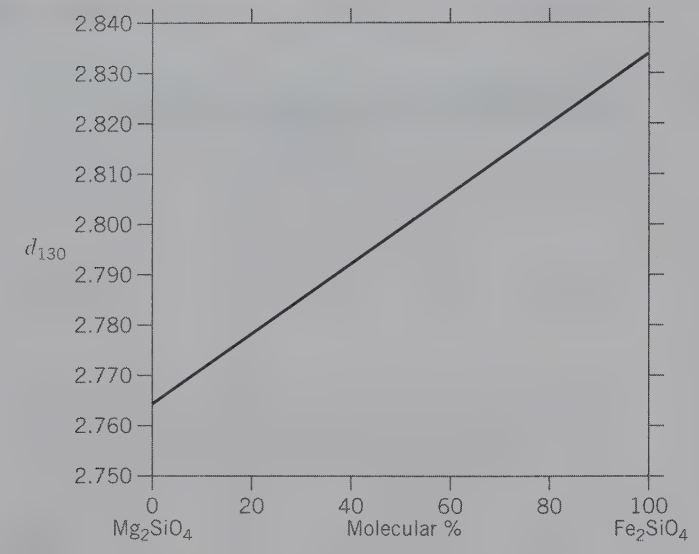

(*a*)

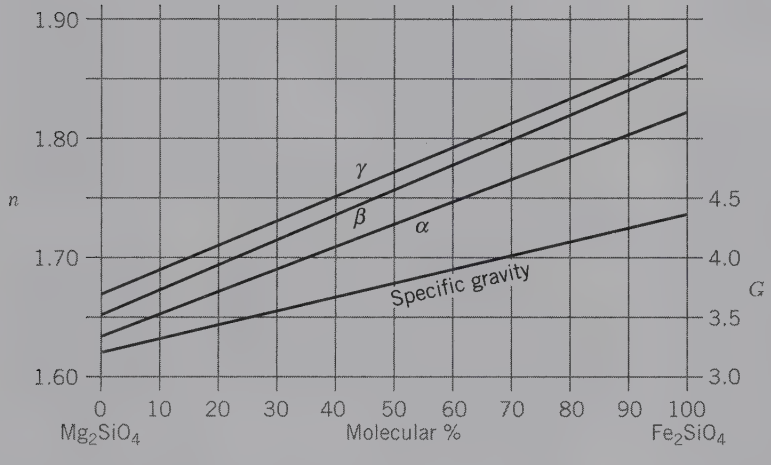

(*b*)

FIG. 19.4 (a) Relationship of the interplanar spacing of 130 (= d_{130}) and composition for the forsterite-fayalite series. (From Deer, W. A., R. A. Howie, and J. Zussman. 1982. *Orthosilicates*, vol. 1A, Wiley, New York; and Longman, London.) (b) Variations of refractive indices and specific gravity with composition.

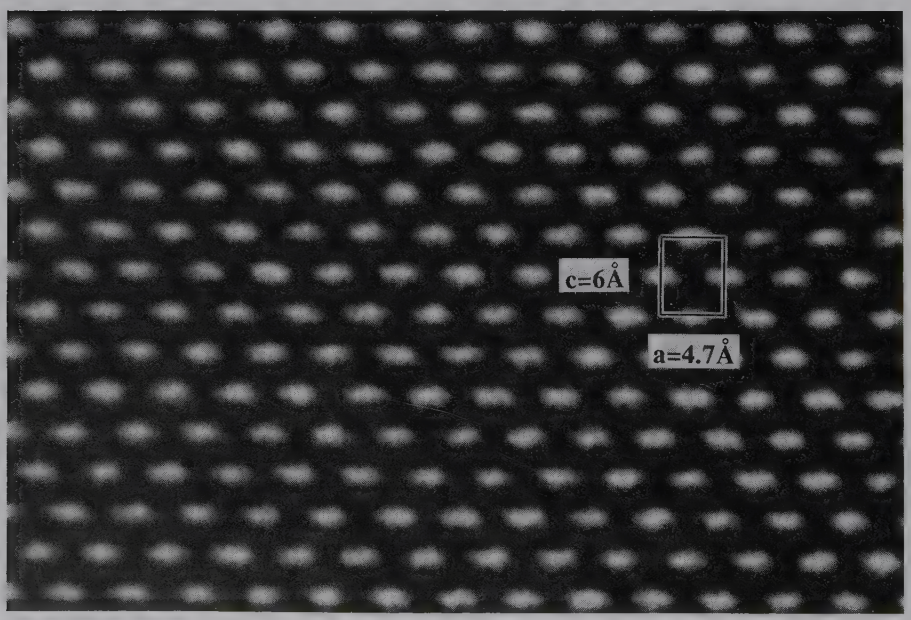

FIG. 19.5 High-resolution transmission electron microscope (HRTEM) image of an *a–c* section of olivine, of composition $(Mg_{1.76}Fe_{0.24})SiO_4$. A unit cell is outlined. This image shows the highly regular and homogeneous nature of the structure of this olivine crystal. (Courtesy of L. M. Wang, University of Michigan.)

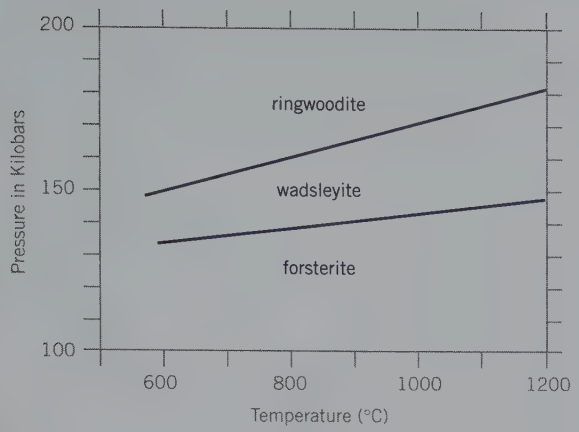

FIG. 19.6 The stability fields of various polymorphs of Mg_2SiO_4: forsterite, wadsleyite, and ringwoodite. (Adapted from Suito, K. 1972. Phase transformations of pure Mg_2SiO_4 into a spinel structure under high pressures and temperatures. *Journal of Physics of the Earth* 20: 225–43.)

SiO_2 and will react with it to form pyroxene, according to this reaction:

$$\underset{\text{forsterite}}{Mg_2SiO_4} + \underset{\text{quartz}}{SiO_2} \rightarrow \underset{\text{enstatite}}{2MgSiO_3}$$

Found as glassy grains in stony and stony-iron meteorites. Occasionally found in metamorphosed dolomitic limestones at high grade, where it is formed by the high-temperature reaction:

$$\underset{\text{dolomite}}{2CaMg(CO_3)_2} + \underset{\text{quartz}}{SiO_2} \rightarrow \underset{\text{forsterite}}{Mg_2SiO_4} + \underset{\text{calcite}}{2CaCO_3} + 2CO_2\uparrow$$

Associated often with pyroxene, plagioclase, magnetite, chromite, and serpentine.

The transparent gem variety is known as *peridot* (see Plate XI, no. 1, Chapter 20). It was used as a gem in ancient times in the East, but the exact locality for the stones is not known. Peridot is found in Myanmar and Pakistan, and in rounded grains associated with pyrope garnet in the surface gravels of Arizona and New Mexico, but the best quality material comes from Zebirget, an island in the Red Sea. Crystals of olivine are found in the lavas of Vesuvius. Larger crystals, altered to serpentine, come from Snarum, Norway. Olivine occurs in granular masses in volcanic bombs in the Eifel district, Germany, and at several localities in Arizona. Dunite rocks are found at Dun Mountain, New Zealand, and with the corundum deposits of North Carolina.

Alteration. Readily altered to *serpentine* minerals, such as *antigorite*, $Mg_3Si_2O_5(OH)_4$. Magnesite, $MgCO_3$ and iron oxides form at the same time as a result of the alteration. Olivines in metamorphosed basic igneous rocks commonly show *coronas*, which are concentric rims consisting of pyroxene and amphibole. Such coronas are the result of the instability of the high-temperature olivine in a lower temperature, H_2O-containing environment.

Use. The clear green variety, *peridot*, is used as a gem. Olivine is mined as refractory sand for the casting industry and for the manufacture of refractory bricks.

Name. Olivine derives its name from the usual olive-green color. *Chrysolite* is a synonym for olivine. Peridot is an old name for the species and now refers to the gem variety.

Similar Species. Other rarer members of the olivine group are *monticellite*, $CaMgSiO_4$, a high-temperature mineral in metamorphosed siliceous dolomitic limestones; and *tephroite*, Mn_2SiO_4.

GARNET GROUP—$(Mg^{2+},Fe^{2+},Mn^{2+})_3Al_2Si_3O_{12}$–$Ca_3(Fe^{3+},Al^{3+},Cr^{3+})_2Si_3O_{12}$

The garnet group includes a series of isostructural species (Table 19.1) with space group *Ia3d*; they crystallize in the hexoctahedral class of the isometric system and are similar in crystal habit. The structural arrangement (see Fig. 18.5) is such that the atomic population of the {100} and {111} families of planes is much depleted. As a result, the cube and octahedon, common on most isometric hexoctahedral crystals, are rarely found on garnets.

Crystallography. Isometric; $4/m\bar{3}2/m$. Common forms are dodecahedron *d* (Fig. 19.7a and 19.8) and trapezohedron, *n* (Fig. 19.7b), often in combination (Figs. 19.7c, d, and 19.9). Hexoctahedrons are observed occasionally (Fig. 19.7e). Other forms are rare. Usually in distinct crystals; also appears in rounded grains; massive granular, coarse or fine.

Ia3d; cell edge (see Table 19.1); $Z = 8$. *d*s for pyrope: 2.89(8), 2.58(9), 1.598(9), 1.542(10), 1.070(8).

Table 19.1 Chemical Compositions and Physical Properties of Garnets

Species	Composition	*n*	G	Unit Cell Edge (Å)
Pyrope	$Mg_3Al_2Si_3O_{12}$	1.714	3.58	11.46
Almandine	$Fe_3Al_2Si_3O_{12}$	1.830	4.32	11.53
Spessartine	$Mn_3Al_2Si_3O_{12}$	1.800	4.19	11.62
Grossular	$Ca_3Al_2Si_3O_{12}$	1.734	3.59	11.85
Andradite	$Ca_3Fe_2Si_3O_{12}$	1.887	3.86	12.05
Uvarovite	$Ca_3Cr_2Si_3O_{12}$	1.868	3.90	12.00
Hydrogrossular	$Ca_3Al_2Si_2O_8(SiO_4)_{1-m}(OH)_{4m}$; $m = 0$–1	1.734 to 1.675	3.59 to 3.13	11.85 to 12.16

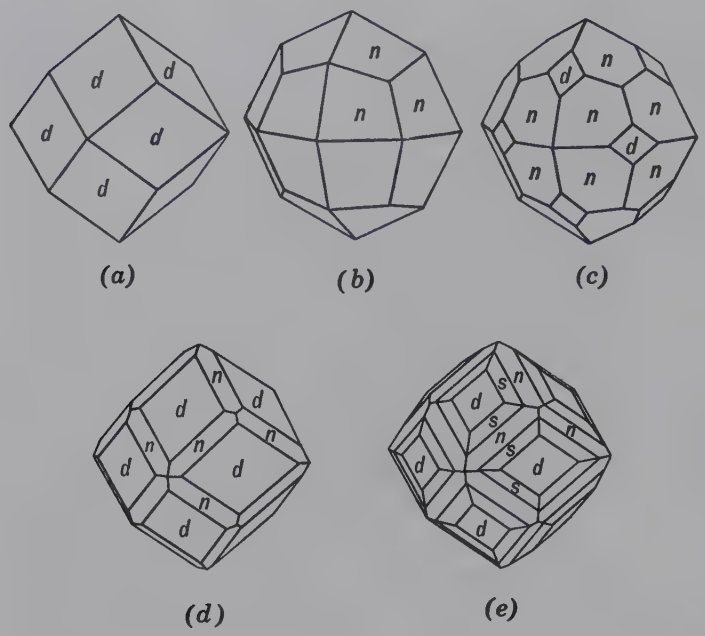

FIG. 19.7 Garnet crystals.

FIG. 19.8 Andradite garnet with dodecahedral faces, from Markhi Khel, Nangahar, Afghanistan. Specimen is 5.5 cm high (Photographs courtesy of Jeff Scovil, collection © Jeff Scovil.)

Physical Properties. **H** $6\frac{1}{2}$–$7\frac{1}{2}$. **G** 3.5–4.3, varying with composition (see Table 19.1). *Luster* vitreous to resinous. *Color* varying with composition (see following text); most commonly red, also brown, yellow, white, green, black. *Streak* white. Transparent to translucent.

Composition and Structure. Garnet compositions are expressed by the general structural formula $A_3\ B_2(SiO_4)_3$ where the *A* site houses Ca, Mg, Fe^{2+}, or Mn^{2+} and the *B* site incorporates Al, Fe^{3+}, and Cr^{3+} (see Fig. 18.5 and page 439). The formulas of the main species are given in Table 19.1, with the refractive indices, specific gravity, and unit cell edges for the end-member compositions. There is extensive substitution among the *pyralspite* group which refers to *py*rope, *al*mandine, and *sp*essartine, with solid solution primarily in the *A* site and Al^{3+} in the *B* site; and also among the *ugrandite* group which refers to *u*varovite, *gr*ossular, and *an*dradite, with Ca^{2+} in the *A* site and solid solution primarily in the *B* site. There is relatively little solid solution between these two major categories (see Fig. 19.10 and garnet groupings on p. 439). Rarely are the pure end-members found. It is difficult to the distinguish the end-members without a chemical analysis. Therefore, *pyralspite* and *ugrandite* are used to indicate the general composition. Hydrous garnets, such as *hydrogrossular*, contain up to 8.5% H_2O. This water, in the form of $(OH)_4^{4-}$ groups, substitutes probably for (SiO_4) tetrahedra in the structure, assuming the replacement $Si^{4+} \rightleftarrows 4H^+$.

Experimental studies at high pressures and temperatures show that the garnet structure is stable in the conditions of the Earth's lower mantle. It appears that pyrope type compositions are most likely in the *P* and *T* regime of the Earth's mantle (see p. 94).

Plate I

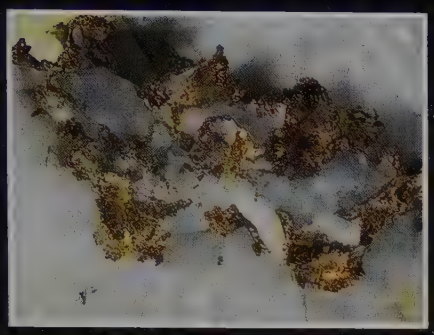

1. Gold in quartz

2. Silver

3. Copper

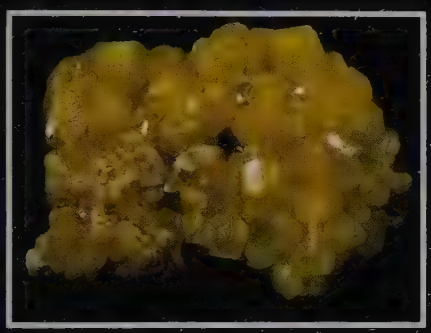

4. Sulfur crystals

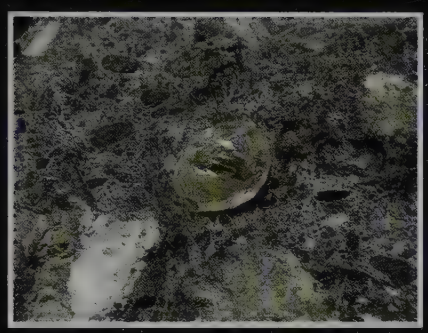

5. Diamond (rounded octahedral crystal) in kimberlite

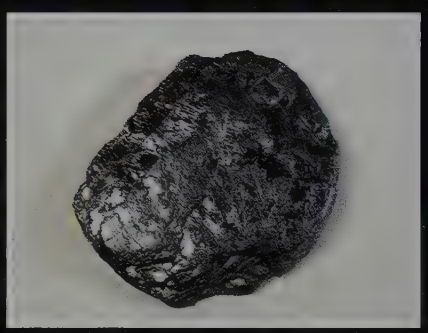

6. Graphite

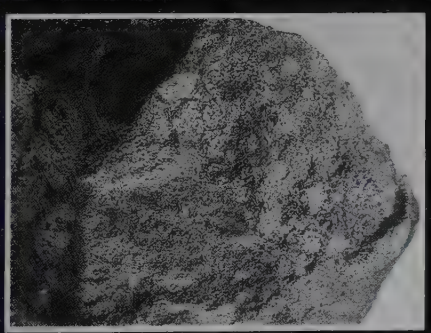

7. Bornite; broken surface with slight purplish tarnish

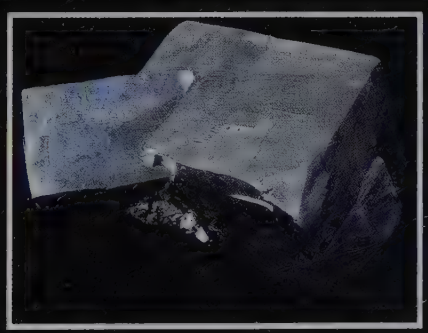

8. Galena (cubic crystals)

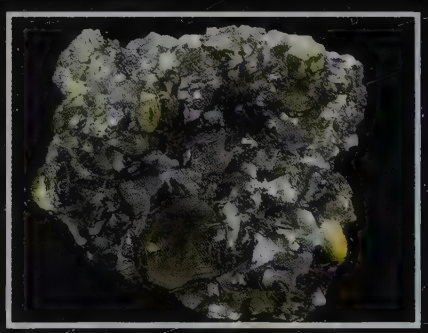

9. Sphalerite crystals

*All of the mineral specimens photographed for these Plates are from the Harvard University Mineralogical Museum. Carl A. Francis and William C. Metropolis provided access to the collections and assisted in selection. Photographs were taken by John Savickas, Albuquerque, New Mexico.

Plate II

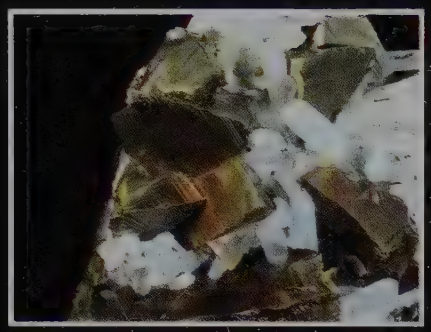

1. Chalcopyrite (tetragonal disphenoid crystals) and white quartz

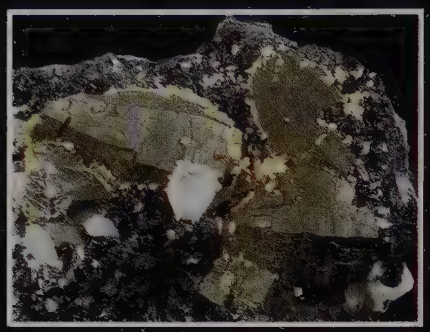

2. Pyrrhotite (curved hexagonal crystals) with white quartz and black sphalerite

3. Stibnite crystals

4. Pyrite (cubic crystals)

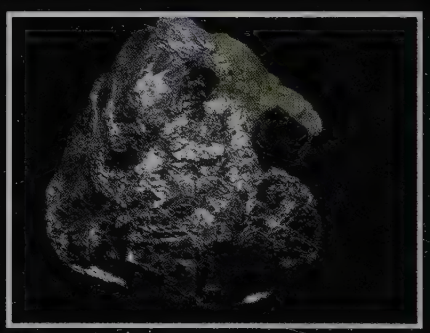

5. Molybdenite

6. Corundum: common corundum in feldspar-mica gneiss and ruby in chromian zoisite

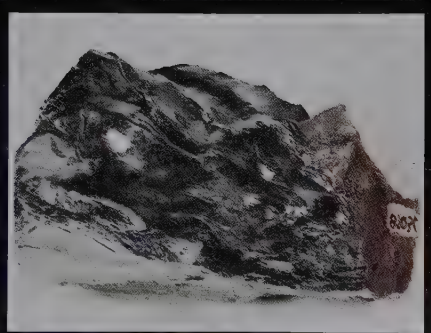

7. Hematite; variety, specularite

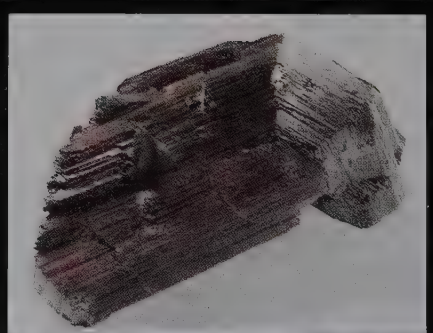

8. Rutile (twinned crystal)

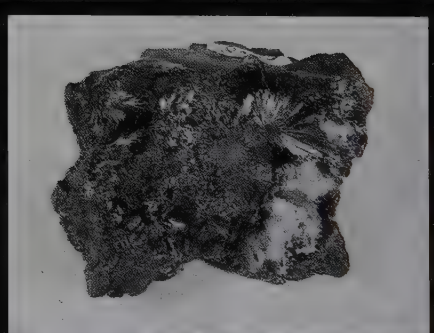

9. Pyrolusite

Plate III

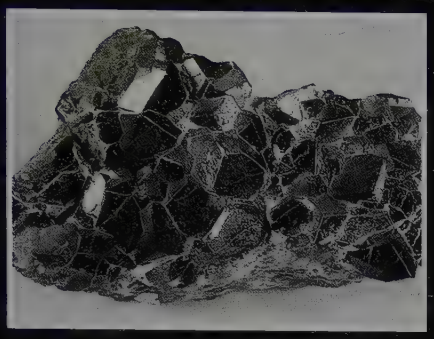

1. Magnetite (octahedral crystals)

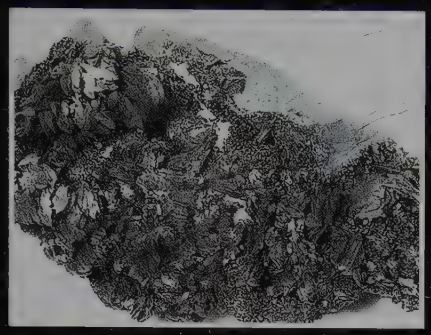

2. Manganite

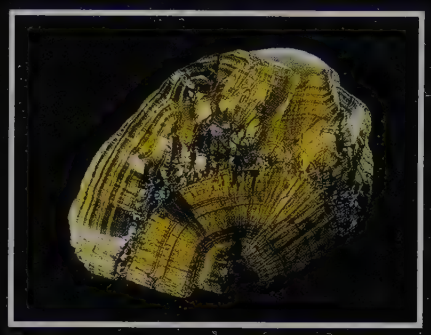

3. Goethite

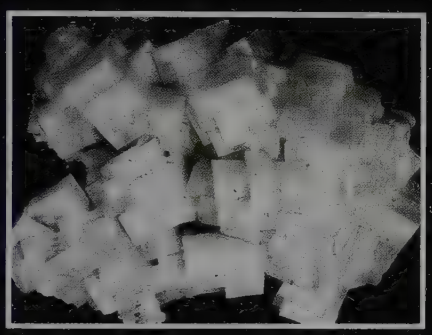

4. Halite (cubic crystals)

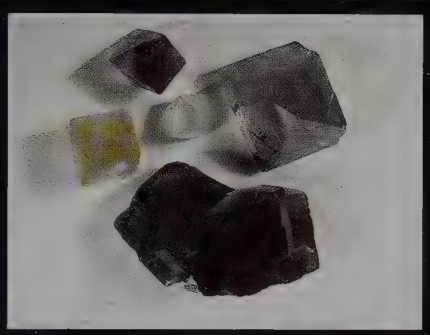

5. Fluorite (cubic crystals and octahedral cleavage fragments)

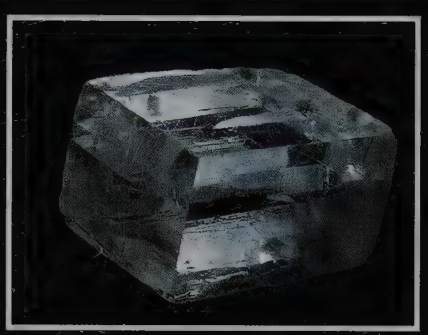

6. Calcite (rhombohedral cleavage fragment); variety, Iceland spar

7. Rhodochrosite (rhombohedral crystals)

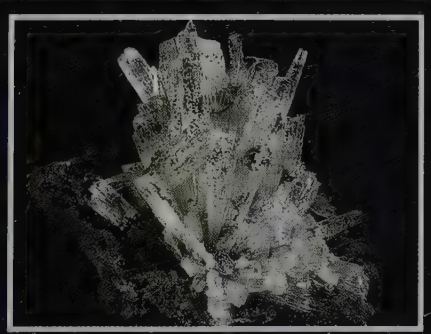

8. Aragonite (prismatic crystals)

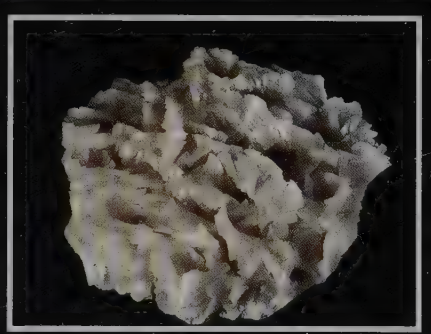

9. Dolomite ("saddle-shaped" crystals)

Plate IV

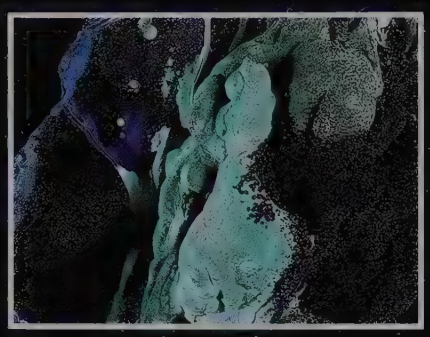

1. Azurite and malachite

2. Barite crystals on botryoidal hematite

3. Gypsum crystals

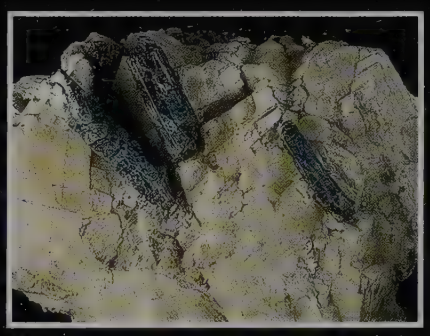

4. Apatite crystals (blue) in coarse-grained calcite

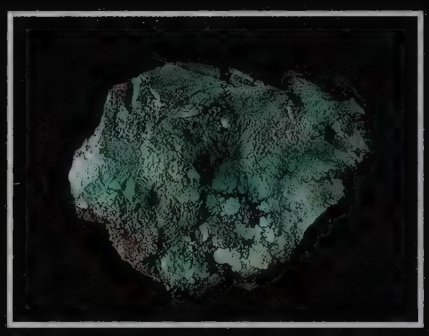

5. Turquoise

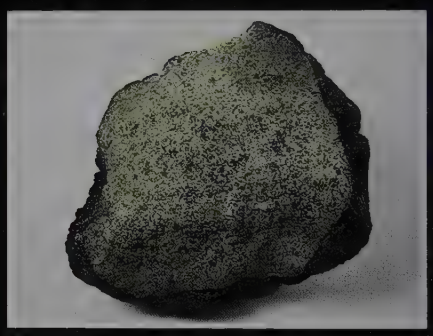

6. Olivine

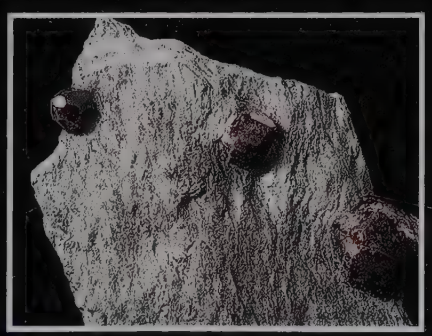

7. Garnet (almandine) crystals in mica schist

8. Zircon crystals

9. Andalusite; variety, chiastolite

Plate V

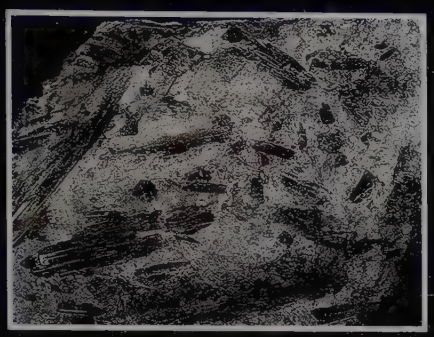

1. Sillimanite in quartz matrix

2. Kyanite and staurolite crystals in paragonite schist

3. Topaz crystal

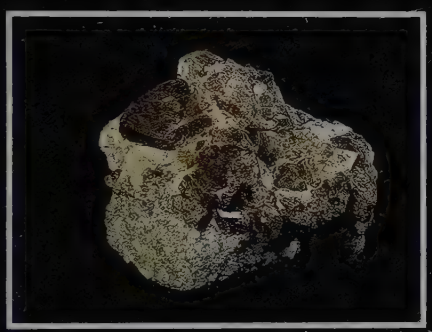

4. Vesuvianite in calcite matrix

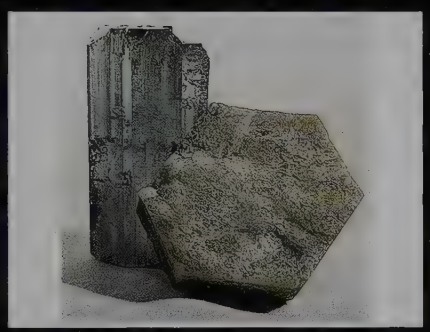

5. Beryl; common beryl and aquamarine

6. Tourmaline crystals; black ("schorl"), pink and green varieties

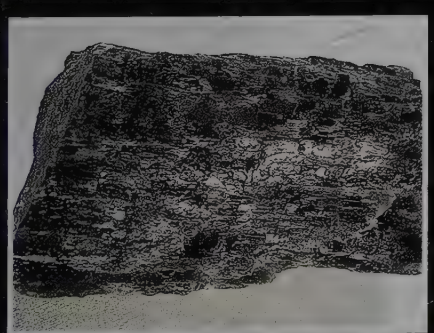

7. Enstatite cleavage fragment

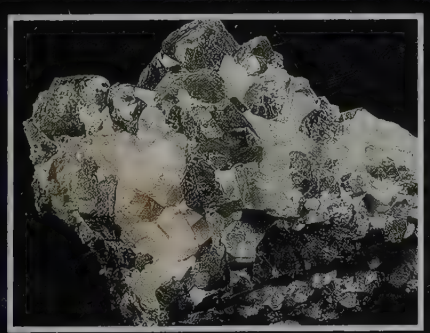

8. Diopside with calcite

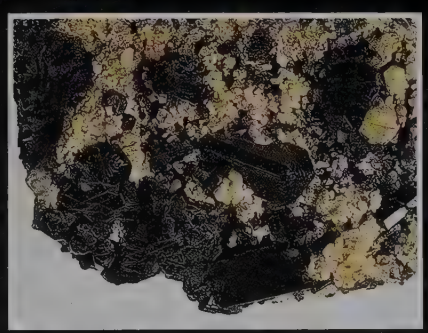

9. Augite with potassium feldspar

Plate VI

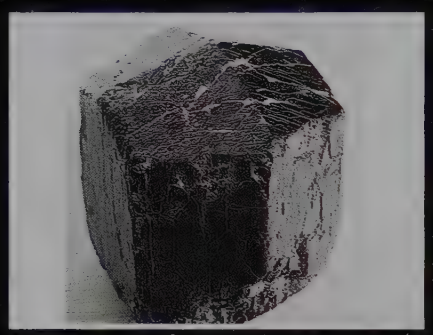

1. Augite crystal

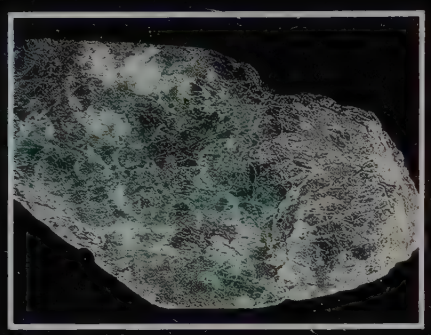

2. Jadeite

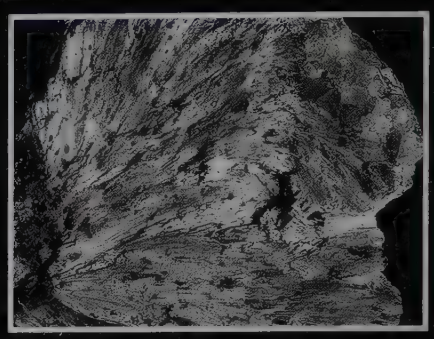

3. Wollastonite and some green diopside grains

4. Rhodonite with calcite and brown willemite

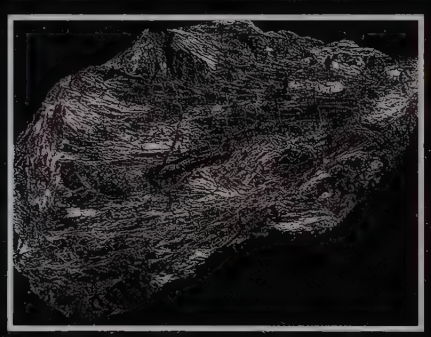

5. Anthophyllite

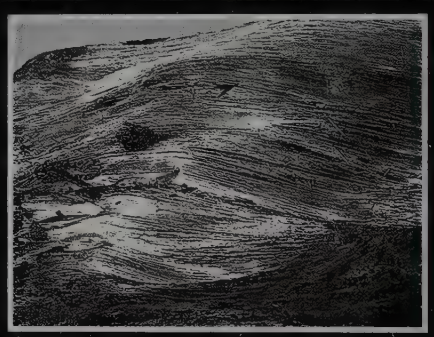

6. Grunerite; asbestiform variety "amosite"

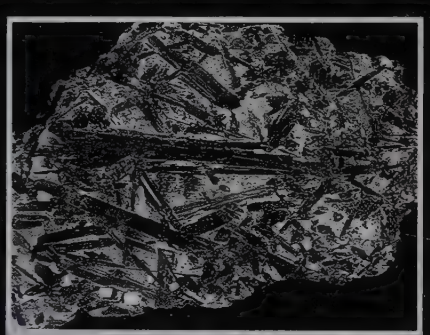

7. Actinolite in chlorite matrix

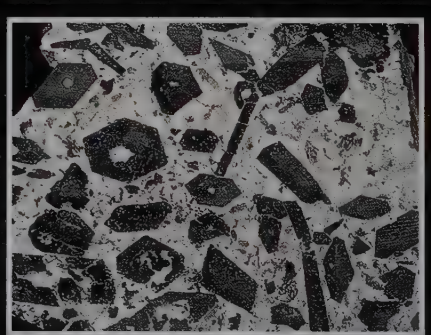

8. Hornblende crystals in cross-section in an albitic matrix

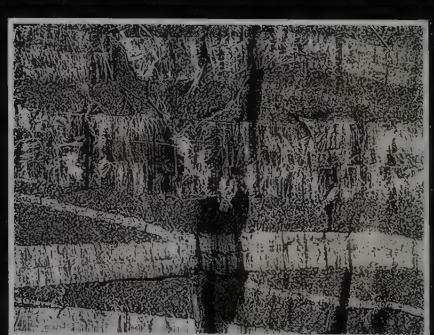

9. Chrysotile asbestos bands within serpentine matrix (a mixture of lizardite and antigorite)

Plate VII

1. Kaolinite, pseudomorphous after Carlsbad-twinned orthoclase

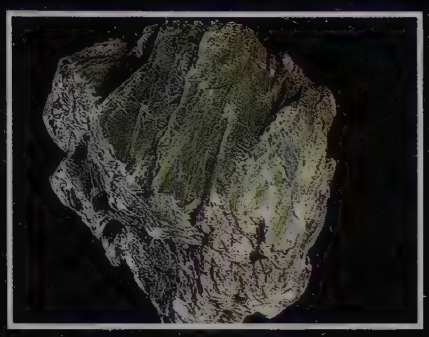

2. Talc

3. Muscovite crystal group

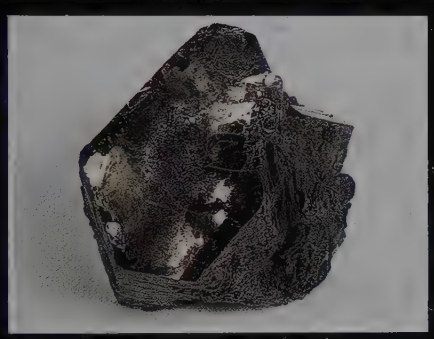

4. Phlogopite

5. Biotite

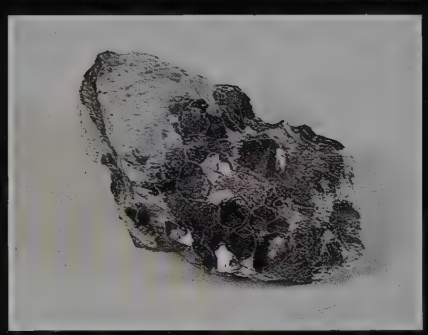

6. Lepidolite with albite

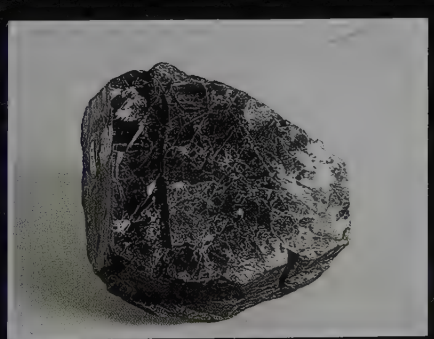

7. Chlorite

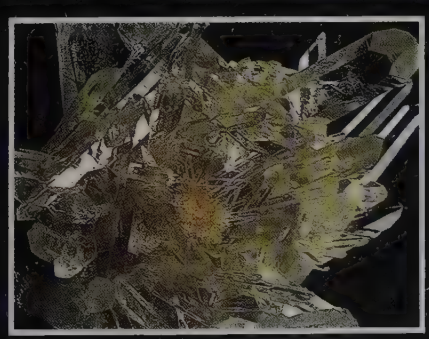

8. Quartz crystals

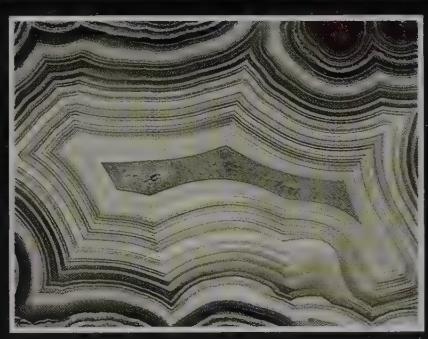

9. Chalcedony; banded, in agate

Plate VIII

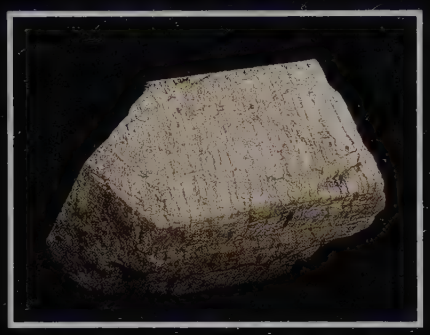

1. Microcline cleavage fragment with perthitic texture

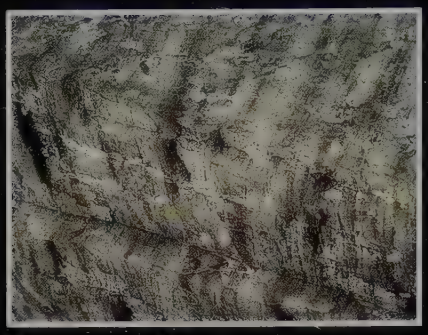

2. Close-up of perthitic texture in microcline of photo no. 1.

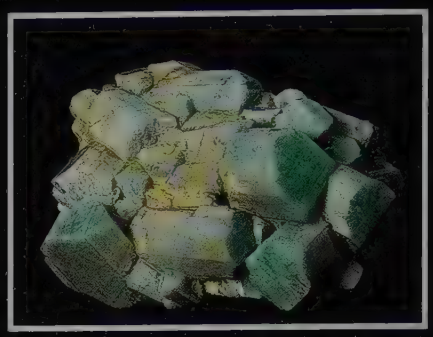

3. Microcline crystals; green variety, amazonite

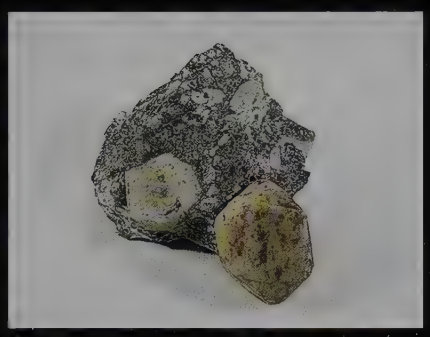

4. Orthoclase; Carlsbad-twinned crystals in trachyte matrix

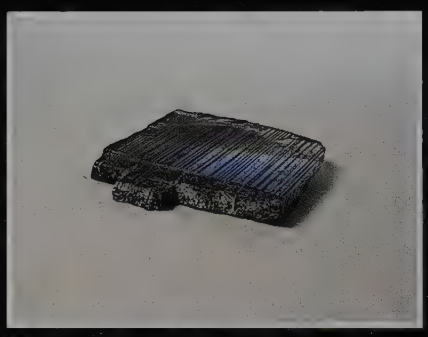

5. Plagioclase; variety, labradorite showing albite twin lamellae and iridescence (also known as labradorescence)

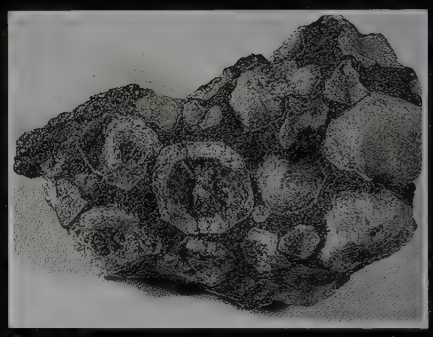

6. Leucite; trapezohedral phenocrysts in phonolite

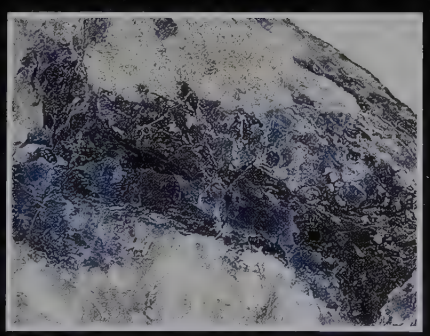

7. Sodalite with nepheline and muscovite

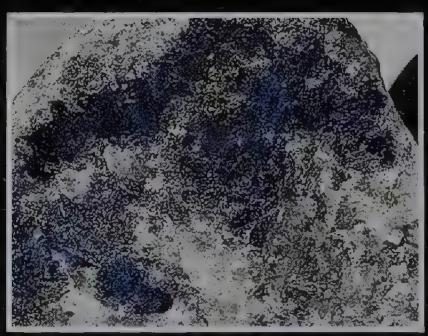

8. Lazurite with pyrite in marble

9. Stilbite

Plate IX

1. Diamond crystals with 5 carat cut stone.

2. The "Patricia Emerald"; 6.6 cm high, 126 grams in weight. (The American Museum of Natural History.)

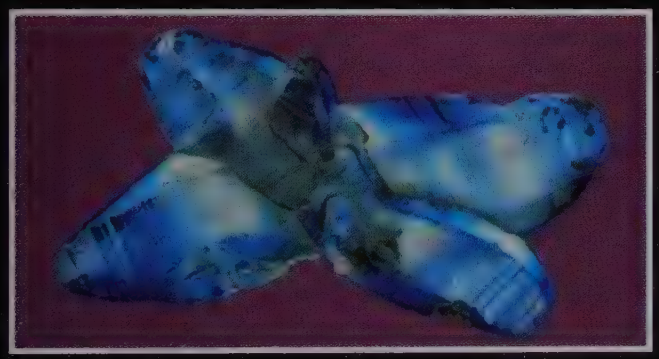

3. Natural sapphire crystals, 3.5 cm long.

4. Ruby crystal on calcite, Jagadalaic, Afghanistan. Crystal 1.3 cm wide.

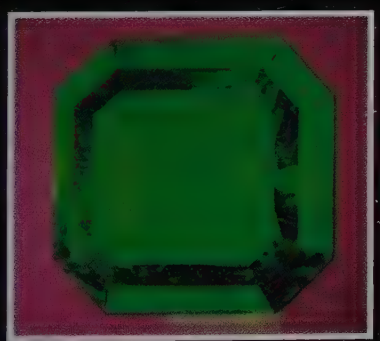

5. The "Denise Emerald," 83.1 carats.

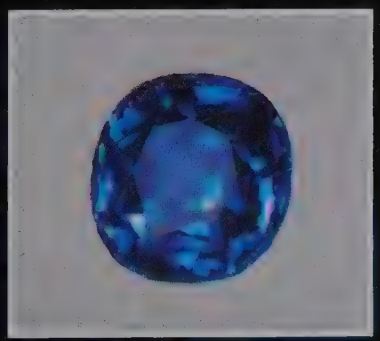

6. Sapphire, 6.5 carats.

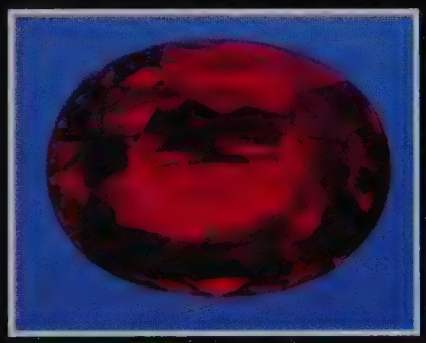

7. Ruby 7.21 carats.

Plate X

1. Smoky quartz.
2. Amethyst.
3. Citrine.
4. Rose quartz.
5. Quartz (with the exception of aventurine) microcrystalline. Clockwise from upper left: aventurine quartz, agate, carnelian, chrysoprase, tiger's eye.
6. Agate snuff bottle and moss agate.
7. Opal.
8. Chrysoberyl.
9. Zircon.
10. Spinel.
11. Tourmaline.

(Harvard Mineralogical Museum.)

Plate XI

1. Olivine (peridot).
2. Garnet.
3. Topaz, natural colors.
4. Topaz. From left to right: colorless stream pebble; colored by irradiation; heat treated after irradiation; below: gem cut from treated material.
5. Lapis lazuli.
6. Jadeite.
7. Turquoise.
8. Beryl.
9. Synthetic emerald crystals.

(Harvard Mineralogical Museum.)

Plate XII

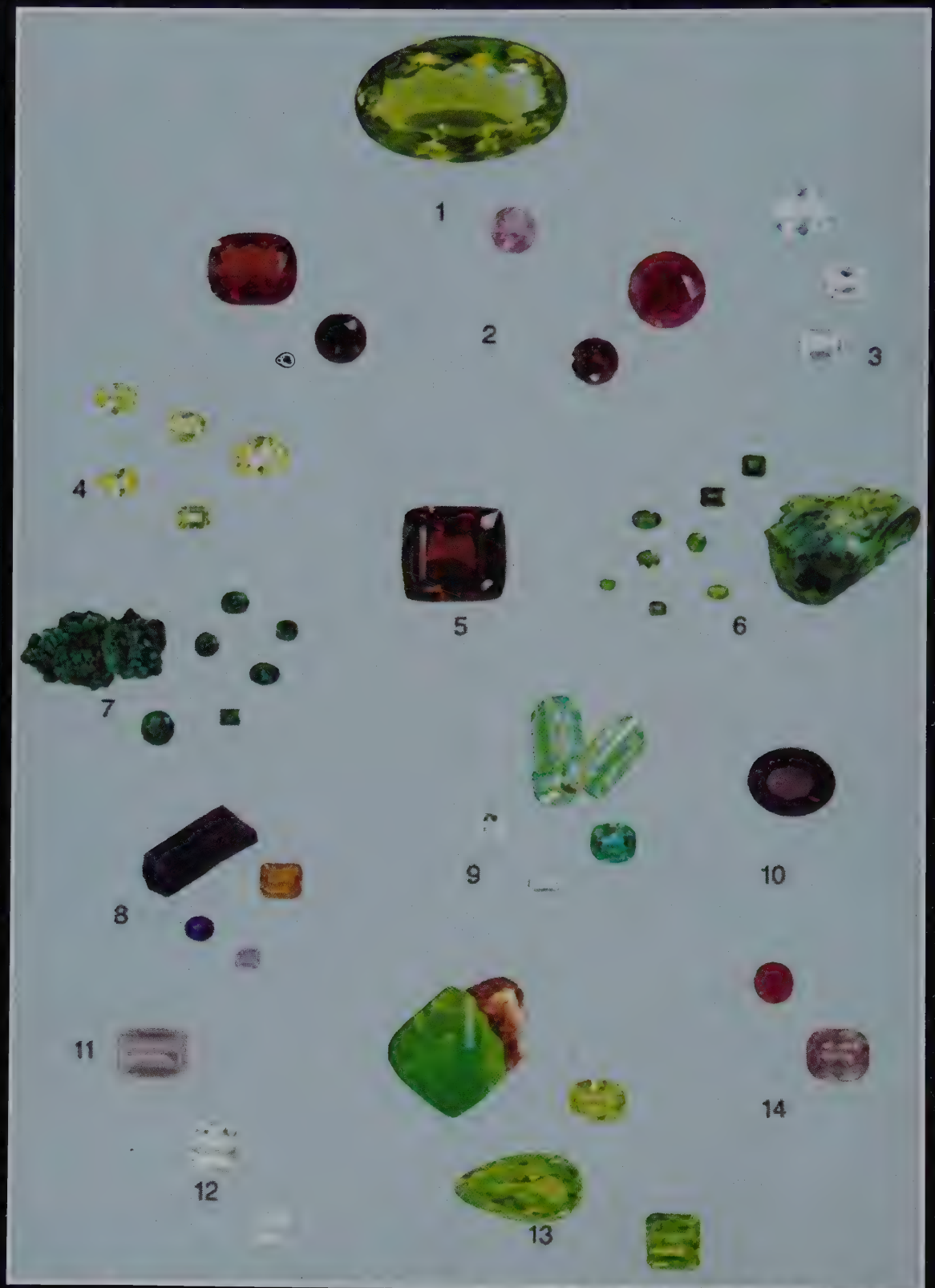

1. Fluorite.
2. Sphalerite.
3. Petalite.
4. Amblygonite.
5. Sinhalite.
6. Diopside.
7. Dioptase.
8. Apatite.
9. Euclase.
10. Enstatite.
11. Barite.
12. Phenakite.
13. Brazilianite.
14. Scheelite.

(Courtesy of A. Rupenthal, Idar-Oberstein, Germany.)

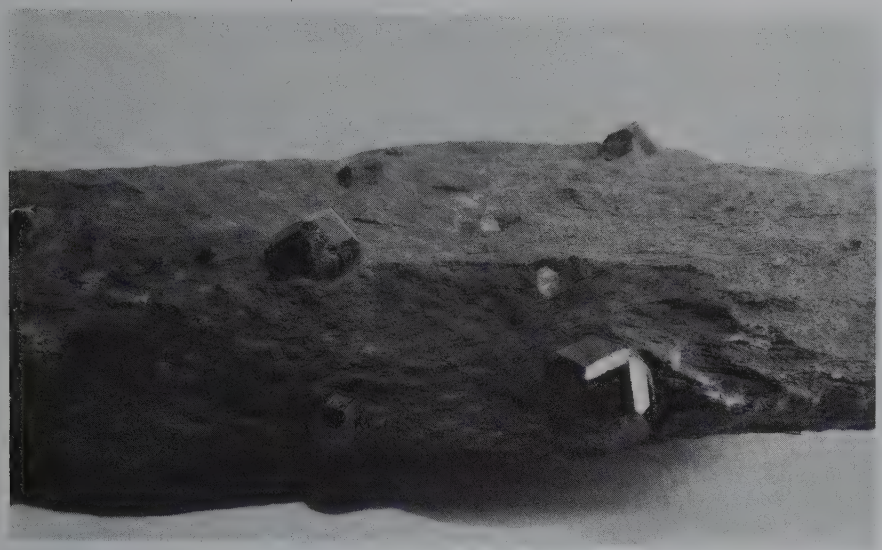

FIG. 19.9 Garnet crystals in chlorite schist.

Pyrope, Mg_3Al_2. Some Ca and Fe^{2+} usually present. Color depends on solid solution and is deep red to nearly black. Often transparent and then used as a gem. Name derived from the Greek word meaning *firelike*. *Rhodolite* is the name given to a pale rose-red or purple garnet, corresponding in composition to two parts of pyrope and one almandine.

Almandine, Fe_3Al_2. Fe^{3+} may replace Al, and Mg and Mn may replace Fe^{2+}. Color is fine deep red, transparent in precious garnet; brownish-red, translucent in common garnet, see Plate IV, no. 7. Name derived from Alabanda in Asia Minor, where in ancient times garnets were cut and polished.

Spessartine, Mn_3Al_2. Fe^{2+} usually replaces some Mn^{2+} and Fe^{3+} some Al. Color is orange to brown to red, depending on composition. Name derived from the locality Spessart, Germany.

Grossular, Ca_3Al_2 (*essonite*, *cinnamon stone*). Often contains Fe^{2+} replacing Ca, and Fe^{3+} replacing Al. Color white, green, yellow, cinnamon-brown, pale red, depending on composition. Name derived from the botanical name for gooseberry, in allusion to the light green color of the original grossular.

Andradite, $Ca_3Fe_2^{3+}$. Al may replace Fe^{3+}; Fe^{2+}, Mn^{2+}, and Mg may replace Ca. Color various shades of yellow, green, brown to black. *Demantoid* is a green variety with a brilliant luster, used as a gem. Named after the Portuguese mineralogist, d'Andrada.

Uvarovite, $Ca_3Cr_2^{3+}$. Color emerald-green. Named after Count Uvarov.

Diagnostic Features. Garnets are usually recognized by their characteristic isometric crystal forms, their hardness, and their color. Specific gravity, refractive index, and unit cell dimension taken together serve to distinguish members of the group.

Occurrence. Garnet is a common and widely distributed mineral; occurring abundantly in some metamorphic rocks (see Fig. 19.9) and as an accessory constituent in some igneous rocks. *Pyralspite* occurs in mica schists, hornblende schists, and gneisses. It is frequently used as an index mineral to delineate isograds in metamorphic rocks. Found in pegmatite dikes, more rarely in granitic rocks. *Pyrope* occurs in ultrabasic rocks, such as peridotites or kimberlites and in serpentines derived from them. The garnets, which in eclogites coexist with pyroxenes and kyanite, vary in composition from pyrope to almandine. *Almandine* is the common garnet in metamorphic rocks, resulting from the regional metamorphism of Al-rich sediments. It is also a widespread detrital garnet in sedimentary rocks. *Ugrandite* is found in metamorphosed rocks rich in calcium. *Spessartine* occurs in skarn deposits and in Mn-rich assemblages containing rhodonite, Mn-oxides, and so forth. *Grossular* is found chiefly as a product of contact or regional metamorphism of impure limestones. *Andradite* occurs in geological environments similar to that of grossularite. It may be the result of metamorphism of impure siliceous limestone, by this reaction:

$$\underset{\text{calcite}}{3CaCO_3} + \underset{\text{quartz}}{3SiO_2} + \underset{\text{hematite}}{Fe_2O_3} \rightarrow \underset{\text{andradite}}{Ca_3Fe_2Si_3O_{12}} + 3CO_2\uparrow$$

Melanite, a black variety of andradite, occurs in alkaline igneous rocks. *Uvarovite* is the rarest of this group of garnets and is found in serpentine associated with chromite. The best known locality is Outokumpu, Finland.

Pyrope of gem quality is found with clear grains of olivine (peridot) in the surface sands near Fort Defiance, close to the New Mexico–Arizona line. A locality near Měrunice (Meronitz), Czech Republic, is famous for pyrope gems. Almandine of gem quality is found in northern India, Sri Lanka, and Brazil. Fine crystals, although for the most part too opaque for cutting, are found in a mica schist on the Stikine River, Alaska. Grossular is used a little in jewelry, but essonite or cinnamon stones of good size and color are found in Sri Lanka. Tangerine orange spessartine is found in Namibia and used as a gem.

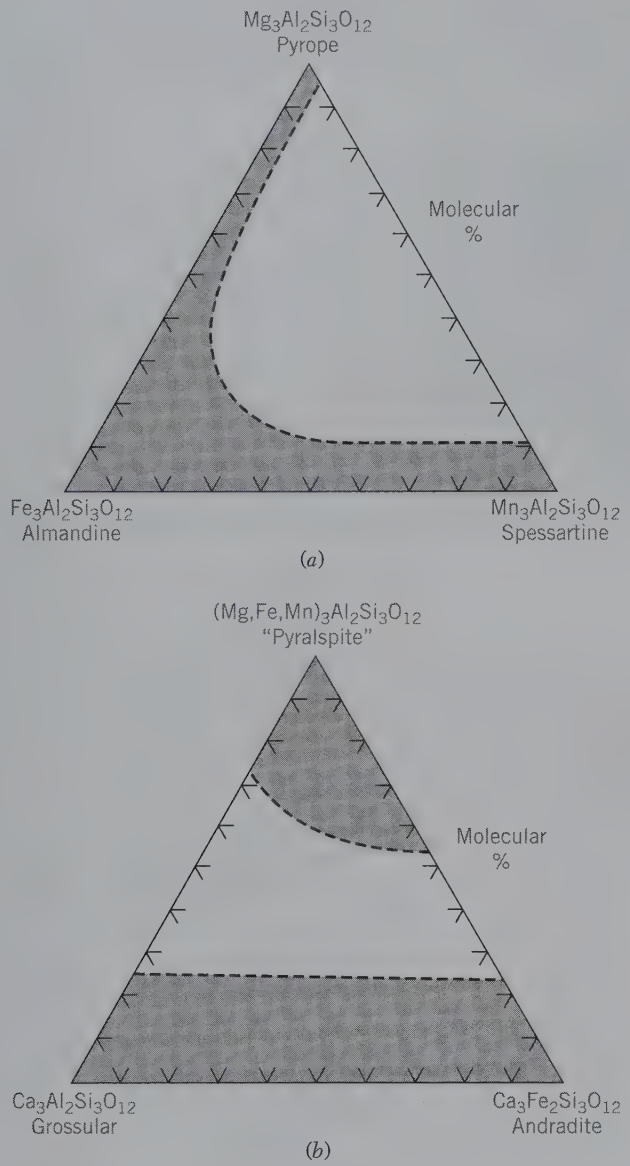

FIG. 19.10 (a) The extent of solid solution in garnets of the *pyralspite* group: pyrope-almandine-spessartine. (b) There is only limited solid solution between members of the *pyralspite* and *ugrandite* groups; ugrandite represents uvavorite-grossular-andradite.

Alteration. Garnet often alters to other minerals, particularly talc, serpentine, and chlorite. Pseudomorphs of chlorite after garnet are common.

Use. All species, except uvarovite, are cut as gemstones (see Plate XI, no. 2, Chapter 20). The most valued is a green andradite, known as *demantoid*, which comes from the Ural Mountains, Russia. At Gore Mountain, New York, large crystals of almandine in an amphibolite are mined. The unusual angular fractures and high hardness of the garnets make them desirable for a variety of abrasive purposes, including garnet paper.

Name. *Garnet* is derived from the Latin word *granatus*, meaning *like a grain*.

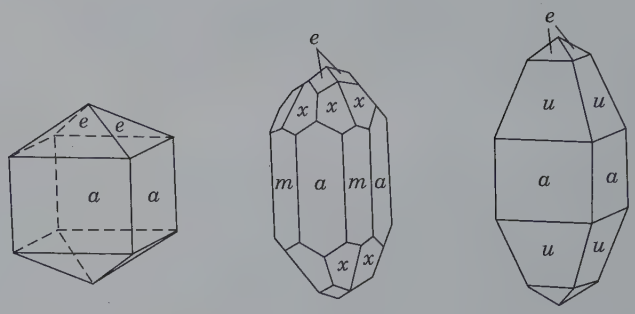

FIG. 19.11 Zircon crystals.

ZIRCON—$ZrSiO_4$

Crystallography. Tetragonal; $4/m2/m2/m$. Crystals usually show a simple combination of prisms and dipyramids, $a\{010\}$ and $e\{011\}$, but $m\{110\}$ and a ditegragonal dipyramid is also observed (Fig. 19.11). Usually in crystals; also in irregular grains.

$I4_1/amd$; a = 6.60, c 5.98 Å; Z = 4. *d*s: 4.41(7), 3.29(10), 2.52(8), 1.710(9).

Physical Properties. *Cleavage* {010} poor. **H** $7\frac{1}{2}$. **G** 4.68. *Luster* adamantine. *Color* commonly some shade of brown, see Plate IV, no. 8; also colorless, gray, green, red. *Streak* uncolored. Usually translucent; in some cases transparent. *Optics*: (+), ω = 1.923–1.960, ϵ = 1.968–2.015. Metamict zircon, n = 1.78.

Composition and Structure. For $ZrSiO_4$, ZrO_2 67.2, SiO_2 32.8%. Zircon contains some hafnium, lead, uranium, and REEs. Although the amount is usually small (1% to 4%), analyses have reported up to 24% HfO_2. The structure of zircon is shown in Fig. 19.12. Zr is in 8-coordination with oxygen in the form of distorted cube-like polyhedra. The eight oxygens surrounding each Zr belong to six different SiO_4 tetrahedra. Although the structure of zircon is resistant to normal chemical attack, it is often in a metamict state (see page 283). This is caused by the structural damage from Th and U,

FIG. 19.12 Structure of zircon, $ZrSiO_4$, consisting of independent SiO_4 tetrahedra and distorted ZrO_8 cubes. (Redrawn from T. Zoltai, *Polyhedral Structure Models*. University of Minnesota, Minneapolis.)

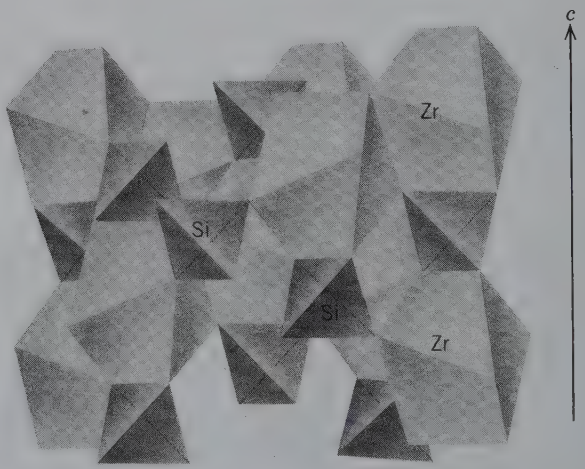

which are present in small amounts in many zircons. The "self-irradiation" from the decay of U and Th produces as a final result an isotropic glass with a reduction in density of about 16% and a lowering of refractive index (see Figs. 12.19 and 12.20).

Diagnostic Features. Usually recognized by its characteristic crystal form, color, luster, hardness, and high specific gravity.

Occurrence. Zircon is a common and widely distributed accessory mineral in all types of igneous rocks. It is especially common in silicic rocks, such as granite, granodiorite, syenite, and monzonite, and very common in nepheline syenite. Found also in marbles, gneisses, and schists. Because zircon is a stable chemical compound, it is a common accessory mineral in many sediments. Its characteristics in the heavy mineral fraction of sandstones are often useful in the evaluation of provenance. Zircon is frequently found as rounded grains in stream and beach sands, often with gold. Zircon has been produced from beach sands in Australia, Brazil, and Florida.

Gem zircons are found in the stream sands at Matura, Sri Lanka; and in the gold gravels in the Ural Mountains, Russia, and Australia. In large crystals from Madagascar. Found in the nepheline syenites of Norway. Found in the United States in Orange and St. Lawrence counties, New York; in considerable quantity in the sands of Henderson and Buncombe counties, North Carolina. Large crystals have been found in Renfrew County, Ontario, Canada.

Use. When transparent, it serves as a gemstone. It is colorless in some specimens, but more often of a brownish or red-orange color. Blue is not a natural color for zircon but is produced by heat treatment. The colorless, yellowish, or smoky stones are called *jargon*, because although resembling diamond they have little value. Serves as the source of zirconium oxide, which is one of the most refractory substances known. Platinum, which fuses at 1755°C, can be melted in crucibles of zirconium oxide.

Overshadowing its other uses since 1945 is the use of zircon as the source of metallic zirconium. Pure zirconium metal is used in the construction of nuclear reactors. Its low neutron-absorption cross-section, coupled with retention of strength at high temperatures and excellent corrosion resistance, makes it a most desirable metal for this purpose.

Mineral grains of zircon in igneous, metamorphic, or sedimentary rocks, are commonly used for radioactive age determinations. The oldest rocks dated thus far were formed 4.4 billion years ago based on a detrital zircon from the Jack Hills region in Western Australia (Wilde et al., 2001).

Name. The name is very old and is believed to be derived from the Persian words *zar*, *gold*, and *gun*, depicting color.

Similar Species. *Thorite*, $ThSiO_4$, is isostructural with zircon. It is usually reddish-brown to black, hydrated, and radioactive.

Al_2SiO_5 GROUP

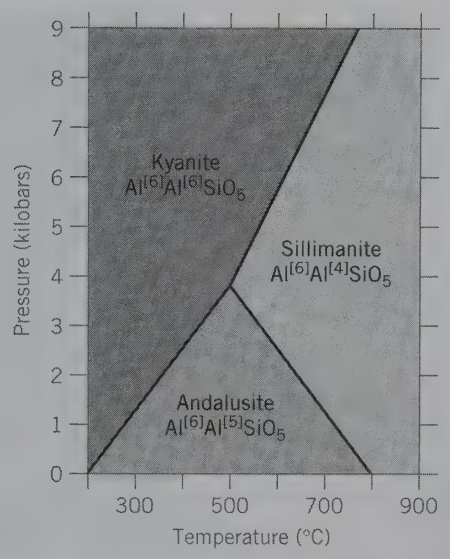

FIG. 19.13 Experimentally determined stability fields for the polymorphs of Al_2SiO_5. (From Holdaway, M. J. 1971. Stability of andalusite and the aluminum silicate stability diagram. *American Journal of Science* 271: 97–131; see also *Orthosilicates, Reviews in Mineralogy*, 1980, Mineralogical Society of America. Washington, D.C., 190.)

The three polymorphs of Al_2SiO_5 are *andalusite*, $Al^{[6]}Al^{[5]}SiO_5$ (space group *Pnnm*), *sillimanite*, $Al^{[6]}Al^{[4]}SiO_5$ (space group *Pbnm*), and *kyanite*, $Al^{[6]}Al^{[6]}SiO_5$ (space group $P\bar{1}$). The structures of the three polymorphs were discussed on pages 439–441 and their structures are shown in Figs. 18.6 and 18.7. All three minerals are found in metamorphosed aluminous rocks, such as mica schists. The stability relations of the three polymorphs have been determined experimentally, as shown in Fig. 19.13. These stability fields are of value in determining the *P–T* conditions of regionally and contact metamorphosed terranes. Rocks rich in aluminum tend to form sillimanite in high-temperature, regionally metamorphosed areas. Andalusite is frequently found in contact metamorphosed aureoles, and kyanite is located in high-pressure metamorphic areas. When all three polymorphs occur together, *P–T* conditions of the rock's origin near 500°C and 3.5 kb can be inferred (see also Fig. 19.13). All three polymorphs are easily recognized, in hand specimen, in medium- to coarse-grained rocks. The ease of recognition of these minerals and their presence in mica schists have led to their use as index minerals in the defining of metamorphic zones, as a function of temperature and pressure. Sillimanite can be used to define metamorphic zones that have been subjected to temperature of about 500°C and up (see Fig. 19.13). The metamorphic zones are named after the index mineral present, for example, sillimanite zone, kyanite zone. The boundaries between different zones are referred to as *isograds*. Kyanite, which has **G** = 3.55 to 3.66 (as compared with **G** = 3.23 for sillimanite and **G** = 3.16–3.20 for andalusite) has the densest structure of the three polymorphs and its stability field is located at lower *T* and higher *P* (Fig. 19.13). Andalusite has the largest specific volume and is the polymorph stable at the lowest pressure conditions.

FIG. 19.14 Successive sections through a chiastolite (andalusite) crystal.

ANDALUSITE—Al_2SiO_5

Crystallography. Orthorhombic; $2/m2/m2/m$. Usually occurs in coarse, nearly square prisms terminated by {001}.

Pnnm; $a = 7.78, b = 7.92, c = 5.57$ Å; $Z = 4$. *ds*: 4.53(10), 3.96(8), 2.76(9), 2.17(10), 1.46(10).

Physical Properties. *Cleavage* {110} good. **H** $7\frac{1}{2}$. **G** 3.16–3.20. *Luster* vitreous. *Color* white when pure, flesh-red, reddish-brown, olive-green with impurities. The variety *chiastolite* has graphite inclusions arranged in a regular manner forming a cruciform design (see Fig. 19.14 and Plate IV, no. 9). Transparent to translucent. *Optics*: (−), $\alpha = 1.632$, $\beta = 1.638$, $\gamma = 1.643$; $2V = 85°$; $X = c$, $Z = a$. In some crystals strong pleochroism; X red, Y and Z green to colorless; $r > v$.

Composition and Structure. Al_2O_3 63.2, SiO_2 36.8%. The structure consists of chains of AlO_6 octahedra parallel to c, cross-linked by SiO_4 tetrahedra and AlO_5 polyhedra (see Fig. 18.7b). Mn substitution for Al up to 38.5 wt. %.

Diagnostic Features. Characterized by the nearly square prism and hardness. Chiastolite is readily recognized by the symmetrically arranged inclusions.

Alteration. Pseudomorphs of muscovite after andalusite are common.

Occurrence. Andalusite is formed typically in the contact aureoles of igneous intrusions in Al-rich rocks. Here, it commonly coexists with cordierite, garnet, and micas. Andalusite can be found in association with kyanite, or sillimanite, or both in regionally metamorphosed terrane. Such occurrences may reflect variations in P and T during metamorphism, as well as the sluggishness of the reconstructive polymorphic transitions (see page 269).

Notable localities are in Andalusia, Spain; the Austrian Tyrol; in gem crystals and water-worn pebbles from Minas Gerais, Brazil. Crystals of chiastolite are found at Bimbowrie, South Australia. In the United States, found in the White Mountains near Laws, California, in Delaware County, Pennsylvania and in Maine. Chiastolite is found at Westford, Lancaster, and Sterling, Massachusetts, and also in California.

Use. Andalusite has been mined in large quantities in California for use in the manufacture of spark plugs and other porcelains of a highly refractory nature. When transparent it may serve as a gemstone.

Name. From Andalusia, a province of Spain.

SILLIMANITE—Al_2SiO_5

Crystallography. Orthorhombic; $2/m2/m2/m$. Occurs in long, slender crystals without distinct terminations, see Plate V, no. 1; often in parallel groups; frequently fibrous and called *fibrolite*.

Pbnm; $a = 7.44, b = 7.60, c = 5.75$ Å; $Z = 4$. *ds*: 3.32(10), 2.49(7), 2.16(8), 1.677(7), 1.579(7).

Physical Properties. *Cleavage* {010} perfect. **H** 6–7. **G** 3.23. *Luster* vitreous. *Color* white. Transparent to translucent. *Optics*: (+), $\alpha = 1.657$, $\beta = 1.658$, $\gamma = 1.677$; $2V = 20°$, $X = b$, $Z = c$; $r > v$.

Composition and Structure. Oxide components as in andalusite. The structure consist of AlO_6 chains parallel to the c axis and linking SiO_4 and AlO_4 tetrahedra, which alternate along the c direction (see Fig. 18.7a).

Diagnostic Features. Characterized by slender crystals with one direction of cleavage.

Occurrence. Sillimanite occurs in high-temperature metamorphosed aluminum-rich rocks, such as almandine-sillimanite-biotite schists and sillimanite-cordierite gneisses. It forms from the breakdown of staurolite and/or muscovite and is used as an index mineral for high-grade metamorphism. In silica-poor rocks it may be associated with corundum.

Notable localities for its occurrence are Maršová (Marschendorf), Czech Republic; Fassa, Austrian Tyrol; Bodenmais, Bavaria; and Freiberg, Saxony, Germany; Ihosy, Madagascar; and waterworn masses in diamantiferous sands from Minas Gerais, Brazil. In the United States, found at Worcester, Massachusetts; at Norwich and Willimantic, Connecticut; and New Hampshire.

Name. In honor of Benjamin Silliman (1779–1864), professor of chemistry at Yale University.

Similar Species. *Mullite*, a nonstoichiometric compound of approximate composition $Al_6Si_3O_{15}$, is rare as a mineral but common in synthetic Al_2O_3-SiO_2 systems at high temperature. *Dumortierite*, $Al_7O_3(BO_3)(SiO_4)_3$, has been used in the manufacture of high-grade porcelain.

KYANITE—Al_2SiO_5

Crystallography. Triclinic; $\bar{1}$. Usually in long, tabular crystals, rarely terminated; see Plate V, no. 2. In bladed aggregates.

P$\bar{1}$; $a = 7.10, b = 7.74, c = 5.57$ Å; $\alpha = 90°6'$, $\beta = 101°2'$, $\gamma = 105°45'$; $Z = 4$. *ds*: 3.18(10), 2.52(4), 2.35(4), 1.93(5), 1.37(8).

Physical Properties. *Cleavage* {100} perfect. **H** = 5 parallel to length of crystals, 7 at right angles to this direction. **G** 3.55–3.66. *Luster* vitreous to pearly. *Color* usually blue, due to titanium, white if pure. Also, in some cases, gray or green. Color may be in irregular streaks and patches. *Optics*: (−); $\alpha = 1.712$, $\beta = 1.720$, $\gamma = 1.728$; $2V = 82°$; $r > v$.

Composition and Structure. Oxide components as in andalusite. The structure consists of AlO_6 octahedral chains parallel to c and AlO_6 octahedra and SiO_4 tetrahedra between the chains (see Fig. 18.6). Substitution of Ti and Cr for Al.

Diagnostic Features. Characterized by its bladed crystals, good cleavage, blue color, and different hardness in different directions.

Occurrence. Kyanite is typically a result of regional metamorphism of aluminous rocks and is often associated with garnet, staurolite, and corundum. It also occurs in some eclogites (rocks with omphacite-type pyroxenes associated with pyrope-rich garnets) and in garnet-omphacite-kyanite occurrences in kimberlite pipes. Both of these rock types reflect high to very high pressures of origin. Crystals of excep-

FIG. 19.15 Bladed kyanite crystals and prismatic staurolite (dark) in mica schist, St. Gotthard, Switzerland (Harvard Mineralogical Museum).

tional quality are found at St. Gotthard, Switzerland (Fig. 19.15); in the Austrian Tyrol; at Minas Gerais, Brazil; and at Pontivy and Morbihan, France. Commercial deposits are located in India, Kenya, and in the United States, in North Carolina and Georgia.

Use. Kyanite is used, as is andalusite, in the manufacture of spark plugs and other high refractory porcelains. Transparent crystals may be cut as gemstones.

Name. Derived from the Greek word *kyanos*, meaning *blue*.

TOPAZ—$Al_2SiO_4(F,OH)_2$

Crystallography. Orthorhombic, *2/m2/m2/m*. Commonly in prismatic crystals terminated by dipyramids, {0*kl*} and {*h*0*l*} prisms and basal pinacoid (see Fig. 19.16 and Plate V, no. 3). Vertical prism faces are frequently striated. Usually in crystals (Fig. 19.17) but also in masses; granular, coarse or fine.

Pbnm; $a = 4.65$, $b = 8.80$, $c = 8.40$ Å; $Z = 4$. *d*s: 3.20(9), 2.96(10), 2.07(9), 1.65(9), 1.403(10).

Physical Properties. *Cleavage* {001} perfect. **H** 8. **G** 3.4–3.6. *Luster* vitreous. *Color* colorless, yellow, pink, wine-yellow, bluish, greenish. Transparent to translucent. *Optics*: (+); $\alpha = 1.606–1.629$, $\beta = 1.609–1.631$, $\gamma = 1.616–1.638$; $2V = 48°–68°$; $X = a$, $Y = b$; $r > v$.

Composition and Structure. $Al_2SiO_4(OH)_2$ contains Al_2O_3 56.6, SiO_2 33.4 and H_2O 10.0%. Most of the $(OH)^-$ is generally replaced by F^-, the maximum fluorine content being 20.7%. The structure of topaz consists of chains parallel to the *c* axis of AlO_4F_2 octahedra, which are cross-linked by independent SiO_4 tetrahedra. This arrangement is morphologically expressed by the prismatic [001] habit. The perfect {001} cleavage of topaz passes through the structure without breaking Si–O bonds; only Al–O and Al–F bonds are broken. The structure is relatively dense because it is based on closest packing of oxygens and fluorine; this packing scheme is neither cubic nor hexagonal, but more complex, *ABAC*.

Diagnostic Features. Recognized chiefly by its crystal form, basal cleavage, hardness (8), and high specific gravity.

Occurrence. Topaz is a mineral formed by fluorine-bearing fluids during the last stages of crystallization of siliceous igneous rocks. Found in cavities in rhyolite lavas and granite; a characteristic mineral in pegmatites, especially in those carrying tin. Associated with tourmaline, cassiterite, apatite, and fluorite; also with beryl, quartz, mica, and feldspar. Found in some localities as rolled pebbles in stream sands.

Notable localities for its occurrence are in Russia in the Nerchinsk district of Siberia in large wine-yellow crystals, and in Mursinsk, Ural Mountains, in pale blue crystals (Fig. 19.17); in Saxony, Germany, from various tin localities; Omi and Mino provinces, Japan; and San Luis Potosi, Mexico. Minas Gerais, Brazil, has long been the principal source of yellow gem-quality topaz. In the 1940s several well-formed, large crystals of colorless topaz were found there; the largest

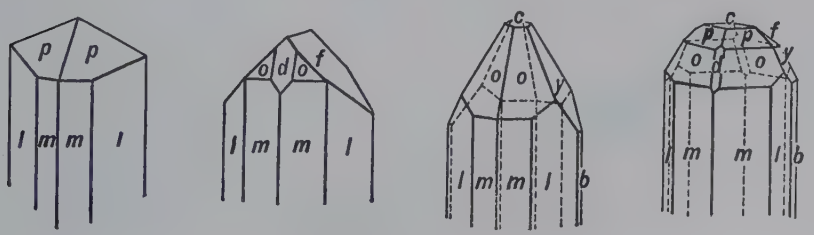

FIG. 19.16 Topaz crystals.

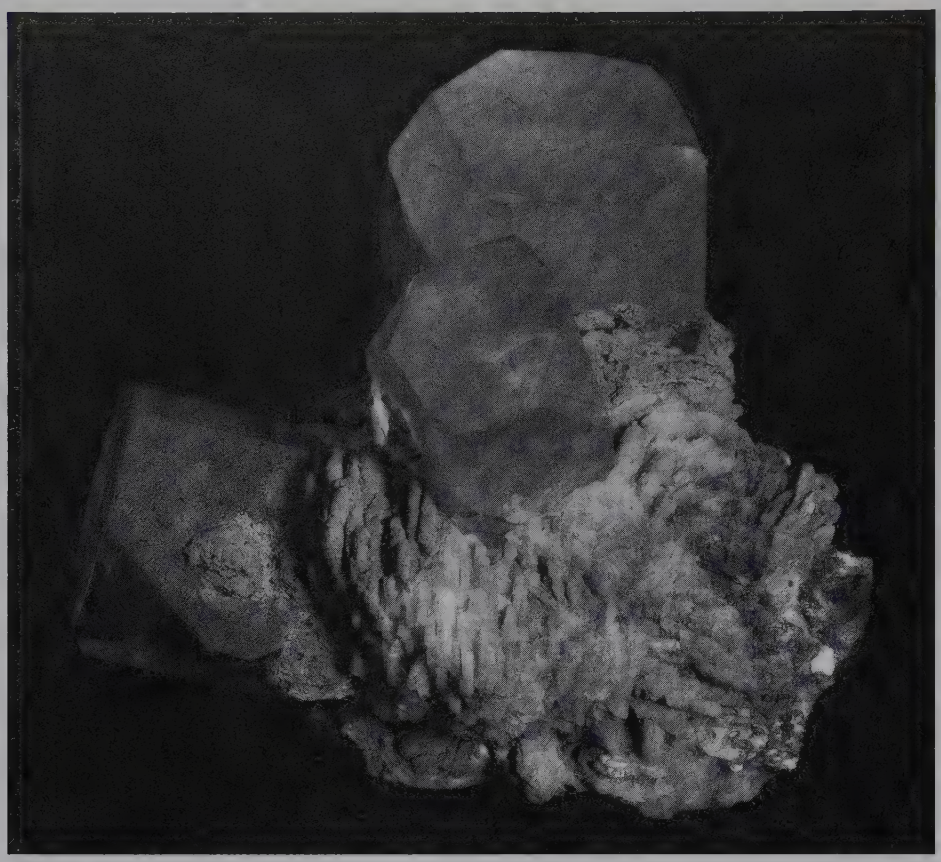

FIG. 19.17 Topaz crystals on feldspar, Siberia, Russia (Harvard Mineralogical Museum).

weighs 596 pounds. In the United States, it has been found at Pikes Peak, near Florissant and Nathrop, Colorado; Thomas Range, Utah; Streeter, Texas; San Diego County, California; Stoneham and Topsham, Maine; Amelia, Virginia; and Jefferson, South Carolina.

Use. As a gemstone. Frequently sold as "precious topaz" to distinguish it from citrine quartz, commonly called topaz. The color of the stones varies, being colorless, wine-yellow, golden brown, pale blue, and pink (see Plate XI, no. 3, Chapter 20). The color of most deep blue topaz has been induced by irradiation plus heat treatment of colorless material (see Plate XI, no. 4, Chapter 20).

Name. Derived from Topazion, the name of an island in the Red Sea, but originally probably applied to some other species.

Similar Species. *Danburite*, $Ca(B_2Si_2O_8)$, a member of the tectosilicates, shows crystal form and physical properties that are similar to those of topaz. It can be distinguished from topaz by testing for boron.

STAUROLITE—$Fe_{3-4}Al_{18}Si_8O_{48}H_{2-4}$ IV

Crystallography. Monoclinic; $2/m$ with $\beta = 90.0–90.45°$ (pseudo-orthorhombic). Prismatic crystals with common forms {110}, {010}, {001}, and {101} (Figs. 19.15 and 19.18a). Cruciform twins common, of two types: (1) with twin plane {031} in which the two individuals cross at nearly 90° (Fig. 19.18b); (2) with twin plane {231} in which they cross at nearly 60° (Fig. 19.18c). In some cases, both types are combined in one twin group. Usually in crystals; rarely massive.

$C2/m$; $a = 7.83$, $b = 16.62$, $c = 5.65$ Å; $\beta = 90.0–90.45°$; $Z = 2$. *ds*: 3.01(8), 2.38(10), 1.974(9), 1.516(5), 1.396(10).

Physical Properties. H 7–7½. **G** 3.65–3.75. *Luster* resinous to vitreous when fresh; dull when altered or impure. *Color* red-brown to brown, see Plate V, no. 2. Translucent.

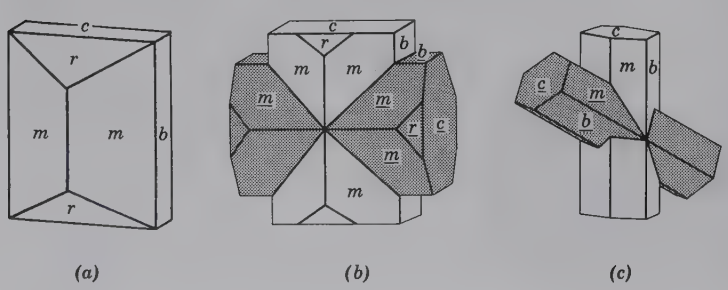

FIG. 19.18 Staurolite.

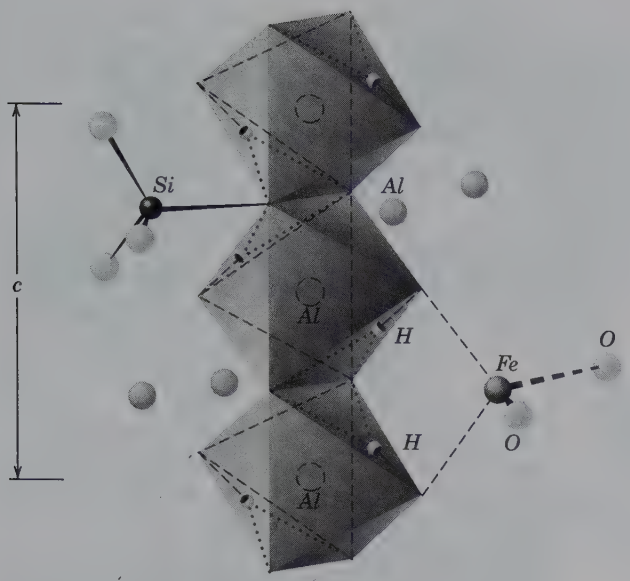

FIG. 19.19 A portion of the staurolite structure showing the iron hydroxide layer. Edge-sharing Al octahedra along *c* are bonded to tetrahedra containing primarily Fe and Si. Hydrogen is bonded to octahedra when Al and Fe sites are vacant, which leads to local order (modified after Holdaway et al., 1986.)

Optics: (+), α = 1.739–1.747, β = 1.745–1.753, γ = 1.752–1.761; 2V = 82°–88°; $X = b$ (colorless), $Y = a$ (pale yellow), $Z = c$ (deep yellow); $r > v$.

Composition and Structure. FeO 16.9, Al_2O_3 53.9, SiO_2 28.2, H_2O 1.6% for the pure Fe_4–H_2 end member. Natural staurolites show a restricted compositional range; however, Zn, Li, Co, Mg, Al and vacancies replace Fe^{2+} up to a few percent, and minor Cr and Ni can be present. Hydrogen content varies from ~ 2.6–4.2 apfu (atoms per formula unit), primarily as a function of *P* and *T*; high *P* staurolite contains more H, high *T* contains less H. Mg-rich staurolite is known from ultra-high *P* metamorphic rocks. Mg, Co, Zn end members have been synthesized. Common substitutions include: $2H^+ \rightleftarrows R^{2+}$, $R^{2+} \rightleftarrows Fe^{2+}$, $3Li + Al^{3+} \rightleftarrows 3R^{2+}$, where R is a divalent cation. The structure has been described to consist of layers of kyanite with 8 Al_2SiO_5 composition (AlO_6 octahedra in chains parallel to the *c* axis) alternating with layers of Fe–Al-O–OH along [010], although the oxide layer is more complicated. Chains of edge-sharing Al octahedra (rutile-like) extend along [001] (Fig. 19.19). Fe in tetrahedral coordination shares vertices with adjacent octahedra and assumes a zig-zag pattern on either side of the chain. Hydrogen is bonded to one O of the Al octahedron; when H is present, Al is typically absent in that octahedron. This leads to order in the structure. Si occupies isolated tetrahedra (Fig. 19.19). Variation in β correlates with occupancy of Al octahedra and order/disorder; monoclinic at room *T*, probably orthorhombic (*Ccmm*) at high *T*.

Diagnostic Features. Recognized by its characteristic crystals and twins. Distinguished from andalusite by its obtuse prism and color.

Occurrence. Staurolite is formed during medium-grade metamorphism of aluminum-rich rocks and is found in schists typically associated with pyralspite garnet, muscovite, and biotite. It may grow on kyanite in parallel orientation (see Fig. 10.11a). Staurolite forms from chloritoid at lower-grades of metamorphism and breaks down to sillimanite and garnet at higher grades. Because of its limited *P–T* stability, it is commonly used as an index mineral for medium-grade aluminous metamorphic rocks.

Notable localities are Monte Campione, Switzerland, and in large twin crystals in Brittany, France; in Scotland and near Taos, New Mexico. Further United States localities are in northwest Maine, New Hampshire, North Carolina, Georgia, Tennessee, Virginia, New Mexico, and Montana.

Use. The right angle twins are sold as amulets under the name "fairy stone," but most of the crosses offered for sale are imitations carved from a fine-grained rock and dyed, or are molded plastic.

Name. Derived from the Greek word *stauros* meaning *cross*, in allusion to its cruciform twins.

Humite Group

The humite group includes the following four members:

Norbergite	$Mg_3(SiO_4)(F,OH)_2$
Chondrodite	$Mg_5(SiO_4)_2(F,OH)_2$
Humite	$Mg_7(SiO_4)_3(F,OH)_2$
Clinohumite	$Mg_9(SiO_4)_4(F,OH)_2$

All four species have similar structures, chemistry, and physical properties. The structure of the members of the humite group is closely related to that of olivine with layers parallel to {100}, which have the atomic arrangement of olivine, and alternating layers of $Mg(OH,F)_2$ composition. For example, the norbergite composition can be rewritten to express this layering as $Mg_2SiO_4{\cdot}Mg(OH,F)_2$. The replacement of F by OH is extensive, but hydroxyl end members are unknown. The members of this group are restricted in their occurrence and are found mainly in metamorphosed and metasomatised limestones and dolomites, and skarns associated with ore deposits. Here only chondrodite, the most common member of the humite group, is discussed in detail.

Chondrodite—$Mg_5(SiO_4)_2(F,OH)_2$

Crystallography. Monoclinic; $2/m$. Crystals are frequently complex with many forms. Usually in isolated grains. Also massive.

$P2_1/c$; a = 7.89, b = 4.74, c = 10.29, β = 109°; Z = 2. *d*s: 3.02(5), 2.76(4), 2.51(5), 2.26(10), 1.740(7).

Physical Properties. **H** 6–6½. **G** 3.1–3.2. *Luster* vitreous to resinous. *Color* light yellow to red. Translucent. *Optics*: (+); α = 1.592–1.615, β = 1.602–1.627, γ = 1.621–1.646; 2V = 71°–85°; $Z = b$, $X \wedge c = 25°$ $r > v$.

Composition and Structure. The composition of chondrodite can be rewritten as $2Mg_2SiO_4{\cdot}Mg(OH,F)_2$ to reflect the olivine-type and brucite-like layering in the structure. The two main substitutions are Mg by Fe^{2+} and F by OH. The Fe substitution is limited to about 6 weight percent FeO.

Diagnostic Features. Characterized by its light yellow to red color and its mineral associations in marble. The members of the humite group cannot be distinguished from one another without optical tests.

Occurrence. Chondrodite occurs most commonly in metamorphosed dolomitic limestones. The mineral association, including phlogopite, spinel, pyrrhotite, and graphite, is highly characteristic. In skarn deposits it is found with wollastonite, forsterite, and monticellite. Noteworthy localities of chondrodite are Monte Somma, Italy; Paragas, Finland; and Kafveltorp, Sweden. In the United States, it was common at the Tilly Foster magnetite deposit near Brewster, New York.

Name. Chondrodite is from the Greek word *chondros*, meaning *a grain*; alluding to its occurrence as isolated grains. Humite is named in honor of Sir Abraham Hume.

Datolite—$CaB(SiO_4)(OH)$

Crystallography. Monoclinic; $2/m$. Crystals are usually nearly equidimensional in the three axial directions and often complex in development (Fig. 19.20). Usually in crystals. Also coarse to finely granular. Compact and massive, resembling unglazed porcelain.

$P2_1/a$; $a = 4.83$, $b = 7.64$, $c = 9.66$ Å, $\beta = 90°9'$; $Z = 4$. *d*s: 3.76(5), 3.40(3), 3.11(10), 2.86(7), 2.19(6).

Physical Properties. **H** 5–$5\frac{1}{2}$. **G** 2.8–3.0. *Luster* vitreous. *Color* white, often with faint greenish tinge. Transparent to translucent. *Optics*: (−); $\alpha = 1.624$, $\beta = 1.652$, $\gamma = 1.668$; $2V = 74°$; $Y = b$, $Z = c$; $r > v$.

Composition and Structure. CaO 35.0, B_2O_3 21.8, SiO_2 37.6, H_2O 5.6%. The structure can be regarded as consisting of layers parallel to {100} of independent SiO_4 and $B(O,OH)_4$ tetrahedra. The layers are bonded by Ca in 8-coordination (6 oxygens and 2 OH groups). Despite the layerlike structure, datolite has no conspicuous cleavage.

Diagnostic Features. Characterized by its glassy luster, pale green color, and its crystals with many faces.

Occurrence. Datolite is a secondary mineral found usually in cavities in basalts and similar rocks. Associated with zeolites, prehnite, apophyllite, and calcite. Notable localities are Andreasberg, Harz Mountains, Germany; in Italy near Bologna, and from Seiser Alpe and Theiso, Trentino; and Arendal, Norway. In the United States, it occurs in Massachusetts, Connecticut, and New Jersey, particularly at Westfield, Massachusetts, and Bergen Hill, New Jersey. Masses of porcelain-like datolite, some white and some red from disseminated native copper, were found in the Lake Superior copper deposits.

Name. Derived from a Greek word meaning *to divide*, in allusion to the granular character of a massive variety.

FIG. 19.20 Datolite.

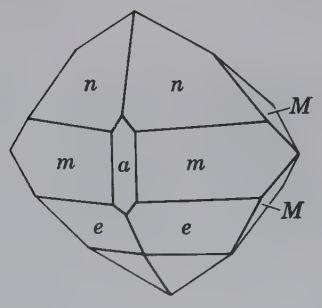

TITANITE (*sphene*)—$CaTiO(SiO_4)$

Crystallography. Monoclinic; $2/m$. Wedge-shaped crystals common resulting from a combination of {001}, {110}, and {111} (Fig. 19.21). May be lamellar or massive.

$C2/c$, $a = 6.56$, $b = 8.72$, $c = 7.44$ Å, $\beta = 119°43'$; $Z = 4$. *d*s: 3.23(10), 2.99(9), 2.60(9), 2.27(3), 2.06(4).

Physical Properties. *Cleavage* {110} distinct. Parting on {100} may be present. **H** 5–$5\frac{1}{2}$. **G** 3.40–3.55. *Luster* resinous to adamantine. *Color* gray, brown, green, yellow, black. Transparent to translucent. *Optics*: (+); $\alpha = 1.900$, $\beta = 1.907$, $\gamma = 2.034$; $2V = 27°$; $Y = b$, $Z \wedge c = 51°$; $r > v$.

Composition and Structure. CaO 28.6, TiO_2 40.8, SiO_2 30.6%. Small amounts of rare earths, Fe, Al, Mn, Mg, and Zr may be present. The structure of titanite is shown in Fig. 19.22. It consists of corner-sharing TiO_6 octahedra that form kinked chains parallel to the *a* axis. These chains are cross-linked by isolated SiO_4 tetrahedra. This tetrahedral-octahedral framework produces cavities that house Ca in 7-coordination.

Diagnostic Features. Characterized by its wedge-shaped crystals and high luster. Hardness is less than that of staurolite and greater than that of sphalerite.

Occurrence. Titanite in small crystals is a common accessory mineral in granites, granodiorites, diorites, syenites, and nepheline syenites. It is found in larger crystals in metamorphic rocks; amphibolites, chlorite schists, and marbles. Also found with iron ores, pyroxene, amphibole, scapolite, zircon, apatite, feldspar, and quartz.

The most notable occurrence of titanite is on the Kola Peninsula, Russia, where it is associated with apatite and nepheline syenite. It is mined there as a source of titanium. It is found in crystals in Tavetsch, Binnental, and St. Gotthard, Switzerland; Zillertal, Tyrol; Ala, Piemonte, and Vesuvius, Italy; Vohemar-Ambilobé region, Madagascar; and Arendal, Norway. In the United States, in Diana, Rossie, Fine, Pitcairn, and Edenville, New York; and Riverside, California. Also in various places in Ontario and Quebec, Canada.

Use. As a source of titanium oxide for use as a paint pigment. A minor gemstone.

FIG. 19.21 Titanite crystals.

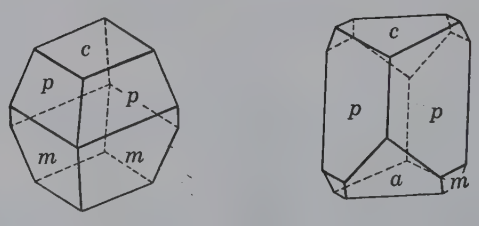

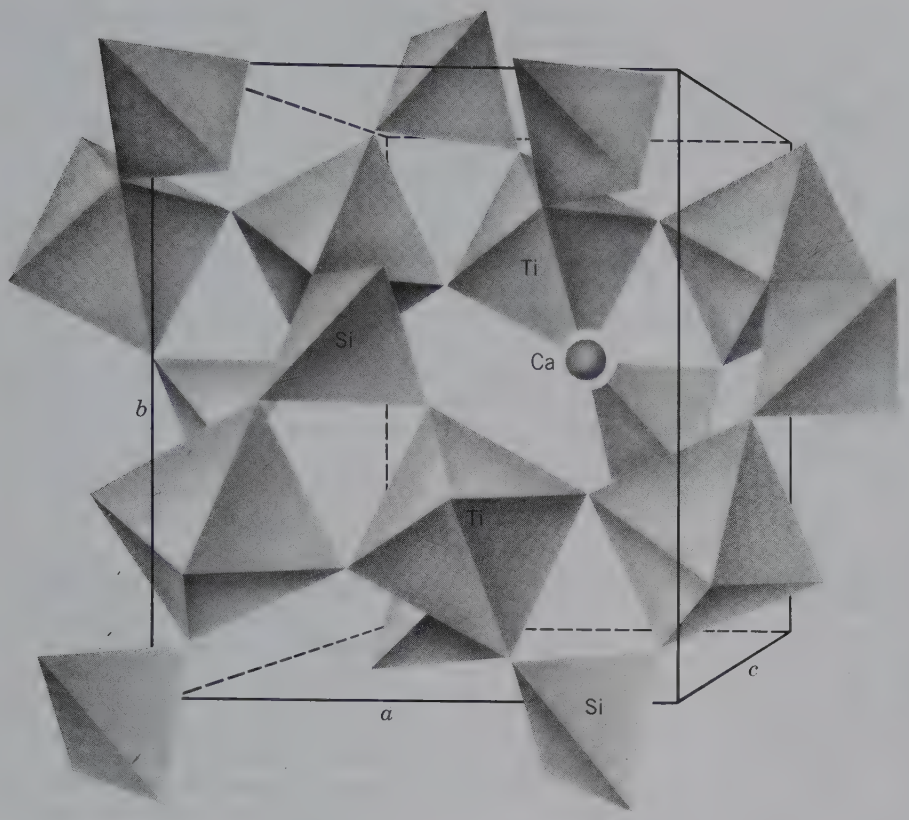

FIG. 19.22 Crystal structure of titanite (sphene) showing Si tetrahedra, Ti octahedra, and a 7-coordinated Ca site. The axes outline a unit cell. (From Papike, J. J. 1987. Chemistry of the rock-forming silicates: Ortho, ring, and single-chain structures. *Reviews of Geophysics* 25: 1483–1526.)

Name. In reference to its titanium content. The element titanium was named after the Titans, the mythical first sons of the Earth.

Similar Species. *Benitoite*, $BaTiSi_3O_9$, a cyclosilicate, occurs in association with *neptunite*, $KNa_2Li(Fe,Mn)_2Ti_2O_2(Si_4O_{11})_2$, a complex inosilicate, in San Benito, California. *Astrophyllite*, *aenigmatite*, *lamprophyllite*, and *fersmanite* are rare Ti-bearing silicates found associated with alkalic rocks. *Benitoite* is a minor gemstone.

Chloritoid—$(Fe,Mg)_2Al_4O_2(SiO_4)_2(OH)_4$

Crystallography. Generally monoclinic, $2/m$; may also be triclinic. Seldom in distinct tabular crystals, usually coarsely foliated, massive. Also in thin scales, small plates, or in radial sprays.

$C2/c$; $a = 9.52$, $b = 5.47$, $c = 18.19$ Å; $\beta = 101°39'$; $Z = 4$. *ds*: 4.50(10), 4.45(10), 3.25(6), 2.97(8), 2.70(7), 2.46(9).

Physical Properties. *Cleavage* {001} good (less so than in micas), producing brittle flakes. **H** $6\frac{1}{2}$ (much harder than chlorite). **G** 3.5–3.8. *Luster* pearly. *Color* dark green, greenish-gray, blue-gray, often grass-green in very thin plates. *Streak* colorless. *Optics*: (+); $\alpha = 1.713–1.730$, $\beta = 1.719–1.734$, $\gamma = 1.723–1.740$; $2V = 36°–60°$; $X = b$, $Z \wedge c = 2°–30°$. Pleochroism strong: Z yellow-green, Y indigo-blue, X olive-green.

Composition and Structure. For the Fe^{2+} end member, SiO_2 23.8, Al_2O_3 40.5, FeO 28.5, and H_2O 7.2%. All chloritoids show some Mg replacing Fe^{2+} but this substitution is limited. Mn^{2+} substitutes Fe^{2+} producing a species known as *ottrelite*. Fe^{3+} substitutes to some extent for Al. The structure of chloritoid is illustrated in Fig. 19.23. It can be described as consisting of two close-packed octahedral layers; one of a bucite-like sheet with composition $[(Fe,Mg)_2AlO_2(OH)_4]^{1-}$ and another of a corundum-type composition, $[Al_3O_8]^{7-}$. These sheets alternate in the direction of the c axis. Independent SiO_4 tetrahedra link the brucite- and corundum-like sheets together. The SiO_4 tetrahedra do not occur in continuous sheets, as in the micas and chlorite. Studies show that chloritoid reacts to staurolite with increasing temperature, according to the reaction: chloritoid + Al_2SiO_5 → staurolite + quartz + fluid.

Diagnostic Features. Chloritoid is difficult to distinguish from chlorite, with which it is generally associated. When in radial sprays, color is diagnostic. Optical study is necessary for unambiguous identification.

Occurrence. Chloritoid is an uncommon constituent of low- to medium-grade regionally metamorphosed iron-rich aluminous rocks. It generally occurs as crystals in association with muscovite, chlorite, staurolite, garnet, and kyanite. The original chloritoid was described from Kosoibrod, in the Ural Mountains, Russia. It is most commonly found in greenschist facies rocks; it is not uncommon in Vermont, northern Michigan and Scotland.

Name. Chloritoid is named for its superficial resemblance to chlorite.

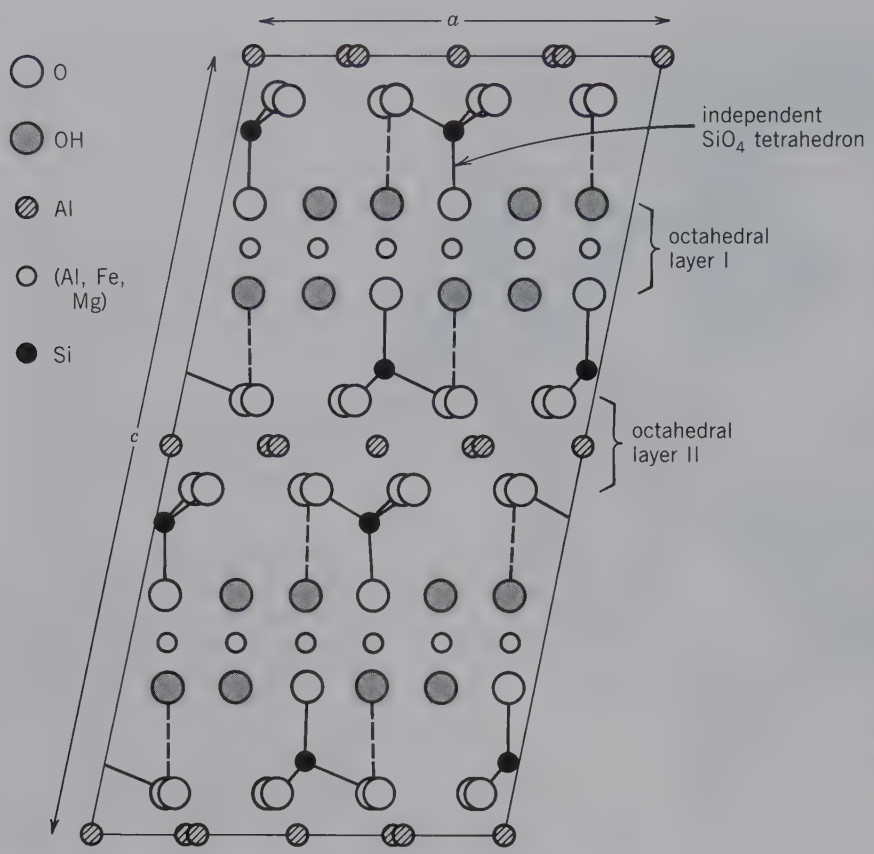

FIG. 19.23 The structure of monoclinic chloritoid projected on (010). Octahedral layer (I) has approximate composition $[Fe_2^{2+}AlO_2(OH)_4]^{1-}$ with some Mg^{2+} and Mn^{2+} substituting for Fe^{2+}; octahedral layer (II) has the composition of $[Al_3O_8]^{7-}$. Isolated tetrahedra link these layers. (From Harrison. F. W., and G. W. Brindley, 1957, The crystal structure of chloritoid. *Acta Crystallographica* 10: 77–82.)

SOROSILICATES

More than 70 minerals have been identified in this group with fundamental building blocks of two silica tetrahedra joined through a single bridging oxygen. Most of them are rare. This section describes six species, of which members of the *epidote group* and *vesuvianite* are most important.

Hemimorphite	$Zn_4(Si_2O_7)(OH)_2{\cdot}H_2O$
Lawsonite	$CaAl_2(Si_2O_7)(OH)_2{\cdot}H_2O$
Epidote group	
Clinozoisite	$Ca_2Al_3O(SiO_4)(Si_2O_7)(OH)$
Epidote	$Ca_2(Fe^{3+},Al)Al_2O(SiO_4)(Si_2O_7)(OH)$
Allanite	$X_2Y_3O(SiO_4)(Si_2O_7)(OH)$
Vesuvianite	$Ca_{19}(Al,Mg,Fe)_{13}(Si_2O_7)_4(SiO_4)_{10}(O,OH,F)_{10}$

HEMIMORPHITE—$Zn_4(Si_2O_7)(OH)_2{\cdot}H_2O$

Crystallography. Orthorhombic; *mm*2. Crystals usually tabular parallel to {010}. They show prism faces and are terminated above usually by a combination of domes and pedion, and below by a pyramid (Fig. 19.24), forming polar crystals. Crystals often divergent, giving rounded groups with slight reentrant notches between the individual crystals, forming knuckle or coxcomb masses. Also mammillary, stalactitic, massive, and granular.

*Imm*2, $a = 8.38$, $b = 10.72$, $c = 5.12$ Å; $Z = 2$. *ds*: 6.60(9), 5.36(6), 3.30(8), 3.10(10), 2.56(5).

Physical Properties. *Cleavage* {110} perfect. **H** $4\frac{1}{2}$–5. **G** 3.4–3.5. *Luster* vitreous. *Color* white to gray, in some cases with faint bluish or greenish shade; also yellow to brown. Transparent to translucent. Strongly pyroelectric and piezoelectric. *Optics*: (+); $\alpha = 1.614$, $\beta = 1.617$, $\gamma = 1.636$; $2V = 46°$; $X = b$, $Z = c$; $r > v$.

Composition and Structure. ZnO 67.5, SiO_2 25.0, H_2O 7.5%. Small amounts of Fe and Al may be present. The structure contains Si_2O_7 groups linked by $ZnO_3(OH)$ tetrahedra. The tetrahedra in the Si_2O_7 groups have their bases parallel to {001} and their apices all point in the same direction along *c*. This orientation causes the polar character of the structure. Each (OH) group is bound to two Zn^{2+} ions. H_2O molecules lie in holes between the tetrahedra. The H_2O molecules are lost continuously by heating hemimorphite up

FIG. 19.24 Hemimorphite.

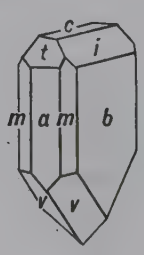

to 500°C. At this temperature all H_2O molecules are driven off and only (OH) groups are retained. These can be driven off only at much higher temperatures with destruction of the crystal structure.

Diagnostic Features. Characterized by the grouping of crystals. Resembles prehnite but has a higher specific gravity.

Occurrence. Hemimorphite is a secondary mineral found in the oxidized portions of zinc deposits, associated with smithsonite, sphalerite, cerussite, anglesite, and galena.

A notable locality for its occurrence is in Chihuahua, Mexico. In the United States, it is found at Sterling Hill, Ogdensburg, New Jersey; Friedensville, Pennsylvania; Wythe County, Virginia; with the zinc deposits of southwestern Missouri; Leadville, Colorado; Organ Mountains, New Mexico; and Elkhorn Mountains, Montana.

Use. An ore of zinc.

Name. From the hemimorphic character of the crystals. The mineral was formerly called *calamine*.

Lawsonite—$CaAl_2(Si_2O_7)(OH)_2{\cdot}H_2O$

Crystallography. Orthorhombic; 222. Usually in tabular or prismatic crystals. Frequently twinned polysynthetically on {110}.

$C222_1$; $a = 8.79$, $b = 5.84$, $c = 13.12$ Å; $Z = 4$. *ds*: 4.17(5), 3.65(6), 2.72(10), 2.62(7), 2.13(7).

Physical Properties. *Cleavage* {010} and {110} good. **H** 8. **G** 3.09. *Color* colorless, pale blue to bluish-gray. *Luster* vitreous to greasy. Translucent. *Optics*: (+); $\alpha = 1.665$, $\beta = 1.674$, $\gamma = 1.684$; $2V = 84°$; $X = a$, $Z = c$; $r > v$.

Composition and Structure. The composition of lawsonite is the same as that of anorthite, $CaAl_2Si_2O_8$, + H_2O. The structure consists of (AlO,OH) octahedra linked by Si_2O_7 groups. Ca^{2+} and H_2O molecules are located between these polyhedra.

Diagnostic Features. Lawsonite is characterized by its high hardness and associated minerals.

Occurrence. Lawsonite is a typical mineral of the high-pressure metamorphism of basaltic rocks (glaucophane facies) associated with chlorite, epidote, titanite, glaucophane, garnet, and quartz. The type locality is on the Tiburon Peninsula, San Francisco Bay, California. It is a common constituent of gneisses and schists formed under low temperature and high pressure.

Name. In honor of Professor Andrew Lawson of the University of California.

Similar Species. *Ilvaite*, $CaFe_2^{2+}Fe^{3+}O(Si_2O_7)(OH)$, is related to lawsonite with a similar although not identical structure.

EPIDOTE GROUP

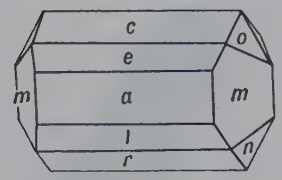

The structure and crystal chemistry of the epidote group are discussed on page 441 (see also Figs. 18.9 and 18.10).

CLINOZOISITE—$Ca_2Al_3O(SiO_4)(Si_2O_7)(OH)$
EPIDOTE—$Ca_2(Al,Fe)Al_2O(SiO_4)(Si_2O_7)(OH)$

Crystallography. Monoclinic; *2/m*. Crystals are usually elongated parallel to *b* with a prominent development of the faces of the [010] zone, giving them a prismatic aspect (Figs. 19.25 and 19.26). Striated parallel to *b*. Twinning on {100} common. Usually coarse to fine granular; also fibrous.

FIG. 19.25 Epidote crystals.

$P2_1/m$; $a = 8.98$, $b = 5.64$, $c = 10.22$ Å, $\beta = 115°24'$; $Z = 2$. *ds*: 5.02(4), 2.90(10), 2.86(6), 2.53(6), 2.40(7).

Physical Properties. *Cleavage* {001} perfect and {100} imperfect. **H** 6–7. **G** 3.25–3.45. *Luster* vitreous. *Color* epidote: pistachio-green to yellowish-green to black; clinozoisite: pale green to gray. Transparent to translucent. *Optics*: Refractive indices and birefringence increase with iron content. Clinozoisite: (+): $\alpha = 1.670$–1.715, $\beta = 1.674$–1.725, $\gamma = 1.690$–1.734; $2V = 14°$–$90°$; $Y = b$, $X \wedge c = -2°$ to $-7°$; $r > v$. Epidote: (−): $\alpha = 1.715$–1.751, $\beta = 1.725$–1.784, $\gamma = 1.734$–1.797; $2V = 64°$–$90°$; $Y = b$, $X \wedge c = 1°$ to $-5°$; $r > v$. Absorption $Y > Z > X$. Transparent crystals may show strong absorption in ordinary light.

Composition and Structure. A complete solid solution series extends from clinozoisite ($Al:Fe^{3+} = 3:0$) to epidote ($Al:Fe^{3+} = 2:1$). *Piemontite*, $Ca_2Mn^{3+}Al_2O(SiO_4)(Si_2O_7)(OH)$, is isostructural with epidote and clinozoisite but contains mainly Mn^{3+} instead of Fe^{3+} or Al^{3+} in the Al site outside the chains of the epidote structure. The structure of epidote has been discussed on page 441 and is illustrated in Fig. 18.9.

Diagnostic Features. Epidote is characterized by its pistachio green color and one perfect cleavage. Piemontite by its pink-rose color and cleavage.

Occurrence. Epidote forms under conditions of regional metamorphism of the epidote-amphibolite facies. Characteristic associations of actinolite–albite–epidote–chlorite occur in the upper part of the greenschist facies. Epidote forms also during retrograde metamorphism and forms as a reaction product of plagioclase, pyroxene, and amphibole. Epidote is common in metamorphosed limestones with calcium-rich garnets, diopside, vesuvianite, and calcite. *Epidotization* is a low-temperature alteration process and is found in veins and joint fillings in granitic rocks.

Epidote is a widespread mineral in igneous and metamorphic rocks. Notable localities for its occurrence in fine crystals are Knappenwand, Untersulzbachthal, Salzburg, Austria (Fig. 19.26a); Bourg d'Oisans, Isère, France; and the Ala Valley and Traversella, Piemonte, Italy. In the United States, found at Riverside, California, and on Prince of Wales Island, Alaska (Fig. 19.26b).

Use. Sometimes cut as a gem.

Name. Epidote from the Greek word meaning *increase*, because the base of the vertical prism has one side longer than the other. Zoisite was named after Baron von Zois and piemontite after the locality, Piemonte, Italy.

Similar Species. *Zoisite* is an orthorhombic polymorph (space group *Pnmc*) of clinozoisite. It is similar in appearance

(*a*)

(*b*)

FIG. 19.26 (a) Epidote, Knappenwand, Austria. (b) Epidote with quartz crystals. Prince of Wales Island, Alaska. (Both specimens from the Harvard Mineralogical Museum.)

and occurrence to clinozoisite but is less common. In 1967 gem quality, blue-colored crystals were found in Tanzania. This variety is known as *tanzanite*.

Allanite—$(Ca,Ce,La)_2(Fe^{2+},Fe^{3+})Al_2O(SiO_4)(Si_2O_7)(OH)$

Crystallography. Monoclinic; $2/m$. Habit of crystals similar to epidote. Commonly massive and in embedded grains. $P2_1/m$; $a = 8.98$, $b = 5.75$, $c = 10.23$ Å, $\beta = 115°0'$; $Z = 2$. *ds*: 3.57(6), 2.94(10), 2.74(8), 2.65(6), 2.14(4).

Physical Properties. **H** $5\frac{1}{2}$–6. **G** 3.5–4.2. *Luster* submetallic to pitchy and resinous. *Color* brown to pitch-black. Often coated with a yellow-brown alteration product. Subtranslucent, will transmit light on thin edges. Slightly radioactive. *Optics*: (−), usually, with $2V = 40°$–$90°$; when (+), $2V = 60°$–$90°$, $\alpha = 1.690$–1.791, $\beta = 1.700$–1.815, $\gamma = 1.706$–1.828; $Y = b$, $X \wedge c$ 1°–40°. Metamict allanites are isotropic with $n = 1.54$–1.72.

Composition and Structure. Of variable composition with Ce, La, Th, and Na in partial substitution for Ca, and Fe^{2+}, Fe^{3+}, Mn^{3+}, and Mg in partial substitution for some of the Al. Referred to as the REE-epidote. The structure of well-crystallized allanite is the same as that of epidote (see Fig. 18.9). Allanite is commonly found in a metamict state as the result of "self-irradiation" by radioactive constituents in the original mineral. Total destruction of the structure leads to a glassy product that adsorbs considerable H_2O (see Fig. 12.20 and related discussion).

Diagnostic Features. Characterized by its black color, pitchy luster, and association with granitic rocks.

Occurrence. Allanite occurs as a minor accessory constituent in many igneous rocks, such as granite, syenite, diorite, and pegmatites. Frequently associated with epidote.

Notable localities are at Miask, Ural Mountains, Russia; Greenland; Falun and Ytterby, Sweden; and Madagascar. In the United States, allanite is found at Franklin, New Jersey, and Barringer Hill, Texas.

Name. In honor of Thomas Allan, who first observed the mineral. *Orthite* is sometimes used as a synonym.

VESUVIANITE (*idocrase*)—$Ca_{19}(Al,Mg,Fe)_{13}(Si_2O_7)_4(SiO_4)_{10}(O,OH,F)_{10}$

Crystallography. Tetragonal; $4/m2/m2/m$. Crystals prismatic often vertically striated. Common forms are {110}, {010}, and {001} (Fig. 19.27). Frequently found in crystals, but striated columnar aggregates more common. Also granular, massive.

$P4/nnc$; $a = 15.66$, $c = 11.85$ Å; $Z = 4$. *ds*: 2.95(4), 2.75(10), 2.59(8), 2.45(5), 1.621(6).

Physical Properties. *Cleavage* {010} poor. **H** $6\frac{1}{2}$. **G** 3.35–3.45. *Luster* vitreous to resinous. *Color* usually green or brown, see Plate V, no. 4; also yellow, blue, red. Subtransparent to translucent. *Streak* white. *Optics*: (−); $\omega = 1.703$–1.752, $\epsilon = 1.700$–1.746.

FIG. 19.27 Vesuvianite.

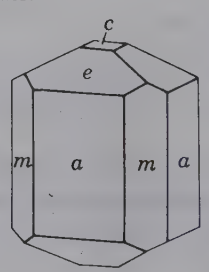

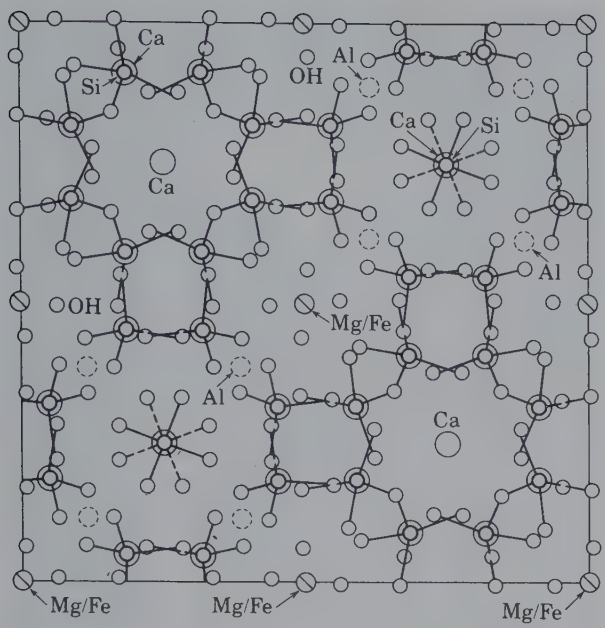

FIG. 19.28 The structure of a unit cell of vesuvianite, projected in (001). In order to compare this structural projection with the projected structure image in Fig. 19.29, regions of high atomic potential are dark areas in Fig. 19.29, whereas white regions represent parts of the structure with low electron density. The two vertical channels, with Ca at their centers, correspond with the darkest regions in the structure image of Fig. 19.29.

Composition and Structure. There is some substitution of Na for Ca; Mn^{2+} for Mg; Fe^{3+} and Ti for Al; and F for (OH). B and Be have been reported in some varieties. The structure of vesuvianite appears to be closely related to that of grossular garnet. Some parts of the structure are common to both minerals. Isolated SiO_4 tetrahedra as well as Si_2O_7 groups occur. Three-fourths of the Ca is in 8-coordination and one-fourth in 6-coordination with oxygen. The Al and Fe (and Mg) are in octahedral coordination with oxygen. A projection of a unit cell of the structure is given in Fig. 19.28. A structure image of this complicated silicate is given in Fig. 19.29. In this photograph, a unit cell is outlined, which is equivalent to the structure shown in Fig. 19.28. Part of the photograph contains a computer-simulated image of the structure. Such calculated images aid in the understanding of features of the experimentally obtained structure image.

Diagnostic Features. Brown, blocky tetragonal prisms and striated columnar masses are characteristic of vesuvianite.

Occurrence. Vesuvianite is usually formed as the result of metamorphism of impure limestones. Associated with grossular and andradite garnet, wollastonite, and diopside. Originally discovered in the ancient ejections of Vesuvius and in the dolomitic blocks of Monte Somma.

Important localities are Zermatt, Switzerland; in Italy, at Ala, Piemonte, at Monzoni, Trentino, and at Vesuvius; Achmatovsk, Ural Mountains, and River Vilui, Siberia, Russia; and Morelos, Mexico. In the United States, it is found at Sanford, Maine; near Olmsteadville, New York; Franklin, New Jersey; Magnet Cove, Arkansas; and Crestmore, California. Found in many contact metamorphic deposits in the western United States. A compact green variety resembling jade found in Siskiyou, Fresno, and Tulare counties, California, is known as *californite*. In Quebec, Canada, found at Litchfield, Pontiac County; at Templeton, Ottawa County; and at Asbestos.

Use. The green, massive variety californite is used as a jade substitute. Transparent crystals may be cut as faceted gems.

Name. From the locality Mount Vesuvius.

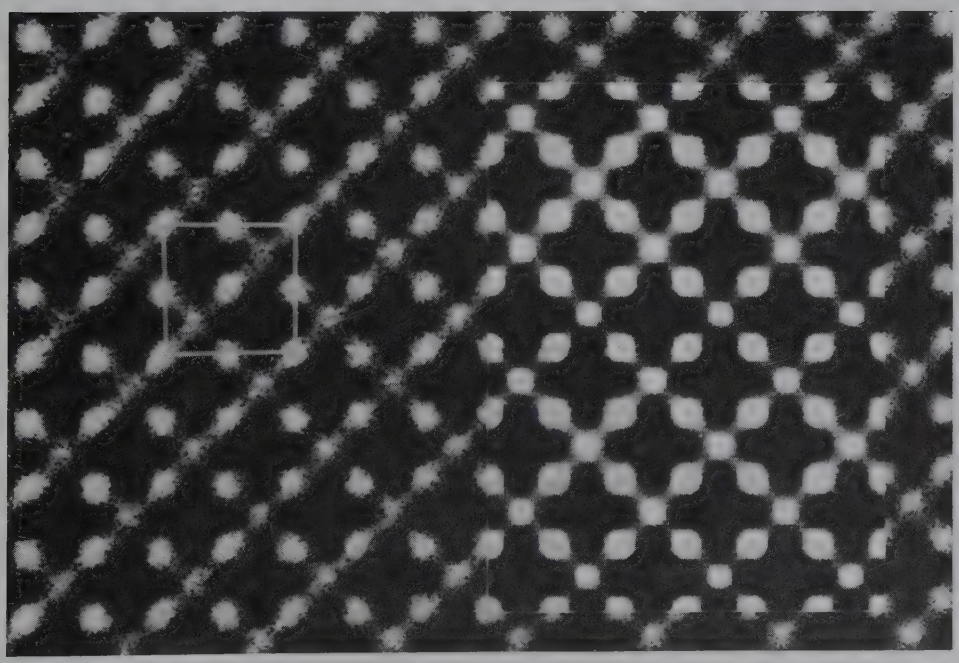

FIG. 19.29 HRTEM image of vesuvianite. The edge of the unit cell, as outlined by a white square, is 15 Å. A computer-calculated image, which simulates the experimental image, is outlined by a rectangular area in the right-hand part of the illustration. The white areas are regions of low electron density in the vesuvianite structure. (From Buseck, P. R. 1978, Computed crystal structure images for high resolution electron microscopy. *Nature* 274: 322–24; reprinted by permission from *Nature*. Copyright © 1978, Macmillan Journals Limited.)

CYCLOSILICATES

The following cyclosilicates, those with linked rings of SiO_4 tetrahedra, are described in detail:

Axinite	$(Ca,Fe^{2+},Mn)_3Al_2BSi_4O_{15}(OH)$
Beryl	$Be_3Al_2(Si_6O_{18})$
Cordierite	$(Mg,Fe)_2Al_4Si_5O_{18}{\cdot}nH_2O$
Tourmaline	$(Na,Ca,\square)(Fe^{2+},Mg,Li,Al)_3$ $(Al,Fe^{3+},Mg)_6(BO_3)_3(Si_6O_{18})$ $(OH)_3(OH,F,O)$

Axinite—$(Ca,Fe^{2+},Mn)_3Al_2BSi_4O_{15}(OH)$

Crystallography. Triclinic; 1. Crystals are usually thin with sharp edges but varied in habit (Fig. 19.30). Frequently in crystals and crystal aggregates; also massive, lamellar to granular.

$P\bar{1}$; $a = 7.15$, $b = 9.16$, $c = 8.96$ Å, $\alpha = 88°04'$, $\beta = 81°36'$, $\gamma = 77°42'$; $Z = 2$. *ds*: 6.30(7), 3.46(8), 3.28(6), 3.16(9), 2.81(10).

Physical Properties. *Cleavage* {100} distinct. **H** $6\frac{1}{2}$–7. **G** 3.27–3.35. *Luster* vitreous. *Color* clove-brown, violet, gray, green, yellow. Transparent to translucent. *Optics*: (−); α = 1.674–1.693, β = 1.681–1.701, γ = 1.684–1.704; $2V = 63°80'$; $r < v$.

Composition and Structure. A considerable range exists in composition with varying amounts of Ca, Mn, and Fe. Some Mg may be present. The complex structure of axinite was originally regarded as made up of Si_4O_{12} rings and BO_3 triangles and (OH) groups. Such Si_4O_{12} rings would classify axinite as one of the cyclosilicates. More recent structure analysis, however, has shown that the axinite structure is best viewed as being made up of $B_2Si_8O_{30}$ groups, in which BO_4 tetrahedra share three corners each, linking together four Si_2O_7 groups. Zoltai (1960) would classify this structure under "complex silicate groups."

Diagnostic Features. Characterized by the triclinic crystals with acute angles.

Occurrence. Axinite occurs in cavities in granite, and in the contact zones surrounding granitic intrusions. Notable localities for its occurrence are Bourg d'Oisans, Isère, France; various points in Switzerland; St. Just, Cornwall, England; and Obira, Japan. In the United States, it occurs at Luning, Nevada, and a as yellow manganous species at Franklin, New Jersey.

Use. A minor gem.

Name. Derived from a Greek word meaning *axe*, in allusion to the wedgelike shape of the crystals.

FIG. 19.30 Axinite.

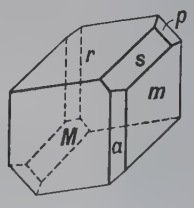

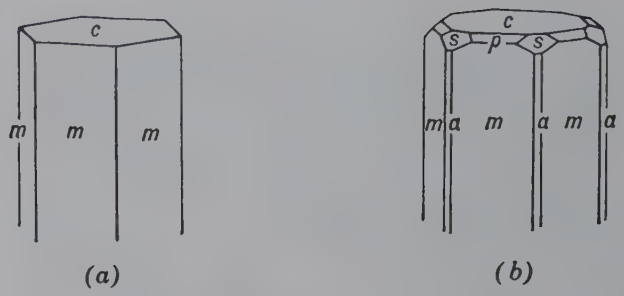

FIG. 19.31 Beryl crystals.

BERYL—$Be_3Al_2(Si_6O_{18})$

Crystallography. Hexagonal; $6/m2/m2/m$. Strong prismatic habit. Cesium beryl frequently flattened on {0001}. Forms usually present consist only of $\{10\bar{1}0\}$ and {0001} (Fig. 19.31b). Pyramidal forms are rare (Figs. 19.32 and 19.33). Crystals frequently of considerable size with rough faces. At Albany, Maine, a tapering crystal 27 feet long weighed over 25 tons.

$P6/mcc$; $a = 9.23$, $c = 9.19$ Å; $Z = 2$. *ds*: 7.98(9), 4.60(5), 3.99(5), 3.25(10), 2.87(10).

Physical Properties. *Cleavage* {0001} imperfect. **H** $7\frac{1}{2}$–8. **G** 2.65–2.8. *Luster* vitreous. *Color* commonly bluish-green or light yellow, may be deep emerald-green, gold-yellow, pink, white, or colorless (see Plate IX, nos. 2 and 5, and Plate XI, no. 8, Chapter 20). Transparent to translucent. Frequently the larger, coarser crystals show a mottled appearance due to the alternation of clear transparent spots with cloudy portions.

Color serves as the basis for several variety names of gem beryl. *Aquamarine* is the pale greenish-blue transparent variety; see Plate V, no. 5. *Morganite*, or rose beryl, is pale pink to deep rose. *Emerald* is the deep green, transparent beryl. *Heliodor* is a clear golden-yellow variety. *Optics*: (−); ω = 1.560–1.602, ϵ = 1.557–1.599.

Composition and Structure. BeO 14.0, Al_2O_3 19.0, SiO_2 67.0 are the theoretical percentages of the oxides in the formula. However, the presence of alkalis (Na and Rb) and Li may considerably reduce the percentage of BeO. Small and variable amounts of H_2O and CO_2 are housed interstitially in the large, hexagonal, vertical channels (see page 444). The structure of beryl is illustrated in Fig. 18.12 and discussed on page 442. See also Fig. A4.2 in Appendix 4 and related text as well as module III on the CD-ROM under the heading "3-dimensional Order: Space Group Elements in Structures."

Diagnostic Features. Recognized usually by its hexagonal crystal form and color. Distinguished from apatite by greater hardness and from quartz by higher specific gravity and higher symmetry.

Occurrence. Beryl, although containing the rare element Be, is rather common and widely distributed. It occurs usually in granitic rocks, or in Be-rich pegmatites. It is also found in mica schists and associated with tin ores. The world's finest emeralds are found in Colombia in a dark bituminous limestone; the most notable localities are Muzo, Cosquez, and Chivor. Emeralds of good quality are found in

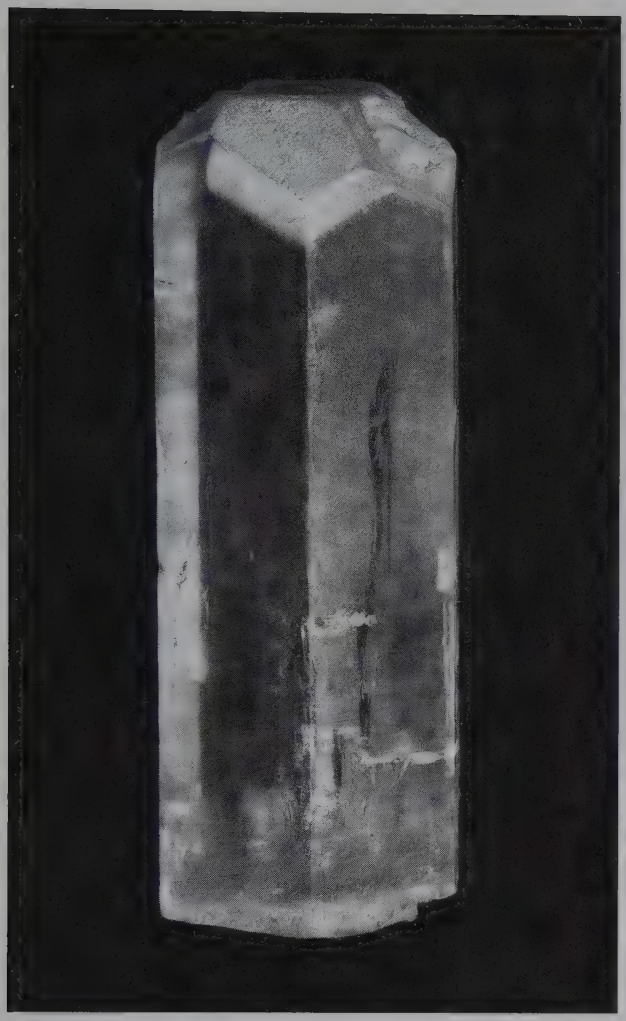

FIG. 19.32 Transparent, light green beryl crystal (length 12.5 cm), from Perm, Ural Mountains, Russia (Harvard Mineralogical Museum).

mica schists in the Transvaal, South Africa; Sandawana, Zimbabwe; and near Sverdlovsk, Russia. Rather pale emeralds have been found in small amount in Alexander County, North Carolina, associated with the green variety of spodumene, *hiddenite*. Beryl of the lighter aquamarine color is much more common and is found in gem quality in many countries.

The world's major source of gem beryl, other than emerald, is Brazil. Fine specimens come from several localities, but the most important are in the state of Minas Gerais. Other important localities are in the Ural Mountains, Russia, Madagascar, and Namibia. In the United States, gem beryl, chiefly *aquamarine*, has been found in various places in New England, Idaho, North Carolina, and Colorado. The most important localities for *morganite* are in the Pala and Mesa Grande districts, San Diego County, California. Common beryl, as an ore of beryllium, is produced in small amounts in many countries but the principal producers are the United States, China, and Mozambique.

Use. As a gemstone, the emerald (see Plate IX, nos. 2 and 5, Chapter 20) ranks as one of the most valuable of stones, and may have a greater value than the diamond. Beryl is also the principal source of beryllium, a lightweight metal similar to aluminum in many of its properties. A major use of beryllium is as an alloy with copper. Beryllium greatly increases the hardness, tensile strength, and fatigue resistance of copper.

Name. The name *beryl* is of ancient origin, derived from the Greek word which was applied to green gemstones.

Similar Species. *Euclase*, $BeAl(SiO_4)(OH)$, and *gadolinite*, $Y_2Fe^{2+}Be_2(SiO_4)_2O_2$, are rare beryllium silicates. Blue *euclase* is sometimes cut as a gemstone.

Cordierite—$(Mg,Fe)_2Al_4Si_5O_{18}\cdot nH_2O$

Crystallography. Orthorhombic: $2/m2/m2/m$. Crystals are usually short prismatic, pseudohexagonal twins twinned on {110}. Also found as imbedded grains and massive, usually anhedral.

Cccm; $a = 17.13$, $b = 9.80$, $c = 9.35$ Å; $Z = 4$. *ds*: 8.54(10), 4.06(8), 3.43(8), 3.13(7), 3.03(8).

Physical Properties. *Cleavage* {010} poor. **H** 7–7½. **G** 2.60–2.66. *Luster* vitreous. *Color* various shades of blue

FIG. 19.33 Light blue crystals of gem beryl (aquamarine) with quartz and spessartine, from Shigar, Pakistan. Specimen is 5 1/2 inches tall (Photographs courtesy of Stuart and Donna Wilensky, Wilensky Fine Minerals, Wurtsboro, NY.)

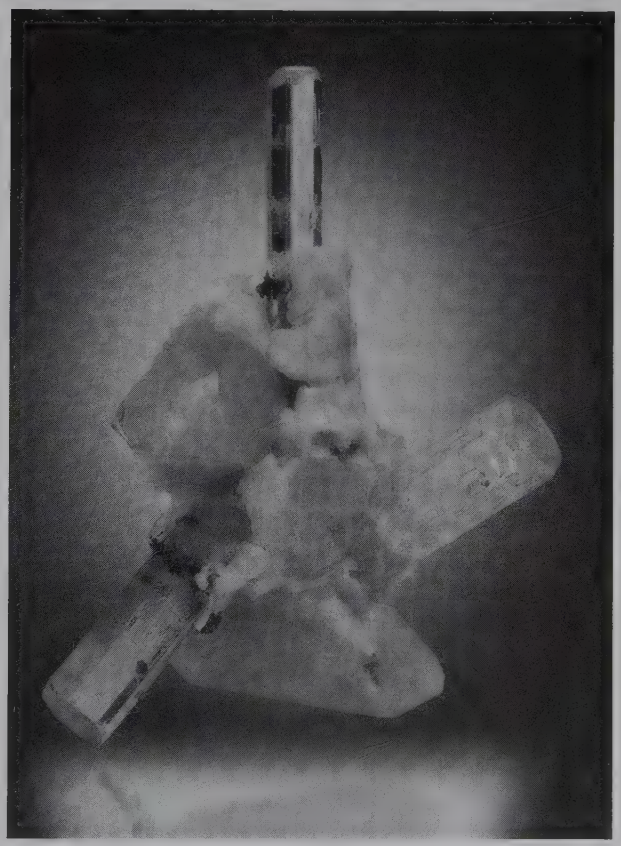

to bluish-gray. Transparent to translucent. *Optics*: usually (−), may be (+). Indices increasing with Fe content. α = 1.522–1.558, β = 1.524–1.574, γ = 1.527–1.578. 2V = 0°–90°. $X = c$, $Y = a$; $r < v$. *Pleochroism*: cordierite is sometimes called *iolite* because of pleochroism. Fe-rich varieties: X colorless, Y and Z violet.

Composition and Structure. Although some substitution of Mg by Fe^{2+} occurs, most cordierites are magnesium-rich. Mn may replace part of the Mg. The Al content of cordierite shows little variation. Most analyses show appreciable but variable H_2O, which is located in the large channels parallel to c. Small amounts of Na and K may be similarly housed. The structure of the low-temperature form, also known as low cordierite, is shown in Fig. 18.13 and is discussed on page 443. A high-temperature polymorph, *indialite*, with random distribution of Al in the $(AlSi)_6O_{18}$ rings, is isostructural with beryl and has space group *P6/mcc*.

Diagnostic Features. Cordierite is distinguished from most quartz by its blue color. Distinguished from corundum by lower hardness. Pleochroism is characteristic if observed.

Alteration. Commonly altered to some form of mica, chlorite, or talc and is then various shades of grayish-green.

Occurrence. Cordierite is a common constituent of contact and regionally metamorphosed Al-rich rocks. Fe-rich cordierite is associated with chlorite, garnet, and muscovite. Common high T assemblages are sillimanite-cordierite-spinel, and cordierite-spinel-plagioclase-orthopyroxene. Cordierite is also found in regionally metamorphosed cordierite-garnet-sillimanite gneisses. Five-centimeter crystals occur in gneisses near Ihosy, Madagascar. Cordierite-anthophyllite coexistences have been described from several localities. It occurs also in norites resulting from the incorporation of aluminous material in gabbroic magmas. It is found in some granites and pegmatites. Gem material has come from Sri Lanka and Madagascar.

Use. Transparent cordierite of good color is used as a gem known by jewelers as *iolite*. Anhydrous varieties are used in the making of high-temperature ceramics.

Name. After the French geologist P. L. A. Cordier (1777–1861). *Iolite* is sometimes used as a synonym.

TOURMALINE—$(Na,Ca,\square)(Fe^{2+},Mg,Al,Mn,Li)_3(Al,Fe^{3+})_6(BO_3)_3(Si_6O_{18})(OH)_3(OH,F,O)$

Crystallography. Hexagonal; $3m$. Usually in prismatic crystals with a prominent trigonal prism and subordinate hexagonal prism, $\{11\bar{2}0\}$, vertically striated. The many different ($hkil$) prism faces may round into each other giving the crystals a cross section like a spherical triangle. When doubly terminated, crystals usually show different forms at the opposite ends of the vertical axis due to the polar nature of the structure (Fig. 19.34). May be massive, compact; also coarse to fine columnar, either radiating or parallel.

$R3m$; a = 15.95, c = 7.24 Å; Z = 3. *ds*: 4.24(7), 4.00(7), 3.51(7), 2.98(9), 2.58(10).

Physical Properties. H 7–7½. G 3.0–3.25. *Luster* vitreous to resinous. *Color* varied, colorless, pink, green, blue, brown, black, depending on the composition and cannot necessarily be correlated with individual species. *Fracture* conchoidal.

Fe-bearing tourmaline (*schorl*) is most common and is usually black; *dravite* contains Mg and is usually brown. The rarer Li-bearing varieties (*elbaite*, containing Na and *liddicoatite*, containing Ca) are light colored in fine shades of green, yellow-red-pink, and blue; see Plate V, no. 6. Rarely white or colorless *rossmanite*. A single crystal may show several different colors arranged either in concentric envelopes about the c axis or in layers transverse to the length. Strongly pyroelectric and piezoelectric. *Optics*: (−); ω = 1.635–1.675, ϵ = 1.610–1.650. Some varieties are strongly pleochroic, $O > E$.

Composition and Structure. A complex silicate of B and Al (see Fig. 18.14) with the following substitutions: Ca for Na along the centers of the ring channels; Mg and Al for Li in 6-coordination between Si_6O_{18} rings and BO_3 groups; Fe^{3+} and Mn^{3+} for Al in polyhedra that link the Si_6O_{18} rings. The structure is discussed on page 444.

Diagnostic Features. Usually recognized by the characteristic rounded triangular cross section of the crystals and conchoidal fracture. Distinguished from hornblende by absence of cleavage and the presence of striated prisms.

Occurrence. The most common and characteristic occurrence of tourmaline is in granite pegmatites (see Box 19.5) and in the rocks immediately surrounding them. It is found also as an accessory mineral in most igneous and metamorphic rocks. It is stable from low temperatures and pressures to very high temperatures and pressures. Most pegmatitic tourmaline is *schorl* or *elbaite* and is associated with the common pegmatite minerals, microcline, albite, quartz, and muscovite. Pegmatites are also the home of the light-colored lithium-bearing tourmalines frequently associated with lepidolite, beryl, apatite, fluorite, and rarer minerals. Mg-rich tourmaline is found in marbles and schists. Occurs as a detrital mineral in sediments due to its mechanical and chemical stability.

Famous localities for the occurrence of the gem tourmalines are the Island of Elba, Italy; the state of Minas Gerais, Brazil; Ural Mountains near Sverdlovsk, Russia; and Madagascar. In the United States, found at Paris and Auburn, Maine; and Mesa Grande, Pala (Fig. 19.35), Rincon, and Ramona in San Diego County, California. Brown crystals are found near Gouverneur, New York, and fine black crystals at Pierrepont, New York.

Use. Tourmaline forms one of the most beautiful of the gemstones (see Plate X, no. 11, Chapter 20). The color of the stones varies, the principal shades being olive-green, pink to red, and blue. A copper-bearing variety is bright turquoise. Sometimes a stone is cut to show different colors in different parts. The green-colored stones are usually known by the mineral name, tourmaline. The red or pink stones are known as *rubellite*, and the rarer dark blue stones are called *indicolite*.

FIG. 19.34 Tourmaline crystals.

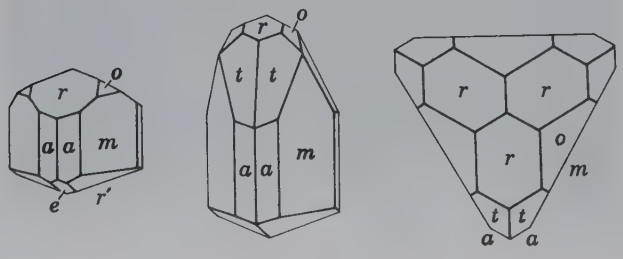

FIG. 19.35 Tourmaline crystals with quartz and white, platy albite, Pala, California (Harvard Mineralogical Museum).

Because of its strong piezoelectric property, tourmaline is used in the manufacture of pressure gauges to measure transient blast pressures (for piezoelectricity, see page 35). Its wide *P–T* stability field and sensitivity to original chemical environment allows tourmaline to be used as a provenance indicator mineral in sediments and their metamorphic equivalents.

Name. *Tourmaline* comes from *turamali*, a name given to the early gems from Sri Lanka.

INOSILICATES

PYROXENE GROUP

The following common pyroxenes, those with single chains of linked SiO_4 tetrahedra, are discussed in detail:

Enstatite-Ferrosilite Series	
Enstatite	$MgSiO_3$
Ferrosilite	$FeSiO_3$
Pigeonite	$Ca_{0.25}(Mg,Fe)_{1.75}Si_2O_6$
Diopside-Hedenbergite Series	
Diopside	$CaMgSi_2O_6$
Hedenbergite	$CaFeSi_2O_6$
Augite	$XY(Z_2O_6)$
Sodium Pyroxene Group	
Jadeite	$NaAlSi_2O_6$
Aegirine	$NaFe^{3+}Si_2O_6$
Spodumene	$LiAlSi_2O_6$

ENSTATITE—$MgSiO_3$-$(Mg,Fe)SiO_3$ FERROSILITE—Fe,SiO_3

Crystallography. Orthorhombic; $2/m2/m2/m$. Prismatic habit, crystals rare. Usually massive, fibrous, or lamellar.

Pbca; $a = 18.22$, $b = 8.81$, $c = 5.17$ Å, for pure enstatite; $Z = 8$. *ds*: 3.17(10), 2.94(4), 2.87(9), 2.53(4), 2.49(5). Unit cell parameters increase with Fe content (see Fig. 19.36).

FIG. 19.36 Variation in unit cell parameters as a function of composition in the orthopyroxene series. (From Deer, W. A., R. A. Howie, and J. Zussman, 1978, *Single-chain silicates*, 2nd ed., v. 2A. Wiley, New York, and Longman, London.)

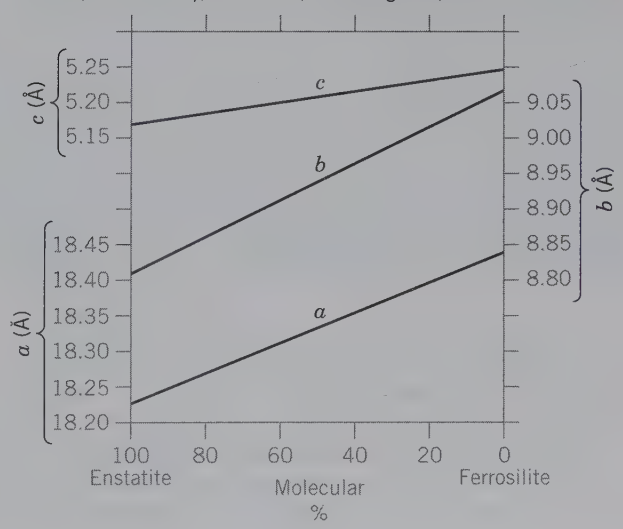

Physical Properties. *Cleavage* {210} good. Because of the doubling of the *a* dimension in orthorhombic pyroxenes, the cleavage form is {210} rather than {110} as in monoclinic pyroxenes. Frequently good parting on {100}, less common on {001}. **H** $5\frac{1}{2}$–6 and **G** 3.2–3.6 for pure enstatite; increasing with Fe content. *Luster* vitreous to pearly on cleavage surfaces; En_{80} has submetallic, bronzelike, and silky luster. *Color* grayish, yellowish, or greenish-white to olive-green and brown, depending on composition; see Plate V, no. 7. Translucent. *Optics*: enstatite (+); En_{90} to En_{10} (−). α = 1.653–1.710, β = 1.653–1.728, γ = 1.663–1.725, for En_{100} to En_{50}. $X = b$, $Z = c$. Indices increase with Fe content (see Fig. 19.37); in ferrosilite β = 1.765.

Composition and Structure. Fe^{2+} may substitute for Mg in all proportions up to nearly 90% $FeSiO_3$. However, in the more common orthopyroxenes the ratio of Fe : Mg rarely exceeds 1 : 1. Pure enstatite contains MgO 40.0, SiO_2 60.0%. The maximum amount of CaO in orthopyroxenes generally does not exceed 1.5 weight percent. The nomenclature for the orthopyroxenes is shown in Fig. 18.15; chemical compositions are generally expressed in terms of molecular percentages, for example, $En_{40}Fs_{60}$. The pure end member $FeSiO_3$, *ferrosilite*, is rarely found in nature because in most geologically observed pressure and temperature ranges the compositionally equivalent assemblage Fe_2SiO_4 (fayalite) + SiO_2 is more stable; all other varieties of the orthopyroxene series are found. The structure of members of the orthopyroxene series can be considered to consist of the monoclinic *t–o–t* strips twinned along {100} so as to essentially double the *a* dimension of orthopyroxenes as compared to the *a* of clinopyroxenes (see Fig. 18.19a). In the *Pbca* structure of orthopyroxenes Fe^{2+} shows a strong preference for the *M2* crystallographic site. Compositions between $MgSiO_3$–$FeSiO_3$ may also occur as members of the monoclinic series, *clinoenstatite–clinoferrosilite*, with space group $P2_1/c$. The common occurrence of orthopyroxenes versus the rare occurrence of clinopyroxenes in the series $MgSiO_3$–$FeSiO_3$ may indicate that the orthorhombic series is generally more stable, and at lower temperatures, than the monoclinic series.

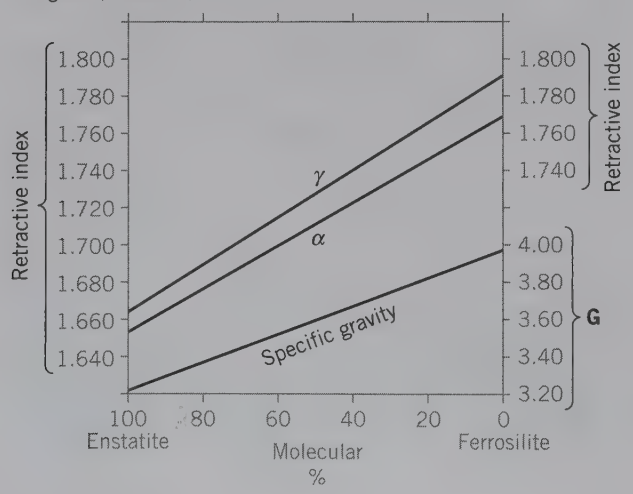

FIG. 19.37 Variation in two refractive indices (α and γ) and specific gravity as a function of composition in the orthopyroxene series. (From Deer, W. A., R. A. Howie, and J. Zussman, 1978, *Single-chain silicates*, 2nd ed., v. 2A. Wiley, New York, and Longman, London.)

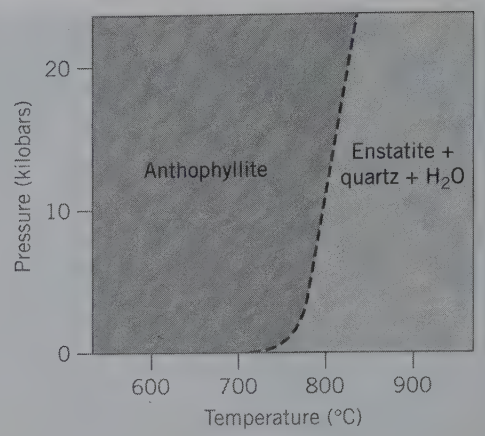

FIG. 19.38 Schematic *P–T* diagram for the stability fields of anthophyllite, $Mg_7Si_8O_{22}(OH)_2$, and reaction products, enstatite, $MgSiO_3$, + quartz + H_2O. (After Greenwood, H. J. 1963. *Journal of Petrology* 4: 325.)

Diagnostic Features. Usually recognized by their color, cleavage, and unusual luster. Varieties high in iron are black and difficult to distinguish from augite without optical tests.

Occurrence. Mg-rich orthopyroxene is a common constituent of peridotites, gabbros, norites, and basalts and is commonly associated with Ca-clinopyroxenes (e.g., augite; see also Box 19.1), olivine, and plagioclase. It may be the major constituent of pyroxenites. Orthopyroxenes may also be found in metamorphic rocks, some types of which are of high *T* and high *P* origin, such as in the granulite facies. Iron-rich members of the orthopyroxene series are common in metamorphosed iron-formation in association with grunerite. In all such occurrences orthopyroxenes commonly coexist with clinopyroxenes because of a large miscibility gap between the two groups (see Fig. 18.15a). Orthopyroxenes frequently show exsolved lamellae of a Ca-rich clinopyroxene. Enstatite as well as clinoenstatite occur in both iron and stony meteorites. In prograde metamorphic rocks orthopyroxenes form commonly at the expense of Mg–Fe amphibole (e.g., anthophyllite) and in retrograde metamorphic rocks orthopyroxenes may give way to Mg–Fe amphiboles (see Fig. 19.38).

Enstatite is found in the United States at the Tilly Foster Mine, Brewster, New York, and at Edwards, St. Lawrence County, New York; at Texas, Pennsylvania; Bare Hills, near Baltimore, Maryland; and Webster, North Carolina. Ferroan enstatite occurs in New York in the norites of the Cortland region, on the Hudson River, and in the Adirondack region. Fe-rich orthopyroxenes are common constituents of the metamorphosed Lake Superior and Labrador Trough iron-formations.

Use. A minor gemstone.

Name. Enstatite is named from the Greek word *enstates*, meaning *opponent*, because of its refractory nature.

BOX 19.1 The Two Most Common Crustal Rock Types: Basalt and Granite

There are two major types of igneous rocks, *extrusive* and *intrusive*. The first group includes those igneous rocks that reached the Earth's surface in a molten or partly molten state. Modern volcanoes produce lava flows that pour from a vent or fracture in the Earth's crust. Such *extrusive* or *volcanic* rocks tend to cool and crystallize rapidly, with the result that their grain size is generally small. **Basalt** is a Mg-rich, Si-poor, very dark, green to black, fine-grained volcanic rock that is common on many volcanic islands, such as the Hawaiian Islands and Iceland. The upper layers of the oceanic crust consist of basalt (see Fig. 5.1b). The photograph illustrates a dark gray *vesicular basalt* (vesicles represent gas bubbles that are entrapped during solidification of the magma). Basalt and its coarser-grained, intrusive equivalent known as **gabbro**, consists commonly of two types of pyroxene (ortho- and clinopyroxene) and calcium-rich plagioclase, but may also contain olivine.

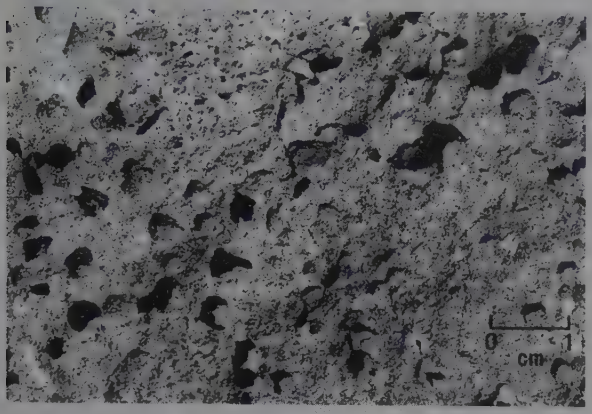

Vesicular, dark gray basalt (composed of two pyroxene types and plagioclase feldspar).

Intrusive or *plutonic* rocks are the result of crystallization from a magma that did not reach the Earth's surface. A magma that is deeply buried in the Earth's crust generally cools slowly, crystallizing minerals that have time to grow to considerable size, giving the rock a medium- to coarse-grained texture. The mineral grains in such rock can generally be identified with the naked eye. **Granite** is generally a coarse-grained rock, Si-rich and Mg-poor, of light color and consists mainly of quartz and potassium feldspar, as well as sodium-rich plagioclase. Muscovite can be present, and so are small amounts of dark silicates such as amphiboles or biotite. The photograph illustrates a coarse-grained quartz–feldspar–hornblende granite. The extrusive equivalent of granite is known as **rhyolite**. The average composition of the continental crust is similar to that of granite because the total amount of sedimentary and metamorphic rocks is insignificant in comparison to the bulk of plutonic igneous rocks (see Fig. 5.1b).

The average chemical composition of basalt (and its plutonic equivalent, gabbro) and granite (and its volcanic equivalent, rhyolite) are listed in the table. Basalt is relatively low in SiO_2 content, as compared with granite. However, basalt is much richer in FeO, MgO, and CaO than granite. The Na_2O, K_2O, and Al_2O_3 contents of granite are higher than those of basalt.

Average Chemical Compositions of Basalt and Granite*

Oxides (Weight %)	Basalt	Granite
SiO_2	48.36	72.08
TiO_2	1.32	0.37
Al_2O_3	16.84	13.86
Fe_2O_3	2.55	0.86
FeO	7.92	1.67
MnO	0.18	0.06
MgO	8.06	0.52
CaO	11.07	1.33
Na_2O	2.26	3.08
K_2O	0.56	5.46
H_2O	0.64	0.53
P_2O_5	0.24	0.18
Total	100.00	100.00

*Analyses from Nockolds, S. R. 1954. *Geological Society of America Bulletin* 65: 1007–1032.

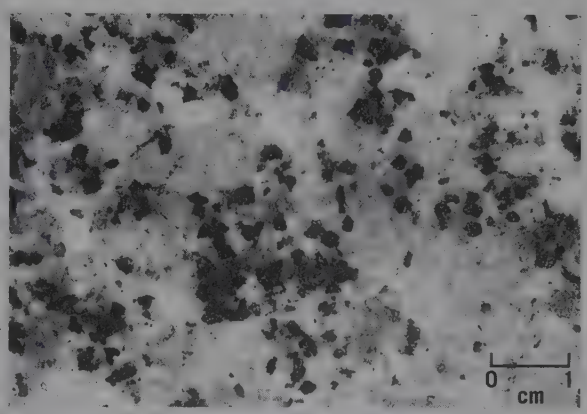

Coarse-grained granite (composed of quartz, K-feldspar, sodic plagioclase, and hornblende).

Pigeonite—$Ca_{0.25}(Mg,Fe)_{1.75}Si_2O_6$

Crystallography. Monoclinic; $2/m$. Rarely as well-formed phenocrysts with a prismatic habit parallel to c.

$P2_1/c$; $a = 9.71$, $b = 8.96$, $c = 5.25$ Å, $\beta = 108°33'$; $Z = 8$. *ds*: 3.21(8), 3.02(10), 2.908(8), 2.904(10), 2.578(6).

Physical Properties. *Cleavage* {110} good; parting on {100} may be present. **H** 6. **G** 3.30–3.46. *Color* brown, greenish-brown, to black. *Optics*: (+); $\alpha = 1.682$–1.722, $\beta = 1.684$–1.722, $\gamma = 1.704$–1.752, increasing with Fe^{2+}. Two orientations occur: (1) with $Y = b$, and (2) more common, $X = b$. $Z \wedge c = 37°$–$44°$, $2V = 0°$–$30°$.

Composition and Structure. Pigeonites are calcium-poor monoclinic pyroxenes that contain between 5 to 15 molecular percent of the $CaSiO_3$ component (see Fig. 18.15;

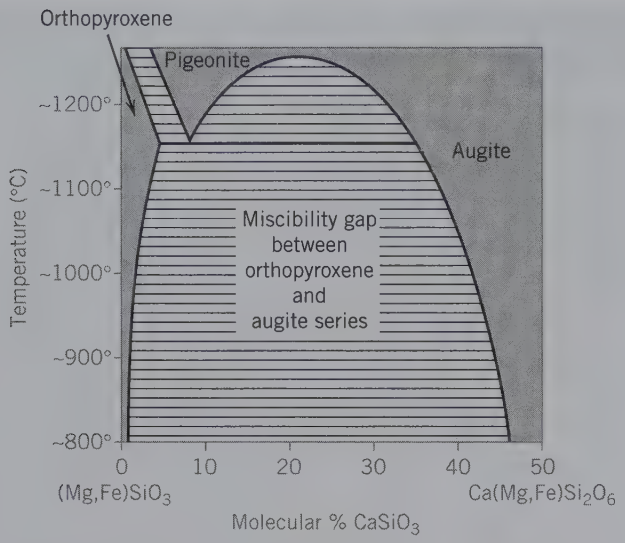

FIG. 19.39 Schematic *T*-composition section across the Wo–En–Fs diagram shown in Fig. 18.15a. The section is at about $En_{65}Fs_{35}$.

field just above orthopyroxene base). The crystal structure of pigeonite is similar to that of diopside with all of the Ca and additional Fe and Mg in the *M2* site, and the remaining Mg and Fe in *M1*. Fe shows a strong preference for the *M2* sites. Pigeonite is stable at high temperatures in igneous rocks and inverts commonly at lower temperatures to orthopyroxene with augite-type exsolution lamellae. A temperature-composition stability diagram is given in Fig. 19.39.

Diagnostic Features. Can be distinguished from other pyroxenes only by optical or X-ray techniques. Augite $2V > 39°$; pigeonite $2V < 32°$.

Occurrence. Pigeonite is common in high-temperature, rapidly cooled lavas and in some intrusives, such as diabases. It is present as phenocrysts in some volcanic rocks, but is not known from metamorphic rocks. If pigeonite formed in an igneous rock that cooled slowly, it may have exsolved augite lamellae on {001} and may subsequently have inverted to orthopyroxene (see Fig. 19.39) through a reconstructive transformation. At even lower temperatures, the orthopyroxene may have developed augite exsolution along {100} planes as well.

Name. After the locality, Pigeon Cove, Minnesota.

DIOPSIDE—$CaMgSi_2O_6$
HEDENBERGITE—$CaFeSi_2O_6$
AUGITE—$(Ca,Na)(Mg,Fe,Al)(Si,Al)_2O_6$

Diopside and hedenbergite form a complete solid solution series with physical and optical properties varying linearly with composition. Augite is a clinopyroxene in which some Na substitutes for Ca, some Al substitutes for both Mg (or Fe) and Si, and in which Fe and Mg contents are higher than in diopside or hedenbergite (see Fig. 18.15a). Although the crystal constants vary slightly from one member to another, a single description suffices for all.

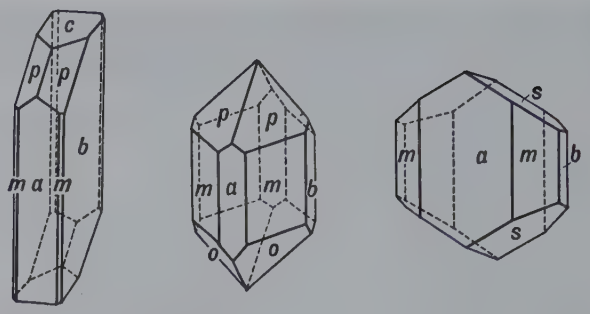

FIG. 19.40 Augite crystals.

Crystallography. Monoclinic; 2/*m*. In prismatic crystals showing square or eight-sided cross section (Fig. 19.40). Also granular massive, columnar, and lamellar. Frequently twinned polysynthetically on {001}; less commonly twinned on {100}.

C2/c; $a = 9.73$, $b = 8.91$, $c = 5.25$ Å; $\beta = 105°50'$; $Z = 4$. *d*s: 3.23(8), 2.98(10), 2.94(7), 2.53(4), 1.748(4). See Fig. A4.1 in Appendix 4 for an illustration of the clinopyroxene structure and related *C2/c* space group, as well as Module III on the CD-ROM under the heading "3-dimensional Order: Space Group Elements in Structures."

Physical Properties. *Cleavage* {110}, at 87° and 93°, imperfect. Frequently parting on {001}, and less commonly on {100}. **H** 5–6. **G** 3.2–3.3. *Luster* vitreous. *Color* white to light green in diopside, see Plate V, no. 8; deepens with increase of Fe. Augite is black; see Plates V, no. 9 and VI, no. 1. Transparent to translucent. *Optics*: (+); α = 1.67–1.74, β = 1.67–1.74, γ = 1.70–1.76 (see Fig. 19.41). $2V = 55°$–$65°$;

FIG. 19.41 Approximate trends of two refractive indices (α and γ) as a function of composition in the diopside-hedenbergite series. There is considerable scatter in the original data from which these lines were obtained. (From Deer, W. A., R. A. Howie, and J. Zussman, 1978, *Single-Chain silicates*, v. 2A. Wiley, New York, and Longman, London.)

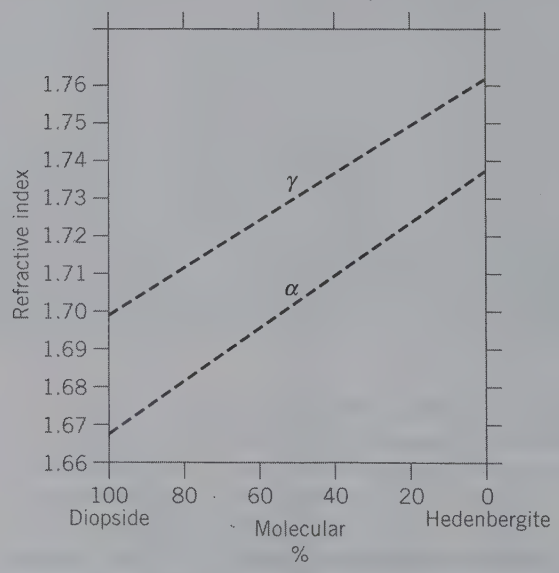

$Y = b$, $Z \wedge c = 39°–48°$; $r > v$. Darker members show pleochroism; X pale green, Y yellow-green, Z dark green.

Composition and Structure. In the diopside–hedenbergite series Mg and Fe^{2+} substitute for each other in all proportions. In the majority of analyses of members of this series the Al_2O_3 content varies between 1 and 3 weight percent. In augite, in addition to varying Mg and Fe^{2+} contents, Al substitutes for both Mg (or Fe^{2+}) and Si. Mn, Fe^{3+}, Ti, and Na may also be present. A complete series exists toward *aegirine–augite*, $(Na,Ca)(Fe^{3+},Fe^{2+},Mg,Al)Si_2O_6$, by the replacement $Ca^{2+}(Mg,Fe^{2+}) \leftrightarrows Na^{+}Fe^{3+}$. Compositional zoning is commonly found in igneous augites with the cores rich in the augite component and the rims tending toward aegirine–augite. Chemical analyses are generally recalculated in terms of molecular percentages of wollastonite (Wo), enstatite (En), and ferrosilite (Fs) and are expressed as $Wo_xEn_yFs_z$, where x, y, and z are molecular percentages (see Table 5.6 and Fig. 18.15). The structures of diopside, hedenbergite, and augite are all based on space group $C2/c$. Their structure is discussed on page 447, and a monoclinic structure is illustrated in Fig. 18.16. The Ca ions in the *M2* site are in 8-coordination, whereas the ions in *M1* are in 6-coordination.

Diagnostic Features. Characterized by crystal form and imperfect prismatic cleavage at 87° and 93°.

Occurrence. *Diopside* and *hedenbergite* are common in metamorphic rocks. Diopside, in association with forsterite and calcite, infrequently with monticellite, is the result of metamorphism of siliceous, Mg-rich limestones, or dolomites. For example:

$$\underset{\text{dolomite}}{CaMg(CO_3)_2} + \underset{\text{quartz}}{2SiO_2} \rightarrow \underset{\text{diopside}}{CaMgSi_2O_6} + 2CO_2\uparrow$$

Other associations include tremolite, scapolite, vesuvianite, garnet, and titanite. Hedenbergite occurs in more Fe-rich metamorphic rocks. Diopside and hedenbergite are also known as products of igneous crystallization. Early formed Ca-rich clinopyroxenes may be very close to diopside in composition, whereas the latest stages of crystallization may be represented by hedenbergite compositions, due to enrichment of the residual magma in Fe. The Skaergaard intrusion, East Greenland, contains late, fine-grained hedenbergite interstitial to earlier formed, coarser grained diopside, and augite grains.

Fine crystals have been found in the Ural Mountains, Russia; Austrian Tyrol; Binnenthal, Switzerland; and Piemonte, Italy. At Nordmark, Sweden, fine crystals range between diopside and hedenbergite. In the United States, they are found at Canaan, Connecticut; and DeKalb Junction and Gouverneur, New York.

Augite is the most common pyroxene and an important rock-forming mineral. It is found chiefly in dark-colored igneous rocks, such as basaltic lavas and intrusives, gabbros, peridotites, and andesites (see Box 19.1). Chemically zoned augites are common in quickly cooled rocks, such as the lunar basalts. The clinopyroxene crystallization history is very well documented for many lunar basalts and gabbros as well as for the Skaergaard intrusion, East Greenland, for example; early formed crystals are more magnesian than later pyroxene grains. Fine crystals of augite have been found in the lavas of Vesuvius and at Val di Fassa, Trentino, Italy; and at Bílina, Czech Republic.

Use. Transparent varieties of diopside have been cut and used as gemstones.

Name. Diopside is from two Greek words meaning *double* and *appearance*, because the vertical prism zone can apparently be oriented in two ways. Hedenbergite is named after M. A. Ludwig Hedenberg, the Swedish chemist who discovered and described it. Augite comes from a Greek word meaning *luster*. The name pyroxene, *stranger to fire*, is a misnomer and was given to the mineral because it was thought that it did not occur in igneous rocks.

Jadeite—$NaAlSi_2O_6$

Crystallography. Monoclinic; $2/m$. Rarely in isolated crystals. Usually granular in compact, massive aggregates.

$C2/c$; $a = 9.50$, $b = 8.61$, $c = 5.24$ Å; $\beta = 107°26'$; $Z = 4$. *ds*: 3.27(3), 3.10(3), 2.92(8), 2.83(10), 2.42(9).

Physical Properties. *Cleavage* {110} at angles of 87° and 93°. Extremely tough and difficult to break. **H** $6\frac{1}{2}$–7. **G** 3.3–3.5. *Color* white; apple-green (see Plate VI, no. 2) to emerald-green with Fe. May be white with spots of green. *Luster* vitreous, pearly on cleavage surfaces. *Optics*: (+); $\alpha = 1.654$, $\beta = 1.659$, $\gamma = 1.667$; $2V = 70°$; $X = b$, $Z \wedge c = 34°$; $r > v$.

Composition and Structure. Na_2O 15.4, Al_2O_3 25.2, SiO_2 59.4 for pure end member. There is no replacement of Si by Al in jadeite and Fe^{3+} substitution for Al is limited. Jadeite has a composition that is intermediate between that of nepheline, $NaAlSiO_4$, and albite, $NaAlSi_3O_8$, but does not form under the crystallization conditions of these two minerals. However, under high pressures (10 to 25 kilobars) and elevated temperatures (between 600° and 1000°C), jadeite forms by:

$$\underset{\text{nepheline}}{NaAlSiO_4} + \underset{\text{albite}}{NaAlSi_3O_8} \leftrightarrows \underset{\text{jadeite}}{2NaAlSi_2O_6}$$

Similarly, jadeite forms at high pressures at the expense of albite alone according to the following reaction:

$$\underset{\text{albite}}{NaAlSi_3O_8} \leftrightarrows \underset{\text{jadeite}}{NaAlSi_2O_6} + \underset{\text{quartz}}{SiO_2}$$

(see Fig. 19.42). The structure of jadeite is shown in Fig. 18.16.

Diagnostic Features. Characterized by its green color and tough aggregates of compact fibers. On polished surfaces nephrite (an amphibole) has an oily luster, jadeite is vitreous.

Occurrence. Jadeite is found only in metamorphic rocks. Laboratory experiments have shown that high pressure and only relatively low temperatures are necessary for the formation of jadeite. Such occurrences are found near the margins of the continental crust (paleo-subduction zones) as in the Alps, California, and Japan. In the Fransiscan Formation of California, jadeitic pyroxene is associated with glaucophane, aragonite, muscovite, lawsonite, and quartz.

Use. Jadeite has long been highly prized in the Orient, especially in China, where it is worked into ornaments and utensils of great variety and beauty. It was also used by primitive people for various weapons and implements.

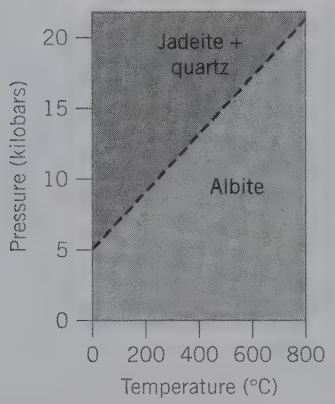

FIG. 19.42 Experimentally determined stability fields of albite and jadeite + quartz. Reaction curve is only approximately located as shown by dashes.

Name. The term *jade* includes both jadeite and the amphibole, nephrite.

Similar Species. *Omphacite* is a bright green variety of augite-type composition rich in $NaAlSi_2O_6$, with space group $C2/c$ or $P2/n$. It occurs in eclogites, which contain omphacite and pyrope-rich garnet as main constituents. These rocks are the result of high pressures and high temperatures of metamorphism. Eclogites are the metamorphosed chemical equivalents of basalts, but contain denser minerals (see Fig. 11.15). Omphacite is also found in kimberlites. The name *omphacite* is from the Greek word *omphax*, meaning *an unripe grape*, in allusion to its characteristic color.

Aegirine—$NaFe^{3+}Si_2O_6$

Crystallography. Monoclinic; $2/m$. Crystals are slender prismatic with steep terminations. Often in fibrous aggregates. Faces are often imperfect.

$C2/c$; $a = 9.66$, $b = 8.79$, $c = 5.26$ Å; $\beta = 107°20'$; $Z = 4$. *ds*: 6.5(4), 4.43(4), 2.99(10), 2.91(4), 2.54(6).

Physical Properties. *Cleavage* {110} imperfect at angles of 87° and 93°. **H** 6–6½. **G** 3.40–3.55. *Luster* vitreous. *Color* black, brown or green. Translucent. *Optics* for aegirine: (−); $\alpha = 1.776$, $\beta = 1.819$, $\gamma = 1.836$; $2V = 60°$; $Y = b$, $Z \wedge c = 8°$; $r > v$. Aegirine–augite: (1) with lower indices and pleochroism in green and brown.

Composition and Structure. Although the term *aegirine* is the recommended name for $NaFe^{3+}Si_2O_6$, both *aegirine* and *acmite* have been used for pyroxenes of this composition. Aegirines show a wide range of composition, but in most species the replacement is according to $Na^+Fe^{3+} \rightleftarrows Ca^{2+}(Mg,Fe^{2+})$, which causes a complete series to augite, with an intermediate member known as *aegirine–augite*. Compositional zoning is very common in aegirine with compositions trending toward augite. Earlier crystallized material is richer in augite (in cores), and rims tend to be enriched in the aegirine component. The structure of aegirine is similar to that of other $C2/c$ pyroxenes (see Fig. 18.16).

Diagnostic Features. The slender, elongate, prismatic crystals, brown to green color, and association are characteristic. However, it is not easily distinguished without optical tests.

Occurrence. Aegirine is a comparatively rare rock-forming mineral found in igneous rocks rich in Na and poor in SiO_2, such as nepheline syenite and phonolite. Associated with orthoclase, feldspathoids, augite, and soda-rich amphiboles. It is also found in some metamorphic rocks associated with glaucophane or riebeckite. It occurs in the nepheline syenites and related rocks of Norway, southern Greenland, and Kola Peninsula, Russia. In the United States, it is found in fine crystals at Magnet Cove, Arkansas. In Canada, at Mount St. Hilaire, Quebec.

Name. After Aegir, the Scandinavian sea god, the mineral being first reported from Norway.

Spodumene—$LiAlSi_2O_6$

Crystallography. Monoclinic; $2/m$. Crystals prismatic, frequently flattened on {100}. Deeply striated vertically. Crystals usually coarse with roughened faces; some very large. Occurs also in cleavable masses. Twinning on {100} common.

$C2/c$; $a = 9.52$, $b = 8.32$, $c = 5.25$ Å; $\beta = 110°28'$; $Z = 4$. *ds*: 4.38(5), 4.21(6), 2.93(10), 2.80(8), 2.45(6).

Physical Properties. *Cleavage* {110} perfect at angles of 87° and 93°. Usually a well-developed parting on {100}. **H** 6½–7. **G** 3.15–3.20. *Luster* vitreous to chalky. *Color* white, gray, pink, yellow, green. Transparent to translucent. *Optics*: (+); $\alpha = 1.660$, $\beta = 1.666$, $\gamma = 1.676$; $2V = 58°$; $Y = b$, $Z \wedge c = 24°$. $r < v$. Absorption: $X > Y > Z$. The clear lilac-colored variety is called *kunzite*, and the clear emerald-green variety *hiddenite*.

Composition and Structure. Li_2O 8.0, Al_2O_3 27.4, SiO_2 64.6%. A small amount of Na usually substitutes for Li. The structure of spodumene is the same as that of other $C2/c$ pyroxenes. The cell volume of spodumene is smaller than that of diopside, for example, because the larger Ca and Mg ions are substituted for by smaller Li and Al. This reduction in ionic sizes causes a somewhat closer packing of the SiO_3 chains.

Diagnostic Features. Characterized by its prismatic cleavage and {100} parting. The angle formed by one cleavage direction and the {100} parting resembles the cleavage angle of tremolite.

Alteration. Spodumene easily alters to other species, becoming dull. The alteration products include clay minerals, albite, *eucryptite*, $LiAlSiO_4$, muscovite, and microcline.

Occurrence. Spodumene is found almost exclusively in lithium-rich pegmatites (see Box 19.5). Although it is a comparatively rare mineral, it occasionally occurs in very large crystals. At the Etta Mine, Black Hills, South Dakota, crystals measuring as much as 40 feet in length and weighing many tons have been found. It formerly was mined as the chief source of lithium, but today other minerals, such as petalite, lepidolite, and amblygonite, are of equal or greater importance. Also, much of the lithium of commerce is extracted as Li_2CO_3 from brines. The major producers of lithium are Russia, China, Chile, and Australia.

The principal countries for the production of gem spodumene are Brazil and Afghanistan. In the United States, beautiful crystals of kunzite have come from California, notably the Pala district in San Diego County. Hiddenite comes from Stony Point, Alexander County, North Carolina.

Use. As a gemstone and as a source of lithium. A major use of lithium is in grease to help it retain its lubricating properties over a wide range of temperatures. It is also used in aluminum, ceramics, glass, storage batteries, air conditioning, and as a welding flux.

Names. *Spodumene* comes from a Greek word meaning *ash-colored*. *Hiddenite* is named for W. E. Hidden; *kunzite*, for G. F. Kunz.

Similar Species. *Eucryptite*, $LiAlSiO_4$, is a major source of lithium at Bikitá, Zimbabwe.

Pyroxenoid Group

The following three members of the pyroxenoid group are discussed in detail:

Wollastonite	$CaSiO_3$
Rhodonite	$MnSiO_3$
Pectolite	$Ca_2NaH(SiO_3)_3$

Wollastonite—$CaSiO_3$

Crystallography. Triclinic; $\bar{1}$. Rarely in tabular crystals with either {001} or {100} prominent. Commonly massive, cleavable to fibrous; also compact. *Pseudowollastonite*, $CaSiO_3$, is a polymorph stable above 1120°C; it is triclinic, pseudohexagonal, with different properties than wollastonite.

$P\bar{1}$; $a = 7.94$, $b = 7.32$, $c = 7.07$ Å; $\alpha = 90°2'$, $\beta = 95°22'$, $\gamma = 103°26'$; $Z = 6$. *d*s: 3.83(8), 3.52(8), 3.31(8), 2.97(10), 2.47(6).

Physical Properties. *Cleavage* {100} and {001} perfect, $\{\bar{1}01\}$ good giving splintery fragments elongated on *b*. **H** 5–5½. **G** 2.8–2.9. *Luster* vitreous, pearly on cleavage surfaces. May be silky when fibrous. *Color* colorless, white, or gray; see Plate VI, no. 3. Translucent. *Optics*: (−); $\alpha = 1.620$, $\beta = 1.632$, $\gamma = 1.634$; $2V = 40°$; Y near b, $X \wedge c = 32°$.

Composition and Structure. CaO 48.3, SiO_2 51.7% for pure $CaSiO_3$. Most analyses are close to the pure end-member in composition, although considerable amounts of Fe and Mn, and lesser Mg, may replace Ca. The structure of wollastonite consists of infinite chains, parallel to the *c* axis, with a unit repeat of three twisted tetrahedra (see Figs. 18.20b and 19.43). Ca is in irregular octahedral coordination and links the SiO_3 chains. *Pseudowollastonite*, stable above 1120°C, has space group $P\bar{1}$ but a much larger unit cell ($Z = 24$ as compared to $Z = 6$ for wollastonite). The basic structure of pseudowollastonite is very similar to that of wollastonite.

FIG. 19.43 The crystal structure of triclinic wollastonite. The tetrahedral silicate chain has a repeat of three tetrahedra. The Ca^{2+} ions are located in octahedral bands that are parallel to *c* and are three octahedra wide. Octahedral sites are identified as *M1*, *M2*, and *M3*. (Adopted from Papike, J. J. 1987. Chemistry of the rock-forming silicates: Ortho, ring, and single-chain structures. *Reviews of Geophysics and Space Physics* 25: 1483–1526.)

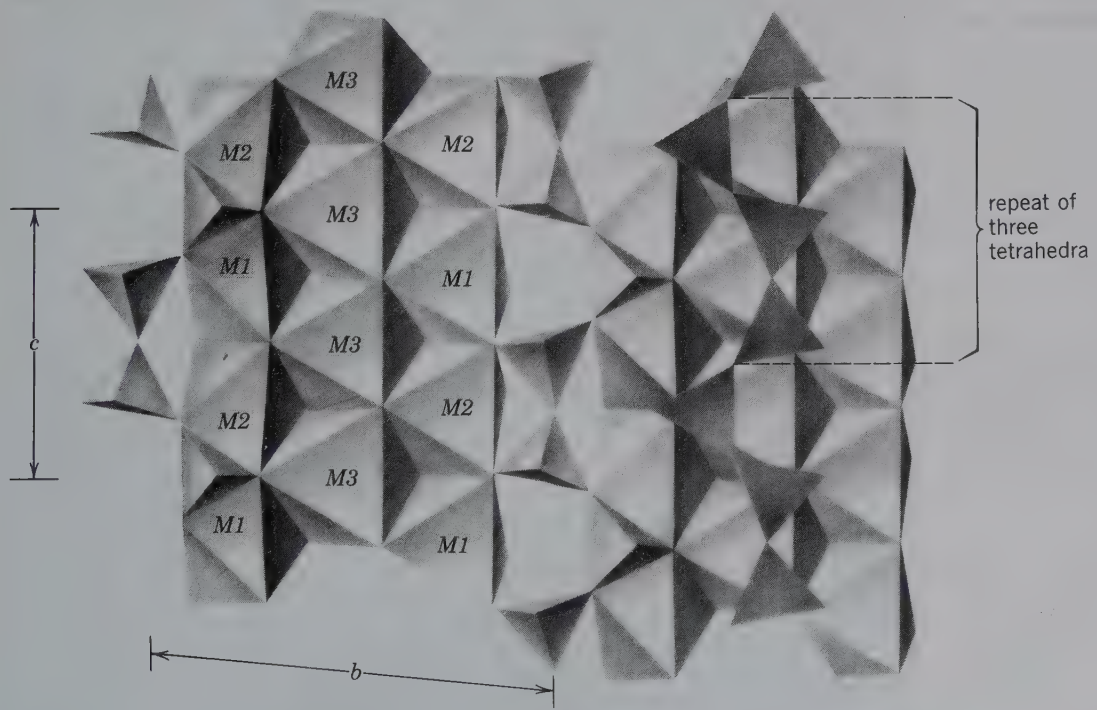

Diagnostic Features. Characterized by its two perfect cleavages of about 84°. It resembles tremolite but is distinguished from it by the cleavage angle.

Occurrence. Wollastonite occurs as a contact metamorphic mineral in metamorphosed Si-rich limestones, and forms by the reaction:

$$\underset{\text{calcite}}{CaCO_3} + \underset{\text{quartz}}{SiO_2} \rightarrow \underset{\text{wollastonite}}{CaSiO_3} + CO_2\uparrow$$

It is associated with calcite, diopside, andradite, grossular, tremolite, plagioclase feldspar, vesuvianite, and epidote. During progressive metamorphism of siliceous dolomites the following approximate sequence of mineral formation is often found, beginning with the lowest-temperature product: talc→tremolite→diopside→forsterite→wollastonite→periclase→monticellite (see Fig. 21.18).

In places it may be so plentiful as to constitute the chief mineral of the rock mass. Such wollastonite rocks are found in the Black Forest, Germany; in Brittany, France; in Willsboro, New York; in California; and in Mexico. Crystals of the mineral are found at Csiklova in Romania; the Harz Mountains, Germany; and Chiapas, Mexico. In the United States found in New York at Diana, Lewis County, and St. Lawrence County. In California at Crestmore, Riverside County.

Use. Wollastonite is mined in those places where it constitutes a major portion of the rock mass and is used in the manufacture of tile.

Name. In honor of the English chemist, W. H. Wollaston (1766–1828).

Rhodonite—$MnSiO_3$

Crystallography. Triclinic; $\bar{1}$. Crystals commonly tabular parallel to {001} (Fig. 19.44); often rough with rounded edges. Commonly massive, cleavable to compact; in embedded grains.

$P\bar{1}$; $a = 7.79$, $b = 12.47$, $c = 6.75$ Å; $a = 85°10'$, $\beta = 94°4'$, $\gamma = 111°29'$; $Z = 10$. *ds*: 4.78(4), 3.15(5), 3.09(3), 2.98(8), 2.93(9), 2.76(10).

Physical Properties. *Cleavage* {110} and $\{1\bar{1}0\}$ perfect. **H** $5\frac{1}{2}$–6. **G** 3.4–3.7. *Luster* vitreous. *Color* rose-red, pink, brown, see Plate VI, no. 4; frequently with black exterior of manganese oxide. Transparent to translucent. *Optics*: (+); $\alpha = 1.716$–1.733, $\beta = 1.720$–1.737, $\gamma = 1.728$–1.747; $2V = 60°$–$75°$, $r < v$.

Composition and Structure. Rhodonite is seldom pure $MnSiO_3$ but contains some Ca, with a maximum $CaSiO_3$ content of about 20 molecular percent. Fe^{2+} may replace Mn up to as much as 14 weight percent FeO (see Fig. 19.45). Zn may be present, and Zn-rich varieties are known as *fowlerite*. The structure of rhodonite consists of SiO_3 chains, parallel to the *c* axis, with a unit repeat of five twisted tetrahedra (see Fig. 18.20c). Layers of cations alternate with the chains. The structure is similar to that of wollastonite (see Fig. 19.43), and pyroxmangite, $(Mn,Fe)SiO_3$.

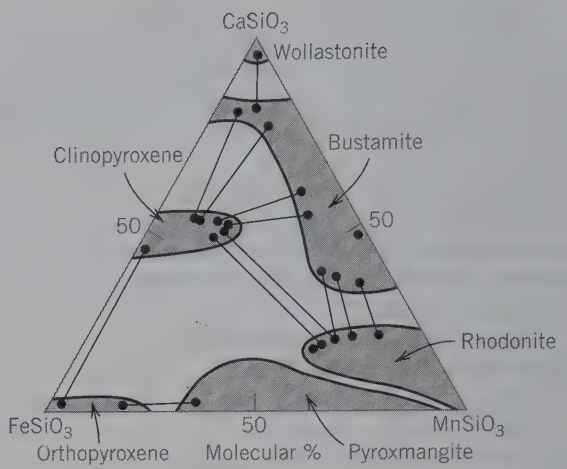

FIG. 19.45 Extent of compositional fields for pyroxenoid and pyroxene compositions in the system $CaSiO_3$–$FeSiO_3$–$MnSiO_3$. The temperature and pressure conditions applicable to this diagram are about 600°C and 6 kilobars, respectively. Tielines join naturally occurring mineral pairs. (Redrawn from Brown, P. E., E. J. Essene, and D. R. Peacor. 1980. Phase relations inferred from field data for Mn pyroxenes and pyroxenoids. *Contributions to Mineralogy and Petrology* 74: 417–25; see also *Pyroxenes, Reviews in Mineralogy*.)

FIG. 19.44 Rhodonite.

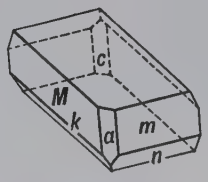

Diagnostic Features. Characterized by its pink color and near 90° cleavages. Distinguished from rhodochrosite by its greater hardness and good cleavage.

Occurrence. Rhodonite is uncommon and occurs in manganese deposits and manganese-rich iron-formations, as a result of metamorphic and commonly associated fluid infiltration. It may form from rhodochrosite by the reaction:

$$\underset{\text{rhodochrosite}}{MnCO_3} + \underset{\text{quartz}}{SiO_2} \rightarrow \underset{\text{rhodonite}}{MnSiO_3} + CO_2\uparrow$$

Rhodonite is found at Långban, Sweden, with other manganese minerals and iron ore; in large masses near Sverdlovsk in the Ural Mountains, Russia; and at Broken Hill, New South Wales, Australia. In the United States rhodonite occurs in good-sized crystals in metamorphosed limestone with franklinite, willemite, zincite, and so forth, at Franklin, New Jersey (Fig. 19.46).

Use. Some rhodonite is polished for use as an ornamental stone. This material is obtained from the Ural Mountains, Russia, and Australia.

Name. Derived from the Greek word for *a rose*, in allusion to the color.

Similar Species. *Pyroxmangite*, $(Mn,Fe)SiO_3$, is structurally very similar to rhodonite, but with a unit repeat of seven tetrahedra in the SiO_3 chain (see Fig. 18.20d). *Pyroxferroite*, $Ca_{0.15}Fe_{0.85}SiO_3$, isostructural with pyroxmangite, is a relatively

FIG. 19.46 Rhodonite, Franklin, New Jersey (Harvard Mineralogical Museum).

common mineral in lunar lavas. *Bustamite*, $(Mn,Ca,Fe)SiO_3$, is very similar in structure to wollastonite. All of these pyroxenoids have extensive fields of solid solution, as shown in Fig. 19.45. *Tephroite*, Mn_2SiO_4, a red to gray mineral associated with rhodonite, is isostructural with olivine.

Pectolite—$NaCa_2(SiO_3)_3O(OH)$ IV

Crystallography. Triclinic; $\bar{1}$. Crystals elongated parallel to the *b* axis. Usually in aggregates of acicular crystals. Commonly radiating, with fibrous appearance (Fig. 19.47). In compact masses.

$P\bar{1}$; $a = 7.99$, $b = 7.04$, $c = 7.02$ Å; $\alpha = 90°31'$, $\beta = 95°11'$, $\gamma = 102°28'$; $Z = 2$. *ds*: 3.28(7), 3.08(9), 2.89(10), 2.31(7), 2.28(7).

Physical Properties. *Cleavage* {001} and {100} perfect. **H** 5. **G** 2.8±. *Luster* vitreous to silky. *Color* colorless, white, green, yellow, or gray. Transparent. *Optics*: (+); $\alpha = 1.595$, $\beta = 1.604$, $\gamma = 1.633$; $2V = 60°$; $Z \approx b$, $X \wedge c = 19°$.

Composition and Structure. CaO 33.8, Na_2O 9.3, SiO_2 54.2, H_2O 2.7%. In some pectolite Mn^{2+} substitutes for Ca. The structure of pectolite contains SiO_3 chains, parallel to the *b* axis, the unit repeat of which consists of three twisted tetrahedra (see Fig. 18.20b) similar to that found in wollastonite. The Ca ions are in octahedral coordination, and Na is present in very distorted octahedral coordination.

Diagnostic Features. Characterized by two directions of perfect cleavage, yielding sharp, acicular fragments that will puncture the skin if not handled carefully. Resembles wollastonite.

Occurrence. Pectolite is a secondary mineral similar in its occurrence to the zeolites. Found lining cavities in basalt, associated with various zeolites, prehnite, calcite, and so forth. Found at Bergen Hill and West Paterson, New Jersey. In Canada, at Asbestos and Mount St. Hilaire, Quebec.

Name. From the Greek word meaning *compact*, in allusion to its habit.

FIG. 19.47 Pectolite (white, fibrous) with small round clusters of prehnite (grey), Paterson, New Jersey (Harvard Mineralogical Museum).

AMPHIBOLE GROUP

The following common double-chain inosilicates, amphiboles, are described in detail:

Anthophyllite	$Mg_7Si_8O_{22}(OH)_2$
Cummingtonite Series	
Cummingtonite	$Mg_7Si_8O_{22}(OH)_2$
Grunerite	$Fe_7Si_8O_{22}(OH)_2$
Tremolite Series	
Tremolite	$Ca_2Mg_5Si_8O_{22}(OH)_2$
Actinolite	$Ca_2(Mg,Fe)_5Si_8O_{22}(OH)_2$
Hornblende	$X_{2-3}Y_5Z_8O_{22}(OH)_2$
Sodium Amphibole Group	
Glaucophane	$Na_2Mg_3Al_2Si_8O_{22}(OH)_2$
Riebeckite	$Na_2Fe^{2+}_3Fe^{3+}_2Si_8O_{22}(OH)_2$

Anthophyllite—$Mg_7Si_8O_{22}(OH)_2$

Crystallography. Orthorhombic; $2/m2/m2/m$. Rarely in distinct crystals. Commonly acicular or fibrous.

Pnma; $a = 18.56$, $b = 18.08$, $c = 5.28$ Å; $Z = 4$. *ds*: 8.26(6), 3.65(4), 3.24(6), 3.05(10), 2.84(4).

Physical Properties. *Cleavage* {210} perfect; $(210) \wedge (2\bar{1}0) = 55°$. **H** $5\frac{1}{2}$–6. **G** 2.85–3.2. *Luster* vitreous. *Color* gray to various shades of green and brown and beige; see Plate VI, no. 5. *Optics*: (−); $\alpha = 1.60$–1.69, $\beta = 1.61$–1.71, $\gamma = 1.62$–1.72. $2V = 70°$–$100°$; $X = a$, $Y = b$. Absorption $Z > Y$ and X. Indices increase with Fe content.

Composition and Structure. *Anthophyllite* is an end-member and part of a solid solution series from $Mg_7Si_8O_{22}(OH)_2$ to $Fe_7Si_8O_{22}(OH)_2$; at higher Fe contents ($Mg/Mg + Fe < 0.5$), it is know as ferro-anthophyllite. *Gedrite* is an Al-containing variety of anthophyllite, with an end-member composition approximating $Mg_5Al_2Si_6Al_2O_{22}(OH)_2$. At moderate temperatures a miscibility gap exists between anthophyllite and gedrite as shown by coexisting anthophyllite and gedrite grains. The structures of anthophyllite and gedrite are similar, both with orthorhombic space group *Pnma*. The relationship of the unit cell of orthoamphibole to that of clinoamphibole is shown in Fig. 18.25a.

Diagnostic Features. Characterized by its clove-brown color but, unless in crystals, cannot be distinguished from other amphiboles such as cummingtonite or grunerite without optical or X-ray tests.

Occurrence. Anthophyllite results from the metamorphism of Mg-rich rocks, such as ultrabasic igneous rocks and impure dolomitic shales. It is common in cordierite-bearing gneisses and schists. It may also form as a retrograde product rimming relict orthopyroxenes and olivine (see Fig. 19.38). It occurs at Kongsberg, Norway, and in many localities in southern Greenland. In the United States, it is found at several localities in Pennsylvania, in southwestern New Hampshire and central Massachusetts, in the Gravelly Range and Tobacco Root Mountains of southwestern Montana, and at Franklin, North Carolina.

Name. From the Latin word *anthophyllum*, meaning *clove*, in allusion to the clove-brown color.

CUMMINGTONITE—$Mg_7Si_8O_{22}(OH)_2$ GRUNERITE—$Fe_7Si_8O_{22}(OH)_2$

Crystallography. Monoclinic; $2/m$. Rarely in distinct crystals. Commonly fibrous or lamellar, often radiated.

$C2/m$; for grunerite, $a = 9.59$, $b = 18.44$, $c = 5.34$ Å, $\beta = 102°0'$; cell lengths decrease with increasing Mg (see Fig. 19.48); $Z = 2$. *ds*: 9.21(5), 8.33(10), 3.07(8), 2.76(9), 2.51(6).

Physical Properties. *Cleavage* {110} perfect. **H** $5\frac{1}{2}$–6. **G** 3.1–3.6. *Luster* silky; fibrous; see Plate VI, no. 6. *Color* various shades of light brown. Translucent; will transmit light on thin edges. *Optics*: (−) for grunerite; (+) for cummingtonite; $\alpha = 1.65$–1.69; $\beta = 1.67$–1.71; $\gamma = 1.69$–1.73; 2V large; $Y = b$, $Z \wedge c = 13°$–$20°$ (see Fig. 19.49). $r < v$ for cummingtonite; $r > v$ for grunerite. Essentially nonpleochroic.

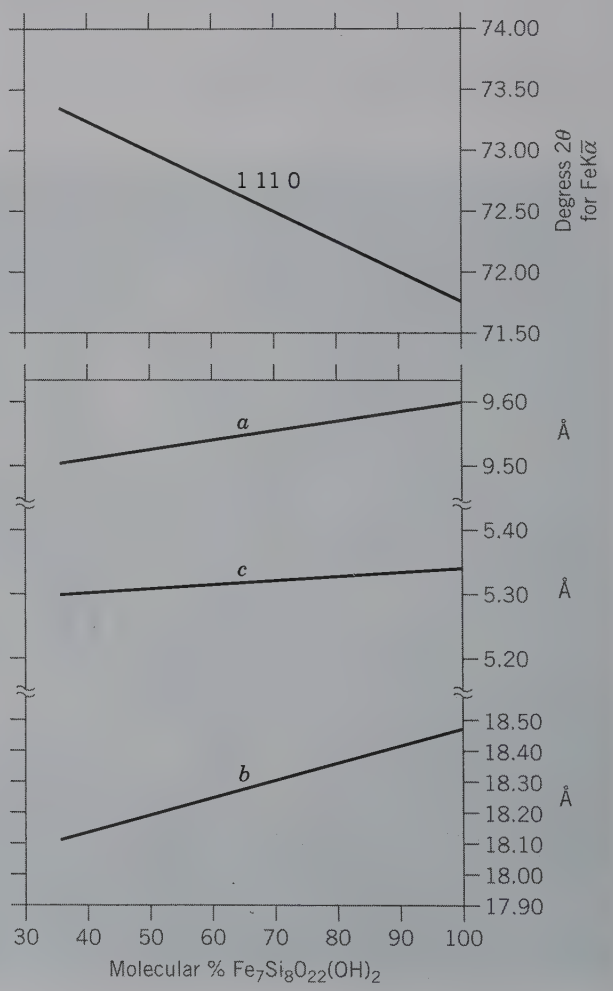

FIG. 19.48 Variation in the unit cell parameters *a*, *b*, and *c* as a function of composition in the cummingtonite–grunerite series. The topmost line relates the angular (2θ) position of the 1, 11, 0 X-ray diffraction peak (as recorded on a diffractometer pattern, or X-ray photograph; see Chapter 14) as a function of composition in the cummingtonite–grunerite series (using FeKα̅ radiation). (From Klein, C. and D. R. Waldbaum. 1967. X-ray crystallographic properties of the cummingtonite-grunerite series. *Journal of Geology* 75: 379–92.)

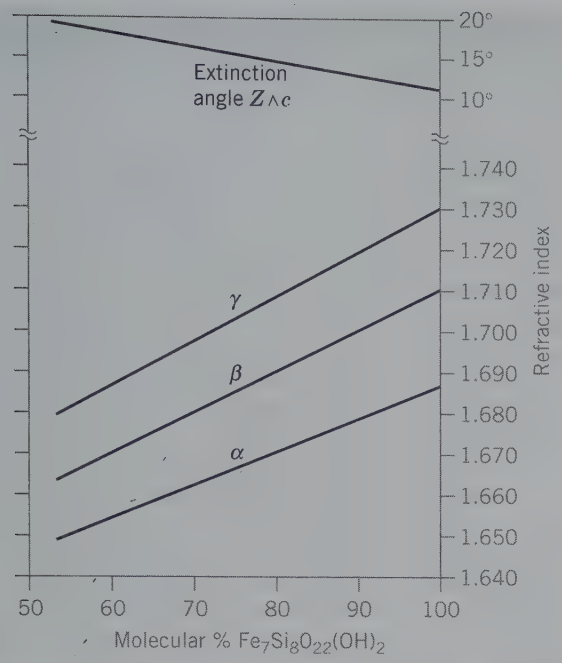

FIG. 19.49 Variation in refractive indices and extinction angle for members of the monoclinic cummingtonite-grunerite series. (From Klein, C. 1964. Cummingtonite-grunerite series: A chemical optical and X-ray study. *American Mineralogist* 49: 963–82.)

Composition and Structure. The *cummingtonite–grunerite* series extends from approximately $Fe_2Mg_5Si_8O_{22}(OH)_2$ to the end-member $Fe_7Si_8O_{22}(OH)_2$. Members with Mg < Fe (atomic percentage) are referred to as cummingtonite; those with Fe > Mg as grunerite (in the literature this division is often taken at 50 atomic percent Fe). Mn^{2+} can be present to as much as $Mn_2Mg_5Si_8O_{22}(OH)_2$, with most of the Mn in the *M4* site. Al_2O_3 and CaO range up to a maximum of 0.4 and 0.9 weight percent, respectively. The structure (see Fig. 18.22) of the majority of members of the cummingtonite–grunerite series is *C2/m*, like that of tremolite; however, some Mg-rich cummingtonites have $P2_1/m$ symmetry.

Diagnostic Features. Characterized by a light brown color and needlelike, often radiating habit. May be impossible to distinguish from anthophyllite or gedrite without optical or X-ray tests.

Occurrence. Cummingtonite is a constituent of regionally metamorphosed rocks and occurs in amphibolites. It commonly coexists with hornblende or actinolite (see tielines in Fig. 18.21). Mg-rich cummingtonite can also coexist with anthophyllite, because of a small miscibility gap between anthophyllite and the Mg-rich part of the cummingtonite–grunerite series (see Fig. 18.25b). Cummingtonite phenocrysts have been reported in some igneous rocks such as dacites. Mn-rich varieties occur in metamorphosed manganese-rich units. Grunerites are characteristic of metamorphosed iron-formations in the Lake Superior region and the Labrador Trough. Upon prograde metamorphism, cummingtonite and grunerite break down to members of the orthopyroxene or olivine series (see Fig. 19.38).

Use. *Amosite*, a very rare asbestiform variety of grunerite, was mined only in the eastern part of the Transvaal Province of South Africa (see Fig. 19.50). The varietal name is derived from the word *Amosa*, an acronym for the company "Asbestos Mines of South Africa." Few data are as yet available on the possible health hazards of this asbestos type (see Ross 1981 and 1982). For comparison and more extensive discussion of asbestos, see *chrysotile* and *crocidolite* and Box 19.2.

Names. Cummingtonite is named after Cummington, Massachusetts, and grunerite after Grüner, nineteenth century French chemist.

TREMOLITE—$Ca_2Mg_5Si_8O_{22}(OH)_2$ ACTINOLITE—$Ca_2(Mg,Fe)_5Si_8O_{22}(OH)_2$

Crystallography. Monoclinic; *2/m*. Crystals usually prismatic. The termination of the crystals is almost always formed by the two faces of a low {0*kl*} prism (similar to hornblende, see Fig. 19.52). Tremolite is often bladed and frequently in radiating columnar aggregates. In some cases in silky fibers. Coarse to fine granular. Compact.

C2/m; $a = 9.84, b = 18.05, c = 5.28$ Å; $\beta = 104°42'$; $Z = 2$. *ds:* 8.38(10), 3.27(8), 3.12(10), 2.81(5), 2.71(9).

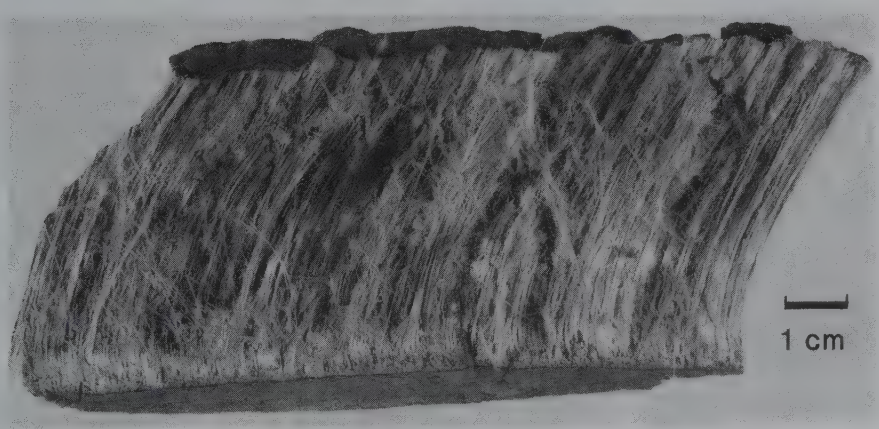

FIG. 19.50 Amosite, an asbestiform variety of the amphibole grunerite (in the trade this is also known as "brown asbestos"), Penge, Transvaal Province, Republic of South Africa (compare with Figs. 19.53 and 19.55).

BOX 19.2 Asbestos: A Mixture and Mix-up of Minerals

News reports frequently cover toxic substances that threaten our environment. One of those threats is asbestos, a name that has come to invoke fear. However, despite popular belief, most asbestos has not been proven to be harmful in concentrations found in the ambient indoor and outdoor environment. Yet regulatory agencies in the United States initiated a program in the 1980s to remove asbestos-containing materials from schools and public buildings at a cost of many billions of dollars. Why is this? Some confusion stems from the use of the term *asbestos*, which is a commercial, and not a mineralogic term.

Asbestos is a collective term encompassing six naturally occurring minerals that exhibit asbestiform habit (see photographs). This fibrous habit imparts superior qualities for use as fire retardants, thermal insulators, and as chemically resistant materials. The fibers are flexible, yet have a tensile strength similar to that of steel wire. Thus, asbestos had widespread commercial appeal. These six different asbestos minerals belong to two silicate groups: the serpentine mineral group is represented by chrysotile asbestos and the amphibole mineral group is represented by riebeckite asbestos (crocidolite), grunerite asbestos (amosite), anthophyllite asbestos, tremolite asbestos and actinolite asbestos. Apart from habit, layered silicates (the serpentines) and double-chained silicates (the amphiboles) display vastly different physical properties.

Approximately 95% of the "asbestos" that was used commercially is chrysotile. Chrysotile, $Mg_3Si_2O_5(OH)_4$, occurs as hollow fibers (like a soda straw; see Figs. 18.38 and 18.39), formed from serpentine sheets rolled like a carpet. Usually, these soft, flexible fibers are bundled together, similar to yarn. Chrysotile exhibits only minor solid solution, and laboratory experiments conclude that a 10 μm chrysotile fiber (the size of those particles found in the lung) dissolves in about nine months in a solution with a pH equivalent to that of the human lung (Hume and Rimstidt, 1992).

The five amphibole asbestos minerals have a greater hardness, and the fibers are smooth, relatively inflexible and generally thicker and more needle-like than chrysotile. Amphiboles exhibit extensive solid solution and, as a consequence, surface reactivity is expected to vary significantly from one amphibole to another. Laboratory experiments on crocidolite demonstrate that it has low solubility and could have a residence time in the lung of hundreds of years (Werner et al., 1995). Health experts agree that of the six asbestos minerals crocidolite is the most carcinogenic. Specifically, in addition to lung cancer, it can cause mesothelioma, a virulent type of cancer that attacks the outer lining of the lung or abdomen. However, crocidolite was used in less than 5% of commercial products.

The difficulty of the regulatory aspects of asbestos are compounded by the chemical variability exhibited by amphiboles. Most recently, fibers of the amphibole *winchite*, have been implicated as an occupational disease agent in the miners from Libby, Montana, USA. However, in the current regulatory classification scheme, winchite asbestos and another fibrous form, richterite asbestos are not classified as asbestos.

Also, the present regulatory definitions do not properly characterize the various asbestos minerals, differentiate between their associated health hazards, nor differentiate between cleavage fragments of the nonasbestiform serpentine and amphibole minerals and true asbestos fibers. The regulatory agencies should not assume that all types of fibers and cleavage fragments present the same health risk. From available data, risks associated with environmental (low-level) exposure to asbestos are minimal. Mineralogists are necessary to evaluate and explain the complexity and heterogeneity of natural asbestiform and nonasbestiform materials to regulatory agencies as well as to medical researchers. Mineralogic information is essential to understanding disease patterns, or the lack therefore, in humans.

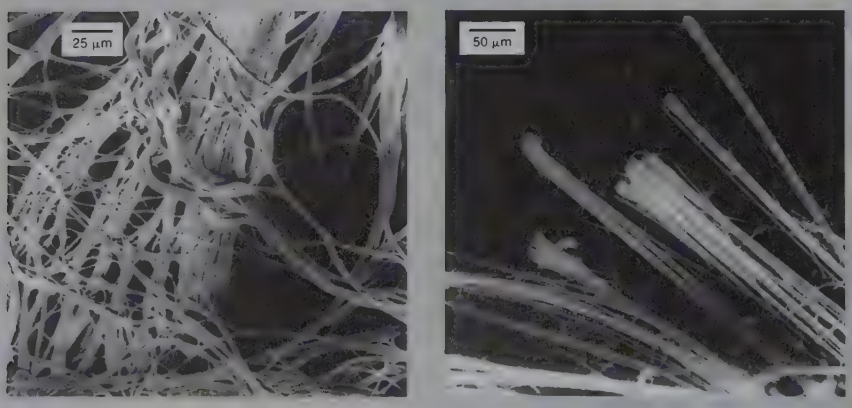

(*a*) (*b*)

Photomicrograph of (a) *chrysotile asbestos and* (b) *crocidolite asbestos. Compare the curly and rope-like nature of the chrysotile fiber bundles to the straight, splintered and needle-like nature of the crocidolite fiber bundles. (Photographs courtesy of M. Ross, U.S. Geological Survey, Reston, Virginia.)*

Physical Properties. *Cleavage* {110} perfect; (110) ∧ (1$\bar{1}$0) = 56° often yielding a splintery surface. **H** 5–6. **G** 3.0–3.3 *Luster* vitreous; often with silky sheen in the prism zone. *Color* varying from white in tremolite to green in actinolite. The color deepens and the specific gravity increases with increase in Fe content, see Plate VI, no. 7. Transparent to translucent. A felted aggregate of tremolite fibers goes under the name of *mountain leather* or *mountain cork*. A tough, compact variety that supplies much of the material known as *jade* is called *nephrite* (see jadeite). *Optics*: (−); α = 1.60–1.68, β = 1.61–1.69, γ = 1.63–1.70; 2V = 80°; $Y = b$, $Z \wedge c = 15°$. Indices increase with iron content.

Composition and Structure. A complete solid solution exists from *tremolite* to *ferro-actinolite*, $Ca_2Fe_5Si_8O_{22}(OH)_2$ (see Fig. 18.21). The name *actinolite* is used for intermediate members. In high-temperature metamorphic and in igneous occurrences a complete series exists from the tremolite–ferro-actinolite series to hornblende as a result of a wide range of Al substitution for Si, and concomitant cation replacements elsewhere in the structure. The names *tremolite* and *ferro-actinolite* are generally used to refer to the Al-poor members of this large compositional range. In lower-temperature occurrences tremolite (or actinolite) may coexist with hornblende as the result of a miscibility gap between tremolite (or actinolite) and hornblende. The structures of the members of the tremolite-ferroactinolite series are of the *C2/m* type (see Figs. 18.22, 18.23, and page 452).

Diagnostic Features. Characterized by slender prisms and good prismatic cleavage. Distinguished from pyroxenes by the cleavage angle and from hornblende by lighter color.

Occurrence. Tremolite is most frequently found in metamorphosed dolomitic limestones where it forms according to this reaction:

$$\underset{\text{dolomite}}{5CaMg(CO_3)_2} + \underset{\text{quartz}}{8SiO_2} + H_2O$$

$$\rightarrow \underset{\text{tremolite}}{Ca_2Mg_5Si_8O_{22}(OH)_2} + \underset{\text{calcite}}{3CaCO_3} + CO_2\uparrow$$

At higher temperatures tremolite is unstable and yields to diopside (see Fig. 19.51). Actinolite is a characteristic mineral of the greenschist facies of metamorphism. It occurs also in glaucophane schists in coexistence with quartz, epidote, glaucophane, pumpellyite, and lawsonite.

Notable localities for crystals of tremolite are Ticino, Switzerland; in the Tyrol; and in Piemonte, Italy. In the United States, from Russell, Gouverneur, Amity, Pierrepont, DeKalb, and Edwards, New York. Crystals of actinolite are found at Greiner, Zillerthal, Tyrol, Austria and at Catalina Island, California. The original jade was probably nephrite that came from the Khotan and Yarkand Mountains of Chinese Turkestan. Nephrite has been found in New Zealand, Mexico, and Central America; and, in the United States, near Lander, Wyoming.

Use. The compact variety, *nephrite*, is used as an ornamental and gem material.

Name. Tremolite is derived from the Tremola Valley near St. Gotthard, Switzerland. Actinolite comes from two Greek words meaning *a ray* and *stone*, in allusion to its frequently somewhat radiated habit.

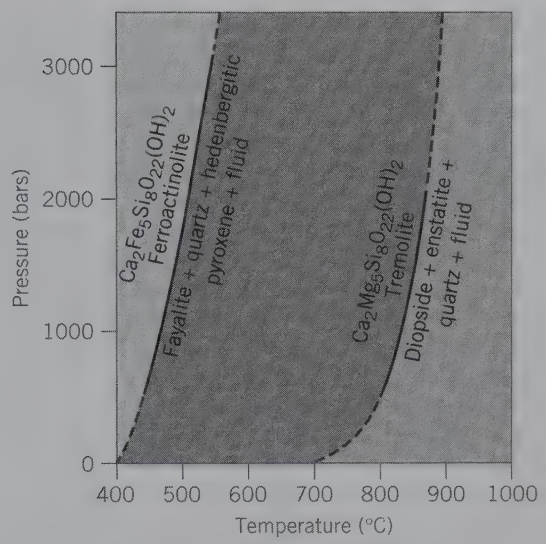

FIG. 19.51 Comparison of the thermal stability limits of tremolite and ferroctinolite. (After Ernst, W. G. 1968. *Amphiboles*. Springer-Verlag, New York, 58.)

HORNBLENDE—
$(Ca,Na)_{2-3}(Mg,Fe,Al)_5Si_6(Si,Al)_2O_{22}(OH)_2$

Crystallography. Monoclinic; 2/*m*. Crystals prismatic, usually terminated by {011}. The vertical prism zone shows, in addition to the prism faces, usually {010}, and more rarely {100} (see Fig. 19.52). May be columnar or fibrous; coarse- to fine-grained.

C2/m; $a = 9.87$, $b = 18.01$, $c = 5.33$ Å; β = 105°44′; $Z = 2$. *ds*: 3.38(9), 3.29(7), 3.09(10), 2.70(10), 2.59(7).

Physical Properties. *Cleavage* {110} perfect. **H** 5–6. **G** 3.0–3.4. *Luster* vitreous; fibrous; fibrous varieties often silky. *Color* various shades of dark green to black; see Plate VI, no. 8. Translucent; will transmit light on thin edges. *Optics*: (−); α = 1.61–1.71, β = 1.62–1.72, γ = 1.63–1.73; 2V = 30°–90°; $Y = b$, $Z \wedge c = 15°–34°$. $r > v$ usually; may be $r < v$. Pleochroism *X* yellow-green, *Y* olive-green, *Z* deep green.

Composition and Structure. What passes under the name of hornblende is in reality a complex and large compositional range with variations in the ratios Ca/Na, Mg/Fe^{2+},

FIG. 19.52 Hornblende crystals.

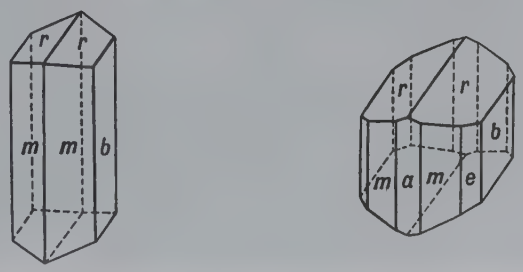

Al/Fe^{3+}, Al/Si, and OH/F. A generalized formula for a "common" hornblende is given previously, and an example of the recalculation of an amphibole analysis is given in Table 5.7. At elevated temperatures, hornblende shows a complete series toward tremolite-ferro-actinolite, but at lower temperatures a miscibility gap exists. In some volcanic rocks, oxyhornblendes are found with considerable Fe^{3+}/Fe^{2+} ratios and low OH contents; an example composition is $NaCa_2Fe_4^{2+}Fe^{3+}(AlSi_7)O_{23}(OH)$. The structure of hornblende is similar to that of *C2/m* tremolite (see Figs. 18.22 and 18.23). Because of the miscibility gap between Ca-amphiboles and Mg-Fe amphiboles, hornblende often contains grunerite exsolution lamellae (see Fig. 12.15).

Diagnostic Features. Crystal form and cleavage angles serve to distinguish hornblende from dark pyroxenes. Usually distinguished from other amphiboles by its dark color, and from tourmaline by its cleavage and lack of striations.

Occurrence. Hornblende is an important and widely distributed rock-forming mineral, occurring in both igneous and metamorphic rocks; it is particularly characteristic of medium-grade metamorphic rocks known as *amphibolites* in which hornblende and associated plagioclase are the major constituents. It characteristically alters from pyroxene both during the late magmatic stages of crystallization of igneous rocks and during metamorphism. Hornblende is a common constituent of syenites and diorites.

Name. From an old German word for any dark prismatic mineral occurring in ores but containing no recoverable metal.

Similar Species. Because of the large chemical variation in the hornblende series, many names have been proposed for members on the basis of chemical composition and physical and optical properties. The most common names on the basis of chemical composition are *edenite*, *pargasite*, *hastingsite*, and *tschermakite*.

Glaucophane—$Na_2Mg_3Al_2Si_8O_{22}(OH)_2$
Riebeckite—$Na_2Fe_3^{2+}Fe_2^{3+}Si_8O_{22}(OH)_2$

Crystallography. Monoclinic; $2/m$. In slender acicular crystals; frequently aggregated; riebeckite sometimes asbestiform.

C2/m; $a = 9.58$, $b = 17.80$, $c = 5.30$ Å; $\beta = 103°48'$; $Z = 2$. *ds*: 8.42(10); 4.52(5), 3.43(6), 3.09(8), 2.72(10).

Physical Properties. *Cleavage* {110} perfect. **H** 6. **G** 3.1–3.4. *Luster* vitreous. *Color* blue to lavender-blue to black, darker with increasing iron content. *Streak* white to light blue. Translucent. *Optics*: (−); $\alpha = 1.61$–1.70, $\beta = 1.62$–1.71, $\gamma = 1.63$–1.72; $2V = 40°$–$90°$; $Y = b$, $Z \wedge c = 8°$. Pleochroism in blue *X*, *Y*, *Z*.

Composition and Structure. Very few glaucophanes are close to the end-member composition, $Na_2Mg_3Al_2Si_8O_{22}(OH)_2$, because of some substitution by Fe^{2+} for Mg and Fe^{3+} for Al. Riebeckite analyses do not conform well with the end-member formulation because the sum of $X + Y$ cations is frequently larger than 7, with Na entering the normally vacant *A* site. A partial series exists between glaucophane and riebeckite, with intermediate compositions known as *crossite*. The structures of both sodic amphiboles are similar to that of *C2/m* tremolite (see Fig. 18.22).

Diagnostic Features. Glaucophane and riebeckite are characterized by their generally fibrous habit and blue color.

Occurrence. *Glaucophane* is found only in metamorphic rocks, such as schists, eclogite, and marble. The occurrences of glaucophane reflect low-temperature, relatively high-pressure metamorphic conditions typical of those found in paleo-subduction zones, in association with jadeite, lawsonite, and aragonite. It is a major constituent of glaucophane schists in the Franciscan Formation of California. It is also found in metamorphic rocks from Mexico, Japan, Taiwan, Indonesia, and eastern Australia. *Riebeckite* occurs most commonly in igneous rocks, such as granites, syenites, nepheline syenites, and related pegmatites. It is a conspicuous mineral in the granite of Quincy, Massachusetts. It is present in some schists of regional metamorphic origin. The asbestiform variety of riebeckite is known as *crocidolite* (see Fig. 19.53 and Box 19.2).

Use. Crocidolite made up about 4% of the total world production of asbestos. All production from mines in the Cape Province, South Africa, was stopped in 1995. There are extensive reserves of crocidolite in the Hamersley Range of Western Australia, but crocidolite has not been mined there since 1966. The crocidolite is closely interbanded with Precambrian banded iron-formation sequences, both in South

FIG. 19.53 Crocidolite, an asbestiform variety of the amphibole riebeckite (in the trade this is also known as "blue asbestos"), Kuruman, Cape Province, Republic of South Africa (compare with Figs. 19.50 and 19.55).

Africa and Western Australia. Medical studies have shown (see Ross, 1981 and 1982; also Mossman and Gee, 1989; and Mossman et al., 1990) that crocidolite is a much greater health hazard than chrysotile asbestos. For comparison, see discussions of *chrysotile* and *amosite*.

In many places in South Africa, oxidized crocidolite fibers occur in quartz. This makes it an attractive ornamental material with a chatoyancy and is widely used for jewelry under the name of *tiger's eye*.

Name. Glaucophane is from the two Greek words meaning *bluish* and *to appear*. Riebeckite is in honor of E. Riebeck.

Similar Species. *Arfvedsonite*, $Na_3Fe_4^{2+}Fe^{3+}Si_8O_{22}(OH)_2$, is a deep green amphibole similar to riebeckite in occurrence. It is commonly associated with aegirine, or aegirine–augite. In the structure of arfvedsonite, the *A* site is completely or almost completely filled by Na (see Table 18.2).

PHYLLOSILICATES

The following common phyllosilicates, those minerals with infinitely extending tetrahedral sheets, are discussed in detail:

Serpentine Group	
Antigorite, Chrysotile, Lizardite	$Mg_3Si_2O_5(OH)_4$
Clay Mineral Group	
Kaolinite	$Al_2Si_2O_5(OH)_4$
Talc	$Mg_3Si_4O_{10}(OH)_2$
Pyrophyllite	$Al_2Si_4O_{10}(OH)_2$
Mica Group	
Muscovite	$KAl_2(AlSi_3O_{10})(OH)_2$
Phlogopite	$KMg_3(AlSi_3O_{10})(OH)_2$
Biotite	$K(Mg,Fe)_3(AlSi_3O_{10})(OH)_2$
Lepidolite	$K(Li,Al)_{2-3}(AlSi_3O_{10})(OH)_2$
Margarite	$CaAl_2(Al_2Si_2O_{10})(OH)_2$
Chlorite Group	
Chlorite	$(Mg,Fe)_3(Si,Al)_4O_{10}(OH)_2{\cdot}(Mg,Fe)_3(OH)_6$

Three minerals closely related to the phyllosilicate group are also covered:

Apophyllite	$KCa_4(Si_4O_{10})_2F{\cdot}8H_2O$
Prehnite	$Ca_2Al(AlSi_3O_{10})(OH)_2$
Chrysocolla	$Cu_4H_4Si_4O_{10}(OH)_8$

SERPENTINE GROUP

ANTIGORITE, LIZARDITE AND CHRYSOTILE—$Mg_3Si_2O_5(OH)_4$

Crystallography. Hexagonal and monoclinic. Crystals, except as pseudomorphs, unknown. Serpentine occurs in three common polymorphs: *antigorite*, *lizardite*, and *chrysotile*. Antigorite and lizardite are commonly massive and fine-grained; chrysotile is fibrous (see Fig. 19.54 and Plate VI, no. 9). Orthorhombic polymorphs of both antigorite and chrysotile are known.

Antigorite either *Pm* or *P2/m*; lizardite-1*T*, *P*31*m*; lizardite-2H_1, *P*6$_3$*cm*; chrysotile, orthorhombic or monoclinic, depending on polytype. For monoclinic antigorite: $a = 5.30$, $b = 9.20$, $c = 7.46$ Å; $\beta = 91°24'$; $Z = 2$. *ds*: 7.30(10), 3.63(8), 2.52(2), 2.42(2), 2.19(1). For monoclinic chrysotile: $a = 5.34$, $b = 9.25$, $c = 14.65$ Å; $\beta = 93°16'$; $Z = 4$.

Physical Properties. **H** 3–5, usually 4. **G** 2.5–2.6. *Luster* greasy, waxlike in the massive varieties, silky when fibrous. *Color* often variegated, showing mottling in lighter and darker shades of green to yellow. Translucent. *Optics*: (−); *Chrysotile*: $\alpha = 1.532–1.549$ (across fiber), $\gamma = 1.545–1.556$ (parallel to fiber length). *Antigorite* : nearly isotropic, $n = 1.55–1.56$.

The characteristic morphology of all asbestos minerals, in their natural form, is a parallel-sided fiber with a length-to-width ratio (referred to as an *aspect ratio*) in excess of 100 : 1 (Champness, Cliff, and Lorimer, 1976). Chrysotile asbestos occurs in very narrow tubular fibers that are often hollow (see Figs. 18.38 and 18.39). Other asbestos minerals are *crocidolite* (Fig. 19.53), an asbestiform variety of the amphibole riebeckite, and *amosite* (Fig. 19.50), an asbestiform variety of the amphibole grunerite. The term *asbestiform* refers to minerals that are mined as asbestos and possess fibrosity typical of asbestos—that is, with small fiber thickness, flexibility, and separability.

Composition and Structure. Close to $Mg_3Si_2O_5(OH)_4$ with MgO 43.0, SiO_2 44.1, and H_2O 12.9%. Small amounts of Fe and Ni may substitute to some extent for Mg and Al for some Si. The idealized structure of lizardite is shown in Fig. 18.34 in terms of trioctahedral *t–o* layers, in analogy with the dioctahedral kaolinite structure. Because of a misfit between the *t* and *o* layers the antigorite structure consists of finite and corrugated layers parallel to {001} (see Fig. 18.37a and page 463). In chrysotile, this same mismatch is responsible for the curvature of the *t–o* layers forming cylindrical tubes (see Fig. 18.37b and page 463). Much of the matrix material of serpentine, known as *lizardite*, is extremely fine-grained and has a platy morphology as seen under the high magnification of the electron microscope (see Fig. 18.39).

Diagnostic Features. Recognized by its variegated green color and its greasy luster or by its fibrous nature.

Occurrence. Serpentine is widely distributed: usually as an alteration of magnesium silicates, especially olivine, pyroxene, and amphibole. From forsterite, it may form by this reaction:

$$\underset{\text{forsterite}}{2Mg_2SiO_4} + 3H_2O \rightarrow \underset{\text{serpentine}}{Mg_3Si_2O_5(OH)_4} + \underset{\text{brucite}}{Mg(OH)_2}$$

It is frequently associated with magnesite, chromite, and magnetite. Found in both igneous and metamorphic rocks, frequently in disseminated particles, in places in such quantity as to make up the entire rock mass. Serpentine, as a rock name, is applied to such rock masses made up mostly of a mixture of fine-grained antigorite and lizardite. The asbestiform variety,

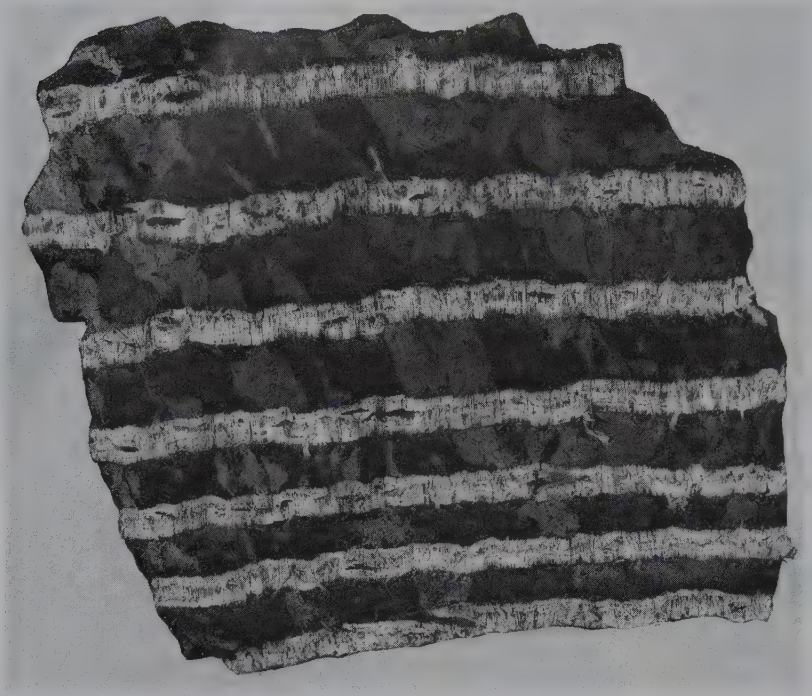

FIG. 19.54 Veins of chrysotile asbestos in serpentine. Thetford, Quebec, Canada.

chrysotile, as the principal asbestos mineral, is mined extensively. More than half of the world's production comes from deposits in Russia, just east of the Ural Mountains. Although for many years asbestos has been mined from large deposits in southeastern Quebec, making Canada the leading world producer, it is now second to Russia. Asbestos is no longer mined in the United States. However, in the eastern townships of Quebec, Canada, chrysotile asbestos continues to be mined from very large open-pit operations. The most productive locations are at Thetford Mines, and the town of Asbestos, Province of Quebec.

Use. Massive serpentine, which is translucent and of a light to dark green color, is often used as an ornamental stone and may be valuable as building material. Mixed with white marble and showing beautiful variegated coloring, it is called *verde antique* marble. A transparent yellow-green variety, *bowenite*, is used as a jade substitute.

The use of chrysotile, as asbestos, depends on its fibrous, flexible nature, which allows it to be made into felt and woven into cloth and other fabrics, and upon its incombustibility and slow conductivity of heat. Asbestos products were used for fireproofing and as an insulation material against heat and electricity (see also Box 19.2).

About 90% of the past and 95% of the present world production of asbestos was or is the chrysotile form (Fig. 19.55). This is known as "white asbestos." The remaining 5% of world production consisted of crocidolite (the asbestiform variety of the amphibole riebeckite), known as "blue asbestos," and amosite (the asbestiform variety of the amphibole grunerite), known as "brown asbestos." Other types of asbestos are of little economic importance.

Over the last many years there has been much attention given, in newspapers and on television, to the health hazards posed by asbestos. In such reports, no distinction is made between the various asbestos types, and furthermore, the health hazards that have been assessed in the dusty workplaces of earlier years (occupational settings, such as sites of asbestos mining and asbestos board manufacturing) are linearly extrapolated to those in nonoccupational settings (e.g., schoolrooms and office buildings with asbestos ceiling and floor tiles). Medical studies on the pathogenicity of the different forms of asbestos (Mossman et al., 1990; Mossman and Gee, 1989; Ross, 1981, 1984) show that crocidolite, the asbestiform variety of the amphibole riebeckite, poses a much greater health hazard (in *occupational settings*) than chrysotile. Occupational exposure to asbestos can cause asbestosis, lung cancer, mesothelioma (cancer of the plural and peritoneal membranes), and benign changes in the pleura (Mossman et al., 1990). Crocidolite fibers appear to be most pathogenic, especially with respect to mesothelioma. Smoking is a strong contributor to the incidence of lung cancer (Ross, 1984).

The main asbestos type used in U.S. buildings is chrysotile. Available data do not support the concept that low-level (*nonoccupational*) exposure to asbestos is a health hazard in buildings and schools (Mossman et al., 1990; see also Klein, C. 1993. Rocks, minerals and a dusty world. *Health Effects of Mineral Dusts. Reviews in Mineralogy* 28, Mineralogical Society of America, Washington, D.C., 7–59). Furthermore, a low-level background of fibers is present globally, in the air and water, as a result of natural weathering processes of rocks with fibrous minerals. Abelson (1990) stated: "We live on a planet on which there is an abundance of serpentine- and amphibole-containing rocks. Natural processes have been releasing fibers throughout Earth history, we breathe about 1 million fibers per year."

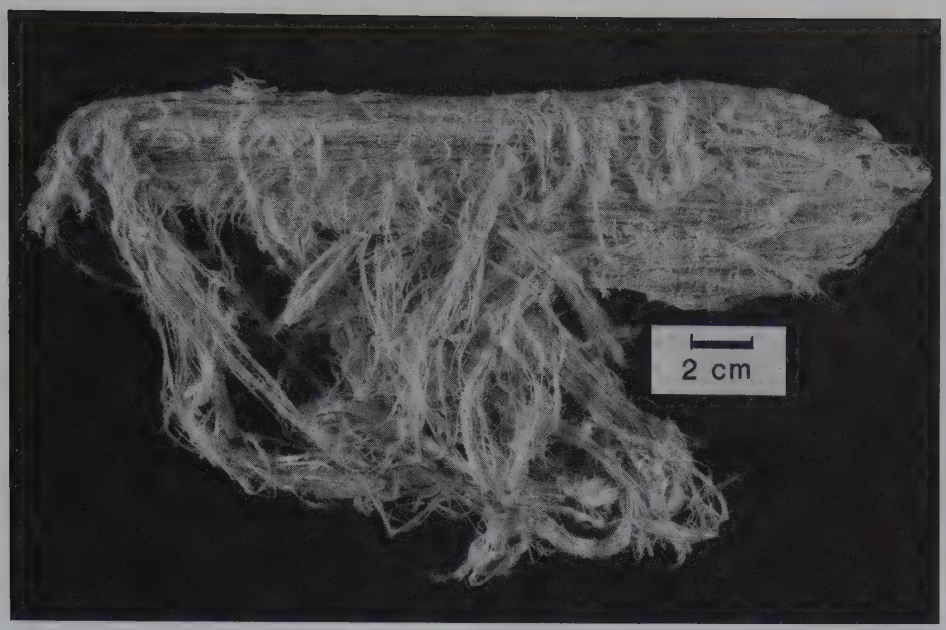

FIG. 19.55 Chrysotile, asbestiform variety of serpentine, Thetford, Quebec, Canada (compare with varieties of amphibole asbestos, Figs. 19.50 and 19.53).

Name. Serpentine refers to the green, serpentlike cloudings of the massive variety. Antigorite after Antigorio in Italy and chrysotile from the Greek words for *golden* and *fiber*.

Similar Species. *Greenalite*, $Fe_6^{2+}Si_4O_{10}(OH)_8$, may be considered as the Fe-rich analogue of the serpentine composition. It has a modulated structure that is very different from that of antigorite, for example; it is fairly common in unmetamorphosed Precambrian iron-formations. *Garnierite*, $(Ni,Mg)_3Si_2O_5(OH)_4$, is an apple-green Ni-bearing serpentine formed as an alteration product of Ni-rich peridotites. It is mined as a nickel ore in New Caledonia, Russia, and Australia. In the United States, it is found at Riddle, Oregon.

CLAY MINERAL GROUP

Clay mineral is a term used for a small number of minerals that occur with a grain size < 2 μm in the largest dimension (Moore and Reynolds, 1997). Most of these are hydrous aluminum silicates with layered structures. They are classified, as are other phyllosilicates, as 1 : 1 (*t–o*) or 2 : 1 (*t–o–t*), some with interlayer cations (see Fig. 18.34). Mg or Fe substitute for Al, and alkalies or alkaline earths may be present as essential constituents. Several polytypes occur for each clay mineral and, in some cases, several clay minerals may be intergrown to form *mixed-layer clays*. Clay minerals have unique properties, in part due to their small grain size and large ratio of surface area to volume. Generally, clay minerals exhibit plastic behavior when wet and will harden when dried or fired. They have highly reactive surfaces, high cation exchange capacities and catalytic activity making them valuable industrial minerals. On the other hand, the ability of some clay minerals to absorb water and increase their volume by 50% leads to problems with slope stability and foundations for houses or airport runways.

Clay minerals should not be confused with the term *clay*. Clay to geologists is a rock term indicating that the grain size of the various minerals comprising the rock is < 2 μm. In this context, the term *clay* has no compositional implication. Here, however, *clay mineral* has implications for both size and composition.

KAOLINITE—$Al_2Si_2O_5(OH)_4$

Crystallography. Triclinic; 1. In very minute, thin, rhombic or hexagonal plates (Fig. 19.56). Usually in claylike masses, either compact or friable.

$C1$; $a = 5.14$. $b = 8.93$, $c = 7.37$ Å; $\alpha = 91°48'$; $\beta = 104°30'$, $\gamma = 90°$; $Z = 2$. *ds*: 7.15(10), 3.57(10), 2.55(8), 2.49(9), 2.33(10).

Physical Properties. *Cleavage* {001} perfect. **H** 2. **G** 2.6. *Luster* usually dull earthy; crystal plates pearly. *Color* white, see Plate VII, no. 1. Often variously colored by impurities. Usually unctuous and plastic. *Optics*: (−); $\alpha = 1.553–1.565$, $\beta = 1.559–1.569$, $\gamma = 1.560–1.570$; $2V = 24°–50°$. $r > v$.

Composition and Structure. Kaolinite shows little compositional variation; for $Al_2Si_2O_5(OH)_4$, Al_2O_3 39.5, SiO_2 46.5, H_2O 14.0%. The dioctahedral structure of kaolinite is shown schematically in Figs. 18.31a and 18.34. It consists of an Si_2O_5 sheet bonded to a gibbsite sheet. The clay minerals *dickite* and *nacrite* are chemically similar to kaolinite but show a *t–o* stacking different from that in kaolinite.

Diagnostic Features. Recognized usually by its claylike character, but without X-ray tests, it is impossible to distinguish from the other clay minerals of similar composition, which collectively make up *kaolin*.

Occurrence. Kaolinite is a common mineral, the primary constituent of kaolin or clay. It forms as an authigenic mineral at low temperatures and pressures in sedimentary

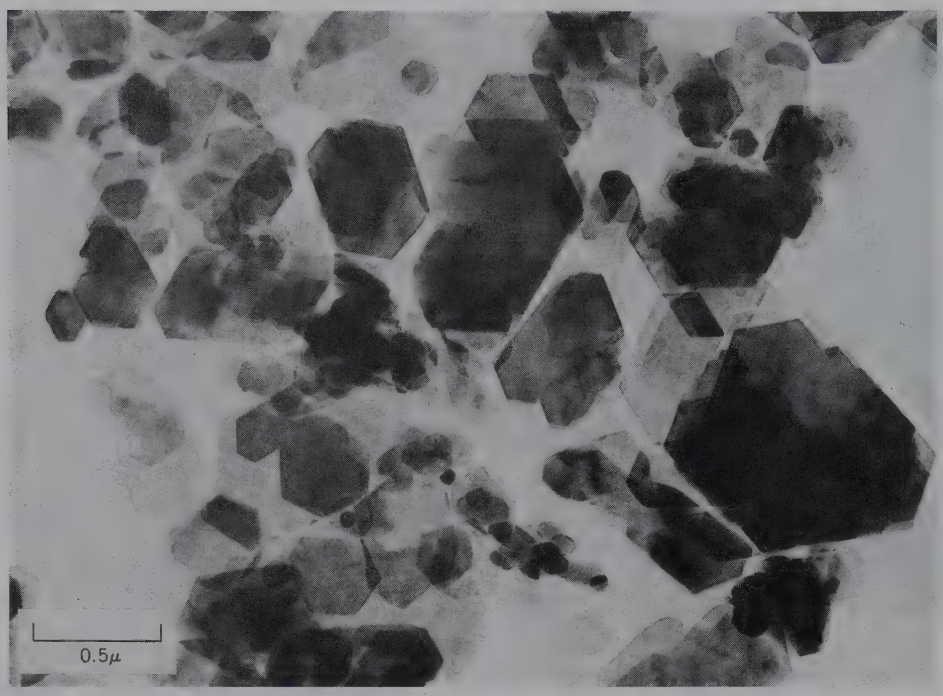

FIG. 19.56 Transmission electron micrograph of well-crystallized kaolinite from Georgia (courtesy of Dr. Kenneth M. Towe, Smithsonian Institution, Washington, D.C.).

rocks. It is also a secondary mineral formed by weathering or hydrothermal alteration of aluminum silicates, particularly feldspar. It is found mixed with feldspar in rocks that are undergoing alteration; in places it forms entire deposits where such alteration has been carried to completion. As one of the common products of the decomposition of rocks, it is found in soils, and transported by water it is deposited, mixed with quartz and other materials, in lakes, and so on, in the form of beds of clay. Kaolinite transforms to dickite at about 120° in sedimentary basins. Good pseudomorphs after potassium feldspar occur in Cornwall, England.

Use. Clay is one of the most important of the natural industrial substances (see also Box 19.3). It is available in every country of the world and is commercially produced in nearly every state in the United States. Many and varied products are made from it, which include common brick, paving brick, drain tile, and sewer pipe. The commercial users of clay recognize many different kinds having slightly different properties, each of which is best suited for a particular purpose. High-grade clay, which is known as *china clay* or *kaolin*, has many uses in addition to the manufacture of china and pottery. Its largest is as a filler in paper, but it is also used in the rubber industry and in the manufacture of refractories.

The chief value of clay for ceramic products lies in the fact that when wet it can be easily molded into any desired shape, and when it is heated, part of the combined water is driven off, producing a hard, durable substance.

Name. Kaolinite is derived from *kaolin*, which is a corruption of the Chinese *kauling*, meaning *high ridge*, the name of a hill near Jauchu Fa, where the material is obtained.

Similar Species. *Dickite* and *nacrite* are of the same composition as kaolinite but differ somewhat in their structure; they are less important constituents of clay deposits.

Halloysite has two forms: one with kaolinite composition, $Al_2Si_2O_5(OH)_4$, the other with composition $Al_2Si_2O_5(OH)_4 \cdot 2H_2O$. The second type dehydrates to the first with loss of interlayer water molecules.

The **smectite** group comprises a number of clay minerals composed of *t–o–t* layers of both dioctahedral and trioctahedral type. The outstanding characteristic of members of this group is their capacity to absorb water molecules between the sheets, thus producing marked expansion of the structure (see Fig. 18.36 for the similar structure of vermiculite; see also Box 19.3) while maintaining crystallographic integrity. The dioctahedral members are *montmorillonite*, *beidellite*, and *nontronite*; the trioctahedral members are *hectorite* and *saponite*.

Montmorillonite is the dominant clay mineral in *bentonite*, altered volcanic ash. Bentonite has the unusual property of expanding several times its original volume when placed in water. This property gives rise to interesting industrial uses. Most important is as a drilling mud in which the montmorillonite is used to give the fluid a viscosity several times that of water. It is also used for stopping leakage in soil, rocks, and dams.

Illite is an alkali-deficient mica near the muscovite composition. The illites differ from the micas in having less substitution of Al for Si, in containing more water, and in having K partly replaced by Ca and Mg. Illite is the primary constituent in many shales.

TALC—$Mg_3Si_4O_{10}(OH)_2$ IV

Crystallography. Triclinic; $\bar{1}$. Crystals rare. Usually tabular with rhombic or hexagonal outline. Foliated and in radiating foliated groups. When compact and massive, known as *steatite* or *soapstone*.

BOX 19.3 Clay Minerals and Some of Their Applications

Commercial clays, or clays utilized as raw materials in manufacturing, are among the most important nonmetallic mineral resources. The various applications of **kaolinite** are described under "use" as part of the systematic descriptions of kaolinite.

Two other clay minerals that have many commercial applications are **montmorillonite** and **vermiculite**. Montmorillonite is the major component of bentonite, which is a soft, plastic, light-colored rock that also contains some colloidal silica. It is the result of devitrification and accompanying chemical alteration of glassy igneous material, usually tuff or volcanic ash. Montmorillonite has the following idealized formula: $(Na,Ca)_{0.3}(Al,Mg)_2Si_4O_{10}\cdot nH_2O$. This clay has the ability to swell as a result of the incorporation of water molecules between the *t–o–t* sheets, in association with the interlayer cations, Na^+ and Ca^{2+}. When montmorillonite is heated in air, the interlayer water is driven off, thereby causing the collapse of the structure around the remaining interlayer cations. This process happens spontaneously in nature during burial metamorphism, leading to water expulsion and layer collapse, thereby transforming the montmorillonite structure to an illite-like structure.

The montmorillonite structure is always somewhat unbalanced, resulting in an overall somewhat negative charge that is balanced by exchangeable cations that are absorbed around the edges of the fine clay particles (see diagram). Such cation absorbance, and the associated cation-exchange capacity, is an important inherent property of many clays and is used in commercial applications, such as soil remediation, and in the fertilization of soils.

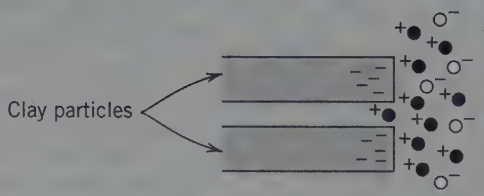

Schematic illustration of cations in solution, or in a water-rich soil, near a negatively charged clay particle.

The above properties are the basis for the use of bentonite in many commercial applications: as drilling muds and catalysts in the petroleum industry, as bonding clays in foundries, as bonding agents in hematite-rich iron ore pellets, and as absorbents. Bentonite clays are also being used as backfill (a buffer material) around high-level radioactive waste (HLW) canisters that are buried underground. Such clays are selected for sealing the space around HLW canisters because (1) they have low hydraulic conductivity, as compared with the host rock in which the repository is located; (2) they have good swelling properties to seal construction-caused joints and rock fractures; (3) their plasticity absorbs rock movements; (4) they show good retention of radionuclides; and (5) they are stable over a period of at least 10^6 years.

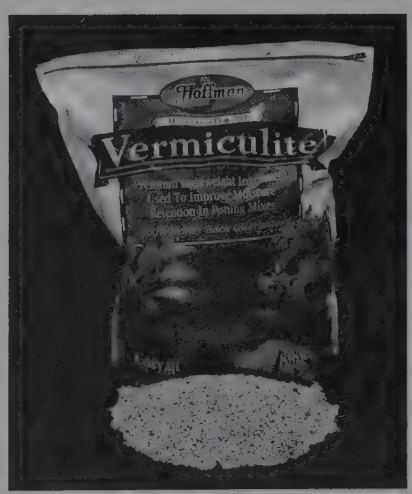

Vermiculite with an idealized formula of $Mg_3(Si,Al)_4O_{10}(OH)_2\cdot 4{\cdot}5H_2O$ $[Mg]_{0.35}$ (see discussion on p. 462 and Fig. 18.36 for a structure illustration) is similar in its properties to those of montmorillonite. The vermiculite structure can expand, as a result of the absorption of H_2O in the interlayer position, but to a lesser degree than observed in montmorillonite. Much of commercial vermiculite is used in agriculture for soil conditioning as a plant-growth medium, chemical fertilizer carrier, and carrier for pesticides and herbicides. When rapidly heated, vermiculite produces a lightweight expanded product that is widely used for thermal insulation and in potting soil. Mixed with plaster and cement, vermiculite is used to make lightweight versions of these materials. Vermiculite is also used as an absorbent for some environmentally hazardous liquids.

Graver, R. 1994. Bentonite as a backfill material in a high-level waste repository. *Materials Research Society Bulletin*: 43–46.

$C\bar{1}$; $a = 5.29, b = 9.17, c = 9.46$ Å; $\alpha = 90°28'$; $\beta = 98°41'$, $\gamma = 90°5'$; $Z = 4$. *ds*: 9.34(10), 4.66(9), 3.12(10), 2.48(7), 1.870(4).

Physical Properties. *Cleavage* {001} perfect. Thin folia somewhat flexible but not elastic. Sectile. **H** 1 (will make a mark on cloth). **G** 2.7–2.8. *Luster* pearly to greasy. *Color* white, apple-green (see Plate VII, no. 2), gray, or silver-white; in soapstone often dark gray or green. Translucent. Greasy feel. *Optics*: (−); $\alpha = 1.539$, $\beta = 1.589$, $\gamma = 1.589$; $2V = 6°–30°$. $Z = b$, $X \perp \{001\}$; $r > v$.

Composition and Structure. There is little variation in the chemical composition of most talc; pure talc contains MgO 31.7, SiO_2 63.5, H_2O 4.8%. Small amounts of Al or Ti may substitute for Si and Fe may replace some of the Mg which causes the color change from white to green. *Minnesotaite*, $Fe_3Si_4O_{10}(OH)_2$, is common in low-grade metamorphic Precambrian iron deposits. Minnesotaite has a modulated structure that is different from that of talc; it is probable that an almost complete solid solution exists between talc and minnesotaite. The trioctahedral structure of talc is similar to that of dioctahedral pyrophyllite and consists of essentially neutral *t–o–t* layers held together by weak residual bonds (see Fig. 18.34).

Diagnostic Features. Characterized by its micaceous habit, cleavage, softness, and greasy feel.

Occurrence. Talc is a secondary mineral formed by the alteration of magnesium silicates, such as olivine, pyroxenes (see Figs. 18.43 and 18.44), and amphiboles, and may be found as pseudomorphs after these minerals. Characteristically in low-grade metamorphic rocks, where, in massive form, *soapstone*, it may make up nearly the entire rock mass. It may also occur as a prominent constituent in schistose rocks, as in the talc schist. Figure 19.57 gives a *P–T* stability diagram for talc and related minerals in the system $MgO–SiO_2–H_2O$.

In the United States, many talc or soapstone quarries are located along the line of the Appalachian Mountains from Vermont to Georgia. The major producing states are Montana, North Carolina, Texas, and Vermont.

Use. Most of the talc and soapstone produced is used in powdered form as an ingredient in paint, ceramics, rubber, insecticides, roofing, paper, cosmetics, and foundry facings. The most familiar use is in talcum powder. Talc is also used as an ornamental material for carving small objects.

Name. The name *talc* is of ancient and doubtful origin, probably derived from the Arabic word, *talk*.

Similar Species. *Minnesotaite*, $Fe_3Si_4O_{10}(OH)_2$, the Fe-rich equivalent of talc. Occurs in Precambrian iron-formations.

Pyrophyllite—$Al_2Si_4O_{10}(OH)_2$

Crystallography. Triclinic; 1. Not in distinct crystals. Foliated, in some cases in radiating lamellar aggregates. Also granular to compact. Identical with talc in appearance.

$C\bar{1}$; $a = 5.16$, $b = 8.97$, $c = 9.35$ Å; $\alpha = 91°11'$; $\beta = 100°28'$, $\gamma = 89°38'$; $Z = 4$. *ds*: 9.21(6), 4.58(5), 4.40(2), 3.08(10), 2.44(2).

Physical Properties. *Cleavage* {001} perfect. Folia somewhat flexible but not elastic. **H** 1–2 (will make a mark on cloth). **G** 2.8. *Luster* pearly to greasy. *Color* white, apple-green, gray, brown. Translucent, will transmit light on thin edges. *Optics*: (−); $\alpha = 1.552$, $\beta = 1.588$, $\gamma = 1.600$; $2V = 57°$; $X \perp \{001\}$; $r > v$.

Composition and Structure. Pyrophyllite shows little deviation from the ideal formula; Al_2O_3 28.3, SiO_2 66.7, H_2O 5.0%. The dioctahedral structure of pyrophyllite con-

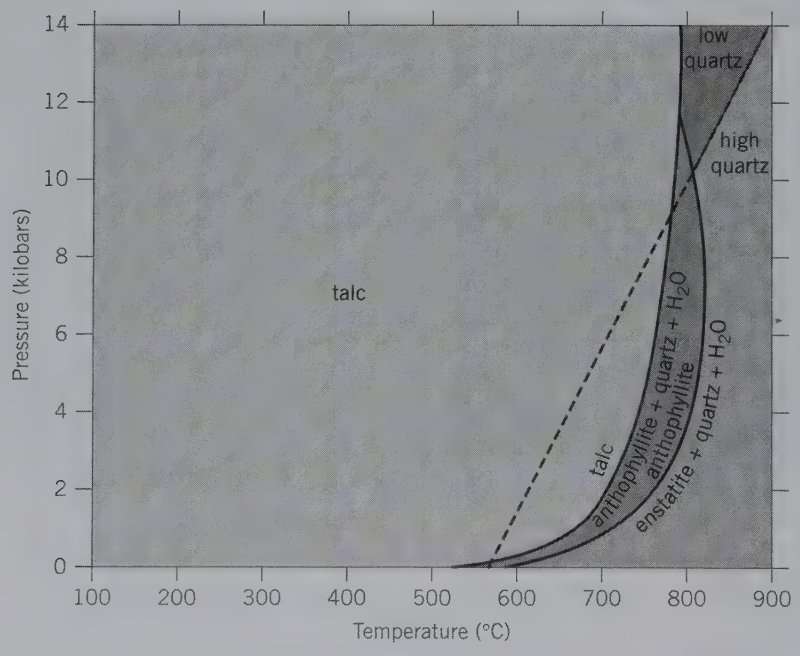

FIG. 19.57 Pressure-temperature diagram for the stability field of talc in the system $MgO–SiO_2–H_2O$. Talc is stable over a wide temperature range, from 100°C to between 500°C and 700°C, depending on the pressure. At high temperature, talc reacts to form anthophyllite, and at even higher temperature, anthophyllite reacts to form enstatite. Compare with Fig. 18.43. The low–high quartz polymorphic transition is also shown. (Adapted from Evans, B. W. and S. Guggenheim. 1988. Talc, pyrophyllite, and related minerals. *Hydrous Phyllosilicates, Reviews in Mineralogy* 19, Mineralogical Society of America, Washington, D.C., 225–94.)

sists of essentially neutral *t–o–t* layers (Figs. 18.32 and 18.34) held together by weak van der Waals bonds.

Diagnostic Features. Characterized chiefly by its micaceous habit, cleavage, and greasy feel. X-ray diffraction techniques are needed for positive identification.

Occurrence. Pyrophyllite is a comparatively rare mineral. Found in low-grade aluminous metamorphic rocks; frequently with kyanite. Occurs in considerable amount in Guilford and Orange counties, North Carolina.

Use. Quarried in North Carolina and used for the same purpose as talc but does not command as high a price as the best grades of talc. A considerable part of the so-called *agalmatolite*, from which the Chinese carve small images, is this species.

Name. From the Greek word meaning *fire* and a *leaf*, because it exfoliates on heating.

MICA GROUP

The micas, composed of *t–o–t* layers with interlayer cations and little or no exchangeable water, crystallize in the monoclinic system but with their crystallographic angle β close to 90°, their monoclinic symmetry is not easily seen. The crystals are usually tabular with prominent basal planes and have either a diamond-shaped or hexagonal outline with angles of approximately 60° and 120°. Consequently, crystals appear to be either orthorhombic or hexagonal. They are characterized by a perfect {001} cleavage. A blow with a somewhat dull-pointed instrument on a cleavage plate develops a six-rayed *percussion figure* (Fig. 19.58), two lines of which are nearly parallel to the prism edges and the third, which is most strongly developed, parallel to the mirror plane {010}. There is limited ionic substitution between various members of the group and two members may crystallize together in parallel with the cleavage extending through both.

MUSCOVITE—$KAl_2(AlSi_3O_{10})(OH)_2$

Crystallography. Monoclinic; $2/m$. Distinct crystals rare; usually tabular with prominent {001}, see Plate VII, no. 3. The presence of prism faces {110} at angles of nearly 60° gives some plates a diamond-shaped outline, making them simulate orthorhombic symmetry (Fig. 19.59). If {010} is also present, the crystals have a hexagonal appearance (Fig. 19.60). The prism faces are roughened by horizontal striations and frequently taper. Penetration twins with [310] the twin axis (see Fig. 19.61). Foliated in large to small sheets; in scales that are, in some cases, aggregated into plumose or globular forms. Also cryptocrystalline and compact massive.

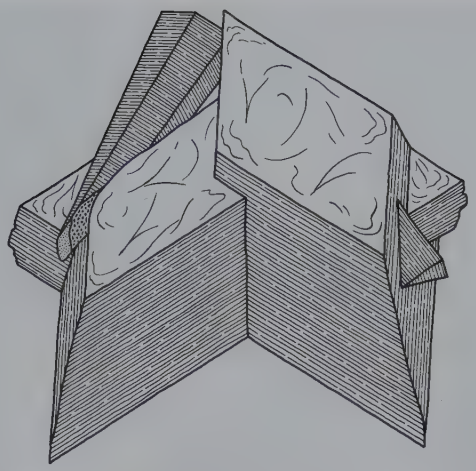

FIG. 19.59 Muscovite. Diamond-shaped crystals (Harvard Mineralogical Museum).

There are several polytypes such as $2M_1$, $1M$, and $3T$. $2M_1$ is most common with space group $C2/c$; $a = 5.19$, $b = 9.04$, $c = 20.08$ Å; $\beta = 95°30'$; $Z = 4$. *ds*: 9.95(10), 3.37(10), 2.66(8), 2.45(8), 2.18(8).

Physical Properties. *Cleavage* {001} perfect, allowing the mineral to be split into very thin sheets; folia flexible and elastic. **H** 2–2½. **G** 2.76–2.88. *Luster* vitreous to silky or pearly. *Color* colorless and transparent in thin sheets. In thicker blocks translucent, with light shades of yellow, brown, green, red. Some crystals allow more light to pass parallel to the cleavage than perpendicular to it. *Optics*: (−); $\alpha = 1.560–1.572$, $\beta = 1.593–1.611$, $\gamma = 1.599–1.615$; $2V = 30°–47°$; $Z = Y$, $X \wedge c = 0°–5°$; $r > v$.

Composition and Structure. Essentially $KAl_2(AlSi_3O_{10})(OH)_2$. Little solid solution occurs among the dioctahedral mica group or between members of the dioctahedral and trioctahedral groups. Minor substitutions may be Na, Rb, Cs for K; Mg, Fe^{2+}, Fe^{3+}, Li, Mn, Ti, Cr for Al; F for OH. *Paragonite*, $NaAl_2(AlSi_3O_{10})(OH)_2$, which is isostructural with muscovite, is practically indistinguishable from it without X-ray methods. At low to moderate temperatures, a large miscibility gap exists between muscovite and paragonite (Fig. 19.62). The structure of muscovite is illustrated in Figs. 18.33 and 18.34. It consists of *t* sheets of composition $(Si,Al)_2O_5$ linked to octahedral gibbsite-like sheets to form *t–o–t* layers. These layers have a net negative charge which is balanced by K or Na ions (in paragonite) between them (see discussion on page 457). Although the muscovite structure may show several polytypic forms due to various ways of stacking succeeding Si_2O_5 sheets (see page 464 and Figs. 18.41 and 18.42b), the most commonly observed polytype is $2M_1$ with space group $C2/c$.

FIG. 19.58 Percussion figure in mica.

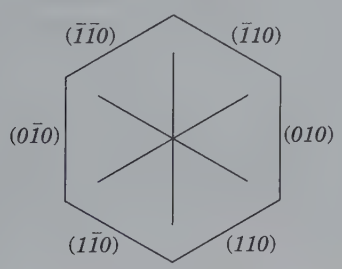

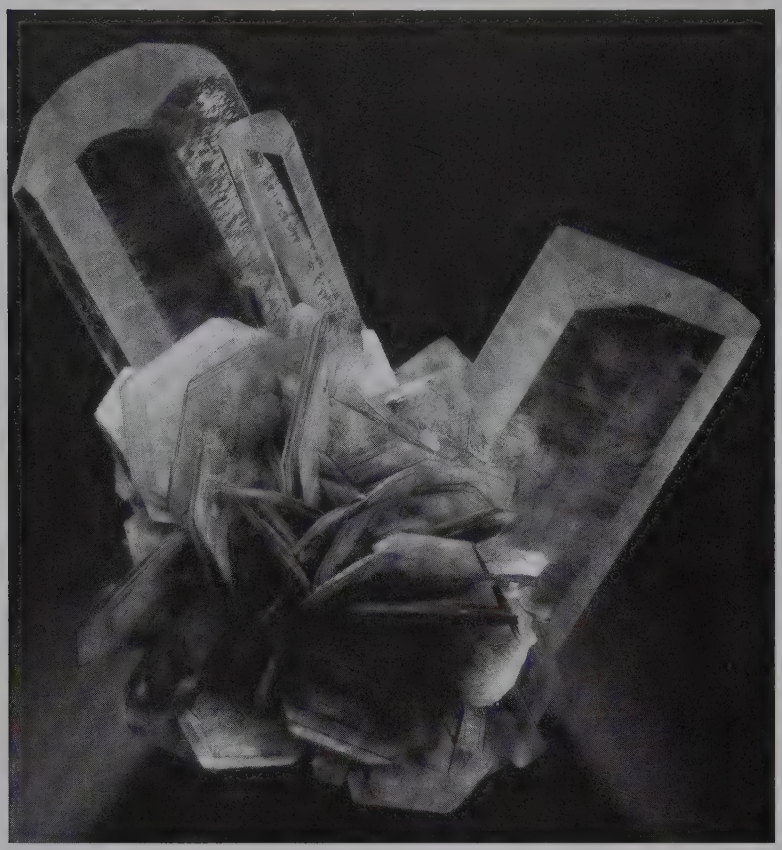

FIG. 19.60 Muscovite displaying hexagonal form with beryl, from Nagar, Pakistan. Specimen is 8.2 cm high. (Photographs courtesy of Jeff Scovil, collection © Jeff Scovil.)

Diagnostic Features. Characterized by its highly perfect cleavage and light color.

Occurrence. Muscovite is a widespread and common rock-forming mineral. Characteristic of granites and granite pegmatites. In pegmatites, muscovite associated with quartz and feldspar may be in large crystals, called *books*, which in some localities are several feet across. It is also very common in metamorphic rocks, forming the primary constituent of mica schists. In the chlorite zone of metamorphism, muscovite is a characteristic constituent of albite–chlorite-muscovite schists (see Fig. 19.63 for a *P–T* stability diagram). Coexistences between muscovite and other micas are shown in Fig. 19.64. In some schistose rocks it occurs as fibrous aggregates of minute scales with a silky luster and is known as *sericite*. The development of sericite from feldspar and other minerals, such as garnet, kyanite, and andalusite, is a common feature of retrograde metamorphism. Sericite also forms as an alteration of the wall rock of hydrothermal ore veins.

FIG. 19.61 Muscovite twin, twin axis [310], producing a penetration twin, with (001) of the individual crystals coplanar. Methuen Township, Ontario, Canada (Harvard Mineralogical Museum).

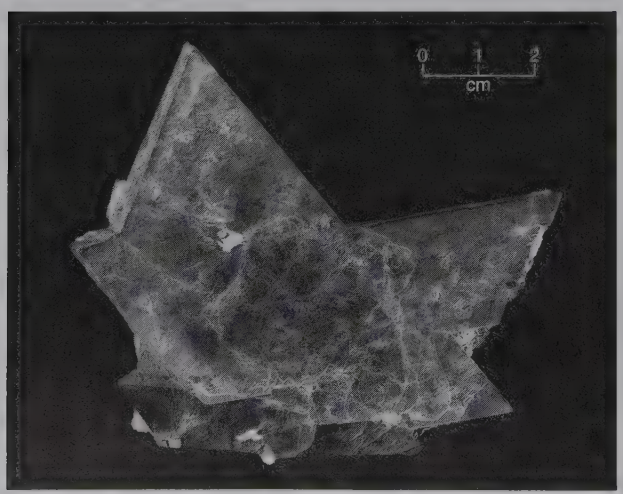

Large and important deposits of muscovite occur in Russia and India. The United States produces only a small amount of sheet mica, but is the largest producer of scrap (flake) mica with major production coming from North and South Carolina, Georgia, New Mexico, and South Dakota. Crystals measuring 7 to 9 feet across have been mined in Mattawan Township, Ontario, Canada. Good specimen material is obtained from pegmatites worldwide.

Use. Because of its high dielectric and heat-resisting properties, *sheet mica*, single cleavage plates, is used as an insulating material in the manufacture of electrical apparatus. The *isinglass* used in furnace and stove doors is sheet mica. Many small parts used for electrical insulation are built up of thin sheets of mica cemented together. They

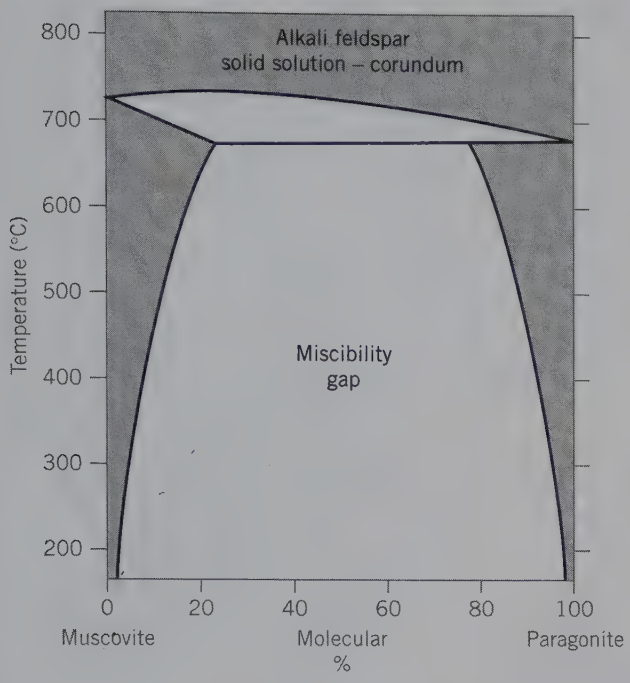

FIG. 19.62 Temperature-composition diagram for the system $KAl_2(AlSi_3O_{10})(OH)_2$–$NaAl_2(AlSi_3O_{10})(OH)_2$. Below about 700°C, this shows a large miscibility gap, and above about 700°C, it shows the reaction relations of (1) muscovite to K-feldspar and (2) paragonite to albite. At that temperature there is complete solid solution between K-feldspar and Na-feldspar (see also Fig. 18.50). Corundum is a reaction product in this reaction:

$$\underset{\text{muscovite}}{KAl_2(AlSi_3O_{10})(OH)_2} \rightarrow \underset{\text{K-feldspar}}{KAlSi_3O_8} + \underset{\text{corundum}}{Al_2O_3} + H_2O\nearrow$$

(From Eugster, H. P. and H. S. Yoder, 1955. The join muscovite–paragonite. Carnegie Institute, Washington, *Annual Report of the Director of the Geophysical Laboratory*, 1954–55, 124.)

may be pressed into shape before the cement hardens. India is the largest supplier of mica used in this way. Ground mica is used in many ways: in the manufacture of wallpapers to give them a shiny luster; as a lubricant when mixed with oils; a filler; as "sparkles" in toothpaste, and as a fireproofing material.

Name. *Muscovite* was so called from the popular name of the mineral, *Muscovy-glass*, because of its use as a substitute for glass in Old Russia (Muscovy). *Mica* was probably derived from the Latin word *micare*, meaning *to shine*.

Phlogopite—$KMg_3(AlSi_3O_{10})(OH)_2$

Crystallography. Monoclinic; $2/m$. Usually in six-sided plates or in tapering prismatic crystals. Crystals frequently large and coarse. Found also in foliated masses.

$C2/m$; $a = 5.33$, $b = 9.23$, $c = 10.26$ Å; $\beta = 100°12'$; $Z = 2$. *ds*: 10.13(10), 3.53(4), 3.36(10), 3.28(4), 2.62(10).

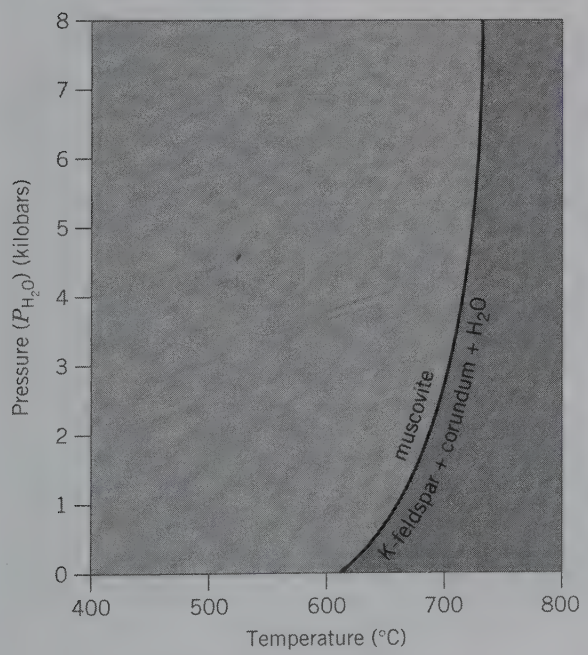

FIG. 19.63 Pressure-temperature stability diagram for muscovite, according to the reaction:

$$\underset{\text{muscovite}}{KAl(Al_2Si_3O_{10})(OH)_2} \rightarrow \underset{\text{K-feldspar}}{KAlSi_3O_8} + \underset{\text{corundum}}{Al_2O_3} + H_2O\nearrow$$

(From Hewitt, D. A., and D. R. Jones, 1984, Experimental phase relations of the micas. *Micas, Reviews in Mineralogy* 13: Mineralogical Society of America, Washington, D.C., 201–56.)

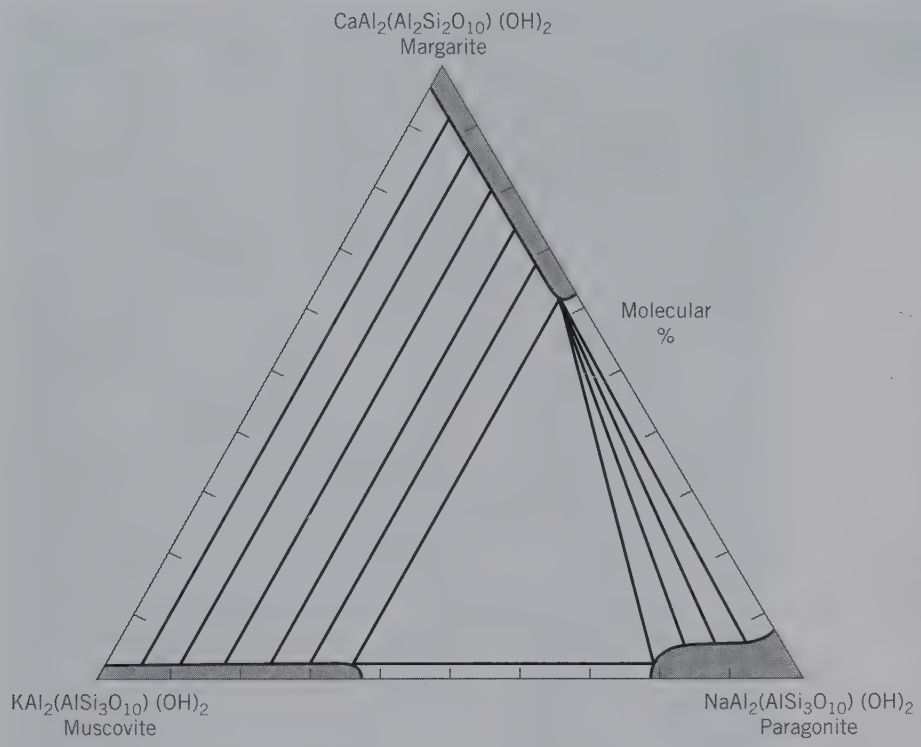

FIG. 19.64 The extent of solid solution for several micas in rocks that have been metamorphosed to a temperature of about 450°C (garnet zone metamorphism). Schematic tielines are drawn between the various solid solution fields, to indicate possible mica pairs, as well as a three-mica triangle (muscovite–paragonite–margarite). (From Guidotti, C. V. 1984. Micas in metamorphic rocks. *Micas, Reviews in Mineralogy* 13: 357–468, Mineralogical Society of America, Washington, D.C.)

Physical Properties. *Cleavage* {001} perfect. Folia flexible and elastic. **H** $2\frac{1}{2}$–3. **G** 2.86. *Luster* vitreous to pearly. *Color* yellowish-brown, green, white, often with copperlike reflections from the cleavage surface; see Plate VII, no. 4. Transparent in thin sheets. When viewed in transmitted light, some phlogopite shows asterism because of tiny oriented inclusions of rutile. *Optics*: (−); $\alpha = 1.53–1.59$, $\beta = 1.56–1.64$, $\gamma = 1.56–1.64$; $2V = 0°–5°$; $Y = b$, $X \wedge c = 0°–5°$; $r < v$.

Composition and Structure. Small amount of Na and lesser amounts of Rb, Cs, and Ba may substitute for K. Fe^{2+} substitutes for Mg, forming a series toward biotite. F may substitute in part for OH. The trioctahedral structure of phlogopite is schematically illustrated in Fig. 18.34. It consists of *t–o–t* layers bonded by interlayer K^+ ions; it is very similar to the muscovite structure except for the difference in the octahedral layer. It occurs most commonly in the 1*M* (space group *C*2/*m*) polytype, but $2M_1$ and 3*T* polytypes occur occasionally (see Figs. 18.41 and 18.42*b*).

Diagnostic Features. Characterized by its micaceous cleavage and brown color. It is, however, impossible to draw a sharp distinction between biotite and phlogopite.

Occurrence. Phlogopite is found in metamorphosed Mg-rich limestones, dolomites, and ultrabasic rocks. It is a common mineral in kimberlite. In the United States, found chiefly in Jefferson and St. Lawrence counties, New York. Found abundantly in Canada in Ontario at North and South Burgess, and in various other localities in Ontario and Quebec. Exceptionally large crystals are found near Sahakara, Madagascar.

Use. Same as for muscovite; chiefly as electrical insulator.

Name. Name from the Greek word *phlogos* meaning *fire*, an allusion to its color.

BIOTITE—$K(Mg,Fe)_3(AlSi_3O_{10})(OH)_2$

Crystallography. Monoclinic; 2/*m*. Rarely in tabular or short prismatic crystals with prominent {001} and pseudohexagonal outline. Usually in irregular foliated masses; often in disseminated scales or in scale aggregates.

*C*2/*m*; $a = 5.31$, $b = 9.23$, $c = 10.18$ Å; $\beta = 99°18'$; $Z = 2$. *ds*: 10.1(10), 3.37(10), 2.66(8), 2.54(8), 2.18(8).

Physical Properties. *Cleavage* {001} perfect. Folia flexible and elastic. **H** $2\frac{1}{2}$–3. **G** 2.8–3.2. *Luster* splendent. *Color* usually brown to black. More rarely light yellow. Thin sheets usually have a smoky color (differing from the almost colorless muscovite). *Optics*: (−); $\alpha = 1.57–1.63$, $\beta = 1.61–1.70$; $\gamma = 1.61–1.70$; $2V = 0°–25°$; $Y = b$, $Z \wedge a = 0°–9°$; $r < v$. Pleochroism in browns or greens depending on Ti or Fe content. *X* yellow, brownish green, brown; *Y* and *Z* brownish red, green, dark green, dark brown.

Composition and Structure. The composition is similar to phlogopite but with considerable substitution of Fe^{2+} for Mg. There is also substitution by Fe^{3+} and Ti and Al for Mg and by Al for Si. In addition Na, Ca, Ba, Rb, and Cs may substitute for K. A complete solid solution series exists between phlogopite and biotite. The trioctahedral biotite structure is the same as that of phlogopite (see Fig. 18.34). The 1*M* polytype with space group *C*2/*m* is most common but $2M_1$ and 3*T* also occur (see Figs. 18.41 and 18.42b).

Diagnostic Features. Characterized by its micaceous cleavage and dark color; see Plate VII, no. 5.

Occurrence. Biotite forms in a variety of geological environments. It is found in igneous rocks ranging from granite pegmatites, to granites, to diorites, to gabbros and peridotites. It occurs also in felsite lavas and porphyries. In metamorphic rocks it is formed over a wide range of temperature and pressure conditions, and it occurs in regionally as well as contact metamorphosed rocks. The crystallization of biotite in Al-rich rocks is taken as the onset of the temperature and pressure conditions of the *biotite zone*. Typical associations at this metamorphic grade are biotite–chlorite and biotite–muscovite. Remains stable above the T of muscovite breakdown. Occurs in fine crystals in blocks included in the volcanics of Mount Vesuvius.

Name. In honor of French physicist J. B. Biot.

Similar Species. *Glauconite*, similar in composition to biotite, is an authigenic mineral found in green pellets in marine sedimentary rocks. *Vermiculite* is a platy mineral formed chiefly as an alteration of biotite. The structure is essentially that of talc with interlayered water molecules (see Fig. 18.36 and Box 19.3). The name comes from the Latin word meaning *to breed worms*, for when heated, the mineral expands into wormlike forms. In the expanded condition it is used extensively in heat and sound insulating. Vermiculite was mined at Libby, Montana, and Macon, North Carolina.

Stilpnomelane, with approximate composition $K(Fe^{2+}, Mg,Fe^{3+})_8(Si,Al)_{12}(O,OH)_{27}$, can be an important constituent of low-grade, regionally metamorphosed schists, of glaucophane metamorphic facies rocks, and of essentially unmetamorphosed Precambrian banded iron-formations. It is impossible to distinguish stilpnomelane in hand specimen from biotite. Stilpnomelane has a modulated layer structure that is very different from that of biotite. Optical microscopic or chemical techniques are necessary to distinguish stilpnomelane from biotite.

LEPIDOLITE—$K(Li,Al)_{2-3}(AlSi_3O_{10})(OH,F)_2$

Crystallography. Monoclinic and hexagonal, depending on the polytype. Crystals usually in small plates or prisms with hexagonal outline. Commonly in coarse- to fine-grained scaly aggregates.

For $1M$ polytype, $C2/m$; $a = 5.21$, $b = 8.97$, $c = 20.16$ Å; $\beta = 100°48'$; $Z = 4$. *ds*: 10.0(6), 5.00(5), 4.50(5), 2.58(10), 1.989(8).

Physical Properties. *Cleavage* {001} perfect. **H** $2\frac{1}{2}$–4. **G** 2.8–2.9. *Luster* pearly. *Color* pink and lilac to grayish-white; see Plate VII, no. 6. Translucent. *Optics*: (−); $\alpha = 1.53$–1.55, $\beta = 1.55$–1.59, $\gamma = 1.55$–1.59; $2V = 0°$–$60°$; $Y = b$, $Z \wedge a = 0°$–$7°$; $r > v$.

Composition and Structure. The composition of lepidolite varies depending on the relative amounts of Al and Li in octahedral coordination. Analyses show a range of Li_2O from 3.3 to 7 weight percent. In addition Na, Rb, and Cs may substitute for K. It is possible that there is a continuous chemical series from dioctahedral muscovite to trioctahedral lepidolite, in which all of the octahedral sites are occupied. Lepidolite can occur as one of three polytypes ($1M$, $2M_2$, and $3T$) (see Figs. 18.41 and 18.42b).

Diagnostic Features. Characterized by its micaceous cleavage and usually by its lilac to pink color. Muscovite may be pink and lepidolite white, and X-ray powder diffraction techniques may be necessary to distinguish them.

Occurrence. Lepidolite is a comparatively rare mineral, found in pegmatites, usually associated with other lithium-bearing minerals such as pink and green tourmaline, amblygonite, and spodumene (see Box 19.5). Often intergrown with muscovite in parallel position. Notable foreign localities for its occurrence are Rožná, Czech Republic; Bikita, Zimbabwe; and Madagascar. In the United States, it is found in several localities in Maine; near Middletown, Connecticut; Pala, California; Dixon, New Mexico; and Black Hills, South Dakota.

Use. A source of lithium. Used in the manufacture of heat-resistant glass.

Name. Derived from the Greek word *lepidos* meaning *scale*.

Margarite—$CaAl_2(Al_2Si_2O_{10})(OH)_2$

Crystallography. Monoclinic; m. Seldom in distinct crystals. Usually in foliated aggregates with micaceous habit.

Cc; $a = 5.13$, $b = 8.92$, $c = 19.50$ Å; $\beta = 100°48'$; $Z = 4$. *ds*: 4.40(8), 3.39(8), 3.20(9), 2.51(10), 2.42(8).

Physical Properties. *Cleavage* {001} perfect. **H** $3\frac{1}{2}$–5 (harder than the true micas). **G** 3.0–3.1. *Luster* vitreous to pearly. *Color* pink, white, and gray. Translucent. Folia somewhat brittle; because of this brittleness margarite is known as a *brittle mica*. *Optics*: (−); $\alpha = 1.632$–1.638; $\beta = 1.643$–1.648; $\gamma = 1.645$–1.650; $2V = 40°$–$67°$; $Z = b$, $Y \wedge a = 7°$.

Composition and Structure. Most analyses are close to the above end-member composition with CaO 14.0, Al_2O_3 51.3, SiO_2 30.2 and H_2O 4.5%. A small amount of Na may replace Ca. The dioctahedral structure of margarite is very similar to that of muscovite (see Fig. 19.65). In margarite, however, the tetrahedral layer has the composition $(Si_2Al_2)O_{10}$ instead of $(Si_3Al)O_{10}$ as in muscovite. Because of the greater electrical charge on the $(Si_2Al_2)O_{10}$ sheet the structure can be balanced by incorporated divalent Ca^{2+} ions instead of monovalent K^+. The bond strength between the layers is therefore greater; this is expressed in the brittle nature of margarite.

Diagnostic Features. Characterized by its micaceous cleavage, brittleness, and association with corundum.

Occurrence. Margarite occurs usually with corundum and diaspore and apparently as an alteration product. It is found in this way in the emery deposits of Asia Minor and on the islands of Naxos and Nicaria, Greece. In the United States, associated with emery at Chester, Massachusetts; Chester County, Pennsylvania; and with corundum deposits in North Carolina.

Name. From the Greek *margarites* meaning *pearl*.

Similar Species. Another *brittle mica* is *clintonite*, $CaMg_2AlAl_3SiO_{10}(OH)_2$, which may be regarded as the Ca analogue of phlogopite.

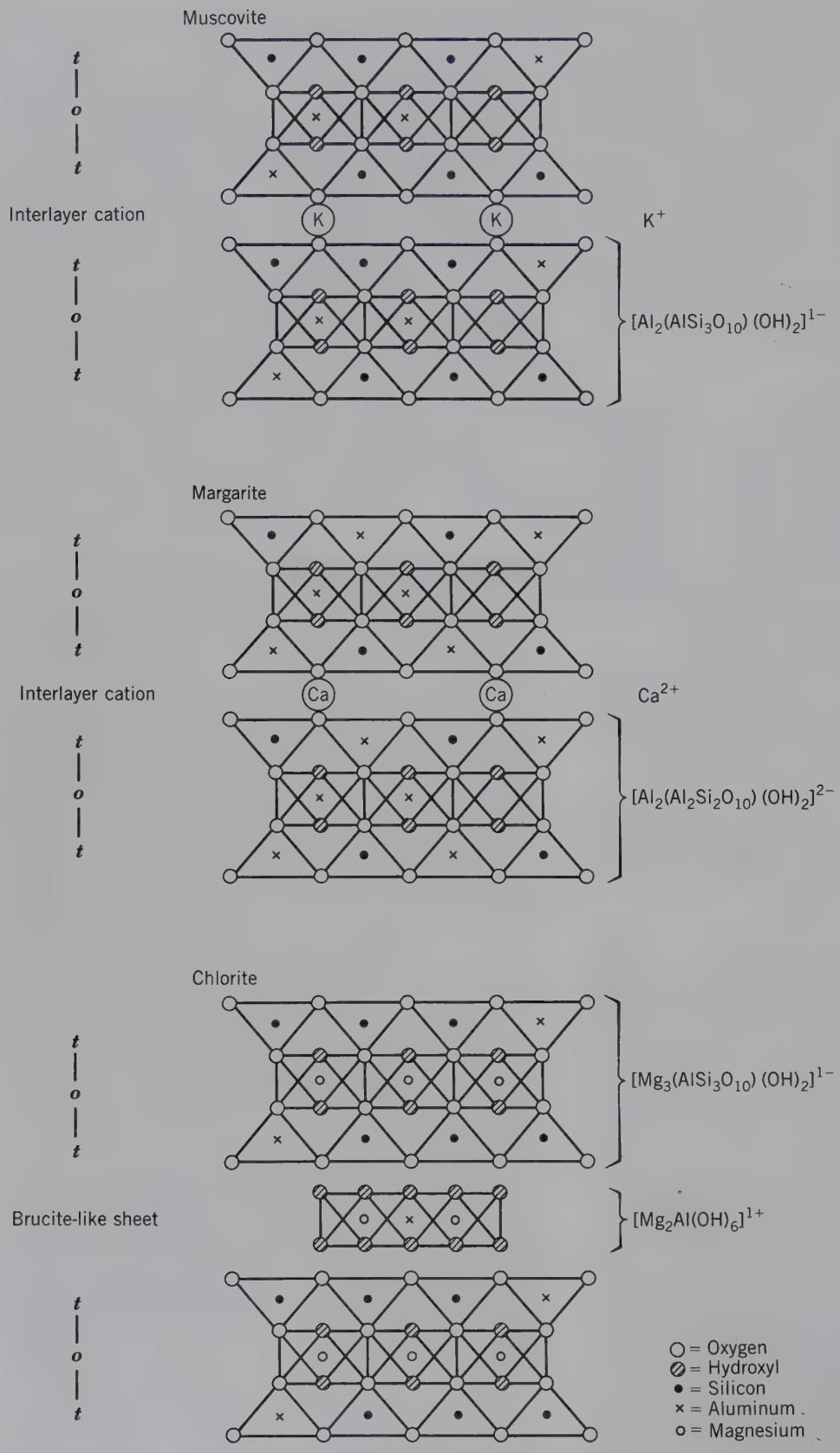

FIG. 19.65 Schematic development of the structures and compositions of muscovite, margarite, and chlorite (compare with Fig. 18.34).

CHLORITE GROUP

A number of minerals are included in the chlorite group, all of which have similar chemical, crystallographic, and physical properties. Without quantitative chemical analyses or careful study of the optical and X-ray properties, it is extremely difficult to distinguish between the members. The following is a composite description of the principal members of the group.

CHLORITE—$(Mg,Fe)_3(Si,Al)_4O_{10}(OH)_2 \cdot (Mg,Fe)_3(OH)_6$

Crystallography. Triclinic or monoclinic depending on the polytype. In pseudohexagonal tabular crystals, with prominent {001}. Similar in habit to crystals of the mica group, but distinct crystals rare. Usually foliated massive or in aggregates of minute scales; also in finely disseminated particles.

Cell parameters vary with composition. $C1$, $C\bar{1}$, Cm and $C2/m$, depending on polytype. For clinochlore: $C2/m$; $a = 5.2$–5.3, $b = 9.2$–9.3, $c = 28.6$ Å; $\beta = 96°50'$; $Z = 4$. *ds*: 3.54(10), 2.53(6), 2.00(6), 1.562(4), 1.534(7).

Physical Properties. *Cleavage* {001} perfect. Folia flexible but not elastic. **H** 2–2½. **G** 2.6–3.3. *Luster* vitreous to pearly. *Color* green of various shades; see Plate VII, no. 7. Rarely yellow, white, rose-red. Transparent to translucent. *Optics*: Most (+), some (−); in all Bxa nearly ⊥ {001}. $\alpha = 1.57$–1.66, $\beta = 1.57$–1.67, $\gamma = 1.57$–1.67; $2V = 20°$–$60°$. Pleochroism in green (+), X, $Y > Z$; (−) $X < Y$, Z. The indices increase with increasing iron content.

Composition and Structure. The composition of chlorite can be regarded as made up of *t–o–t* layers of composition $[Mg_3(AlSi_3O_{10})(OH)_2]^{1-}$ interleaved with a "brucite-like" sheet in which one out of three Mg^{2+} ions is replaced by one Al^{3+}, resulting in a composition of $[Mg_2Al(OH)_6]^{1+}$. This is illustrated schematically in Fig. 19.65. When the composition of the *t–o–t* layer and the "brucitelike" sheet are added, the composition $(Mg,Al)_6(Si,Al)_4O_{10}(OH)_8$ results, which is a general formula for magnesian chlorite. In most chlorites, there is considerable deviation from this formula because of Fe^{2+}, Fe^{3+}, and additional Al substitution. A diagrammatic sketch of the chlorite structure is given in Fig. 18.35.

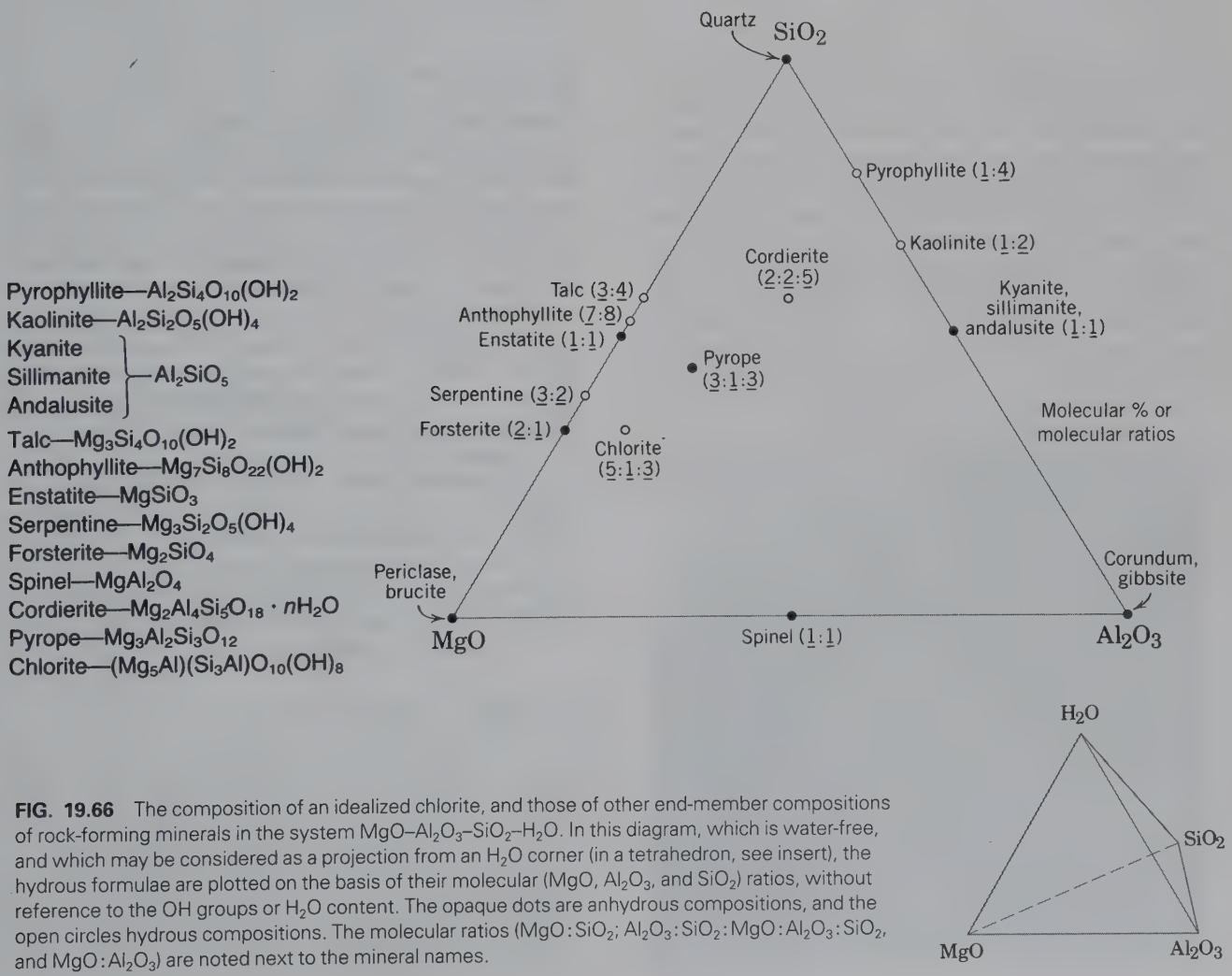

FIG. 19.66 The composition of an idealized chlorite, and those of other end-member compositions of rock-forming minerals in the system MgO–Al_2O_3–SiO_2–H_2O. In this diagram, which is water-free, and which may be considered as a projection from an H_2O corner (in a tetrahedron, see insert), the hydrous formulae are plotted on the basis of their molecular (MgO, Al_2O_3, and SiO_2) ratios, without reference to the OH groups or H_2O content. The opaque dots are anhydrous compositions, and the open circles hydrous compositions. The molecular ratios ($MgO:SiO_2$; $Al_2O_3:SiO_2$; $MgO:Al_2O_3:SiO_2$, and $MgO:Al_2O_3$) are noted next to the mineral names.

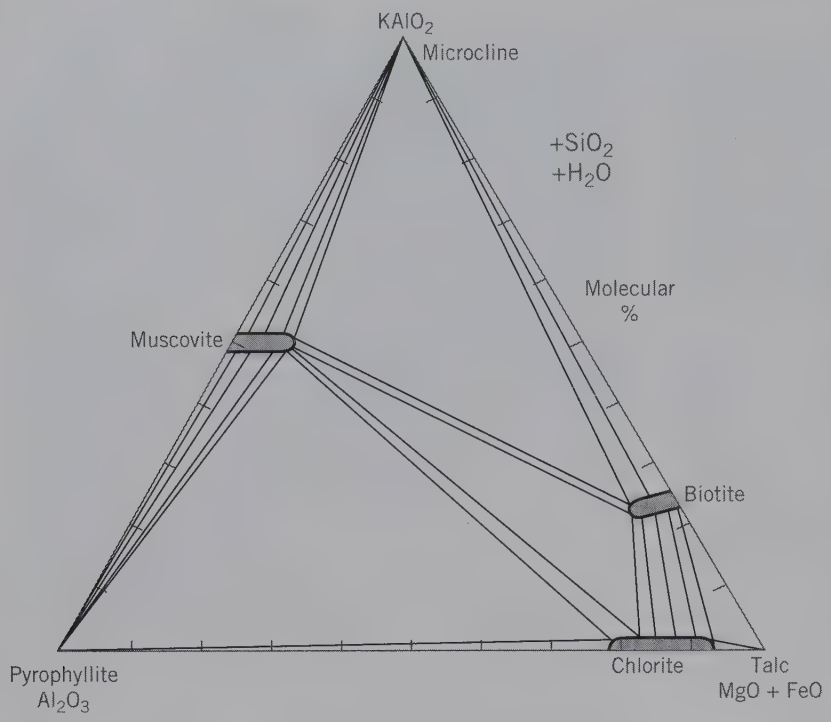

FIG. 19.67 Common assemblages involving chlorite, and other layer silicates, as well as microcline in metamorphic rocks of the biotite zone of the greenschist facies. The chemistry of this system is: $KAlO_2$–Al_2O_3–(Mg + Fe)O –(SiO_2)–(H_2O). The right-hand corner of the triangle shows two components, allowing for the representation of some solid solution extent in natural minerals. SiO_2 and H_2O are assumed to be present for the representation of the composition of anhydrous and hydrous silicates. Tielines connect coexisting mineral pairs. Triangles represent three-mineral assemblages. (Adapted from *Petrologic phase equilibria*, 21st edition, by W. G. Ernst. Copyright © 1976 by W. H. Freeman and Company. Reprinted by permission.)

The general formula of chlorite may be represented as follows: $A_{5\text{-}6}Z_4O_{10}(OH)_8$, where A = Al, Fe^{2+}, Fe^{3+}, Li, Mg, Mn, Ni, and Z = Al, Si, Fe^{3+}. Because of the extensive solid solution, many species names have been given to members of the chlorite group. Examples are *chamosite*, $(Fe,Al,Mg)_6(Si,Al)_4O_{10}(OH)_8$, *clinochlore*, $(Mg,Al)_6(Si,Al)_4O_{10}(OH)_8$, *pennantite*, $Mn_5^{2+}Al(Si_3Al)O_{10}(OH)_8$, and *sudoite*, $Mg_2Al_3(Si_3Al)O_{10}(OH)_8$. The composition of an idealized Mg end member chlorite, $(Mg_5Al)(Si_3Al)O_{10}(OH)_8$, is plotted on an anhydrous basis in Fig. 19.66. Figure 19.67 illustrates the common occurrence of chlorite, in association with other layer silicates, as well as microcline, in metamorphic rocks of the biotite zone of the greenschist facies.

The great range in composition of chlorite is reflected in variations in physical and optical properties as well as X-ray parameters (e.g., interplanar spacings and variation in unit cell size).

Diagnostic Features. Characterized by its green color, micaceous habit and cleavage, and by the fact that the folia are not elastic.

Occurrence. Chlorite is a common mineral in metamorphic rocks and it is the diagnostic mineral of the *greenschist facies*. In mica schists it occurs in quartz-albite-chlorite-muscovite-garnet assemblages. It is also commonly found as a primary mineral with actinolite and epidote. Chlorite is also a common constituent of igneous rocks where it has formed as an alteration of Mg–Fe silicates, such as pyroxenes, amphiboles, biotite, and garnet. The green color of many igneous rocks is due to the chlorite to which the ferromagnesian silicates have altered; and the green color of many schists and slates is due to finely disseminated particles of the mineral.

Name. Chlorite is derived from the Greek word *chloros* meaning *green*, in allusion to the common color of the mineral.

RELATED SPECIES

Apophyllite—$KCa_4(Si_4O_{10})_2F{\cdot}8H_2O$

Crystallography. Tetragonal; $4/m2/m2/m$. Usually in crystals showing a combination of {110}, {011}, and {001} (Fig. 19.68). Crystals may resemble a combination of cube and octahedron (Fig. 19.69), but are shown to be tetragonal by difference in luster between faces of prism and base.

$P4/mnc$; $a = 9.02$, $c = 15.8$ Å; $Z = 2$. *ds*: 4.52(2), 3.94(10), 3.57(1), 2.98(7), 2.48(3).

Physical Properties. *Cleavage* {001} perfect. **H** $4\frac{1}{2}$–5. **G** 2.3–2.4. *Luster* of base pearly, other faces vitreous. *Color* colorless, white, or grayish; pale shades of green, yellow, rose. Transparent to translucent. *Optics*: (+); $\omega = 1.537$, $\epsilon = 1.535$. May be optically (−).

Composition and Structure. The structure of apophyllite differs from that of the other phyllosilicates in that the sheets are composed of four-fold and eight-fold rings. These sheets are linked to each other by Ca, K, and F ions. Water, which is bonded to the Si_2O_5 sheet by hydrogen bonding, is lost at about 250°C. This indicates that the water

FIG. 19.68 Apophyllite.

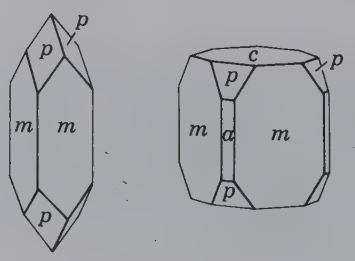

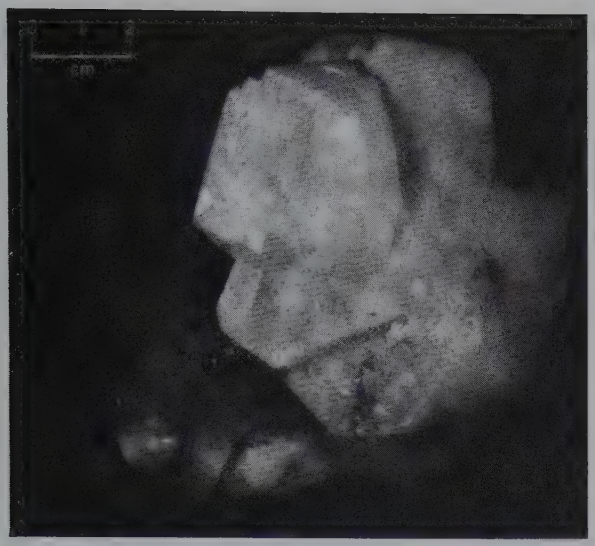

FIG. 19.69 Apophyllite crystals with stilbite, India.

is more strongly held than adsorbed water, but less strongly than structural (OH) groups.

Diagnostic Features. Recognized usually by its crystals, color, luster, and basal cleavage.

Occurrence. Apophyllite occurs as a secondary mineral lining cavities in basalt and related rocks, associated with zeolites, calcite, datolite, and pectolite.

It is found in fine crystals at Andreasberg, Harz Mountains, Germany; near Bombay, India; Iceland; and Guanajuato, Mexico. In the United States, at Bergen Hill and Paterson, New Jersey; and Lake Superior copper district. Found in fine crystals in Nova Scotia.

Name. Apophyllite is derived from two Greek words meaning *from* and *a leaf*, because of its tendency to exfoliate when ignited.

Prehnite—$Ca_2Al(AlSi_3O_{10})(OH)_2$ IV

Crystallography. Orthorhombic; *2mm*. Distinct crystals are rare, commonly tabular parallel to {001}. Usually reniform, stalactitic (Fig. 19.70), and in rounded groups of tabular crystals.

P2cm; $a = 4.65$, $b = 5.48$, $c = 18.49$ Å; $Z = 2$. *ds*: 3.48(9), 3.28(6), 3.08(10), 2.55(10), 1.77(7).

Physical Properties. **H** 6–6½. **G** 2.8–2.95. *Luster* vitreous. *Color* usually light green, passing into white. Translucent. *Optics*: (+); $\alpha = 1.616$, $\beta = 1.626$, $\gamma = 1.649$; $2V = 66°$; $X = a$, $Z = c$; $r > v$.

Composition and Structure. CaO 27.1, Al_2O_3 24.8, SiO_2 43.7, H_2O 4.4%. Some Fe^{3+} may replace Al. The structure of prehnite contains sheets of Al and Si tetrahedra parallel to {001}. Ca is in 7-coordination and lies between Si tetrahedra in adjoining sheets.

Diagnostic Features. Characterized by its green color and crystalline aggregates forming reniform surfaces.

Occurrence. Prehnite occurs as a secondary mineral lining cavities in basalt and related rocks. Associated with zeolites, datolite, pectolite, and calcite. In the United States, it occurs notably at Paterson and Bergen Hill, New Jersey. In Canada, it occurs at Asbestos, Quebec, also found in Australia.

Use. Sometimes used as an ornamental and gem material.

Name. In honor of Colonel Prehn, who brought the mineral from the Cape of Good Hope.

Chrysocolla≈$Cu_4H_4Si_4O_{10}(OH)_8 \cdot nH_2O$ IV

Crystallography and Structure. Generally amorphous and, thus, in the strict sense cannot be considered a mineral. Partially crystalline material shows the presence of Si_4O_{10} layers in a defect structure. Massive, compact; in some cases earthy. Individual specimens inhomogeneous.

Physical Properties. Fracture conchoidal. **H** 2–4. **G** 2.0–2.4. *Luster* vitreous to earthy. *Color* green to greenish-blue; brown to black when impure. Refractive index variable, usually about 1.50.

Composition. Chrysocolla is a hydrogel or gelatinous precipitate and shows a wide range in composition. Chemical analyses report: CuO 32.4–42.2, SiO_2 37.9–42.5, H_2O 12.2–18.8%. In addition Al_2O_3 and Fe_2O_3 are usually present in small amounts.

Diagnostic Features. Characterized by its green or blue color and conchoidal fracture. Distinguished from turquoise by lower hardness.

Occurrence. Chrysocolla forms in the oxidized zones of copper deposits (see Box 15.3) associated with malachite, azurite, cuprite, or native copper, for example. It is commonly found in the oxidized portions of porphyry copper ores. Found in the copper districts of Arizona and New Mexico; at Chuquicamata, Chile; and Zaire.

Use. A minor ore of copper. Sometimes cut as a gemstone, but most chrysocolla used in jewelry is intergrown with chalcedony and has the refractive index of chalcedony.

FIG. 19.70 Prehnite, Paterson, New Jersey.

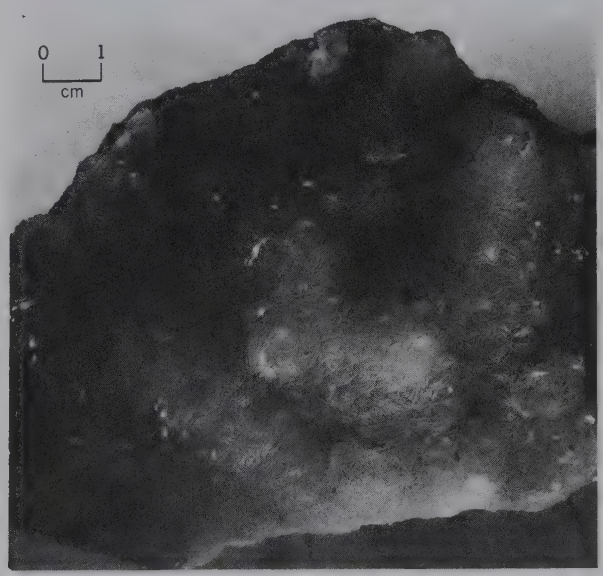

Name. Chrysocolla is derived from two Greek words meaning *gold* and *glue*, which was the name of a similar-appearing material used to solder gold.

Similar Species. *Dioptase*, $Cu_6(Si_6O_{18})\cdot 6H_2O$, is a rhombohedral cyclosilicate occurring in well-defined green rhombohedral crystals. It is a minor gem mineral. *Planchéite*, $Cu_8(Si_4O_{11})_2(OH)_4\cdot H_2O$, and *shattuckite*, $Cu_5(SiO_3)_4(OH)_2$, have inosilicate structures.

TECTOSILICATES

The following tectosilicate groups and species, those with 4 bridging oxygens for each SiO_4 tetrahedron, are described in detail:

SiO_2 Group	
Quartz, Tridymite, Cristobalite	SiO_2
Opal	$SiO_2\cdot nH_2O$
Feldspar Group	
K-Feldspars	
Microcline, Orthoclase, Sanidine	$KAlSi_3O_8$
Plagioclase Feldspars	
Albite	$NaAlSi_3O_8$
Anorthite	$CaAl_2Si_2O_8$
Feldspathoid Group	
Leucite	$KAlSi_2O_6$
Nepheline	$(Na,K)AlSiO_4$
Sodalite	$Na_8(AlSiO_4)_6Cl_2$
Lazurite	$(Na,Ca)_8(AlSiO_4)_6(SO_4,S,Cl)_2$
Petalite	$LiAlSi_4O_{10}$
Scapolite Series	
Marialite	$Na_4(AlSi_3O_8)_3(Cl_2,CO_3,SO_4)$
Meionite	$Ca_4(Al_2Si_2O_8)_3(Cl_2,CO_3,SO_4)$
Analcime	$NaAlSi_2O_6\cdot H_2O$
Zeolite Group	
Natrolite	$Na_2Al_2Si_3O_{10}\cdot 2H_2O$
Habazite	$CaAl_2Si_4O_{12}\cdot 6H_2O$
Heulandite	$(Ca_{0.5},Na,K)_9(Al_9Si_{27}O_{72})\cdot\sim 24H_2O$
Stilbite	$(Na,K,Ca_{0.5})_9(Al_9Si_{27}O_{72})\cdot 28H_2O$

SiO_2 GROUP

QUARTZ—SiO_2

FIG. 19.71 Purple quartz (amethyst) displaying striations and pyramidal terminations, from Amatitlan, Mexico. Specimen is 12 cm high (Photographs courtesy of Jeff Scovil, collection © Jeff Scovil.)

Crystallography. Quartz, hexagonal; 32. High-quartz, hexagonal; 622. Crystals commonly prismatic, with prism faces horizontally striated (Fig. 19.71). Terminated usually by a combination of positive and negative rhombohedra (Fig. 19.71), which often are so equally developed as to give the effect of a hexagonal dipyramid (see Fig. 19.72a and Plate VII, no. 8). In some crystals one rhombohedron predominates or occurs alone (Figs. 19.71 and 19.72b). It is chosen as $r\{10\bar{1}1\}$. The prism faces may be poorly developed, and the combination of the two rhombohedra gives what appears to be a hexagonal dipyramid (a *quartzoid*) (Fig. 19.72c). Some crystals are malformed, but the recognition of the prism faces by their horizontal striations assists in the orientation. The trigonal trapezohedral faces x are occasionally observed and reveal the true symmetry. They occur at the upper right of alternate prism faces in right-hand quartz and to the upper left of alternate prism faces in left-hand quartz (Figs. 19.72d and e). The right- and left-hand trigonal trapezohedrons are enantimorphous forms and reflect the arrangement of the SiO_4 tetrahedra, either in the form of a right- or left-hand screw (see space groups). In the absence of x faces, and when viewed under the microscope, the "hand" can be recognized by observing whether plane polarized light passing parallel to c is rotated to the left or right.

Crystals may be elongated in tapering and sharply pointed forms, and some appear twisted or bent. Equant crystals with apparent six-fold symmetry (Figs. 19.72a and c) are characteristic of high-temperature quartz, but the same habit is found in quartz that crystallized as the low-temperature form. Most quartz is twinned according to one or both of two laws (see Figs. 10.22c and d). These are *Dauphiné*, c the twin axis; and *Brazil* $\{11\bar{2}0\}$ the twin plane. Both types are penetration twins and external evidence of them is rarely seen.

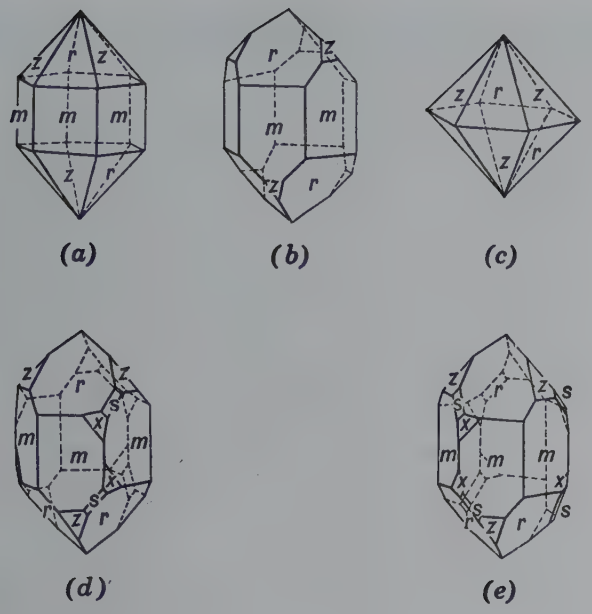

FIG. 19.72 Quartz crystals.

The size of crystals varies from individuals weighing several tons to finely crystalline coatings, forming "drusy" surfaces (see Fig. 12.22). Also common in massive forms of great variety. From coarse- to fine-grained crystalline to flintlike or cryptocrystalline, giving rise to many variety names, discussed in the next section. May form in concretionary masses.

$P3_221$ or $P3_121$, $a = 4.91$, $c = 5.41$ Å; $Z = 3$. *ds*: 4.26(8), 3.34(10), 1.818(6), 1.541(4), 1.081(5) (see Fig. 14.18).

Physical Properties. **H** 7. **G** 2.65. *Fracture* conchoidal. *Luster* vitreous, in some specimens greasy. *Color* usually colorless or white, but frequently colored by impurities and may then be any color. Transparent to translucent. Strongly piezoelectric and pyroelectric. *Optics*: (+); $\omega = 1.544$, $\epsilon = 1.553$.

Composition and Structure. Of all the minerals, quartz is most nearly a pure chemical compound with constant physical properties. Si 46.7, O 53.3%. The structure of low (α) quartz with one of two enantiomorphic space groups, $P3_121$ or $P3_221$, is discussed on page 271 and illustrated in Fig. 12.5b. At 573°C, and at atmospheric pressure, this structure transforms instantaneously to high (β) quartz, with hexagonal symmetry and one of two enantiomorphic space groups, $P6_222$ or $P6_422$. (This structure is shown in Fig. 12.5a). The displacive transformation from low to high quartz involves only minor atomic adjustments without breaking of Si–O bonds. Upon cooling high quartz, through the inversion point at 573°C, Dauphiné twinning may be produced (see page 272).

Diagnostic Features. Characterized by its glassy luster, conchoidal fracture, and crystal form. Distinguished from calcite by its hardness and from white varieties of beryl by its lower hardness.

Varieties. Many different forms of quartz exist, to which varietal names have been given. The more important varieties, with a brief description of each, follow.

Coarsely Crystalline Varieties

Rock Crystal. Colorless quartz, commonly in distinct crystals.

Amethyst. Quartz colored various shades of violet, often in crystals. The color results from the presence of trace amounts of iron as $[FeO_4]^{4-}$ color centers (see Table 10.3).

Rose Quartz. Usually massive, rarely in crystals, color a rose-red or pink. Often fades on exposure to light. Fibers related to dumortierite, $Al_7(BO_3)(SiO_4)_3O_3$ but containing Fe + Ti, appear to be the coloring agent.

Smoky Quartz; Cairngorm Stone. Frequently in crystals; smoky yellowish-brown to almost black. Named *cairngorm* for the locality of Cairngorm in Scotland. The dark color is attributed to the presence of trace amounts of Al^{3+} ions, which produce $[AlO_4]^{4-}$ color centers upon irradiation of originally colorless quartz (see Table 10.3 and related discussion).

Citrine. Light yellow, resembling topaz, in color to orange to orange-brown, (see Plate X, nos. 1 to 4, Chapter 20 for illustrations of colored varieties of quartz). Commonly heat treated to enhance color.

Milky Quartz. Milky white owing to minute fluid inclusions. Some specimens have a greasy luster.

Quartz may contain parallel fibrous inclusions that give the mineral a chatoyancy. When stones are cut *en cabochon* they are called *quartz cat's eye* (see Fig. 2.10). *Tiger's eye*, a gem material, is characterized by a radiant golden-brown chatoyancy. This chatoyancy derives from minute, oxidized crocidolite (amphibole) fibers that are included in quartz columns (Heaney and Fisher, 2003).

With Inclusions. Many other minerals occur as inclusions in quartz and give rise to varietal names. *Rutilated quartz* has fine needles of rutile penetrating it (Fig. 19.73). Tourmaline

FIG. 19.73 Rutilated quartz. Brazil (Harvard Mineralogical Museum).

and other minerals are found in quartz in the same way. *Aventurine quartz* includes brilliant scales of colored minerals such as hematite (red) or chromium mica (green) and is used as a gem material. Liquids and gases may occur as fluid inclusions; both liquid and gaseous carbon dioxide exist in some quartz.

Microcrystalline Varieties

The microcrystalline varieties of quartz are divided into two types, depending on their structure: *fibrous* and *granular*. It is difficult to distinguish between them macroscopically.

A. Fibrous Varieties

Chalcedony is the general term applied to fibrous varieties. It is generally a brown to gray, translucent variety, with a waxy luster, often mammillary and in other imitative shapes. Chalcedony has been deposited from aqueous solutions and is frequently found lining or filling cavities in rocks. Color and banding give rise to the following varieties:

Carnelian, a red chalcedony, grades into brown sand.

Chrysoprase is an apple-green chalcedony colored by nickel oxide.

Agate is a variety with alternating layers of chalcedony having different colors and porosity. The colors are usually in delicate, fine parallel bands. The bands are commonly curved, in some specimens concentric (see Fig. 19.74 and Plate VII, no. 9). Most agate used for commercial purposes is colored by artificial means. Some agates have the different colors not arranged in bands but irregularly distributed. *Moss agate* is a variety in which the variation in color is caused by visible impurities, commonly manganese oxide in mosslike patterns (see Plate X, nos. 5 and 6, Chapter 20).

Wood that has been petrified by replacement by clouded agate is known as *silicified* or *agatized wood*.

Onyx, like agate, is a layered chalcedony, with layers arranged in parallel planes. *Sardonyx* is an onyx with sard alternating with white or black layers.

FIG. 19.74 Agate cut and polished. Brazil (Harvard Mineralogical Museum).

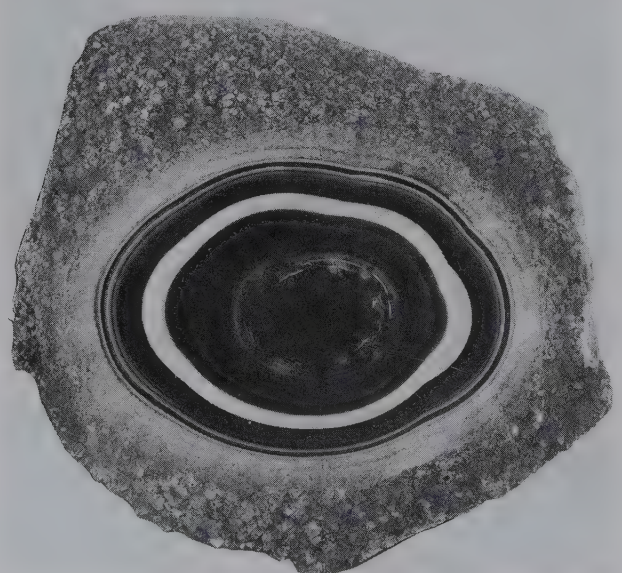

Heliotrope or *bloodstone* is a green chalcedony with small red spots of jasper in it.

B. Granular Varieties

Flint and *chert* resemble each other, and there is no sharp distinction between them. Dark, siliceous nodules, usually found in chalk, are called flint, whereas lighter-colored bedded deposits are called chert.

Jasper is a granular microcrystalline quartz with dull luster usually colored red by included hematite.

Prase has a dull green color; otherwise it is similar to jasper, and occurs with it.

Occurrence. Quartz is a common and abundant mineral occurring in a wide variety of geological environments. It is present in many igneous and metamorphic rocks and is a major constituent of granite pegmatites (see Boxes 19.1 and 19.5). It is the most common gangue mineral in hydrothermal and metal-bearing veins and in many veins is essentially the only mineral present. In the form of flint and chert, quartz is deposited on the sea floor as microorganisms contemporaneously with the enclosing rock; or solutions carrying silica may replace limestone to form chert horizons. On the breakdown of quartz-bearing rocks, the quartz, because of its mechanical and chemical stability, persists as detrital grains to accumulate as sand (see Box 19.4). Quartz-rich sandstone and its metamorphic equivalent, quartzite, are composed mainly of quartz.

Rock crystal is found widely distributed, some of the more notable localities being the Alps; Minas Gerais, Brazil; Madagascar; and Japan. The best quartz crystals from the United States are found near Hot Springs, Arkansas, and Little Falls, Herkimer County, New York. Important occurrences of amethyst are in the Ural Mountains, Russia, Czech Republic, Uruguay, Zambia, and Brazil. Found at Thunder Bay on the north shore of Lake Superior. In the United States, rock crystal is found in Delaware and Chester counties, Pennsylvania; Oxford County, Maine. Smoky quartz is found in large and fine crystals in Switzerland; and in the United States at Pikes Peak, Colorado; Alexander County, North Carolina; and Oxford County, Maine. Rose quartz is found in the Black Hills, South Dakota and in California.

The chief source of agates at present is in southern Brazil and northern Uruguay. Most of these agates are cut at Idar-Oberstein, Germany, itself a famous agate locality. In the United States, agate is found in numerous places, notably in Oregon and Wyoming. The chalk cliffs at Dover, England, are famous for the flint nodules that weather from them. Similar nodules are found on the French coast of the English Channel and on islands off the coast of Denmark. Massive quartz, occurring in veins or with feldspar in pegmatite dikes, is mined in Connecticut, New York, Maryland, and Wisconsin for its various commercial uses.

Use. Quartz has many and varied uses. It is widely used as gemstones or ornamental material, as amethyst, rose quartz, smoky quartz, tiger's eye, aventurine, carnelian, agate, and onyx. As fine particles, quartz is used in mortar, in concrete, as a flux, as an abrasive, and in the manufacture of glass and silica brick. In powdered form it is used in porcelain, paints, sandpaper, scouring soaps, and as a wood filler. In the form of quartzite and sandstone it is used as a building stone and for paving purposes.

BOX 19.4 Mineral Dust in the Environment

The issue of adverse human health effects caused by mineral dusts, especially asbestos and crystalline silica (SiO_2) dusts, has been a major concern. The incidence of cancer and asbestosis among professional asbestos workers and silicosis among hard-rock miners and sand blasters was the basis for subsequent evaluations of the interaction of mineral dust and health. Aspects of the asbestos question are discussed under the headings of crocidolite ("blue asbestos") use on p. 519 and chrysotile ("white asbestos") use on p. 520 (see also Box 19.2 and Klein 1993, Rocks, Minerals, and a Dusty World*).

Here, we will address the question of whether there is good reason to be concerned about silica (SiO_2) dust in the air. Although there are several polymorphs of SiO_2 (see Table 18.3), the three that are of concern are quartz, cristobalite, and tridymite, with quartz by far the most common of the three. Quartz is a common constituent of many rock types and may constitute 100% of some beach sands. The photograph shows well-sorted, rounded sand-size grains, in the size range of grains in a sandbox.

Inhalation of large quantities of fine quartz dust, over extended periods of time, may result in silicosis, in which the lung develops scar tissue and loses its air exchange capacity. On the basis of some animal experiments in which rats, mice, and hamsters were exposed to intense airborne quartz dusts, the International Agency for Research on Cancer (IARC) declared quartz a carcinogen in 1987. The results in these animal experiments were extremely inconsistent (see Saffiotti et al. 1993, Biological Studies on the carcinogenic mechanisms of quartz*), and there is always the fundamental question of how well such animal studies relate to human beings. As a result of this IARC decision, the U.S. Occupational Safety and Health Administration (OSHA) now requires that any U.S. product that contains more than 0.1 percent "free silica" display a warning label. For example, bags of sand and other quartz-bearing products now carry labels, such as the one printed here labeling quartz as a carcinogen. What happens if quartz-rich beaches, sandboxes, dirt roads, farmlands, all kinds of commercial products, and the desert regions of Arizona, Nevada, California, and New Mexico (with commonly fierce dust storms) become identified, in the public mind, as carcinogenic to humans? Ross et al. 1993 (Health effects of mineral dusts other than asbestos*) reviews many epidemiological studies of workers employed since 1950 and exposed to mineral dusts, but finds no evidence for nonmalignant chronic disease (such as silicosis) and no justification for the prediction of increased cancer risk due to silica dust exposure. As such, declaring quartz, in the natural environment, a carcinogen is not only confusing but highly alarming to the public at large.

THIS PRODUCT MAY CONTAIN SILICA. SILICA DUST IF INHALED MAY CAUSE RESPIRATORY OR OTHER HEALTH PROBLEMS. PROLONGED INHALATION MAY CAUSE DELAYED LUNG INJURY, INCLUDING SILICOSIS AND POSSIBLY CANCER.

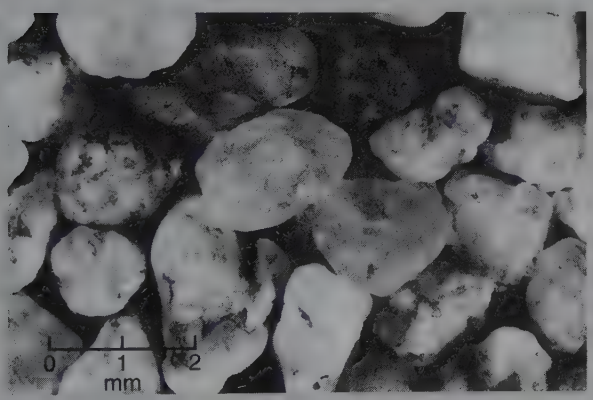

Well-sorted, rounded mineral grains described as sand, on the basis of the size of the grains ranging between $\frac{1}{16}$ mm and 2 mm in diameter. Some of the sand grains in this photograph are made of quartz, others are feldspar. Sand from the Great Sand Dunes National Monument, Colorado.

*All above three articles are part of *Reviews in Mineralogy* 28, entitled Health effects of mineral dusts, G. D. Guthrie, Jr., and Brooke T. Mossman, editors. Mineralogical Society of America, Washington, D.C. Articles are on pp. 7–59 for C. Klein; on pp. 361–401 for Ross et al.; pp. 523–543 for Saffiotti et al.

Quartz has many uses in scientific equipment. Because of its transparency in both the infrared and ultraviolet portions of the spectrum, quartz is made into lenses and prisms for optical instruments. The *optical activity* of quartz (the ability to rotate the plane of polarization of light) is utilized in the manufacture of an instrument to produce monochromatic light of differing wavelengths. Quartz wedges, cut from transparent crystals, are used as an accessory to the polarizing microscope. Because of its piezoelectric property, quartz has specialized uses. It is cut into small oriented plates and used as

radio oscillators to permit both transmission and reception on a fixed frequency. The tiny quartz plate used in digital quartz watches serves the same function as quartz oscillators used to control radio frequencies (see page 351). This property also makes it useful in the measurement of instantaneous high pressures, such as result from firing a gun or an atomic explosion.

Synthesis. Since 1947, much of the quartz used for optical and piezoelectrical purposes has been manufactured by hydrothermal methods. More recently yellow, brown, blue, and violet quartz has been synthesized for use as gem material.

Name. The name *quartz* is a German word of ancient derivation.

Similar Species. *Lechatelierite*, SiO_2, is fused silica or silica glass. Found in **fulgurites**, tubes of fused sand formed by lightning, and in cavities in some volcanic rocks. *Lechatelierite* is also found at Meteor Crater, Arizona, where sandstone has been fused by the heat generated by the impact of a meteorite.

Tridymite–SiO_2

Crystallography. Low (α) tridymite: monoclinic or orthorhombic; 2/*m*, *m*, or 222. High (β) tridymite: hexagonal; 6/*m*2/*m*2/*m*. Crystals are small and commonly twinned and at room temperature are pseudomorphs after high tridymite.

Low tridymite, for *C*2/*c* or *Cc*; $a = 18.54$, $b = 5.01$, $c = 25.79$ Å; $\beta = 117°40'$; $Z = 48$; for $C222_1$; $a = 8.74$, $b = 5.04$, $c = 8.24$ Å; $Z = 8$. *d*s: (low tridymite): 4.30(10), 4.08(9), 3.81(9), 2.96(6), 2.47(6). High tridymite, $P6_3/mmc$; $a = 5.04$, $c = 8.24$ Å; $Z = 4$.

Physical Properties. **H** 7. **G** 2.26. *Luster* vitreous. *Color* colorless to white. Transparent to translucent. *Optics*: (+); $\alpha = 1.468–1.479$; $\beta = 1.470–1.480$, $\gamma = 1.475–1.483$; $2V = 40°–90°$.

Composition and Structure. Ideally SiO_2. However, small amounts of Na and Al may be in solid solution. The crystal structure of low (α) tridymite is closely related to that of high tridymite but the framework is slightly distorted which lowers the symmetry. The high (β) tridymite structure consists of sheets of tetrahedra that lie parallel to {0001}; the tetrahedra within each sheet share corners to form six-membered rings (see Fig. 18.45a) and in these rings tetrahedra alternatively point up or down, providing linkage between the sheets. Tridymite is the stable form of SiO_2 at temperatures between 870° and 1470°C, at atmospheric pressure (see Fig. 18.46). At higher temperatures it transforms to cristobalite, at lower temperatures to high quartz. These transformations are reconstructive and extremely sluggish.

Diagnostic Features. It is impossible to identify tridymite by macroscopic means, but under the microscope its crystalline outline and refractive index distinguish it from the other silica minerals.

Occurrence. Tridymite occurs commonly in certain siliceous volcanic rocks, such as rhyolite, obsidian, and dacite, and for this reason may be considered an abundant mineral. It is most commonly the result of devitrification of volcanic glass, such as obsidian, and is commonly associated with sanidine and cristobalite. It is found in large amounts in the rocks of the San Juan district of Colorado. It is also found in stony meteorites and the lunar basalts.

Name. From the Greek word meaning *three-fold*, in allusion to its common occurrence in trillings.

Cristobalite—SiO_2

Crystallography. Low (α) cristobalite: tetragonal; 422. High (β) cristobalite: isometric; $4/m\bar{3}2/m$. Crystals small octahedra; this form is retained on inversion from high to low cristobalite. Also in spherical aggregates.

Low cristobalite, $P4_12_12_1$ (or $P4_32_12$): $a = 4.97$, $c = 6.93$ Å; $Z = 4$. *d*s (low cristobalite): 4.05(10), 2.84(1), 2.48(2), 1.929(1), 1.870(1). High cristobalite, $Fd3m$: $a = 7.13$ Å; $Z = 8$.

Physical Properties. **H** $6\frac{1}{2}$. **G** 2.32. *Luster* vitreous. Colorless. Translucent. *Optics*: (+); ω 1.484, $\epsilon = 1.487$.

Composition and Structure. Ideally SiO_2, but most natural material contains some Na and Al in solid solution. The low cristobalite structure is tetragonal, whereas high cristobalite is isometric. In high cristobalite six-membered tetrahedral rings are stacked parallel to {111}; see Fig. 18.45b. High cristobalite is stable from 1470°C to the melting point, 1728°C, at atmospheric pressure (see Fig. 18.46). The transformation at 1470°C to tridymite is of the reconstructive type.

Diagnostic Features. The occurrence in small lava cavities as spherical aggregates is characteristic, but it cannot be determined with certainty without optical or X-ray measurements.

Occurrence. Cristobalite is present in many siliceous volcanic rocks, both as the lining of cavities and as an important constituent in the fine-grained groundmass. It is, therefore, an abundant mineral. It is most commonly the result of devitrification of volcanic glass, such as obsidian. Associated with tridymite in the rocks of the San Juan district, Colorado.

Name. From the Cerro San Cristobal near Pachuca, Mexico.

OPAL—$SiO_2 \cdot nH_2O$

Crystallography. Generally amorphous. Massive; often botryoidal, stalactitic. Although X-ray studies indicate that much opal is essentially amorphous, it contains silica spheres in an ordered packing (see Structure, below, and also Figs. 2.6 and 2.7).

Physical Properties. *Fracture* conchoidal. **H** 5–6. **G** 2.0–2.25. *Luster* vitreous; often somewhat resinous. *Color* colorless, white, pale shades of yellow, red, brown, green, gray, and blue. The darker colors result from impurities. Often has a milky or "opalescent" effect and may show a fine play of colors. Transparent to translucent. Some opal, especially *hyalite*, shows a greenish-yellow fluorescence in ultraviolet light. *Optics*: Refractive index 1.44–1.46.

Composition and Structure. $SiO_2 \cdot nH_2O$. The water content, usually between 4% and 9%, may be as high as 20%. The specific gravity and refractive index decrease with increasing water content.

Although opal is essentially amorphous, it has been shown to have an ordered structure. It is not a crystal structure with atoms in a regular three-dimensional array but is made up of closely packed spheres of silica in hexagonal

and/or cubic closest packing (see Figs. 2.6 and 2.7). Air or water occupies the voids between the spheres. In common opal the domains of equal-size spheres with uniform packing are small or nonexistent, but in precious opal, large domains are made up of regularly packed spheres of the same size. The sphere diameters vary from one opal to another and range from 1500 Å to 3000 Å. When white light passes through the essentially colorless opal and strikes planes of voids between spheres, certain wavelengths are diffracted and flash out of the stone as nearly pure spectral colors. This phenomenon has been described as analogous to the diffraction of X-rays by crystals. In X-ray diffraction the interplanar spacings (d) are of the same order of magnitude as the wavelengths of X-rays. In precious opal the spacings, determined by sphere diameters, are far greater but so are the wavelengths of visible light (4,000–7,000 Å). The different wavelengths that satisfy the Bragg equation are diffracted with change in the angle of incident light (θ). Because light is refracted when it enters precious opal, the equation must include the refractive index, μ (= 1.45), and the equation is written $n\lambda = \mu 2d \sin\theta$ (see Fig. 2.7).

Diagnostic Features. Distinguished from microcrystalline varieties of quartz by lesser hardness and specific gravity and by the presence of water.

Varieties. *Precious opal* is characterized by a brilliant internal play of colors that may be red, orange, green, or blue (see Plate X, no. 7, Chapter 20). The body color is white, milky-blue, yellow, or black (*black opal*). *Fire opal* is a variety with intense orange to red reflectins.

Common Opal. Milk-white, yellow, green, red, etc., without internal reflections.

Hyalite. Clear and colorless opal with a globular or botryoidal surface.

Geyserite or *Siliceous Sinter.* Opal deposited by hot springs and geysers. Found about the geysers in Yellowstone National Park, Wyoming.

Wood Opal. Fossil wood with opal as the petrifying material.

Diatomite. Fine-grained deposits, resembling chalk in appearance. Formed by sinking from near the surface and the accumulation on the sea floor of the siliceous tests of diatoms. Also known as *diatomaceous earth* or *infusorial earth*.

Occurrence. Opal may be deposited by hot springs at shallow depths, by meteoric waters, or by low-temperature hypogene solutions. It is found lining and filling cavities in rocks and may replace wood buried in volcanic tuff. The largest accumulations of opal are as siliceous tests of silica-secreting organisms.

Precious opals are found at Caernowitza, Hungary; in Querétaro, Mexico; Queensland and New South Wales, Australia; and Brazil. Black opal has been found in the United States in Virgin Valley, Nevada. Diatomite is mined in several western states, principally at Lompoc, California.

Synthesis. Pierre Gilson in Switzerland has synthesized precious opal that is identical to natural material in chemical and physical properties, including a beautiful play of colors.

Use. As a gem. Opal is usually cut in round shapes, *en cabochon*. Stones of large size and exceptional quality are very highly prized. Diatomite is used extensively as an abrasive, filler, filtration powder, and in insulation products.

Name. The name *opal* originated in the Sanskrit, *upala*, meaning stone or precious stone.

FELDSPAR GROUP

K-FELDSPARS

MICROCLINE—$KAlSi_3O_8$

Crystallography. Triclinic; $\bar{1}$. The habit and crystal forms are similar to those of orthoclase, and microcline may be twinned according to the same laws as orthoclase; *Carlsbad* twins are common, but *Baveno* and *Manebach* twins are rare (see Fig. 19.75). It is also twinned according to the *albite law*, with {010} the twin plane, and the *pericline law*, with {010} the twin axis. These two types of twinning are usually present in microcline and on {001} the lamellae cross at nearly 90° giving a characteristic "tartan" structure (see Fig. 10.18). Microcline is found in cleavable masses, in crystals, and as a rock constituent in irregular grains. Microcline probably forms some of the largest known crystals. In a pegmatite in Karelia, Russia, a mass weighing more than 2,000 tons showed the continuity of a single crystal. Also in pegmatites microcline may be intimately intergrown with quartz, forming *graphic granite* (Fig. 19.76).

Microcline frequently has irregular and discontinuous bands crossing {001} and {010} that result from the exsolution of albite. The intergrowth as a whole is called *perthite*, see Plate VIII, nos. 1 and 2, or, if fine, *microperthite* (see page 475 and Fig. 19.77).

$C\bar{1}$; for low microcline $a = 8.59$, $b = 12.97$, $c = 7.22$ Å; $\alpha = 90°41'$, $\beta = 115°59'$, $\gamma = 87°39'$; $Z = 4$. *d*s: 4.21(5), 3.83(3), 3.48(3), 3.37(5), 3.29(5), 3.25(10).

Physical Properties. *Cleavage* {001} perfect, {010} good at an angle of 89°30′. **H** 6. **G** 2.54–2.57. *Luster* vitreous. *Color* white to pale yellow, more rarely red or green. Green microcline is known as *amazonite*. Translucent to transparent. *Optics*: (−); $\alpha = 1.522$, $\beta = 1.526$, $\gamma = 1.530$; $2V = 83°$; $r > v$.

Composition and Structure. For $KAlSi_3O_8$, K_2O 16.9, Al_2O_3 18.4, SiO_2 64.7%; there is some substitution of Na for K (see Fig. 18.50). The structure of microcline is triclinic and, therefore, less symmetrical than that of sanidine,

FIG. 19.75 Twinning in feldspar. (a) Carlsbad twin. (b) Manebach twin. (c) Baveno twin.

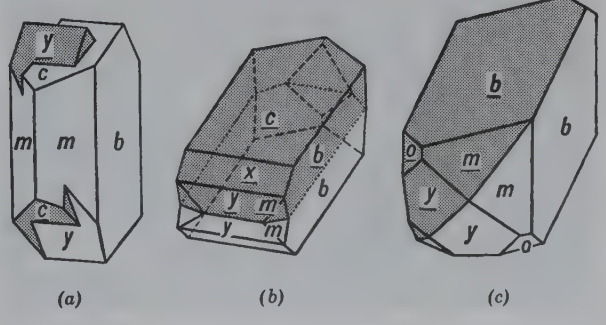

(a) (b) (c)

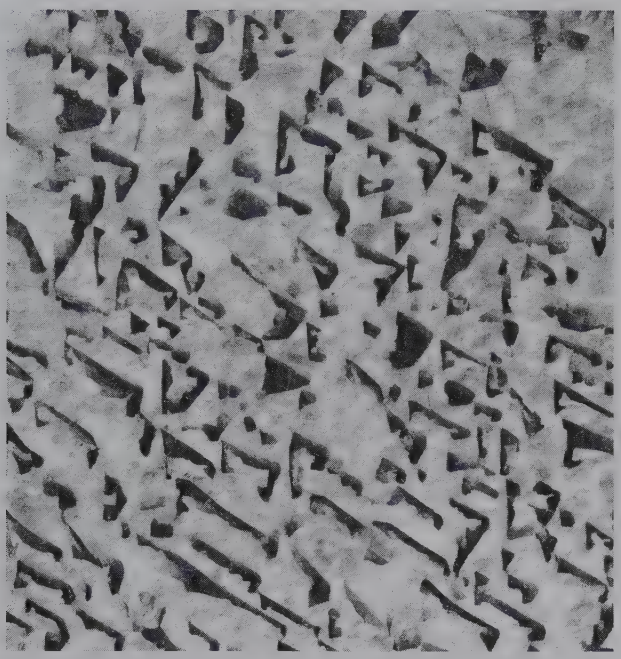

FIG. 19.76 Graphic granite, Hybla, Ontario. Quartz dark, microcline light.

which is shown in Fig. 18.48. Maximum low microcline shows perfect Al–Si order in the tetrahedral framework. With increasing disorder (increasing T) the terms *low*, *intermediate*, and *high* microcline are applied. At considerably higher T, the microcline structure transforms to orthoclase or sanidine (see Fig. 18.50 and also Fig. 12.9 and related text).

Diagnostic Features. Distinguished from orthoclase by its triclinic crystals and by observing the presence of microcline ("tartan") twinning, which can rarely be determined without the aid of the microscope. With minor exceptions, deep green feldspar is microcline.

FIG. 19.77 Microperthite as seen in polarized light under the microscope.

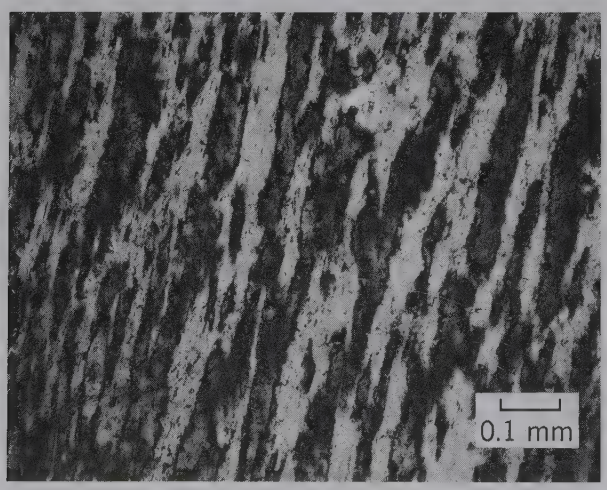

Occurrence. Microcline is a prominent constituent of igneous rocks, such as granites and syenites that cooled slowly and at considerable depth. In sedimentary rocks it is present in arkose and conglomerate. In metamorphic rocks in gneisses. Microcline is the common K-feldspar of pegmatites and was quarried extensively in North Carolina, North and South Dakota, Colorado, Virginia, Wyoming, Maine, and Connecticut (see Box 19.5). *Amazonite*, a green variety of microcline, is found in the Ural Mountains, Russia, and in various places in Norway and Madagascar. In the United States, it is found at Pikes Peak, Colorado (see photograph at the very beginning of this chapter), and Amelia Court House, Virginia; see Plate VIII, no. 3.

Use. Feldspar is used chiefly in the manufacture of porcelain. It is ground very fine and mixed with kaolin or clay, and quartz. When heated to high temperature the feldspar fuses and acts as a cement to bind the material together. Fused feldspar also furnishes the major part of the glaze on porcelain ware. A small amount of feldspar is used in the manufacture of glass to contribute alumina to the batch. Amazonite is polished and used as an ornamental material.

Name. *Microcline* is derived from two Greek words meaning *little* and *inclined*, referring to the slight variation of the cleavage angle from 90°. *Feldspar* is derived from the German word *feld*, field.

ORTHOCLASE—$KAlSi_3O_8$ IV

Crystallography. Monoclinic; $2/m$. Crystals are usually short prismatic elongated parallel to a, or elongated parallel to c and flattened on {010}. The prominent forms are $b\{010\}$, $c\{001\}$, and $m\{110\}$, often with smaller $\{0kl\}$ and $\{hkl\}$ prisms (Fig. 19.78). Frequently twinned according to the following laws: *Carlsbad* penetration twin with c as twin axis, see Plate VIII, no. 4; *Baveno* with {021} as twin and composition plane; *Manebach* with {001} as twin and composition plane (see Figs. 19.75*b* and *c*). Commonly in crystals or in coarsely cleavable to granular masses; more rarely fine-grained, massive, and cryptocrystalline. Most abundantly in rocks as formless grains.

$C2/m$; $a = 8.56$, $b = 12.96$, $c = 7.21$ Å; $\beta = 115°50'$; $Z = 4$. *ds*: 4.22(6), 3.77(7), 3.46(5), 3.31(10), 3.23(8).

Physical Properties. *Cleavage* {001} perfect, {010} good, {110} imperfect. **H** 6. **G** 2.57. *Luster* vitreous. *Color* colorless, white, gray, flesh-red, rarely yellow or green. *Streak* white. *Optics*: (−); $\alpha = 1.518$, $\beta = 1.524$, $\gamma = 1.526$; $2V = 10°–70°$; $Z = b$, $X \wedge a = 5°$; $r > v$.

Composition and Structure. Most analyses contain small amounts of Na, but a complete solid solution series is

FIG. 19.78 Orthoclase and sanidine crystals.

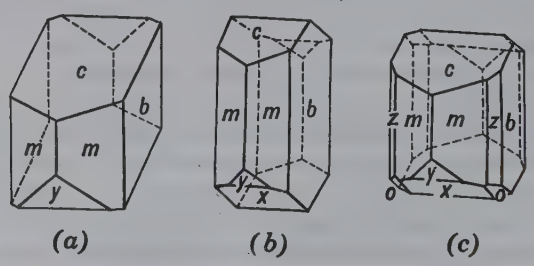

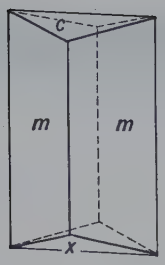

FIG. 19.79 Adularia.

possible at high temperature (see Fig. 18.50). Orthoclase represents a K-feldspar structure that crystallizes at intermediate temperature and has a partially ordered Al–Si distribution. At higher temperatures the Al–Si distribution in the structure becomes less ordered and is known as sanidine (see Fig. 12.9 and related text).

Diagnostic Features. Is usually recognized by its color, hardness, crystal form, and cleavage. Distinguished from the other feldspars by its right-angle cleavage and the lack of twin striations on the best cleavage surface.

Occurrence. Orthoclase is a major constituent of granites, granodiorites, and syenites, which have cooled at moderate depth and at reasonably fast rates. In more slowly cooled granites and syenites microcline will be the characteristic K-feldspar.

Name. The name *orthoclase* refers to the right-angle cleavage possessed by the mineral.

Similar Species. *Adularia*, $KAlSi_3O_8$, is a colorless, translucent to transparent variety of K-feldspar which is commonly found in pseudo-orthorhombic crystals (Fig. 19.79). It occurs mainly in low-temperature veins in gneisses and schists. Some adularia shows an opalescent play of colors and is called *moonstone*.

SANIDINE—$(K,Na)AlSi_3O_8$

Crystallography. Monoclinic; $2/m$. Crystals are often tabular parallel to {010}; also elongated on *a* with square cross section as in Fig. 19.78a. Carlsbad twins common.

$C2/m$; for high sanidine, $a = 8.56$, $b = 13.03$, $c = 7.17$ Å; $\beta = 115°59'$; $Z = 4$. *ds*: 4.22(6), 3.78(8), 3.31(10), 3.278(6), 3.225(8).

Physical Properties. *Cleavage* {001} perfect, {010} good. **H** = 6. **G** = 2.56–2.62. *Luster* vitreous. *Color* colorless and commonly transparent. *Streak* white. *Optics*: (−); $\alpha = 1.518–1.525$; $\beta = 1.523–1.530$, $\gamma = 1.525–1.531$. Occurs in two orientations with optic plane parallel with {010} and $2V = 0°–60°$, and with optic plane normal to {010} and $2V = 0°–25°$.

Composition and Structure. A complete solid solution exists at high temperature between sanidine and high albite; part of the intermediate region is known as *anorthoclase* (see Fig. 18.47). The structure of sanidine shows a disordered (random) distribution of Al and Si in the tetrahedral framework (see Fig. 18.48). The Al and Si distribution in orthoclase is more ordered (see Fig. 12.9 and related text).

Diagnostic Features. Can be characterized with confidence only by optical or X-ray techniques. Optic orientation and 2V differ from orthoclase. Microcline and plagioclase show different types of twinning.

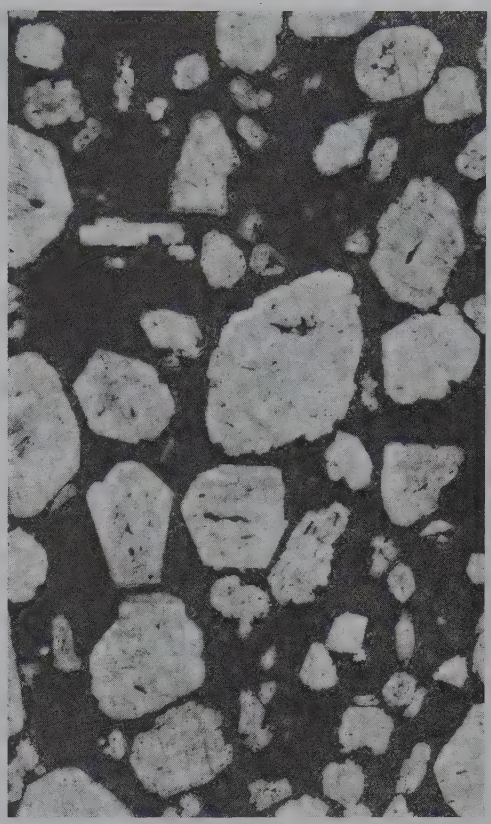

FIG. 19.80 Polished slab of basalt with sanidine phenocrysts.

Occurrence. As phenocrysts (see Fig. 19.80) in extrusive igneous, rocks such as rhyolites and trachytes. Sanidine is characteristic of rocks that cooled quickly from an initial high temperature of eruption. Most sanidines are cryptoperthitic.

Name. Sanidine is derived from the Greek word *sanis* meaning *tablet*, and the Greek word *idos*, meaning *appearance*, in allusion to its typical tabular habit.

PLAGIOCLASE FELDSPAR SERIES

The plagioclase feldspars form, at elevated temperatures, an essentially complete solid solution series from pure *albite* (Ab), $NaAlSi_3O_8$, to pure *anorthite* (An), $CaAl_2Si_2O_8$ (see Fig. 18.54). Discontinuities in this series, as shown by the existence of peristerite and other intergrowths (see page 475), can be detected only by careful electron optical and X-ray studies. The nomenclature for the series, as based on six arbitrary divisions, is given in Fig. 18.47. If species names are not given, the composition is expressed by $Ab_{20}An_{80}$, for example, which may be shortened to An_{80}. Most of the properties of the various species in this series vary in a uniform manner with the change in chemical composition (see Fig. 19.81). For this reason, the series can be more easily understood if one comprehensive description is given, rather than six individual descriptions, and the dissimilarities between members are indicated. The

BOX 19.5 Minerals in Pegmatites

Pegmatites are extremely coarse-grained rocks that are commonly closely related genetically and in space to large masses of plutonic rocks. They are found as veins or dikes traversing the granular igneous rock, but more commonly they extend out from it into the surrounding country rock. Granites more commonly than any other rock have pegmatites genetically associated with them; consequently, unless modified by other terms, pegmatite refers to *granite pegmatite.* The minerals in most pegmatites are the common minerals in granite (quartz, feldspar, mica) but of extremely large size. Crystals of these minerals measuring a foot (approximately 30 cm) across are common, and in some localities they reach gigantic sizes. Quartz crystals weighing thousands of pounds and mica crystals more than 10 feet across have been found. A common characteristic of pegmatites is the simultaneous and interpenetrating crystallization of quartz and K-feldspar (usually microcline) to form *graphic granite.*

Although most pegmatites are composed entirely of the minerals found abundantly in granite, those of greatest interest contain other, rarer minerals. In these pegmatites, there has been a definite sequence in deposition. The earliest minerals are microcline and quartz, with smaller amounts of garnet and black tourmaline (see photo). These are followed and partly replaced by albite, lepidolite, gem tourmaline, beryl, spodumene, amblygonite, topaz, apatite, and fluorite. A host of rarer minerals such as triphylite, columbite, monazite, molybdenite, and uranium minerals may be present. In some places the above minerals are abundant and form large crystals that are mined for their rare constituent elements. Spodumene crystals more than 40 feet long have been found in the Black Hills of South Dakota, and beryl crystals from Albany, Maine, have measured as much as 27 feet long and 6 feet in diameter.

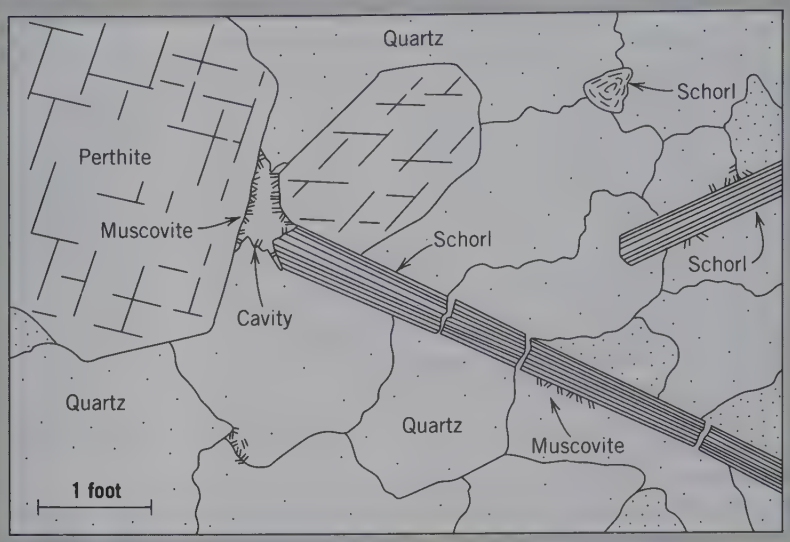

The drawing, with a scale bar = 1 foot = 30.4 cm, is of the giant pegmatite texture in a quartz–perthite–schorl (tourmaline) occurrence in a pegmatite dike near Sage, Riverside County, California. (Jahns, R. H. 1953. The genesis of pegmatites. I. Occurrence and origin of giant crystals. *American Mineralogist* 38: 563–98.) The photo shows black tourmaline with beryl and is from a similar occurrence.

The formation of pegmatite dikes is directly connected with the crystallization of the larger masses of associated plutonic rock. The process of crystallization concentrates the volatile constituents in the residual melt of the magma. The presence of these volatiles (H_2O, B, F, Cl, and P) decreases the melt viscosity and facilitates crystallization. Such an end product of magmatic crystallization is also enriched in the rare elements (Be,Li) originally disseminated through the magma. When this residual liquid is injected into the cooler surrounding rock, it crystallizes from the borders inward, frequently giving a zonal distribution of minerals with massive quartz at the center.

The world's most important gemstone-producing pegmatites are in the northeastern part of the state of Minas Gerais, Brazil. These pegmatites have produced large quantities of gem tourmaline, topaz, kunzite (a pink gem spodumene), morganite (a rose-colored gem beryl), aquamarine (a green-blue gem beryl), and chrysoberyl (see also Chapter 20).

Schorl crystal on beryl, from the Shigar Valley, Skardu District, N. A. Pakistan. Specimen is 10.3 cm high (Photographs courtesy of Jeff Scovil, collection © Jeff Scovil).

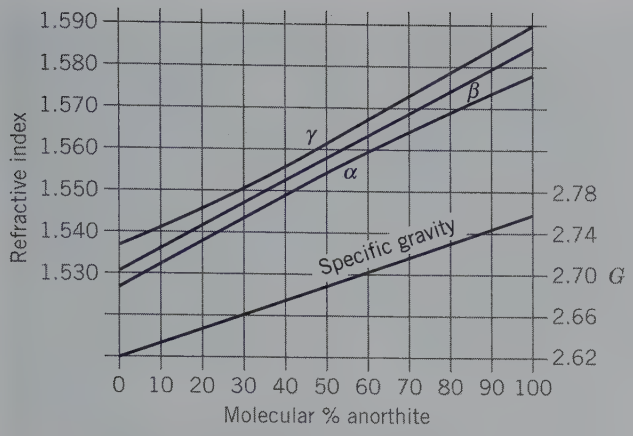

FIG. 19.81 Variation of refractive indices and specific gravity with composition in the plagioclase feldspar series.

distinction between high- and low-temperature forms of the series can be made only by X-ray and optical means.

ALBITE—$NaAlSi_3O_8$
ANORTHITE—$CaAl_2Si_2O_8$

Crystallography. Triclinic; $\bar{1}$. Crystals commonly tabular parallel to {010}; occasionally elongated on *b* (Fig. 19.82). In anorthite crystals may be prismatic elongated on *c*.

Crystals frequently twinned according to the various laws governing the twins of orthoclase, that is *Carlsbad*, *Baveno*, and *Manebach*. In addition, they are nearly always twinned according to the *pericline law*. Albite twinning with twin plane {010} is commonly polysynthetic and because $(010) \wedge (001) \approx 86°$, {001} either as a crystal face or cleavage is crossed by parallel groovings or striations (Figs. 19.83 and 10.16a). Often these striations are so fine as to be invisible to the unaided eye, but on some specimens they are coarse and easily seen. The presence of the striations on the basal cleavage is one of the best proofs that a feldspar belongs to the plagioclase series. Pericline twinning with *b* as the twin axis is also polysynthetic. Striations resulting from it can be seen on {010}. Their direction on {010} is not constant but varies with the composition.

Distinct crystals are rare. Usually in twinned, cleavable masses; as irregular grains in igneous rocks.

For albite, $C\bar{1}$: $a = 8.14, b = 12.8, c = 7.16$ Å; $\alpha = 94°20'$, $\beta = 116°34'$, $\gamma = 87°39'$; $Z = 4$. For anorthite, $I\bar{1}$ or $P\bar{1}$: $a = 8.18, b = 12.88, c = 14.17$ Å; $\alpha = 93°10'$, $\beta = 115°51'$, $\gamma = 91°13'$; $Z = 8$. *d*s (Ab–An): 4.02–4.03(7), 3.77–3.74(5), 3.66–3.61(6), 3.21(7)–3.20(10), 3.18(10)–3.16(7).

FIG. 19.82 Albite crystals.

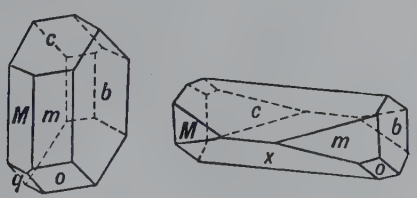

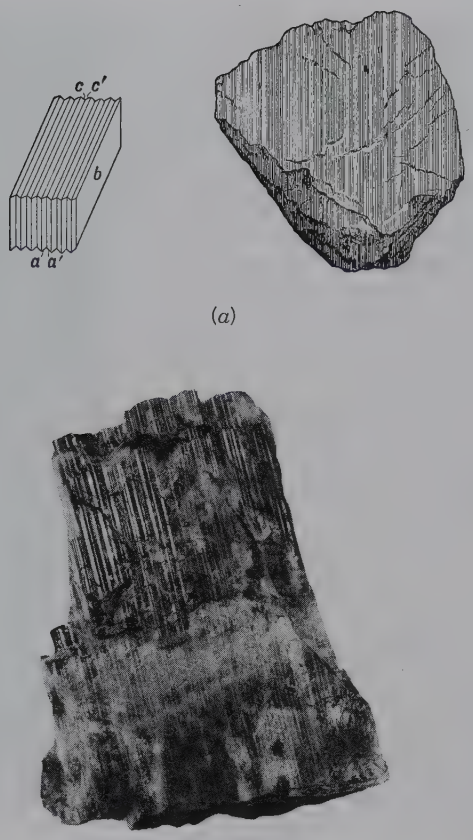

FIG. 19.83 (a) Albite twinning (see also Fig. 10.16). (b) Labradorite feldspar showing albite twinning striations on the basal pinacoid (001) (Harvard Mineralogical Museum).

Physical Properties. *Cleavage* {001} perfect, {010} good. **H** 6. **G** 2.62 in albite to 2.76 in anorthite (Fig. 19.81). *Color* colorless, white, gray; less frequently greenish, yellowish, flesh-red. *Luster* vitreous to pearly. Transparent to translucent. A beautiful play of colors is frequently seen, especially in labradorite (see Plate VIII, no. 5) and andesine. *Optics*: Albite: (+); $\alpha = 1.527$, $\beta = 1.532$, $\gamma = 1.538$; $2V = 74°$. Anorthite: (−); $\alpha = 1.577$, $\beta = 1.585$, $\gamma = 1.590$, $2V = 77°$ (see Fig. 19.81).

Composition and Structure. An essentially complete solid solution series extends from $NaAlSi_3O_8$ to $CaAl_2Si_2O_8$ at elevated temperatures (see Fig. 18.54). Considerable K may be present, especially toward the albite end of the series (see Figs. 18.53 and 18.56). Very fine scale discontinuities in the series, which can be detected only by electron optical and X-ray means, are reflected in the occurrence of very fine lamellar intergrowths: peristerite, Bøggild and Huttenlocher intergrowths (see page 475). The structure of albite is triclinic ($C\bar{1}$) at low to moderate temperatures, and shows a highly ordered Al–Si distribution; low albite is structurally analogous to low microcline. High albite is also triclinic and has a highly disordered Al–Si distribution. At temperatures above 980°C a monoclinic variety of albite, known as monalbite, with a totally disordered Al–Si distribution exists. Anorthite has

space group $P\bar{1}$ at low temperatures. At elevated temperatures the structure of anorthite inverts to $I\bar{1}$ (see Fig. 18.54).

Diagnostic Features. The plagioclase feldspars can be distinguished from other feldspars by the presence of albite twin striations on {001}. They can be placed accurately in their proper places in the series only by quantitative chemical analysis or optical tests, but they can be roughly distinguished from one another by specific gravity (see Fig. 19.81).

Occurrence. The plagioclase feldspars, as rock-forming minerals, are even more widely distributed and more abundant than the potash feldspars. They are found in igneous, metamorphic, and, more rarely, sedimentary rocks.

The classification of igneous rocks is based largely on the kind and amount of feldspar present. As a rule, the greater the percentage of SiO_2 in a rock the fewer the dark minerals, the greater amount of potash feldspar, and the more sodic the plagioclase; and conversely, the lower the percentage of SiO_2 the greater the percentage of dark minerals and the more calcic the plagioclase.

In an igneous crystallization sequence, the more refractory minerals crystallize before the less refractory ones. The *An* end member of the plagioclase series has a much higher melting point than the *Ab* end member (see Fig. 18.54). For this reason plagioclase feldspars that crystallize early from a magma are generally more Ca-rich than those that crystallize later. Continuous chemical zoning occurs commonly in phenocrysts with Ca-rich centers and more Na-rich rims.

Albite is included with orthoclase and microcline in what are known as the *alkali* feldspars, all of which have a similar occurrence. They are commonly found in granites, syenites, rhyolites, and trachytes. Albite is common in pegmatites, where it may replace earlier microcline; as the platy variety, *cleavelandite*. Some albite and oligoclase shows an opalescent play of colors and is known as *moonstone*. The name *albite* is derived from the Latin word *albus*, meaning *white*, in allusion to the color.

Oligoclase is characteristic of granodiorites and monzonites. In some localities, notably at Tvedestrand, Norway, it contains inclusions of hematite, which give the mineral a golden shimmer and sparkle. Such feldspar is called *aventurine* oligoclase, or *sunstone*. The name is derived from two Greek words meaning *little* and *fracture* because it was believed to have less perfect cleavage than albite.

Andesine is rarely found except as grains in andesites and diorites. It is named for the Andes Mountains, where it is the primary feldspar in andesites.

Labradorite is the common feldspar in gabbros and basalts and in anorthosite it is the only important constituent. Found on the coast of Labrador in large cleavable masses that show a fine iridescent play of colors. The name is derived from this locality. Spectacular crystals occur also in Madagascar.

Bytownite is rarely found except as grains in gabbros. Named for Bytown, Canada (now the city of Ottawa).

Anorthite is rarer than the more sodic plagioclases. Found in rocks rich in dark minerals and in druses of ejected volcanic blocks and in recrystallized limestones of contact metamorphic deposits. Name derived from the Greek word meaning *oblique*, because its crystals are triclinic.

Use. Plagioclase feldspars are less widely used than potash feldspars. Albite, or *soda spar*, as it is called commercially, is used in ceramics in a manner similar to microcline. Labradorite that shows a play of colors is polished and used as an ornamental stone. Those varieties that show opalescence are cut and sold under the name of *moonstone*.

Name. The name *plagioclase* is derived from the Greek word *plagios*, meaning *oblique*, an allusion to the oblique angle between the cleavages. (See under "Occurrence" for names of specific species.)

FELDSPATHOID GROUP

LEUCITE—$KAlSi_2O_6$

Crystallography. Tetragonal; $4/m$ below 605°C. Isometric, $4/m\bar{3}2/m$ above 605°C. Usually in trapezohedral crystals that at low temperature are pseudomorphs of the high-temperature form (Fig. 19.84).

Below 605°C: $I4_1/a$; a = 13.04, c = 13.85 Å; Z = 16. Above 605°C: $Ia3d$; a = 13.43 Å; Z = 16. *ds* (low T form): 5.39(8), 3.44(9), 2.27(10), 2.92(7), 2.84(7).

Physical Properties. **H** $5\frac{1}{2}$–6. **G** 2.47. *Luster* vitreous to dull. *Color* white to gray. Translucent. *Optics*: (+); ω = 1.508, ϵ = 1.509.

Composition and Structure. Most leucites are close to $KAlSi_2O_6$ with K_2O 21.5, Al_2O_3 23.5, SiO_2 55.0%. Small amounts of Na may replace K. The structure of the low-temperature polymorph is shown in Fig. 18.58.

Diagnostic Features. Characterized by its trapezohedral form. Leucite is a primary crystallization product and is usually embedded in a fine-grained matrix (see Fig. 19.85 and Plate VIII, no. 6), whereas analcime is usually a secondary mineral filling cavities in volcanic rocks.

Occurrence. Although leucite is a rather rare mineral it is abundant in certain volcanic rocks. It is found only in silica-deficient rocks and thus never in rocks containing quartz. Its most notable occurrence is as phenocrysts in the rocks of Mount Vesuvius. In the United States, it is found in rocks of the Leucite Hills, Wyoming, and in certain of the rocks in the Highwood and Bear Paw Mountains, Montana. Pseudomorphs of a mixture of nepheline, orthoclase, and analcime after leucite, *pseudoleucite*, are found in syenites of Arkansas, Montana, and Brazil.

Name. From the Greek word *leukos* meaning *white*.

FIG. 19.84 Leucite.

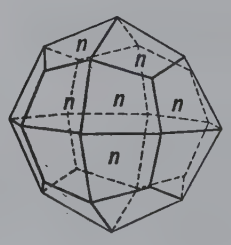

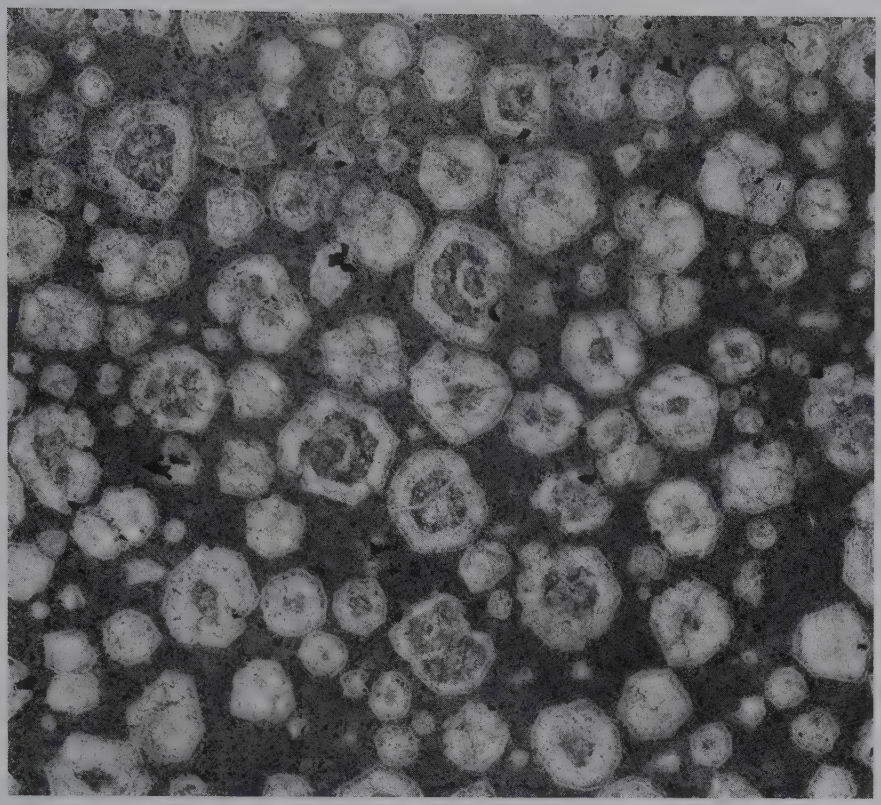

FIG. 19.85 Polished slab of basalt showing large leucite phenocrysts.

Similar Species. *Pollucite*, $CsAlSi_2O_6 \cdot H_2O$, isostructural with leucite, is a rare isometric mineral usually occurring in pegmatites, notably at Bernie Lake, Manitoba.

NEPHELINE—(Na,K)AlSiO$_4$

Crystallography. Hexagonal; 6. Rarely in small prismatic crystals with base. Almost invariably massive, compact, and in embedded grains.

$P6_3$; a = 10.01, c = 8.41 Å; Z = 8. *d*s: 4.18(7), 3.27(7), 3.00(10), 2.88(7), 2.34(6).

Physical Properties. *Cleavage* $\{10\bar{1}0\}$ distinct. **H** $5\frac{1}{2}$–6. **G** 2.60–2.65. *Luster* vitreous in clear crystals; greasy to waxy in the massive variety. *Color* colorless, white, or yellowish. In the massive variety, gray, greenish, and reddish. Transparent to translucent. *Optics*: (−); ω = 1.529–1.546, ϵ = 1.526–1.542.

Composition and Structure. The end-member composition $NaAlSiO_4$ contains Na_2O 21.8, Al_2O_3 35.9, SiO_2 42.3%. The amount of K in natural nephelines may range from 3 to 12 weight percent K_2O. A large miscibility gap exists at low to moderate temperatures between $NaAlSiO_4$ and *kalsilite*, $KAlSiO_4$. However, at temperatures above about 1000°C a complete solid solution series exists between Na and K end members. Figure 19.86 illustrates the large miscibility gap in this chemical system. As a function of decreasing temperature, the Na^+ and K^+ ions in an originally homogeneous solid solution become segregated, forming finely intergrown exsolution lamellae of differing compositions. The process of exsolution in this chemical system is analogous to that discussed for the alkali feldspars (see Fig. 18.50 and page 474). The structure of nepheline is illustrated in Fig. 18.59 and discussed on page 477.

Diagnostic Features. Characterized in massive varieties by its greasy luster. Distinguished from quartz by lower hardness and lack of conchoidal fracture.

Occurrence. Nepheline is a rock-forming mineral found in silica-deficient intrusive and extrusive rocks. Crystals are present in the volcanic rocks of Mount Vesuvius. The largest known mass of intrusive nepheline rocks is on the Kola Peninsula, Russia, where, locally, nepheline is associated with apatite. Extensive masses of nepheline rocks are found in Norway and South Africa. In the United States, nepheline, both massive and in crystals, is found at Litchfield, Maine, associated with cancrinite. Found near Magnet Cove, Arkansas, and Beemerville, New Jersey. Common in the syenites of the Bancroft region of Ontario, Canada, where the associated pegmatites contain large masses of nearly pure nepheline.

Use. Iron-free nepheline, because of its high Al_2O_3 content, has been used in place of feldspar in the glass industry. Most nepheline for this purpose comes from Ontario, Canada. Nepheline produced as a by-product of apatite mining on the Kola Peninsula, Russia, is used by the Russians in several industries including ceramics, leather, textile, wood, rubber, and oil.

Name. *Nepheline* is derived from the Greek word *nephele* meaning a *cloud*, because when immersed in acid the mineral becomes cloudy.

Similar Species. *Cancrinite*, $Na_6Ca(CO_3)(AlSiO_4)_6 \cdot 2H_2O$, is a rare mineral similar to nepheline in occurrence and associations.

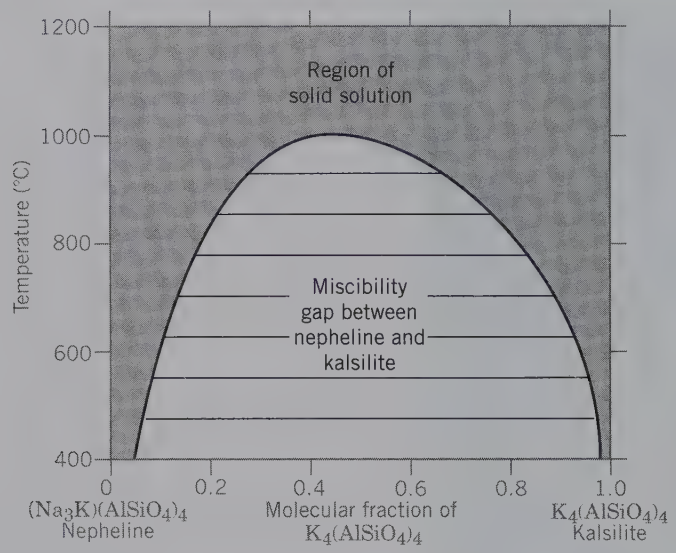

FIG. 19.86 Temperature-composition section for the join nepheline, $Na_3K(AlSiO_4)_4$–kalsilite, $K_4(AlSiO_4)_4$. Compare with Fig. 18.50, which is a similar diagram for the alkali feldspar system. (From Ferry, J. and J. G. Blencoe. 1978. Subsolidus phase relations in the nepheline–kalsilite system at 0.5, 2.0, and 5.0 Kbar. *American Mineralogist* 63: 1225–40.)

Sodalite—$Na_8(AlSi_4O_6Cl_2$

Crystallography. Isometric; $\bar{4}3m$. Crystals rare, usually dodecahedra. Commonly massive, in embedded grains.

$P\bar{4}3n$; a = 8.83–8.91 Å; Z = 2. *ds*: 6.33(8), 3.64(10), 2.58(5), 2.10(2), 1.75(3).

Physical Properties. *Cleavage* {011} poor. **H** $5\frac{1}{2}$–6. **G** 2.15–2.3. *Luster* vitreous. *Color* usually blue, also white, gray, green. Transparent to translucent. *Optics*: refractive index 1.483.

Composition and Structure. Na_2O 25.6, Al_2O_3 31.6, SiO_2 37.2, Cl 7.3%. Only small substitution of K for Na. In the structure of sodalite the $AlSiO_4$ framework is linked such as to produce cagelike, cubooctahedral cavities in which the Cl is housed (see Fig. 18.60).

Diagnostic Features. Usually identified by its blue color, and distinguished from lazurite by the different occurrence and absence of associated pyrite; see Plate VIII, no. 7. If color is not blue, a test for chlorine is necessary to distinguish it from analcime, leucite, and haüyne.

Occurrence. Sodalite is a comparatively rare rock-forming mineral associated with nepheline, cancrinite, and other feldspathoids in nepheline syenites, trachytes, phonolites, and so forth. Found in transparent crystals in the volcanic rocks of Mount Vesuvius. The massive blue variety is found at Bancroft, Ontario; Ice River, British Columbia; Pakistan, and Namibia.

Use. May be carved as an ornamental material.

Name. Named in allusion to its sodium content.

Similar Species. Other rare feldspathoids are *haüyne*, $Na_6Ca_2(AlSiO_4)_6(SO_4)_2$, and *nosean*, $Na_8(AlSiO_4)_6(SO_4)_2{\cdot}H_2O$.

Lazurite—$(Na,Ca)_8(AlSiO_4)_6(SO_4,S,Cl,OH)$

Crystallography. Isometric; $\bar{4}3m$. Crystals rare, usually dodecahedral. Commonly massive, compact.

$P\bar{4}3m$; a = 9.08 Å; Z = 1. *ds*: 3.74(10), 2.99(10), 2.53(9), 1.545(9), 1.422(7).

Physical Properties. Cleavage {011} imperfect. **H** 5–$5\frac{1}{2}$. **G** 2.4–2.45. *Luster* vitreous. *Color* deep azure-blue, greenish-blue. Translucent. *Optics*: refractive index 1.50±.

Composition and Structure. Small amounts of Rb, Cs, Sr, and Ba may substitute for Na. There is considerable variation in the amounts of SO_4, S, OH, and Cl. Lazurite appears isostructural with sodalite (see Fig. 18.60 and discussion on page 477). The large cagelike cavities in the structure house the Cl and S anions and the (SO_4) anionic groups.

Diagnostic Features. Characterized by its blue color and the presence of associated pyrite; see Plate VIII, no. 8.

Occurrence. Lazurite is a rare mineral, occurring usually in recrystallized limestones as a product of contact metamorphism. *Lapis lazuli* is a mixture of lazurite with small amounts of calcite, pyroxene, and other silicates, and commonly contains small disseminated particles of pyrite. The best quality of lapis lazuli comes from northeastern Afghanistan. Also found at Lake Baikal, Siberia, Russia, and in Chile.

Use. Lapis lazuli is highly prized as an ornamental stone, for carvings, and so on (see Plate XI, no. 5, Chapter 20). As a powder it was formerly used as the paint pigment ultramarine. Now ultramarine is produced synthetically.

Name. Lazurite is an obsolete synonym for azurite, and hence the mineral is named because of its color resemblance to azurite.

Petalite—$Li(AlSi_4O_{10})$

Crystallography. Monoclinic; $2/m$. Crystals rare, flattened on {010} or elongated on [100]. Usually massive or in foliated cleavable masses.

$P2/a$; a = 11.76, b = 5.14, c = 7.62 Å; β = 112°24′; Z = 2. *ds*: 3.73(10), 3.67(9), 3.52(3), 2.99(1), 2.57(2).

Physical Properties. *Cleavage* {001} perfect, {201} good. Brittle. **H** 6–$6\frac{1}{2}$. **G** 2.4. *Luster* vitreous, pearly on {001}. *Color* colorless, white, gray. Transparent to translucent. *Op-*

tics: (+); $\alpha = 1.505$, $\beta = 1.511$, $\gamma = 1.518$; $2V = 83°$; $Z = b$. $X \wedge a = 2°–8°$. $r > v$.

Composition and Structure. LiO 4.9, Al_2O_3 16.7, SiO_2 78.4%. The structure of petalite consists of a framework of AlO_4 and SiO_4 tetrahedra that contains Si_4O_{10} layers linked by AlO_4 tetrahedra. The Li is in tetrahedral coordination with oxygen.

Diagnostic Features. Characterized by its platy habit. Distinguished from spodumene by its cleavage and lesser specific gravity.

Occurrence. Petalite is found in pegmatites where it is associated with other lithium-bearing minerals, such as spodumene, tourmaline, and lepidolite. Petalite was considered a rare mineral until it was found to be abundant at the Varutrask pegmatite, Sweden. More recently, it has been found abundantly in Bikita, Zimbabwe, and in Namibia. At these localities, associated with lepidolite and eucryptite, it is mined extensively.

Use. An important ore of lithium. (See spodumene, page 510.) Colorless petalite may be faceted as a gem.

Name. From the Greek word *petalos* meaning *leaf*, alluding to the cleavage.

Scapolite Series

The *scapolites* are metamorphic minerals with compositions suggestive of the feldspars. There is a complete solid solution series between *marialite*, $3NaAlSi_3O_8 \cdot NaCl$, and *meionite*, $3CaAl_2Si_2O_8 \cdot CaSO_4$ (or $CaCO_3$). When the formulas are written in this way, it is clear that the composition of marialite is the equivalent of three formula weights of albite, $NaAlSi_3O_8$, plus one formula weight NaCl, and that the meionite composition is equivalent to three formula weights of anorthite, $CaAl_2Si_2O_8$, plus one formula weight of $CaCO_3$ or $CaSO_4$. In this series, there is complete substitution of Ca for Na with charge compensation effected as in the feldspars by concomitant substitution of Al for Si. There is also complete substitution of CO_3, SO_4, and Cl_2 for each other. The name *wernerite* has been used for members intermediate in composition between marialite and meionite.

The structure of scapolite consists of a framework of SiO_4 and AlO_4 tetrahedra with large cavities containing the (Ca,Na) ions and (CO_3,Cl_2,SO_4) anionic groups (see Fig. 19.87).

Marialite—Meionite

Crystallography. Tetragonal; $4/m$. Crystals usually prismatic. Prominent forms are prisms {010} and {110} and dipyramid {011}; rarely shows the faces of the tetragonal dipyramid *z* (Fig. 19.88). Crystals are usually coarse, or with faint fibrous appearance.

$I4/m$; $a = 12.2$, $c = 7.6$ Å; $Z = 2$. *a* varies slightly with composition. *d*s: (marialite), 4.24(7), 3.78(9), 3.44(10), 3.03(10), 2.68(9).

Physical Properties. *Cleavage* {100} and {110} imperfect but distinct. **H** 5–6. **G** 2.55–2.74. The specific gravity

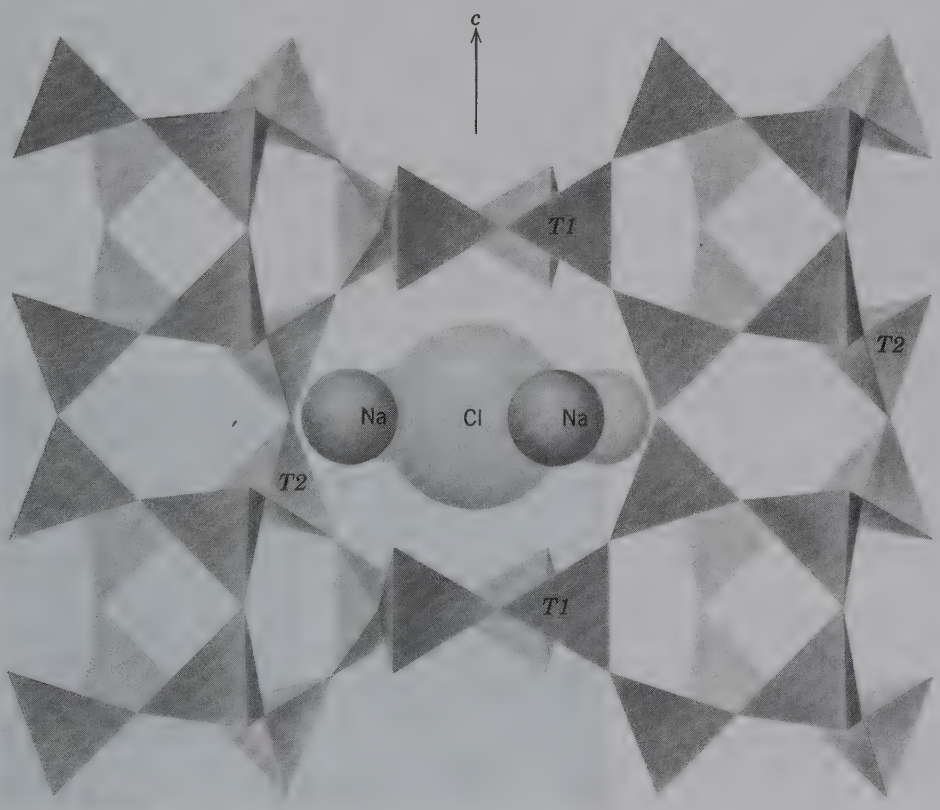

FIG. 19.87 The structure of scapolite projected on (100). (After Papike, J. J. and M. Cameron. 1976. Crystal chemistry of silicate minerals of geophysical interest. *Reviews of Geophysics and Space Physics* 14: 75.)

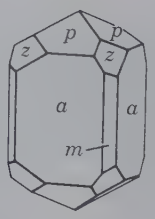

FIG. 19.88 Scapolite.

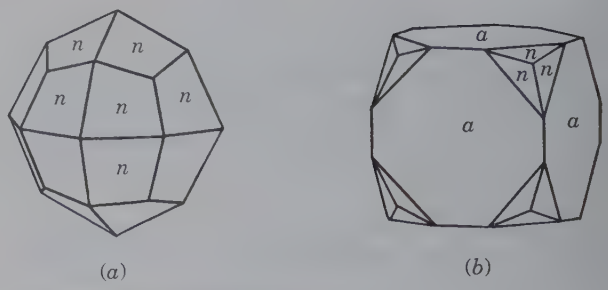

(*a*) (*b*)

FIG. 19.89 Analcime crystals.

and refractive indices increase with increasing Ca content. *Luster* vitreous when fresh. *Color* white, gray, pale green; more rarely yellow, bluish, or reddish. Transparent to translucent. *Optics*: (−); ω 1.55–1.60, ϵ = 1.54–1.56.

Composition and Structure. The extent of solid solution between *marialite*, $Na_4(AlSi_3O_8)_3(Cl_2,CO_3,SO_4)$, and *meionite*, $Ca_4(Al_2Si_2O_8)_3(Cl_2,CO_3,SO_4)$, is discussed on page 547. The structure, illustrated in Fig. 19.87, contains two crystallographically distinct tetrahedra, *T*1 and *T*2. In marialite compositions, Al is confined to the *T*2 tetrahedra (46% Al, 54% Si) and only Si occupies the *T*1 sites. In meionite compositions Al is housed in both tetrahedral sites.

Diagnostic Features. Characterized by its crystals with square cross-section and four cleavage directions at 45°. When massive, resembles feldspar but has a characteristic fibrous appearance on the cleavage surfaces.

Occurrence. Scapolite occurs in schists, gneisses, amphibolites, and granulite facies rocks. In many cases, it is derived by alteration from plagioclase feldspars. It is also characteristic in recrystallized limestones as a contact metamorphic mineral. Associated with diopside, amphibole, garnet, apatite, titanite, and zircon.

Crystals of gem quality with a yellow color occur in Madagascar. In the United States, it is found in various places in Massachusetts, notably at Bolton; and in Orange, Lewis, and St. Lawrence counties, New York. Also found at various points in Ontario, Canada.

Use. Colorless crystals may be cut as faceted gemstones.

Name. From the Greek word *skapos* meaning a *shaft*, in allusion to the prismatic habit of the crystals.

Analcime—$NaAlSi_2O_6{\cdot}H_2O$[1]

Crystallography. Isometric; $4/m\bar{3}2/m$. Usually in trapezohedra (Figs. 19.89a and 19.90). Cubes with trapezohedral truncations also known (Fig. 19.89b). Usually in crystals, also massive granular.

$Ia3d$; a = 13.71 Å; Z = 16. *ds*: 5.61(8), 4.85(4), 3.43(10), 2.93(7), 2.51(5).

Physical Properties. **H** 5–5½. **G** 2.27. *Luster* vitreous. *Color* colorless or white. Transparent to translucent. *Optics*: refractive index 1.48–1.49.

Composition and Structure. The chemical composition of most analcimes is fairly constant with minor amounts of K or Ca substituting for Na; also some Al substitution for Si. $NaAlSi_2O_6{\cdot}H_2O$ contains Na_2O 14.1, Al_2O_3 23.2, SiO_2 54.5, H_2O 8.2%. The structure is made of a framework of AlO_4 and SiO_4 tetrahedra with four- and six-membered tetrahedral rings. This framework contains continuous channels along the three-fold axes of the structure, which are occupied by H_2O molecules. The octahedrally coordinated Na is housed in somewhat smaller voids in the structure.

Diagnostic Features. Usually recognized by its free-growing crystals and its vitreous luster. Crystals resemble leucite, but leucite is always embedded in rock matrix.

Occurrence. Analcime occurs as a primary mineral in some igneous rocks, but more commonly as the product of hydrothermal action in the filling of basaltic cavities. It is an original constituent of analcime basalts and may occur in alkaline rocks, such as aegirine–analcime–nepheline syenites. It is also found in vesicles of igneous rocks in association with prehnite, calcite, and zeolites. Fine crystals are found in the Cyclopean Islands near Sicily; in the Val di Fassa and on the Seiser Alpe, Trentino, Italy; in Victoria, Australia; and Kerguelen Island in the Indian Ocean. In the United States, it is found at Bergen Hill, New Jersey; in the Lake Superior copper district; and at Table Mountain, near Golden, Colorado. Also found at Cape Blomidon, Nova Scotia.

FIG. 19.90 Analcime from Ischia, Italy. Scanning electron microscope (SEM) photograph. (From Gottardi, G. and E. Galli, 1985, *Natural zeolites*. Springer-Verlag, New York, with permission.)

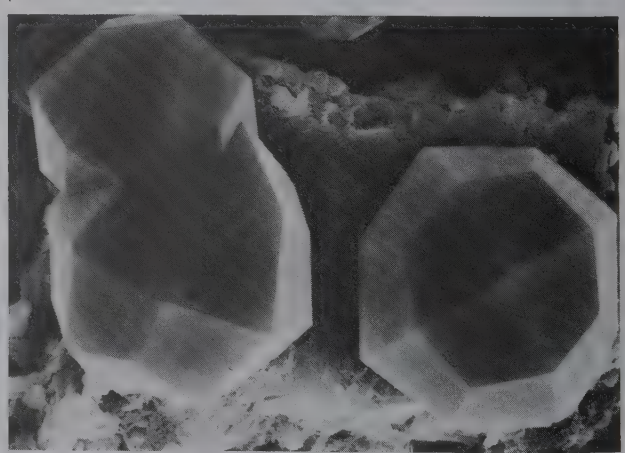

[1]Analcime may be classified as a member of the zeolite group; however, its structure, chemistry, and occurrence are very similar to those of the feldspathoids.

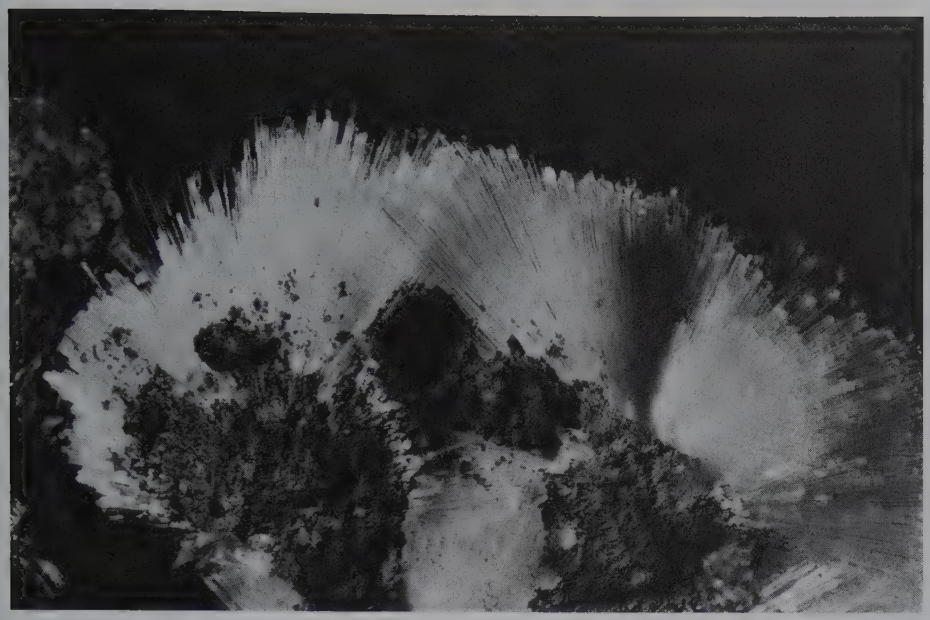

FIG. 19.91 Natrolite from Altavilla, Vicenza, Italy. (From Gottardi, G. and E. Galli, 1985, *Natural zeolites*. Springer-Verlag, New York, with permission.)

Name. Derived from the Greek word *analkidos* meaning *weak*, in allusion to its weak electrical property when heated or rubbed.

Zeolite Group

The number of naturally occurring zeolites is about 60, and here only four species are described in detail. These are: *natrolite* with a fibrous habit; *chabazite* with an equant habit; and *heulandite* and *stilbite* with platy habit and cleavage.

Natrolite—$Na_2Al_2Si_3O_{10}{\cdot}2H_2O$

Crystallography. Orthorhombic; *mm*2. Prismatic, often acicular with prism zone vertically striated. Usually in radiating crystal groups (Fig. 19.91); also fibrous, massive, granular, or compact.

*Fdd*2; $a = 18.29$, $b = 18.64$, $c = 6.59$ Å; $Z = 8$. *ds*: 6.6(9), 5.89(8), 3.19(9), 2.86(10), 2.42(6).

Physical Properties. *Cleavage* {110} perfect. **H** 5–5½. **G** 2.25. *Luster* vitreous. *Color* colorless or white, rarely tinted yellow to red. Transparent to translucent. *Optics*: (+); $\alpha = 1.480$, $\beta = 1.482$, $\gamma = 1.493$; $2V = 63°$; $X = a$; $Y = b$; $r < v$.

Composition and Structure. Na_2O 16.3, Al_2O_3 26.8, SiO_2 47.4, H_2O 9.5%. Some K and Ca may replace Na. Natrolite is one of the group of fibrous zeolites. Its structure consists of an Si–Al–O framework in which chains parallel to the *c* axis are prominent (see Fig. 18.61). The chains are linked laterally by the sharing of some oxygens of opposing tetrahedra. Na is coordinated between the chains to six oxygens, four of which are tetrahedral oxygens and two of which are from water molecules. The perfect {110} cleavage in natrolite is due to the relatively small number of bonds between chains as compared to the large number of bonds within the chainlike structure.

Diagnostic Features. Light color and commonly fibrous habit.

Occurrence. Natrolite is characteristically found lining cavities in basalt associated with other zeolites and calcite. Notable localities are Ústí nad Labém (Aussig), Czech Republic; Puy-de-Dôme, France; and Val di Fassa, Trentino, Italy. In the United States, it is found at Bergen Hill, New Jersey. Also found in various places in Nova Scotia.

Name. From the Latin word *natrium*, meaning *sodium*, in allusion to its composition.

Similar Species. *Scolecite*, $CaAl_2Si_3O_{10}{\cdot}3H_2O$, is another fibrous zeolite, similar in structure to natrolite but monoclinic in symmetry.

Chabazite—$Ca_2Al_2Si_4O_{12}{\cdot}6H_2O$

Crystallography. Hexagonal, $\bar{3}2/m$ or triclinic, $\bar{1}$. Usually in rhombohedral crystals, $\{10\bar{1}1\}$, with nearly cubic angles. May show several different rhombohedrons (Fig. 19.92). Often in penetration twins.

$R\bar{3}m$ or $P\bar{1}$; $a = 9.41$, $b = 9.42$, $c = 9.42$ Å; $\alpha = 94°11'$, $\beta = 94°16'$, $\gamma = 94°21'$; $Z = 6$. *ds*: 9.35(5), 5.03(3), 4.33(7), 3.87(3), 2.925(10).

Physical Properties. *Cleavage* $\{10\bar{1}1\}$ poor. **H** 4–5. **G** 2.05–2.15. *Luster* vitreous. *Color* white, yellow, pink, red.

FIG. 19.92 Chabazite.

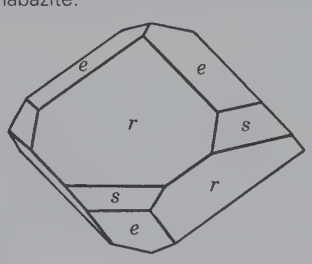

BOX 19.6 Zeolites and Their Many Unique Properties

There is considerable discussion of the various behavioral properties of zeolites in Chapter 18, pp. 472 to 482. The focus here is on some of their additional commercial applications. About 60 natural zeolite minerals have been identified, and more than 100 zeolites have been synthesized (see Holmes, D. A. 1994. Zeolites. *Industrial minerals and rocks*, 6th ed. Edited by D. C. Carr (senior editor). Society for Mining, Metallurgy, and Exploration, Inc., Littleton, Colorado.)

Zeolites are characterized by the following properties (from Holmes):

- High degree of hydration
- Low density and large void volume when dehydrated
- Stability of the crystal structure of many of them when dehydrated
- Cation exchange properties
- Uniform molecular-sized channels in the dehydrated crystals
- Ability to absorb gases and vapors
- Catalytic properties

Potential commercial utilization includes hundreds of possible applications. The principal uses are as follows:

- Ammonium ion removal in waste stream treatment, sewage treatment, pet litter and aquaculture
- Odor control
- Heavy metal ion removal from nuclear, mine, and industrial wastes
- Agricultural use, such as soil conditioner and animal feed supplement

Synthetic zeolites can be tailored in physical and chemical properties to serve many applications more closely, and they are more uniform in quality than their natural counterparts. However, natural zeolites are generally much lower in cost than synthetic zeolite products. Much ongoing research in zeolite synthesis is focused on the production of zeolite structures with larger pore diameters and cage sizes. Pore diameters in zeolites are typically less than 10 Å. Synthetic zeolites with very large ring and cage sizes have recently been produced (examples of various such cages are shown in the diagram of the erionite structure).

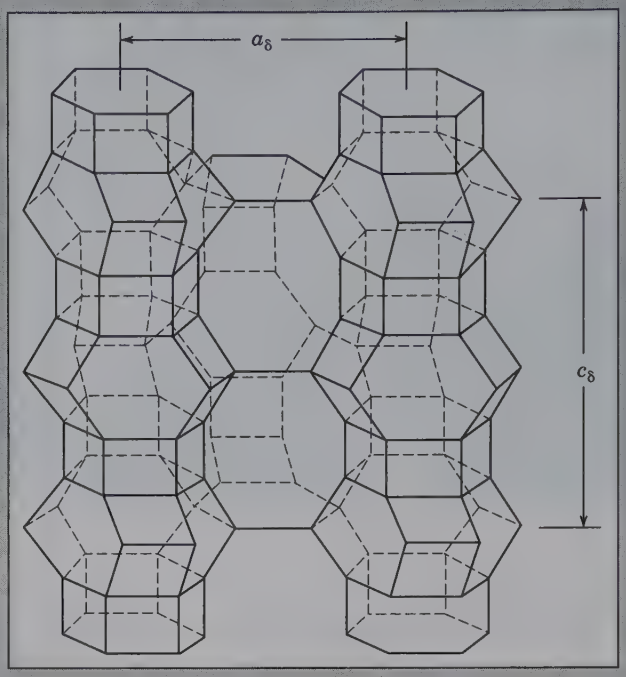

View of the framework structure of erionite. The lines connect Si and Al positions only; oxygen atoms and cations are not shown. (From Kokotailo, G. T., K. S. Sawru, and S. L. Lawton. 1972. Direct observation of stacking faults in the zeolite erionite. American Mineralogist *57: 439–44.)*

An unusually fibrous natural zeolite, erionite, with formula $Na_6K_2(Al_8Si_{28}O_{72})\cdot 25H_2O$, has been identified as an especially serious health hazard in the region of the town of Karain, Turkey. The local geology in that area consists of recent volcanic ash (tuff) deposits that are easily worked with tools to produce dimension stone for housing. These building materials represent the alteration of the original volcanic tuff by groundwater to produce relatively unconsolidated material consisting of montmorillonite clay and erionite. The erionite needles in the local geology and building stones have been identified as the cause of many cases of malignant mesothelioma (a fatal tumor arising from mesothelial cells in the pleura) in the region.

Transparent to translucent. *Optics*: (+) or (−); $\alpha = 1.4848$, $\beta = 1.4852$, $\gamma = 1.4858$, $2V \sim 70°$.

Composition and Structure. The ideal composition is $Ca_2Al_2Si_4O_{12}\cdot 6H_2O$, but there is considerable replacement of Ca by Na and K as well as (Na,K)Si for CaAl. The structure of chabazite consists of an Al–Si–O framework with large cagelike openings bounded by rings of tetrahedra (see Fig. 18.62). The cages are connected to each other by channels that allow for the diffusion of molecules through the structure of a size comparable to the diameter (3.9 Å) of the channels. Argon (3.84 Å in diameter) is rapidly absorbed by the chabazite structure, but *iso*-butane (5.6 Å in diameter) cannot enter the structure. In this way chabazite can act as a molecular sieve (see Fig. 18.64).

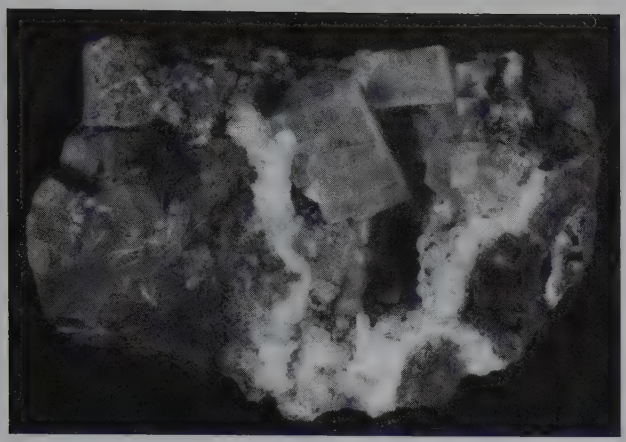

FIG. 19.93 Chabazite in basalt cavity. Paterson, New Jersey (Harvard Mineralogical Museum).

Diagnostic Features. Recognized usually by its rhombohedral-appearing crystals (Fig. 19.93), and distinguished from calcite by its poorer cleavage and lack of effervescence in HCl.

Occurrence. Chabazite is found, usually with other zeolites, lining cavities in basalt. Notable localities are the Faeroe Islands; the Giant's Causeway, Ireland; Ústí nad Labém (Aussig), Czech Republic; Seiser Alpe, Trentino, Italy; Oberstein, Germany; and Poona, India. In the United States, it is found in West Paterson, New Jersey, and Goble Station, Oregon. Also found in Nova Scotia and there known as *acadialite*.

Name. Chabazite is derived from a Greek word that was an ancient name for a *stone*.

Heulandite—$(Ca_{0.5},Na,K)_9(Al_9Si_{27}O_{72})\cdot\sim 24H_2O$

Crystallography. Monoclinic; $2/m$ but crystals often simulate orthorhombic symmetry (Figs. 19.94 and 19.95); often diamond-shaped with {010} prominent.

$C2/m$; $a = 17.71$, $b = 17.94$, $c = 7.46$ Å; $\beta = 116°20'$; $Z = 4$. *ds*: 8.9(7), 5.10(4), 3.97(10), 3.42(5), 2.97(7).

Physical Properties. *Cleavage* {010} perfect. **H** $3\frac{1}{2}$–4. **G** 2.18–2.2. *Luster* vitreous, pearly on {010}. *Color* colorless, white, yellow, red. Transparent to translucent. *Optics*: (+); $\alpha = 1.482$, $\beta = 1.485$, $\gamma = 1.489$; $2V = 50°$; $X = b$. $Y \wedge c = 35°$. $r > v$.

Composition and Structure. There is considerable variation in the Si/Al ratio with concomitant variation in the proportions of Ca, Na, and K. The structure of heulandite consists of a very open Si–Al–O framework in which two-thirds of the $(Si,Al)O_4$ tetrahedra are linked to form networks of six-membered rings parallel to {010}; this is responsible for the perfect {010} cleavage. The framework contains several sets of channels that house the water molecules as well as Ca.

FIG. 19.94 Heulandite.

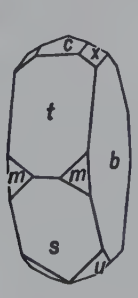

FIG. 19.95 Heulandite from Val di Fassa, Italy. (From Gottardi, G. and E. Galli, 1985, *Natural zeolites*. Springer-Verlag, New York, with permission.)

Diagnostic Features. Characterized by its crystal form and one direction of perfect cleavage with pearly luster.

Occurrence. Heulandite is usually found in cavities of basic igneous rocks associated with other zeolites and calcite. Found in notable quality in Iceland; the Faeroe Islands; Andreasberg, Harz Mountains, Germany; Tyrol, Austria; and India, near Bombay. In the United States, it is found at West Paterson, New Jersey. Also found in Nova Scotia.

Name. In honor of the English mineral collector, H. Heuland.

Stilbite—$(Na,K,Ca_{0.5})_9(Al_9Si_{27}O_{72})\cdot 28H_2O$

Crystallography. Monoclinic; $2/m$. Crystals usually tabular on {010} or in sheaflike aggregates (Figs. 19.96, 19.97 and Plate VIII, no. 9). They may also form cruciform penetration twins.

$C2/m$; $a = 13.61$, $b = 18.24$, $c = 11.27$ Å; $\beta = 127°51'$; $Z = 4$. *ds*: 9.1(9), 4.68(7), 4.08(10), 3.41(5), 3.03(7).

Physical Properties. *Cleavage* {010} perfect. **H** $3\frac{1}{2}$–4. **G** 2.1–2.2. *Luster* vitreous; pearly on {010}. *Color* white, more rarely yellow, brown, red. Translucent. *Optics*: (−); $\alpha = 1.494$, $\beta = 1.498$, $\gamma = 1.500$; $2V = 33°$; $Y = b$, $X \wedge a = 5°$.

Composition and Structure. Na and K are usually present, substituting for Ca by the coupled substitution mechanisms $Na^+Si^{4+} \leftrightarrows Ca^{2+}Al^{3+}$ and $(Na,K)^+Al^{3+} \leftrightarrows Si^{4+}$. The structure of stilbite is similar to that of heulandite with sheets of six-membered $(Si,Al)O_4$ tetrahedra parallel to {010}. This accounts for the tabular habit and excellent {010} cleavage.

FIG. 19.96 Stilbite.

Diagnostic Features. Characterized chiefly by its cleavage, pearly luster on the cleavage face, and common sheaflike groups of crystals.

Occurrence. Stilbite is found in cavities in basalts and related rocks associated with other zeolites and calcite. Notable localities are Poona, India; Isle of Skye; Faeroe Islands; Kilpatrick, Scotland; and Iceland. In the United States, it is found in northeastern New Jersey. Also found in Nova Scotia.

Name. Derived from the Greek word *stilbo* meaning *luster*, in allusion to the pearly luster.

Similar Species. Other zeolites of lesser importance than those described are:

Phillipsite, $(K,Ca_{0.5},Na)_9(Al_9Si_{27}O_{72})\cdot\sim 24H_2O$, monoclinic
Harmotome, $Ba_2(Na,K,Ca_{0.5})(Al_5Si_{11}O_{32})\cdot 12H_2O$, monoclinic
Gmelinite, $Na_{7.5}(Al_{7.5}Si_{16.5}O_{48})\cdot 21.5H_2O$, hexagonal

FIG. 19.97 Stilbite. Jewel Tunnel, Bombay, India (Harvard Mineralogical Museum).

Laumontite, $Ca_4(Al_8Si_{16}O_{48})\cdot 18H_2O$, monoclinic
Scolecite, $Ca(Al_2Si_3O_{10})\cdot 3H_2O$, monoclinic
Thomsonite, $NaCa_2(Al_5Si_5O_{20})\cdot 6H_2O$, orthorhombic. A compact, massive type is used as a gem. When polished, red, yellow, or green "eyes" are seen on a rounded surface.

REFERENCES AND FURTHER READING

In addition to these references, see references from Chapter 18.

Abelson, P. H. 1990. The asbestos removal fiasco (editorial). *Science* 247: 1017.

Carr, D. (ed.). *Industrial minerals and rocks.* 1994. 6th ed. Society for Mining, Metallurgy, and Exploration, Inc., Littleton, Colorado.

Champness, P. E., G. Cliff, and G. W. Lorimer. 1976. The identification of asbestos. *Journal of Microscopy* 108: 231–49.

Darragh, P. J., A. J. Gaskin, and J. V. Sanders. 1976. Opals. *Scientific American* 234, 4: 84–95.

Deer, W. A., R. A. Howie, and J. Zussman. 1962 and 1963. *Rock-forming minerals*, v. 1–4. Wiley, New York.

———. 1978. *Single-chain silicates*, v. 2A. 1982, *Orthosilicates*, v. 1A; 1986; *Disilicates and ring silicates* v. 1B; *Double-chain silicates*, v. 2B. For vols. 2A, 1A, and 1B. Wiley, New York. For vol. 2B, London: The Geological Society.

———. 1992. *An introduction to the rock-forming minerals.* 2nd ed. Wiley, New York.

Dutrow, B. L., M. J. Holdaway and R. W. Hinton. 1986. Lithium in staurolite and its petrologic significance. *Contributions to Mineralogy and Petrology*, 94: 496–506.

Feldspar mineralogy. 1983. *Reviews in Mineralogy* 2. Mineralogical Society of America, Washington, D.C.

Frondel, C. 1962. *The system of mineralogy* 3. *Silica Minerals.* Wiley, New York.

Gottardi, G., and E. Galli. *Natural zeolites.* Springer-Verlag, New York.

Grim, R. E. 1968. *Clay mineralogy.* 2nd ed. McGraw-Hill, New York.

Guthrie, G. D. Jr. 1992. Biological effects of inhaled minerals. *American Mineralogist.* 77: 225–43.

Hawthorne, F. C., L. Ungaretti, R. Oberti, F. Caucia, and A. Callegari. 1993. The crystal chemistry of staurolite. I. Crystal structure and site populations. *The Canadian Mineralogist* 31: 551–82.

———. 1993. The crystal chemistry of staurolite. II. Order-disorder and the monoclinic orthorhombic phase transition. *The Canadian Mineralogist* 31: 583–595.

Heaney, P., and D. M. Fisher. 2003. New interpretation of the origin of tiger's eye. *Geology* 31: 323–26.

Holdaway, M. J., B. L. Dutrow, and P. Shore. 1986. A model for the crystal chemistry of staurolite. *American Mineralogist* 71: 1142–59.

Hume, L. Ann, and J. D. Rimstidt. 1992. The biodurability of chrysotile asbestos. *American Mineralogist* 77: 1125–28.

Klein, C., 1993, Rocks, minerals, and a dusty world, in *Health Effects of Mineral Dust*, G. D. Guthrie and B. T. Mossman, Eds. *Reviews in Mineralogy* 28, Mineralogical Society of America, Washington, D.C.

Mandarino, J. H., and M. E. Back. 2004. *Fleischer's glossary of mineral species 2004.* The Mineralogical Record, Inc., Tucson.

Moore, D. M., and R. C. Reynolds, Jr. 1997. *X-ray diffraction and the identification and analysis of clay minerals.* 2nd ed. Oxford University Press, Oxford.

Morimoto, N., J. Fabries, A. K. Ferguson, I. V. Ginzburg, M. Ross, F. A. Siefert, J. Zussman, K. Aoki, and G. Gottardi. 1988. Nomenclature of pyroxenes. *American Mineralogist*: 73: 1123–1133.

Mossman, B. T., J. Bignon, J. Corn, A. Seaton, and J. B. L. Gee. 1990. Asbestos: Scientific developments and implications for public policy. *Science*: 247: 294–301.

Mossman, B. T., and J. B. L. Gee. 1989. Asbestos-related diseases. *New England Journal of Medicine*: 320: 1721–29.

Natural Zeolites: Occurrence, properties, applications. 2001. D. L. Bish and D. W. Ming, eds. *Reviews in Mineralogy and Geochemistry* 45. Mineralogical Society of America, Washington, D.C.

Nesse, W. D. 1991. *Introduction to optical mineralogy.* 2nd ed. Oxford University Press, New York.

Nolan, R. P., A. M. Langer, M. Ross, F. J. Wicks, and R. F. Martin (eds.). 2001. The health effects of chrysotile asbestos. Contribution of science to risk-management decisions. *The Canadian Mineralogist*, Special Publication 5. Mineralogical Society of Canada, Ottawa.

Pyroxenes. 1980. *Reviews in Mineralogy* 7. Mineralogical Society of America, Washington, D.C.

Ross, M. 1981. The geologic occurrences and health hazards of amphiboles and serpentine asbestos, in *Amphiboles, Reviews in Mineralogy* 9: 279–325.

———. 1984. A survey of asbestos related disease in trades and mining occupations and in factory and mining communities as a means of predicting health risks of nonoccupational exposure to fibrous minerals. *American Society for Testing and Materials*, Special Publication no. 834: 51–104.

———. 1998. The health effects of mineral dusts. *The Environmental Geochemistry in Mineral Deposits*, G. S. Plumlee and M. J. Logsdon (eds.) *Reviews in Economic Geology*, v. 6A, Society of Economic Geologists, Inc., Littleton, Colorado, 339–56.

Ross, M. and R. P. Nolan. 2003. History of asbestos discovery and use and asbestos-related disease in context with the occurrence of asbestos within ophiolite complexes. *Geological Society America Special Paper* 233: 447–70.

Ross, M., R. A. Kuntze, and R. A. Clifton. 1984. A definition of asbestos. *American Society of Testing and Materials*, Special Technical Publication 834: 139–47.

Werner, Andres, M. Hochella, G. Guthrie et al. 1995. Asbestiform riebeckite (crocidolite) dissolution in the presence of Fe chelators: Implications for mineral-induced disease. *American Mineralogist.* 80: 1093–1103.

Wildavsky, A., and D. Schulte. 1995. No runs, no hits, all errors: the asbestos and alar scares. *But is it true? A citizen's guide to environmental health and safety issues.* A.Wildavsky (ed.). Harvard University Press, Cambridge. 185–201.

Wilde, S. A., J. W. Valley, W. H. Peck, and C. M. Graham. 2001. Evidence from detrital zircons for the existence of continental crust and oceans on the Earth 4.4 Gyr ago. *Nature* 409: 175–78.

CHAPTER 20

Gem Minerals

Contemporary gold (18K; K = karat) pendant with a 7.7 carat blue-green Namibian fancy cut tourmaline and a total of 2.2 carats of brilliant cut diamonds (designed by Gordon Aatlo, San Carlos, California; photograph courtesy of B. Dutrow).

Because most gems are minerals, a brief section is devoted to gemology, the science of gemstones. The use of the term *gem* is legally restricted in the American gem trade to refer to stones of natural origin.

Gemstones have always been a fascinating subject. Revered for centuries, gems and jewelry were mainly reserved for the ruling classes. Today, however, nearly everyone owns or has purchased gemstones as part of jewelry items. These items contain gemstones that range from the inexpensive to the highly valuable, from quartz to diamonds.

This chapter introduces a few new concepts or techniques but draws on subject matter covered in prior chapters. After reading this chapter, you will be a more well-informed customer in jewelry stores.

A **gem** is defined as follows:

> a gem is a mineral which, by cutting and polishing, possesses sufficient beauty to be used in jewelry or for personal adornment.

Although beauty is the prime requirement, the more desirable and more valuable gems are *both rare and durable*. Included in the term *gem* are several organic gem materials, pearl, amber, coral, and jet, which, although products of nature, are not strictly minerals. These will be omitted from our discussion. The reason for the restricted use of the term *gem* is to exclude all manufactured simulants; but in spite of the legislation, they are frequently referred to as *synthetic gems*. In a study of gems, these synthetics are important because

one of the major and difficult tasks of the gemologist is to determine whether a stone is natural or synthetic. Such determinations are important because the rare natural gem may have a value several hundred times greater than a similar-appearing synthetic substitute. It is also important to know whether the color of a gemstone is natural or has been artificially induced. Thus, this chapter discusses how synthetics are manufactured, how they can be distinguished from the gems they simulate, and the manner in which the color of gems can be enhanced by treatment.

GEM MINERALS

Because a mineral must have certain qualifications to be placed in the special category of gem minerals, the number is limited. Of the approximately 4,200 known mineral species, approximately 70 meet the requirements, and of these about 15 can be considered as important gem minerals.

Chapters 15 to 19 on "Systematic Mineralogy" include all the minerals commonly used as gems as well as many others less frequently encountered as cut stones. Table 20.1 lists these minerals by chemical groups with the names of the more important gem minerals in boldface type. However, the list is not all-inclusive and other rarer minerals occasionally appear as gemstones. The gemologist is frequently called upon to identify the minerals from which ornamental objects have been carved. Therefore, Table 20.1 includes some minerals that are commonly used in carvings.

Table 20.1 Gem Minerals*

NATIVE ELEMENTS	TUNGSTATES	SILICATES (*continued*)
Diamond	Scheelite	Axinite
SULFIDES	PHOSPHATES	**Beryl**
Sphalerite	Beryllonite	Cordierite
Pyrite	Apatite	**Tourmaline**
OXIDES	Amblygonite	Enstatite-hypersthene
Zincite	Brazilianite	Diopside
Corundum	**Turquoise**	**Jadeite** (jade)
Hematite	Variscite	Spodumene
Rutile	SILICATES	Rhodonite
Anatase	Phenacite	**Tremolite-actinolite** (nephrite jade)
Cassiterite	Willemite	Serpentine
Spinel	**Olivine**	Talc
Gahnite	**Garnet**	Prehnite
Chrysoberyl	**Zircon**	Chrysocolla
HALIDES	Euclase	Dioptase
Fluorite	Andalusite	**Quartz**
CARBONATES	Sillimanite	**Opal**
Calcite	Kyanite	Feldspar
Rhodochrosite	**Topaz**	Danburite
Smithsonite	Staurolite	Sodalite
Aragonite	Datolite	Lazurite
Malachite	Titanite	Petalite
Azurite	Benitoite	Scapolite
SULFATES	Zoisite	
Gypsum	Epidote	
	Vesuvianite	

*Colored photographs of many of these minerals and gems cut from them are given in Plates IX–XII.

GEM QUALIFICATIONS

Of the several attributes of gemstones, beauty is most important. Factors contributing to beauty are color, luster, transparency, and, through skillful cutting, brilliance and fire. Most gems possess two or more of these qualities, but in some nontransparent stones, such as turquoise, beauty lies in color alone. Opal, one of the most colorful gems, owes its attractiveness to flashes of spectral colors diffracted from the stone's interior, a phenomenon known as play of color.

Because most gemstones are used for personal adornment, they should be able to resist scratching and abrasion, which would dull their luster and mar their beauty. Thus, durability, which depends on hardness and toughness, is the second requisite of a gem mineral. It is generally considered that a gemstone hard enough to resist abrasion should have a minimum hardness of 7, that of quartz. Only 10 or 12 gems satisfy this requirement, but others fashioned from softer minerals will retain their luster for many years if treated with care. This does not mean that care should not be exercised in wearing hard gemstones, for some are brittle and a sharp blow may cause them to fracture or cleave. A few minerals with a hardness less than 7 may be extremely tough. This is true of nephrite jade. A blow that would shatter a diamond would have little effect on the nephrite.

In addition to the two intrinsic properties of beauty and durability, other factors influence the desirability of a gem. First of these is *rarity*, long an attribute of the highly prized gems—diamond, emerald, ruby, and sapphire. As the supply diminishes and they become rarer, their value increases. If, on the other hand, a gem through new discoveries becomes abundant, it decreases in value and loses its appeal to the few that formerly could afford it. The desirability of gems is also subject to the vagaries of *fashion*. For example, the dark red pyrope garnet was much in vogue during the nineteenth century but is in little demand today. A final factor that can be added to the desirable properties of gems is *portability*. Gemstones are unique in combining high value with small volume and weight and can be transported easily from one country to another during periods of political unrest and economic instability.

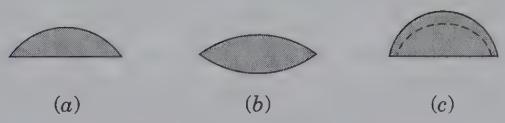

FIG. 20.1 Cross sections of cabochon cut stones. (a) Simple cabochon with domed top and flat base. (b) Double cabochon. (c) Hollow cabochon.

When gemstones are used to finance political unrest, they have been termed "conflict stones." Such stones are less desirable and are of lesser value.

TYPES OF GEM CUTS

Two basic types of gem cuts are significant because mention is frequently made of them on the following pages. They are the *cabochon* cut and the *faceted* cut. The cabochon has a smooth-domed top and most commonly a flat base (Fig. 20.1). Faceted gemstones are bounded by polished plane surfaces (facets) to which different names are given depending on their position. When viewed from above, the outline of faceted stones may be round, oval, rectangular, square, triangular, or other "fancy" shapes. The brilliant cut, most common for diamond, is shown in Fig. 20.2. The upper part of the stone is called the *bezel*, *crown*, or *top*; the lower part is called the *pavilion*, *base*, or *back*. The central top facet is the *table* and the small facet parallel to it is the *culet*. The edge between bezel and pavilion is the *girdle*.

FIG. 20.2 A faceted gemstone (brilliant cut) with 58 facets. (a) Top view of the bezel showing the upper facets. (b) Bottom view of the pavilion showing the lower facets. (c) Side view showing the table (*T*), culet (*C*), and girdle (*G*).

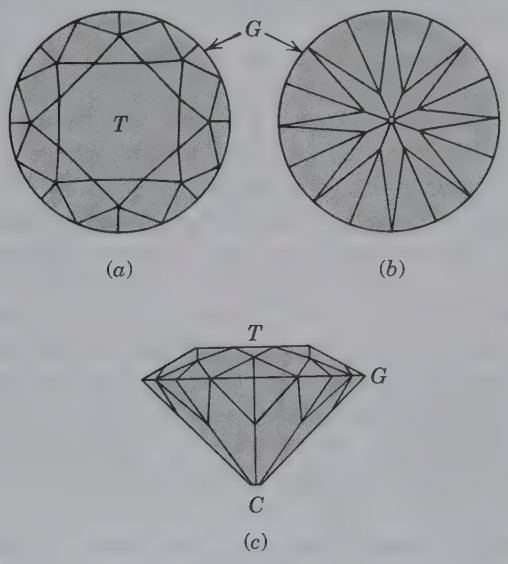

THE EARLY USES OF GEMS

Although gemology as a science is modern, interest in gems is ancient and extends back beyond the dawn of history. Archaeological finds present clear evidence that our remote ancestors collected and treasured gem minerals as objects of beauty. By the beginning of history, numerous gems were not only known but were shaped to enhance their beauty and even pierced, permitting them to be strung together and worn as necklaces or bracelets. Four thousand years before the Christian Era, gems of lapis lazuli, chalcedony, amazonite, and jasper were cut and carved in Babylonia. The presence of lapis lazuli, undoubtedly from Afghanistan, shows that gem trade routes existed at that time. Later, trade extended as far as Egypt, for lapis lazuli has been found in Egyptian tombs of the Twelfth Dynasty erected 4400 years ago. But far earlier in the predynastic period (5000–3000 B.C.) ornaments were fashioned in Egypt from a large number of minerals. They included several varieties of quartz—rock crystal, chalcedony, agate, carnelian, chrysoprase, and jasper—as well as turquoise, chrysocolla, amazonite, olivine, fluorite, and malachite. Emerald was also a gem well known to the early Egyptians. But unlike many of the other gems found in Egyptian tombs, whose source is unknown, emeralds were obtained from the Zabara Mountains in upper Egypt near the shore of the Red Sea. Even today, one can see abundant evidence of these ancient mining activities.

By the time of the ancient Greek and Roman civilizations, many of the gem minerals were known, and the art of carving them was well advanced. The people of these civilizations valued gems as objects of beauty and used them, as they are used today, for personal adornment. But of equal or perhaps greater importance were the presumed supernatural powers that they bestowed on the wearer. The belief in these mystical properties of gems was already old by Roman times, and each successive culture or civilization has added to the lore or independently created its own. Wearing gems as talismans or amulets was widespread, with different virtues attributed to different stones. There was virtually no disaster or human ailment that some gem would not guard against. They protected the wearer from disease, poison, lightning, fire, and intoxication; others rendered one invisible or invulnerable or endowed one with strength and wisdom.

Astrology played a part in the superstitions surrounding gems, remnants of which persist today. A particular stone was believed to possess special virtues if worn under zodiacal control, that is, during a given month. A definite gem was assigned to each sign of the

zodiac and, thus, for most effective influence, a different stone should be worn each month. Because this required 12 gems, which few could possess, and because the most potent stone corresponded to the sign in which the birthday of the wearer fell, the use of month stones or birthstones gradually evolved.

The astrologers who assigned gems to zodiac signs were influenced by earlier religious symbolism of gems, because the early lists of birthstones bear a striking resemblance to gems mentioned in the Bible. In Exodus 28, instructions are given for preparing the breastplate of the high priest of the 12 tribes of Israel as follows: "And thou shall set it in settings of stones, even four rows of stones; the first row shall be a sardius, a topaz, and a carbuncle. And the second row shall be an emerald, a sapphire, and a diamond; and the third row a ligure, an agate, and an amethyst; and the fourth row a beryl, and an onyx, and a jasper." With the exception of *ligure* (possibly zircon), all the names of the various stones are still in use, but certainly many do not refer to stones so known today. In ancient times, minerals were classified primarily by color, with a single name given to what we now recognize as several species. Carbuncle was red and could refer to ruby or spinel but most likely to garnet. Topaz was a green stone, possibly olivine, and a sapphire a blue one, perhaps lapis lazuli. What was called diamond could not have been today's gem, for one large enough for the breastplate was rare, if indeed known, and was too hard to engrave with the name of one of the tribes. It is possible that emerald, amethyst, beryl, red-brown chalcedony (sard), and onyx refer to gems as we know them.

Although the relation of some early described gems to modern gem and mineral names is uncertain, it seems probable that the gem minerals listed as "important" (Table 20.1) were, with few exceptions, known 2000 years ago. The esteem in which individual gems are held, and hence their value, has changed from time to time through the centuries and is still subject to change. Even at the current time, there is no unanimity among gemologists as to the ordering of gems according to value.

IMPORTANT GEMS—PAST AND PRESENT

DIAMOND—C

For most of historic time, diamond has held the preeminent position as the most coveted gem but it was rare among the ancients. Pliny, writing in 100 A.D., said it is "the most valuable of gemstones, but known only to kings." Its great value results from its high hardness, brilliant luster, and high dispersion, giving rise to flashes of spectral colors (Plate IX, no. 1). Moreover, it is quite insoluble in acids or alkalis. Because of these resistant properties it was called *adamas*, from the Greek word meaning *the invincible*, from which the name *diamond* is derived.

India was the primary source of early diamonds. Diamonds were extracted from three separate alluvial diggings, but the most important area was Golconda. This was not a mine but a trading center whose name was given to a district in the southern part of the country that yielded many famous stones. Some of these gems are known today; the whereabouts of others are unknown. But each in its time has left a trail of treachery, intrigue, murder, and wars. The most celebrated of these ancient diamonds is the Koh-i-nor, which, after recutting, weighs 108.83 carats,[1] and is included in the British crown jewels. The Great Mogul (180 carats), described in detail by the French gem merchant Tavernier in the middle of the seventeenth century, vanished after the sack of Delhi in 1739. The blue Hope diamond (45.52 carats), with a long history of tragedy and disaster, now occupies a central position in the gem display of the Smithsonian Institution, Washington, D.C.

With the discovery of diamonds in river gravels in Brazil in 1725, that country became and remained for 140 years the world's leading diamond producer. In 1866, diamonds were discovered in South Africa, first in stream gravels but shortly thereafter in diamond "pipes," the rock in which they originally occurred. During the following 100 years, numerous finds of diamonds, both alluvial and in situ, were made in a dozen African countries, but South Africa remains the largest producer of African gem diamonds. It was at the Premier Mine in that country that the Cullinan (3106 carats), the world's largest gem diamond, was found in 1905. In recent years, diamonds have been coming from Russia. Although the figures are unreliable, it is estimated that Russia accounts for about 25% of the world production and is expanding its capacity. In 2004, the world diamond production totaled about 115 million carats, but the supply is increasing. Each year brings reports of new finds and expanded production from old mines. For example, Botswana produces about 22% and Australia about 15% of total world diamond production, which includes gem as well as industrial diamonds.

About 75% of the diamonds produced are of industrial grade, not suitable for gems. Stones cut from the remaining 25% have great variation in value, which

[1]One carat equals 0.2 gram.

depends on what is called the four Cs; these are color, clarity, cut, and carat weight. Diamonds are graded into many categories on the basis of color and clarity (imperfections). The most used color scale grades from D (colorless) to Z (light yellow or brown). Typically, the most valuable stones are an icy blue-white. The clarity scale includes seven divisions ranging from F (Flawless) to I_3 (Included). Clarity grades are prefixed by V for very and S for slight. For example, a stone with a clarity of VVS_1 is very very slightly included. These inclusions are difficult to detect under 10× magnification. "I" stones have inclusions that are visible under 10× magnification as well as to the human eye. Flawless stones are exceedingly rare. At the top of the scale, the flawless stone of best color has a value at least ten times that of a stone of equal weight at the bottom of the scale. To give the optimum brilliance and fire, a diamond must be properly proportioned. A well-cut stone may be worth 50% more than one poorly cut but of equal weight, color, and clarity. For this reason, many old diamonds are recut to increase their value even though they lose weight in the process. The price of a diamond is related to its weight but it is a nonlinear correlation. If a 1-carat stone is worth $9,300, a 2-carat stone of like quality may be worth $34,000 per carat, and one of 3 carats $65,000 per carat. Examples of several diamond cuts are shown in Fig. 20.3.

BERYL—$Be_3Al_2Si_6O_{18}$

As a gem mineral, beryl occurs in transparent crystals in several color varieties to which special names have been given. These are *goshenite*, colorless; *morganite*, pink; *aquamarine*, blue-green; and *heliodor*, yellow. These beryls make gorgeous gems but it is only the deep green variety, *emerald*, that is ranked as a "precious" stone (Plate IX, nos. 2 and 5). Since ancient times a high value has been placed on emerald, and today its value may equal, or even exceed, that of diamond and ruby.

Although emeralds were mined in ancient Egypt, nearly 4,000 years ago, it was not until the Spanish conquest in the sixteenth century that large, high-quality stones reached Europe and the rest of the world. When the Spanish arrived in what is now Colombia, Ecuador, and Peru, they found the Indians there had large stones of emerald. These they seized, but it was not until later that they learned that the source was Colombia. Other emerald deposits have since been found in Russia (1830), Australia (about 1900), South Africa (1927), and Zimbabwe (1956). But Colombia remains the unquestioned source of fine stones, as it has been for over 400 years. There are two separate mining districts: Chivor, 75 km northeast of Bogota, and Muzo, 100 km north of Bogota. The mines at both localities have been at various times under private and government

FIG. 20.3 Diamond, octahedral crystal in kimberlite matrix with faceted gems. The types of cuts, clockwise from upper left, are brilliant, marquise, heart-shaped, emerald cut, pear-shaped, oval. The brilliant cut stone (upper left) is approximately 4 carats (courtesy of the Diamond Information Center, New York, New York).

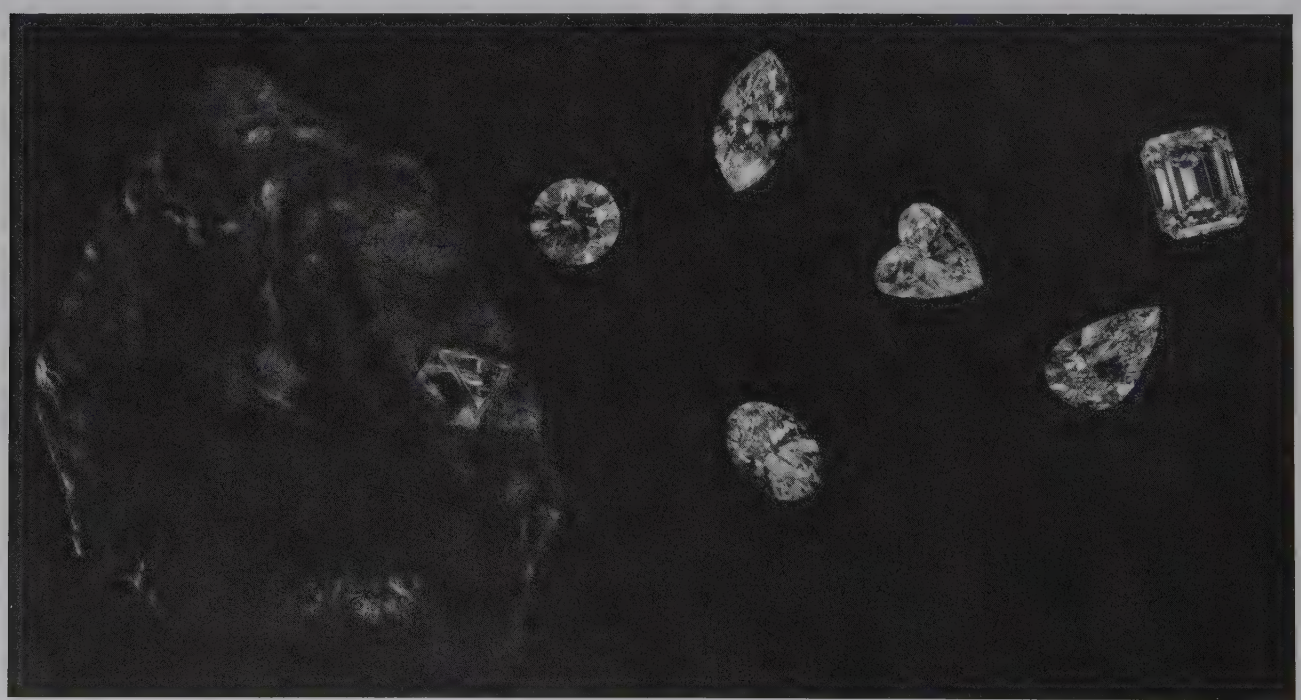

ownership. But whoever the operator, stealing, bribery, and even murder have accompanied the mining operation. Today at nationalized mines, the work is carried out under armed guard. Still, the same problems exist and a high percentage of Colombian emerald production is mined and sold illegally.

RUBY AND SAPPHIRE—Al_2O_3

These gem varieties of corundum have since ancient times been held in high esteem, and with diamond and emerald, they are regarded as the most valuable of gemstones. Ruby receives its name from the Latin word *ruber*, meaning *red* (Plate IX, nos. 4 and 7). Sapphire comes from the Latin word *sapphirus*, meaning *blue*, and was first used to denote any blue gemstone (Plate IX, nos. 3 and 6). Today, all gem corundum, except red, is called sapphire, but the color is specified as yellow sapphire, purple sapphire, and so on. In the gem trade, however, *sapphire* is assumed to be blue.

Rubies are various shades of red, but the deep red, known as pigeon-blood, is of greatest value. Flawless stones of this color are seldom larger than three carats, and those that exceed ten carats are extremely rare. In the past, large rubies were reported, but the whereabouts of most of them are unknown. Travernier in the seventeenth century described a ruby owned by the King of Bijapur as weighing more than 50 carats. The German Emperor Rudolph II is reported to have possessed a ruby the size of a hen's egg. Because rubies have been confused with other red stones, particularly spinel and tourmaline, it may be that some of the earlier reported large rubies "disappeared" on the discovery that they were other gems. Blue sapphires are far more abundant than rubies of similar quality and thus are of less value. Also, large sapphire crystals are not uncommon and numerous stones exceeding 100 carats have been described, many of which are known today. Transparent rubies and sapphires are commonly faceted, but nontransparent stones of fine color may be cut cabochon. This is particularly true if there is indication of asterism in the rough. Care must be taken in cutting such a stone to have the *c* axis perpendicular to the base of the cabochon so that the star appearing on the upper curved surface will be centered. Since the advent of synthetic star rubies and star sapphires, the popularity of natural "stars" has decreased, and they are of no greater value than cabochons of similar size and color that lack asterism.

Since the fifteenth century, Burma (now Myanmar) has been the source of the finest rubies. They come from three separate areas, but the most important is near Mogok. The rubies originated in a metamorphic limestone (marble), and mining of the parent rock has yielded some fine stones. However, most of the gems are recovered, as they have been since ancient times, from the soil of the mountain slopes and from the gravels of the stream valleys. Stones of poorer quality than the Burmese have long come from alluvial deposits in Cambodia, Thailand, and Sri Lanka. The most recent major ruby discovery is in the Tsavo National Park, Kenya. Mining, which began there in 1980, has produced stones of high quality said to rival those from Burma.

Because ruby and sapphire are both varieties of corundum, it is not surprising that they form under similar conditions and have similar occurrences. Excellent sapphires of a cornflower blue—the most desirable color—come from alluvial deposits near Batambang in Thailand and adjacent areas of Cambodia. In Sri Lanka, sapphires of good quality are recovered from the gem gravels. More recently, an array of multicolored sapphires has been discovered and mined in Madagascar. In 1881 in Kashmir in the Himalaya Mountains, a landslide revealed the presence of sapphires. These "Kashmir" blue stones are highly prized but are somewhat lighter in color than those from Cambodia and Thailand.

OPAL—$SiO_2 \cdot nH_2O$

Precious opal lacks the high hardness, clarity, and brilliance of most of the other important gems. But even without these properties, it is highly prized. The great value of precious opal lies in a subtle beauty resulting from an internal display of flashing colors (Plate X, no. 7). Various names have been given to precious opal, such as *black opal*, from which a brilliant play of color is emitted from a dark body color; and *fire opal*, in which a translucent background produces flashes of red to orange colors. Attractive carvings have been executed from opal but as a gem it is always cut cabochon. Many opal gemstones are doublets; that is, a thin slice of precious opal is cemented to a slice of nongem opal, or other material, and the assembly is cut and polished. Because most opals are nontransparent, and the color flashes a surface phenomenon, the doublet resembles a stone cut from a single piece and the deception, if such is intended, is difficult to detect. Some doublets are capped with colorless quartz, which protects the softer opal from damage, yet does not detract from the appeal of the stone.

Opal was well-known and greatly valued in Roman times. The high esteem in which it was held is indicated by Pliny in the story of Nonius, a Roman senator who possessed an opal the size of a hazelnut. The emperor Marcus Antonius demanded the stone, but rather than part with it, Nonius abandoned his other possessions

and fled the country. With only minor fluctuations, opals maintained their high value until early in the nineteenth century. At that time, a decrease in popularity and a consequent lessening of value may have resulted from the superstition that opal was an unlucky stone. Today, with the superstition either forgotten or ignored, opal commands a high place among important gems.

Ancient opals of fine quality are suggested to have come from India and those of poorer quality from Egypt. From Roman times until late in the nineteenth century, most precious opal came from mines near Cervenica, Eastern Slovakia. Today, Australia is the principal source, with production from several widely separated localities. Opal occurs in several locations in Mexico, making that country the second major producer.

JADE

The name *jade* is given to two different minerals: jadeite, $\mathbf{NaAlSi_2O_6}$, a pyroxene, and tremolite-actinolite, $\mathbf{Ca_2(Mg,Fe)_5Si_8O_{22}(OH)_2}$, an amphibole (called nephrite). The two types have in common an extreme toughness and generally a green color (Plate XI, no. 6). Although nephrite is composed of a felted mass of fibers and jadeite is an aggregate of interlocking grains, the textural differences are obscured on polished pieces, making identification difficult. Distinction is best made by specific gravity: nephrite **G** = 3.0±; jadeite **G** = 3.3.

When the Spanish conquistadores arrived in Mexico and Central America, they found carved jadeite that was greatly valued by the natives for the important role it played in their social and religious life. It is reported that Montezuma considered a gift of two pieces of jade to Cortez equal to two cartloads of gold. Recent finds of jadeite in Central America have been made, but it is uncertain as to whether they are the source of the ancient jade of the Aztecs and Mayas.

On the discovery of New Zealand in 1769, Captain Cook found that the native Maoris also placed a high value on jade and carved it into ornaments, utensils, and weapons. This was nephrite found in stream boulders and along the west coast of the south island. The source of this jade has been located in the mountains to the east and is actively worked today.

Many centuries before the West knew of jade in America and New Zealand, it was valued in China above all other substances, and the art of working it into elaborate carvings was ancient. The early Chinese jade was nephrite from Chinese Turkestan; it was much later that jadeite, the rarer and more valued jade, was brought from Burma to be carved by Chinese artisans. Jadeite is still being recovered as stream boulders from the Uru River in Upper Myanmar.

CHRYSOBERYL—$BeAl_2O_4$

The most common chrysoberyl occurs in shades of yellow, green, or brown (Plate X, no. 8). Its high hardness ($8\frac{1}{2}$), transparency, and pleasing color make it a desirable gemstone. However, it is for the rare varieties of *cat's eye* and *alexandrite* that this gem is best known and most valued. A cabochon cut cat's eye shows a marked chatoyancy, a sharp band of light crossing a yellow, green, or brown background. Numerous other gems show a chatoyancy, but the term *cat's eye* should be reserved for chatoyant chrysoberyl. These rare and highly prized stones come mostly from Sri Lanka.

Alexandrite is a dark-colored chrysoberyl with the remarkable property of appearing green in daylight and red in artificial (incandescent) light. Because of this color change, it has been described as "an emerald by day and a ruby by night." Alexandrite was discovered in the Ural Mountains, Russia, in 1830 on the day the Czarevitch, later Czar Alexander II of Russia, reached his majority, and was named for him. Alexandrites are also found in the gem gravels of Sri Lanka and, although their color change is less dramatic than in the Russian stones, they command a high price.

TOPAZ—$Al_2SiO_4(F,OH)_2$

For centuries the name *topaz* has been subject to much confusion, a situation that still exists with both jeweler and layperson. The ancients undoubtedly used the word for gem olivine, *peridot*, that came from Zebirget, an island in the Red Sea. The first use of the name for the mineral we know today as topaz was by Henckel in 1737 for yellow to sherry-colored gems from Saxony (Plate XI, nos. 3 and 4). Since then it has been used for stones of this color, sometimes called *precious topaz*, to set it apart from other similar-appearing gems that may be called topaz. The most common confusion is with yellow quartz, citrine, for which various names have been used to imply the stone is topaz or a close relative.

The confusion regarding topaz is compounded by the fact that gem-quality crystals of the mineral are not always wine-yellow. They are most commonly colorless, but may be pink, red, orange, greenish, pale blue, or brown. Furthermore, certain colorless topaz can be turned a deep aquamarine-blue by irradiation followed by heat treatment. Most of this treated topaz comes from Brazil, which is also the source of most of the precious topaz.

TOURMALINE—$(Na,Ca)(Fe^{2+},Mg,Li,Al)_3(Al,Fe^{3+})_6(Si_6O_{18})(BO_3)_3OH_3(F,O,OH)$

Tourmaline is unique among gem minerals in occurring in shades of all colors as well as in multicolored crystals. This is due to the extensive solid solution exhibited by tourmaline (Plate X, no. 11). Names have been given to the various colored varieties, but it is more meaningful to call them tourmaline with the appropriate color modifier. Tourmaline is a widespread mineral and undoubtedly has long been used as a gem, but it was not until early in the eighteenth century that its identity became known. At that time, it received its name from the Singhalese word, *turamali*, used in Ceylon (now Sri Lanka) for yellow zircon. It is reported that when a parcel of turamali sent to Holland turned out to be yellow tourmaline, the name was given to that mineral, and, although a misnomer, it has persisted.

There are numerous worldwide occurrences of gem tourmaline. Some of the more important are in Minas Gérais, Brazil; Madagascar; Mozambique; and Namibia. In the United States the first significant gem find was of tourmaline at Mount Mica, Maine. In 1972 another major deposit was discovered not far away in Newry, Maine. Other important localities are in California, mostly in San Diego County. Mining of gem tourmaline began there 100 years ago and, with reopening of old mines and the discovery of new deposits, is still producing superb specimens.

QUARTZ—SiO_2

Quartz is listed with the "important" gem minerals not for its rarity or high value but because of its many common and abundant gem varieties (Plate X, nos. 1–6). In all likelihood, quartz was the first mineral used for personal adornment and has occupied a prominent place among gems ever since. Of the 12 stones in the breastplate of the high priest, at least half appear to have been a quartz variety. Theophrastus in his treatise *On Stones*, written about 300 B.C., mentions quartz and its varieties more than any other mineral, and states "among the ancients, there was no precious stone in more common use." It is still in common use, and all but two or three of its many coarsely crystalline and fine-grained varieties are used as gem materials. One should refer to "Quartz" (Chapter 19) for the names and properties of the gem varieties.

TURQUOISE—$Cu^{2+}Al_6(PO_4)_4(OH)_8 \cdot 4H_2O$

Turquoise, valued chiefly for its color, is an ancient gem material (Plate XI, no. 7). The oldest mines are at Sarabit Elkhadem on the Sinai Peninsula and date as far back as 4000 B.C. It appears certain that carved turquoise in bracelets of Queen Zer of Egypt's First Dynasty came from this locality. Nishapur, Iran (Persia), is the source of the finest turquoise today just as it has been since mining began there more than 2,000 years ago. The only other deposits of importance today are in China, Tibet, and in southwestern United States.

Turquoise came from many localities in the American Southwest, but the most famous is in the Los Cerillos Mountains, New Mexico, where the American Indians may have begun mining as early as 1,000 years ago. Indian jewelry set with turquoise has become very popular in recent years. The result has been not only a large increase in price but the use of substitutes and the manufacture of synthetic turquoise.

GARNET—$(Mg^{2+},Fe^{2+},Mn^{2+})_3Al_2Si_3O_{12}$–$Ca_3(Fe^{3+},Al^{3+},Cr^{3+})_2Si_3O_{12}$

The large range in the chemistry of garnet is reflected in the diversity of color (Plate XI, no. 2) and other physical properties of its several varieties. For a description of the various species and the extensive solid solution between them, refer to the discussion of the garnet group in Chapters 18 and 19. Since biblical times, the garnet used as gems is dark red and to many is the only color associated with the mineral. Yet garnet occurs in all colors except blue. Mention is made here of only the more unusual colors that may be encountered in garnet gemstones.

Pyrope and *almandine*, and solid solutions between them, are various shades of red and violet. These are the garnets used in early times as gems. *Grossular* may also be red, but it is the orange-yellow (hessonite) to orange-brown (essonite) material that has been most widely used as gemstones. Recently, a transparent, emerald-green vanadium-bearing variety, called *tsavorite*, has been found in the Tsavo National Park, Kenya. Stones of tsavorite are small but highly valued. A jade-green, massive variety of grossular from South Africa has been used as a jade substitute. *Andradite* may be yellow-green to black, but it is only the transparent green variety, *demantoid*, that is important as a gem. It is the garnet of greatest value and occupies a high position among all gems. *Spessartine* of gem quality is rare, but yellow, yellow-brown, tangerine orange, and orange-brown crystals are cut into lovely stones. *Uvarovite*, the chromium garnet, occurs in brilliant, deep green crystals. The crystals are too small for cutting but were they larger, they would make striking gems.

ZIRCON—$ZrSiO_4$

Zircon is an Eastern gem that for centuries has come from the gem gravels of Sri Lanka and Indochina. It is recovered as water-worn crystals, usually in shades of red or brown, but it may be green, gray, or colorless (Plate X, no. 9). For a long time, the reddish-brown crystals have been heat treated to produce more attractive colors. Heating in air usually yields a yellow stone, but blue or colorless stones result when heated in a reducing environment. The most popular colored stone is blue, which is sold under the name of *starlite*.

Zircon has a high refractive index and a high dispersion, giving a brilliance and fire to a cut stone approaching those of a diamond. Because of the resemblance, colorless zircons from Matura, Sri Lanka, were called "Matura diamonds."

There are two types of zircon used as gems: a crystalline variety and a metamict type. The chemical composition is $ZrSiO_4$, but hafnium is always present, and sometimes small amounts of thorium and uranium are present as well. Originally all zircon was crystalline, but irradiation by these radioactive elements destroys the structure, making the crystals amorphous. Metamict zircons are usually green and have lower refractive indices and density than the crystalline variety (see p. 282 for a discussion of the metamict state).

OLIVINE—$(Mg,Fe)_2SiO_4$

The olive-green gem variety of olivine is known as *peridot* (Plate XI, no. 1), but was called chrysolite (a synonym for olivine) and "evening emerald." The gem was known to the ancients as topazian, a name presumably derived from Topazias, an island in the Red Sea. It was called topaz until the eighteenth century, when the name was transferred to another gem, our present-day topaz. Although the early stones undoubtedly came from the Red Sea island, for centuries their source remained a mystery until it was rediscovered early in the twentieth century. Since rediscovery, the island, known as Zebirget (formerly Saint John's Island), has yielded a large quantity of fine peridot crystals. In 1958, the deposit was nationalized by the Egyptian government. Although peridot has come from Myanmar, Australia, Norway, Pakistan, and the United States, Zebirget remains the outstanding locality for large stones of high quality.

GEM PROPERTIES AND INSTRUMENTS FOR THEIR DETERMINATION

Gems are basically minerals, and the material in Chapters 15 through 19 describes their physical and chemical properties which form the basis for their definition and identification. This section reviews physical properties as they pertain to gem identification and describes identification tools.

PHYSICAL PROPERTIES

Because the characterizing properties of gems are obviously the same as for the minerals from which they were fashioned, one should refer to descriptions of the individual minerals. Chapter 22, however, has two tables helpful in gem identification: (1) a list of minerals in order of increasing specific gravity (Table 22.2), and (2) a list of nonopaque minerals in order of increasing refractive index (Table 22.3). In most cases, an unknown gem can be identified by determination of these two properties. Specific gravity—along with cleavage, fracture, hardness, and fluorescence—are covered in the next few paragraphs. Refractive indices are described in the "Instruments" section.

Cleavage and Fracture

These properties that commonly enable one to identify a mineral specimen are far less important in gem identification. Evidence of them is usually obliterated in a well-cut and polished gemstone. However, careful inspection of a cut stone with a hand lens or microscope may reveal interior reflecting surfaces, indicating incipient cleavage cracks and fractures. A mounted stone should also be examined at the points of contact with the prongs where pressure of mounting may have produced tiny fractures or cleavages.

Hardness

A scratch test for hardness of a gemstone should be made only when other identifying tests have failed, and then with extreme caution. To determine hardness the gemologist uses a set of *hardness points*. These are metal tubes set with sharp-pointed mineral fragments usually having hardnesses of 10, 9, $8\frac{1}{2}$, 8, $7\frac{1}{2}$, 7, and 6. When it is necessary to check hardness on a faceted stone, the scratch, as short as possible, should be attempted on a back facet near the girdle or on the girdle itself. To avoid scratching an unset stone, the gem girdle can be used as the "scratcher" with attempts to scratch the scale minerals. Begin with a mineral low in the scale and work toward those of higher hardness until no scratch is produced. A short scratch usually can be made on the back of a cabochon without injury to the stone.

Specific Gravity

The specific gravity is as characteristic a property of gems as it is of minerals. Its determination, coupled

with refractive index, in many cases suffices for identification. But unlike the refractive index, discussed later, it cannot be determined for a mounted stone. The most reliable methods of determining specific gravity are by hydrostatic weighing or by suspension in a heavy liquid (page 33). The definite values obtained by these methods are more helpful in pinpointing a gem than approximate specific gravities obtained in the manner outlined below.

It is common practice for gemologists to maintain a number of bottles containing liquids of known densities. Densities found most convenient are 2.67 (bromoform + acetone), in which quartz floats and beryl sinks; 2.89 (bromoform), in which beryl floats and tourmaline sinks; 3.10 (methylene iodide + acetone), in which gem tourmaline just floats and fluorite sinks; 3.33 (methylene iodide), in which fluorite sinks and jadeite is suspended or sinks slowly. By making successive tests, the specific gravity of a gem can be bracketed or determined as greater than 3.33 or less than 2.67. For example, a gemstone that sinks in the 3.10 liquid but floats in the 3.33 liquid has a specific gravity between these limits. To avoid contamination, the stone should be well cleaned before transferring from one liquid to another.

Fluorescence

Some gemstones fluoresce under ultraviolet light but for only a few, as for their parent minerals, is the fluorescent color constant and therefore diagnostic. Of this small number that are occasionally cut as gems, willemite fluoresces a yellow-green, scheelite a pale blue, and benitoite a bright blue in shortwave ultraviolet. Gems cut from some minerals are always nonfluorescent, but those cut from other minerals may or may not fluoresce. Thus, in most cases, fluorescence cannot be used as a definitive test for gem identification.

INSTRUMENTS FOR STUDYING GEMS

Many of the methods developed by the mineralogist for mineral determination are applied equally effectively to gemstone identification. In the study of rough gem material, the procedures are identical. In general, however, there is a fundamental difference in approach. Whereas the mineralogist can scratch, powder, or dissolve the mineral under investigation, the gemologist is restricted to nondestructive tests when working with cut and polished gemstones. As a result, specialized instruments and techniques have been developed for their study. The following pages describe the importance of these methods used in determining the properties of gems.

Observation

The first step in identification of a gem is to look at it with the unaided eye, for several properties are seen as surface phenomena. These include luster, color, and, in a faceted stone, fire caused by dispersion of the spectral colors. Other surface features, observed best in cabochon stones, are (with examples) play of color, *opal*; opalescence, *moonstone*; iridescence or labradorescence, *labradorite*; asterism, *star ruby*; and chatoyancy, *cat's eye*, (page 26). Such observations may yield sufficient information for the experienced gemologist to identify a gem.

Hand Lens

Perhaps the most important gemological instrument is a simple hand lens; one with a 10× magnification is most commonly used. With it one can determine the quality of the cut. Are the facets well polished, are they symmetrically disposed, do they meet at common points, and are the edges between them sharp or rounded? The cut of an imitation is usually poorer than that of the gem it simulates. The hand lens will also reveal major flaws or inclusions that detract from the value of a stone.

The Microscope

For a critical examination, one that will reveal imperfections not seen with a hand lens, it is necessary to use a microscope. The type most useful in gemology is a low-power binocular microscope with magnification ranging from 10× to 60×. This instrument differs from the polarizing microscope (page 291) in that it gives true stereoscopic vision with an erect rather than an inverted image. Provision is made to view the stone in both incident and transmitted light. With the light source above the microscope stage, the external features are observed in light reflected from the surface. The interior of the stone is best seen in transmitted light, that is, in light passing through it from a substage illuminator. However, it is difficult to inspect the complete interior of a gemstone in normal transmitted light because of reflection and refraction by the facets. This problem is largely overcome in the gemological microscope (Fig. 20.4) by a substage adapter, giving what is called dark field illumination. Using this lighting technique, the gemstone is illuminated by a hollow cone of light that does not fall directly on the microscope objective. The gemstone is held at the apex of this cone, and any flaws or inclusions within it appear bright against a dark background. Study of these internal imperfections aids both in identification and in quality determination. Also, it frequently provides a means of determining whether a stone is of natural origin or is a synthetic imitation.

FIG. 20.4 A low-power stereoscopic wide-field microscope, designed to provide several different methods for illuminating gemstones (courtesy of Gemological Institute of America, GEM Instruments Corporation, Santa Monica, California).

The Polariscope

The most informative tests are based on the optical properties and are usually the first made in gemstone identification. A determination as to whether a stone is isotropic or anisotropic can be made quickly using a polarizing microscope (Fig. 13.10). Equally effective for the purpose is a simple polariscope used by most gemologists. It is composed of two polarizing plates, one held above the other with a light source below, see Fig. 20.5. The plates are adjusted to the crossed position by turning the upper polar until a minimum of light passes through it. A transparent gemstone placed on the lower plate and slowly turned will remain dark if it is isotropic (isometric or noncrystalline), but will become alternately light and dark if anisotropic (page 295).

Refractive Index and the Refractometer

Of the several measurable properties of gems, refractive index is most informative and is determined most easily. The **RI** (the abbreviation used by gemologists for refractive index) can be determined on both set and unset gemstones, using especially designed refractometers. Several makes of refractometers are available, but all operate on the same principle: total reflection and the critical angle (page 290). But they are so constructed that, instead of measuring the angle, the refractive index is read directly from a scale. Central to all the instruments is a lead glass of high refractive index cut in the form of a hemisphere, hemicylinder, or prism with a flat, polished upper surface. The refractometer developed by the Gemological Institute of America (Fig. 20.6) uses a hemicylinder.

To make an **RI** determination, a facet of the gemstone, usually the table, is placed on the polished surface but separated from it by a film of liquid. Light entering through a ground glass at the back of the instrument passes through the hemicylinder, striking the gemstone at varying angles of incidence. When the light rays are at angles greater than the critical angle, they are totally reflected back through the hemicylinder to fall on a transparent scale. The image of the scale is reflected by a mirror and is observed through a telescope (Fig. 20.7a). The position of the boundary separating light from dark portions (the shadow edge) is determined by the refractive index, which can be read from the scale (Fig. 20.7b).

The contact liquid usually used with a standard jeweler's refractometer is a mixture of methelyne io-

FIG. 20.5 Polariscope used for distinguishing isotropic from anisotropic materials, determining pleochroism, and obtaining interference figures (courtesy of Gemological Institute of America, GEM Instruments Corporation, Santa Monica, California).

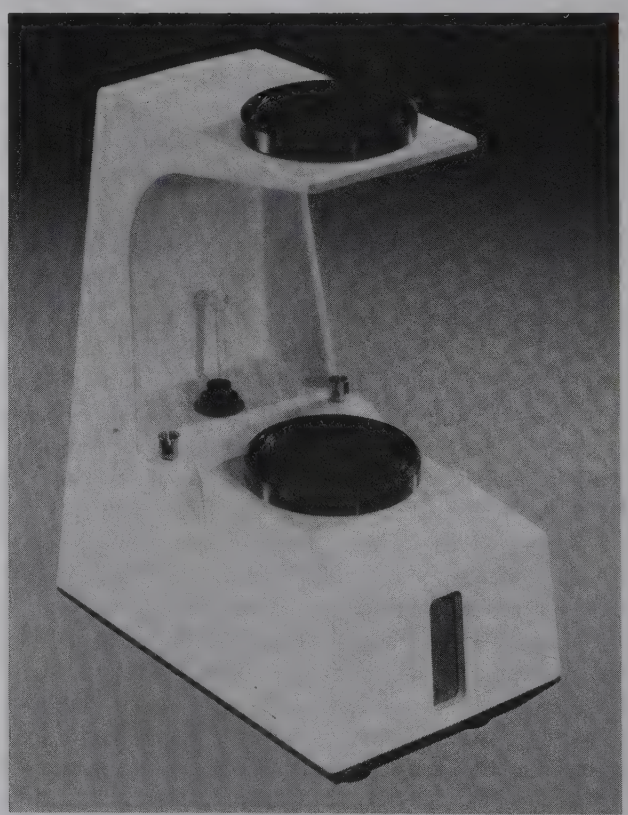

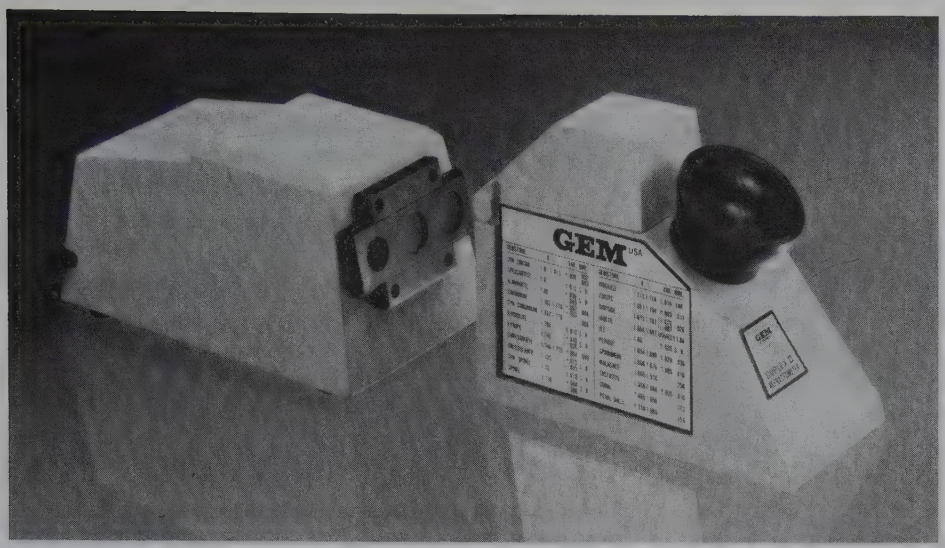

FIG. 20.6 Jeweler's refractometer (courtesy of Gemological Institute of America, GEM Instruments Corporation, Santa Monica, California).

dide, sulfur, and tetraiodoethylene with an **RI** of 1.81. Because the liquid must have an **RI** greater than that of the gemstone, the maximum refractive index determination is about 1.80. *Caution:* Refractive index liquids available in most mineralogical laboratories with **RI** greater than 1.78 should not be used. They are corrosive and will etch the lead glass of the refractometer. However, they may be used in a refractometer in which the glass is replaced by chemically inert cubic zirconia (**RI** 2.16). With this instrument, using a liquid of **RI** 2.10, measurements of refractive index as high as 2.08 can be made.

Anisotropic Gems. Although, basically, the method of refractive index determination is applicable to all gemstones, it strictly applies only to those that are isotropic with a single refractive index. Anisotropic crystals have two refractive indices if uniaxial and three if biaxial.

Uniaxial stones, in general, give rise to two shadow edges on the refractometer, one resulting from vibrations of the *O* ray, the other from vibrations of the *E* ray. If the stone is turned on the hemicylinder, one edge remains constant; this is ω, the **RI** of the *O* ray. The other edge, resulting from the E ray, varies as the stone is

FIG. 20.7 (a) Schematic diagram of light rays entering a refractometer and striking a gemstone of spinel at varying angles of incidence. Rays at angles less than the critical angle (CA) pass upward through the stone. Rays at angles greater than CA are totally reflected through the hemicylinder. (b) Image of scale as seen through the optical system with reading at 1.720, the **RI** of spinel. The faint edge at 1.81 is the **RI** of the contact liquid.

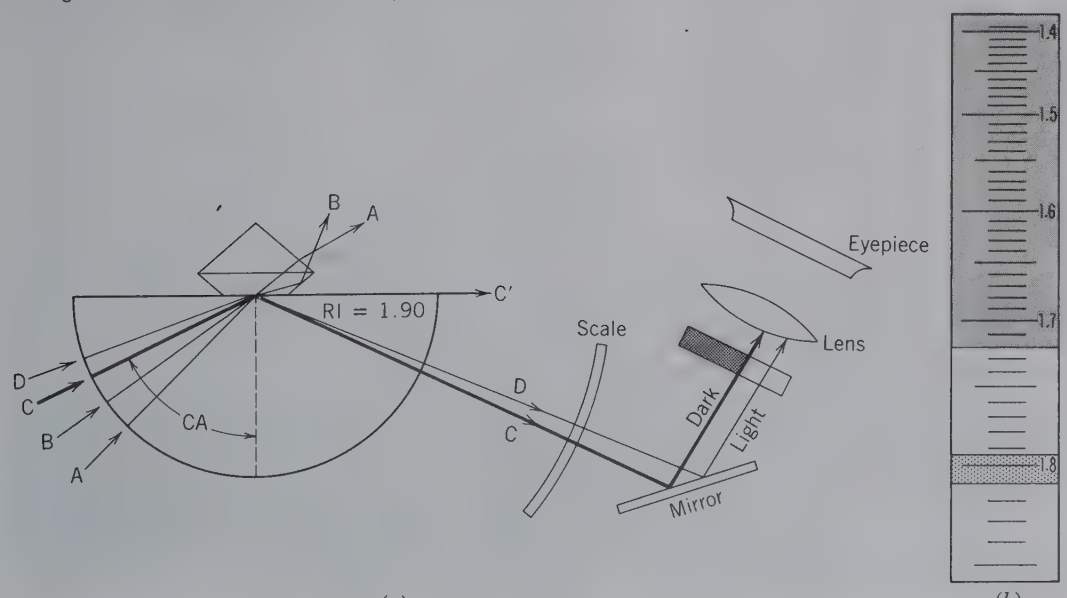

(a) (b)

turned, giving values of ϵ'. The true value of ϵ is read when the two edges are farthest apart. The difference between ω and ϵ is the *birefringence*. The stone is optically positive if $\omega < \epsilon$ and negative if $\omega > \epsilon$. If the polished surface of the gem in contact with the refractometer is perpendicular to the optic axis (*c* crystal axis), both shadow edges remain constant as the stone is turned. In this situation, measurements should be made with the stone lying on another facet. One can then determine whether the high or low index is variable and thus the optic sign.

Biaxial gemstones normally show two shadow edges on the refractometer but, unlike uniaxial, both edges move as the stone is turned. The maximum reading of the higher edge is γ, the minimum reading of the lower edge is α, and their difference is the birefringence. To determine the optic sign, it is necessary to know the third index, β. For $(\gamma - \beta) > (\beta - \alpha)$ is positive and $(\gamma - \beta) < (\beta - \alpha)$ is negative. As the stone is rotated, the value of β is observed as *either* (1) the lowest reading of the higher edge or (2) the highest reading of the lower edge. If (1) is less than the midpoint between α and γ, β is nearer to α than to γ and the stone is positive; if (2) is greater than this midpoint, β nearer to γ than to α and the stone is negative. If neither shadow edge passes the midpoint, the gemstone should be placed on a different face and readings (1) and (2), the two possibilities for β, again determined. The value common to both sets of readings is β.

Dispersion

Refractive index varies with the wavelength of light and is less for red than for violet light, a phenomenon called *dispersion*. Dispersion is a characterizing feature of gemstones and is given as a number representing the difference of **RI** determined in red light and in violet light. For diamond it is 0.044 and for quartz 0.013. The high dispersion of diamond gives it its fire, the flashes of color from a cut stone. If white light is used in determining the **RI** of a gemstone, the shadow edge on the scale is not a line but, because of dispersion, is a band of spectral colors. For precise measurements it is necessary to use a monochromatic source such as sodium light. The refractive index usually reported is that determined in sodium light.

The Dichroscope

Light passing through an anisotropic crystal may be absorbed differently in different vibration directions. The phenomenon is called *dichroism* in uniaxial crystals (page 299) and *pleochroism* in biaxial crystals (page 304) although the term *pleochroism* is commonly used for both. It may be evidenced only in a difference in intensity of light of a given wavelength, but frequently different wavelengths are absorbed in each vibration direction, resulting in color variations characteristic of a given gem.

Uniaxial gemstones with only two rays, *O* and *E*, can show only two pleochroic colors, which vary as do the refractive indices. When light moves parallel to the optic axis, only one color is seen, that of the *O* ray. The color of the *E* ray is most pronounced when light moves perpendicular to the optic axis. In some uniaxial gems the color difference is only in intensity. For example, in green tourmaline, the absorption of the *O* ray is much greater than that of the *E* ray and is expressed as $O > E$ or $\omega > \epsilon$. When absorption results in different pleochroic colors, the colors are given. For example in emerald: *O* (ω) yellow-green, *E* (ϵ) blue-green. In biaxial crystals light absorption may be different for light vibrating in each of the principal crystallographic directions, *X*, *Y*, *Z*. For example, the variety of chrysoberyl, *alexandrite*, has strong pleochroism expressed as *X* (α) red, *Y* (β) orange, and *Z* (γ) green.

Because pleochroic colors result from rays vibrating at right angles to each other, it is possible to observe one by eliminating the other. This can be done with a polariscope by rotating the stone to an extinction position. The upper polar is then removed and the color noted in plane polarized light. If the stone is pleochroic, a different color or color intensity will be observed on rotating it 90°. A gemstone either uniaxial or biaxial may be pleochroic, yet no color difference will be seen if light passes through it parallel to an optic axis. Thus, in testing for pleochroism, it is advisable to make observations with light passing through the stone in several directions.

The dichroscope is an instrument long used by gemologists for detecting pleochroism. The instrument is a metal tube with a square or rectangular opening at one end and a lens at the other. Within the tube is an elongated cleavage piece of optical calcite (Iceland spar). Because of the strong double refraction of calcite, two images of the opening are seen through the instrument (Fig. 20.8). If a pleochroic stone is held over a bright light source and viewed through the

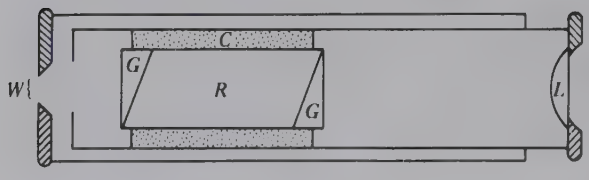

FIG. 20.8 Dichroscope, diagrammatic section. *R* is a calcite cleavage rhombohedron held in a metal tube by a cork setting, *C*. Glass prisms, *G*, are cemented to the calcite to aid in light transmission. To the right of the drawing is a double image of the window. *W*, as seen through lens, *L*.

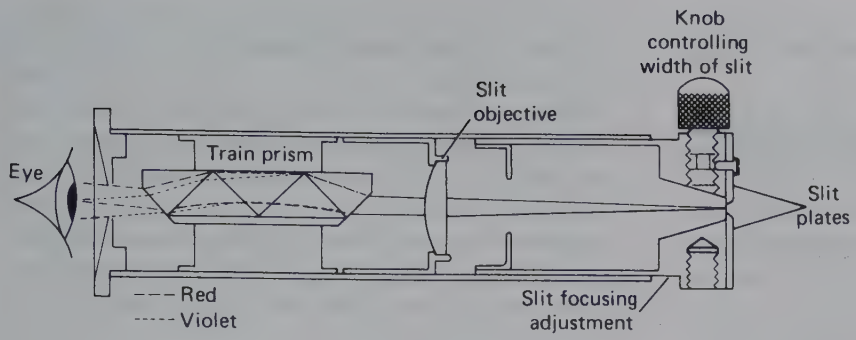

FIG. 20.9 Section through a direct vision prism spectroscope of the type manufactured by R. and J. Beck, London.

dichroscope, the two images have different colors. Although the same colors are seen with a polariscope, they are observed simultaneously with the dichroscope and are compared more easily.

Color Filters

A colored gemstone absorbs certain wavelengths of white light, and the color results from a combination of the unabsorbed wavelengths. To the eye, two gems may have nearly identical colors but the color of one may result from quite a different mixture of wavelengths than the color of the other. Color filters offer a means of resolving the basic difference and aid in gem identification.

The most commonly used filter is the *Chelsea*, sometimes called the "emerald filter" because its principal use is to distinguish emerald from other green gems and imitations. The filter transmits only the long red wavelengths and a band in the yellow-green portion of the spectrum. Emerald transmits red light but absorbs some of the yellow-green. It, therefore, appears red when illuminated by a bright incandescent light and viewed through the filter. Most other green gems as well as glass imitations absorb red light and appear green. Although this is a helpful test in emerald identification, it must be used with caution because a few other green gems as well as synthetic emerald may appear red and the color of emerald from some localities remains unchanged.

The Spectroscope

Gemologists use a small, direct vision spectroscope. It is essentially a metal tube with an adjustable slit at one end and an eyecap window at the other end. Between the ends are arranged a lens to focus on the slit and a train of prisms, as shown in Fig. 20.9. When the slit is directed toward a source of white light, one observes a ribbon of the complete visible spectrum, red at one end, violet at the other. Different portions of the spectrum are brought into sharp focus by pulling out or pushing in the drawtube carrying the slit.

When a gemstone is interposed between the bright light and the spectroscope, the continuous spectrum is visible but it may be crossed by dark bands or lines where certain wavelengths have been eliminated (Fig. 20.10). This is an absorption spectrum. The dark bands or lines fall in positions identical to the bright bands or lines of the emission spectrum but are not as sharp or as well defined. Nevertheless, their distribution depends on the elements present and yields information that aids in the identification of certain gems. Bands or lines resulting from both major elements and minor elements, acting as coloring agents, may be present. In some cases with data obtained with the spectroscope, one can differentiate between a natural or synthetic gem or tell whether the color is natural or has been artificially induced.

FIG. 20.10 Absorption spectrum of a pale yellow diamond. Seen through the spectroscope the background would be a continuous spectrum of violet through red, crossed by dark lines (courtesy of Gemological Institute of America, Santa Monica, California).

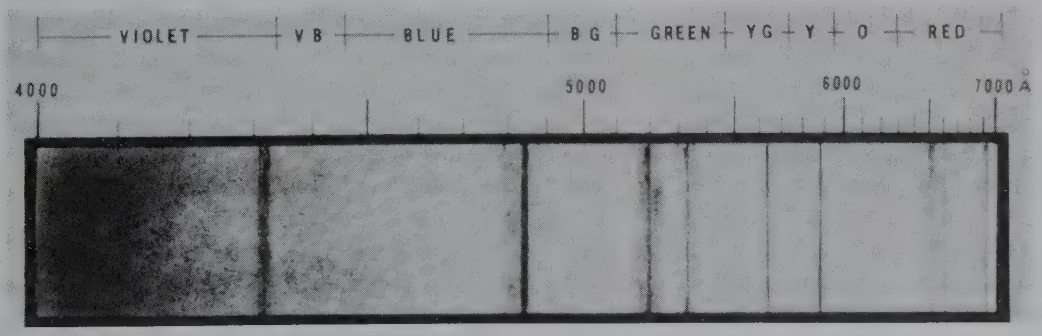

X-ray Diffraction

Of the several methods used today for mineral identification, the one yielding the most definitive information is an X-ray powder photograph or powder diffractogram (p. 308). Thus, in studying a mineral, this is frequently the first, and perhaps the only, test made, even though other, simpler tests might have been adequate.

In studying a gem, the reverse is true. Only when all other tests have failed to identify a gem is resort made to an X-ray powder photograph. This is due in part to the difficulty in obtaining the requisite sample. However, with care and without injury to the stone, sufficient material can be ground from the back of a cabochon or scraped from the girdle of a faceted gemstone to make a powder mount.

SYNTHESIS OF GEM MATERIALS

During the twentieth century, mineralogical research resulted in the laboratory synthesis of many minerals. Most of these are fine-grained aggregates or in small crystals, but a few have been grown in large, single crystals. These latter are of concern—particularly those that duplicate gem minerals. Because duplication is not only in appearance but in all respects—chemistry, crystal structure, and physical properties—detection is difficult.

The method of synthesis varies, depending on the desired product. Some techniques have been developed to produce only a single gem (e.g., diamond and opal), whereas others are used to synthesize several. The methods of more general application, outlined next, are followed by a consideration of the most important synthetic gem materials. Included are not only synthetic minerals but also synthetic products without natural equivalents.

VERNEUIL PROCESS

On a commercial scale, gem synthesis had its beginning in 1902. In that year Auguste Verneuil announced that by a process of flame fusion he had synthesized ruby in sizes large enough and clear enough to be cut as gemstones. An industry based on the Verneuil technique grew rapidly, and within a decade millions of carats, not only of ruby, but of sapphires both colorless and in a variety of colors, were being produced annually. Later (ca. 1920) spinel and still later (ca. 1947) rutile were manufactured by the same process. The Verneuil method with only minor changes remains today the principal means of gem synthesis.

In the Verneuil process, a powder with the chemical composition of the desired crystal (for ruby, Al_2O_3 plus a coloring agent) is melted as it passes through an oxygen–hydrogen flame. Droplets of the fused powder fall on a ceramic plate and, on cooling, form a carrot-shaped single crystal of corundum called a *boule*. Most crystals grown by the Verneuil method contain small gas bubbles, usually spherical but sometimes elongated. Also present are curved striae resulting from successive layers of molten material spreading over the curved surface of the growing boule. Detection in a gemstone of these bubbles and growth striations signifies a synthetic origin.

CZOCHRALSKI PROCESS

By this technique, also called *crystal pulling*, large, high-quality crystals of several compounds including corundum can be grown. A melt of the composition of the desired crystal is contained in an iridium crucible. A "seed" crystal, held on the end of a rotating rod, is touched to the surface of the melt and then slowly withdrawn. On withdrawal, material continually crystallizes, forming a rod-shaped crystal. Ruby crystals 40 cm long and 5 cm in diameter are grown in this manner.

FLUX GROWTH

In this method, a powder of the composition of the desired crystal is mixed with a flux, a material having a relatively low melting point. As the mixture is heated in an inert crucible, the flux melts and, in the molten state, dissolves the other material. After the melt is thoroughly mixed, it is allowed to cool slowly. On reaching a critical temperature, crystal nuclei of the desired material form and gradually increase in size as the temperature is further lowered. When cool, the crystals are recovered by dissolving the flux. Several gem materials, including emerald and ruby, are grown by this method.

HYDROTHERMAL GROWTH

In nature, many minerals crystallize from hot, water-rich solutions. The constituent elements, held in solution at high temperatures, are precipitated as the solutions move toward the surface into regions of lower temperature. Using equipment designed to withstand high temperature and high pressure, hydrothermal growth in the laboratory closely duplicates the natural process. The apparatus, called an autoclave or "bomb," is a heavy-walled steel cylinder closed at one end. To prepare an autoclave for crystal growth of quartz, for example, pure quartz fragments as source material are placed in the bottom, and seed plates of thin slices of single quartz crystals are held in the upper part. The bomb is then 85% filled with water to which a crystal-

lization catalyst has been added to increase the solubility of the quartz fragments. After sealing, the bomb is placed in a furnace and heated to about 400°C in the lower part and to about 340°C in the upper part. As the temperature is raised, the water expands to fill the bomb and the pressure reaches 1,300 to 2,000 bars. The convection current generated by the temperature gradient causes the solution to rise, carrying silica dissolved from the feed material. When it reaches the zone of lower temperature, the silica is deposited on the seed plates. Although ruby and emerald are grown hydrothermally, quartz is by far the most important product grown by this method.

TREATMENT OF GEMSTONES

The color of a number of gemstones can be changed or enhanced by "treatment." The change in some is temporary, lasting only a few days or weeks, but in others it is permanent, resulting in a color identical to that of a naturally colored stone. The principal methods of treatment are dyeing, heating, and irradiation, or, for some gems, a combination of heating and irradiation.

DYEING

An old and an obvious way to color a gemstone is to stain it with an appropriate dye. Because the material must be sufficiently porous to permit penetration of the pigmenting solution, the method is restricted to relatively few gems. Dyeing has been used most effectively in coloring chalcedony, jade, and turquoise.

HEAT TREATMENT

It has long been known that heating certain gemstones will result in a color change or will render an off-color stone colorless. It is likely that most, if not all, gem materials have been subjected to heat treatment in both oxidizing and reducing environments with the hope that they too could be similarly enhanced. However, only a few have responded favorably, and some have been downgraded by heating. The gems for which heat treatment is most successful are zircon, quartz, beryl, topaz, and zoisite (tanzanite).

IRRADIATION

Irradiation has produced desirable color changes in numerous gems but in only a few is the color permanent. There are several irradiation sources: X-rays, alpha particles from a cyclotron, neutrons from atomic piles, and gamma rays from cobalt 60. Irradiation is most effective in producing desirable color changes in diamond, topaz, and quartz.

SYNTHETIC AND TREATED GEMS

Gems that have been synthesized and those that have responded most favorably to treatment are listed below, designated *s* for synthesis and *t* for treatment.

Beryl (*s*, *t*)	Quartz (*s*, *t*)
Chrysoberyl (*s*)	Rutile (*s*)
Corundum (*s*, *t*)	Spinel (*s*)
Diamond (*s*, *t*)	Topaz (*t*)
Jade (*t*)	Turquoise (*s*, *t*)
Opal (*s*, *t*)	Zoisite (*t*)

These gems are discussed briefly, describing the method by which each is synthesized and/or treated. Also mentioned, under "Imitation," are the materials, both natural and synthetic, that are sometimes used to imitate the natural gem. Glass is not included with the materials used as imitations, but it could be in each case. Therefore, the gemologist should be ever alert to the possibility that a stone is glass. Although glass may correspond in color to the gem it simulates, usually the deception can be quickly detected by determination of other properties.

BERYL

Synthesis. Beryl synthesis has been directed chiefly to emerald because of its high value compared with other gem beryls. Efforts have been highly successful and emerald has been synthesized by both flux-growth and hydrothermal methods. Also, a special hydrothermal method (the Lechtleitner process) has been developed by which an overgrowth of emerald can be produced on gemstones of colorless beryl.

Most natural emeralds are nonfluorescent but synthetics usually fluoresce a dull red under longwave ultraviolet. Also, natural emeralds usually appear red when viewed through the Chelsea filter, whereas most synthetics and imitations appear green. Unfortunately neither test is unequivocal. Flux-grown emeralds contain wisplike inclusions that signify a synthetic origin. The refractive indices and specific gravity of synthetics made by the different processes differ slightly from one another as well as from natural emerald, as shown below.

Emerald Type	ω	ϵ	G
Natural Colombian	1.583	1.577	2.71–2.77
Hydrothermal	1.573	1.568	2.66–2.70
Flux grown (some)	1.579	1.571	2.65–2.68
Flux grown (normal)	1.564	1.561	2.65–2.66

Treatment. Gems of green, yellow, and pink beryl are usually of natural colors, but the deep blue of many aquamarines has been produced by heat treatment of greenish-yellow beryl. Emeralds with surface cracks may be "oiled," that is, immersed in an oil of the same refractive index as emerald. The cracks, filled with oil, are obscured and the color of the stone deepened.

Imitation. A composite stone simulating emerald, called a triplet, is made with a crown and pavilion of colorless beryl (or colorless synthetic spinel), between which there is a layer of green-colored cement.

CHRYSOBERYL

Synthesis. Alexandrite, the variety of chrysoberyl that appears green in daylight and red in incandescent light, has been synthesized by flux growth. The properties of these synthetics, including the color change, are very similar to those of natural crystals.

Imitation. Synthetic corundum and, to a lesser extent, synthetic spinel, are made to resemble alexandrite. However, the color change in these synthetics is less marked than in alexandrite, being more violet in artificial light and a grayish-green in daylight.

CORUNDUM (RUBY AND SAPPHIRE)

Synthesis. Synthetic corundum is produced most extensively by the Verneuil process. It is synthesized as ruby (red) and as sapphire both colorless and in a wide variety of colors, some of which do not occur in nature. Synthetic sapphire in colors usually displayed by other gems may be sold erroneously under the names of those gems; for example, purple as "amethyst" and yellow as "topaz." Since 1947, star rubies and blue star sapphires have been manufactured by the Verneuil method. As cabochon stones they rival in beauty the natural stones they imitate. Tiny bubbles and curved growth striae are characteristic of corundum grown by the Verneuil process.

Corundum is also synthesized hydrothermally and by crystal pulling and flux-growth methods. Rubies made by flux growth lack the characterizing features of Verneuil-grown crystals and detection as a synthetic is difficult, and in some cases impossible. Moreover, the color of synthetic rubies is strikingly similar to that of natural rubies and, for this reason they command a relatively high price.

Treatment. The color of some rubies and blue sapphires can be enhanced by heat treatment. Gray sapphires heated to a high temperature in the proper gaseous environment may become a deep blue. Also a surface color can be induced by diffusion of impurities (e.g., TiO_2) into a stone during heat treatment.

DIAMOND

Synthesis. Using apparatus designed to maintain both high temperature and high pressure, diamonds were synthesized in 1955 by the General Electric Company (see Box 15.2). Although these were small crystals, not suitable for gems, they signaled the beginning of an industry to manufacture abrasive diamond. By 1980, diamond grit was being made in several countries, with a total annual production of more than 100 million carats. In 1970, General Electric announced the synthesis of gem quality diamonds large enough (about 1 carat each) to be cut into gemstones. Currently, gem quality synethic diamonds of up to 3 carats are sold at prices lower than those for natural stones.

Treatment. Color can be produced or changed in diamonds by irradiation and heat treatment. Early in the twentieth century, diamonds were colored green by exposure to radiation from radium compounds. This treatment induced not only color but a radioactivity that remains dangerously high. Today diamonds are colored green, without induced radioactivity, in a nuclear reactor and with a cyclotron. Heat treatment of these green stones changes the color to yellow or brown. Diamonds have been colored blue by high-energy electron bombardment. Distinguishing between treated and naturally colored stones presents a difficult problem for the gemologist.

Imitation. For a long time various colorless gems have been used to imitate diamond, but the properties of most of them are so different from those of diamonds as to permit easy recognition. Zircon, with **RI** beyond the range of the jeweler's refractometer and relatively high dispersion, is most deceptive, but unlike diamond, it is birefringent. With the manufacture of gem materials that have no natural counterparts, detection of diamond simulants became more difficult. These substances are briefly described at the end of this chapter under "Manufactured Gem Materials Without Natural Counterparts." They and the minerals used to imitate diamond are listed in Table 20.2 with several diagnostic properties, in order of decreasing refractive index. For comparison, diamond and its properties are given first.

JADE

Jade is not a single mineral, but includes the pyroxene, jadeite, and the amphibole, tremolite-actinolite, known as nephrite. Although the two types of jade are quite distinct mineralogically, they are frequently difficult to distinguish from one another.

Treatment. Jadeite occurs in all colors but the most highly prized has a deep emerald-green color.

Table 20.2 Properties of Diamond and Diamond Imitations

Material	RI*	Disp†	Opt.‡	G§	H
Diamond	2.42	0.044	I	3.52	10
Rutile (syn.)	2.75±	0.33	A	4.26	6
Strontium titanate‖	2.41	0.19	I	5.13	$5\frac{1}{2}$
Cubic zirconia‖	2.16	0.06	I	5.9±	8
GGG‖	1.97	0.038	I	7.02	7
Zircon	1.95±	0.039	A	4.70	7+
YAG‖	1.83	0.028	I	4.55	8+
Sapphire (nat., syn.)	1.77	0.018	A	4.02	9
Spinel (syn.)	1.73±	0.020	I	3.64	8
Topaz	1.62±	0.014	A	3.5±	8
Beryl	1.58±	0.014	A	2.70	8
Quartz	1.55	0.013	A	2.65	7

*RI is average refractive index; ± indicates a variation greater than 0.01.
†Disp. is dispersion
‡Opt. I, isotropic; A, anisotropic.
§G is average specific gravity; ± indicates a variation of 0.1 or greater.
‖ Manufactured materials without natural counterparts.

White jadeite has been dyed the color of this "imperial" jade. Under magnification, the color can be seen distributed along veinlets and grain boundaries.

Imitation. Several minerals have been used as jade substitutes, some of which closely resemble true jade. These include massive green vesuvianite, *californite*; massive grossular garnet; and particularly *bowenite*, a translucent yellow-green serpentine. Other substitutes, more easily distinguished because of low hardness, are *pseudophite*, a massive form of chlorite; *agalmatolite*, a compact talc or pyrophyllite; and *verdite*, a green rock containing a chrome-bearing muscovite.

OPAL

Synthesis. The determination in 1964 that opal is made up of close-packed silica spheres (page 25) pointed the way to its eventual synthesis. By developing a process that would closely duplicate this "structure," Pierre Gilson produced synthetic opal in 1974. These synthetics have chemical and physical properties, including a play of color, that are essentially identical to those of natural precious opal. Detection of the synthetic product is difficult. Under magnification in transmitted light, however, synthetic opal shows a mosaic structure not seen in natural opal.

Treatment. A play of color can be induced in some opals by immersing them in water, which apparently fills voids between the spheres. But as the water slowly leaves, so does the color effect. In such an opal, the play of color is retained if it is impregnated with paraffin or plastic.

Imitation. A material simulating opal is basically a glass with included platelets from which emanate color flashes. It can be distinguished from opal by its greater refractive index (1.49–1.51) and specific gravity (2.41–2.50). In addition, it has lower water content (natural opals have 5% to 15% H_2O) and typically contains zirconium. A realistic opal imitation is made of plastic spheres embedded in a plastic matrix, but it has much lower hardness and specific gravity than does opal.

QUARTZ

Synthesis. The many efforts to synthesize quartz during and immediately following World War II met with success in 1947, when optical grade crystals large enough for scientific uses were grown by the hydrothermal method. Since then, increasingly large amounts have been produced each year, with an estimated world production today of more than 700 tons! Most of this quartz is colorless and used for technological purposes. But colored quartz is also synthesized, duplicating the natural colors of citrine, amethyst, and smoky quartz. Other synthetic crystals are grown in colors in which natural quartz does not occur, for example, dark green and deep blue. If not of an unusual color, it is difficult if not impossible to distinguish synthetic from natural quartz in a cut stone.

Because it is general practice in quartz synthesis to use seed plates cut from single, untwinned crystals, the resulting synthetic product is also in single, untwinned crystals. Although natural citrine and amethyst gems may be single crystals, they are commonly twinned according to the Brazil law (optical twinning). Thus, the presence of this twinning in a gemstone points to a natural origin.

Treatment. Most colorless quartz, natural and synthetic, will turn smoky on irradiation but, on heating, again becomes colorless. With heat treatment,

amethyst usually becomes an orange-brown citrine but some turn green. In either case, the violet amethyst color returns on irradiation.

Dyed Microcrystalline Quartz. Although agate and other types of chalcedony occur in several natural colors, much of this material used for ornamental purposes has been dyed. Depending on the dye, a gray to white agate may be rendered black or colored red, pink, yellow, blue, purple, or brown. Chert dyed the blue color of lapis lazuli has been sold under the name of "Swiss lapis."

RUTILE

Although natural rutile is too dark to be used as a gem, synthetic rutile of gem quality has been produced by the Verneuil process since 1947. The boules as grown are black, but on annealing in oxygen, become transparent and pale yellow. When first made, synthetic rutile was a popular diamond substitute, but it is little used today. With its high refractive index (average 2.75) and extremely high dispersion (0.33), it outshines diamond and is easily detected. Furthermore, its high birefringence (0.287) causes a pronounced doubling of the back facets, giving a "fuzzy" appearance to cut stones.

SPINEL

Synthetic spinel is made by the Verneuil process in a variety of colors not found in the mineral and, as such, is used more to imitate other gems than to simulate natural spinel. Most commonly it is colorless or blue to imitate diamond, blue sapphire, and aquamarine. Different shades of green imitate tourmaline, peridot, emerald, and chrysoberyl. Alexandrite-colored synthetic spinel is used to simulate alexandrite, and a cloudy form makes a rather convincing imitation of moonstone.

Synthetic spinel has the curved striations and gas bubbles characteristic of Verneuil-grown crystals. Its refractive index (1.73) and specific gravity (3.64) are both slightly greater than of natural spinel, which are respectively 1.72 and 3.60.

TURQUOISE

Synthesis. Synthetic turquoise was introduced to the gem market in 1972 by Pierre Gilson as Gilson-created Turquoise. It is of a fine color and made both with and without "matrix," but the method of manufacture has not been revealed.

Treatment. Natural turquoise may be impregnated with oil, paraffin, or plastic to enhance its color and increase its hardness. Such treatment can usually be detected by touching the material with a red-hot needle.

Imitation. Glass, dyed chalcedony or chert, enamel, and plastic are used to imitate turquoise. Powdered turquoise, when compacted and bonded with plastic, forms a realistic imitation of the naturally massive material. When scratched with a knife, such impregnated turquoise tends to cut rather than to powder.

MANUFACTURED GEM MATERIALS WITHOUT NATURAL COUNTERPARTS

These manufactured materials that do not duplicate gem minerals are used primarily as diamond substitutes, although colored varieties of some make attractive cut stones in their own right. Included with them is, paradoxically, the mineral name *garnet*. It seems appropriate to do this because manufactured "garnets" differ both chemically and physically from natural garnets.

GARNET

The chemical composition of garnet is expressed by the general structural formula, $A_3B_2(SiO_4)_3$. Several different ions may occupy both the *A* and *B* sites, giving rise to a wide range in chemical composition. In synthetic garnets the general structure is preserved, but unusual elements substitute in the *A* and *B* sites, and the silicon site may be occupied by aluminum or gallium. The synthetic "garnets" used as diamond imitations are rare earth compounds and usually are designated by the abbreviations "YAG" and "GGG," reflecting the elements present.

YAG is yttrium aluminum "garnet," $Y_3Al_2(AlO_4)_3$. It is isometric with the following properties: **H** 8+, **G** 4.55, **RI** 1.833, disp. 0.028. In addition to colorless material, YAG is produced in red, yellow, green, and blue colors.

GGG is gadolinium gallium "garnet," $Gd_3Ga_2(GaO_4)_3$. It is isometric with the following properties; **H** $6\frac{1}{2}$, **G** 7.05, **RI** 1.97, disp. 0.038. Because of its higher refractive index and dispersion, GGG is a more impressive diamond substitute than YAG. Both YAG and GGG are produced by flux-growth and Czochralski techniques.

STRONTIUM TITANATE—$SrTiO_3$

Strontium titanate has been produced since 1955 by the Verneuil process. The boules as they come from the furnace are black due to a deficiency of oxygen, but on annealing in an oxygen atmosphere, they become quite colorless. Strontium titanate is isometric, with

H $5\frac{1}{2}$ and **G** 5.13. The **RI** is 2.41, only slightly below that of diamond (2.42); but the dispersion, 0.19, over four times that of diamond (0.044), gives the faceted stone an excessive fire. Furthermore, because of the low hardness, polishing scratches and rounded facet junctions are usually present.

CUBIC ZIRCONIA

Since its introduction to the gem market in 1976, cubic zirconia, sometimes abbreviated CZ, has become the most important diamond simulant. It is isometric and has the following properties: **H** 8, **G** 5.9±, **RI** 2.16±, disp. 0.06. On consideration of these properties, it becomes immediately apparent why CZ is the most convincing diamond substitute. Because of its high hardness, it takes a good polish and resists scratching. The high refractive index produces a brilliance approaching that of diamond, and the dispersion, although high, is not excessive.

A unique type of melt growth called "skull melting" has been devised for the manufacture of cubic zirconia; the melting point of ZrO_2 (2750°C) is so high that conventional crucibles cannot be used. The "skull" is a container that is open at the top with a cylindrical wall composed of closely spaced, vertical fingers of water-cooled copper tubes. The material to be melted is placed in the "skull," which remains relatively cool while, by use of a radio frequency generator, the central material is brought to the necessary temperature and melts within a shell of its own powder. On cooling, crystals grow upward from the bottom as CZ, the isometric polymorph of zirconia. To prevent the crystals from inverting to the low-temperature monoclinic form on further cooling, a stabilizer of yttrium oxide or calcium oxide is added to the ZrO_2 powder to be melted. The refractive index and specific gravity vary with the kind and amount of stabilizer.

REFERENCES AND FURTHER READING

Anderson, B. W. 1990. *Gem testing.* 10th ed. Butterworth & Co., London.

Arem, J. E. 1987. *Color encyclopedia of gemstones*, 2nd ed. Van Nostrand Reinhold, New York.

Branson, O. T. 1976. *Turquoise, the gem of the centuries.* Treasure Chest Publications, Inc., Tucson, Arizona.

Gübelin, E. J., and J. I. Koivula. 1986. *Photoatlas of inclusions in gemstones.* ABC Edition, Zurich.

Harlow, G. E. (ed). 1998. *The nature of diamonds.* Cambridge University Press, Cambridge.

Hurlbut, C. S., Jr., and R. C. Kammerling. 1991. *Gemology.* Wiley, New York.

Keller, P. 1990. *Gemstones and their origins.* Van Nostrand Reinhold, New York.

Liddicoat, R. T. 1989. *Handbook of gem identification.* 12th ed. Gemological Institute of America, Santa Monica, California.

Nassau, K. 1980. *Gems made by man.* Gemological Institute of America, Santa Monica, California.

Schumann, W. 1997. *Gemstones of the world.* Rev. and expanded edition. Sterling Publishing Co., New York.

Sinkankas, J. 1959, 1976. *Gemstones of North America*, v. 1, 2. Van Nostrand Reinhold, New York.

Ward, F. 1993. *Diamonds.* Gem Book Publishers, Bethesda, Maryland.

———. 1993. *Emeralds.* Gem Book Publishers, Bethesda, Maryland.

———. 2001. *Jade.* Gem Book Publishers, Bethesda, Maryland.

Webster, R. 1994. *Gems.* 5th ed. Butterworth & Co., London.

CHAPTER 21

Mineral Assemblages: Introduction to Rock Types

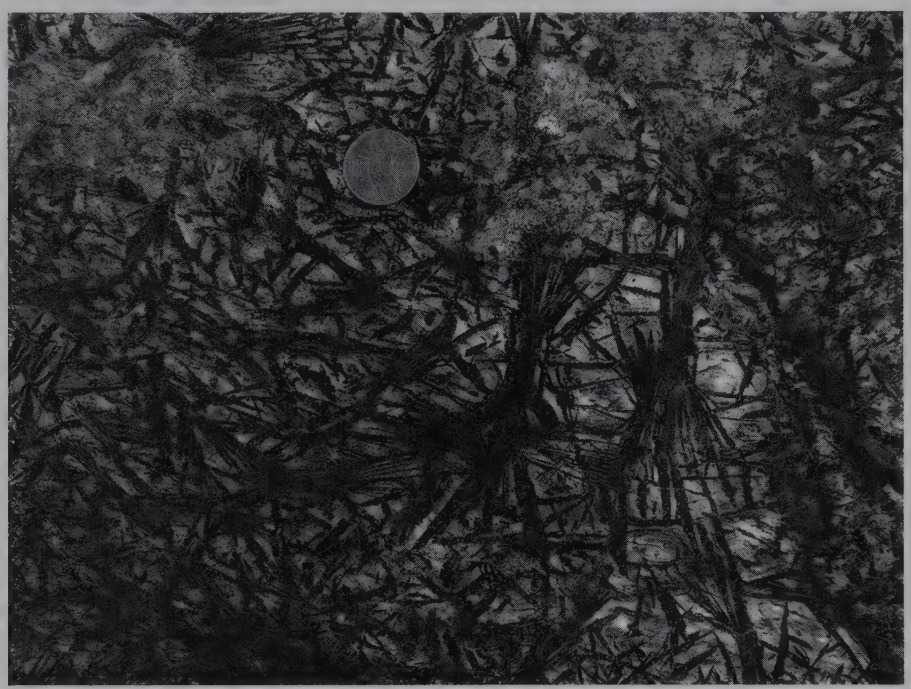

Outcrop photograph of a garbenschiefer (a German rock term meaning a schist with a sheaf-like texture*) consisting of radiating bundles of dark green hornblende in a fine-grained matrix of muscovite and plagioclase. Scale is indicated by the coin, about 15 mm in diameter. From the Stillup Valley, Austria. (Photograph courtesy of Jane Selverstone, University of New Mexico, Albuquerque).*

In most mineralogy (mineral science) courses, the mineral specimens that were chosen for study are mainly monomineralic (meaning, consisting of a single mineral). Such specimens are best suited for the evaluation and study of their physical properties. All these single-mineral specimens were specifically selected from rock types that most commonly contain several minerals. Indeed, most rocks consist of many more minerals than just one. These groupings of minerals are also referred to as the mineral assemblage. Such mineral assemblages reflect the environment of formation and commonly can be used as a diagnostic tool. That is, specific mineral assemblages are diagnostic of specific rock types. Minerals that occur in the same environment are related—this is one of the criteria for classifying minerals in the current scheme.

Rocks can be divided into three primary groups: igneous, sedimentary, and metamorphic. Igneous rocks crystallize from a magma; sedimentary rocks form from the consolidation of chemical or mechanical sediments at low pressures and temperatures; and metamorphic rocks form from pre-existing rocks due to recrystallization in the solid state at temperatures and pressures in the range between igneous and sedimentary rocks. A brief overview of the most common varieties of rock types, as well as a cursory discussion of the origins of the various rocks, provides the mineralogist with an introduction to the closely related field of petrology (the study of rocks).

Petrology requires identification of individual minerals in a rock, their textures, compositions, abundances, and grain sizes. This information is fundamental to understanding the origin of the rock, its classification, subsequent modifications, and its relationship to the tectonic environment in which it formed. A petrologist must have a strong background in mineralogy and mineral identification. In addition, he (or she) must be conversant with processes associated with the origin of rocks and with experimental studies that elucidate their temperature stability range.

IGNEOUS ROCKS

Igneous rocks make up approximately 95% of the upper 16 km of the Earth's crust. However, their great abundance is hidden on the Earth's surface by a relatively thin but widespread layer of sedimentary and metamorphic rocks. Igneous rocks have crystallized from a silicate melt, known as a **magma**. The temperatures (about 600° to 1400°C) necessary to generate magmas, concluded from laboratory experiments and from active volcanoes, suggest that their source lies within the Earth. A magma is principally made up of O, Si, Al, Fe, Ca, Mg, Na, and K, but it also contains considerable amounts of H_2O and CO_2 as well as lesser gaseous components, such as H_2S, HCl, CH_4, and CO. As a magma cools, there is a definite order of crystallization of the various mineral constituents, as a function of bulk composition. In a magma consisting mainly of O, Si, Mg, and Fe, for example, the mineral with the highest melting point, Mg-rich olivine, Mg_2SiO_4, crystallizes first, followed by more Fe-rich olivines approaching fayalite, Fe_2SiO_4 (see Figs. 11.6a and 19.2). In a magma of the appropriate composition for pyroxene crystallization, the Mg-rich ortho- and clinopyroxenes (Fig. 18.15), such as enstatite and diopsidic augite, would crystallize before hedenbergite and Fe-rich orthopyroxenes that have lower relative melting points. In magmas rich in the plagioclase component (Figs. 11.6b, 18.54 and 18.56) the An-rich plagioclases will crystallize before the Ab-rich members. All of the previously mentioned crystallization sequences are the result of **continuous reactions** that take place under equilibrium conditions between the melt and the precipitated crystals as a function of decreasing temperature. If chemical equilibrium is not maintained between melt and crystals during cooling, the resulting crystals may show *compositional zoning*. This is especially common in the plagioclase feldspars and in members of the pyroxene series. Igneous rocks also illustrate **discontinuous reactions** that occur at fairly definite temperatures in contrast to those that take place over a range of temperatures such as continuous reactions. In igneous rocks of appropriate bulk composition, it is common to find early-formed olivine crystals rimmed by later orthopyroxenes.

Early-formed crystals produced in a cooling melt may separate from the liquid by gravitational settling or may be removed from the melt by tectonic deformation. Therefore, the crystals may not remain in equilibrium with the melt from which they crystallized and systematic changes will occur in the bulk composition of the remaining (residual) magma.

The continuous and discontinuous reactions as well as separation of magma and crystals lead to what is known as **magmatic differentiation**. This concept was first developed by N. L. Bowen on the basis of his studies of the textures and mineralogical constituents of many igneous rock types and his correlative experimental studies. Mg–Fe-rich igneous silicates constitute a series of mineral groups that are related to each other by discontinuous reactions. For example, early-formed olivine may be rimmed by pyroxene; amphiboles form at the expense of the pyroxene rims; and biotite may form as a reaction product of the earlier crystallized amphiboles. On the other hand, members of the plagioclase feldspar series represent a continuous reaction series in which An-rich plagioclase crystallizes early from the melt, enriching the residual melt in alkalies (Na and K). This leads to chemical differentiation of the melt and the production of more Na-rich feldspars. Fig. 21.1 illustrates schematically what is known as **Bowen's reaction series**. As a magma of basaltic composition cools, olivine and An-rich plagioclase may crystallize first. If these minerals remain in contact with the magma they tend to form pyroxene and more Ab-rich plagioclase and the resulting rock will be a gabbro or a basalt. If, however, the bulk of the early olivine and An-rich plagioclase is removed, by crystal settling, the bulk composition of the remaining melt will tend to become enriched in Si, Al, Fe^{2+}, alkalies and H_2O and CO_2. Such a melt could produce a mineral assemblage consisting mainly of amphiboles, some mica, alkali feldspar, and SiO_2. It should be noted in Fig. 21.1 that amphiboles, micas, alkali feldspars, and quartz are relatively low-temperature, late stage crystallization products. The various processes that cause magmatic differentiation produce a large variety of igneous rocks from a common parent magma. These rocks also exhibit a wide variety of textures. The texture of a rock refers to its degree of crystallinity, its grain size, and the geometric and spatial relationships between various constituents of the rock.

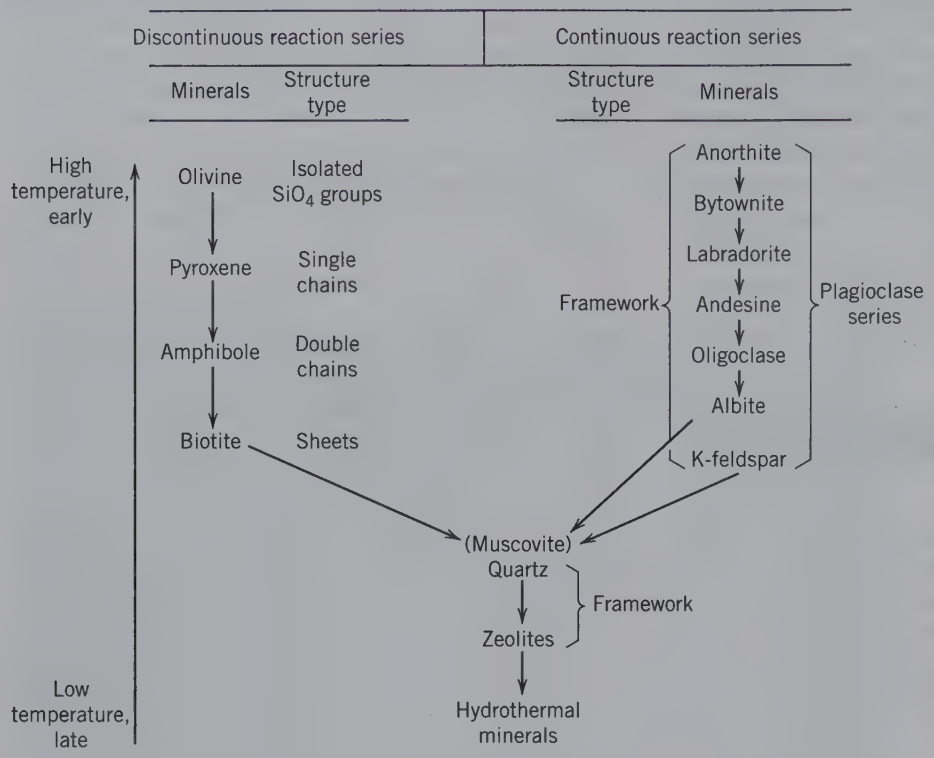

FIG. 21.1 Bowen's reaction series, relating changes in mineral groups (in discontinuous reactions) and changes in mineral composition (in continuous reactions) to a general decrease in temperature during the crystallization of a cooling magma.

GENERAL OCCURRENCE AND TEXTURE

There are two major types of igneous rocks, **extrusive** and **intrusive**. The first group includes those igneous rocks that reached the Earth's surface in a molten or partly molten state. Modern volcanoes produce lava flows that pour from a vent or fracture in the Earth's crust. Such extrusive or **volcanic** rocks tend to cool and crystallize rapidly with the result that their grain size is generally small. If the cooling has been so rapid as to prevent the formation of even small crystals of the mineral constituents, the resulting rock may be a **glass**. (A glass lacks long-range crystalline order.) Ordinarily, the mineral constituents of fine-grained extrusive rocks can be determined only by microscopic examination of thin sections of the rocks (see Chapter 13). **Intrusive** or **plutonic** rocks are the result of crystallization from a magma that did not reach the Earth's surface. Magmatic intrusions that are discordant with the surrounding country rock are referred to as **batholiths** (very large) or **plutons**, depending on their size and shape; when the intrusive is tabular and concordant it is known as a **sill**. A magma that is deeply buried in the Earth's crust generally cools slowly and the crystallizing minerals have time to grow to considerable size (mm-cm), giving the rock a medium- to coarse-grained texture. The mineral grains in such rocks can generally be identified with the naked eye. When a magma intrudes in **dikes** (discordant tabular bodies) the textures are usually finer grained than those of plutonic rocks but coarser than those of volcanic rocks; these rocks of intermediate grain size are known as **hypabyssal**.

Some igneous rocks have a bimodal distribution of grain size. Large crystals of some minerals are embedded in a much finer-grained matrix. The larger crystals are *phenocrysts*, and the finer-grained material is the *groundmass* (see Fig. 19.80). Such rocks are known as **porphyries**. The phenocrysts vary in size from a centimeter or more across down to millimeters. The groundmass may be composed of fairly coarse-grained material, or its grains may be microscopic. The difference in size between the phenocrysts and the particles of the groundmass is the distinguishing feature of a porphyry. The porphyritic texture develops in a two stage process. Some of the crystals grow to considerable size before being incorporated into the main mass of the magma prior to emplacement or eruption. Any of the types of igneous rocks described may have a porphyritic variety, such as *granite porphyry*, *diorite porphyry*, *rhyolite porphyry*. Porphyritic varieties are most common in volcanic rocks, especially in the more Si-rich types.

CHEMICAL COMPOSITION

The chemical bulk compositions of igneous rocks exhibit a limited range. The largest oxide component, SiO_2, ranges from about 40 to 75 weight percent in common igneous rock types (see Table 21.1 and Fig.

Table 21.1 Average Chemical Composition of Some Igneous Rocks*

Oxide	Nepheline syenite	Syenite	Granite	Tonalite	Diorite	Gabbro	Periodotite	Dunite
SiO_2	54.83	59.41	72.08	66.15	51.86	48.36	43.54	40.16
TiO_2	0.39	0.83	0.37	0.62	1.50	1.32	0.81	0.20
Al_2O_3	22.63	17.12	13.86	15.56	16.40	16.84	3.99	0.84
Fe_2O_3	1.56	2.19	0.86	1.36	2.73	2.55	2.51	1.88
FeO	3.45	2.83	1.67	3.42	6.97	7.92	9.84	11.87
MnO	trace	0.08	0.06	0.08	0.18	0.18	0.21	0.21
MgO	trace	2.02	0.52	1.94	6.12	8.06	34.02	43.16
CaO	1.94	4.06	1.33	4.65	8.40	11.07	3.46	0.75
Na_2O	10.63	3.92	3.08	3.90	3.36	2.26	0.56	0.31
K_2O	4.16	6.53	5.46	1.42	1.33	0.56	0.25	0.14
H_2O	0.18	0.63	0.53	0.69	0.80	0.64	0.76	0.44
P_2O_5	—	0.38	0.18	0.21	0.35	0.24	0.05	0.04
Total	99.77	100.00	100.00	100.00	100.00	100.00	100.00	100.00

*All analyses except the nepheline syenite from Nockolds, S. R. 1954. *Geological Society of American Bulletin*, v. 65, 1007–1032.

21.2). Al_2O_3 ranges from about 10 to 20 weight percent (except for peridotite and dunite, Table 21.1) and each of the other major components generally does not exceed 10 weight percent (except MgO in periodite and dunite, see Table 21.1).

When the magma is low in SiO_2, the resulting rocks will contain mainly silica-poor minerals, such as olivine, pyroxene, hornblende, or biotite and little or no free SiO_2 (i.e., quartz, cristobalite, tridymite; Figs. 21.2 and 21.3). These rocks, which tend to be dark because of their high percentage of ferromagnesian minerals, are known as **mafic** rock types. When the melt is poor in SiO_2 (*subsiliceous*, or silica undersaturated) and high in alkalies and Al_2O_3 (as in a nepheline syenite composition,

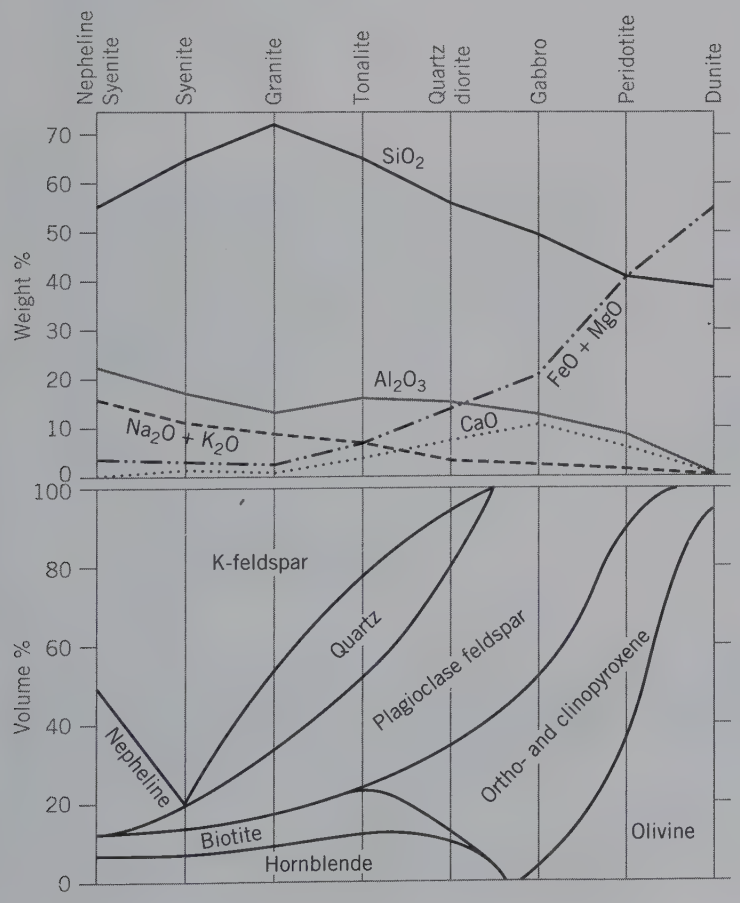

FIG. 21.2 Relationships of variation in chemical and mineral compositions in igneous rocks.

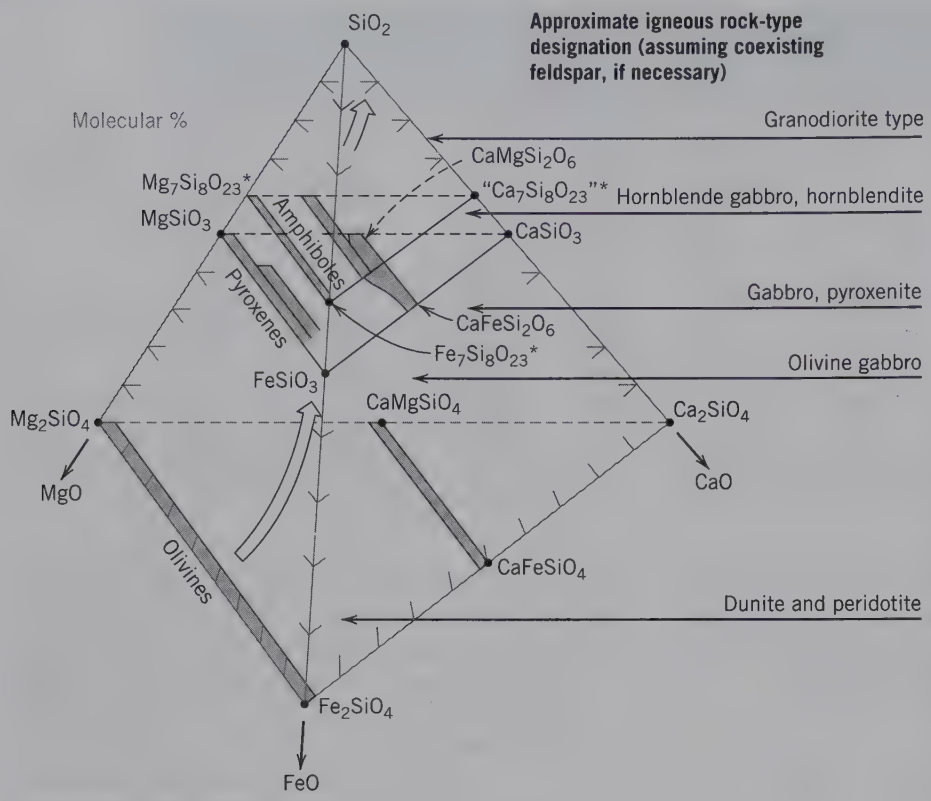

*amphiboles, in this anhydrous systems, are represented by anhydrous formulae, in which 2(OH) are replaced by one oxygen, (e.g., $Mg_7Si_8O_{22}(OH)_2$ becomes $Mg_7Si_8O_{23}$).

FIG. 21.3 End-member compositions, and approximate extents of solid solution in major mafic mineral groups, in terms of molecular percentages of SiO_2, MgO, FeO, and CaO. The triangular diagrams for olivines, pyroxenes, and amphiboles are equivalent to those given in Figs. 19.1, 18.15, and 18.21, respectively). In this representation all compositions are given as anhydrous; in the amphiboles $2(OH)^{1-}$ are replaced by one oxygen, O^{2-}, for reasons of charge balance.

The large arrow inside the tetrahedron shows the general, discontinuous progression in mafic silicate groups from subsiliceous to more SiO_2-rich (compare with Fig. 21.1). Some igneous rock types, on the right of the tetrahedron, are correlated with approximate bulk compositions at various heights above the base of the tetrahedron.

Table 21.1) the resultant crystallization products will contain SiO_2-poor minerals, such as feldspathoids and will lack free SiO_2 as quartz (Figs. 21.2 and 21.4). Crystallization of a melt high in SiO_2 (silica oversaturated) results in rocks with abundant quartz and alkali feldspars, with or without muscovite, and only minor amounts of ferromagnesian minerals. Such rock types are referred to as **felsic** (alkali feldspar-rich) or **silicic**, and are lighter in overall color than mafic rocks. In general, the darker the rock the greater the abundance of ferromagnesian minerals, and the lighter the rock the greater the abundance of quartz, or feldspars, or feldspathoids.

CLASSIFICATION

Because of considerable variation in magmas both in chemistry and in conditions of crystallization, igneous rock types show a wide variation in mineralogy and texture. There is a complete gradation from one rock type into another so the names of igneous rocks, and the boundaries between types, are largely arbitrary (Figs. 21.2 and 21.5).

FIG. 21.4 Feldspar and feldspathoid compositions in the system SiO_2 (quartz)–$NaAlSiO_4$ (nepheline)–$KAlSiO_4$ (kalsilite)–$CaAl_2O_4$. Bars and fields indicate average extent of solid solution. A melt of composition x_1 (*silica oversaturated*) would produce a quartz-feldspar assemblage; a melt of x_2 composition (*silica saturated*) and lying in the feldspar plane would produce only feldspars, and a melt of composition x_3 (*silica undersaturated*) would produce feldspar–feldspathoid assemblages.

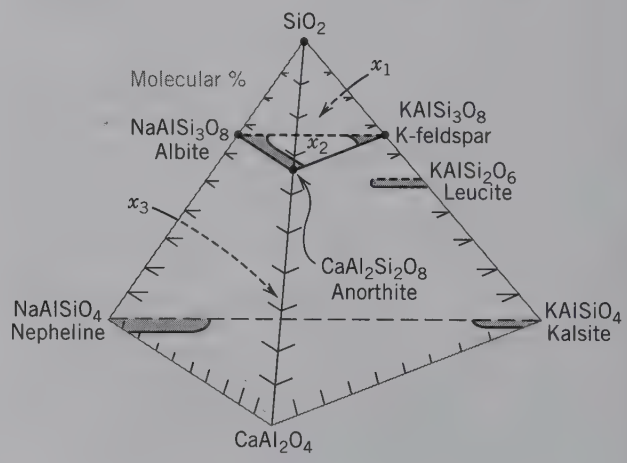

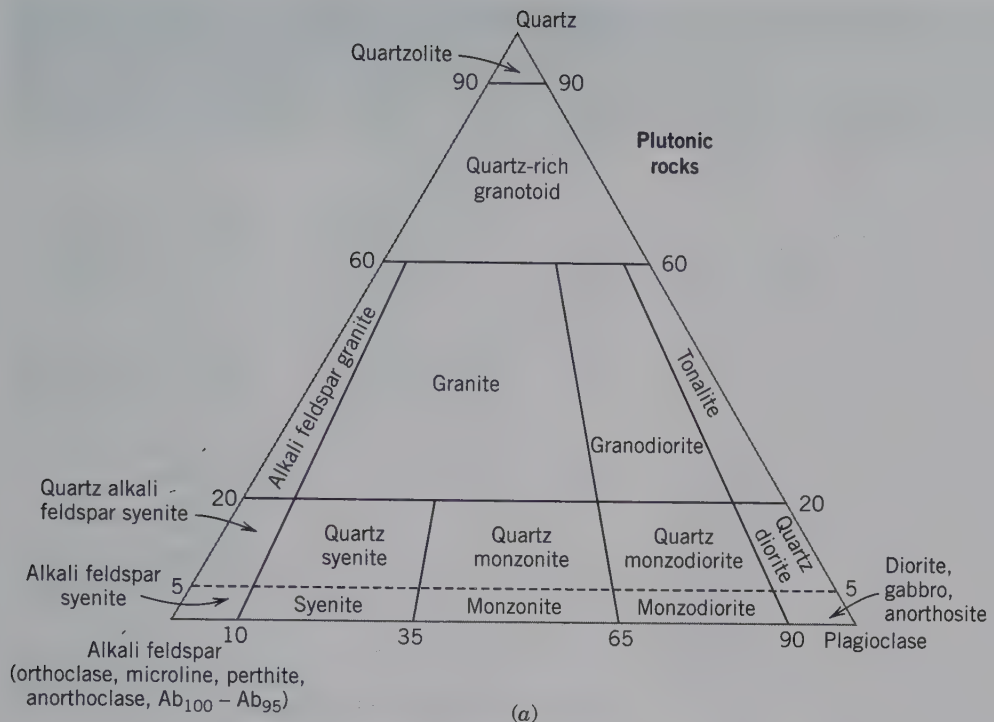

(*a*)

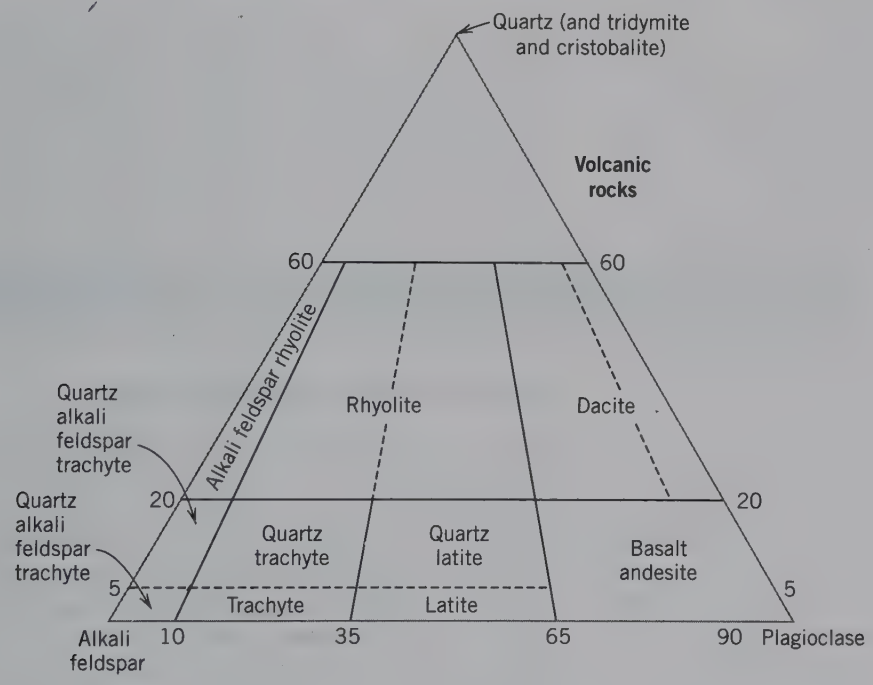

(*b*)

FIG. 21.5 General classification and nomenclature of some common plutonic rock types (a) and some common volcanic rock types (b). This classification is based on the relative percentages of quartz, alkali feldspar, and plagioclase, measured in volume percent. (Adapted from Subcommission on the Systematics of Igneous Rocks. 2002, and Hyndman, D. W. 1972. *Petrology of igneous and metamorphic rocks.* McGraw-Hill Book Co., New York, 35.)

Table 21.2 Simplified Classification of the Igneous Rocks

	Quartz > 5%		No Quartz; No Feldspathoids		Nepheline or Leucite > 5%	
Feldspar	Coarse	Fine	Coarse	Fine	Coarse	Fine
K-feldspar* > plagioclase	Granite	Rhyolite	Syenite	Trachyte	Foid syenite	Phonolite
					Foid monzosyenite	Tephritic phonolite
Plagioclase> K-feldspar	Granodiorite	Dacite	Monzonite	Latite	Foid monzodiorite	Phonolitic basanite (olivine > 10%)
Plagioclase (oligoclase or andesine)	Tonalite	Dacite	Monzodiorite	Andesite basalt	Foid monzogabbro	Phonolitic tephrite (olivine < 10%)
Plagioclase (labradorite) to anorthite)	Quartz diorite	Andesite	Gabbro	Basalt	Foid diorite Foid gabbro	Basanite (olivine > 10%) Tephrite (olivine < 10%)
No feldspar			Peridotite (olivine dominant) Pyroxenite (pyroxene dominant) Hornblendite (hornblende dominant)		Ijolite	Nephelinite (– olivine) Nepheline basalt (+ olivine)

*K-feldspar includes orthoclase, microcline, and microperthite; in high *T* volcanic rocks it can be sanidine or anorthoclase.

Many schemes have been proposed for the classification of igneous rocks, but the most practical is based on mineralogy and texture. In general, four criteria are to be considered in classifying an igneous rock. (1) The relative amount of silica; quartz (or tridymite, or cristobalite) indicates an excess of silica; feldspathoids indicate a deficiency of silica. (2) The kinds of feldspar (alkali feldspar versus plagioclase) and the relative amount of each kind. (3) The relative amount and type of dark (ferromagnesian) minerals. (4) The texture or size of the grains. Is the rock coarse- or fine-grained; that is, is it plutonic or volcanic?

The exact determination of the kind of feldspar or a correct estimate of the amount of each kind is impossible in the field or in the hand specimen. It is also impossible in many fine-grained rocks to recognize individual minerals. Such precise work must be left for the laboratory and carried out by the microscopic examination of thin sections of rocks (refer to Chapter 13). Nevertheless, it is important that the basis for the general classification be understood in order that a simplified field classification have more meaning.

Three major divisions may be made on the basis of the silica content (Fig. 21.4). (1) Quartz present in amounts greater than 5% (silica oversaturated). (2) No quartz and no feldspathoids present (silica saturated). (3) Feldspathoids in amounts greater than 5% (silica undersaturated). The above divisions made on the basis of silica content are further subdivided according to the kind and amount (or the absence) of feldspar. Most of the rocks classified have a coarse- and fine-grained variety, which receive different names. Figure 21.5 illustrates the classification of the principal plutonic and volcanic rock types. Table 21.2 gives examples of the principal rock types according to such a classification. Although these rock names are the most important, more than 600 have been proposed to indicate specific types of igneous rocks.

MINERALOGICAL COMPOSITION

Many minerals are found in the igneous rocks, but those called *rock-forming minerals* are comparatively few. Table 21.3, which lists the major mineral constituents of igneous rocks, is divided into two parts: (1) the common rock-forming minerals of igneous rocks, and (2) the accessory minerals of igneous rocks. See Table 21.4 for a listing of common mineral assemblages in some plutonic rocks and Table 21.5 for a volume percentage listing of mineral constituents in some common plutonic rock types.

PLUTONIC ROCKS

Granite–Granodiorite. Granite is a granular rock of light color and even texture consisting primarily of feldspar and quartz (see also Box 19.1). Usually both K-feldspar and oligoclase (or albite) are present;

Table 21.3 Mineralogy of Igneous Rocks

Common Rock-Forming Minerals	Common Accessory Minerals
Quartz, tridymite, cristobalite	Zircon
Feldspars	Titanite
Orthoclase	Magnetite
Microcline	Ilmenite
Sanidine	Hematite
Plagioclase	Apatite
Nepheline	Pyrite
Sodalite	Rutile
Leucite	Tourmaline
Micas	Monazite
Muscovite	Garnet
Biotite	
Phlogopite	
Pyroxenes	
Augite	
Orthopyroxene	
Aegirine	
Amphiboles	
Hornblende	
Arfvedsonite	
Riebeckite	
Olivine	

K-feldspar may be flesh-colored or red, whereas oligoclase (or albite) is commonly white and can be recognized by the presence of albite twinning striations. The quartz can be recognized by its glassy luster and lack of cleavage. Granites usually carry a small amount (about 8%) of mica or hornblende. The mica is commonly biotite, but muscovite may also be present. The minor accessory minerals are zircon, titanite, apatite, magnetite, ilmenite and/or tourmaline. Figure 21.6 illustrates the liquidus diagram for the hydrous granite system, $NaAlSi_3O_8$–$KAlSi_3O_8$–SiO_2–H_2O, with a temperature minimum of about 770°C in the central part of a low-temperature trough between the liquidus fields of K–Na feldspar solid solutions and high quartz. When the mineral compositions of hundreds of granites are expressed in terms of percentages of albite, K-feldspar, and quartz, they can be plotted on Fig. 21.6. The distribution of the resulting data points represents the residual melt compositions from which the granites formed during their crystallization history. These melt compositions coincide broadly with the experimentally determined region of minimum temperature, between 860° and 770°C. Many granites, therefore, are concluded to be the result of crystallization from melts at these temperatures.

There is a complete series grading from granite, with feldspar almost entirely the K-rich varieties, to granodiorite with feldspar mostly plagioclase and only slightly more than 10% K-feldspar. The boundary between the two types is arbitrarily set. Granites are those rocks in which K-feldspar generally exceeds plagioclase; granodiorites are those in which plagioclase exceeds K-feldspar. In most instances, as the plagioclase increases in amount, the percentage of dark minerals also increases. Thus, in general, granodiorites are darker than granites. However, in the field or in a hand

Table 21.4 Typical Mineral Assemblages of Some Plutonic Rocks (See also Table 21.5)

	Major Constituents (> 10%)	Minor Constituents (each < 10%)
Granite	mc (often perthitic) + Ab (or olg) + qtz	bt, ms, hbl, mt, zrc, ap, ttn, tur
Granodiorite	ads + kfs + qtz + hbl	bt, ttn, ap, mt
Syenite	mc + Ab (or olg)	qtz, bt, hbl, ttn, ap, zrc
Nepheline syenite	or + ne	ab, aeg, arf, sod, ap, zrc, ttn
Monzonite	pl + or + aug	hbl, qtz, bt, mt, ap, ttn
Diorite	olg (or ads) + hbl	bt, or, qtz, hbl, pyx, ap, zrc, mt
Gabbro	pl (An_{50}-An_{90}) + aug + opx + ol	bt, mt, sp, ilm, hbl
Norite	lab (or byt) + opx + some ol	aug, hbl, bt, ap, mt
Anorthosite	lab (~90%)	aug, hbl, bt
Peridotite	ol (Fo) + opx	hbl, chr, pl
Dunite	ol (Fo) ~90%	chr, mt, ilm, po

Abbreviations: Ab = albite, aeg = aegirine, ads = andesine, ap = apatite, arf = arfvedsonite, aug = augite, bt = biotite, byt = bytownite, chr = chromite, hbl = hornblende, ilm = ilmenite, Kfs = K-feldspar, lab = labradorite, mt = magnetite, mc = microcline, ms = muscovite, ne = nepheline, olg = oligoclase, ol = olivine, opx = orthopyroxene, or = orthoclase, pl = plagioclase, po = pyrrhotite, pyx = pyroxene, qtz = quartz, sp = spinel, sod = sodalite, ttn = titanite, tur = tourmaline, zrc = zircon (abbreviations after Kretz, 1983, Symbols for rock-forming minerals. *American Mineralogist*, 68. 277–279).

Table 21.5 Approximate Mineral Compositions of Some Plutonic Rock Types (In Volume Percent)*

	Granite	Syenite	Granodiorite	Quartz Diorite	Diorite	Gabbro	Olivine Diabase	Diabase	Dunite
Quartz	25		21	20	2				
Orthoclase and microperthite	40	72	15	6	3				
Oligoclase	26	12							
Andesine			46	56	64				
Labradorite						65	63	62	
Biotite	5	2	3	4	5	1		1	
Amphibole	1	7	13	8	12	3		1	
Orthopyroxene				1	3	6			2
Clinopyroxene		4		3	8	14	21	29	
Olivine						7	12	3	95
Magnetite	2	2	1	2	2	2	2	2	3
Ilmenite	1	1				2	2	2	
Apatite	Trace	Trace	Trace	Trace	Trace				
Titanite	Trace	Trace	1	Trace	Trace				
Color Index†	9	16	18	18	30	35	37	38	98–100

*After Larsen, E. S. 1942. *Handbook of physical constants*, Birch, F., Schairer, Y. F., and Spicer, H. C. (eds.), *Geological Society of America, Special Paper* 36, Table 1.2, 3. The percentage values are based on grain counts of minerals in a thin section using a polarizing microscope. This is known as *modal analysis*.

†Color index—a number that represents the percentage, by volume, of dark-colored (i.e., mafic) minerals in a rock.

FIG. 21.6 Isobaric equilibrium diagram for the system $NaAlSi_3O_8$–$KAlSi_3O_8$–SiO_2–H_2O projected onto the anhydrous base of the $NaAlSi_3O_8$–$KAlSi_3O_8$–SiO_2–H_2O tetrahedron. Contour lines indicate melting temperatures. Stability fields are approximately located. The shaded area in the center represents percentages of quartz, albite, and K-feldspar, as calculated for hundreds of chemically analyzed granites. (From Tuttle, O. F., and Bowen, N. L. 1958. Origin of granite in the light of experimental studies in the system $NaAlSi_3O_8$–$KAlSi_3O_8$–SiO_2–H_2O. *Geological Society of America Memoir*, 74.)

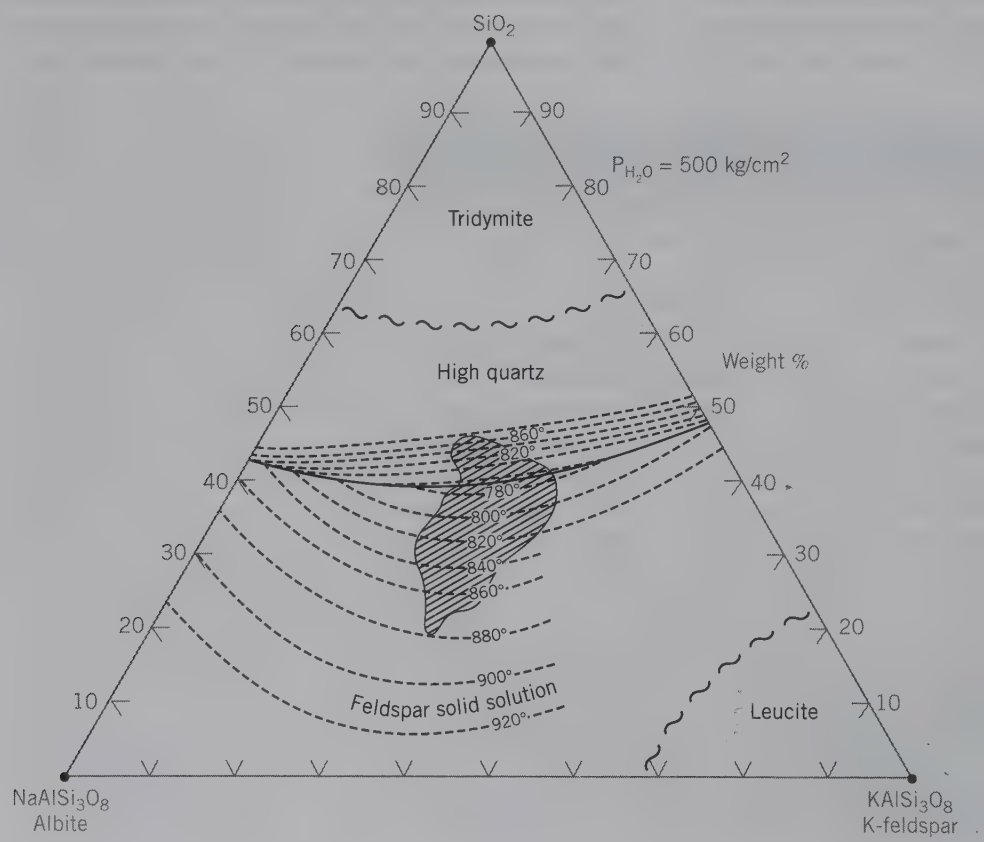

specimen, it is usually difficult to distinguish between the two rock types with certainty. As a consequence, the general term *granitoid* is used in field descriptions.

Syenite–Monzonite. A syenite is a granular rock of light color and even texture composed essentially of K-feldspar and oligoclase, with lesser amounts of hornblende, biotite, and pyroxene. It resembles granite but differs from granite in that it contains less than 5% quartz. Accessory minerals are apatite, titanite, zircon, and magnetite.

A series exists between syenite and monzonite, with increasing plagioclase content in the monzonite (Fig. 21.5). Monzonites are usually darker than syenites, because an increase in dark minerals frequently accompanies an increase in plagioclase. However, without microscopic aid, it is rarely possible to distinguish between the two types.

Nepheline is present in some syenites; if the amount exceeds 5%, the rock is called a *nepheline syenite*. The nepheline has a greasy luster and may be mistaken for quartz, but can be distinguished by its hardness ($5\frac{1}{2}$–6) and lack of transparency. Some nepheline syenites may contain sodalite; others, corundum.

Syenites in which leucite is present in amounts greater than 5% are called *leucite syenites*. The leucite can be recognized by its trapezohedral form (see Fig. 19.85). Such rocks are extremely rare.

Tonalite-Quartz Diorite. A tonalite is composed essentially of plagioclase feldspar and quartz with only minor amounts of K-feldspar (less than 5%). The plagioclase is oligoclase or andesine. Dark minerals, especially biotite and hornblende, are plentiful; pyroxene is more rarely present. Apatite, magnetite, and titanite are common accessory minerals. Although not essential to the classification, dark minerals are usually abundant, and thus, in general, tonalites are darker in color than granites; see color index at the bottom of Table 21.5.

As the plagioclase becomes more An-rich and with a lessening of the amount of quartz, tonalite grades into a *quartz–diorite* and into a *diorite*.

Diorite-Gabbro. A diorite is a granular rock characterized by plagioclase feldspar (oligoclase to andesine) but lacking quartz and K-feldspar in appreciable amounts. Hornblende is the principal dark mineral, but biotite is usually present. Pyroxenes are minor constituents. Magnetite, ilmenite, apatite, and less commonly, titanite and zircon are accessory minerals. Normally dark minerals are present in sufficient amount to give the rock a dark appearance (Table 21.5).

If the plagioclase is more calcic in composition than andesine (labradorite to anorthite), the rock is a *gabbro*. Although the distinction is made on this criterion alone, rocks with labradorite or more calcic plagioclase usually have pyroxene as the chief dark constituent, whereas the diorites with more sodic plagioclase usually have amphiboles as dark minerals. Olivine and orthopyroxene are also present in most gabbros. The association of pyroxene–olivine–An-rich plagioclase is diagnostic of the relatively high temperatures of crystallization of mafic rock types. In Fig. 11.9 forsterite and protoenstatite are shown crystallizing together from 1557°C to about 1300°C (along the crystallization path between the two fields). These temperatures are much higher than those determined for granites, for example, in Fig. 21.5. See also Fig. 21.1, which expresses these relative temperature differences qualitatively.

The name *norite* is given to a gabbro in which the pyroxene is essentially orthopyroxene; it is usually impossible to make this distinction without microscopic aid. A type of igneous rock known as *anorthosite* is composed of greater than 90% plagioclase feldspar and may, therefore, be light in color.

If amounts of nepheline in diorites and gabbros exceed 5%, the rocks are called respectively *nepheline diorite* and *nepheline gabbro*. These rocks are rare.

The term *diabase* is sometimes used to indicate a fine-grained gabbro characterized by a certain texture. This "diabasic" texture is shown microscopically to have augite filling the interstices of tabular plagioclase grains.

Peridotite. A peridotite is a granular rock composed of more than 40% olivine; feldspar is negligible (less than 5%). The minerals are chiefly pyroxene and olivine in varying proportions, but hornblende may be present. If the rock is composed of greater than 60% pyroxene, it is called a *pyroxenite*; if it is composed of greater than 90% olivine, it is called a *dunite*. The name *hornblendite* is given to a rare type of rock composed almost wholly of hornblende. Magnetite, chromite, ilmenite, and garnet are frequently associated with peridotites. Platinum is associated with chromite in some peridotites, usually dunites, whereas diamond is found in a variety of altered peridotite known as *kimberlite*.

The olivine in peridotites can be altered to the mineral serpentine. If the entire rock is altered, the name *serpentinite* is given to it (see also page 602).

VOLCANIC ROCKS

Because of their fine-grained texture, it is much more difficult to distinguish between the different types of volcanic rocks than between their plutonic equivalents in hand specimen. In the field, only an approximate classification, based primarily on whether the rock is light or dark in color, can be made. The term *felsite* is used to include the dense, fine-grained rocks of all colors except dark gray, dark green, or black.

Felsite embraces the following types described next: rhyolite, trachyte, quartz latite, latite, dacite, and andesite. Experienced petrologists may be able, by the aid of a hand lens, to discern differences in texture or mineral composition that enable them to classify these rocks, but, to the untrained observer, they frequently appear much the same.

Rhyolite is a dense, fine-grained rock, the volcanic equivalent of a granite. It is composed essentially of alkali feldspar and quartz, but much of the silica may be present as cristobalite. Phenocrysts of quartz, sanidine, and oligoclase are common. Dark minerals are not abundant, but dark brown biotite is most common. Augite and hornblende are found in some rhyolites.

Rhyolites may be uniform in appearance or may show a flow structure, giving a banded or streaked appearance to the rock. The groundmass may be partly or entirely glassy. When the rock is completely glassy and compact, it is known as *obsidian* and is usually black. *Pumice* is rhyolite glass in which expanding gas bubbles have distended the magma to form a highly vesicular material. In pumice, cavities are so numerous as to make up the bulk of the rock and give it low specific gravity.

Trachyte is the volcanic equivalent of syenite. It is composed chiefly of alkali feldspar with some dark minerals but lacks quartz. Small amounts of tridymite and cristobalite are often found in gas cavities. Phenocrysts of sanidine are frequently present and characteristically show Carlsbad twinning; phenocrysts of oligoclase, biotite, hornblende, and pyroxene are less common. Olivine may be present.

Flow banding or streaking is common in trachytes. Unlike rhyolites, glass is seldom found in the groundmass, and there are few glassy or vesicular types. The tabular feldspar frequently shows a subparallel orientation (due to flow) which is so common in trachytes that it is called *trachytic texture*.

Phonolite is the volcanic equivalent of nepheline syenite and is poorer in silica than trachyte. This is expressed mineralogically by the presence of feldspathoids. Orthoclase or sanidine is the common feldspar; albite is rarely present. Nepheline occurs in the groundmass as minute hexagonal crystals and can be observed only by microscopic aid. Sodalite and other feldspathoids may be present, usually altered to zeolites. Leucite is present in *leucite phonolite*. It is in well-formed crystals that range from microscopic sizes to a centimeter in diameter. Aegirine is the common dark mineral and normally occurs as tabular phenocrysts, but biotite may be abundant in the leucite-rich rocks. The phonolites are completely crystalline, and there are no glassy varieties.

Latite and **quartz latite** are the volcanic equivalents of monzonite and quartz monzonite, respectively. They contain about equal amounts of plagioclase and alkali feldspar. The dark minerals are primarily biotite and hornblende. The distinction between them is based on the amount of quartz present; quartz latites contain more than 5% quartz, latites less than 5% quartz. Both of these rock types occur infrequently.

Dacite is the dense volcanic equivalent of granodiorite. It contains plagioclase feldspar and quartz, both of which may occur as phenocrysts. The dark mineral is usually hornblende, but biotite is found in some varieties. Some glass may be present in the groundmass, but glassy equivalents of dacites are rare.

Andesite is the volcanic equivalent of quartz diorite and is composed chiefly of oligoclase or andesine feldspar. K-feldspar and quartz are absent or present in amounts of less than 10%. Hornblende, biotite, augite, or orthopyroxene may be present, frequently as phenocrysts. In some cases, olivine phenocrysts may be present. Andesites are usually named according to the dark mineral present, such as *hornblende andesite* or *olivine andesite*. In some andesites, the groundmass is partly glassy and in rarer types completely so.

Andesites are abundant in certain localities, notably in the Andes Mountains of South America, from which locality the rock receives its name.

Basalt is a dark-colored, fine-grained rock, the volcanic equivalent of gabbro (see also Box 19.1). Labradorite feldspar is the primary constituent of the groundmass, whereas more calcic plagioclase (bytownite or anorthite) may be present as phenocrysts. Augite and olivine are usually present; the augite is frequently found both as phenocrysts and in the groundmass, but olivine, as a rule, is only in phenocrysts. Brown hornblende and brown biotite are present in some basalts.

The groundmass of some basalts contains small amounts of interstitial glass and in rare instances is entirely glassy. Gas cavities (vesicles) near the top of basalt flows may be abundant enough to make the rock vesicular.

The presence of nepheline or leucite in basalt gives rise to the rare rock types *tephrite* and *leucite tephrite*.

Basalts are the most abundant of the volcanic rocks and form extensive lava flows in many regions; the most noted are the Columbia River flows in the western United States and the Deccan "traps" of western India. The oceanic basins are underlain by extensive flows of basaltic composition. Many of the great volcanoes, such as form the Hawaiian Islands, are built up of basaltic material. In addition to forming extrusive rock masses, basalt is widely found forming many small dikes and other intrusives.

Fragmental Igneous Rocks

During periods of igneous activity, volcanoes eject fragmental material, which accumulates and forms the *fragmental igneous rocks*, or *pyroclastic rocks*. The ejecta vary greatly in size. Rock composed of finer particles of *volcanic ash*, and *volcanic dust* is called *tuff* and can be an *airfall tuff*, or an *ashflow tuff*; that composed of coarser volcanic bombs and spatter from volcanic vents is called *agglomerate*, or *volcanic breccia*. If such rocks are waterlaid and bedded, they form a transition between the igneous and sedimentary rocks.

Pegmatites

Pegmatites are extremely coarse-grained igneous rocks that are commonly closely related genetically and in space to large masses of plutonic rocks. They are found as veins or dikes traversing igneous rocks but more commonly extend out from it into the surrounding country rock. Pegmatites are geochemically complex. They are classified, in part, on the basis of their different geochemical signatures as expressed in their mineralogical constituents. Other classifications rely on their differentiation from a parent rock and are related to the type of granite from which they were derived (see Cerný and Ercit, 2005, for details). For example, a family of pegmatites classified as NYF is characterized by high concentrations of Nb, Y, and F (in addition to Be, REEs, Sc, Ti, Zr, Th, and U) whereas LCT pegmatites are characterized by high concentrations of Li, Cs, and Ta (in addition to Rb, Be, Sn, B, P, and F). Box 19.5 provides additional discussion of pegmatites and has an illustration of their characteristically large grain size.

SEDIMENTARY ROCKS

Sedimentary rocks cover approximately 80% of the Earth's land surface, but their total contribution to the upper 16 km of the Earth's crust is estimated to be only about 5%. As such, the sedimentary sequences we see represent only a veneer over a crust, consisting mainly of igneous and metamorphic rocks.

The constituents of most sedimentary rocks are derived from the weathering of previously existing rock masses. **Chemical weathering** decomposes minerals in the rocks, and **mechanical weathering** is responsible for the physical fragmentation of the original rock. The decomposition and disintegration products are transported to, and deposited in, areas of accumulations by the action of water or, less frequently, by glacial or wind action. Such unconsolidated sediments are converted into rocks by the processes of *diagenesis* and *lithification*, which include compaction and cementation of the loose materials.

The products of *chemical* decomposition may be transported in solution by water into lakes and seas, where chemical changes (such as due to evaporation) or organisms, may cause precipitation. Upon induration, diagenesis and lithification, these chemical (or biochemical) precipitates result in *chemical sedimentary rocks* (Fig. 21.7). Such chemically deposited sediments are represented by carbonate (such as *travertine*) and evaporite sequences and finely banded sedimentary ironformations. These truly chemical sediments are also known as *orthochemical* (from the Greek word meaning *correct* or *true*) sedimentary rocks. If organisms have

FIG. 21.7 Schematic diagram for the sequence: source rock→weathering→sedimentary rock. The arrows represent processes; the boxes represent products. (Modified after Suttner, L. J., and J. Meyers. 1991. Field study of the petrology of sedimentary rocks. *Manual for geological field study of Northern Rocky Mountains.* Indiana University, Bloomington, 305–26.)

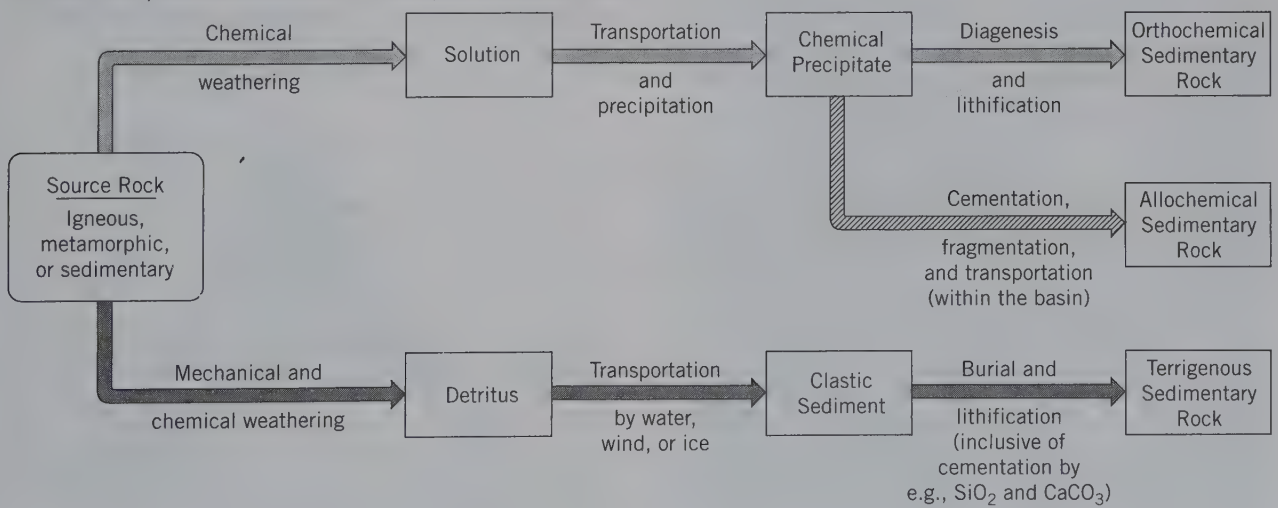

Table 21.6 Chemical Composition of Average Igneous Rock Compared with Average Compositions of Some Sedimentary Rock Types*

	Average Continental Igneous Rock	Average Sandstone	Average Shale	Average Limestone
SiO_2	59.14	78.33	58.10	5.19
TiO_2	1.05	0.25	0.65	0.06
Al_2O_3	15.34	4.77	15.40	0.81
Fe_2O_3	3.08	1.07	4.02	0.54
FeO	3.80	0.30	2.45	—
MgO	3.49	1.16	2.44	7.89
CaO	5.08	5.50	3.11	42.57
Na_2O	3.84	0.45	1.30	0.05
K_2O	3.13	1.31	3.24	0.33
H_2O	1.15	1.63	5.00	0.77
P_2O_5	0.30	0.08	0.17	0.04
CO_2	0.10	5.03	2.63	41.54
SO_3	—	0.07	0.64	0.05
C(elemental)	—	—	0.80	—
Total	99.50	99.95	99.95	99.84

*After Clarke, F. W. 1924. Data of geochemistry. *U.S. Geological Survey Bulletin*, no. 770.

caused the precipitation of the major sedimentary mineral components, or if the precipitated minerals have undergone substantial movement (and redeposition) after their crystallization, the resulting sediment is referred to as *allochemical* (from the Greek word meaning *different*). Examples of such allochemical sedimentary rocks are oolitic and fossiliferous limestone.

More generally, weathering includes both chemical decomposition and mechanical disintegration. Thus, the end-products consist of sedimentary materials that are the products of chemical as well as mechanical action. Both processes produce solid fragments and particles known as *detritus*, or clastic material. Mechanically deposited loose sediments include gravel and sand, which, upon lithification (compaction and cementation) form conglomerates and sandstones (Fig. 21.7). These sediments, with clastic textures, are known as *terrigenous* sediments. Detrital materials consist most commonly of chemically inert minerals, such as quartz, K-feldspar, garnet, zircon, rutile, and magnetite, and of rock fragments made of these minerals.

The two categories, *chemical* and *detrital*, are not exclusive because most chemical sediments contain some detrital material and most clastic rocks also carry some chemical sediment.

CHEMICAL COMPOSITION

The range in chemical compositions of igneous rocks (see Table 21.1) is generally relatively small because the crystallization sequence of a magma is governed by physiochemical and chemical principles that control the sequence of products crystallizing from the melt. In contrast, sedimentary rocks present a much larger compositional range (Table 21.6). For example, a sandstone consisting essentially of quartz grains may contain as much as 99% SiO_2; FeO + Fe_2O_3 may be as high as 58% in banded iron-formations rich in hematite and magnetite; CaO may reach 55% in limestones. This large range in compositions, illustrated in Fig. 21.8, is caused by the weathering cycle that tends to produce mechanical sediments that are compositionally different from chemical sediments.

MINERALOGICAL COMPOSITION

The minerals of sedimentary rocks can be divided into two major groups: (1) minerals that are resistant to the mechanical and chemical breakdown of the weathering cycle, and (2) minerals that are newly formed from the

FIG. 21.8 Compositional variations of common sediments. (After Mason, B., and Moore, C. B. 1982. *Principles of geochemistry*, 4th ed. John Wiley & Sons, New York.)

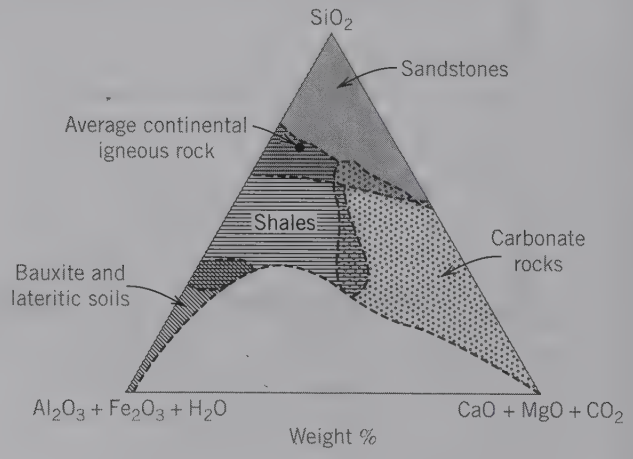

Table 21.7 Relative Stabilities of Some Rock-Forming Minerals in the Weathering Cycle

High stability	Quartz
Increasing stability	Muscovite
	K-feldspar
	Biotite
	Albite
	intermediate plagioclases
	Anorthite
	Hornblende
	Augite
Low stability	Olivine

products of chemical weathering. The relative stabilities of minerals to weathering are shown in Table 21.7. This listing means that quartz is one of the chemically and mechanically most resistant minerals, whereas olivine is easily altered chemically. The positions of minerals listed between quartz and olivine represent intermediate stabilities ("survival rates") during the weathering process. This sequence is very similar to Bowen's reaction series in reverse (see Fig. 21.1). This similarity indicates that the minerals formed at the lowest temperature in the crystallization of a melt are also the most stable at surface temperatures and pressures (atmospheric conditions).

Important chemical breakdown reactions involving high-temperature igneous (or metamorphic) minerals, as the reactants in a hydrous (weathering) environment at low temperature and pressure (atmospheric conditions), have reaction products that fall into three categories: (1) layer silicates, such as kaolinite and montmorillonite, (2) silica in solution, as H_4SiO_4, and (3) Na^+, K^+, Ca^{2+}, and Mg^{2+} ions in solution. Fe^{2+} released from the breakdown of mafic minerals, is oxidized to Fe^{3+} and is precipitated as $Fe(OH)_3$, as a precursor to goethite, or hematite. Examples of three such actions are as follows:

$$\underset{\text{augite}}{(Ca,Na)(Mg,Fe^{2+},Al)(Si,Al)_2O_6} + H_2O + H^+ \rightarrow$$

$$\text{Na- and Ca-montmorillonite} + H_2SiO_4 + Na^+ + Ca^2 + Fe(OH)_3,$$

$$3KAlSi_3O_8 + 12H_2O + 2H^+ \rightarrow$$
$$\underset{\text{orthoclase}}{} \qquad \underset{\text{muscovite}}{KAl_3Si_3O_{10}(OH)_2} + 6H_4SiO_4 + 2K^+,$$

where muscovite continues its alteration to kaolinite by the following reaction:

$$\underset{\text{muscovite}}{KAl_3Si_3O_{10}(OH)_2} + 3H_2O + 2H^+ \rightarrow$$
$$\rightarrow 3\underset{\text{kaolinite}}{Al_2Si_2O_5(OH)_4} + K^+$$

Figure 21.9 is a high-resolution transmission electron microscope (HRTEM) image of an arrested reaction in which sillimanite is giving way to kaolinite according to the following low-temperature hydration reaction:

$$\underset{\text{sillimanite}}{Al_2SiO_5} + \underset{\text{quartz}}{SiO_2} + H_2O \rightarrow \underset{\text{kaolinite}}{Al_2Si_2O_5(OH)_4}$$

Detrital sedimentary rocks consist mainly of the most resistant rock-forming minerals, quartz, K-feldspar, mica, and lesser plagioclase, as well as small amounts of garnet, zircon, tourmaline, and spinel (magnetite). The detrital rock types may be regarded as accidental, mechanical mixtures of genetically unrelated resistant minerals. For example, a feldspar-rich sandstone may contain orthoclase and microcline, as well as several members of the plagioclase series. Such a random variety of feldspar compositions is not found in igneous assemblages because of physical-chemical controls in the crystallization sequence.

Chemical sedimentary rocks that result from the inorganic or organic precipitation of minerals can be interpreted, in large part, in terms of chemical and physico-chemical principles that apply at low temperatures (25°C) and atmospheric pressure (see, for example,

FIG. 21.9 High-resolution transmission electron microscope (HRTEM) image of the arrested reaction of sillimanite (sill) altering to kaolinite (kao) during low-temperature, hydrous conditions. (Courtesy of A. J. Brearley, Department of Earth and Planetary Sciences, University of New Mexico, Albuquerque.)

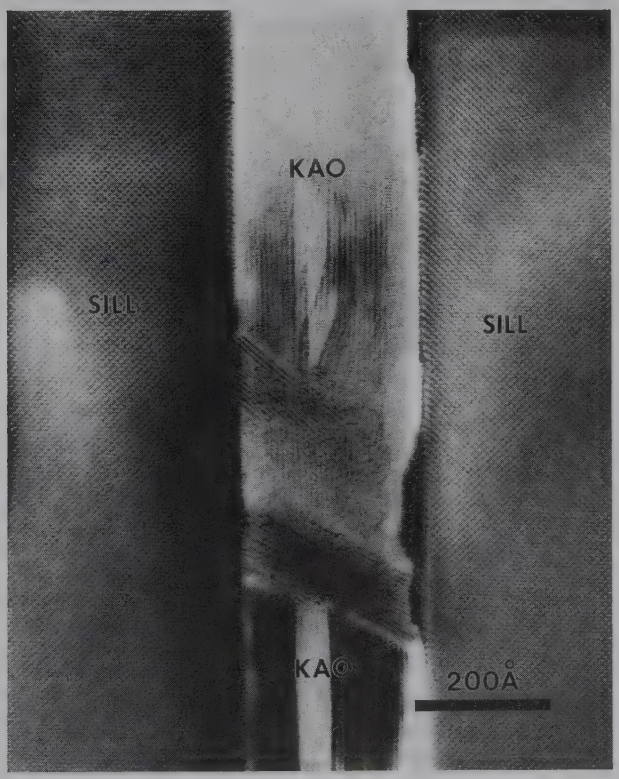

Table 21.8 Sedimentary Rocks Subdivided into Three Major Categories

I	II	III
Terrigenous Sedimentary Rocks (Clastic Texture)	Allochemical Sedimentary Rocks (Biochemical/Biogenic; with Clastic Texture)	Orthochemical Sedimentary Rocks
conglomerates, breccias, sandstones, and mudstones	limestones, dolostones, phosphorites, chert, and coal	evaporites, chert, travertine and iron-formations
agglomerates and volcaniclastic sandstones		

Figs. 11.18 and 11.19). Such chemical sedimentary assemblages, therefore, are not random or accidental but reflect the concentrations of ions in solution, as well as conditions, such as temperature, pressure, and salinity of the sedimentary basin. For example, the sequence of minerals in evaporite beds can be related to the concentration of ions in solution in the brine from which the sequence precipitated (see Box 16.2). Examples of common chemical precipitates are calcite, aragonite, gypsum, anhydrite, and halite. In sedimentary iron-formations hematite, magnetite, siderite and ankerite as well as chert are considered products of chemical sedimentation.

CLASSIFICATION

Sedimentary rocks are, in general, *stratified*, that is, they are characterized by layers or beds distinguished from each other by differences in grain size, mineral composition, color, or internal structure. Other features that are uniquely diagnostic of a sedimentary origin are: primary sedimentary structures, such as ripple marks; the presence of fossils; the occurrence of grains whose shape is the result of transportation (referred to as *clasts* or *detrital grains*); and the presence of a mineral that is invariably of sedimentary origin, such as glauconite.

All sedimentary rocks can be grouped in three broad categories, terrigenous, allochemical, and orthochemical, as shown in Table 21.8. The identification of a sedimentary rock type within each of these three broad categories is based upon its mineralogical composition and its texture (inclusive of grain size and grain shape).

Terrigenous Sedimentary Rocks

Terrigenous sedimentary rocks consist of *detrital grains*, which form the framework of the rock, and which are joined together by *cement*; these detrital grains (or clasts) are known as the *framework grains*. Variable amounts of *matrix*, which consists of fragmental material substantially smaller than the mean size of the framework grains, may also be present. Because of the normally very fine grain size of matrix material, it may be difficult to determine whether this is of detrital rather than diagenetic origin. The textural expression of rocks dominated by detrital material is a composite of the grain size, grain shapes, sorting, and angularity of the framework grains. A universally adopted grain size scale for *detrital* (or *clastic*) sediments is given in Table 21.9. Examples of various degrees of sorting are given in Fig. 21.10.

Clastic rocks are dominated by detrital (framework) grains and include conglomerates, breccias, sandstones, and mudrocks. *Conglomerates* and *breccias* consist of large clasts (boulder, cobbles, pebbles, and granules) with or without a sandy matrix; conglomer-

Table 21.9 Terms and Sizes for Clastic Sediments and Clastic Sedimentary Rock Types*

	Name	Millimeters	Micrometers	Φ
GRAVEL		4,096		−12
	Boulder	256		−8
	Cobble	64		−6
	Pebble	4		−2
	Granule			
		2		−1
SAND	Very coarse sand	1		0
	Coarse sand	0.5	500	1
	Medium sand	0.25	250	2
	Fine sand	0.125	125	3
	Very fine sand			
		0.062	62	4
MUD	Coarse silt	0.031	31	5
	Medium silt	0.016	16	6
	Fine silt	0.008	8	7
	Very fine silt			
		0.004	4	8
	Clay			

*After J. A. Udden, J. A. (1898) and C. K. Wentworth (1924). The Φ scale, devised by W. C. Krumbein (1934), is based on a logarithmic transformation, $\Phi = -\log_2 S$, where S is grain size in millimeters. The Φ scale is commonly used in sedimentological studies because it is more convenient in presenting data than if values are given in millimeters.

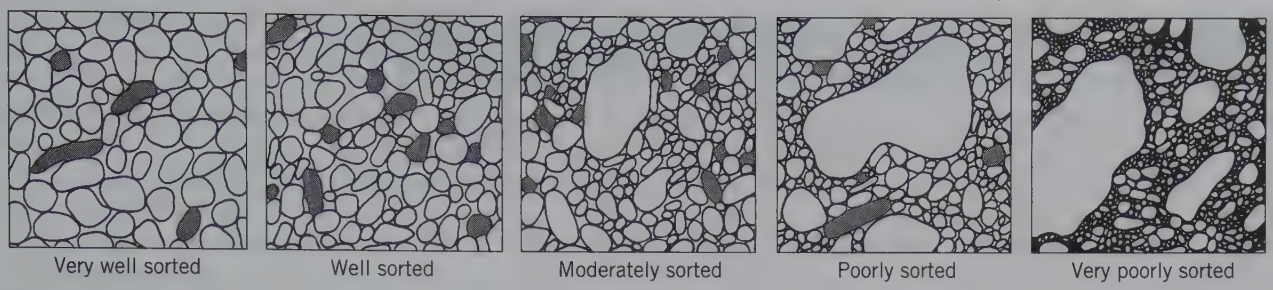

FIG. 21.10 Degrees of sorting in sandstones and conglomerates. (From Compton, R. R. 1962. *Manual of field geology.* John Wiley & Sons, New York.)

ates show pronounced rounding of the clasts and breccias contain more angular clasts. Volcanic debris may be a predominant component of some sedimentary rocks; such are commonly referred to as *pyroclastic rocks*. Coarse-grained pyroclastics with a grain size over 32 mm are known as *agglomerates* (with rounded clasts) or volcanic breccias (with angular clasts). *Sandstones* are finer-grained (grain size between 2 and 0.062 mm) and most easily classified by recognizing the amounts of clastic (framework) grains composed of quartz (and chert), feldspar, and lithic fragments. A commonly accepted scheme of sandstone classification, as based on the population of these three components in the clastic grains, is given in Fig. 21.11. Such a classification scheme is most applicable to the study of sandstones in thin section under the microscope, because the name assignment is based on a modal (volume percent) analysis of the constituent clastic grains. However, with close inspection in the field with a hand lens, a reasonably correct name can be assigned. The matrix material of sandstones is commonly made of clay minerals and very fine-grained quartz. When the matrix of a sandstone constitutes more than about 10 volume percent of the rock, it is classified as a *wacke*. *Greywackes* are mostly dark gray sandstones with abundant matrix. *Volcaniclastic* sandstones are made primarily of volcanic fragments, volcanic glass, and crystals. Many tend to be green because chlorite replaces original ferromagnesian minerals. Common cements in sandstones are quartz, calcite, and clay minerals. Diagenetic hematite may stain sandstones red. In volcaniclastic sandstones, common cements are zeolites, such as laumontite.

Mudstone is a general term for sediments composed mainly of silt-sized (0.062 to 0.004 mm) and clay-sized (< 0.004 mm) particles. Mudstones are essentially impossible to study in hand specimen because of their fine grain size. Laboratory methods of study for these very fine-grained rock types include X-ray diffraction, electron microprobe, and scanning and transmission electron microscope techniques. *Siltstones*

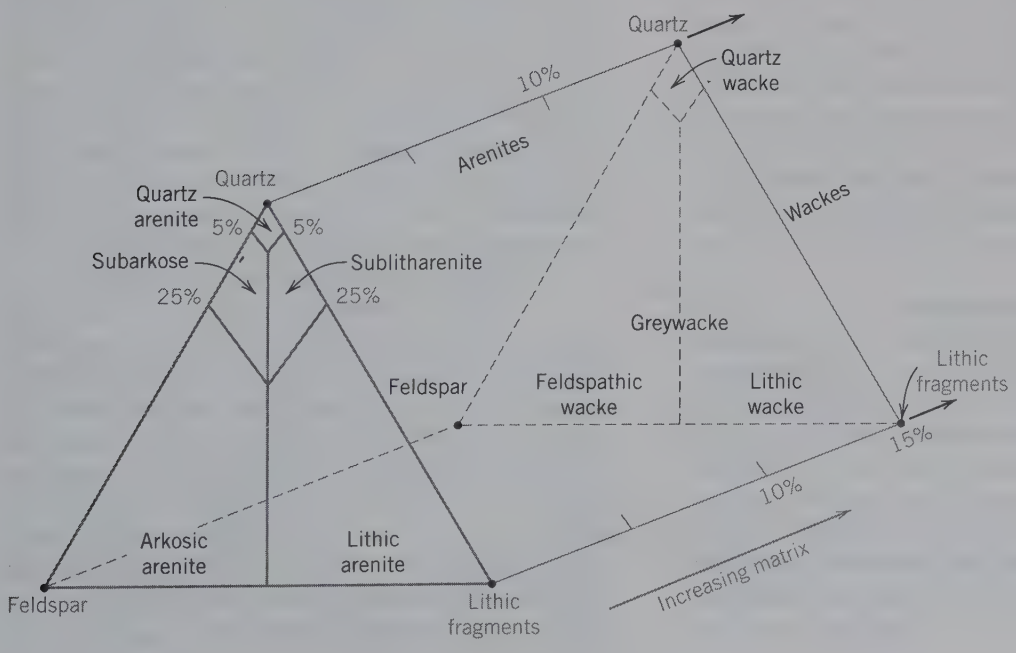

FIG. 21.11 Classification of common sandstones. (From Tucker, M. E. 1982. *Field description of sedimentary rocks.* John Wiley & Sons, New York.)

Table 21.10 Classification of terrigenous rocks* (compare with Fig. 21.11 for sandstone classification)

GRAIN SIZE			Composition			
			Lithic fragments (e.g., chert, limestone, volcanic, granite)		Quartz	Feldspar
Sand	Cobble	Conglomerate (rounded), breccia (angular)	Cobble conglomerate (or breccia) (e.g., granite cobble conglomerate)		Quartz cobble conglomerate (or breccia)	
Sand	Pebble	Conglomerate (rounded), breccia (angular)	Pebble conglomerate (or breccia) (e.g., chert pebble conglomerate)		Quartz pebble conglomerate (or breccia)	
Sand	Granule	Conglomerate (rounded), breccia (angular)	Granule conglomerate (or breccia) (e.g., limestone granule conglomerate)		Quartz granule conglomerate (or breccia)	Feldspar granule conglomerate (or breccia)
Sand	Sand	Sandstone	**Wacke (> 10% matrix)**	Lithic† wacke	Quartz wacke wacke	Feldspathic‡
Sand	Sand	Sandstone	**Arenite (< 10% matrix)**	Lithic arenite	Quartz arenite arenite	Feldspathic‡
Silt		(composition cannot be evaluated because of the fine grain size)				
Silt		Siltstone				
Mud		Mudstone—lacking fissility Shale—showing fissility				

*Modified after Suttner, L. J., and Meyers, J. 1991. Field study of the petrology of sedimentary rocks. *Manual for geologic field study of Northern Rocky Mountains.* Indiana University, Bloomington, 306–326.

†Dark, highly indurated lithic wackes are also referred to as greywackes.

‡Red- or pink-colored feldspathic wackes and arenites can be referred to as *arkoses.*

and *claystones* are rock types made up mainly of silt and clay particle size materials, respectively. *Shale* is characterized by *fissility*, the ability to split into thin sheets, generally parallel to the bedding. Mudstones are nonfissile, commonly with a massive or blocky texture. *Slate* refers to a mudstone with a well-developed cleavage (which may or may not be parallel to the bedding and is commonly the result of metamorphism).

A schematic classification of common terrigenous sedimentary rocks is given in Table 21.10.

Allochemical Carbonate Rocks

Allochemical carbonate rocks show clastic (fragmental) textures analogous to those seen in terrigenous rocks, but the textural interpretation in these mineralogically simple rocks is not always straightforward. Because calcite recrystallizes easily and because secondary dolmite (replacing original calcium carbonates; this process is known as *dolomitization*) often destroys the texture of the original carbonate, textural interpretations of such limestones or dolostones may be impossible in hand specimens.

Limestones consist of two classes of constituents, orthochemical and allochemical. These constituents originate from within the basin of deposition of the limestone, and are referred to as *intrabasinal*. The orthochemical components are of two types: (1) *microcrystalline calcite ooze*, which is a very fine-grained carbonate precipitate that has settled to the bottom of the basin, and (2) *sparry calcite cement*, which is coarser in grain size than the ooze, and tends to be clear or translucent. This coarser-grained type of calcite is a pore-filling cement that was precipitated in place from solution. The allochemical components of limestone are of four types: *intraclasts*, *oolites*, *fossils*, and *pellets*. *Intraclasts* represent fragments of weakly consolidated carbonate sediment that has been torn up, transported, and redeposited by currents within the basin of deposition. They consist of various types of limestone and can range in size from very fine to pebble or boulder size. *Oolites*, in a size range of 0.1 to 1.0 mm in diameter, are spherical and show radial and concentric structures, and resemble fish roe. They are commonly formed around nuclei, such as shell fragments, pellets, or quartz-sand grains. They de-

velop by chemical accretion under the rolling influence of waves in shallow marine environments. *Fossils* of many types are common constituents of limestones. *Pellets* are well-rounded, homogeneous aggregates of microcrystalline calcite in a size range of 0.03 to 0.20 mm in diameter. They are mainly the feces of mollusks, worms, and crustaceans.

Because carbonate rocks tend to be mixtures of (1) the allochemical components noted previously, (2) microcrystalline ooze, and (3) sparry calcite cement, Folk (1959) notes that, as a first-order approach, limestones can be classified on the basis of the volumetric abundance of these three types of materials. Such a classification of limestones, which ignores any of the possibly present terrigenous components (e.g., detrital quartz-sand grains), is given in Fig. 21.12. In this figure, the *allochems* (intraclasts, oolites, fossils, and pellets) represent the framework material of the rock. The microcrystalline matrix is equivalent to a clay-rich matrix in a poorly sorted sandstone. The sparry cement in the filling of pore spaces, as in quartz-rich sandstones, is a chemical precipitate. A rock composed only of microcrystalline limestone is referred to as a *micrite*. Folk (1959) recommends that after limestones have been divided into type I, type II, and type III (see caption of Fig. 21.12) it is essential to note which allochemical components (intraclasts, oolites, fossils, or pellets) predominate. Once this is known, it can be incorporated into a scheme of nomenclature by using parts of the allochem names (*intra* from *intraclast*; *oo* from *oolite*; *pel* from *pellet*; and *bio* for *biogenic*, in place of *fossil*) as prefixes. This leads, for example, to biosparite and biomicrite, both consisting of fossil fragments but in different matrix types (*biosparite* = a limestone with more than 10% allochems in a dominantly sparry calcite matrix; *biomicrite* = a limestone with more than 10% allochems set in a micritic matrix). Other such terms are shown at the upper part of the triangle in Fig. 21.12.

FIG. 21.12 Classification of limestones in terms of volume percentage of allochem grains, microcrystalline calcite matrix, and sparry calcite cement. (After Folk, R. L. 1959. Practical petrographic classification of limestones. *Bulletin of the American Association of Petroleum Geologists* 43: 1–38.) The field of common limestones is shaded. Type I limestones consist of a mixture of allochemical constituents and sparry calcite cement; type II of a variable percentage of allochemical grains in a microcrystalline matrix; and type III of microcrystalline calcite matrix only (referred to as *micrite*).

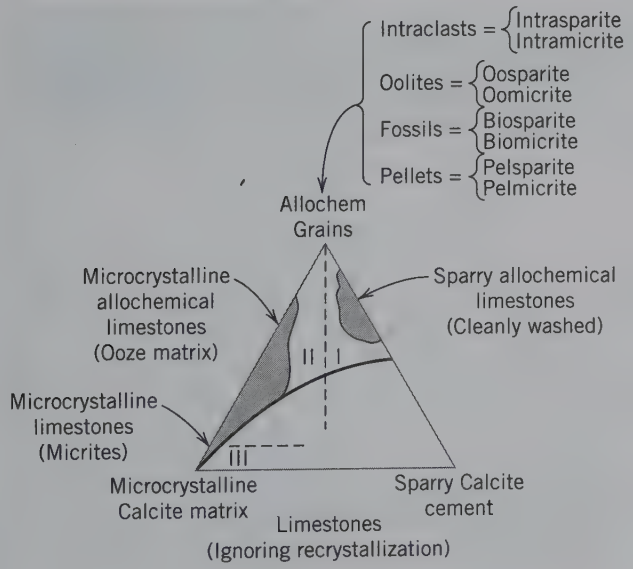

There is another commonly used classification of limestones, as outlined by R. J. Dunham (1962), with emphasis on the depositional texture of limestones, instead of Folk's emphasis on the micritic content of the rock. Dunham's classification stresses the question of "were the framework grains (Folk's allochems) in close contact with each other, that is, were they well packed when they were deposited?" Because both classifications are almost equally popular, both are combined in a graphic representation in Fig. 21.13. The terms *mudstone*, *wackestone*, *packstone*, *grainstone*, and *boundstone* were introduced by Dunham (1962) so as to reflect, at one extreme, less than 10% grains (mudstone) and, at the other extreme, the predominance of original components that are closely bound together (boundstone). The term *boundstone* is equivalent to *biolithite*, a limestone made up of organic structures that grew *in situ* (in place), forming a coherent rock mass during growth. *Wackestone* reflects more than 10% grains in a microcrystalline ooze (micrite), *packstone* is a grain-supported limestone with micrite matrix and sparry calcite cement, and *grainstone* is a grain-supported limestone with very little micrite, if any. Either of the two schemes of Fig. 21.13 can be used to classify limestones on the basis of careful observation by hand lens in the field, or binocular microscope in the laboratory.

Dolostones are Ca–Mg-rich carbonate rocks consisting mainly of the mineral dolomite. The term *dolomite* is commonly used for both the rock type and the mineral. Dolostones in limestone–dolostone sequences may show irregular or cross-cutting relationships with the limestones, indicating that the dolostone has formed by replacement of early calcite by later dolomite. Such observations form the basis for the interpretation of the process of *dolomitization*, which involves the replacement of original calcium carbonate in limestone by Ca–Mg-carbonate (dolomite) at any time during or after deposition. Sometimes it is possible with a hand lens to see rhombic outlines of dolomite grains cutting across fossil fragments; however, such observations are best made in thin section with petrographic microscope.

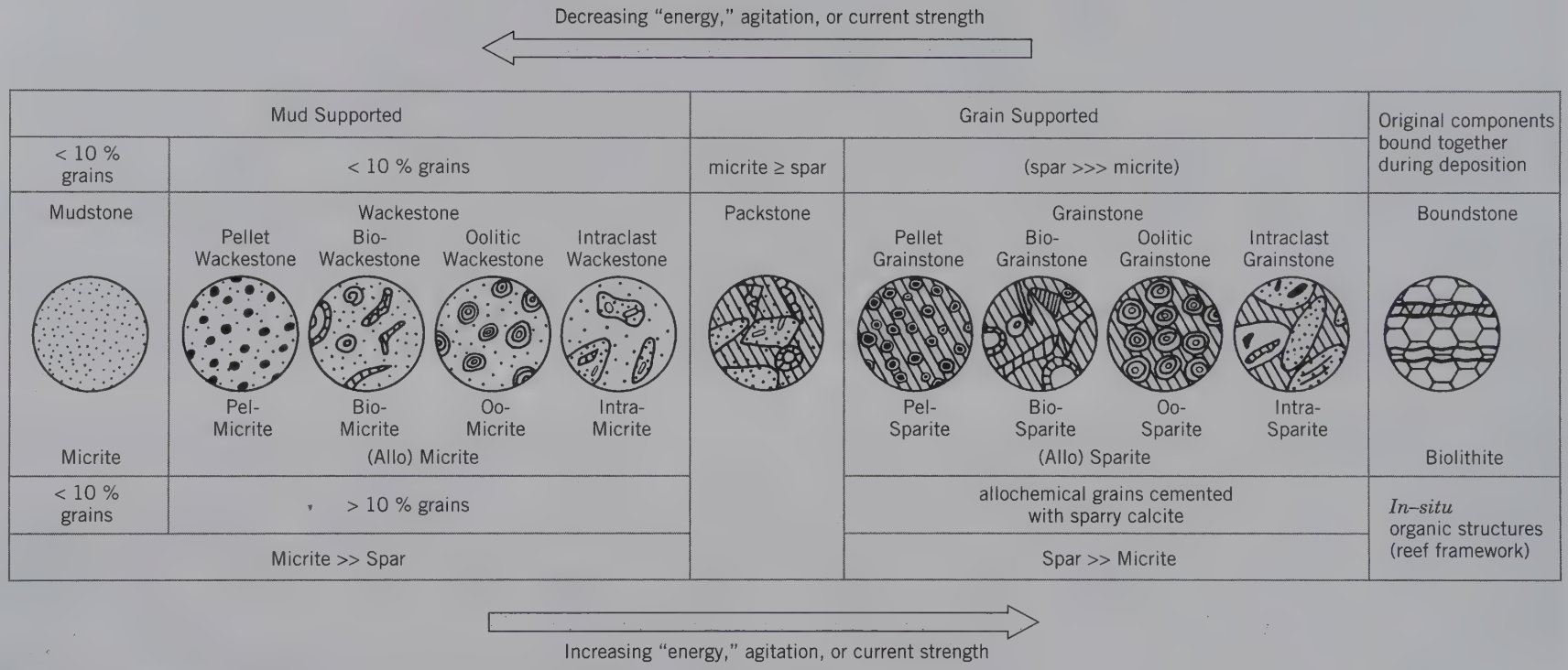

FIG. 21.13 Classification of carbonate rocks after Folk (1959) and Dunham (1962). The headings at the bottom of the chart represent the classification of R. L. Folk; those at the top of the chart, the classification of R. J. Dunham. (From Suttner, L. J., and J. Meyers. 1991. *Manual for geological study of Northern Rocky Mountains*. Indiana University, Bloomington, 305–26.

Orthochemical Sedimentary Rocks

Orthochemical sedimentary rocks are the result of direct precipitation by chemical action in the depositional basin as a result of environmental (e.g., climatic) changes. Three sedimentary rock occurrences that fall into this category are: evaporites, banded iron-formation, and travertine. Bedded cherts may also be of direct chemical origin.

Evaporites. When a restricted body of seawater or the waters of saline lakes evaporate, the elements in solution (see Box 16.2) are precipitated in what are known as evaporites. More than 80 minerals (excluding clastic material) have been recorded in evaporites and most of these are chlorides, sulfates, carbonates, and borates; only about 11 rank as major constituents (see Box 16.2). On evaporation, the general sequence of precipitation is: some calcite, $CaCO_3$ (when the original volume of seawater is reduced by evaporation to about one-half), gypsum, $CaSO_4 \cdot 2H_2O$, or anhydrite, $CaSO_4$, (with the volume reduced to one-fifth of the original), halite, NaCl, (with the volume reduced to one-tenth of the original), and finally sulfates and chlorides of Mg and K. If all the salt in a 1,000 foot (305 m) column of seawater were precipitated, it would form 0.5 feet (0.15 m) of calcium sulfate, 11.8 feet (3.6 m) of NaCl, and 2.6 feet (0.8 m) of K- and Mg-bearing salts, producing a total salt column of 15 feet (4.6 m) thick.

In natural deposits, the minerals that precipitate early in the sequence tend to show increased abundance. Gypsum and anhydrite are by far the most abundant evaporate minerals and commonly form massive beds. The deposition of gypsum or anhydrite depends on the temperature and salinity of the brine; anhydrite is formed at higher salt concentrations and at higher temperatures than gypsum. Halite forms about 95% of the chloride minerals in an evaporite sequence. Deposits of the more soluble salts, such as sylvite, KCl; carnallite, $KMgCl_3 \cdot 6H_2O$; and polyhalite, $K_2Ca_2Mg(SO_4)_4 \cdot 2H_2O$, are rare because they are not deposited until nearly complete dryness is attained. Nevertheless, in places, large deposits (particularly of sylvite) have formed and are mined extensively as the primary source of potassium.

Iron-formation. Sedimentary, banded iron-formations are common in rock sequences of Precambrian age. These iron-rich formations, which commonly weather to a dark, reddish-brown color as a result of the formation of red hematite and yellow-brown goethite (and/or limonite), may show well-developed sedimentary stratification (such as banding on a scale of millimeters, centimeters, or meters) as well as oolitic textures. The overall bulk chemistry of these iron-formations reflects the highly unusual chemistry of the original waters from which these sedimentary sequences precipitated. Table 21.11 gives the major oxide components of a sedimentary carbonate-silicate-chert-magnetite iron-formation. Its major components are SiO_2, FeO, Fe_2O_3, MgO, CaO, and CO_2, with only small amounts of Al_2O_3, MnO, Na_2O, and K_2O. When the average chemical compositions of many well-studied iron-formations are recalculated on an H_2O- and CO_2-free basis, the curves in Fig. 21.14 result. The chemical data plotted on this graph represent the bulk compositions of sedimentary (and, thus, unmetamorphosed) iron-formations as well as metamorphosed iron-formation sequences. During metamorphism of iron-formations, CO_2 and H_2O are lost in decarbonation and dehydration reactions. Therefore, in order to compare the chemistry of unmetamorphosed and metamorphosed materials, it is best to compare them

Table 21.11 Chemical Composition of a Carbonate Silicate-Chert-Magnetite Iron-Formation from the Labrador Trough Area, Canada, and Common Minerals in Iron-Formation*

	Weight Percent	Common Minerals
SiO_2	29.60	Chert—SiO_2
Al_2O_3	0.78	Magnetite—Fe_3O_4
Fe_2O_3	11.70	Hematite—Fe_2O_3
FeO	32.00	Siderite—$FeCO_3$
MnO	0.85	Ankerite—$CaFe(CO_3)_2$
MgO	3.62	Calcite—$CaCO_3$
CaO	2.73	Greenalite—$(Fe,Mg)_3Si_2O_5(OH)_4$
Na_2O	0.01	Minnesotaite—$(Fe,Mg)_3Si_4O_{10}(OH)_2$
K_2O	0.25	Stilpnomelane~$K(Fe^{2+},Mg,Fe^{3+})_8(Si,Al)_{12}(O,OH)_{27}$
H_2O	0.83	Riebeckite—$Na_2Fe_3^{2+}Fe_2^{3+}Si_8O_{22}(OH)_2$†
CO_2	18.10	
Total	100.47	

*From Klein, C., and Fink. R. P. 1976. Petrology of the Sokoman iron-formation in the Howells River area, at the western edge of the Labrador Trough. *Economic Geology* 71: 453:87.
†Common as crocidolite in Western Australia and South African iron-formations.

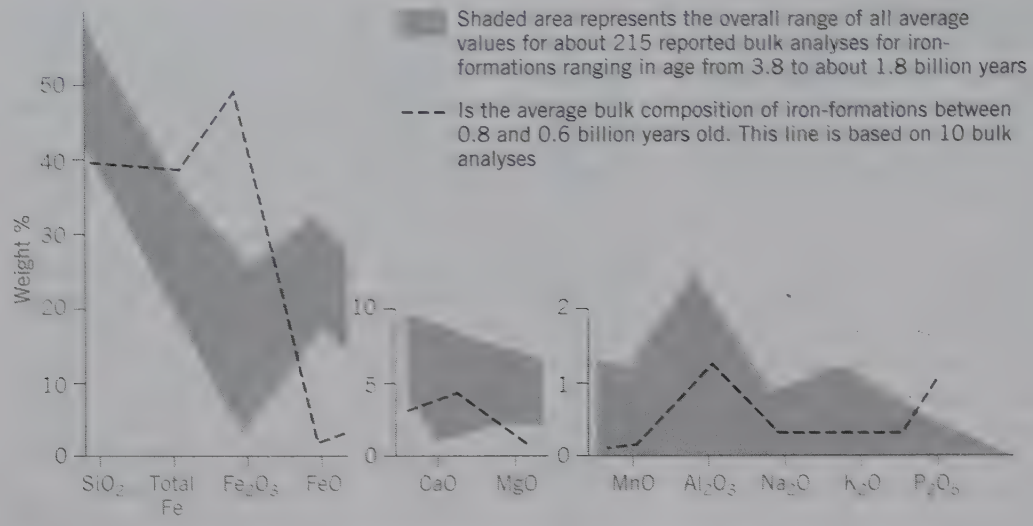

FIG. 21.14 Plot of the major chemical oxide components of Precambrian iron-formations with the original analytical results recalculated to 100% on an H_2O-free basis. Note that the data for the various components are presented relative to three different (vertical) weight percentage scales. See Box 16.1 for age distribution. (From Klein, C. 2005. Some Precambrian banded iron-formations (BIFs) from around the world: Their age, geologic setting, mineralogy, metamorphism, and origin. *American Mineralogist* 90: 1473–99).

without reference to CO_2 and H_2O. Figure 21.14 shows the unique average chemical composition of these sedimentary sequences.

Common minerals in Precambrian iron-formations are listed in Table 21.11. Generally, chert, magnetite, and Fe-rich carbonates (siderite and ankerite) are the most common constituents. Hematite and various Fe-rich silicates (greenalite, minnesotaite, and stilpnomelane) can be locally abundant as well. Greenalite, $(Fe,Mg)_3Si_2O_5(OH)_4$, is the Fe-rich analogue of antigorite; minnesotaite, $(Fe,Mg)_3Si_4O_{10}(OH)_2$, is the Fe-rich equivalent of talc; and stilpnomelane, $K(Fe^{2+},Mg,Fe^{3+})_8(Si,Al)_{12}(O,OH)_{27}$, is a complex layer-silicate structure closely related to that of biotite. Riebeckite, $Na_2Fe_3^{2+}Fe_2^{3+}Si_8O_{22}(OH)_2$, is abundant, in its fibrous variety *crocidolite*, in the Precambrian, banded iron-formations of Western Australia and South Africa. This sodium-rich amphibole is considered diagenetic in origin in these sedimentary sequences.

Regions of vast Precambrian iron-formations are found in the Lake Superior region of the United States, the Labrador Trough of Canada, the Hamersley Range of Western Australia, the Transvaal region of South Africa, and in Brazil (see also Box 16.1).

Travertine. This is a calcareous material deposited from spring waters (frequently thermal springs) under atmospheric conditions. If the deposit is porous, it is known as *calcareous tufa*. Such deposits are prevalent in limestone regions where circulating groundwater containing CO_2 has incorporated considerable calcium carbonate in solution. When the groundwater reaches the surface as springs, some of the CO_2 is given off, resulting in the precipitation of the calcium carbonate as travertine.

Further Description of Rock Types

Conglomerate. Conglomerates may be considered consolidated gravels. They are composed of coarse clasts, ranging from boulder to granule size, that have been rounded by transportation. The individual clasts may be composed entirely of quartz (e.g., *quartz pebble conglomerate*, or *quartzose conglomerate*), or may be rock fragments that have not been decomposed (e.g., *granite cobble conglomerate*, or *limestone granule conglomerate*). Fine conglomerates grade into coarse sandstones.

Agglomerate. This is a pyroclastic rock containing abundant subangular or rounded fragments (bombs) in a fine-grained volcanic matrix. The rounding of the boulders and pebbles is due to the erosion by running water. Agglomerates are common near volcanic vents. A *volcanic breccia* is of similar composition, but the fragments are more angular.

Sandstone. A cemented or indurated sedimentary rock with grain sizes between 0.062 and 2 mm. The constituent grains are usually rounded and waterworn but may be more or less angular. The detrital particles (clasts) may be quartz, rock fragments, volcanic debris, organic material, or any other clastic material. Sandstones are subdivided texturally into *arenites* and *wackes* on the basis of detrital matrix contents (see Fig. 21.11). The term *arenite* or *wacke* is prefixed with a compositional modifier as in *lithic arenite*, *arkosic aren-*

ite, *feldspathic wacke*, and *quartz wacke*. The cement that binds the sand grains together may be silica, a carbonate (usually calcite), an iron oxide (hematite or geothite), or clay minerals. The color of the rock depends in large measure on the character of the cement. The rocks with silica or calcite as their binding materials are light in color, usually white to gray, pale yellow, or buff; those that contain an iron oxide are red to reddish-brown. When a sandstone breaks, it is commonly the cement that is fractured, the individual grains remaining unbroken so that the fresh surfaces of the rock may have a granular appearance and feeling. *Arkose* is an arenite with more than 25% feldspar among the clastic grains. Arkoses are often pink or red because of the large content of K-feldspar, and they may resemble a granite in appearance. These rocks have undergone little chemical weathering. A *greywacke* is a type of sandstone with grayish-green color, clay matrix, poor sorting of sand grains, and abundant lithic fragments.

Siltstone, Mudstone, and Shale. These rock names are based on the fine grain size ($< \frac{1}{16}$ mm) of the sedimentary particles. It is not possible to describe the composition of these rocks in hand specimen because of the fine grain size. *Siltstones* lack fissility, that is, they lack ease of splitting along bedding planes. *Mudstone* is a nonfissile rock consisting of mud-sized detritus. A *shale* is a fissile sedimentary silicate-rich rock with particles mostly in the silt and clay size. The color of these rocks is commonly some tone of gray, although they may be brown, red, or green to black. They are composed chiefly of clay minerals with quartz and mica but are too fine-grained to permit the recognition of their mineral constituents by the eye alone. By the introduction of quartz and an increase in their grain size, they grade into greywackes and arenites, and with the presence of calcite, they grade into limestones.

Limestone. Limestone composed essentially of calcite, $CaCO_3$, is the most abundant chemically precipitated sedimentary rock. Although the calcite may be precipitated directly from seawater, most limestone is the result of organic precipitation. Many organisms living in the sea extract calcium carbonate from the water to build hard protective shells. On the death of the organisms, the hard calcareous parts accumulate on the sea floor. When marine life is abundant, great thicknesses of shells and other hard parts may build up and, when consolidated, become limestone. There are many varieties of limestone. *Chalk* is a soft, micritic limestone composed for the most part of foraminiferal shells. *Coquina* is a loosely cemented fragmental limestone made of fossil shells and fragments; it is found along the coasts of Florida and Mexico. *Lithographic limestone* is a compact, very fine-grained limestone, formerly used in printing. It is predominantly a micrite, with the most famous example occurring in Solenhofen, Germany. A *mudstone* is a mud-supported limestone that contains less than 10% sand- or gravel-sized grains; this is equivalent to a *micrite*. The term *micrite*, for a limestone of microcrystalline calcium carbonate, is strongly preferred over mudstone, which can be confused with terrigenous mudstone. A *wackestone* is a mud-supported limestone with more than 10% sand- or gravel-sized particles. Subdivisions of wackestone (according to R. J. Dunham, 1962, and R. L. Folk, 1959, respectively, see Fig. 21.13) are: pellet wackestone (pelmicrite), biowackestone (biomicrite), oolitic wackestone (oomicrite), and intraclast wackestone (intramicrite). *Packstone* is a classic limestone in which the grains rest on each other, but some micrite is present. *Grainstone* is carbonate rock in which the grains are in contact with each other and which contains only a minor amount of mud. Grainstones have been divided by R. J. Dunham (1962) into pellet grainstone, biograinstone, oolitic grainstone, and intraclast grainstone (Fig. 21.13). Equivalent terms (according to R. L. Folk, 1959) are: pelsparite, biosparite, oosparite, and intrasparite. A *boundstone* is a carbonate rock in which the skeletal parts were cemented in place during their formation and remain in their growth position. This is equivalent to *biolithite*, which is typical of reef frameworks (organic structures) in which skeletal elements and fragments are cemented by biogenic carbonate.

Dolostone. This name was introduced to distinguish the rock, dolomite, from the mineral, dolomite. Dolostone resembles limestone so closely in its appearance that it is usually impossible to distinguish the two rock types without a chemical test. Dolostones have generally not formed as original chemical precipitates but are the result of alteration of limestone in which part of the calcium is replaced by magnesium. This process of *dolomization* is suggested to have taken place either by the action of seawater shortly after original deposition, or by the action of circulating groundwater after the rock has been consolidated and raised above sea level.

Siliceous Sinter. In certain volcanic regions hot springs deposit an opaline material known as siliceous sinter or *geyserite*. The deposit apparently results from both evaporation and secretion of silica by algae.

Diatomaceous Earth. This is a light-colored, soft, friable, and porous siliceous deposit made of diatoms. Diatoms are minute one-celled organisms that live in both fresh and seawater and have the power of secreting tests of opaline material. When the organisms die, their tiny shells accumulate to build up a chalk-like deposit of *diatomaceous* earth.

Evaporites, **iron-formation**, and **travertine** are described on pages 593–594.

METAMORPHIC ROCKS

Metamorphic rocks are derived from preexisting rocks (igneous, sedimentary, or metamorphic) by recrystallization in the solid state. This results in mineralogical, textural, and structural changes. Such changes may be the result of marked variations in temperature, pressure, fluids, and shearing stress at considerable depth in the Earth's crust. Weathering effects, at atmospheric conditions, are not considered part of metamorphism, nor are chemical reactions involving partial melting as these are part of igneous processes. Although metamorphic changes, such as recrystallization and chemical reactions among mineral constituents, take place essentially in the solid state, the solids may exchange chemical species with small amounts of a liquid phase consisting mainly of H_2O (as water, steam, or supercritical fluid, depending on the temperature and pressure at which the reactions took place). The general conditions of formation of metamorphic rocks lie between those of sedimentary rocks that form at essentially atmospheric conditions of T and P and those of igneous rocks that are the result of crystallization from a melt at high T. Metamorphic rocks may be the result also of large changes in pressure in conjunction with increasing metamorphic temperature; mineral assemblages in the Earth's mantle have formed in response to very high confining pressures (see page 93). Excluding gain or loss of fluids, many metamorphic reactions are generally considered to be essentially **isochemical**; this implies that during recrystallization and chemical reactions, the bulk chemistry of rocks remains essentially constant. If this is not the case, and if additional elements have been introduced into the rock by circulating fluids, for example, the rock is said to have undergone **metasomastism**.

The most obvious textural feature of most metamorphic rocks (except those of contact metamorphic origin, see the following text) is the alignment of minerals along planar surfaces. For example, a shale that has undergone only slight metamorphic changes may show well-developed cleavage along planar surfaces when recrystallized under directed stress, producing a *slate*. With increased temperature of metamorphism, recrystallization of originally very fine-grained minerals produces coarser-grained *schists*, which exhibit minerals aligned in parallel layers (known as *schistosity*). The coarsest-grained metamorphic rocks that show distinct mineralogical banding are known as *gneisses* (exhibiting *gneissosity*).

In general, metamorphic rocks can be divided into two groups: (1) those formed by contact metamorphism, typically without directed stress, and (2) those formed by regional metamorphism, with directed stress. **Contact metamorphic rocks** occur as concentric zones (*aureoles*) around hot igneous intrusions. Such metamorphic rocks typically lack schistosity, and the relatively large temperature gradient from the intrusive contact to the unaffected country rock gives rise to zones that differ in mineral assemblages. Sandstones are converted to *quartzites*, and shales are changed to *hornfels*, a fine-grained dense rock. **Regional metamorphic rocks** are the result of increases in T or P, or both, and deformation, on a regional scale (areas a few hundred to thousands of miles in extent) in response to mountain building, or deep burial of rocks. Contact and regionally metamorphosed rocks generally reflect an increase in temperature (progressive or **prograde** metamorphism) in their assemblages. However, when assemblages of high-temperature origin (e.g., igneous or high-temperature metamorphic rocks) are overprinted by conditions of lower-temperature metamorphism, the process is referred to as **retrograde** (or retrogressive) metamorphism. Retrograde metamorphism usually requires the addition of fluids.

A transmission electron microscope (TEM) photograph, of a *prograde* metamorphic reaction in which muscovite gives way to the reaction products potassium feldspar, biotite, spinel, and corundum, is shown in Fig. 21.15. This arrested reaction shows the original reactant, muscovite (with some Mg and Fe replacing octahedral Al in the structure), and two of the products, potassium feldspar and biotite. The complete reaction is:

$$\text{muscovite (containing some Mg and Fe)} \rightarrow \text{K-feldspar} + \text{biotite} + \text{spinel} + \text{corundum} + H_2O\uparrow$$

An example of an arrested *retrograde* metamorphic reaction of an original high-temperature pyroxene (of enstatite composition, $MgSiO_3$, but with monoclinic symmetry, referred to as *clinoenstatite*) altering to a complex mixture of hydrous silicate products (including *biopyriboles*, see page 455), is shown in an HRTEM image in Figure 21.16. The original clinoenstatite (marked as *cpx*, which is an abbreviation for the generic term *clinopyroxene*) is riddled with lamellae that represent silicate structures with chains of variable width (these are wider than the structural chain units that are found in the structure of the original pyroxene). The homogeneous wide band at the left is the ultimate, stable alteration product talc. A qualitative equation for this reaction is:

$$\underset{\text{clinoenstatite}}{xMgSiO_3} + nH_2O \rightarrow \underset{\text{anthophyllite}}{yMg_7Si_8O_{22}(OH)_2} + \text{“biopyriboles”} + \underset{\text{talc}}{zMg_3Si_4O_{10}(OH)_2}$$

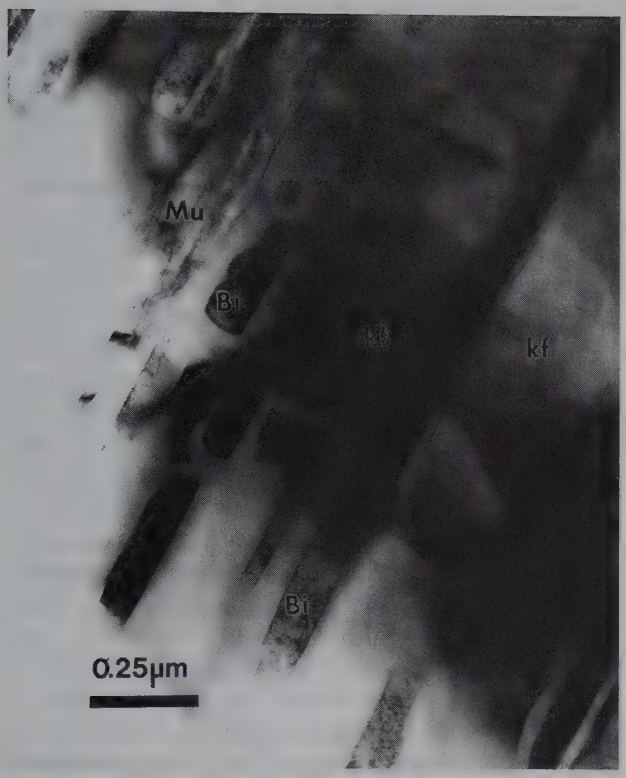

FIG. 21.15 Transmission electron micrograph of an original muscovite (Mu) that has partially reacted to biotite platelets (Bi) and potassium feldspar (kf) as a result of metamorphism between 750° and 900°C. The other reaction products mentioned in the text (spinel and corundum) are not present in this image (From Brearley, A. J. 1986. An electron optical study of muscovite breakdown in pelitic xenoliths during pyrometamorphism, *Mineralogical Magazine* 50: 385–97).

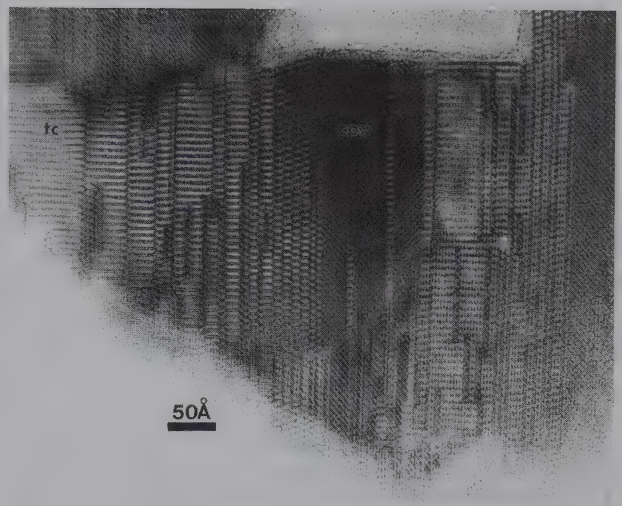

FIG. 21.16 High-resolution transmission electron microscope (HRTEM) image of an arrested retrograde reaction in which the original, high-temperature pyroxene has transformed into a mixture of amphiboles, "biopyriboles" as well as talc. The original pyroxene is identified by cpx (clinopyroxene; it is a monoclinic form with enstatite composition). The amphiboles are the thinnest vertical stripes, with variable widths; and talc (tc) is present in the far left corner. (Compare with Fig. 18.43.) This mixture of silicates occurs in the Allende meteorite. (Courtesy A. J. Brearley, Department of Earth and Planetary Sciences, University of Mexico, Albuquerque.)

CHEMICAL COMPOSITION

Because metamorphic rocks are the recrystallized and generally foliated (from the Latin word *folia* meaning *leaves*) products of rocks of igneous or sedimentary bulk compositions, the general range of their chemical compositions is as large as that of igneous and sedimentary rocks combined. Although most metamorphic reactions take place without addition of chemical species to the rock, some chemical components may be lost, especially during the higher-temperature ranges of metamorphism. For example, a shale, which is largely composed of hydrous minerals, such as clays, may convert into a slate and subsequently into a schist with increasing temperatures, during which the mineral assemblage becomes less and less hydrous, due to progressive *dehydration*. In other words, with an increase in temperatures during metamorphism, water is generally lost from the rock. Similarly, carbonate-rich sedimentary rocks, while undergoing increasing temperatures of metamorphism, will tend to lose CO_2, which is known as *decarbonation*. Such processes can be illustrated as follows:

$$\underset{\text{kaolinite}}{Al_4Si_4O_{10}(OH)_8} \rightarrow \underset{\text{pyrophyllite}}{Al_2Si_4O_{10}(OH)_2} + \underset{\text{corundum}}{Al_2O_3} + 3H_2O\uparrow$$

and

$$\underset{\text{calcite}}{CaCO_3} + \underset{\text{quartz}}{SiO_2} \rightarrow \underset{\text{wollastonite}}{CaSiO_3} + CO_2\uparrow$$

Although such losses of H_2O and CO_2 to a thin layer of fluid phase surrounding the mineral grains are common during the conditions of progressive metamorphism, additions of chemical species from the fluid phase to the rock are considered part of metasomatic processes.

MINERALOGICAL COMPOSITION

The mineralogical composition of a rock that has not undergone metamorphic conditions will generally be very different from that of its metamorphosed equivalent. The extent of the differences is largely controlled by the marked changes of T and P during metamorphism; the relative degrees of metamorphism can be expressed in terms of *grades*, such as very low, low, medium, and high grade (Fig. 21.17). *Changes in metamorphic grade are reflected in changes in*

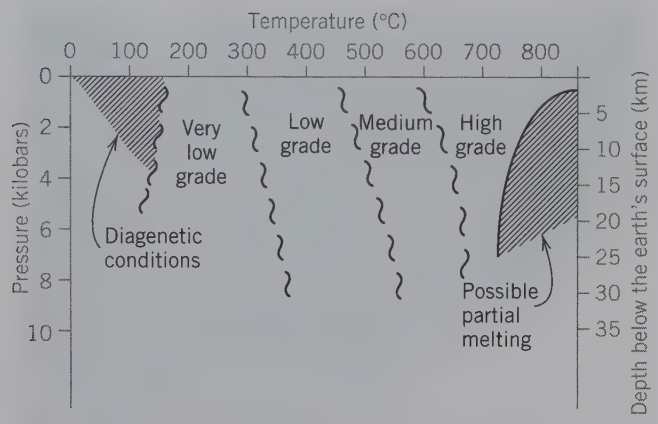

FIG. 21.17 Schematic *P–T* diagram outlining approximate fields for various metamorphic grades. The shaded area marked "diagenetic conditions" represents the general condition of lithification of a sediment at low temperature. (After Winkler, H. G. F. 1974. *Petrogenesis of metamorphic rocks*. Springer-Verlag, New York, 5, with some modifications.)

the mineral assemblages of the rocks. Petrologists, in their description of the mineralogical changes in rocks as a function of increasing metamorphic temperature, commonly represent such changes graphically. Such a graphical approach is shown in Fig. 21.18 for a sedimentary cherty dolomitic limestone that has been subjected to various metamorphic temperature conditions. The cation components of the mineral assemblage in the original sedimentary rock (Fig. 21.18*a*) are correctly accounted for by the components of the corners of the triangle. However, CO_2, although present in the dolomite and calcite composition, is not depicted. Similarly, the cation proportions of any hydrous minerals, as in Fig. 21.18*c* (e.g., talc and tremolite) are accounted for, but (OH) is not shown. This is a relatively common practice in metamorphic petrology so as to allow for the representation of anhydrous, hydrous, and carbonate minerals on the same composition diagrams. The theoretical justification for this is that H_2O (or OH) and CO_2 are major constituents of the metamorphic fluid which, in most cases, is considered to have been present and in equilibrium with the various minerals throughout the

FIG. 21.18 Some of the assemblage changes as a result of increasing temperature in the system $CaO–MgO–SiO_2–CO_2–H_2O$. Triangle in (*a*) represents the original, sedimentary assemblage in this system (the composition of a naturally occurring cherty, dolomitic limestone is only partly represented in this triangle because it also contains small amounts of FeO). The triangle in (*f*) represents the highest-temperature (contact metamorphic) assemblage, and the other triangles represent intermediate grades of metamorphism.

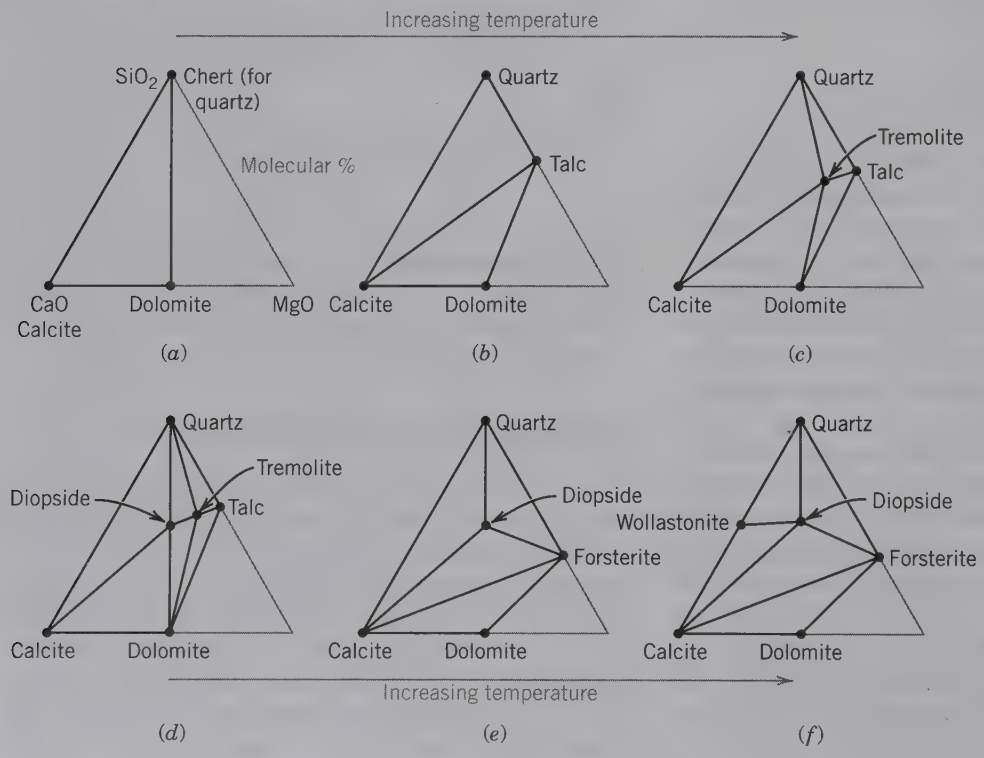

metamorphic process; such components are often referred to as *perfectly mobile components*.

In graphical terms, this means that all CO_2-containing and hydrous minerals in the system CaO–MgO–SiO_2–CO_2–H_2O have been projected from their chemical location in a 4-component system (e.g., CaO–MgO–SiO_2–CO_2 for the carbonates; and CaO–MgO–SiO_2–H_2O for the hydrous silicates) onto a carbonate-free and anhydrous plane, respectively. The CaO–MgO–SiO_2–CO_2 or CaO–MgO–SiO_2–H_2O systems can be regarded as tetrahedra in which the apex (above the plane of the page) is the CO_2 or H_2O component. The triangles shown in Fig. 21.18 are the triangular bases of these tetrahedra onto which the carbonates or hydrous compositions have been projected.

In going from Fig. 21.18*a* to 21.18*b*, the original sediment has undergone very low-grade metamorphic conditions (*T* between about 150° and 250°C; Fig. 21.17) as shown by the formation of talc according to:

$$\underset{\text{dolomite}}{3CaMg(CO_3)_2} + \underset{\text{quartz}}{4SiO_2} + H_2O \rightarrow$$

$$\underset{\text{talc}}{Mg_3Si_4O_{10}(OH)_2} + \underset{\text{calcite}}{3CaCO_3} + 3CO_2\uparrow$$

This is represented on the diagrams by the reorientation of tielines connecting stable mineral assemblages.

At low-grade metamorphic conditions (*T* between 250°C and 450°C) the assemblage on the right of the above equation may react as follows:

$$\underset{\text{talc}}{2Mg_3Si_4O_{10}(OH)_2} + \underset{\text{calcite}}{3CaCO_3} \rightarrow$$

$$\underset{\text{tremolite}}{Ca_2Mg_5Si_8O_{22}(OH)_2} + \underset{\text{dolomite}}{CaMg(CO_3)_2} + CO_2\uparrow + H_2O\uparrow$$

The tremolite product is plotted in Fig. 21.18*c*.

At medium-grade metamorphic conditions (about 450°C to 600°C) tremolite gives way to diopside according to:

$$\underset{\text{tremolite}}{Ca_2Mg_5Si_8O_{22}(OH)_2} + \underset{\text{calcite}}{3CaCO_3} + \underset{\text{quartz}}{2SiO_2} \rightarrow$$

$$\underset{\text{diopside}}{5CaMgSi_2O_6} + 3CO_2\uparrow + H_2O\uparrow$$

As a result, diopside is now part of the assemblage, as shown in Fig. 21.18*d*.

At high-grade metamorphic conditions (above 600°C) forsterite may form as follows:

$$\underset{\text{diopside}}{CaMgSi_2O_6} + \underset{\text{dolomite}}{3CaMg(CO_3)_2} \rightarrow$$

$$\underset{\text{forsterite}}{2Mg_2SiO_4} + \underset{\text{calcite}}{4CaCO_3} + 2CO_2\uparrow$$

The occurrence of forsterite is noted in Fig. 21.18*e*.

At higher temperatures, such as near the contact zone of an igneous intrusive (contact metamorphism) wollastonite may be formed by the reaction with high CO_2 fluids:

$$\underset{\text{calcite}}{CaCO_3} + \underset{\text{quartz}}{SiO_2} \rightarrow \underset{\text{wollastonite}}{CaSiO_3} + CO_2\uparrow$$

The wollastonite reaction product is shown in Fig. 21.18*f*.

The previously mentioned types of reactions can be studied experimentally, providing us with quantitative information in terms of temperature and pressure ranges at which reactants give way to products (see Figs. 11.16 and 11.17). This provides us with reasonably close estimates of the conditions of metamorphism of rocks that are similar in bulk chemistry and fluid composition to those studied in the laboratory.

To depict graphically the mineralogical and assemblage changes that take place in rocks of more complex composition than the example shown in Fig. 21.18, some chemical components by which the chemical system is defined must be combined. The cation (or cation-oxide) components most commonly combined in graphical representations, are those that substitute for each other in the same cation site in a crystal structure. For this reason (MgO + FeO + MnO), (K_2O + Na_2O), and (Al_2O_3 + SiO_2) are commonly selected as combined components. The triangular composition diagram in Fig. 21.19 allows for the graphical representation of a relatively large number of common metamorphic silicate compositions as a result of the combination of (MgO + FeO) in the lower left corner; the other corners represent single oxide components. In this diagram, hydrous minerals are plotted by ignoring the (OH) or H_2O contents in their formulae. This is equivalent to stating that the hydrous mineral compositions have been projected onto the (MgO + FeO)–Al_2O_3-SiO_2 triangular base from an H_2O apex in a tetrahedral configuration. Such composition diagrams are very useful in a visual overview of all possible minerals that can occur in a specific chemical system. They also may be used to indicate, in a general sense, what minerals are found together at a specific metamorphic grade. In Fig. 21.19, tielines connect only those minerals that may be found to coexist at high metamorphic temperatures (over an estimated range of about 600° to 850°C).

A major drawback in this diagram is that binary Fe–Mg series (e.g., Mg_2SiO_4 to Fe_2SiO_4) appear only as points instead of line segments (or compositional bars). To avoid the need for combining components in triangular composition diagrams, various other graphical

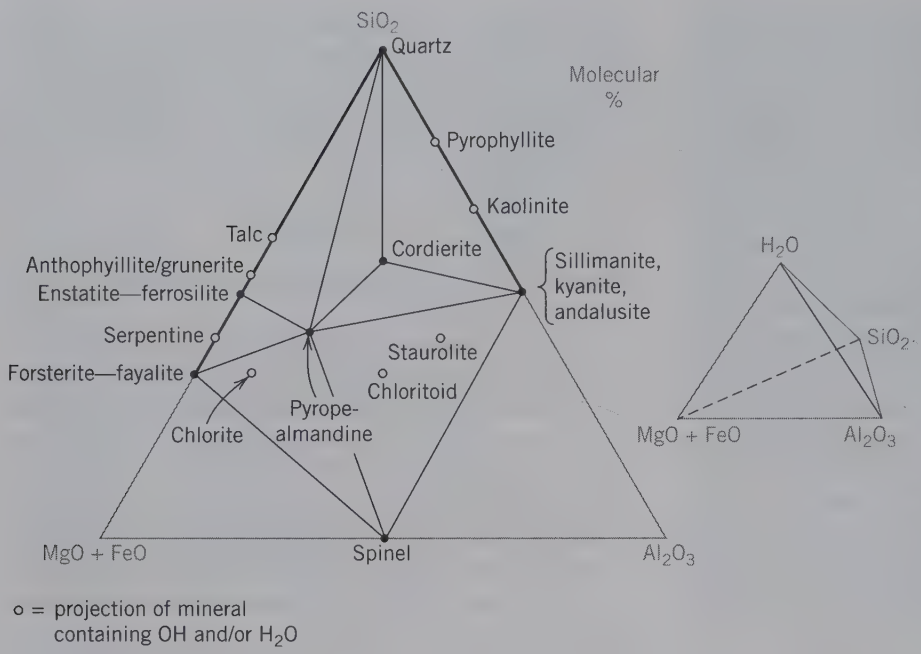

FIG. 21.19 The composition of common diagenetic and metamorphic silicates in the system $MgO–FeO–Al_2O_3–SiO_2–H_2O$. The triangle, which is water-free, can be considered as a projection from an H_2O corner in a tetrahedron (see insert). All minerals containing OH and/or H_2O are shown by open circles; all anhydrous minerals with opaque dots. Within the triangle, tielines are shown which connect the compositions of minerals that commonly form at very high temperatures of metamorphism (between about 600° and 850°C). These tielines represent coexistence (i.e., compatabilities). For the graphical location of mineral compositions in this triangle see Fig. 19.66.

projection schemes have been devised in metamorphic petrology.

In a systematic study of shales and their metamorphic equivalents in the Scottish Highlands, published in 1912, G. Barrow delineated various metamorphic zones on the basis of the occurrence of *index minerals*.[1] At successively higher grades of metamorphism, he noted that the argillaceous rocks showed the development of the following index minerals: first chlorite, then biotite, next almandine, subsequently staurolite, then kyanite, and at the highest temperatures sillimanite. Similar progressions of minerals are found in other metamorphic regions containing argillaceous rocks, such as in the New England region. When areas of specific index mineral occurrence are outlined on a geological map, such as a chlorite-rich region or a biotite-rich region, the line that marks the first appearance of an index mineral is known as an *isograd* (for "equal grade."). The isograds reflect positions of similar metamorphic grade in terms of *T* and *P*. Isograds are labeled with the name of the appropriate index mineral, or mineral pair, such as biotite isograd, garnet isograd, staurolite isograd, sillimanite–K-feldspar isograd, and so on.

In regions where very high pressures have been generated during metamorphism the final mineral assemblages will be different, for a specific bulk rock composition, from those where high temperatures have been most prevalent. Aluminum-rich rocks metamorphosed at high temperature commonly contain sillimanite, whereas those subjected to high pressures (with some increase in temperature, see Fig. 11.17) contain kyanite. Similarly, high-temperature basalt assemblages occur as coarse-grained eclogites (see Fig. 11.15) in the high-pressure regions of the lower crust of the Earth.

In addition to the subdivision of *P* and *T* fields in terms of very low, low, medium, and high grades of metamorphism (Fig. 21.17) metamorphic rocks are often classified in terms of metamorphic facies. *A metamorphic facies is a set of metamorphic mineral assemblages, repeatedly associated in space and time, such that there is a constant and, therefore, predictable relation between mineral composition and chemical composition.* A metamorphic facies is defined not in terms of a single index mineral but by an association of mineral assemblages; some examples of metamorphic facies follow. *Zeolite* facies represents the lowest grade of metamorphism. The mineral assemblages include zeolites, chlorite, muscovite, and quartz. *Greenschist facies* is the low-grade metamorphic facies of many regionally metamorphosed terranes. The mineral assemblages may include chlorite, epidote,

[1]An index mineral is a mineral that developed under a particular set of temperature and pressure conditions, thus, characterizing a particular degree of metamorphism. When dealing with progressive (or prograde) metamorphism, it is a mineral whose first appearance (in going from low to higher grades of metamorphism) marks the outer limit of the lower grade.

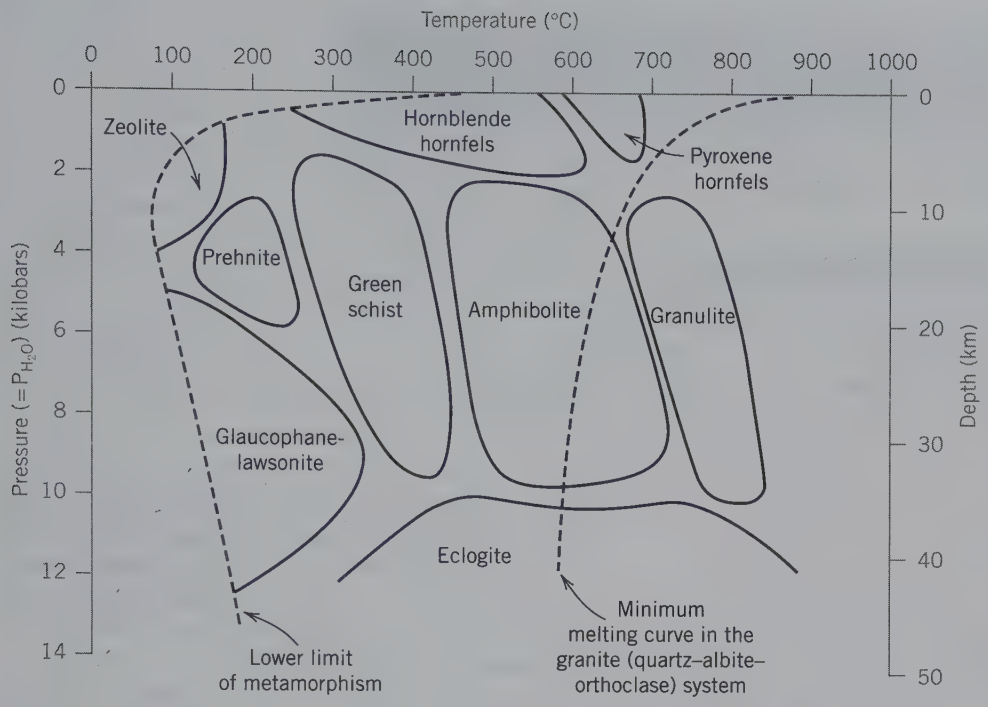

FIG. 21.20 Tentative scheme of metamorphic facies in relation to pressure (P_{H_2O}) and temperature. All boundaries are gradational. (Modified from Turner, F. J. 1968. *Metamorphic petrology.* McGraw-Hill Book Co., New York, 366. Copyright 1968 by McGraw-Hill, Inc. Used with permission of McGraw-Hill Book Co.) Compare with Fig. 21.17.

muscovite, albite, and quartz. *Amphibolite facies* occurs in medium- to high-grade metamorphic terranes. The mineral constituents include hornblende, plagioclase, and almandine in metamorphosed basalts and staurolite and sillimanite in metamorphosed shales. *Glaucophane-lawsonite schist* (or *blueschist*) *facies* is represented by relatively low temperatures but elevated pressures of metamorphism in young orogenic zones, such as California and Japan. Characteristic constituents are lawsonite, jadeite, albite, glaucophane, muscovite, and garnet in metamorphosed basalts. *Granulite facies* reflects the maximum temperature conditions of regional metamorphism, such as have been commonly attained in Archean (Precambrian) terranes. Characteristic mineral constituents are plagioclase, orthopyroxene, garnet, and diopside. *Eclogite facies* represents the deep-seated conditions of metamorphism. Characteristic mineral constituents are pyrope-rich garnet and omphacite in metamorphosed basalts. Such assemblages are common in *kimberlite* pipes, many of which carry associated diamond. A diagram outlining the approximate fields of the various metamorphic facies in terms of P and T is given in Fig. 21.20.

Minerals that are especially common in metamorphic rocks are listed in Table 21.12. Examples of mineral assemblages in carbonate-rich and aluminum-rich rocks as a function of increasing metamorphic grade are given in Table 21.13.

Table 21.12 Common Silicates of Metamorphic Rocks

Phyllosilicates	talc
	serpentine
	chlorite
	muscovite
	biotite
Inosilicates	anthophyllite
	cummingtonite-grunerite
	tremolite-actinolite
	hornblende
	glaucophane
	clinopyroxene with jadeite component (high pressure)
	diopside
	orthopyroxene
	wollastonite*
Tectosilicates	quartz
	plagioclase, except for very An-rich compositions
	microline and orthoclase
Nesosilicates and *Sorosilicates*	garnet (pyrope at high pressures)
	epidote
	kyanite, sillimanite, andalusite
	vesuvianite*
	forsterite
	staurolite
	chloritoid

*Especially common in contact metamorphic rocks.

Table 21.13 Examples of Metamorphic Mineral Assemblages Produced During Prograde Metamorphism in Carbonate-Rich Rocks and Al-rich Shale

	Ca Carbonate-rich rock (see Fig. 21.18)	Shale (Al-rich)
Very low grade	calcite–dolomite–talc and calcite–quartz–talc	muscovite–chlorite–quartz–feldspar
Low grade	calcite–dolomite–tremolite and calcite–tremolite–quartz	biotite–muscovite–chlorite–quartz–feldspar
Medium grade	calcite–dolomite–diopside and calcite–diopside–quartz	staurolite–garnet–biotite–muscovite–quartz–feldspar
High grade	calcite–dolomite–forsterite and calcite–diopside–quartz	sillimanite–garnet–biotite–muscovite–quartz–feldspar

Rock Types

Some of the most common metamorphic rocks are briefly described next.

Slate. Slates are exceedingly fine-grained rocks that have a remarkable property known as *slaty cleavage*, which permits them to be split into thin, broad sheets. Their color is commonly gray to black but may be green, yellow, brown, and red. Slates are usually the result of the metamorphism of shales. Their characteristic slaty cleavage may or may not be parallel to the bedding planes of the original shales. Slate is rather common in occurrence.

Marble. A marble is a metamorphosed limestone. It is a recrystallized rock composed of grains of calcite or, more rarely, dolomite. The individual grains may be so small that they cannot be distinguished by the eye, and again they may be coarse and show clearly the characteristic calcite cleavage. Like limestone, a marble is characterized by its softness and its effervescence with acids. When pure, marble is white, but various impurities may create a wide range of color. It is found in many localities and may be in thick and extensive beds. Commercially, *marble* is used to indicate any Ca-carbonate rock capable of taking a polish and, thus, includes some limestones.

Schist. Schists are metamorphic rocks that are distinguished by the presence of well-developed foliation or schistosity, along which the rock may be easily broken. A common example is a *mica schist*, which consists essentially of quartz and mica, usually muscovite or biotite, or both. Mica is the prominent mineral, occurring in irregular leaves and in foliated masses. The mica plates all lie with their cleavage planes parallel to each other and give to the rock a striking laminated appearance. Mica schists frequently carry characteristic accessory minerals, such as garnet, staurolite, kyanite, sillimanite, and andalusite; thus, the rock may be called *garnet–mica schist* or *staurolite–mica schist*. Other varieties of schists that are derived chiefly by the metamorphism of mafic igneous rocks are *talc schist*, *chlorite schist*, *hornblende schist*, and *amphibolite*. They are characterized, as their names indicate, by the preponderance of some metamorphic ferromagnesian mineral.

Gneiss. When the word *gneiss* is used alone, it refers to a coarsely foliated metamorphic rock. The banding is caused by the segregation of quartz and feldspar into layers alternating with layers of dark minerals. Because the metamorphism of many igneous or sedimentary rocks may result in a gneiss, there are many varieties with varied mineral associations. Thus, they are given such names as *plagioclase–biotite gneiss*, *hornblende gneiss*, or *pyroxene–garnet gneiss*. When it is certain that a gneiss is the result of metamorphism of an earlier-formed igneous rock, the igneous rock name is used in the metamorphic terminology, such as *granite gneiss* or *syenite gneiss*. Granitic gneisses, that is, rocks derived from the metamorphism of granites, are common especially in Precambrian terranes.

Quartzite. As its name indicates, a quartzite is a rock composed essentially of quartz. It has been derived from a quartz-rich sandstone by metamorphism. It is a common and widely distributed rock in which solution and redeposition of silica have yielded a compact rock of interlocking quartz grains. It is distinguished from an unmetamorphosed quartz arenite by the fracture, which in a metamorphic quartzite passes through the grains but in a sandstone, passes around them.

Serpentine. A serpentine is a rock composed essentially of the mineral serpentine, derived by retrograde metamorphism and hydration of high-temperature igneous rocks, such as dunite or peridotite. The primary forsteritic olivine gives way, in a lower temperature (retrograde) and hydrous metamorphic environment, to serpentine and brucite according to:

$$\underset{\text{forsterite}}{4Mg_2SiO_4} + 6H_2O \rightarrow \underset{\text{serpentine}}{Mg_6Si_4O_{10}(OH)_8} + \underset{\text{brucite}}{2Mg(OH)_2}$$

Serpentinites are compact, of a green to greenish-yellow color, and may have a slightly greasy feel. Serpentinites may be a source for associated chromite and platinum, as in the Ural Mountains, Russia, or a source of nickel from associated garnierite (ore rich in nickel-bearing minerals), as in New Caledonia.

Soapstone. A metamorphic rock with a massive or schistose texture and soft feel, composed essentially of fine-grained talc. It is generally the metamorphic alteration production of an originally ferromagnesian silicate-rich rock.

Amphibolite. An unfoliated or somewhat foliated metamorphic rock composed essentially of amphibole and plagioclase. Some varieties may consist almost completely of hornblende. Mineral qualifiers are used as prefixes to indicate the presence of specific minerals, for example, *garnet–amphibolite*, *biotite–amphibolite*. Amphibolites may be the metamorphic products of basic igneous rocks or of argillaceous carbonate rocks.

Greenschist. A well-foliated greenish rock consisting largely of chlorite, actinolite (or hornblende), epidote, and albite. *Greenstone* is a field term applied to somewhat metamorphosed basaltic or doleritic rocks with a characteristic green color caused by the presence of chlorite, actinolite, and epidote.

Granulite. A high-grade, relatively coarse-grained metamorphic rock with a strong layering due to the occurrence of well-oriented, flattened lenses of quartz and feldspar. Other major constituents may be pyroxene, garnet, cordierite, kyanite, or sillimanite. It contains little or no mica, and lacks prismatic minerals. The term *granulite* can be prefaced by a mineral name, or a series of mineral names, such as *garnet–granulite* or *granulite–kyanite–granulite*. Similarly, the mineralogical and chemical composition of the rock may be expressed by the use of a prefix, for example, *syenite–granulite*.

Eclogite. A dense, granular rock, which has resulted from high-pressure and high-temperature metamorphism. It is composed chiefly of omphacite (a pyroxene composition along the diopside–jadeite series) and pyrope–rich garnet. It has the bulk composition of a gabbro (or basalt; see Fig. 11.15). Other minerals that may be present are: quartz, kyanite, enstatite, olivine, and rutile. Commonly mineral names are used as qualifiers, as in *kyanite–eclogite*.

Skarn Rock. A contact metamorphic and metasomatic rock within the aureole of an intrusive igneous body. It is the result of considerable metasomatic replacement of the original rock type, which commonly is a limestone. Mineral prefixes are used to indicate the dominant mineral, for example, *andradite skarn*.

Hornfels. An old German name for a compact, horn-looking rock. Its use is now restricted to a massive, fine-grained, contact-metamorphosed rock. It is commonly made up of quartz, mica, feldspar, garnet, andalusite and/or cordierite, and minor amounts of amphibole and pyroxene showing no preferred orientation of mineral grains. The name may be modified by noting the most important constituents, for example, *cordierite–andalusite–hornfels*.

REFERENCES AND FURTHER READING

Best, M. G. 2003. *Igneous and metamorphic petrology*, 2nd ed. Blackwell Publishing, 729 pp.

Blatt, H. 1992. *Sedimentary petrology*, 2nd ed. W.H. Freeman and Co., San Francisco.

Blatt, H., Middleton, G. and Murray, R. 1980. *Origin of sedimentary rocks*, 2nd ed. Prentice Hall, Englewood Cliffs, N.J.

Blatt, H., and R. J. Tracy. 1996. *Petrology: Igneous, sedimentary, and metamorphic*. W. J. Freeman and Company, New York.

Boggs, S. 1992. *Petrology of sedimentary rocks*. Macmillan Publishing Co., New York.

Burns, R. G., ed. 1979. *Marine minerals. Reviews in Mineralogy* 6. Mineralogical Society of America, Washington, D.C.

Cerný, P., and T. S. Ercit. 2005. The classification of granitic pegmatites. *The Canadian Mineralogist* 43: 2005–2026.

Dietrich, R. V., and Skinner, B. J. 1979. *Rocks and rock minerals*. John Wiley & Sons, New York.

Dunham, R. J. 1962. Classification of carbonate rocks according to depositional texture. *American Association of Petroleum Geologists Memoir* 1: 108–21.

Folk, R. L. 1959. Practical petrographic classification of limestones. *American Association of Petroleum Geologists Bulletin* 43: 1–38.

Fry, N. 1983. *The field description of metamorphic rocks*. John Wiley & Sons, New York.

Hess, P. C. 1989. *Origins of igneous rocks*. Harvard University Press, Cambridge, Massachusetts.

Hyndman, D. W. 1972. *Petrology of igneous and metamorphic rocks*. McGraw-Hill Book Co., New York.

Igneous rocks: A classification and glossary of terms. 2002. Recommendations of the International Union of Geological Sciences, Subcommission of the Systematics of Igneous Rocks. R. W. Le Maitre (ed.). 2nd ed. Cambridge University Press, Cambridge.

Jahns, R. H. 1952. The study of pegmatites. *Economic Geology*, 50th anniversary volume. 1025–1130.

Klein, C. 2008. *Mineral rocks: Exercises in crystal chemistry and mineral chemistry, crystallography, x-ray powder diffraction, mineral and rock identification, and ore mineralogy*, 3rd ed., Wiley, New York.

Spear, F. S. 1993. *Metamorphic phase equilibria and pressure-temperature time paths*. Mineralogical Society of America, Washington, D.C.

Stewart, F. H. 1963. Marine evaporites. U.S. Geological Survey Professional Paper no. 440-Y.

Tucker, M. E. 1982. *The field description of sedimentary rocks*. John Wiley & Sons, New York.

Turner, F. J. 1980. *Metamorphic petrology*, 2nd ed. McGraw-Hill Book Co., New York.

Winkler, H. G. F. 1979. *Petrogenesis of metamorphic rocks*, 5th ed. Springer-Verlag, New York.

Winter, J. D. 2001. *An introduction to igneous and metamorphic petrology*. Prentice Hall, Upper Saddle River, New Jersey.

Yardley, B. W. D. 1989. *An introduction to metamorphic petrology*, John Wiley & Sons, New York.

CHAPTER 22

Determinative Tables

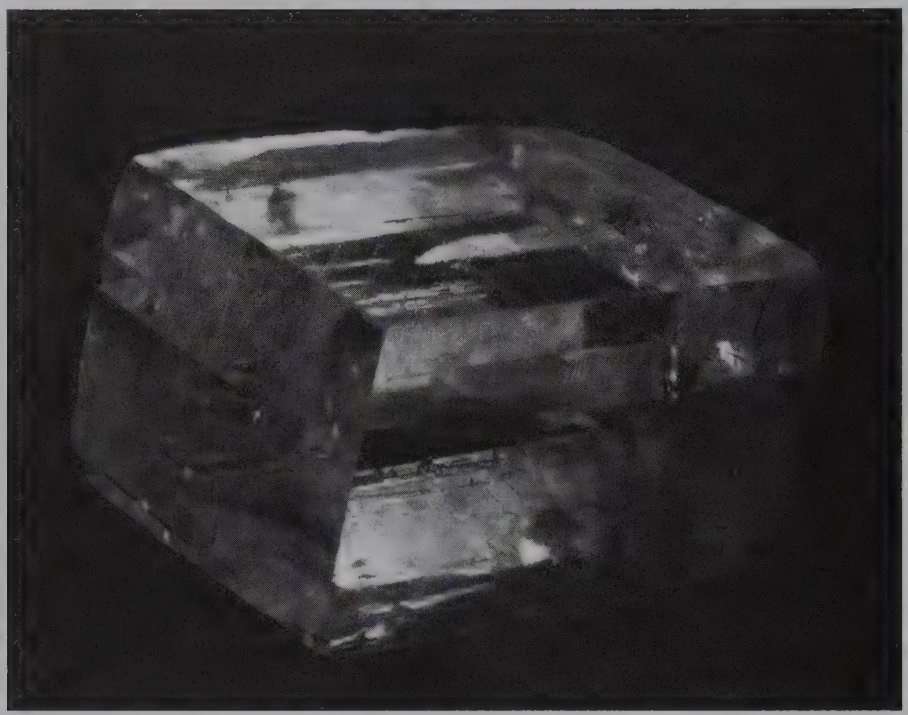

Rhombohedral $\{10\bar{1}1\}$ cleavage fragment of Iceland spar, which is the chemically pure, optically clear, and colorless variety of calcite, $CaCO_3$. Rhombohedral cleavage and effervescence in cold HCl are highly diagnostic in the identification of calcite. From the Helgustadir Calcite Mine, Eskifjordur, Sudur Mula Sysla, Iceland (Harvard Mineralogical Museum).

This chapter contains three determinative tables. Table 22.1 is based on those physical properties of minerals that can be easily and quickly determined in hand specimen. Table 22.2 lists increasing specific gravity by which minerals can be identified. Table 22.3 lists increasing refractive indices (for nonopaque minerals) by which a mineral's identity can be established.

Table 22.1 allows a mineral to be identified on the basis of easily assessed physical properties. These properties should be used with the understanding that for many minerals there is a variation in physical properties from specimen to specimen. Color for some minerals is constant, but for others it is extremely variable (refer to Chapter 10). Hardness, although more definite, may vary slightly and, by change in the state of aggregation of a mineral, may appear to vary more widely. Cleavage may also be obscured in a fine-grained aggregate of a mineral. In using the tables, it is often impossible to differentiate between two or three similar species. However, by consulting the descriptions of the possible minerals in the sections "Systematic Descriptions" and the specific tests given there, a definite decision can usually be made.

In the determinative tables, only the common minerals or those that, though rarer, are of economic importance have been included. The chances of having to identify a mineral that is not included in these tables are small, but it must be noted that there is such a possibility. The names of the minerals have been printed in three different styles of type, as **PYRITE**, CHALCOCITE, and Covellite, to indicate their relative importance and frequency of occurrence, respectively. Whenever there is ambiguity in placing a mineral, it has been included in the two or more possible divisions.

The general scheme of classification is outlined on page 332. The proper division in which to look for a mineral can be determined by means of the tests indicated there. The tables are divided into two main sections on the basis of luster: (1) metallic and submetallic and (2) nonmetallic. The metallic minerals are opaque and give black or dark-colored streaks, whereas nonmetallic minerals are nonopaque and give either colorless or light-colored streaks. The tables are next subdivided according to hardness. These

divisions are easily determined. For nonmetallic minerals they are as follows:

- $\leq 2\frac{1}{2}$, can be scratched by a fingernail
- $>2\frac{1}{2}-\leq 3$, cannot be scratched by a fingernail, can be scratched by a copper cent
- $>3-\leq 5\frac{1}{2}$, cannot be scratched by a copper cent, can be scratched by a knife
- $>5\frac{1}{2}-\leq 7$, cannot be scratched by a knife, can be scratched by quartz
- >7 cannot be scratched by quartz

Metallic minerals have fewer divisions of hardness; they are $\leq 2\frac{1}{2}$; $>2\frac{1}{2}-\leq 5\frac{1}{2}$; $>5\frac{1}{2}$.

Nonmetallic minerals are further subdivided according to whether they show a *prominent* cleavage. If the cleavage is not prominent and imperfect or obscure, the mineral is included with those that have no cleavage. Minerals in which cleavage may not be observed easily, because of certain conditions in the state of aggregation, have been included in both divisions.

The minerals that fall in a given division of the tables have been arranged according to various methods. In some cases, those that possess similar cleavages have been grouped together; frequently color determines the order, and so on. The column farthest to the left will indicate the method of arrangement.

The figures given in the column headed **G** are specific gravity. This is an important diagnostic physical property but less easily determined than luster, hardness, color, and cleavage. For a discussion of specific gravity and methods for its accurate determination, see page 33. However, if a specimen is pure and of sufficient size, its approximate specific gravity can be determined by simply weighing it in the hand. The following is a list of common minerals over a wide range of specific gravity. By experimenting with specimens of these, one can become expert in the approximate determination of specific gravity. Following the determinative tables (Table 22.1) is a list of the common minerals arranged according to increasing specific gravity (Table 22.2).

Gypsum	2.32	Pyrite	5.02
Orthoclase	2.57	Arsenopyrite	6.07
Quartz	2.65	Cassiterite	6.95
Calcite	2.71	Galena	7.50
Fluorite	3.18	Cinnabar	8.10
Topaz	3.53	Copper	8.90
Corundum	4.02	Silver	10.5
Barite	4.45		

Many minerals are polymorphic. The crystal system given in the tables is that of the most commonly observed form.

GENERAL CLASSIFICATION OF THE TABLES

LUSTER—METALLIC OR SUBMETALLIC

I. Hardness: $\leq 2\frac{1}{2}$ will leave a mark on the paper). Page 606

II. Hardness: $>2\frac{1}{2}$, $<5\frac{1}{2}$ (can be scratched by a knife; will not readily leave a mark on paper). Page 607

III. Hardness: $>5\frac{1}{2}$ (cannot be scratched by a knife). Page 610

LUSTER—NONMETALLIC

I. Streak definitely colored. Page 612

II. Streak colorless.
   - A. Hardness: $\leq 2\frac{1}{2}$ (can be scratched by a fingernail). Page 614
   - B. Hardness: $>2\frac{1}{2}$, ≤ 3 (cannot be scratched by a fingernail; can be scratched by a copper cent).
     1. Cleavage prominent. Page 616
     2. Cleavage not prominent.
        - a. A small splinter is fusible in the candle flame. Page 617
        - b. Infusible in candle flame. Page 618
   - C. Hardness; >3, $\leq 5\frac{1}{2}$ (cannot be scratched by a copper cent; can be scratched by a knife).
     1. Cleavage prominent. Page 619
     2. Cleavage not prominent. Page 623
   - D. Hardness; $>5\frac{1}{2}$, ≤ 7 (cannot be scratched by a knife, can be scratched by quartz).
     1. Cleavage prominent. Page 626
     2. Cleavage not prominent. Page 629
   - E. Hardness: >7 (cannot be scratched by quartz).
     1. Cleavage prominent. Page 632
     2. Cleavage not prominent. Page 633

Table 22.1 Minerals Arranged by Several Physical Properties

LUSTER: METALLIC OR SUBMETALLIC
1. Hardness: $\leq 2\frac{1}{2}$,
(Will leave a mark on paper)

Streak	Color	G	H	Remarks	Name, Composition, Crystal System
Black	Iron-black	4.7	1–2	Usually splintery or in radiating fibrous aggregates.	**PYROLUSITE** p. 382 MnO_2 Tetragonal
	Steel-gray to iron-black	2.23	$1-1\frac{1}{2}$	Cleavage perfect {0001}. May be in hexagonal-shaped plates. Greasy feel.	**GRAPHITE** p. 350 C Hexagonal
Black to greenish black	Blue-black	4.7	$1-1\frac{1}{2}$	Cleavage perfect {0001}. May be in hexagonal-shaped leaves. Greenish streak on glazed porcelain (graphite, black). Greasy feel.	MOLYBDENITE p. 365 MoS_2 Hexagonal
Gray-black	Blue-black to lead-gray	7.6	$2\frac{1}{2}$	Cleavage perfect cubic {100}. In cubic crystals. Massive granular.	**GALENA** p. 353 PbS Isometric
	Blue-black	4.5	2	Cleavage perfect {010}. Bladed with cross striations. Fuses in candle flame.	**STIBNITE** p. 361 Sb_2S_3 Orthorhombic
Bright red	Red to vermillion	8.1	$2-2\frac{1}{2}$	Cleavage perfect $\{10\bar{1}0\}$. Luster adamantine. Usually granular massive.	**CINNABAR** p. 360 HgS Hexagonal
	Ruby-red	5.55	$2-2\frac{1}{2}$	Cleavage $\{10\bar{1}1\}$. Fusible in candle flame. Associated with pyrargyrite.	Prousite p. 367 Ag_3AsS_3 Hexagonal
Red-brown	Red to vermillion	5.2	1+	Earthy. Frequently as pigment in rocks. Crystalline hematite is harder and black.	**HEMATITE** p. 377 Fe_2O_3 Hexagonal
Red-brown to brown-red	Deep red to black	5.85	$2\frac{1}{2}$	Cleavage $\{10\bar{1}1\}$. Fusible in candle flame. Shows dark ruby-red color in thin splinters. Associated with other silver minerals.	Pyrargyrite p. 367 Ag_3SbS_3 Hexagonal
Black; may mark paper	Steel-gray on fresh surface. Tarnishes to dull gray	7.3	$2-2\frac{1}{2}$	Usually massive or earthy. Easily sectile. Bright steel-gray on fresh surfaces; darkens on exposure.	ACANTHITE p. 351 Ag_2S Isometric
	Blue; may tarnish to blue-black	4.6	$1\frac{1}{2}-2$	Usually in platy masses or in thin six-sided platy crystals. Moistened with water turns purple.	Covellite p. 359 CuS Hexagonal

Table 22.1 (continued)

LUSTER: METALLIC OR SUBMETALLIC
II. Hardness: $>2\frac{1}{2}-\leq 5\frac{1}{2}$,
(Can be scratched by a knife; will not readily leave a mark on paper)

Streak	Color	G	H	Remarks	Name, Composition, Crystal System
Black	Gray-black	4.4	3	Cleavage {110}. Usually in bladed masses showing cleavage. Associated with other copper minerals.	ENARGITE p. 366 Cu_3AsS_4 Orthorhombic
	Pale copper-red; may be silver-white, pinkish	7.8	$5-5\frac{1}{2}$	Usually massive. May be coated with green nickel bloom. Associated with cobalt and nickel minerals.	NICKELINE p. 358 NiAs Hexagonal
	Fresh surface brownish-bronze; purple tarnish	5.1	3	Usually massive. Associated with other copper minerals; primarily chalcocite and chalcopyrite. "Peacock ore."	**BORNITE** p. 351 Cu_5FeS_4 Isometric
	Brownish-bronze	4.6	4	Small fragments magnetic. Usually massive. Often associated with chalcopyrite and pyrite.	**PYRRHOTITE** p. 357 $Fe_{1-x}S$ Hexagonal
		4.6 to 5.0	$3\frac{1}{2}-4$	Octahedral parting. Resembles pyrrhotite with which it usually is associated but nonmagnetic.	Pentlandite p. 359 $(Fe,Ni)_9S_8$ Isometric
	Brass-yellow	4.1 to 4.3	$3\frac{1}{2}-4$	Usually massive, but may be in crystals resembling tetrahedrons. Associated with other copper minerals and pyrite.	**CHALCOPYRITE** p. 356 $CuFeS_2$ Tetragonal
	Brass-yellow; slender crystals greenish	5.5	$3-3\frac{1}{2}$	Cleavage $\{10\bar{1}1\}$, rarely seen. Usually in radiating groups of hairlike crystals	MILLERITE p. 358 NiS Hexagonal
Gray-black; will mark paper	Lead-gray	4.6	2	Cleavage perfect {010}. Fuses easily in candle flame. In bladed crystal aggregates with cross striations.	**STIBNITE** p. 361 Sb_2S_3 Orthorhombic
		7.5	$2\frac{1}{2}$	Cleavage perfect {100}. In cubic crystals and granular masses. If held in the candle flame, does not fuse but small globules of metallic lead collect on the surface. Octahedra rare.	**GALENA** p. 353 PbS Isometric
Black; may mark paper	Steel-gray on fresh surface. Tarnishes to dull gray	7.3	$2-2\frac{1}{2}$	Easily sectile. Usually massive or earthy. Rarely in cubic crystals.	Acanthite p. 351 Ag_2S Isometric

Table 22.1 (continued)

LUSTER: METALLIC OR SUBMETALLIC
II. Hardness: $>2\frac{1}{2}-\leq5\frac{1}{2}$,
(Can be scratched by a knife; will not readily leave a mark on paper)

Streak	Color	G	H	Remarks	Name, Composition, Crystal System
Usually black; may be brownish	Black	3.7 to 4.7	5–6	Massive botryoidal and stalactitic. Usually associated with pyrolusite	ROMANECHITE p. 391 $(Ba,H_2O)_2(Mn^{4+},Mn^{3+})_5O_{10}$ Appears amorphous
Black; may have brown tinge	Steel-gray. May tarnish to dead black on exposure	4.7 to 5.0	$3-4\frac{1}{2}$	Massive or in tetrahedral crystals. Often associated with silver ores.	TETRAHEDRITE p. 367 $(Cu,Fe,Ag,Zn)_{12}Sb_4S_{13}$ Isometric
Gray-black		5.7	$2\frac{1}{2}-3$	Somewhat sectile. Usually compact massive. Associated with other copper minerals. Steel gray on freshly cut surface.	CHALCOCITE p. 351 Cu_2S Orthorhombic
Dark brown to black	Iron-black to brownish-black	4.6	$5\frac{1}{2}$	Luster pitchy. May be accompanied by yellow or green oxidation products. Usually in masses in peridotites.	**CHROMITE** p. 388 $FeCr_2O_4$ Isometric
	Brown to black	7.0 to 7.5	$5-5\frac{1}{2}$	Cleavage perfect {010}. With greater amounts of Mn streak and color are darker. Tabular crystals.	WOLFRAMITE p. 425 $(Fe,Mn)WO_4$ Monoclinic
Dark brown to black	Steel-gray to iron-black	4.3	4	In radiating fibrous or crystalline masses. Distinct prismatic crystals often grouped in bundles. Associated with pyrolusite.	MANGANITE p. 390 MnO(OH) Orthorhombic
Light to dark brown	Dark brown to coal-black. More rarely yellow or red	3.9 to 4.1	$3\frac{1}{2}-4$	Cleavage perfect {110} (6 directions). Usually cleavable, granular; may be in tetrahedral crystals. The streak is always of a lighter color than the specimen.	**SPHALERITE** p. 356 ZnS Isometric
Red-brown to brown-red	Dark brown to steel-gray to black	4.8 to 5.3	$5\frac{1}{2}-6\frac{1}{2}$	Usually harder than a knife. Massive, radiating, reniform, micaceous.	**HEMATITE** p. 377 Fe_2O_3 Hexagonal
	Red-brown to deep red. Ruby-red if transparent	6.0	$3\frac{1}{2}-4$	Massive or in cubes or octahedrons. May be in very slender crystals. Associated with malachite, azurite, native copper.	CUPRITE p. 375 Cu_2O Isometric
Yellow-brown; yellow ocher	Dark brown to black	4.37	$5-5\frac{1}{2}$	Cleavage {010}. In radiating fibers, mammillary and stalactitic forms. Rarely in crystals.	**GOETHITE** p. 392 $\alpha FeO(OH)$ Orthorhombic
Dark red (some varieties mark paper)	Dark red to vermillion	8.10	$2\frac{1}{2}$	Cleavage $\{10\bar{1}1\}$. Usually granular or earthy. Commonly impure and dark red or brown. When pure, translucent or transparent and bright red.	**CINNABAR** p. 360 HgS Hexagonal

Table 22.1 (continued)

LUSTER: METALLIC OR SUBMETALLIC
II. Hardness: $>2\frac{1}{2}-\leq5\frac{1}{2}$,
(Can be scratched by a knife; will not readily leave a mark on paper)

Streak	Color	G	H	Remarks	Name, Composition, Crystal System
Copper-red, shiny	Copper-red on fresh surface. Black or green tarnish	8.9	$2\frac{1}{2}-3$	Malleable. Usually in irregular grains. May be in branching crystal groups or in rude isometric crystals.	COPPER p. 344 Cu Isometric
Silver-white, shiny	Silver-white on fresh surface. Black tarnish	10.5	$2\frac{1}{2}-3$	Malleable. Usually in irregular grains. May be in wire, plates, branching crystal groups.	SILVER p. 343 Ag Isometric
Gray, shiny	White or steel-gray	14 to 19	$4-4\frac{1}{2}$	Malleable. Irregular grains or nuggets. Unusually hard for a metal. Rare.	Platinum p. 345 Pt Isometric
Gold-yellow, shiny	Gold-yellow	15.0 to 19.3	$2\frac{1}{2}-3$	Malleable. Irregular grains, nuggets, leaves. Very heavy; specific gravity varies with silver content.	GOLD p. 341 Au Isometric

Table 22.1 (continued)

LUSTER: METALLIC OR SUBMETALLIC
III. Hardness: $>5\frac{1}{2}$
(Cannot be scratched by a knife)

Streak	Color	G	H	Remarks	Name, Composition, Crystal System
Black	Silver- or tin-white	6.0 to 6.2	$5\frac{1}{2}$–6	Usually massive. Crystals pseudo-orthorhombic.	**ARSENOPYRITE** p. 366 FeAsS Monoclinic
		6.1 to 6.9	$5\frac{1}{2}$	Usually massive. Crystals pyritohedral. May be coated with pink nickel bloom.	Skutterudite–Nickel skutterudite p. 366 $CoAs_{2-3}$–$(Ni,Co,Fe)As_{2-3}$ Isometric
		6.33	$5\frac{1}{2}$	Commonly in pyritohedral crystals with pinkish cast. Also massive.	Cobaltite–Gersdorffite p. 365 CoAsS–NiAsS Pseudo-isometric
	Copper-red to silver-white with pink tone	7.5	5–$5\frac{1}{2}$	Usually massive. May be coated with green nickel bloom.	NICKELINE p. 358 NiAs Hexagonal
	Pale brass-yellow	5.0	6–$6\frac{1}{2}$	Often in pyritohedrons or striated cubes. Massive granular. Most common sulfide.	**PYRITE** p. 363 FeS_2 Isometric
	Pale yellow to almost white	4.9	6–$6\frac{1}{2}$	Frequently in "cock's comb" crystal groups and radiating fibrous masses.	**MARCASITE** p. 364 FeS_2 Orthorhombic
	Black	5.18	6	Strongly magnetic. Crystals octahedral. May show octahedral parting.	**MAGNETITE** p. 386 Fe_3O_4 Isometric
Dark brown to black	Black	9.0 to 9.7	$5\frac{1}{2}$	Luster pitchy. Massive granular, botryoidal crystals.	Uraninite p. 383 UO_2 Isometric
		4.7	$5\frac{1}{2}$–6	May be slightly magnetic. Often associated with magnetite. Massive granular; platy crystals; as sand.	**ILMENITE** p. 379 $FeTiO_3$ Hexagonal
		3.7 to 4.7	5–6	Compact massive, stalactitic, botryoidal. Associated with other manganese minerals and told by greater hardness.	ROMANECHITE p. 391 $(Ba,H_2O)_2(Mn^{4+},Mn^{3+})_5O_{10}$ Monoclinic
Dark brown to black	Black	5.3 to 7.3	6	Luster black and shiny on fresh surface. May have slight bluish tarnish. Granular or in stout prismatic crystals.	Ferrocolumbite-Ferrotantalite p. 389 $(Fe,Mn)(Nb,Ta)_2O_6$ Orthorhombic

Table 22.1 (continued)

LUSTER: METALLIC OR SUBMETALLIC
III. Hardness: $>5\frac{1}{2}$
(Cannot be scratched by a knife)

Streak	Color	G	H	Remarks	Name, Composition, Crystal System
Dark brown	Iron-brown to brownish-black	7.0 to 7.5	$5-5\frac{1}{2}$	Cleavage perfect {010}. With greater amounts of Mn streak and color are darker. Tabular crystals.	WOLFRAMITE p. 425 $(Fe,Mn)WO_4$ Monoclinic
		4.6	$5\frac{1}{2}$	Luster pitchy. Frequently accompanied by green oxidation products. Usually in granular masses in peridotites.	**CHROMITE** p. 388 $FeCr_2O_4$ Isometric
		5.15	6	Slightly magnetic. Granular or in octahedral crystals. Common only at Franklin, NJ, associated with zincite and willemite.	FRANKLINITE p. 387 $(Fe,Zn,Mn)(Fe,Mn)_2O_4$ Isometric
Red-brown, brown-red	Red to dark brown to steel-gray to black	4.8 to 5.3	$5\frac{1}{2}-6\frac{1}{2}$	Radiating, reniform, massive, micaceous. Rarely in steel-black rhombohedral crystals. Some varieties softer.	**HEMATITE** p. 377 Fe_2O_3 Hexagonal
Pale brown	Brown to black	4.18 to 4.25	$6-6\frac{1}{2}$	In prismatic crystals, vertically striated; often slender acicular. Crystals frequently twinned. Found in black sands.	**RUTILE** p. 379 TiO_2 Tetragonal
Yellow-brown to yellow-ocher	Dark brown to black	4.37	$5-5\frac{1}{2}$	Cleavage {010}. Radiating, colloform, stalactitic.	**GOETHITE** p. 392 $\alpha FeO(OH)$ Orthorhombic

Table 22.1 (continued)

LUSTER: NONMETALLIC
I. Streak definitely colored

Streak	Color	G	H	Remarks	Name, Composition, Crystal System
Dark red	Dark red to vermillion	8.10	$2\frac{1}{2}$	Cleavage $\{10\bar{1}0\}$. Usually granular or earthy. Commonly impure and dark red or brown. When pure, translucent or transparent and bright red.	**CINNABAR** p. 360 HgS Hexagonal
	Red-brown. Ruby-red when transparent	6.0	$3\frac{1}{2}$–4	Massive or in cubes or octahedrons. May be in very slender crystals. Associated with malachite, azurite, native copper.	CUPRITE p. 375 Cu_2O Isometric
Red-brown	Red to dark brown to steel-gray to black	4.8 to 5.3	$5\frac{1}{2}$–$6\frac{1}{2}$	Radiating, reniform massive, micaceous. Rarely in steel-black rhombohedral crystals. Some varieties softer.	**HEMATITE** p. 377 Fe_2O_3 Hexagonal
	Deep red to black	5.8	$2\frac{1}{2}$	Cleavage $\{10\bar{1}1\}$. Fusible in candle flame. Shows dark ruby-red color in thin splinters. Associated with other silver minerals.	Pyrargyrite p. 367 Ag_3SbS_3 Hexagonal
Bright red	Ruby-red	5.55	2–$2\frac{1}{2}$	Cleavage $\{10\bar{1}1\}$. Fusible in candle flame. Light "ruby silver." Associated with pyrargyrite.	Proustite p. 367 Ag_3AsS_3 Hexagonal
Pink	Red to pink	2.95	$1\frac{1}{2}$–$2\frac{1}{2}$	Cleavage perfect {010}. Usually reniform or as powdery or earthy crusts. Found as coatings on cobalt minerals.	Erythrite (cobalt bloom) p. 431 $Co_3(AsO_4)_2 \cdot 8H_2O$ Monoclinic
Yellow-brown to yellow-ocher	Dark brown to black	4.4	5–$5\frac{1}{2}$	Cleavage {010}. In radiating fibers, mammillary and stalactitic forms. Rarely in crystals.	**GOETHITE** p. 392 $\alpha FeO(OH)$ Orthorhombic
Brown	Dark brown	7.0 to 7.5	5–$5\frac{1}{2}$	Cleavage perfect {010}. With greater amounts of manganese the streak and color are darker. Tabular crystals.	WOLFRAMITE p. 425 $(Fe,Mn)WO_4$ Monoclinic
	Light to dark brown	3.83 to 3.88	$3\frac{1}{2}$–4	In cleavable masses or in small curved rhombohedral crystals. Becomes magnetic after heating in candle flame.	**SIDERITE** p. 409 $FeCO_3$ Hexagonal

Table 22.1 (continued)

LUSTER: NONMETALLIC
I. Streak definitely colored

Streak	Color	G	H	Remarks	Name, Composition, Crystal System
Light brown	Light to dark brown	3.9 to 4.1	$3\frac{1}{2}$–4	Cleavage perfect {011}. (6 directions).Usually cleavable, granular; may be in tetrahedral crystals. The streak is always of a lighter color than the specimen.	**SPHALERITE** p. 356 ZnS Isometric
	Brown to black	6.8 to 7.1	6–7	Occurs in twinned crystals. Fibrous, reniform, and irregular masses; in rolled grains.	**CASSITERITE** p. 382 SnO_2 Tetragonal
	Reddish-brown to black	4.18 to 4.25	6–$6\frac{1}{2}$	Crystals vertically striated; often acicular. Twinning common.	**RUTILE** p. 379 TiO_2 Tetragonal
Orange-yellow	Deep red to orange-yellow	5.68	4–$4\frac{1}{2}$	Cleavage {0001}. Found only at Franklin, NJ, associated with franklinite and willemite.	ZINCITE p. 376 ZnO Hexagonal
	Bright red to orange	5.9 to 6.1	$2\frac{1}{2}$–3	Luster adamantine. In long slender crystals, often interlacing groups. Decrepitates in candle flame.	Crocoite p. 422 $PbCrO_4$ Monoclinic
	Deep red	3.48	$1\frac{1}{2}$–2	Frequently earthy. Associated with orpiment. Fusible in candle flame.	REALGAR p. 360 AsS Monoclinic
Pale yellow	Lemon-yellow	3.49	$1\frac{1}{2}$–2	Cleavage {010}. Luster resinous. Associated with realgar. Fusible in candle flame.	ORPIMENT p. 361 As_2S_3 Monoclinic
	Pale yellow	2.05 to 2.09	$1\frac{1}{2}$–$2\frac{1}{2}$	Burns with blue flame giving odor of SO_2. Orthorhombic crystals. Granular, earthy.	**SULFUR** p. 345 S Orthorhombic
Light green	Dark emerald-green	3.75 to 3.77	3–$3\frac{1}{2}$	One perfect cleavage {010}. In granular cleavable masses or small prismatic crystals.	Atacamite p. 397 $Cu_2Cl(OH)_3$ Orthorhombic
Light green	Dark emerald-green	3.9±	$3\frac{1}{2}$–4	One good cleavage {010}. In small prismatic crystals or granular masses.	Antlerite p. 424 $Cu_3(SO_4)(OH)_4$ Orthorhombic
	Bright green	3.9 to 4.03	$3\frac{1}{2}$–4	Radiating fibrous, mammillary. Associated with azurite and may alter to it. Effervesces in cold acid.	**MALACHITE** p. 415 $Cu_2CO_3(OH)_2$ Monoclinic
Light blue	Intense azure-blue	3.77	$3\frac{1}{2}$–4	In small crystals, often in groups. Radiating fibrous, usually as alteration from malachite. Effervesces in cold acid.	**AZURITE** p. 416 $Cu_3(CO_3)_2(OH)_2$ Monoclinic
Very light blue	Light green to turquoise-blue	2.0 to 2.4	2–4	Massive compact. Associated with oxidized copper minerals.	CHRYSOCOLLA p. 533 $\sim Cu_4H_4Si_4O_{10}(OH)_8 \cdot nH_2O$ Amorphous

Table 22.1 (continued)

LUSTER: NONMETALLIC
II. Streak colorless
A. Hardness: $\leq 2\frac{1}{2}$
(Can be scratched by a fingernail)

Cleavage, Fracture	Color	G	H	Remarks	Name, Composition, Crystal System
Perfect cleavage in one direction The micas or related micaceous minerals possess such a perfect cleavage that they can be split into exceedingly thin sheets. They may occur as aggregates of minute scales, when the micaceous structure may not be readily apparent.	Pale brown, green, yellow, white	2.76 to 2.88	$2-2\frac{1}{2}$	In foliated masses and scales. Crystals tabular with hexagonal or diamond-shaped outline. Cleavage flakes elastic.	**MUSCOVITE** p. 525 $KAl_2(AlSi_3O_{10})(OH)_2$ Monoclinic
	Dark brown, green to black; may be yellow	2.95 to 3	$2\frac{1}{2}-3$	Usually in irregular foliated m asses. Crystals have hexagonal outline, but rare. Cleavage flakes elastic.	**BIOTITE** p. 528 $K(Mg,Fe)_3(AlSi_3O_{10})(OH)_2$ Monoclinic
	Yellowish-brown, green white	2.86	$2\frac{1}{2}-3$	Often in six-sided tabular crystals; in irregular foliated masses. May show copperlike reflection from cleavage.	PHLOGOPITE p. 528 $KMg_3(AlSi_3O_{10})(OH)_2$ Monoclinic
	Green of various shades	2.6 to 2.9	$2-2\frac{1}{2}$	Usually in irregular foliated masses. May be in compact masses of minute scales. Thin sheets flexible but not elastic.	**CHLORITE** p. 531 $(Mg,Fe)_3(Si,Al)_4O_{10}(OH)_2 \cdot -(Mg,Fe)_3(OH)_6$ Monoclinic
	White, apple-green, gray. When impure as in soapstone, dark gray, dark green to almost black	2.7 to 2.8	1	Greasy feel. Frequently distinctly foliated or micaceous. Cannot be positively identified by physical tests.	**TALC** p. 524 $Mg_3Si_4O_{10}(OH)_2$ Monoclinic
		2.8 to 2.9	1–2		Pyrophyllite p. 525 $Al_2Si_4O_{10}(OH)_2$ Monoclinic
	White, gray, green	2.39	$2\frac{1}{2}$	Pearly luster on cleavage face, elsewhere vitreous. Sectile. Commonly foliated massive, may be in broad tabular crystals. Thin sheets flexible but not elastic.	BRUCITE p. 390 $Mg(OH)_2$ Hexagonal
{001} perfect seldom seen. Fracture earthy.	White; may be darker	2.6 to 2.63	$2-2\frac{1}{2}$	Compact, earthy. Breathed upon, gives argillaceous odor. Will adhere to the dry tongue.	**KAOLINITE** p. 522 $Al_2Si_2O_5(OH)_4$ Triclinic
Cubic {100}	Colorless or white to orange	1.99	2	Soluble in water, bitter taste. Resembles halite but softer. In granular cleavable masses or cubic crystals.	Sylvite p. 394 KCl Isometric

Table 22.1 (continued)

LUSTER: NONMETALLIC
II. Streak colorless
A. Hardness: $\leq 2\frac{1}{2}$
(Can be scratched by a fingernail)

Cleavage, Fracture	Color	G	H	Remarks	Name, Composition, Crystal System
{010} perfect, {100}, {011} good	Colorless, white, gray. May be colored by impurities	2.32	2	Occurs in crystals, broad cleavage flakes. May be compact massive without cleavage, or fibrous with silky luster.	**GYPSUM** p. 423 $CaSO_4 \cdot 2H_2O$ Monoclinic
Rhombohedral {10$\bar{1}$1} poor	Colorless or white	2.29	1–2	Occurs in saline crusts. Readily soluble in water; cooling and salty taste. Fusible in candle flame.	NITRATITE p. 416 $NaNO_3$ Hexagonal
Prismatic {110}, seldom seen. Fracture conchoidal		2.09 to 2.14	2	Usually in crusts, silky tufts and delicate acicular crystals. Readily soluble in water; cooling and salty taste. Fusible in the candle flame.	Niter, p. 416 KNO_3 Orthorhombic
Fracture uneven	Pearl-gray or colorless. Turns to pale brown on exposure to light	5.5±	2–3	Perfectly sectile. Translucent in thin plates. In irregular masses, rarely in crystals. Distinguished from other silver halides only by chemical tests.	Chlorargyrite p. 395 AgCl Isometric
	Pale yellow	2.05 to 2.09	$1\frac{1}{2}$–$2\frac{1}{2}$	Burns with blue flame, giving odor of SO_2. Orthorhombic crystals. Granular, earthy.	**SULFUR** p. 345 S Orthorhombic
	Yellow, brown, gray, white	2.0 to 2.55	1–3	In rounded grains, often earthy and claylike. Usually harder than $2\frac{1}{2}$.	**BAUXITE** p. 392 A mixture of Al hydroxides
Cleavage seldom seen	White	1.95	1	Usually in rounded masses of fine fibers and acicular crystals.	ULEXITE p. 419 $NaCaB_5O_6(OH) \cdot 5H_2O$ Triclinic

Table 22.1 (continued)

LUSTER: NONMETALLIC
II. Streak colorless
B. Hardness: $>2\frac{1}{2}-\leq 3$
(Cannot be scratched by a fingernail; can be scratched by a copper cent)
1. Cleavage prominent

Cleavage, Fracture		Color	G	H	Remarks	Name, Composition, Crystal System
Perfect cleavage in one direction. See also the minerals of the mica group, p. 614, which may be harder than the fingernail.	{001}	Lilac, grayish white, pink	2.8 to 3.0	$2\frac{1}{2}-4$	Crystals six-sided prismatic. Usually in small irregular sheets and scales. A pegmatite mineral.	LEPIDOLITE p. 529 $K(Li,Al)_{2-3}(AlSi_3O_{10})(OH,F)_2$ Monoclinic
	{001}	Pink, gray, white	3.0 to 3.1	$3\frac{1}{2}-5$	Usually in irregular foliated masses; folia brittle. Associated with emery.	MARGARITE p. 529 $CaAl_2(Al_2Si_2O_{10})(OH)_2$ Monoclinic
	{010}	Colorless or white	4.3	$3\frac{1}{2}$	Usually massive, with radiating habit. Effervesces in cold acid.	**WITHERITE** p. 412 $BaCO_3$ Orthorhombic
Cleavage in two directions {001} {100}		Colorless or white to gray	1.95	3	Occurs in cleavable crystalline aggregates.	KERNITE p. 416 $Na_2B_4O_6(OH)_2{\cdot}3H_2O$ Monoclinic
Cleavage in three directions at right angles	Cubic {100}	Colorless, white, red, blue	2.1 to 2.3	$2\frac{1}{2}$	Common salt. Soluble in water, taste salty, fusible in candle flame. In granular masses or in cubic crystals.	**HALITE** p. 393 NaCl Isometric
	Cubic {100}	Colorless or white to orange	1.99	2	Resembles halite, but distinguished from it by more bitter taste and lesser hardness.	Sylvite p. 394 KCl Isometric
	{001} {010} {100}	Colorless, white, blue, gray, red	2.89 to 2.98	$3-3\frac{1}{2}$	Commonly in massive aggregates, not showing cleavage, appears 'sugary'; then distinguished only by chemical tests.	**ANHYDRITE** p. 422 $CaSO_4$ Orthorhombic
Cleavage in three directions, not at right angles. Rhombohedral $\{10\bar{1}1\}$		Colorless, white, and variously tinted	2.71	3	Effervesces in cold acid. Crystals show many forms. Occurs as limestone and marble. Clear varieties show strong double refraction.	**CALCITE** p. 407 $CaCO_3$ Hexagonal
Cleavage in three directions, not at right angles. Rhombohedral $\{10\bar{1}1\}$.		Colorless, white, pink	2.85	$3\frac{1}{2}-4$	Usually harder than 3. Often in curved rhombohedral crystals with pearly luster; as dolomitic limestone and marble. Powdered mineral will effervesce in cold acid.	**DOLOMITE** p. 413 $CaMg(CO_3)_2$ Hexagonal

Table 22.1 (continued)

LUSTER: NONMETALLIC
II. Streak colorless
B. Hardness: $>2\frac{1}{2}-\leq 3$
(Cannot be scratched by a fingernail; can be scratched by a copper cent)
1. Cleavage prominent

Cleavage, Fracture	Color	G	H	Remarks	Name, Composition, Crystal System
Cleavage in three directions. Basal {001} at right angles to prismatic {210}	Colorless, white, blue, yellow red	4.5	$3-3\frac{1}{2}$	Frequently in aggregates of platy crystals. Pearly luster on basal cleavage. Characterized by high specific gravity and thus distinguished from celestite.	**BARITE** p. 420 $BaSO_4$ Orthorhombic
	Colorless, white, blue, red	3.95 to 3.97	$3-3\frac{1}{2}$	Similar to barite but lower specific gravity.	**CELESTITE** p. 421 $SrSO_4$ Orthorhombic
	Colorless or white; gray-brown when impure	6.2 to 6.4	3	Adamantine luster. Usually massive but may be in small tabular crystals. Alteration of galena. When massive may need test for SO_4 to distinguish from cerrusite ($PbCO_3$).	**ANGLESITE** p. 421 $PbSO_4$ Orthorhombic

2. Cleavage not prominent
a. Small splinter is fusible in the candle flame

	Color	G	H	Remarks	Name, Composition, Crystal System
	Colorless or white	1.7±	$2-2\frac{1}{2}$	Soluble in water. One good cleavage, seldom seen. In crusts and prismatic crystals. In candle, flame swells and then fuses. Sweetish alkaline taste.	**BORAX** p. 417 $Na_2B_4O_5(OH)_4{\cdot}8H_2O$ Monoclinic
		2.95 to 3.0	$2\frac{1}{2}$	Massive with peculiar translucent appearance. Fine powder becomes nearly invisible when placed in water. Ivigtut, Greenland, only important locality. Pseudocubic parting.	CRYOLITE p. 395 Na_3AlF_6 Monoclinic
		6.55	$3-3\frac{1}{2}$	Luster adamantine. In granular masses and platy crystals, usually associated with galena. Effervesces in cold nitric acid.	**CERUSSITE** p. 413 $PbCO_3$ Orthorhombic

Table 22.1 (continued)

LUSTER: NONMETALLIC
II. Streak colorless
B. Hardness: $>2\frac{1}{2}$, ≤ 3
(Cannot be scratched by a fingernail; can be scratched by a copper cent)
2. Cleavage not prominent
b. Infusible in candle flame

Color	G	H	Remarks	Name, Composition, Crystal System
Colorless or white	4.3	$3\frac{1}{2}$	Often in radiating masses; granular; rarely in pseudohexagonal crystals. Effervesces in cold acid	**WITHERITE** p. 412 $BaCO_3$ Orthorhombic
	2.6 to 2.63	$2-2\frac{1}{2}$	Usually compact, earthy. When breathed upon, gives an argillaceous odor.	**KAOLINITE** p. 522 $Al_2Si_2O_5(OH)_4$ Triclinic
Colorless, white, blue, gray, red	2.89 to 2.98	$3-3\frac{1}{2}$	Commonly in massive fine aggregates, not showing cleavage, but may appear 'sugary,' and can be distinguished only by chemical tests.	**ANHYDRITE** p. 422 $CaSO_4$ Orthorhombic
Yellow, brown, gray, white	2.0 to 2.55	1–3	Usually pisolitic; in rounded grains and earthy masses. Often impure.	**BAUXITE** p. 392 A mixture of aluminum hydroxides
Ruby-red, brown, yellow	6.7 to 7.1	3	Luster resinous. In slender prismatic and cavernous crystals; in barrel-shaped forms.	Vanadinite p. 430 $Pb_5(VO_4)_3Cl$ Hexagonal
Yellow, green, white, brown	2.33	$3\frac{1}{2}-4$	Characteristically in radiating hemispherical globular aggregates. Cleavage seldom seen.	Wavellite p. 431 $Al_3(PO_4)_2(OH)_3 \cdot 5H_2O$ Orthorhombic
Olive- to blackish-green, yellow-green, white	2.3 to 2.66	2–5	Massive. Fibrous in the asbestos variety, chrysotile. Frequently mottled green in the massive variety.	**SERPENTINE** p. 519 $Mg_3Si_2O_5(OH)_4$ Monoclinic

Table 22.1 (continued)

LUSTER: NONMETALLIC
II. Streak colorless
C. Hardness: $>3-\leq 5\frac{1}{2}$
(Cannot be scratched by a copper cent; can be scratched by a knife)
1. Cleavage prominent

Cleavage	Color	G	H	Remarks	Name, Composition, Crystal System
One cleavage direction					
{100}	Blue, usually darker at center; white	3.56 to 3.66	5–7	In bladed aggregates with cleavage parallel to length. Can be scratched by a knife parallel to the length of the crystal but not in a direction at right angles to this.	**KYANITE** p. 492 Al_2SiO_5 Triclinic
{010}	White, yellow, brown, red	2.1 to 2.2	$3\frac{1}{2}-4$	Characteristically in sheaflike crystal aggregates. May be in flat tabular crystals. Luster pearly on cleavage face.	**STILBITE** p. 551 $(Na,K,Ca_{0.5})_9(Al_9Si_{27}O_{72})\cdot 28H_2C$ Monoclinic
{001}	Colorless, white, pale green, yellow, rose	2.3 to 2.4	$4\frac{1}{2}-5$	In prismatic crystals vertically striated. Crystals often resemble cubes truncated by the octahedron. Luster pearly on base, elsewhere vitreous.	APOPHYLLITE p. 532 $KCa_4(Si_4O_{10})_2F\cdot 8H_2O$ Tetragonal
{010}	White, yellow, red	2.18 to 2.20	$3\frac{1}{2}-4$	Luster pearly on cleavage, elsewhere vitreous. Crystals often tabular parallel to cleavage plane. Found in cavities in igneous rocks.	HEULANDITE p. 551 $(Ca_{0.5},Na,K)_9(Al_9Si_{27}O_{72})\cdot \sim 24H_2C$ Monoclinic
{010}	Colorless, white	2.42	$4-4\frac{1}{2}$	In crystals and in cleavable aggregates. Decrepitates violently in the candle flame.	COLEMANITE p. 419 $CaB_3O_4(OH)_3\cdot H_2O$ Monoclinic
{010}	Colorless, white	4.3	$3\frac{1}{2}$	Often in radiating crystal aggregates; granular. Rarely in pseudohexagonal crystals.	WITHERITE p. 412 $BaCO_3$ Orthorhombic
{010} {110} poor	Colorless, white	2.95	$3\frac{1}{2}-4$	Effervesces in cold acid. Frequently in radiating groups of acicular crystals; in pseudohexagonal twins.	**ARAGONITE** p. 411 $CaCO_3$ Orthorhombic
Two cleavage directions					
{001} {100}	Bluish gray, salmon to clove-brown	3.42 to 3.56	$4\frac{1}{2}-5$	Commonly cleavable, massive. Found in pegmatites with other lithium minerals.	Triphylite-lithiophilite p. 427 $Li(Fe,Mn)PO_4$ Orthorhombic
{001} {100}	Colorless, white, gray	2.8 to 2.9	$5-5\frac{1}{2}$	Usually cleavable, massive to fibrous. Also compact. Associated with calcite, diopside.	WOLLASTONITE p. 511 $CaSiO_3$ Triclinic
{001} {100}	Colorless, white, gray	2.7 to 2.8	5	In radiating aggregates of sharp acicular crystals. Associated with zeolites in cavities in igneous rocks.	Pectolite p. 513 $NaCa_2(SiO_3)_3O(OH)$ Triclinic

Table 22.1 (continued)

LUSTER: NONMETALLIC
II. Streak colorless
C. Hardness: >3–≤5½
(Cannot be scratched by a copper cent; can be scratched by a knife)
1. Cleavage prominent

Cleavage		Color	G	H	Remarks	Name, Composition, Crystal System
Two cleavage directions	{110}	Colorless, white	2.25	5–5½	Slender prismatic crystals, prism faces vertically striated. Often in radiating groups. Found lining cavities in igneous rocks.	**NATROLITE** p. 549 $Na_2Al_2Si_3O_{10}·2H_2O$ Orthorhombic
	{110}	Colorless, white	3.7	3½–4	In prismatic crystals and pseudohexagonal twins. Also fibrous and massive. Effervesces in cold acid.	**STRONTIANITE** p. 413 $SrCO_3$ Orthorhombic
	{110}	White, pale green, blue, gray	3.4 to 3.5	4½–5	Often in radiating crystal groups. Also stalactitic, mammillary. Prismatic cleavage seldom seen.	**HEMIMORPHITE** p. 498 $Zn_4(Si_2O_7)(OH)_2·H_2O$ Orthorhombic
	{110}	Brown, gray, green, yellow	3.4 to 3.55	5–5½	Luster adamantine to resinous. In thin wedge-shaped crystals with sharp edges. Prismatic cleavage seldom seen.	TITANITE p. 496 $CaTiO(SiO_4)$ Monoclinic
	Prismatic at angles of 56° and 124°	White, green, black	3.0 to 3.3	5–6	Crystals usually slender, fibrous; may be asbestiform. Tremolite (white, gray, violet), actinolite (green) common in metamorphic rocks. Hornblende and arfvedsonite (dark green to black) common in igneous and metamorphic rocks.	**AMPHIBOLE GROUP** p. 514 Essentially hydrous Ca–Mg–Fe silicates Monoclinic
		Gray, clove-brown, green	2.85 to 3.2	5½–6	An amphibole. Distinct crystals rare. Commonly in aggregates and fibrous masses.	Anthophyllite p. 514 or grunerite p. 514 $(Mg,Fe)_7Si_8O_{22}(OH)_2$ Orthorhombic or monoclinic
	Prismatic at nearly 90° angles	White, green black, brown	3.1 to 3.5	5–6	In stout prisms with rectangular cross section. Often in granular crystalline masses. Diopside (colorless, white, green), aegirine (brown, green), augite (dark green to black), members of the orthopyroxene series (light brown)	**PYROXENE GROUP** p. 505 Essentially Ca–Mg–Fe silicates Monoclinic and orthorhombic
Prismatic at nearly 90° angles		Rose-red, pink, brown	3.58 to 3.70	5½–6	Color diagnostic. Usually massive, cleavable to compact, in imbedded grains; in large rough crystals, with rounded edges.	RHODONITE p. 512 $MnSiO_3$ Triclinic

Table 22.1 (continued)

LUSTER: NONMETALLIC
II. Streak colorless
C. Hardness: $>3-\leq 5\frac{1}{2}$
(Cannot be scratched by a copper cent; can be scratched by a knife)
1. Cleavage prominent

Cleavage	Color	G	H	Remarks	Name, Composition, Crystal System
Three cleavage directions; Three directions not at right angles. Rhombohedral {10$\bar{1}$1}	Colorless, white, and variously tinted	2.72	3	Effervesces in cold acid. Crystals show many forms. Occurs as limestone and marble. Clear varieties show strong double refraction.	**CALCITE** p. 407 $CaCO_3$ Hexagonal
	Colorless, white, pink	2.85	$3\frac{1}{2}-4$	Often in curved rhombohedral crystals with pearly luster. In coarse masses as dolomitic limestone and marble. Powdered mineral will effervesce in cold acid.	**DOLOMITE** p. 413 $CaMg(CO_3)_2$ Hexagonal
	White, yellow gray, brown	3.0 to 3.2	$3\frac{1}{2}-5$	Commonly in dense compact masses; also in fine to coarse cleavable masses. Effervesces in hot hydrochloric acid.	MAGNESITE p. 409 $MgCO_3$ Hexagonal
	Light to dark brown	3.83 to 3.88	$3\frac{1}{2}-4$	In cleavable masses or in small curved rhombohedral crystals. Becomes magnetic after heating.	**SIDERITE** p. 409 $FeCO_3$ Hexagonal
	Pink, rose-red, brown	3.45 to 3.6	$3\frac{1}{2}-4\frac{1}{2}$	In cleavable masses or in small rhombohedral crystals. Characterized by its color.	RHODOCHROSITE p. 410 $MnCO_3$ Hexagonal
	Brown, green, blue, pink, white	4.35 to 4.40	5	In rounded botryoidal aggregates and honeycombed masses. Effervesces in cold hydrochloric acid. Cleavage rarely seen.	SMITHSONITE p. 411 $ZnCO_3$ Hexagonal
{10$\bar{1}$1}	White, yellow, flesh-red	2.05 to 2.15	4–5	In small rhombohedral crystals with nearly cubic angles. Found lining cavities in igneous rocks.	CHABAZITE p. 549 $Ca_2Al_2Si_4O_{12}{\cdot}6H_2O$ Hexagonal
Three cleavage directions; {001} {010} {100}	Colorless, white, blue, gray, red	2.89 to 2.98	$3-3\frac{1}{2}$	Commonly in massive fine aggregates, not showing cleavage, but may appear 'sugary,' and can be distinguished only by chemical tests.	**ANHYDRITE** p. 422 $CaSO_4$ Orthorhombic
{001} at right angles to {110}	Colorless, white, blue, yellow, red	4.5	$3-3\frac{1}{2}$	Frequently in aggregates of platy crystals. Pearly luster on basal cleavage. Characterized by high specific gravity and, thus, distinguished from celestite.	**BARITE** p. 420 $BaSO_4$ Orthorhombic
	Colorless, white, blue, red	3.95 to 3.97	$3-3\frac{1}{2}$	Similar to barite but lower specific gravity. Adamantine luster.	**CELESTITE** p. 421 $SrSO_4$ Orthorhombic

Table 22.1 (continued)

LUSTER: NONMETALLIC
II. Streak colorless
C. Hardness: $>3-\leq 5\frac{1}{2}$
(Cannot be scratched by a copper cent; can be scratched by a knife)
1. Cleavage prominent

Cleavage		Color	G	H	Remarks	Name, Composition, Crystal System
Four cleavage directions	{111} Octahedral	Colorless, blue, violet, green, yellow, pink	3.18	4	In cubic crystals often in penetration twins. Characterized by cleavage.	**FLUORITE** p. 396 CaF_2 Isometric
Four cleavage directions	{100} {110}	White, pink gray, green, brown	2.65 to 2.74	5–6	In prismatic crystals, granular or massive. Commonly altered. Prismatic cleavage obscure.	SCAPOLITE p. 547 Essentially Na, Ca aluminum silicate Tetragonal
Six cleavage directions Dodecahedral {011}		Yellow, brown, colorless	3.9 to 4.1	$3\frac{1}{2}-4$	Luster resinous. Small tetrahedral crystals rare. Usually in cleavable masses. If massive, difficult to determine.	**SPHALERITE** p. 356 ZnS Isometric
Six cleavage directions Dodecahedral {011}		Blue, white, gray, green	2.15 to 2.3	$5\frac{1}{2}$–6	Massive or in embedded grains; rarely in crystals. A feldspathoid associated with nepheline, never with quartz.	SODALITE p. 546 $Na_6(AlSiO_4)_6Cl_2$ Isometric

Table 22.1 (continued)

LUSTER: NONMETALLIC
II. Streak colorless
C. Hardness: $>3-\leq 5\frac{1}{2}$
(Cannot be scratched by a copper cent; can be scratched by a knife)
2. Cleavage not prominent

Color	G	H	Remarks	Name, Composition, Crystal System
Colorless, white	2.25	$5-5\frac{1}{2}$	In slender prismatic crystals, prism faces vertically striated. Often in radiating groups. Found lining cavities in igneous rocks. Poor prismatic cleavage.	NATROLITE p. 549 $Na_2Al_2Si_3O_{10}\cdot 2H_2O$ Orthorhombic
	2.95	$3\frac{1}{2}-4$	Effervesces in cold acid. Falls to powder in the candle flame. Frequently in radiating groups of acicular crystals; in pseudohexagonal twins. Cleavage indistinct.	ARAGONITE p. 411 $CaCO_3$ Orthorhombic
	2.27	$5-5\frac{1}{2}$	Usually in trapezohedrons with vitreous luster. Found lining cavities in igneous rocks.	ANALCIME p. 548 $NaAlSi_2O_6\cdot H_2O$ Isometric
	3.7	$3\frac{1}{2}-4$	Occurs in prismatic crystals and pseudohexagonal twins. Also fibrous and massive. Effervesces in cold hydrochloric acid.	STRONTIANITE p. 413 $SrCO_3$ Orthorhombic
	3.0 to 3.2	$3\frac{1}{2}-5$	Commonly in dense compact masses showing no cleavage. Effervesces in hot hydrochloric acid.	MAGNESITE p. 409 $MgCO_3$ Hexagonal
	4.3	$3\frac{1}{2}$	Often in radiating masses; granular; rarely in pseudohexagonal crystals. Effervesces in cold hydrochloric acid.	WITHERITE p. 412 $BaCO_3$ Orthorhombic
	2.7 to 2.8	5	Commonly fibrous in radiating aggregates of sharp acicular crystals. Associated with zeolites in cavities in igneous rocks.	Pectolite p. 513 $NaCa_2(SiO_3)_3O(OH)$ Triclinic
Colorless, pale green, yellow	2.8 to 3.0	$5-5\frac{1}{2}$	Usually in crystals with many brilliant faces. Occurs with zeolites lining cavities in igneous rocks.	DATOLITE p. 496 $CaB(SiO_4)(OH)$ Monoclinic
White, pale green, blue, gray	3.4 to 3.5	$4\frac{1}{2}-5$	Often in radiating crystal groups. Also stalactitic, mammillary. Prismatic cleavage seldom seen.	HEMIMORPHITE p. 498 $Zn_4(Si_2O_7)(OH)_2\cdot H_2O$ Orthorhombic
White, pink, gray, green, brown	2.65 to 2.74	5–6	In prismatic crystals, granular or massive. Commonly altered. Prismatic cleavage obscure.	SCAPOLITE p. 547 Essentially Na, Ca–aluminum silicate Tetragonal
White, grayish, red	2.6 to 2.8	4	May be in rhombohedral crystals. Usually massive granular. Definitely determined only by chemical tests. Cleavage {0001}, poor.	ALUNITE p. 425 $KAl_3(SO_4)_2(OH)_6$ Hexagonal

Table 22.1 (continued)

LUSTER: NONMETALLIC
II. Streak colorless
C. Hardness: $>3-\leq 5\frac{1}{2}$
(Cannot be scratched by a copper cent; can be scratched by a knife)
2. Cleavage not prominent

Color	G	H	Remarks	Name, Composition, Crystal System
Colorless, white, yellow, red, brown	1.9 to 2.2	5–6	Conchoidal fracture. Precious opal shows internal play of colors. Specific gravity and hardness less than fine-grained quartz.	**OPAL** p. 538 $SiO_2 \cdot nH_2O$ Essentially amorphous
Brown, green, blue, pink, white	4.35 to 4.40	5	Usually in rounded botryoidal aggregates and in honeycombed masses. Effervesces in cold hydrochloric acid. Cleavage rarely seen.	**SMITHSONITE** p. 411 $ZnCO_3$ Hexagonal
Brown, gray, green, yellow	3.4 to 3.55	$5-5\frac{1}{2}$	Adamantine to resinous luster. In thin wedge-shaped crystals with sharp edges. Prismatic cleavage seldom seen.	TITANITE p. 496 $CaTiO(SiO_4)$ Monoclinic
Colorless, white, yellow, red, brown	2.72	3	May be fibrous or fine granular, banded in Mexican onyx variety. Effervesces in cold hydrochloric acid.	**CALCITE** p. 407 $CaCO_3$ Hexagonal
Yellowish- to reddish-brown	5.0 to 5.3	$5-5\frac{1}{2}$	In small crystals or as rolled grains. Found in pegmatites.	Monazite p. 427 $(Ce,La,Y,Th)PO_4$ Monoclinic
Light to dark brown	3.38 to 3.88	$3\frac{1}{2}-4$	Usually cleavable but may be in compact concretions in clay or shale—clay ironstone variety. Becomes magnetic on heating. Curved rhombohedra.	**SIDERITE** p. 409 $FeCO_3$ Hexagonal
White, yellow, green, brown	5.9 to 6.1	$4\frac{1}{2}-5$	Luster vitreous to adamantine. Massive and in octahedral-like crystals. Frequently associated with quartz. Will fluoresce.	SCHEELITE p. 426 $CaWO_4$ Tetragonal
Yellow, orange, red, gray, green	6.8±	3	Luster adamantine. Usually in square tabular crystals. Also granular massive. Characterized by color and high specific gravity.	WULFENITE p. 426 $PbMoO_4$ Tetragonal
White, yellow brown, gray, blue	2.6 to 2.9	3–5	Occurs massive as rock phosphate. Difficult to identify without chemical tests.	**APATITE** p. 428 $Ca_5(PO_4)_3(F,Cl,OH)$ Appears amorphous
Yellow, brown, gray, white	2.0 to 2.55	1–3	Usually pisolitic; in rounded grains and earthy masses. Often impure.	**BAUXITE** p. 392 A mixture of aluminum hydroxides
Green, blue, violet, brown, colorless	3.15 to 3.20	5	Usually in hexagonal prisms with pyramid. Also massive. Poor basal cleavage.	**APATITE** p. 428 $Ca_5(PO_4)_3(F,Cl,OH)$ Hexagonal
Green, brown, yellow, gray	6.5 to 7.1	$3\frac{1}{2}-4$	In small hexagonal crystals, often curved and barrel-shaped. Crystals may be cavernous. Often globular and botryoidal.	Pyromorphite p. 430 $Pb_5(PO_4)_3Cl$ Hexagonal

Table 22.1 (continued)

LUSTER: NONMETALLIC
II. Streak colorless
C. Hardness: $>3-\leq 5\frac{1}{2}$
(Cannot be scratched by a copper cent; can be scratched by a knife)
2. Cleavage not prominent

Color	G	H	Remarks	Name, Composition, Crystal System
Yellow, green, white, brown	2.33	$3\frac{1}{2}-4$	Characteristically in radiating, hemispherical globular aggregates. Cleavage seldom seen.	Wavellite p. 431 $Al_3(PO_4)_2(OH)_3 \cdot 5H_2O$ Orthorhombic
Olive- to blackish-green, yellow-green, white	2.3 to 2.6	2–5	Massive. Fibrous in the asbestos variety, chrysotile. Frequently mottled green in the massive variety.	**SERPENTINE** p. 519 $Mg_3Si_2O_5(OH)_4$ Monoclinic
Yellow-green, white, blue, gray, brown	3.9 to 4.2	$5\frac{1}{2}$	Massive and in disseminated grains. Rarely in hexagonal prisms. Associated with red zincite and black franklinite at Franklin, NJ. Will fluoresce.	WILLEMITE p. 484 Zn_2SiO_4 Hexagonal
White, gray, blue, green	2.15 to 2.3	$5\frac{1}{2}-6$	Massive or in embedded grains; rarely in crystals. A feldspathoid associated with nepheline, never with quartz. Dodecahedral cleavage poor.	SODALITE p. 546 $Na_6(AlSiO_4)_6Cl_2$ Isometric
Deep azure-blue, greenish-blue	2.4 to 2.45	$5-5\frac{1}{2}$	Usually massive. Associated with feldspathoids and pyrite. Poor dodecahedral cleavage.	Lazurite p. 546 $(Na,Ca)_8(AlSiO_4)_6(SO_4,S,Cl,OH)_2$ Isometric

Table 22.1 (continued)

LUSTER: NONMETALLIC
II. Streak colorless
D. Hardness: $>5\frac{1}{2} \leq 7$
(Cannot be scratched by a knife; can be scratched by quartz)
1. Cleavage prominent

	Cleavage	Color	G	H	Remarks	Name, Composition, Crystal System
One cleavage direction	{010}	White, gray, pale lavender, yellow-green	3.35 to 3.45	$6\frac{1}{2}-7$	In thin tabular crystals. Luster pearly on cleavage face. Associated with emery, margarite, chlorite.	Diaspore p. 391 $\alpha AlO(OH)$ Orthorhombic
	{010} perfect	Hair-brown, grayish-green, white	3.23	6–7	In long, prismatic crystals. May be in parallel groups—columnar or fibrous. Found in mica schists.	SILLIMANITE p. 492 Al_2SiO_5 Orthorhombic
	{001}	Yellowish to blackish-green	3.35 to 3.45	6–7	In prismatic crystals striated parallel to length. Found in metamorphic rocks and recrystallized limestones.	**EPIDOTE** p. 499 $Ca_2(Al,Fe)Al_2O(SiO_4)$-$(Si_2O_7)(OH)$ Monoclinic
	{100}	Blue; may be gray, green, white	3.56 to 3.66	5–7	In bladed aggregates with cleavage parallel to length. H = 5 parallel to length of crystal.	**KYANITE** p. 492 Al_2SiO_5 Triclinic
Two cleavage directions	{100} good {110} poor	White, pale green, or blue	3.0 to 3.1	6	Usually cleavable, resembling feldspar. Found in pegmatites associated with other lithium minerals.	AMBLYGONITE p. 431 $LiAlFPO_4$ Triclinic
	{100} good {001}	Colorless, white, gray	2.8 to 2.9	$5-5\frac{1}{2}$	Usually cleavable, massive to fibrous. Also compact. Associated with calcite, diopside.	WOLLASTONITE p. 511 $CaSiO_3$ Triclinic
	{001} {100}	Grayish-white, green, pink	3.25 to 3.37	$6-6\frac{1}{2}$	In prismatic crystals, deeply striated. Also massive, columnar, compact. Luster pearly on cleavage, elsewhere vitreous.	Clinozoisite p. 499 $Ca_2Al_3O(SiO_4)(Si_2O_7)(OH)$ Monoclinic
	{110}	Colorless, white	2.25	$5-5\frac{1}{2}$	In slender prismatic crystals, prism faces vertically striated. Often in radiating groups lining cavities in volcanic rocks.	**NATROLITE** p. 549 $Na_2Al_2Si_3O_{10}\cdot 2H_2O$ Orthorhombic
	{110}	Brown, gray, green, yellow	3.4 to 3.55	$5-5\frac{1}{2}$	Luster adamantine to resinous. In thin wedge-shaped crystals with sharp edges. Prismatic cleavage seldom seen.	TITANITE p. 496 $CaTiO(SiO_4)$ Monoclinic

Table 22.1 (continued)

LUSTER: NONMETALLIC
II. Streak colorless
D. Hardness: $>5\frac{1}{2} \leq 7$
(Cannot be scratched by a knife; can be scratched by quartz)
1. Cleavage prominent

Two cleavage directions at 90° or nearly 90°

Cleavage	Color	G	H	Remarks	Name, Composition, Crystal System
{001} {010}	Colorless, white, gray, cream, red, green	2.54 to 2.56	6	In cleavable masses or in irregular grains as rock constituents. May be in crystals in pegmatites. Distinguished with certainty only with the microscope. Green amazonite is microcline.	**ORTHOCLASE** p. 540 Monoclinic **MICROCLINE** p. 539 Triclinic $KAlSi_3O_8$
{001} {010}	Colorless, white, gray, bluish. Often shows play of colors	2.62 (ab) to 2.76 (an)	6	In cleavable masses or in irregular grains as a rock constituent. On the better cleavage, can be seen a series of fine parallel striations due to albite twinning; these distinguish it from orthoclase.	**PLAGIOCLASE** p. 541 Various proportions of albite, $NaAlSi_3O_8$, and anorthite, $CaAl_2Si_2O_8$ Triclinic
{110}	White, gray, pink, green	3.15 to 3.20	$6\frac{1}{2}$–7	In flattened prismatic crystals, vertically striated. Also massive, cleavable. Found in pegmatites. Frequently shows good {100} parting.	SPODUMENE p. 510 $LiAlSi_2O_6$ Monoclinic
{110}	White, green, black	3.1 to 3.5	5–6	In stout prisms with rectangular cross section. Often in granular masses. Diopside (colorless, white, green), aegirine (brown, green), augite (dark green to black). Characterized by cleavage.	**PYROXENE GROUP** p. 505 Essentially Ca–Mg–Fe silicates Monoclinic
{110}	Gray-brown, green, bronze-brown, black	3.2 to 3.5	$5\frac{1}{2}$	Crystals are usually prismatic but rare. Commonly massive, fibrous, lamellar. Fe may replace Mg and mineral is darker.	ENSTATITE p. 505 $MgSiO_3$ Orthorhombic
{110}	Rose-red, pink, brown	3.58 to 3.70	$5\frac{1}{2}$–6	Color diagnostic. Usually massive; cleavable to compact, in embedded grains; in large rough crystals with rounded edges.	RHODONITE p. 512 $MnSiO_3$ Triclinic

Table 22.1 (continued)

LUSTER: NONMETALLIC
II. Streak colorless
D. Hardness: $>5\frac{1}{2} \leq 7$
(Cannot be scratched by a knife; can be scratched by quartz)
1. Cleavage prominent

Cleavage		Color	G	H	Remarks	Name, Composition, Crystal System
Two cleavage directions at 54° and 126° angles	{110}	White, green black	3.0 to 3.3	5–6	Crystals usually slender fibrous; may be asbestiform. Tremolite (white, gray, violet) and actinolite (green) are common in metamorphic rocks. Hornblende and arfvedsonite (dark green to black) are common in igneous rocks. Characterized by cleavage angle.	**AMPHIBOLE GROUP** p. 514 Essentially hydrous Ca–Mg–Fe silicates Monoclinic
	{110}	Gray, clove-brown, green	2.85 to 3.2	$5\frac{1}{2}$–6	An amphibole. Distinct crystals rare. Commonly in aggregates and fibrous, massive.	Anthophyllite p. 514 and grunerite p. 514 $(Mg,Fe)_7(Si_8O_{22})(OH)_2$ Orthorhombic and monoclinic
Six cleavage directions	{110}	Blue, gray, white, green	2.15 to 2.3	$5\frac{1}{2}$–6	Massive or embedded grains; rarely in crystals. A feldspathoid associated with nepheline, never with quartz.	SODALITE p. 546 $Na_8(AlSiO_4)_6Cl_2$ Isometric

Table 22.1 (continued)

LUSTER: NONMETALLIC
II. Streak colorless
D. Hardness: $>5\frac{1}{2} \leq 7$
(Cannot be scratched by a knife; can be scratched by quartz)
2. Cleavage not prominent

Color	G	H	Remarks	Name, Composition, Crystal System
Colorless	2.26	7	Occurs as small crystals in cavities in volcanic rocks. Difficult to determine without optical aid.	Tridymite p. 538 SiO_2 Pseudohexagonal
Colorless or white	2.27	$5-5\frac{1}{2}$	Usually in trapezohedrons with vitreous luster. Found lining cavities in igneous rocks.	ANALCIME p. 548 $NaAlSi_2O_6 \cdot H_2O$ Isometric
	2.32	7	Occurs in spherical aggregations in volcanic rocks. Difficult to determine without optical aid.	Cristobalite p. 538 SiO_2 Pseudoisometric
Colorless, yellow, red, brown, green, gray, blue	1.9 to 2.2	5–6	Conchoidal fracture. Precious opal shows internal play of colors. Gravity and hardness less than fine-grained quartz.	**OPAL** p. 538 $SiO_2 \cdot nH_2O$ Essentially amorphous
Gray, white, colorless	2.45 to 2.50	$5\frac{1}{2}-6$	In trapezohedral crystals embedded in dark igneous rock. Does not line cavities as analcime does.	LEUCITE p. 544 $KAlSi_2O_6$ Pseudoisometric
Colorless, pale, green, yellow	2.8 to 3.0	$5-5\frac{1}{2}$	Usually in crystals with many brilliant faces. Occurs with zeolites lining cavities in igneous rocks.	DATOLITE p. 496 $CaB(SiO_4)(OH)$ Monoclinic
Colorless, white, smoky. Variously colored	2.65	7	Crystals usually show horizontally striated prism with rhombohedral terminations. Conchoidal fracture. Often massive.	**QUARTZ** p. 534 SiO_2 Hexagonal
Colorless, gray, greenish, reddish	2.55 to 2.65	$5\frac{1}{2}-6$	Greasy luster. A rock constituent, usually massive; rarely in hexagonal prisms. Poor prismatic cleavage. A feldspathoid.	NEPHELINE p. 545 $(Na,K)AlSiO_4$ Hexagonal
White, gray, light to dark green, brown	2.65 to 2.74	5–6	In prismatic crystals, granular or massive. Commonly altered and prismatic cleavage obscure.	SCAPOLITE p. 547 Essentially Na–Ca aluminum silicate Tetragonal
Light yellow, brown, orange	3.1 to 3.2	$6-6\frac{1}{2}$	Occurs in disseminated crystals and grains. Commonly in crystalline limestones.	Chondrodite p. 495 $Mg_5(SiO_4)_2(F,OH)_2$ Monoclinic
Light brown, yellow, red, green	2.6	7	Chalcedony, waxy luster, commonly colloform; as agate lining cavities. Dull luster, massive: jasper red, flint black, chert gray.	**MICROCRYSTALLINE QUARTZ** p. 536 SiO_2
Blue, bluish-green, green	2.6 to 2.8	6	Usually appears amorphous in reniform and stalactitic masses.	TURQUOISE p. 432 $CuAl_6(PO_4)_4(OH)_8 \cdot 4H_2O$ Triclinic

Table 22.1 (continued)

LUSTER: NONMETALLIC
II. Streak colorless
D. Hardness: $>5\frac{1}{2} \leq 7$
(Cannot be scratched by a knife; can be scratched by quartz)
2. Cleavage not prominent

Color	G	H	Remarks	Name, Composition, Crystal System
Apple-green, gray, white	2.8 to 2.95	$6-6\frac{1}{2}$	Reniform and stalactitic with crystalline surface. In subparallel groups of tabular crystals.	PREHNITE p. 533 $Ca_2Al(AlSi_3O_{10})(OH)_2$ Orthorhombic
Yellow-green, white, blue, gray, brown	3.9 to 4.2	$5\frac{1}{2}$	Massive and in disseminated grains. Rarely in hexagonal prisms. Associated with red zincite and black franklinite at Franklin, NJ. Will fluoresce.	WILLEMITE p. 484 Zn_2SiO_4 Hexagonal
Olive to grayish-green, brown	3.27 to 4.37	$6\frac{1}{2}-7$	Usually in disseminated grains in basic igneous rocks. May be massive, granular.	OLIVINE p. 485 $(Mg,Fe)_2SiO_4$ Orthorhombic
Black, green, brown, blue, red, pink, colorless	3.0 to 3.25	$7-7\frac{1}{2}$	In slender prismatic crystals with triangular cross section. Crystals may be in radiating groups. Found usually in pegmatites. Black most common, often striated; light colors associated with lithium minerals.	**TOURMALINE** p. 503 Complex boron silicate of Na–Ca–Al–Mg–Fe–Mn Hexagonal-rhombohedral
Green, brown, yellow, blue, red	3.35 to 4.45	$6\frac{1}{2}$	In square prismatic crystals, vertically striated. Often columnar and granular massive. Found in recrystallized limestones.	VESUVIANITE p. 500 Complex hydrous Ca–Mg–Fe–Al silicate Tetragonal
Clove-brown, gray, green, yellow	3.27 to 3.35	$6\frac{1}{2}-7$	In wedge-shaped crystals with sharp edges. Also lamellar.	AXINITE p. 502 $(Ca,Fe,Mn)_3Al_2B(Si_4O_{15})(OH)$ Triclinic
Red-brown to brown	3.65 to 3.75	$7-7\frac{1}{2}$	In prismatic crystals; commonly in cruciform penetration twins. Frequently altered on the surface and then soft. Found in schists.	**STAUROLITE** p. 494 $Fe_{3-4}Al_{18}Si_8O_{48}H_{2-4}$ Pseudo-orthorhombic
Reddish-brown, flesh-red, olive-green, white	3.16 to 3.20	$7\frac{1}{2}$	Prismatic crystals with nearly square cross section. Cross section may show black cross (chiastolite). May be altered to mica and then soft. Found in mica schists.	**ANDALUSITE** p. 492 Al_2SiO_5 Orthorhombic
Brown, gray, green, yellow	3.4 to 3.55	$5-5\frac{1}{2}$	Luster adamantine to resinous. In thin wedge-shaped crystals with sharp edges. Prismatic cleavage seldom seen.	**TITANITE** p. 496 $CaTiO(SiO_4)$ Monoclinic
Yellowish- to reddish-brown	5.0 to 5.3	$5-5\frac{1}{2}$	In isolated crystals, granular. Commonly found in pegmatites.	Monazite p. 427 $(Ce,La,Y,Th)PO_4$ Monoclinic
Brown to black	6.8 to 7.1	6–7	Rarely in prismatic crystals, twinned. Fibrous, giving reniform surface. Rolled grains. Usually gives light brown streak.	**CASSITERITE** p. 382 SnO_2 Tetragonal

Table 22.1 (continued)

LUSTER: NONMETALLIC
II. Streak colorless
D. Hardness: $>5\frac{1}{2} \leq 7$
(Cannot be scratched by a knife; can be scratched by quartz)
2. Cleavage not prominent

Color	G	H	Remarks	Name, Composition, Crystal System
Reddish-brown to black	4.18 to 4.25	$6-6\frac{1}{2}$	In prismatic crystals, vertically striated; often slender, acicular. Crystals frequently twinned. A constituent of black sands.	**RUTILE** p. 379 TiO_2 Tetragonal
Brown to pitch-black	3.5 to 4.2	$5\frac{1}{2}-6$	Crystals often tabular. Massive and in embedded grains. An accessory mineral in igneous rocks.	Allanite p. 500 Ce, La, Th epidote Monoclinic
Blue, rarely colorless	2.60 to 2.66	$7-7\frac{1}{2}$	In embedded grains and massive, resembling quartz. Commonly altered and foliated; then, softer than a knife.	Cordierite p. 503 $(Mg,Fe)_2Al_4Si_5O_{18}{\cdot}nH_2O$ Orthorhombic (Pseudohexagonal)
Deep azure-blue, greenish-blue	2.4 to 2.45	$5-5\frac{1}{2}$	Usually massive. Associated with feldspathoids and pyrite. Poor dodecahedral cleavage.	LAZURITE p. 546 $(Na,Ca)_8(AlSiO_4)_6$-$(SO_4,S,Cl,OH)_2$ Isometric
Azure-blue	3.0 to 3.1	$5-5\frac{1}{2}$	Usually in pyramidal crystals, which distinguishes it from massive lazurite. A rare mineral.	LAZULITE p. 431 $(Mg,Fe)Al_2(PO_4)_2(OH)_2$ Monoclinic
Blue, green, white, gray	2.15 to 2.3	$5\frac{1}{2}-6$	Massive or in embedded grains; rarely in crystals. A feldspathoid associated with nepheline, never with quartz. Poor dodecahedral cleavage.	SODALITE p. 546 $Na_8(AlSiO_4)_6Cl_2$ Isometric

Table 22.1 (continued)

LUSTER: NONMETALLIC
II. Streak colorless
E. Hardness: >7
(Cannot be scratched by quartz)
1. Cleavage prominent

Cleavage		Color	G	H	Remarks	Name, Composition, Crystal System
One cleavage direction	{001}	Colorless, yellow, pink, bluish, greenish	3.4 to 3.6	8	Usually in crystals, also coarse to fine granular. Found in pegmatites.	**TOPAZ** p. 493 $Al_2SiO_4(F,OH)_2$ Orthorhombic
	{010}	Brown, gray, greenish-gray, white	3.23	6–7	Commonly in long slender prismatic crystals. May be in parallel groups, columnar or fibrous. Found in schistose rocks.	**SILLIMANITE** p. 492 Al_2SiO_5 Orthorhombic
Two cleavage directions	{110}	White, gray, pink, green	3.15 to 3.20	$6\frac{1}{2}$–7	In flattened prismatic crystals, vertically striated. Also massive, cleavable. Pink variety, kunzite; green, hiddenite. Found in pegmatites. Frequently shows good {100} parting.	SPODUMENE p. 510 $LiAlSi_2O_6$ Monoclinic
Three cleavage directions	{010} {110}	Colorless pale blue, gray	3.09	8	Commonly in tabular or prismatic crystals associated with blue amphibole.	Lawsonite p. 499 $CaAl_2(Si_2O_7)(OH_2)\cdot H_2O$ Orthorhombic
Four cleavage directions	{111}	Colorless, yellow, red, blue, black	3.5	10	Adamantine luster. In octahedral crystals, frequently twinned. Faces may be curved.	Diamond p. 346 C Isometric
No cleavage. Rhombohedral and basal parting		Colorless, gray, blue, red, yellow, brown, green	3.95 to 4.1	9	Luster adamantine to vitreous. Parting fragments may appear nearly cubic. In hexagonal barrel-shaped crystals.	**CORUNDUM** p. 376 Al_2O_3 Hexagonal

Table 22.1 (continued)

LUSTER: NONMETALLIC
II. Streak colorless
E. Hardness: >7
(Cannot be scratched by quartz)
2. Cleavage not prominent

Color	G	H	Remarks	Name, Composition, Crystal System
Colorless, white, smoky, variously colored	2.65	7	Crystals usually show horizontally striated prism with rhombohedral terminations. Conchoidal fracture. Often massive.	**QUARTZ** p. 534 SiO_2 Hexagonal
White, colorless	2.97 to 3.0	$7\frac{1}{2}$–8	In small rhombohedral crystals. A rare mineral.	Phenacite p. 484 Be_2SiO_4 Hexagonal
White and almost any color	3.95 to 4.1	9	Luster adamantine to vitreous. Parting fragments may appear nearly cubic. In hexagonal barrel-shaped crystals.	**CORUNDUM** p. 376 Al_2O_3 Hexagonal
Red, black, blue, green, brown	3.6 to 4.0	8	In octahedrons; twinning common. Associated with recrystallized limestones.	**SPINEL** p. 384 $MgAl_2O_4$ Isometric
Bluish-green, yellow, pink, colorless	2.65 to 2.8	$7\frac{1}{2}$–8	Commonly in hexagonal prisms terminated by the base; pyramid faces are rare. Crystals large in places. Poor basal cleavage.	**Beryl** p. 502 $Be_3Al_2(Si_6O_{18})$ Hexagonal
Yellowish to emerald-green	3.65 to 3.8	$8\frac{1}{2}$	In tabular crystals; frequently in pseudohexagonal twins. Found in pegmatites.	CHRYSOBERYL p. 388 $BeAl_2O_4$ Orthorhombic
Green, brown, blue, red, pink, black	3.0 to 3.25	7–$7\frac{1}{2}$	In slender prismatic crystals with triangular cross section. Found usually in pegmatites. Black most common, light colors associated with lithium minerals.	TOURMALINE p. 503 Complex boron silicate of Na–Ca–Al–Mg–Fe–Mn Hexagonal-rhombohedral
Green, gray, white	3.3 to 3.5	$6\frac{1}{2}$–7	Massive, closely compact. Poor prismatic cleavage at nearly 90° angles. A pyroxene.	Jadeite p. 509 $NaAlSi_2O_6$ Monoclinic
Olive to grayish-green, brown	3.27 to 4.37	$6\frac{1}{2}$–7	Usually in disseminated grains in basic igneous rocks. May be massive granular.	**OLIVINE** p. 485 $(Mg,Fe)_2SiO_4$ Orthorhombic
Green, brown, yellow, blue, red	3.35 to 3.45	$6\frac{1}{2}$	In square prismatic crystals, vertically striated. Often columnar and granular, massive. Found in recrystallized limestones.	VESUVIANITE p. 500 Complex hydrous Ca–Mg–Fe–Al silicate Tetragonal
Dark green	4.55	$7\frac{1}{2}$–8	Usually in octahedrons, characteristically striated. A zinc spinel.	Gahnite p. 385 $ZnAl_2O_4$ Isometric
Reddish-brown to black	6.8 to 7.1	6–7	Rarely in prismatic crystals, twinned. Fibrous, giving reniform surface. Rolled grains. Usually gives light brown streak.	**CASSITERITE** p. 382 SnO_2 Tetragonal

Table 22.1 (continued)

LUSTER: NONMETALLIC
II. Streak colorless
E. Hardness: >7
(Cannot be scratched by quartz)
2. Cleavage not prominent

Color	G	H	Remarks	Name, Composition, Crystal System
Reddish-brown, flesh-red, olive-green, white	3.16 to 3.20	$7\frac{1}{2}$	Prismatic crystals with nearly square cross section. Cross section may show black cross (chiastolite). May be altered to mica and then soft. Found in schists.	**ANDALUSITE** p. 492 Al_2SiO_5 Orthorhombic
Clove-brown, green, yellow, gray	3.27 to 3.35	$6\frac{1}{2}$–7	In wedge-shaped crystals with sharp edges. Also lamellar.	AXINITE p. 416 $Ca_2(Fe,Mn)Al_2(BO_3)(Si_4O_{12})(OH)$ Triclinic
Red-brown to brown	3.65 to 3.75	7–$7\frac{1}{2}$	In prismatic crystals; commonly in cruciform penetration twins. Frequently altered on the surface and then soft. Found in mica schists.	**STAUROLITE** p. 494 $Fe_{3-4}Al_{18}Si_8O_{48}H_{2-4}$ Pseudo-orthorhombic
Brown, red, gray, green, colorless	4.68	$7\frac{1}{2}$	Usually in small prisms truncated by the pyramid. An accessory mineral in igneous rocks. Found as rolled grains in sand.	**ZIRCON** p. 490 $ZrSiO_4$ Tetragonal
Usually brown to red. Also yellow, green, pink	3.5 to 4.3	$6\frac{1}{2}$–$7\frac{1}{2}$	Usually in dodecahedrons or trapezohedrons or in combinations of the two. An accessory mineral in igneous rocks and pegmatites. Commonly in metamorphic rocks. As sand.	**GARNET** p. 387 $A_3B_2(SiO_4)_3$ Isometric

Table 22.2 Minerals Arranged According to Increasing Specific Gravity

G	Name
1.6	Carnallite
1.7	**Borax**
1.95	**Kernite**
1.96	**Ulexite**
1.99	Sylvite
2.0–2.19	
2.0–2.55	**Bauxite**
2.0–2.4	**Chrysocolla**
2.05–2.09	**Sulfur**
2.05–2.15	**Chabazite**
1.9–2.2	**Opal**
2.09–2.14	Niter
2.1–2.2	**Stilbite**
2.16	**Halite**
2.18–2.20	**Heulandite**
2.2–2.39	
2.0–2.4	**Chrysocolla**
2.2–2.65	**Serpentine**
2.23	**Graphite**
2.25	**Natrolite**
2.26	Tridymite
2.27	**Analcime**
2.29	Nitratite
2.30	Cristobalite
2.30	**Sodalite**
2.32	**Gypsum**
2.33	Wavellite
2.3–2.4	**Apophyllite**
2.39	**Brucite**
2.4–2.59	
2.0–2.55	**Bauxite**
2.2–2.65	**Serpentine**
2.42	**Colemanite**
2.42	Petalite
2.4–2.45	**Lazurite**
2.45–2.50	**Leucite**
2.2–2.8	**Garnierite**
2.54–2.57	**Microcline**
2.57	**Orthoclase**
2.6–2.79	
2.55–2.65	**Nepheline**
2.6–2.63	**Kaolinite**
2.62	**Albite**
2.60–2.66	Cordierite
2.65	**Oligoclase**
2.65	**Quartz**
2.69	**Andesine**
2.6–2.8	Alunite
2.6–2.8	Turquoise
2.71	**Labradorite**
2.65–2.74	**Scapolite**
2.65–2.8	**Beryl**
2.72	**Calcite**
2.6–3.3	**Chlorite**
2.62–2.76	**Plagioclase**
2.6–2.9	**Collophane**
2.74	**Bytownite**
2.7–2.8	Pectolite
2.7–2.8	**Talc**
2.76	**Anorthite**
2.8–2.99	
2.6–2.9	**Collophane**
2.8–2.9	Pyrophyllite
2.8–2.9	**Wollastonite**
2.85	**Dolomite**
2.86	Phlogopite
2.76–2.88	**Muscovite**
2.8–2.95	**Prehnite**
2.8–3.0	**Datolite**
2.8–3.0	**Lepidolite**
2.89–2.98	**Anhydrite**
2.9–3.0	Boracite
2.95	**Aragonite**
2.95	Erythrite
2.8–3.2	**Biotite**
2.95–3.0	**Cryolite**
2.97–3.00	Phenacite
3.0–3.19	
2.97–3.02	Danburite
2.85–3.2	Anthophyllite
3.0–3.1	**Amblygonite**
3.0–3.1	**Lazulite**
3.0–3.2	**Magnesite**
3.0–3.1	Margarite
3.0–3.25	**Tourmaline**
3.0–3.3	**Tremolite**
3.09	Lawsonite
3.1–3.2	Autunite
3.1–3.2	Chondrodite
3.15–3.20	**Apatite**
3.15–3.20	**Spodumene**
3.16–3.20	**Andalusite**
3.18	**Fluorite**
3.2–3.39	
3.1–3.3	Scorodite
3.2	**Hornblende**
3.23	**Sillimanite**
3.2–3.3	**Diopside**
3.2–3.4	**Augite**
3.25–3.37	Clinozoisite
3.26–3.36	Dumortierite
3.27–3.35	Axinite
3.27–4.37	**Olivine**
3.2–3.5	**Enstatite**
3.4–3.59	
3.27–4.27	Olivine
3.3–3.5	Jadeite
3.35–3.45	**Diaspore**
3.35–3.45	**Epidote**
3.35–3.45	**Vesuvianite**
3.4–3.5	**Hemimorphite**
3.45	Arfvedsonite
3.40–3.55	Aegirine
3.4–3.55	**Titanite**
3.48	**Realgar**
3.42–3.56	Triphylite
3.49	**Orpiment**
3.4–3.6	**Topaz**
3.5	**Diamond**
3.45–3.60	**Rhodochrosite**
3.5–4.3	Garnet
3.6–3.79	
3.27–4.37	Olivine
3.5–4.2	Allanite
3.5–4.3	**Garnet**
3.6–4.0	**Spinel**
3.56–3.66	**Kyanite**
3.58–3.70	**Rhodonite**
3.65–3.75	**Staurolite**
3.7	**Strontianite**
3.65–3.8	**Chrysoberyl**
3.75–3.77	Atacamite
3.77	**Azurite**
3.8–3.99	
3.7–4.7	**Romanechite**
3.6–4.0	**Spinel**
3.6–4.0	Limonite
3.83–3.88	**Siderite**
3.5–4.2	Allanite
3.5–4.3	**Garnet**
3.9	Antlerite
3.9–4.03	**Malachite**
3.95–3.97	**Celestite**
4.0–4.19	
3.9–4.1	**Sphalerite**
4.02	**Corundum**
3.9–4.2	**Willemite**
4.2–4.39	
4.1–4.3	**Chalcopyrite**
3.7–4.7	**Romanechite**
4.18–4.25	**Rutile**
4.3	**Manganite**
4.3	**Witherite**
4.37	**Goethite**
4.35–4.40	**Smithsonite**
4.4–4.59	
4.43–4.45	**Enargite**
4.5	**Barite**
4.55	Gahnite
4.52–4.62	**Stibnite**

Table 22.2 (continued)

G	Name	G	Name	G	Name
4.6–4.79		**5.4–5.59**		**6.5–6.99**	
3.7–4.7	**Romanechite**	5.5	Millerite	6.5	**Skutterudite**
4.6	**Chromite**	5.5±	**Chlorargyrite**	6.55	**Cerussite**
4.58–4.65	**Pyrrhotite**	5.55	**Proustite**	6.78	Bismuthinite
4.7	**Ilmenite**			6.5–7.1	Pyromorphite
4.75	**Pyrolusite**	**5.6–5.79**		6.8	**Wulfenite**
4.6–4.76	Covellite			6.7–7.1	Vanadinite
4.62–4.73	**Molybdenite**	5.5–5.8	**Chalcocite**	6.8–7.1	**Cassiterite**
4.68	**Zircon**	5.68	**Zincite**		
		5.5–6.0	Jamesonite	**7.0–7.49**	
4.8–4.99		5.3–7.3	Columbite		
				7.0–7.5	**Wolframite**
4.6–5.0	Pentlandite	**5.8–5.99**		7.3	**Acanthite**
4.6–5.1	**Tetrahedrite-Tennantite**	5.8–5.9	Bournonite	**7.5–7.99**	
4.89	**Marcasite**	5.85	**Pyrargyrite**		
				7.4–7.6	**Galena**
5.0–5.19		**6.0–6.49**		7.3–7.9	Iron
				7.78	**Nickeline**
5.02	**Pyrite**	5.9–6.1	Crocoite		
4.8–5.3	**Hematite**	5.9–6.1	**Scheelite**	**>8.0**	
5.06–5.08	**Bornite**	6.0	**Cuprite**		
5.15	**Franklinite**	6.07	**Arsenopyrite**	8.10	**Cinnabar**
5.0–5.3	Monazite	6.0–6.2	Polybasite	8.9	**Copper**
5.18	**Magnetite**	6.2–6.4	**Anglesite**	9.0–9.7	Uraninite
		5.3–7.3	Columbite	10.5	**Silver**
5.2–5.39		6.33	**Cobaltite**	15.0–19.3	**Gold**
				14–19	**Platinum**

Table 22.3 Nonopaque Minerals and Some Synthetic Compounds Arranged According to Increasing Refractive Index*

n, ω, β	ϵ, α	γ	Optic Sign	Name
1.338	1.338	1.339	B+	Cryolite
1.433			I	Fluorite
1.45			I	Opal
1.469	1.447	1.472	B−	Borax
1.472	1.454	1.485	B−	Kernite
1.475	1.473	1.479	B+	Tridymite
1.482	1.480		U−	Chabazite
1.482	1.480	1.493	B+	Natrolite
1.483			I	Sodalite
1.492	1.490	1.493	B+	Heulandite
1.487	1.484		U−	Cristobalite
1.487			I	Analcime
1.490			I	Sylvite
1.498	1.494	1.500	B−	Stilbite
1.50			I	Lazurite
1.50			≈I	Chrysocolla
1.504	1.332	1.504	B−	Niter
1.504	1.491	1.520	B+	Ulexite
1.508	1.509		U+	Leucite
1.511	1.505	1.518	B+	Petalite
1.526	1.522	1.530	B−	Microcline
1.523	1.520	1.530	B+	Gypsum
1.524	1.518	1.526	B−	Orthoclase
1.524–1.574	1.522–1.560	1.527–1.578	B±	Cordierite
1.526	1.521	1.528	B−	Sanidine
1.532	1.527	1.538	B+	Albite
1.54–1.59	1.52–1.56		U−	Scapolite
1.537	1.550		U+	Chalcedony
1.537	1.534		U−	Nepheline
1.533	1.536		U+	Apophyllite
1.535	1.525	1.550	B+	Wavellite
1.540	1.540	1.550	B+	Chrysotile
1.542	1.540		U−	Apophyllite
1.543	1.539	1.547	B−	Oligoclase
1.544			I	Halite
1.544	1.531		U−	Marialite
1.544	1.553		U+	Quartz
1.547	1.540	1.550	B−	Cordierite
1.553	1.550	1.557	B+	Andesine
1.55			≈I	Antigorite
1.55–1.59	1.53–1.55	1.55–1.59	B−	Lepidolite
1.588	1.552	1.561	B−	Beryllonite
1.56–1.64	1.53–1.59	1.56–1.64	B−	Phlogopite
1.563	1.559	1.568	B+	Labradorite
1.564	1.559	1.565	B−	Kaolinite
1.57–1.60	1.56–1.60		U−	Beryl
1.570	1.590		U+	Brucite
1.57–1.67	1.57–1.66	1.57–1.67	B±	Chlorite
1.572	1.567	1.576	B−	Bytownite
1.577	1.595		U+	Alunite
1.575	1.570	1.614	B+	Anhydrite
1.577	1.553		U−	Autunite
1.579	1.579	1.584	B+	Clinochlore
1.58			I	Variscite
1.581	1.572	1.586	B−	Anorthite
1.583	1.577		U−	Emerald
1.587	1.336		U−	Nitratite
1.587–1.610	1.575–1.595	1.590–1.622	B−	Amblygonite
1.588	1.544	1.598	B−	Pyrophyllite
1.589	1.539	1.589	B−	Talc
1.59			I	Howlite
1.592	1.586	1.614	B+	Colemanite
1.598	1.551	1.598	B−	Phlogopite
1.594	1.585		U−	Beryl (gem)
1.602	1.556	1.603	B−	Muscovite
1.604	1.595	1.633	B+	Pectolite
1.61–1.70	1.57–1.63	1.61–1.70	B−	Biotite
1.609	1.602	1.621	B+	Brazilianite
1.609–1.631	1.606–1.630	1.616–1.638	B+	Topaz
1.61–1.71	1.60–1.69	1.62–1.72	B±	Anthophyllite
1.612	1.598	1.626	B±	Chondrodite
1.61–1.66	1.59–1.65	1.61–1.66	B−	Glaucophane
1.616	1.600	1.627	B−	Tremolite
1.617	1.614	1.636	B+	Hemimorphite
1.62–1.72	1.61–1.71	1.63–1.73	B−	Hornblende
1.62	1.61	1.65	B+	Turquoise
1.624	1.622	1.631	B+	Celestite
1.627	1.600	1.649	B+	Prehnite
1.630	1.619	1.640	B−	Anthophyllite
1.63–1.67	1.62–1.67		U−	Apatite
1.632	1.620	1.634	B−	Wollastonite
1.633	1.630	1.636	B−	Danburite
1.634	1.612	1.643	B−	Lazulite
1.640–1.60	1.61–1.66		U−	Tourmaline
1.637	1.622	1.649	B−	Actinolite
1.637	1.636	1.648	B+	Barite
1.638	1.632	1.643	B−	Andalusite
1.638	1.633	1.652	B+	Anthophyllite
1.64–1.68	1.63–1.66	1.65–1.70	B+	Cummingtonite
1.643	1.626	1.643	B−	Glaucophane
1.645	1.634	1.647	B−	Margarite
1.646	1.622	1.658	U−	Tourmaline (gem)
1.648	1.584		B−	Biotite
1.649	1.644		U−	Apatite
1.651	1.703		U+	Dioptase
1.65–1.88	1.63–1.88	1.67–1.87	B±	Olivine
1.651	1.635	1.670	B+	Forsterite
1.652	1.624	1.668	B−	Datolite
1.654	1.670		U+	Phenacite
1.658	1.486		U−	Calcite
1.658	1.657	1.677	B+	Sillimanite
1.659	1.654	1.667	B+	Jadeite
1.662	1.636		U−	Tourmaline
1.661	1.626	1.699	B±	Erythrite
1.665	1.650	1.679	B+	Cummingtonite
1.665	1.660	1.674	B+	Enstatite
1.666	1.654	1.670	B−	Hornblende
1.666	1.655	1.672	B+	Spodumene
1.667	1.520	1.669	B−	Strontianite
1.683	1.678	1.688	B−	Bronzite (orthopyroxene)
1.672	1.654	1.690	B+	Olivine (peridot)
1.69–1.72	1.68–1.74	1.71–1.75	B+	Augite

*A continuous listing of minerals is given according to increasing refractive index: n (isotropic), ω (uniaxial), β (biaxial). Under optic sign: I = isotropic; U = uniaxial, + or −; B = biaxial, + or −. Although only a few minerals have constant refractive indices, a single listing is given for most. A range of refractive indices is given when the variation is appreciably greater than ±0.01.

Table 22.3 (continued)

n, ω, β	ϵ, α	γ	Optic Sign	Name
1.674	1.665	1.684	B+	Lawsonite
1.676	1.623	1.677	B−	Biotite
1.676	1.529	1.677	B−	Witherite
1.676	1.667	1.699	B+	Diopside
1.679	1.676	1.680	B+	Lithiophilite
1.680	1.530	1.685	B−	Aragonite
1.681	1.500		U−	Dolomite
1.688	1.681	1.692	B−	Axinite
1.690	1.670	1.708	B−	Grunerite
1.691	1.719		U+	Willemite
1.692	1.690	1.694	B±	Triphylite
1.694	1.679	1.698	B−	Hornblende
1.694	1.693	1.702	B+	Zoisite
1.699	1.668	1.707	B−	Sinhalite
1.700	1.696	1.711	B−	Riebeckite
1.700	1.509		U−	Magnesite
1.701	1.680	1.720	B−	Olivine
1.702	1.703	1.728	B+	Pigeonite
1.703–1.752	1.700–1.746		U−	Vesuvianite
1.704	1.698	1.723	B+	Augite
1.704	1.694	1.707	B−	Hypersthene (orthopyroxene)
1.714–1.750			I	Pyrope
1.72–1.74	1.71–1.74	1.72–1.75	B+	Rhodonite
1.720–1.734	1.713–1.730	1.723–1.740	B−	Chloritoid
1.720	1.712	1.728	B−	Kyanite
1.722	1.702	1.850	B+	Diaspore
1.724			I	Spinel
1.72–1.78	1.71–1.75	1.73–1.80	B−	Epidote
1.725	1.718	1.748	B+	Hedenbergite
1.734			I	Grossular
1.737	1.733	1.747	B+	Rhodonite
1.738	1.726	1.789	B+	Antlerite
1.748	1.746	1.756	B+	Chrysoberyl
1.749	1.743	1.757	B+	Staurolite
1.755	1.733	1.765	B−	Epidote
1.757	1.804		U+	Benitoite
1.758	1.730	1.838	B+	Azurite
1.769	1.760		U−	Corundum
1.794	1.792	1.845	B+	Monazite
1.78–1.87	1.76–1.78	1.80–1.84	B−	Aegirine
1.80			I	Gahnite
1.80			I	Spessartine
1.816	1.579		U−	Rhodochrosite
1.819	1.776	1.836	B−	Aegirine
1.820			I	Almandine
1.833			I	YAG
1.861	1.831	1.880	B−	Atacamite
1.883	1.877	1.894	B+	Anglesite
1.850	1.623		U−	Smithsonite
1.875	1.633		U−	Siderite
1.875	1.655	1.909	B−	Malachite
1.877	1.835	1.886	B−	Fayalite
1.868			I	Uvarovite
1.887			I	Andradite
1.907	1.900	2.034	B+	Titanite
1.920	1.934		U+	Scheelite
1.920–1.960	1.967–2.015		U+	Zircon
1.93	1.75	1.95	B−	Carnotite
1.975			I	GGG
1.997	2.093		U+	Cassiterite
2.013	2.029		U+	Zincite
2.058	2.048		U−	Pyromorphite
2.077	1.804	2.079	B−	Cerussite
2.11			I	Chromite
2.16			I	Zirconia (cubic)
2.39	2.26	2.40	B−	Goethite
2.35	2.27		U−	Vanadinite
2.37			I	Sphalerite
2.37	2.31	2.66	B+	Crocoite
2.404	2.283		U−	Wulfenite
2.409			I	Strontium titanate
2.417			I	Diamond
2.554	2.493		U−	Anatase
2.586	2.583	2.704	B+	Brookite
2.684	2.538	2.704	B−	Realgar
2.61	2.90		U+	Rutile
2.81	2.40	3.02	B−	Orpiment
2.85			I	Cuprite
2.85	3.20		U+	Cinnabar
2.98	2.71		U−	Proustite
3.08	2.88		U−	Pyrargyrite
3.22	2.94		U−	Hematite

APPENDIX 1

Outstanding Contributions to the Mineral Sciences

The Roebling Medal was established in 1937 by the Mineralogical Society of America in memory of Colonel Washington A. Roebling (1837–1926), who made a generous financial gift to the Society. Colonel Roebling, the designer of such well-known suspension bridges as those over the Niagara River at Niagara Falls, the Allegheny River at Pittsburgh, the Ohio River in Cincinnati, and the East River in New York City (the Brooklyn Bridge), and who worked on bridges during the Civil War, had a deep, life-long interest in the study of minerals. The Roebling medal signifies the highest recognition of achievement that mineralogy can bestow on outstanding investigators in the United States or abroad (for more information see www.minsocam.org). In 1927, Roebling's son John donated his father's mineral collection of about 16,000 specimens to the National Museum of Natural History (Smithsonian Institution) in Washington, D.C. This collection, known as the Washington A. Roebling Mineral Collection, was undoubtedly one of the largest and finest private collections of its time. This acquisition, together with another collection of about 9,100 specimens (the Canfield Collection), made the Smithsonian mineral collection one of the best in the world. (Roe, A. 1990. Washington A. Roebling, his life and his mineral collection. *Mineralogical Record* 21: 13–30).

Table A1.1 is a listing of all Roebling medalists since 1937. The table also provides a very short description of the type of scientific work for which the medalist was recognized.

Table A1.1 Recipients of the Roebling Medal Awarded by the Mineralogical Society of America

Award Year	Recipient and Institutional Affiliation	Examples of Outstanding Contributions to Mineralogy
1937	Charles Palache, Harvard University	goniometric studies in crystallography and mineral paragenesis; minerals of Franklin Furnace, NJ
1938	Waldemar T. Schaller, U.S. Geological Survey	chemical mineralogy; crystallography and paragenesis of pegmatite minerals
1940	Leonard James Spencer, British Museum (Natural History)	mineral systematics; long-time editor of *Mineralogical Magazine and Mineralogical Abstracts*
1941	Esper S. Larsen, Jr., Harvard University	mineralogy and petrology; the determination of the optical properties of nonopaque minerals
1945	Edward H. Kraus, University of Michigan	occurrence and origin of minerals; crystallographic forms; development of apparatus for mineral testing
1946	Clarence S. Ross, U.S. Geological Survey	petrography and petrology, particularly clay minerals; microscopic techniques; geochemistry of ore deposits
1947	Paul Niggli, Technische Hochschule, Zurich	crystallography and structure of minerals; igneous and metamorphic rocks; minerals of the Swiss Alps
1948	William Lawrence Bragg, Cavendish Laboratory, University of Cambridge	crystal structure determinations by X-ray diffraction techniques; recipient (jointly with his father, William Henry Bragg) of the Nobel Prize for Physics in 1915
1949	Herbert E. Merwin, Geophysical Laboratory, Carnegie Institution	crystal optics; characterization of synthetic, transparent, and opaque phases
1950	Norman L. Bowen, Geophysical Laboratory, Carnegie Institution	application of experimental physico-chemical data and principles to petrological problems
1952	Federick E. Wright, Geophysical Laboratory, Carnegie Institution	optical properties of minerals; design of improved petrographic microscope and test plates
1953	William F. Foshag, U.S. National Museum	characterization of new minerals; minerals of the United States and Mexico; gemology

(*Continued*)

Table A1.1 *(continued)*

Award Year	Recipient and Institutional Affiliation	Examples of Outstanding Contributions to Mineralogy
1954	Cecil Edgar Tilley, University of Cambridge	application of physico-chemical principles to the study of mineral assemblages in metamorphic and igneous rocks
1955	Alexander N. Winchell, University of Wisconsin	evaluation of major rock-forming silicate groups; textbooks on optical mineralogy
1956	Arthur F. Buddington, Princeton University	quantitative petrologic studies of many rock types and of ore deposits
1957	Walter F. Hunt, University of Michigan	mineralogy; editor for 35 years of *The American Mineralogist*
1958	Martin J. Buerger, Massachusetts Institute of Technology	structural crystallography; development of single crystal X-ray techniques; textbooks in crystallography
1959	Felix L. Machatschki, University of Vienna	atomic arrangement of major silicate groups, atomic substitution; relation of crystal structure to paragenesis
1960	Thomas F. W. Barth, Oslo University	petrology and X-ray crystallography; petrogenetic relations of rocks in regions of Norway (e.g., the Oslo region) and North America
1961	Paul Ramdohr, University of Heidelberg	reflected light microscopy; mineralogy and genesis of ore deposits; major text on ore mineralogy
1962	John W. Gruner, University of Minnesota	X-ray crystallography of clay minerals; mineralogy and petrology of iron-formations; uranium mineralizations
1963	John Frank Schairer, Geophysical Laboratory, Carnegie Institution	experimental studies of silicate phase equilibria
1964	Clifford Frondel, Harvard University	structural mineralogy; characterization of many new minerals; mineralogy of uranium and thorium; co-author of *Dana's System*
1965	Adolph Pabst, University of California Berkeley	X-ray crystallographic and structural mineralogy; evaluation of the metamict state and of sheet silicates
1966	Max H. Hey, British Museum (Natural History)	mineral chemistry of zeolites, the chlorite group, and meteorites; author of *Index of Mineral Species*; long-time editor of *Mineralogical Magazine*
1967	Linus Pauling, University of California, San Diego	crystal and molecular structures; quantum chemistry; theory of chemical bonding; author of *The Nature of the Chemical Bond*; recipient of the Nobel Prize in Chemistry in 1954 and the Nobel Peace Prize in 1962
1968	Tei-ichi Ito, University of Tokyo	structural crystallography; polymorphism; X-ray powder diffraction
1969	Fritz Laves, Technische Hochscule, Zurich	structure and paragenesis of feldspars; crystal chemistry of metallic compounds
1970	George W. Brindley, Pennsylvania State	structural crystallography of layer silicates; clay mineralogy; crystallography
1971	J. D. H. Donnay, Johns Hopkins University	crystal optics; relationship of morphology and structure; twinning; author of *Crystal Data*
1972	Elburt F. Osborn, Bureau of Mines, U.S. Department of Interior	experimental petrology in rock-forming systems; crystallization and differentiation trends in magmas
1973	George Tunell, University of California, Santa Barbara	experimental investigations of oxidized ore minerals; physical-chemical evaluations of ore-forming processes
1974	Ralph E. Grim, University of Illinois, Champaign-Urbana	clay mineralogy; author of *Clay Mineralogy* and *Applied Clay Mineralogy*
1975	O. Frank Tuttle, Stanford University	experimental petrology; development of hydrothermal research equipment; experimental studies on the origin of granite
1975	Michael Fleischer, U. S. Geological Survey	trace element geochemistry; evaluation of new mineral species; long-time chairman of international commission on new minerals; long-time editor of section on mineralogy in *Chemical Abstracts*
1976	Carl W. Correns, University of Göttingen	physical-chemical evaluations of sedimentology; chemical and physical oceanography; mineralogy of sediments
1977	Raimond Castaing, University of Paris	inventor of the electron microprobe and pioneering work on theory of quantitative analysis; development of ion beam microprobe
1978	James B. Thompson, Jr., Harvard University	theoretical evaluation of petrologic systems; thermodynamics of systems; metamorphic reactions in pelitic schists; crystal chemistry of amphiboles
1979	William H. Taylor, Cavendish Laboratory, University of Cambridge	structural crystallography; structural features of feldspar, zeolite, and aluminosilicate minerals
1980	D. S. Korzhinskii, Academy of Sciences, Moscow	application of chemical thermodynamics to petrology; author of *Physicochemical Basis for the Analysis of the Paragenesis of Minerals* and of *Theory of Metasomatic Zoning*
1981	Robert M. Garrels, University of South Florida	theoretical studies of ore formation; chemical thermodynamics of mineral systems; phase diagrams for minerals at low temperature; chemical evolution of the ocean and atmosphere; co-author of *Solutions, Minerals and Equilibria*

Table A1.1 (continued)

Award Year	Recipient and Institutional Affiliation	Examples of Outstanding Contributions to Mineralogy
1982	Joseph V. Smith, University of Chicago	structural crystallography of rock-forming minerals; zeolites and feldspars; lunar mineralogy and petrology; author of *Feldspars* (2 volumes)
1983	Hans P. Eugster, Johns Hopkins University	solid-fluid equilibria in hydrothermal systems; chemical sedimentation and water chemistry such as in active salt lakes
1984	Paul B. Barton, Jr., U.S. Geological Survey	petrology of ores; the chemistry and physics of the ore-forming process
1985	Francis J. Turner, University of California, Berkeley	metamorphic petrology
1986	Edwin Roedder, U.S. Geological Survey	fluid inclusions in minerals
1987	Gerald V. Gibbs, Virginia Polytechnic Institute and State University	mathematical foundations of crystallography; application of molecular orbital theory to chemical bonding
1988	Julian R. Goldsmith, University of Chicago	order-disorder in feldspars; phase equilibria of carbonates; oxygen-isotope fractionations among minerals
1989	Helen D. Megaw, University of Cambridge	X-ray crystal structure of feldspars; origin of ferroelectricity in oxides
1990	Sturges W. Bailey, University of Wisconsin	structural and crystal chemical studies of layer silicate minerals
1991	E-an Zen, U.S. Geological Survey	application of thermodynamics in petrology; the temperature-pressure regime of the Appalachian mountain belt; igneous thermobarometry
1992	Hatten S. Yoder, Jr., Geophysical Laboratory, Carnegie Institution	experimental petrology and its application to mineral paragenesis; study of the role of water in metamorphism and the petrogenesis of igneous rocks; author of *Generation of Basaltic Magma*
1993	Brian Mason, National Museum of Natural History (Smithsonian Institution)	characterization of a broad range of terrestrial and meteoritic mineralogy; author of *Principles of Geochemistry*, and of *Meteorites*; co-author of *Mineralogy*
1994	William A. Bassett, Cornell University	experimental studies in high-pressure mineral physics using the diamond cell that he developed
1995	William S. Fyfe, University of Western Ontario	experimental phase equilibria, crystal chemistry, aqueous geochemistry, mineral spectroscopy, high temperature processes, and environmental geochemistry
1996	Donald H. Lindsley, State University of New York at Stony Brook	experimental and theoretical work on phase relations in Fe–Ti oxides, pyroxenes, and olivines; thermometry, barometry, and oxybarometry of rock types with these ferromagnesian minerals
1997	Ian S. E. Carmichael, University of California, Berkeley	studies of volcanic regions in the Pacific rim; tectonic and volcanic history of Western Mexico; thermodynamic properties of silicate liquids
1998	C. Wayne Burnham, Pennsylvania State University	experimental and thermodynamic evaluations of the behavior of volatiles in igneous petrogenesis
1999	Ikuo Kushiro, University of Tokyo	experimental studies on the genesis of basaltic and andesitic magmas and on the properties of magmas at higher pressures
2000	Robert C. Reynolds, Jr., Dartmouth College	X-ray diffraction studies of mixed-layered clay minerals and computer simulations of diffraction patterns of disordered minerals
2001	Peter J. Wyllie, California Institute of Technology	experimental petrology on various aspects of igneous processes, producing a long series of phase diagrams that have elucidated many magmatic processes
2002	Werner F. Schreyer, Ruhr-Universität, Bochum, Germany	application of experimental mineralogy to petrologic problems; study of ultra-high pressure metamorphic rocks; synthesis of new mineral phases, boron-bearing minerals
2003	Charles T. Prewitt, Geophysical Laboratory, Carnegie Institute of Washington	application of synchrotron radiation to mineralogical crystallography; contributions to comparative crystal chemistry; mineral physics, high-pressure research and development of structural principles for high-pressure phases
2004	Frances R. (Joe) Boyd, Geophysical Laboratory, Carnegie Institute of Washington	development of high-pressure, high-temperature experimental equipment (press); its application to mineral stability; significant contributions to mantle petrology and evolution of continental lithosphere
2005	Ho-kwang Mao, Geophysical Laboratory, Carnegie Institute of Washington	experimental mineralogy, innovative application of high-pressure, high-temperature experiments to understanding of the Earth's mantle and core
2006	W. Gary Ernst, Stanford University, California	experimental studies of amphibole stability; connecting blueschist terranes to subduction zone metamorphism; global comparisons of subduction zone and ultra-high pressure metamorphic terranes

Development of Models for the Atom

This appendix provides additional details on the theoretical development of the model now in use for the **atom**, to supplement the information covered in Chapter 3.

THE BOHR MODEL OF THE ATOM

The first widely accepted picture of the atom was developed in 1913 by the Danish physicist Niels Bohr. This model is based on the fact that when an electrical charge is passed through a tube containing hydrogen, light is emitted, and the light's spectrum is found to consist of several sharp lines with specific wavelength (λ) values (Fig. A2.1). Four of these lines, in the visible part of the spectrum, can be seen with the naked eye, and the others, in the ultraviolet region, can be recorded on photographic film. Because of the specific and characteristic wavelength (λ) values of the light lines emitted by all chemical elements heated to a high temperature, Niels Bohr concluded that electrons of the elements occur in specific energy levels at various distances away from the nucleus. He postulated that when an electron absorbs energy it jumps to a higher

FIG. A2.1 The line spectrum of hydrogen obtained by refraction through a glass prism. The wavelengths of the lines in the visible spectrum are given in nanometers (nm). The lines to the left of these are in the ultraviolet region of the spectrum. The distinct line separation is due to the fact that the light energy released has only distinct quantities of energy and none in between (from Brady, J. E., and G. E. Humiston. 1982. *General chemistry: Principles and structure, 3rd ed. Wiley, New York; copyright © John Wiley & Sons; reprinted by permission).*

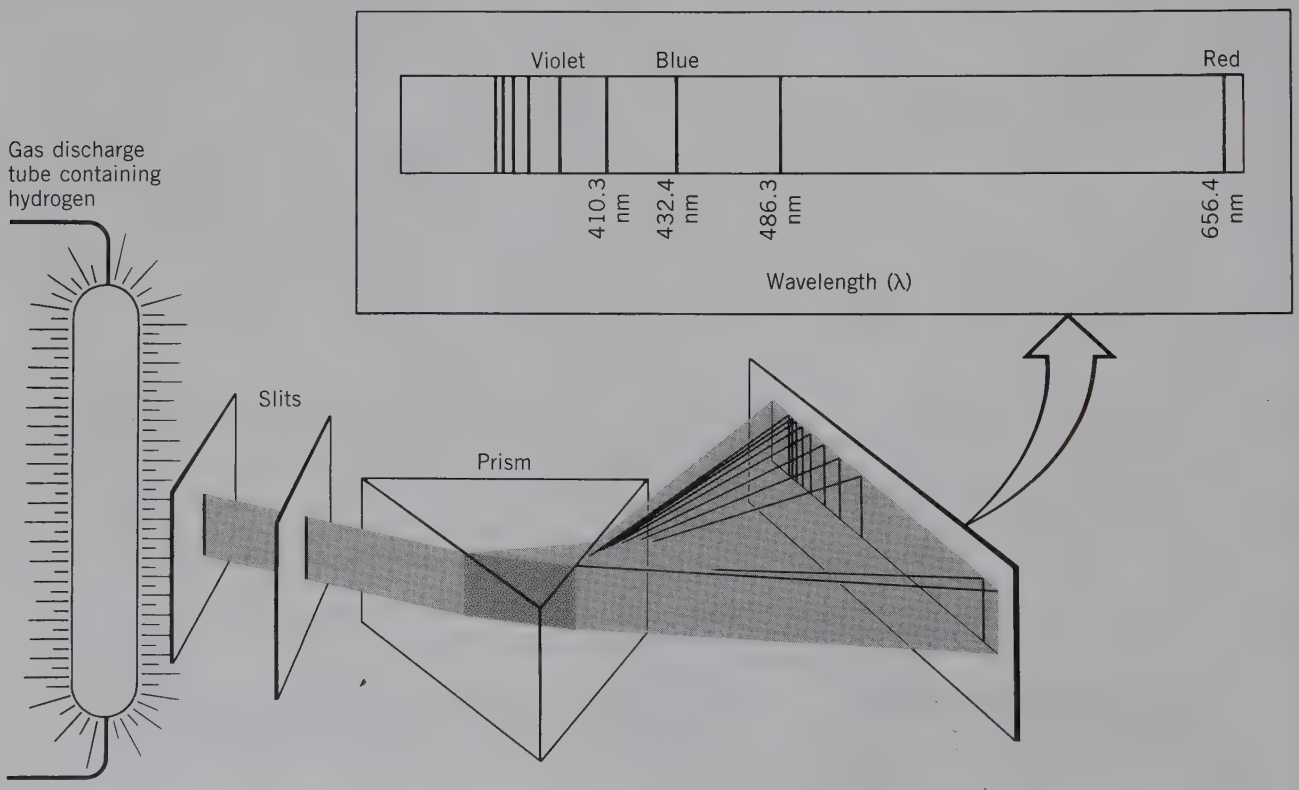

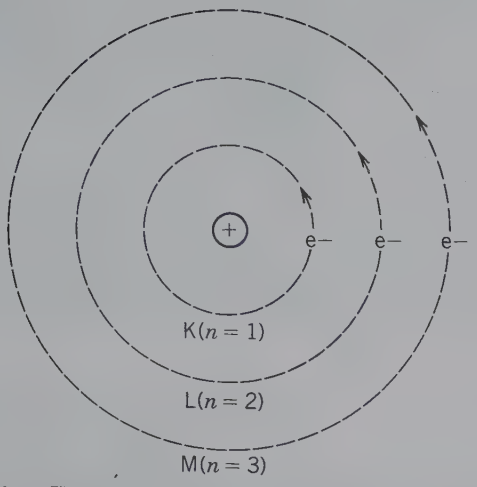

FIG. A2.2 The Bohr model of the atom. Electrons travel along specific orbits of fixed energy levels (known as K, L, M, N, . . . shells, with principal quantum number, $n = 1, 2, 3, 4, \ldots, \infty$).

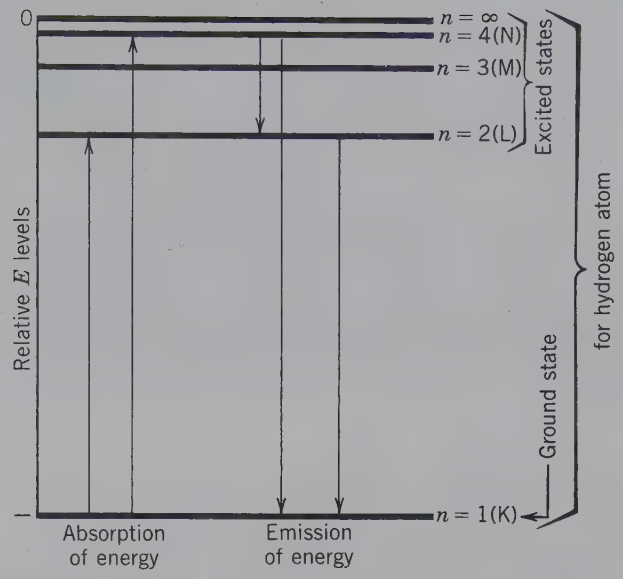

FIG.A2.3 Schematic representation of the energy levels of electrons (for $n = 1, 2, 3, 4, \ldots, \infty$) in the Bohr atomic mode. The two vertical "up" arrows show two possibilities for the increase in energy level of an electron as a result of the absorption of energy; the three "down" arrows show three possibilities for how electron energy is lost as a result of the emission of energy.

energy level, and when it loses energy, it drops to a lower energy level (Fig. A2.2). This led Niels Bohr to conclude that electrons occur in discrete, or *quantized*, energy levels. The energy of the emitted radiation is proportional to the wavelength of the radiation, in accordance with the Einstein equation

$$E = \frac{hc}{\lambda}$$

where E is the energy, c is the velocity of light, λ is the wavelength of the radiation emitted, and h is a proportionality constant known as Planck's constant. This is a universal constant of nature that relates the energy of a quantum of radiation to the frequency of the oscillator that emitted it. Its numerical value is 6.62517×10^{-27} erg sec.

In the Bohr model of the atom, the electrons are visualized as circling the nucleus in "orbits" (as in a planetary system), or energy levels, at fixed distances from the nucleus, depending on their energies. A schematic illustration of the hydrogen atom as based on the Bohr theory is given in Chapter 3 (see Fig. 3.1). At the center is the *nucleus*, which, except in the hydrogen atom, is made up of *protons* and *neutrons* (the hydrogen nucleus is made up of a single proton).

In chemical elements with more than one electron, the electrons are distributed in shells designated by n (e.g., $n = 1$, $n = 2$, $n = 3$, etc.) and known as the *principal quantum numbers*. The corresponding electron shells (or orbits) are designated K, L, M, N, etc. (Fig. A2.3). For this model, Bohr derived an equation for the energy of the electron, as follows:

$$E = -A\frac{1}{n^2}$$

where A is a constant involving knowledge of the mass and charge of the electron and Planck's constant, and n is the principal quantum number, which identifies the electron orbit. This equation shows that the energy of an electron in a particular orbit depends on the value of n. The greatest absolute value of energy is represented by $n = 1$ because this yields the largest value for the fraction $1/n^2$. Because of the negative sign in the equation, this is the lowest (most negative) energy, E (see Fig. A2.3). In Fig. A2.3, the energy (E) scale is expressed in negative units, in accordance with the previously mentioned equation. Although this may appear unusual, note that the electron orbits represent energy levels with various distinct energy differences between them.

THE SCHRÖDINGER MODEL OF THE ATOM

Although the concept of electrons circling the nucleus in well-defined orbits (as in the Bohr model) gained wide acceptance, it did not satisfactorily explain a number of important observations. It was not applicable to the line spectra of complex atoms (with atomic numbers higher than those of hydrogen). Additional spectral lines were interpreted as the result of the axial spin (clockwise or counterclockwise) of the electrons, which

was not accounted for in the Bohr model. A single quantum number, n, furthermore, did not account for possible elliptical electron orbits. It also gave no basic understanding for the quantization of energy between various orbital levels, and it failed to explain why an orbiting electron did not radiate energy.

In 1923, the French physicist Louis-Victor de Broglie demonstrated that electrons, instead of behaving solely as particles whose positions can be determined in space (as in the Bohr model), had properties identical to those of waves. The wavelength (λ) of a particle with mass m and velocity v is expressed as

$$\lambda = \frac{h}{mv}$$

where h is Planck's constant.

With electrons having wavelike properties, it becomes impossible to visualize them as being in a specific place at a particular time. This notion, expressed as the *uncertainty principle*, was introduced by the German scientist Werner Heisenberg. It implies that the motion of an electron around the nucleus of an atom cannot be satisfactorily described in terms of orbits, be they circular or elliptical.

In 1926, all the previously mentioned developments were incorporated into a new atomic model by Erwin Schrödinger and were expressed as a wave equation. In this equation, the electrons are described by wave functions, and the theoretical model is founded on the quantum properties of energy, that is, the theory of *quantum mechanics*. The Schrödinger equation relates the probability of finding an electron at a given time, in a specific place, to the mass and potential energy of the particle at that time and place.

One form of the Schrödinger equation is as follows:

$$\frac{\partial^2\Psi}{\partial x^2} + \frac{\partial^2\Psi}{\partial y^2} + \frac{\partial^2\Psi}{\partial z^2} + \frac{8\pi^2 m}{h^2}(E - V)\Psi = 0$$

where Ψ is a wave function in terms of three coordinate axial directions (x, y, z), m is the mass of the electron, E is the total energy of the electron, V is the potential energy of the electron at some specified point, and h is Planck's constant.

The Schrödinger equation is also stated as follows;

$$\nabla^2\Psi + \frac{8\pi^2 m}{h^2}(E - V)\Psi = 0$$

where the ∇^2 symbol is a differential operator with

$$\nabla^2\Psi = \frac{\partial^2\Psi}{\partial x^2} + \frac{\partial^2\Psi}{\partial y^2} + \frac{\partial^2\Psi}{\partial z^2} \quad ,$$

The unique contribution of the Schrödinger equation is its representation of physical observations in a way that had not been possible in earlier developed models. The function $\Psi(x, y, z)$, which occurs in the wave equation, describes the behavior of an electron. The square of this function, $\Psi^2(x, y, z)$, defines a region in space (x, y, z) where the electron may be found with a certain probability. This is shown schematically in Fig. A2.4. This illustration might be considered the final print of millions of superimposed photographs of the position of an electron in three-dimensional space, defined by x, y, and z axial directions. With the electron in rapid motion, the final composite photograph would produce an array of dots (like a cloud) with dense and more openly spaced regions. The dense regions would be those of a high probability of finding an electron, and those of low density would represent a lower probability of locating an electron. The wave theory, therefore, portrays the motion of electrons only in terms of the probability of finding a certain electron within a small volume unit. It does not describe the movement of electrons in well-defined, simple orbits.

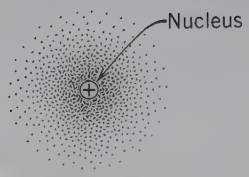

FIG.A2.4 Schematic illustration of the electron probability density distribution (Ψ^2) of an electron around a nucleus (an electron cloud). The dots do not show the location of the electron but only the probability of finding the electron in that location. The greater the density of dots, the greater the probability of finding the electron in that region.

The electron behavior summarized by the Schrödinger wave equation can be compared to the vibrations of a string stretched between two fixed points. Figure A2.5 shows some of the ways in which a string can vibrate. In Fig. A2.5a, the string vibrates in the simplest way, that is, between two fixed end points. In Fig. A2.5b, the string distorts like a standing sinusoidal wave, with a central point where there is no displacement. The points of no displacement are known as *nodes*. Figure A2.5c shows a string vibrating between two fixed end nodes, and with two nodes at one-third and two-thirds of the length of the string. Each of these different vibration patterns can be defined by a fundamental audio frequency, v audio (where v audio $= v/\lambda$; v = velocity of sound; and λ = wavelength of the string) and a principal quantum number, n. In the one-dimensional example of a string, the quantum number, n, gives the number of half-wavelengths in the vibrations, and $(n = 1)$ is the number of nodes (including the nodes at the ends of the string). In the case of a three-dimensional electron wave, nodes may form along each of the three axial directions.

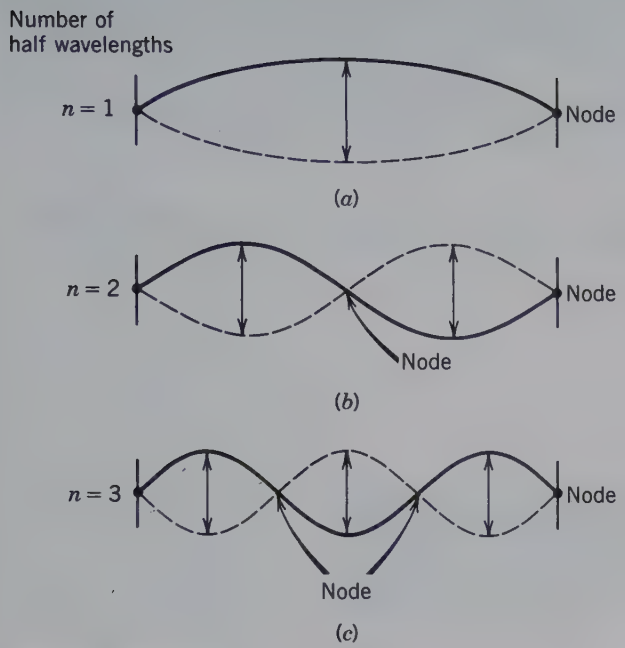

FIG.A2.5 Relationship between principal quantum number n and the number of half wavelengths in a standing wave. In solutions to the wave equation, nodes represent regions with no electron density (see Fig. A2.4). The wave functions that describe the motions of an electron are known as "orbitals," to distinguish them from the "orbits" in the Bohr atomic model.

To completely specify the position of an electron in three-dimensional space, *three quantum numbers* are needed:

1. the *principal quantum number*, n
2. the *azimuthal quantum number* (or *orbital shape quantum number*), l, and
3. the *magnetic quantum number*, m.

These three quantum numbers follow from the solution of the Schrödinger wave equation and represent specified parameters in the mathematical formulation of Ψ. These quantum numbers are discussed, in detail, in Chapter 3 and form the basis for the current view of the atom.

APPENDIX 3

Distribution of Forms in 32 Point Groups, Arranged by Crystal System

The point groups shown in bold are discussed, in detail, in Chapter 9. (Tables from Buerger, M. J. 1956. *Elementary crystallography*. Wiley, New York.)

Table A3.1 Forms in the Triclinic, Monoclinic, and Orthorhombic Systems

No. of Faces	Name of Form	Point group (crystal class) 1	$\bar{1}$	2	*m*	**2/*m***	222	***mm*2**	**2/*m*2/*m*2/*m***	Unique Form for
1	Pedion	+		+	+			+		
2	Pinacoid		+	+	+	+	+	+	+	
2	Dome			+	+			+		
2	Sphenoid									
4	Prism					+	+	+	+	
4	Disphenoid						+			222
4	Pyramid							+		*mm*2
8	Dipyramid								+	2/*m*2/*m*2/*m*

Table A3.2 Forms in the Tetragonal System

No. of Faces	Name of Form	Point group (crystal class) 4	$\bar{4}$	**4/*m***	422	4*mm*	**$\bar{4}$2*m***	**4/*m*2/*m*2/*m***	Unique Form for
1	Pedion	+				+			
2	Pinacoid		+	+	+		+	+	
4	Tetragonal prism	+	+	+	+	+	+	+	
4	Tetragonal pyramid	+				+			
4	Tetragonal disphenoid		+				+		
8	Ditetragonal prism				+	+	+	+	
8	Tetragonal dipyramid			+	+		+	+	
8	Tetragonal trapezohedron				+				422
8	Tetragonal scalenohedron						+		$\bar{4}$2*m*
8	Ditetragonal pyramid					+			4*mm*
16	Ditetragonal dipyramid							+	4/*m*2/*m*2/*m*

Table A3.3 Forms in the Hexagonal System

No. of Faces	Name of Form	Point group (crystal class)											Unique Form for
		3	$\bar{3}$	32	3*m*	$\bar{3}2/m$	6	$\bar{6}$	6/*m*	622	6*mm*	$\bar{6}m2$	6/*m*2/*m*2/*m*	
1	Pedion	+			+		+				+			
2	Pinacoid		+	+		+		+	+	+		+	+	
3	Trigonal prism	+		+	+			+				+		
3	Trigonal pyramid	+			+									
6	Ditrigonal prism			+	+							+		
6	Hexagonal prism		+	+	+	+	+		+	+	+	+	+	
6	Trigonal dipyramid			+				+				+		
6	Rhombohedron		+	+		+								
6	Trigonal trapezohedron			+										32
6	Ditrigonal pyramid				+									3*m*
6	Hexagonal pyramid				+		+				+			
12	Hexagonal dipyramid					+			+	+		+	+	
12	Hexagonal scalenohedron					+								$\bar{3}2/m$
12	Dihexagonal prism					+				+	+		+	
12	Ditrigonal dipyramid											+		$\bar{6}/m2$
12	Hexagonal trapezohedron									+				622
12	Dihexagonal pyramid										+			6*mm*
24	Dihexagonal dipyramid												+	6/*m*2/*m*2/*m*

Table A3.4 Forms in the Isometric System

No. of Faces	Name of Form	Point Group (crystal class)					Unique Form for
		23	432	2/$m\bar{3}$	$\bar{4}$3*m*	4*m*$\bar{3}$2/*m*	
4	Tetrahedron	+			+		
6	Cube	+	+	+	+	+	
8	Octahedron		+	+		+	
12	Dodecahedron	+	+	+	+	+	
	Pyritohedron	+		+			
	Tristetrahedron	+			+		
	Deltoid dodecahedron	+			+		
	Tetartoid	+					23
24	Tetrahexahedron		+		+	+	
	Trapezohedron		+	+		+	
	Trisoctahedron		+	+		+	
	Hextetrahedron				+		$\bar{4}$3*m*
	Diploid			+			2/$m\bar{3}$
	Gyroid		+				432
48	Hexoctahedron					+	4/$m\bar{3}$2/*m*

Space Groups as an Expression of Morphology and Structure

A clearer understanding of what space groups mean can be gained from correlations between point group symmetry (as based on morphology), internal structure, and the resultant space group symbolism. A point group is the translation-free residue of an isogonal space group. A crystal structure that might contain screw axes and/or glide planes will exhibit morphology that reflects only rotation axes and/or mirrors. The angular relations between the faces of a crystal are not affected by the translational nature of the internally present axes and planes. Screw axes and glide planes cause displacements in the structure, but these are so small (2 to 5 Å) that they cannot be observed morphologically and are, therefore, absent in the notation of point group symmetry.

The most informative way to evaluate an internal structure is by the visual study and inspection of three-dimensional models of the structure. (Various views of crystal structures and their space group elements are given in module III of the CD-ROM under the heading "3-dimensional Order: Space Group Elements in Structures.") However, Figs. A4.1, A4.2, and A4.3 are restricted to two-dimensional representations of three-dimensional arrangements.

DIOPSIDE (MONOCLINIC EXAMPLE)

Figure A4.1 shows the correlation between the symmetry deduced from the morphology of diopside, $CaMgSi_2O_6$ (a member of the clinopyroxene series) and its internal structure as well as the derived space group. The diopside crystal (see Fig. A4.1a) has point group symmetry $2/m$ (projected in Fig. A4.1b), and the simplest possible lattice compatible with point group symmetry $2/m$ is P (primitive, shown in Fig. A4.1c). In order to arrive at the correct (not just the simplest) choice of lattice type (and unit cell), refer to the atomic structure of diopside (and similar clinopyroxenes) to identify some of the basic repeat units (Figs. A4.1d, e): these are a cross-section and a frontal view of tetrahedral–octahedral–tetrahedral (t–o–t) chains that parallel the c axis (see the section on the pyroxene group in Chapter 18). These structural units (t–o–t) are repeated in a centered pattern in the plan view (Fig. A4.1d). In three dimensions, this is compatible with a c-centered monoclinic lattice (C). The locations of two-fold rotation axes (parallel to the b axis) and interleaved two-fold screw axes (the result of the centering) are shown. The vertical section in Fig. A4.1e shows the presence of a glide component of $c/2$ in the tetrahedral chain. This is expressed by the c in the space group symbol $C2/c$, in place of m in the point group notation $2/m$. The locations of these glide planes are shown in the plan view of the pyroxene structure (Fig. A4.1d) and are marked g. Interleaved, halfway between these glides, will be additional glide planes that result from the centering of the unit cell choice. The three-dimensional lattice that is appropriate to the structure of diopside is monoclinic and C-centered (Fig. A4.1f). For purposes of clarity, the drawing shows only some of the symmetry elements present; additional glides, two-fold rotation, and screw axes would be present in locations equivalent to those shown in Fig. A4.1c. In Fig. A4.1g, the conventional space group representation is given for $C2/c$. This discussion omitted the location of the various positions of inversion symmetry (centers of symmetry). It is conventional to choose the origin of a space group at the location of such a center of symmetry. Therefore, the two-fold rotation and screw axes appear at $+1/4c$ in Fig. A4.1g; the centers, at the positions noted, lie $1/4c$ below the symmetry axes.

BERYL (HEXAGONAL EXAMPLE)

The correlation between point group symmetry, structure, and resultant space group for the hexagonal mineral beryl, $Be_3Al_2Si_6O_{18}$, is shown in Fig. A4.2. Due to its hexagonal crystal form, apparent in its external morphology (Figs. A4.2a, b) and its internal structure (Figs. A4.2c, d), the choice of lattice type for this mineral must be hexagonal. The horizontal projection onto (0001) (Fig. A4.2c) shows the unique six-fold Si_6O_{18} rings. If the centers of four of these rings are chosen as

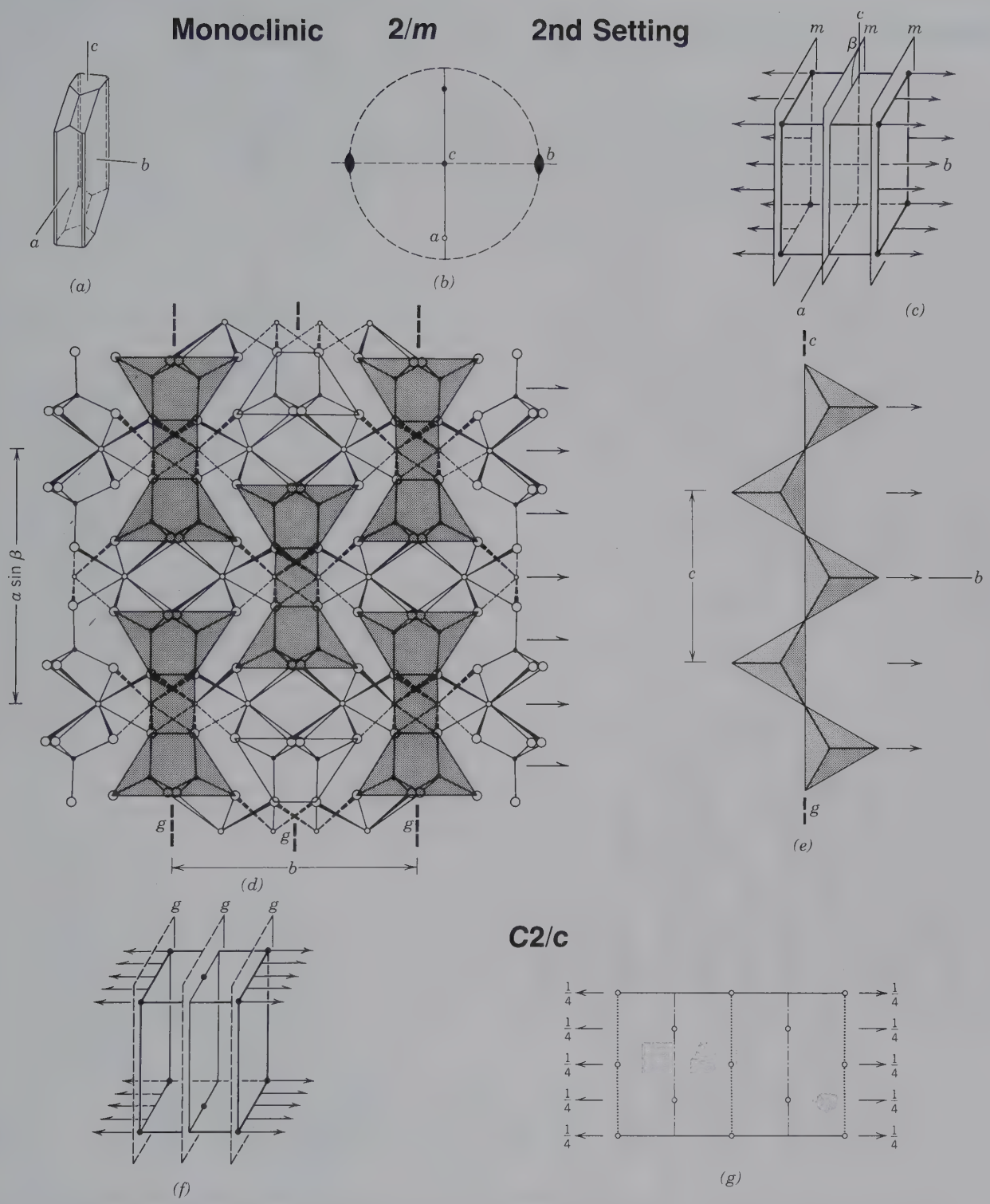

FIG. A4.1 Relationship of point group symmetry to space group representation for diopside, a member of the clinopyroxene group. (a) Crystal of diopside. (b) Stereogram of 2/*m* symmetry. (c) Sketch of a possible monoclinic, primitive lattice compatible with 2/*m*. Locations of two-fold axes and mirrors are noted. (d) A view of the clinopyroxene structure along the *c* axis. (Redrawn from Cameron, M., and J. J. Papike. 1980. Crystal chemistry of pyroxenes. *Reviews in Mineralogy* 7.) Centering of the cell is outlined by the distribution of shaded units in the structure. Rotation and screw axes parallel to *b* are noted, as are glide planes (marked *g*). (e) The location of vertical glide planes, with a *c*/2 component, in an idealized tetrahedral pyroxene chain. (f) A sketch of the centered, monoclinic lattice, as based on the structural information of parts (d) and (e). For simplicity, only some of the rotation axes, screw axes, and glide planes are shown. (g) An illustration of the *C*/2*c* space group of diopside.

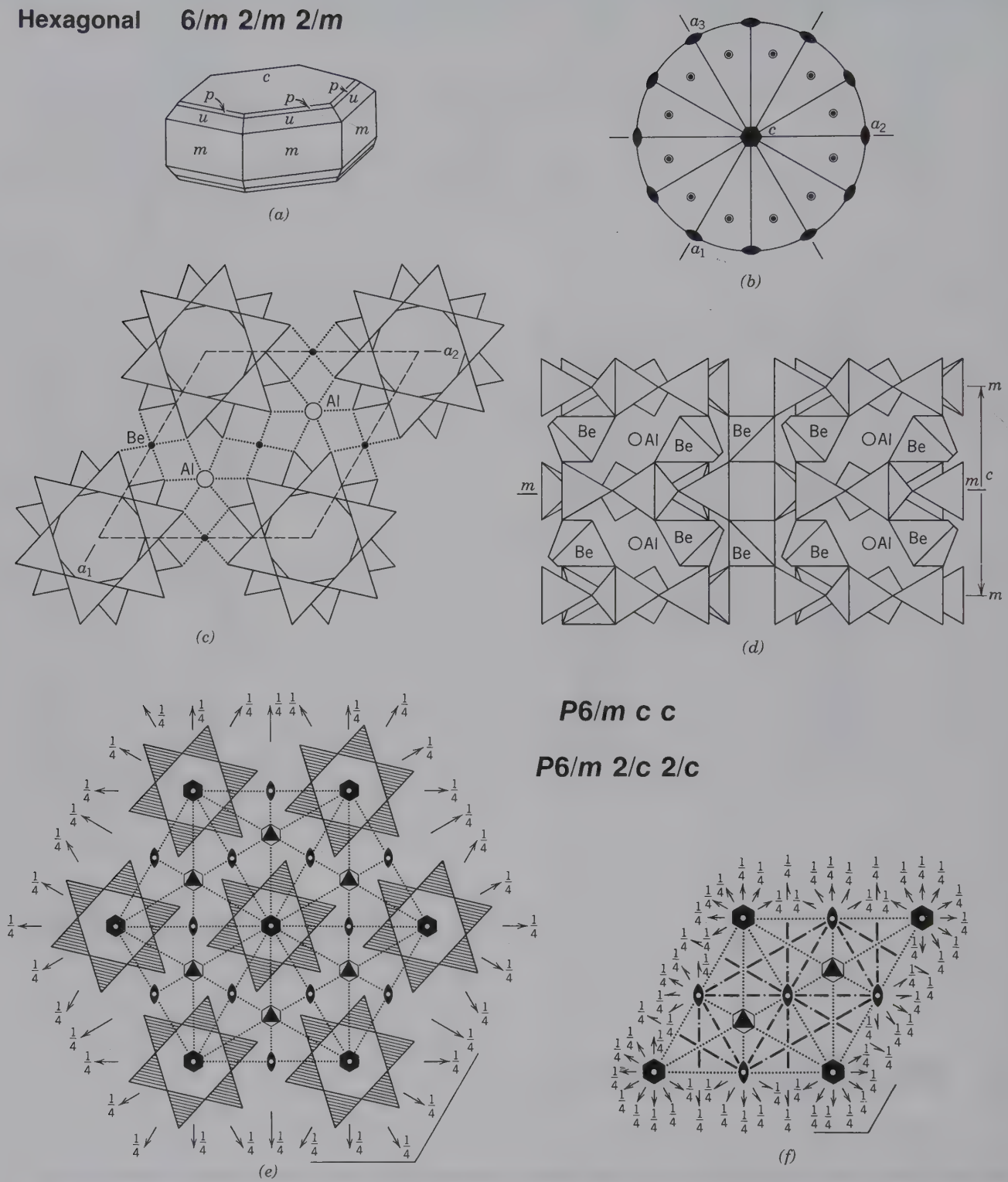

FIG. A4.2 Relationship of point group symmetry to space group representation for the mineral beryl. (a) A beryl crystal flattened on (0001), typical of cesium-rich beryl. (b) A stereogram of the point group symmetry 6/*m*2/*m*2/*m* as reflected by the morphology. (c) The structure of beryl as projected onto (0001). A unit cell is shown by dashed lines. (d) A vertical section through the beryl structure. (e) A projection of some of the structural elements of beryl and their relationships to each other as shown by the presence of some of the symmetry elements. (From Shubnikov, A. V., and V. A. Koptsik. 1974. *Symmetry in science and art*. Plenum Press, New York.) (f) The conventional representation of the space group *P*6/*m*2/*c*2/*c*, which is compatible with the beryl structure.

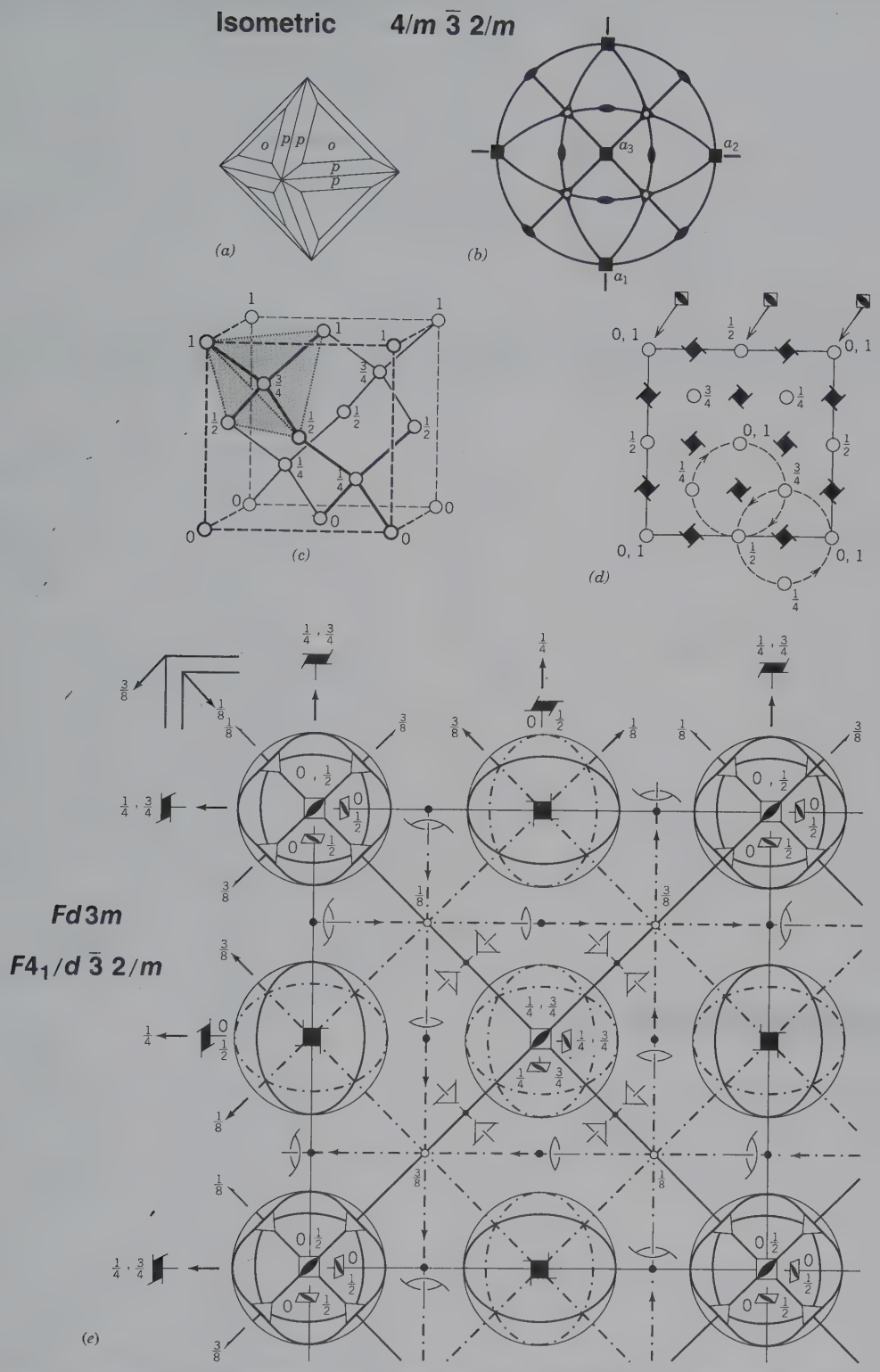

FIG. A4.3 Relationship of point group symmetry to space group representation for diamond. (a) A diamond crystal showing an octahedron (*o*) modified by a trisoctahedron (*p*). (b) A stereogram of the point group symmetry 4/*m* $\bar{3}$ 2/*m* compatible with the morphology shown in (a). (c) A sketch of a unit cell of the diamond structure. (d) A projection of the diamond structure in (c) onto a horizontal cube face. The carbon atoms are related to each other by four-fold screw axes of opposite hand (4_1 and 4_3). Four-fold rotoinversion axes are coincident with the positions of each of the carbon atoms. Only three are shown by the graphical symbol (◥) so as not to clutter the diagram. (e) The conventional representation of the space group $F4_1/d\bar{3}2/m$, which is compatible with the diamond structure. (From *International Tables for Crystallography.* 1983. vol. A.)

the positions for possible lattice nodes, the rhombus shape of the lattice becomes obvious (a primitive hexagonal lattice choice, as in *P* of the space group symbol). The six-fold symmetry about the centers of the rings is also apparent. In a vertical cross section of the structure (Fig. A4.2d), the location of horizontal mirrors through the centers of the rings is clear (the hexagonal outline of, and horizontal mirrors through, these rings account for 6/*m* in the space group symbol). Be and Al provide cross-links between the Si_6O_{18} rings; Be is in tetrahedral (four-fold) coordination and Al in octahedral (six-fold) coordination. The Be ions occupy positions where three directions of two-fold rotation axes intersect (222) and the Al ions occupy locations where vertical three-fold axes intersect with horizontal two-fold axes (32). These symmetry locations are superimposed on the horizontal section through the beryl structure in Fig. A4.2e. (For reasons of clarity not all possible symmetry elements have been shown in this representation.) The location of the horizontal mirror (perpendicular to the *c* axis) is indicated by the 120° bracket at the bottom right of the figure. The many horizontal two-fold rotation axes are located at +1/4*c*. The six-fold rings above and below are not equivalent in orientation (Fig. A4.2d) because they are rotated by 30° with respect to each other. These rotations between interleaved rings (along the *c* direction) are the result of reflections by vertical glide planes (marked as *c*s in the space group symbol). The resulting conventional representation of the space group, *P6/mcc*, which reflects the beryl structure, is shown in Fig. A4.2f. The rhombus reflects the shape that results when the centers of four hexagonal rings are connected (Fig. A4.2c).

DIAMOND (ISOMETRIC EXAMPLE)

The last illustration correlating point group, space group, and internal structure is that of the mineral diamond, C. Diamonds crystallize in the most symmetric point group ($4/m\bar{3}2/m$) of the isometric system, and crystals are usually octahedral (Fig. A4.3a) but may be cubic or dodecahedral. The structure of diamond consists of carbon atoms in tetrahedral coordination with four nearest carbon neighbors (see the upper-left part of the unit cell of Fig. A4.3c). The unit cell of diamond is based on a cubic lattice (Fig. A4.3c). A close look at the distribution of carbon atoms in the unit cell reveals that each of the faces of the cube contains one carbon atom at its center (in addition to carbon atoms at all the corners). This "all-face-centered" distribution of nodes in the lattice is reflected in *F* of the space group notation. When this same unit cell is projected onto a horizontal cube face at the bottom of the unit cell, the drawing in Fig. A4.3d results. This projection reveals the presence, at positions halfway between the carbon atoms (or projected carbon atoms) of 2 types of four-fold screw axes. These two enantiomorphic screw-axis types (4_1 and 4_3) are located in alternate rows and are parallel to the four-fold rotation axes in the point group notation. The helical paths for two of the screw rotations are shown by a sequence of increasing fractions. The symmetry about each of the carbon atoms is $\bar{4}\,3m$, because of tetrahedral coordination. A projection of the symmetry elements in the space group of diamond is shown in Fig. A4.3e. In addition to the 4_1 and 4_3 axes, there are four-fold rotoinversion axes (◪) interspaced with the screw rotations. Centers of symmetry (small circles with fractions, such as 1/8 and 3/8) are given. Diamond glide planes (*d*) (shown by dot-dash lines with arrows) are parallel to the cube faces of the unit cell. These planes are inclined to the plane of the figure because they have translation components of the type *b*/4 + *c*/4, *a*/4 + *c*/4. Vertical mirror planes (and interleaved glide planes) occur in diagonal directions.

MINERAL INDEX

In this index, the mineral name is followed by the commonly sought information: composition, crystal system (Xl Sys.), specific gravity (**G**), hardness (**H**), and index of refraction (n). For uniaxial crystals $n = \omega$, for biaxial crystals $n = \beta$. The refractive index is given as a single entry when the range is usually no greater than ± 0.01. Remarks include cleavage (Cl), and useful properties. Mineral names in boldface (e.g., **Arsenopyrite**) represent species for which complete descriptions are given in the chapters on systematic mineralogy (Chapters 15 to 19), those in lightface (e.g., Arfvedsonite) refer to minerals that are briefly treated or only mentioned in the text.

Name, Page	Composition	Xl Sys.	G	H	n	Remarks
A						
Acadialite, 549	.....					See chabazite
Acanthite, 351	Ag_2S	Mon / Iso	7.3	$2-2\frac{1}{2}$	—	Low temp. Ag_2S
Achroite, 503	.....					Colorless tourmaline
Acmite, 510	.....					See aegirine
Actinolite, 515	$Ca_2(Mg,Fe)_5Si_8O_{22}(OH)_2$	Mon	3.1–3.3	5–6	1.64	Green amphibole
Adularia, 540	$KAlSi_3O_8$	Mon	.....			Colorless, translucent K-feldspar
Aegirine, 510	$NaFe^{3+}Si_2O_6$	Mon	3.5	$6-6\frac{1}{2}$	1.82	Na-pyroxene
Aegirine-augite, 509	$(Na,Ca)(Fe^{3+},Fe^{2+},Mg,Al)$-$Si_2O_6$	Mon	3.4–3.5	6	1.71–1.78	Pyroxene, in acicular crystals
Aenigmatite, 497	$Na_2Fe_5^{2+}TiO_2(Si_2O_6)_3$	Tric	3.75	$5\frac{1}{2}$	1.80	In prismatic crystals, black
Agalmatolite, 525	.....					Compact talc substitute for gem jade
Agate, 536	.....					Concentric layers of chalcedony
Alabandite, 356, 382	MnS	Iso	4.0	$3\frac{1}{2}-4$	—	Black
Alabaster, 423	.....					See gypsum
Albite, 542	$NaAlSi_3O_8(An_0$-$An_{10})$	Tric	2.62	6	1.53	Na end-member of plagioclase
Alexandrite, 388	.....					Gem chrysoberyl
Alkali feldspar, 539	.....					Na- or K-feldspar
Allanite, 500	$(Ca,Ce)_3(Fe^{2+},Fe^{3+})Al_2O$-$(SiO_4)(Si_2O_7)(OH)$	Mon	3.5–4.2	$5\frac{1}{2}-6$	1.70–1.81	Brown-black, pitchy luster
Almandine, 489	$Fe_3Al_2Si_3O_{12}$	Iso	4.32	7	1.83	A garnet, red-purple
Altaite, 356	PbTe	Iso	8.16	3	—	Tin-white
Alumstone, 425	.....					See alunite
Alunite, 425	$KAl_3(SO_4)_2(OH)_6$	Hex	2.6–2.8	4	1.57	Usually massive
Amalgam, 343	Ag-Hg	.....				See silver
Amazonite, 539	.....					Green microcline
Amblygonite, 431	$LiAlFPO_4$	Tric	3.0–3.1	6	1.60	Cleavable masses
Amethyst, 535	SiO_2	.....				Purple quartz
Amosite, 515	.....					Asbestiform cummingtonite; "brown asbestos"
Amphibole, 514	.....					A mineral group
Analcime, 548	$NaAlSi_2O_6{\cdot}H_2O$	Iso	2.27	$5-5\frac{1}{2}$	1.48–1.49	Usually in trapezohedrons
Anatase, 380	TiO_2	Tet	3.9	$5\frac{1}{2}-6$	2.6	Adamantine luster
Anauxite, 522	.....	Mon	2.6	2	1.56	Si-rich kaolinite
Andalusite, 492	Al_2SiO_5	Orth	3.16–3.20	$7\frac{1}{2}$	1.64	Square cross sections

Name, Page	Composition	Xl Sys.	G	H	*n*	Remarks
Andesine, 544	$Ab_{70}An_{30}$-$Ab_{50}An_{50}$	Tric	2.69	6	1.55	Plagioclase feldspar
Andradite, 489	$Ca_3Fe_2Si_3O_{12}$	Iso	3.86	7	1.89	A garnet
Anglesite, 421	$PbSO_4$	Orth	6.2–6.4	3	1.88	Cl{001} {210}
Anhydrite, 422	$CaSO_4$	Orth	2.89–2.98	$3–3\frac{1}{2}$	1.58	Cl{010} {100} {001}
Ankerite, 413	$CaFe(CO_3)_2$	Hex	2.95–3	$3\frac{1}{2}$	1.70–1.75	Cl{10$\bar{1}$1}
Annabergite, 431	$Ni_3(AsO_4)_2{\cdot}8H_2O$	Mon	3.0	$2\frac{1}{2}–3$	1.68	Nickel bloom; green
Anorthite, 542	$CaAl_2Si_2O_8$(An_{90}-An_{100})	Tric	2.76	6	1.58	Ca end-member of plagioclase
Anorthoclase, 541	$(K,Na)AlSi_3O_8$	Tric	2.58	6	1.53	An alkali feldspar between K-spar and Ab
Anthophyllite, 514	$Mg_7Si_8O_{22}(OH)_2$	Orth	2.85–3.2	$5\frac{1}{2}–6$	1.61–1.71	An amphibole
Antigorite, 519	$Mg_3Si_2O_5(OH)_4$	Mon	2.5–2.6	~4	1.55	Platy serpentine
Antimony, 335	Sb	Hex	6.7	3	—	Cl{0001}
Antlerite, 424	$Cu_3SO_4(OH)_4$	Orth	3.9±	$3\frac{1}{2}–4$	1.74	Green
Apatite, 428	$Ca_5(PO_4)_3(F,Cl,OH)$	Hex	3.15–3.20	5	1.63	Cl{0001} poor
Apophyllite, 532	$KCa_4(Si_4O_{10})_2F{\cdot}8H_2O$	Tet	2.3–2.4	$4\frac{1}{2}–5$	1.54	Cl{001}
Aquamarine, 502	.....					Greenish-blue gem beryl
Aragonite, 411	$CaCO_3$	Orth	2.95	$3\frac{1}{2}–4$	1.68	Cl{010} {110}
Arfvedsonite, 519	$Na_3Fe_4^{2+}Fe^{3+}Si_8O_{22}(OH)_2$	Mon	3.45	6	1.69	Deep green amphibole
Argentite, 351	Ag_2S	.....				Now known as acanthite
Arsenopyrite, 366	FeAsS	Mon	6.07	$5\frac{1}{2}–6$	—	Pseudo-orthorhombic
Asbestos, 519, 520	.....					See amphibole and serpentine
Astrophyllite, 497	$(K,Na)_3(Fe,Mn)_7(Ti,Zr)_2$-$Si_8(O,OH)_{31}$	Tric	3.35	3	1.71	Micaceous cleavage
Atacamite, 397	$Cu_2Cl(OH)_3$	Orth	3.75–3.77	$3–3\frac{1}{2}$	1.86	Green, Cl{010}
Augite, 508	$(Ca,Na)(Mg,Fe,Al)(Si,Al)_2O_6$	Mon	3.2–3.4	5–6	1.67–1.73	Dark green to black pyroxene
Aurichalcite, 416	$(Zn,Cu)_5(CO_3)_2(OH)_3$	Orth	3.64	2	1.74	Green to blue
Autunite, 432	$Ca(UO_2)_2(PO_4)_2{\cdot}10–12\ H_2O$	Tet	3.1–3.2	$2–2\frac{1}{2}$	1.58	Yellow-green
Aventurine, 536, 544	.....					Quartz or oligoclase
Axinite, 502	$(Ca,Fe,Mn)_3Al_2BSi_4O_{15}(OH)$	Tric	3.27–3.35	$6\frac{1}{2}–7$	1.69	Crystal angles acute
Azurite, 416	$Cu_3(CO_3)_2(OH)_2$	Mon	3.77	$3\frac{1}{2}–4$	1.76	Always blue

B

Balas ruby, 385	.....					Red gem spinel
Barite, 420	$BaSO_4$	Orth	4.5	$3–3\frac{1}{2}$	1.64	Cl{001} {210}
Bauxite, 392	mixture of diaspore, gibbsite, boehmite	—	2.0–2.55	1–3	—	An earthy rock
Beidellite, 524	$(Ca,Na)_{0.3}Al_2(OH)_2$-$(Al,Si)_4O_{10}{\cdot}4H_2O$	Mon	2–3	1–2	—	Member of montmorillonite group
Benitoite, 497	$BaTiSi_3O_9$	Hex	3.6	$6\frac{1}{2}$	1.76	Blue
Bentonite, 524	.....					Montmorillonite alteration of volcanic ash
Beryl, 502, 558, 569	$Be_3Al_2(Si_6O_{18})$	Hex	2.65–2.8	$7\frac{1}{2}–8$	1.57–1.61	Usually green
Beryllonite, 431	$NaBePO_4$	Mon	2.81	$5\frac{1}{2}$	1.56	Rare gem mineral
Biotite, 528	$K(Mg,Fe)_3(AlSi_3O_{10})(OH)_2$	Mon	2.8–3.2	$2\frac{1}{2}–3$	1.61–1.70	Black mica
Bismuthinite, 363	Bi_2S_3	Orth	6.78 ± 0.03	2	—	Cl{010}
Black-band ore, 409	.....					See siderite
Black jack, 356	.....					See sphalerite
Bloodstone, 536	.....					Green and red chalcedony
Boehmite, 391, 392	$\gamma AlO(OH)$	Orth	3.01–3.06	$3\frac{1}{2}–4$	1.65	In bauxite
Bog-iron ore, 392	.....					See limonite
Boracite, 419	$Mg_3ClB_7O_{13}$	Orth	2.9–3.0	7	1.66	Pseudoisometric
Borax, 417	$Na_2B_4O_5(OH)_4{\cdot}8H_2O$	Mon	1.7±	$2–2\frac{1}{2}$	1.47	Cl{100}
Bornite, 351	Cu_5FeS_4	Tet	5.06–5.08	3	—	Purple-blue tarnish
Bort, 346	C	Iso so	3.5	10	2.4	Variety of diamond

Name, Page	Composition	Xl Sys.	G	H	*n*	Remarks
Bowenite, 521	.....					Yellow-green variety of serpentine; substitute for jade
Bravoite, 363	$(Ni,Fe)S_2$	Iso	4.66	$5\frac{1}{2}-6$	—	Steel-gray
Brazilianite, 431	$NaAl_3(PO_4)_2(OH)_4$	Mon	2.98	$5\frac{1}{2}$	1.61	Yellow-green gem mineral
Breithauptite, 358	NiSb	Hex	8.23	$5\frac{1}{2}$	—	Copper-red
Brittle mica, 529	.....					A type of mica
Brochantite, 424	$Cu_4SO_4(OH)_6$	Mon	3.9	$3\frac{1}{2}-4$	1.78	Cl{010}; green
Bromargyrite, 395	AgBr	Iso	5.9	$1-1\frac{1}{2}$	2.25	Sectile
Bronzite, 505	$(Mg,Fe)SiO_3$	Orth	3.3±	$5\frac{1}{2}$	1.68	Member of orthopyroxene series
Brookite, 380	TiO_2	Orth	3.9–4.1	$5\frac{1}{2}-6$	2.6	Adamantine luster
Brucite, 390	$Mg(OH)_2$	Hex	2.39	$2\frac{1}{2}$	1.57	Cl{0001}
Bustamite, 513	$(Mn,Ca,Fe)SiO_3$	Tric	3.3–3.4	$5\frac{1}{2}-6\frac{1}{2}$	1.67–1.70	Pink to brownish pyroxenoid
Bytownite, 544	$Ab_{10}An_{90}$	Tric	2.74	6	1.57	Plagioclase feldspar
C						
Cairngorm Stone, 535	SiO_2	.....				Smoky quartz
Calamine, 411	.....					See smithsonite, hemimorphite
Calaverite, 343	$AuTe_2$	Mon	9.35	$2\frac{1}{2}$		Rare gold ore
Calcite, 407	$CaCO_3$	Hex	2.71	3	1.66	Cl{10$\bar{1}$1}
Californite, 501	.....					See vesuvianite; used as gem substitute for jade
Cancrinite, 546	$Na_6Ca(CO_3)(AlSiO_4)_6{\cdot}2H_2O$	Hex	2.45	5–6	1.52	Feldspathoid
Carbonado, 346	C	Iso	3.5	10	2.4	Black, cryptocrystalline diamond
Carbonate-apatite, 428	$Ca_5F(CO_3,PO_4,OH)_3$	.....				See apatite
Carnallite, 395	$KMgCl_3{\cdot}6H_2O$	Orth	1.6	1	1.48	Deliquescent
Carnelian, 536	.....					Red chalcedony
Carnotite, 433	$K_2(UO_2)_2(VO_4)_2{\cdot}3H_2O$	Mon	4.7–5	Soft	1.93	Yellow
Cassiterite, 382	SnO_2	Tet	6.8–7.1	6–7	2.00	Luster adamantine
Cat's eye, 535	.....					See chrysoberyl and quartz
Celestite, 421	$SrSO_4$	Orth	3.95–3.97	$3-3\frac{1}{2}$	1.62	Cl{001} {210}
Celsian, 470	$BaAl_2Si_2O_8$	Mon	3.37	6	1.59	Ba-feldspar
Cerargyrite, 395	.....					See chlorargyrite
Cerianite, 384	$(Ce,Th)O_2$	Iso	.....	.....	>2.0	Very rare
Cerussite, 413	$PbCO_3$	Orth	6.55	$3-3\frac{1}{2}$	2.08	Efferv. in HNO_3
Chabazite, 549	$Ca_2Al_2Si_4O_{12}{\cdot}6H_2O$	Hex	2.05–2.15	4–5	1.48	Cubelike crystals
Chalcanthite, 424	$CuSO_4{\cdot}5H_2O$	Tric	2.12–2.30	$2\frac{1}{2}$	1.54	Soluble in water
Chalcedony, 536	.....					Microcryst. quartz
Chalcocite, 351	Cu_2S	Mon / Hex	5.5–5.8	$2\frac{1}{2}-3$	—	Imperfectly sectile
Chalcopyrite, 356	$CuFeS_2$	Tet	4.1–4.3	$3\frac{1}{2}-4$	—	Brittle, yellow
Chalcosiderite, 432	$CuFe_6(PO_4)_4(OH)_8{\cdot}4H_2O$	Tric	3.22	$4\frac{1}{2}$	1.84	Light green
Chalcotrichite, 375	.....					Fibrous cuprite
Chalk, 407	.....					See calcite
Chalybite, 409	.....					See siderite
Chamosite, 532	$(Fe^{2+},Al,Mg)_6(Si,Al)_4O_{10}(OH)_8$ $(Si_3Al)O_{10}(OH,O)_8$	Mon	—	2–3	1.60	See chlorite group
Chert, 536	SiO_2	—	2.65	7	1.54	Microcryst. quartz
Chesterite, 455	$(Mg,Fe)_{17}Si_{20}O_{54}(OH)_6$	Orth	.....			Microscopic alteration of anthophyllite; a "biopyribole"
Chiastolite, 492	.....					Variety of andalusite
Chloanthite, 366	$(Ni,Co)As_{3-x}$	Iso	6.5	$5\frac{1}{2}-6$		Arsenic-deficient variety of Ni-skutterudite

Name, Page	Composition	Xl Sys.	G	H	*n*	Remarks
Chlorapatite, 428	$Ca_5(PO_4)_3Cl$	.....				See apatite
Chlorargyrite, 395	AgCl	Iso	5.5±	2–3	2.07	Perfectly sectile
Chlorite, 531	$(Mg,Fe)_3(Si,Al)_4O_{10}$-$(OH)_2$·$(Mg,Fe)_3(OH)_6$	Mon Tric	2.6–3.3	$2-2\frac{1}{2}$	1.57–1.67	Green, Cl{001}
Chloritoid, 497	$(Fe,Mg)_2Al_4O_2(SiO_4)_2(OH)_4$	Mon Tric	3.5–3.8	$6\frac{1}{2}$	1.72–1.73	Appears similar to chlorite
Chondrodite, 495	$Mg_5(SiO_4)_2(F,OH)_2$	Mon	3.1–3.2	$6-6\frac{1}{2}$	1.60–1.63	Yellow-red
Chromite, 388	$FeCr_2O_4$	Iso	4.6	$5\frac{1}{2}$	2.16	Luster submetallic; a spinel
Chrysoberyl, 388, 560, 570	$BeAl_2O_4$	Orth	3.65–3.8	$8\frac{1}{2}$	1.75	Crystals tabular
Chrysocolla, 533	~$Cu_4H_4Si_4O_{10}(OH)_8$·nH_2O	?	2.0–2.4	2–4	1.40±	Bluish-green
Chrysolite, 485	.....					See olivine
Chrysoprase, 536	.....					Green chalcedony
Chrysotile, 519	$Mg_3Si_2O_5(OH)_4$	Mon	2.5–2.6	4	1.55	Fibrous variety of serpentine; "white asbestos"
Cinnabar, 360	HgS	Hex	8.10	$2\frac{1}{2}$	2.81	Red
Cinnamon stone, 489	.....					See grossularite
Citrine, 535	SiO_2	.....				Yellow quartz
Clay ironstone, 409	.....					See siderite
Clay minerals, 521	.....					A mineral group
Cleavelandite, 544	.....					White, platy albite
Clinochlore, 532	.....				1.58	See chlorite
Clinoenstatite, 506	$MgSiO_3$	Mon	3.19	6	1.66	In meteorites
Clinoferrosilite, 506	$FeSiO_3$	Mon	.....			Clinopyroxene end-member
Clinohumite, 495	$Mg_9(SiO_4)(F,OH)_2$	Mon	3.1–3.2	6	1.64	See chondrodite
Clinohypersthene, 506	$(Mg,Fe)SiO_3$	Mon	3.4–3.5	5–6	1.68–1.72	In meteorites
Clinozoisite, 499	$Ca_2Al_3O(SiO_4)(Si_2O_7)(OH)$	Mon	3.35–3.37	$6-6\frac{1}{2}$	1.67–1.72	Crystals striated
Clintonite, 529	$Ca(Mg,Al)_{3-2}Al_3SiO_{10}(OH)_2$	Mon	3–3.1	$3\frac{1}{2}$	1.65	Brittle mica
Cobalt bloom, 431	$Co_3(AsO_4)_2$·$8H_2O$	.....				See erythrite
Cobaltite, 365	CoAsS	Orth	6.33	$5\frac{1}{2}$	—	In pseudoisometric pyritohedrons
Coesite, 470	SiO_2	Mon	3.01	7	1.59	High-pressure form of SiO_2
Colemanite, 419	$CaB_3O_4(OH)_3$·H_2O	Mon	2.42	$4-4\frac{1}{2}$	1.59	Cl{010} perfect
Collophane, 428	.....					See apatite
Columbite (ferro), 389	$(Fe,Mn)Nb_2O_6$	Orth	5.2–7.3	6	—	see ferrocolumbite
Common salt, 393	.....					See halite
Copper, 344	Cu	Iso	8.9	$2\frac{1}{2}-3$		Malleable
Cordierite, 503	$(Mg,Fe)_2Al_4Si_5O_{18}$·nH_2O	Orth	2.60–2.66	$7-7\frac{1}{2}$	1.53–1.57	Light bluish-gray
Corundum, 376, 559	Al_2O_3	Hex	4.02	9	1.77	Rhombohedral parting
Cotton balls, 419	.....					See ulexite
Covellite, 359	CuS	Hex	4.6–4.76	$1\frac{1}{2}-2$	—	Blue
Cristobalite, 538	SiO_2	Tet Iso	2.32	$6\frac{1}{2}$	1.48	In volcanic rocks
Crocidolite, 519	$NaFe_3^{2+}Fe_2^{3+}Si_8O_{22}(OH)_2$	Mon	3.2–3.3	4	1.70	Blue amphibole asbestos
Crocoite, 422	$PbCrO_4$	Mon	5.9–6.1	$2\frac{1}{2}-3$	2.36	Orange-red
Crossite, 519	.....					Amphibole between glaucophane and riebeckite
Cryolite, 395	Na_3AlF_6	Mon	2.95–3.0	$2\frac{1}{2}$	1.34	White
Cryptomelane, 391	KMn_8O_{16}	.....				See romanechite
Cryptoperthite, 475	.....					Extremely fine-grained intergrowth of K- and Na-feldspar
Cummingtonite, 517	$(Mg,Fe)_7Si_8O_{22}(OH)_2$	Mon	3.1–3.3	$5\frac{1}{2}-6$	1.66–1.68	Light beige, needlelike amphibole
Cuprite, 375	Cu_2O	Iso	6.1	$3\frac{1}{2}-4$	—	Ruby-red in transparent crystals
Cymophane, 388	.....					Chatoyant chrysoberyl

Name, Page	Composition	Xl Sys.	G	H	*n*	Remarks
D						
Danburite, 494	$Ca(B_2Si_2O_8)$	Orth	2.97–3.02	7	1.63	In crystals
Datolite, 496	$CaB(SiO_4)(OH)$	Mon	2.8–3.0	$5–5\frac{1}{2}$	1.65	Usually in crystals
Demantoid, 490	.....					Green andradite garnet
Diallage, 508	.....					Variety of diopside
Diamond, 346, 557, 570	C	Iso	3.51	10	2.42	Adamantine luster
Diaspore, 391, 392	$\alpha AlO(OH)$	Orth	3.35–3.45	$6\frac{1}{2}–7$	1.72	Cl{010} perfect
Diatomaceous earth, 538	.....					See opal
Diatomite, 539	.....					See opal
Dichroite, 503	.....					See cordierite
Dickite, 524	$Al_2Si_2O_5(OH)_4$	Mon	2.6	$2–2\frac{1}{2}$	1.56	Clay mineral
Digenite, 351	Cu_9S_5	Iso	5.6	$2\frac{1}{2}–3$	—	Similar to chalcocite
Diopside, 508	$CaMgSi_2O_6$	Mon	3.2	5–6	1.67	White to light green pyroxene
Dioptase, 534	$Cu_6(Si_6O_{18})\cdot 6H_2O$	Hex	3.3	5	1.65	Green; minor gem
Djurleite, 351	$Cu_{31}S_6$	Mon	5.75	2.5–3	—	Black; dark gray
Dolomite, 413	$CaMg(CO_3)_2$	Hex	2.85	$3\frac{1}{2}–4$	1.68	Cl{10$\bar{1}$1}
Dravite, 504	.....					Na,Mg,Al-tourmaline
Dry-bone ore, 411	.....					See smithsonite
Dumortierite, 492	$Al_7O_3(BO_3)(SiO_4)_3$	Orth	3.26–3.36	7	1.69	Radiating
E						
Edenite, 517	$NaCa_2Mg_5AlSi_7O_{22}(OH)_2$	Mon	3.0	6	1.63	See hornblende
Elbaite, 503	.....					Na,Li,Al-tourmaline
Electrum, 341	.....					See gold
Emerald, 502	.....					Deep green gem beryl
Emery, 377	.....					Corundum with magnetite
Enargite, 366	Cu_3AsS_4	Orth	4.45	3	—	Cl{110}
Endlichite, 430	.....					See vanadinite
Enstatite, 505	$MgSiO_3$	Orth	3.2–3.5	$5\frac{1}{2}$	1.65	Cl{210} ~ 90°
Epidote, 499	$Ca_2(Al,Fe)Al_2O(SiO_4)$-$(Si_2O_7)(OH)$	Mon	3.35–3.45	6–7	1.72–1.78	Cl{001}, {100}, green
Epsomite, 424	$MgSO_4\cdot 7H_2O$	Orth	1.75	$2–2\frac{1}{2}$	1.46	Bitter taste
Epsom salt, 424	.....					See epsomite
Erythrite, 431	$Co_3(AsO_4)_2\cdot 8H_2O$	Mon	3.06	$1\frac{1}{2}–2\frac{1}{2}$	1.66	Pink; cobalt bloom
Essonite, 489	.....					See grossular; garnet
Euclase, 503	$BeAl(SiO_4)(OH)$	Mon	3.1	$7\frac{1}{2}$	1.66	Cl{010}
Eucryptite, 511	$LiAlSiO_4$	Hex	2.67	—	1.55	Spodumene alteration
F						
Fairy stone, 494	.....					See staurolite
Famatinite, 367	Cu_3SbS_4	Tet	4.52	$3\frac{1}{2}$	—	Gray
Fayalite, 485	Fe_2SiO_4	Orth	4.39	$6\frac{1}{2}$	1.86	Olivine, Fe end-member
Feldspar, 539	.....					A mineral group
Feldspathoid, 544	.....					A mineral group
Ferberite, 425	$FeWO_4$	Mon	7.0–7.5	5	—	See wolframite
Fergusonite, 390	$(Y,Er,Ce,Fe)NbO_4$	Tet	5.8	$5\frac{1}{2}–6$	—	Brown-black
Ferrimolybdite, 365	$Fe_2(MoO_4)_3\cdot 8H_2O$	Orth?	2.99	~1	1.73–1.79	Canary-yellow, soft
Ferroactinolite, 516	$Ca_2Fe_5Si_8O_{22}(OH)_2$	Mon	3.2–3.3	5–6	1.68	Dark green amphibole
Ferrocolumbite, 389, 390	$(Fe,Mn)N6_2O_6$	Orth	5.2–7.3	6	—	Iron-black; submetallic
Ferropseudobrookite, 379	$FeTi_2O_5$	.....				See ilmenite
Ferrosilite, 505	$FeSiO_3$	Orth	3.9	6	1.79	Orthopyroxene end-member
Ferrotantalite, 389, 390	$(Fe,Mn)Ta_2O_6$	Orth	±6.5	6	—	Iron-black; submetallic
Fersmannite, 497	$Na_4Ca_4Ti_4(SiO_4)_3(O,OH,F)_3$	Mon	3.44	$5\frac{1}{2}$	1.93	Brown; rare; in alkalic rocks
Fibrolite, 492	.....					See sillimanite
Fischesserite, 343	Ag_3AuSe_2	.....				Rare gold ore
Flint, 536	SiO_2	—	2.65	7	1.54	Microcryst. quartz

Name, Page	Composition	Xl Sys.	G	H	*n*	Remarks
Flos ferri, 411	.....					See aragonite
Fluorapatite, 428	$Ca_5(PO_4)_3F$	.....				See apatite
Fluorite, 396	CaF_2	Iso	3.18	4	1.43	Cl octahedral
Forsterite, 485	Mg_2SiO_4	Orth	3.2	$6\frac{1}{2}$	1.63	Olivine; Mg end-member
Fowlerite, 512	.....					Zn-bearing rhodonite
Franklinite, 387	$(Zn,Fe,Mn)(Fe,Mn)_2O_4$	Iso	5.15	6	—	Spinel from Franklin, NJ
Freibergite, 367	.....					Ag-bearing tetrahedrite
Fuchsite, 525	.....					Chrome-rich muscovite
G						
Gadolinite, 503	$YFeBe_2(SiO_4)_2O_2$	Mon	4.0–4.5	$6\frac{1}{2}$–7	1.79	Black
Gahnite, 385	$ZnAl_2O_4$	Iso	4.55	$7\frac{1}{2}$–8	1.80	Spinel; dark green octahedrons
Galaxite, 385	$MnAl_2O_4$	Iso	4.03	$7\frac{1}{2}$–8	1.92	Mn spinel
Galena, 353	PbS	Iso	7.4–7.6	$2\frac{1}{2}$	—	Cl cubic
Garnet, 487, 561, 572	$A_3B_2(SiO_4)_3$	Iso	3.5–4.3	$6\frac{1}{2}$–$7\frac{1}{2}$	1.71–1.88	A mineral group; commonly in crystals
Garnierite, 521	$(Ni,Mg)_3Si_2O_5(OH)_4$	Mon	2.2–2.8	2–3	1.59	Green Ni serpentine
Gaylussite, 416	$Na_2Ca(CO_3)_2{\cdot}5H_2O$	Mon	1.99	2–3	1.52	Cl{110} perfect
Gedrite, 514	$\sim Na_{0.5}(Mg,Fe)_2(Mg,Fe)_{3.5}$-$(Al,Fe^{3+})_{1.5}Si_6Al_2O_{22}(OH)_2$	Orth	.....			See anthophyllite
Geikielite, 379	$MgTiO_3$	Hex	4.05	$5\frac{1}{2}$–6	—	Cl{$10\bar{1}1$}
Gersdorffite, 365	NiAsS	Iso	5.9	$5\frac{1}{2}$	—	See cobaltite
Geyserite, 539	.....					Opal in hot springs
Gibbsite, 390, 392	$Al(OH)_3$	Mon	2.3–2.4	$2\frac{1}{2}$–$3\frac{1}{2}$	1.57	Basal Cl{001}
Glaucodot, 366	(Co,Fe)AsS	Orth	6.04	5	—	Tin-white
Glauconite, 529	$(K,Na,Ca)_{0.5-1}(Fe^{3+},Al,$-$Fe^{2+},Mg)_2(Si,Al)_4O_{10}(OH)_2{\cdot}nH_2O$	Mon	2.4±	2	1.62	In green sands
Glaucophane, 518	$Na_2Mg_3Al_2Si_8O_{22}(OH)_2$	Mon	3.1–3.3	6–$6\frac{1}{2}$	1.62–1.67	Blue to black amphibole
Gmelinite-Na, 552	$Na_{7.5}(Al_{7.5}Si_{16.5}O_{48}){\cdot}21.5H_2O$	Hex	2.1±	$4\frac{1}{2}$	1.49	A zeolite
Goethite, 391	$\alpha FeO(OH)$	Orth	4.37	5–$5\frac{1}{2}$	2.39	Cl{010} perfect
Gold, 341	Au	Iso	15–19.3	$2\frac{1}{2}$–3	—	Yellow, soft
Goshenite, 502	.....					Colorless gem beryl
Graphite, 350	C	Hex	2.23	1–2	—	Black, platy
Greenalite, 521	$Fe_3Si_2O_5(OH)_4$	Mon	3.2	—	1.67	In iron-formations
Greenockite, 356	CdS	Hex	4.9	3–$3\frac{1}{2}$	—	Yellow-orange
Grossular, 489	$Ca_3Al_2Si_3O_{12}$	Iso	3.59	$6\frac{1}{2}$	1.73	A garnet
Grunerite, 514	$Fe_7Si_8O_{22}(OH)_2$	Mon	3.6	6	1.71	Light brown, needlelike amphibole
Gypsum, 423	$CaSO_4{\cdot}2H_2O$	Mon	2.32	2	1.52	Cl{010} {100} {011}
H						
Halite, 393	NaCl	Iso	2.16	$2\frac{1}{2}$	1.54	Cl cubic; salty
Halloysite, 524	$Al_2Si_2O_5(OH)_4$ and $Al_2Si_2O_5(OH)_4{\cdot}2H_2O$	Mon	2.0–2.2	1–2	1.54	Clay mineral
Harmotome, 552	$Ba_2(Na,K,Ca_{0.5})(Al_5Si_{11}O_{32}){\cdot}12H_2O$	Mon	2.45	$4\frac{1}{2}$	1.51	A zeolite
Hastingsite, 517	$NaCa_2Fe_4(Al,Fe)Al_2Si_6$-$O_{22}(OH)_2$	Mon	3.2	6	1.66	See hornblende
Haüyne, 546	$(Na_6,Ca_2)(AlSiO_4)_6(SO_4)_2$	Iso	2.4–2.5	$5\frac{1}{2}$–6	1.50	A feldspathoid
Hectorite, 524	$(Mg,Li)_3Si_4O_{10}(OH)_2Na_{0.3}{\cdot}4H_2O$	Mon	2.5	1–$1\frac{1}{2}$	1.52	Li montmorillonite
Hedenbergite, 508	$CaFeSi_2O_6$	Mon	3.55	5–6	1.73	Clinopyroxene end-member
Helidor, 502	.....					Golden beryl
Heliotrope, 536	.....					Green and red chalcedony
Hematite, 377	Fe_2O_3	Hex	5.26	$5\frac{1}{2}$–$6\frac{1}{2}$	—	Red streak
Hemimorphite, 498	$Zn_4(Si_2O_7)(OH)_2{\cdot}H_2O$	Orth	3.4–3.5	$4\frac{1}{2}$–5	1.62	Cl{110}
Hercynite, 385	$FeAl_2O_4$	Iso	4.39	$7\frac{1}{2}$–8	1.80	Fe spinel
Heulandite-Ca, 551	$(Ca_{0.5},Na,K)_9(Al_9Si_{27}O_{72}){\cdot}\sim 24H_2O$	Mon	2.18–2.20	$3\frac{1}{2}$–4	1.48	Cl{010} perfect
Hiddenite, 510	.....					Green gem spodumene

Name, Page	Composition	Xl Sys.	G	H	*n*	Remarks
Hollandite, 391	$Ba_2Mn_8O_{16}$	Tet / Mon	4.9	6	—	Silver-gray to black
Holmquistite, 453	$Li_2(Mg,Fe)_3(Al,Fe^{3+})_2Si_8O_{22}(OH)_2$	Orth	3.06–3.13	5–6	1.64–1.66	Blue to violet-blue; near Li-pegmatites
Hornblende, 517	$(Ca,Na)_{2-3}(Mg,Fe,Al)_5Si_6(Si,Al)_2O_{22}(OH)_2$	Mon	3.0–3.4	5–6	1.62–1.72	Green to black amphibole
Horn silver, 395	.....					See chlorargyrite
Huebnerite, 425	$MnWO_4$	Mon	7.0	5	—	See wolframite
Humite, 495	$Mg_7(SiO_4)_3(F,OH)_2$	Orth	3.1–3.2	6	1.64	See chondrodite
Hyalite, 539	.....					Colorless, globular opal
Hyalophane, 470	$(K,Ba)(Al,Si)_2Si_2O_8$	Mon	2.8	6	1.54	A feldspar
Hydroboracite, 419	$CaMgB_6O_8(OH)_6{\cdot}3H_2O$	Mon	2.17	2	1.53	Clear, colorless to white
Hydrogrossular, 488	$Ca_3Al_2Si_2O_8(SiO_4)_{1-m}(OH)_{4m}$	Iso	3.13–3.59	6–7	1.67–1.73	Hydrous garnet
Hydroxylapatite, 428	$Ca_5(PO_4)_3(OH)$		.....			See apatite
Hydrozincite, 411	$Zn_5(CO_3)_2(OH)_6$	Mon	3.6–3.8	2–$2\frac{1}{2}$	1.74	Secondary mineral
Hypersthene, 505	$(Mg,Fe)SiO_3$	Orth	3.4–3.5	5–6	1.68–1.73	An intermediate member of the orthopyroxene series

I

Iceland spar, 407	.....					See calcite
Idocrase, 500	.....					See vesuvianite
Illite, 524	.....				1.57–1.61	Mica-like clay mineral
Ilmenite, 379	$FeTiO_3$	Hex	4.7	$5\frac{1}{2}$–6	—	May be slightly magnetic
Ilvaite, 499	$CaFe_2^{2+}Fe^{3+}O(Si_2O_7)(OH)$	Orth	4.0	$5\frac{1}{2}$–6	1.91	Black
Indialite, 503	$(Mg,Fe)_2Al_4Si_5O_{18}{\cdot}nH_2O$	Hex	~2.6	7	—	High *T* form of cordierite
Indicolite, 503	.....					Blue tourmaline
Inyoite, 419	$CaB_3O_3(OH)_5{\cdot}4H_2O$	Mon	1.88	2	1.51	Colorless, transparent
Iodargyrite, 395	AgI	Hex	5.5–5.7	1–$1\frac{1}{2}$	2.18	Sectile
Iodobromite, 395	Ag(Cl,Br,I)	Iso	5.71	1–$1\frac{1}{2}$	2.20	Sectile; same as iodian bromargyrite
Iolite, 503	.....					See cordierite
Iridium, 345	Ir	Iso	22.7	6–7	—	A platinum metal
Iridosmine, 345	Ir-Os	Hex	19.3–21.1	6–7	—	See platinum
Iron, 345	Fe	Iso	7.3–7.9	$4\frac{1}{2}$	—	Very rare

J

Jacobsite, 387	$MnFe_2O_4$	Iso	5.1	$5\frac{1}{2}$–$6\frac{1}{2}$	2.3	A spinel
Jade, 509, 516, 560	.....					See nephrite and jadeite
Jadeite, 509	$NaAlSi_2O_6$	Mon	3.3–3.5	$6\frac{1}{2}$–7	1.66	Green, compact
Jargon, 490	.....					See zircon
Jarosite, 425	$KFe_3(SO_4)_2(OH)_6$	Hex	3.2±	3	1.82	Yellow-brown
Jasper, 536	.....					Red, microcryst. quartz
Jimthompsonite, 455	$(Mg,Fe)_{10}Si_{12}O_{32}(OH)_4$	Orth	.....			Microscopic alteration of anthophyllite; a "biopyribole"
Johannsenite, 453	$CaMnSi_2O_6$	Mon	3.4–3.5	6	1.71–1.73	Mn analogue of diopside

K

Kainite, 395	$KMg(Cl,SO_4){\cdot}2\frac{3}{4}H_2O$	Mon	2.1	3	1.51	Cl{001}; salty, bitter
Kalsilite, 545	$KAlSiO_4$	Hex	2.61	6	1.54	Isostructural with nepheline
Kamacite, 345	Fe-Ni	Iso	7.3–7.9	4	—	In meteorites
Kaolin, 522	.....					Mixture of clay minerals
Kaolinite, 522	$Al_2Si_2O_5(OH)_4$	Tric	2.6	2	1.55	Earthy
Keatite, 468	SiO_2	Tet	2.50	7	1.52	Synthetic
Kernite, 516	$Na_2B_4O_6(OH)_2{\cdot}3H_2O$	Mon	1.9	3	1.47	Cl{001} {100}

Name, Page	Composition	Xl Sys.	G	H	*n*	Remarks
K-feldspar, 539	.....					See microcline, orthoclase, sanidine
Kieserite, 394	$MgSO_4 \cdot H_2O$	Mon	2.57	$3\frac{1}{2}$	1.53	Massive, granular; whitish gray
Kirschteinite, 484	$CaFeSiO_4$	.....				An olivine
Kostovite, 343	$CuAuTe_4$	.....				Rare gold ore
Krennerite, 343	$AuTe_2$	Orth	8.62	2–3	—	Basal Cl{001}
Kunzite, 510	.....					Pink gem spodumene
Kutnahorite, 415	$CaMn(CO_3)_2$	Hex	3.12	$3\frac{1}{2}$–4	1.74	Mn-dolomite
Kyanite, 492	Al_2SiO_5	Tric	3.55–3.66	5–7	1.72	Blue, bladed
L						
Labradorite, 544	$Ab_{50}An_{50}$-$Ab_{30}An_{70}$	Tric	2.71	6	1.56	A member of the plagioclase feldspar series
Lamprophyllite, 497	$Na_3Sr_2Ti_3(Si_2O_7)_2(O,OH,F)_2$	Orth	3.45	4	1.75	Platy
Langbeinite, 394	$K_2Mg_2(SO_4)_3$	Iso	2.83	$3\frac{1}{2}$–4	1.53	Colorless; in evaporites
Lapis lazuli, 546	.....					See lazurite
Laumontite, 552	$Ca_4(Al_8Si_{16}O_{48}) \cdot 18H_2O$	Mon	2.28	4	1.52	A zeolite
Lawsonite, 499	$CaAl_2(Si_2O_7)(OH)_2 \cdot H_2O$	Orth	3.09	8	1.67	In gneisses and schists
Lazulite, 431	$(Mg,Fe)Al_2(PO_4)_2(OH)_2$	Mon	3.0–3.1	5–$5\frac{1}{2}$	1.64	Blue
Lazurite, 546	$(Na,Ca)_8(AlSiO_4)_6(SO_4,S,Cl,OH)_2$	Iso	2.4–2.45	5–$5\frac{1}{2}$	1.50	Blue; associated with pyrite
Lechatelierite, 538	SiO_2	Amor	2.2	6–7	1.46	Fused silica
Lepidochrosite, 392	$\gamma FeO(OH)$	Orth	4.09	5	2.2	Red
Lepidolite, 529	$K(Li,Al)_{2-3}(AlSi_3O_{10})(O,OH,F)_2$	Mon	2.8–2.9	$2\frac{1}{2}$–4	1.55–1.59	Pink, lilac, gray mica
Leucite, 544	$KAlSi_2O_6$	Tet Iso	2.47	$5\frac{1}{2}$–6	1.51	In trapezohedrons
Leucoxene, 381	.....					Brownish alteration of Ti minerals
Liddicoatite, 504	.....					See tourmaline
Ligure, 490	.....					Possible ancient name for zircon
Limonite, 392	$FeO \cdot OH \cdot nH_2O$	Amor	3.6–4.0	5–$5\frac{1}{2}$	—	Streak yellow-brown
Linnaeite, 366	Co_3S_4	Iso	4.8	$4\frac{1}{2}$–$5\frac{1}{2}$	—	Steel-gray
Litharge, 355	PbO	Tet	9.14	2	2.66	Red
Lithiophilite, 427	$Li(Mn,Fe)PO_4$	Orth	3.5	5	1.67	Cl{001} {010}
Lizardite, 519	$Mg_3Si_2O_5(OH)_4$	.....				Massive; a polymorph of serpentine
Lodestone, 386	.....					Natural magnet
Lonsdaelite, 346	C	Hex	3.3+	10	2.42	Hexagonal diamond
Luzonite, 366	Cu_3AsS_4	Tet	4.4	3–4	—	Low *T* form of enargite
M						
Maghemite, 378	γFe_2O_3	.....				Hematite dimorph
Magnesiochromite, 388	$MgCr_2O_4$	Iso	4.2	$5\frac{1}{2}$	—	A spinel
Magnesioferrite, 387	$MgFe_2O_4$	Iso	4.5–4.6	$5\frac{1}{2}$–$6\frac{1}{2}$	—	A spinel
Magnesite, 409	$MgCO_3$	Hex	3.0–3.2	$3\frac{1}{2}$–5	1.70	Commonly massive
Magnetite, 385	Fe_3O_4	Iso	5.18	6	—	Strongly magnetic; a spinel
Malachite, 415	$Cu_2(CO_3)(OH)_2$	Mon	3.9–4.03	$3\frac{1}{2}$–4	1.88	Green
Manganite, 390	$MnO(OH)$	Mon	4.3	4	—	Prismatic, pseudo-orthorhombic crystals
Manganotantalite, 389	$(Mn,Fe)Ta_2O_6$	Orth	6.6±	$4\frac{1}{2}$	—	See columbite
Manjiroite, 391	$(Na,K)Mn_8O_{16} \cdot nH_2O$	.....				See romanechite
Marcasite, 364	FeS_2	Orth	4.89	6–$6\frac{1}{2}$	—	Polymorphous with pyrite
Margarite, 529	$CaAl_2(Al_2Si_2)_{10}(OH)_2$	Mon	3.0–3.1	$3\frac{1}{2}$–5	1.65	Brittle mica
Marialite, 548	$Na_4(AlSi_3O_8)_3(Cl_2,CO_3,SO_4)$	Tet	2.60±	$5\frac{1}{2}$–6	1.55	See scapolite
Martite, 377	.....					See hematite
Meionite, 548	$Ca_4(Al_2Si_2O_8)_3(Cl_2,CO_3,SO_4)$	Tet	2.69	$5\frac{1}{2}$–6	1.59	See scapolite
Melanite, 489	$Ca_3Fe_2(SiO_4)_3$	Iso	3.7	7	1.94	Black andradite garnet

Name, Page	Composition	Xl Sys.	G	H	*n*	Remarks
Melanterite, 364, 424	$FeSO_4 \cdot 7H_2O$	Mon	1.90	2	1.48	Green-blue
Metacinnabar, 360	$Hg_{1-x}S$	Iso	7.65	3	—	Grayish-black
Mica, 525	.....					A mineral group
Microcline, 539	$KAlSi_3O_8$	Tric	2.54–2.57	6	1.53	Low *T* K-feldspar
Microlite, 390	$Ca_2Ta_2O_6(O,OH,F)$	Iso	5.48–5.56	$5\frac{1}{2}$	1.92–1.99	Streak yellow to brown
Microperthite, 474	.....					Intergrowth of K-spar and albite
Millerite, 358	NiS	Hex	5.5 ± 0.2	$3-3\frac{1}{2}$	—	Capillary crystals
Mimetite, 430	$Pb_5(AsO_4)_3Cl$	Hex	7.0–7.2	$3\frac{1}{2}$	2.1–2.2	Pale yellow, yellow-brown
Minium, 355	Pb_3O_4	?	8.9–9.2	$2\frac{1}{2}$	2.42	Earthy, brownish-red
Minnesotaite, 524	$Fe_3Si_4O_{10}(OH)_2$	Mon	3.01	1 ?	~1.60	In iron-formations
Molybdenite, 365	MoS_2	Hex	4.62–4.73	$1-1\frac{1}{2}$	—	Lead-gray, platy
Monalbite, 475	$NaAlSi_3O_8$	Mon	.....			Monoclinic, high *T* albite
Monazite, 427	$(Ce,La,Y,Th)PO_4$	Mon	4.6–5.4	$5-5\frac{1}{2}$	1.79	Parting {001}
Montebrasite, 431	$(Li,Na)Al(PO_4)(OH,F)$	Tric	~2.98	$5\frac{1}{2}-6$	1.61	See amblygonite
Montbrayite, 343	$(Au,Sb)_2Te_3$		.....			Rare gold ore
Monticellite, 484	$CaMgSiO_4$	Orth	3.2	5	1.65	An olivine
Montmorillonite, 524	$(Al,Mg)_8(Si_4O_{10})_4(OH)_8 \cdot 12H_2O$	Mon	2.5	$1-1\frac{1}{2}$	1.50–1.64	A clay mineral
Moonstone, 540	.....					See adularia, albite, and orthoclase
Morganite, 502	.....					Rose gem beryl
Moss agate, 536	.....					Agate with mosslike patterns
Mountain cork, 515	.....					Felted tremolite
Mountain leather, 515	.....					Felted tremolite
Mullite, 492	$\sim Al_6Si_3O_{15}$	Orth	3.23	6–7	1.67	Cl{010}
Muscovite, 525	$KAl_2(AlSi_3O_{10})(OH)_2$	Mon	2.76–2.88	$2-2\frac{1}{2}$	1.60	Cl{001} perfect
Muthmannite, 343	(Ag,Au)Te		.....			Rare gold ore

N

Nacrite, 524	$Al_2Si_2O_5(OH)_4$	Mon	2.6	$2-2\frac{1}{2}$	1.56	Clay mineral
Nagyagite, 343	$Pb_5Au(Te,Sb)_4S_{5-8}$	Hex	7.4	$1-1\frac{1}{2}$	—	Blackish lead-gray
Natroalunite, 425	$(Na,K)Al_3(SO_4)_2(OH)_6$	Hex	2.6–2.9	$3\frac{1}{2}-4$	1.57	White, grayish, massive
Natrolite, 549	$Na_2Al_2Si_3O_{10} \cdot 2H_2O$	Orth	2.25	$5-5\frac{1}{2}$	1.48	Cl{110} perfect
Nepheline, 545	$(Na,K)AlSiO_4$	Hex	2.60–2.65	$5\frac{1}{2}-6$	1.54	Greasy luster
Nephrite, 515	.....					Tough, compact tremolite
Neptunite, 497	$KNa_2Li(Fe,Mn)_2TiO_2(Si_4O_{11})_2$	Mon	3.23	5–6	1.70	Black
Nickeline, 358	NiAs	Hex	7.78	$5-5\frac{1}{2}$	—	Copper-red
Nickel bloom, 431	.....					See annabergite
Nickel iron, 345	Fe-Ni	Iso	7.8–8.2	5	—	Kamacite, taenite
Nickel skutterudite, 366	$(Ni,Co)As_3$	Iso	6.5 ± 0.4	$5\frac{1}{2}-6$	—	Tin-white
Niter, 416	KNO_3	Orth	2.09–2.14	2	1.50	Cooling taste
Nitratite, 416	$NaNO_3$	Hex	2.29	1–2	1.59	Cooling taste
Nontronite, 524	$Fe_2(Al,Si)_4O_{10}(OH)_2Na_{0.3} \cdot nH_2O$	Mon	2.5	$1-1\frac{1}{2}$	1.60	Clay mineral
Norbergite, 495	$Mg_3(SiO_4)(F,OH)_2$	Orth	3.1–3.2	6	1.57	See chondrodite
Nosean, 546	$Na_8(AlSiO_4)_6SO_4 \cdot H_2O$	Iso	2.3±	6	1.50	A feldspathoid

O

Oligoclase, 544	$Ab_{90}An_{10}$-$Ab_{70}An_{30}$	Tric	2.65	6	1.54	A member of the plagioclase feldspar series
Olivine, 485, 562	$(Mg,Fe)_2SiO_4$	Orth	3.27–4.37	$6\frac{1}{2}-7$	1.69	Green rock-forming mineral
Omphacite, 510	$(Ca,Na)(Mg,Fe,Al)Si_2O_6$	Mon	3.2–3.4	5–6	1.67–1.70	Green pyx. in eclogite
Onyx, 536	.....					Layered chalcedony
Onyx marble, 407	.....					See calcite and aragonite
Opal, 538, 559, 571	$SiO_2 \cdot nH_2O$	Amor	2.0–2.25	5–6	1.44	Conchoidal fracture
Orpiment, 361	As_2S_3	Mon	3.49	$1\frac{1}{2}-2$	2.8	Cl{010}; yellow
Orthite, 500	.....					See allanite
Orthoclase, 540	$KAlSi_3O_8$	Mon	2.57	6	1.52	Medium *T* K-feldspar

Name, Page	Composition	Xl Sys.	G	H	*n*	Remarks
Orthoferrosilite, 505	$FeSiO_3$	Orth	3.9	6	1.79	Orthopyroxene end-member (= ferrosilite)
P						
Palladium, 345	Pd	Iso	11.9	$4\frac{1}{2}$–5	—	See platinum
Paragonite, 526	$NaAl_2(AlSi_3O_{10})(OH)_2$	Mon	2.85	2	1.60	Similar to muscovite
Pargasite, 517	$NaCa_2Fe_4(Al,Fe)Al_2Si_6O_{22}(OH)_2$	Mon	3–3.5	$5\frac{1}{2}$	1.62	See hornblende
Patronite, 430	VS_4	Mon	.....			Ore of vanadium
Pectolite, 513	$NaCa_2(SiO_3)_3O(OH)$	Tric	2.8	5	1.60	Crystals acicular
Pennantite, 532	.....				1.66	See chlorite
Pentlandite, 359	$(Fe,Ni)_9S_8$	Iso	4.6–5.0	$3\frac{1}{2}$–4	—	Generally with pyrrhotite
Periclase, 376	MgO	Iso	3.56	$5\frac{1}{2}$	1.73	Cl{001}, cubic
Peridot, 485	.....					Gem olivine
Peristerite, 475	.....					Intergrowths between Ab_{98} and Ab_{85}; "moonstone"
Perovskite, 379	$CaTiO_3$	Orth	4.03	$5\frac{1}{2}$	2.38	Pseudoisometric crystals
Perthite, 474	.....					Coarse K-feldspar–albite intergrowth
Petalite, 547	$Li(AlSi_4O_{10})$	Mon	2.4	6–$6\frac{1}{2}$	1.51	Cl{001} {201}
Petzite, 343	$(Ag,Au)_2Te$	Iso	8.7–9.0	$2\frac{1}{2}$–3	—	Steel-gray to iron-black
Phenacite, 484	Be_2SiO_4	Hex	2.97–3.0	$7\frac{1}{2}$–8	1.65	In pegmatites
Phillipsite-K, 552	$(K,Ca_{0.5},Na)_9(Al_9Si_{27}O_{72})\cdot\sim 24H_2O$	Mon	2.2	$4\frac{1}{2}$–5	1.50	A zeolite
Phlogopite, 528	$KMg_3(AlSi_3O_{10})(OH)_2$	Mon	2.86	$2\frac{1}{2}$–3	1.56–1.64	Yellow-brown mica
Phosgenite, 413	$Pb_2CO_3Cl_2$	Tet	6.0–6.3	3	2.12	Adamantine luster
Phosphorite, 428	.....					See apatite
Piemontite, 499	$Ca_2MnAl_2O(SiO_4)(Si_2O_7)(OH)$	Mon	3.4	$6\frac{1}{2}$	1.75–1.81	Reddish-brown
Pigeonite, 507	$\sim Ca_{0.25}(Mg,Fe)_{1.75}Si_2O_6$	Mon	3.30–3.46	6	1.64–1.72	High *T* pyroxene
Pitchblende, 383	.....					Massive UO_2
Plagioclase, 541	$Ab_{100}An_0$-Ab_0An_{100}	Tric	2.62–2.76	6	1.53–1.59	The Na–Ca–feldspar series
Plancheite, 534	$Cu_8(Si_4O_{11})_2(OH)_2\cdot H_2O$	Orth	3.3	$5\frac{1}{2}$	1.66	Fibrous, mammillary, blue
Platinum, 345	Pt	Iso	14–19	4–$4\frac{1}{2}$	—	Steel-gray with bright luster; malleable
Pleonaste, 384	.....					Ferroan spinel
Pollucite, 545	$CsAlSi_2O_6\cdot H_2O$	Iso	2.9	$6\frac{1}{2}$	1.52	Colorless; in pegmatites
Polyhalite, 395	$K_2Ca_2Mg(SO_4)_2\cdot 2H_2O$	Tric	2.78	$2\frac{1}{2}$–3	1.56	Bitter taste
Potash feldspar, 539	$KAlSi_3O_8$	.....				Microcline, orthoclase, sanidine
Powellite, 426	$CaMoO_4$	Tet	4.23	$3\frac{1}{2}$–4	1.97	Fluoresces yellow
Prase, 536	.....					Dull green, microcrystalline quartz
Prehnite, 533	$Ca_2Al(AlSi_3O_{10})(OH)_2$	Orth	2.8–2.95	6–$6\frac{1}{2}$	1.63	Tabular crystals, green
Proustite, 367	Ag_3AsS_3	Hex	5.57	2–$2\frac{1}{2}$	3.09	Light ruby silver
Pseudobrookite, 379	Fe_2TiO_5	.....				See ilmenite
Pseudoleucite, 544	.....					See leucite
Pseudophite, 571	.....					Massive form of chlorite; substitute for jade
Pseudowollastonite, 511	$CaSiO_3$	Tric	.....			High *T* form of wollastonite
Psilomelane, 391	.....					See romanechite
Pyrargyrite, 367	Ag_3SbS_3	Hex	5.85	2–$2\frac{1}{2}$	3.08	Dark ruby-silver
Pyrite, 363	FeS_2	Iso	5.02	6–$6\frac{1}{2}$	—	Crystals striated
Pyrochlore, 390	$(Ca,Na)_2(Nb,Ta)_2O_6(O,OH,F)$	Iso	4.3±	5	—	Usually metamict
Pyrolusite, 382	MnO_2	Tet	4.75	1–2	—	Sooty black
Pyromorphite, 406, 430	$Pb_5(PO_4)_3Cl$	Hex	7.04	$3\frac{1}{2}$–4	2.06	Adamantine luster
Pyrope, 489	$Mg_3Al_2Si_3O_{12}$	Iso	3.58	7	1.71	A garnet
Pyrophanite, 379	$MnTiO_3$	Hex	4.54	5–6	2.48	Cl{22$\bar{1}$1}
Pyrophyllite, 525	$Al_2Si_4O_{10}(OH)_2$	Mon	2.8	1–2	1.59	Smooth feel; micaceous habit
Pyroxene, 505	.....					A mineral group
Pyroxenoid, 511	.....					A mineral group

Name, Page	Composition	Xl Sys.	G	H	*n*	Remarks
Pyroxferroite, 512	$Ca_{0.15}Fe_{0.85}SiO_3$	Tric	3.7	—	1.75	Pyroxenoid; in lunar rocks
Pyroxmangite, 512	$(Mn,Fe)SiO_3$	Tric	3.6–3.8	$5\frac{1}{2}$–6	1.72–1.75	From metamorphic Mn-rich rocks
Pyrrhotite, 357	$Fe_{1-x}S$	Mon Hex	4.58–4.65	4	—	Magnetic
Q						
Quartz, 534, 561, 571	SiO_2	Hex	2.65	7	1.54	Conchoidal fracture
R						
Ramsayite, 497	$Na_2Ti_2Si_2O_9$	Orth	3.43	6	2.01	Rare Ti-bearing silicate in alkalic rocks
Realgar, 360	AsS	Mon	3.48	$1\frac{1}{2}$–2	2.60	Cl{010}; red
Red ocher, 377	.....					See hematite
Rhodochrosite, 410	$MnCO_3$	Hex	3.5–3.7	$3\frac{1}{2}$–4	1.82	Cl{10$\bar{1}$1}; pink
Rhodolite, 489	.....					Pale rose-red to purple garnet
Rhodonite, 512	$MnSiO_3$	Tric	3.4–3.7	$5\frac{1}{2}$–6	1.73–1.75	Pink pyroxenoid
Riebeckite, 519	$Na_2Fe_3^{2+}Fe_2^{3+}Si_8O_{22}(OH)_2$	Mon	3.4	5	1.66–1.71	Bluish-colored amphibole; may be fibrous
Ringwoodite, 485	Mg_2SiO_4	.....				High-pressure polymorph of olivine
Rock crystal, 535	SiO_2	.....				Colorless quartz crystal
Rock salt, 393	.....					See halite
Romanechite, 391	$(Ba,H_2O)_2(Mn^{4+},Mn^{3+})_5O_{10}$	Orth	3.7–4.7	5–6	—	Botryoidal; formerly known as psilomelane
Roscoelite, 430	$KV_2(AlSi_3O_{10})(OH)_2$	Mon	2.97	$2\frac{1}{2}$	1.69	Vanadium mica
Rose quartz, 535	SiO_2	.....				Pink quartz
Rubellite, 504	.....					Red to pink tourmaline
Ruby, 376, 559, 570	.....					Red gem corundum
Ruby copper, 375	.....					See cuprite
Ruby silver, 367	.....					See pyrargyrite and proustite
Ruby spinel, 384	$MgAl_2O_4$	.....				Red gem spinel
Rutile, 379	TiO_2	Tet	4.18–4.25	6–$6\frac{1}{2}$	2.61	Adamantine luster; reddish-brown
S						
Saltpeter, 416	.....					See niter
Sanidine, 540	$(K,Na)AlSi_3O_8$	Mon	2.56–2.62	6	1.53	High *T* K-feldspar
Saponite, 524	$(Mg,Fe)_3(Al,Si)_4O_{10}(OH)_2$-$(\frac{1}{2}Ca,Na)_{0.3}\cdot 4H_2O$	Mon	2.5	1–$1\frac{1}{2}$	1.52	Clay mineral
Sapphire, 376	.....					Blue gem corundum
Sard, 536	.....					Brown chalcedony
Sardonyx, 536	.....					Onyx with sard
Satin spar, 423	.....					Fibrous gypsum
Scapolite, 547	$3NaAlSi_3O_8\cdot NaCl$ to $3CaAl_2Si_2O_8\cdot CaCO_3$	Tet	2.55–2.74	5–6	1.55–1.60	Cl{100} {110}
Scheelite, 426	$CaWO_4$	Tet	5.9–6.1	$4\frac{1}{2}$–5	1.92	Cl{101}
Schorl, 504	.....					Na,Fe,Al-tourmaline
Scolecite, 549, 552	$CaAl_2Si_3O_{10}\cdot 3H_2O$	Mon	2.2±	5–$5\frac{1}{2}$	1.52	A zeolite
Scorzalite, 431	$(Fe,Mg)Al_2(PO_4)_2(OH)_2$	Mon	3.35	$5\frac{1}{2}$–6	1.67	Blue; see lazulite
Selenite, 423	.....					Broad, colorless cleavage folia of gypsum
Sericite, 525	.....					Fine-grained muscovite

Name, Page	Composition	Xl Sys.	G	H	*n*	Remarks
Serpentine, 519	$Mg_3Si_2O_5(OH)_4$	Mon Orth	2.3	3–5	1.55	Green to yellow; waxlike to silky (when fibrous)
Shattuckite, 534	$Cu_5(SiO_3)_4(OH)_2$	Orth	3.8	—	1.78	Blue
Siderite, 409	$FeCO_3$	Hex	3.96	$3\frac{1}{2}$–4	1.88	Cl{10$\bar{1}$1}
Sillimanite, 492	Al_2SiO_5	Orth	3.23	6–7	1.66	Cl{010} perfect
Silver, 343	Ag	Iso	10.5	$2\frac{1}{2}$–3	—	White, malleable
Sinhalite, 419	$Mg(Al,Fe)BO_4$	Orth	3.48	$6\frac{1}{2}$	1.70	Brown gem mineral
Skutterudite, 366	$CoAs_{2-3}$	Iso	6.5 ± 0.4	$5\frac{1}{2}$–6	—	Tin-white
Smaltite, 366	$(Co,Ni)As_{3-x}$	Iso	6.5 ± 0.4	$5\frac{1}{2}$–6	—	See skutterudite
Smectite, 524	.....					Clay mineral
Smithsonite, 411	$ZnCO_3$	Hex	4.30–4.45	4–$4\frac{1}{2}$	1.85	Reniform; many colors
Smoky quartz, 535	SiO_2	.....				Brown to black
Soapstone, 524	.....					See talc
Sodalite, 546	$Na_8(AlSiO_4)_6Cl_2$	Iso	2.15–2.30	$5\frac{1}{2}$–6	1.48	Usually blue
Soda niter, 416	.....					See nitratite
Specularite, 377	.....					Platy, metallic hematite
Sperrylite, 345	$PtAs_2$	Iso	10.50	6–7	—	See platinum
Spessartine, 489	$Mn_3Al_2Si_3O_{12}$	Iso	4.19	7	1.80	A garnet
Sphalerite, 356	ZnS	Iso	3.9–4.1	$3\frac{1}{2}$–4	2.37	Cl{011}; 6 directions
Sphene, 496	.....					See titanite
Spinel, 384, 572	$MgAl_2O_4$	Iso	3.5–4.1	8	1.72	In octahedrons
Spodumene, 510	$LiAlSi_2O_6$	Mon	3.15–3.20	$6\frac{1}{2}$–7	1.67	Cl{110} ~ 90°; in pegmatites
Staetite, 524	.....					See talc
Stannite, 357, 383	Cu_2FeSnS_4	Tet	4.3–4.5	4	—	Metallic, gray to black
Starlite, 562	.....					Blue, heat treated zircon; a gem
Staurolite, 494	$Fe_{3-4}Al_{18}Si_8O_{48}H_{2-4}$	Mon	3.65–3.75	7–$7\frac{1}{2}$	1.75	Pseudo-orthorhombic; cruciform twins
Stibnite, 361	Sb_2S_3	Orth	4.52–4.62	2	—	Cl{010} perfect; prismatic crystals
Stilbite, 551	$(Na,K,Ca_{0.5})_9(Al_9Si_{27}O_{72})\cdot 28H_2O$	Mon	2.1–2.2	$3\frac{1}{2}$–4	1.50	A zeolite; sheaflike aggregates
Stiplnomelane, 529	~$K(Mg,Fe^{2+},Fe^{3+})_8(Si,Al)_{12}(O,OH)_{27}\cdot 2$–$4H_4O$	Mon	2.59–2.96	3–4	1.58–1.74	Brownish; in micalike plates
Stishovite, 470	SiO_2	Tet	4.35	7	1.80	In meteorite craters; high *P* form of quartz
Stolzite, 405	$PbWO_4$	Tet	7.9–8.3	$2\frac{1}{2}$–3	2.27	Cl{001} {011}
Stream tin, 382	SnO_2	.....				See cassiterite
Strontianite, 413	$SrCO_3$	Orth	3.7	$3\frac{1}{2}$–4	1.67	Effervescence in HCl
Sudoite, 532	$Mg_2(Al,Fe^{3+})_3Si_3AlO_{10}(OH)_8$	Mon	.....			Member of the chlorite group
Sulfur, 345	S	Orth	2.05–2.09	$1\frac{1}{2}$–$2\frac{1}{2}$	2.04	Burns with blue flame
Sunstone, 544	.....					See oligoclase
Sylvanite, 343	$(Au,Ag)Te_2$	Mon	8.0–8.2	$1\frac{1}{2}$–2	—	Cl{010} perfect
Sylvite, 394	KCl	Iso	1.99	2	1.49	Cl cubic; bitter

T

Taenite, 345	Fe-Ni	Iso	7.8–8.2	5	—	In meteorites
Talc, 522	$Mg_3Si_4O_{10}(OH)_2$	Tric	2.7–2.8	1	1.59	Greasy feel; sectile
Tantalite (ferro), 389	$(Fe,Mn)Ta_2O_6$	Orth	6.5±	6	—	See ferrifanfailite
Tanzanite, 499	.....					Blue gem zoisite
Tennantite, 367	$Cu_{12}As_4S_{13}$	Iso	4.6–5.1	3–$4\frac{1}{2}$	—	In tetrahedrons
Tenorite, 376	CuO	Tric	6.5	3–4	—	Black
Tephroite, 513	Mn_2SiO_4	Orth	4.1	6	1.70–1.80	An olivine
Tetrahedrite, 367	$Cu_{12}Sb_4S_{13}$	Iso	4.6–5.1	3–$4\frac{1}{2}$	—	In tetrahedrons
Thomsonite, 552	$NaCa_2(Al_5Si_5O_{20})\cdot 6H_2O$	Orth	2.3	5	1.52	A zeolite
Thorianite, 383, 384	ThO_2	Iso	9.7	$6\frac{1}{2}$	—	Dark gray, brownish-black
Thorite, 491	$ThSiO_4$	Tet	5.3	5	1.8	Brown to black; radioactive

Name, Page	Composition	Xl Sys.	G	H	*n*	Remarks
Tiger's eye, 535	.....					Brown chatoyant gem material; see crocidolite and quartz
Tincalconite, 417	$Na_2B_4O_5(OH)_4{\cdot}3H_2O$	Hex	1.88	1	1.46	Alteration of borax
Titanite, 496	$CaTiO(SiO_4)$	Mon	3.40–3.55	$5–5\frac{1}{2}$	1.91	Wedge-shaped crystals; formerly known as sphene
Todorokite, 391	$(Mn,Ca,Mg)Mn_3O_7{\cdot}H_2O$	.....				See romanechite
Topaz, 493, 560	$Al_2SiO_4(F,OH)_2$	Orth	3.4–3.6	8	1.61–1.63	Cl{001} perfect
Torbernite, 433	$Cu(UO_2)_2(PO_4)_2{\cdot}8–12H_2O$	Tet	3.22	$2–2\frac{1}{2}$	1.59	Green
Tourmaline, 503, 561	$(Na,Ca)(Fe,Li,Mg,Al)_3(Al,Fe,Mn)_6(BO_3)_3(Si_6O_{18})(OH)_3(OH,F,O)$	Hex	3.0–3.25	$7–7\frac{1}{2}$	1.64–1.68	Trigonal cross sections and conchoidal fracture
Travertine, 407	.....					See calcite
Tremolite, 515	$Ca_2Mg_5Si_8O_{22}(OH)_2$	Mon	3.0–3.2	5–6	1.61	Cl{110}; white to light green
Tridymite, 538	SiO_2	Mon Orth	2.26	7	1.47	In volcanic rocks
Triphylite, 427	$Li(Fe,Mn)PO_4$	Orth	3.42–3.56	$4\frac{1}{2}–5$	1.69	Cl{001} {010}
Troilite, 358	FeS	Hex	4.7	4	—	In meteorites
Trona, 416	$Na_3H(CO_3)_2{\cdot}2H_2O$	Mon	2.13	3	1.49	Alkaline taste
Troostite, 484	.....					Manganiferous willemite
Tsavorite, 561	.....					Emerald green gem garnet
Tschermakite, 517	$Ca_2Mg_3(Al,Fe)_2Al_2Si_6O_{22}(OH)_2$	.....				See hornblende
Tufa, 407	.....					See calcite
Turquoise, 432, 561, 572	$CuAl_6(PO_4)_4(OH)_8{\cdot}4H_2O$	Tric	2.6–2.8	6	1.62	Blue-green; gem material
Tyuyamunite, 433	$Ca(UO_2)_2(VO_4)_2{\cdot}5–8\frac{1}{2}H_2O$	Orth	3.7–4.3	2	1.86	Yellow; radioactive; secondary alteration
U						
Ulexite, 419	$NaCaB_5O_6(OH)_6{\cdot}5H_2O$	Tric	1.96	$1–2\frac{1}{2}$	1.50	"Cotton balls"; fiber optic
Ulvöspinel, 387	Fe_2TiO_4	Iso	4.78	$7\frac{1}{2}–8$	—	Commonly as exsolution in magnetite
Uraninite, 383	UO_2	Iso	7.5–9.7	$5\frac{1}{2}$	—	Pitchy luster; radioactive
Uvarovite, 489	$Ca_3Cr_2Si_3O_{12}$	Iso	3.90	$7\frac{1}{2}$	1.87	Rare green garnet
Uytenbogaardite, 343	Ag_3AuS_3	.....				Rare gold ore
V						
Vanadinite, 430	$Pb_5(VO_4)_3Cl$	Hex	6.9	3	2.25–2.42	Adamantine luster; red to yellow
Variscite, 432	$Al(PO_4){\cdot}2H_2O$	Orth	2.57	$3\frac{1}{2} – 4\frac{1}{2}$	1.58	Green, massive
Verde antique, 521	.....					Marble and green serpentine
Verdelite, 503	.....					Green tourmaline
Verdite, 571	.....					Green rock material containing fuchsite; substitute for gem jade
Vermiculite, 529	$(Mg,Ca)_{0.3}(Mg,Fe,Al)_{3.0}(Al,Si)_4O_{10}(OH)_4{\cdot}8H_2O$	Mon	2.4	$1\frac{1}{2}$	1.55–1.58	Altered biotite
Vesuvianite, 500	$Ca_{19}(Al,Mg,Fe)_{13}(Si_2O_7)_4(SiO_4)_{10}(O,OH,F)_{10}$	Tet	3.35–3.45	$6\frac{1}{2}$	1.70–1.75	Prismatic crystals; formerly known as idocrase
Vivianite, 431	$Fe_3(PO_4)_2{\cdot}8H_2O$	Mon	2.58–2.68	$1\frac{1}{2} – 2$	1.60	Cl{010} perfect
W						
Wad	.....					Manganese ore; mixture of manganese minerals
Wadsleyite, 485	Mg_2SiO_4	.....				High-pressure polymorph of olivine

Name, Page	Composition	Xl Sys.	G	H	*n*	Remarks
Wavellite, 431	$Al_3(PO_4)_2(OH)_3{\cdot}5H_2O$	Orth	2.36	$3\frac{1}{2} - 4$	1.54	Radiating aggregates
Wernerite, 547	.....				1.55–1.60	See scapolite
White iron pyrites, 364	.....					See marcasite
Willemite, 484	Zn_2SiO_4	Hex	3.9–4.2	$5\frac{1}{2}$	1.69	From Franklin, NJ
Witherite, 412	$BaCO_3$	Orth	4.3	$3\frac{1}{2}$	1.68	Effervescence in HCl
Wolframite, 425	$(Fe,Mn)WO_4$	Mon	7.0–7.5	$4 - 4\frac{1}{2}$	—	Cl{010} perfect, tabular crystals
Wollastonite, 511	$CaSiO_3$	Tric	2.8–2.9	$5 - 5\frac{1}{2}$	1.63	Cl{100}, {001} perfect
Wood opal, 538	.....					Fossil wood with opal
Wood tin, 382	.....					See cassiterite
Wulfenite, 426	$PbMoO_4$	Tet	6.8±	3	2.40	Orange-red
Wurtzite, 356	ZnS	Hex	3.98	4	2.35	Polymorph of sphalerite
X						
Xanthophyllite, 529	$Ca(Mg,Al)_{3-2}(Al_2Si_2O_{10})(OH)_2$	Mon	3–3.1	$3\frac{1}{2}$	1.65	Brittle mica
Z						
Zeolite, 549	.....					A mineral group
Zinc blende, 356	.....					See sphalerite
Zincite, 376	ZnO	Hex	5.68	4	2.01	From Franklin, NJ
Zircon, 490, 562	$ZrSiO_4$	Tet	4.68	$7\frac{1}{2}$	1.92–1.96	Commonly in small crystals
Zoisite, 499	$Ca_2Al_3O(SiO_4)(Si_2O_7)(OH)$	Orth	3.35	6	1.69	Gray, green-brown, metamorphic

SUBJECT INDEX

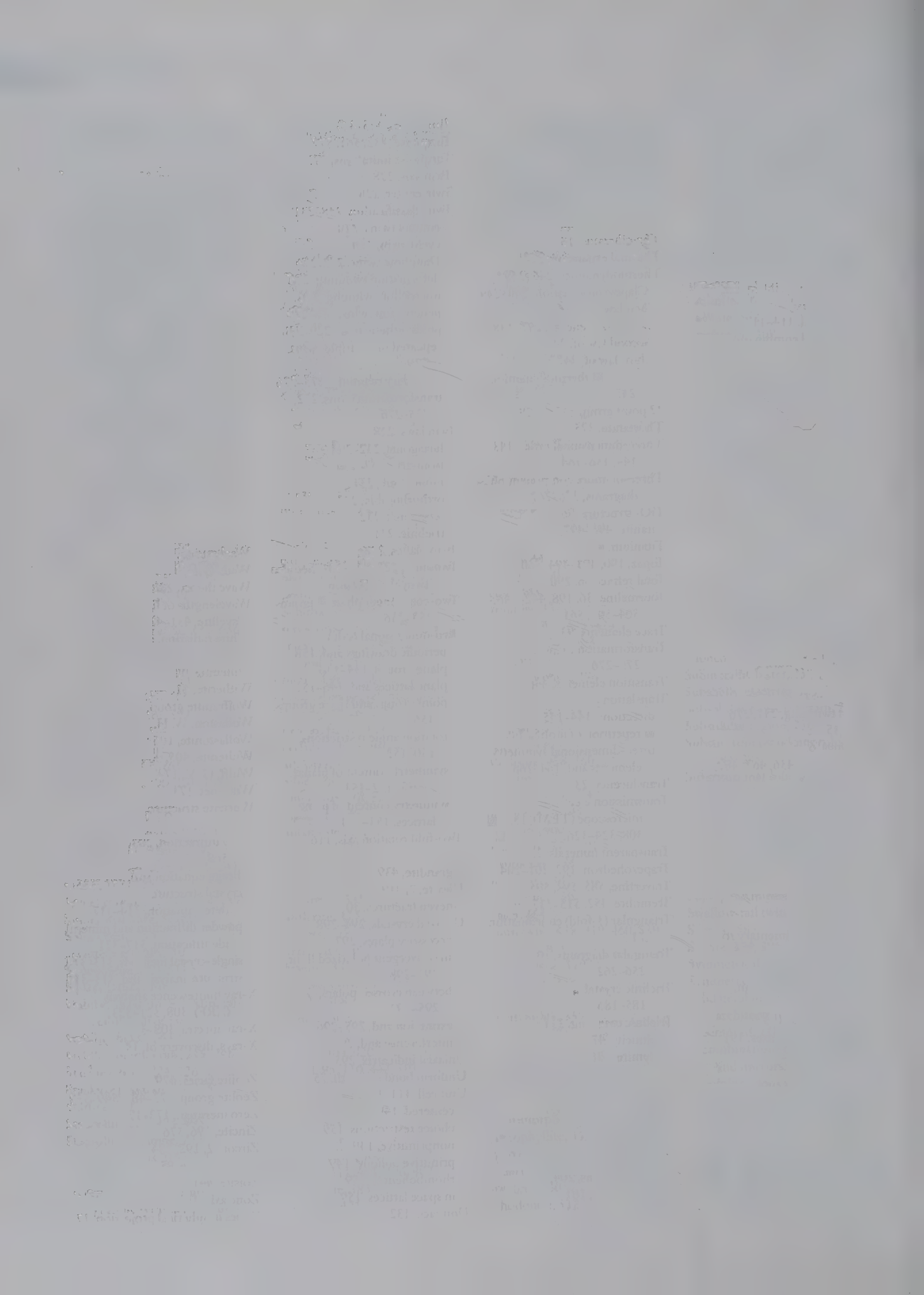

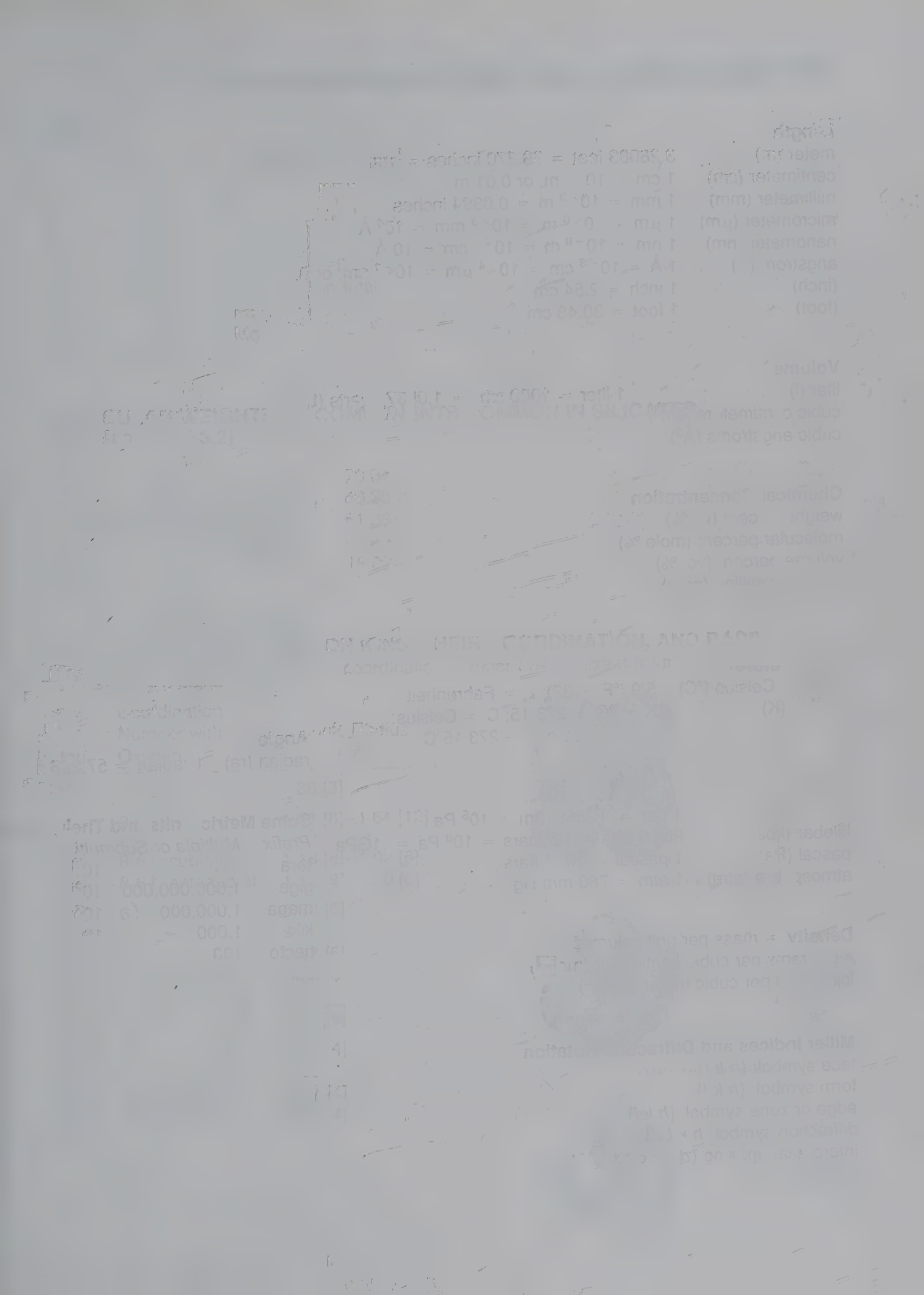

SOME UNITS, SYMBOLS, AND CONVERSION FACTORS

Length

meter (m)	3.28083 feet = 39.370 inches = 100 cm = 10^{10} Å
centimeter (cm)	1 cm = 10^{-2} m, or 0.01 m
millimeter (mm)	1 mm = 10^{-3} m = 0.0394 inches
micrometer (μm)	1 μm = 10^{-6} m = 10^{-3} mm = 10^{4} Å
nanometer (nm)	1 nm = 10^{-9} m = 10^{-7} cm = 10 Å
angstrom (Å)	1 Å = 10^{-8} cm = 10^{-4} μm = 10^{-1} nm, or 0.1 nm
(inch)	1 inch = 2.54 cm
(foot)	1 foot = 30.48 cm

Volume

liter (l)	1 liter = 1000 cm^3 = 1.0567 quarts (U.S.)
cubic centimeters (cm^3)	
cubic angstroms ($Å^3$)	

Chemical Concentration

weight percent (wt %)
molecular percent (mole %)
volume percent (vol %)
parts per million (ppm)
parts per billion (ppb)

Temperature

degrees Celsius (°C)	5/9 (°F − 32); F = Fahrenheit
kelvins (K)	K = °C + 273.15; C = Celsius; absolute zero = −273.15°C

Pressure

bar	1 bar = 0.9869 atm = 10^5 Pa
kilobar (kbar)	986.9 atm = 10^3 bars = 10^8 Pa = .1GPa
pascal (Pa)	1 pascal = 10^{-5} bars
atmosphere (atm)	1 atm = 760 mm Hg

Density = mass per unit volume;
e.g. grams per cubic centimeter (g/cm^3)
kilograms per cubic meter (kg/m^3)

Miller Indices and Diffraction Notation

face symbol: (*h k l*)
form symbol: {*h k l*}
edge or zone symbol: [*h k l*]
diffraction symbol: *h k l*
interplanar spacing (*d*); e.g. $d_{h\,k\,l}$

Unit Cell Measurements

edge lengths (*a*, *b*, *c*)
angles (α, β, γ)

Optical Parameters

refractive indices (*n*; ε, ω; α, β, γ)
optic axial angle (2*V*)
extinction angle (*X*, *Y* or *Z* ∧ *a* or *c*)

Angle

radian (ra) 1 radian = 57.296 degre

Some Metric Units and Their Prefixe

Prefix	*Multiple or Submultiple*	
tera		10^{12}
giga	1,000,000,000	10^{9}
mega	1,000,000	10^{6}
kilo	1,000	10^{3}
hecto	100	10^{2}
deka	10	10^{1}
	1	10^{0}
deci	0.1	10^{-1}
centi	0.01	10^{-2}
milli	0.001	10^{-3}
micro	0.000 001	10^{-6}
nano	0.000 000 001	10^{-9}
pico		10^{-12}

THE EIGHT MOST COMMON ELEMENTS IN THE EARTH'S CRUST (See Figure 3.2)

Weight Percentage		Volume Percentage	
O	46.60	O	~94
Si	27.72	K	~6 in total
Al	8.13	Na	
Fe	5.00	Ca	
Ca	3.63	Si	
Na	2.83	Al	
K	2.59	Fe	
Mg	2.09	Mg	
Total	98.59		

MOLECULAR WEIGHTS OF COMPONENTS COMMON IN SILICATES (See also Table 3.2)

SiO_2	60.08	MnO	70.94
TiO_2	79.90	MgO	40.30
Al_2O_3	101.96	Na_2O	61.98
FeO	71.85	K_2O	94.20
Fe_2O_3	159.69	H_2O	18.02
CaO	56.08		

SOME OF THE MOST COMMON IONS, THEIR COORDINATION, AND RADII

(The number in brackets is **C.N.** = coordination number.) See Table 3.8 for a complete listing.

Ion	Coordination Number with Oxygen		Ionic Radius Å
O^{2-}			1.36 [3]
K^+	8-12		1.51 [8]–1.64 [12]
Na^+	8-6	cubic to octahedral	1.18 [8]–1.02 [6]
Ca^{2+}	8-6	cubic to octahedral	1.12 [8]–1.00 [6]
Mn^{2+}	6	octahedral	0.83 [6]
Fe^{2+}	6	octahedral	0.78 [6]
Mg^{2+}	6	octahedral	0.72 [6]
Fe^{3+}	6	octahedral	0.65 [6]
Ti^{4+}	6	octahedral	0.61 [6]
Al^{3+}	6	octahedral	0.54 [6]
Al^{3+}	4	tetrahedral	0.39 [4]
Si^{4+}	4	tetrahedral	0.26 [4]
P^{5+}	4	tetrahedral	0.17 [4]
S^{6+}	4	tetrahedral	0.12 [4]

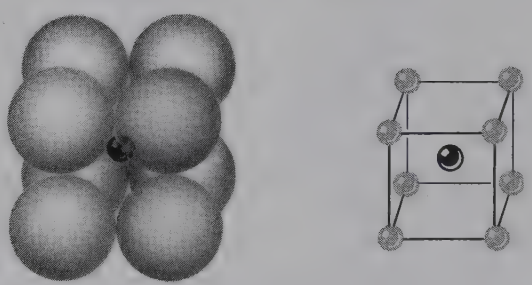

Cubic coordination

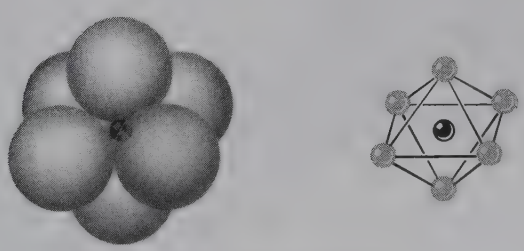

Octahedral coordination

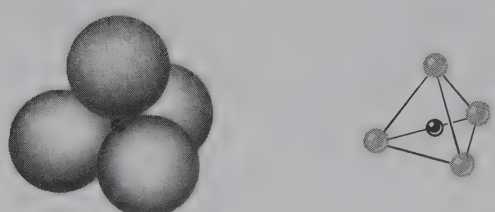

Tetrahedral coordination

Selected Abbreviations for Minerals

(after Kretz, 1983; Spear, 1993; and Winter, 2001*)

Act	actinolite	Elb	elbaite	Ol	olivine
Ab	albite	En	enstatite (ortho)	Omp	omphacite
Aln	allanite	Ep	epidote	Oam	orthoamphibole
Alm	almandine	Fa	fayalite	Or	orthoclase
Als	aluminosilicate	Fac	ferro-actinolite	Opx	orthopyroxene
Amp	amphibole	Fs	ferrosilite	Pg	paragonite
Anl	analcime	Fl	fluorite	Per	periclase
And	andalusite	Fo	forsterite	Prv	perovskite
Ads	andesine	Gn	galena	Phl	phlogopite
Adr	andradite	Grt	garnet	Pgt	pigeonite
Anh	anhydrite	Ged	gedrite	Pl	plagioclase
Ank	ankerite	Glt	glauconite	Pmp	pumpellyite
An	anorthite	Gln	glaucophane	Py	pyrite
Atg	antigorite	Gt	goethite	Prp	pyrope
Ath	anthophyllite	Gr	graphite	Prl	pyrophyllite
Ap	apatite	Grs	grossularite	Po	pyrrhotite
Arg	aragonite	Gru	grunerite	Qtz	quartz
Aug	augite	Gp	gypsum	Rbk	riebeckite
Brt	barite	Hl	halite	Rds	rhodochrosite
Bt	biotite	Hd	hedenbergite	Rt	rutile
Brl	beryl	Hem	hematite	Sa	sanidine
Bn	bornite	Hul	heulandite	Srl	schorl
Brc	brucite	Hbl	hornblende	Scp	scapolite
Cam	Ca-clinoamphibole	Ill	illite	Srp	serpentine
Cpx	Ca-clinopyroxene	Ilm	ilmenite	Sd	siderite
Cal	calcite	Jd	jadeite	Sil	sillimanite
Cls	celestite	Kln	kaolinite	Sps	spessartine
Cc	chalcocite	Kfs	K-feldspar	Sp	sphalerite
Ccp	chalcopyrite	Ky	kyanite	Spn	sphene
Chl	chlorite	Lab	labradorite	Spl	spinel
Cld	chloritoid	Lmt	laumontite	Spd	spodumene
Chr	chromite	Lws	lawsonite	St	staurolite
Ctl	chrysotile	Lpd	lepidolite	Stb	stilbite
Cen	clinoenstatite	Lct	leucite	Sti	stishovite
Cfs	clinoferrosilite	Lz	lizardite	Tlc	talc
Czo	clinozoisite	Mt	magnetite	Ttn	titanite
Coe	coesite	Mrg	margarite	Toz	topaz
Crd	cordierite	Mc	microcline	Tur	tourmaline
Crn	corundum	Mo	molybdenum	Tr	tremolite
Cv	covellite	Mnz	monazite	Trd	tridymite
Crs	cristobalite	Mnt	montmorillonite	Vrm	vermiculite
Cum	cummingtonite	Ms	muscovite	Ves	vesuvianite
Di	diopside	Ntr	natrolite	Wo	wollastonite
Dol	dolomite	Ne	nepheline	Zrc	zircon
Drv	dravite	Olg	oligoclase	Zo	zoisite

From Kretz, R., 1983. Symbols for Rock-forming minerals. *American Mineralogist*, p. 280–282. Spear, F. S., 1993. *Metamorphic Phase Equilibria and Pressure-Temperature-Time Paths.* Mineralogical Society of America. Winter, J., D., 2001. *An Introduction to Igneous and Metamorphic Petrology.* Prentice-Hall.

STEREOGRAPHIC NET WITH 10CM RADIUS

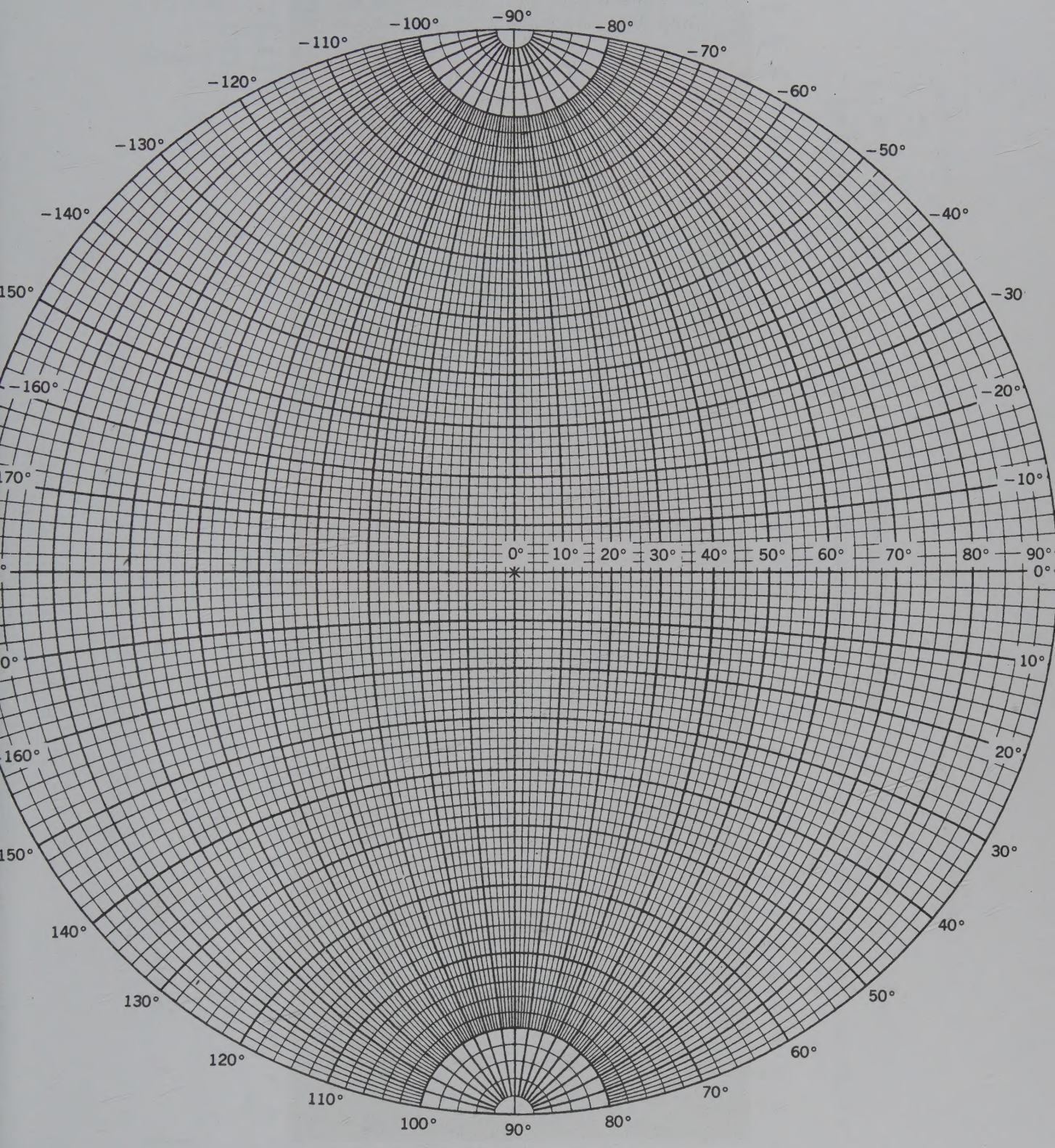

Interference Color Chart

Graphical representation of the relationship between retardation, birefringence, and crystal thickness: $\Delta = d(n_2 - n_1)$

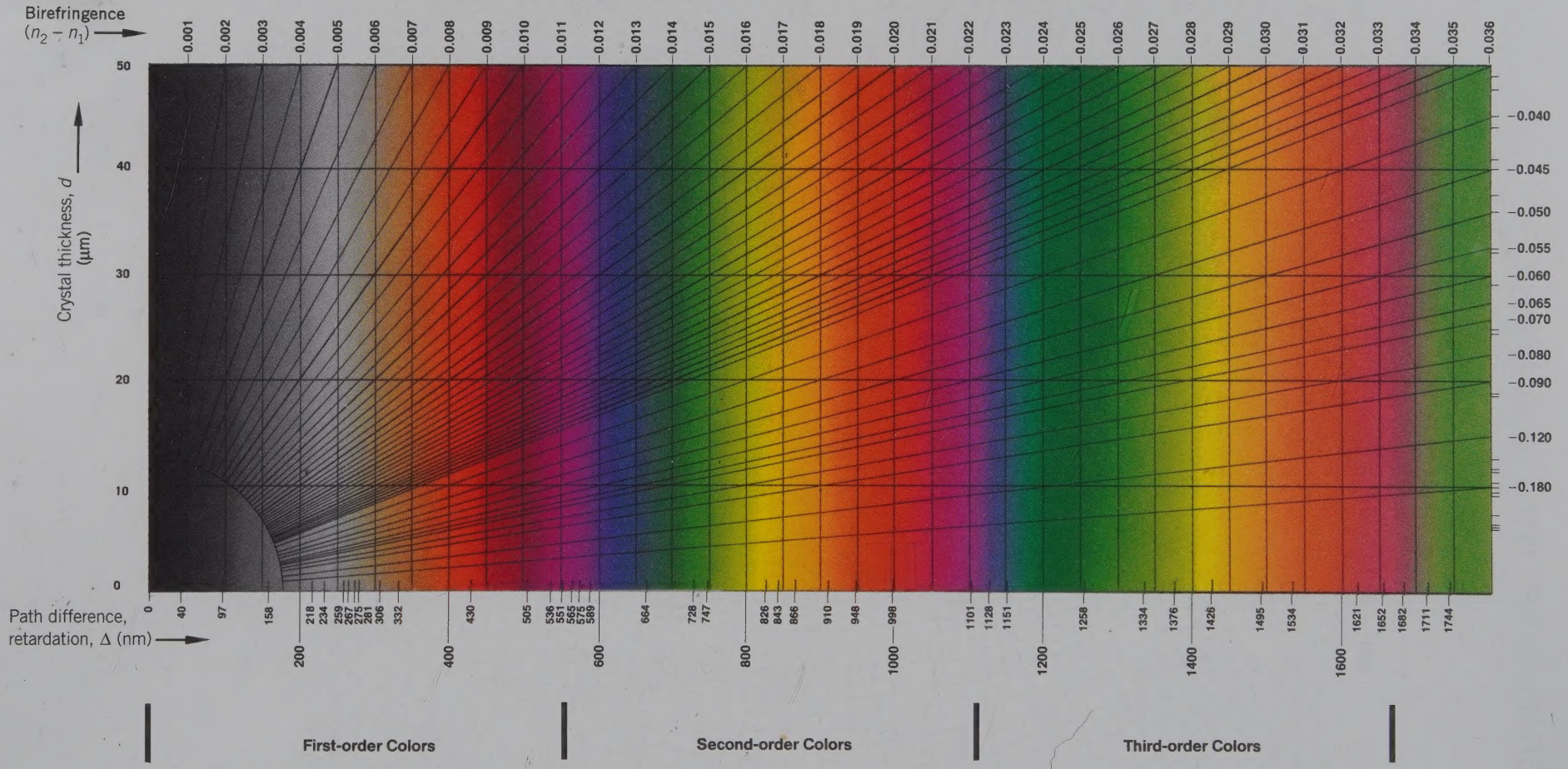

Periodic Table of the Elements

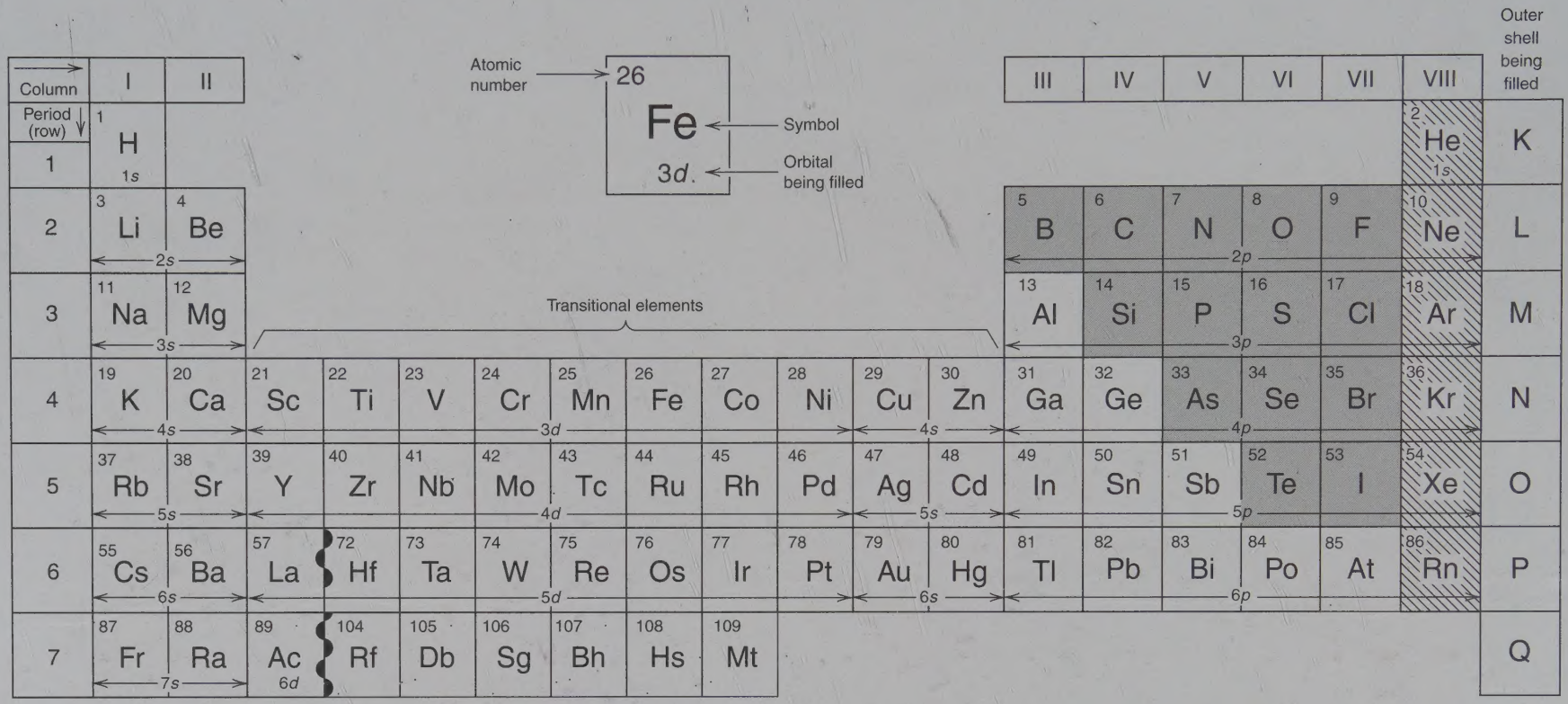

Lanthanide series	58 Ce	59 Pr	60 Nd	61 Pm	62 Sm	63 Eu	64 Gd	65 Tb	66 Dy	67 Ho	68 Er	69 Tm	70 Yb	71 Lu		
							4f									
Actinide series	90 Th	91 Pa	92 U	93 Np	94 Pu	95 Am	96 Cm	97 Bk	98 Cf	99 Es	100 Fm	101 Md	102 No	103 Lr		
	6d															

Metallic elements | Nonmetallic elements | Inert gases | Elements that do not occur naturally

First published in 1848, authored by J.D. Dana, the *Manual of Mineral Science* now enters its 23rd edition. This new edition, authored by Cornelis Klein of the University of New Mexico and Barbara Dutrow of Louisiana State continues in the tradition of its predecessors as the standard textbook in Mineralogy, Mineral Science, Earth Materials, and Rocks and Minerals courses. Over the years, the *Manual of Mineral Science* has brought its authority and comprehensive approach to students the world over: Since the 19th edition, the *Manual of Mineral Science* has been translated into 4 different languages; Russian, Spanish, Chinese, and Italian, and will soon be available in Slovak.

Readable, User-friendly, and Searchable: Now organized into 22 chapters, the 23rd edition of the *Manual of Mineral Science*, packages coherent subject matter into smaller, more easily accessible units. Each of the 22 chapters has a new and expanded introductory statement, which gives the user a quick overview of what is to come. This feature is preceded by a new illustration that highlights some aspect of the subject in that particular chapter. Additionally, many of the first 14 chapters are independent of each other, allowing for greater flexibility in an instructor's preferred subject sequence.

Expanded CD-ROM: The accompanying Mineralogy Tutorial CD-ROM (3.0) has been expanded to include new sections on "graphical representation of mineral chemistry" and "twinning." These additions compliment the already robust CD-ROM, which includes a large number of animations that deal with three-dimensional concepts (in crystal chemistry and crystallography) that are difficult to visualize from a book illustration, as well as brief text pages for 104 of the most common minerals, with links to crystal structure illustrations, compositional and assemblage diagrams, stability and phase diagrams, and solid solution mechanisms.

Digital Images for Classroom Presentation: PowerPoint images, organized by chapter, are now available to enhance classroom presentation. Available on the instructor's companion site, the PowerPoints include: 160 scientific illustrations, 72 color photographs of minerals in Plates I through VIII, 23 new color specimen photos, and gemstones from Plates IX through XII. Additionally, all black and white figures from the textbook are available in digital form in the online Image Gallery. The 23rd edition also offers a complete online glossary.

Updated Visuals: The majority of illustrations in this edition were re-rendered and/or redesigned and many new photographs, mainly of mineral specimens, have been added.

Thoroughly Revised Lab Manual: Also published by John Wiley & Sons, the thoroughly updated *Laboratory Manual: Minerals and Rocks: Exercises in Crystal and Mineral Chemistry, Crystallography, X-ray Powder Diffraction, Mineral and Rock Identification, and Ore Mineralogy*, 3e, is for use in the mineralogy laboratory and covers the subject matter in the same sequence as the *Manual of Mineral Science*, 23e.

ISBN 978-0-471-72157-4

WILEY
1807-2007 KNOWLEDGE FOR GENERATIONS
www.wiley.com/college/klein